CHEM 361: INORGANIC CHEMISTRY



Lori Ann Watson
Earlham College

LibreTexts™

CHEM 361: Inorganic Chemistry (Watson)

This text is disseminated via the Open Education Resource (OER) LibreTexts Project (https://LibreTexts.org) and like the thousands of other texts available within this powerful platform, it is freely available for reading, printing, and "consuming."

The LibreTexts mission is to bring together students, faculty, and scholars in a collaborative effort to provide an accessible, and comprehensive platform that empowers our community to develop, curate, adapt, and adopt openly licensed resources and technologies; through these efforts we can reduce the financial burden born from traditional educational resource costs, ensuring education is more accessible for students and communities worldwide.

Most, but not all, pages in the library have licenses that may allow individuals to make changes, save, and print this book. Carefully consult the applicable license(s) before pursuing such effects. Instructors can adopt existing LibreTexts texts or Remix them to quickly build course-specific resources to meet the needs of their students. Unlike traditional textbooks, LibreTexts' web based origins allow powerful integration of advanced features and new technologies to support learning.



LibreTexts is the adaptable, user-friendly non-profit open education resource platform that educators trust for creating, customizing, and sharing accessible, interactive textbooks, adaptive homework, and ancillary materials. We collaborate with individuals and organizations to champion open education initiatives, support institutional publishing programs, drive curriculum development projects, and more.

The LibreTexts libraries are Powered by NICE CXone Expert and was supported by the Department of Education Open Textbook Pilot Project, the California Education Learning Lab, the UC Davis Office of the Provost, the UC Davis Library, the California State University Affordable Learning Solutions Program, and Merlot. This material is based upon work supported by the National Science Foundation under Grant No. 1246120, 1525057, and 1413739.

Any opinions, findings, and conclusions or recommendations expressed in this material are those of the author(s) and do not necessarily reflect the views of the National Science Foundation nor the US Department of Education.

Have questions or comments? For information about adoptions or adaptions contact info@LibreTexts.org or visit our main website at https://LibreTexts.org.

This text was compiled on 01/11/2026

TABLE OF CONTENTS

Licensing

1: Intro, Review, and Effective Nuclear Charge

- 1.1: Introduction to Inorganic Chemistry
  - 1.1.1: What is Inorganic Chemistry?
  - 1.1.2: Inorganic vs Organic Chemistry
  - 1.1.3: History of Inorganic Chemistry
- 1.2: Atomic Structure
  - 1.2.1: Historical Development of Atomic Theory
    - 1.2.1.1: The Periodic Table
    - 1.2.1.2: Discovery of Subatomic Particles and the Bohr Atom
  - 1.2.2: The Schrödinger equation, particle in a box, and atomic wavefunctions
    - 1.2.2.1: Particle in a Box
    - 1.2.2.2: Quantum Numbers and Atomic Wave Functions
    - 1.2.2.3: Aufbau Principle
    - 1.2.2.4: Shielding
  - 1.2.3: Periodic Properties of Atoms
    - 1.2.3.1: Ionization energy
    - 1.2.3.2: Electron Affinity
    - 1.2.3.3: Covalent and Ionic Radii
    - 1.2.3.4: Hard and Soft Acids and Bases
      - 1.2.3.4.1: Quantitative Measures of Hardness, Softness, and Acid-Base Interactions from a Hard Soft Acid-Base Principle perspective involve orbital energies and or apportioning acid-base bonding in terms of electrostatic and covalent factors
      - 1.2.3.4.2: Hard-Hard and Soft-Soft preferences may be explained and quantified in terms of electrostatic and covalent and electronic stabilization on the stability of Lewis acid-base adducts
- 1.3: Simple Bonding Theory
  - 1.3.1: Lewis Electron-Dot Diagrams
    - 1.3.1.1: Resonance
    - 1.3.1.2: Breaking the octet rule with higher electron counts (hypervalent atoms)
    - 1.3.1.3: Formal Charge
    - 1.3.1.4: Lewis fails to predict unusual cases- Boron and Beryllium
  - 1.3.2: Valence Shell Electron-Pair Repulsion
    - 1.3.2.1: Lone Pair Repulsion
    - 1.3.2.2: Multiple Bonds
    - 1.3.2.3: Electronegativity and Atomic Size Effects
    - 1.3.2.4: Ligand Close Packing
  - 1.3.3: Molecular Polarity
  - 1.3.4: Hydrogen Bonding
  - 1.3.5: Valence Bond Theory
  - 1.3.6: Hybrid Atomic Orbitals

2: Molecular Symmetry and Point Groups

- 2.1: Symmetry Elements and Operations
- 2.2: Point Groups
  - 2.2.1: Groups of Low and High Symmetry
  - 2.2.2: Other Groups
- 2.3: Properties and Representations of Groups
  - 2.3.1: Matrices
  - 2.3.2: Representations of Point Groups
  - 2.3.3: Character Tables
- 2.4: Examples and Applications of Symmetry
  - 2.4.1: Molecular Vibrations
  - 2.4.2: Chirality

3: Molecular Orbital Theory

- 3.1: Prelude to Molecular Orbital Theory
- 3.2: Formation of Molecular Orbitals from Atomic Orbitals
  - 3.2.1: Molecular Orbitals from s Orbitals
  - 3.2.2: Molecular Orbitals from p Orbitals
  - 3.2.3: Molecular orbitals from d orbitals
  - 3.2.4: Nonbonding Orbitals and Other Factors
- 3.3: Homonuclear Diatomic Molecules
  - 3.3.1: Molecular Orbitals
  - 3.3.2: Orbital Mixing
  - 3.3.3: Diatomic Molecules of the First and Second Periods
  - 3.3.4: Photoelectron Spectroscopy
- 3.4: Heteronuclear Diatomic Molecules
  - 3.4.1: Polar bonds
  - 3.4.2: Ionic Compounds and Molecular Orbitals
- 3.5: Larger (Polyatomic) Molecules
  - 3.5.1: Bifluoride anion
  - 3.5.2: Carbon Dioxide
  - 3.5.3: H_2O
  - 3.5.4: NH_3
  - 3.5.5: CO_2 (Revisted with Projection Operators)
  - 3.5.6: BF_3

4: d Block Chemistry

- 4.1: Coordination Chemistry I - Structure and Isomers
  - 4.1.1: History
  - 4.1.2: Nomenclature and Ligands
  - 4.1.3: Isomerism
  - 4.1.4: Coordination Numbers and Structures
- 4.2: Coordination Chemistry II - Bonding
  - 4.2.1: Evidence for Electronic Structures
    - 4.2.1.1: Thermodynamic Data

- 4.2.1.2: Magnetic Susceptibility
- 4.2.1.3: Electronic Spectra
- 4.2.1.4: Coordination Number and Molecular Shapes
- 4.2.2: Bonding Theories
  - 4.2.2.1: Crystal Field Theory
    - 4.2.2.1.1: Crystal Field Theory
    - 4.2.2.1.2: Colors of Coordination Complexes
    - 4.2.2.1.3: Crystal Field Stabilization Energy
    - 4.2.2.1.4: Factors That Affect the Magnitude of Δo
    - 4.2.2.1.5: Jahn-Teller Distortions
    - 4.2.2.1.6: Magnetic Moments of Transition Metals
    - 4.2.2.1.7: Magnetism
    - 4.2.2.1.8: Thermodynamics and Structural Consequences of d-Orbital Splitting
  - 4.2.2.2: Ligand Field Theory
- 4.3: Ligand Exchange Reactions (Thermodynamics)
  - 4.3.1: Associative Ligand Substitution
  - 4.3.2: Dissociative Ligand Substitution
- 4.4: Electronic Spectra of Coordination Compounds

5: Solid State Chemistry

- 5.1: Prelude to Metals and Alloys
- 5.2: Unit Cells and Crystal Structures
- 5.3: Crystal Structures of Metals
  - 5.3.1: Conduction in Metals
- 5.4: Atomic Orbitals and Magnetism
  - 5.4.1: Ferro-, Ferri- and Antiferromagnetism
  - 5.4.2: Hard and Soft Magnets
  - 5.4.3: Defects in Metallic Crystals
- 5.5: X-ray Crystallography
  - 5.5.1: Miller Indices (hkl)
  - 5.5.2: Powder X-ray Diffraction
- 5.6: Prelude to Ionic and Covalent Solids - Structures
  - 5.6.1: Close-packing and Interstitial Sites
  - 5.6.2: Structures Related to NaCl and NiAs
  - 5.6.3: Tetrahedral Structures
  - 5.6.4: Layered Structures and Intercalation Reactions
  - 5.6.5: Spinel, Perovskite, and Rutile Structures
- 5.7: Ionic Radii and Radius Ratios
- 5.8: Energetics of Crystalline Solids- The Ionic Model
  - 5.8.1: Born-Haber Cycles for NaCl and Silver Halides
  - 5.8.2: Lattice Energies and Solubility
  - 5.8.3: Kapustinskii Equation
- 5.9: Electronic Properties of Materials - Superconductors and Semiconductors
  - 5.9.1: Prelude to Electronic Properties of Materials - Superconductors and Semiconductors
  - 5.9.2: Superconductors
  - 5.9.3: Periodic Trends- Metals, Semiconductors, and Insulators

- 5.9.4: Semiconductors- Band Gaps, Colors, Conductivity and Doping
- 5.9.5: Semiconductor p-n Junctions
- 5.9.6: Diodes, LEDs and Solar Cells
- 5.9.7: References

6: Organometallic Chemistry

- 6.1: 18 Valence Electron Rule
- 6.2: Synthesis and Stability
  - 6.2.1: Transition Metal Alkyl Complexes
  - 6.2.2: Metal-Carbenes
  - 6.2.3: Metal Hydrides
  - 6.2.4: Metal Carbonyls
  - 6.2.5: Metal Phosphines
  - 6.2.6: Complexes of π−bound Ligands
    - 6.2.6.1: Metal Alkene Complexes
    - 6.2.6.2: Metal Allyl and Diene Complexes
    - 6.2.6.3: Metal Cyclopentadienyl Complexes
- 6.3: Reaction Mechanisms
  - 6.3.1: Oxidative Addition and Reductive Elimination
  - 6.3.2: Insertion and Elimination Reactions
  - 6.3.3: Nucleophilic and Electrophilic Addition and Abstraction
- 6.4: Applications
  - 6.4.1: Homogeneous Catalysis - I
  - 6.4.2: Homogeneous Catalysis - II
  - 6.4.3: Catalytic Applications of Organometallic Compounds- Alkene Metathesis

7: Bioinorganic Chemistry

- 7.1: Biological Significance of Iron, Zinc, Copper, Molybdenum, Cobalt, Chromium, Vanadium, and Nickel
- 7.2: Introduction to Amino Acids and Proteins
- 7.3: Overview of Hemoglobin and Myoglobin
  - 7.3.1: Myoglobin, Hemoglobin, and their Ligands
  - 7.3.2: Oxygen Transport by the Proteins Myoglobin and Hemoglobin
- 7.4: Ferrodoxins, Hydrogenases, and Nitrogenases - Metal-Sulfide Proteins
  - 7.4.1: Iron-sulfur Proteins and Models
  - 7.4.2: Iron-sulfur Proteins and Models (Part 2)
  - 7.4.3: Iron-sulfur Proteins and Models (Part 3)
  - 7.4.4: Iron-sulfur Proteins and Models (Part 4)
- 7.5: The Reaction Pathways of Zinc Enzymes and Related Biological Catalysts
  - 7.5.1: About Carbonic Anhydrase
  - 7.5.2: Catalytic Mechanism
  - 7.5.3: Metal Substitution
- 7.6: Metals in Medicine
  - 7.6.1: Metal Deficiency and Disease
  - 7.6.2: Toxic Effects of Metals
  - 7.6.3: Aspects of Platinum Binding to DNA
  - 7.6.4: Survey of Metals Used for Diagnosis and Chemotherapy
  - 7.6.5: Platinum Anticancer Drugs- A Case Study

- 7.6.6: Mapping the Major Adducts of cis- and trans-DDP on DNA; Sequence Specificity
- 7.6.7: Structure of Platinum-DNA Complexes
- 7.6.8: Site-specifically Platinated DNA \(\;^{154}\)
- 7.6.9: Bioinorganic Chemistry of Platinum Anticancer Drugs- How Might They Work?
- 7.6.10: Bioinorganic Chemistry of Platinum Anticancer Drugs; How Might They Work? (Part 2)
- 7.6.11: Design of New Inorganic Anticancer Drugs

Index

Glossary

Detailed Licensing

Licensing

*A detailed breakdown of this resource's licensing can be found in **Back Matter/Detailed Licensing**.*

CHAPTER OVERVIEW

1: Intro, Review, and Effective Nuclear Charge

1.1: Introduction to Inorganic Chemistry

1.2: Atomic Structure

1.3: Simple Bonding Theory

1.1: Introduction to Inorganic Chemistry
1.1.1: What is Inorganic Chemistry?
1.1.2: Inorganic vs Organic Chemistry
1.1.3: History of Inorganic Chemistry
1.2: Atomic Structure
1.2.1: Historical Development of Atomic Theory
1.2.1.1: The Periodic Table
1.2.1.2: Discovery of Subatomic Particles and the Bohr Atom
1.2.2: The Schrödinger equation, particle in a box, and atomic wavefunctions
1.2.2.1: Particle in a Box
1.2.2.2: Quantum Numbers and Atomic Wave Functions
1.2.2.3: Aufbau Principle
1.2.2.4: Shielding
1.2.3: Periodic Properties of Atoms
1.2.3.1: Ionization energy
1.2.3.2: Electron Affinity
1.2.3.3: Covalent and Ionic Radii
1.2.3.4: Hard and Soft Acids and Bases
1.2.3.4.1: Quantitative Measures of Hardness, Softness, and Acid-Base Interactions from a Hard Soft Acid-Base Principle perspective involve orbital energies and or apportioning acid-base bonding in terms of electrostatic and covalent factors
1.2.3.4.2: Hard-Hard and Soft-Soft preferences may be explained and quantified in terms of electrostatic and covalent and electronic stabilization on the stability of Lewis acid-base adducts
1.3: Simple Bonding Theory
1.3.1: Lewis Electron-Dot Diagrams
1.3.1.1: Resonance
1.3.1.2: Breaking the octet rule with higher electron counts (hypervalent atoms)
1.3.1.3: Formal Charge
1.3.1.4: Lewis fails to predict unusual cases- Boron and Beryllium
1.3.2: Valence Shell Electron-Pair Repulsion
1.3.2.1: Lone Pair Repulsion
1.3.2.2: Multiple Bonds
1.3.2.3: Electronegativity and Atomic Size Effects
1.3.2.4: Ligand Close Packing
1.3.3: Molecular Polarity
1.3.4: Hydrogen Bonding

1.3.5: Valence Bond Theory
1.3.6: Hybrid Atomic Orbitals

1: Intro, Review, and Effective Nuclear Charge is shared under a not declared license and was authored, remixed, and/or curated by LibreTexts.

SECTION OVERVIEW

1.1: Introduction to Inorganic Chemistry

This chapter introduces some history and context about the field of Inorganic Chemistry.

1.1.1: What is Inorganic Chemistry?

1.1.2: Inorganic vs Organic Chemistry

1.1.3: History of Inorganic Chemistry

1.1: Introduction to Inorganic Chemistry is shared under a not declared license and was authored, remixed, and/or curated by LibreTexts.

1.1.1: What is Inorganic Chemistry?

Where did the name "Inorganic Chemistry" come from? Well, the term "Organic Chemistry" literally means the *chemistry of life*. Organic chemistry is the study of carbon-based molecules because the first molecules that were isolated from living organisms contained carbon. On the other hand, minerals and other non-living things seemed to be made of other elements. For some time in our history, scientists believed that the chemical difference between living and non-living things was carbon. So, if "organic" molecules are the molecules of life, then is "inorganic chemistry" the "chemistry of death"? Almost? "Inorganic" chemistry historically meant the chemistry of "non-living" things; and these were non-carbon based molecules and ions.

The names "organic" and "inorganic" come from science history, and still today a generally-accepted definition of *Inorganic Chemistry is the study of non-carbon molecules, or all the elements on the periodic table except carbon (*Figure **1.1.1.1**. But, this definition is not completely correct because the field of Inorganic Chemistry also includes organometallic compounds and the study of some carbon-based molecules that have properties that are familiar to metals (like conduction of electricity). This makes the field of inorganic chemistry very broad, and practically limitless. A great way to understand the breadth of the field is to take a look at the abstracts in the latest article of Inorganic Chemistry. Or, check out the 20 most-read articles from this past year using the links below.

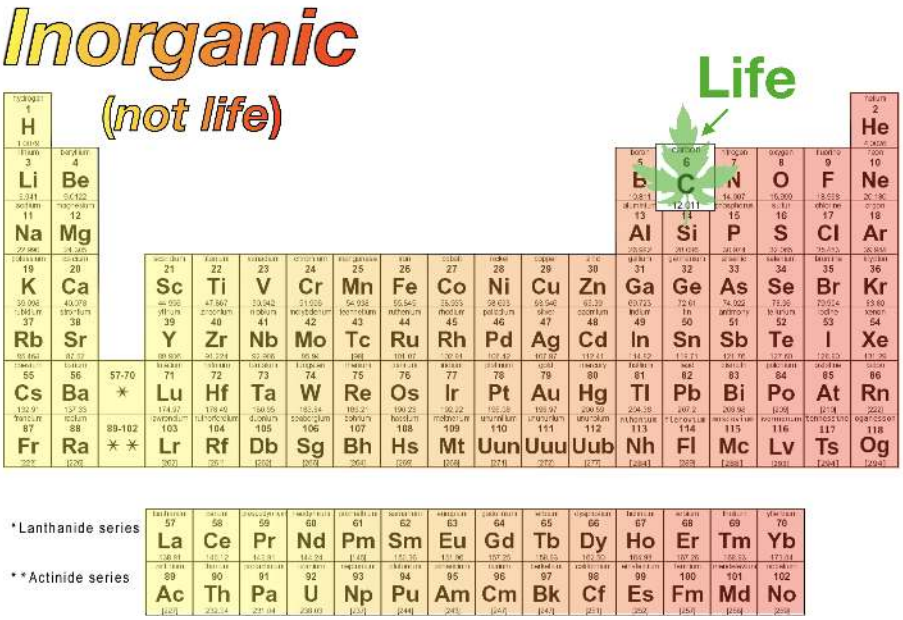


Figure **1.1.1.1**. An illustration of the historic meaning of "organic" and "inorganic". The modern understanding of organic and inorganic chemistry is not consistent with these historical meanings. (Kathryn Haas; CC-NC-BY-SA)

External links:

- The journal, Inorganic Chemistry: https://pubs.acs.org/journal/inocaj
- The latest issue of Inorganic chemistry: https://pubs.acs.org/toc/inocaj/current
- The most popular Inorganic Chemistry articles from the past month and the past year: https://pubs.acs.org/action/showMostReadArticles?journalCode=inocaj

Practice

? What are the Sub-Fields of Inorganic Chemistry?

To appreciate the breadth of Inorganic Chemistry, go to the most recent issue of Inorganic Chemistry and look at the titles and visual abstracts. Identify at least 4 sub-fields of Inorganic Chemistry.

Answer

> There are a lot of correct answers here! The point here is that you notice that Inorganic Chemistry is a very broad field. It has something for almost everyone because many other fields overlap with Inorganic Chemistry. You might notice that some of the sub-fields you identified are also interdisciplinary fields between inorganic chemistry and another discipline. For a list of some of the subfields of Inorganic Chemistry, check this Wikipedia article.

1.1.1: What is Inorganic Chemistry? is shared under a not declared license and was authored, remixed, and/or curated by LibreTexts.

- **1.1: What is Inorganic Chemistry?** by Kathryn Haas is licensed CC BY-NC-SA 4.0.

1.1.2: Inorganic vs Organic Chemistry

The division between the fields of Inorganic and Organic chemistry has become blurred. For example, let's look at one of the major classes of catalysts used for organic synthesis reactions: organometalic catalysts (Figure **1.1.2.1**). Organometallic catalysts like these, and all organometallic compounds, contain metals that are bonded to carbon or carbon-containing molecules. So, are they "inorganic" because they contain metals, or "organic" because they contain carbon? These illustrate that clear divisions between organic and inorganic chemistry do not exist. Further, metal ions are common in biology and so the idea that metals are "inorganic" and thus classed as "non-living or non-biological" is incorrect. A canonical example is the organometallic catalyst adenosylcobalbumin, which is an important biological cofactor containing a cobalt (Co) ion (Figure **1.1.2.1**, right) and a cobalt-carbon bond.

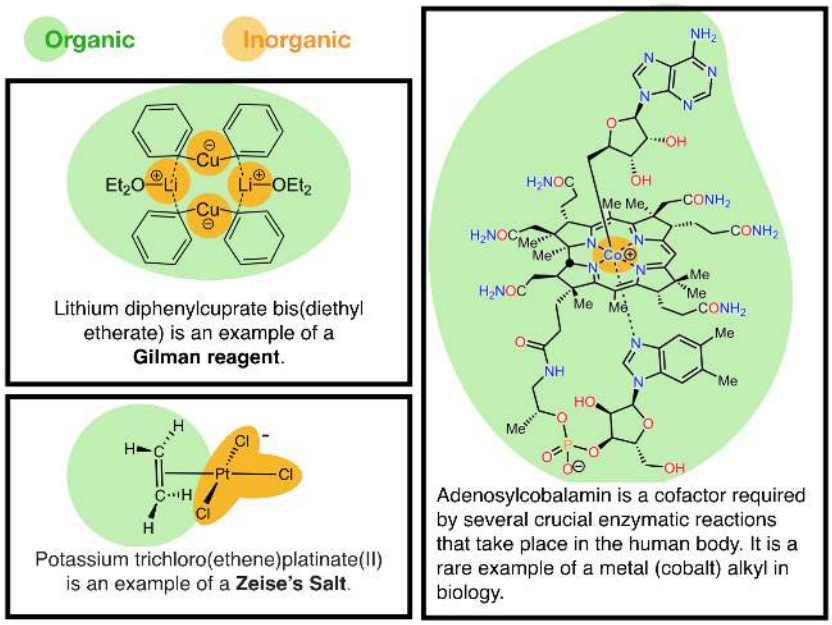
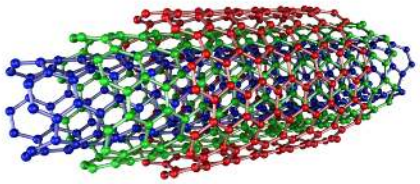


Figure **1.1.2.1**: Some examples of organometallic catalysts. These compounds catalyze organic reactions or biochemical reactions and they are compounds that contain both carbon and metals. These compounds are examples of molecules that cannot be defined only as organic molecules or only as inorganic molecules. Adenosylcobalbumin is an example of an organometallic catalyst that is present in biology, further illustrating that "inorganic" metals are important cofactors in biology. This image is based on information on the Wikipedia article on Organometallic Chemistry and is created from images found there; attribution to images created by Alsosaid1987, AdoCbl-ColorCoded, CC BY-SA 4.0 and Smokefoot, Zeise'sSalt, CC BY-SA 3.0. (Kathryn Haas; CC-BY-SA)

Some of the subfields of Inorganic Chemistry focus on electrical conductivity of inorganic materials (i.e., conduction, superconduction, and semiconduction) and on the study of optical and electronic properties of inorganic nanomaterials. Electrical conductivity is a canonical property of metals, but carbon-based materials also demonstrate electrical conductivity. For example, carbon nanotubes conduct electricity through their extended conjugated π systems. Fullerenes, of which the most famous is Buckminsterfullerene, or Buckeyball (C_{60}), demonstrate interesting properties that are similar to nanoparticles, and when combined with metals and crystallized can demonstrate superconductivity.



Buckminsterfullerene is a type of fullerene with the formula C_{60}



Triple-walled armchair **carbon nanotube**

Figure **1.1.2.2**: This figure is created from information found on the Wikipedia articles for Buckmisterfullerene and carbon nanotubes. Attribution Eric Wieser, Multi-walled Carbon Nanotube, CC BY-SA 3.0. (Kathryn Haas; CC-BY-SA)

Although carbon nanotubes and fullerenes are allotropes of carbon, their material properties are somewhat foreign to many organic chemists, who traditionally have focused on smaller organic molecules having very different properties. However, these properties are familiar to inorganic chemists. Thus, inorganic chemists have embraced these molecules as "inorganic" due to the fact that they behave more like inorganic materials than smaller organic molecules. This class of carbon-based molecules serves as another example of molecules that are not perfectly matched to the traditional definitions of "organic" and "inorganic" chemistry. Certainly, the future will hold more and more examples of molecules that do not fit into the traditional disciplines of chemistry.

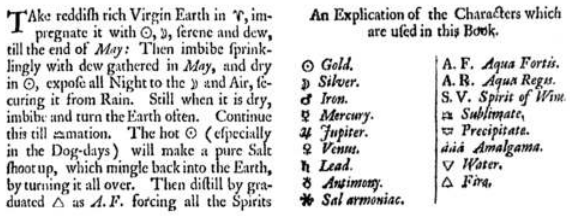
This page titled 1.1.2: Inorganic vs Organic Chemistry is shared under a not declared license and was authored, remixed, and/or curated by Kathryn Haas.

- **1.2: Inorganic vs Organic Chemistry** by Kathryn Haas is licensed CC BY-NC-SA 4.0.

1.1.3: History of Inorganic Chemistry

Metals serve an essential role in many aspects of human civilization and have defined ages of human history. The period of time from about 3300 BC to 1200 BC is often referred to as the Bronze Age. During this period our ancestors first started using metal and learned to mix various elements with copper to make a strong alloy, called bronze. This age yielded significant advancement in the crafting of sharper knives and stronger weapons out of metal instead of rock, wood and bone. Around 1200 BC the human race found an even harder metal and discovered a much stronger alloy called steel. This period is known as the Iron Age. More recently, periods of time known as Gold Rushes have caused huge changes in population distributions and wealth in some countries. Metal has obvious importance in our modern way of life. Today, iron and steel are used for making buildings, machines, automobiles, jewelry, cooking pots, tools, weapons, vehicles, electronics, surgical instruments and symbolic structures like the Eiffel Tower and the Statue of Liberty. Gold, silver, and copper still serve as currency for trade and exchange of goods and services.

The existence of chemistry as a field of study owes much to the fact that gold was a valuable commodity throughout our history. In both the ancient Egyptian society and during the Roman Empire, gold mines were the property of the state, not an individual or group. So there were few ways for most people to legally get any gold for themselves. The Alchemists were a varied group of scholars and charlatans who aimed to solve this problem by creating the **Philosopher's Stone** (which caused the transmutation of lead into gold). Three major streams of alchemy are known: Chinese, Indian, and European, with all three streams having some factors in common. Techniques developed in the European stream ultimately influenced the development of the science of chemistry.


TAke reddiſh rich Virgin Earth in ♈, impregnate it with ☉, ☽, ſerene and dew, till the end of *May*: Then imbibe ſprinklingly with dew gathered in *May*, and dry in ☉, expoſe all Night to the ☽ and Air, ſecuring it from Rain. Still when it is dry, imbibe and turn the Earth often. Continue this till ♎mation. The hot ☉ (eſpecially in the Dog-days) will make a pure Salt ſhoot up, which mingle back into the Earth, by turning it all over. Then diſtill by graduated △ as *A. F.* forcing all the Spirits

An Explication of the Characters which are uſed in this Book.

☉ *Gold.*
☽ *Silver.*
♂ *Iron.*
☿ *Mercury.*
♃ *Jupiter.*
♀ *Venus.*
♄ *Lead.*
♁ *Antimony.*
❋ *Sal armoniac.*

A. F. *Aqua Fortis.*
A. R. *Aqua Regis.*
S. V. *Spirit of Wine.*
♎ *Sublimate.*
♈ *Precipitate.*
ȧȧȧ Amalgama.
▽ *Water.*
△ *Fire.*

Figure 1.1.3.1. Alchemist recipe. Many of the specific approaches that alchemists used when they tried changing lead into gold are vague and unclear. Each alchemist had his own code for recording his data. The processes were kept secret so others could not profit from them. Different scholars developed their own set of symbols as they recorded the information they came up with. Many alchemists were not very honest, taking money from a nobleman by claiming to be able to make gold from lead, then leaving town in the middle of the night. Sometimes the nobleman would detect the fraud and have the alchemist hung. By the 1300's, several European rules had declared alchemy to be illegal and set out strict punishments for those practicing the alchemical arts.

Although alchemists were never successful in changing lead into gold, they made several contributions to modern-day chemistry. Strong acids and bases were discovered, including nitric acid (*ce*$HNO3$), sulfuric acid (H_2SO_4), and hydrochloric acid (HCl), as well as sodium hydroxide ($NaOH$). Glassware for running chemical reactions was developed, as were methods for distillation, crystallization, and sublimation. Alchemy helped improve the study of metallurgy and the extraction of metals from ores. More systematic approaches to research were developed that allowed the discovery of atoms and laid the groundwork for development of the periodic table. For more about the History of Chemistry in general, try the LibreText page A Brief History of Chemistry.

Inorganic compounds have been known and used since antiquity; probably the oldest is the deep blue pigment called Prussian blue ($Fe_4[Fe(CN)_6]_3$). However, the chemical nature of these substances was unknown until the late nineteenth and early twentieth century when the modern field of coordination chemistry emerged. Much of what we know about inorganic chemistry is based largely on the work of and debates between Alfred Werner (1866–1919; Nobel Prize in Chemistry in 1913) and Sophus Mads Jørgensen (1837 –1914). After Werner succeeded in these debates, the field of inorganic chemistry declined in popularity until the mid-twentieth century, when the second world war stimulated renewed interest. During the post-war era, several important discoveries and theories were developed. For example, important theories of bonding in coordination compounds were developed.

Soon after World War II, Crystal Field Theory (CFT) and Ligand Field Theory (LFT) were developed. These are two critical and complimentary theories that provide explanations of spectroscopic, chemical, and structural properties of inorganic coordination compounds, CFT being more simple, and LFT more accurate. In the 1950's, organometallic catalysts were discovered that catalyzed important organic reactions and the Haber-Bosch Process was discovered. The Haber-Bosch Process is catalyzed by an inorganic oxide catalyst and is one of the world's most important industrial reactions. It provides for the synthesis of ammonia directly from elemental nitrogen, N_2, and hydrogen, H_2.

$$N_2(g) + 3H_2(g) \rightleftharpoons 2NH_3(g) \quad (1.1.3.1)$$

Since its development in the early twentieth century, it has led to the production of an enormous quantity of fertilizer, vastly increasing global food production. As a result, it is estimated that a significant fraction of the nitrogen content in the typical human body is ultimately derived from this process. Yet while the reaction must be run at high temperatures and pressures in the industrial setting, the nitrogenase enzyme in the roots of plants can carry out this reaction at the mild conditions within the soil. Intense investigations were then aimed at improving inorganic catalysts through understanding the metal cofactors in enzymes. The link between the Haber-Bosch industrial process and the nitrogenase enzyme was an early bridge between the fields of organometallic chemistry and biochemistry.

Contributions

Part of this page is adapted from K.Haas Ph.D. dissertation

Part of this page is adapted from the following LibreTexts pages

- Alchemy contributed by CK-12 Foundation by Sharon Bewick, Richard Parsons, Therese Forsythe, Shonna Robinson, and Jean Dupon.
- Werner's Theory of Coordination Compounds
- The Haber-Bosch Process Worksheet

1.1.3: History of Inorganic Chemistry is shared under a CC BY-NC-SA 4.0 license and was authored, remixed, and/or curated by LibreTexts.

- **1.3: History of Inorganic Chemistry** by Kathryn Haas is licensed CC BY-NC-SA 4.0.

SECTION OVERVIEW

1.2: Atomic Structure

1.2.1: Historical Development of Atomic Theory

- 1.2.1.1: The Periodic Table
- 1.2.1.2: Discovery of Subatomic Particles and the Bohr Atom

1.2.2: The Schrödinger equation, particle in a box, and atomic wavefunctions

- 1.2.2.1: Particle in a Box
- 1.2.2.2: Quantum Numbers and Atomic Wave Functions
- 1.2.2.3: Aufbau Principle
- 1.2.2.4: Shielding

1.2.3: Periodic Properties of Atoms

- 1.2.3.1: Ionization energy
- 1.2.3.2: Electron Affinity
- 1.2.3.3: Covalent and Ionic Radii
- 1.2.3.4: Hard and Soft Acids and Bases
  - 1.2.3.4.1: Quantitative Measures of Hardness, Softness, and Acid-Base Interactions from a Hard Soft Acid-Base Principle perspective involve orbital energies and or apportioning acid-base bonding in terms of electrostatic and covalent factors
  - 1.2.3.4.2: Hard-Hard and Soft-Soft preferences may be explained and quantified in terms of electrostatic and covalent and electronic stabilization on the stability of Lewis acid-base adducts

---

1.2: Atomic Structure is shared under a not declared license and was authored, remixed, and/or curated by LibreTexts.

1.2.1: Historical Development of Atomic Theory

Notes about this page

The page below is a brief overview on the history of atomic theory. It contains lots of video media.

Alternatives pages on the history of atomic theory are:

- A more detailed overview that includes practice problems is here (click).
- Another brief overview is here (click).

Skills to Develop

By the end of this section, you will be able to:

- State the postulates of Dalton's atomic theory
- Use postulates of Dalton's atomic theory to explain the laws of definite and multiple proportions
- Outline milestones in the development of modern atomic theory
- Summarize and interpret the results of the experiments of Thomson, Millikan, and Rutherford

A Video Introduction to Atomic Theory through the Nineteenth Century From Crash Course Chemistry



***Video* 1.2.1.1*:* Lavoisier's discovery of The Law of Conservation of Matter led to the Laws of Definite and Multiple Proportions and eventually Dalton's Atomic Theory.**

Atomic Theory through the Nineteenth Century

The earliest recorded discussion of the basic structure of matter comes from ancient Greek philosophers, the scientists of their day. In the fifth century BC, Leucippus and Democritus argued that all matter was composed of small, finite particles that they called *atomos*, a term derived from the Greek word for "indivisible." They thought of atoms as moving particles that differed in shape and size, and which could join together. Later, Aristotle and others came to the conclusion that matter consisted of various combinations of the four "elements"—fire, earth, air, and water—and could be infinitely divided. Interestingly, these philosophers thought about atoms and "elements" as philosophical concepts, but apparently never considered performing experiments to test their ideas.

The Aristotelian view of the composition of matter held sway for over two thousand years, until English schoolteacher John Dalton helped to revolutionize chemistry with his hypothesis that the behavior of matter could be explained using an atomic theory. First published in 1807, many of Dalton's hypotheses about the microscopic features of matter are still valid in modern atomic theory. Here are the postulates of Dalton's atomic theory.

1. Matter is composed of exceedingly small particles called atoms. An atom is the smallest unit of an element that can participate in a chemical change.

2. An element consists of only one type of atom, which has a mass that is characteristic of the element and is the same for all atoms of that element (Figure **1.2.1.1**). A macroscopic sample of an element contains an incredibly large number of atoms, all of which have identical chemical properties.
3. Atoms of one element differ in properties from atoms of all other elements.
4. A compound consists of atoms of two or more elements combined in a small, whole-number ratio. In a given compound, the numbers of atoms of each of its elements are always present in the same ratio (Figure **1.2.1.2**).
5. Atoms are neither created nor destroyed during a chemical change, but are instead rearranged to yield substances that are different from those present before the change (Figure **1.2.1.3**).

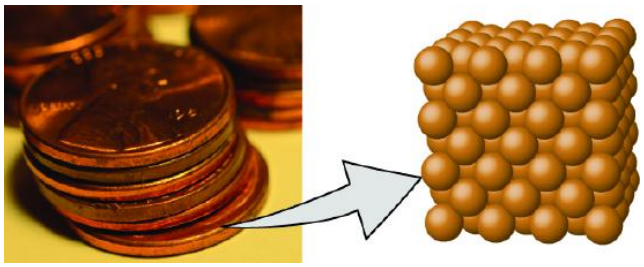


Figure* 1.2.1.1*: *A pre-1982 copper penny (left) contains approximately 3×10^{22} copper atoms (several dozen are represented as brown spheres at the right), each of which has the same chemical properties. (credit: modification of work by "slgckgc"/Flickr)*

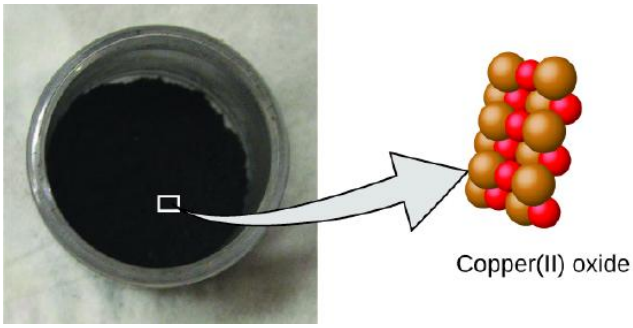


Figure* 1.2.1.2*: *Copper(II) oxide, a powdery, black compound, results from the combination of two types of atoms—copper (brown spheres) and oxygen (red spheres)—in a 1:1 ratio. (credit: modification of work by "Chemicalinterest"/Wikimedia Commons)*

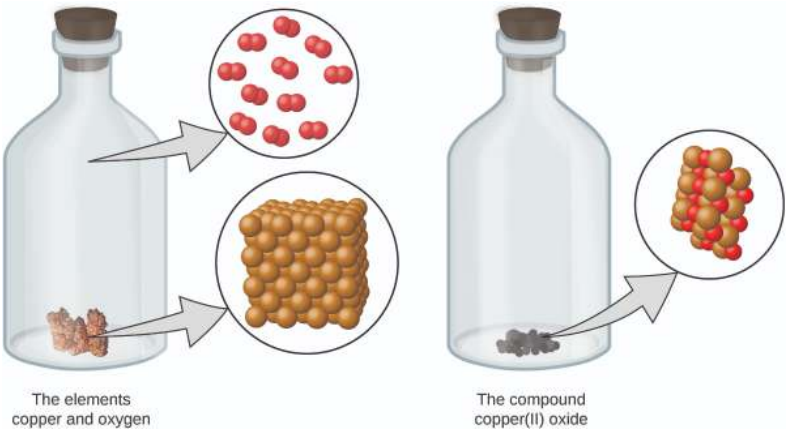


Figure* 1.2.1.3: When the elements copper (a shiny, red-brown solid, shown here as brown spheres) and oxygen (a clear and colorless gas, shown here as red spheres) react, their atoms rearrange to form a compound containing copper and oxygen (a powdery, black solid). (credit copper: modification of work by http://images-of-elements.com/copper.php).*

Dalton's atomic theory provides a microscopic explanation of the many macroscopic properties of matter that you've learned about. For example, if an element such as copper consists of only one kind of atom, then it cannot be broken down into simpler substances, that is, into substances composed of fewer types of atoms. And if atoms are neither created nor destroyed during a

chemical change, then the total mass of matter present when matter changes from one type to another will remain constant (the law of conservation of matter (or mass)).

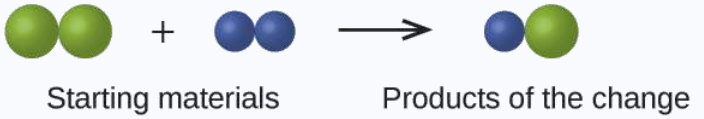
Want to learn more about the Law of Conservation of Mass?



Video* 1.2.1.2*: "We are made of star stuff" - Carl Sagan.

Example 1.2.1.1: Testing Dalton's Atomic Theory

In the following drawing, the green spheres represent atoms of a certain element. The purple spheres represent atoms of another element. If the spheres touch, they are part of a single unit of a compound. Does the following chemical change represented by these symbols violate any of the ideas of Dalton's atomic theory? If so, which one?



Solution

The starting materials consist of two green spheres and two purple spheres. The products consist of only one green sphere and one purple sphere. This violates Dalton's postulate that atoms are neither created nor destroyed during a chemical change, but are merely redistributed. (In this case, atoms appear to have been destroyed.)

Exercise 1.2.1.1

In the following drawing, the green spheres represent atoms of a certain element. The purple spheres represent atoms of another element. If the spheres touch, they are part of a single unit of a compound. Does the following chemical change represented by these symbols violate any of the ideas of Dalton's atomic theory? If so, which one



Answer

The starting materials consist of four green spheres and two purple spheres. The products consist of four green spheres and two purple spheres. This does not violate any of Dalton's postulates: Atoms are neither created nor destroyed, but are redistributed in small, whole-number ratios.

Dalton knew of the experiments of French chemist Joseph Proust, who demonstrated that *all samples of a pure compound contain the same elements in the same proportion by mass*. This statement is known as the law of definite proportions or the law of constant composition. The suggestion that the numbers of atoms of the elements in a given compound always exist in the same ratio is

consistent with these observations. For example, when different samples of isooctane (a component of gasoline and one of the standards used in the octane rating system) are analyzed, they are found to have a carbon-to-hydrogen mass ratio of 5.33:1, as shown in Table **1.2.1.1**.

***Table* 1.2.1.1**: *Constant Composition of Isooctane*

Sample	Carbon	Hydrogen	Mass Ratio
A	14.82 g	2.78 g	$\frac{\text{14.82 g carbon}}{\text{2.78 g hydrogen}} = \frac{\text{5.33 g carbon}}{\text{1.00 g hydrogen}}$
B	22.33 g	4.19 g	$\frac{\text{22.33 g carbon}}{\text{4.19 g hydrogen}} = \frac{\text{5.33 g carbon}}{\text{1.00 g hydrogen}}$
C	19.40 g	3.64 g	$\frac{\text{19.40 g carbon}}{\text{3.63 g hydrogen}} = \frac{\text{5.33 g carbon}}{\text{1.00 g hydrogen}}$

It is worth noting that although all samples of a particular compound have the same mass ratio, the converse is not true in general. That is, samples that have the same mass ratio are not necessarily the same substance. For example, there are many compounds other than isooctane that also have a carbon-to-hydrogen mass ratio of 5.33:1.00.

Dalton also used data from Proust, as well as results from his own experiments, to formulate another interesting law. The law of multiple proportions states that *when two elements react to form more than one compound, a fixed mass of one element will react with masses of the other element in a ratio of small, whole numbers*. For example, copper and chlorine can form a green, crystalline solid with a mass ratio of 0.558 g chlorine to 1 g copper, as well as a brown crystalline solid with a mass ratio of 1.116 g chlorine to 1 g copper. These ratios by themselves may not seem particularly interesting or informative; however, if we take a ratio of these ratios, we obtain a useful and possibly surprising result: a small, whole-number ratio.

$$\frac{\frac{\text{1.116 g Cl}}{\text{1 g Cu}}}{\frac{\text{0.558 g Cl}}{\text{1 g Cu}}} = \frac{2}{1} \tag{1.2.1.1}$$

This 2-to-1 ratio means that the brown compound has twice the amount of chlorine per amount of copper as the green compound.

This can be explained by atomic theory if the copper-to-chlorine ratio in the brown compound is 1 copper atom to 2 chlorine atoms, and the ratio in the green compound is 1 copper atom to 1 chlorine atom. The ratio of chlorine atoms (and thus the ratio of their masses) is therefore 2 to 1 (Figure **1.2.1.4**).

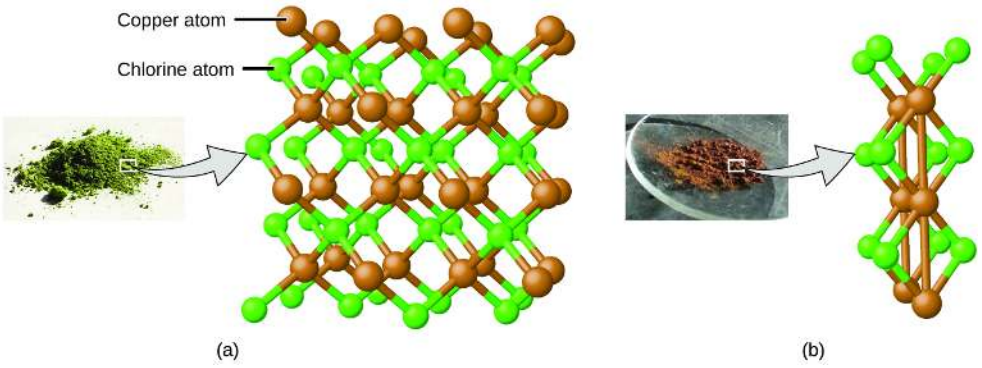


***Figure* 1.2.1.4**: *Compared to the copper chlorine compound in (a), where copper is represented by brown spheres and chlorine by green spheres, the copper chlorine compound in (b) has twice as many chlorine atoms per copper atom. (credit a: modification of work by "Benjah-bmm27"/Wikimedia Commons; credit b: modification of work by "Walkerma"/Wikimedia Commons)*

Example 1.2.1.2: Laws of Definite and Multiple Proportions

A sample of compound A (a clear, colorless gas) is analyzed and found to contain 4.27 g carbon and 5.69 g oxygen. A sample of compound B (also a clear, colorless gas) is analyzed and found to contain 5.19 g carbon and 13.84 g oxygen. Are these data an example of the law of definite proportions, the law of multiple proportions, or neither? What do these data tell you about substances A and B?

Solution

In compound A, the mass ratio of carbon to oxygen is:

$$\frac{1.33\text{ g O}}{1\text{ g C}}$$

In compound B, the mass ratio of carbon to oxygen is:

$$\frac{2.67\text{ g O}}{1\text{ g C}}$$

The ratio of these ratios is:

$$\frac{\frac{1.33\text{ g O}}{1\text{ g C}}}{\frac{2.67\text{ g O}}{1\text{ g C}}} = \frac{1}{2}$$

This supports the law of multiple proportions. This means that A and B are different compounds, with A having one-half as much carbon per amount of oxygen (or twice as much oxygen per amount of carbon) as B. A possible pair of compounds that would fit this relationship would be A = CO_2 and B = CO.

Exercise 1.2.1.2

A sample of compound X (a clear, colorless, combustible liquid with a noticeable odor) is analyzed and found to contain 14.13 g carbon and 2.96 g hydrogen. A sample of compound Y (a clear, colorless, combustible liquid with a noticeable odor that is slightly different from X's odor) is analyzed and found to contain 19.91 g carbon and 3.34 g hydrogen. Are these data an example of the law of definite proportions, the law of multiple proportions, or neither? What do these data tell you about substances X and Y?

Answer

In compound X, the mass ratio of carbon to hydrogen is $\frac{14.13\text{ g C}}{2.96\text{ g H}}$.

In compound Y, the mass ratio of carbon to oxygen is $\frac{19.91\text{ g C}}{3.34\text{ g H}}$.

The ratio of these ratios is

$$\frac{\frac{14.13\text{ g C}}{2.96\text{ g H}}}{\frac{19.91\text{ g C}}{3.34\text{ g H}}} = \frac{4.77\text{ g C/g H}}{5.96\text{ g C/g H}} = 0.800 = \frac{4}{5}.$$

This small, whole-number ratio supports the law of multiple proportions. This means that X and Y are different compounds.

In the two centuries since Dalton developed his ideas, scientists have made significant progress in furthering our understanding of atomic theory. Much of this came from the results of several seminal experiments that revealed the details of the internal structure of atoms. Here, we will discuss some of those key developments, with an emphasis on application of the scientific method, as well as understanding how the experimental evidence was analyzed. While the historical persons and dates behind these experiments can be quite interesting, it is most important to understand the concepts resulting from their work.

Atomic Theory after the Nineteenth Century

If matter were composed of atoms, what were atoms composed of? Were they the smallest particles, or was there something smaller? In the late 1800s, a number of scientists interested in questions like these investigated the electrical discharges that could be produced in low-pressure gases, with the most significant discovery made by English physicist J. J. Thomson using a cathode ray tube. This apparatus consisted of a sealed glass tube from which almost all the air had been removed; the tube contained two metal electrodes. When high voltage was applied across the electrodes, a visible beam called a cathode ray appeared between them.

This beam was deflected toward the positive charge and away from the negative charge, and was produced in the same way with identical properties when different metals were used for the electrodes. In similar experiments, the ray was simultaneously deflected by an applied magnetic field, and measurements of the extent of deflection and the magnetic field strength allowed Thomson to calculate the charge-to-mass ratio of the cathode ray particles. The results of these measurements indicated that these particles were much lighter than atoms (Figure 1.2.1.1).

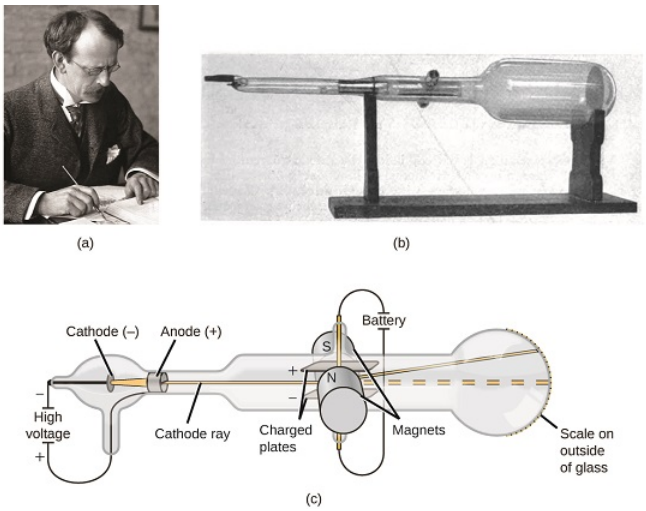
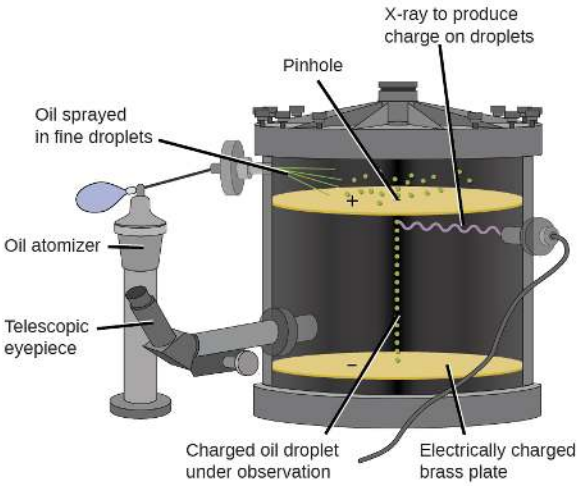


***Figure* 1.2.1.5**: *(a) J. J. Thomson produced a visible beam in a cathode ray tube. (b) This is an early cathode ray tube, invented in 1897 by Ferdinand Braun. (c) In the cathode ray, the beam (shown in yellow) comes from the cathode and is accelerated past the anode toward a fluorescent scale at the end of the tube. Simultaneous deflections by applied electric and magnetic fields permitted Thomson to calculate the mass-to-charge ratio of the particles composing the cathode ray. (credit a: modification of work by Nobel Foundation; credit b: modification of work by Eugen Nesper; credit c: modification of work by "Kurzon"/Wikimedia Commons).*

Based on his observations, here is what Thomson proposed and why: The particles are attracted by positive (+) charges and repelled by negative (−) charges, so they must be negatively charged (like charges repel and unlike charges attract); they are less massive than atoms and indistinguishable, regardless of the source material, so they must be fundamental, subatomic constituents of all atoms. Although controversial at the time, Thomson's idea was gradually accepted, and his cathode ray particle is what we now call an electron, a negatively charged, subatomic particle with a mass more than one thousand-times less that of an atom. The term "electron" was coined in 1891 by Irish physicist George Stoney, from "*electr*ic i*on*."

In 1909, more information about the electron was uncovered by American physicist Robert A. Millikan via his "oil drop" experiments. Millikan created microscopic oil droplets, which could be electrically charged by friction as they formed or by using X-rays. These droplets initially fell due to gravity, but their downward progress could be slowed or even reversed by an electric field lower in the apparatus. By adjusting the electric field strength and making careful measurements and appropriate calculations, Millikan was able to determine the charge on individual drops (Figure 1.2.1.2).



Oil drop	Charge in coulombs (C)
A	4.8×10^{-19} C
B	3.2×10^{-19} C
C	6.4×10^{-19} C
D	1.6×10^{-19} C
E	4.8×10^{-19} C

***Figure* 1.2.1.6:** *Millikan's experiment measured the charge of individual oil drops. The tabulated data are examples of a few possible values.*

Looking at the charge data that Millikan gathered, you may have recognized that the charge of an oil droplet is always a multiple of a specific charge, 1.6×10^{-19} C. Millikan concluded that this value must therefore be a fundamental charge—the charge of a single electron—with his measured charges due to an excess of one electron (1 times 1.6×10^{-19} C), two electrons (2 times 1.6×10^{-19} C), three electrons (3 times 1.6×10^{-19} C), and so on, on a given oil droplet. Since the charge of an electron was now known due to Millikan's research, and the charge-to-mass ratio was already known due to Thomson's research (1.759×10^{11} C/kg), it only required a simple calculation to determine the mass of the electron as well.

$$\text{Mass of electron} = 1.602 \times 10^{-19} \cancel{\text{C}} \times \frac{1 \text{ kg}}{1.759 \times 10^{11} \cancel{\text{C}}} = 9.107 \times 10^{-31} \text{ kg} \tag{2.3.1}$$

Scientists had now established that the atom was not indivisible as Dalton had believed, and due to the work of Thomson, Millikan, and others, the charge and mass of the negative, subatomic particles—the electrons—were known. However, the positively charged part of an atom was not yet well understood. In 1904, Thomson proposed the "plum pudding" model of atoms, which described a positively charged mass with an equal amount of negative charge in the form of electrons embedded in it, since all atoms are electrically neutral. A competing model had been proposed in 1903 by Hantaro Nagaoka, who postulated a Saturn-like atom, consisting of a positively charged sphere surrounded by a halo of electrons (Figure 1.2.1.3).

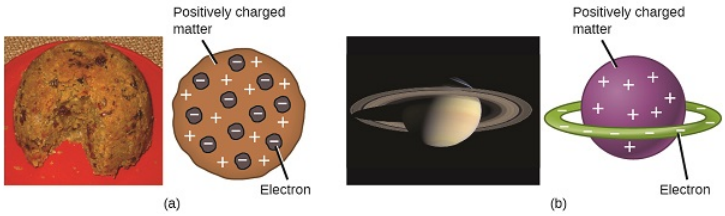


***Figure* 1.2.1.7:** *(a) Thomson suggested that atoms resembled plum pudding, an English dessert consisting of moist cake with embedded raisins ("plums"). (b) Nagaoka proposed that atoms resembled the planet Saturn, with a ring of electrons surrounding a positive "planet." (credit a: modification of work by "Man vyi"/Wikimedia Commons; credit b: modification of work by "NASA"/Wikimedia Commons).*

The next major development in understanding the atom came from Ernest Rutherford, a physicist from New Zealand who largely spent his scientific career in Canada and England. He performed a series of experiments using a beam of high-speed, positively charged alpha particles (α particles) that were produced by the radioactive decay of radium; α particles consist of two protons and two neutrons (you will learn more about radioactive decay in the chapter on nuclear chemistry). Rutherford and his colleagues Hans Geiger (later famous for the Geiger counter) and Ernest Marsden aimed a beam of α particles, the source of which was

embedded in a lead block to absorb most of the radiation, at a very thin piece of gold foil and examined the resultant scattering of the α particles using a luminescent screen that glowed briefly where hit by an α particle.

What did they discover? Most particles passed right through the foil without being deflected at all. However, some were diverted slightly, and a very small number were deflected almost straight back toward the source (Figure **1.2.1.4**). Rutherford described finding these results: “It was quite the most incredible event that has ever happened to me in my life. It was almost as incredible as if you fired a 15-inch shell at a piece of tissue paper and it came back and hit you”[1] (p. 68).

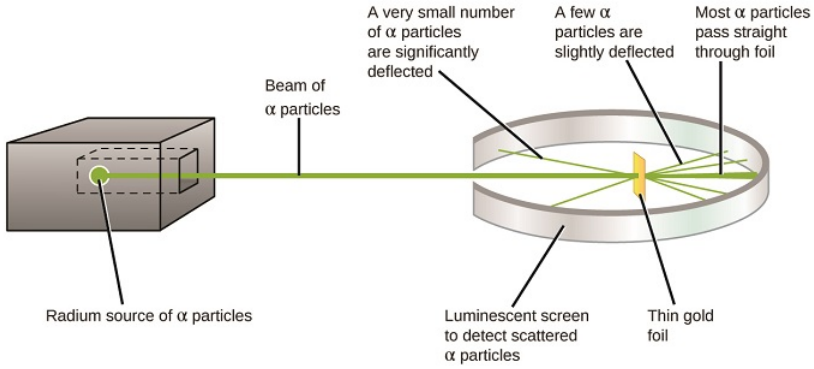


Figure* 1.2.1.8*: *Geiger and Rutherford fired α particles at a piece of gold foil and detected where those particles went, as shown in this schematic diagram of their experiment. Most of the particles passed straight through the foil, but a few were deflected slightly and a very small number were significantly deflected.*

Here is what Rutherford deduced: Because most of the fast-moving α particles passed through the gold atoms undeflected, they must have traveled through essentially empty space inside the atom. Alpha particles are positively charged, so deflections arose when they encountered another positive charge (like charges repel each other). Since like charges repel one another, the few positively charged α particles that changed paths abruptly must have hit, or closely approached, another body that also had a highly concentrated, positive charge. Since the deflections occurred a small fraction of the time, this charge only occupied a small amount of the space in the gold foil. Analyzing a series of such experiments in detail, Rutherford drew two conclusions:

1. The volume occupied by an atom must consist of a large amount of empty space.
2. A small, relatively heavy, positively charged body, the nucleus, must be at the center of each atom.

This analysis led Rutherford to propose a model in which an atom consists of a very small, positively charged nucleus, in which most of the mass of the atom is concentrated, surrounded by the negatively charged electrons, so that the atom is electrically neutral (Figure **1.2.1.5**).

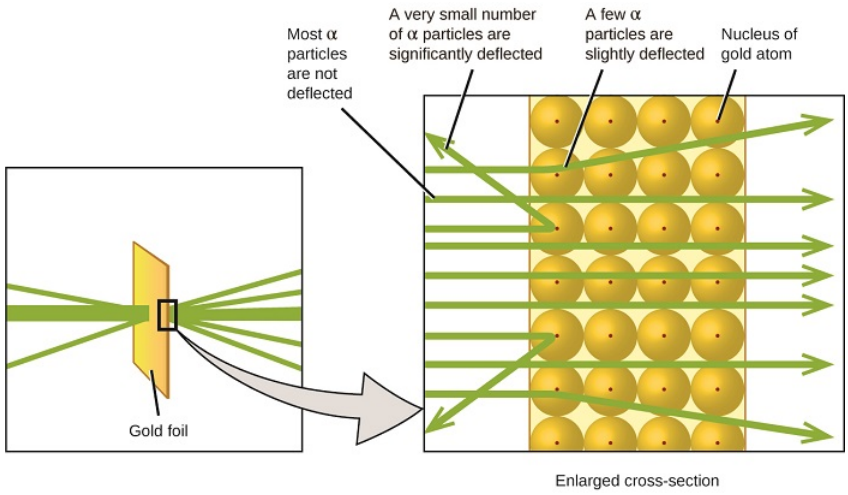
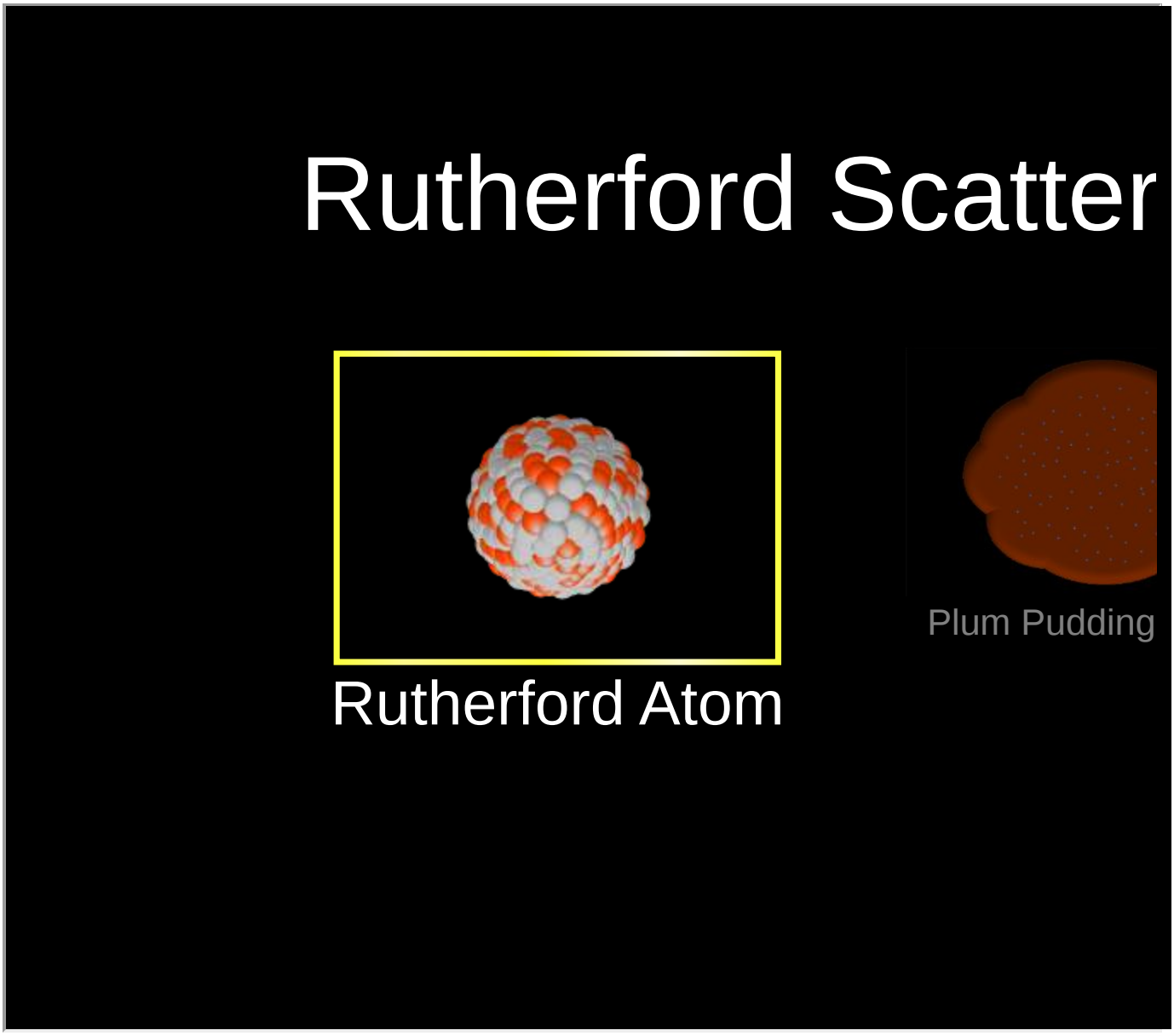


Figure* 1.2.1.9*: *The α particles are deflected only when they collide with or pass close to the much heavier, positively charged gold nucleus. Because the nucleus is very small compared to the size of an atom, very few α particles are deflected. Most pass through*

the relatively large region occupied by electrons, which are too light to deflect the rapidly moving particles.

After many more experiments, Rutherford also discovered that the nuclei of other elements contain the hydrogen nucleus as a "building block," and he named this more fundamental particle the proton, the positively charged, subatomic particle found in the nucleus. With one addition, which you will learn next, this nuclear model of the atom, proposed over a century ago, is still used today.



Another important finding was the discovery of isotopes. During the early 1900s, scientists identified several substances that appeared to be new elements, isolating them from radioactive ores. For example, a "new element" produced by the radioactive decay of thorium was initially given the name mesothorium. However, a more detailed analysis showed that mesothorium was chemically identical to radium (another decay product), despite having a different atomic mass. This result, along with similar findings for other elements, led the English chemist Frederick Soddy to realize that an element could have types of atoms with different masses that were chemically indistinguishable. These different types are called isotopes—atoms of the same element that differ in mass. Soddy was awarded the Nobel Prize in Chemistry in 1921 for this discovery.

One puzzle remained: The nucleus was known to contain almost all of the mass of an atom, with the number of protons only providing half, or less, of that mass. Different proposals were made to explain what constituted the remaining mass, including the

existence of neutral particles in the nucleus. As you might expect, detecting uncharged particles is very challenging, and it was not until 1932 that James Chadwick found evidence of neutrons, uncharged, subatomic particles with a mass approximately the same as that of protons. The existence of the neutron also explained isotopes: They differ in mass because they have different numbers of neutrons, but they are chemically identical because they have the same number of protons. This will be explained in more detail later in this unit.



Video* 1.2.1.2*: An Introduction to Subatomic Particles

Summary



***Video* 1.2.1.3*:** A summary of discoveries in atomic theory.*



***Video* 1.2.1.4*:** A different summary of discoveries in atomic theory.*

The ancient Greeks proposed that matter consists of extremely small particles called atoms. Dalton postulated that each element has a characteristic type of atom that differs in properties from atoms of all other elements, and that atoms of different elements can combine in fixed, small, whole-number ratios to form compounds. Samples of a particular compound all have the same elemental proportions by mass. When two elements form different compounds, a given mass of one element will combine with masses of the other element in a small, whole-number ratio. During any chemical change, atoms are neither created nor destroyed.

Although no one has actually seen the inside of an atom, experiments have demonstrated much about atomic structure. Thomson's cathode ray tube showed that atoms contain small, negatively charged particles called electrons. Millikan discovered that there is a fundamental electric charge—the charge of an electron. Rutherford's gold foil experiment showed that atoms have a small, dense, positively charged nucleus; the positively charged particles within the nucleus are called protons. Chadwick discovered that the nucleus also contains neutral particles called neutrons. Soddy demonstrated that atoms of the same element can differ in mass; these are called isotopes.

Footnotes

1. Ernest Rutherford, "The Development of the Theory of Atomic Structure," ed. J. A. Ratcliffe, in *Background to Modern Science*, eds. Joseph Needham and Walter Pagel, (Cambridge, UK: Cambridge University Press, 1938), 61–74. Accessed September 22, 2014, https://ia600508.us.archive.org/3/it...e032734mbp.pdf.

Glossary

Dalton's atomic theory
set of postulates that established the fundamental properties of atoms

law of constant composition
(also, law of definite proportions) all samples of a pure compound contain the same elements in the same proportions by mass

law of multiple proportions
when two elements react to form more than one compound, a fixed mass of one element will react with masses of the other element in a ratio of small whole numbers

law of definite proportions
(also, law of constant composition) all samples of a pure compound contain the same elements in the same proportions by mass

alpha particle (α particle)
positively charged particle consisting of two protons and two neutrons

electron
negatively charged, subatomic particle of relatively low mass located outside the nucleus

isotopes
atoms that contain the same number of protons but different numbers of neutrons

neutron
uncharged, subatomic particle located in the nucleus

proton
positively charged, subatomic particle located in the nucleus

nucleus
massive, positively charged center of an atom made up of protons and neutrons

Contributors

- Paul Flowers (University of North Carolina - Pembroke), Klaus Theopold (University of Delaware) and Richard Langley (Stephen F. Austin State University) with contributing authors. Textbook content produced by OpenStax College is licensed under a Creative Commons Attribution License 4.0 license. Download for free at http://cnx.org/contents/85abf193-2bd...a7ac8df6@9.110).
- Adelaide Clark, Oregon Institute of Technology
- Crash Course Chemistry: Crash Course is a division of Complexly and videos are free to stream for educational purposes.
- TED-Ed's commitment to creating lessons worth sharing is an extension of TED's mission of spreading great ideas. Within TED-Ed's growing library of TED-Ed animations, you will find carefully curated educational videos, many of which represent collaborations between talented educators and animators nominated through the TED-Ed website.

Feedback

Have feedback to give about this text? Click here.

Found a typo and want extra credit? Click here.

1.2.1: Historical Development of Atomic Theory is shared under a not declared license and was authored, remixed, and/or curated by LibreTexts.

- **2.1: Historical Development of Atomic Theory** is licensed CC BY-NC-SA 4.0.

1.2.1.1: The Periodic Table

Learning Objectives

- To become familiar with the history of the periodic table.

The modern periodic table has evolved through a long history of attempts by chemists to arrange the elements according to their reactivity and other properties as an aid in predicting chemical behavior. Now that we have arranged the table according to electronic structure, it makes sense to go back and look at earlier efforts in the light of what we know about electronic structure.

One of the first to suggest such an arrangement was the German chemist Johannes Dobereiner (1780–1849), who noticed that many of the known elements could be grouped in triads, sets of three elements that have similar properties—for example, chlorine, bromine, and iodine; or copper, silver, and gold. Dobereiner proposed that all elements could be grouped in such triads, but subsequent attempts to expand his concept were unsuccessful. We now know that portions of the periodic table—the *d* block in particular—contain triads of elements with substantial similarities. The middle three members of most of the other columns, such as sulfur, selenium, and tellurium in group 16 or aluminum, gallium, and indium in group 13, also have remarkably similar chemistry.

By the mid-19th century, the atomic masses of many of the elements had been determined. The English chemist John Newlands (1838–1898), hypothesizing that the chemistry of the elements might be related to their masses, arranged the known elements in order of increasing atomic mass and discovered that every seventh element had similar properties (Figure 3.4.1). Newlands therefore suggested that the elements could be classified into octaves: a group of seven elements (not counting the noble gases, which were unknown at the time) that correspond to the *horizontal* rows in the main group elements. Unfortunately, Newlands's "law of octaves" did not seem to work for elements heavier than calcium, and his idea was publicly ridiculed. At one scientific meeting, Newlands was asked why he didn't arrange the elements in alphabetical order instead of by atomic mass, since that would make just as much sense! Actually, Newlands was on the right track—with only a few exceptions, atomic mass does increase with atomic number, and similar properties occur every time a set of ns^2np^6 subshells is filled. Despite the fact that Newlands's table had no logical place for the *d*-block elements, he was honored for his idea by the Royal Society of London in 1887.

John Newlands (1838–1898)

Newlands noticed that elemental properties repeated every seventh (or multiple of seven) element, as musical notes repeat every eighth note.

No.	No.	No.	No.	No.	No.	No.	No.
H 1	F 8	Cl 15	Co & Ni 22	Br 29	Pd 36	I 42	Pt & Ir 50
Li 2	Na 9	K 16	Cu 23	Rb 30	Ag 37	Cs 44	Tl 51
G 3	Mg 10	Ca 17	Zn 25	Sr 31	Bd [sic-Cd] 38	Ba & V 45	Pb 54
Bo 4	Al 11	Cr 19	Y 24	Ce & La 33	U 40	Ta 46	Th 56
C 5	Si 12	Ti 18	In 26	Zr 32	Sn 39	W 47	Hg 52
N 6	**P 13**	Mn 20	**As 27**	Di & Mo 34	**Sb 41**	Nb 48	**Bi 55**
O 7	S 14	Fe 21	Se 28	Ro & Ru 35	Te 43	Au 49	Os 51

NOTE. Where two elements happen to have the same equivalent, both are designated by the same number.

Figure 3.4.1 The arrangement of the elements into octaves as proposed by **Newlands:** *The table shown here accompanied a letter from a 27-year-old Newlands to the editor of the journal Chemical News in which he wrote: "If the elements are arranged in the order of their equivalents, with a few slight transpositions, as in the accompanying table, it will be observed that elements belonging to the same group usually appear on the same horizontal line. It will also be seen that the numbers of analogous elements generally differ either by 7 or by some multiple of seven; in other words, members of the same group stand to each other in the same relation as the extremities of one or more octaves in music. Thus, in the nitrogen group, between nitrogen and phosphorus there are 7 elements; between phosphorus and arsenic, 14; between arsenic and antimony, 14; and lastly, between antimony and bismuth, 14 also. This peculiar relationship I propose to provisionally term the Law of Octaves. I am, &c. John A. R. Newlands, F.C.S. Laboratory, 19, Great St. Helen's, E.C., August 8, 1865."*

The periodic table achieved its modern form through the work of the German chemist Julius Lothar Meyer (1830–1895) and the Russian chemist Dimitri Mendeleev (1834–1907), both of whom focused on the relationships between atomic mass and various physical and chemical properties. In 1869, they independently proposed essentially identical arrangements of the elements. Meyer aligned the elements in his table according to periodic variations in simple atomic properties, such as "atomic volume" (Figure

3.4.2), which he obtained by dividing the atomic mass (molar mass) in grams per mole by the density of the element in grams per cubic centimeter. This property is equivalent to what is today defined as molar volume, the molar mass of an element divided by its density (measured in cubic centimeters per mole):

$$\frac{molar\ mass\ \left(g/mol\right)}{density\ \left(g/cm^3\right)} = molar\ volume\ \left(cm^3/mol\right)$$

As shown in Figure 3.4.2 , the alkali metals have the highest molar volumes of the solid elements. In Meyer's plot of atomic volume versus atomic mass, the nonmetals occur on the rising portion of the graph, and metals occur at the peaks, in the valleys, and on the down slopes.

Dimitri Mendeleev (1834–1907)

When his family's glass factory was destroyed by fire, Mendeleev moved to St. Petersburg, Russia, to study science. He became ill and was not expected to recover, but he finished his PhD with the help of his professors and fellow students. In addition to the periodic table, another of Mendeleev's contributions to science was an outstanding textbook, *The Principles of Chemistry*, which was used for many years.

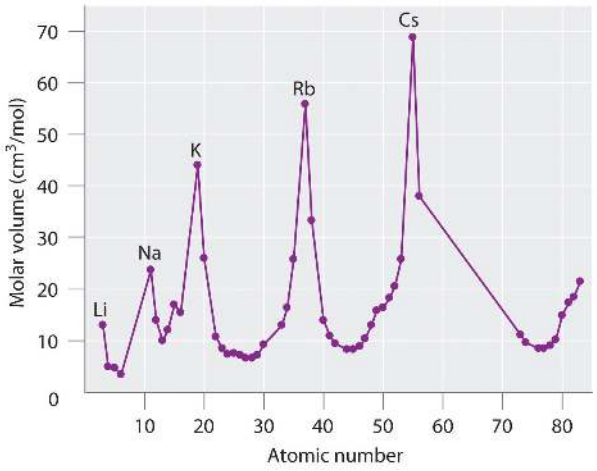


Figure 3.4.2 Variation of atomic volume with atomic number, adapted from Meyer's plot of **1870:** *Note the periodic increase and decrease in atomic volume. Because the noble gases had not yet been discovered at the time this graph was formulated, the peaks correspond to the alkali metals (group 1).*

Mendeleev's Periodic Table

Mendeleev, who first published his periodic table in 1869 (Figure 3.4.3), is usually credited with the origin of the modern periodic table. The key difference between his arrangement of the elements and that of Meyer and others is that Mendeleev did not assume that all the elements had been discovered (actually, only about two-thirds of the naturally occurring elements were known at the time). Instead, he deliberately left blanks in his table at atomic masses 44, 68, 72, and 100, in the expectation that elements with those atomic masses would be discovered. Those blanks correspond to the elements we now know as scandium, gallium, germanium, and technetium.

Reihen	Gruppe I. — R^2O	Gruppe II. — RO	Gruppe III. — R^2O^3	Gruppe IV. RH^4 RO^2	Gruppe V. RH^3 R^2O^5	Gruppe VI. RH^2 RO^3	Gruppe VII. RH R^2O^7	Gruppe VIII. — RO^4
1	H=1							
2	Li=7	Be=9,4	B=11	C=12	N=14	O=16	F=19	
3	Na=23	Mg=24	Al=27,3	Si=28	P=31	S=32	Cl=35,5	
4	K=39	Ca=40	—=44	Ti=48	V=51	Cr=52	Mn=55	Fe=56, Co=59, Ni=59, Cu=63.
5	(Cu=63)	Zn=65	—=68	—=72	As=75	Se=78	Br=80	
6	Rb=85	Sr=87	?Yt=88	Zr=90	Nb=94	Mo=96	—=100	Ru=104, Rh=104, Pd=106, Ag=108.
7	(Ag=108)	Cd=112	In=113	Sn=118	Sb=122	Te=125	J=127	
8	Cs=133	Ba=137	?Di=138	?Ce=140	—	—	—	— — — —
9	(—)	—				—	—	
10	—	—	?Er=178	?La=180	Ta=182	W=184	—	Os=195, Ir=197, Pt=198, Au=199.
11	(Au=199)	Hg=200	Tl=204	Pb=207	Bi=208	—	—	
12	—	—	—	Th=231	—	U=240	—	— — — —

Figure 3.4.3 Mendeleev's periodic table, as published in the German journal *Annalen der Chemie und Pharmacie* in 1872: *The column headings "Reihen" and "Gruppe" are German for "row" and "group." Formulas indicate the type of compounds formed by each group, with "R" standing for "any element" and superscripts used where we now use subscripts. Atomic masses are shown after equal signs and increase across each row from left to right.*

The groups in Mendeleev's table are determined by how many oxygen or hydrogen atoms are needed to form compounds with each element. For example, in Group I, two atoms of hydrogen (H), lithium (Li), sodium (Na), and potassium (K) form compounds with one atom of oxygen. In Group VII, one atom of fluorine (F), chlorine (Cl), and bromine (Br), reacts with one atom of hydrogen. Notice how this approach has trouble with the transition metals. Until roughly 1960, a rectangular table developed from Mendeleev's table and based on reactivity was standard at the front of chemistry lecture halls.

The most convincing evidence in support of Mendeleev's arrangement of the elements was the discovery of two previously unknown elements whose properties closely corresponded with his predictions (Table 3.4.1). Two of the blanks Mendeleev had left in his original table were below aluminum and silicon, awaiting the discovery of two as-yet-unknown elements, *eka*-aluminum and *eka*-silicon (from the Sanskrit *eka*, meaning "one," as in "one beyond aluminum"). The observed properties of gallium and germanium matched those of *eka*-aluminum and *eka*-silicon so well that once they were discovered, Mendeleev's periodic table rapidly gained acceptance.



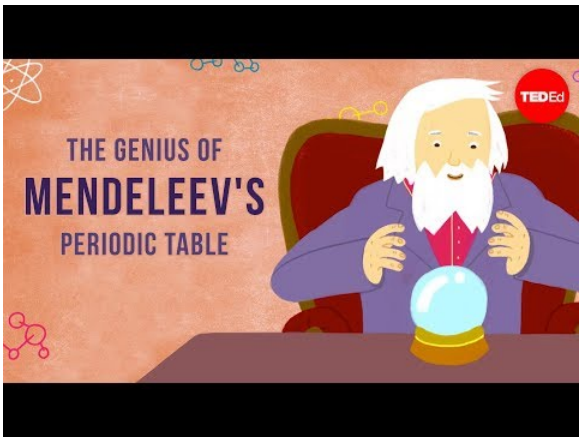


Table 3.4.1 Comparison of the properties predicted by Mendeleev in 1869 for *eka*-aluminum and *eka*-silicon with the properties of gallium (discovered in 1875) and germanium (discovered in 1886)

Property	*eka*-Aluminum (predicted)	Gallium (observed)	*eka*-Silicon (predicted)	Germanium (observed)
atomic mass	68	69.723	72	72.64
element	metal	metal	dirty-gray metal	gray-white metal
	low mp*	mp = 29.8°C	high mp	mp = 938°C
	d = 5.9 g/cm^3	d = 5.91 g/cm^3	d = 5.5 g/cm^3	d = 5.323 g/cm^3
oxide	E_2O_3	Ga_2O_3	EO_2	GeO_2
	d = 5.5 g/cm^3	d = 6.0 g/cm^3	d = 4.7 g/cm^3	d = 4.25 g/cm^3
chloride	ECl_3	$GaCl_3$	ECl_4	$GeCl_4$
	volatile	mp = 78°C bp* = 201°C	bp < 100°C	bp = 87°C

*mp = melting point; bp = boiling point.

When the chemical properties of an element suggested that it might have been assigned the wrong place in earlier tables, Mendeleev carefully reexamined its atomic mass. He discovered, for example, that the atomic masses previously reported for beryllium, indium, and uranium were incorrect. The atomic mass of indium had originally been reported as 75.6, based on an assumed stoichiometry of InO for its oxide. If this atomic mass were correct, then indium would have to be placed in the middle of the nonmetals, between arsenic (atomic mass 75) and selenium (atomic mass 78). Because elemental indium is a silvery-white *metal*, however, Mendeleev postulated that the stoichiometry of its oxide was really In_2O_3 rather than InO. This would mean that indium's atomic mass was actually 113, placing the element between two other metals, cadmium and tin.

One group of elements absent from Mendeleev's table was the noble gases, all of which were discovered more than 20 years later, between 1894 and 1898, by Sir William Ramsay (1852–1916; Nobel Prize in Chemistry 1904). Initially, Ramsay did not know where to place these elements in the periodic table. Argon, the first to be discovered, had an atomic mass of 40. This was greater than chlorine's and comparable to that of potassium; so Ramsay, using the same kind of reasoning as Mendeleev, decided to place the noble gases between the halogens and the alkali metals.

The Role of the Atomic Number in the Periodic Table

Despite its usefulness, Mendeleev's periodic table was based entirely on empirical observation supported by very little understanding. It was not until 1913, when a young British physicist, H. G. J. Moseley (1887–1915), while analyzing the frequencies of x-rays emitted by the elements, discovered that the underlying foundation of the order of the elements was the

atomic number, not the atomic mass. Moseley hypothesized that the placement of each element in his series corresponded to its atomic number *Z*, which is the number of positive charges (protons) in its nucleus. Argon, for example, although having an atomic mass greater than that of potassium (39.9 amu versus 39.1 amu, respectively), was placed *before* potassium in the periodic table. While analyzing the frequencies of the emitted x-rays, Moseley noticed that the atomic number of argon is 18, whereas that of potassium is 19, which indicated that they were indeed placed correctly. Moseley also noticed three gaps in his table of x-ray frequencies, so he predicted the existence of three unknown elements: technetium (Z = 43), discovered in 1937; promethium (Z = 61), discovered in 1945; and rhenium (Z = 75), discovered in 1925.

H. G. J. Moseley (1887–1915)

Moseley left his research work at the University of Oxford to join the British army as a telecommunications officer during World War I. He was killed during the Battle of Gallipoli in Turkey.

Example 3.4.1

Before its discovery in 1999, some theoreticians believed that an element with a Z of 114 existed in nature. Use Mendeleev's reasoning to name element 114 as *eka*-_____; then identify the known element whose chemistry you predict would be most similar to that of element 114.

Given: atomic number

Asked for: name using prefix *eka*-

Strategy:

A Using the periodic table locate the n = 7 row. Identify the location of the unknown element with Z = 114; then identify the known element that is directly above this location.

B Name the unknown element by using the prefix *eka*- before the name of the known element.

Solution:

A The n = 7 row can be filled in by assuming the existence of elements with atomic numbers greater than 112, which is underneath mercury (Hg). Counting three boxes to the right gives element 114, which lies directly below lead (Pb). **B** If Mendeleev were alive today, he would call element 114 *eka*-lead.

Exercise

Use Mendeleev's reasoning to name element 112 as *eka*-_____; then identify the known element whose chemistry you predict would be most similar to that of element 112.

Answer: *eka*-mercury

Summary

The periodic table arranges the elements according to their electron configurations, such that elements in the same column have the same valence electron configurations. Periodic variations in size and chemical properties are important factors in dictating the types of chemical reactions the elements undergo and the kinds of chemical compounds they form. The modern periodic table was based on empirical correlations of properties such as atomic mass; early models using limited data noted the existence of **triads** and **octaves** of elements with similar properties. The periodic table achieved its current form through the work of Dimitri Mendeleev and Julius Lothar Meyer, who both focused on the relationship between atomic mass and chemical properties. Meyer arranged the elements by their atomic volume, which today is equivalent to the **molar volume**, defined as molar mass divided by molar density. The correlation with the electronic structure of atoms was made when H. G. J. Moseley showed that the periodic arrangement of the elements was determined by atomic number, not atomic mass.

Key Takeaways

- The elements in the periodic table are arranged according to their properties, and the periodic table serves as an aid in predicting chemical behavior.

Conceptual Problems

1. Johannes Dobereiner is credited with developing the concept of chemical triads. Which of the group 15 elements would you expect to compose a triad? Would you expect B, Al, and Ga to act as a triad? Justify your answers.
2. Despite the fact that Dobereiner, Newlands, Meyer, and Mendeleev all contributed to the development of the modern periodic table, Mendeleev is credited with its origin. Why was Mendeleev's periodic table accepted so rapidly?
3. How did Moseley's contribution to the development of the periodic table explain the location of the noble gases?
4. The *eka*- naming scheme devised by Mendeleev was used to describe undiscovered elements.
    1. Use this naming method to predict the atomic number of *eka*-mercury, *eka*-astatine, *eka*-thallium, and *eka*-hafnium.
    2. Using the *eka*-prefix, identify the elements with these atomic numbers: 79, 40, 51, 117, and 121.

Numerical Problem

1. Based on the data given, complete the table.

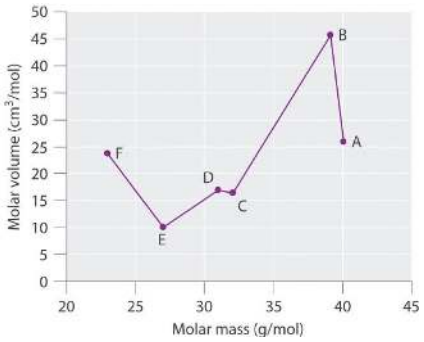
Species	Molar Mass (g/mol)	Density (g/cm^3)	Molar Volume (cm^3/mol)
A	40.078		25.85
B	39.09	0.856	
C	32.065		16.35
D		1.823	16.98
E	26.98		9.992
F	22.98	0.968	

Plot molar volume versus molar mass for these substances. According to Meyer, which would be considered metals and which would be considered nonmetals?

Answer

1.

Species	Molar Mass (g/mol)	Density (g/cm^3)	Molar Volume (cm^3/mol)
A	**40.078**	1.550	**25.85**
B	**39.09**	**0.856**	45.67
C	**32.065**	1.961	**16.35**
D	30.95	**1.823**	**16.98**
E	**26.98**	2.700	**9.992**
F	**22.98**	**0.968**	23.7



Meyer found that the alkali metals had the highest molar volumes, and that molar volumes decreased steadily with increasing atomic mass, then leveled off, and finally rose again. The elements located on the rising portion of a plot of molar volume versus molar mass were typically nonmetals. If we look at the plot of the data in the table, we can immediately identify those elements with the largest molar volumes (A, B, F) as metals located on the left side of the periodic table. The element with the smallest molar volume (E) is aluminum. The plot shows that the subsequent elements (C, D) have molar volumes that are larger than that of E, but smaller than those of A and B. Thus, C and D are most likely to be nonmetals (which is the case: C = sulfur, D = phosphorus).

Contributors and Attributions

- Anonymous

Modified by Joshua Halpern

Video from TED-Ed Lou Serocp

1.2.1.1: The Periodic Table is shared under a not declared license and was authored, remixed, and/or curated by LibreTexts.

- **2.1.1: The Periodic Table** is licensed CC BY-NC-SA 4.0.

1.2.1.2: Discovery of Subatomic Particles and the Bohr Atom

Hydrogen Absorption and Emission Spectra

When a high-voltage electrical discharge is passed through a sample of hydrogen gas (H_2) at low pressure, the result is individual isolated hydrogen atoms that emit a red light. Unlike blackbody radiation, the color of the light emitted by the hydrogen atoms does not depend greatly on the temperature of the gas in the tube. When the emitted light is passed through a prism, only a few narrow lines of particular wavelengths, called a line spectrum, are observed rather than a continuous range of wavelengths (Figure **1.2.1.2.1**). The light emitted by hydrogen atoms is red because, of its four characteristic lines, the most intense line in its spectrum is in the red portion of the visible spectrum, at 656 nm.

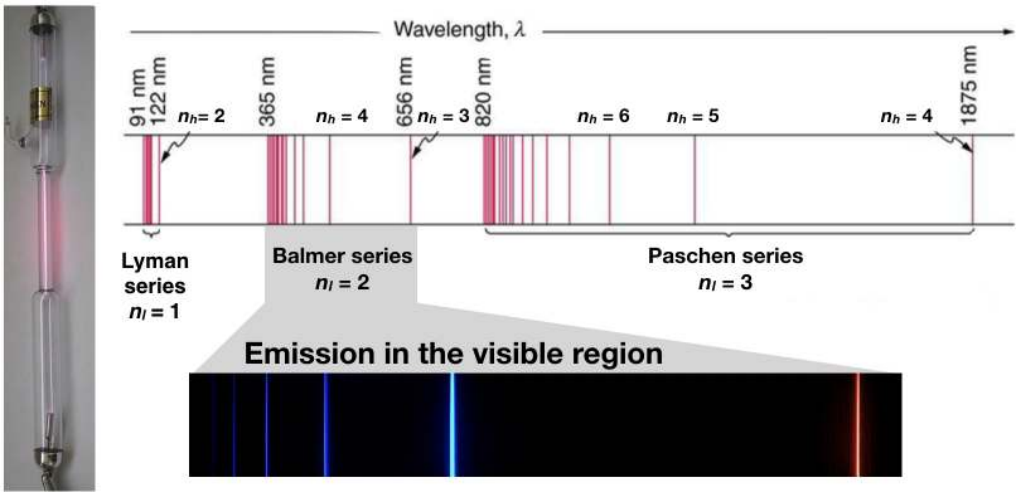


Figure **1.2.1.2.1**: The emission of light by hydrogen atoms. (left) A sample of excited hydrogen atoms emits a characteristic red light. (bottom) When the light emitted by a sample of excited hydrogen atoms is split into its component wavelengths by a prism, four characteristic violet, blue, green, and red emission lines can be observed, with the most intense at 656 nm. (top) A diagram showing extended regions of the electromagnetic spectrum and the hydrogen line spectra that are observed. (Kathryn Haas; CC-BY-SA)

The Balmer Series

In 1885, a Swiss mathematics teacher, Johann Balmer (1825–1898), showed that the frequencies of the lines observed in the visible region of the hydrogen line spectrum fit a simple equation that can be expressed as follows:

$$u = constant\left(\frac{1}{2^2} - \frac{1}{n^2}\right) \tag{1.2.1.2.1}$$

where n = 3, 4, 5, 6. As a result, these lines are known as the *Balmer series*. The Swedish physicist Johannes Rydberg (1854–1919) subsequently restated and expanded Balmer's result in the *Rydberg equation*:

$$\frac{1}{\lambda} = R_H\left(\frac{1}{n_l^2} - \frac{1}{n_h^2}\right) \tag{1.2.1.2.2}$$

,

where n_l and n_h are positive integers, $n_h > n_l$, and R_H, the *Rydberg constant*, has a value of 1.09737 × 10^7 m^{-1}. Like Balmer's equation, Rydberg's simple equation described the wavelengths of the visible lines in the emission spectrum of hydrogen (with $n_l = 2, n_h = 3, 4, 5, ...$). More importantly, Rydberg's equation also predicted the wavelengths of other series of lines that would be observed in the emission spectrum of hydrogen: one in the ultraviolet ($n_l = 1, n_h = 2, 3, 4, ...$) and one in the infrared ($n_l = 3, n_h = 4, 5, 6$).

Other Series

The results given by Balmer and Rydberg for the spectrum in the visible region of the electromagnetic spectrum start with $n_h = 3$, and $n_l = 2$.

Is there a different series with the following formula (e.g., $n_l = 1$)?

$$\frac{1}{\lambda} = R_H \left(\frac{1}{1^2} - \frac{1}{n^2} \right) \tag{1.2.1.2.3}$$

The values for n_h and wavenumber u for this series would be:

Table 1.2.1.2.1: The Lyman Series of Hydrogen Emission Lines ($n_l = 1$)

n_h	2	3	4	5
λ (nm)	121	102	97	94
$\tilde{u}$ (cm^{-1})	82,2291	97,530	102,864	105,332

Do you know what region of the electromagnetic radiation these lines are in? Of course, these lines are in the UV region, and they are not visible, but they are detected by instruments; these lines form a **Lyman series**. The existences of the Lyman series and Balmer's series suggest the existence of more series. For example, the series with $n_2^2 = 3$ and n_1^2 = 4, 5, 6, 7, ... is called the **Pashen series**.

Multiple series

The spectral lines are grouped into series according to n_1 values. Lines are named sequentially starting from the longest wavelength/lowest frequency of the series using Greek letters within each series. For example, the ($n_1 = 1/n_2 = 2$) line is called "Lyman-alpha" (Ly-α), while the ($n_1 = 3/n_2 = 7$) line is called "Paschen-delta" (Pa-δ). The first six series have specific names:

- Lyman series with $n_1 = 1$
- Balmer series with $n_1 = 2$
- Paschen series (or Bohr series) with $n_1 = 3$
- Brackett series with $n_1 = 4$
- Pfund series with $n_1 = 5$
- Humphreys series with $n_1 = 6$



The spectral series of hydrogen based on the Rydberg Equation (on a logarithmic scale).

Example 1.2.1.2.1: The Lyman Series

The so-called Lyman series of lines in the emission spectrum of hydrogen corresponds to transitions from various excited states to the *n* = 1 orbit. Calculate the wavelength of the lowest-energy line in the Lyman series to three significant figures. In what region of the electromagnetic spectrum does it occur?

Given: lowest-energy orbit in the Lyman series

Asked for: wavelength of the lowest-energy Lyman line and corresponding region of the spectrum

Strategy:

A. Substitute the appropriate values into Equation ***Ref*2.1.2.2** (the Rydberg equation) and solve for λ.
B. Locate the region of the electromagnetic spectrum corresponding to the calculated wavelength.

Solution:

We can use the Rydberg equation (Equation $Ref2.1.2.2$ to calculate the wavelength:

$$\frac{1}{\lambda} = R_H \left(\frac{1}{n_l^2} - \frac{1}{n_h^2} \right)$$

A For the Lyman series, $n_1 = 1$.

$$\begin{aligned} \frac{1}{\lambda} &= R_H \left(\frac{1}{n_l^2} - \frac{1}{n_h^2} \right) \\ &= 1.097 \times m^{-1} \left(\frac{1}{1} - \frac{1}{4} \right) \\ &= 8.228 \times 10^6 \; m^{-1} \end{aligned}$$

Spectroscopists often talk about energy and frequency as equivalent. The cm^{-1} unit (wavenumbers) is particularly convenient. We can convert the answer in part A to cm^{-1}.

$$\begin{aligned} \tilde{u} &= \frac{1}{\lambda} \\ &= 8.228 \times 10^6 \cancel{m^{-1}} \left(\frac{\cancel{m}}{100 \; cm} \right) \\ &= 82,280 \; cm^{-1} \end{aligned}$$

and

$$\lambda = 1.215 \times 10^{-7} \; m = 122 \; nm$$

This emission line is called Lyman alpha and is the strongest atomic emission line from the sun; it drives the chemistry of the upper atmosphere of all the planets producing ions by stripping electrons from atoms and molecules. It is completely absorbed by oxygen in the upper stratosphere, dissociating O_2 molecules to O atoms, which react with other O_2 molecules to form stratospheric ozone (O_3).

B This wavelength is in the ultraviolet region of the spectrum.

? Exercise 1.2.1.2.1: The Pfund Series

The Pfund series of lines in the emission spectrum of hydrogen corresponds to transitions from higher excited states to $n_1 = 5$. Calculate the wavelength of the *second* line in the Pfund series to three significant figures. In which region of the spectrum does it lie?

Answer

$4.65 \times 10^3 \; nm$; infrared

The above discussion presents only a phenomenological description of hydrogen emission lines. Balmer and Rydberg could predict where emission lines could occur, but they could not explain why lines followed this pattern using any useful theory. For an explanation of why atoms demonstrate discrete emission spectra, quantum theories were developed.

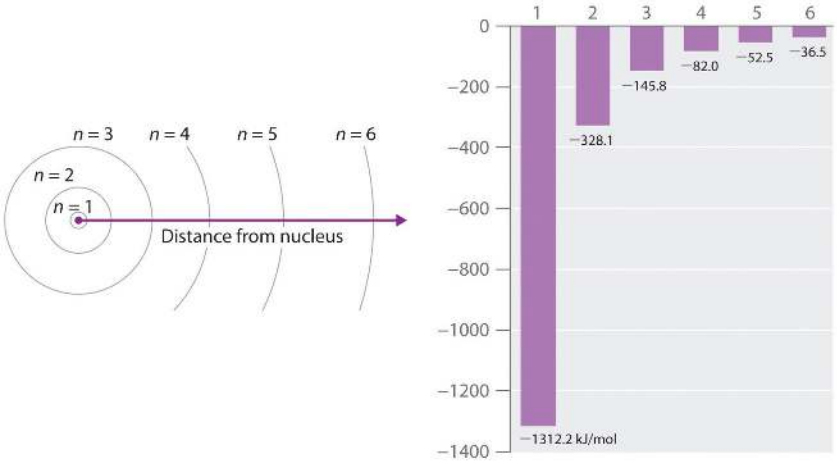
The Bohr Model

In 1913, a Danish physicist, Niels Bohr (1885–1962; Nobel Prize in Physics, 1922), proposed a theoretical model for the hydrogen atom that explained its emission spectrum. Bohr's model required only one assumption: *The electron moves around the nucleus in circular orbits that can have only certain allowed radii*. Rutherford's earlier model of the atom had also assumed that electrons moved in circular orbits around the nucleus and that the atom was held together by the electrostatic attraction between the positively charged nucleus and the negatively charged electron. Although we now know that the assumption of circular orbits was incorrect, Bohr's insight also posited that *the electron could occupy only certain regions of space*.

Using classical physics, Niels Bohr showed that the energy of an electron in a particular orbit is given by

$$E_n = \frac{-R_H hc}{n^2} \tag{1.2.1.2.4}$$

where R_H is the Rydberg constant, h is Planck's constant, c is the speed of light, and n is a positive integer corresponding to the number assigned to the orbit, with $n = 1$ corresponding to the orbit closest to the nucleus. In this model $n = \infty$ corresponds to the level where the energy holding the electron and the nucleus together is zero. In that level, the electron is unbound from the nucleus and the atom has been separated into a negatively charged (the electron) and a positively charged (the nucleus) ion. In this state the radius of the orbit is also infinite. The atom has been ionized.

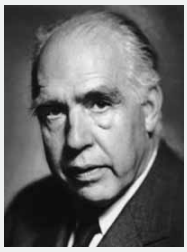


(a) Hydrogen orbits (Bohr model). Orbits are not drawn to scale. **(b) Hydrogen orbit energy (kJ/mol) vs. *n***

Figure **1.2.1.2.2**: *The Bohr Model of the hydrogen atom (a) The distance of the orbit from the nucleus increases with increasing n. (b) The energy of the orbit becomes increasingly less negative with increasing n.*

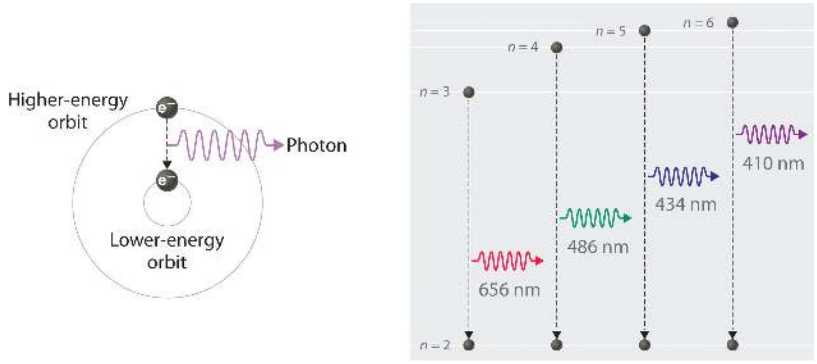
Niels Bohr (1885–1962)

During the Nazi occupation of Denmark in World War II, Bohr escaped to the United States, where he became associated with the Atomic Energy Project.



In his final years, he devoted himself to the peaceful application of atomic physics and to resolving political problems arising from the development of atomic weapons.

As n decreases, the energy holding the electron and the nucleus together becomes increasingly negative; the radius of the orbit shrinks and more energy is needed to ionize the atom. The orbit with n = 1 is the lowest lying and most tightly bound. The negative sign in Equation ??? indicates that the electron-nucleus pair is more tightly bound (i.e. at a lower potential energy) when they are near each other than when they are far apart. Because a hydrogen atom with its one electron in this orbit has the lowest possible energy, this is the **ground state** (the most stable arrangement of electrons for an element or a compound) for a hydrogen atom. As n increases, the radius of the orbit increases; the electron is farther from the proton, which results in a less stable arrangement with higher potential energy (Figure **1.2.1.2.2*a***). A hydrogen atom with an electron in an orbit with n > 1 is therefore in an **excited state**, defined as any arrangement of electrons that is higher in energy than the ground state. When an atom in an excited state undergoes a transition to the ground state in a process called decay, it loses energy by emitting a photon whose energy corresponds to the *difference* in energy between the two states (Figure **1.2.1.2.1**).



(a) Electronic emission transition (b) Balmer series transitions

Figure **1.2.1.2.3**: *The emission of light by a hydrogen atom in an excited state. (a) Light is emitted when the electron undergoes a transition from an orbit with a higher value of n (at a higher energy) to an orbit with a lower value of n (at lower energy). (b) The Balmer series of emission lines is due to transitions from orbits with n ≥ 3 to the orbit with n = 2. The differences in energy between these levels correspond to light in the visible portion of the electromagnetic spectrum.*

So the difference in energy (ΔE) between any two orbits or energy levels is given by $\Delta E = E_{n_l} - E_{n_h}$, where n_l is the final orbit and n_h the initial orbit. Substituting from Bohr's equation (Equation 2.1.2.4) for each energy value gives

$$\Delta E = E_{final} - E_{initial} = -\frac{R_H hc}{n_h^2} - \left(-\frac{R_H hc}{n_l^2}\right) = -R_H hc\left(\frac{1}{n_h^2} - \frac{1}{n_l^2}\right) \tag{1.2.1.2.5}$$

If $n_h > n_l$, the transition is from a higher energy state (larger-radius orbit) to a lower energy state (smaller-radius orbit), as shown by the dashed arrow in part (a) in Figure **1.2.1.2.3**. Substituting hc/λ for ΔE gives

$$\Delta E = \frac{hc}{\lambda} = -R_H hc\left(\frac{1}{n_h^2} - \frac{1}{n_l^2}\right) \tag{1.2.1.2.6}$$

Canceling *hc* on both sides gives

$$\frac{1}{\lambda} = -R_H\left(\frac{1}{n_h^2} - \frac{1}{n_l^2}\right) \tag{1.2.1.2.7}$$

Except for the negative sign, this is the same equation that Rydberg obtained experimentally. The negative sign in Equations 1.2.1.2.6 and 1.2.1.2.7 indicates that energy is released as the electron moves from orbit n_h to orbit n_l because orbit n_h is at a higher energy than orbit n_l. Bohr calculated the value of R_H from fundamental constants such as the charge and mass of the electron and Planck's constant and obtained a value of 1.0974×10^7 m^{-1}, the same number Rydberg had obtained by analyzing the emission spectra.

We can now understand the physical basis for the Balmer series of lines in the emission spectrum of hydrogen (**1.2.1.2.3***b*); the lines in this series correspond to transitions from higher-energy orbits (n > 2) to the second orbit (n = 2). Thus, the hydrogen atoms in the sample have absorbed energy from the electrical discharge and decayed from a higher-energy excited state (n > 2) to a lower-energy state (n = 2) by emitting a photon of electromagnetic radiation whose energy corresponds exactly to the difference in energy between the two states (Figure **1.2.1.2.3***a*). The n = 3 to n = 2 transition gives rise to the line at 656 nm (red), the n = 4 to n = 2 transition to the line at 486 nm (green), the n = 5 to n = 2 transition to the line at 434 nm (blue), and the n = 6 to n = 2 transition to the line at 410 nm (violet). Because a sample of hydrogen contains a large number of atoms, the intensity of the various lines in a line spectrum depends on the number of atoms in each excited state. At the temperature in the gas discharge tube, more atoms are in the n = 3 than the n ≥ 4 levels. Consequently, the n = 3 to n = 2 transition is the most intense line, producing the characteristic red color of a hydrogen discharge (Figure **1.2.1.2.1***a*). Other families of lines are produced by transitions from excited states with n > 1 to the orbit with n = 1 or to orbits with n ≥ 3. These transitions are shown schematically in Figure **1.2.1.2.4** :

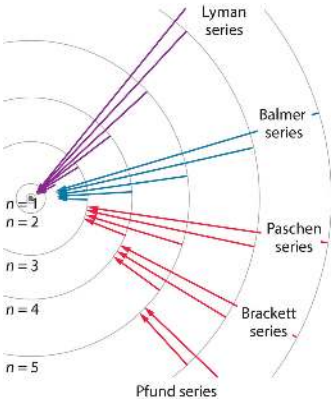


Figure 1.2.1.2.4: Electron transitions responsible for the various series of lines observed in the emission spectrum of hydrogen. The Lyman series of lines is due to transitions from higher-energy orbits to the lowest-energy orbit (n = 1); these transitions release a great deal of energy, corresponding to radiation in the ultraviolet portion of the electromagnetic spectrum. The Paschen, Brackett, and Pfund series of lines are due to transitions from higher-energy orbits to orbits with n = 3, 4, and 5, respectively; these transitions release substantially less energy, corresponding to infrared radiation. (Orbits are not drawn to scale.)

Using Atoms to Time

In contemporary applications, electron transitions are used in timekeeping that needs to be exact. Telecommunications systems, such as cell phones, depend on timing signals that are accurate within a millionth of a second per day; the same goes for the devices that control the US power grid. Global positioning system (GPS) signals must be accurate within a billionth of a second per day, which is equivalent to gaining or losing no more than one second in 1,400,000 years. Quantifying time requires finding an event with an interval that repeats on a regular basis.

To achieve the accuracy required for modern purposes, physicists have turned to the atom. The current standard used to calibrate clocks is the cesium atom. Supercooled cesium atoms are placed in a vacuum chamber and bombarded with microwaves whose frequencies are carefully controlled. When the frequency is exactly right, the atoms absorb enough energy to undergo an electronic transition to a higher-energy state. Decay to a lower-energy state emits radiation. The microwave frequency is continually adjusted, serving as the clock's pendulum.

In 1967, the second was defined as the duration of 9,192,631,770 oscillations of the resonant frequency of a cesium atom, called the *cesium clock*. Research is currently under way to develop the next generation of atomic clocks that promise to be even more accurate. Such devices would allow scientists to monitor vanishingly faint electromagnetic signals produced by nerve pathways in the brain and allow geologists to measure variations in gravitational fields, which cause fluctuations in time, that would aid in the discovery of oil or minerals.

Example 1.2.1.2.1: The Lyman Series

The so-called Lyman series of lines in the emission spectrum of hydrogen corresponds to transitions from various excited states to the n = 1 orbit. Calculate the wavelength of the lowest-energy line in the Lyman series to three significant figures. In what region of the electromagnetic spectrum does it occur?

Given: lowest-energy orbit in the Lyman series

Asked for: wavelength of the lowest-energy Lyman line and corresponding region of the spectrum

Strategy:

A. Substitute the appropriate values into Equation 2.1.2.4 (the Rydberg equation) and solve for λ.
B. Use Figure 2.2.1 to locate the region of the electromagnetic spectrum corresponding to the calculated wavelength.

Solution:

We can use the Rydberg equation to calculate the wavelength:

$$\frac{1}{\lambda} = -R_H \left(\frac{1}{n_h^2} - \frac{1}{n_l^2} \right)$$

A For the Lyman series, /(n_l = 1\). The lowest-energy line is due to a transition from the n = 2 to n = 1 orbit because they are the closest in energy.

$$\frac{1}{\lambda} = -R_H \left(\frac{1}{n_h^2} - \frac{1}{n_l^2} \right) = 1.097 \times m^{-1} \left(\frac{1}{1} - \frac{1}{4} \right) = 8.228 \times 10^6 \; m^{-1}$$

It turns out that spectroscopists (the people who study spectroscopy) use cm^{-1} rather than m^{-1} as a common unit. Wavelength is inversely proportional to energy but frequency is directly proportional as shown by Planck's formula, E=hu.

Spectroscopists often talk about energy and frequency as equivalent. The cm^{-1} unit is particularly convenient. The infrared range is roughly 200 - 5,000 cm^{-1}, the visible from 11,000 to 25,000 cm^{-1} and the UV between 25,000 and 100,000 cm^{-1}. The units of cm^{-1} are called wavenumbers, although people often refer to the unit as inverse centimeters. We can convert the answer in part A to cm^{-1}.

$$\tilde{u} = \frac{1}{\lambda} = 8.228 \times 10^6 \; \cancel{m^{-1}} \left(\frac{\cancel{m}}{100 \; cm} \right) = 82,280 \; cm^{-1}$$

and

$$\lambda = 1.215 \times 10^{-7} \; m = 122 \; nm$$

This emission line is called Lyman alpha. As the strongest atomic emission line from the sun, it drives the chemistry of the upper atmosphere of all the planets, producing ions by stripping electrons from atoms and molecules. It is completely absorbed by oxygen in the upper stratosphere, dissociating O_2 molecules to O atoms which react with other O_2 molecules to form stratospheric ozone.

B This wavelength is in the ultraviolet region of the spectrum.

? Exercise 1.2.1.2.1: The Pfund Series

The Pfund series of lines in the emission spectrum of hydrogen corresponds to transitions from higher excited states to the n = 5 orbit. Calculate the wavelength of the *second* line in the Pfund series to three significant figures. In which region of the spectrum does it lie?

Answer

4.65×10^3 nm; infrared

Bohr's model of the hydrogen atom gave an exact explanation for its observed emission spectrum. The following are his key contributions to our understanding of atomic structure:

- Electrons can occupy only certain regions of space, called *orbits*.
- Orbits closer to the nucleus are lower in energy.
- Electrons can move from one orbit to another by absorbing or emitting energy, giving rise to characteristic spectra.

Unfortunately, Bohr could not explain *why* the electron should be restricted to particular orbits. Also, despite a great deal of conjecturing, such as assuming that orbits could be ellipses rather than circles, his model could not quantitatively explain the emission spectra of any element other than hydrogen (Figure **1.2.1.2.5**). In fact, Bohr's model worked only for species that contained just one electron: H, He^+, Li^{2+}, and so forth. Scientists needed a fundamental change in their way of thinking about the electronic structure of atoms to advance beyond the Bohr model.

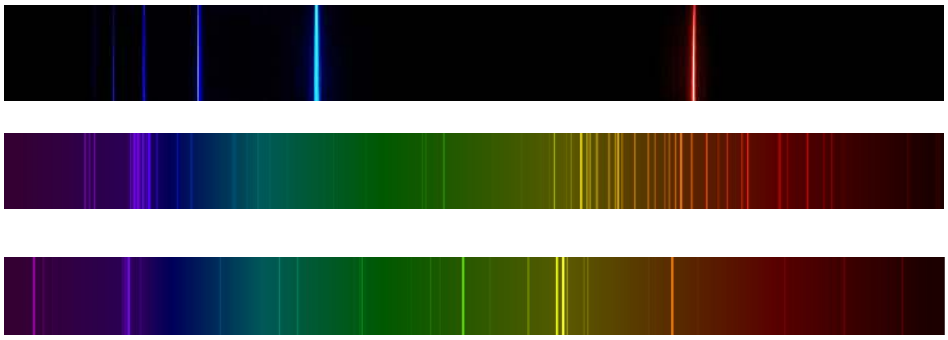


Figure 1.2.1.2.5: The emission spectra of elements compared to hydrogen. **Top:** hydrogen gas (atomized to hydrogen atoms in the discharge tube). **Middle:** neon. **Bottom:** mercury. The strongest lines in the hydrogen spectrum are in the far UV Lyman series starting at 124 nm and below. The strongest lines in the mercury spectrum are at 181 and 254 nm, also in the UV. These are not shown. Attribution: Hydrogen (Jan Homann / CC BY-SA); Neon (Teravolt at en.Wikipedia / Public domain); Mercury (Teravolt at en.Wikipedia / Public domain)

The Energy States of the Hydrogen Atom

Thus far, we have explicitly considered only the emission of light by atoms in excited states, which produces an emission spectrum (a spectrum produced by the emission of light by atoms in excited states). The converse, absorption of light by ground-state atoms to produce an excited state, can also occur, producing an absorption spectrum (a spectrum produced by the absorption of light by ground-state atoms).

> When an atom emits light, it decays to a lower energy state; when an atom absorbs light, it is excited to a higher energy state.

If white light is passed through a sample of hydrogen, hydrogen atoms absorb energy as an electron is excited to higher energy levels (orbits with $n \geq 2$). If the light that emerges is passed through a prism, it forms a continuous spectrum with *black* lines (corresponding to no light passing through the sample) at 656, 468, 434, and 410 nm. These wavelengths correspond to the $n = 2$ to $n = 3$, $n = 2$ to $n = 4$, $n = 2$ to $n = 5$, and $n = 2$ to $n = 6$ transitions. Any given element therefore has both a characteristic emission spectrum and a characteristic absorption spectrum, which are essentially complementary images.

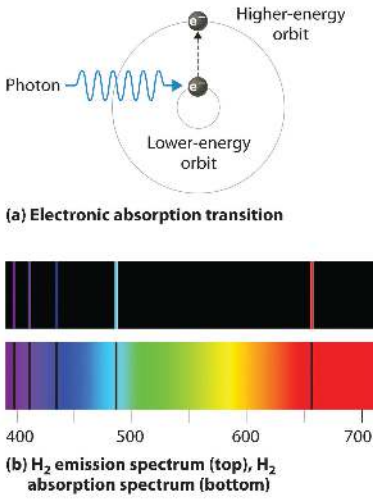


Figure 1.2.1.2.6: Absorption and emission spectra. Absorption of light by a hydrogen atom. (a) When a hydrogen atom absorbs a photon of light, an electron is excited to an orbit that has a higher energy and larger value of n. (b) Images of the emission and absorption spectra of hydrogen are shown here.

Emission and absorption spectra form the basis of *spectroscopy*, which uses spectra to provide information about the structure and the composition of a substance or an object. In particular, astronomers use emission and absorption spectra to determine the composition of stars and interstellar matter. As an example, consider the spectrum of sunlight shown in Figure 1.2.1.2.7. Since the sun is very hot, it emits light in the form of a continuous emission spectrum. Superimposed on the spectrum, however, is a series of

dark lines primarily resulting from the absorption of specific frequencies of light by cooler atoms in the outer atmosphere of the sun. By comparing these lines with the spectra of elements measured on Earth, we now know that the sun contains large amounts of hydrogen, iron, and carbon, along with smaller amounts of other elements. During the solar eclipse of 1868, the French astronomer Pierre Janssen (1824–1907) observed a set of lines that did not match those of any known element. He suggested that they were due to the presence of a new element, which he named *helium*, from the Greek *helios*, meaning "sun." Helium (He) was finally discovered in uranium ores on Earth in 1895. Alpha particles are helium nuclei. Alpha particles emitted by radioactive uranium nuclei pick up electrons from the rocks to form helium atoms.

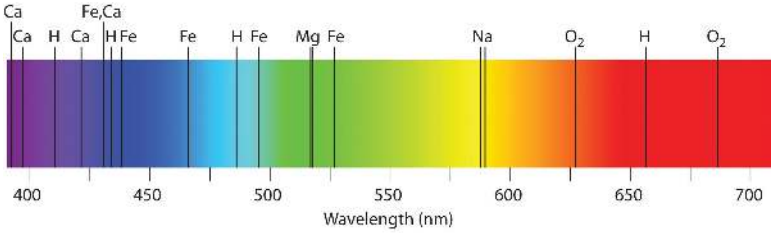


Figure **1.2.1.2.7**: *The visible spectrum of sunlight. The characteristic dark lines are mostly due to the absorption of light by elements that are present in the cooler outer part of the sun's atmosphere; specific elements are indicated by the labels. The lines at 628 and 687 nm, however, are due to the absorption of light by oxygen molecules in Earth's atmosphere.*

The familiar red color of neon signs used in advertising is due to the emission spectrum of neon shown in part (b) in Figure **1.2.1.2.5**. Similarly, the blue and yellow colors of certain street lights are caused, respectively, by mercury and sodium discharges. In all these cases, an electrical discharge excites neutral atoms to a higher energy state, and light is emitted when the atoms decay to the ground state. In the case of mercury, most of the emission lines are below 450 nm, which produces a blue light (part (c) in Figure **1.2.1.2.5**). In the case of sodium, the most intense emission lines are at 589 nm, which produces an intense yellow light.

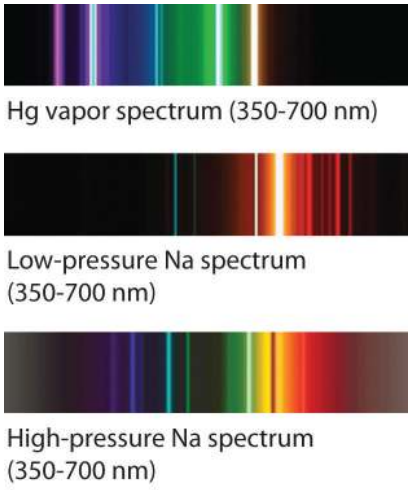


Figure **1.2.1.2.8**: *The emission spectra of sodium and mercury. Many street lights use bulbs that contain sodium or mercury vapor. Due to the very different emission spectra of these elements, they emit light of different colors. The lines in the sodium lamp are broadened by collisions. The dark line in the center of the high pressure sodium lamp where the low pressure lamp is strongest is caused by absorption of light in the cooler outer part of the lamp.*

Summary

There is an intimate connection between the atomic structure of an atom and its spectral characteristics. Atoms of individual elements emit light at only specific wavelengths, producing a **line spectrum** rather than the continuous spectrum of all wavelengths produced by a hot object. Niels Bohr explained the line spectrum of the hydrogen atom by assuming that the electron moved in circular orbits and that orbits with only certain radii were allowed. Lines in the spectrum were due to transitions in which an electron moved from a higher-energy orbit with a larger radius to a lower-energy orbit with smaller radius. The orbit closest to the nucleus represented the **ground state** of the atom and was most stable; orbits farther away were higher-energy **excited states**. Transitions from an excited state to a lower-energy state resulted in the emission of light with only a limited number of wavelengths. Atoms can also absorb light of certain energies, resulting in a transition from the ground state or a lower-energy

excited state to a higher-energy excited state. This produces an **absorption spectrum**, which has dark lines in the same position as the bright lines in the **emission spectrum** of an element. Bohr's model revolutionized the understanding of the atom but could not explain the spectra of atoms heavier than hydrogen.

Contributors and Attributions

- Modified by Joshua Halpern (Howard University)

1.2.1.2: Discovery of Subatomic Particles and the Bohr Atom is shared under a not declared license and was authored, remixed, and/or curated by LibreTexts.

- **2.1.2: Discovery of Subatomic Particles and the Bohr Atom** is licensed CC BY-NC-SA 3.0.

1.2.2: The Schrödinger equation, particle in a box, and atomic wavefunctions

2.02: The Schrödinger equation particle in a box and atomic wavefunctions

This page titled 1.2.2: The Schrödinger equation, particle in a box, and atomic wavefunctions is shared under a CC BY-NC-SA 4.0 license and was authored, remixed, and/or curated by Kathryn Haas.

1.2.2.1: Particle in a Box

2.2.01: Particle in a Box

This page titled 1.2.2.1: Particle in a Box is shared under a CC BY-NC-SA 4.0 license and was authored, remixed, and/or curated by Kathryn Haas.

1.2.2.2: Quantum Numbers and Atomic Wave Functions

2.2.02: Quantum Numbers and Atomic Wave Functions

This page titled 1.2.2.2: Quantum Numbers and Atomic Wave Functions is shared under a CC BY-NC-SA 4.0 license and was authored, remixed, and/or curated by Kathryn Haas.

1.2.2.3: Aufbau Principle

2.2.03: Aufbau Principle

This page titled 1.2.2.3: Aufbau Principle is shared under a Public Domain license and was authored, remixed, and/or curated by Kathryn Haas.

1.2.2.4: Shielding

2.2.04: Shielding

1.2.2.4: Shielding is shared under a CC BY-NC-SA 4.0 license and was authored, remixed, and/or curated by LibreTexts.

SECTION OVERVIEW

1.2.3: Periodic Properties of Atoms

General periodic trends are specific patterns that are present within the periodic table; these are patterns in properties like electronegativity, ionization energy, electron affinity, atomic radius, melting point, and metallic character. General periodic trends provide chemists with an invaluable tool to quickly predict an element's properties. These trends exist because of the similar atomic structure of the elements within their respective group families or periods, and because of the periodic nature of the elements. Some of the general periodic trends are described in this section.

1.2.3.1: Ionization energy

1.2.3.2: Electron Affinity

1.2.3.3: Covalent and Ionic Radii

1.2.3.4: Hard and Soft Acids and Bases

1.2.3.4.1: Quantitative Measures of Hardness, Softness, and Acid-Base Interactions from a Hard Soft Acid-Base Principle perspective involve orbital energies and or apportioning acid-base bonding in terms of electrostatic and covalent factors

1.2.3.4.2: Hard-Hard and Soft-Soft preferences may be explained and quantified in terms of electrostatic and covalent and electronic stabilization on the stability of Lewis acid-base adducts

References

1. Russo, Steve, and Mike Silver. Introductory Chemistry. San Francisco: Pearson, 2007.
2. Petrucci, Ralph H, et al. General Chemistry: Principles and Modern Applications. 9th Ed. New Jersey: Pearson, 2007.
3. Atkins, Peter et. al, *Physical Chemistry*, 7th Edition, 2002, W.H Freeman and Company, New York, pg. 390.
4. Alberty, Robert A. et. al, *Physical Chemistry*, 3rd Edition, 2001, John Wiley & Sons, Inc, pg. 380.
5. Kots, John C. et. al, *Chemistry & Chemical Reactivity*, 5th Edition, 2003, Thomson Learning Inc, pg. 305-309.

1.2.3: Periodic Properties of Atoms is shared under a not declared license and was authored, remixed, and/or curated by LibreTexts.

1.2.3.1: Ionization energy

Ionization energy (IE) is the energy required to **remove an electron from a neutral atom or cation in its gaseous phase**. IE is also known as *ionization potential*.

$$A^{n+}_{(g)} \longrightarrow A^{(n+1)+}_{(g)} + e^- \qquad IE = \Delta U$$

Conceptually, ionization energy is the affinity of an element for its outermost electron (an electron it already has in its valence shell).

1st, 2nd, and 3rd Ionization Energies

The symbol I_1 stands for the ***first ionization energy*** (energy required to take away an electron from a neutral atom, where $n = 0$). The symbol I_2 stands for the ***second ionization energy*** (energy required to take away an electron from an atom with a +1 charge, $n = 2$.)

- **First Ionization Energy,** I_1 (general element, A):

$$A_{(g)} \rightarrow A^{1+}_{(g)} + e^-$$

- **Second Ionization Energy,** I_2 (general element, A):

$$A^{1+}_{(g)} \rightarrow A^{2+}_{(g)} + e^-$$

- **Third Ionization Energy,** I_3 (general element, A):

$$A^{2+}_{(g)} \rightarrow A^{3+}_{(g)} + e^-$$

Each succeeding ionization energy is larger than the preceding energy. This means that $I_1 < I_2 < I_3 < ... < I_n$ will always be true. For example, ionization energy increases as succeeding electrons are taken away from **Mg**.

$$Mg_{\,(g)} \rightarrow Mg^{+}{}_{(g)} + e^- \quad I_1 = 738\,kJ/mol$$

$$Mg^{+}{}_{(g)} \rightarrow Mg^{2+}{}_{(g)} + e^- \quad I_2 = 1451\,kJ/mol$$

Ionization energy is correlated with the strength of attraction between the positively-charged nucleus and the negatively-charged valence electrons. The higher the ionization energy, the stronger the attractive force between nucleus and valence electrons, and the more energy is required to remove a valence electron. The lower the ionization energy, the weaker the attractive force between nucleus and valence electrons, and the less energy required to remove a valence electron.

General periodic trends in electron affinity

In general, ionization energies increase from left to right and decrease down a group; however, there are variations in these trends that would be expected from the effects of penetration and shielding. The trends in **first ionization energy** are shown in Figure 1.2.3.1.1 and are summarized below.

- **Across a period:** As Z* increases across a period, the ionization energy of the elements generally increases from left to right. However there are breaks or variation in the trends in the following cases:
  - IE is especially low when removal of an electron creates a newly empty p subshell (examples include I_1 of B, Al, Sc)
  - IE energy is especially low where removal of an electron results in a half-filled p or d subshell (examples include I_1 of O, S)
  - IE increases more gradually across the d- and f-subshells compared to s- and p- subshells. This is because d- and f- electrons are weakly penetrating and experience especially low Z*.
- **From one period to the next:** There is an especially large decrease in IE with the start of every new period (from He to Li or from Ne to Na for example). This is consistent with the idea that IE is especially low when removal of an electron creates a newly empty s-subshell.
- **Noble gases:** The noble gases posses very high ionization energies. Note that helium has the highest ionization energy of all the elements.

- **Down a group:** Although Z* increases going down a group, there is no reliable trend in IE going down any group; in some cases IE increases going down a group, while in other cases IE decreases going down a group.

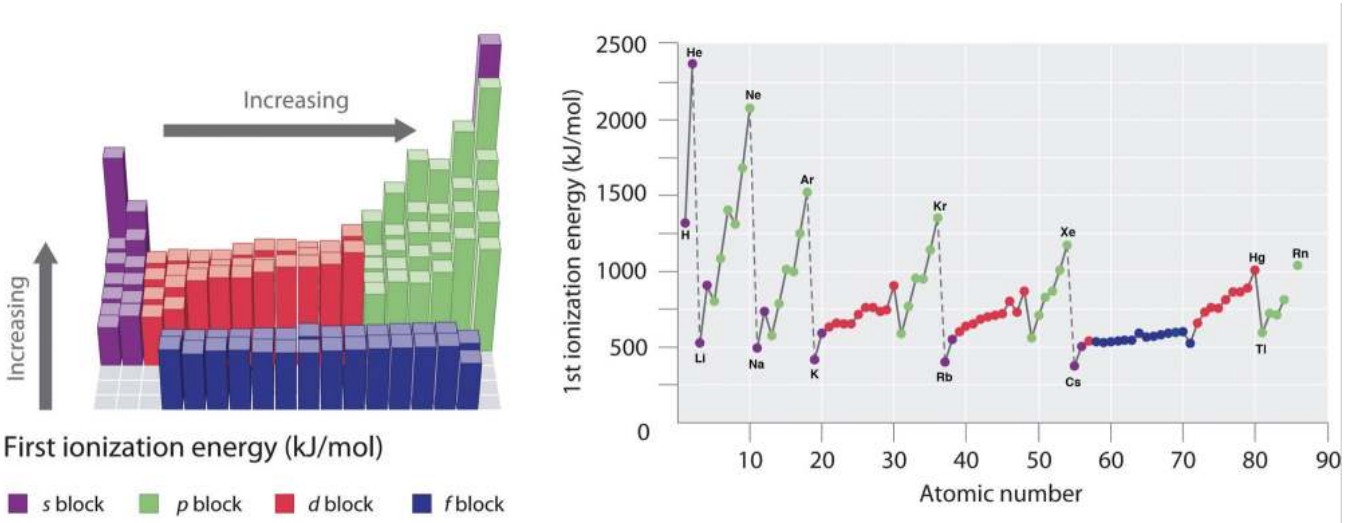


Figure 1.2.3.1.1: Graph showing the First Ionization Energy of the Elements. Left: ionization energies are mapped onto the periodic table, where the magnitude of ionization energy is depicted as a bar graph. Right: the first ionization energy is plotted against atomic number. In both panels the elements of the s-block are shown in purple, p-block are shown in green, d-block are shown in red, and f-block are shown in blue. (CC BY-NC-SA 3.0; anonymous)

Plots of the I_1, I_2, and I_3 of elements from hydrogen to krypton (first four periods) are shown in Figure 1.2.3.1.2. Notice that $I_3 > I_2 > I_1$. Also notice that trends mentioned above for I_1 hold true for subsequent ionizations when electron configurations are considered!

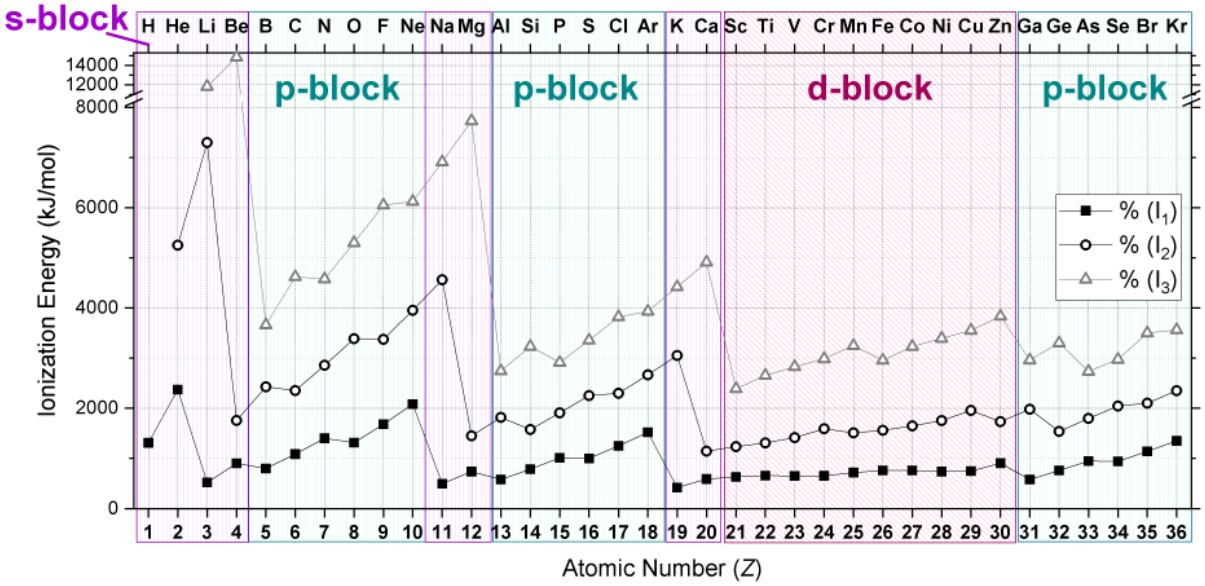


Figure 1.2.3.1.2. The first (I_1), second (I_2), and third (I_3) ionization energies plotted for elements with Z = 1 to 36 (H to Kr). The position of each element in its atomic form is indicated as s- p- or d-block. (CC-BY-NC-SA; Kathryn Haas)

1.2.3.1: Ionization energy is shared under a not declared license and was authored, remixed, and/or curated by LibreTexts.

- **2.3.1: Ionization energy** by Bingyao Zheng, Emily Nguyen, Kathryn Haas, Swetha Ramireddy is licensed CC BY-NC-SA 3.0.

1.2.3.2: Electron Affinity

Definitions of Electron Affinity

According to IUPAC, there are two different, but equivalent, definitions of **electron affinity (EA)**.[1]

Definition: Electron Affinity defined as removal of an electron

Electron affinity can be defined as the energy *required* when an electron is removed from a gaseous anion. The reaction as shown in equation 1.2.3.2.1 is *endothermic* (positive ΔU) for elements except noble gases and alkaline earth metals. Under this definition, the more positive the EA value, the higher an atom's affinity for electrons.

$$A^-_{(g)} \longrightarrow A_{(g)} + e^- \qquad EA = \Delta U \tag{1.2.3.2.1}$$

The reaction shown in Equation 1.2.3.2.1 is similar those that define ionization energy. For this reason, the EA is also described as the *zeroth ionization energy*.

Definition: Electron Affinity defined as addition of an electron

An alternate and more common definition is the microscopic reverse of Equation 1.2.3.2.1. This more common definition states that electron affinity is the energy *released* when an electron is added to a gaseous atom, as shown in Equation 1.2.3.2.2. The reaction as shown in equation 1.2.3.2.2 is *exothermic* (negative ΔU) for elements except noble gases and alkaline earth metals. The more negative this EA value, the higher an atom's affinity for electrons.

$$A_{(g)} + e^- \longrightarrow A^-_{(g)} \qquad EA = \Delta U \tag{1.2.3.2.2}$$

Conceptually, this second definition is quite similar to the concept of electronegativity; but unlike electronegativity, EA is a well-defined quantitative measurement.

Trends in Electron Affinity

For this discussion, we will use the definition of EA that is consistent with it being a *zeroth ionization energy:* a more positive (larger) value means that the EA is higher (meaning stronger affinity toward an electron).

- **Across a period**: Similar to ionization energy, EA generally increases across a row of the periodic table; this observation is consistent with the increase in effective nuclear charge (Z*) from left to right across a period. However, there are variations across a period that are similar to variations in ionization energy and that can be explained by shielding, penetration, and electron configuration.
- **Down a group**: Like the case of ionization energy trends, EA does not consistently decrease going down a column of the periodic table despite the fact that Z^* increases down a group.

The trend in EA follows a zig-zag pattern similar to the one seen with ionization energies, except that it is displaced by one unit from the trend in I_1, two units from I_2, and so on. For example, EA peaks at F, while I_1 peaks at Ne, I_2 peaks at Na, and I_3 peaks at Mg. A plot of EA for the first 13 elements is shown overlaid on plots of I_1, I_2 and I_3 in Figure 1.2.3.2.1., where the shifts in the peaks and valleys within each zig-zag trend are indicated.

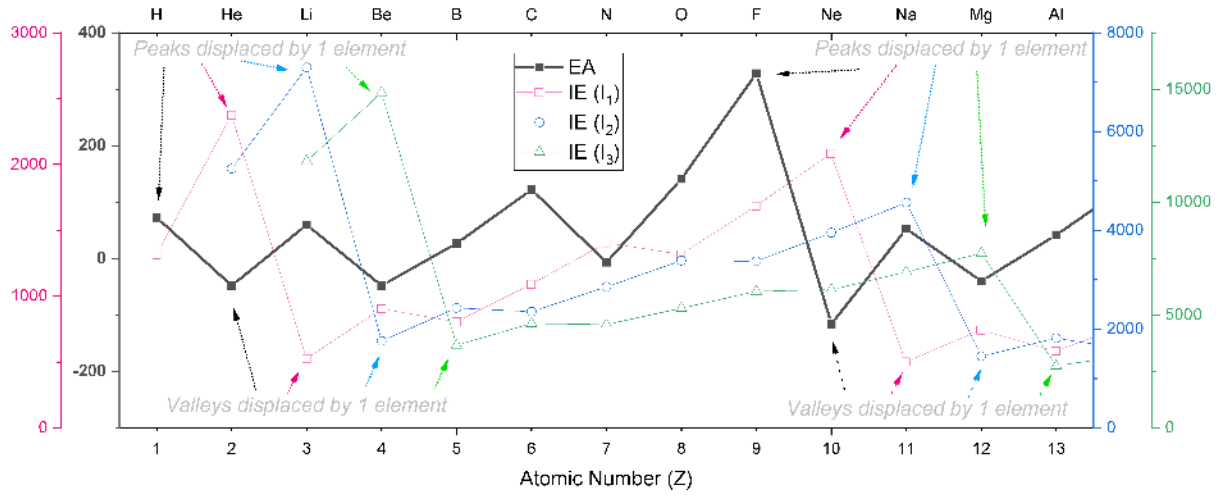


Figure **1.2.3.2.1**. A plot of electron affinity (the zeroth ionization energy) is overlaid on plots of the first (I_1), second (I_2), and third (I_3) ionization energies. Each plot is shown using separate y-axes. Trends in EA are similar to those in ionization energies, except that the peaks and valleys of the trends are shifted by one unit, as indicated. These plots are shown in units of kJ/mole. (CC-BY-NC-SA; Kathryn Haas)

Sources

1. IUPAC. Compendium of Chemical Terminology, 2nd ed. (the "Gold Book"). Compiled by A. D. McNaught and A. Wilkinson. Blackwell Scientific Publications, Oxford (1997). Online version (2019-) created by S. J. Chalk. ISBN 0-9678550-9-8. doi.org/10.1351/goldbook.
2. Electron Affinity (data page), Wikipedia. en.Wikipedia.org/wiki/Electron_affinity_(data_page) Accessed 12/3/19.

1.2.3.2: Electron Affinity is shared under a not declared license and was authored, remixed, and/or curated by LibreTexts.

- **2.3.2: Electron Affinity** by Kathryn Haas is licensed CC BY-NC-SA 4.0.

1.2.3.3: Covalent and Ionic Radii

Measurement of Radius

There are several methods that can be used to determine radii of atoms and ions:

- **Nonpolar atomic radii:** The radius of an atom is derived from the bond lengths within nonpolar molecules; one-half the distance between the nuclei of two atoms within a covalent bond.
- **van der Waals radius:** The radius of an atom is determined by collision with other atoms.
- **Crystal radii**: The atomic or ionic radius is determined using electron density maps from X-ray data.

The measurement of atomic or ionic size will depend on a number of factors, including the covalent character of bonding in any particular molecule, coordination number, physical state (liquid, solid, gas), the identity of nearby atoms/ions, variation in crystal structure, and distortions within regular crystal structures. You should keep in mind that the size of an atom or ion is a "fuzzy" measure, and the radius under a different set of conditions will probably change slightly.

Regardless, measured atomic and ionic radii reveal obvious trends across the periodic table and between atoms and ions. The relative atomic sizes shown in Figure **1.2.3.3.1** were derived from crystallographic data.[1]

Trends in Atomic Radius

Atomic size generally decreases gradually from left to right across a period of elements. As nuclear charge (Z) increases, we expect the effective nuclear charge (Z*) of the valence electrons to also increase. Increasing Z pulls electrons closer to the nucleus. However, with each additional unit of Z, there is also an additional electron. The change in size is a balance of a compression caused by increasing Z and an expansion in the number of electrons. As a result, the atomic radius decreases *gradually* across a period.

Atomic size generally increases going down a group. As valence electrons occupy higher level shells due to the increasing quantum number (n), size increases despite the fact that Z and Z* are increasing going down the group.

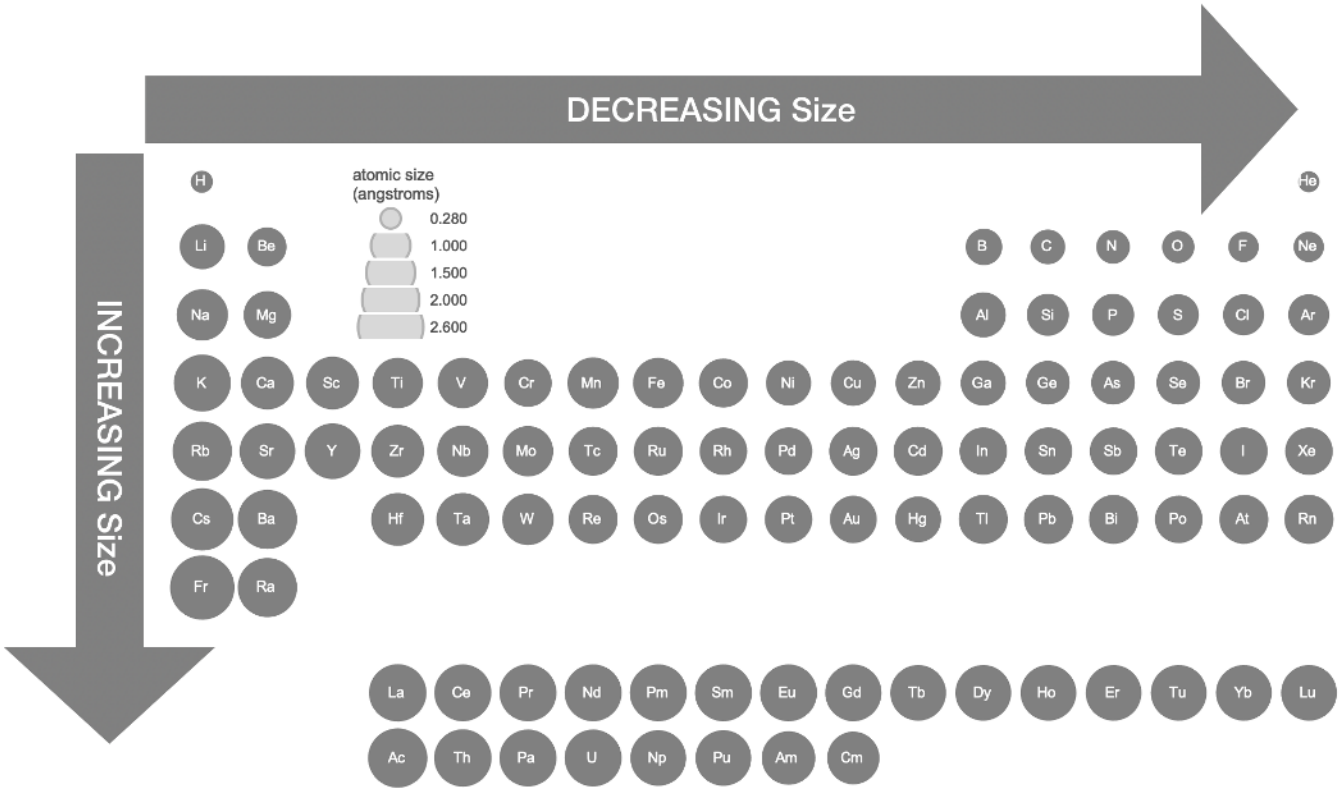


Figure **1.2.3.3.1**. *Atomic Radii Calculated from Crystalographic Data. Data from Cordero, Beatriz, Veronica Gomez, Ana E. Platero-Prats, Marc Reves, Jorge Echeverria, Eduard Cremades, Flavia Barragan, and Santiago Alvarez. "Covalent Radii Revisited." Dalton Transactions, no. 21 (2008): 2832–38. doi:10.1039/b801115j.* (Kathryn Haas; CC-NC-BY-SA)

Trends in Ionic Radius

Trends in ionic radius follow general trends in atomic radius for ions of the same charge. Ionic radius varies with the charge of the ion (and number of electrons) and the electron configuration (e.g. high spin or low spin).

Cations

Compared to their atoms, cations have the same Z but fewer electrons. Removal of electrons from an atom to form a cation results in a significant increase in effective nuclear charge, resulting in all other electrons being more strongly attracted to the nucleus, and having a lower energy level. The result is a contraction in size from the atom to cation. Figure **1.2.3.3.2** visually illustrates the relative size of atoms and some cations of the first four periods; the data is available in tabular format in Figure **1.2.3.3.3**.

Anions

Compared to their atoms, anions have the same Z but more electrons. Addition of electrons to an atom to form an anion results in a decrease in effective nuclear charge, which corresponds to a decrease in attractive force between the nucleus and electrons. Lower attractive force leads to expansion, where the size of the atom becomes larger in the formation of an anion. Figure **1.2.3.3.2** visually illustrates the relative size of atoms and some anions of the first four periods, while the data is available in tabular format in Figure **1.2.3.3.3**.

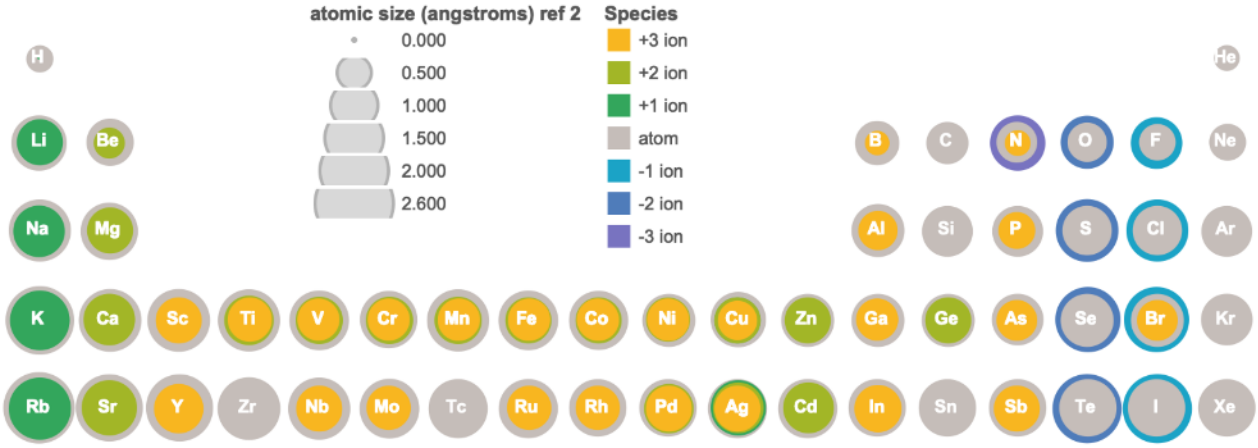


Figure **1.2.3.3.2**. This figure illustrates relative size of atoms and ions of the first four periods of the periodic table. Atomic radius is indicated by grey circles. Radius of cations is shown in green (+1), lime (+2), and yellow (+3) circles. Radius of anions are shown as aqua (-1), blue (-2), and purple (-3) circles. Data from sources 1-3. (Kathryn Haas; CC-NC-BY-SA)

H 0.31 (atom) 0 (+1)																	He 0.28 (atom)
Li 1.28 (atom) 0.9 (+1) - -	Be 0.96 (atom) 0.41 (+2) - -											B 0.84 (atom) 0.25 (+1)	C 0.76 (atom) 0.29 (+4)	N 1.32 (-3) 0.71 (atom) 0.3 (+3) 0.27 (+5)	O 1.21 (-2) 0.66 (atom)	F 1.145 (-1) 0.57 (atom)	Ne 0.58 (atom)
Na 1.66 (atom) 1.16 (+1)	Mg 1.41 (atom) 0.86 (+2)											Al 1.21 (atom) 0.675 (+3)	Si 1.11 (atom) 0.4 (+4)	P 1.07 (atom) 0.58 (+3) 0.31 (+5)	S 1.7 (-2) 1.05 (atom) 0.51 (+4) 0.26 (+6)	Cl 1.67 (-1) 1.02 (atom)	Ar 1.06 (atom)
K 2.03 (atom) 1.52 (+1)	Ca 1.76 (atom) 1.14 (+2)	Sc 1.7 (atom) 0.885 (+3)	Ti 1.6 (atom) 1 (+2) 0.81 (+3) 0.745 (+4)	V 1.53 (atom) 0.93 (+2) 0.78 (+3) 0.72 (+4)	Cr 1.39 (atom) 0.94 (+2 hs) 0.87 (+2 ls) 0.7555 (+3) 0.69 (+4) 0.63 (+5) 0.58 (+6)	Mn 1.61 (atom) 0.97 (+2 hs) 0.81 (+2 ls) 0.785 (+3 hs) 0.72 (+3 ls) 0.67 (+4) 0.47 (+5) 0.395 (+6) 0.39 (+7)	Fe 1.52 (atom) 0.92 (+2 hs) 0.765 (+3 hs) 0.75 (+2 ls) 0.725 (+4) 0.69 (+3 ls) 0.39 (+6)	Co 1.5 (atom) 0.885 (+2 hs) 0.79 (+2 ls) 0.75 (+3 hs) 0.685 (+3 ls) 0.67 (+4 hs)	Ni 1.24 (atom) 0.83 (+2) 0.74 (+3 hs) 0.7 (+3 ls) 0.62 (+4)	Cu 1.32 (atom) 0.91 (+1, cn6) 0.87 (+2, cn6) 0.68 (+3, cn6)	Zn 1.22 (atom) 0.88 (+2)	Ga 1.22 (atom) 0.76 (+3)	Ge 1.2 (atom) 0.87 (+2) 0.67 (+4)	As 1.19 (atom) 0.72 (+3) 0.6 (+5)	Se 1.84 (-2) 1.2 (atom) 0.64 (+4) 0.56 (+6)	Br 1.82 (-1) 1.2 (atom) 0.73 (+3) 0.53 (+7) 0.45 (+5)	Kr 1.16 (atom)
Rb 2.2 (atom) 1.66 (+1)	Sr 1.95 (atom) 1.32 (+2)	Y 1.9 (atom) 1.04 (+3)	Zr 1.75 (atom) 0.86 (+4)	Nb 1.64 (atom) 0.86 (+3) 0.82 (+4) 0.78 (+5)	Mo 1.54 (atom) 0.83 (+3) 0.79 (+4) 0.75 (+5) 0.73 (+6)	Tc 1.47 (atom) 0.785 (+4) 0.74 (+5) 0.7 (+7)	Ru 1.46 (atom) 0.82 (+3) 0.76 (+4) 0.705 (+5) 0.52 (+7) 0.5 (+8)	Rh 1.42 (atom) 0.805 (+3) 0.74 (+4) 0.69 (+5)	Pd 1.39 (atom) 0.73 (+1) 1 (+2) 0.9 (+3) 0.755 (+4)	Ag 1.45 (atom) 1.29 (+1) 1.08 (+2) 0.89 (+3)	Cd 1.44 (atom) 1.09 (+2)	In 1.42 (atom) 0.94 (+3)	Sn 1.39 (atom) 0.83 (+4)	Sb 1.39 (atom) 0.9 (+3) 0.74 (+5)	Te 2.07 (-2) 1.38 (atom) 1.1 (+4) 0.7 (+6)	I 2.06 (-1) 1.39 (atom) 1.09 (+5) 0.67 (+7)	Xe 1.4 (atom) 0.62 (+8)

Figure 1.2.3.3.3.

This figure shows radii (in Angstroms) of atoms and ions of the first four periods of the periodic table. Radii from each element are listed from largest to smallest, ionic charge indicated in parentheses (); hs = high spin, ls = low spin, cn6 = coordination number is 6. Data from sources 1-3. (Kathryn Haas; CC-NC-BY-SA)

References

1. Cordero, Beatriz, Veronica Gomez, Ana E. Platero-Prats, Marc Reves, Jorge Echeverria, Eduard Cremades, Flavia Barragan, and Santiago Alvarez. *"Covalent Radii Revisited." Dalton Transactions, no. 21 (2008): 2832–38. doi:10.1039/b801115j.*
2. R. D. Shannon (1976). "Revised effective ionic radii and systematic studies of interatomic distances in halides and chalcogenides". *Acta Crystallogr A.* **32** (5): 751–767. Bibcode:1976AcCrA..32..751S. doi:10.1107/S0567739476001551.
3. Wikipedia articles on Atomic Radius and Ionic Radius.

1.2.3.3: Covalent and Ionic Radii is shared under a not declared license and was authored, remixed, and/or curated by LibreTexts.

- **2.3.3: Covalent and Ionic Radii** by Bingyao Zheng, Emily Nguyen, Kathryn Haas, Swetha Ramireddy is licensed CC BY-NC-SA 4.0.

1.2.3.4: Hard and Soft Acids and Bases

Origin of the Hard-Soft Acid-Base Principle

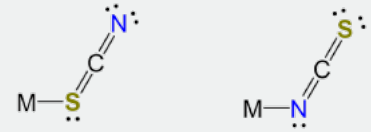
One of the strengths of the Lewis acid-base concept is the readiness with which it illuminates the role that covalent and electrostatic interactions in acid base behavior, specifically through its ability to explain chemical interactions in terms of frontier orbitals and the interactions between charged groups as electrons are donated from a base to an acid. However, simply acknowledging the presence of such interactions does little to illuminate the degree to which each mode of explanation best explains the bonding in a given system? To what extent is a given adduct better described as held together by covalent bonds as opposed to ionic ones - *e.g.* better described as a molecule rather than an ion pair? Moreover, does it even matter, given that the orbitals of quantum mechanics result from the combination of electrons' wavelike behavior with their electrostatic attraction to nuclei in either case?[1] These questions and more are addressed by one of the most important conceptual tools in contemporary inorganic chemistry, the Hard-Soft acid-base principle.

The **Hard-Soft acid-base principle (HSAB principle)** stems from the recognition that some Lewis acids and bases seem to have a natural affinity for one another.* Consider the following:

- Some metals are commonly found in nature as salts of chloride or as oxide ores while others are found in combination with sulfur. Geochemists even use the Goldschmidtt classification scheme to classify the halide and oxide formers as lithophiles and the sulfide formers as chalcophiles.
- In living systems small highly charged metals ions like Fe^{3+} are usually found bound to N and O atoms while larger metals with lower charges such as Zn^{2+} are often found attached to at least one S atom. Similarly, metals prefer to bind to one coordination site over the other when forming complexes with ambidentate ligands. The most well-known instances involve complexes of cyanate and thiocyanate, which can coordinate metals through either the N or chalcogen atom. For instance, Cu^{2+} and Zn^{2+} form *N*-thiocyanato complexes in species like $[Cu(NCS)_2(py)_2]$ and $[Zn(NCS)_4]^{2-}$ while their larger cogeners Au^{3+} and Hg^{2+} preferentially forms *S*-thiocyanato complexes, giving species like $[Hg(SCN)_4]^{2-}$.

Ambidentate ligands

Ambidentate ligands possess multiple coordination sites through which a metal may bind. For instance, thiocyanate may coordinate metals (M) at either the S or N to give *S*-thiocyanato or *N*-thiocyanato complexes.



S-thiocyanato *N*-thiocyanato

- The solubility trends for the alklai metal halides and silver halides are opposite, even though both involve salts of formula M^+X^- (salts can be thought of as involving Lewis acid-base adduct formation between the anions and cations). Specifically, although the silver halides are all relatively insoluble in water, the very modest solubility they possess follows the order:

$$X = F >> Cl > Br > I \text{ (for the solubility of AgX)}$$

In contrast, the much more ample solubility of the alkali metal halides** follows the opposite order. For example, the order for the lithium halides is

$$X = F << Cl < Br << I \text{ (for the solubility of LiX)}$$

Notes

1. Albeit suitably fudged through such niceties as the Aufbau principle and other approximations.

* Despite the fruitfulness of this observation, in general it is important to reduce the potential for observer bias by checking observations like these against compounds reported in the chemical literature and databases like the Inorganic Crystal Structure and Cambridge Crystallographic Databases.

** These are very soluble in water, to the point where some solutions are perhaps better described as solutions of water in the halide.

† This can be predicted based on the relative hardness of BF_3, BR_3, and BH_3 in the list of hard and soft acids. However, for those of you who may be confused as to why H is considered a better electron donor for the purposes of softening a Lewis acid center while alkyl groups are better electron donors for the purposes of stabilizing carbocations in organic chemistry, the dominant effect is the lower electronegativity of H relative to carbon (in CH_3). The effect of electron donation due to hyperconjugation isn't as great for thermodynamically stable bases like BX_3/BR_3.

1.2.3.4: Hard and Soft Acids and Bases is shared under a not declared license and was authored, remixed, and/or curated by LibreTexts.

- **6.6: Hard and Soft Acids and Bases** by Stephen M. Contakes is licensed CC BY 4.0.

1.2.3.4.1: Quantitative Measures of Hardness, Softness, and Acid-Base Interactions from a Hard Soft Acid-Base Principle perspective involve orbital energies and or apportioning acid-base bonding in terms of electrostatic and covalent factors

Pearson Absolute Hardness is a useful metric of hardness based on orbital energies

The recognition that hard acids and bases possess a large HOMO-LUMO gap suggests that the gap size itself might serve as a useful index of hardness. The basis for this idea may be found by considering Pearson's definition of absolute hardness, η.[1] **Pearson's absolute hardness, η**, is half the second derivative of a species' energy with respect to changes in total number of electrons, N_{e^-}.

$$\text{Pearson's absolute hardness} = \eta = \frac{1}{2}\frac{d^2E}{dN_{e^-}^2}$$

$$(in \;\; eV)$$

and, since acids' and bases' hardness and softness are inversely related, Pearson's absolute softness, σ, is just the inverse of hardness.

$$\text{Pearson's softness} = \frac{1}{\eta}$$

Of these, Pearson's absolute hardness is related to the **Mulliken definition of electronegativity** as the first derivative of a species' energy with respect to changes in total number of electrons.

$$\text{Mulliken electronegativity} = \chi = \frac{dE}{dN_{e^-}}$$

$$(in \;\; eV)$$

Operationally, both the Pearson hardness and Mulliken electronegativity are approximated in terms of the energies associated with unit changes in the number of electrons – *i.e.*, in terms of ionization energies and electronegativities. Specifically,

$$\text{Pearson's absolute hardness} = \eta \approx \frac{IE - EA}{2}$$

$$\text{Mulliken electronegativity} = \chi \approx \frac{IE + EA}{2}$$

where IE and EA are in eV.

The connection between Pearson's absolute hardness/softness and the HOMO-LUMO gap then follows from Koopman's theorem, in which the ionization energy (IE) is just the opposite of the HOMO energy.

$$IE = -E_{HOMO}$$

Similarly, the electron affinity (EA), defined as the opposite of the energy released on absorption of an electron, may be taken as an approximation of the LUMO energy.

$$E_{LUMO} \approx -EA$$

So Pearson's absolute hardness is just half the HOMO-LUMO gap (band gap) size in electron volts:

$$\text{Pearson's absolute hardness} = \eta \approx \frac{E_{LUMO} - E_{HOMO}}{2}$$

where all values are given in eV,

and the Mulliken electronegativity is just the average of the HOMO and LUMO energies (~Fermi energy):

$$Mulliken\ electronegativity, \chi \approx -\frac{E_{LUMO} + E_{HOMO}}{2}$$

$$where\ all\ values\ are\ given\ in\ eV$$

The relationships between the Pearson absolute hardness, Mulliken electronegativity, and HOMO and LUMO energies are depicted schematically for the group 1A monocations in Figure **1.2.3.4.1.1**.

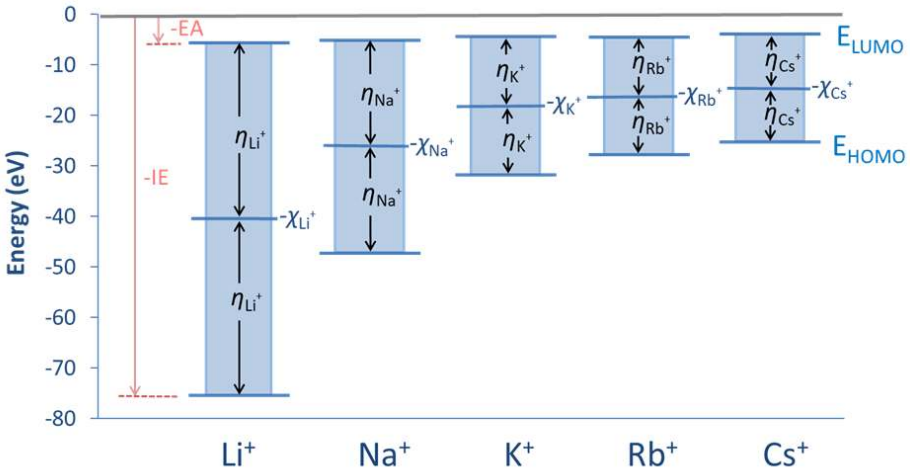


Figure **1.2.3.4.1.1**. Relationships between Pearson absolute hardness, Mulliken electronegativity, and HOMO and LUMO energies for the group 1A monocations.

Values of the Pearson hardness and Mulliken electronegativity for several acids and bases are given in Table **1.2.3.4.1.1**. The values in the table confirm the expected trends, showing an increase in hardness with size (down a group), with increasing charge, and as substituent electronegativity increases for a series of isolobal ions.

Table **1.2.3.4.1.1**: Pearson Absolute Hardness and Related Parameters for Selected Acids and Bases.[2] Taken from Pearson, R. G., Absolute electronegativity and hardness: application to inorganic chemistry. Inorganic Chemistry 1988, 27 (4), 734-740.

Species	Ionization Energy, IE or I (eV)	Electron Affinity, EA or A (eV)	Mulliken Electronegativity, χ (eV)	Pearson Absolute Hardness, η (eV)
Selected Acids				
Group 1A monocations				
Li^+	75.64	5.39	40.52	35.12
Na^+	47.29	5.14	26.21	21.08
K^+	31.63	4.34	17.99	13.64
Rb^+	27.28	4.18	15.77	11.55
Cs^+	25.1	3.89	14.5	10.6
Group 11 monocations				
Cu^+	20.29	7.73	14.01	6.28
Ag^+	21.49	7.58	14.53	6.96
Au^+	20.5	9.23	14.9	5.6
Isoelectronic Row 3 Metal Cations				
Na^+	47.29	5.14	26.21	21.08
Mg^{2+}	80.14	15.04	47.59	32.55
Al^{3+}	119.99	28.45	74.22	45.77
Changes with Transition Metal Ion Charge				
Fe^{2+}	30.65	16.18	23.42	7.24
Fe^{3+}	54.8	30.65	42.73	12.08
Co^{2+}	33.50	17.06	25.28	8.22
Co^{3+}	51.3	22.5	42.4	8.9
Boron trihalides				
BF_3	15.81	-3.5	6.2	9.7
BCl_3	11.60	0.33	5.97	5.64
BBr_3	10.51	0.82	5.67	4.85
CO_2	13.8	-3.8	5.0	8.8
CS_2	10.08	0.62	5.35	5.56
Selected Bases				
Group 17 monoanions (taken to be identical to the free atom values; for arguments as to why this is reasonable see Pearson, R. G., Inorg. Chem. 1988, 27 (4), 734-740.)				
F^-	17.42	3.40	10.41	7.01
Cl^-	13.01	3.62	8.31	4.70
Br^-	11.84	3.36	7.60	4.24
I^-	10.45	3.06	6.76	3.70

Species	Ionization Energy, IE or I (eV)	Electron Affinity, EA or A (eV)	Mulliken Electronegativity, χ (eV)	Pearson Absolute Hardness, η (eV)
Group 15 hydrides				
NH_3	10.7	-5.6	2.6	8.2
PH_3	10.0	-1.9	4.1	6.0
Trimethylpnictides				
NMe_3	7.8	-4.8	1.5	6.3
PMe_3	8.6	-3.1	2.8	5.9
$AsMe_3$	8.7	-2.7	3.0	5.7
Group 16 hydrides				
H_2O	12.6	-6.4	3.1	9.5
H_2S	10.5	-2.1	4.2	6.2
Phosphorous trihalides				
PF_3	12.3	-1.0	5.7	6.7
$PC1_3$	10.2	0.8	5.5	4.7
PBr_3	9.9	1.6	5.6	4.2

Drago-Wayland Acid-Base Parameters allow for estimation of the electrostatic and covalent contributions to the enthalpy of formation of a Lewis acid-base adduct.

Although Pearson hardness values are a useful metric of acids' and bases' hardness, they cannot easily be used to estimate the Lewis acid-base interaction energy. This is not the case for the EC model developed by Drago and Wayland.[3] In the **Drago and Wayland's EC Model,** the enthalpy of formation of an acid-base adduct, AB,

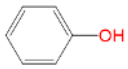
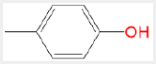
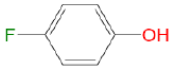
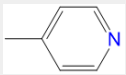
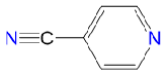
$$A + B \rightleftharpoons AB \qquad \Delta H_{AB\ adduct}$$

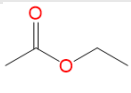
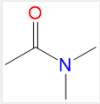
from the acid (A) and base (B) can be calculated as the sum of products of electrostatic (E) and covalent (C) factors that reflect the propensity of the acid and base to engage in strong electrostatic and covalent interactions with one another:

$$-\Delta H_{AB\ adduct} = E_A E_B + C_A C_B$$

where E_A and C_A are the electrostatic and covalent parameters for the acid and E_B and C_B the electrostatic and covalent parameters for the base given in units of $kcal^{½}\ mol^{-½}$. E and C parameters for selected acids and bases are given in Table **1.2.3.4.1.2** .

Table **1.2.3.4.1.2**: E and C Parameters for selected Lewis acids and bases according to the ECW model.[4,5] Taken from Vogel, G. C.; Drago, R. S., The ECW Model. *Journal of Chemical Education* 1996, 73 (8), 701 and Drago, R. S. A modern approach to acid-base chemistry. *Journal of Chemical Education* 1974, 51 (5), 300 (for BF_3).

Species	E (kcal^{½} mol$^{-½}$)	C (kcal^{½} mol$^{-½}$)	W (kcal mol^{-1})	C/E
Acids				
I_2	0.5†	2†	0	4
ICl	2.92	1.66	0	0.57
H_2O	1.31	0.78	0	0.59
SO_2	0.51	1.56	0	3.1
$HCCl_3$ (chloroform)	1.56	0.44	0	0.28
$(CH_3)_3COH$	1.07	0.69	0	0.65
$(CF_3)_3COH$	3.06	1.88	-0.87	0.61
	2.27	1.07	0	0.47
	2.23	1.03	0	0.46
	2.30	1.11	0	0.48
	1.38	0.68	0	0.49
BF_3	1.62	9.88		6.10
$B(CH_3)_3$	2.90	3.60	0	1.2
$Al(CH_3)_3$	8.66	3.68	0	0.43
$Ga(C_2H_5)_3$	6.95	1.48	0	0.21
$In(CH_3)_3$	6.60	2.15	0	0.33
$Zn[N(Si(CH_3)_3)]_2$	2.75	2.32	0	0.84
$Cd[N(Si(CH_3)_3)]_2$	2.50	1.83	0	0.73
Bases				
NH_3	2.31	2.04		0.88
CH_3NH_2	2.16	3.13		1.4
$(CH_3)_2NH$	1.80	4.21		2.3
$(CH_3)_3N$	1.21	5.61		4.6
	1.78	3.54		2.0
	1.81	3.73		2.0
	1.53	2.94		1.9

Species	E (kcal^{½} mol$^{-½}$)	C (kcal^{½} mol$^{-½}$)	W (kcal mol^{-1})	C/E
CH_3CN	1.64	0.71		0.43
$ClCH_2CN$	1.67	0.33		0.20
$CH_3C(O)CH_3$	1.74	1.26		0.72
$(C_2H_5)_2O$	1.80	1.63		0.91
	1.64	2.18		1.3
 (EtOAc)	1.63	0.95		0.58
	2.35†	1.31		0.56
$(CH_3)_2S$	0.25	3.75		15
$(CH_3CH_2)_2S$	0.24	3.92†		15
	0.26	4.07		16
$(CH_3)_2Se$	0.05	4.24		83
$(CH_3)_2SO$	2.4	1.47		0.61
$(CH_3)_3P$	0.25	5.81		24
$(CH_3O)_3P$	0.13	4.83		37
$(C_6H_5)_3PO$	2.59	1.67		0.64
$(C_6H_5)_3PS$	0.35	3.65		10
C_6H_6	0.70	0.45		0.64

† These values were fixed to parameterize the rest of the E and C parameters.

Trends in the relative values of C and E for the acids and bases in Table **1.2.3.4.1.2** are very roughly consistent with the trends in hardness and softness outlined earlier. However, the parameters suggest that some trends in hardness reflect changes in species' ability to engage in ionic interactions while others reflect changes in species' ability to engage in strong covalent interactions. For example, C_B for the dimethylchalcogenides increases steadily from 1.5 to 4.25 kcal^{½} mol$^{-½}$ on going from Me_2O to Me_2Se while E_B decreases from 1.68 to 0.05 kcal^{½} mol$^{-½}$, suggesting that electrostatic and covalent factors are both involved in a decrease in base hardness down group 16. However, in the case of phosphines and amines it appears that electrostatic factors are primarily responsible for the decrease in hardness down group 15. On going from Me_3N to Me_3P, C_B only increases slightly from 5.61 to 5.81 kcal^{½} mol$^{-½}$ while E_B decreases from 1.21 to 0.25 kcal^{½} mol$^{-½}$ - *i.e.*, to 20% of the Me_3N value.

However, some species tend to have very high values for both E and C, reflecting their ability to engage in strong electrostatic and covalent interactions, while others have small values for both, reflecting their relative stability as free species in solution.

As can be seen by comparing the acids and bases listed in the absolute hardness table (Table **1.2.3.4.1.1**) and the EC parameters table (Table **1.2.3.4.1.2**). The EC model has primarily been applied to organic and main group organometallic acids and bases. However, a variety of extensions have been proposed that enable its wider applicability.

The simple EC model only includes electrostatic and covalent considerations and thus ignores steric, lattice energy, and other contributions to the interaction energy. Thus it is only useful for analyzing the interaction energies of sterically unhindered adducts in which solvation energy and other contributions to the overall interaction energy are insignificant. However, additional refinements of the model attempt to extend its usefulness by accomodating various factors, such as

- *Steric strain.* Specifically, Hancock and Martell[6] introduced a D parameter to account for any additional steric strain introduced upon adduct formation,* giving

$$-\Delta H_{AB\ adduct} = E_A E_B + C_A C_B - D_A D_B$$

- *Charge transfer upon adduct formation.* As discussed in section 6.4.2, the formation of a Lewis acid-base complex results in a net transfer of electron density from the electron donor (base) to the acceptor (acid). Drago and Wong[7] extended the EC model to include that charge transfer by adding what they called receptance factors that account for the acid's ability to receive electron density (R_A) and transference factors that account for the base's ability to donate electron density (T_B), giving

$$-\Delta H_{AB\ adduct} = E_A E_B + C_A C_B + R_A T_B$$

  This extension of the EC model is called the **electrostatic-covalent-transfer or ECT model**. Notably, it has been applied successfully to adducts involving ions, for which the $R_A T_B$ term can account for as much as 31% of the interaction energy.

- *Any constant energy term, such as the energy needed to cleave a dimer in order to make the Lewis acid (e.g., $Al_2Cl_6 \rightarrow 2AlCl_3$).* Drago and Vogel[4] extended the EC model to accommodate these constant energy terms, which they designated W. The resulting model is called the **ECW model,** for which

$$-\Delta H_{AB\ adduct} = E_A E_B + C_A C_B + W$$

where

$$W = W_A + W_B$$

A simple application of EC and extended EC models is that they allow the enthalpy of adduct formation to be calculated. These enthalpy calculations based on the EC model are consistent with the superior interaction energy of hard-hard and soft-soft interactions compared to hard-soft ones. Consider, for example, the transfer of I_2 between BF_3 and $InMe_3$, H_3N-BF_3, and H_3N-$InMe_3$.

$$H_3N - BF_3 + InMe_3 \rightleftharpoons BF_3 + H_3N - InMe_3$$

Since H_3N is a hard base and BF_3 and $InMe_3$ are harder and softer acids, respectively, the equilibrium is expected to favor the reactant, H_3N-BF_3. Assuming the equilbrium is enthalpically driven, this qualitative analysis is consistent with the expected endothermic enthalpy of the reaction, as may be seen from the calculated enthalpies of adduct formation for both H_3N-BF_3 and H_3N-$InMe_3$.

For H_3N-BF_3:

$$-\Delta H_{H_3N-BF_3} = E_{BF_3} E_{NH_3} + C_{BF_3} C_{NH_3}$$

$$-\Delta H_{H_3N-BF_3} = (1.62)(2.31) + (9.88)(2.04)$$

$$-\Delta H_{H_3N-BF_3} = 3.74\ kcal/mol + 20.1\ kcal/mol = 23.8\ kcal/mol$$

$$\Delta H_{H_3N-BF_3} = -23.8\ kcal/mol$$

For H_3N-$InMe_3$:

$$-\Delta H_{H_3N-InMe_3} = E_{InMe_3} E_{NH_3} + C_{InMe_3} C_{NH_3}$$

$$-\Delta H_{H_3N-InMe_3} = (6.6)(2.31) + (2.15)(2.04)$$

$$-\Delta H_{H_3N-InMe_3} = 15.25\ kcal/mol + 4.39\ kcal/mol = 19.63\ kcal/mol$$

$$\Delta H_{H_3N-InMe_3} = -19.63\ kcal/mol$$

So H_3N-BF_3 is enthalpically favored by -4.2 kcal/mol [=-23.8 kcal/mol - (-19.63 kcal/mol) according to Hess' Law].

In addition to their utility for estimating enthalpies of Lewis acid-base complex formation, EC and related models serve as a useful tool for estimating the relative importance of ionic, covalent, and steric factors in complex formation. Specifically,

- The relative contributions of ionic and covalent factors can be calculated directly, as from the E and C terms. This can provide insight into why some complexes are more stable than others. Such calculations reveal that the hard-hard adduct H_3N-BF_3 is favored over the hard-soft adduct H_3N-$InMe_3$ because of the strong covalent interaction holding together H_3N-BF_3. The covalent term accounts for 84% of the energy of the H_3N-BF_3 interaction and is largely lost upon formation of H_3N-$InMe_3$, for which it contributes only 22% of the interaction energy. When the electrostatic term is accounted for, it can be seen that the formation of H_3N-$InMe_3$ from H_3N-BF_3 is disfavored, since it would result in a loss of 15.7 kcal/mol of covalent stabilization that would be incompletely compensated for by a gain of 11.5 kcal/mol of electrostatic stabilization.
- The role of other contributions to the bonding in a Lewis acid-base complex may be estimated from the discrepancy between the experimental and EC model calculated stabilization energies. This is because the EC parameters assume sigma bonding and so any deviation between the calculated and experimental enthalpies of complex formation can be attributed to non-sigma contributions.
    - This is done explicitly in extensions of the EC model. For instance, in the case of the Hancock and Martell, ECT, and ECW extensions of the EC model, the contributions of the steric, charge transfer, and constant energy factors (like dimer dissociation) are directly computed in the model.
    - Comparisons of the difference between the energies calculated using ordinary EC parameters and the observed enthalpies has also been used as an estimate of the
        - steric strain energy in strained adducts, which exhibit a less exothermic heat of adduct formation than expected
        - π-backbonding energy in adducts which are capable of such interactions and exhibit a more exothermic heat of formation than expected.[8-10]
    - For examples see (a) Drago, R. S., The interpretation of reactivity in chemical and biological systems with the E and C model. Coordination Chemistry Reviews 1980, 33 (3), 251-277; (b) Drago, R. S.; Bilgrien, C. J., Inductive transfer and coordination of ligands in metal—metal bonded systems. Polyhedron 1988, 7 (16), 1453-1468; (c) Drago, R. S., The question of a synergistic metal-metal interaction leading to .pi.-back-bond stabilization in dirhodium tetrabutyrate adducts. Inorganic Chemistry 1982, 21 (4), 1697-1698.
- The role of electrostatic, covalent, and other contributions to the spectroscopic behavior of Lewis acid-base complexes can be assessed similarly using specialized versions of the ECW or ECT model that allow for calculation of changes in spectroscopic parameters upon adduct formation - *e.g.*, OH stretching frequencies. Details are beyond the scope of this text but may be found in the original literature,[11] for example, Drago, R. S.; Vogel, G. C. *JACS* 1992, 114 (24), 9527-9532; Vogel, G. C.; Drago, R. S., *J. Chem. Educ.* 1996, 73 (8), 701; Drago, R. S.; Wong, N. M., *J. Chem. Educ.* 1996, 73 (2), 123.).

Pearson Softness Parameters have been proposed as a means of calculating the equilibrium constant for formation of a Lewis acid-base adduct, although they are more commonly used to estimate metal toxicity

Pearson also proposed a softness parameter that can be used to estimate the thermodynamics of Lewis acid-base complex formation, this time in the form of the equilibrium constant for

$$A + B \overset{K}{\rightleftharpoons} AB$$

for which Pearson proposed

$$logK = S_A S_B + \sigma_A \sigma_B$$

where S_A and S_B are acid and base parameters related to the strength of the acid-base interaction and σ_A and σ_B are acid and base parameters related to softness. This approach hasn't found as wide an acceptance in studies of chemical reactivity as the Drago-Wayland and absolute hardness parameters. However, because the toxicity of metal ions sometimes depends on their propensity to bind soft Lewis bases in living systems, the softness parameters which Pearson and Mawby subsequently proposed based on the relative energies of metal fluorine and metal iodine bonds[12] have been widely used as a tool for predicting metal ion toxicity.[13]

References

1. Pearson, R. G., Absolute electronegativity and absolute hardness of Lewis acids and bases. *Journal of the American Chemical Society* 1985, 107 (24), 6801-6806.

2. Pearson, R. G., Absolute electronegativity and hardness: application to inorganic chemistry. *Inorganic Chemistry* 1988, 27 (4), 734-740.

3. Drago, R. S.; Wayland, B. B., A Double-Scale Equation for Correlating Enthalpies of Lewis Acid-Base Interactions. *Journal of the American Chemical Society* 1965, 87 (16), 3571-3577.

4. Vogel, G. C.; Drago, R. S., The ECW Model. *Journal of Chemical Education* 1996, 73 (8), 701.

5. Drago, R. S. A modern approach to acid-base chemistry. *Journal of Chemical Education* 1974, 51 (5), 300

6. Hancock, R. D.; Martell, A. E., Hard and Soft Acid-Base Behavior in Aqueous Solution: Steric Effects Make Some Metal Ions Hard: A Quantitative Scale of Hardness-Softness for Acids and Bases. *Journal of Chemical Education* 1996, 73 (7), 654.

7. Drago, R. S.; Wong, N. M., The Role of Electron-Density Transfer and Electronegativity in Understanding Chemical Reactivity and Bonding. *Journal of Chemical Education* 1996, 73 (2), 123.

8. Drago, R. S., The interpretation of reactivity in chemical and biological systems with the E and C model. Coordination Chemistry Reviews 1980, 33 (3), 251-277.

9. Drago, R. S.; Bilgrien, C. J., Inductive transfer and coordination of ligands in metal—metal bonded systems. Polyhedron 1988, 7 (16), 1453-1468.

10. Drago, R. S., The question of a synergistic metal-metal interaction leading to .pi.-back-bond stabilization in dirhodium tetrabutyrate adducts. Inorganic Chemistry 1982, 21 (4), 1697-1698.

11. Drago, R. S.; Vogel, G. C., Interpretation of spectroscopic changes upon adduct formation and their use to determine electrostatic and covalent (E and C) parameters. *Journal of the American Chemical Society* 1992, 114 (24), 9527-9532.

12. Pearson, R. G.; Mawby, R. J. The Nature of Metal-Halogen Bonds in Gutmann, V. *Halogen Chemistry, vol. 3.* Academic Press: London, 1967, pp. 55-84.

13. Kinraide, T. B. Improved Scales for Metal Ion Softness and Toxicity *Environmental Toxicology and Chemistry* 2009, 28 (3), 525-533.

Notes

* More precisely, the D parameters account for the difference in steric strain in the adduct relative to a water adduct of the Lewis acid.

1.2.3.4.1: Quantitative Measures of Hardness, Softness, and Acid-Base Interactions from a Hard Soft Acid-Base Principle perspective involve orbital energies and or apportioning acid-base bonding in terms of electrostatic and covalent factors is shared under a not declared license and was authored, remixed, and/or curated by LibreTexts.

- **6.6.1: Quantitative Measures of Hardness, Softness, and Acid-Base Interactions from a Hard Soft Acid-Base Principle Perspective Involve Orbital Energies and/or Apportioning Acid-Base Bonding in Terms of Electrostatic and Covalent Factors** by Stephen M. Contakes is licensed CC BY 4.0.

1.2.3.4.2: Hard-Hard and Soft-Soft preferences may be explained and quantified in terms of electrostatic and covalent and electronic stabilization on the stability of Lewis acid-base adducts

The Hard Soft Acid Base Principle is a Conceptual Tool for Thinking About Patterns of Lewis Acid-Base Reactivity

The explanation of the trends in metal distribution, halide salt solubility, and preferred metal coordination patterns is rooted in Arland, Chatt, and Davies' observation that *Lewis acids and bases could be classified into two groups based on their propensity to form stable compounds with one another* (*e.g.* acids in a class tend to form more stable adducts with bases in the same class than they did with bases in the other).[1] Arland, Chatt, and Davies somewhat boringly termed these groups class a and class b but today they are known by Ralph Pearson's name for them. Pearson called the class a acids and bases hard and class b acids and bases soft. These terms reflect how "soft" these substance's electron clouds are towards distortion or, in other words, their polarizability (Figure **1.2.3.4.2.1**). Pearson terms acids and bases which are relatively polarizable **soft** and those which are difficult to polarize **hard.**

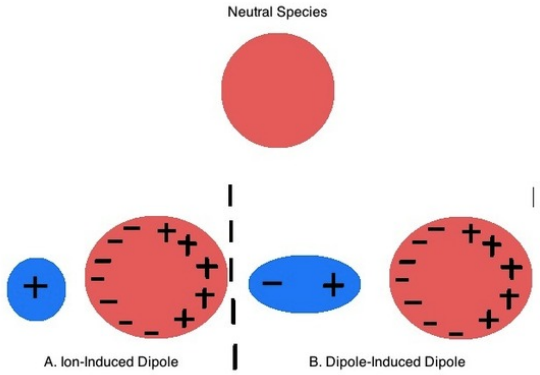


Figure **1.2.3.4.2.1**: Polarizability refers to the ease with which a substance's electron cloud may be distorted under the action of an electric field. A fragment's polarizability determines the degree to which its electron cloud is distorted by A.) an Ion and B.) a polar molecule to induce a dipole moment. The figure is taken from (and the caption expanded from) Cox, Kelly and Dana Reusser "Polarizability"

Recognizing Hard and Soft Acids and Bases

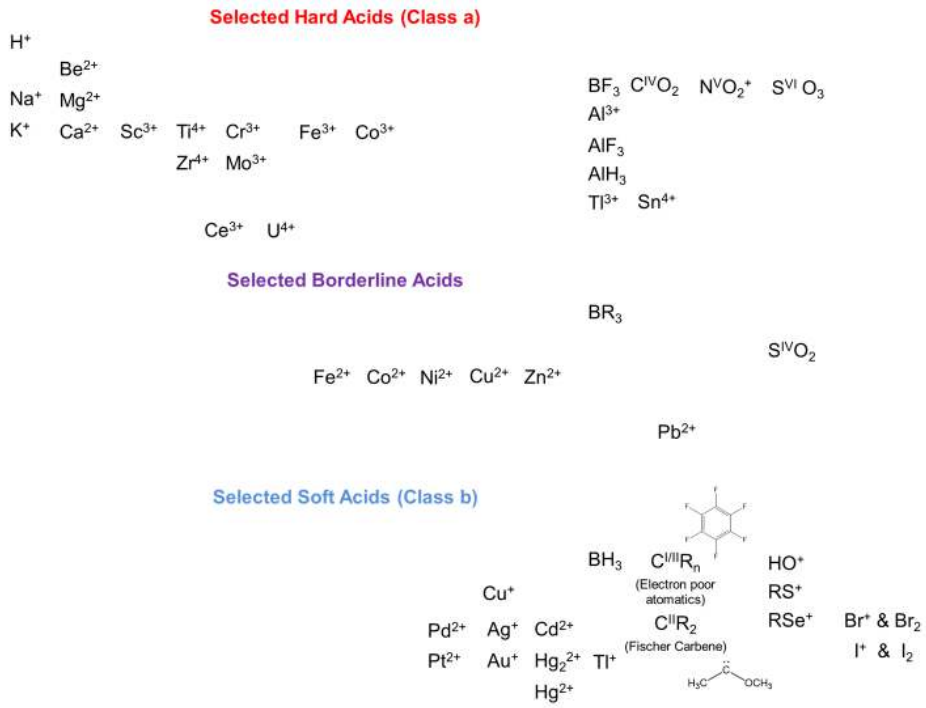
Hard acids and bases come in two varieties:

1. hard acid and base sites that possess few valence electrons and for which polarization therefore involves distorting core electrons, which are difficult to distort because they are close to the nucleus and experience a high nuclear charge. The most common examples of such substances are Lewis acid hard acids towards the left of the periodic table.
2. hard acid and base sites with a high charge density (highly charged relative to size) and/or which are electron deficient. In these cases polarization involves distorting electrons that already experience strong unshielded electrostatic interactions.

Soft acids and bases also come in two varieties

1. soft acids and bases which posses many valence electrons and so are more readily polarized. In consequence, all other things being equal, soft acids and bases are more likely to be found towards the middle or right of the periodic table.
2. soft acids and bases with little charge density and/or which are relatively electron rich.

Note that the hard-soft classification should not be thought of as if all hard acids and bases are equally hard and all soft acids and bases equally soft. There is a graduation in hardness and softness and a number of intermediate acids and bases which do not fit neatly in either category. With this caveat in mind, representative **hard, soft, and borderline acids** are given below. Notice how they illustrate the trends just outlined.



As expected, hard acids tend to be found towards the left side of the periodic table and involve higher oxidation states and/or electron donating substituents while soft acids are more common to the right of the periodic table and involve lower oxidation states and/or electron donating substituents.

Illustrative hard, soft, and borderline bases are given below. Again, notice how these substances illustrate the general trends.

Selected Hard Bases (Class a)

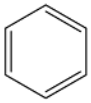
Nitrogen bases	Oxygen bases		small halides
NH_2^-	OH^-	CO_3^{2-}	F^-
NH_3	H_2O	RCO_2^-	Cl^-
RNH_2	ROH	NO_3^-	
NH_2NH_2	ROR	PO_4^{3-}	
		SO_4^{2-}	

Selected Borderline Bases

electron-poor Nitrogen bases		low oxidation state element oxyanions	intermediate halides
N_3^-		NO_2^-	
NO_2^-			
SCN^-		SO_3^{2-}	Br^-
N_2			

Selected Soft Bases (Class b)

Carbon bases	P and As bases	Sulfur bases	large halides & pseudohalides
R^-	PR_3	RS^-	H^-
CO	$P(OR)_3$	RSH	I^-
CN^-	AsR_3	RSR	
RNC		SCN^-	
$R_2C{=}CR_2$ (alkenes)			



(electron-rich aromatics)

Qualitative Estimation of the Relative Hardness and Softness of Lewis Acids and Bases

As can be seen from the examples above, **hard acids are relatively electron-poor and hard bases electron-rich** since they have comparatively

- small frontier orbitals, reflective of their relatively small atom/ion/fragment sizes
- high (for acids) or low (for bases) oxidation states on the base atom, reflected in a large positive formal charge (for acids) or negative formal charge (for bases)
- low polarizability, due to loss or gain of substantial numbers of electrons, or the localization of
  - positive charge on an electropositive element or an atom bearing electron-withdrawing substituents
  - negative charge on an electronegative element or an atom bearing electron-donating substituents

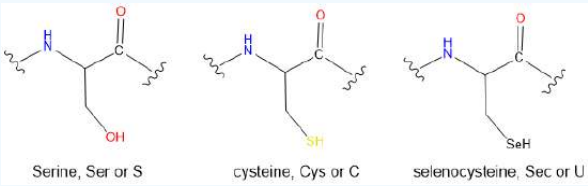
In contrast to hard acids and bases, **soft acids are relatively electron-rich and soft bases larger and more electron poor** since they have comparatively

- large frontier orbitals, reflective of their relatively large atom/ion/fragment sizes
- low oxidation states, often resulting in small or nonexistent atomic charges
- high polarizability, as might be expected of species in which electron-electron repulsions are lower and electrons are spread over a large volume. Sometimes this is indicated by
  - positive charge on an electronegative element or an atom bearing electron-donating substituents
  - negative charge on an electropositive element or an atom bearing electron-withdrawing substituents

Exercise 1.2.3.4.2.1

Rank the acids or bases in each set in increasing order of expected hardness.

a. Cr^{2+} and Cr^{3+}
b. H^+, Cs^+, and Tl^+
c. SCN^- (acting as a base at N) and SCN^- (acting as a base at S)
d. AlF_3, AlH_3, $AlMe_3$
e. The side chains of the following proteinogenic amino acids

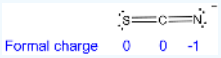


Answer

(a) $Cr^{2+} < Cr^{3+}$ All other things being equal, hardness increases with oxidation state.

(b) $Tl^+ < Cs^+ < H^+$ The order reflects Cs^+ and Tl^+'s larger size relative to H^+ (which doesn't possess any electrons that can be polarized anyway) and that Tl^+ still possesses two valence electrons while Cs^+ possesses none.

(c) SCN^- (acting as a base at S) < SCN^- (acting as a base at N). The order reflects the greater electronegativity of N than S and N's possession of a more negative formal charge of -1.



(d) $AlH_3 < AlMe_3 < AlF_3$. The hardness increases as the substituents on the Lewis acid Al center become less electron donating and more electron withdrawing (and, incidentally, harder bases) as their electronegativity increases in the order H^- < CH_3^- < F^-. Note that the order of electron donating ability for H^- and CH_3^- is the opposite observed for carbocations, for which hyperconjugation plays a larger role.

(e) Sec < Cys < Ser. The hardness increases as the electronegativity of the Lewis base chalcogen increases on going from a selenol to a thiol to an alcohol.

The Hard-Soft Acid-Base Principle (HSAB Principle)

The **Hard-Soft acid-base principle (HSAB Principle) explains patterns in Lewis acid-base reactivity in terms of a *like reacts with like preference***. Both thermodynamically and kinetically, hard acids prefer hard bases and soft acids soft bases. Specifically,

- Thermodynamically, hard acids form stronger acid-base complexes with hard bases while soft acids form stronger complexes with soft bases.
- Kinetically, hard acids/electrophiles react more quickly with hard bases/nucleophiles while soft acids/electrophiles react more quickly with soft bases/neucleophiles.

Applications of the HSAB principle include

1. Predicting the equilibrium or speed of *Lewis acid-base metathesis and displacement reactions.* In a Lewis acid-base **metathesis reaction** the acids and bases swap partners

$$\mathbf{A_1 : B_1 + A_2 : B_2 \overset{k_1,\, K_{eq_1}}{\rightleftharpoons} A_1 : B_2 + A_2 : B_1}$$

For example, the equilibrium position of the metathesis reaction between $\mathbf{TlF}$ and $\mathbf{K_2S}$ favors the products:

$$\mathbf{2\,TlF + H_2S \rightleftharpoons Tl_2S + 2\,KF}$$

consistent with the HSAB's hard-hard and soft-soft preference.



The HSAB principle also allows for prediction of the position of displacement reactions, in which a Lewis acid or base forms an adduct using a base or acid from an existing Lewis acid-base complex. In these reactions, the displacement of acid or base from the reactant complex may be thought of as a sort of metathesis reaction, one in which in the unbound acid or base switches places with one in the complex. For example, the reaction between **HI** and methylmercury cation

$$\mathbf{HI + HgSCH_3^+ \rightleftharpoons CH_3SHgI + H^+}$$

involves displacement of an iodide from **HI** to give $\mathbf{CH_3HgI}$. The position of the equilibrium favors $\mathbf{CH_3HgI}$ since both $\mathbf{CH_3Hg^+}$ and $\mathbf{I^-}$ are soft, while $\mathbf{H^+}$ is a hard acid.



Exercise 1.2.3.4.2.2

Predict the position of equilibrium for the following reaction.

$$\mathbf{Fe_2O_3 + 3\,Ag_2S \rightleftharpoons Fe_2S_3 + 3\,Ag_2O}$$

Answer

The equilibrium will favor the reactants (K<1) since the hard-hard and soft-soft interactions in the reactants are more stable than the hard-soft interactions in the products.



Exercise 1.2.3.4.2.3

Predict whether K for the following equilibria will be <<1, ~1, or >>1.

a. $\mathbf{2\,HF + (CH_3Hg)_2S \rightleftharpoons 2\,CH_3HgF + H_2S}$
b. $\mathbf{Ag(NH_3)_2^+ + 2\,PH_3 \rightleftharpoons Ag(PH_3)_2^+ + 2\,NH_3}$
c. $\mathbf{Ag(PH_3)_2^+ + 2\,H_3B{-}SH_2 \rightleftharpoons 2\,H_3B{-}PH_3 + Ag(SH_2)_2^+}$
d. $\mathbf{H_3B{-}NH_3 + F_3B{-}SH_2 \rightleftharpoons H_3B{-}SH_2 + F_3B{-}NH_3}$

Answer

a. K< < 1 since the reactant adducts are hard-hard and soft-soft while the products involve hard-soft interactions.

b. K>>1 since the reactant complex, diamine silver(I), is a complex of a hard base, NH_3, with the soft acid, Ag^+, while the product is a complex of the same soft acid with the soft base phosphine.

c. K~1 since all the adducts amongst the reactants and products involve soft acids and bases.

d. K>>1 since BH_3 is a softer acid than BF_3, so it will form a stronger complex with the softer base H_2S while the harder BF_3 forms a stronger complex with the harder base NH_3.

2. Predicting the relative strengths of a given set of *Lewis acids or bases towards a particular substrate*. Consider, for example, the relative strengths of a BH_3, BMe_3, and BF_3 towards group 15 hydrides like NH_3, PH_3, and AsH_3. Of the

boranes listed, the hardest acid BF_3 is the strongest acid towards the hard base NH_3 while BH_3 is the strongest towards AsH_3.[†]

? Exercise 1.2.3.4.2.4

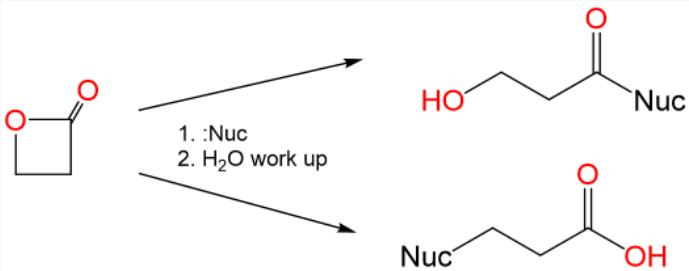
Which acid will form the most stable complex with **CO**: $\mathbf{BH_3}$, $\mathbf{BF_3}$, or $\mathbf{BMe_3}$?

Answer

$\mathbf{BH_3}$. Since **CO** forms complexes primarily through its carbon lone pair, it is a soft base and so will form the strongest complex with the softest Lewis acid.

? Exercise 1.2.3.4.2.5

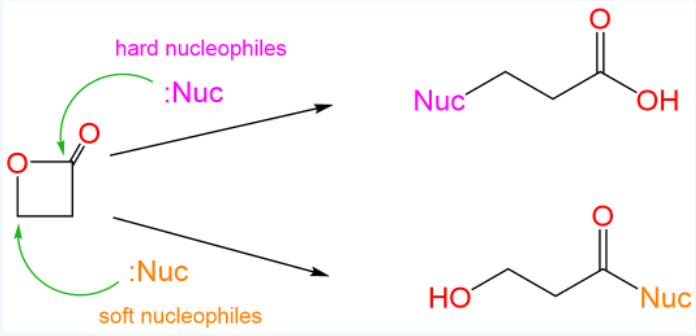
When lactones react with nucleophiles, they can undergo ring opening reactions to give either an alcohol or a carboxylic acid, as shown for propiolactone below:



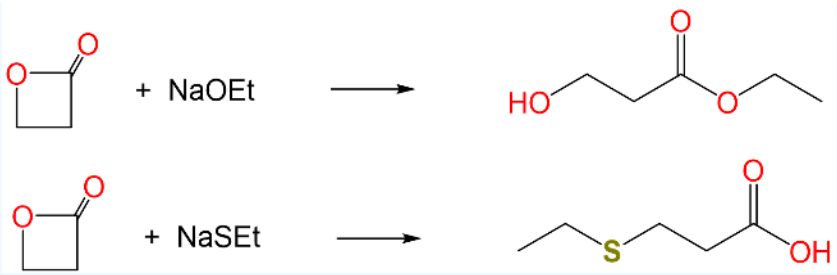
In the reaction above, sterically unhindered alkoxides give one product and sterically unhindered thioalkoxides the other. Explain why this is the case and predict the products of the reaction between propiolactone and the sodium salts of ethoxide and thioethoxide.

Answer

The two reaction products correspond to nucleophilic attack at the lactones' two electrophilic carbon centers. Specifically, the acid is produced by attack at the softer C^{I} center of the CH_2 directly attached to the ester oxygen and the alcohol by nucleophilic attack at the harder C^{III} center of the ester carbonyl.



Consequently, it is reasonable to expect that the harder base ethoxide will nucleophilically attack the harder carbonyl carbon while the softer thioethoxide will attack the softer methylene carbon.



The theoretical interpretation of the hard-soft acid-base principle is that hard-hard preferences reflect superior electrostatic stabilization while soft-soft preferences reflect superior covalent stabilization.

The hard-hard and soft-soft preferences in Lewis acid-base interactions reflect that

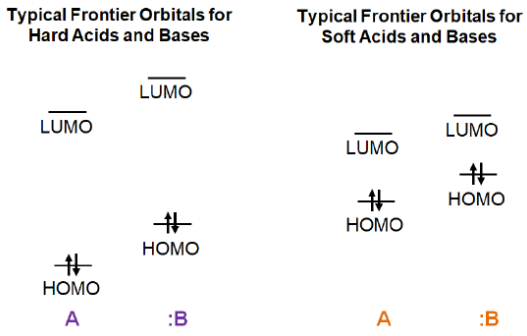
- The lone pair of a hard base is strongly stabilized electrostatically by a hard acid.
- The lone pair of a soft base is strongly stabilized by forming a covalent bond with a soft acid.
- The lone pair of a hard or soft base is comparatively weakly stabilized by an acid opposite to it in hardness or softness since the overall electrostatic and covalent stabilization of the adduct is comparatively weak.

To see why this is the case it is helpful to divide the contributions to the interaction energy between an acid and a base as follows:

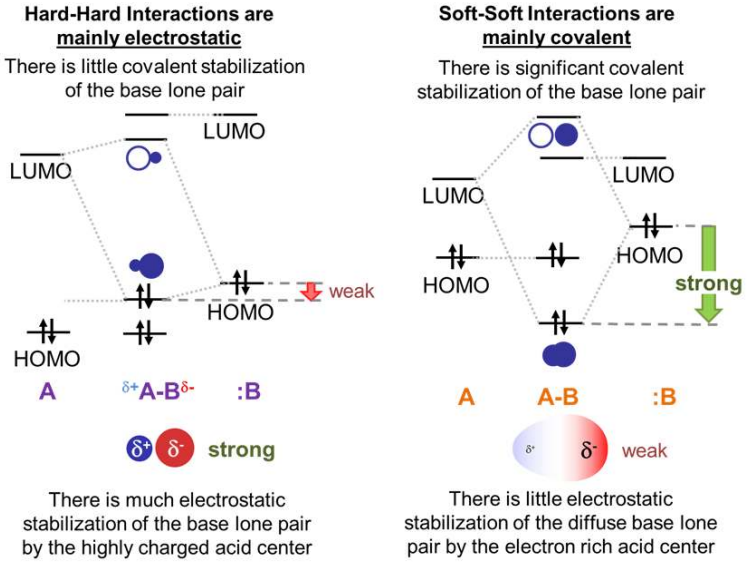
$$\text{Interaction Energy} = \underbrace{\text{Electrostatic attractions and repulsions of partial atomic charges}}_{\text{Ionic term}} + \underbrace{\text{Interactions between filled orbitals on one fragment and unfilled orbitals on the other}}_{\text{Covalent term}} + \underbrace{\text{Electrostatic repulsions between filled orbitals on the two fragments}}_{\text{Steric term}}$$

Of the three contributions to the interaction energy, only the ionic and covalent terms directly relate to the hardness of the interacting acid and base. One approach to thinking about how hardness influences the ionic and covalent contributions is to consider the frontier orbitals involved in the acid-base interaction. This is sometimes done through the use of the Salem-Klopman equation,[1,*] although in the treatment which follows a more qualitative approach will be employed.

Both hard acids and bases will have comparatively low energy HOMO levels and high energy LUMO levels, with a correspondingly high HOMO-LUMO gap. In contrast, soft acids and bases will have comparatively high-energy HOMO levels and low-energy LUMO levels, giving a comparatively smaller HOMO-LUMO gap.



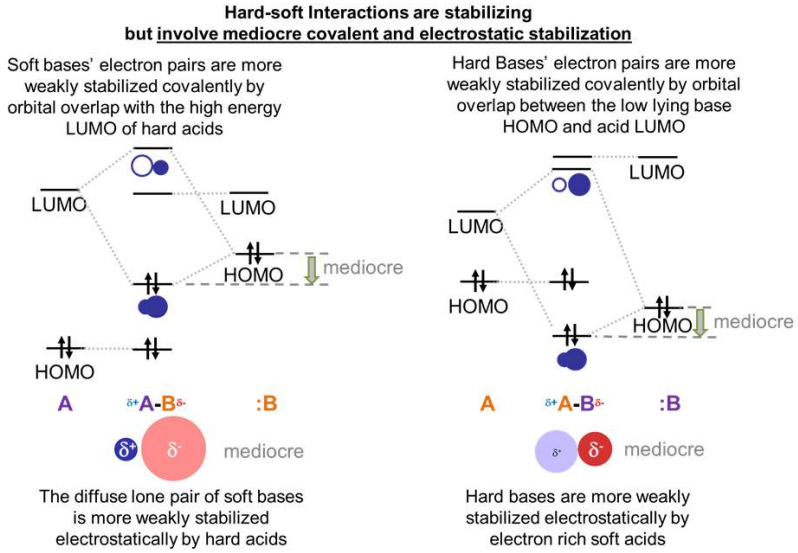
Given this, consider the frontier orbital interactions involved in the formation of an acid-base complex for the possible cases, as illustrated schematically below.



The large gap in energy between hard bases' highly stabilized HOMO lone pairs and the high energy LUMO of hard acids ensures that in **hard acid-hard base adducts the dominant stabilizing interaction will involve electrostatic attraction between the base lone pair and the electropositive Lewis acid center**. Fortunately, since the electron clouds in hard bases are relatively dense and electron rich while hard Lewis acids are highly charged and small, these electrostatic interactions are strong.

In contrast, in **soft acid-soft base adducts, the dominant stabilizing interaction will be covalent.** This is because the small gap in energy between a soft base HOMO and soft acid LUMO enables the formation of a well-stabilized bonding orbital with significant electron density between the acid and base.

The orbitals' interactions between hard acids and soft bases and soft acids and hard bases are intermediate between the hard acid-hard base and soft acid-soft base cases.



This means that the adducts are stable relative to free acid and base – just not as well stabilized as in the hard acid and hard base case. In the case of hard acids and soft bases the hard acids are less able to stabilize the soft bases' relatively diffuse electron pair electrostatically and there isn't as much covalent stabilization as in adducts of soft acids and bases due to the hard acid's high energy.

References

1. Ahrland, S.; Chatt, J.; Davies, N. R., The relative affinities of ligand atoms for acceptor molecules and ions. Quarterly Reviews, Chemical Society 1958, 12 (3), 265-276.

2. Pearson, R. G., Hard and Soft Acids and Bases. Journal of the American Chemical Society 1963, 85 (22), 3533-3539.

3. Fleming, I., Molecular orbitals and organic chemical reactions. Reference ed.; Wiley: Hoboken, N.J., 2010.

Notes

* Despite the fruitfulness of this observation, in general it is important to reduce the potential for observer bias by checking observations like these against compounds reported in the chemical literature and databases like the Inorganic Crystal Structure and Cambridge Crystallographic Databases.

** These are very soluble in water, to the point where some solutions are perhaps better described as solutions of water in the halide.

† This can be predicted based on the relative hardness of BF_3, BR_3, and BH_3 in the list of hard and soft acids. However, for those of you who may be confused as to why H is considered a better electron donor for the purposes of softening a Lewis acid center while alkyl groups are better electron donors for the purposes of stabilizing carbocations in organic chemistry, the dominant effect is the lower electronegativity of H relative to carbon (in CH_3). The effect of electron donation due to hyperconjugation isn't as great for thermodynamically stable bases like BX_3/BR_3.

†† For more on the Salem-Klopman equation see Fleming, I., Molecular orbitals and organic chemical reactions. Reference ed.; Wiley: Hoboken, N.J., 2010; pp. 138-143.

1.2.3.4.2: Hard-Hard and Soft-Soft preferences may be explained and quantified in terms of electrostatic and covalent and electronic stabilization on the stability of Lewis acid-base adducts is shared under a not declared license and was authored, remixed, and/or curated by LibreTexts.

- **6.6.2: Hard-Hard and Soft-Soft preferences may be explained and quantified in terms of electrostatic and covalent and electronic stabilization on the stability of Lewis acid-base adducts** by Stephen M. Contakes is licensed CC BY 4.0.

SECTION OVERVIEW

1.3: Simple Bonding Theory

1.3.1: Lewis Electron-Dot Diagrams

- 1.3.1.1: Resonance
- 1.3.1.2: Breaking the octet rule with higher electron counts (hypervalent atoms)
- 1.3.1.3: Formal Charge
- 1.3.1.4: Lewis fails to predict unusual cases- Boron and Beryllium

1.3.2: Valence Shell Electron-Pair Repulsion

- 1.3.2.1: Lone Pair Repulsion
- 1.3.2.2: Multiple Bonds
- 1.3.2.3: Electronegativity and Atomic Size Effects
- 1.3.2.4: Ligand Close Packing

1.3.3: Molecular Polarity

1.3.4: Hydrogen Bonding

1.3.5: Valence Bond Theory

1.3.6: Hybrid Atomic Orbitals

1.3: Simple Bonding Theory is shared under a not declared license and was authored, remixed, and/or curated by LibreTexts.

1.3.1: Lewis Electron-Dot Diagrams

In 1916, Gilbert Lewis Newton introduced a simple way to show the bonding between atoms in a molecule though Lewis electron dot diagrams. Creating Lewis diagrams is rather simple and requires only a few steps and some accounting of the valence electrons on each atom. Valence electrons are represented as dots. When two electrons are paired (lone pairs), they are represented by two adjacent dots located on an atom, and when two paired electrons are shared between atoms (bonds), they are shown as lines. For example, below are the electron dot structures of atoms and the Lewis electron dot structures of the molecules.

These diagrams are helpful because they allow us to show how atoms are connected, and when coupled with Valence Shell Electron Repulsion Theory (VSEPR), we can use Lewis structures to predict the shape of the molecule.

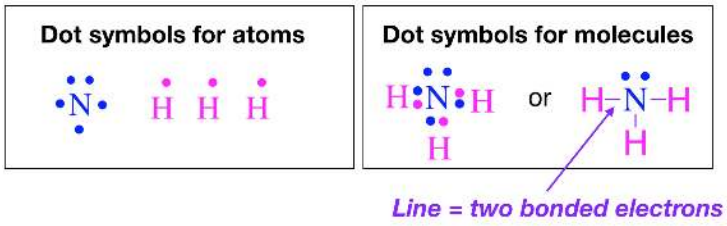


Figure 1.3.1.1: Lewis dot structure of atoms comprising ammonia and the dot structure of the molecule. (Kathryn Haas; CC-NC-BY-SA)

The drawing of Lewis electron-dot structures is guided largely by the **octet rule**: that atoms form bonds to achieve eight electrons in their valence shell. For many elements, a full valence shell has an electron configuration of s^2p^6, or eight electrons. A common exception to this rule is the first row elements, H and He. These two elements have $n = 1$ as their valence shell, and so they have only two electrons in a full valence shell ($1s^2$ electron configuration). Although H and He are exceptions to the "octet rule", they still form bonds to achieve a full valence shell. It may be better to think of this as the "full valence" rule of bonding. We will see many more violations to the "octet" rule as we progress through this course. In the case of metals and metalloids, breaking of the rules is particularly common. (CC-BY-NC-SA; Kathryn Haas)

Common violations of the octet rule

- **Less than eight electrons (hypovalency)**: H and He are examples of elements that cannot have more than two electrons in their full valence shell. Additionally, there are cases where a valid Lewis structure contains atoms with ***hypovalency:*** *partially-filled valence shells*. An example of this is a *carbocation, a positively charged carbon with only six electrons in its valence shell.* Carbocations are important intermediates in organic chemistry, and they are highly reactive (unstable) Lewis acids (electrophiles). Another example of hypovalency is the Lewis structure for BH_3, which shows boron with three bonds, and only six electrons in its valence shell. Boron hydride is a strong Lewis Acid. (Side note: the actual chemical form of BH_3 is not well-predicted by the Lewis structure and we'll see more about this in Section 3.1.4.)
- **More than eight electrons (hypervalency)**: This is a case where an element has more than eight electrons in its valence shell. It is common for larger atoms ($n \geq 3$), and it is discussed further in Section 3.1.2.

Pitfall alert! There are different rules for counting electrons depending on the purpose of the counting. These are the rules for counting for "octets". The rules for counting for calculation of an atom's formal charge are !!different!! and are described in Section 3.1.1. When an atom is part of a molecule, all electrons that are associated with the atom are counted as contributing to the atom's valence. This includes electrons that are lone pairs on the atoms, and *all* electrons that are shared in bonds. If four electrons are shared between two atoms, it is a double bond. If six electrons are shared between atoms, it is a triple bond.

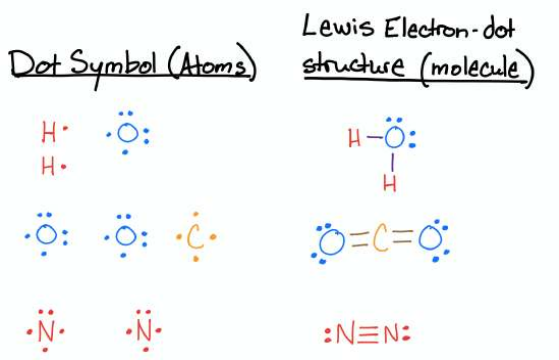
Electrons in valence (octet) = total unbonded electrons on the atom + total bonded electrons (2 electrons per bond)

Even if you're an old pro at drawing Lewis structures, it's a good idea to polish up. Please complete the practice exercises below. You should get out an actual piece of paper (I know...just do it. It's good for you.) and a writing tool and try to complete each problem before checking the answer.

Exercise 1.3.1.1

Draw the Lewis structures for H_2O, CO_2, and N_2.

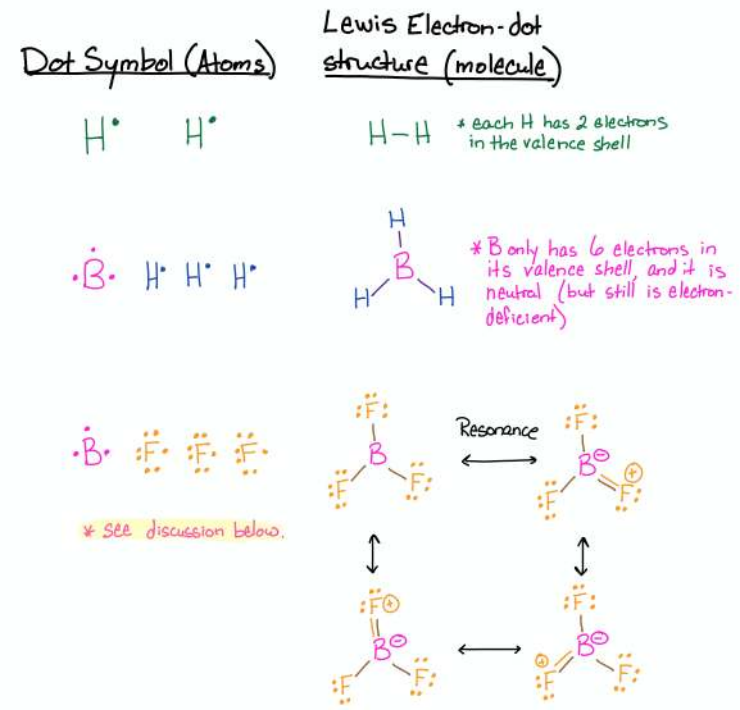
Answer



Exercise 1.3.1.2

Draw the Lewis structures for H_2, BH_3 and BF_3.

Answer



These three examples include atoms that have less than eight electrons in their valence shell. In the case of H, it is satisfied with only two electrons in its valence, as was discussed earlier in this section. The case of BH_3 was also discussed above. In the Lewis structure of BH_3, the boron can only have six electrons in its octet and it is neutral in charge. The boron is electron deficient even though it has neutral charge.

The case of BF_3 deserves a discussion: If you are unfamiliar with resonance and formal charge, see Sections 3.1.1 (Resonance) and 3.1.3 (Formal Charge) first and come back to this afterward. You might have drawn the BF_3 structure similar to the one that is drawn for BH_3, where boron has three bonds and only six electrons in its valence shell. If you did that, then you are correct; but if you only gave this structure, then your answer is not complete. There are three other correct

ways to draw the structure. Since F has lone pairs of electrons, other valid Lewis structures would each have a double bond to one of the fluorines (three total). All of these structures are called resonance structures, and based on the four of them, we could predict that BF_3 would have B-F bonds that have some double-bond character. If fact, this is the case for BF_3; it has bond lengths that are shorter than single bonds, but longer than double bonds. Read more about it on its Wikipedia page here (click).

Outside Links

- en.Wikipedia.org/wiki/Lewis_structures
- http://www.ausetute.com.au/lewisstr.html
- cost.georgiasouthern.edu/chem...cule/lewis.htm

This page titled 1.3.1: Lewis Electron-Dot Diagrams is shared under a not declared license and was authored, remixed, and/or curated by Kathryn Haas.

- **3.1: Lewis Electron-Dot Diagrams** by Kathryn Haas is licensed CC BY-NC-SA 4.0.
- **2.1B: Lewis Structures** by Andrew Iskandar is licensed CC BY 4.0.

1.3.1.1: Resonance

Learning Objectives

- To understand the concept of resonance.

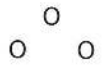
Resonance structures are a set of two or more Lewis Structures that collectively describe the electronic bonding of a single polyatomic species including fractional bonds and fractional charges. Resonance structures are capable of describing delocalized electrons that cannot be expressed by a single Lewis formula with an integral number of covalent bonds.

Sometimes one Lewis Structure is not Enough

Sometimes, even when formal charges are considered, the bonding in some molecules or ions cannot be described by a single Lewis structure. Resonance is a way of describing delocalized electrons within certain molecules or polyatomic ions where the bonding cannot be expressed by a single Lewis formula. A molecule or ion with such delocalized electrons is represented by several contributing structures (also called resonance structures or canonical forms). Such is the case for ozone ($\mathbf{O_3}$), an allotrope of oxygen with a V-shaped structure and an O–O–O angle of 117.5°.

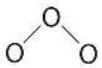
Ozone (O_3)

1. We know that ozone has a V-shaped structure, so one O atom is central:



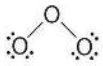
2. Each O atom has 6 valence electrons, for a total of 18 valence electrons.

3. Assigning one bonding pair of electrons to each oxygen–oxygen bond gives



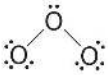
with 14 electrons left over.

4. If we place three lone pairs of electrons on each terminal oxygen, we obtain

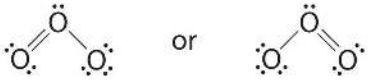


and have 2 electrons left over.

5. At this point, both terminal oxygen atoms have octets of electrons. We therefore place the last 2 electrons on the central atom:

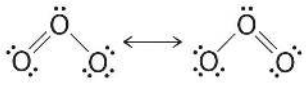


6. The central oxygen has only 6 electrons. We must convert one lone pair on a terminal oxygen atom to a bonding pair of electrons—but which one? Depending on which one we choose, we obtain either



Which is correct? In fact, neither is correct. Both predict one O–O single bond and one O=O double bond. As you will learn, if the bonds were of different types (one single and one double, for example), they would have different lengths. It turns out, however, that both O–O bond distances are identical, 127.2 pm, which is shorter than a typical O–O single bond (148 pm) and longer than the O=O double bond in O_2 (120.7 pm).

Equivalent Lewis dot structures, such as those of ozone, are called **resonance structures**. The position of the *atoms* is the same in the various resonance structures of a compound, but the position of the *electrons* is different. Double-headed arrows link the different resonance structures of a compound:



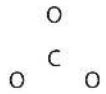
The double-headed arrow indicates that the actual electronic structure is an *average* of those shown, not that the molecule oscillates between the two structures.

> *When it is possible to write more than one equivalent resonance structure for a molecule or ion, the actual structure is the average of the resonance structures.*

The Carbonate (CO_3^{2-}) Ion

Like ozone, the electronic structure of the carbonate ion cannot be described by a single Lewis electron structure. Unlike O_3, though, the actual structure of CO_3^{2-} is an average of *three* resonance structures.

1. Because carbon is the least electronegative element, we place it in the central position:



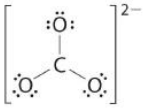
The three oxygens are drawn in the shape of a triangle with the carbon at the center of the triangle.

2. Carbon has 4 valence electrons, each oxygen has 6 valence electrons, and there are 2 more for the −2 charge. This gives 4 + (3 × 6) + 2 = 24 valence electrons.

3. Six electrons are used to form three bonding pairs between the oxygen atoms and the carbon:



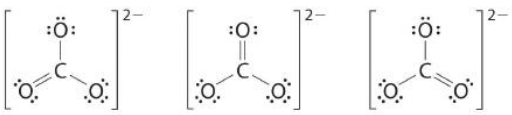
4. We divide the remaining 18 electrons equally among the three oxygen atoms by placing three lone pairs on each and indicating the −2 charge:



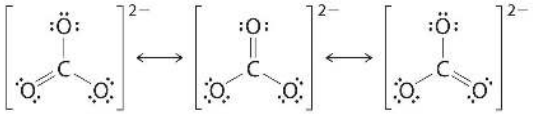
The Lewis dot structure has a central carbon that is bonded to 3 oxygens. Each oxygen has 3 lone pairs. The molecule is inside square brackets and has a charge of minus 2.

5. No electrons are left for the central atom.

6. At this point, the carbon atom has only 6 valence electrons, so we must take one lone pair from an oxygen and use it to form a carbon–oxygen double bond. In this case, however, there are *three* possible choices:



As with ozone, none of these structures describes the bonding exactly. Each predicts one carbon–oxygen double bond and two carbon–oxygen single bonds, but experimentally all C–O bond lengths are identical. We can write resonance structures (in this case, three of them) for the carbonate ion:



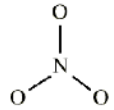
The resonance structure includes all three Lewis dot structures with double headed arrows between them.

The actual structure is an average of these three resonance structures.

The Nitrate (NO_3^-) ion

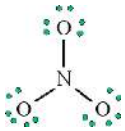
1. Count up the valence electrons: (1*5) + (3*6) + 1(ion) = **24** electrons

2. Draw the bond connectivities:

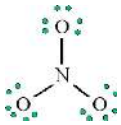


The three oxygens are drawn in the shape of a triangle with the nitrogen at the center of the triangle.

3. Add octet electrons to the atoms bonded to the center atom:

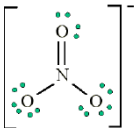


4. Place any leftover electrons (24-24 = **0**) on the center atom:



5. Does the central atom have an octet?

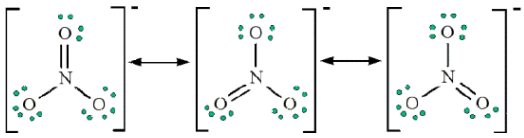
- **NO**, it has 6 electrons
- Add a multiple bond (first try a double bond) to see if the central atom can achieve an octet:



A double bond is added between one oxygen and the central nitrogen. The molecule has a negative charge.

6. Does the central atom have an octet?

- YES
- Are there possible resonance structures? YES



Note: We would expect that the bond lengths in the $\mathbf{NO_3^-}$ ion to be somewhat shorter than a single bond.



Example 1.3.1.1.1: Benzene

Benzene is a common organic solvent that was previously used in gasoline; it is no longer used for this purpose, however, because it is now known to be a carcinogen. The benzene molecule (C_6H_6) consists of a regular hexagon of carbon atoms, each of which is also bonded to a hydrogen atom. Use resonance structures to describe the bonding in benzene.

Given: molecular formula and molecular geometry

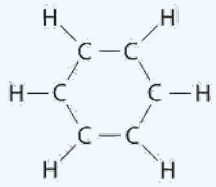
Asked for: resonance structures

Strategy:

A. Draw a structure for benzene illustrating the bonded atoms. Then calculate the number of valence electrons used in this drawing.
B. Subtract this number from the total number of valence electrons in benzene and then locate the remaining electrons such that each atom in the structure reaches an octet.
C. Draw the resonance structures for benzene.

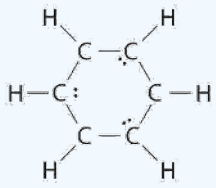
Solution:

A Each hydrogen atom contributes 1 valence electron, and each carbon atom contributes 4 valence electrons, for a total of (6 × 1) + (6 × 4) = 30 valence electrons. If we place a single bonding electron pair between each pair of carbon atoms and between each carbon and a hydrogen atom, we obtain the following:



Each carbon atom in this structure has only 6 electrons and has a formal charge of +1, but we have used only 24 of the 30 valence electrons.

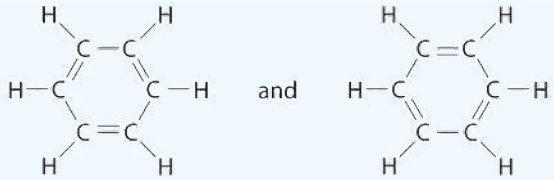
B If the 6 remaining electrons are uniformly distributed pairwise on alternate carbon atoms, we obtain the following:



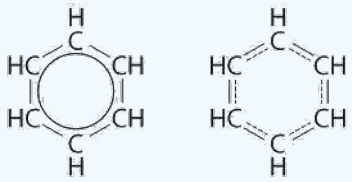
Three carbon atoms now have an octet configuration and a formal charge of −1, while three carbon atoms have only 6 electrons and a formal charge of +1. We can convert each lone pair to a bonding electron pair, which gives each atom an octet of

electrons and a formal charge of 0, by making three C=C double bonds.

C There are, however, two ways to do this:



Each structure has alternating double and single bonds, but experimentation shows that each carbon–carbon bond in benzene is identical, with bond lengths (139.9 pm) intermediate between those typically found for a C–C single bond (154 pm) and a C=C double bond (134 pm). We can describe the bonding in benzene using the two resonance structures, but the actual electronic structure is an average of the two. The existence of multiple resonance structures for aromatic hydrocarbons like benzene is often indicated by drawing either a circle or dashed lines inside the hexagon:

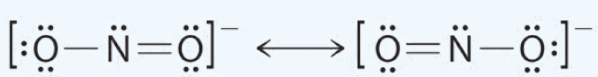


Benzene

Exercise 1.3.1.1.1: Nitrite Ion

The sodium salt of nitrite is used to relieve muscle spasms. Draw two resonance structures for the nitrite ion (NO_2^-).

Answer



There is a double bond between one oxygen and the nitrogen, It can be found on the left oxygen or the right oxygen.

Resonance structures are particularly common in oxoanions of the *p*-block elements, such as sulfate and phosphate, and in aromatic hydrocarbons, such as benzene and naphthalene.

Warning

If several reasonable resonance forms for a molecule exists, the "actual electronic structure" of the molecule will probably be intermediate between all the forms that you can draw. The classic example is benzene in Example **1.3.1.1.1**. One would expect the double bonds to be shorter than the single bonds, but if one overlays the two structures, you see that one structure has a single bond where the other structure has a double bond. The best measurements that we can make of benzene do not show two bond lengths - instead, they show that the bond length is intermediate between the two resonance structures.

Resonance structures is a mechanism that allows us to use all of the possible resonance structures to try to predict what the actual form of the molecule would be. Single bonds, double bonds, triple bonds, +1 charges, -1 charges, these are our limitations in explaining the structures, and the true forms can be in between - a carbon-carbon bond could be mostly single bond with a little bit of double bond character and a partial negative charge, for example.

Summary

Some molecules have two or more chemically equivalent Lewis electron structures, called resonance structures. Resonance is a mental exercise and method within the Valence Bond Theory of bonding that describes the delocalization of electrons within molecules. These structures are written with a **double-headed arrow** between them, indicating that none of the Lewis structures accurately describes the bonding but that the actual structure is an average of the individual resonance structures. Resonance

structures are used when one Lewis structure for a single molecule cannot fully describe the bonding that takes place between neighboring atoms relative to the empirical data for the actual bond lengths between those atoms. The net sum of valid resonance structures is defined as a resonance hybrid, which represents the overall delocalization of electrons within the molecule. A molecule that has several resonance structures is more stable than one with fewer. Some resonance structures are more favorable than others.

1.3.1.1: Resonance is shared under a not declared license and was authored, remixed, and/or curated by LibreTexts.

- **8.6: Resonance Structures** is licensed CC BY-NC-SA 3.0.

1.3.1.2: Breaking the octet rule with higher electron counts (hypervalent atoms)

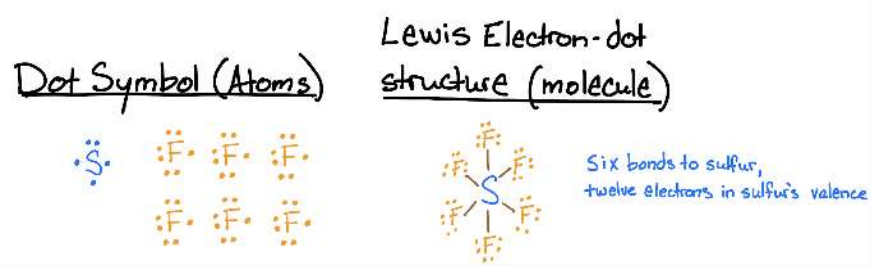
The octet rule applies well to atoms in the second row of the periodic table, where a full valence shell includes eight electrons with an electron configuration of s^2p^6. Even elements in the third and fourth row are known to follow this rule *sometimes*, but not always. In larger atoms, where $n \geq 3$ the valence shell contains additional subshells: the $d, f, g...$ subshells. Therefore, atoms with $n \geq 3$ can have higher valence shell counts by "expanding" into these additional subshells. When atoms contain more than eight electrons in their valence shell, they are said to be **hypervalent**. Hypervalency allows atoms with $n \geq 3$ to break the octet rule by having more than eight electrons. This also means they can have five or more bonds; something that is nearly unheard of for atoms with $n \leq 2$. Complete the exercises below to see examples of molecules containing hypervalent atoms.

? Exercise 1.3.1.2.1

Draw the Lewis structures for sulfur hexafluoride (SF_6).

Answer

Each fluorine atom has one valence electron and will make one bond each. The sulfur has six valence electrons, and must make six bonds to form a molecule with the six fluorine atoms. The molecular structure has six bonds to sulfur, with twelve valence electrons. The sulfur is hypervalent.

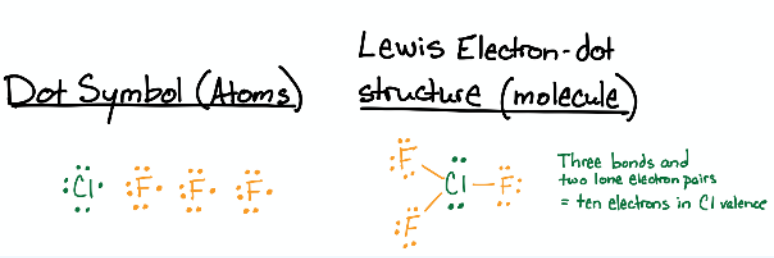


? Exercise 1.3.1.2.1

Draw the Lewis structure for chlorine trifluoride (ClF_3.

Answer

All atoms are halogens and each has seven valence electrons. Chlorine is capable of hypervalency because it is in the third row of the periodic table; however fluorine cannot have more than eight valence electrons in its valence because it is in the second row. The structure has the three fluorine atoms bonded to a central chlorine atom. The chlorine has a valence of ten electrons due to its three bonds and two lone pairs.



Is hypervalency real? Not exactly. Hypervalency is a concept associated with hybrid orbital theory and Lewis theory. It's useful for some simple things, like predicting how atoms are connected and predicting molecular shape. But the idea that the d-orbitals are involved in bonding isn't accurate according to wave mechanics.

For main group molecules, chemists (like Pauling) thought a long time ago that hypervalence is due to expanded s^2p^6 octets. The consensus is now clear that d orbitals are NOT involved in bonding in molecules like SF_6 any more than they are in SF_4 and SF_2. In all three cases, there is a small and roughly identical participation of d-orbitals in the wavefunctions. This has been established in both MO and VB theory. However, using hybrid orbitals with d-orbital contributions equips us with a language which can pragmatically describe the geometries of highly coordinated substances.

While hybrid orbitals are a powerful tool to describe the geometries and shape of molecules and metal complexes, in "real" molecules their significance may be debated. Often a more realistic molecular orbitals approach is needed. However, from an epistemologically simple point of view, bonding theories can only be judged by their predictions. To the extent that hybridization can explain the shapes of PF_5 and SF_6, valence bond theory is a perfectly good theory. To the extent that if you write out the valence bond wavefunction using hybridized orbitals and calculate energies and other properties à la Pauling (i.e., ionization energy and electron affinities) and find them to be off from experimental results (by tens of kcals/mol), then valence bond theory is not accurate.

> *Bonding theories can only be judged by their predictions.*

A simple explanation that can be given is that molecular wavefunctions constructed out of hybridized atomic orbitals are accurate enough to predict some things, but not others. Predictions of any theory must be compared with empirical evidence to assess when they work and when they fail. When a theory gives the wrong answer, at least one assumption must not hold. In this case, the valence bond wavefunction is not accurate enough to capture some important features of a system's electronic structure. It may not be the most intellectually satisfying answer, but to say more would result in a much more complicated answer and certainly far beyond the level reasonably expected from general chemistry discussions.

This page titled 1.3.1.2: Breaking the octet rule with higher electron counts (hypervalent atoms) is shared under a not declared license and was authored, remixed, and/or curated by Kathryn Haas.

- **3.1.2: Breaking the octet rule with higher electron counts (hypervalent atoms)** by Kathryn Haas is licensed CC BY-NC-SA 4.0.

1.3.1.3: Formal Charge

The formal charge of an atom in a molecule is the *hypothetical* charge the atom would have if we could redistribute the electrons in the bonds evenly between the atoms. Another way of saying this is that formal charge results when we take the number of valence electrons of a neutral atom, subtract the nonbonding electrons, and then subtract the number of bonds connected to that atom in the Lewis structure.

Calculating Formal Charges

We calculate the formal charge of an atom in a molecule or polyatomic ions as follows:

$$\text{Formal Charge} = (\text{valence electrons of the "free" element}) - (\text{unshared electrons}) - (\text{bonds}).$$

We can double-check formal charge calculations by determining the sum of the formal charges for the whole structure. The sum of the formal charges of all atoms in a molecule must be zero; the sum of the formal charges in an ion should equal the charge of the ion.

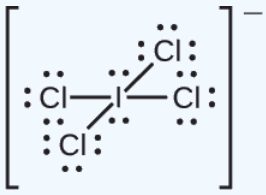
We must remember that the formal charge calculated for an atom is not the *actual* charge of the atom in the molecule. Formal charge is only a useful bookkeeping procedure; it does not indicate the presence of actual charges.

Calculating Formal Charge from Lewis Structures

Assign formal charges to each atom in the interhalogen ion $\mathbf{ICl_4^-}$.

Solution

We divide the bonding electron pairs equally for all **I–Cl** bonds:



We assign lone pairs of electrons to their atoms. Each **Cl** atom now has seven electrons assigned to it, and the I atom has eight.

Subtract this number from the number of valence electrons for the neutral atom:

- I: 7 – 8 = –1
- Cl: 7 – 7 = 0

The sum of the formal charges of all the atoms equals –1, which is identical to the charge of the ion (–1).

Exercise 1.3.1.3.1

Calculate the formal charge for each atom in the carbon monoxide molecule:



Answer

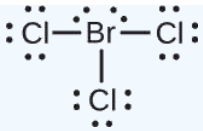
C −1, O +1

Example: Calculating Formal Charge from Lewis Structures

Assign formal charges to each atom in the interhalogen molecule $\mathbf{BrCl_3}$.

Solution

Assign one of the electrons in each Br–Cl bond to the Br atom and one to the Cl atom in that bond:



Assign the lone pairs to their atom. Now each Cl atom has seven electrons and the Br atom has seven electrons.

Subtract this number from the number of valence electrons for the neutral atom. This gives the formal charge:

- Br: 7 – 7 = 0
- Cl: 7 – 7 = 0

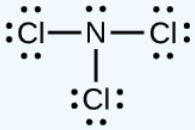
All atoms in $\mathbf{BrCl_3}$ have a formal charge of zero, and the sum of the formal charges totals zero, as it must in a neutral molecule.

? Exercise 1.3.1.3.2

Determine the formal charge for each atom in $\mathbf{NCl_3}$.

Answer

N: 0; all three Cl atoms: 0



1.3.1.3: Formal Charge is shared under a not declared license and was authored, remixed, and/or curated by LibreTexts.

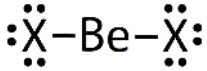
- **7.5: Formal Charges and Resonance** by OpenStax is licensed CC BY 4.0. Original source: https://openstax.org/details/books/chemistry-2e.

1.3.1.4: Lewis fails to predict unusual cases- Boron and Beryllium

Two notable cases where Lewis theory fails to predict structure are the cases of beryllium (**Be**) and boron (**B**). These two atoms are in period 2 ($n = 2$) of the periodic table and their atoms have the valence electron configurations of $2s^2$ and $2s^2 2p^1$, respectively.

Beryllium

The Lewis electron dot structures are shown below for BeX_2, where **X** is one of the halogens, **F** or **Cl**.



Each of the structures above would predict a linear geometry for the BeX_2 molecule. Together the three resonance structures suggest partial double-bond character in the Be-X bond, which results in an intermediate bond length between a single and double bond.

There are issues with each of these resonance structures. The structure on the left would predict only four electrons around **Be**; thus, the atom does not fulfill the octet rule. The structure on the left suggests multiple bonds for the halogen (**X**) and high separation of charge with formal charge on each atom. The structure in the middle is a mix of these problems. None of these situations is ideal according to Lewis theory. Further, experimental data is not consistent with any of these structures or their resonance hybrid (except in the case of $BeCl_2$ at very high temperatures).

It turns out that the monomer of BeX_2 does exist, but only at very high temperatures and low pressures. Even under extreme conditions, the monomer is not particularly stable due to the electron deficiency around **Be**.

BeF_2

At ambient temperature and pressure, BeF_2 is a solid that looks similar to quartz (Figure **1.3.1.4.1**) The Be is four-coordinate with tetrahedral geometry; each F is two-coordinate and the Be-F bond length is 1.54 Å. This structure is possible due to an extended 3-dimensional network in the solid where adjacent BeF_2 units are bonded to one another, as shown in Figure **1.3.1.4.1**.

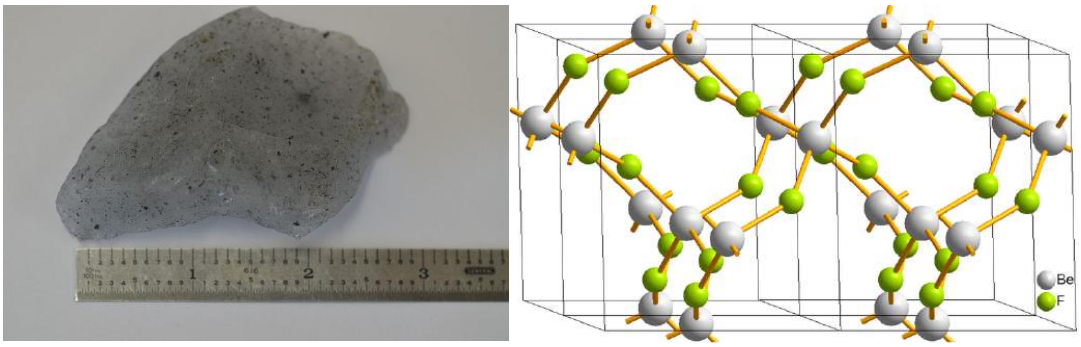


Figure **1.3.1.4.1**: (left) A nugget of beryllium fluoride obtained from Materion. Black spots are carbon (CC BY-SA 3.0; Bckelleher via Wikipedia). (right) BeF2 structure (CC BY-SA 3.0 Unported; Materialscientist via Wikipedia)

In the liquid phase, BeF_2 has a fluctuating tetrahedral structure where Be and F ions exchange. The vapor phase is reached at temperatures higher than 1000 °C (at ~ 1 atm). In the vapor phase, BeF_2 exists as a monomer with linear geometry and a bond length of 1.43 Å, consistent with a double bond between **Be** and **F**.

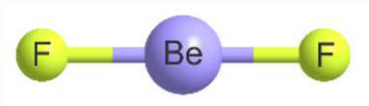


Figure **1.3.1.4.2**: Geometries of BeF_2. (CC BY; Ibon Alkorta and Anthony C. Legoe via Inorganics)

$BeCl_2$

At ambient temperature and pressure, $BeCl_2$ is a solid. As in BeF_2 described above, $BeCl_2$ has four-coordinate, tetrahedral Be and two-coordinate Cl. In contrast to BeF_2, solid $BeCl_2$ is a 1-dimensional polymer consisting of edge-shared tetrahedral.

In the gas phase, $BeCl_2$ exists as a dimer with two chlorine atoms bridging two Be atoms. In the dimer, the Be atoms are 3-coordinate. Bridging Cl atoms are two-coordinate, while terminal Cl atoms are one-coordinate. At higher temperatures in the vapor phase, the linear monomer also exists.

Boron ($2s^2 2p^1$)

Prediction based on Lewis structures:

Lewis structures of $\mathbf{BH_3}$ and $\mathbf{BF_3}$ were described in Exercise 3.1.2, and are drawn again below for convenience.

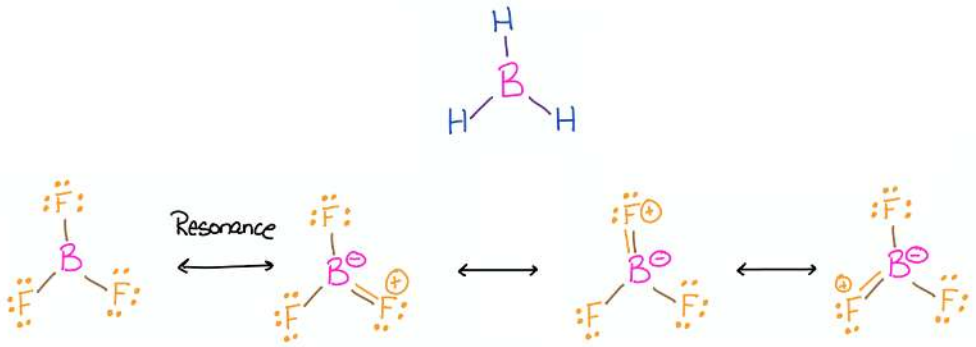


Figure 1.3.1.4.2: Lewis structures of $\mathbf{BH_3}$ and $\mathbf{BF_3}$. (Kathryn Haas; CC-NC-BY-SA)

Boron trihalides

Boron trihalides, like $\mathbf{BF_3}$, have properties that are largely predicted by Lewis structures and VSEPR theory. The Lewis structure for $\mathbf{BF_3}$ includes several resonance structures. The structure with only single bonds is the most common representation for this molecule because the charge separation shown in the other structures is considered to be unfavorable. The highly polarized B-F bond has a dipole moment that lies opposite to the indicated formal charges shown in the resonance structures with double bonds between boron and fluorine.

The resonance hybrid of $\mathbf{BF_3}$ predicts partial double bond character between boron and fluorine, thus a bond length shorter than a single bond. Using the Lewis structures and VSEPR theory, we would predict a trigonal planar geometry around boron. In fact, the actual structure of $\mathbf{BF_3}$ is a monomer with trigonal planar geometry and with bond length that is shorter than a single bond. The case is similar to structures of other boron trihalides as well.

Boron trihalides are electron deficient at the boron center and react readily with Lewis bases. In other words they are strong Lewis acids (electrophiles).

Boron trihydride (BH_3 is really B_2H_6)

The properties of boron trihydride ($\mathbf{BH_3}$) are not predicted by the simple predictions made through Lewis structures and VSEPR. The monomer, BH_3, is not stable, but when dissolved in the presence of a Lewis base, BH_3 can form a stable acid-base adduct. In its pure form, the compound actually exists as a dimeric gas with a molecular unit of B_2H_6 (try drawing a valid Lewis structure for that!). Its unexpected structure includes two H's that bridge the two boron atoms in 3-center-2-electron bonds. You can read more about B_2H_6 on the Wikipedia page for Diborane(6). The unique bonding observed for boron is described more in Chapter 8 and Chapter 15.

This page titled 1.3.1.4: Lewis fails to predict unusual cases- Boron and Beryllium is shared under a not declared license and was authored, remixed, and/or curated by Kathryn Haas.

- **3.1.4: Lewis Fails to Predict Unusual Cases - Boron and Beryllium** by Kathryn Haas is licensed CC BY-NC-SA 4.0.

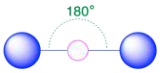
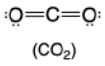
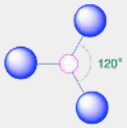
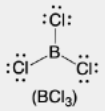
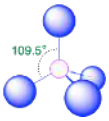
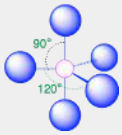
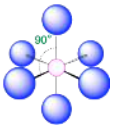
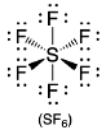
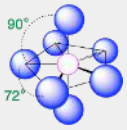
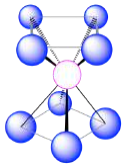
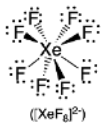
1.3.2: Valence Shell Electron-Pair Repulsion

Introduction to VSEPR

The **Valence Shell Electron Repulsion (VSEPR)** model can predict the structure of most molecules and polyatomic ions in which the central atom is a nonmetal; it also works for some structures in which the central atom is a metal. VSEPR builds on Lewis electron dot structures (discussed in Section 3.1); Lewis structures alone predict only connectivity while the Lewis structure and VSEPR together can predict the geometry of each atom in a molecule. The main idea of VSEPR theory is that pairs of electrons (in bonds and in lone pairs) repel each other. The pairs of electrons (in bonds and in lone pairs) are called "groups". Because electrons repel each other electrostatically, the most stable arrangement of electron groups (i.e., the one with the lowest energy) is the one that minimizes repulsion. Groups are positioned around the central atom in a way that produces the molecular structure with the lowest energy. In other words, the repulsion between groups around an atom favors a geometry in which the groups are as far apart from each other as possible. Although VSEPR is simplistic because it does not account for the subtleties of orbital interactions that influence molecular shapes, it accurately predicts the three-dimensional structures of a large number of compounds.

We can use the VSEPR model to predict the geometry around the atoms in a polyatomic molecule or ion by focusing on the number of electron pairs (groups) around a *central atom* of interest. Groups include bonded and unbonded electrons; a single bond, a double bond, a triple bond, a lone pair of electrons, or even a single unpaired electron each count as one group. The molecule or polyatomic ion is given an AX_mE_n designation, where **A is the central atom**, **X is a bonded atom**, **E is a nonbonding** valence electron group (usually a lone pair of electrons), and m and n are integers. The number of groups is equal to the sum of m and n. Using this information, we can describe the molecular geometry around a central atom, that is, the arrangement of the *bonded atoms* in a molecule or polyatomic ion. The geometries that are predicted from VSEPR when a central atom has only bonded groups ($n = 0$) are listed below in Table **1.3.2.1**. The cases where lone pairs contribute to the total groups ($n \geq 1$) are discussed in the next section about lone pair repulsion.

Table **1.3.2.1**. Geometries predicted using VSEPR theory (bonded groups only).

Groups around central atom (m + n)	Geometry Name	Geometry Sketch	Predicted bond Angle	Example
2	linear		180°	
3	trigonal plane		120°	
4	tetrahedron		109.5°	
5	trigonal bipyramid		90° and 120°	
6	octahedron		90°	
7	pentagonal bipyramid		90° and 72°	
8	square antiprism		70.5°, 99.6° and 109.5°	

Practice

VSEPR to predict Molecular Geometry

You can follow these four steps to predict the geometry around an atom using VSEPR:

1. Draw the Lewis electron structure of the molecule or polyatomic ion.
2. For the central atom of interest, assign the AX_mE_n designation and the total number of groups (m+n).
3. Determine the electron group arrangement around the central atom that minimizes repulsions.
4. Describe the molecular geometry.

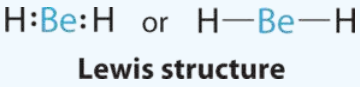
Use the procedure above to complete the exercises below

Exercise 1.3.2.1

Predict the geometry around the central atom in BeH_2 and CO_2.

Answer BeH_2

1. The central atom, beryllium, contributes two valence electrons, and each hydrogen atom contributes one. The Lewis electron structure is



Lewis structure

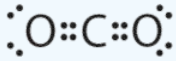
2. There are two groups around the central atom, and both groups are single bonds. Thus BeH_2 is designated as AX_2.

3. We see from Table **1.3.2.1** that the arrangement that minimizes repulsions places the groups 180° apart.

4. From Table **1.3.2.1** we see that with two bonding pairs, the molecular geometry that minimizes repulsions in BeH_2 is *linear.*

Answer CO_2

1. The central atom, carbon, contributes four valence electrons, and each oxygen atom contributes six. The Lewis electron structure is



2. The carbon atom forms two double bonds. Each double bond is counted as one group, so there are two groups around the central atom. Once again, both groups around the central atom are bonds, so CO_2 is designated as AX_2.

3. Like BeH_2, the arrangement that minimizes repulsions places the groups 180° apart.

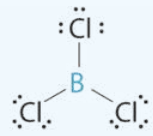
4. VSEPR only recognizes groups around the *central* atom (the carbon). Thus the lone pairs on the oxygen atoms do not influence the molecular geometry. With two bonded groups on the central atom and no lone pairs, the molecular geometry of CO_2 is linear (Table **1.3.2.1**). The structure of CO_2 is shown in Table **1.3.2.1**.

? Exercise 1.3.2.2

Predict the geometry around the central atom in BCl_3 and CO_3^{2-}.

Answer BCl_3

1. The central atom, boron, contributes three valence electrons, and each chlorine atom contributes seven valence electrons. The Lewis electron structure is



Lewis structure

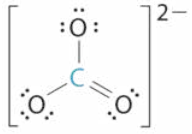
2. There are three groups around the central atom and all are single bonds. The structure is designated as AX_3.

3. To minimize repulsions, the groups are placed 120° apart (Table **1.3.2.1**).

4. From Table **1.3.2.1** we see that with three bonding pairs around the central atom, the molecular geometry of BCl_3 is *trigonal planar*.

Answer CO_3^{2-}

1. The central atom, carbon, has four valence electrons, and each oxygen atom has six valence electrons. The Lewis electron structure of one of three resonance forms is represented as

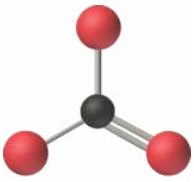


Lewis structure

2. The structure of CO_3^{2-} is a resonance hybrid. It has three identical bonds, each with a bond order of $1\frac{1}{3}$. All electron groups are bonds. With three bonding groups around the central atom, the structure is designated as AX_3.

3. We minimize repulsions by placing the three groups 120° apart (Table **1.3.2.1**).

4. We see from Table **1.3.2.1** that the molecular geometry of CO_3^{2-} is trigonal planar with bond angles of 120°.



Molecular geometry
(trigonal planar)

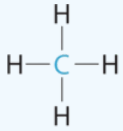
In our next example we encounter the effects of lone pairs and multiple bonds on molecular geometry for the first time.

? Exercise 1.3.2.3

Predict the geometry around the central atom in CH_4, PCl_5 and SF_6.

Answer CH_4

1. The central atom, carbon, contributes four valence electrons, and each hydrogen atom has one valence electron, so the full Lewis electron structure is

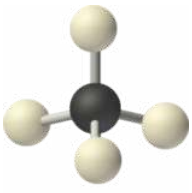


Lewis structure

2. There are four electron groups around the central atom. All electron groups are bonding pairs, so the structure is designated as AX_4.

3. As shown in Table **1.3.2.1**, repulsions are minimized by placing the groups in the corners of a tetrahedron with bond angles of 109.5°.

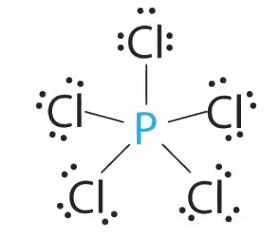
4. With four bonding pairs, the molecular geometry of methane is *tetrahedral* (Table **1.3.2.1**).



Molecular geometry
(tetrahedral)

Answer PCl_5

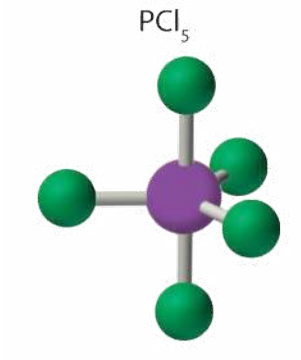
1. Phosphorus has five valence electrons and each chlorine has seven valence electrons, so the Lewis electron structure of PCl_5 is



2. There are five bonding groups around phosphorus, the central atom. All electron groups are bonds, so the structure is designated as AX_5.

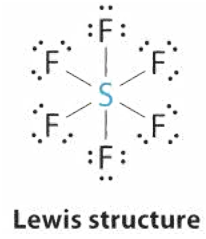
3. The structure that minimizes repulsions is a *trigonal bipyramid*, which consists of two trigonal pyramids that share a base (Table 1.3.2.1).

4. The molecular geometry of PCl_5 is *trigonal bipyramidal*, as shown below. The molecule has three atoms in a plane in *equatorial* positions and two atoms above and below the plane in *axial* positions. The three equatorial positions are separated by 120° from one another, and the two axial positions are at 90° to the equatorial plane. The axial and equatorial positions are not chemically equivalent.



Answer SF_6

1. The central atom, sulfur, contributes six valence electrons, and each fluorine atom has seven valence electrons, so the Lewis electron structure is

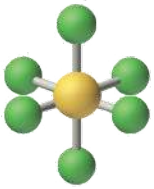


With an expanded valence, this species is an exception to the octet rule.

2. There are six electron groups around the central atom, each a bonding pair. We see from Figure 1.3.2.2 that the geometry that minimizes repulsions is *octahedral*.

3. With only bonding pairs, SF_6 is designated as AX_6. All positions are chemically equivalent, so all electronic interactions are equivalent.

4. There are six nuclei, so the molecular geometry of SF_6 is octahedral.



Molecular geometry
(octahedral)

This page titled 1.3.2: Valence Shell Electron-Pair Repulsion is shared under a CC BY-NC-SA 4.0 license and was authored, remixed, and/or curated by Kathryn Haas.

- **3.2: Valence Shell Electron-Pair Repulsion** by Kathryn Haas is licensed CC BY-NC-SA 4.0.

1.3.2.1: Lone Pair Repulsion

In the previous section, we saw how to use VSEPR to predict the geometry around a central atom based on the number of groups attached to a central atom. However, our previous discussion was limited to the simple cases where all of the groups were bonded groups (i.e., in the designation AX_mE_n , n=0). When all of the groups are bonds, the geometries can be predicted using information in Table 3.2.1 in the previous section. Now we will consider cases where one or more of these groups are lone pairs.

Lone pairs have stronger repulsive forces than bonded groups.

When one or more of the groups is a lone pair of electrons (non-bonded electrons), the experimentally-observed geometry around an atom is slightly different than in the case where all groups are bonds. The actual bond angles are similar, but not exactly the same, as those predicted based on the *total number of groups* (the "parent" geometry). When there is a mixture of group types (**lone pairs (E)** ***and*** **bonded groups (X)**) there are three different types of angles to consider: bond angles between two bonded atoms (**X-X** angles), angles between a bonded atom and a lone pair (**X-E** angles), and angles between two lone pairs (**E-E** angles). Empirical evidence shows the following trend in the degree of bond angles around atoms with a mixture of group types:

Trend in bond angles:

E-E >**X-E** >**X-X**

Using empirical evidence as a guide, we can predict that lone pairs repel other electron groups more strongly than bonded pairs. The molecular geometry of molecules with lone pairs of electrons is better predicted when we consider that electronic repulsion created by lone pairs is stronger than the repulsion from bonded groups. It is difficult to predict the exact bond angle based on this principle, but we can predict approximate angles, as described and summarized below in Table **1.3.2.1.1**.

Table **1.3.2.1.1**: Predictions of molecular geometry and bond angles around atoms with a mixture of bonded (X) and unbonded (E) electron groups.

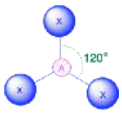
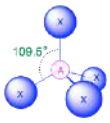
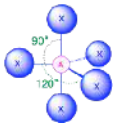
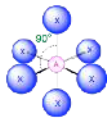
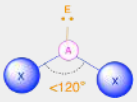
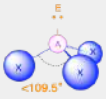
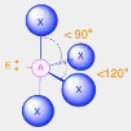
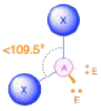
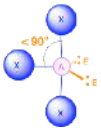
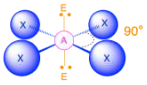
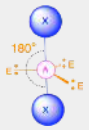
Electron Groups (m + n)					
	2 (steric number = 2)	**3** (steric number = 3)	**4** (steric number = 4)	**5** (steric number = 5)	**6** (steric number = 6)
Parent Geometry (0 lone pairs) AX_m	 AX_2, linear 180°	 AX_3, trig. plane 120°	 $AX4$, tetrahedron 109.5°	 AX_5, trig. bipyramid 90°, 120°	 AX_6, octahedron 90°
1 lone pair AX_mE_1		 $AX2E_1$, bent <120°	 AX_3E_1, trig. pyramid <109.5°	 AX_4E_1, see-saw <90°, <120°	 AX_5E_1, square pyramid 90°, <90°
2 lone pairs AX_mE_2			 AX_2E_2, bent <109.5°	 AX_3E_2, T-shape <90°	 AX_4E_2, square plane 90°
3 lone pairs AX_mE_3				 AX_2E_3, linear 180°	

Table **1.3.2.1.1** summarizes the geometries and bond angles predicted for nearest-neighbor bonded groups on central atoms with a mixture of lone pairs and bonded groups. The table does not cover all possible situations; it only includes cases where there are two bonded groups in which an X-X angle is measurable between nearest-neighbors. A more detailed description of some selected cases is given below.

Two Electron Groups (m + n = 2)

(Steric number = 2) In the case that there are only two electron groups around a central atom, those groups will lie 180° from one another. This results in a linear molecular geometry with 180° bond angles.

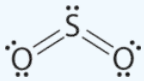
Three Electron Groups (m + n = 3)

(Steric number = 3) In the case that there are three electron groups around a central atom, those groups will lie approximately 120° from one another in space. This results in an electronic geometry that is approximately **trigonal planar**. There are two different molecular geometries that are possible in this category:

- When all of the electron groups are bonds (m = 3 or AX_3), the molecular geometry is a ***trigonal plane*** with **120°** bond angles.
- When there is one lone pair (m=2, n=1 or AX_2E_1), the molecular geometry is ***bent*** with a bond angle that is slightly **less than 120°**.

✔ AX_2E Molecules: Example SO_2

1. The central atom, sulfur, has 6 valence electrons, as does each oxygen atom. With 18 valence electrons, the Lewis electron structure is shown below.



2. There are three electron groups around the central atom: two double bonds and one lone pair. We initially place the groups in a trigonal planar arrangement to minimize repulsions (Table **1.3.2.1.1**).

3. With two bonding pairs and one lone pair, the structure is designated as AX_2E. This designation has a total of three electron pairs, two X and one E. The lone pair occupies more space around the central atom than a bonding pair (even double bonds!). Bonding pairs and lone pairs repel each other electrostatically in the order BP–BP < LP–BP < LP–LP. In SO_2, we have one BP–BP interaction and two LP–BP interactions.

4. The molecular geometry is described only by the positions of the nuclei, *not* by the positions of the lone pairs. Thus, with two nuclei and one lone pair the shape is *bent*, or *V shaped*, which can be viewed as a trigonal planar arrangement with a missing vertex. The O-S-O bond angle is expected to be *less than* 120° because of the extra space taken up by the lone pair.

Four Electron Groups (m + n = 4)

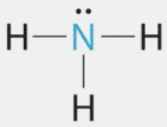
(Steric number = 4) In the case that there are four electron groups around a central atom, those groups will lie approximately 109.5° from one another in space. This results in an electronic geometry that is approximately **tetrahedral**. There are three different molecular geometries that are possible in this category:

- When all electron groups are bonds (m=4 or AX_4), the molecular geometry is a ***tetrahedron*** with bond angles of **109.5°**.
- When there is one lone pair (m=3, n=1 or AX_3E_1), the molecular geometry is a ***trigonal pyramid*** with bond angles of **slightly less than 109.5°**.
- When there are two lone pairs (m=2, n=2 or AX_2E_2), the molecular geometry is ***bent*** with bond angles of **slightly less than 109.5°**.

📌 AX_3E Molecules: Example NH_3

One of the limitations of Lewis structures is that they depict molecules and ions in only two dimensions. With four electron groups, we must learn to show molecules and ions in three dimensions.

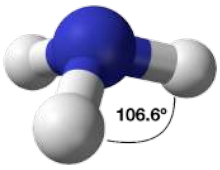
1. In ammonia, the central atom, nitrogen, has five valence electrons and each hydrogen donates one valence electron, producing the Lewis electron structure



Lewis structure

2. There are four electron groups around nitrogen, three bonding pairs and one lone pair. Repulsions are minimized by directing each hydrogen atom and the lone pair to the corners of a tetrahedron.

3. With three bonding pairs and one lone pair, the structure is designated as AX_3E. This designation has a total of four electron pairs, three X and one E. We expect the LP–BP interactions to cause the bonding pair angles to deviate significantly from the angles of a perfect tetrahedron.



The Difference in the Space Occupied by a Lone Pair of Electrons and by a Bonding Pair

As with SO_2, this composite model of electron distribution and negative electrostatic potential in ammonia shows that a lone pair of electrons occupies a larger region of space around the nitrogen atom than does a bonding pair of electrons that is shared with a hydrogen atom.

4. There are three nuclei and one lone pair, so the molecular geometry is *trigonal pyramidal*. In essence, this is a tetrahedron with a vertex missing. However, the H–N–H bond angles are less than the ideal angle of 109.5° because of LP–BP repulsion. The bond angles in ammonia are 106.6°.

AX_2E_2 Molecules: Example H_2O

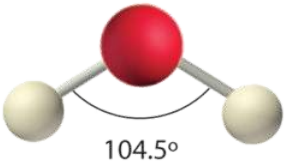
1. Oxygen has six valence electrons and each hydrogen has one valence electron, producing the Lewis electron structure



2. There are four groups around the central oxygen atom, two bonding pairs and two lone pairs. Repulsions are minimized by directing the bonding pairs and the lone pairs to the corners of a tetrahedron.

3. With two bonding pairs and two lone pairs, the structure is designated as AX_2E_2 with a total of four electron pairs. Due to LP–LP, LP–BP, and BP–BP interactions, we expect a significant deviation from idealized tetrahedral angles.

4. With two hydrogen atoms and two lone pairs of electrons, the structure has significant lone pair interactions. There are two nuclei about the central atom, so the molecular shape is *bent*, or *V shaped*, with an H–O–H angle that is even less than the H–N–H angles in NH_3, as we would expect because of the presence of two lone pairs of electrons on the central atom rather than one. This molecular shape is essentially a tetrahedron with two missing vertices.



Five Electron Groups (m + n = 5)

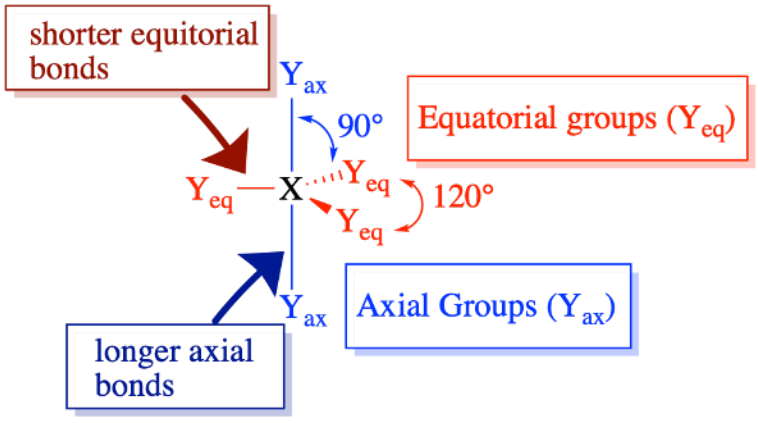


Figure: Trigonal pyramidal molecules (steric number 5) possess different bond angles and lengths for axial (ax) and equatorial (eq) pendant atoms. (CC-BY-NC-SA; Kathryn Haas).

(Steric number = 5) In the case that there are five electron groups around a central atom, there are two different types of positions around the central atom: equatorial positions and axial positions. The three equatorial ligands are 120° from one another and are 90° from each of the two axial ligands. The axial positions have three adjacent groups oriented 90° away in space. Axial groups are thus more crowded than the equatorial positions with only two adjacent groups at 90°. The crowding of axial positions results in slight differences in bond distances; crowded axial groups have longer bonds than the less crowded equatorial groups. Lone pairs of electrons generally prefer to occupy equatorial positions rather than axial positions. The justification for this preference, according to VSEPR theory, is that the lone electron pairs are more repulsive than bonding electron pairs, and thus the lone pairs prefer the less crowded equatorial positions.

The arrangement of five groups around a central atom results in a **trigonal bipyramidal** electronic geometry. There are four different molecular geometries that are possible in this category, depending upon the number of bonded groups and lone pairs of electrons:

- When all electron groups are bonds (m=5 or AX_5), the molecular geometry is a ***trigonal bipyramid*** with bond angles of **120°** and **90°** between adjacent ligands.
- When there is one lone pair (m=4, n=1 or AX_4E_1), the lone pair occupies one of the equatorial positions. The molecular geometry is called a ***see saw*** with bond angles of **slightly less than 120°** and **slightly less than 90°**.
- When there are two lone pairs (m=3, n=2 or AX_3E_2), each lone pair occupies one of the three equatorial positions. The molecular geometry is ***T-shaped*** with bond angles of **slightly less than 120°** and **slightly less than 90°**.
- When there are three lone pairs (m=1, n=3 or AX_3E_2), the lone pairs occupy the three equatorial positions. The molecular geometry is ***linear*** with bond angles of **180°**.

AX_4E Molecules: SF_4

1. The sulfur atom has six valence electrons and each fluorine has seven valence electrons, so the Lewis electron structure is



Lewis structure

With an expanded valence, this species is an exception to the octet rule.

2. There are five groups around sulfur, four bonding pairs and one lone pair. With five electron groups, the lowest energy arrangement is a trigonal bipyramid.

3. We designate SF_4 as AX_4E; it has a total of five electron pairs. However, because the axial and equatorial positions are not chemically equivalent, where do we place the lone pair? If we place the lone pair in the axial position, we have three LP–BP repulsions at 90°. If we place it in the equatorial position, we have two 90° LP–BP repulsions at 90°. With fewer 90° LP–BP repulsions, we can predict that the structure with the lone pair of electrons in the *equatorial position is more stable than the one with the lone pair in the axial position*. We also expect a deviation from ideal geometry because a lone pair of electrons occupies more space than a bonding pair.

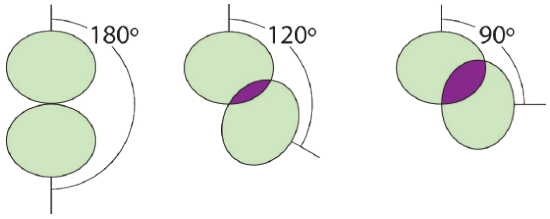
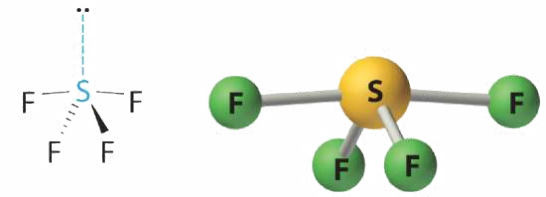


Illustration of the Area Shared by Two Electron Pairs versus the Angle between Them

At 90°, the two electron pairs share a relatively large region of space, which leads to strong repulsive electron–electron interactions.

4. With four nuclei and one lone pair of electrons, the molecular structure is based on a trigonal bipyramid with a missing equatorial vertex; it is described as a *seesaw*. The F_{axial}–S–F_{axial} angle is 173° rather than 180° because of the lone pair of electrons

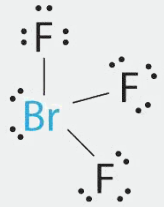
in the equatorial plane.



Molecular geometry (seesaw)

AX_3E_2 Molecules: BrF_3

1. The bromine atom has seven valence electrons, and each fluorine has seven valence electrons, so the Lewis electron structure is

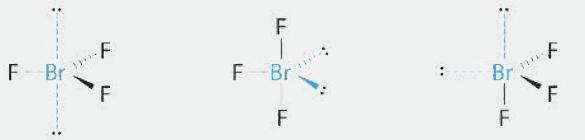


Lewis structure

Once again, we have a compound that is an exception to the octet rule.

2. There are five groups around the central atom, three bonding pairs and two lone pairs. We again direct the groups toward the vertices of a trigonal bipyramid.

3. With three bonding pairs and two lone pairs, the structural designation is AX_3E_2 with a total of five electron pairs. Because the axial and equatorial positions are not equivalent, we must decide how to arrange the groups to minimize repulsions. If we place both lone pairs in the axial positions, we have six LP–BP repulsions at 90°. If both are in the equatorial positions, we have four LP–BP repulsions at 90°. If one lone pair is axial and the other equatorial, we have one LP–LP repulsion at 90° and three LP–BP repulsions at 90°:



Lone pairs axial (a) | Lone pairs equatorial (b) | Lone pairs axial and equatorial (c)

Interactions	(a)	(b)	(c)
90° LP–LP	0	0	1
90° LP–BP	6	4	3

Structure (c) can be eliminated because it has a LP–LP interaction at 90°. Structure (b), with fewer LP–BP repulsions at 90° than (a), is lower in energy. However, we predict a deviation in bond angles because of the presence of the two lone pairs of electrons.

4. The three nuclei in BrF_3 determine its molecular structure, which is described as *T shaped*. This is essentially a trigonal bipyramid that is missing two equatorial vertices. The F_{axial}–Br–F_{axial} angle is 172°, less than 180° because of LP–BP repulsions.

Because lone pairs occupy more space around the central atom than bonding pairs, electrostatic repulsions are more important for lone pairs than for bonding pairs.

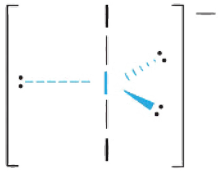
AX_2E_3 Molecules: I_3^-

1. Each iodine atom contributes seven electrons and the negative charge one, so the Lewis electron structure is



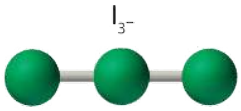
2. There are five electron groups about the central atom in I_3^-, two bonding pairs and three lone pairs. To minimize repulsions, the groups are directed to the corners of a trigonal bipyramid.

3. With two bonding pairs and three lone pairs, I_3^- has a total of five electron pairs and is designated as AX_2E_3. We must now decide how to arrange the lone pairs of electrons in a trigonal bipyramid in a way that minimizes repulsions. Placing them in the equatorial positions eliminates 90° LP–LP repulsions and minimizes the number of 90° LP–BP repulsions.



The three lone pairs of electrons have equivalent interactions with the three iodine atoms, so we do not expect any deviations in bonding angles.

4. With three nuclei and three lone pairs of electrons, the molecular geometry of I_3^- is linear. This can be described as a trigonal bipyramid with three equatorial vertices missing. The ion has an I–I–I angle of 180°, as expected.



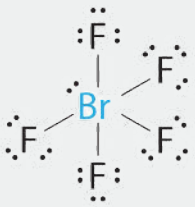
Six Electron Groups (m + n = 6)

(Steric number = 6) In the case that there are six electron groups around a central atom, the nearest groups will lie approximately 90° from one another in space. This results in an electronic geometry that is approximately **octahedral**. There are three relevant molecular geometries in this category:

- When all electron groups are bonds (m=6 or AX_6), the molecular geometry is an ***octahedron*** with bond angles of **90°** between adjacent bonds.
- When there is one lone pair (m=5, n=1 or AX_5E_1) we now distinguish between the axial and equitorial positions; the lone pair is considered to be in one of the axial positions, while the bond directly opposite of the lone pair is the axial bond. The molecular geometry is a ***square pyramid*** with bond angles of **90°** between adjacent equatorial bonds and **slightly less than 90°** between the axial bond and equatorial groups.
- When there are two lone pairs (m=4, n=2 or AX_4E_2), the lone pairs are opposite of one another and each occupy an axial position. The molecular geometry is ***square planar*** with bond angles of **90°**.

AX_5E Molecules: BrF_5

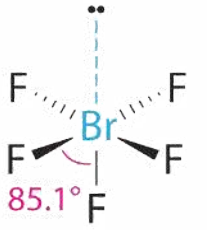
1. The central atom, bromine, has seven valence electrons, as does each fluorine, so the Lewis electron structure is



Lewis structure

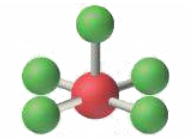
With its expanded valence, this species is an exception to the octet rule.

2. There are six electron groups around the Br, five bonding pairs and one lone pair. Placing five F atoms around Br while minimizing BP–BP and LP–BP repulsions gives the following structure:



3. With five bonding pairs and one lone pair, BrF_5 is designated as AX_5E; it has a total of six electron pairs. The BrF_5 structure has four fluorine atoms in a plane in an equatorial position and one fluorine atom and the lone pair of electrons in the axial positions. We expect all F_{axial}–Br–$F_{equatorial}$ angles to be less than 90° because of the lone pair of electrons, which occupies more space than the bonding electron pairs.

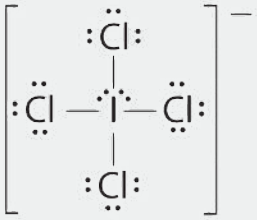
4. With five nuclei surrounding the central atom, the molecular structure is based on an octahedron with a vertex missing. This molecular structure is *square pyramidal*. The F_{axial}–B–$F_{equatorial}$ angles are 85.1°, less than 90° because of LP–BP repulsions.



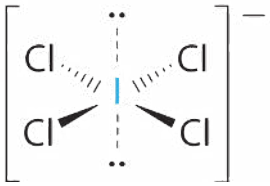
Molecular geometry
(square pyramidal)

AX_4E_2 Molecules: ICl_4^-

1. The central atom, iodine, contributes seven electrons. Each chlorine contributes seven, and there is a single negative charge. The Lewis electron structure is

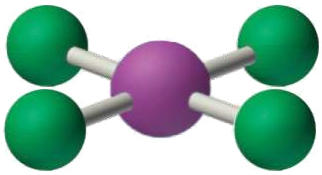


2. There are six electron groups around the central atom, four bonding pairs and two lone pairs. The structure that minimizes LP–LP, LP–BP, and BP–BP repulsions is



3. ICl_4^- is designated as AX_4E_2 and has a total of six electron pairs. Although there are lone pairs of electrons, with four bonding electron pairs in the equatorial plane and the lone pairs of electrons in the axial positions, all LP–BP repulsions are the same. Therefore, we do not expect any deviation in the Cl–I–Cl bond angles.

4. With five nuclei, the ICl4− ion forms a molecular structure that is *square planar*, an octahedron with two opposite vertices missing.



Summary

The arrangement of bonded atoms in a molecule or polyatomic ion is crucial to understanding the chemistry of a molecule, but Lewis electron structures give no information about **molecular geometry**. The **valence-shell electron-pair repulsion (VSEPR) model** allows us to predict which of the possible structures is actually observed in most cases. VSEPR is based on the assumption that pairs of electrons occupy space, and the lowest-energy structure is the one that minimizes repulsions between electron pairs. In the VSEPR model, the molecule or polyatomic ion is given an AX_mE_n designation, where A is the central atom, X is a bonded atom, E is a nonbonding valence electron group (usually a lone pair of electrons), and *m* and *n* are integers. Each group around the central atom is designated as a bonding pair (BP) or lone (nonbonding) pair (LP). From the BP and LP interactions we can predict both the relative positions of the atoms and the angles between the bonds, called the **bond angles**. From this we can describe the **molecular geometry**. The VSEPR model can be used to predict the shapes of many molecules and polyatomic ions, but it gives no information about bond lengths and the presence of multiple bonds. A combination of VSEPR and a bonding model, such as Lewis electron structures, is necessary to understand the presence of multiple bonds.

The relationship between the number of electron groups around a central atom, the number of lone pairs of electrons, and the molecular geometry is summarized in Table **1.3.2.1.1**.

Example Excercises

✔ Example 1.3.2.1.1

Using the VSEPR model, predict the molecular geometry of each molecule or ion.

1. PF_5 (phosphorus pentafluoride, a catalyst used in certain organic reactions)
2. H_3O^+ (hydronium ion)

Given: two chemical species

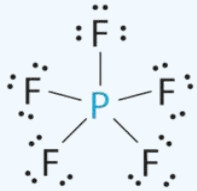
Asked for: molecular geometry

Strategy:

A. Draw the Lewis electron structure of the molecule or polyatomic ion.
B. Determine the electron group arrangement around the central atom that minimizes repulsions.
C. Assign an AX_mE_n designation; then identify the LP–LP, LP–BP, or BP–BP interactions and predict deviations in bond angles.
D. Describe the molecular geometry.

Solution:

1. **A** The central atom, P, has five valence electrons and each fluorine has seven valence electrons, so the Lewis structure of PF_5 is



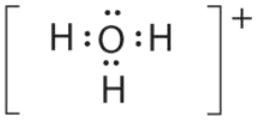
B There are five bonding groups about phosphorus. The structure that minimizes repulsions is a trigonal bipyramid.

C All electron groups are bonding pairs, so PF_5 is designated as AX_5. Notice that this gives a total of five electron pairs. With no lone pair repulsions, we do not expect any bond angles to deviate from the ideal.

D The PF_5 molecule has five nuclei and no lone pairs of electrons, so its molecular geometry is trigonal bipyramidal.



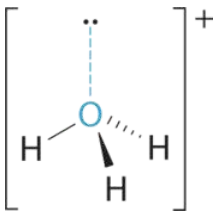
- **A** The central atom, O, has six valence electrons, and each H atom contributes one valence electron. Subtracting one electron for the positive charge gives a total of eight valence electrons, so the Lewis electron structure is



B There are four electron groups around oxygen, three bonding pairs and one lone pair. Like NH_3, repulsions are minimized by directing each hydrogen atom and the lone pair to the corners of a tetrahedron.

C With three bonding pairs and one lone pair, the structure is designated as AX_3E and has a total of four electron pairs (three X and one E). We expect the LP–BP interactions to cause the bonding pair angles to deviate significantly from the angles of a perfect tetrahedron.

D There are three nuclei and one lone pair, so the molecular geometry is *trigonal pyramidal*, in essence a tetrahedron missing a vertex. However, the H–O–H bond angles are less than the ideal angle of 109.5° because of LP–BP repulsions:



? Exercise 1.3.2.1.1

Using the VSEPR model, predict the molecular geometry of each molecule or ion.

a. XeO_3
b. PF_6^-
c. NO_2^+

Answer a

trigonal pyramidal

Answer b

octahedral

Answer c

linear

Example 1.3.2.1.2

Predict the molecular geometry of each molecule.

1. XeF_2
2. $SnCl_2$

Given: two chemical compounds

Asked for: molecular geometry

Strategy:

Use the strategy given in Example 1.3.2.1.1.

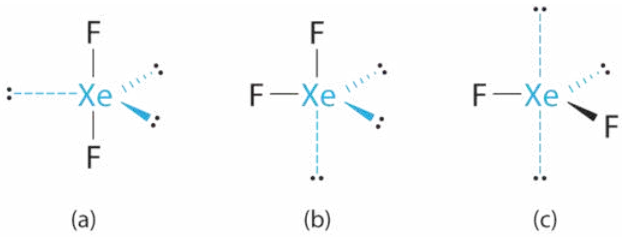
Solution:

1. **A** Xenon contributes eight electrons and each fluorine seven valence electrons, so the Lewis electron structure is



B There are five electron groups around the central atom, two bonding pairs and three lone pairs. Repulsions are minimized by placing the groups in the corners of a trigonal bipyramid.

C From B, XeF_2 is designated as AX_2E_3 and has a total of five electron pairs (two X and three E). With three lone pairs about the central atom, we can arrange the two F atoms in three possible ways: both F atoms can be axial, one can be axial and one equatorial, or both can be equatorial:

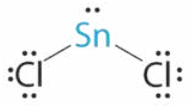


Interactions			
90 LP–LP	0	2	2

The structure with the lowest energy is the one that minimizes LP–LP repulsions. Both (b) and (c) have two 90° LP–LP interactions, whereas structure (a) has none. Thus both F atoms are in the axial positions, like the two iodine atoms around the central iodine in I_3^-. All LP–BP interactions are equivalent, so we do not expect a deviation from an ideal 180° in the F–Xe–F bond angle.

D With two nuclei about the central atom, the molecular geometry of XeF_2 is linear. It is a trigonal bipyramid with three missing equatorial vertices.

- **A** The tin atom donates 4 valence electrons and each chlorine atom donates 7 valence electrons. With 18 valence electrons, the Lewis electron structure is



B There are three electron groups around the central atom, two bonding groups and one lone pair of electrons. To minimize repulsions the three groups are initially placed at 120° angles from each other.

C From B we designate $SnCl_2$ as AX_2E. It has a total of three electron pairs, two X and one E. Because the lone pair of electrons occupies more space than the bonding pairs, we expect a decrease in the Cl–Sn–Cl bond angle due to increased LP–BP repulsions.

D With two nuclei around the central atom and one lone pair of electrons, the molecular geometry of $SnCl_2$ is bent, like SO_2, but with a Cl–Sn–Cl bond angle of 95°. The molecular geometry can be described as a trigonal planar arrangement with one vertex missing.

? Exercise 1.3.2.1.2

Predict the molecular geometry of each molecule.

a. SO_3
b. XeF_4

Answer a

trigonal planar

Answer b

square planar

This page titled 1.3.2.1: Lone Pair Repulsion is shared under a not declared license and was authored, remixed, and/or curated by Kathryn Haas.

- **3.2.1: Lone Pair Repulsion** by Kathryn Haas is licensed CC BY-NC-SA 4.0.
- **3.2.2: Multiple Bonds** by Kathryn Haas is licensed CC BY-NC-SA 4.0.

1.3.2.2: Multiple Bonds

In the previous sections, we saw how to predict the approximate geometry around an atom using VSEPR theory, and we learned that lone pairs of electrons slightly distort bond angles from the "parent" geometry. This page discusses the effect of multiple (double and triple) bonds between bonded atoms.

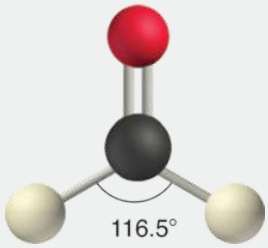
Double and triple bonds are more repulsive than single bonds

VSEPR theory predicts that double and triple bonds have stronger repulsive forces than single bonds. Like lone pairs of electrons, multiple bonds occupy more space around the central atom than a single bond. The result is that bond angles are slightly distorted compared to the parent geometry. Since a multiple bond has a higher electron density than a single bond, its electrons occupy more space than those of a single bond. Double and triple bonds distort bond angles in a way similar to what lone pairs do. Due to the stronger repulsion, double and triple bonds occupy positions similar to those of lone pairs in groups with 5 and 6 electron groups.

Examples 1.3.2.2.1

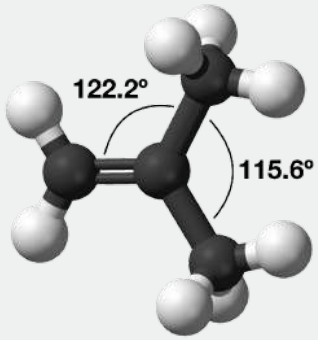
CH_2O

In a molecule such as CH_2O (AX_3), whose structure is shown below, the double bond repels the single bonds more strongly than the single bonds repel each other. This causes a deviation from ideal geometry (an H–C–H bond angle of 116.5° rather than 120°).



2-methybutene

In the molecule, $CH_2C(CH_3)_2$, the methyl—C—methyl bond angle is 115.6°, which is less than the 120° bond angle that would be expected of the parent geometry. On the other hand, the acetyl—C—methyl bond angle is greater than 120°, with an actual bond angle of 122.2°.



Atoms with both lone pairs and multiple bonds

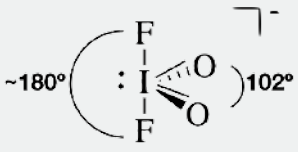
In general, we expect that a lone pair has slightly greater repulsive force than a multiple bond, and that a multiple bond has slightly greater repulsive force than a single bond. The **order of expected repulsive force** is:

$$\text{lone pair} > \text{double or triple bond} > \text{single bond}$$

Examples1.3.2.2.1

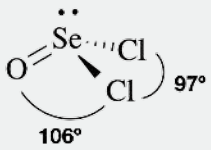
$IO_2F_2^-$

With five electron groups, the IO_2F_2 molecule has an approximately trigonal bipyramidal electronic (parent) geometry. The central iodine atom has a single bond to each of the fluorine atoms, a double bond to each oxygen, and a lone pair. The lone pair and the double bonds will occupy more space around iodine than each of the single bonds. Thus, we expect the lone pair and double bonds to occupy equatorial positions around the central iodine. The O=I=O bond angle is 102° (*much* smaller than the 120° angle expected from the parent geometry). This dramatically smaller angle is a result of the increased repulsion between the lone pair and the double bond.



$SeOCl_2$

With four electron groups, the $SeOCl_2$ molecule has four electron groups and approximately tetrahedral electronic (parent) geometry. It has both a lone pair and a double bond on the central selenium atom. The two chlorine atoms are singly bonded to selenium, while the oxygen is double bonded. The lone pair is most repulsive, followed by the double bonded oxygen, and then the chlorine bonds. This gives a Cl—Se—Cl bond angle of 97° and a Cl—Se—O bond angle of 106°; both angles are less than the 109.5° angles expected for the ideal tetrahedral geometry.



Practice

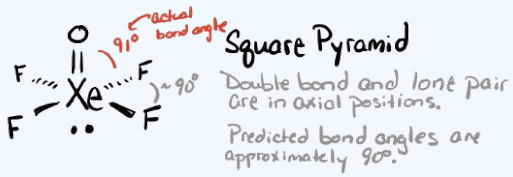
Exercise 1.3.2.2.1

Use VSEPR theory to predict the geometries and draw the structures of the following.

a. $XeOF_4$
b. NO_2^-
c. $SOCl_2$
d. IOF_3^-

Answer a

This molecule has six electron groups around the central Xe atom (steric number 6), and thus has an approximately octahdral electronic (parent) geometry. There is a double bond to O and a lone pair, both of which are more strongly repulsive than the single bonds to F. The double bond and lone pair will be directly opposite to each other, designated as axial positions. The result is a square pyramidal molecular geometry. VSEPR theory predicts F—Xe—F bond angles of 90°. As a general rule, lone pairs are slightly more repulsive than multiple bonds, and so we might expect the O—Xe—F bond angles to be <90°; *however in this case the actual O—Xe—F bond angle is observed to be 91°* (you could not have predicted the latter).



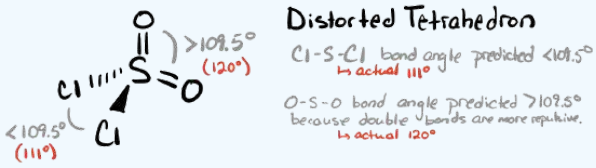
Answer b

This molecule has three electron groups around the central atom: one lone pair and two double bonds to oxygen atoms. This results in an approximately trigonal planar electronic (parent geometry). We expect the lone pair to be slightly more repulsive than double bonds, and so we expect the O—N—O bond angle to be slightly less than 120°. *The actual O—N—O angle is 115°.*



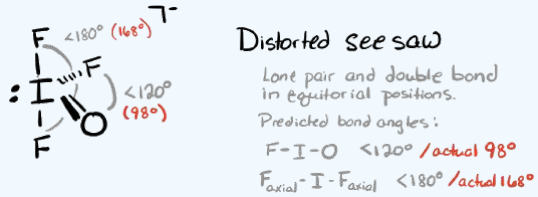
Answer c

This molecule has four electron groups (steric number 4) with an approximately tetrahedral electronic (parent) geometry. Each double bonded oxygen will take up more space around the central S than the single bonded Cl atoms. We should expect the double bonds to repel each other more strongly than they repel each single bond, with the least repulsive interaction being between the two single bonds. The bond angle for Cl—S—Cl is expected to be <109.5° according to VSEPR theory (however, it is actually 111°). We would expect the bond angle for O—S—O to be larger than the angle for Cl—S—Cl and for Cl—S—O. The O—S—O bond angle is predicted to be >109.5° (and the actual bond angle is 120°). The molecular geometry is a distorted tetrahedron.



Answer d

This molecule has five electron groups (steric number 5) with an approximately trigonal bipyramidal electronic (parent) geometry. There is one lone pair, a double bond to O, and three single bonds to F atoms around the central I atom. The lone pair and double bond are most repulsive, and should occupy the less crowded equatorial positions rather than the more crowded axial positions. This results in a seesaw molecular geometry. With the more repulsive lone pair and the strongest equatorial repulsive force being between the double bond and lone pair, we should expect the $F_{equatorial}$—I—O bond angle to be less than the 120° angle expected for the parent geometry (*it is actually much less, at 98°*). Due to repulsion between the axial F atoms and both the lone pair and double bond, we should expect the F—S—F bond angles to be compressed. The F_{axial}—I—F_{axial} is actually 168°.



References

- Miessler, G.; Fischer, P.J.; Tarr, D. (2014). Inorganic Chemistry. New Jersey: Prentice-Hall. pp. 55

This page titled 1.3.2.2: Multiple Bonds is shared under a not declared license and was authored, remixed, and/or curated by Kathryn Haas.

- **3.2.2: Multiple Bonds** by Kathryn Haas is licensed CC BY-NC-SA 4.0.

1.3.2.3: Electronegativity and Atomic Size Effects

Introduction

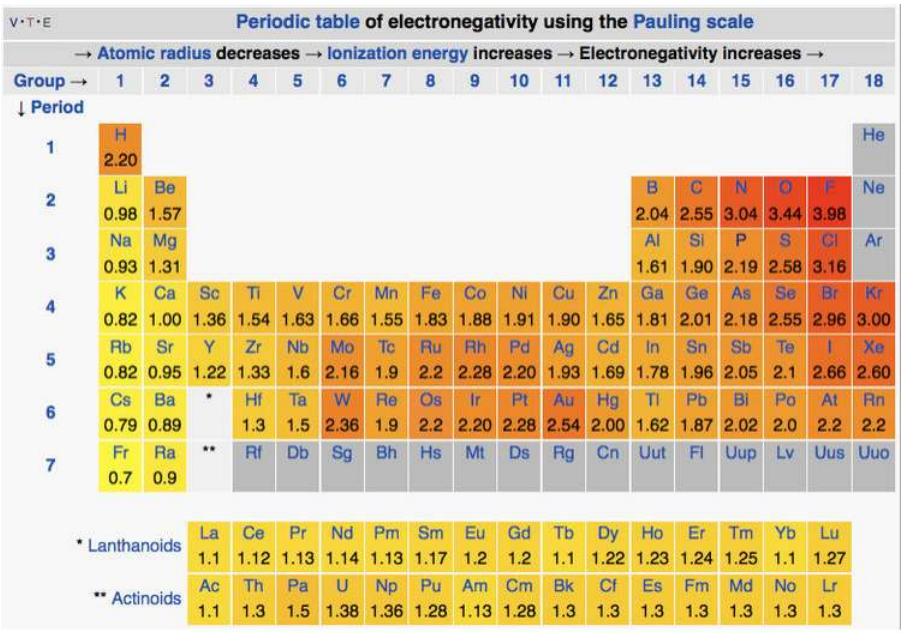
We saw in previous sections how lone pairs of electrons and multiple bonds distort bond angles between non-central atoms (ligands) around a central atom. This section describes how ligand **electronegativity and size also influence bond angles and molecular geometry**. Electronegativity is generally correlated with atomic size going down any group of the periodic table. There are some cases where bond angles can be predicted by these correlations. However, size and electronegativity can also work as competing factors in determining bond angles.

Definitions of Electronegativity

Linus Pauling introduced the first electronegativity scale in 1932 in order to explain the extra stability of molecules with polar bonds.[1] The electronegativity of an atom, represented by the Greek letter χ (chi), can be defined as the tendency of an atom to draw electrons to itself in a chemical bond. On the Pauling scale, the electronegativity difference between two atoms A and B was defined in terms of the dissociation energies E_d of the A-A, B-B, and A-B bonds:

$$\chi_A - \chi_B = \sqrt{E_d(AB) - [E_d(AA) + E_d(BB)]/2}$$

where the energies are expressed in electron volts. Pauling's scale of electronegativity ranges from Fluorine (most electronegative = 4.0) to Francium (least electronegative = 0.7). [2,3] The polarity of bonds and assignment of formal charges is predicted by electronegativity differences.



Periodic table of electronegativity using the Pauling scale

→ Atomic radius decreases → Ionization energy increases → Electronegativity increases →

Group →	1	2	3	4	5	6	7	8	9	10	11	12	13	14	15	16	17	18
↓ Period																		
1	H 2.20																	He
2	Li 0.98	Be 1.57											B 2.04	C 2.55	N 3.04	O 3.44	F 3.98	Ne
3	Na 0.93	Mg 1.31											Al 1.61	Si 1.90	P 2.19	S 2.58	Cl 3.16	Ar
4	K 0.82	Ca 1.00	Sc 1.36	Ti 1.54	V 1.63	Cr 1.66	Mn 1.55	Fe 1.83	Co 1.88	Ni 1.91	Cu 1.90	Zn 1.65	Ga 1.81	Ge 2.01	As 2.18	Se 2.55	Br 2.96	Kr 3.00
5	Rb 0.82	Sr 0.95	Y 1.22	Zr 1.33	Nb 1.6	Mo 2.16	Tc 1.9	Ru 2.2	Rh 2.28	Pd 2.20	Ag 1.93	Cd 1.69	In 1.78	Sn 1.96	Sb 2.05	Te 2.1	I 2.66	Xe 2.60
6	Cs 0.79	Ba 0.89	*	Hf 1.3	Ta 1.5	W 2.36	Re 1.9	Os 2.2	Ir 2.20	Pt 2.28	Au 2.54	Hg 2.00	Tl 1.62	Pb 1.87	Bi 2.02	Po 2.0	At 2.2	Rn 2.2
7	Fr 0.7	Ra 0.9	**	Rf	Db	Sg	Bh	Hs	Mt	Ds	Rg	Cn	Uut	Fl	Uup	Lv	Uus	Uuo

* Lanthanoids	La 1.1	Ce 1.12	Pr 1.13	Nd 1.14	Pm 1.13	Sm 1.17	Eu 1.2	Gd 1.2	Tb 1.1	Dy 1.22	Ho 1.23	Er 1.24	Tm 1.25	Yb 1.1	Lu 1.27
** Actinoids	Ac 1.1	Th 1.3	Pa 1.5	U 1.38	Np 1.36	Pu 1.28	Am 1.13	Cm 1.28	Bk 1.3	Cf 1.3	Es 1.3	Fm 1.3	Md 1.3	No 1.3	Lr 1.3

Figure 1.3.2.3.1: Table of Pauling electronegativities from Wikipedia's Electronegativity page (click).

While directly relevant to the strength of chemical bonds, the Pauling definition of electronegativity has a significant limitation: calculating each value requires data from several compounds in which specific atoms are bonded. This means that the scale cannot be successfully applied to all situations. To overcome this limitation, alternative electronegativity scales were developed based on different thermochemical measurements or calculations. These other scales are listed in the table below. More thorough descriptions of how values in each scale are calculated are described on Wikipedia's Electronegativity page (click) and a concise history of electronegativity scales is summarized in ref 4.

Scale Developer	Year first described	Characteristics
Linus Pauling[1]	1932	Based on bond energies
Robert S. Mulliken[5,6]	1934	Based on valence electron properties of atoms (electron affinity and ionization energy)
Louis Allred & Eugene G. Rochow[7]	1958	Based on electrostatic force (effective nuclear charge)
Robert T. Sanderson[8]	1983	Based on atomic electron density
Ralph G. Pearson[9]	1985	Related to Hard-Soft Acid-Based theory
Leland C. Allen, Joseph Mann, Terry L. Meek[10,11,12]	1989, 2000	Average ionization energies of valence shell electrons, configuration energies (CE) $$\mathrm{CE} = \frac{n\varepsilon_s + m\varepsilon_p}{n+m}$$ n = number of s electrons m = number of p electrons $\varepsilon_s, \varepsilon_p$ = experimental 1-electron s and p energies

The primary advantage to this scale developed by Mann, Meek, and Allen[12] is that it is based on configuration energy (CE), the average ionization energies of valence electrons in ground state free atoms. A scale based on ionization energies can be calculated more directly for any element. However, a critique of all electronegativity scales, including this one, is that they are all based on assumptions that fail in some cases.

There is a relationship between electronegativity and atomic size because both are related to ionization energy. Like ionization energy, there is a general trend across the periodic table for both electronegativity and atomic size; in general, smaller atoms toward the top right-hand side of the periodic table have greater electronegativity values and smaller atomic size. We will see below that both electronegativity and atomic size influence bond angles and absolute molecular geometry around a central atom. In some cases, the size and electronegativity affects are aligned; in some cases these effects compete.

Electronegativity and Size Influence Bond Angles

Let's begin by examining the bond angles of several trigonal pyramidal molecules. The molecules shown in Figure **1.3.2.3.2** each have three identical "pendant groups" on the central atom (Figure **1.3.2.3.2**). *Pendant atoms* or *pendant groups* are the atoms, or groups of atoms, that are bonded directly to the central atom. The molecules shown here are arranged according to the size of the central and pendant atoms. Central atoms increase in size going down this figure, and pendant atoms increase in size going across from left to right. The bond angles and bond lengths are labeled in each case.

What trends can you identify?

Trends in Size

First, let's examine how the size of the central and pendant groups might influence bond angle. In VSEPR theory, **the size of atoms (or groups of atoms) will affect bond angles due to changes in steric interactions between pendant groups.**

Size of the central atom

Examine the relationship between the size of the central atom and the bond angles in Figure **1.3.2.3.2** (go down any column in the figure). For example, compare NH_3, PH_3, AsH_3, and SbH_3, with bond angles 106.6°, 93.2°, 92.1°, and 91.6°, respectively. In this series, the size of the central atom increases from N to Sb while the size of the pendant atom (hydrogen) remains constant. *As the size of the central atom increases, the bond angles decrease; thus, we observe a negative relationship between size of the central atom and the bond angle in these molecules*. This relationship is explained by sterics. As the central atom increases in size, the

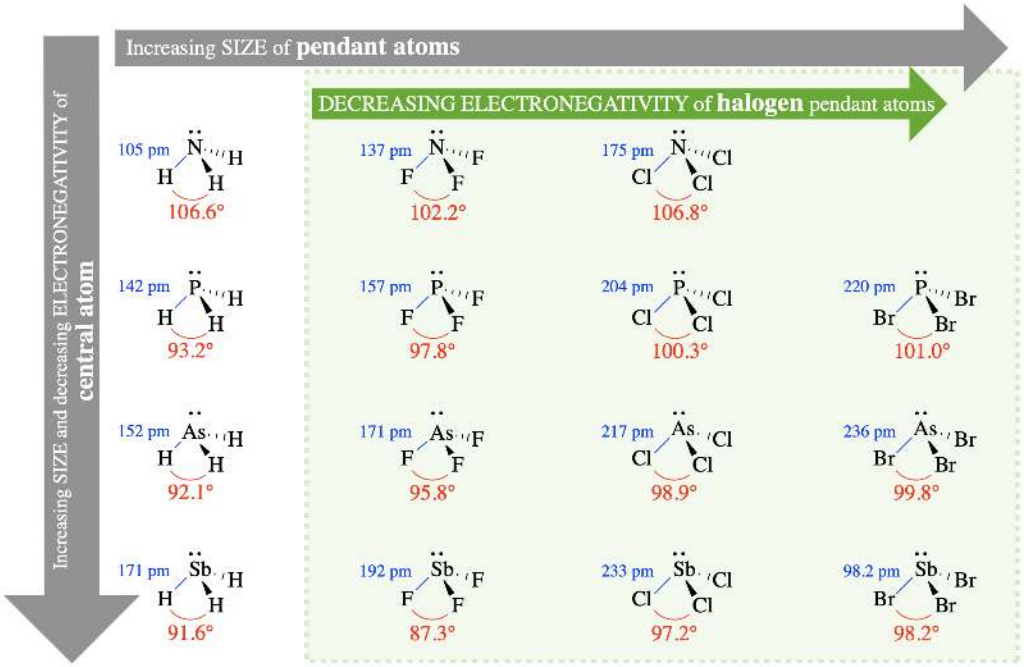


Figure **1.3.2.3.2**: Several molecules with trigonal pyramidal electronic geometry are shown arranged according to size of the central atom (increasing size of central atom from top to bottom) and pendant atom (increasing size of pendant atoms from left to right). Bond angles and bond lengths are indicated. (Kathryn Haas; CC-NC-BY-SA)

bond lengths also increase and the pendant atoms are farther from each other in space. In VSEPR theory, this will reduce steric interactions between the pendant groups. Since the lone pair on these molecules is more repulsive than bonded groups, the decrease in steric interactions between bonded groups results in a decrease in bond angles.

Size of the pendant atoms (or groups)

Examine the relationships between size of the halogen pendant atoms and bond angle in Figure **1.3.2.3.2** (go across any row within the shaded region). For example, compare PF_3, PCl_3, and PBr_3, with bond angles 97.8°, 100.3°, and 101.0°, respectively. In this series, the size of the pendant atom increases from F to Br while the central atom remains constant (phosphorous). *As the size of pendant atoms increases, the bond angle increases; thus, we observe a direct relationship between size of the pendant group and the bond angle in these molecules*. Again, we can explain this using sterics. As the size of the pendant atoms increases, sterics between the pendant groups will increase (despite small changes in bond length). Increased steric interactions between pendant groups will prefer larger bond angles between the groups.

This trend fails, however, if we consider the molecules with hydrogen as the pendant atoms. Notice, for example, that H is the smallest pendant atom. If we consider the trend described above, we should assume that XH_3 (where X is a variable atom) would have the smallest bond angle in the series of XH_3, XF_3, XCl_3, and XBr_3. However this is not the case of NH_3, NF_3, and NCl_3, with bond angles 106.6°, 102.2°, and 106.8°, respectively. To explain the variation in these bond angles, we need to consider electronegativity.

Trends in Electronegativity

Now let's examine how electronegativity influences bond angles around a central atom. In VSEPR theory, **electronegativity of atoms/groups will affect bond angles due to changes in the distribution of electron pairs around the central atom (and thus changes in the severity of electron pair repulsion).** This really comes down to bond polarity caused by the difference in electronegativity between the central atom and pendant groups (bond polarity in the context of valence bond theory). In a polar bond, the more electronegative atom will pull electron density towards itself. When a pendant atom is more electronegative, it will pull the bonded electron pair towards itself and away from the central atom; this will reduce the electron pair repulsion between bonded electron pairs on the central atom. A decrease in electron pair repulsion on the central atom should decrease bond angles between the groups (Figure **1.3.2.3.3**).

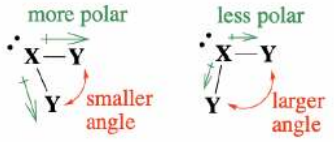


Figure **1.3.2.3.3**. When electron pairs are distributed away from the central atom, repulsions are decreased, allowing smaller bond angles. (Kathryn Haas; CC-NC-BY-SA)

Electronegativity is an alternative explanation to the trends we already examined above in Figure **1.3.2.3.2** . For example, when we compare the halogen pendant atoms (shaded region in Figure **1.3.2.3.2**) , the electronegativity of pendant groups decreases, bond polarity of the bonds decreases, and bond angles increase going from left to right and from F to Br. As more electron density remains on the central atom, electron repulsion between the bonded pairs increases and bond angles increase.

The electronegativity argument can also be used to explain the fact that NH_3 (106.6°) has a larger bond angle than NF_3 (102.2°). This particular case illustrates how electronegativity and size can be competing factors. While electronegativity differences seem to dominate in the case of NH_3 (106.6°) compared to NF_3 (102.2°), size differences still dominate in the cases of other XH_3 and XF_3 examples in Figure **1.3.2.3.2**).

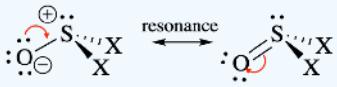
? Exercise 1.3.2.3.1

Predict the geometry and approximate bond angles. Then put the molecules in each series in order of smallest to largest bond angle. Defend your answer.

a. The X-S-X bond angle in OSF_2, $OSCl_2$, $OSBr_2$
b. H_2O, H_2S, H_2Se, H_2Te
c. H_2O, OF_2, OCl_2

Answer (a)

Geometry and predicted bond angles: These are molecules with steric number 4. They can be written as two different resonance structures, and the resonance hybrid would have double bond character between S and O.



We would expect a trigonal pyramidal geometry with all bond angles <109.5° because the lone pair is more repulsive than bonds. Because the double bond is more repulsive than single bonds, we should also expect the O-S-X bond angles to be greater than the X-S-X bond angles.

Trend: This is a series of molecules that varies in the identity of the pendant atoms; the variation is within the halogens. The size of the halogens increases, and the electronegativity decreases in the order F, Cl, Br. Both size and electronegativity would lead us to conclude that the X-S-X bond angles would increase in the order $OSF_2 < OSCl_2 < OSBr_2$

Explanation: (1) Increasing electonegativity of the pendant atom (F > Cl > Br) increases the polarity of the bond and reduces the electron density of the bonded pair on the central atom. This reduces the e-e repulsions of adjacent bonded electron pairs on S, allowing the halogens to become closer. The more electronegative pendant atoms can have smaller bond angles. (2) Increasing size of pendant atoms (F < Cl < Br) increases steric repulsions and increases bond angle. Both explanations lead to the same predicted trend.

The actual measured X-S-X bond angles are OSF_2 (92.3°) / $OSCl_2$ (96.2°) / $OSBr_2$ (98.2°). The trend in these bond angles is consistent with the prediction.

Answer (b)

Geometry and predicted bond angles: These are molecules with steric number 4, bent molecular geometry, with predicted bond angles <109.5° because the two lone pairs are each more repulsive than the bonds. There are two lone pairs and two single bonds to H around each central atom.

Trend: This is a series of molecules that varies in the identity of the central atom. The central atom increases in the order O < S < Se < Te, where Te is the largest element and O is the smallest. Arguments based on size would lead us to predict that the pendant groups of H_2Te would be less sterically crowded and thus have a smaller bond angle than the pendant groups of H_2O. The electronegativity decreases in the order O > S > Se > Te, where O is the most electronegative element and Te is the least. Thus, we expect the bonding electro pairs to be closer to the central atom on O than they would be on Te; we should expect H_2Te to have the least electron pair repulsions and thus smallest bond angle in this series, while H_2O would have the strongest electron pair repulsions and largest bond angles.

Both arguments lead to the same conclusion, that the order of increasing bond angle is $H_2Te < H_2Se < H_2S < H_2O$.

The actual measured bond angles are H_2Te (90.2°) / H_2Se (90.6°) / H_2S (92.1°) / H_2O (104.5). The trend in these bond angles is consistent with prediction.

Answer (c)

Geometry and predicted bond angles: These are molecules with steric number 4, bent molecular geometry, with predicted bond angles <109.5° because the two lone pairs are each more repulsive than the bonds. There are two lone pairs and two single bonds to H around each central atom. (This is similar to the case in (b)).

Trend: This is a series of molecules that varies in the identity of the pendant atoms; two of the molecules have halogens, and the other has hydrogen pendant atoms. This is a case where size and electronegativity will be conflicting factors because trends in electronegativity do not mirror the trend in size.

- *Size:* The size of pendant atoms increases in the order H < F < Cl where H is smallest and Cl is largest. Prediction of bond angles based on size alone would lead to the predicted order of increasing bond angle $H_2O < OF_2 < OCl_2$.
- *Electronegativity*: The electronegativity decreases in the order F > Cl > H where F has the greatest electronegativity and H has the least. Since we expect the most electronegative pendant atoms to have the smallest bond angles, prediction based on electronegativity alone would lead to the predicted order of increasing bond angle $OF_2 < OCl_2 < H_2O$.

The points above illustrate how the two different arguments would lead to different predictions about the trend in bond angle. This makes it difficult to predict the actual order of increasing bond angle. However, we saw above in the example of NH_3 vs NF_3 that electronegativity is more important than size; yet in the case of NH_3 vs NCl_3, the much larger size of the pendant atom is more important. If we apply this lesson to the current problem, we might predict the order $OF_2 < H_2O < OCl_2$, and in fact this more nuanced prediction, based on a similar case, matches the actual order for measured bond angles: OF_2 (103.3°) < H_2O (104.5°) < OCl_2 (110.9°).

Group Electronegativities

You probably heard the terms "electron donating group" and "electron withdrawing group" from your coursework in Organic Chemistry. For example, the acid trifluoroacetic acid (TFA) is more acidic than acetic acid due to the electron withdrawing effects of the CF_3 group compared to CH_3. CF_3 is an electron withdrawing group, while CH_3 is an electron donating group. In other words, CF_3 is more electronegative than CH_3.

The electron withdrawing ability (electronegativity) of groups can be estimated and compared, just as they are with atoms. Although there is no one scale that is used for group electronegativities, and published values even for the same groups vary widely, there are reliable trends within similar groups. The same size and electronegativity factors discussed above that affect bond angles for *pendant atoms*, also can be used to rationalize distorted bond angles for *pendant groups* around a central atom.

? Exercise 1.3.2.3.2

Consider the relative electronegativities and sizes of the pendant atoms/groups in the following examples. Is the trend in bond angles what you would expect from the relative group electronegativities and relative sizes? What, if any, is the more dominant factor in determining the trend?

a. $N(CH_3)_3$ has an C-N-C bond angle of 110.9°, while $N(CF_3)_3$ has a bond angle of 117.9°.
b. The X-S-X bond angles in molecules of the form $SO_2(X)_2$ are: $SO_2(OH)_2$ 101.3°; $SO_2(CF_3)_2$ 102.0°; $SO_2(CH_3)_2$ 102.6°.

Answer (a)

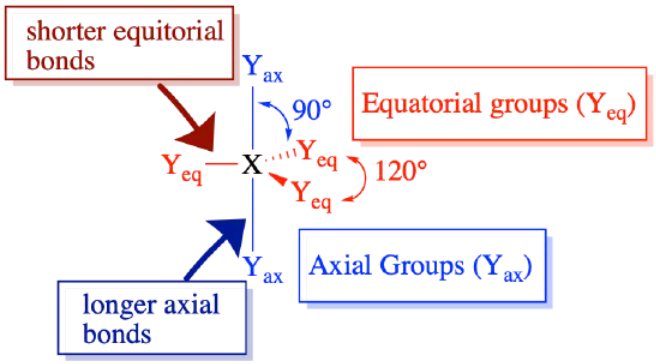
Add texts here. Do not delete this text first.

Answer (b)

Add texts here. Do not delete this text first.

Special case of electronegativity and size in steric number 5 (trigonal bypyramid)

Molecules with steric number 5 are interesting because they posses two different types of positions (equatorial and axial). These positions have unique bond angles and bond lengths. Pendant atoms/groups have different preferences for the axial and equatorial positions that depend somewhat on their electronegativity.



Molecules with steric number 5 possess different bond angles and lengths for axial (ax) and equatorial (eq) pendant atoms. (CC-BY-NC-SA; Kathryn Haas)

In a previous section, we discussed the preference of lone pairs and multiple bonds for the equatorial positions in trigonal bipyramidal molecules. VSEPR theory rationalizes this by assuming that lone pairs and multiple bonds are more repulsive than the electron pairs in single bonds. Equatorial positions are less crowded (with only two closest neighbors at 90°, and two farther neighbors at 120°) compared to axial positions (with three closest neighbors at 90°), thus the more repulsive groups prefer the less crowded equatorial positions.

Pendant groups that are more electronegative result in weaker electron pair repulsion around the central atom, while groups that are less electronegative result in stronger electron-pair repulsion around the central atom (as described above). The result for steric number 5: **bonding pairs to *less electronegative elements* are *more repulsive*, and *generally prefer equatorial* positions.** Still, lone pairs and multiple bonds are more repulsive than single bonds and would show a stronger preference for equatorial positions.

Examples and Nuances

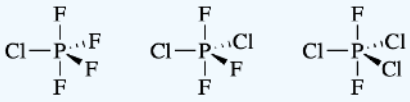
? Exercise 1.3.2.3.3

Some examples of molecule that demonstrate the equatorial preference of less electronegative groups are below. Predict (draw) their structures.

a. PF_4Cl, PF_3Cl_2, and PF_2Cl_3
b. $PF_4(CH_3)$ $PF_3(CH_3)_2$, and $PF_2(CH_3)_3$

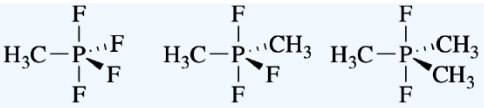
Answer (a)

Cl is less electronegative than F; thus we expect Cl to have stronger preference for the equatorial positions.

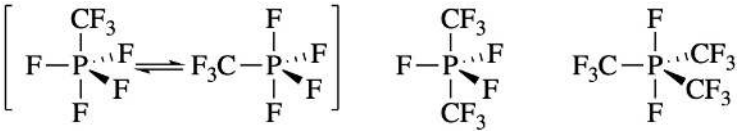


Answer (b)

CH_3, an electron donating group, is less electronegative than F. We expect CH_3 to have a stronger preference for the equatorial positions.



In the exercise above, the structures can be explained by the electronegativity of the pendant groups; less electronegative groups prefer the equatorial positions. There are other similar molecules for which explanations (or predictions) are difficult. For example, the series of molecules below seems to have completely random placement of F and CF_3 groups. **These structures could not be predicted based on VSEPR theory.** It seems that in this case, the more symmetrical arrangements of pendant groups is preferred.



References and resources

1. Pauling, L. (1932). "The Nature of the Chemical Bond. IV. The Energy of Single Bonds and the Relative Electronegativity of Atoms". *J. Am. Chem. Soc.* **54**(9): 3570–3582. doi:10.1021/ja01348a011.
2. Housecroft, Catherine E. et. al. "Inorganic Chemistry" 3rd Edition. Pearson Education Limited 2008. Chapter 2.5 "Electronegativity Values" pgs. 42-44
3. International Union of Pure and Applied Chemistry. "Electronegativity". goldbook.iupac.org/E01990.html.
4. Pearson, R.G. *Acc. Chem. Res.* 1990, 23, 1, 1–2. https://doi.org/10.1021/ar00169a001
5. Mulliken, R. S. (1934). "A New Electroaffinity Scale; Together with Data on Valence States and on Valence Ionization Potentials and Electron Affinities". *J. Chem. Phys.***2** (11): 782–793. doi:10.1063/1.1749394.
6. Mulliken, R. S. (1935). "Electronic Structures of Molecules XI. Electroaffinity, Molecular Orbitals and Dipole Moments". J. Chem. Phys. **3** (9): 573–585. doi:10.1063/1.1749731.
7. Allred, A. L.; Rochow, E. G. (1958). "A scale of electronegativity based on electrostatic force". *Journal of Inorganic and Nuclear Chemistry*. **5** (4): 264–268. doi:10.1016/0022-1902(58)80003-2
8. Sanderson, R. T. (1983). "Electronegativity and bond energy". *Journal of the American Chemical Society*. **105** (8): 2259–2261. doi:10.1021/ja00346a026
9. Pearson, R. G. (1985). "Absolute electronegativity and absolute hardness of Lewis acids and bases". J. Am. Chem. Soc. 107 (24): 6801. doi:10.1021/ja00310a009.
10. Allen, Leland C. (1989). "Electronegativity is the average one-electron energy of the valence-shell electrons in ground-state free atoms". Journal of the American Chemical Society. 111 (25): 9003–9014. doi:10.1021/ja00207a003.
11. Mann, Joseph B.; Meek, Terry L.; Allen, Leland C. (2000). "Configuration Energies of the Main Group Elements". Journal of the American Chemical Society. 122 (12): 2780–2783. doi:10.1021/ja992866e.
12. Mann, Joseph B.; Meek, Terry L.; Knight, Eugene T.; Capitani, Joseph F.; Allen, Leland C. (2000). "Configuration energies of the d-block elements". Journal of the American Chemical Society. 122 (21): 5132–5137. doi:10.1021/ja9928677

Acknowledgment

- Matthew Salem (UC Davis) (Pauling Electronegativity)
- Introduction to Inorganic Chemistry Wikibook (https://chem.libretexts.org/Bookshel..._Bond_Strength)
- Curated or created by Kathryn Haas

This page titled 1.3.2.3: Electronegativity and Atomic Size Effects is shared under a not declared license and was authored, remixed, and/or curated by Kathryn Haas.

- **3.2.3: Electronegativity and Atomic Size Effects** by Kathryn Haas is licensed CC BY-NC-SA 4.0.

1.3.2.4: Ligand Close Packing

Introduction

Ligand Close Packing (LCP) theory is complimentary to VSEPR, except that LCP focuses on repulsions between pendant *atoms* ("outer" atoms that are not directly bonded to one another), rather than focusing on the chemical environment around the central atom in a molecule. Both LCP and the VSEPR models were developed by Robert Gillespie.

The LCP model assumes that ligands (or pendant atoms) "pack" as closely as possible around a central atom. A given ligand will have a specific atomic radius when bound to a central atom. The distance between two ligands around the same central atom is simply the sum of the atomic radii of the pendant atoms. Therefore for a specific set of ligands around a specific central atom, the ligand-ligand distances are constant despite the coordination number or bond angles. In other words, for a series of similar molecules with the same central atom, while bond angles and bond distances of pendant atoms may change, the distances between two pendant atoms remain the same.

Ligand Close Packing Theory

According to LCP, distances between two pendant atoms are similar...

- even when steric number changes
- even when bond angles change
- Reason: pendant atoms "pack" around the central atom.

Ligand Close Packing and Bond Distances

If the distance between non-bonded atoms remains constant even while bond angles change, then the bond length between the pendant and central atom must change to accommodate. For example, $\mathbf{PF_4^+}$ and $\mathbf{PF_3O}$ have almost identical $\mathbf{F-F}$ distances of 238 and 237 pm, respectively. As expected from VSEPR, the $\mathbf{F-P-F}$ bond angle in $\mathbf{PF_4^+}$ is 109.5°. The $\mathbf{F-P-F}$ bond angle in $\mathbf{PF_3O}$ (101.1°) is smaller due to the increased repulsion of the oxygen double bond. Therefore the P-F bond lengths must be different. In fact, the P-F bond distances are 145.7 pm in $\mathbf{PF_4^+}$ and 154 pm in $\mathbf{PF_3O}$.

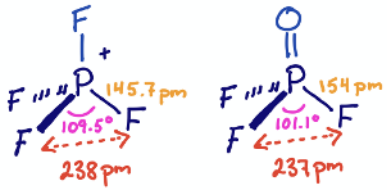


Figure **1.3.2.4.1**: The molecular structures of $\mathbf{PF_4^+}$ and $\mathbf{PF_3O}$. The distances between neighboring F atoms are similar in the two molecules, while bond lengths and angles differ. The $\mathbf{PF_4^+}$ ion has a $\mathbf{P-F}$ bond length of 145.7 pm, an $\mathbf{F-P-F}$ bond angle of 109.5°, and a distance of 238 pm between neighboring F atoms. The $\mathbf{PF_3O}$ molecule has a $\mathbf{P-F}$ bond length of 154 pm, an $\mathbf{F-P-F}$ bond angle of 101.1°, and a distance of 237 pm between neighboring F atoms. (CC-BY-NC-SA; Kathryn Haas)

The relationship between bond angles, bond lengths, and close-packing distance is described by right angle trigonometry (recall SOA-CAH-TOA). In a right triangle, the hypotenuse is the longest side, opposite to the right angle. For either of the other two angles in the triangle, the angle (θ) and lengths of the sides (*opposite* and *adjacent* to θ) are related by the trigometric functions shown in Figure **1.3.2.4.2** .

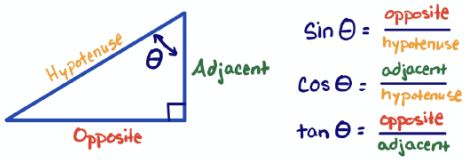


Figure **1.3.2.4.2**: Visual depiction of SOA-CAH-TOA. (CC-BY-NC-SA; Kathryn Haas)

In the case of a molecule, we can apply right angle trigonometry by imagining that the bond angle is divided into two right angles, as illustrated in Figure **1.3.2.4.2**. The hypotenuse of the triangles is the bond length, the opposite side is one half of the close-

packing distance, and θ is one half the bond angle.

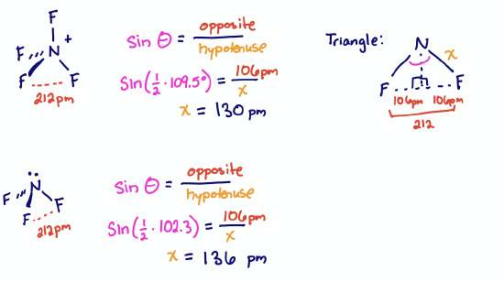


Figure 1.3.2.4.1: Illustration of how right angle trigonometry can be applied to determine bond angle, bond length, or distance between neighboring atoms: any bond angle can be divided into two right angles where the bond length is the hypotenuse, the distance between neighbors is twice the opposite side, and the bond angle is twice θ. (CC-BY-NC-SA; Kathryn Haas)

Exercise 1.3.2.4.1

The distance between F atoms is 212 pm in both NF_4^+ and NF_3. The bond angles are 109.5° and 102.3°, respectively. What are the expected $N-F$ bond lengths?

Answer



The actual measured bond lengths are 130 pm for NF_4^+ and 136.5 pm for NF_3.

Sources and Resources

- https://en.Wikipedia.org/wiki/LCP_th...ieNyholm1957-3

This page titled 1.3.2.4: Ligand Close Packing is shared under a not declared license and was authored, remixed, and/or curated by Kathryn Haas.

- **3.2.4: Ligand Close Packing** by Kathryn Haas is licensed CC BY-NC-SA 4.0.

1.3.3: Molecular Polarity

Dipole moments occur when there is a separation of charge. They can occur between two ions in an ionic bond or between atoms in a covalent bond; dipole moments arise from differences in electronegativity. The larger the difference in electronegativity, the larger the dipole moment. The distance between the charge separation is also a deciding factor in the size of the dipole moment. The dipole moment is a measure of the polarity of the molecule.

Introduction

When atoms in a molecule share electrons unequally, they create what is called a dipole moment. This occurs when one atom is more electronegative than another, resulting in that atom pulling more tightly on the shared pair of electrons, or when one atom has a lone pair of electrons and the difference of electronegativity vector points in the same way. One of the most common examples is the water molecule, made up of one oxygen atom and two hydrogen atoms. The differences in electronegativity and lone electrons give oxygen a partial negative charge and each hydrogen a partial positive charge.

Dipole Moment

When two electrical charges, of opposite sign and equal magnitude, are separated by a distance, an electric dipole is established. The size of a dipole is measured by its dipole moment (μ). Dipole moment is measured in Debye units, which is equal to the distance between the charges multiplied by the charge (1 Debye equals $3.34 \times 10^{-30}\ C\,m$). The dipole moment of a molecule can be calculated by Equation 1.3.3.1:

$$\vec{\mu} = \sum_i q_i \vec{r}_i \tag{1.3.3.1}$$

where

- $\vec{\mu}$ is the dipole moment vector
- q_i is the magnitude of the ith charge, and
- $\vec{r}_i$ is the vector representing the position of ith charge.

The dipole moment acts in the direction of the vector quantity. An example of a polar molecule is H_2O. Because of the lone pair on oxygen, the structure of H_2O is bent (via VSEPR theory), which means that the vectors representing the dipole moment of each bond do not cancel each other out. Hence, water is polar.

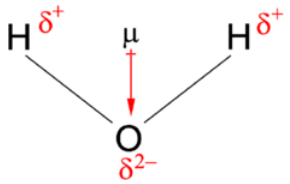


Figure 1.3.3.1: Dipole moment of water. The convention in chemistry is that the arrow representing the dipole moment goes from positive to negative. Physicist tend to use the opposite orientation.

The vector points from positive to negative, on both the molecular (net) dipole moment and the individual bond dipoles. Table A2 shows the electronegativity of some of the common elements. The larger the difference in electronegativity between the two atoms, the more electronegative that bond is. To be considered a polar bond, the difference in electronegativity must be large. The dipole moment points in the direction of the vector quantity of each of the bond electronegativities added together.

It is relatively easy to measure dipole moments: just place a substance between charged plates (Figure 1.3.3.2); polar molecules increase the charge stored on the plates, and the dipole moment can be obtained (i.e., via the capacitance of the system). Nonpolar CCl_4 is not deflected; moderately polar acetone deflects slightly; highly polar water deflects strongly. In general, polar molecules will align themselves: (1) in an electric field, (2) with respect to one another, or (3) with respect to ions (Figure 1.3.3.2).

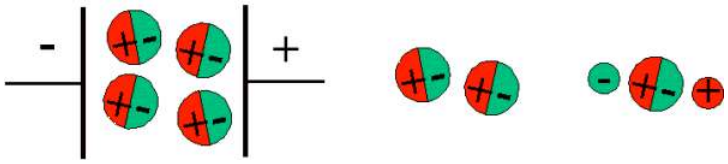


Figure 1.3.3.2: Polar molecules align themselves in an electric field (left), with respect to one another (middle), and with respect to ions (right)

Equation 1.3.3.1 can be simplified for a simple separated two-charge system like diatomic molecules or when considering a bond dipole within a molecule

$$\mu_{diatomic} = Q \times r \tag{1.3.3.2}$$

This bond dipole is interpreted as the dipole from a charge separation over a distance r between the partial charges Q^+ and Q^- (or the more commonly used terms δ^+ - δ^-); the orientation of the dipole is along the axis of the bond. Consider a simple system of a single electron and proton separated by a fixed distance. When the proton and electron are close together, the dipole moment (degree of polarity) decreases. However, as the proton and electron get farther apart, the dipole moment increases. In this case, the dipole moment is calculated as (via Equation 1.3.3.2):

$$\begin{aligned}\mu &= Qr \\ &= (1.60 \times 10^{-19}\, C)(1.00 \times 10^{-10}\, m) \\ &= 1.60 \times 10^{-29}\, C \cdot m\end{aligned}$$

The Debye characterizes the size of the dipole moment. When a proton and electron are 100 pm apart, the dipole moment is $4.80\ D$:

$$\begin{aligned}\mu &= (1.60 \times 10^{-29}\, C \cdot m)\left(\frac{1\ D}{3.336 \times 10^{-30}\, C \cdot m}\right) \\ &= 4.80\ D\end{aligned}$$

$4.80\ D$ is a key reference value and represents a pure charge of +1 and -1 separated by 100 pm. If the charge separation is increased then the dipole moment increases (linearly):

- If the proton and electron are separated by 120 pm:

$$\mu = \frac{120}{100}(4.80\ D) = 5.76\ D \tag{1.3.3.3}$$

- If the proton and electron are separated by 150 pm:

$$\mu = \frac{150}{100}(4.80\ D) = 7.20\ D \tag{1.3.3.4}$$

- If the proton and electron are separated by 200 pm:

$$\mu = \frac{200}{100}(4.80\ D) = 9.60\ D \tag{1.3.3.5}$$

Example 1.3.3.1: Water

The water molecule in Figure 1.3.3.1 can be used to determine the direction and magnitude of the dipole moment. From the electronegativities of oxygen and hydrogen, the difference in electronegativity is 1.2e for each of the hydrogen-oxygen bonds. Next, because the oxygen is the more electronegative atom, it exerts a greater pull on the shared electrons; it also has two lone pairs of electrons. From this, it can be concluded that the dipole moment points from between the two hydrogen atoms toward the oxygen atom. Using the equation above, the dipole moment is calculated to be 1.85 D by multiplying the distance between the oxygen and hydrogen atoms by the charge difference between them and then finding the components of each that point in the direction of the net dipole moment (the angle of the molecule is 104.5˚).

The bond moment of the O-H bond =1.5 D, so the net dipole moment is

$$\mu = 2(1.5)\cos\left(\frac{104.5^\circ}{2}\right) = 1.84\ D$$

Polarity and Structure of Molecules

The shape of a molecule and the polarity of its bonds determine the OVERALL POLARITY of that molecule. A molecule that contains polar bonds might not have any overall polarity, depending upon its shape. The simple definition of whether a complex molecule is polar or not depends upon whether its overall centers of positive and negative charges overlap. If these centers lie at the same point in space, then the molecule has no overall polarity (and is non polar). If a molecule is completely symmetric, then the dipole moment vectors on each molecule will cancel each other out, making the molecule nonpolar. A molecule can only be polar if the structure of that molecule is not symmetric.

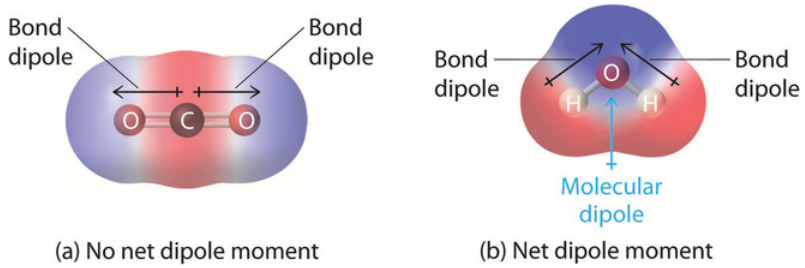


Figure 1.3.3.3: Charge distributions of CO_2 and H_2O\). Blue and red colored regions are negatively and positively signed regions, respectively. (CC BY-SA-NC 3.0; anonymous)

A good example of a nonpolar molecule that contains polar bonds is carbon dioxide (Figure 1.3.3.3*a*). This is a linear molecule and each C=O bond is, in fact, polar. The central carbon will have a net positive charge, and the two outer oxygen atoms a net negative charge. However, since the molecule is linear, these two bond dipoles cancel each other out (i.e. the vector addition of the dipoles equals zero) and the overall molecule has a zero dipole moment ($\mu = 0$).

> *Although a polar bond is a prerequisite for a molecule to have a dipole, not all molecules with polar bonds exhibit dipoles*

For AB_n molecules, where A is the central atom and B are all the same types of atoms, there are certain molecular geometries which are symmetric. Therefore, they will have no dipole even if the bonds are polar. These geometries include linear, trigonal planar, tetrahedral, octahedral and trigonal bipyramid.

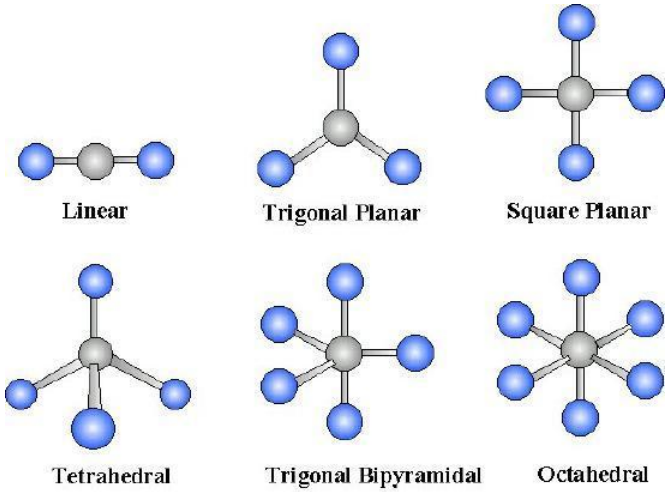
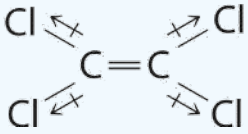


Figure 1.3.3.4: Molecular geometries with exact cancellation of polar bonding to generate a non-polar molecule ($\mu = 0$)

Example 1.3.3.3: C_2Cl_4

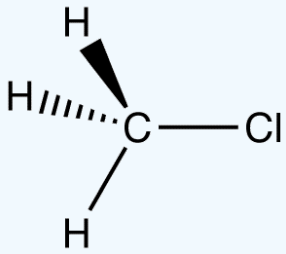
Although the C–Cl bonds are rather polar, the individual bond dipoles cancel one another in this symmetrical structure, and $Cl_2C{=}CCl_2$ does not have a net dipole moment.



Example 1.3.3.3: CH_3Cl

C-Cl, the key polar bond, is 178 pm. Measurement reveals 1.87 D. From this data, % ionic character can be computed. If this bond were 100% ionic (based on proton & electron),

$$\mu = \frac{178}{100}(4.80\ D)$$
$$= 8.54\ D$$



Although the bond length is ***increasing***, the dipole is ***decreasing*** as you move down the halogen group. The electronegativity decreases as we move down the group. Thus, the greater influence is the electronegativity of the two atoms (which influences the ***charge*** at the ends of the dipole).

Table **1.3.3.1**: Relationship between Bond length, Electronegativity and Dipole moments in simple Diatomics

Compound	Bond Length (Å)	Electronegativity Difference	Dipole Moment (D)
HF	0.92	1.9	1.82
HCl	1.27	0.9	1.08
HBr	1.41	0.7	0.82
HI	1.61	0.4	0.44

References

1. *Housecroft, Catherine E. and Alan G. Sharpe. Inorganic Chemistry. 3rd ed. Harlow: Pearson Education, 2008. Print. (Pages 44-46)*
2. *Tro, Nivaldo J. Chemistry: A Molecular Approach. Upper Saddle River: Pearson Education, 2008. Print. (Pages 379-386)*

1.3.3: Molecular Polarity is shared under a not declared license and was authored, remixed, and/or curated by LibreTexts.

- **Dipole Moments** by Delmar Larsen, Mike Blaber is licensed CC BY 4.0.

1.3.4: Hydrogen Bonding

A hydrogen bond is an intermolecular force (IMF) that forms a special type of dipole-dipole attraction when a hydrogen atom bonded to a strongly electronegative atom exists in the vicinity of another electronegative atom with a lone pair of electrons. Intermolecular forces (IMFs) occur between molecules. Other examples include ordinary dipole-dipole interactions and dispersion forces. Hydrogen bonds are are generally stronger than ordinary dipole-dipole and dispersion forces, but weaker than true covalent and ionic bonds.

The evidence for hydrogen bonding

Many elements form compounds with hydrogen. If you plot the boiling points of the compounds of the group 14 elements with hydrogen, you find that the boiling points increase as you go down the group.

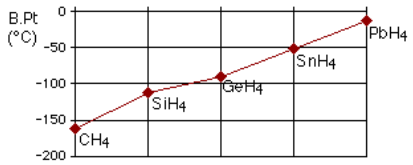


Figure 1: Boiling points of group 14 elemental halides.

The increase in boiling point happens because the molecules are getting larger with more electrons, and so van der Waals dispersion forces become greater. If you repeat this exercise with the compounds of the elements in groups 15, 16, and 17 with hydrogen, something odd happens.

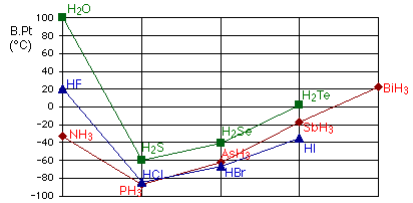


Figure 2: Boiling points of group 15-17 elemental halides.

Although the same reasoning applies for group 4 of the periodic table, the boiling point of the compound of hydrogen with the first element in each group is abnormally high. In the cases of NH_3, H_2O and HF there must be some additional intermolecular forces of attraction, requiring significantly more heat energy to break the IMFs. These relatively powerful intermolecular forces are described as hydrogen bonds.

Origin of Hydrogen Bonding

The molecules capable of hydrogen bonding include the following:

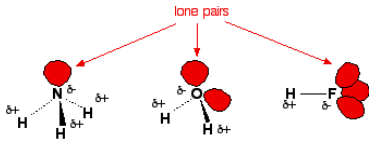


Figure 3: The lone pairs responsible for hydrogen bonding in NH_3, H_2O, and HF. The solid line represents a bond in the plane of the screen or paper. Dotted bonds are going back into the screen or paper away from you, and wedge-shaped ones are coming out towards you.

Notice that in each of these molecules:

- The hydrogen is attached directly to a highly electronegative atoms, causing the hydrogen to acquire a highly positive charge.
- Each of the highly electronegative atoms attains a high negative charge and has at least one "active" lone pair. Lone pairs at the 2-level have electrons contained in a relatively small volume of space, resulting in a high negative charge density. Lone pairs at higher levels are more diffuse and, resulting in a lower charge density and lower affinity for positive charge.

> *If you are not familiar with electronegativity, you should follow this link before you go on.*

Consider two water molecules coming close together.

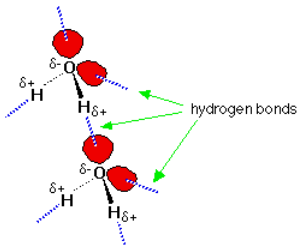


Figure 4: Hydrogen bonding in water

The δ^+ hydrogen is so strongly attracted to the lone pair that it is almost as if you were beginning to form a co-ordinate (dative covalent) bond. It doesn't go that far, but the attraction is significantly stronger than an ordinary dipole-dipole interaction. Hydrogen bonds have about a tenth of the strength of an average covalent bond, and are constantly broken and reformed in liquid water. If you liken the covalent bond between the oxygen and hydrogen to a stable marriage, the hydrogen bond has "just good friends" status.

Water is an ideal example of hydrogen bonding. Notice that each water molecule can potentially form four hydrogen bonds with surrounding water molecules: two with the hydrogen atoms and two with the with the oxygen atoms. There are exactly the right numbers of δ^+ hydrogens and lone pairs for every one of them to be involved in hydrogen bonding.

This is why the boiling point of water is higher than that of ammonia or hydrogen fluoride. In the case of ammonia, the amount of hydrogen bonding is limited by the fact that each nitrogen only has one lone pair. In a group of ammonia molecules, there are not enough lone pairs to go around to satisfy all the hydrogens. In hydrogen fluoride, the problem is a shortage of hydrogens. In water, two hydrogen bonds and two lone pairs allow formation of hydrogen bond interactions in a lattice of water molecules. Water is thus considered an ideal hydrogen bonded system.

More complex examples of hydrogen bonding

The hydration of negative ions

When an ionic substance dissolves in water, water molecules cluster around the separated ions. This process is called hydration. Water frequently attaches to positive ions by co-ordinate (dative covalent) bonds. It bonds to negative ions using hydrogen bonds.

> *If you are interested in the bonding in hydrated positive ions, you could follow this link to co-ordinate (dative covalent) bonding.*

The diagram shows the potential hydrogen bonds formed with a chloride ion, Cl-. Although the lone pairs in the chloride ion are at the 3-level and would not normally be active enough to form hydrogen bonds, they are made more attractive by the full negative charge on the chlorine in this case.

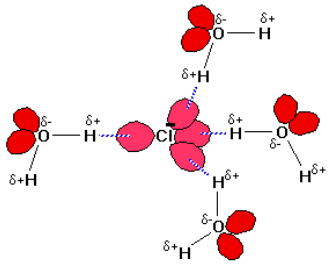


Figure 5: Hydrogen bonding between chloride ions and water.

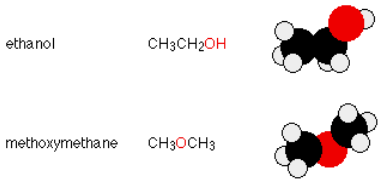
However complicated the negative ion, there will always be lone pairs that the hydrogen atoms from the water molecules can hydrogen bond to.

Hydrogen bonding in alcohols

An alcohol is an organic molecule containing an -OH group. Any molecule which has a hydrogen atom attached directly to an oxygen or a nitrogen is capable of hydrogen bonding. Hydrogen bonds also occur when hydrogen is bonded to fluorine, but the HF

group does not appear in other molecules. Molecules with hydrogen bonds will always have higher boiling points than similarly sized molecules which don't have an -O-H or an -N-H group. The hydrogen bonding makes the molecules "stickier," such that more heat (energy) is required to separate them. This phenomenon can be used to analyze boiling point of different molecules, defined as the temperature at which a phase change from liquid to gas occurs.

Ethanol, $\mathbf{CH_3CH_2{-}O{-}H}$, and methoxymethane, $\mathbf{CH_3{-}O{-}CH_3}$, both have the same molecular formula, $\mathbf{C_2H_6O}$.

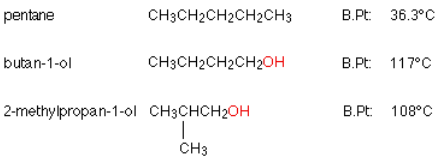


They have the same number of electrons, and a similar length. The van der Waals attractions (both dispersion forces and dipole-dipole attractions) in each will be similar. However, ethanol has a hydrogen atom attached directly to an oxygen; here the oxygen still has two lone pairs like a water molecule. Hydrogen bonding can occur between ethanol molecules, although not as effectively as in water. The hydrogen bonding is limited by the fact that there is only one hydrogen in each ethanol molecule with sufficient $\delta+$ charge.

In methoxymethane, the lone pairs on the oxygen are still there, but the hydrogens are not sufficiently $\delta+$ for hydrogen bonds to form. Except in some rather unusual cases, the hydrogen atom has to be attached directly to the very electronegative element for hydrogen bonding to occur. The boiling points of ethanol and methoxymethane show the dramatic effect that the hydrogen bonding has on the stickiness of the ethanol molecules:

ethanol (with hydrogen bonding)	78.5°C
methoxymethane (without hydrogen bonding)	-24.8°C

The hydrogen bonding in the ethanol has lifted its boiling point about 100°C. It is important to realize that hydrogen bonding exists in addition to van der Waals attractions. For example, all the following molecules contain the same number of electrons, and the first two have similar chain lengths. The higher boiling point of the butan-1-ol is due to the additional hydrogen bonding.



Comparing the two alcohols (containing -OH groups), both boiling points are high because of the additional hydrogen bonding; however, the values are not the same. The boiling point of the 2-methylpropan-1-ol isn't as high as the butan-1-ol because the branching in the molecule makes the van der Waals attractions less effective than in the longer butan-1-ol.

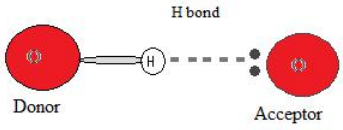
Hydrogen bonding in organic molecules containing nitrogen

Hydrogen bonding also occurs in organic molecules containing N-H groups; recall the hydrogen bonds that occur with ammonia. Examples range from simple molecules like CH_3NH_2 (methylamine) to large molecules like proteins and DNA. The two strands of the famous double helix in DNA are held together by hydrogen bonds between hydrogen atoms attached to nitrogen on one strand, and lone pairs on another nitrogen or an oxygen on the other one.

Donors and Acceptors

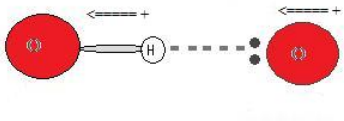
In order for a hydrogen bond to occur there must be both a hydrogen donor and an acceptor present. The donor in a hydrogen bond is usually a strongly electronegative atom such as N, O, or F that is covalently bonded to a hydrogen bond.

The hydrogen acceptor is an electronegative atom of a neighboring molecule or ion that contains a lone pair that participates in the hydrogen bond.



Why does a hydrogen bond occur?

Since the hydrogen donor (N, O, or F) is strongly electronegative, it pulls the covalently bonded electron pair closer to its nucleus, and away from the hydrogen atom. The hydrogen atom is then left with a partial positive charge, creating a dipole-dipole attraction between the hydrogen atom bonded to the donor and the lone electron pair of the acceptor. This results in a hydrogen bond.(see Interactions Between Molecules With Permanent Dipoles)

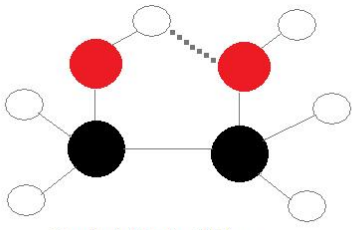


Types of hydrogen bonds

Although hydrogen bonds are well-known as a type of IMF, these bonds can also occur within a single molecule, between two identical molecules, or between two dissimilar molecules.

Intramolecular hydrogen bonds

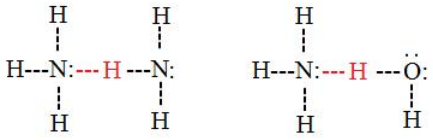
Intramolecular hydrogen bonds are those which occur *within* one single molecule. This occurs when two functional groups of a molecule can form hydrogen bonds with each other. In order for this to happen, both a hydrogen donor a hydrogen acceptor must be present within one molecule, and they must be within close proximity of each other in the molecule. For example, intramolecular hydrogen bonding occurs in ethylene glycol ($C_2H_4(OH)_2$) between its two hydroxyl groups due to the molecular geometry.



Intramolecular h-bonding in Ethylene Glycol molecule

Intermolecular hydrogen bonds

Intermolecular hydrogen bonds occur *between* separate molecules in a substance. They can occur between any number of like or unlike molecules as long as hydrogen donors and acceptors are present in positions where they can interact with one another. For example, intermolecular hydrogen bonds can occur between NH_3 molecules alone, between H_2O molecules alone, or between NH_3 and H_2O molecules.



Properties and effects of hydrogen bonds

On Boiling Point

When we consider the boiling points of molecules, we usually expect molecules with larger molar masses to have higher normal boiling points than molecules with smaller molar masses. This, without taking hydrogen bonds into account, is due to greater dispersion forces (see Interactions Between Nonpolar Molecules). Larger molecules have more space for electron distribution and thus more possibilities for an instantaneous dipole moment. However, when we consider the table below, we see that this is not always the case.

Compound	Molar Mass	Normal Boiling Point
H_2O	18 g/mol	373 K
HF	20 g/mol	292.5 K
NH_3	17 g/mol	239.8 K
H_2S	34 g/mol	212.9 K
HCl	36.4 g/mol	197.9 K
PH_3	34 g/mol	185.2 K

We see that H_2O, HF, and NH_3 each have higher boiling points than the same compound formed between hydrogen and the next element moving down its respective group, indicating that the former have greater intermolecular forces. This is because H_2O, HF, and NH_3 all exhibit hydrogen bonding, whereas the others do not. Furthermore, H_2O has a smaller molar mass than HF but partakes in more hydrogen bonds per molecule, so its boiling point is higher.

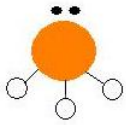
On Viscosity

The same effect that is seen on boiling point as a result of hydrogen bonding can also be observed in the viscosity of certain substances. Substances capable of forming hydrogen bonds tend to have a higher viscosity than those that do not form hydrogen bonds. Generally, substances that have the possibility for multiple hydrogen bonds exhibit even higher viscosities.

Factors preventing Hydrogen bonding

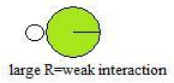
Electronegativity

Hydrogen bonding cannot occur without significant electronegativity differences between hydrogen and the atom it is bonded to. Thus, we see molecules such as PH_3, which do not participate in hydrogen bonding. PH_3 exhibits a trigonal pyramidal molecular geometry like that of ammonia, but unlike NH_3 it cannot hydrogen bond. This is due to the similarity in the electronegativities of phosphorous and hydrogen. Both atoms have an electronegativity of 2.1, and thus, there is no dipole moment. This prevents the hydrogen atom from acquiring the partial positive charge needed to hydrogen bond with the lone electron pair in another molecule. (see Polarizability)



Atom Size

The size of donors and acceptors can also affect the ability to hydrogen bond. This can account for the relatively low ability of Cl to form hydrogen bonds. When the radii of two atoms differ greatly or are large, their nuclei cannot achieve close proximity when they interact, resulting in a weak interaction.

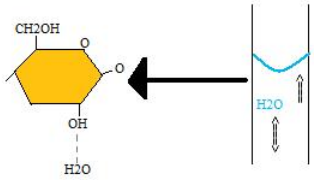


Hydrogen Bonding in Nature

Hydrogen bonding plays a crucial role in many biological processes and can account for many natural phenomena such as the Unusual properties of Water. In addition to being present in water, hydrogen bonding is also important in the water transport system of plants, secondary and tertiary protein structure, and DNA base pairing.

Plants

The cohesion-adhesion theory of transport in vascular plants uses hydrogen bonding to explain many key components of water movement through the plant's xylem and other vessels. Within a vessel, water molecules hydrogen bond not only to each other, but also to the cellulose chain that comprises the wall of plant cells. Since the vessel is relatively small, the attraction of the water to the cellulose wall creates a sort of capillary tube that allows for capillary action. This mechanism allows plants to pull water up into their roots. Furthermore, hydrogen bonding can create a long chain of water molecules, which can overcome the force of gravity and travel up to the high altitudes of leaves.



Proteins

Hydrogen bonding is present abundantly in the secondary structure of proteins, and also sparingly in tertiary conformation. The secondary structure of a protein involves interactions (mainly hydrogen bonds) between neighboring polypeptide backbones which contain nitrogen-hydrogen bonded pairs and oxygen atoms. Since both N and O are strongly electronegative, the hydrogen atoms bonded to nitrogen in one polypeptide backbone can hydrogen bond to the oxygen atoms in another chain and vice-versa. Though they are relatively weak, these bonds offer substantial stability to secondary protein structure because they repeat many times and work collectively.

In tertiary protein structure, interactions are primarily between functional R groups of a polypeptide chain; one such interaction is called a hydrophobic interaction. These interactions occur because of hydrogen bonding between water molecules around the hydrophobe that further reinforces protein conformation.

References

1. Brown, et al. Chemistry:The Central Science. 11th ed. Upper Saddle River, New Jersey: Pearson/Prentice Hall, 2008.
2. Chang, Raymond. General Chemistry:The Essential Concepts. 3rd ed. New York: Mcgraw Hill, 2003
3. Petrucci, et al. General Chemistry: Principles & Modern Applications. 9th ed. Upper Saddle River, New Jersey: Pearson/Prentice Hall, 2007.

1.3.4: Hydrogen Bonding is shared under a not declared license and was authored, remixed, and/or curated by LibreTexts.

- **Hydrogen Bonding** by Jim Clark, Jose Pietri is licensed CC BY-NC-SA 4.0.

1.3.5: Valence Bond Theory

Learning Objectives

- Describe the formation of covalent bonds in terms of atomic orbital overlap
- Define and give examples of σ and π bonds

As we know, a scientific theory is a strongly supported explanation for observed natural laws or large bodies of experimental data. For a theory to be accepted, it must explain experimental data and be able to predict behavior. For example, VSEPR theory has gained widespread acceptance because it predicts three-dimensional molecular shapes that are consistent with experimental data collected for thousands of different molecules. However, VSEPR theory does not provide an explanation of chemical bonding.

There are successful theories that describe the electronic structure of atoms. We can use quantum mechanics to predict the specific regions around an atom where electrons are likely to be located: A spherical shape for an *s* orbital, a dumbbell shape for a *p* orbital, and so forth. However, these predictions only describe the orbitals around free atoms. When atoms bond to form molecules, atomic orbitals are not sufficient to describe the regions where electrons will be located in the molecule. A more complete understanding of electron distributions requires a model that can account for the electronic structure of molecules. One popular theory holds that a covalent bond forms when a pair of electrons is shared by two atoms and is simultaneously attracted by the nuclei of both atoms. In the following sections, we will discuss how such bonds are described by valence bond theory and hybridization.

Valence bond theory describes a covalent bond as the overlap of half-filled atomic orbitals (each containing a single electron) that yield a pair of electrons shared between the two bonded atoms. We say that orbitals on two different atoms overlap when a portion of one orbital and a portion of a second orbital occupy the same region of space. According to valence bond theory, a covalent bond results when two conditions are met:

1. an orbital on one atom overlaps an orbital on a second atom and
2. the single electrons in each orbital combine to form an electron pair.

The mutual attraction between this negatively charged electron pair and the two atoms' positively charged nuclei serves to physically link the two atoms through a force we define as a covalent bond. The strength of a covalent bond depends on the extent of overlap of the orbitals involved. Orbitals that overlap extensively form bonds that are stronger than those that have less overlap.

The energy of the system depends on how much the orbitals overlap. Figure **1.3.5.1** illustrates how the sum of the energies of two hydrogen atoms (the colored curve) changes as they approach each other. When the atoms are far apart there is no overlap, and by convention we set the sum of the energies at zero. As the atoms move together, their orbitals begin to overlap. Each electron begins to feel the attraction of the nucleus in the other atom. In addition, the electrons begin to repel each other, as do the nuclei. While the atoms are still widely separated, the attractions are slightly stronger than the repulsions, and the energy of the system decreases. (A bond begins to form.) As the atoms move closer together, the overlap increases, so the attraction of the nuclei for the electrons continues to increase (as do the repulsions among electrons and between the nuclei). At some specific distance between the atoms, which varies depending on the atoms involved, the energy reaches its lowest (most stable) value. This optimum distance between the two bonded nuclei is the bond distance between the two atoms. The bond is stable because at this point, the attractive and repulsive forces combine to create the lowest possible energy configuration. If the distance between the nuclei were to decrease further, the repulsions between nuclei and the repulsions as electrons are confined in closer proximity to each other would become stronger than the attractive forces. The energy of the system would then rise (making the system destabilized), as shown at the far left of Figure **1.3.5.1**.

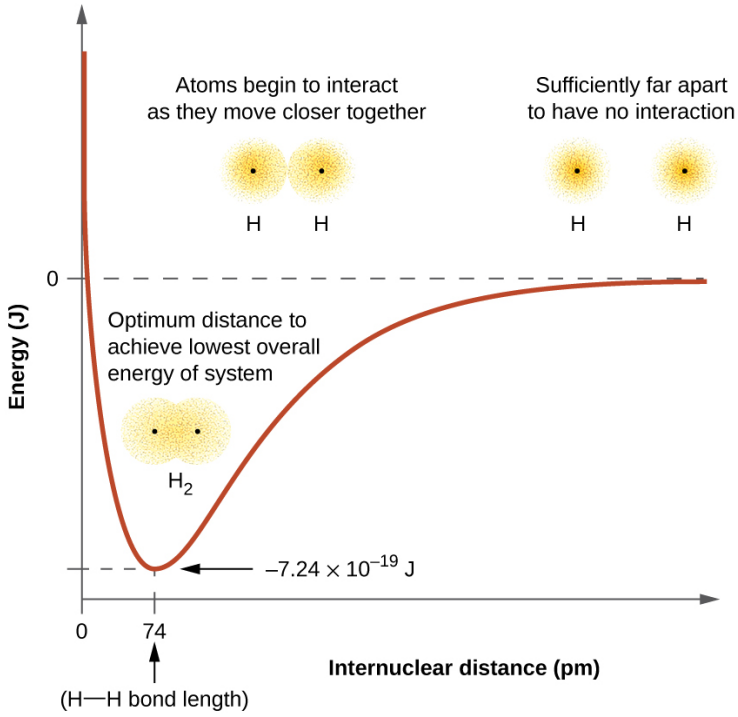


Figure 1.3.5.1: The interaction of two hydrogen atoms changes as a function of distance. The energy of the system changes as the atoms interact. The lowest (most stable) energy occurs at a distance of 74 pm, which is the bond length observed for the H_2 molecule.

A pair of diagrams are shown and labeled “a” and “b”. Diagram a shows three consecutive images. The first image depicts two separated blurry circles, each labeled with a positive sign and the term “H atom.” The phrase written under them reads, “Sufficiently far apart to have no interaction.” The second image shows the same two circles, but this time they are much closer together and are labeled, “Atoms begin to interact as they move closer together.” The third image shows the two circles overlapping, labeled, “H subscript 2,” and, “Optimum distance to achieve lowest overall energy of system.” Diagram b shows a graph on which the y-axis is labeled “Energy (J),” and the x-axis is labeled, “Internuclear distance (p m).” The midpoint of the y-axis is labeled as zero. The curve on the graph begins at zero p m and high on the y-axis. The graph slopes downward steeply to a point far below the zero joule line on the y-axis and the lowest point reads “0.74 p m” and “H bonded to H bond length.” It is also labeled “ negative 7.24 times 10 superscript negative 19 J.” The graph then rises again to zero J. The graph is accompanied by the same images from diagram a; the first image correlates to the point in the graph where it crosses the zero point on the y-axis, the third image where the graph is lowest.

The bond energy is the difference between the energy minimum (which occurs at the bond distance) and the energy of the two separated atoms. This is the quantity of energy released when the bond is formed. Conversely, the same amount of energy is required to break the bond. For the H_2 molecule shown in Figure 1.3.5.1, at the bond distance of 74 pm the system is $7.24 \times 10^{-19}\ J$ lower in energy than the two separated hydrogen atoms. This may seem like a small number. However, we know from our earlier description of thermochemistry that bond energies are often discussed on a per-mole basis. For example, it requires $7.24 \times 10^{-19}\ J$ to break one H–H bond, but it takes $4.36 \times 10^{5}\ J$ to break 1 mole of H–H bonds. A comparison of some bond lengths and energies is shown in Table 1.3.5.1. We can find many of these bonds in a variety of molecules, and this table provides average values. For example, breaking the first C–H bond in CH4 requires 439.3 kJ/mol, while breaking the first C–H bond in $H{-}CH_2C_6H_5$ (a common paint thinner) requires 375.5 kJ/mol.

Table 1.3.5.1: Representative Bond Energies and Lengths

Bond	Length (pm)	Energy (kJ/mol)		Bond	Length (pm)	Energy (kJ/mol)
H–H	74	436		C–O	140.1	358
H–C	106.8	413		C = O	119.7	745
H–N	101.5	391		C ≡ O	113.7	1072
H–O	97.5	467		H–Cl	127.5	431
C–C	150.6	347		H–Br	141.4	366
C = C	133.5	614		H–I	160.9	298
C ≡ C	120.8	839		O–O	148	146
C–N	142.1	305		O = O	120.8	498
C = N	130.0	615		F–F	141.2	159
C ≡ N	116.1	891		Cl–Cl	198.8	243

In addition to the distance between two orbitals, the orientation of orbitals also affects their overlap (other than for two *s* orbitals, which are spherically symmetric). Greater overlap is possible when orbitals are oriented such that they overlap on a direct line between the two nuclei. Figure **1.3.5.2** illustrates this for two *p* orbitals from different atoms; the overlap is greater when the orbitals overlap end to end rather than at an angle.

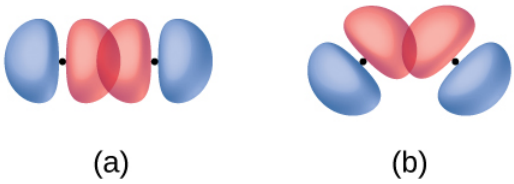


Figure **1.3.5.2**: (a) The overlap of two p orbitals is greatest when the orbitals are directed end to end. (b) Any other arrangement results in less overlap. The dots indicate the locations of the nuclei.

The overlap of two *s* orbitals (as in H_2), the overlap of an *s* orbital and a *p* orbital (as in HCl), and the end-to-end overlap of two *p* orbitals (as in Cl_2) all produce sigma bonds (σ bonds), as illustrated in Figure **1.3.5.3**. A σ bond is a covalent bond in which the electron density is concentrated in the region along the internuclear axis; that is, a line between the nuclei would pass through the center of the overlap region. Single bonds in Lewis structures are described as σ bonds in valence bond theory.

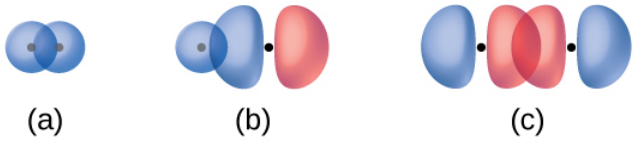


Figure **1.3.5.3**: Sigma (σ) bonds form from the overlap of the following: (a) two s orbitals, (b) an s orbital and a p orbital, and (c) two p orbitals. The dots indicate the locations of the nuclei.

Three diagrams are shown and labeled “a,” “b,” and “c.” Diagram a shows two spherical orbitals lying side by side and overlapping. Diagram b shows one spherical and one peanut-shaped orbital lying near one another so that the spherical orbital overlaps with one end of the peanut-shaped orbital. Diagram c shows two peanut-shaped orbitals lying end to end so that one end of each orbital overlaps the other.

A pi bond (π bond) is a type of covalent bond that results from the side-by-side overlap of two *p* orbitals, as illustrated in Figure **1.3.5.4**. In a π bond, the regions of orbital overlap lie on opposite sides of the internuclear axis. Along the axis itself, there is a node, that is, a plane with no probability of finding an electron.

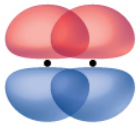
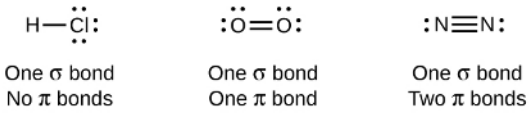


Figure 1.3.5.4: Pi (π) bonds form from the side-by-side overlap of two p orbitals. The dots indicate the location of the nuclei.

While all single bonds are σ bonds, multiple bonds consist of both σ and π bonds. As the Lewis structures suggest, O_2 contains a double bond, and N_2 contains a triple bond. The double bond consists of one σ bond and one π bond, and the triple bond consists of one σ bond and two π bonds. Between any two atoms, the first bond formed will always be a σ bond, but there can only be one σ bond in any one location. In any multiple bond, there will be one σ bond, and the remaining one or two bonds will be π bonds. These bonds are described in more detail later in this chapter.

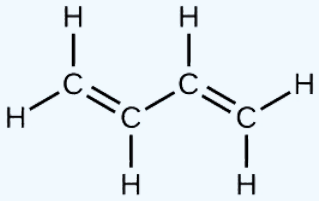


A diagram contains three Lewis structures. The left most structure shows an H atom bonded to a C l atom by a single bond. The C l atom has three lone pairs of electrons. The phrase “One sigma bond No pi bonds” is written below the drawing. The center structure shows two O atoms bonded by a double bond. The O atoms each have two lone pairs of electrons. The phrase “One sigma bond One pi bond” is written below the drawing. The right most structure shows two N atoms bonded by a triple bond. Each N atom has a lone pairs of electrons. The phrase “One sigma bond Two pi bonds” is written below the drawing.

As seen in Table 1.3.5.1, an average carbon-carbon single bond is 347 kJ/mol, while in a carbon-carbon double bond, the π bond increases the bond strength by 267 kJ/mol. Adding an additional π bond causes a further increase of 225 kJ/mol. We can see a similar pattern when we compare other σ and π bonds. Thus, each individual π bond is generally weaker than a corresponding σ bond between the same two atoms. In a σ bond, there is a greater degree of orbital overlap than in a π bond.

Example 1.3.5.1: Counting σ and π Bonds

Butadiene, C_4H_6, is used to make synthetic rubber. Identify the number of σ and π bonds contained in this molecule.



Butadiene

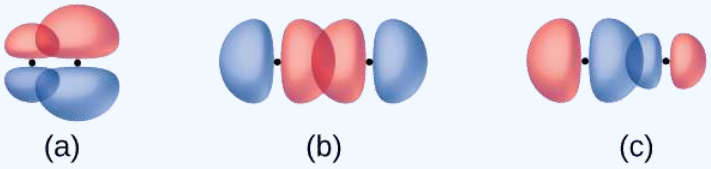
Solution

There are six σ C–H bonds and one σ C–C bond, for a total of seven from the single bonds. There are two double bonds that each have a π bond in addition to the σ bond. This gives a total nine σ and two π bonds overall.

Exercise 1.3.5.1

Identify each illustration as depicting a σ or π bond:

a. side-by-side overlap of a 4*p* and a 2*p* orbital
b. end-to-end overlap of a 4*p* and 4*p* orbital
c. end-to-end overlap of a 4*p* and a 2*p* orbital



Answer

(a) is a π bond with a node along the axis connecting the nuclei while (b) and (c) are σ bonds that overlap along the axis.

Summary

Valence bond theory describes bonding as a consequence of the overlap of two separate atomic orbitals on different atoms that creates a region with one pair of electrons shared between the two atoms. When the orbitals overlap along an axis containing the nuclei, they form a σ bond. When they overlap in a fashion that creates a node along this axis, they form a π bond.

Glossary

overlap
coexistence of orbitals from two different atoms sharing the same region of space, leading to the formation of a covalent bond

node
plane separating different lobes of orbitals, where the probability of finding an electron is zero

pi bond (π bond)
covalent bond formed by side-by-side overlap of atomic orbitals; the electron density is found on opposite sides of the internuclear axis

sigma bond (σ bond)
covalent bond formed by overlap of atomic orbitals along the internuclear axis

valence bond theory
description of bonding that involves atomic orbitals overlapping to form σ or π bonds, within which pairs of electrons are shared

This page titled 1.3.5: Valence Bond Theory is shared under a CC BY license and was authored, remixed, and/or curated by OpenStax.

- **8.2: Valence Bond Theory** by OpenStax is licensed CC BY 4.0. Original source: https://openstax.org/details/books/chemistry-2e.

1.3.6: Hybrid Atomic Orbitals

Learning Objectives

- Explain the concept of atomic orbital hybridization
- Determine the hybrid orbitals associated with various molecular geometries

Thinking in terms of overlapping atomic orbitals is one way for us to explain how chemical bonds form in diatomic molecules. However, to understand how molecules with more than two atoms form stable bonds, we require a more detailed model. As an example, let us consider the water molecule, in which we have one oxygen atom bonding to two hydrogen atoms. Oxygen has the electron configuration $1s^2 2s^2 2p^4$, with two unpaired electrons (one in each of the two 2*p* orbitals). Valence bond theory would predict that the two O–H bonds form from the overlap of these two 2*p* orbitals with the 1*s* orbitals of the hydrogen atoms. If this were the case, the bond angle would be 90°, as shown in Figure **1.3.6.1**, because *p* orbitals are perpendicular to each other. Experimental evidence shows that the bond angle is 104.5°, not 90°. The prediction of the valence bond theory model does not match the real-world observations of a water molecule; a different model is needed.

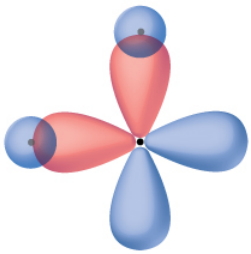


Figure **1.3.6.1**: The hypothetical overlap of two of the 2p orbitals on an oxygen atom (red) with the 1s orbitals of two hydrogen atoms (blue) would produce a bond angle of 90°. This is not consistent with experimental evidence.[1]

Two peanut-shaped orbitals lie perpendicular to one another. They overlap with spherical orbitals to the left and top of the diagram.

Quantum-mechanical calculations suggest why the observed bond angles in H_2O differ from those predicted by the overlap of the 1*s* orbital of the hydrogen atoms with the 2*p* orbitals of the oxygen atom. The mathematical expression known as the wave function, ψ, contains information about each orbital and the wavelike properties of electrons in an isolated atom. When atoms are bound together in a molecule, the wave functions combine to produce new mathematical descriptions that have different shapes. This process of combining the wave functions for atomic orbitals is called hybridization and is mathematically accomplished by the *linear combination of atomic orbitals*, LCAO, (a technique that we will encounter again later). The new orbitals that result are called hybrid orbitals. The valence orbitals in an *isolated* oxygen atom are a 2*s* orbital and three 2*p* orbitals. The valence orbitals in an oxygen atom in a water molecule differ; they consist of four equivalent hybrid orbitals that point approximately toward the corners of a tetrahedron (Figure **1.3.6.2**). Consequently, the overlap of the O and H orbitals should result in a tetrahedral bond angle (109.5°). The observed angle of 104.5° is experimental evidence for which quantum-mechanical calculations give a useful explanation: Valence bond theory must include a hybridization component to give accurate predictions.

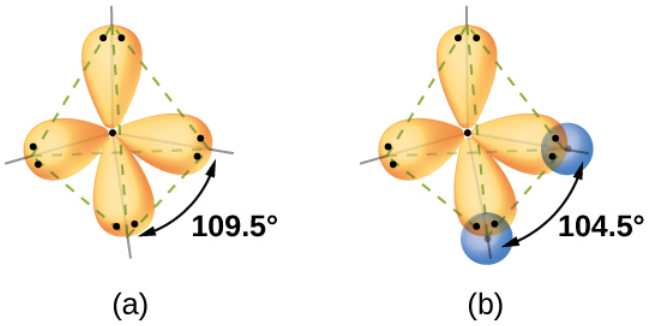


Figure **1.3.6.2**: (a) A water molecule has four regions of electron density, so VSEPR theory predicts a tetrahedral arrangement of hybrid orbitals. (b) Two of the hybrid orbitals on oxygen contain lone pairs, and the other two overlap with the 1s orbitals of hydrogen atoms to form the O–H bonds in H_2O. This description is more consistent with the experimental structure.

Two diagrams are shown and labeled “a” and “b.” Diagram a shows two peanut-shaped orbitals lying in a tetrahedral arrangement around the letter “O.” Diagram b shows the same two orbitals, but they now overlap to the top and to the left with two spherical orbitals, each labeled “H.” A pair of electrons occupies each lobe of the peanut-shaped orbitals.

The following ideas are important in understanding hybridization:

1. Hybrid orbitals do not exist in isolated atoms. They are formed only in covalently bonded atoms.
2. Hybrid orbitals have shapes and orientations that are very different from those of the atomic orbitals in isolated atoms.
3. A set of hybrid orbitals is generated by combining atomic orbitals. The number of hybrid orbitals in a set is equal to the number of atomic orbitals that were combined to produce the set.
4. All orbitals in a set of hybrid orbitals are equivalent in shape and energy.
5. The type of hybrid orbitals formed in a bonded atom depends on its electron-pair geometry as predicted by the VSEPR theory.
6. Hybrid orbitals overlap to form σ bonds. Unhybridized orbitals overlap to form π bonds.

In the following sections, we shall discuss the common types of hybrid orbitals.

1.3.6.1: sp Hybridization

The beryllium atom in a gaseous $BeCl_2$ molecule is an example of a central atom with no lone pairs of electrons in a linear arrangement of three atoms. There are two regions of valence electron density in the $BeCl_2$ molecule that correspond to the two covalent Be–Cl bonds. To accommodate these two electron domains, two of the Be atom’s four valence orbitals will mix to yield two hybrid orbitals. This hybridization process involves mixing of the valence *s* orbital with one of the valence *p* orbitals to yield two equivalent *sp* hybrid orbitals that are oriented in a linear geometry (Figure **1.3.6.3**). In this figure, the set of *sp* orbitals appears similar in shape to the original *p* orbital, but there is an important difference. The number of atomic orbitals combined always equals the number of hybrid orbitals formed. The *p* orbital is one orbital that can hold up to two electrons. The *sp* set is two equivalent orbitals that point 180° from each other. The two electrons that were originally in the *s* orbital are now distributed to the two *sp* orbitals, which are half filled. In gaseous $BeCl_2$, these half-filled hybrid orbitals will overlap with orbitals from the chlorine atoms to form two identical σ bonds.

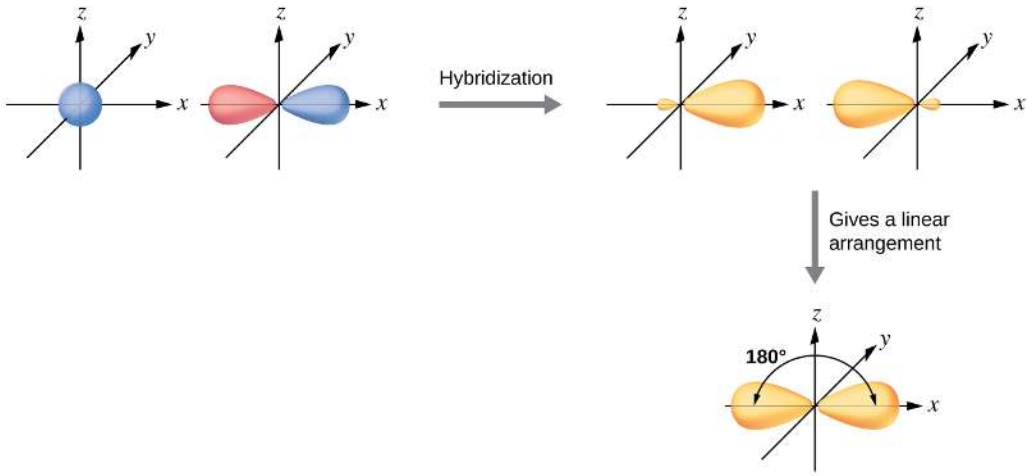


Figure **1.3.6.3**: Hybridization of an s orbital (blue) and a p orbital (red) of the same atom produces two sp hybrid orbitals (yellow). Each hybrid orbital is oriented primarily in just one direction. Note that each sp orbital contains one lobe that is significantly larger than the other. The set of two sp orbitals are oriented at 180°, which is consistent with the geometry for two domains.

A series of three diagrams connected by a right-facing arrow that is labeled, “Hybridization,” and a downward-facing arrow labeled, “Gives a linear arrangement,” are shown. The first diagram shows a blue spherical orbital and a red, peanut-shaped orbital, each placed on an X, Y, Z axis system. The second diagram shows the same two orbitals, but they are now purple and have one enlarged lobe and one smaller lobe. Each lies along the x-axis in the drawing. The third diagram shows the same two orbitals, but their smaller lobes now overlap along the x-axis while their larger lobes are located at and labeled as “180 degrees” from one another.

We illustrate the electronic differences in an isolated Be atom and in the bonded Be atom in the orbital energy-level diagram in Figure **1.3.6.4**. These diagrams represent each orbital by a horizontal line (indicating its energy) and each electron by an arrow. Energy increases toward the top of the diagram. We use one upward arrow to indicate one electron in an orbital and two arrows (up and down) to indicate two electrons of opposite spin.

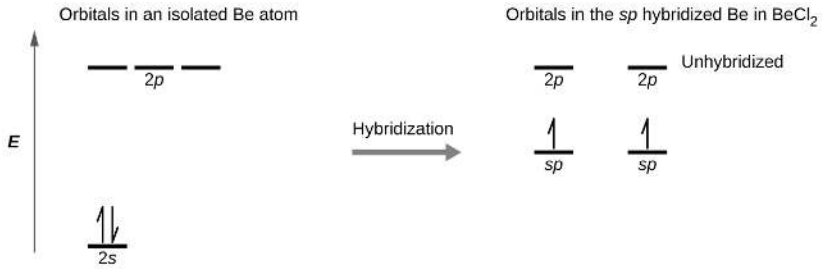


Figure **1.3.6.4**: This orbital energy-level diagram shows the sp hybridized orbitals on Be in the linear $BeCl_2$ molecule. Each of the two sp hybrid orbitals holds one electron and is thus half filled and available for bonding via overlap with a Cl 3p orbital.

A diagram is shown in two parts, connected by a right facing arrow labeled, “Hybridization.” The left diagram shows an up-facing arrow labeled, “E.” To the lower right of the arrow is a short, horizontal line labeled, “2 s,” that has two vertical half-arrows facing up and down on it. To the upper right of the arrow are a series of three short, horizontal lines labeled, “2 p.” Above these two sets of lines is the phrase, “Orbitals in an isolated B e atom.” The right side of the diagram shows two short, horizontal lines placed halfway up the space and each labeled, “s p.” An upward-facing half arrow is drawn vertically on each line. Above these lines are two other short, horizontal lines, each labeled, “2 p.” Above these two sets of lines is the phrase, “Orbitals in the s p hybridized B e in B e C l subscript 2.”

When atomic orbitals hybridize, the valence electrons occupy the newly created orbitals. The Be atom had two valence electrons, so each of the *sp* orbitals gets one of these electrons. Each of these electrons pairs up with the unpaired electron on a chlorine atom when a hybrid orbital and a chlorine orbital overlap during the formation of the Be–Cl bonds. Any central atom surrounded by just two regions of valence electron density in a molecule will exhibit *sp* hybridization. Other examples include the mercury atom in the linear $HgCl_2$ molecule, the zinc atom in $Zn(CH_3)_2$, which contains a linear C–Zn–C arrangement, and the carbon atoms in HCCH and CO_2.

1.3.6.2: sp^2 Hybridization

The valence orbitals of a central atom surrounded by three regions of electron density consist of a set of three sp^2 hybrid orbitals and one unhybridized p orbital. This arrangement results from sp^2 hybridization, the mixing of one s orbital and two p orbitals to produce three identical hybrid orbitals oriented in a trigonal planar geometry (Figure **1.3.6.5**).

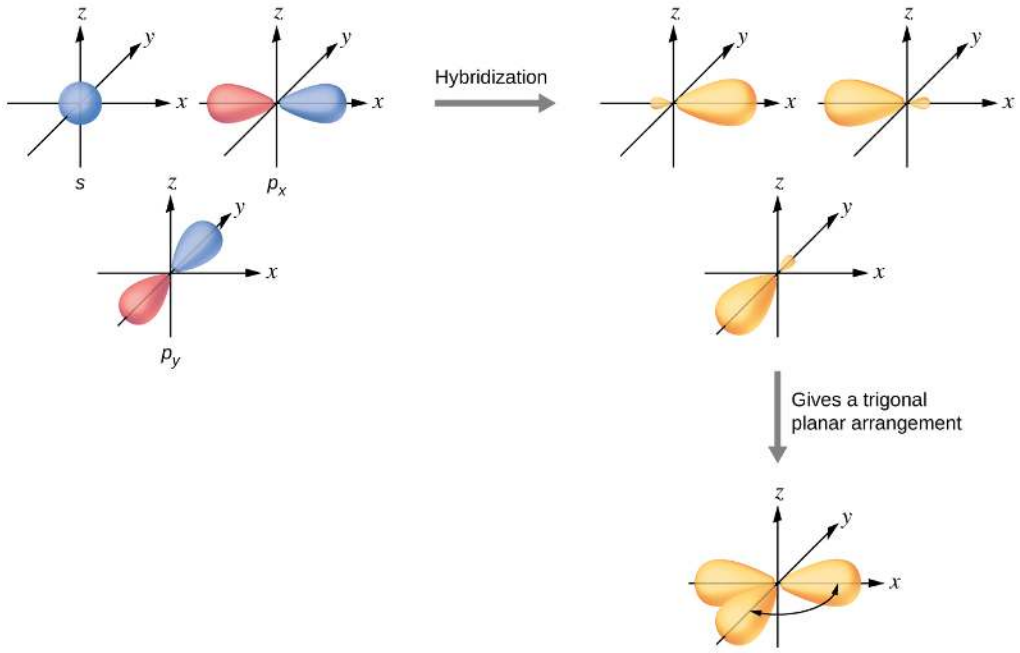


Figure **1.3.6.5**: The hybridization of an s orbital (blue) and two p orbitals (red) produces three equivalent sp^2 hybridized orbitals (yellow) oriented at 120° with respect to each other. The remaining unhybridized p orbital is not shown here, but is located along the z axis.

A series of three diagrams connected by a right-facing arrow that is labeled, “Hybridization,” and a downward-facing arrow labeled, “Gives a trigonal planar arrangement,” are shown. The first diagram shows a blue spherical orbital and two red, peanut-shaped orbitals, each placed on an X, Y, Z axis system. The two red orbitals are located on the x and z axes, respectively. The second diagram shows the same three orbitals, but they are now purple and have one enlarged lobe and one smaller lobe. Each lies in a different axis in the drawing. The third diagram shows the same three orbitals, but their smaller lobes now overlap while their larger lobes are located at and labeled as “120 degrees” from one another.

Although quantum mechanics yields the “plump” orbital lobes as depicted in Figure **1.3.6.5**, sometimes for clarity these orbitals are drawn thinner and without the minor lobes, as in Figure **1.3.6.6**, to avoid obscuring other features of a given illustration. We will use these “thinner” representations whenever the true view is too crowded to easily visualize.

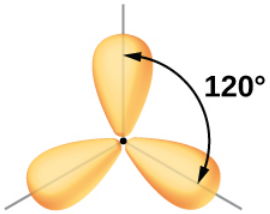


Figure **1.3.6.6**: This alternate way of drawing the trigonal planar sp^2 hybrid orbitals is sometimes used in more crowded figures.

Three balloon-like orbitals are shown, and connect together near their narrower ends in one plane. The angle between a pair of lobes is labeled, “120 degrees.”

The observed structure of the borane molecule, BH_3, suggests sp^2 hybridization for boron in this compound. The molecule is trigonal planar, and the boron atom is involved in three bonds to hydrogen atoms (Figure **1.3.6.7**).

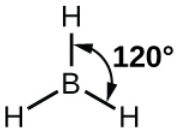


Figure **1.3.6.7**: BH_3 is an electron-deficient molecule with a trigonal planar structure.

A boron atom is shown connected to three hydrogen atoms, which are arranged around it like a pyramid. The angle from one line connecting the boron atom to a hydrogen atom to another line connecting the boron atom to a hydrogen atom is labeled, “120 degrees.”

We can illustrate the comparison of orbitals and electron distribution in an isolated boron atom and in the bonded atom in BH_3 as shown in the orbital energy level diagram in Figure **1.3.6.8**. We redistribute the three valence electrons of the boron atom in the three sp^2 hybrid orbitals, and each boron electron pairs with a hydrogen electron when B–H bonds form.

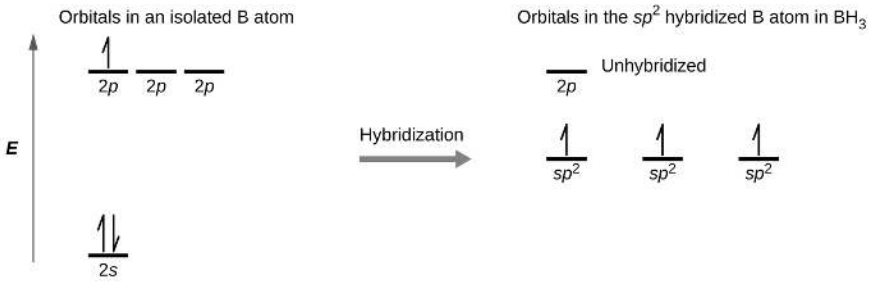


Figure **1.3.6.8**: In an isolated B atom, there are one 2s and three 2p valence orbitals. When boron is in a molecule with three regions of electron density, three of the orbitals hybridize and create a set of three sp^2 orbitals and one unhybridized 2p orbital. The three half-filled hybrid orbitals each overlap with an orbital from a hydrogen atom to form three σ bonds in BH_3.

A diagram is shown in two parts, connected by a right facing arrow labeled, “Hybridization.” The left diagram shows an up-facing arrow labeled “E.” To the lower right of the arrow is a short, horizontal line labeled, “2 s,” that has two vertical half-arrows facing up and down on it. To the upper right of the arrow are a series of three short, horizontal lines labeled, “2 p.” Above both sets of these lines is the phrase, “Orbitals in an isolated B atom.” One of the lines has a vertical, up-facing arrow drawn on it. The right side of the diagram shows three short, horizontal lines placed halfway up the space and each labeled, “s p superscript 2.” An upward-facing half arrow is drawn vertically on each line. Above these lines is one other short, horizontal line, labeled, “2 p.” Above both sets of lines is the phrase, “Orbitals in the s p superscript 2 hybridized B atom in B H subscript 3.”

Any central atom surrounded by three regions of electron density will exhibit sp^2 hybridization. This includes molecules with a lone pair on the central atom, such as ClNO (Figure **1.3.6.9**), or molecules with two single bonds and a double bond connected to the central atom, as in formaldehyde, CH_2O, and ethene, H_2CCH_2.

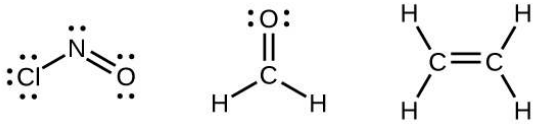


Figure **1.3.6.9**: The central atom(s) in each of the structures shown contain three regions of electron density and are sp^2 hybridized. As we know from the discussion of VSEPR theory, a region of electron density contains all of the electrons that point in one direction. A lone pair, an unpaired electron, a single bond, or a multiple bond would each count as one region of electron density.

Three Lewis structures are shown. The left-hand structure shows a chlorine atom surrounded by three lone pairs of electrons single bonded to a nitrogen atom with one lone pair of electrons and double bonded to an oxygen atom with two lone pairs of electrons. The middle structure shows a carbon atom single bonded to two hydrogen atoms and double bonded to an oxygen atom that has two lone pairs of electrons. The right-hand structure shows two carbon atoms, double bonded to one another and each single bonded to two hydrogen atoms.

1.3.6.3: sp^3 Hybridization

The valence orbitals of an atom surrounded by a tetrahedral arrangement of bonding pairs and lone pairs consist of a set of four sp^3 hybrid orbitals. The hybrids result from the mixing of one *s* orbital and all three *p* orbitals that produces four identical sp^3 hybrid orbitals (Figure **1.3.6.10**). Each of these hybrid orbitals points toward a different corner of a tetrahedron.

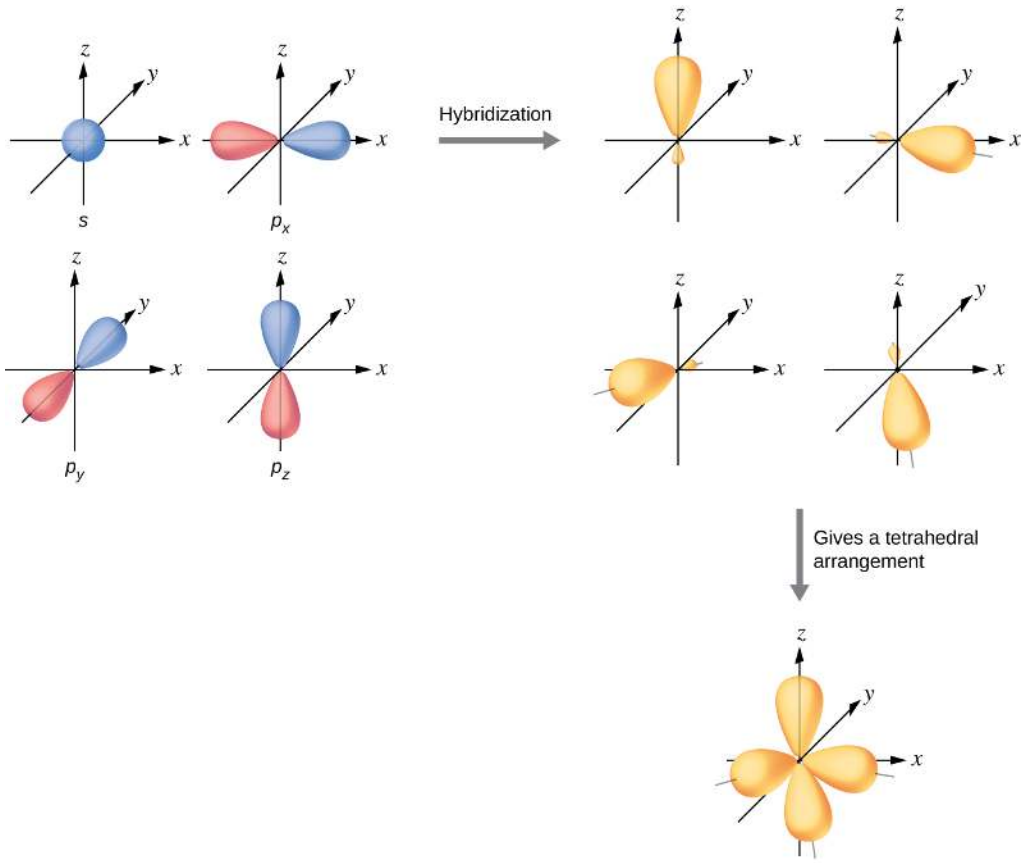


Figure **1.3.6.10**: The hybridization of an s orbital (blue) and three p orbitals (red) produces four equivalent sp^3 hybridized orbitals (yellow) oriented at 109.5° with respect to each other.

A series of three diagrams connected by a right-facing arrow that is labeled, “Hybridization,” and a downward-facing arrow labeled, “Gives a tetrahedral arrangement,” are shown. The first diagram shows a blue spherical orbital and three red, peanut-shaped orbitals, each placed on an x, y, z axis system. The three red orbitals are located on the x , y and z axes, respectively. The second diagram shows the same four orbitals, but they are now purple and have one enlarged lobe and one smaller lobe. Each lies in a different axis in the drawing. The third diagram shows the same four orbitals, but their smaller lobes now overlap to form a tetrahedral structure.

A molecule of methane, CH_4, consists of a carbon atom surrounded by four hydrogen atoms at the corners of a tetrahedron. The carbon atom in methane exhibits sp^3 hybridization. We illustrate the orbitals and electron distribution in an isolated carbon atom and in the bonded atom in CH_4 in Figure **1.3.6.11**. The four valence electrons of the carbon atom are distributed equally in the hybrid orbitals, and each carbon electron pairs with a hydrogen electron when the C–H bonds form.

https://chem.libretexts.org/@go/page/360807

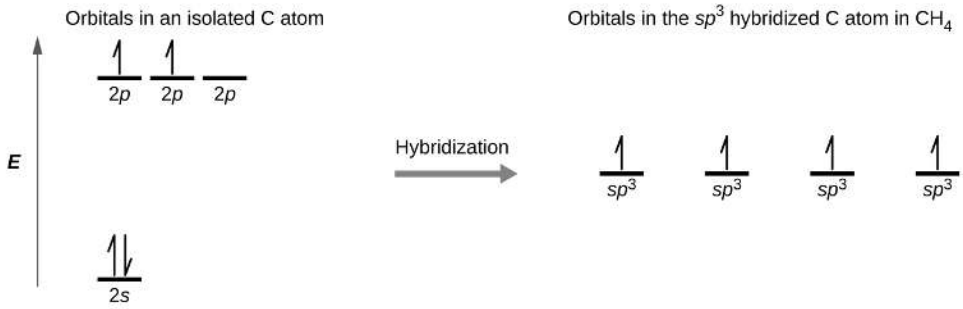


Figure **1.3.6.11**: The four valence atomic orbitals from an isolated carbon atom all hybridize when the carbon bonds in a molecule like CH_4 with four regions of electron density. This creates four equivalent sp^3 hybridized orbitals. Overlap of each of the hybrid orbitals with a hydrogen orbital creates a C–H σ bond.

A diagram is shown in two parts, connected by a right facing arrow labeled, “Hybridization.” The left diagram shows an up-facing arrow labeled “E.” To the lower right of the arrow is a short, horizontal line labeled, “2 s,” that has two vertical half-arrows facing up and down on it. To the upper right of the arrow are a series of three short, horizontal lines labeled, “2 p.” Two of the lines have a vertical, up-facing arrow drawn on them. Above both sets of lines is the phrase, “Orbitals in an isolated C atom.” The right side of the diagram shows four short, horizontal lines placed halfway up the space and each labeled, “s p superscript 3.” An upward-facing half arrow is drawn vertically on each line. Above these lines is the phrase, “Orbitals in the s p superscript 3 hybridized C atom in C H subscript 4.”

In a methane molecule, the 1*s* orbital of each of the four hydrogen atoms overlaps with one of the four sp^3 orbitals of the carbon atom to form a sigma (σ) bond. This results in the formation of four strong, equivalent covalent bonds between the carbon atom and each of the hydrogen atoms to produce the methane molecule, CH_4.

The structure of ethane, C_2H_6, is similar to that of methane in that each carbon in ethane has four neighboring atoms arranged at the corners of a tetrahedron—three hydrogen atoms and one carbon atom (Figure **1.3.6.10**). However, in ethane an sp^3 orbital of one carbon atom overlaps end to end with an sp^3 orbital of a second carbon atom to form a σ bond between the two carbon atoms. Each of the remaining sp^3 hybrid orbitals overlaps with an *s* orbital of a hydrogen atom to form carbon–hydrogen σ bonds. The structure and overall outline of the bonding orbitals of ethane are shown in Figure **1.3.6.12**. The orientation of the two CH_3 groups is not fixed relative to each other. Experimental evidence shows that rotation around σ bonds occurs easily.

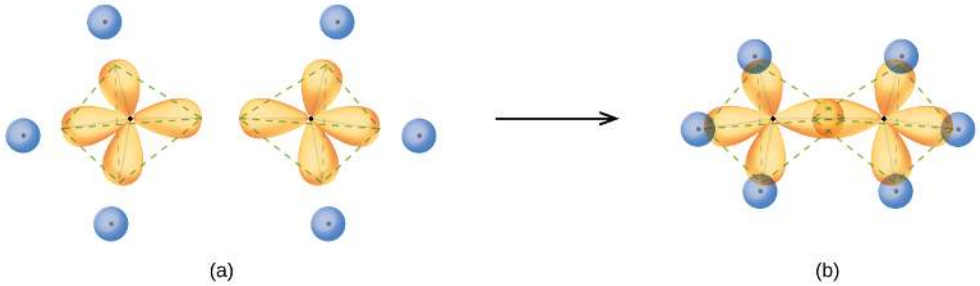


Figure **1.3.6.12**: (a) In the ethane molecule, C_2H_6, each carbon has four sp^3 orbitals. (b) These four orbitals overlap to form seven σ bonds.

Two diagrams are shown and labeled “a” and “b.” Diagram a shows two carbon atoms, each surrounded by their four s p subscript three hybridized orbitals in a three dimensional arrangement. Each of the orbitals is shown overlapping with a spherical hydrogen atom. Diagram b shows the same general arrangement, but the hydrogen atoms are just represented by an, “H” and their spherical orbitals are not shown.

An sp^3 hybrid orbital can also hold a lone pair of electrons. For example, the nitrogen atom in ammonia is surrounded by three bonding pairs and a lone pair of electrons directed to the four corners of a tetrahedron. The nitrogen atom is sp^3 hybridized with one hybrid orbital occupied by the lone pair.

The molecular structure of water is consistent with a tetrahedral arrangement of two lone pairs and two bonding pairs of electrons. Thus we say that the oxygen atom is sp^3 hybridized, with two of the hybrid orbitals occupied by lone pairs and two by bonding pairs. Since lone pairs occupy more space than bonding pairs, structures that contain lone pairs have bond angles slightly distorted from the ideal. Perfect tetrahedra have angles of 109.5°, but the observed angles in ammonia (107.3°) and water (104.5°) are slightly smaller. Other examples of sp^3 hybridization include CCl_4, PCl_3, and NCl_3.

1.3.6.4: sp^3d and sp^3d^2 Hybridization

To describe the five bonding orbitals in a trigonal bipyramidal arrangement, we must use five of the valence shell atomic orbitals (the *s* orbital, the three *p* orbitals, and one of the *d* orbitals), which gives five sp^3d hybrid orbitals. With an octahedral arrangement of six hybrid orbitals, we must use six valence shell atomic orbitals (the *s* orbital, the three *p* orbitals, and two of the *d* orbitals in its valence shell), which gives six sp^3d^2 hybrid orbitals. These hybridizations are only possible for atoms that have *d* orbitals in their valence subshells (that is, not those in the first or second period).

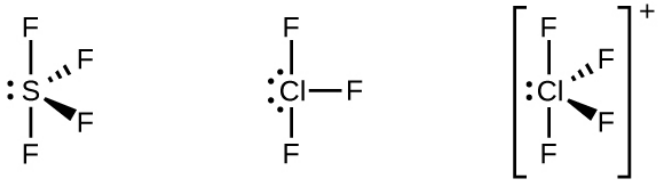


Figure **1.3.6.13**: The three compounds pictured exhibit sp^3d hybridization in the central atom and a trigonal bipyramid form. SF_4 and ClF_4^+ *have one lone pair of electrons on the central atom, and* ClF_3 *has two lone pairs giving it the T-shape shown.*

Three Lewis structures are shown along with designations of molecular shape. The left image shows a sulfur atom singly bonded to four fluorine atoms. The sulfur atom has one lone pair of electrons while each fluorine has three. Two fluorine atoms are drawn vertically up and down from the sulfur while the other two are shown going into and out of the page. The second structure shows one chlorine atom singly bonded to three fluorine atoms. The chlorine has two lone pairs of electrons while each fluorine has three. Two fluorine atoms are drawn vertically up and down from the sulfur while the other is shown horizontally. The right structure shows a chlorine atom singly bonded to four fluorine atoms. The chlorine atom has one lone pair of electrons and a superscript plus sign, while each fluorine has three lone pairs of electrons. Two fluorine atoms are drawn vertically up and down from the sulfur while the other two are shown going into and out of the page.

In a molecule of phosphorus pentachloride, PCl_5, there are five P–Cl bonds (thus five pairs of valence electrons around the phosphorus atom) directed toward the corners of a trigonal bipyramid. We use the 3*s* orbital, the three 3*p* orbitals, and one of the 3*d* orbitals to form the set of five sp^3d hybrid orbitals (Figure **1.3.6.13**) that are involved in the P–Cl bonds. Other atoms that exhibit sp^3d hybridization include the sulfur atom in SF_4 and the chlorine atoms in ClF_3 and in ClF_4^+. (The electrons on fluorine atoms are omitted for clarity.)

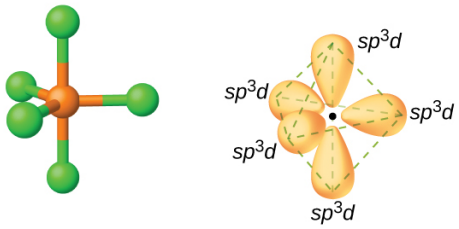


Figure **1.3.6.14**: (a) The five regions of electron density around phosphorus in PCl_5 require five hybrid sp^3d orbitals. (b) These orbitals combine to form a trigonal bipyramidal structure with each large lobe of the hybrid orbital pointing at a vertex. As before, there are also small lobes pointing in the opposite direction for each orbital (not shown for clarity).

Two images are shown and labeled “a” and “b.” Image a depicts a ball-and-stick model in a trigonal bipyramidal arrangement. Image b depicts the hybrid orbitals in the same arrangement and each is labeled, “s p superscript three d.”

The sulfur atom in sulfur hexafluoride, SF_6, exhibits sp^3d^2 hybridization. A molecule of sulfur hexafluoride has six bonding pairs of electrons connecting six fluorine atoms to a single sulfur atom. There are no lone pairs of electrons on the central atom. To bond six fluorine atoms, the 3*s* orbital, the three 3*p* orbitals, and two of the 3*d* orbitals form six equivalent sp^3d^2 hybrid orbitals, each directed toward a different corner of an octahedron. Other atoms that exhibit sp^3d^2 hybridization include the phosphorus atom in PCl_6^-, the iodine atom in the interhalogens IF_6^+, IF_5, ICl_4^-, IF_4^- and the xenon atom in XeF_4.

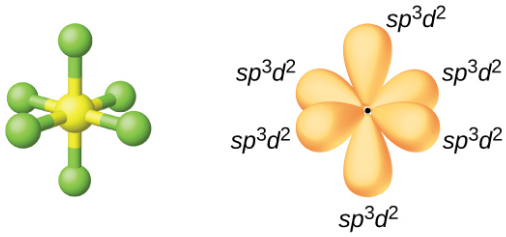


Figure **1.3.6.15**: (a) Sulfur hexafluoride, SF_6, has an octahedral structure that requires sp^3d^2 hybridization. (b) The six sp^3d^2 orbitals form an octahedral structure around sulfur. Again, the minor lobe of each orbital is not shown for clarity.

Two images are shown and labeled “a” and “b.” Image a depicts a ball-and-stick model in an octahedral arrangement. Image b depicts the hybrid orbitals in the same arrangement and each is labeled, “s p superscript three d superscript two.”

1.3.6.5: Assignment of Hybrid Orbitals to Central Atoms

The hybridization of an atom is determined based on the number of regions of electron density that surround it. The geometrical arrangements characteristic of the various sets of hybrid orbitals are shown in Figure **1.3.6.16**. These arrangements are identical to those of the electron-pair geometries predicted by VSEPR theory. VSEPR theory predicts the shapes of molecules, and hybrid orbital theory provides an explanation for how those shapes are formed. To find the hybridization of a central atom, we can use the following guidelines:

1. Determine the Lewis structure of the molecule.
2. Determine the number of regions of electron density around an atom using VSEPR theory, in which single bonds, multiple bonds, radicals, and lone pairs each count as one region.
3. Assign the set of hybridized orbitals from Figure **1.3.6.16** that corresponds to this geometry.

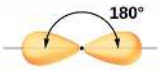
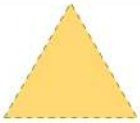
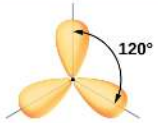
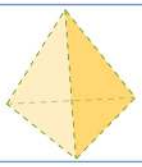
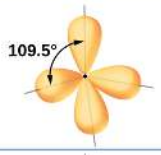
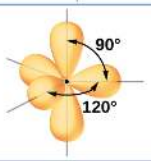
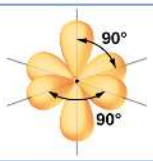
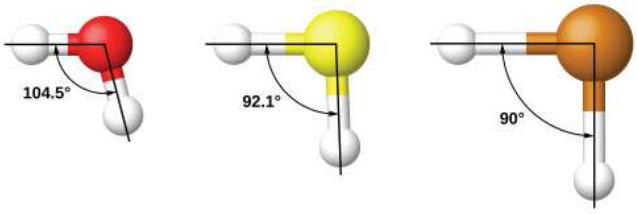
Regions of Electron Density	Arrangement		Hybridization	
2		linear	*sp*	
3		trigonal planar	sp^2	
4		tetrahedral	sp^3	
5		trigonal bipyramidal	sp^3d	
6		octahedral	sp^3d^2	

Figure **1.3.6.16**: The shapes of hybridized orbital sets are consistent with the electron-pair geometries. For example, an atom surrounded by three regions of electron density is sp^2 hybridized, and the three sp^2 orbitals are arranged in a trigonal planar fashion.

A table is shown that is composed of five columns and six rows. The header row contains the phrases, “Regions of electron density,” “Arrangement,” (which has two columns below it), and “Hybridization,” (which has two columns below it). The first column contains the numbers “2,” “3,” “4,” “5,” and “6.” The second column contains images of a line, a triangle, a three sided pyramid, a trigonal bipyramid, and an eight-faced ocatahedron. The third column contains the terms, “Linear,” “Trigonal planar,” “Tetrahedral,” “Trigonal bipyramidal,” and “Octahedral.” The fourth column contains the terms “s p,” “s p superscript 2,” “s p superscript 3,” “s p superscript 3 d,” and “s p superscript 3 d superscript 2.” The last column contains drawings of the molecules beginning with a peanut-shaped structure marked with an angle of “180 degrees.” The second structure is made up of three equal-sized, rounded structures connected at one point with an angle of “120 degrees,” while the third structure is a three-dimensional arrangement of four equal-sized, rounded structures labeled as “109.5 degrees.” The fourth structure is made up of five equal-sized, rounded structures connected at “120 and 90 degrees,” while the fifth structure has six equal-sized, rounded structures connected at “90 degrees.”

> *It is important to remember that hybridization was devised to rationalize experimentally observed molecular geometries, not the other way around.*

The model works well for molecules containing small central atoms, in which the valence electron pairs are close together in space. However, for larger central atoms, the valence-shell electron pairs are farther from the nucleus, and there are fewer repulsions. Their compounds exhibit structures that are often not consistent with VSEPR theory, and hybridized orbitals are not necessary to explain the observed data.



Three Lewis structures are shown. The left structure shows an oxygen atom with two lone pairs of electrons single bonded to two hydrogen atoms. The middle structure is made up of a sulfur atom with two lone pairs of electrons single bonded to two hydrogen atoms. The right structure is made up of a tellurium atom with two lone pairs of electrons single bonded to two hydrogen atoms. From left to right, the bond angles of each molecule decrease.

For example, we have discussed the H–O–H bond angle in H_2O, 104.5°, which is more consistent with sp^3 hybrid orbitals (109.5°) on the central atom than with 2*p* orbitals (90°). Sulfur is in the same group as oxygen, and H_2S has a similar Lewis structure. However, it has a much smaller bond angle (92.1°), which indicates much less hybridization on sulfur than oxygen. Continuing down the group, tellurium is even larger than sulfur, and for H_2Te, the observed bond angle (90°) is consistent with overlap of the 5*p* orbitals, without invoking hybridization. We invoke hybridization where it is necessary to explain the observed structures.

Example 1.3.6.1: Assigning Hybridization

Ammonium sulfate is important as a fertilizer. What is the hybridization of the sulfur atom in the sulfate ion, SO_4^{2-}?

Solution

The Lewis structure of sulfate shows there are four regions of electron density.

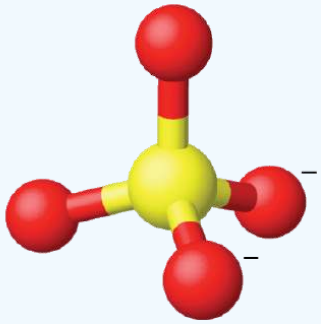
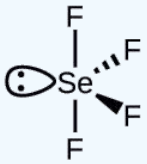


Figure 1.3.6.16).

A structure is shown in which a sulfur atom is bonded to four oxygen atoms in a tetrahedral arrangement. Two of the oxygen atoms have a negative charge.

Exercise 1.3.6.1

What is the hybridization of the selenium atom in SeF_4?



A Lewis structure is shown in which four fluorine atoms are each attached to one sulfur atom. Two of the attached fluorine atoms are vertically attached up and down, while two are attached into and out of the page to the right. The sulfur also has one lone pair of electrons attached to the left of the structure.

Answer

The selenium atom is sp^3d hybridized.

Example 1.3.6.2: Assigning Hybridization

Urea, $NH_2C(O)NH_2$, is sometimes used as a source of nitrogen in fertilizers. What is the hybridization of each nitrogen and carbon atom in urea?

Solution

The Lewis structure of urea is

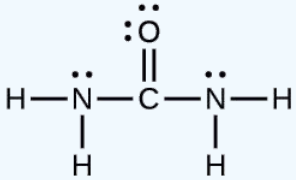


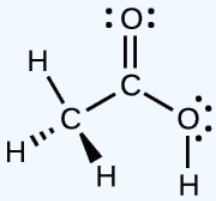
Figure **1.3.6.16**). This is the hybridization of the nitrogen atoms in urea.

A Lewis structure is shown in which a carbon atom is double bonded to an oxygen atom that has two lone pairs of electrons. The carbon atom forms single bonds to two nitrogen atoms. Each nitrogen is single bonded to two hydrogen atoms, and each nitrogen atoms has one lone pair of electrons.

The carbon atom is surrounded by three regions of electron density, positioned in a trigonal planar arrangement. The hybridization in a trigonal planar electron pair geometry is sp^2 (Figure **1.3.6.16**), which is the hybridization of the carbon atom in urea.

Exercise 1.3.6.1

Acetic acid, $H_3CC(O)OH$, is the molecule that gives vinegar its odor and sour taste. What is the hybridization of the two carbon atoms in acetic acid?



A Lewis structure is shown in which a carbon atom is double bonded to an oxygen atom that has two lone pairs of electrons and single bonded to another oxygen atom that is single boned to a hydrogen atom. This second oxygen atom has two lone pairs of electrons. The carbon is also single bonded to a carbon atom that is single bonded to three hydrogen atoms.

Answer

$H_3\underline{C}$, sp^3; $\underline{C}(O)OH$, sp^2

Summary

We can use hybrid orbitals, which are mathematical combinations of some or all of the valence atomic orbitals, to describe the electron density around covalently bonded atoms. These hybrid orbitals either form sigma (σ) bonds directed toward other atoms of the molecule or contain lone pairs of electrons. We can determine the type of hybridization around a central atom from the geometry of the regions of electron density about it. Two such regions imply *sp* hybridization; three, sp^2 hybridization; four, sp^3 hybridization; five, sp^3d hybridization; and six, sp^3d^2 hybridization. Pi (π) bonds are formed from unhybridized atomic orbitals (*p* or *d* orbitals).

1.3.6.5.1: Footnotes

1. Note that orbitals may sometimes be drawn in an elongated “balloon” shape rather than in a more realistic “plump” shape in order to make the geometry easier to visualize.

1.3.6.5.2: Glossary

hybrid orbital
orbital created by combining atomic orbitals on a central atom

hybridization
model that describes the changes in the atomic orbitals of an atom when it forms a covalent compound

***sp* hybrid orbital**
one of a set of two orbitals with a linear arrangement that results from combining one *s* and one *p* orbital

***sp*^{2} hybrid orbital**
one of a set of three orbitals with a trigonal planar arrangement that results from combining one *s* and two *p* orbitals

***sp*^{3} hybrid orbital**
one of a set of four orbitals with a tetrahedral arrangement that results from combining one *s* and three *p* orbitals

***sp*^{3}*d* hybrid orbital**
one of a set of five orbitals with a trigonal bipyramidal arrangement that results from combining one *s*, three *p*, and one *d* orbital

***sp*^{3}*d*^{2} hybrid orbital**
one of a set of six orbitals with an octahedral arrangement that results from combining one *s*, three *p*, and two *d* orbitals

---

This page titled 1.3.6: Hybrid Atomic Orbitals is shared under a CC BY license and was authored, remixed, and/or curated by OpenStax.

- **8.3: Hybrid Atomic Orbitals** by OpenStax is licensed CC BY 4.0. Original source: https://openstax.org/details/books/chemistry-2e.

CHAPTER OVERVIEW

2: Molecular Symmetry and Point Groups

2.1: Symmetry Elements and Operations

2.2: Point Groups

2.2.1: Groups of Low and High Symmetry

2.2.2: Other Groups

2.3: Properties and Representations of Groups

2.3.1: Matrices

2.3.2: Representations of Point Groups

2.3.3: Character Tables

2.4: Examples and Applications of Symmetry

2.4.1: Molecular Vibrations

2.4.2: Chirality

2: Molecular Symmetry and Point Groups is shared under a not declared license and was authored, remixed, and/or curated by LibreTexts.

2.1: Symmetry Elements and Operations

Introduction

The symmetry of a molecule consists of **symmetry operations** and **symmetry elements**. A symmetry operation is an operation that is performed to a molecule which leaves it indistinguishable and superimposable on the original position. Symmetry operations are performed with respect to symmetry elements (points, lines, or planes).

An example of a symmetry operation is a 180° rotation of a water molecule in which the resulting position of the molecule is indistinguishable from the original position (see Figure **2.1.1**). In this example, the symmetry operation is the rotation and the symmetry element is the axis of rotation.

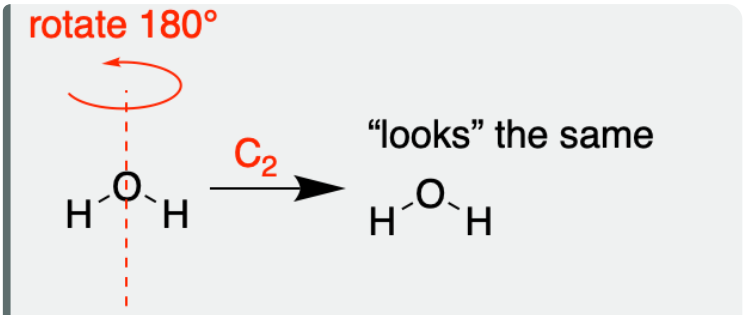


Figure 2.1.1: An example of a symmetry operation is a 180° rotation where the resulting position is indistinguishable from the original. A 180° rotation is called a C_2 operation; the axis of rotation is the symmetry element.

There are five types of symmetry operations: **identity**, **reflection**, **inversion**, **proper rotation**, and **improper rotation**. The symmetry elements that correspond to the five types of symmetry operations are listed in Table **2.1.1**.

Table **2.1.1***: Table of elements and operations*

Element	Operation	Symbol
Identity	identity	E
Proper rotation	rotation by (360/n)°	C_n
Reflection	reflection in a plane	σ
Inversion	inversion of a point at (x,y,z) to (-x,-y,-z)	*i*
Improper rotation	rotation by (360/n)°, followed by reflection in the plane perpendicular to the rotation axis	S_n

Symmetry Operations and Elements

Identity (E)

All molecules have the identity element. The identity operation is doing nothing to the molecule (it doesn't rotate, reflect, or invert...it just is).

Proper Rotation and Proper Axis (C_n)

A "proper" rotation is just a simple rotation operation about an axis. The symbol for any proper rotation or proper axis is $C_{(360/n)}$, where n is the degree of rotation. Thus, a 180° rotation is a C_2 rotation around a C_2 axis, and a 120° rotation is a C_3 rotation about a C_3 axis.

PRINCIPLE AXIS: The principle axis of a molecule is the highest order proper rotation axis, in other words, the largest value of n. For example, if a molecule had C_2 and C_4 axes, the C_4 is the principle axis.

Reflection and Symmetry Planes (σ)

Mirror planes are symmetry planes within the molecule. A reflection operation occurs with respect to a plane of symmetry. There are three classes of symmetry elements:

1. σ_h (horizontal): horizontal planes are perpendicular to principal axis
2. σ_v (vertical): vertical planes are parallel to the principal axis
3. σ_d (dihedral): dihedral planes are parallel to the principle axis and bisect two C_2 axes

Inversion and Inversion Center (i)

The inversion operation requires a point of symmetry (a center of symmetry within a molecule). In other words, a point at the center of the molecule that can transform (x,y,z) into (-x,-y,-z) coordinate. Structures of tetrahedron, triangles, and pentagons lack an inversion center.

Improper rotation (S_n)

Improper rotation is a combination of a rotation with respect to an axis of rotation (C_n), followed by a reflection through a plane perpendicular to that C_n axis. In short, an S_n operation is equivalent to C_n followed by σ_h.

References

1. Introduction to Molecular Symmetry by J. S Ogden
2. Inorganic Chemistry by Catherine Housecroft And Alan G. Sharpe.

2.1: Symmetry Elements and Operations is shared under a not declared license and was authored, remixed, and/or curated by LibreTexts.

SECTION OVERVIEW

2.2: Point Groups

Introduction

A **Point Group** describes all the symmetry operations that can be performed on a molecule that result in a conformation indistinguishable from the original. Point groups are used in Group Theory, the mathematical analysis of groups, to determine properties such as a molecule's molecular orbitals.

Assigning Point Groups

While a point group contains all of the symmetry operations that can be performed on a given molecule, it is not necessary to identify all of these operations to determine the molecule's overall point group. Instead, a molecule's point group can be determined by following a set of steps which analyze the presence (or absence) of particular symmetry elements.

Steps for assigning a molecule's point group:

1. Determine if the molecule has an infinite rotation axis.
2. If yes, determine if there is an inversion center. If no, find the highest order rotation axis, C_n, and continue.
3. If the molecule does not contain a rotation axis, look for either a mirror plane or an inversion center. If you find at least one rotation axis, look for multiple rotation axes where the n value is greater than 2.
4. Determine if the molecule has any C_2 axes perpendicular to the principal C_n axis. If so, then there are n such C_2 axes, and the molecule is in the D set of point groups. If not, it is in either the C or S set of point groups.
5. Determine if the molecule has a horizontal mirror plane (σ_h) perpendicular to the principal C_n axis. If so, the molecule is either in the C_{nh} or D_{nh} set of point groups.
6. Determine if the molecule has a vertical mirror plane (σ_v) containing the principal C_n axis. If so, the molecule is either in the C_{nv} or D_{nd} set of point groups. If not, and if the molecule has n perpendicular C_2 axes, then it is part of the D_n set of point groups.
7. Determine if there is an improper rotation axis, S_{2n}, collinear with the principal C_n axis. If so, the molecule is in the S_{2n} point group. The S_{2n} point group is extremely unlikely to appear in this course. If not, the molecule is in the C_n point group.

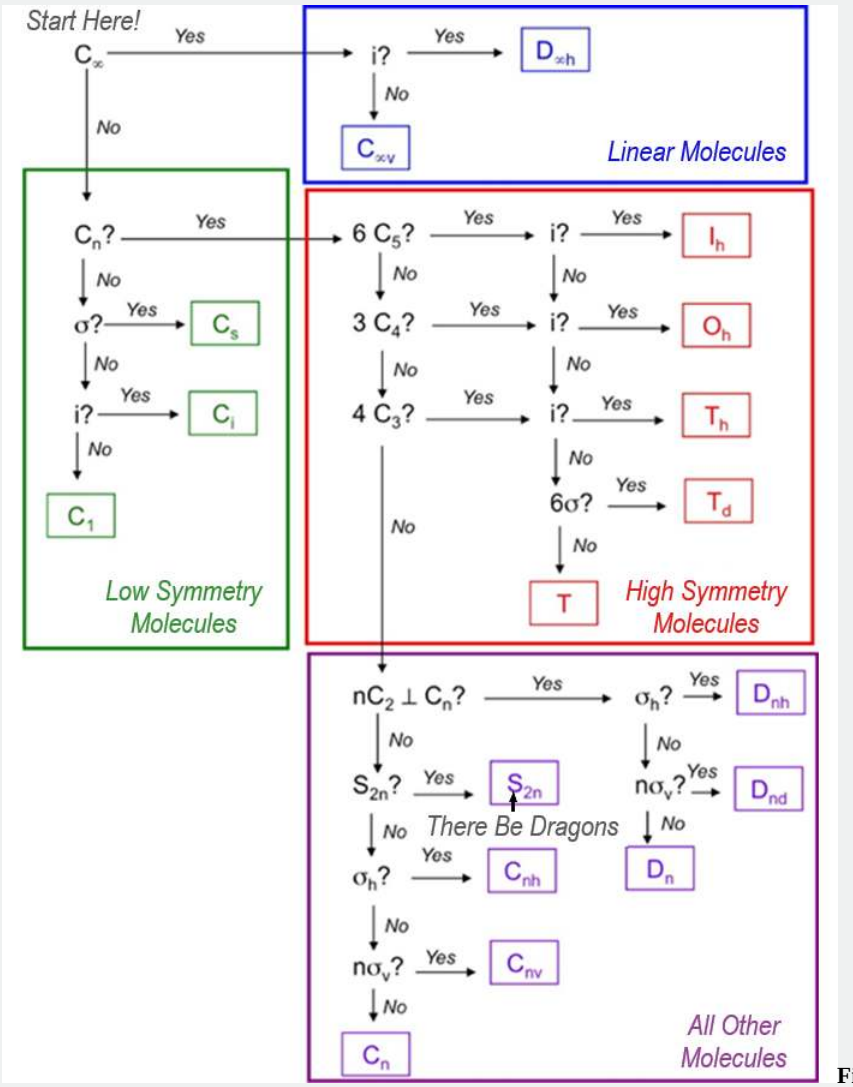


Figure 2.2.1: Decision tree for determining a molecule's point group (CC-BY-NC-SA; Chip Nataro)

Example 2.2.1

Find the point group of borane (BH3).

Answer

Solution

1. Borane does not have an infinite rotation axis.
2. Highest order rotation axis: C3
3. There are not multiple axes with n greater than 2.
4. There are 3 C_2 axes perpendicular to the principal axis
5. There is a horizontal mirror plane (σ_h)

Borane is in the D_{3h} point group.

See Also

Symmetry Challenge

2.2.1: Groups of Low and High Symmetry

2.2.2: Other Groups

2.2: Point Groups is shared under a not declared license and was authored, remixed, and/or curated by LibreTexts.

2.2.1: Groups of Low and High Symmetry

Low Symmetry Point Groups

Low symmetry point groups include the C_1, C_s, and C_i groups

Group	Description	Example
C_1	only the identity operation (E)	CHFClBr
C_s	only the identity operation (E) and one mirror plane	C_2H_2ClBr
C_i	only the identity operation (E) and a center of inversion (i)	$C_2H_2Cl_2Br$

High Symmetry Point Groups

High symmetry point groups include the T_d, O_h, I_h, $C_{\infty v}$, and $D_{\infty h}$ groups. The table below describes their characteristic symmetry operations. The full set of symmetry operations included in the point group is described in the corresponding character table.

Group	Description	Example
$C_{\infty v}$	linear molecule with an infinite number of rotation axes and vertical mirror planes (σ_v)	HBr
$D_{\infty h}$	linear molecule with an infinite number of rotation axes, vertical mirror planes (σ_v), perpendicular C_2 axes, a horizontal mirror plane (σ_h), and an inversion center (i)	CO_2
T_d	typically have tetrahedral geometry, with 4 C_4 axes, 3 C_2 axes, 3 S_4 axes, and 6 dihedral mirror planes (σ_d)	CH_4
O_h	typically have octahedral geometry, with 3 C_4 axes, 4 C_3 axes, and an inversion center (i) as characteristic symmetry operations	SF_6
I_h	typically have an icosahedral structure, with 6 C_5 axes as characteristic symmetry operations	$B_{12}H_{12}^{2-}$

2.2.1: Groups of Low and High Symmetry is shared under a not declared license and was authored, remixed, and/or curated by LibreTexts.

2.2.2: Other Groups

D Groups

The D set of point groups are classified as D_{nh}, D_{nd}, or D_n, where n refers to the principal axis of rotation. Overall, the D groups are characterized by the presence of n C_2 axes perpendicular to the principal C_n axis. Further classification of a molecule in the D groups depends on the presence of horizontal or vertical/dihedral mirror planes.

Group	Description	Example
D_{nh}	n perpendicular C_2 axes, and a horizontal mirror plane (σ_h)	benzene, C_6H_6 is D_{6h}
D_{nd}	n perpendicular C_2 axes, and a vertical mirror plane (σ_v)	propadiene, C_3H_4 is D_{2d}
D_n	n perpendicular C_2 axes, no mirror planes	$[Co(en)_3]^{3+}$ is D_3

C Groups

The C set of point groups are classified as C_{nh}, C_{nv}, or C_n, where n refers to the principal axis of rotation. The C set of groups are characterized by the absence of n C_2 axes perpendicular to the principal C_n axis. Further classification of a molecule in the C groups depends on the presence of horizontal or vertical/dihedral mirror planes.

Group	Description	Example
C_{nh}	horizontal mirror plane (σ_h) perpendicular to the principal C_n axis	boric acid, H_3BO_3 is C_{3h}
C_{nv}	vertical mirror plane (σ_v) containing the principal C_n axis	ammonia, NH_3 is C_{3v}
C_n	no mirror planes	$P(C_6H_5)_3$ is C_3

S Groups

The S set of point groups are classified as S_{2n}, where n refers to the principal axis of rotation. The S set of groups are characterized by the absence of n C_2 axes perpendicular to the principal C_n axis, as well as the absence of horizontal and vertical/dihedral mirror planes. However, there is an improper rotation (or a rotation-reflection) axis collinear with the principal C_n axis.

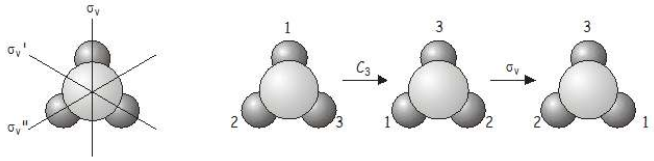
Group	Description	Example
S_{2n}	improper rotation (or a rotation-reflection) axis collinear with the principal C_n axis	12-crown-4 is S_4

2.2.2: Other Groups is shared under a not declared license and was authored, remixed, and/or curated by LibreTexts.

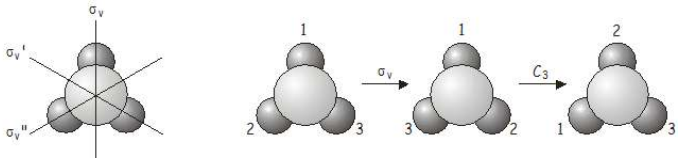
2.3: Properties and Representations of Groups

Group Multiplication

Now we will investigate what happens when we apply two symmetry operations in sequence. As an example, consider the NH_3 molecule, which belongs to the C_{3v} point group. Consider what happens if we apply a C_3rotation (120˚ counter-clockwise) followed by a σ_v reflection (reflection over the σ_v axis). We write this combined operation $\sigma_v C_3$ (when written, symmetry operations operate on the thing directly to their right, just as operators do in quantum mechanics – we therefore have to work backwards from right to left from the notation to get the correct order in which the operators are applied). As we shall soon see, the order in which the operations are applied is important.



The combined operation $\sigma_v C_3$ is equivalent to σ_v'' (note the double prime on σ_v''!), which is also a symmetry operation of the C_{3v} point group. Now let's see what happens if we apply the operators in the reverse order, i.e., $C_3\sigma_v$ is (σ_v followed by C_3).



Again, the combined operation $C_3\sigma_v$ is equivalent to another operation of the point group, this time σ_v' (note the single prime on σ_v'!).

There are two important points that are illustrated by this example:

1. The order in which two operations are applied is important. For two symmetry operations A and B, AB is not necessarily the same as BA, i.e. symmetry operations do not in general ***commute***. In some groups the symmetry elements do commute; such groups are said to be ***Abelian***.
2. If two operations from the same point group are applied in sequence, the result will be equivalent to another operation from the point group. Symmetry operations that are related to each other by other symmetry operations of the group are said to belong to the same ***class***. In NH_3, the three mirror planes σ_v, σ_v' and σ_v'' belong to the same class (related to each other through a C_3 rotation), as do the rotations C_3^+ and C_3^- (anticlockwise and clockwise rotations about the principal axis, related to each other by a vertical mirror plane).

Four Properties of Mathematical Groups

Now that we have explored some of the properties of symmetry operations and elements and their behavior within point groups, we are ready to introduce the formal mathematical definition of a group. The definitions below will be put into the context of *molecular* symmetry.

A mathematical group is defined as a set of elements (A_1, A_2, A_3...) together with a rule for forming combinations A_i,A_j... For our purposes, A_1, A_2, A_3, etc. are symmetry elements and A_i, A_j, etc. are symmetry operations described in a previous section. The elements of the group and the rule for combining them must satisfy the following four criteria.

1. The group must include the **identity** E, which commutes with other members of the group. In other terms, $EA_i = A_i$ for all the elements of the group. Application of the identity operation before or after another operation, A_i, results in the same outcome as A_i alone.
2. The elements must satisfy the group property that the combination of any pair of elements is also an element of the group. For example, in the C_{3v} point group, a C_3 rotation followed by a σ_v gives another operation that is already part of the group: a σ_v''.

3. Each symmetry operation A_i must have an inverse A_i^{-1}, which is also an element of the group, such that

$$A_i A_i^{-1} = A_i^{-1} A_i = E$$

   The inverse g_i^{-1} effectively 'undoes' the effect of the symmetry operation g_i. For example, in the C_{3v} point group, the inverse of C_3^+ is C_3^-.
4. The rule of combination must be associative

$$(A_i A_j)(A_k) = A_i(A_j A_k)$$

   Or $A(BC) = (AB)C$. In other words, the order of operations should not matter.

Group theory is an important area in mathematics, and luckily for chemists the mathematicians have already done most of the work for us. Along with the formal definition of a group comes a comprehensive mathematical framework that allows us to carry out a rigorous treatment of symmetry in molecular systems and learn about its consequences.

Many problems involving operators or operations (such as those found in quantum mechanics or group theory) may be reformulated in terms of matrices. Any of you who have come across transformation matrices before will know that symmetry operations such as rotations and reflections may be represented by matrices. It turns out that the set of matrices representing the symmetry operations in a group obey all the conditions laid out above in the mathematical definition of a group, and using matrix representations of symmetry operations simplifies carrying out calculations in group theory. Before we learn how to use matrices in group theory, it will probably be helpful to review some basic definitions and properties of matrices.

*This page was adapted from here (click).

Contributors and Attributions

- Claire Vallance (University of Oxford)
- Curated or created by Kathryn Haas

2.3: Properties and Representations of Groups is shared under a not declared license and was authored, remixed, and/or curated by LibreTexts.

- **4.3: Properties and Representations of Groups** by Kathryn Haas is licensed CC BY-NC-SA 4.0.

2.3.1: Matrices

The symmetry of molecules is essential for understanding the structures and properties of organic and inorganic compounds. The properties of chemical compounds are often easily explained by consideration of symmetry. For example, the symmetry of a molecule determines whether the molecule has a permanent dipole moment or not. The theories that describe optical activity, infrared and ultraviolet spectroscopy, and crystal structure involve the application of symmetry considerations. Matrix algebra is the most important mathematical tool in the description of symmetry.

The properties of symmetry groups are organized in character tables (discussed later in this chapter). Character tables are constructed based on matrices. This page is a brief description of matrices and matrix multiplication.

What is a matrix?

An $m \times n$ matrix $\mathbf{A}$ is a rectangular array of numbers with m rows and n columns. The numbers m and n are the dimensions of $\mathbf{A}$. The numbers in the matrix are called its entries. The entry in row i and column j is called a_{ij}.

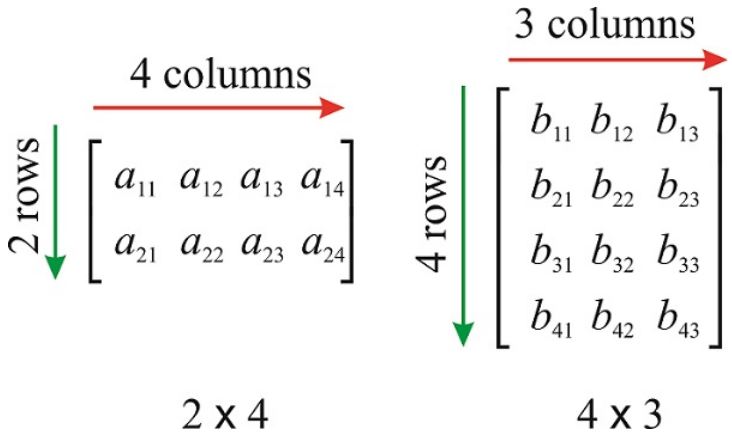


Figure **2.3.1.1**: Matrices of different dimensions

Some types of matrices have special names:

- A square matrix:

$$\begin{pmatrix} 3 & -2 & 4 \\ 5 & 3i & 3 \\ -i & 1/2 & 9 \end{pmatrix}$$

  with $m = n$
- A rectangular matrix:

$$\begin{pmatrix} 3 & -2 & 4 \\ 5 & 3i & 3 \end{pmatrix}$$

  with $m \neq n$
- A column vector:

$$\begin{pmatrix} 3 \\ 5 \\ -i \end{pmatrix}$$

  with $n = 1$
- A row vector:

$$\begin{pmatrix} 3 & -2 & 4 \end{pmatrix}$$

  with $m = 1$
- The identity matrix:

$$\begin{pmatrix} 1 & 0 & 0 \\ 0 & 1 & 0 \\ 0 & 0 & 1 \end{pmatrix}$$

with $a_{ij} = \delta_{i,j}$, where $\delta_{i,j}$ is a function defined as $\delta_{i,j} = 1$ if $i = j$ and $\delta_{i,j} = 0$ if $i \neq j$.

- A diagonal matrix:

$$\begin{pmatrix} a & 0 & 0 \\ 0 & b & 0 \\ 0 & 0 & c \end{pmatrix}$$

with $a_{ij} = c_i \delta_{i,j}$.

- An upper triangular matrix:

$$\begin{pmatrix} a & b & c \\ 0 & d & e \\ 0 & 0 & f \end{pmatrix}$$

All the entries below the main diagonal are zero.

- A lower triangular matrix:

$$\begin{pmatrix} a & 0 & 0 \\ b & c & 0 \\ d & e & f \end{pmatrix}$$

All the entries above the main diagonal are zero.

- A triangular matrix is one that is either lower triangular or upper triangular.

The Trace of a Matrix

The trace of an $n \times n$ square matrix $\mathbf{A}$ is the sum of the diagonal elements, and formally defined as $Tr(\mathbf{A}) = \sum_{i=1}^{n} a_{ii}$.

For example,

$$\mathbf{A} = \begin{pmatrix} 3 & -2 & 4 \\ 5 & 3i & 3 \\ -i & 1/2 & 9 \end{pmatrix} ; Tr(\mathbf{A}) = 12 + 3i$$

Singular and Nonsingular Matrices

A square matrix with nonzero determinant is called *nonsingular*. A matrix whose determinant is zero is called *singular*. (Note that you cannot calculate the determinant of a non-square matrix).

For a 2x2 matrix,

$$\mathbf{B} = \begin{pmatrix} a & b \\ c & d \end{pmatrix} ; det(\mathbf{B}) = ad - cb$$

For a 3x3 matrix,

$$\mathbf{C} = \begin{pmatrix} a & b & c \\ d & e & f \\ g & h & i \end{pmatrix}$$

$$det(\mathbf{C}) = a \begin{pmatrix} e & f \\ h & i \end{pmatrix} - b \begin{pmatrix} d & f \\ g & i \end{pmatrix} + c \begin{pmatrix} d & e \\ g & h \end{pmatrix}$$

$$det(\mathbf{C}) = aei - ahf - bdi + bgf + cdh - cge$$

The Matrix Transpose

The matrix transpose, most commonly written $\mathbf{A}^T$, is the matrix obtained by exchanging $\mathbf{A}$'s rows and columns. It is obtained by replacing all elements a_{ij} with a_{ji}. For example:

$$\mathbf{A} = \begin{pmatrix} 3 & -2 & 4 \\ 5 & 3i & 3 \end{pmatrix} \rightarrow \mathbf{A}^T = \begin{pmatrix} 3 & 5 \\ -2 & 3i \\ 4 & 3 \end{pmatrix}$$

Matrix Multiplication

To multiply two matrices, the number of vertical columns in the first matrix must be the same as the number of rows in the second matrix. If $\mathbf{A}$ has dimensions $m \times n$ and $\mathbf{B}$ has dimensions $n \times p$, then the product $\mathbf{AB}$ is defined, and has dimensions $m \times p$.

$$c_{ij} = \sum a_{ij} \times b_{ij}$$

The entry $a_{ij} \times b_{ij}$ is obtained by multiplying row i of $\mathbf{A}$ by column j of $\mathbf{B}$, which is done by multiplying corresponding entries together and then adding the results:

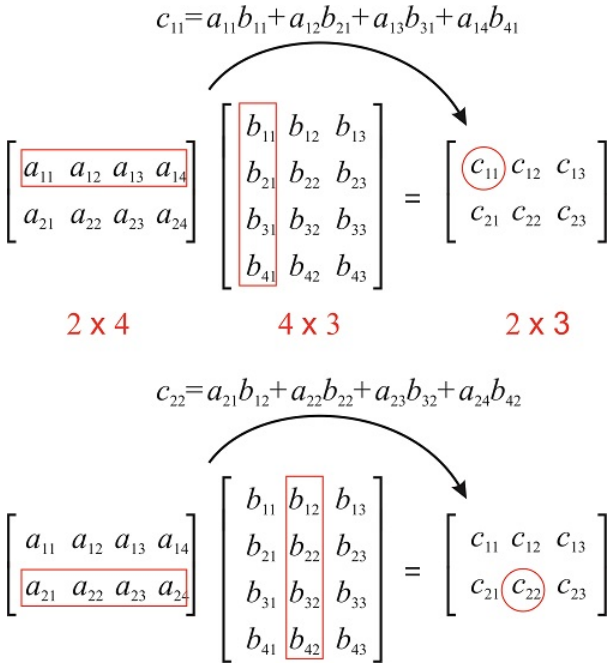


Figure 2.3.1.1: Matrix multiplication

Example 2.3.1.1

Calculate the product

$$\begin{pmatrix} 1 & -2 & 4 \\ 5 & 0 & 3 \\ 0 & 1/2 & 9 \end{pmatrix} \begin{pmatrix} 1 & 0 \\ 5 & 3 \\ -1 & 0 \end{pmatrix}$$

Solution

We need to multiply a 3×3 matrix by a 3×2 matrix, so we expect a 3×2 matrix as a result.

$$\begin{pmatrix} 1 & -2 & 4 \\ 5 & 0 & 3 \\ 0 & 1/2 & 9 \end{pmatrix} \begin{pmatrix} 1 & 0 \\ 5 & 3 \\ -1 & 0 \end{pmatrix} = \begin{pmatrix} a & b \\ c & d \\ e & f \end{pmatrix}$$

To calculate a, which is entry (1,1), we use row 1 of the matrix on the left and column 1 of the matrix on the right:

$$\begin{pmatrix} 1 & -2 & 4 \\ 5 & 0 & 3 \\ 0 & 1/2 & 9 \end{pmatrix} \begin{pmatrix} 1 & 0 \\ 5 & 3 \\ -1 & 0 \end{pmatrix} = \begin{pmatrix} a & b \\ c & d \\ e & f \end{pmatrix} \rightarrow a = 1 \times 1 + (-2) \times 5 + 4 \times (-1) = -13$$

To calculate b, which is entry (1,2), we use row 1 of the matrix on the left and column 2 of the matrix on the right:

$$\begin{pmatrix}1 & -2 & 4\\ 5 & 0 & 3\\ 0 & 1/2 & 9\end{pmatrix}\begin{pmatrix}1 & 0\\ 5 & 3\\ -1 & 0\end{pmatrix}=\begin{pmatrix}a & b\\ c & d\\ e & f\end{pmatrix}\rightarrow b=1\times 0+(-2)\times 3+4\times 0=-6$$

To calculate c, which is entry (2,1), we use row 2 of the matrix on the left and column 1 of the matrix on the right:

$$\begin{pmatrix}1 & -2 & 4\\ 5 & 0 & 3\\ 0 & 1/2 & 9\end{pmatrix}\begin{pmatrix}1 & 0\\ 5 & 3\\ -1 & 0\end{pmatrix}=\begin{pmatrix}a & b\\ c & d\\ e & f\end{pmatrix}\rightarrow c=5\times 1+0\times 5+3\times(-1)=2$$

To calculate d, which is entry (2,2), we use row 2 of the matrix on the left and column 2 of the matrix on the right:

$$\begin{pmatrix}1 & -2 & 4\\ 5 & 0 & 3\\ 0 & 1/2 & 9\end{pmatrix}\begin{pmatrix}1 & 0\\ 5 & 3\\ -1 & 0\end{pmatrix}=\begin{pmatrix}a & b\\ c & d\\ e & f\end{pmatrix}\rightarrow d=5\times 0+0\times 3+3\times 0=0$$

To calculate e, which is entry (3,1), we use row 3 of the matrix on the left and column 1 of the matrix on the right:

$$\begin{pmatrix}1 & -2 & 4\\ 5 & 0 & 3\\ 0 & 1/2 & 9\end{pmatrix}\begin{pmatrix}1 & 0\\ 5 & 3\\ -1 & 0\end{pmatrix}=\begin{pmatrix}a & b\\ c & d\\ e & f\end{pmatrix}\rightarrow e=0\times 1+1/2\times 5+9\times(-1)=-13/2$$

To calculate f, which is entry (3,2), we use row 3 of the matrix on the left and column 2 of the matrix on the right:

$$\begin{pmatrix}1 & -2 & 4\\ 5 & 0 & 3\\ 0 & 1/2 & 9\end{pmatrix}\begin{pmatrix}1 & 0\\ 5 & 3\\ -1 & 0\end{pmatrix}=\begin{pmatrix}a & b\\ c & d\\ e & f\end{pmatrix}\rightarrow f=0\times 0+1/2\times 3+9\times 0=3/2$$

The result is:

$$\begin{pmatrix}1 & -2 & 4\\ 5 & 0 & 3\\ 0 & 1/2 & 9\end{pmatrix}\begin{pmatrix}1 & 0\\ 5 & 3\\ -1 & 0\end{pmatrix}=\begin{pmatrix}-13 & -6\\ 2 & 0\\ -13/2 & 3/2\end{pmatrix}$$

Example 2.3.1.2

Calculate

$$\begin{pmatrix}1 & -2 & 4\\ 5 & 0 & 3\end{pmatrix}\begin{pmatrix}1\\ 5\\ -1\end{pmatrix}$$

Solution

We are asked to multiply a 2×3 matrix by a 3×1 matrix (a column vector). The result will be a 2×1 matrix (a vector).

$$\begin{pmatrix}1 & -2 & 4\\ 5 & 0 & 3\end{pmatrix}\begin{pmatrix}1\\ 5\\ -1\end{pmatrix}=\begin{pmatrix}a\\ b\end{pmatrix}$$

$$a=1\times 1+(-2)\times 5+4\times(-1)=-13$$

$$b=5\times 1+0\times 5+3\times(-1)=2$$

The solution is:

$$\begin{pmatrix}1 & -2 & 4\\ 5 & 0 & 3\end{pmatrix}\begin{pmatrix}1\\ 5\\ -1\end{pmatrix}=\begin{pmatrix}-13\\ 2\end{pmatrix}$$

Need help? The link below contains solved examples: Multiplying matrices of different shapes (three examples): http://tinyurl.com/kn8ysqq

External links:

- Multiplying matrices, example 1: http://patrickjmt.com/matrices-multiplying-a-matrix-by-another-matrix/
- Multiplying matrices, example 2: http://patrickjmt.com/multiplying-matrices-example-2/
- Multiplying matrices, example 3: http://patrickjmt.com/multiplying-matrices-example-3/

The Commutator

Matrix multiplication is not, in general, commutative. For example, we can perform

$$\begin{pmatrix} 1 & -2 & 4 \\ 5 & 0 & 3 \end{pmatrix} \begin{pmatrix} 1 \\ 5 \\ -1 \end{pmatrix} = \begin{pmatrix} -13 \\ 2 \end{pmatrix}$$

but cannot perform

$$\begin{pmatrix} 1 \\ 5 \\ -1 \end{pmatrix} \begin{pmatrix} 1 & -2 & 4 \\ 5 & 0 & 3 \end{pmatrix}$$

Even with square matrices, that can be multiplied both ways, multiplication is not commutative. In this case, it is useful to define the **commutator**, defined as:

$$[\mathbf{A}, \mathbf{B}] = \mathbf{AB} - \mathbf{BA}$$

Example 2.3.1.3

Given $\mathbf{A} = \begin{pmatrix} 3 & 1 \\ 2 & 0 \end{pmatrix}$ and $\mathbf{B} = \begin{pmatrix} 1 & 0 \\ -1 & 2 \end{pmatrix}$

Calculate the commutator $[\mathbf{A}, \mathbf{B}]$

Solution

$$[\mathbf{A}, \mathbf{B}] = \mathbf{AB} - \mathbf{BA}$$

$$\mathbf{AB} = \begin{pmatrix} 3 & 1 \\ 2 & 0 \end{pmatrix} \begin{pmatrix} 1 & 0 \\ -1 & 2 \end{pmatrix} = \begin{pmatrix} 3 \times 1 + 1 \times (-1) & 3 \times 0 + 1 \times 2 \\ 2 \times 1 + 0 \times (-1) & 2 \times 0 + 0 \times 2 \end{pmatrix} = \begin{pmatrix} 2 & 2 \\ 2 & 0 \end{pmatrix}$$

$$\mathbf{BA} = \begin{pmatrix} 1 & 0 \\ -1 & 2 \end{pmatrix} \begin{pmatrix} 3 & 1 \\ 2 & 0 \end{pmatrix} = \begin{pmatrix} 1 \times 3 + 0 \times 2 & 1 \times 1 + 0 \times 0 \\ -1 \times 3 + 2 \times 2 & -1 \times 1 + 2 \times 0 \end{pmatrix} = \begin{pmatrix} 3 & 1 \\ 1 & -1 \end{pmatrix}$$

$$[\mathbf{A}, \mathbf{B}] = \mathbf{AB} - \mathbf{BA} = \begin{pmatrix} 2 & 2 \\ 2 & 0 \end{pmatrix} - \begin{pmatrix} 3 & 1 \\ 1 & -1 \end{pmatrix} = \begin{pmatrix} -1 & 1 \\ 1 & 1 \end{pmatrix}$$

$$[\mathbf{A}, \mathbf{B}] = \begin{pmatrix} -1 & 1 \\ 1 & 1 \end{pmatrix}$$

Multiplication of a vector by a scalar

The multiplication of a vector $\vec{v}_1$ by a scalar n produces another vector of the same dimensions that lies in the same direction as $\vec{v}_1$;

$$n \begin{pmatrix} x \\ y \end{pmatrix} = \begin{pmatrix} nx \\ ny \end{pmatrix}$$

The scalar can stretch or compress the length of the vector, but cannot rotate it (figure [fig:vector_by_scalar]).

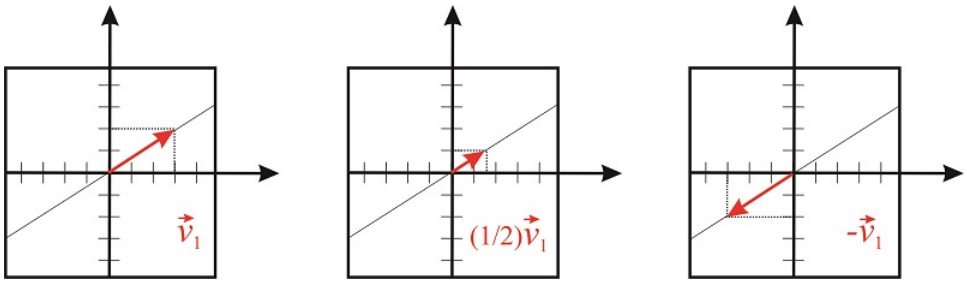


Figure **2.3.1.2**: Multiplication of a vector by a scalar

Multiplication of a square matrix by a vector

The multiplication of a vector $\vec{v_1}$ by a square matrix produces another vector of the same dimensions of $\vec{v_1}$. For example, we can multiply a 2×2 matrix and a 2-dimensional vector:

$$\begin{pmatrix} a & b \\ c & d \end{pmatrix} \begin{pmatrix} x \\ y \end{pmatrix} = \begin{pmatrix} ax + by \\ cx + dy \end{pmatrix}$$

For example, consider the matrix

$$\mathbf{A} = \begin{pmatrix} -2 & 0 \\ 0 & 1 \end{pmatrix}$$

The product

$$\begin{pmatrix} -2 & 0 \\ 0 & 1 \end{pmatrix} \begin{pmatrix} x \\ y \end{pmatrix}$$

is

$$\begin{pmatrix} -2x \\ y \end{pmatrix}$$

We see that 2×2 matrices act as operators that transform one 2-dimensional vector into another 2-dimensional vector. This particular matrix keeps the value of y constant and multiplies the value of x by -2 (Figure **2.3.1.3**).

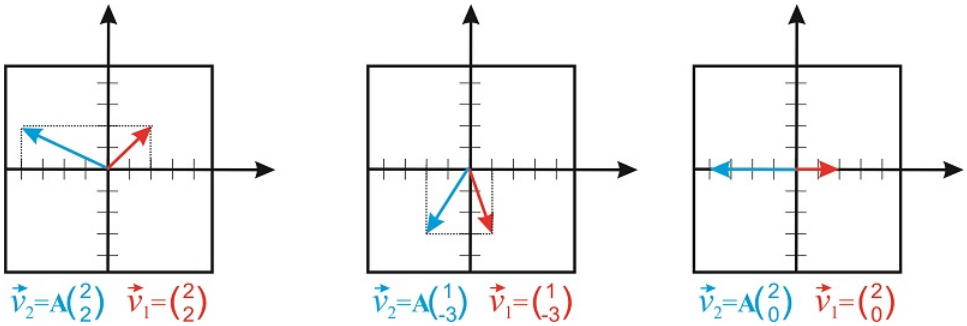


Figure **2.3.1.3**: Multiplication of a vector by a square matrix

Notice that matrices are useful ways of representing operators that change the orientation and size of a vector. An important class of operators that are of particular interest to chemists are the so-called symmetry operators.

Attribution

This page was adapted from Matrices (click here), contributed by Marcia Levitus, Associate Professor (Biodesign Institute) at Arizona State University.

Curated or created by Kathryn Haas

2.3.1: Matrices is shared under a not declared license and was authored, remixed, and/or curated by LibreTexts.

- **4.3.1: Matrices** by Kathryn Haas is licensed CC BY-NC-SA 4.0.

2.3.2: Representations of Point Groups

Symmetry Operations: Matrix Representations

A **symmetry operation**, such as a rotation around a symmetry axis or a reflection through a plane, is an operation that, when performed on an object, results in a new orientation of the object that is indistinguishable from the original. For example, if we rotate a square in the plane by $\pi/2$ or π, the new orientation of the square is superimposable on the original one (Figure **2.3.2.1**).

If rotation by an angle θ of a molecule (or object) about some axis results in an orientation of the molecule (or object) that is superimposable on the original, the axis is called a rotation axis. The molecule (or object) is said to have an n-fold rotational axis, where n is $2\pi/\theta$. The axis is denoted as C_n. The square of Figure **2.3.2.1** has a C_4 axis perpendicular to the plane because a $90°$ rotation leaves the figure indistinguishable from the initial orientation. This axis is also a C_2 axis because a $180°$ degree rotation leaves the square indistinguishable from the original square. In addition, the figure has several other C_2 axis that lie on the same plane as the square:

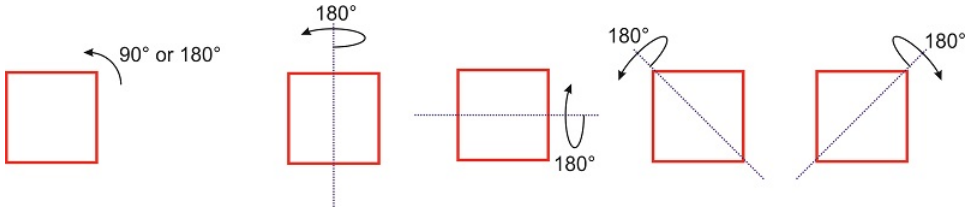


Figure **2.3.2.1**: Symmetry operations performed on a square

A symmetry operation moves all the points of the object from one initial position to a final position, and that means that symmetry operators are 3×3 square matrices (or 2×2 in two dimensions). Each symmetry operation can be expressed as a **transformation matrix** where the vector (x', y', z') represents the new coordinates of the point (x, y, z) after the symmetry operation.

$$[\text{New Coordinates}(x', y', z')] = [\text{Transformation Matrix}] \times [\text{Old Coordinates}(x, y, z)]$$

We will use the example of water, which is in the C_{2v} point group, to illustrate how transformation matrices can be used to represent the symmetry of a group.

Figure **2.3.2.2** shows the three symmetry elements of the molecule of water (H_2O). This molecule has only one rotation axis, which is 2-fold, and therefore we call it a "C_2 axis." It also has two mirror planes, one that contains the two hydrogen atoms (σ_{yz}), and another one perpendicular to it (σ_{xz}). Both planes contain the C_2 axis.

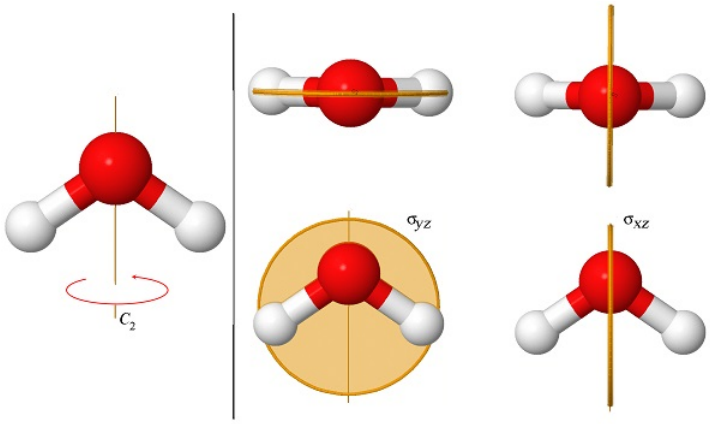


Figure **2.3.2.2**: The symmetry elements of the molecule of water

Transformation Matrix of C_2 rotation

A 2-fold rotation around the z−axis changes the location of a point (x, y, z) to $(-x, -y, z)$ (see Figure **2.3.2.3**). By convention, rotations are always taken in the counterclockwise direction.

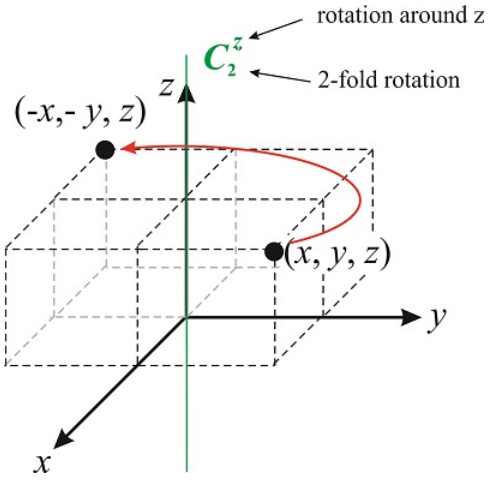


Figure 2.3.2.3: A 2-fold rotation around the z-axis

What is the matrix that represents the C_2 rotation? The matrix transforms the vector (x, y, z) into $(-x, -y, z)$, so

$$C_2(x, y, z) = (-x, -y, z)$$

$$\begin{pmatrix} a_{11} & a_{12} & a_{13} \\ a_{21} & a_{22} & a_{23} \\ a_{31} & a_{32} & a_{33} \end{pmatrix} \begin{pmatrix} x \\ y \\ z \end{pmatrix} = \begin{pmatrix} -x \\ -y \\ z \end{pmatrix}$$

We know the matrix is a 3×3 square matrix because it needs to multiply a 3-dimensional vector. In addition, we write the vector as a vertical column to satisfy the requirements of matrix multiplication.

$$\begin{pmatrix} a_{11} & a_{12} & a_{13} \\ a_{21} & a_{22} & a_{23} \\ a_{31} & a_{32} & a_{33} \end{pmatrix} \begin{pmatrix} x \\ y \\ z \end{pmatrix}$$

$$a_{11}x + a_{12}y + a_{13}z = -x$$

$$a_{21}x + a_{22}y + a_{23}z = -y$$

$$a_{31}x + a_{32}y + a_{33}z = z$$

and we conclude that $a_{11} = -1$, $a_{12} = a_{13} = 0$, $a_{22} = -1$, $a_{21} = a_{23} = 0$ and $a_{33} = 1$, $a_{31} = a_{32} = 0$. The transformation matrix of the C_2 operation of the C_{2v} point group is:

$$C_2 = \begin{pmatrix} -1 & 0 & 0 \\ 0 & -1 & 0 \\ 0 & 0 & 1 \end{pmatrix}$$

Transformation Matrix of σ_{xz} reflection

Rotations are not the only symmetry operations we can perform on a molecule. Figure 2.3.2.4 illustrates the reflection of a point through the xz plane. This operation transforms the vector (x, y, z) into the vector $(x, -y, z)$. Symmetry operators involving reflections through a plane are usually denoted with the letter σ, so the operator that reflects a point through the xz plane is $\hat{\sigma}_{xz}$:

$$\sigma_{xz}(x, y, z) = (x, -y, z)$$

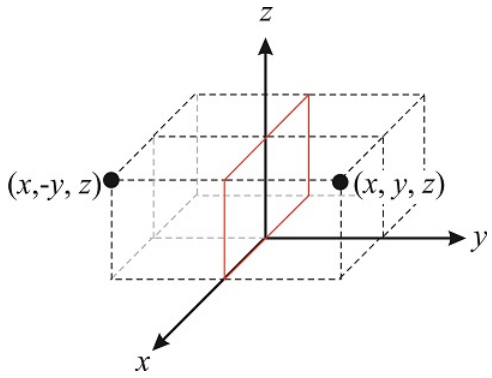


Figure **2.3.2.3**: A reflection through the xz plane

Following the same logic we used for the rotation matrix, we can write the σ_{xz} transformation matrix as:

$$\sigma_{x,z} = \begin{pmatrix} 1 & 0 & 0 \\ 0 & -1 & 0 \\ 0 & 0 & 1 \end{pmatrix}$$

This is true because

$$\begin{pmatrix} 1 & 0 & 0 \\ 0 & -1 & 0 \\ 0 & 0 & 1 \end{pmatrix} \begin{pmatrix} x \\ y \\ z \end{pmatrix} = \begin{pmatrix} x \\ -y \\ z \end{pmatrix}$$

? Exercise 2.3.2.1

Find the transformation matrix of the identity (E) and the $\sigma_{y,z}$ operations under the C_{2v} point group.

Answer

The transformation matrix for E is $\begin{pmatrix} 1 & 0 & 0 \\ 0 & 1 & 0 \\ 0 & 0 & 1 \end{pmatrix}$.

The transformation matrix for $\sigma_{v(yz)''}$ is $\begin{pmatrix} -1 & 0 & 0 \\ 0 & 1 & 0 \\ 0 & 0 & 1 \end{pmatrix}$.

Characters

For a square matrix, the ***character*** is the trace of the matrix. For the C_2 operation, with the transformation matrix

$$\begin{pmatrix} -1 & 0 & 0 \\ 0 & -1 & 0 \\ 0 & 0 & 1 \end{pmatrix},$$

the trace is $(-1) + (-1) + 1 = -1$.

The set of characters for a point group is called a **reducible representation (Γ)**. The reducible representation for the C_{2v} point group is:

C_{2v}	E	C_2	σ_v	σ'_v
Γ	3	−1	1	1

? Exercise 2.3.2.1

Prove that the characters in the reducible representation for C_{2v} are correct:

C_{2v}	E	C_2	σ_v	σ'_v
Γ	3	−1	1	1

Answer

For the E operation, with the transformation matrix $\begin{pmatrix}1&0&0\\0&1&0\\0&0&1\end{pmatrix}$, the trace is $1+1+1=3$.

For the C_2^z operation, with the transformation matrix $\begin{pmatrix}-1&0&0\\0&-1&0\\0&0&1\end{pmatrix}$, the trace is $(-1)+(-1)+1=-1$.

For the $\sigma_{v(xz)'}$ operation, with the transformation matrix $\begin{pmatrix}1&0&0\\0&-1&0\\0&0&1\end{pmatrix}$, the trace is $1+(-1)+1=1$.

For the $\sigma_{v(yz)''}$ operation, with the transformation matrix $\begin{pmatrix}-1&0&0\\0&1&0\\0&0&1\end{pmatrix}$, the trace is $-1+1+1=1$.

This gives the reducible representation

C_{2v}	E	C_2	σ_v	σ_v'
Γ	3	−1	1	1

Reducible and Irreducible Representations

Let us now go back and look in more detail at the transformation matrices of the C_{2v} point group that we derived above. If we look at the matrices carefully we see that they all take the same block diagonal form (a square matrix is said to be **block diagonal** if all the elements are zero except for a set of submatrices lying along the diagonal).

$$E=\begin{pmatrix}[1]&0&0\\0&[1]&0\\0&0&[1]\end{pmatrix},\ C_2=\begin{pmatrix}[-1]&0&0\\0&[-1]&0\\0&0&[1]\end{pmatrix},$$
$$\sigma'_{v(xz)}=\begin{pmatrix}[1]&0&0\\0&[-1]&0\\0&0&[1]\end{pmatrix},\ \sigma_{v(yz)''}=\begin{pmatrix}[-1]&0&0\\0&[1]&0\\0&0&[1]\end{pmatrix}$$

All the non-zero elements become 1x1 matrices that each represent individual x, y, z coordinates. In other words, the element a_{11} represents x, a_{22} represents y, and a_{33} represents z. The matrix elements for x from each transformation matrix combine to form an irreducible representation of the C_{2v} point group. Likewise, the matrix elements for y combine to form a second irreducible representation, and the same is true for z elements. These irreducible representations are shown below:

C_{2v}	E	C_2	σ_v	σ_v'	Coordinate Used
	1	−1	1	−1	x
	1	−1	−1	1	y
	1	1	1	1	z
Γ	3	−1	1	1	

The irreducible representations add to form the reducible representation, Γ. This Γ, which is the set of 3x3 matrices, can be reduced to the set of 1x1 matrices of the irreducible representations. The irreducible representations cannot be reduced further, hence their name.

Sources & Attribution

- Parts of this page was adapted from Matrices (click here) (Symmetry Operators), contributed by Marcia Levitus, Associate Professor (Biodesign Institute) at Arizona State University.
- Parts of this page were adapted from Reductions of Representations, contributed by

  Claire Vallance (University of Oxford)
- Curated or created by Kathryn Haas

2.3.2: Representations of Point Groups is shared under a not declared license and was authored, remixed, and/or curated by LibreTexts.

- **4.3.2: Representations of Point Groups** by Kathryn Haas is licensed CC BY-NC-SA 4.0.

2.3.3: Character Tables

Introduction to Character Tables, using C_{2v} as example

A character table is the complete set of irreducible representations of a symmetry group. In the previous section, we derived three of the four irreducible representations for the C_{2v} point group. These three irreducible representations are labeled A_1, B_1, and B_2. The fourth irreducible representation, A_2, can be derived using the properties (or "rules") for irreducible representations listed below.

Properties of Characters of Irreducible Representations in Point Groups

1. There is always a totally symmetric representation in which all the characters are 1.
   e.g. In C_{2v}, A_1 is totally symmetric.
2. The order of the group (h) is the total number of symmetry operations in the group.
   e.g. In C_{2v}, $h = 4$
3. Similar operations are listed as classes (R) and appear as columns in the table.
   e.g. In C_{2v}, there are four classes of operations, E, C_2, $\sigma_{v(xz)}$, and $\sigma'_{v(yz)}$
4. The number of irreducible representations (rows) must equal the number of classes (columns). This results in all character tables being square.
   e.g. In C_{2v}, there are four classes and four irreducible representations.
5. The sum of squares of all characters under E is equal to the order of the group: $h = \sum [\chi_i]^2$
   e.g. In C_{2v}, $h = 1^2 + 1^2 + 1^2 + 1^2 = 4$
6. For any irreducible representation (i), the sum of squares of its characters multiplied by the number of operations in the class is the order of the group: $h = \sum [\chi_i(R)]^2$
   e.g. For A_2 in C_{2v}, $h = (1 \times 1)^2 + (1 \times 1)^2 + (-1 \times 1)^2 + (-1 \times 1)^2 = 4$
7. Irreducible representations are orthogonal. For any two representations (i and j): $\sum [\chi_i * (R) \chi_j(R)] = 0$
   e.g. For B_1 and B_2 of C_{2v}, $[1 \times 1] + [-1 \times -1] + [1 \times -1] + [-1 \times 1] = 0$

The complete character table for C_{2v} is given below.

C_{2v}	E	C_2	σ_v	σ'_v	$h = 4$	
A_1	1	1	1	1	z	x^2, y^2, z^2
A_2	1	1	−1	−1	R_z	xy
B_1	1	−1	1	−1	x, R_y	xz
B_2	1	−1	−1	1	y, R_x	yz

The various sections of the table are as follows:

i. The first element in the table gives the name of the point group, usually in Schoenflies (C_{2v}) notation.
ii. Along the first row are the symmetry operations of the group, E, C_2, σ_v and σ_v'', followed by the order of the group, h.
iii. In the first column are the irreducible representations of the group, represented by Mulliken Labels. In C_{2v} the irreducible representations are A_1, A_2, B_1 and B_2. The Mulliken labels indicate the symmetry of each representation (explained further below).
iv. The characters (χ) of the irreducible representations under each symmetry operation are given in the bulk of the table.
v. The final column(s) of the table lists a number of functions that transform as the various irreducible representations of the group. These are the Cartesian axes (x, y, z), the Cartesian products ($z^2, x^2 + y^2, xy, xz, yz$), and the rotations ($R_x, R_y, R_z$) (explained further below).

Another example: C_{3v}

Th C_{3v} point group has three classes of operations: E, C_3, and $\sigma_{v(xz)}$. The derivation of transformation matrices for E and $\sigma_{v(xz)}$ is similar to the case for C_{2v}. However, the C_{3v} operation does not give simple 1 or -1 characters. If we carry out a rotation about z by an angle θ, our x and y axes are transformed onto new axes x' and y'. The new axes can each be written as a linear combination of our original x and y axes. The derivation of the rotation matrices will not be covered in this text, but is described elsewhere:

$$x' = x\cos\theta + y\sin\theta$$
$$y' = -x\sin\theta + y\cos\theta$$

For a C_3 rotation counterclockwise through 120° (or $\frac{2\pi}{3}$):

$$x' = x\cos(2\pi/3) + y\sin(2\pi/3) = -\tfrac{1}{2}x - \tfrac{\sqrt{3}}{2}y$$
$$y' = -x\sin(2\pi/3) + y\cos(2\pi/3) = \tfrac{\sqrt{3}}{2}x - \tfrac{1}{2}y$$

The transformation matrices for symmetry operations of C_{3v} are as follows:

$$E = \begin{pmatrix} 1 & 0 & 0 \\ 0 & 1 & 0 \\ 0 & 0 & 1 \end{pmatrix} \quad C_3 = \begin{pmatrix} -\frac{1}{2} & -\frac{\sqrt{3}}{2} & 0 \\ \frac{\sqrt{3}}{2} & -\frac{1}{2} & 0 \\ 0 & 0 & 1 \end{pmatrix} \quad \sigma'_{v(xz)} = \begin{pmatrix} 1 & 0 & 0 \\ 0 & -1 & 0 \\ 0 & 0 & 1 \end{pmatrix}$$

The C_3 transformation matrix contains off-diagonal entries, and therefore it cannot be block diagonalized as 1x1 matrices. However, the first two lines can be diagonalized as a 2x2 and the last line as a 1x1 matrix (Figure **2.3.3.1**):

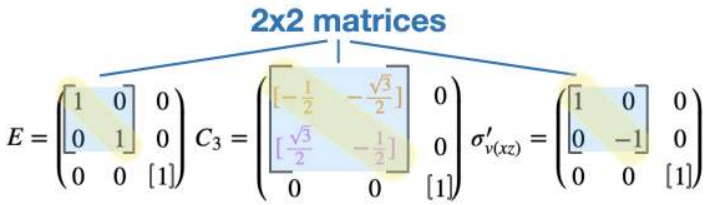


Figure **2.3.3.1**: The C_3 transformation matrix contains off-diagonal entries, and therefore it cannot be block diagonalized as 1x1 matrices. However, the first two lines can be diagonalized as a 2x2 and the last line as a 1x1 matrix. (CC-BY-NC-SA; Kathryn Haas)

The character from a 2x2 matrix is the sum of the trace of that matrix. So, for the C_3 operation, the 2x2 matrix gives the character -1 (from $-\frac{1}{2} + -\frac{1}{2}$).

The character table for C_{3v} is shown below.

C_{3v}	E	$2C_3$	$3\sigma_v$	$h = 6$
A_1	1	1	1	$z, z^2, x^2 + y^2$
A_2	1	1	−1	R_z
E	2	−1	0	$(x, y), (xy, x^2 + y^2), (xz, yz), (R_x, R_y)$

Additional features of character tables

Additional Features of Character Tables

1. Symmetry operations of the same class are grouped into the same column (class) in the character table and not listed separately.
   e.g. In the C_{3v} point group, there are four operations: E, C_3, C_3^2, and σ_v. The C_3 and C_3^2 operations are listed together in the character table as $2C_3$.
2. IF there are multiple C_2 axes (in a D group), the C_2 axes that are perpendicular to the principle axis are labeled with primes (e.g. C_2' and C_2''); when there are multiple types of perpendicular C_2 axes, one prime (C_2') means that it passes through more atoms, while a double prime (C_2'') means it goes between atoms.
3. Mirror planes that are perpendicular to the principle axis are "horizontal" mirror planes and are designated with an h subscript (σ_h). Mirror planes that are in-plane with the principle axis are "vertical" mirror planes, σ_v. When there are two types of vertical mirror planes, those that run through more atoms are σ_v while those that run between atoms are "dihedral", σ_d.
4. Matching the symmetry operations listed in the character table to the symmetry operations of a molecule can confirm its point group.

5. Irreducible representations are each assigned a Mulliken label, listed in the left-hand column, that indicates the symmetry of that representation as follows:

Mulliken Labels	**meaning**
A	singly degenerate (1x1), symmetric to principle axis
B	singly degenerate (1x1), antisymmetric to principle axis
E	doubly degenerate (2x2)
T	triply degenerate (3x3)
Subscripts and superscripts	**meaning**
1	symmetric to $\sigma_v$or perpendicular to C_2
2	anti-symmetric to $\sigma_v$or perpendicular to C_2
g	symmetric to inversion center
u	anti-symmetric to inversion center
$'$	symmetric to σ_h
$''$	anti-symmetric to σ_h

6. The right-hand columns of the character table list a number of functions that transform as the various irreducible representations of the group. These are the Cartesian axes (x, y, z), the Cartesian products $(z^2, x^2 + y^2, xy, xz, yz)$, and the rotations (R_x, R_y, R_z). These expressions indicate the properties of orbitals within the symmetry group. The s-orbital, which is totally symmetric, corresponds to the irreducible representation that possesses symmetry of x^2, y^2 and z^2 combined. The p -orbitals each possess the symmetry of the corresponding axis (e.g. p_x corresponds to the x axis). Each of the d-orbitals possess the symmetry of the corresponding binary product (e.g. d_{xy} corresponds to the binary product, xy, in the character table).

The functions listed in the final column of the table are important in many chemical applications of group theory, particularly in spectroscopy. For example, by looking at the transformation properties of x, y and z (sometimes given in character tables as T_x, T_y, T_z) we can discover the symmetry of translations along the x, y, and z axes. Similarly, R_x, R_y and R_z represent rotations about the three Cartesian axes. The transformation properties of x, y, and z can be used to determine whether or not a molecule is IR-active or whether or not it can absorb a photon of x-, y-, or z-polarized light and undergo a spectroscopic transition. The Cartesian products play a similar role in determining selection rules for Raman transitions, which involve two photons.

A visual summary of the sections and their significance is given in Figure **2.3.3.2**. Character tables for common point groups are given in the References section of LibreTexts Bookshelves.

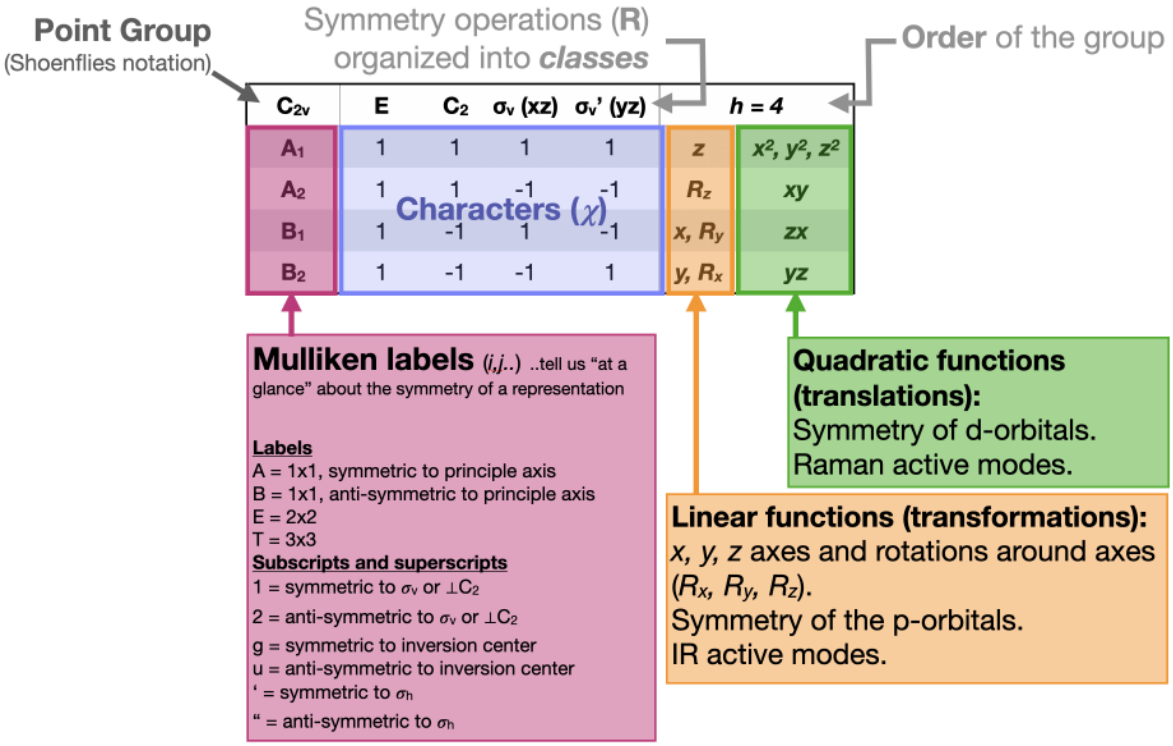


Figure **2.3.3.2**: Visual summary of the sections of a character table and their meaning. (CC-BY-NC-SA; Kathryn Haas)

Contributors and Attributions

- Curated or created by Kathryn Haas
- Claire Vallance (University of Oxford)

  adapted from Character Tables (click here)

This page titled 2.3.3: Character Tables is shared under a not declared license and was authored, remixed, and/or curated by Kathryn Haas.

- **4.3.3: Character Tables** by Kathryn Haas is licensed CC BY-NC-SA 4.0.

SECTION OVERVIEW

2.4: Examples and Applications of Symmetry

The purpose of learning group theory is that molecular symmetry can be applied to understand the properties of molecules. This chapter introduces two applications of symmetry: chirality and molecular vibrations (in the context of analyzing IR and Raman spectra). An additional application of symmetry, to understand molecular bonding, deserves its own chapter and will be explored in Chapter 5.

2.4.1: Molecular Vibrations

2.4.2: Chirality

2.4: Examples and Applications of Symmetry is shared under a not declared license and was authored, remixed, and/or curated by LibreTexts.

2.4.1: Molecular Vibrations

Symmetry and group theory can be applied to understand molecular vibrations. This is particularly useful in the context of predicting the number of peaks expected in the infrared (IR) and Raman spectra of a given compound.

We will use water as a case study to illustrate how group theory is used to predict the number of peaks in IR and Raman spectra.

How many IR and Raman peaks would we expect for H_2O?

To answer this question with group theory, a pre-requisite is that you **assign the molecule's point group and assign an axis system** to the entire molecule. By convention, the z axis is collinear with the principle axis, the x axis is in-plane with the molecule or the most number of atoms. It is a good idea to stick with this convention (see Figure 2.4.1.1).

What is the point group for H_2O? (click to see answer)

H_2O has the following operations: E, C_2, σ_v, σ_v'. The point group is C_{2v}.

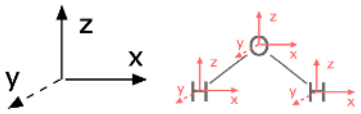


Figure 2.4.1.1: The first step to finding normal modes is to assign a consistent axis system to the entire molecule and to each atom. (CC-BY-SA; Kathryn Haas)

Now that we know the molecule's point group, we can use group theory to determine the symmetry of all motions in the molecule, or the symmetry of each of its degrees of freedom. Then we will subtract rotational and translational degrees of freedom to find the vibrational degrees of freedom. The number of degrees of freedom depends on the number of atoms (N) in a molecule. Each atom in the molecule can move in three dimensions (x, y, z), and so the number of degrees of freedom is three dimensions times N number of atoms, or $3N$. The total degrees of freedom include a number of vibrations, three translations (in x, y, and z), and either two or three rotations. Linear molecules have two rotational degrees of freedom, while non-linear molecules have three. The vibrational modes are represented by the following expressions:

$$\begin{aligned} \text{Linear Molecule Degrees of Freedom} &= 3N-5 \\ \text{Non-Linear Molecule Degrees of Freedom} &= 3N-6 \end{aligned}$$

Our goal is to find the symmetry of all degrees of freedom, and then determine which are vibrations that are IR- and Raman-active.

STEP 1: Find the reducible representation for all normal modes Γ_{modes}.

The first major step is to **find a reducible representation (Γ)** for the movement of all atoms in the molecule (including rotational, translational, and vibrational degrees of freedom). We'll refer to this as Γ_{modes}. To find normal modes using group theory, **assign an axis system** to each individual atom to represent the three dimensions in which each atom can move. Each axis on each atom should be consistent with the conventional axis system you previously assigned to the entire molecule (see Figure 2.4.1.1).

Γ_{modes} is the sum of the characters (trace) of the transformation matrix for the entire molecule (in the case of water, there are 9 degrees of freedom and this is now a 9x9 matrix). Let's walk through this step-by-step. The transformation matrix of E and C_2 are shown below:

$$E = \begin{pmatrix} 1 & 0 & 0 & 0 & 0 & 0 & 0 & 0 & 0 \\ 0 & 1 & 0 & 0 & 0 & 0 & 0 & 0 & 0 \\ 0 & 0 & 1 & 0 & 0 & 0 & 0 & 0 & 0 \\ 0 & 0 & 0 & 1 & 0 & 0 & 0 & 0 & 0 \\ 0 & 0 & 0 & 0 & 1 & 0 & 0 & 0 & 0 \\ 0 & 0 & 0 & 0 & 0 & 1 & 0 & 0 & 0 \\ 0 & 0 & 0 & 0 & 0 & 0 & 1 & 0 & 0 \\ 0 & 0 & 0 & 0 & 0 & 0 & 0 & 1 & 0 \\ 0 & 0 & 0 & 0 & 0 & 0 & 0 & 0 & 1 \end{pmatrix} \begin{pmatrix} x_{oxygen} \\ y_{oxygen} \\ z_{oxygen} \\ x_{hydrogen-a} \\ y_{hydrogen-a} \\ z_{hydrogen-a} \\ x_{hydrogen-b} \\ y_{hydrogen-b} \\ z_{hydrogen-b} \end{pmatrix} = \begin{pmatrix} x'_{oxygen} \\ y'_{oxygen} \\ z'_{oxygen} \\ x'_{hydrogen-a} \\ y'_{hydrogen-a} \\ z'_{hydrogen-a} \\ x'_{hydrogen-b} \\ y'_{hydrogen-b} \\ z'_{hydrogen-b} \end{pmatrix}, \chi = 9$$

$$C_2 = \begin{pmatrix} -1 & 0 & 0 & 0 & 0 & 0 & 0 & 0 & 0 \\ 0 & -1 & 0 & 0 & 0 & 0 & 0 & 0 & 0 \\ 0 & 0 & 1 & 0 & 0 & 0 & 0 & 0 & 0 \\ 0 & 0 & 0 & 0 & 0 & 0 & -1 & 0 & 0 \\ 0 & 0 & 0 & 0 & 0 & 0 & 0 & -1 & 0 \\ 0 & 0 & 0 & 0 & 0 & 0 & 0 & 0 & 1 \\ 0 & 0 & 0 & -1 & 0 & 0 & 0 & 0 & 0 \\ 0 & 0 & 0 & 0 & -1 & 0 & 0 & 0 & 0 \\ 0 & 0 & 0 & 0 & 0 & 1 & 0 & 0 & 0 \end{pmatrix} \begin{pmatrix} x_{oxygen} \\ y_{oxygen} \\ z_{oxygen} \\ x_{hydrogen-a} \\ y_{hydrogen-a} \\ z_{hydrogen-a} \\ x_{hydrogen-b} \\ y_{hydrogen-b} \\ z_{hydrogen-b} \end{pmatrix} = \begin{pmatrix} x'_{oxygen} \\ y'_{oxygen} \\ z'_{oxygen} \\ x'_{hydrogen-a} \\ y'_{hydrogen-a} \\ z'_{hydrogen-a} \\ x'_{hydrogen-b} \\ y'_{hydrogen-b} \\ z'_{hydrogen-b} \end{pmatrix}, \chi = 1$$

It is unnecessary to find the transformation matrix for each operation since it is only the TRACE that gives us the character, and any off-diagonal entries do not contribute to Γ_{modes}. The values that contribute to the trace can be found simply by performing each operation in the point group and assigning a value to each individual atom to represent how it is changed by that operation. If the atom moves away from itself, that atom gets a character of zero (this is because any non-zero characters of the transformation matrix are off of the diagonal). If the atom remains in place, each of its three dimensions is assigned a value of $\cos\theta$. For the example of H_2O under the C_{2v} point group, the axes that remain unchanged ($\theta = 0°$) are assigned a value of $\cos(0°) = 1$, while those that are moved into the negative of themselves (rotated or reflected to $\theta = 180°$) are assigned $\cos(180°) = -1$. The character for Γ is the sum of the values for each transformation.

Let's walk through the steps to assign characters of Γ_{modes} for H_2O to illustrate how this works:

For the operation E, performed on H_2O, all three atoms remain in place. The three axes x, y, z on each atom remain unchanged. Thus, each of the three axes on each of three atom (nine axes) is assigned the value $\cos(0°) = 1$, resulting in a sum of $\chi = 9$ for the Γ_{modes}.

For the operation C_2, the two hydrogen atoms are moved away from their original position, and so the hydrogens are assigned a value of zero. The oxygen remains in place; the z-axis on oxygen is unchanged ($\cos(0°) = 1$), while the x and y axes are inverted ($\cos(180°)$). The sum of these characters gives $\chi = -1$ in the Γ_{modes}.

Now you try! Find the characters of $\sigma_{v(xz)}$ and $\sigma_{v(yz)}$ under the C_{2v} point group. Compare what you find to the Γ_{modes} for all normal modes given below.

C_{2v}	E	C_2	σ_v	σ'_v
Γ_{modes}	9	−1	3	1

(2.4.1.1)

STEP 2: Break Γ_{modes} into its component irreducible representations.

Now that we've found the Γ_{modes} (2.4.1.1), we need to break it down into the individual irreducible representations ($i, j, k...$) for the point group. We can do this systematically using the following formula:

Misplaced '#'

In other words, the number of irreducible representations of type i is equal to the sum of the number of operations in the class × the character of the Γ_{modes} × the character of i, and that sum is divided by the order of the group (h).

Using equation ???, we find that for all normal modes of H_2O:

$$\Gamma_{modes} = 3A_1 + 1A_2 + 3B_1 + 2B_2 \tag{2.4.1.2}$$

.

Notice there are 9 irreducible representations in Equation 2.4.1.2. These irreducible representations represent the symmetries of all 9 motions of the molecule: vibrations, rotations, and translations.

? Exercise 2.4.1.1: Derive the irreducible representation in equation 2.4.1.2.

Derive the nine irreducible representations of Γ_{modes} for H_2O, expression 2.4.1.2.

Hint

To find the number of each kind of irreducible representation that combine to form the Γ_{modes}, we need the characters of Γ_{modes} that we found above (2.4.1.1), the C_{2v} character table (below), and equation ???.

C_{2v}	$1E$	$1C_2$	$1\sigma_v$	$1\sigma_v'$	$h=4$	
A_1	1	1	1	1	z	x^2, y^2, z^2
A_2	1	1	−1	−1	R_z	xy
B_1	1	−1	1	−1	x, R_y	xz
B_2	1	−1	−1	1	y, R_x	yz

In the C_{2v} point group, each class has only one operation, so the number of operations in each class (from equation ???) is 1 for each class. This has been explicitly added to the character table above for emphasis.

Answer

The number of $A_1 = \frac{1}{4}[(1\times 9\times 1) + (1\times(-1)\times 1) + (1\times 3\times 1) + (1\times 1\times 1)] = 3A_1$

The number of $A_2 = \frac{1}{4}[(1\times 9\times 1) + (1\times(-1)\times 1) + ((-1)\times 3\times 1) + ((-1)\times 1\times 1)] = 1A_2$

The number of $B_1 = \frac{1}{4}[(1\times 9\times 1) + ((-1)\times(-1)\times 1) + (1\times 3\times 1) + ((-1)\times 1\times 1)] = 3B_1$

The number of $B_2 = \frac{1}{4}[(1\times 9\times 1) + ((-1)\times(-1)\times 1) + ((-1)\times 3\times 1) + (1\times 1\times 1)] = 2B_2$

STEP 3: Subtract rotations and translations to find vibrational modes.

Because we are interested in molecular vibrations, we need to subtract the rotations and translations from the total degrees of freedom.

$$\text{Vibrations} = \Gamma_{modes} - \text{Rotations} - \text{Translations}$$

In the example of H_2O, the total degrees of freedom are given above in equation 2.4.1.2, and therefore the vibrational degrees of freedom can be found by:

$$H_2O \text{ vibrations} = (3A_1 + 1A_2 + 3B_1 + 2B_2) - \text{Rotations} - \text{Translations} \tag{2.4.1.3}$$

But which of the irreducible representations are ones that represent rotations and translations? The symmetry of rotational and translational degree modes can be found by inspecting the right-hand columns of any character table. Rotational modes correspond to irreducible representations that include R_x, R_y, and R_z in the table, while each of the three translational modes has the same symmetry as the x, y and z axes. For a non-linear molecule, subtract three rotational irreducible representations and three translational irreducible representations from the total Γ_{modes}.

In the specific case of water, we refer to the C_{2v} character table:

C_{2v}	E	C_2	σ_v	σ_v'	$h=4$	
A_1	1	1	1	1	z	x^2, y^2, z^2
A_2	1	1	−1	−1	R_z	xy
B_1	1	−1	1	−1	x, R_y	xz
B_2	1	−1	−1	1	y, R_x	yz

In C_{2v}, translations correspond to B_1, B_2, and A_1 (respectively for x, yz), and rotations correspond to B_2, B_1, and A_1 (respectively for R_x, R_y, R_z). Subtracting these six irreducible representations from Γ_{modes} will leave us with the irreducible representations for vibrations.

$$\begin{aligned} H_2O \text{ vibrations} &= \Gamma_{modes} - \text{Rotations} - \text{Translations} \\ &= (3A_1 + 1A_2 + 3B_1 + 2B_2) - (A_1 + B_1 + B_2) - (A_2 + B_1 + B_2) \\ &= 2A_1 + 1B_1 \end{aligned}$$

The three vibrational modes for H_2O are $2A_1 + 1B_1$. Note that we have the correct number of vibrational modes based on the expectation of $3N - 6$ vibrations for a non-linear molecule.

STEP 4: Determine which of the vibrational modes are IR-active and Raman-active.

The next step is to determine which of the vibrational modes is IR-active and Raman-active. To do this, we apply the IR and Raman Selection Rules below:

IR and Raman Selection Rules

Infrared selection rules:

If a vibration results in the change in the molecular dipole moment, it is IR-active. In the character table, we can recognize the vibrational modes that are IR-active by those with symmetry of the x, y, and z axes.

In C_{2v}, any vibrations with A_1, B_1 or B_2 symmetry would be IR-active.

Raman selection rules:

If a vibration results in a change in the molecular polarizability, it will be Raman-active. In the character table, we can recognize the vibrational modes that are Raman-active by those with symmetry of any of the binary products (xy, xz, yz, x^2, y^2, and z^2) or a linear combination of binary products (e.g. $x^2 - y^2$).

In C_{2v}, any vibrations with A_1, A_2, B_1 or B_2 symmetry would be Raman-active.

In our H_2O example, we found that of the three vibrational modes, two have A_1 and one has B_1 symmetry. Both A_1 and B_1 are IR-active, and both are also Raman-active. ***There are two possible IR peaks and three possible Raman peaks expected for water***.*

*It is important to note that this prediction tells only what is possible, but not what we might actually see in the IR and Raman spectra. For example, if the two IR peaks overlap, we might actually notice only one peak in the spectrum. Or, if one or more peaks is off-scale, we wouldn't see it in actual data. Group theory tells us what is *possible and allows us to make predictions or interpretations of spectra*.

Summary of Analysis for Water

Each molecular motion for water, or any molecule, can be assigned a symmetry under the molecule's point group. For water, we found that there are a total of 9 molecular motions; $3A_1 + A_2 + 3B_1 + 2B_2$. Six of these motions are not the translations and rotations. The remaining motions are vibrations; two with A_1 symmetry and one with B_1 symmetry.

We can tell what these vibrations would look like based on their symmetries. The two A_1 vibrations must be completely symmetric, while the B_1 vibration is antisymmetric with respect to the principal C_2 axis.

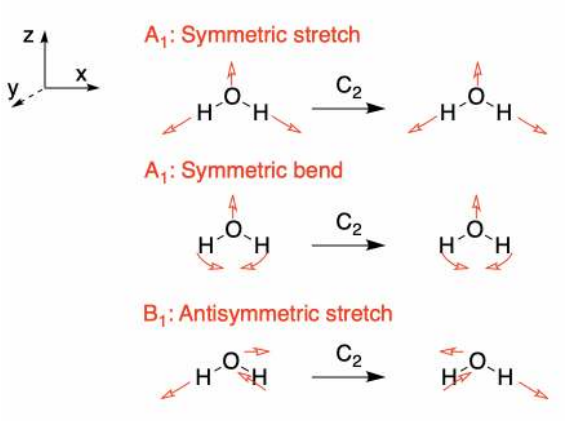


Figure 2.4.1.2: Illustration of the vibrational motions of water. The antisymmetric stretch has B_1 symmetry, while the symmetric stretch and symmetric bend both have A_1 symmetry. (Click here to see animation) (CC-BY-NC-SA; Kathryn Haas)

Table 2.4.1.1: Summary of the Symmetry of Molecular Motions for Water

All Motions (step 2 above)	Translations (x,y,z)	Rotations (R_x, R_y, R_z)	**Remaining Vibrations**	Description of Vibration
$3A_1$	$1A_1$		$2A_1$	One is a symmetric stretch. The other is a symmetric bend. Both are *IR-active* and *Raman-active*
A_2		$1A_2$		
$3B_1$	$1B_1$	$1B_1$	$1B_1$	Antisymmetric stretch that is *IR-active* and *Raman-active*.
$2B_2$	$1B_2$	$1B_2$		

? Exercise 2.4.1.2

Find the symmetries of all motions of the square planar complex, tetrachloroplatinate (II). Determine which are rotations, translations, and vibrations. Determine which vibrations are IR and Raman active.

Answer

The point group of $[PtCl_4]^{2-}$ is D_{4h} (refer to its character table). There are five atoms and 15 vectors (x, y, z for each atom × 5 atoms).

STEP 1: The first major step is to **find a reducible representation (Γ)** for the movement of all atoms in the molecule.

C_{2v}	E	$2C_4$	C_2	$2C_2'$	$2C_2''$	i	$2S_4$	σ_h	$2\sigma_v$	$2\sigma_d$
Γ_{modes}	15	1	−1	−3	−1	−3	−1	5	3	1

(2.4.1.4)

.

STEP 2: Break Γ_{modes} into its component irreducible representations.

Following the process described earlier, we come to $A_{1g} + A_{2g} + B_{1g} + B_{2g} + E_g + 2A_{2u} + B_{2u} + 3E_u$. This accounts for all modes of movement, including rotations and translations.

STEP 3: Subtract rotations and translations to find vibrational modes.

The translations are $A_{2u} + E_u$ and the rotations are $A_{2g} + E_g$.
The remaining normal modes are: $A_{1g} + B_{1g} + B_{2g} + A_{2u} + B_{2u} + 2E_u$

STEP 4: Determine which of the vibrational modes are IR-active and Raman-active:

$A_{2u} + E_u$ are IR-active. Since A_{2u} is singly degenerate and E_u is doubly degenerate, we expect three possible IR bands.
$A_{1g} + B_{1g} + B_{2g}$ are Raman-Active. Each of these is singly degenerate, so we expect three possible Raman bands.

Selected Vibrational Modes

The interpretation of CO stretching vibrations in an IR spectrum is particularly useful. Symmetry and group theory can be applied to predict the number of CO stretching bands that appear in a vibrational spectrum for a given metal coordination complex. A classic example of this application is in distinguishing isomers of metal-carbonyl complexes. For example, the *cis*- and *trans*-isomers of square planar metal dicarbonyl complexes ($ML_2(CO)_2$) have a different number of IR stretches that can be predicted and interpreted using symmetry and group theory. Another example is the case of *mer*- and *fac*- isomers of octahedral metal tricarbonyl complexes ($ML_3(CO)_3$). Structures of the two types of metal carbonyl configurations and their isomers are shown in Figure **2.4.1.1**. The isomers in each case can be distinguished using vibrational spectroscopy.

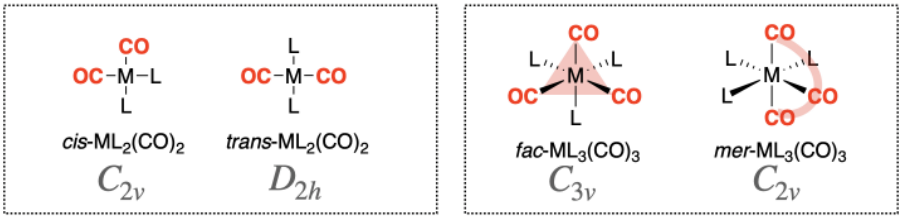


Figure **2.4.1.3**: Cis- and *trans*- isomers of square planar metal dicarbonyl complexes ($ML_2(CO)_2$) are shown in the left box. *Mer*- and *fac*- isomers of octahedral metal tricarbonyl complexes ($ML_3(CO)_3$) are shown in the right box. The point group for each of the general structures is also shown. (CC-BY-NC-SA; Kathryn Haas)

EXAMPLE 1: Distinguishing *cis*- and *trans*- isomers of square planar metal dicarbonyl complexes

General structures of the *cis*- and *trans*- isomers of square planar metal dicarbonyl complexes ($ML_2(CO)_2$) are shown in the left box in Figure **2.4.1.1**. We can use symmetry and group theory to predict how many carbonyl stretches we should expect for each isomer following the steps below.

Step 1: Assign the point group and Cartesian coordinates for each isomer.

The *cis*-isomer has C_{2v} symmetry and the *trans*-isomer has D_{2h} symmetry. We assign the Cartesian coordinates so that z is colinear with the principle axis in each case. For the D_2h isomer, there are several orientations of the z axis possible. The axes shown in Figure **2.4.1.2** will be used here.



Figure **2.4.1.4**: Cis- and *trans*- isomers of square planar metal dicarbonyl complexes ($ML_2(CO)_2$) are shown and oriented with respect to the Cartesian coordinates shown at the left so that the highest-order rotation axis is colinear with z and the molecule is co-planar with the xz plane. The vector along each C—O bond is shown using a red arrow (→). These vectors represent the direction of C—O stretching motions. (CC-BY-NC-SA; Kathryn Haas)

Step 2: Produce a reducible representation (Γ) for CO stretches in each isomer

First, assign a vector along each C—O bond in the molecule to represent the direction of C—O stretching motions, as shown in Figure **2.4.1.2** (red arrows →). These vectors are used to produce a reducible representation (**Γ**) for the C—O stretching motions in each molecule. Using the symmetry operations under the appropriate character table, assign a value of 1 to each vector that remains in place during the operation, and a value of 0 if the vector moves out of place. There will be no occasion where a vector remains in place but is inverted, so a value of -1 will not occur.

cis- $ML_2(CO)_2$:

For *cis*- $ML_2(CO)_2$, the point group is C_{2v} and so we use the operations under the C_{2v} character table to create the Γ_{cis-CO}.

C_{2v}	E	C_2	$\sigma_v(xz)$	$\sigma_v'(yz)$
Γ_{cis-CO}	2	0	2	0

trans- $ML_2(CO)_2$:

For trans- $ML_2(CO)_2$, the point group is D_{2h} and so we use the operations under the D_{2h} character table to create the $\Gamma_{trans-CO}$.

D_{2h}	E	$C_2(z)$	$C_2(y)$	$C_2(x)$	i	$\sigma(xy)$	$\sigma(xz)$	$\sigma(yz)$
$\Gamma_{trans-CO}$	2	0	0	2	0	2	2	0

Step 3: Break each Γ into its component irreducible representations

Each Γ can be reduced using inspection or by the systematic method described previously.

In the case of the *cis*- $ML_2(CO)_2$, the CO stretching vibrations are represented by A_1 and B_1 irreducible representations:

C_{2v}	E	C_2	$\sigma_v(xz)$	$\sigma_v'(yz)$		
Γ_{cis-CO}	2	0	2	0		
A_1	1	1	1	1	z	x^2, y^2, z^2
B_1	1	−1	1	−1	x, R_y	xz

(2.4.1.5)

In the case of *trans*- $ML_2(CO)_2$, the CO stretching vibrations are represented by A_1 and B_{3u} irreducible representations:

D_{2h}	E	$C_2(z)$	$C_2(y)$	$C_2(x)$	i	$\sigma(xy)$	$\sigma(xz)$	$\sigma(yz)$	
$\Gamma_{trans-CO}$	2	0	0	2	0	2	2	0	
A_g	1	1	1	1	1	1	1	1	$x^2,\ y^2,\ z^2$
B_{3u}	1	−1	−1	1	−1	1	1	−1	x

These irreducible representations correspond to the symmetries of only the selected C—O vibrations. Since these motions are isolated to the C—O group, they do not include any rotations or translations of the entire molecule, and so we do not need to find and subtract rotationals or translations (unlike the previous cases where all motions were considered).

Step 4: Determine which vibrational modes are IR-active and/or Raman-active

Apply the infrared selection rules described previously to determine which of the CO vibrational motions are IR-active and Raman-active. The two isomers of $ML_2(CO)_2$ are described below.

In the case of the *cis*- $ML_2(CO)_2$, the CO stretching vibrations are represented by A_1 and B_1 irreducible representations. The characters of both representations and their functions are shown above, in 2.4.1.5 (and can be found in the C_{2v} character table). Under C_{2v}, both the A_1 and B_1 CO vibrational modes are IR-active and Raman-active. Therefore, two bands in the IR spectrum and two bands in the Raman spectrum are possible.

In the case of the trans- $ML_2(CO)_2$, the CO stretching vibrations are represented by A_g and B_{3u} irreducible representations. The characters of both representations and their functions are shown above, in 2.4.1.5 (and can be found in the D_{2h} character table). Under D_{2h}, the A_g vibrational mode is is Raman-active only, while the B_{3u} vibrational mode is IR-active only. Therefore, only one IR band and one Raman band are possible for this isomer.

Summary

It is possible to distinguish between the two isomers of square planar $ML_2(CO)_2$ using either IR or Raman vibrational spectroscopy. The *cis*- $ML_2(CO)_2$ can produce two CO stretches in an IR or Raman spectrum, while the *trans*- $ML_2(CO)_2$ isomer can produce only one band in either type of vibrational spectrum. If a sample of $ML_2(CO)_2$ produced two CO stretching bands, we could rule out the possibility of a pure sample of *trans*-$ML_2(CO)_2$.

Exercise 2.4.1.3

Repeat the steps outlined above to determine how many CO vibrations are possible for *mer*-$ML_3(CO)_3$ and *fac*-$ML_3(CO)_3$ isomers (see Figure **2.4.1.1**) in both IR and Raman spectra. Could either of these vibrational spectroscopies be used to distinguish the two isomers?

Answer

Step 1: Assign the point group and Cartesian coordinates for each isomer.
The *fac*-isomer is C_{3v}. The *mer*-isomer is C_{2v}.

Step 2: Produce a reducible representation for CO stretches in each isomer.

Step 3: Break each into its component irreducible representations.

Step 4: Determine which vibrational modes are IR-active and/or Raman-active.

***For fac*-$ML_3(CO)_3$**, the point group is C_{3v} and so we use the operations under the C_{3v} character table to create the Γ_{fac-CO}. Then break it into its irreducible representations and determine which are IR and Raman active:

C_{3v}	E	$2C_2$	$3\sigma_v$
Γ_{fac-CO}	3	0	1

This reduces to $A_1 + E$. Both of these are IR active, and since one is singly degenerate while the other is doubly degenerate, we expect three possible IR bands from this isomer. Both vibrational modes are also Raman active, and again we would expect three possible bands in the Raman spectrum.

For mer-$ML_3(CO)_3$, the point group is C_{2v} and so we use the operations under the C_{2v} character table to create the Γ_{mer-CO}. Then break it into its irreducible representations and determine which are IR and Raman active:

C_{2v}	E	C_2	$\sigma_v(xz)$	$\sigma'_v(yz)$
Γ_{mer-CO}	3	1	3	1

This reduces to $2A_1 + B_1$; both A_1 and B_1 are IR and Raman active. So this isomer would have three possible IR bands and three possible Raman Bands.

These two isomers have the same number of possible bands in both IR and Raman spectroscopy. It would not be straightforward to distinguish them from each other based on the number of possible bands in the vibrational spectrum.

This page titled 2.4.1: Molecular Vibrations is shared under a not declared license and was authored, remixed, and/or curated by Kathryn Haas.

- **4.4.2: Molecular Vibrations** by Kathryn Haas is licensed CC BY-NC 4.0.

2.4.2: Chirality

Introduction

Around the year 1847, the French scientist Louis Pasteur provided an explanation for the optical activity of tartaric acid salts. When he carried out a particular reaction, Pasteur observed that two types of crystals precipitated. Patiently and carefully using tweezers, Pasteur was able to separate the two types of crystals. Pasteur noticed that the types rotated plane-polarized light by the same amount but in different directions. These two compounds are called enantiomers.

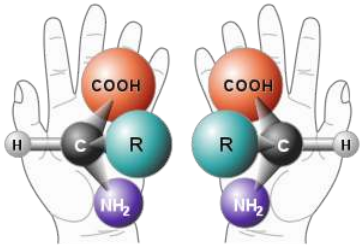


Figure 2.4.2.1: Two enantiomers of an amino acid (with side chain R).

What is chirality?

A molecule is **chiral** (or **dissymetric**) if it is non-superimposable on its mirror image. The two mirror images of a chiral molecule are called enantiomers. Enantiomers have the same physical properties (e.g., melting point, etc.). They differ in their ability to rotate plane polarized light and in their reactivity with other chiral molecules. Due to their ability to rotate plane polarized light, they are referred to as being *optically active*.

Using Symmetry to Determine Chirality

There are some general rules of thumb that help determine whether a molecule is chiral or achiral. The point group of the molecule, and the symmetry operations within that point group, can give clues as to whether the molecule is chiral.

Symmetry operations of chiral molecules

A chiral molecule cannot possess a plane of symmetry (σ), a center of inversion (i), or an improper rotation (S_n). Due to the fact that all groups that lack both σ and i also lack S_n, **a molecule that belongs to any group that lacks S_n is chiral**.

An example of an inorganic coordination complex is tris(ethylenediamine)cobalt(III) (Figure 2.4.2.1). Figure 2.4.2.1 shows the two enantiomers of tris(ethylenediamine)cobalt(III): the **Δ** and **Λ** isomers.

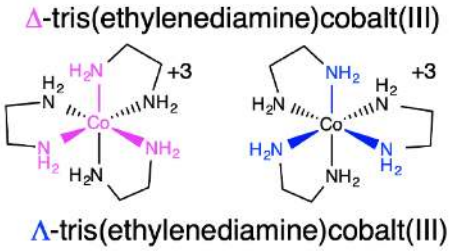


Figure 2.4.2.2: Two chiral enantiomers of tris(ethylenediamine)coalt(III).

You can visualize the **Λ** and **Δ** isomers by imagining that the ligands around the metal centers are blades of a fan. To push the air toward you, you would need to rotate the **Δ** isomer clockwise, and the **Λ** isomer counter-clockwise.

Exercise 2.4.2.1

Which point groups are possible for chiral molecules?

Answer

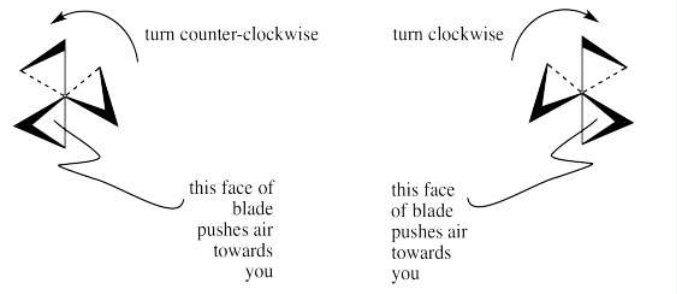


Figure **2.4.2.3**: Another way of thinking about the chirality of the two chiral enantiomers of tris(ethylenediamine)coalt(III) shown in Figure **2.4.2.2**. This figure was taken from Structure and Reactivity in Organic, Biological, and Inorganic Chemistry.

As a result of the previous discussion, there are a few classes of point groups that lack an improper axis. Those classes are C_1, C_n, and D_n.

2.4.2: Chirality is shared under a CC BY-NC license and was authored, remixed, and/or curated by LibreTexts.

- **4.4.1: Chirality** by Kathryn Haas is licensed CC BY-NC 4.0.

CHAPTER OVERVIEW

3: Molecular Orbital Theory

3.1: Prelude to Molecular Orbital Theory
3.2: Formation of Molecular Orbitals from Atomic Orbitals
3.2.1: Molecular Orbitals from s Orbitals
3.2.2: Molecular Orbitals from p Orbitals
3.2.3: Molecular orbitals from d orbitals
3.2.4: Nonbonding Orbitals and Other Factors
3.3: Homonuclear Diatomic Molecules
3.3.1: Molecular Orbitals
3.3.2: Orbital Mixing
3.3.3: Diatomic Molecules of the First and Second Periods
3.3.4: Photoelectron Spectroscopy
3.4: Heteronuclear Diatomic Molecules
3.4.1: Polar bonds
3.4.2: Ionic Compounds and Molecular Orbitals
3.5: Larger (Polyatomic) Molecules
3.5.1: Bifluoride anion
3.5.2: Carbon Dioxide
3.5.3: H_2O
3.5.4: NH_3
3.5.5: CO_2 (Revisted with Projection Operators)
3.5.6: BF_3

3: Molecular Orbital Theory is shared under a not declared license and was authored, remixed, and/or curated by LibreTexts.

3.1: Prelude to Molecular Orbital Theory

Valence bond (VB) theory gave us a qualitative picture of chemical bonding, which was useful for predicting the shapes of molecules, bond strengths, etc. It fails to describe some bonding situations accurately because it ignores the wave nature of the electrons. Molecular orbital (MO) theory has the potential to be more quantitative. With it we can also get a picture of where the electrons are in the molecule, as shown in the image at the right. This can help us understand patterns of bonding and reactivity that are otherwise difficult to explain.

Although MO theory in principle gives us a way to calculate the energies and wavefunctions of electrons in molecules very precisely, usually we settle for simplified models. These models do not give very accurate orbital and bond energies, but they do explain concepts such as resonance (e.g., in the ferrocene, $C_{10}H_{10}Fe$, molecule) that are hard to represent otherwise. We can get more accurate energies from MO theory using computational methods. While MO theory is more correct than VB theory and can be very accurate in predicting the properties of molecules, it is also rather complicated even for fairly simple molecules. For example, you should be able to draw the VB pictures for CO, NH_3, and benzene, but we will find that these are increasingly challenging with MO theory.

3.1: Prelude to Molecular Orbital Theory is shared under a not declared license and was authored, remixed, and/or curated by LibreTexts.

- **2.1: Prelude to Molecular Orbital Theory** by Chemistry 310 is licensed CC BY-SA 4.0. Original source: https://en.wikibooks.org/wiki/Introduction_to_Inorganic_Chemistry.

3.2: Formation of Molecular Orbitals from Atomic Orbitals

Molecular orbital theory extends from quantum theory and the atomic orbital wavefunctions (ψ) described by the Schrödinger equation. While the Schrödinger equation defines a Ψ for electrons in individual atoms, we can approximate the molecular wavefunction (what Ψ would look like if we combined the ψ of individual atoms). The addition or subtraction of wavefunctions is termed **linear combination of atomic orbitals** (LCAO). Molecular orbital theory is applied to LCAO to describe bonding.

The LCAO for the wavefunction of two atoms (ψ_a and ψ_b) is represented by the general expression below. The coefficients c_a and c_b quantify the contribution of each atomic ψ to the molecular Ψ.

$$\Psi = c_a\psi_a + c_b\psi_b$$

For two atomic ψs to form a bond, three conditions must be satisfied:

- First, the **distance between the atoms** must be small enough to provide good overlap. This is because the two orbitals must be able to overlap using regions of ψ^2 where the probability of finding electrons is significant. If atoms are not close enough, ψ_a and ψ_b cannot interact productively. At the same time, the atoms must be far enough apart that their nuclei do not repel each other.
- The **symmetry of the orbitals** must be compatible such that regions of ψ_a and ψ_b with the same sign constructively interfere more than regions with opposite sign destructively interfere. In other words, for a productive interaction, there must be a relatively high probability of finding an electron between the two nuclei, and this depends on the symmetry (and sign of the ψ) of the atomic orbitals.
- Third, the **energies of the atomic orbitals** must be similar. Orbitals with similar energy combine to make the most stable bonding molecular orbitals. Atomic orbitals with very different energies form less stable bonding interactions, and the larger the difference in the atomic orbitals, the weaker the bonding interaction will be.

Atomic orbitals combine to form molecular orbitals when these three conditions are met. The result is a set of bonding molecular orbitals that are lower in energy than the original atomic orbital energies.

This page titled 3.2: Formation of Molecular Orbitals from Atomic Orbitals is shared under a CC BY-NC-SA 4.0 license and was authored, remixed, and/or curated by Kathryn Haas.

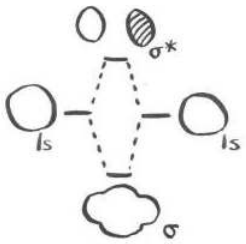
- **5.1: Formation of Molecular Orbitals from Atomic Orbitals** by Kathryn Haas is licensed CC BY-SA 4.0.

3.2.1: Molecular Orbitals from s Orbitals

In the case of the hydrogen molecule, we took two atomic orbitals and combined them to form two molecular orbitals. These new molecular orbitals had different wavelengths than the two atomic orbitals: one had a longer wavelength and was a little lower in energy, while the other had a shorter wavelength and was a little higher in energy. If we take into account the energy of the two original atomic wavefunctions, and compare them to the total energy of the two new molecular wavefunctions, there is no change overall.

We started with two atomic orbitals, and by combining them we produced two molecular orbitals. Both of these ideas are useful in considering the formation of more complex molecules from individual atoms.

- The average energy of the orbitals has remained almost constant.
- Also, the number of wavefunctions has remained constant.



Of course, from the point of view of the two real electrons, some remarkable changes have occurred. Both of these electrons have adopted a longer wavelength and a lower energy and that has made all the difference. There is an occupied molecular orbital and an unoccupied molecular orbital; only the occupied orbital makes a real energetic contribution to the overall stability of the molecule. The unoccupied orbital is completely imaginary.

A bonding picture of He_2 would look exactly the same, because it would also involve the overlap of 1s electrons on one atom with 1s electrons on the other atom. There would be a different electronic energy, however. That difference would affect the prospects of helium-helium bond formation.

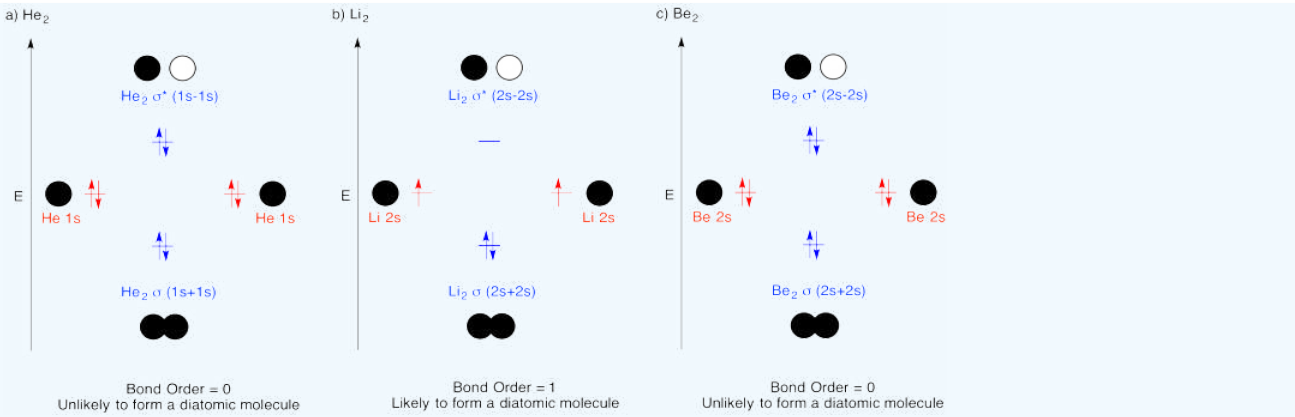
- The electrons have lower kinetic energy in the bond than they had before bonding.
- Electronic energy has decreased. A stable bond has formed.

? Exercise 3.2.1.1

Construct molecular orbital diagrams for the following diatomic species and discuss the likelihood of bond formation in each case.

a. He_2.
b. Li_2.
c. Be_2.

Answer



This page titled 3.2.1: Molecular Orbitals from s Orbitals is shared under a CC BY-NC-SA 4.0 license and was authored, remixed, and/or curated by Chris Schaller.

3.2.2: Molecular Orbitals from p Orbitals

Bonding with P-orbitals

Sigma bonding with p-orbitals

Other diatomic molecules in the upper right corner of the periodic table can be constructed in a similar way. Look at dinitrogen, N_2.

We can think about how dinitrogen would form if two nitrogen atoms were placed close enough together to share electrons. Nitrogen has more electrons than hydrogen, so this interaction is more complicated.

In our qualitative examination of bonding in main group diatomics, we will take the approach used in Lewis structures and just look at the valence electrons. A quantitative molecular orbital calculation with a computer would not take this shortcut, but would include all of the electrons in the atoms that are bonding together.

Nitrogen has five valence electrons, and these electrons are found in the 2s and 2p levels. There are three possible atomic orbitals in the 2p level where some of these electrons could be found: p_x, p_y and p_z. We need to look at the interaction between the s and p_x, p_y and p_z orbitals on one nitrogen atom with the s and p_x, p_y and p_z orbitals on the other nitrogen. That process could be extremely complicated, but:

- Orbital interactions are governed by symmetry.

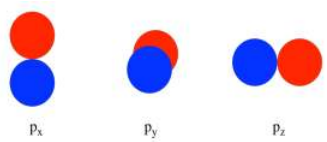
Orbitals interact most easily with other orbitals that have the same element of symmetry. For now, we can simplify and say that orbitals on one atom only interact with the same type of orbitals on the other atom.

- s orbitals interact with s orbitals. We can already see how that will work out in dinitrogen, because that is what happened in dihydrogen.
- p_x orbitals interact with p_x orbitals.
- p_y orbitals interact with p_y orbitals.
- p_z orbitals interact with p_z orbitals.

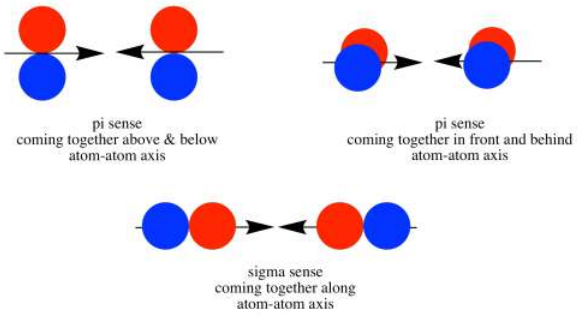
Another complication here is that the s and p orbitals do not start out at the same energy level. When the orbitals mix, one combination goes up in energy and one goes down. Does the s antibonding combination go higher in energy than the combinations from p orbitals? Do the p bonding combinations go lower in energy than the combinations from s orbitals? We will **simplify** and **assume** that the s and p levels remain completely separate from each other. This is not always true, but the situation varies depending on what atoms we are dealing with.

- The combination of one s orbital with another is just like in hydrogen. Two original orbitals will combine and rearrange to produce two new orbitals.
- There is a bonding combination in which the orbitals are in phase. The new orbital produced has a longer wavelength than the original orbital. It is lower in energy.
- There is an antibonding combination in which the orbitals are out of phase. The new orbital produced has a shorter wavelength than the original orbital. It is higher in energy.

In considering the interaction of two p orbitals, we have to keep in mind that p orbitals are directional. A p orbital lies along a particular axis: x, y or z. The three p orbitals on nitrogen are all mutually perpendicular (or orthogonal) to each other. That situation is in contrast to s orbitals, which are spherical and thus look the same from any direction.

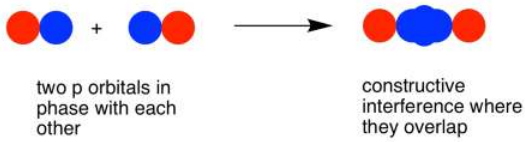


We first need to define one axis as lying along the N-N bond. It does not really matter which one. We arbitrarily say the N-N bond lies along the z axis. The p_z orbitals have a different spatial relationship to each other compared to the p_y and p_x. The p_z orbitals lie along the bond axis, whereas the p_y and p_x are orthogonal to it.

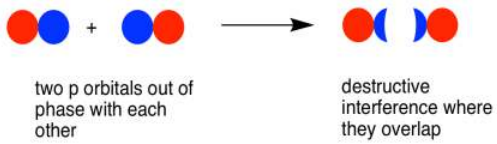


As the nitrogen atoms are brought together, one lobe on one p_z orbital overlaps strongly with one lobe on the other p_z orbital. The other lobes point away from each other and do not interact in any obvious way.

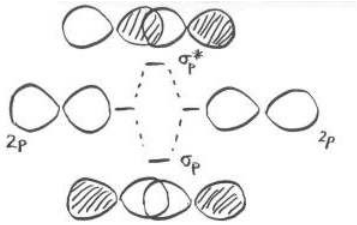
As with the s orbital, the p_z orbitals can be in-phase or out-of-phase. The in-phase combination results in constructive interference. (Here, "in-phase" means the lobes that overlap are in-phase; for that to happen the two p orbitals are actually completely out-of-phase with each other mathematically, so that one orbital is the mirror image of the other.) This combination is at a longer wavelength than the original orbital. It is a lower energy combination.



The out-of-phase combination (meaning in this case that the overlapping lobes are out-of-phase) results in destructive interference. This combination is at shorter wavelength than the original orbital. It is a higher energy combination.



As a result, we have two different combinations stemming from two different p orbitals coming together in two different ways. We get a low-energy, in-phase, bonding combination and a high-energy, out-of-phase, antibonding combination.

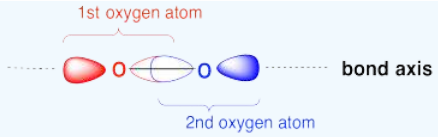


What about those other p orbitals, the ones that do not lie along the bond axis? We'll take a look at that problem on the next page.

? Exercise 3.2.2.2

Draw an MO cartoon of a sigma bonding orbital formed by the overlap of two p orbitals between two oxygen atoms. Label the positions of the oxygen nuclei with the symbol "O". Label the O-O bond axis.

Answer



Exercise 3.2.2.3

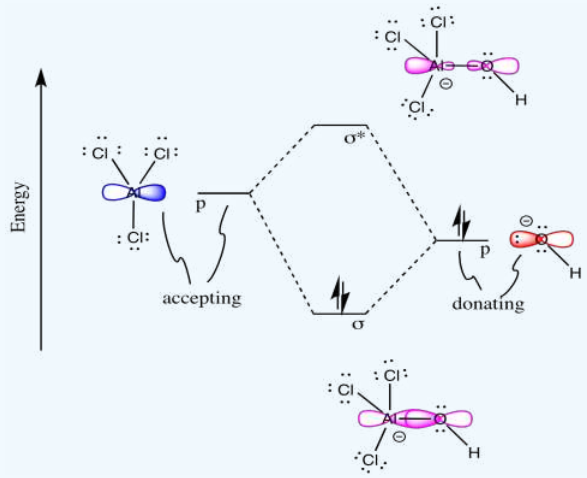
Chemical reactions can be described by MO diagrams too! Consider the following reaction in which a new sigma bond is formed.



Draw an MO diagram for the reaction above. In other words, start from the one frontier MO on each reactant to build the MO's of the new sigma bond in the product.

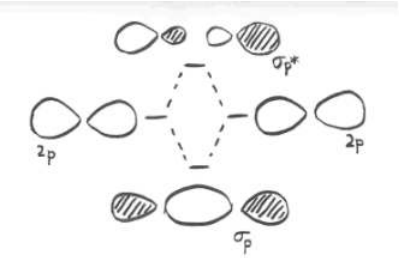
- o Draw the orbital from the base (hydroxide) that is likely to donate its electrons.
- o Draw the orbital from the acid (aluminum chloride) that is likely to accept electrons.
- o Complete the MO mixing diagram of these two orbitals:
  - • Label the electron donating orbital
  - • Label the electron accepting orbital
  - • Populate the MO mixing diagram with electrons
- o Draw a cartoon showing each reactant and product MO that contributes to the bonding interaction.

Answer



Pi-bonding with p-orbitals

Earlier, we saw that p orbitals that lie along the same axis can interact to form bonds.



Parallel, but not collinear, p orbitals can also interact with each other. They would approach each other side by side, above and below the bond axis between the two atoms. They can be close enough to each other to overlap, although they do not overlap as strongly as orbitals lying along the bond axis. They can make an in-phase combination, as shown below.

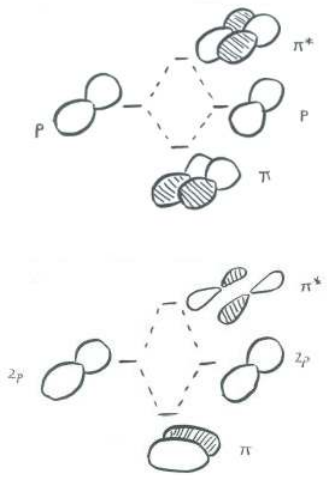


They could also make an out-of-phase combination, as shown below.



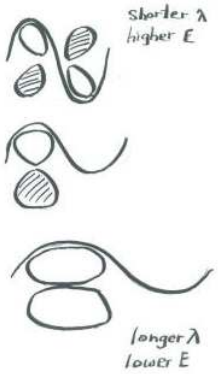
- parallel p orbitals can overlap to produce bonding and antibonding combinations.
- the resulting orbitals contain nodes along the bond axis.
- the electron density is found above and below the bond axis.
- this is called a p (pi) bond.

The illustration above is for one set of p orbitals that are orthogonal to the bond axis. The second picture shows the result of the constructive (or destructive) interference. A similar picture could be shown for the other set of p orbitals.

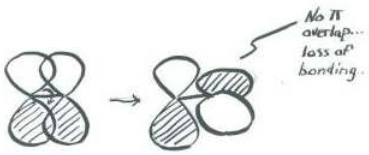


In a main group diatomic species like dinitrogen, one p orbital lying along the bond axis can engage in s bonding. The two p orbitals orthogonal to the bond axis can engage in p bonding. There will be both bonding and antibonding combinations.

Just as the sigma-bonding orbitals display progressively shorter wavelengths along the bonding axis as they go to higher energy, so do the pi bonding orbitals. In other words, there are more nodes in the higher-energy orbitals than in the lower-energy ones.



An important consequence of the spatial distribution or "shape" of a p orbital is that it is not symmetric with respect to the bond axis. An s orbital is not affected when the atom at one end of the bond is rotated with respect to the other. A p orbital is affected by such a rotation. If one atom turns with respect to the other, the p orbital would have to stretch to maintain the connection. The orbitals would not be able to overlap, so the connection between the atoms would be lost.



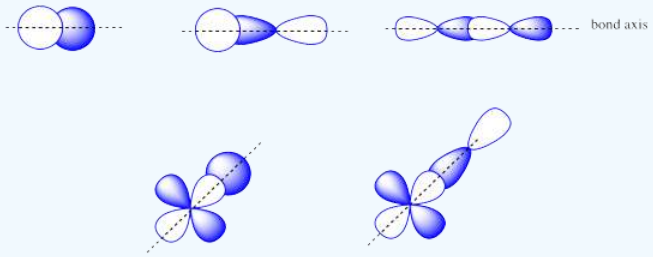
? Exercise 3.2.2.4

The combinations of _____ atomic orbitals leads to σ orbitals.

Draw pictures.

Answer

The combinations of ***s*** + ***s*** OR ***s*** + ***p*** OR ***p*** + ***p*** OR ***s*** + ***d*** OR ***p*** + ***d*** atomic orbitals can lead to σ orbitals.



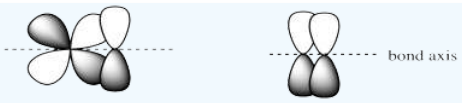
? Exercise 3.2.2.5

The combinations of _____ atomic orbitals leads to π orbitals.

Draw pictures.

Answer

The combinations of side by side p + p or p + d atomic orbitals leads to π orbitals.



Exercise 3.2.2.6

Which molecular orbital is typically the highest in energy?

a. p
b. σ
c. π*
d. π
e. σ*

Answer

e) σ*

Exercise 3.2.2.7

Why would a *core* 1s orbital not interact with a *valence* 2s orbital?

Hint: Why is a Li_2O bond stronger than a K_2O bond?

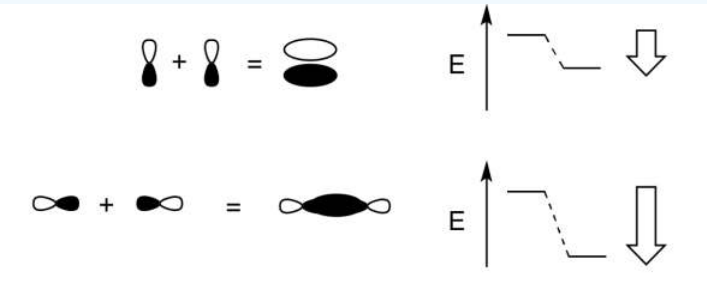
Answer

Li^+ and O^{2-} are more similar in size than K^+ and O^{2-}, so the bond between Li^+ and O^{2-} is stronger.

The energy difference between any core orbitals and valence orbitals is too large, so they cannot interact. In order for orbitals to interact, the orbitals need to have the same symmetry, be in the same plane, and be similar in energy.

Exercise 3.2.2.8

Add a few words to explain the ideas conveyed in these drawings.



Answer

When two parallel p orbitals combine out-of-phase, destructive interference occurs.

There is a node between the atoms.

The energy of the electrons increases.

When two parallel p orbitals combine in-phase, constructive interference occurs.

There is no node between the atoms; the electrons are found above and below the axis connecting the atoms.

The energy of the electrons decreases.

Attribution

Chris P Schaller, Ph.D., (College of Saint Benedict / Saint John's University)

Curated or created by Kathryn Haas

This page titled 3.2.2: Molecular Orbitals from p Orbitals is shared under a CC BY-NC-SA 4.0 license and was authored, remixed, and/or curated by Chris Schaller.

- **5.1.2: Molecular Orbitals from p Orbitals** by Chris Schaller is licensed CC BY-NC 3.0.

3.2.3: Molecular orbitals from d orbitals

In transition metals and other heavier elements, the d orbitals may combine with other orbitals of compatible symmetry (and energy) to form molecular orbitals. Generally, there are three types of bonding and antibonding interactions that may occur with d orbitals: sigma (σ), pi (π), and delta (δ) bonds.

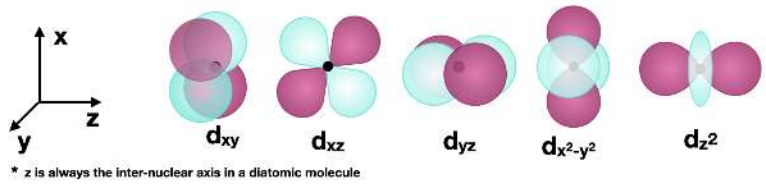


Figure 3.2.3.1: The five $3d$ orbitals are shown. The orientation of the axes is consistent and the z axis is horizontal for convenience in drawing bonding along the z axis (see examples below). (CC-BY-SA; Kathryn Haas)

Sigma (σ) bonding with d orbitals

σ bonds are symmetric with respect to the inter-nuclear axis (in a diatomic molecule, this is the z axis). An example of a σ bond formed by d orbitals is that of two d_{z^2} orbitals (see Figure 3.2.3.2). If a bonded atom is in a position other than on the z axis (in an octahedral geometry, for example), σ bonds can also form. For example, two $d_{x^2-y^2}$ orbitals on atoms bonded along the x or y axes could also form a σ bond.

d orbitals can also form σ bonds with other types of orbitals with the appropriate symmetry. Examples of orbitals with appropriate symmetry are the s orbital and certain p orbitals on another atom, as shown below in Figure 3.2.3.2.

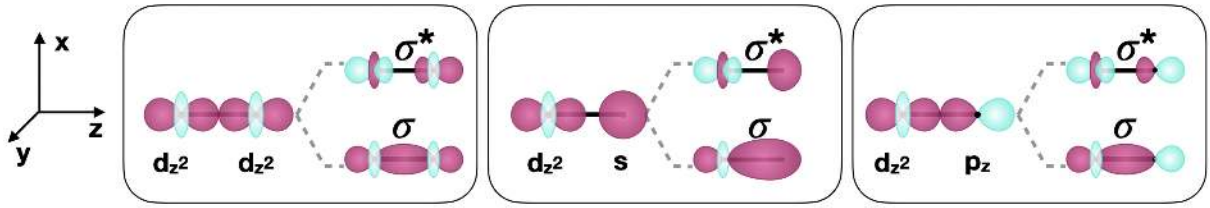


Figure 3.2.3.2: Selected examples of σ bonds involving d orbitals along the z internuclear axis (shown as a bold horizontal line) between two atoms. (CC-BY-SA; Kathryn Haas)

Pi (π) bonding with d orbitals

π bonds are those with one node that is in-plane with the internuclear axis. A π bond can form between two d orbitals or between d orbitals and other types of orbitals with comparable symmetry. An example of a π bond between two d orbitals is that formed by two d_{xz} orbitals along the z axis (shown in Figure 3.2.3.3). d orbitals can also form π bonds using p orbitals with compatible symmetry, as shown in Figure 3.2.3.3.

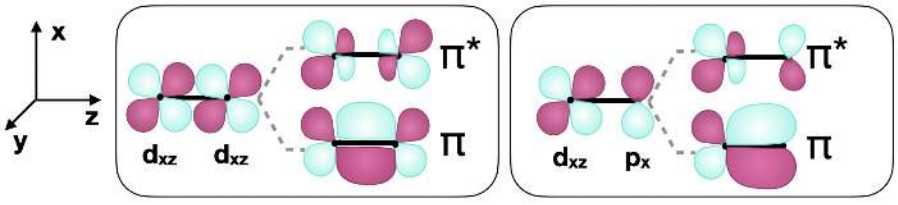


Figure 3.2.3.3: Selected examples of π bonds involving d orbitals along the z internuclear axis (shown as a bold horizontal line) between two atoms. (CC-BY-SA; Kathryn Haas)

Delta (δ) bonding with d orbitals

δ bonds are those with two nodes that are in-plane with the internuclear axis. δ bonds can form between two d orbitals with appropriate symmetry. For example, when two atoms bond along the z axis, the d_{xy} orbitals and the two $d_{x^2-y^2}$ orbitals can form δ bonds (Figure 3.2.3.4).

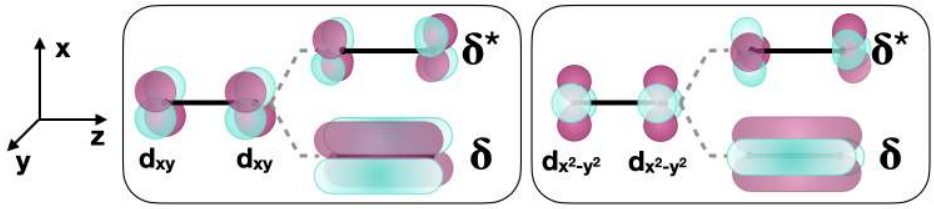


Figure 3.2.3.4: Selected examples of δ bonds involving d orbitals along the z internuclear axis (shown in bold horizontal line) between two atoms. (CC-BY-SA; Kathryn Haas)

Incompatible orbitals

In the descriptions above, we focused on how bonds (and antibonds) can be formed with d orbitals. All bonding and non-bonding interactions require that orbitals have compatible symmetry to form productive interactions. It is worth mentioning that orbitals with symmetry that is incompatible with the d orbitals will not have bonding or antibonding interactions with d orbitals. The figure below shows several sets of orbitals that are incompatible for bonding.

Curated or created by Kathryn Haas

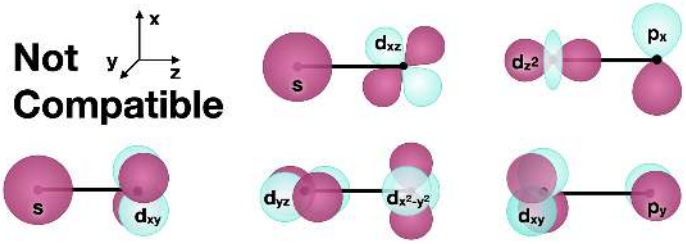


Figure 3.2.3.5: Several incompatible pairs of orbitals. (CC-BY-SA; Kathryn Haas)

This page titled 3.2.3: Molecular orbitals from d orbitals is shared under a CC BY-NC-SA 4.0 license and was authored, remixed, and/or curated by Kathryn Haas.

- **5.1.3: Molecular orbitals from d orbitals** by Kathryn Haas is licensed CC BY-SA 4.0.

3.2.4: Nonbonding Orbitals and Other Factors

The simplest case is when there is an even number of atomic orbitals that all combine to form strong bonding and antibonding orbitals. But what if there is an uneven number of atomic orbitals? Or what if there are some orbitals that don't meet the criteria for bonding? Or what if the bonding interactions are weak? In these cases, there will be molecular orbitals on the molecule that have non-bonding character.

It is important to note that the bonding, non-bonding, and antibonding nature of orbitals exist on a spectrum. Some bonding and anti-bonding orbitals may have some non-bonding character depending on where their energies lie with respect to the original atomic orbital energies. When molecular orbitals have energies similar to their original atomic orbitals, they will have some non-bonding character. The closer the energies of atomic and molecular orbitals, the more non-bonding the molecular orbitals.

Two major factors to consider

Uneven number of atomic orbitals: In the case that there is an uneven number of atomic orbitals with compatible symmetry, orbitals with non-bonding character will form. For example, in the case where three atomic orbitals combine, the most common result is formation of a low-energy bonding orbital, a high energy antibonding orbital, and a non-bonding orbital of intermediate energy (Figure 3.2.4.1).

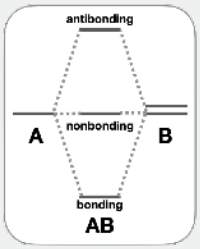


Figure 3.2.4.1. This figure illustrates the most common case for three atomic orbitals that combine to form three molecular orbitals; formation of one low-energy bonding, one high-energy antibonding, and one intermediate energy non-bonding molecular orbital. (CC-BY-NC-SA, Kathryn Haas)

Differences in energy: Combination of orbitals with different energies may lead to orbitals with non-bonding character. Atomic orbitals that have similar energies will have the strongest interactions, and result in bonding molecular orbitals with much lower energies than the component atomic orbitals. On the other hand, atomic orbitals with very unequal energies have a weaker interaction because the molecular orbitals are closer in energy to the atomic orbital energies, thus there is less energy benefit to putting electrons in the bonding molecular orbitals (Figure 3.2.4.2). When bonding or antibonding orbitals are close to the energies of the contributing atomic orbitals, those molecular orbitals may have some non-bonding character.

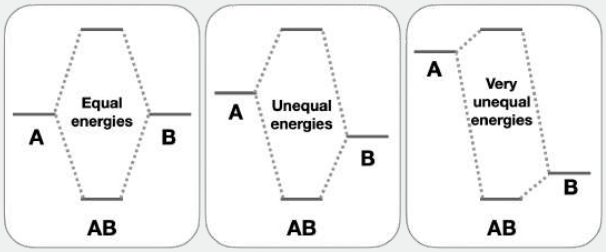


Figure 3.2.4.2. This figure illustrates how relative energies of atomic orbitals result in molecular orbitals that are more or less favorable. The greater the energy difference between atomic orbitals and the bonding molecular orbital, the more eneretically favorable it is for bonding to occur. (CC-BY-NC-SA, Kathryn Haas)

This page titled 3.2.4: Nonbonding Orbitals and Other Factors is shared under a CC BY-NC-SA 4.0 license and was authored, remixed, and/or curated by Kathryn Haas.

- **5.1.4: Nonbonding Orbitals and Other Factors** by Kathryn Haas is licensed CC BY-SA 4.0.

SECTION OVERVIEW

3.3: Homonuclear Diatomic Molecules

In this section you will be introduced to the molecular orbital diagrams of several homonuclear diatomic molecules. Homonuclear diatomic molecules are molecules made of exactly two identical atoms, and they are relatively simple.

3.3.1: Molecular Orbitals

3.3.2: Orbital Mixing

3.3.3: Diatomic Molecules of the First and Second Periods

3.3.4: Photoelectron Spectroscopy

This page titled 3.3: Homonuclear Diatomic Molecules is shared under a CC BY-NC-SA 4.0 license and was authored, remixed, and/or curated by Kathryn Haas.

3.3.1: Molecular Orbitals

There are several cases where our more elementary models of bonding (like Lewis Theory and Valence Bond Theory) fail to predict the actual molecular properties and reactivity. A classic example is the case of O_2 and its magnetic properties. At very cold temperatures, O_2 is attracted to a magnetic field, and thus it must be paramagnetic (unpaired electrons give rise to magnetism). Watch the video below!



The magnetic properties of O_2 are easily rationalized by its **molecular orbital diagram**. A molecular orbital diagram is a diagram that shows the relative energies and identities of each molecular orbital in a molecule. Figure 3.3.1.1 shows a simplified and generic molecular orbital diagram for a second-row homonuclear diatomic molecule. The diagram is simplified in that it assumes that interactions are limited to degenerate orbitals from two atoms (see next section).

There are some things you should note as you inspect Figure 3.3.1.1 (and keep these in mind as you draw your own diagrams!). First, notice that there are the **same number of molecular orbitals as there are atomic orbitals**. Second, notice that **each orbital in the diagram is rigorously labeled** using labels (σ and π) that include the subscripts u and g. These labels and subscripts indicate the symmetry of the orbitals. The σ symbol indicates that the orbital is symmetric with respect to the internuclear axis, while the π label indicates that there is one node along that axis. The g and u stand for *gerade* and *ungerade*, the German words for *even* and *uneven*, respectively. The subscript g is given to orbitals that are *even*, or *symmetric*, with respect to an inversion center. The subscript u is given to orbitals that are *uneven*, or *antisymetric*, with respect to an inversion center. The pictures of calculated molecular orbitals are shown in Figure 3.3.1.1 to illustrate the symmetry of each orbital.

Another important thing to notice is that the diagram in Figure 3.3.1.1 lacks electrons (because it is generic for any second-row diatomic molecule). If this were a *complete* molecular orbital diagram it would **include the electrons for each atom and for the molecule**. Electrons in molecular orbitals are filled in the same way an atomic orbital diagram would be filled, where electrons occupy lower energy orbitals before higher energy orbitals, and electrons occupy empty degenerate orbitals before pairing. A complete molecular orbital diagram would show whether the molecule is diamagnetic or paramagnetic. It can also be used to calculate the bond order of the molecule (the number of bonds between atoms) using the formula below:

$$\text{Bond order } = \frac{1}{2}\left[\begin{pmatrix}\text{number of electrons}\\ \text{in bonding orbitals}\end{pmatrix} - \begin{pmatrix}\text{number of electrons}\\ \text{in antibonding orbitals}\end{pmatrix}\right]$$

In general, non-valence (core) electrons can be ignored because they contribute nothing to the bond order. In fact, many molecular orbital diagrams will ignore the core orbitals, as they are insignificant for bonding interactions and reactivity.

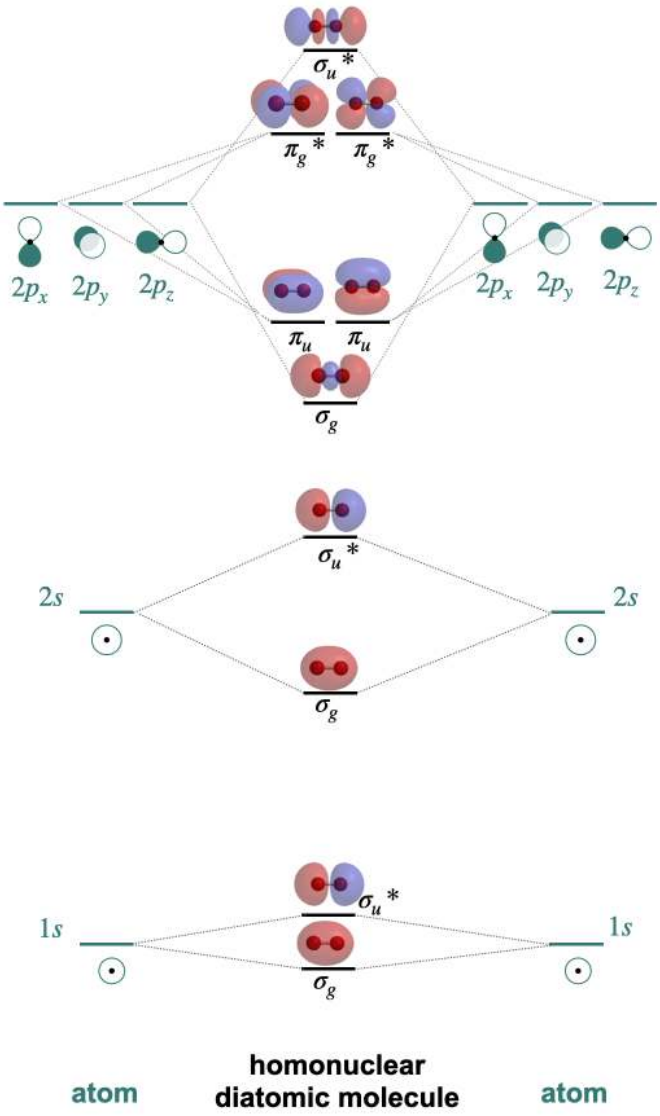


Figure **3.3.1.1**: A generic molecular orbital diagram for a homonuclear diatomic molecule of second-row elements assuming no orbital mixing (interactions are formed by orbitals of the same energy from each atom). (CC-BY-NC-SA, Kathryn Haas)

Now, to see how this molecular orbital diagram can explain the magnetic behaviour of O_2, complete the example below.

✔ Example **3.3.1.1**

Let's change Figure **3.3.1.1** to make it specific for O_2. Re-draw the MO diagram (no need to draw the shapes of orbitals). Fill in the correct number of electrons for each oxygen atom on either side of the diagram. Then, fill in the total molecular electrons in the center. Calculate the bond order and determine whether it is diamagnetic or paramagnetic.

Solution

The diagram in Figure **3.3.1.1** includes core orbitals (the 1s) and valence electrons (2s, 2p). Therefore, we will consider all the electrons in an oxygen atom and a dioxygen molecule. An oxygen atom has eight total electrons. So we fill eight electrons into the atomic orbitals for the oxygen atom on the right, and eight electrons into the atomic orbitals for oxygen on the left. The total number of electrons for the molecule is sixteen, so fill in 16 electrons into the molecular orbitals, being sure to apply Hund's rule and the Aufbau principle. The result is a diagram that looks like the one drawn below in Figure **3.3.1.2**.

The bond order is calculated using the molecular orbitals (we can ignore atomic orbitals). There are 10 electrons in binding orbitals and 6 electrons in antibonding orbitals). This gives a bond order of $\frac{1}{2}(10-6)=2$. This bond order is consistent with valence bond theory!

This diagram indicates that dioxygen is paramagnetic; it has two unpaired electrons in the π^* orbitals. This paramagnetic electron configuration explains why dioxygen is attacted to magnetic fields!

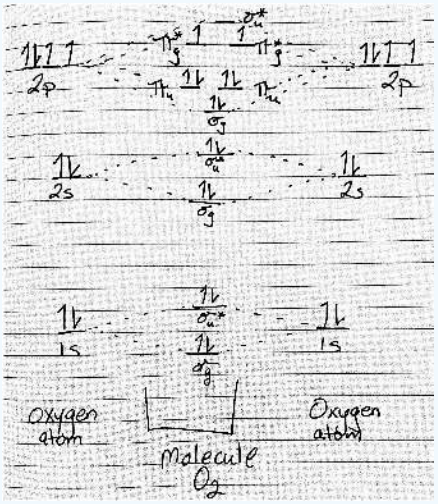


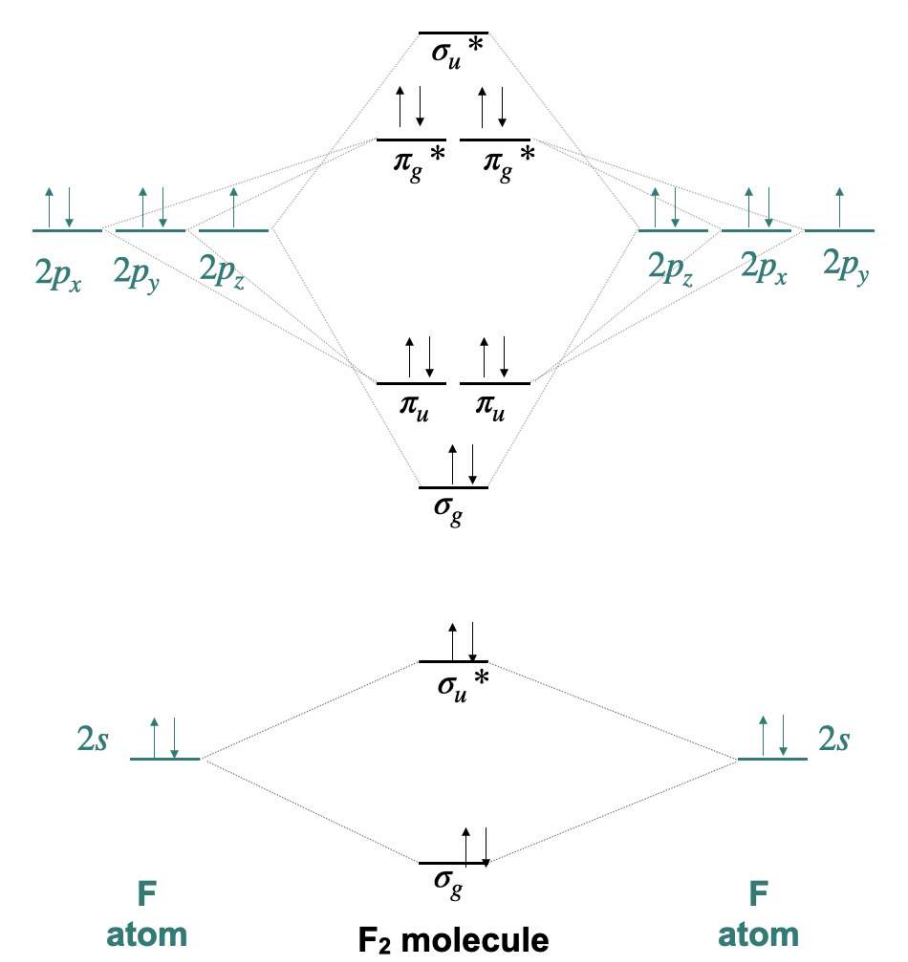
Figure 3.3.1.2: Hand-drawn molecular orbital diagram for dioxygen. (CC-BY-SA; Kathryn Haas)

? Exercise 3.3.1.1

Draw the molecular orbital diagram for F_2; be sure to label your orbitals with the appropriate symmetry and count your orbitals to make sure that the total number of atomic orbitals and molecular orbitals is the same. As a shortcut, include only the valence orbitals and electrons. What is the bond order? Is the molecule diamagnetic or paramagnetic?

Answer

The valence orbitals on an F atom are 2s and 2p. And, there are seven valence electrons in F. This gives fourteen total valence electrons. The MO diagram of the valence molecular orbitals can be constructed by combining the valence 2s and valence 2p orbitals from each F atom. The bond order is 1 and the molecule is diamagnetic.



This page titled 3.3.1: Molecular Orbitals is shared under a CC BY-NC-SA 4.0 license and was authored, remixed, and/or curated by Kathryn Haas.

- **5.2.1: Molecular Orbitals** by Kathryn Haas is licensed CC BY-SA 4.0.

3.3.2: Orbital Mixing

In the previous section, we introduced a simplified molecular orbital (MO) diagram, assuming that interactions were limited to degenerate orbitals of compatible symmetry. A version of that *simplified* diagram for second-row homonuclear diatomics is shown on the left side of Figure **3.3.2.1** (only valence orbitals shown).

In reality, orbitals of compatible symmetry can combine, or mix, even when they have different energies. When sets of orbitals mix, it has the effect of decreasing the energy of the lower-energy set and increasing the energy of the higher-energy set. There are two ways to explain mixing, described in the points below. The diagram on the right of side of Figure **3.3.2.1** shows how energy levels are affected by orbital mixing.

- **Starting from the simplified MO diagram and mixing molecular orbitals of like symmetry**: If we start with the "no mixing" simplified diagram shown on the left, we can pick out the orbitals with like symmetry and consider what will happen if these molecular orbitals mix. For example, starting from the MO diagram on the left side of Figure **3.3.2.1**, we see that there are two σ_g orbitals that have identical symmetry (hence they have identical symmetry labels). Upon mixing, the lower-energy $\sigma_g(2s)$ will decrease in energy while the higher-energy $\sigma_g(2p)$ will increase in energy. Likewise, there are two σ_u^* orbitals that will mix, decreasing the energy of $\sigma_u^*(2s)$ while increasing the energy of $\sigma_u^*(2p)$.
- **Starting from and mixing atomic orbitals of compatible symmetry**: Starting from the atomic orbitals, we can select the orbitals that have compatible symmetry to make productive interactions, and combine them as a set to make molecular orbitals. From the two sets of atomic orbitals on the right panel in Figure **3.3.2.1**, there are two sets of four orbitals with compatable symmetry; one is the set of two $2s$ and two $2p_z$ orbitals. These four orbitals can combine to form molecular orbitals with σ symmetry. They combine to form one lowest-energy bonding σ_g, a highest-energy σ_u^*, and two orbitals with intermediate energy (σ_g, and σ_u^*). This treatment can be expressed as the linear combination of four atomic orbitals:

  $$\Psi = c_1\psi(2s_a) \pm c_2\psi(2s_b) \pm c_3\psi(2p_a) \pm c_4\psi(2p_b)$$

  where the coefficients $c_1 = c_2$ and $c_3 = c_4$ for homonuclear diatomic molecules.

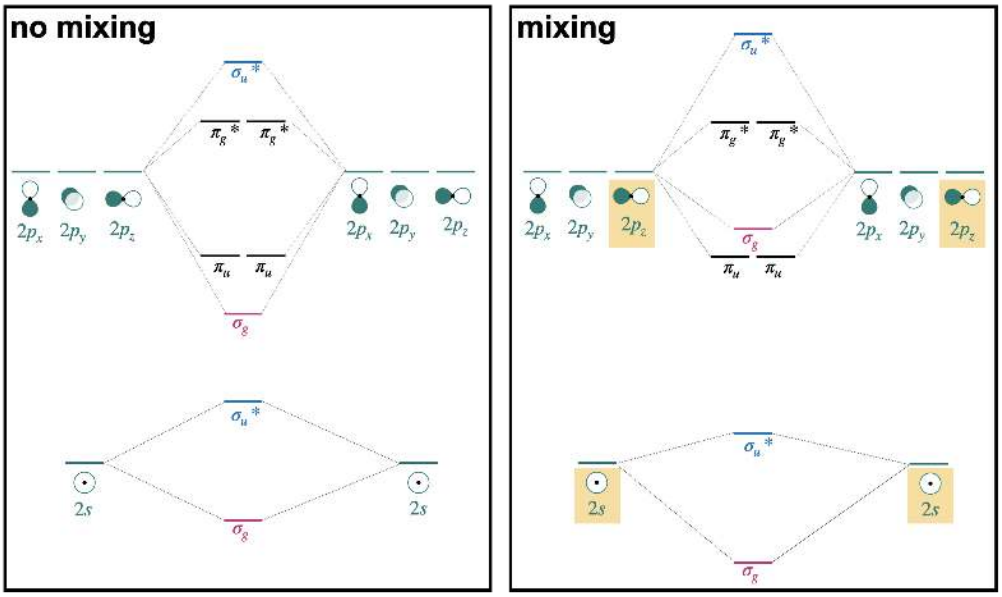


Figure **3.3.2.1**: Mixing of orbitals with like symmetry affects the energies of molecular orbitals. The simplified case where no mixing occurs is shown on the left. The effects of mixing are shown on the right. The σ_g orbitals of like symmetry are highlighted in fuschia and the σ_u^* orbitals of like symmetry are highlighted in blue. A group of atomic orbitals of similar symmetry are highlighted in yellow boxes; these atomic orbitals combine to give all σ molecular orbitals. (CC-BY-SA, Kathryn Haas)

In the case of homonuclear diatomic molecules of the second row, orbital mixing has important consequences for the energetic order of the $\sigma_g(2p)$ and $\pi_u(2p)$ orbitals. This will be discussed in the next section.

This page titled 3.3.2: Orbital Mixing is shared under a CC BY-NC-SA 4.0 license and was authored, remixed, and/or curated by Kathryn Haas.

- **5.2.2: Orbital Mixing** by Kathryn Haas is licensed CC BY-SA 4.0.

https://chem.libretexts.org/@go/page/360829

3.3.3: Diatomic Molecules of the First and Second Periods

First Period Homonuclear Diatomic Molecules

In the first row of the periodic table, the valence atomic orbitals are $1s$. There are two possible homonuclear diatomic molecules of the first period:

Dihydrogen, H_2 $[\sigma_g^2(1s)]$: This is the simplest diatomic molecule. It has only two molecular orbitals (σ_g and σ_u^*), two electrons, a bond order of 1, and is diamagnetic. Its bond length is 74 pm. MO theory would lead us to expect bond order to decrease and bond length to increase if we either add or subtract one electron. The calculated bond length for the H_2^+ ion is approximately 105 pm.[1]

Dihelium, He_2 $[\sigma_g^2\sigma_u^{*2}(1s)]$: This molecule has a bond order of zero due to equal number of electrons in bonding and antibonding orbitals. Like other nobel gases, He exists in the atomic form and does not form bonds at ordinary temperatures and pressures.

? Exercise 3.3.3.1

Draw the complete molecular orbital diagrams for H_2 and for He_2. Include sketches of the atomic and molecular orbitals.

Answer

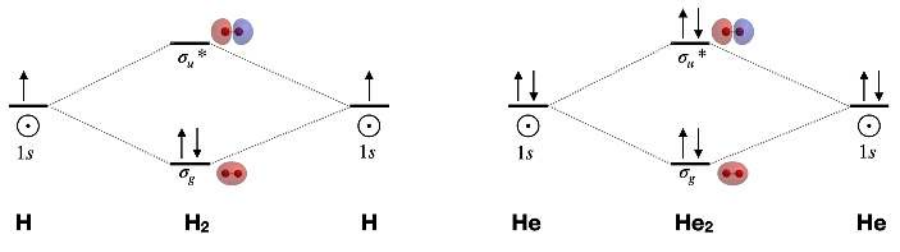


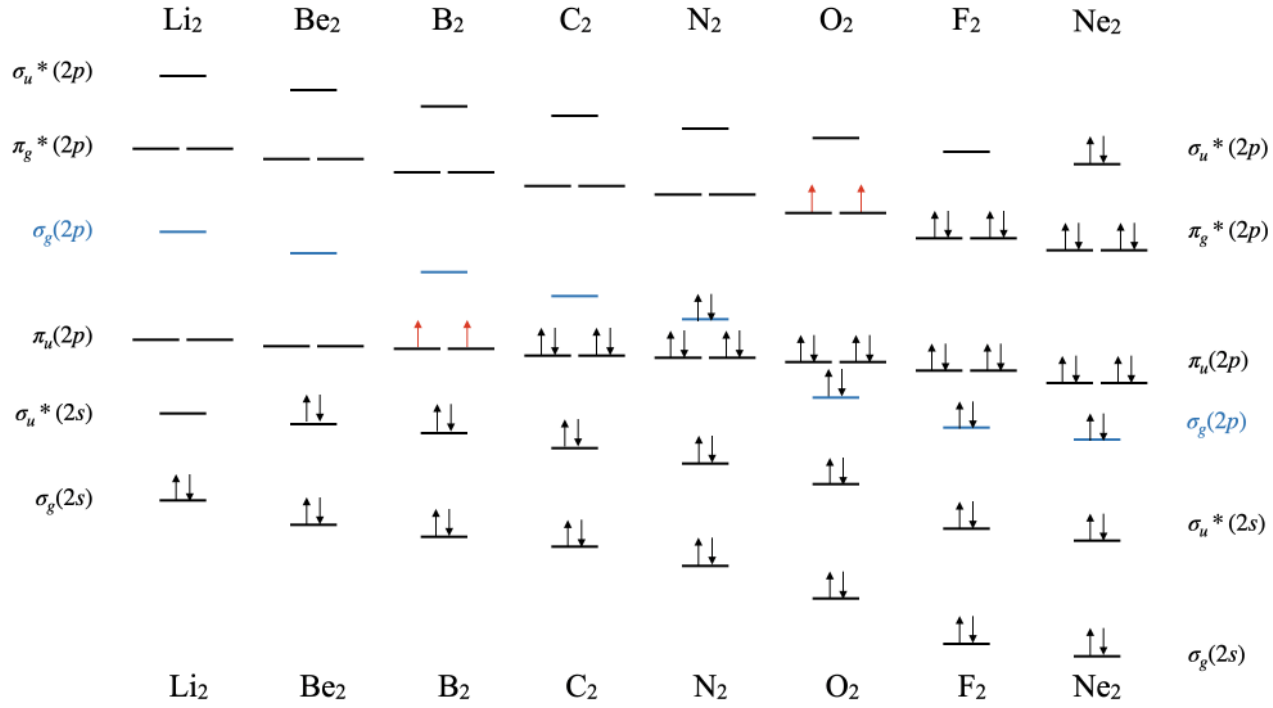
Figure for Exercise 3.3.3.1: Molecular orbital diagrams for dihydrogen and dihelium. Molecular orbital surfaces calculated using Spartan software. (CC-BY-NC-SA; Kathryn Haas)

A complete molecular orbital diagram includes all atomic orbitals and molecular orbitals, their symmetry labels, and electron filling.

Second Period Homonuclear Diatomic Molecules

The second period elements span from Li to Ne. The valence orbitals are 2s and 2p. In their molecular orbital diagrams, non-valence orbitals (1s in this case) are often disregarded in molecular orbital diagrams.

Orbital mixing has significant consequences for the magnetic and spectroscopic properties of second period homonuclear diatomic molecules because it affects the order of filling of the $\sigma_g(2p)$ and $\pi_u(2p)$ orbitals. Early in period 2 (up to and including nitrogen), the $\pi_u(2p)$ orbitals are lower in energy than the $\sigma_g(2p)$ (see Figure 3.3.3.1). However, later in period 2, the $\sigma_g(2p)$ orbitals are pulled to a lower energy. This lowering in energy of $\sigma_g(2p)$ is not unique; all of the σ orbitals in the molecule are pulled to lower energy due to the increasing positive charge of the nucleus. The π orbitals in the molecule are also affected, but to a much lesser extent than σ orbitals. The reason has to do with the high penetration of s atomic orbitals compared to p atomic orbitals (recall our previous discussion on penetration and shielding, and its effect on periodic trends). The σ molecular orbitals have more s character and thus their energy is more influenced by increasing nuclear charge. As nuclear charge increases, the energy of the $\sigma_g(2p)$ orbital is lowered significantly more than the energy of the $\pi_u(2p)$ orbitals (Figure 3.3.3.1).



	Li_2	Be_2	B_2	C_2	N_2	O_2	F_2	Ne_2
Unpaired e⁻	0	0	2	0	0	2	0	0
Bond Order	1	0	1	2	3	2	1	0
Experimental* Bond Length (pm)	267.3	246.0	159.0	124.3	109.8	120.8	141.2	310.0

*Experimental bond lengths from "List of Experimental Diatomic Bond Lengths", NIST, https://cccbdb.nist.gov/diatomicexpbondx.asp

Figure 3.3.3.1: Molecular orbital energy-level diagrams for the diatomic molecules of the period 2 elements. Unlike earlier diagrams, *only the valence molecular orbital energy levels for the **molecules** are shown here (atomic orbitals not shown for simplicity).* For Li_2 through N_2, the $\sigma_g(2p)$ orbital is higher in energy than the $\pi_u(2p)$ orbitals. In contrast, from O_2 onward, the $\sigma_g(2p)$ orbital is *lower* in energy than the $\pi_u(2p)$ orbitals because the nuclear charge increases across the row. The experimental bond lengths correlate with the calculated bond order. (CC-BY-NC-SA, Kathryn Haas)

Dilithium, Li_2 $[\sigma_g^2(2s)]$: This molecule has a bond order of one and is observed experimentally in the gas phase to have one Li-Li bond.

Diberylium, Be_2 $[\sigma_g^2\sigma_u^{*2}(2s)]$: This molecule has a bond order of zero due to the equal number of electrons in bonding and antibonding orbitals. Although Be_2 does not exist under ordinary conditions, it can be produced in a laboratory and its bond length measured (Figure 3.3.3.2). Although the bond is very weak, its bond length is surprisingly ordinary for a covalent bond of the second period elements.[2]

Diboron, B_2 $[\sigma_g^2\sigma_u^{*2}(2s)\pi_u^1\pi_u^1(2p)]$: The case of diboron is one that is much better described by molecular orbital theory than by Lewis structures or valence bond theory. This molecule has a bond order of one. The molecular orbital description of diboron also predicts, accurately, that diboron is paramagnetic. The paramagnetism is a consequence of orbital mixing, resulting in the σ_g orbital's being at a higher energy than the two degenerate π_u^* orbitals.

Dicarbon, C_2 $[\sigma_g^2\sigma_u^{*2}(2s)\pi_u^2\pi_u^2(2p)]$: This molecule has a bond order of two. Molecular orbital theory predicts two bonds with π symmetry, and no σ bonding. C_2 is rare in nature because its allotrope, diamond, is much more stable.

Dinitrogen, N_2 $[\sigma_g^2\sigma_u^{*2}(2s)\pi_u^2\pi_u^2\sigma_g^2(2p)]$: This molecule is predicted to have a triple bond. This prediction is consistent with its short bond length and bond dissociation energy. The energies of the $\sigma_g(2p)$ and $\pi_u(2p)$ orbitals are very close, and their relative energy levels have been a subject of some debate (see next section for discussion).

Dioxygen, O_2 $[\sigma_g^2\sigma_u^{*2}(2s)\sigma_g^2\pi_u^2\pi_u^2\pi_g^{*1}\pi_g^{*1}(2p)]$: This is another case where valence bond theory fails to predict actual properties. Molecular orbital theory correctly predicts that dioxygen is paramagnetic, with a bond order of two. Here, the molecular orbital diagram returns to its "normal" order of orbitals where orbital mixing could be somewhat ignored, and where $\sigma_g(2p)$ is lower in energy than $\pi_u(2p)$.

Difluorine, F_2 $[\sigma_g^2\sigma_u^{*2}(2s)\sigma_g^2\pi_u^2\pi_u^2\pi_g^{*2}\pi_g^{*2}(2p)]$: This molecule has a bond order of one and like oxygen, the $\sigma_g(2p)$ is lower in energy than $\pi_u(2p)$.

Dineon, Ne_2 $[\sigma_g^2\sigma_u^{*2}(2s)\sigma_g^2\pi_u^2\pi_u^2\pi_g^{*2}\pi_g^{*2}\sigma_u^{*2}(2p)]$: Like other noble gases, Ne exists in the atomic form and does not form bonds at ordinary temperatures and pressures. Like Be_2, Ne_2 is an unstable species that has been created in extreme laboratory conditions and its bond length has been measured (Figure **3.3.3.2**)

? Exercise 3.3.3.2

Draw the complete molecular orbital diagram for O_2. Show calculation of its bond order and tell whether it is diamagnetic or paramagnetic.

Answer

O_2 is paramagnetic with a bond order of 2. Its $\sigma_g(2p)$ molecular orbital is lower in energy that the set of $\pi_u(2p)$ orbitals.

$$\text{Bond order} = \frac{1}{2}\left[\left(\begin{array}{c}\textbf{8 electrons in}\\ \textbf{valence bonding orbitals}\end{array}\right) - \left(\begin{array}{c}\textbf{4 electrons in}\\ \textbf{valence antibonding orbitals}\end{array}\right)\right]$$

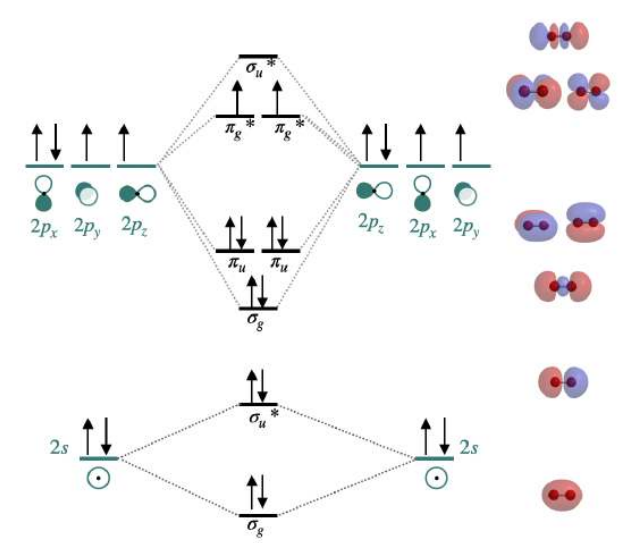


Figure for Exercise **3.3.3.2**. Molecular orbital diagram of O_2. (CC-BY-NC-SA, Kathryn Haas)

? Exercise 3.3.3.3: The Peroxide Ion

Use a qualitative molecular orbital energy-level diagram to predict the electron configuration, the bond order, and the number of unpaired electrons in the peroxide ion (O_2^{2-}).

Answer

This diagram looks similar to that of $\mathbf{O_2}$, except that there are two additional electrons.
$(\sigma_g(2s))^2\,(\sigma_u^*(2s))^2\,(\sigma_g(2p))^2\,(\pi_u(2p))^4\,(\pi_g(2p))^4$; bond order of 1; no unpaired electrons.

Bond Lengths in Homonuclear Diatomic Molecules

The trends in experimental bond lengths are predicted by molecular orbital theory, specifically by the calculated bond order. The values of bond order and experimental bond lengths for the second period diatomic molecules are given in Figure **3.3.3.1**, and

shown in graphical format on the plot in Figure **3.3.3.2**. From the plot, we can see that bond length correlates well with bond order, with a minimum bond length occurring where the bond order is greatest ($\mathbf{N_2}$). The shortest bond distance is at $\mathbf{N_2}$ due to its high bond order of 3. From $\mathbf{N_2}$ to $\mathbf{F_2}$ the bond distance increases despite the fact that atomic radius decreases.

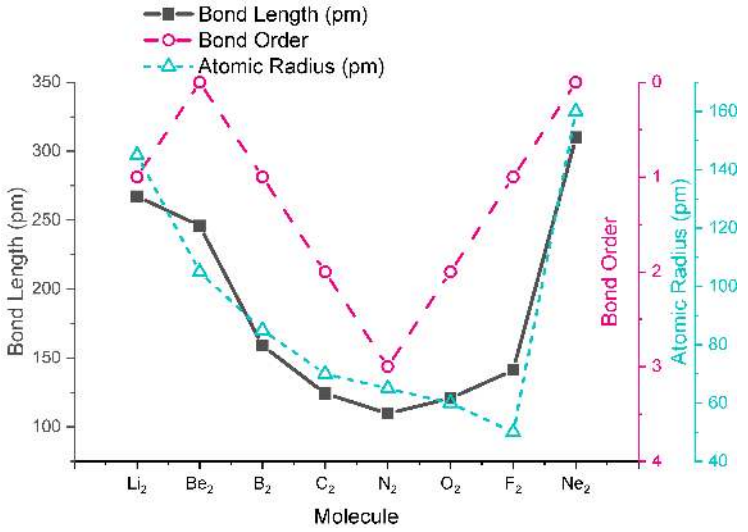


Figure **3.3.3.2**: Overlayed plots of bond length (black squares), bond order (pink circles), and atomic radius (teal triangles) versus atomic number for second period homonuclear diatomic molecules. (CC-BY-NC-SA; Kathryn Haas)

References

1. NIST, Calculated Geometries available for H_2^+ (Hydrogen cation) 2Σg+ D∞h, available at https://cccbdb.nist.gov/diatomicexpbondx.asp
2. Merritt, J. M.; Bondybey, V. E.; Heaven, M. C., Beryllium Dimer-Caught in the Act of Bonding. *Science* **2009,** *324* (5934), 1548-1551.

This page titled 3.3.3: Diatomic Molecules of the First and Second Periods is shared under a CC BY-NC-SA 4.0 license and was authored, remixed, and/or curated by Kathryn Haas.

- **5.2.3: Diatomic Molecules of the First and Second Periods** by Kathryn Haas is licensed CC BY-SA 4.0.
- **5.P: Problems** is licensed CC BY-SA 4.0.

3.3.4: Photoelectron Spectroscopy

A photoelectron spectrum can show the relative energies of occupied molecular orbitals by ionization. The *ionization energy* is a direct measure of the energy required to just remove the electron concerned from its initial level to the vacuum level (free electron). Photoelectron spectroscopy measures the relative energies of the ground and excited positive ion states that are obtained by removal of single electrons from the neutral molecule.

$$A + \text{photon} \rightarrow A^+ + e^-$$

The information obtained from photoelectron spectroscopy is typically discussed in terms of the electronic structure and bonding in the ground states of neutral molecules, with ionization of electrons occurring from bonding molecular orbitals, lone pairs, antibonding molecular orbitals, or atomic cores. These descriptions reflect the relationship of ionization energies to the molecular orbital model of electronic structure.

Ionization energies are directly related to the energies of molecular orbitals (by Koopmans' theorem).

Example: Photoelectron spectrum of dihydrogen

The molecular orbital description of dihydrogen involves two $1s$ atomic orbitals generating two molecular orbitals: a bonding σ_g and an antibonding σ_u^*. The two electrons occupy the σ_g bonding orbital, leaving the molecule with a bond order of one (Figure **3.3.4.1**). The PES spectrum of dihydrogen (Figure **3.3.4.1**) has a single band that corresponds to the ionization of one electron from the σ_g. The multiple peaks are due to electrons ejecting from a range of stimulated vibrational energy levels. When extensive vibrational structure is resolved in a PES molecular orbital, then the removal of an electron from that molecular orbital induces a significant change in the bonding (in this case an increase in the bond length due to decrease in bond order).

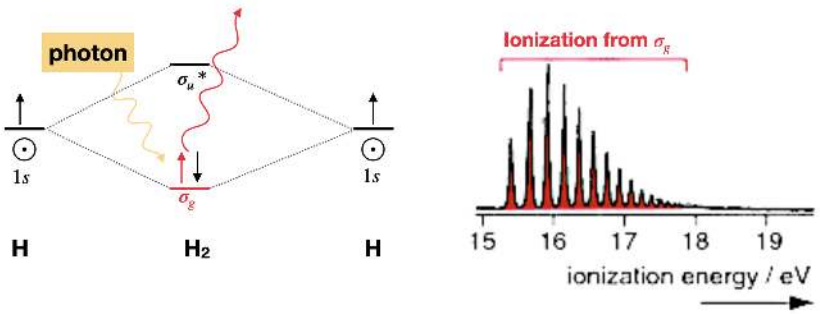


Figure **3.3.4.1**: The molecular orbital diagram and photoelectron spectrum of dihydrogen. (CC-BY-NC-SA; Libretexts)

Example: Photoelectron spectrum of dinitrogen

Diatomic nitrogen is more complex than hydrogen since multiple molecular orbitals are occupied. Five molecular orbitals are occupied; two of them are degenerate. Three bands in the photoelectron spectrum correspond to ionization of an electron in $\sigma_g(2p)$, $\pi_u(2p)$ and $\sigma_u^*(2s)$ molecular orbitals. Ionization of the fourth type of orbital, $\sigma_g(2s)$, does not appear in Figure **3.3.4.2** because it is either off scale or because the incident light $h\nu$ used did not have sufficient energy to ionize electrons in that deeply stabilized molecular orbital. Note that extensive vibrational structure for the $\pi_u(2p)$ band indicates that the removal of an electron from this molecular orbital causes a significant change in the bonding.

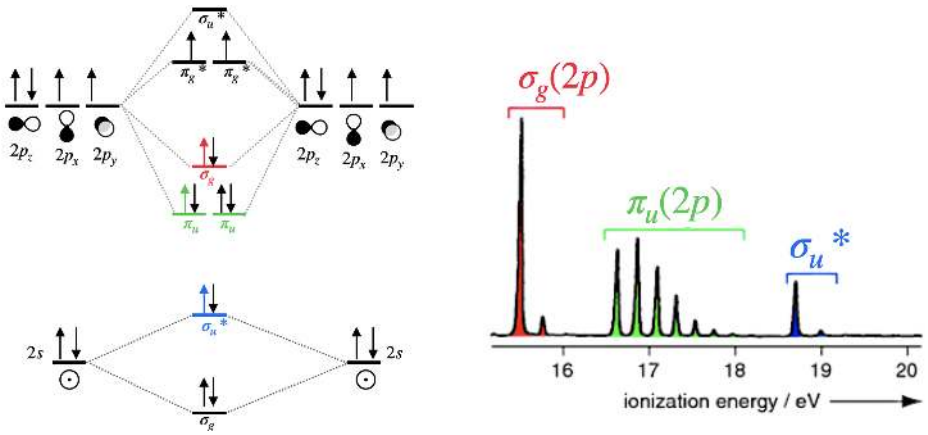


Figure **3.3.4.2**: The molecular orbital diagram and photoelectron spectrum of dinitrogen. (CC-BY-NC-SA; Libretexts)

From the photoelectron spectrum of dinitrogen, we can see that the electrons in the $\sigma_g(2p)$ orbital can be ionized using less energy than required to ionize electrons in the $\pi_u(2p)$ orbital. This is evidence for $\sigma_g(2p)$ existing at a higher energy than the $\pi_u(2p)$ orbitals.

This page titled 3.3.4: Photoelectron Spectroscopy is shared under a CC BY-NC-SA 4.0 license and was authored, remixed, and/or curated by Kathryn Haas.

- **10.4: Photoelectron Spectroscopy** by Roger Nix is licensed CC BY 4.0.

SECTION OVERVIEW

3.4: Heteronuclear Diatomic Molecules

Diatomic molecules with two non-identical atoms are called **heteronuclear** diatomic molecules. When atoms are not identical, the molecule forms by combining atomic orbitals of unequal energies. *The result is a polar bond in which atomic orbitals contribute unevenly to each molecular orbital*.

The application of molecular orbital theory to heteronuclear diatomic molecules is similar to the case of homonuclear diatomics, except that the atomic orbitals from each atom have different energies and contribute unequally to molecular orbitals. Recall that atomic orbitals must have compatible symmetry and similar energy to combine into molecular orbitals. In the case where atomic orbitals of like symmetry have different energies, they combine less favorably than orbitals that are closer to one another in energy. As a general rule, orbitals that have energy differences of greater than 10-14 eV do not combine favorably. In the molecular orbital diagram, the closer a molecular orbital is to an atomic orbital, the more that atomic orbital contributes to the molecular orbital. This last point is helpful for back-of-the napkin estimations of what the molecular orbitals "look" like.

In this section, you should learn how to generate molecular orbital diagrams of heteronuclear diatomic molecules. To approach such a problem, we must start with a knowledge of the relative energies of electrons in different atomic orbitals. In other words, we need knowledge of the orbital potential energies (or orbital ionization energies).

3.4.1: Polar bonds

3.4.2: Ionic Compounds and Molecular Orbitals

Sources:

- Gray, Harry. *Electrons and Chemical Bonding*, Benjamin, 1964.
- Miessler, Gary L, and Donald A. Tarr. *Inorganic Chemistry*. Upper Saddle River, N.J: Pearson Education, 2014. Print.

3.4: Heteronuclear Diatomic Molecules is shared under a CC BY-NC-SA 4.0 license and was authored, remixed, and/or curated by LibreTexts.

3.4.1: Polar bonds

Molecular orbital diagrams for heteronuclear diatomic molecules

The molecular orbital diagram of a heteronuclear diatomic molecule is approached in a way similar to that of a homonuclear diatomic molecule. The orbital diagrams may also look similar. A major difference is that the more electronegative atom will have orbitals at a lower energy level. Two examples of heteronuclear diatomic molecules will be explored below as illustrative examples.

Carbon monoxide MO diagram

Carbon monoxide is an example of a heteronuclear diatomic molecule where both atoms are second-row elements. The valence molecular orbitals in both atoms are the $2s$ and $2p$ orbitals. The molecular orbital diagram for carbon monoxide (Figure **3.4.1.1**) is constructed in a way similar to how you would construct dicarbon or dioxygen, except that the oxygen orbitals have a lower potential energy than analogous carbon orbitals. The labeling of molecular orbitals in this diagram follows a convention by which orbitals are given serial labels according to type of orbital (σ, π, etc.). The lowest energy orbitals of any type are assigned a value of 1 and higher energy orbitals of the same type are assigned by increasing intervals (..2, 3, 4...). The orbital labeling system described previously is inappropriate for heteronuclear diatomic molecules that cannot be assigned g and u subscripts.

A consequence of unequal atomic orbital energy levels is that orbital mixing is significant. Notice the order of the molecular orbitals labeled 1π and 3σ in Figure **3.4.1.1**. This is a similar order of π and σ orbitals to the one we saw in the case of the σ_g and π_u orbitals of N_2 and lighter diatomics of the second period. Because the oxygen $2p_z$ orbital is close in energy to both the carbon $2p_z$ and carbon $2s$, these three orbitals will have significant interaction (mixing). The result is an increase in the energy of the 3σ orbital and a decrease in energy of the $2\sigma^*$ orbital, resulting in the diagram shown in Figure **3.4.1.1**.

In the case of carbon monoxide (Figure **3.4.1.1**), atomic orbitals contribute unequally to each molecular orbital. For example, because the $2s$ orbital of oxygen is very close in energy to the 2σ moelcular orbital, it contributes to that molecular orbital more than the $2s$ orbital from carbon. Notice the shape of this 2σ orbital and how it is unevenly distributed over the two atoms; it is more heavily distributed on the oxygen because it is most like the oxygen $2s$. This is in line with the assumption that electron density is distributed more on oxygen because it is more electronegative than carbon. Likewise, the 1π orbitals are unevenly distributed, with more distribution close to the oxygen.

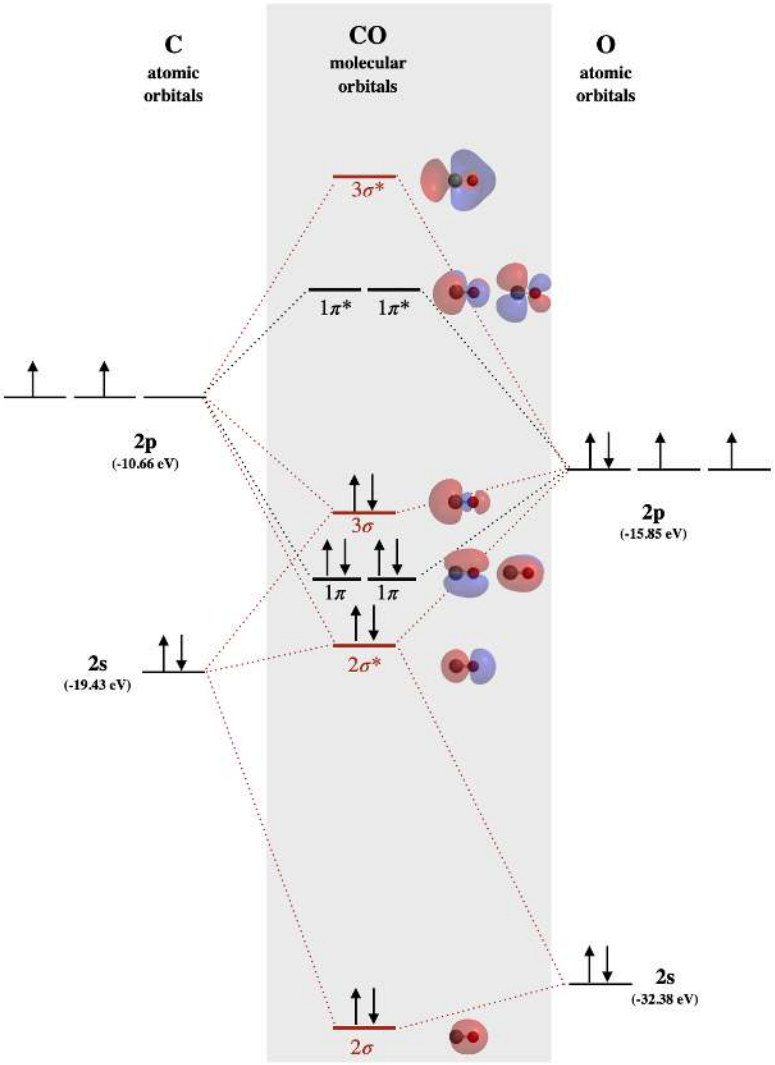
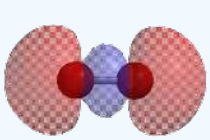


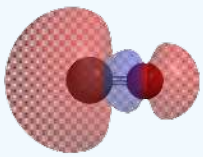
Figure 3.4.1.1: Molecular orbital diagram of carbon monoxide. The labeling of molecular orbitals in this diagram follows a convention by which orbitals are given serial names according to the type of orbital (σ, π, etc.). The lowest energy orbitals of any type are assigned a value of 1 and higher energy orbitals of the same type are assigned by increasing intervals (..2, 3, 4...). The orbital labeling system described previously is inappropriate for heteronuclear diatomic molecules that cannot be assigned g and u subscripts. Molecular orbital surfaces were calculated using Spartan software. (Kathryn Haas, CC-BY-NC-SA)

? Exercise 3.4.1.1

Examine the shape of the 3σ orbital of carbon monoxide in Figure 3.4.1.1. Describe what ways this shape is different from the shape of the σ_g orbitals from second period homonuclear diatomic molecules (see Fig. 5.2.1.1). Rationalize these differences. Both orbitals are re-created below for convenience.



σ_g of homonuclear diatomic



3σ of CO

Answer

The 3σ orbital is like the σ_g in that it has three lobes and two nodes distributed along the internuclear bond. They are different in their distribution. The two external lobes of σ_g are evenly distributed because they are an equal combination of two p_z orbitals (one from each atom). The 3σ orbital is more heavily distributed toward the carbon atom, the less electronegative atom, than toward the oxygen. The unequal distribution of 3σ is apparent in the unequal sizes of its exterior lobes and the uneven shape of the interior lobe. The heavier distribution within the exterior lobe on carbon is caused by the mixing of the carbon $2s$ orbital with carbon and oxygen $2p_z$ orbitals. The uneven shape of the interior lobe, where it leans toward oxygen, is best explained by the fact that the 3σ orbital is closer in energy to the oxygen $2p_z$ than the carbon $2p_z$.

Hydrogen fluoride MO diagram

Hydrogen fluoride is an example of a heteronuclear diatomic molecule in which the two atoms are from different periods. In this case, the valence orbital of H is $1s$ while those of F are $2s$ and $2p$. The molecular orbital diagram for HF is shown in Figure 3.4.1.2.

Three of these orbitals have compatible symmetry for mixing; these are the hydrogen $1s$, fluorine $2s$, and fluorine $2p$. However, the extent to which they will interact depends on their relative energies. Fluorine is more electronegative than H, and the fluorine atom has a higher first ionization energy than does hydrogen. From these trends, we can expect that the fluorine valence orbitals are lower in energy than that of hydrogen. From Table 5.3.1, we find that the 1s orbital of H (-13.6 eV) is higher in energy than both fluorine orbitals (-18.7 and -40.2 eV, respectively for $2p$ and $2s$). The energies of hydrogen $1s$ and fluorine $2p$ are a good match for combination; however, the fluorine $2s$ orbital is much too different to create a productive interaction. Therefore, we expect that the fluorine $2s$ will create a non-bonding molecular orbital, while the $1s$ and $2p_z$ orbitals combine to make σ bonding and σ^* antibonding molecular orbitals. The remaining $2p_x$ and $2p_y$ orbitals do not have compatible symmetry for bonding with hydrogen, and they will form non-bonding π molecular orbitals. The non-bonding orbitals will have similar energy and character as their component atomic orbitals.

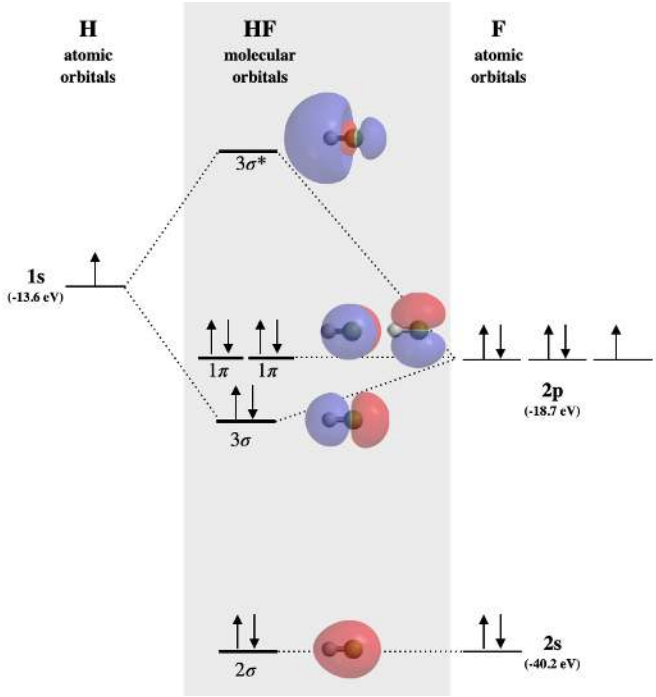


Figure 3.4.1.2: Molecular Orbital diagram of hydrogen fluoride. Molecular orbitals calculated using Spartan software. (Kathryn Haas, CC-BY-NC-SA)

Chemical reactions take place at the HOMO and LUMO orbitals

Knowledge of molecular orbital diagrams, and the shapes of molecular orbitals, can be used to accurately explain and predict chemical reactivity. Chemical reactions take place using the highest occupied molecular orbitals (HOMO) of a nucleophile or Lewis base, and the lowest unoccupied molecular orbital (LUMO) of an electrophile or Lewis acid.

> *Lewis bases react using electrons in the HOMO, while Lewis acids react using the empty LUMO.*

Example: Reactivity of CO with metal ions

CO is an excellent ligand for many metal ions. In fact, the strong affinity between CO and the heme iron (Fe) ions in hemoglobin can explain the mechanism of carbon monoxide poisoning. When CO binds in place of O_2 to hemoglobin, that hemoglobin can no longer carry O_2 to tissue cells. CO binding to hemoglobin is strong and practically irreversible. When CO binds to metal ions, it does so through the carbon atom. This is contrary to expectations based on the Lewis structure and the known bond polarity, where electron density is polarized toward oxygen. The distribution of the electron density of the HOMO of CO can explain this observation!

? Exercise 3.4.1.2

Refer to the MO diagram for CO. Identify the HOMO and explain why CO bonds to metal ions through the carbon atom rather than through the oxygen atom.

Answer

In the interaction between CO and a metal ion, CO would act as a Lewis base; thus it will react using electrons in its HOMO. The MO diagram for CO is shown in Figure 3.4.1.1: the HOMO is the 3σ orbital (also discussed in ? Exercise 3.4.1.1). The electron density of that MO is centered around the carbon atom, thus the carbon atom will be a better Lewis base than the O atom.

This page titled 3.4.1: Polar bonds is shared under a CC BY-NC-SA 4.0 license and was authored, remixed, and/or curated by Kathryn Haas.

- **5.3.2: Polar bonds** by Kathryn Haas is licensed CC BY-SA 4.0.

3.4.2: Ionic Compounds and Molecular Orbitals

Ionic interactions lie at one extreme on a spectrum of bonding. On the opposite end of the spectrum are the non-polar covalent bonds (e.g., homonuclear diatomics). In these molecules, molecular orbitals are formed by equal-energy atomic orbitals, resulting in electron density evenly distributed over the molecule. In the middle of the spectrum are the cases of polar covalent bonds (e.g., heteronuclear diatomics), in which atomic orbitals of unequal energies contribute unequally to molecular orbitals, resulting in uneven distribution of electron density across the molecule. In the case of polar bonds, the electron density is shifted toward the more electronegative atom since that atom contributes more to the lowest energy bonding molecular orbitals. Molecular orbital diagrams can be drawn for ionic compounds as if they are extremely polar bonds in which electrons are not only shifted toward, but are transferred completely to the more electronegative atom.

Example: NaCl

In **NaCl**, the sodium **3*s*** orbital (-5.2 eV) is significantly higher in energy than the chlorine valence orbitals. The chlorine **3*s*** and **3p_z** orbitals have compatible symmetry, yet only the **3p_z** orbital (-13.8 eV) is close enough in energy to interact with the Na **3*s***; still, the energy difference is large enough to make bonding weak. The Na **3*s*** orbital combines with Cl **3p_z** to form the molecular orbitals labeled **4σ** and **4σ*** in Figure **3.4.2.1**. The **4σ** orbital is weakly bonding, but is very close in energy to the Cl **3p_z** orbital, and is mostly Cl-like in character. Notice that all **σ** orbitals look very much like either **s** or **p** orbitals centered on the **Cl** atom, while the **4σ*** orbital is centered almost entirely on Na. The lack of molecular orbitals that are distributed over both atoms at once is consistent with a lack of significant covalent bond character in **NaCl**. The bonding here is characterized by transfer of one electron from **Na** to **Cl** and is almost entirely electrostatic. Bonding that is mostly electrostatic in character is non-directional, unlike true covalent bonding.

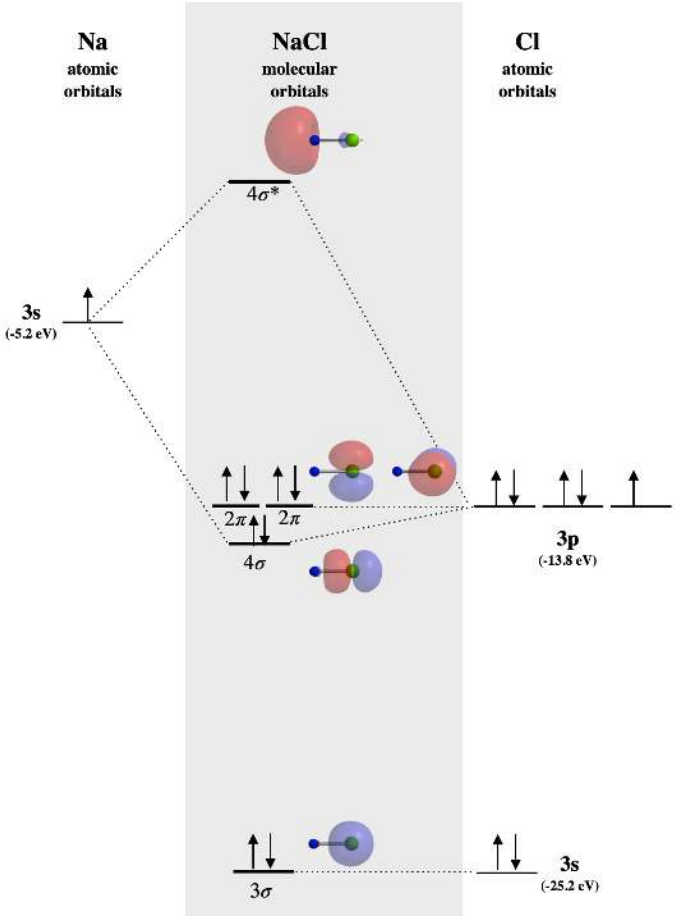


Figure **3.4.2.1**: The molecular orbital diagram for sodium chloride. Molecular orbital surfaces calculated using Spartan software indicate almost no covalent nature of bonding. (CC-BY-NC-SA, Kathryn Haas)

Exercise 3.4.2.1

Draw the molecular orbital diagram for **LiF**. Make sure to label all molecular orbitals appropriately, and specify whether they are mostly bonding, non-bonding, or antibonding. Identify the HOMO and LUMO. Sketch the approximate shapes of all orbitals.

Answer

We expect **LiF** to be an ionic compound because the energy difference in valence orbitals is at least 10-14 eV. (See Table 5.3.1) There are a variety of ways used to label molecular orbitals. In the figure below, we are using the convention of labeling each type of orbital with numbers starting from the lowest-energy orbitals. The 1σ orbital would be mostly F $1s$ in character and is not shown. The 2σ orbital is mostly non-bonding in nature, although it has a very small contribution from $2s$ of Li due to compatible symmetry. The 3σ orbital is slightly bonding but it is mostly F$2p$ in character. The two 1π orbitals are completely non-bonding. The $3\sigma^*$ orbital is antibonding.

- HOMO is 1π
- LUMO is $3\sigma^*$

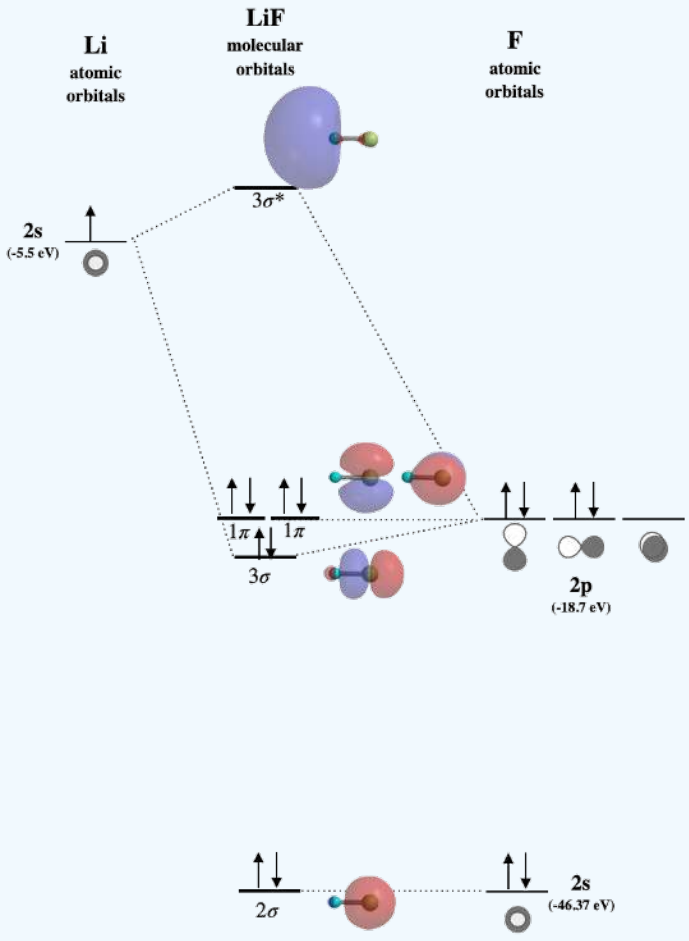


Figure for Exercise 3.4.2.1: Molecular orbital diagram for the ionic compund, LiF. (CC-BY-NC-SA, Kathryn Haas)

This page titled 3.4.2: Ionic Compounds and Molecular Orbitals is shared under a CC BY-NC-SA 4.0 license and was authored, remixed, and/or curated by Kathryn Haas.

- **5.3.3: Ionic Compounds and Molecular Orbitals** by Kathryn Haas is licensed CC BY-SA 4.0.

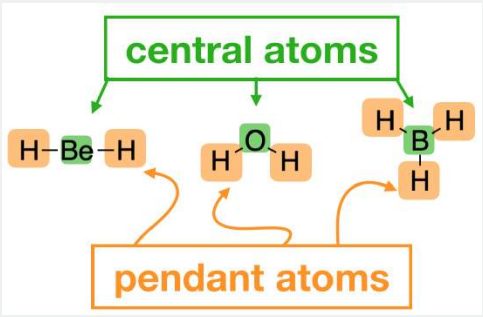
SECTION OVERVIEW

3.5: Larger (Polyatomic) Molecules

We can extend the method we used for diatomic molecules to draw the molecular orbitals of more complicated, polyatomic molecules (molecules with more than two atoms). To combine several different atoms in a molecular orbital diagram, we will group orbitals from different atoms into sets that match the symmetry of a central atom. These **group orbitals** are also referred to as **symmetry adapted linear combinations (SALCs)**. We'll use a stepwise approach to do this as summarized below.

Symmetry adapted linear combinations (SALCs)

We need SALCs (aka group orbitals) to draw molecular orbital (MO) diagrams of *polyatomic* molecules. SALCs are groups of orbitals on **pendant atoms**. These groups of orbitals much match the symmetry of valence orbitals on the **central atom** in order to create a productive interaction. When we combine SALCs with the atomic orbitals on the central atom, we can generate an MO diagram that gives us information about the molecule's bonding and electronic states.



Below is a set of steps you can follow to find SALCs and draw an MO Diagram. Each step will be illustrated in detail through the examples in the subsections that follow this page.

1. Find the **point group** of the molecule and assign Cartesian coordinates so that z is the principal axis.
   Sometimes we can simplify things by looking only at the point group of the relevant orbitals. Only simplify when instructed to do so.*
2. Identify and count the pendant atoms' valence orbitals.
   Is there more than 1 type for each atom (ex. just s, or s and p?) We expect 1 SALC for each ligand orbital.
3. Generate a **reducible representation (Γ)** for the group of pendant atom orbitals using the appropriate character table.
   You have to do this for each set of orbital types. If you only have s orbitals for each ligand, you only need to generate 1 reducible representation. If you have p orbitals, you would generate additional Γ*'s for p_x, p_y, and p_z.*
4. Break the Γ into its component **irreducible representations** from the character table. Note the symmetry of each irreducible representation, its associated orbitals, and their degeneracy.
5. If you are asked to sketch the shapes of SALCs, determine what they "look like" using one of the following strategies.
   (a) Shortcut: if the reducible representations are listed with s, p, or d orbitals in the character table, just draw them (… and skip steps b-c)
   (b) Systematic (Projection Operator) method: Draw an expanded character table and draw your molecule with each ligand identified by letters or numbers (*a,b,c...* or *i,j,k...* or *1,2,3...*) Determine where each pendant atom/orbital ends up under each of the operations of your expanded table. Project the values for each irreducible representation onto the chart you created and then add up the values. Positive and negative values are opposite signed orbitals.
6. Draw the MO diagram by combining SALCs with AO's of like symmetry. When drawing SALC energy levels, remember that the more nodal planes in your SALC orbital drawing, the higher the energy for that SALC orbital.

** When we are focused on orbitals, as in the case for finding group orbitals and drawing molecular orbital diagrams, the symmetry of the orbitals is what we are interested in. In the case of high-symmetry point groups, like $D_{\infty h}$ and $C_{\infty v}$, even though the molecule may have a C_∞ axis, the orbitals do not necessarily retain this symmetry element. For example, the p_x orbital would not have a C_∞ axis, but rather a C_2 axis. It is sufficient and useful to substitute D_{2h} for $D_{\infty h}$ and C_{2v} for $C_{\infty v}$ to simplify the problem.*

3.5.1: Bifluoride anion

3.5.2: Carbon Dioxide

3.5.3: H_2O

3.5.4: NH_3

3.5.5: CO_2 (Revisted with Projection Operators)

3.5.6: BF_3

3.5: Larger (Polyatomic) Molecules is shared under a CC BY-NC-SA 4.0 license and was authored, remixed, and/or curated by LibreTexts.

3.5.1: Bifluoride anion

Finding SALCs and drawing the MO diagram for [F-H-F]⁻

The linear anion [F-H-F]⁻ is a good place to start as an example to illustrate the process of generating pendant atom SALCs and then constructing a molecular orbital diagram for a polyatomic molecule. We will proceed using the steps outlined on the previous page for generating SALCs and a molecular orbital diagram.

Step 1. Find the point group of the molecule and assign Cartesian coordinates so that z is the principal axis.

We begin by assigning the appropriate point group for this molecule: $D_{\infty h}$ (Figure 3.5.1.1). As mentioned in the previous page, it is useful to substitute D_{2h} for $D_{\infty h}$ when generating SALCs and molecular orbital diagrams. The z axis is assigned to be colinear with the principal axis, and in this case is the same as the C_∞ axis (Figure 3.5.1.1).

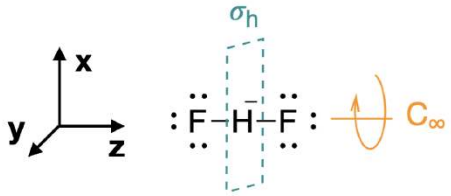


Figure 3.5.1.1: The [FHF]⁻ anion belongs to the $D\infty_h$ point group. (CC-BY-NC-SA; Kathryn Haas)

Step 2. Identify and count the pendant atoms' valence orbitals.

The next step is to identify the valence orbitals on the pendant F atoms that will form SALCs. In most cases, you should consider all of the valence orbitals. In this case, each of the fluorine atoms has four valence orbitals ($2s$, $2p_x$, $2p_y$, and $2p_z$). From these eight fluorine valence orbitals, we should expect eight group orbitals (SALCs).

3. - 5. Generate SALCS (shortcut)

To draw these SALCs for this molecule is rather simple, and we don't need to follow all the steps of finding the Γ's and reducing them. Rather, you can proceed as if you are creating bonding and antibonding molecular orbitals between the two F atoms, except that the F orbitals are separated by the H atom. Approximate sketches of the eight SALCs from F valence orbitals are shown in Figure 3.5.1.2.

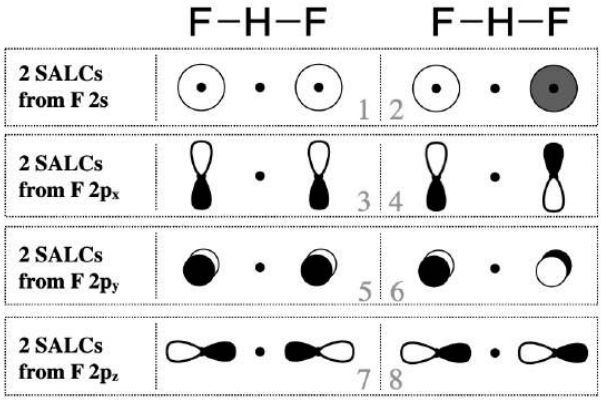


Figure 3.5.1.2: Eight SALCs from the valence orbitals of two fluorine atoms. (CC-BY-NC-SA; Kathryn Haas)

6. Draw the MO diagram by combining SALCs with AO's of like symmetry.

SALCs can productively interact with the central atom only when symmetry is compatible. Just some of the groups of orbitals in Figure 3.5.1.2 possess appropriate symmetry to combine with the hydrogen atom valence orbital (the H $1s$). In this simple case, you can decide whether orbitals have compatible symmetry by visually inspecting the shapes of the group orbitals. The F $2p_y$ and $2p_x$ orbitals do not have appropriate symmetry to bond to the H $1s$ orbital because the nodes of these orbitals run through the center of the H $1s$ orbital, thus we can eliminate all SALCs composed from F $2p_x$ and $2p_y$ (*these are SALCs numbered 3-6 in Figure* 3.5.1.2). On the other hand, the F $2s$ and $2p_z$ orbitals individually do have appropriate shape and direction in space for productive interaction

with an H $1s$ orbital. However only SALCs where the *entire group* has appropriate symmetry will combine with H $1s$ to produce bonding or antibonding molecular orbitals. Only the SALCs labeled with numbers 1 and 7 can combine with an s orbital in the center of the group. The ways in which these SALCs are able to combine with H $1s$ are illustrated in Figure **3.5.1.3**.

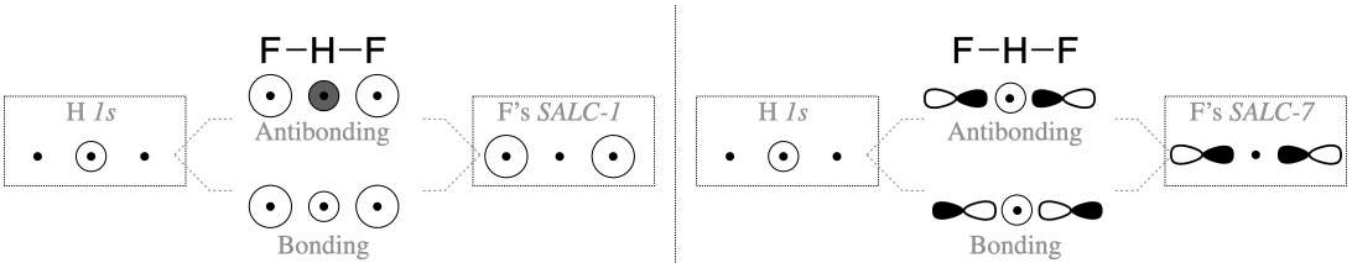
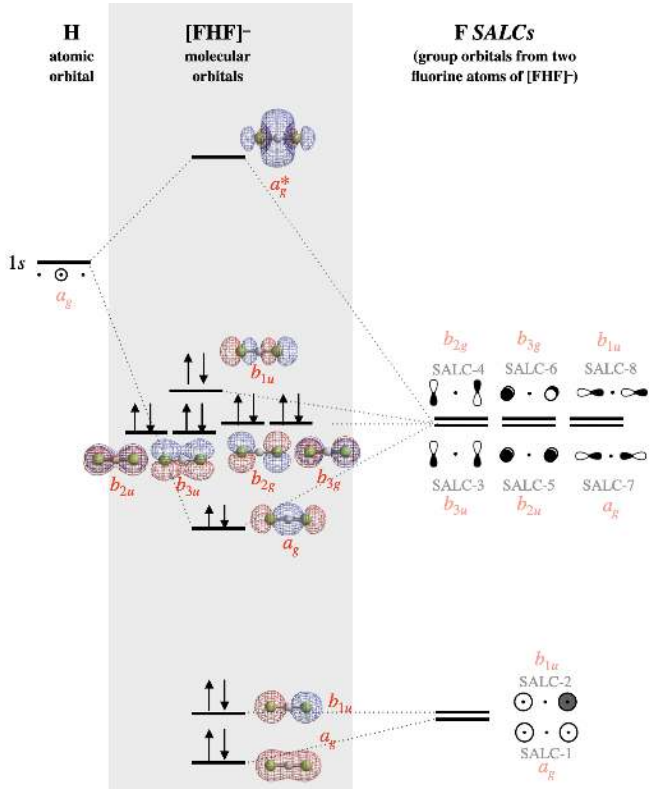


Figure **3.5.1.3**: Combinations of a central H $1s$ orbital with the group orbitals, SALC-1 and SALC-7 from Figure **3.5.1.2**, to create bonding and antibonding interactions. (CC-BY-NC-SA; Kathryn Haas)

Before we assume that both SALC-1 and SALC-7 will combine with the H $1s$ orbital, we must consider the energies of all atomic orbitals. The F $2p_z$ orbital has a potential energy of -18.7 eV (see Table 5.3.1). This is a good match for the H $1s$ orbital (-13.6 eV). However, the F $2s$ orbital has a much lower energy of -46.37 eV and would have weak interaction with the H $1s$.

The molecular orbital diagram for $[F\text{-}H\text{-}F]^-$ is shown in Figure **3.5.1.4**. Notice that all atomic orbitals, group orbitals (SALCs), and molecular orbitals in Figure **3.5.1.4** are assigned a symmetry label that corresponds to each element's symmetry under the D_{2h} point group. The molecular orbital labels correspond to **lower-case Mulliken Labels** of individual reducible representations from the D_{2h} character table. Upper-case symbols are used to indicate symmetry and irreducible representations, while lower-case symbols are used to indicate the identity of an orbital with that symmetry. The labeling methods described for simple diatomic linear molecules (σ, π) are not sufficient to indicate the more complex symmetries of the molecular orbitals in polyatomic molecules. The use of lower-case Mulliken symbols is the most rigorous way to label the orbitals. Refer to your instructor for how you should label orbitals for any graded work.

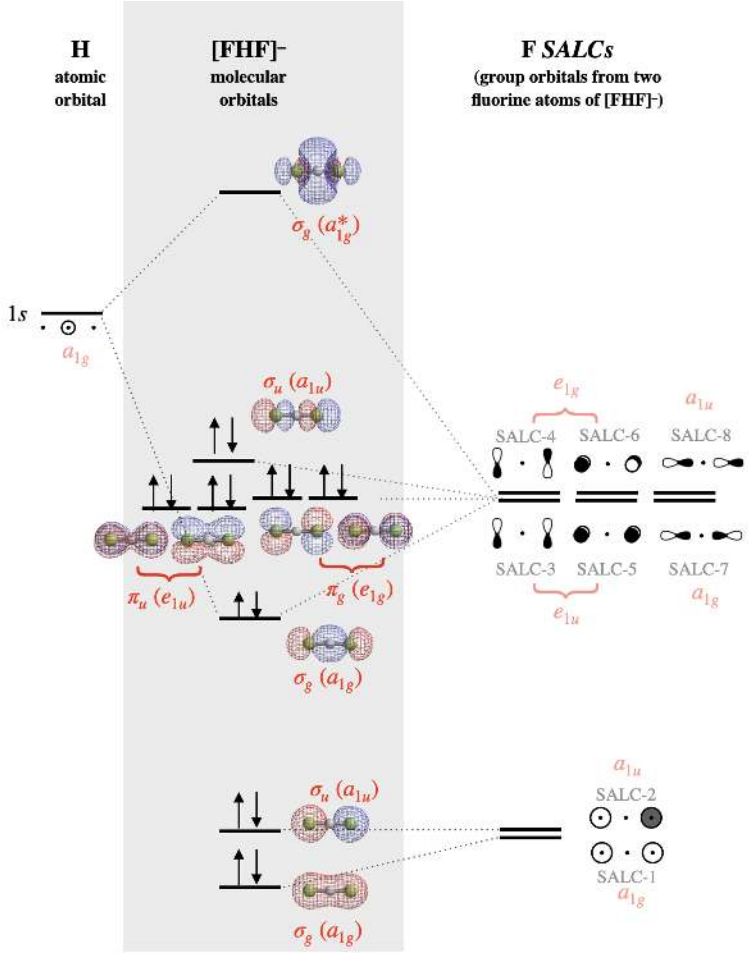


https://chem.libretexts.org/@go/page/360836

Figure **3.5.1.4**:The molecular orbital diagram for [F-H-F]⁻. The molecular orbital surfaces and relative energy levels were calculated using Spartan software. SALCs are labeled according to numbers assigned in Figure **3.5.1.2**. The symmetry of each SALC and orbital under the D_{2h} **point group** is shown in red font. (CC-BY-NC-SA; Kathryn Haas)

Click here for a version of Figure 3.5.1.4 using $D_{\infty h}$ labeling:

For high-symmetry groups, a shortcut is to use a lower-symmetry group that maintains the critical symmetry elements. In the case of the $D_{\infty h}$ point group, it is often sufficient to use the approximation of the D_{2h} point group and character table. This is the same MO diagram as shown above, but using the symmetry labels appropriate for the D_{2h} approximation.



Alternate Figure **3.5.1.4**: The molecular orbital diagram for [F-H-F]⁻. The molecular orbital surfaces and relative energy levels were calculated using Spartan software. SALCs are labeled according to numbers assigned in Figure **3.5.1.2**. The symmetry of each SALC and orbital under the D_{2h} **point group** is shown in red font. (CC-BY-NC-SA; Kathryn Haas)

Constructing the MO diagram

After identifying the atomic orbitals and constructing SALCs, place the atomic orbitals of H on one side of the diagram and all SALCs from F on the other side. Molecular orbitals are in the center.

The lowest-energy fluorine SALCs will be those composed of the lowest-energy atomic orbitals of fluorine; these would be SALC-1 (a_{1g}) and SALC-2 (a_{1u}) that are constructed from fluorine s atomic orbitals. Of these two orbitals, the one with zero nodes would be slightly lower in energy than the one with one node. When these two orbitals form molecular orbitals, the completely symmetric SALC-1 will be mostly non-bonding with slight bonding character from minor combination with the hydrogen $1s$ orbital. SALC-2, however is symmetrically incompatible with hydrogen $1s$ and will be a truly non-bonding orbital distributed over both F atoms.

The six SALCs constructed of fluorine p orbitals will have higher energy since the fluorine p atomic orbitals are higher in energy than the s orbitals (SALC-3 through SALC-8). Again, we expect SALCs with more nodes (SALC-4, -6, -8) to have slightly higher

energy than those with fewer nodes (SALC-3, -5, -7). SALC-7 will form a bonding and antibonding interaction with the hydrogen **1*s*** orbital. All other SALCS are truly non-bonding, but are non-degenerate non-bonding orbitals.

In bifluoride, there is an important distinction between the Lewis structure and molecular orbital description of lone pairs. In Lewis theory, the lone pairs are localized to individual fluorine atoms, while in the molecular orbital description each lone pair is distributed over both fluorine atoms at once (see surface depiction of each molecular orbital in Figure **3.5.1.4**).

3.5.1: Bifluoride anion is shared under a CC BY-NC-SA 4.0 license and was authored, remixed, and/or curated by LibreTexts.

- **5.4.1: Bifluoride anion** is licensed CC BY-SA 4.0.

3.5.2: Carbon Dioxide

Construct SALCs and the molecular orbital diagram for CO_2

Carbon dioxide is another linear molecule. This example is slightly more complex than the previous example of the bifluoride anion. While bifluoride had only one valence orbital to consider in its central H atom (the $1s$ orbital), carbon dioxide has a larger central atom, and thus more valence orbitals that will interact with SALCs.

Preliminary Steps

Step 1. Find the point group of the molecule and assign Cartesian coordinates so that z is the principal axis.

The CO_2 molecule is linear and its point group is $D_{\infty h}$. The z axis is collinear with the C_∞ axis. We will use the D_{2h} point group as a substitute since the orbital symmetries are retained in the D_{2h} point group.

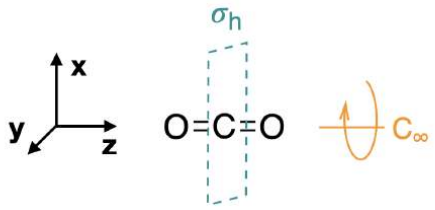


Figure 3.5.2.1: CO_2 belongs to the $D_{\infty h}$ point group. (CC_BY-NC-SA; Kathryn Haas)

Step 2. Identify and count the pendant atoms' valence orbitals.

Each of the two pendant oxygen atoms has four valence orbitals; $2s$, $2p_x$, $2p_y$, and $2p_z$. Thus, we can expect a total of eight SALCs.

Generate SALCs

The SALCs for CO_2 are identical in shape and symmetry to those described in the previous example for the bifluoride anion. But instead of cutting to the shortcut, we will systematically derive the SALCs here to demonstrate the process.

Step 3. Generate the Γ's

Use the D_{2h} character table to generate four reducible representations ($\Gamma's$); one for each of the four types of pendant atom orbitals (s, p_x, p_y, p_z). For each s orbital, assign a value of 1 if it remains in place during the operation or zero if it moves out of its original place. For each p orbital, assign 1 if there is no change, -1 if it remains in place but is inverted, and 0 if it moves out of its original position. The four Γ's are given below:

D_{2h}	E	$C_2(z)$	$C_2(y)$	$C_2(x)$	i	$\sigma(xy)$	$\sigma(xz)$	$\sigma(yz)$
Γ_{2s}	2	2	0	0	0	0	2	2
Γ_{2p_x}	2	−2	0	0	0	0	2	−2
Γ_{2p_y}	2	−2	0	0	0	0	−2	2
Γ_{2p_z}	2	2	0	0	0	0	2	2

Step 4. Break Γ's into irreducible representations for individual SALCs

Reduce each Γ into its component irreducible representations. There are two strategies that can be used to do this. The quick and easy way is to do it "by inspection", but this only works well for simple cases. The other is by using the systematic approach for breaking a Γ into reducible representations described previously in section 4.4.2 using the following formula:

$$\text{number of } i = \frac{1}{h}\sum(\text{number of operations in class}) \times (\chi_\Gamma) \times (\chi_i) \tag{3.5.2.1}$$

In other words, the number of irreducible representations of type i is equal to the sum of the number of operations in the class × the character of the Γ_{modes} × the character of i, and that sum is divided by the order of the group (h).

Using either approach results in the following eight irreducible representations ($2A_g + 2B_{1u} + B_{2g} + B_{3u} + B_{3g} + B_{2u}$):

$\mathbf{D_{2h}}$	E	$C_2(z)$	$C_2(y)$	$C_2(x)$	i	$\sigma(xy)$	$\sigma(xz)$	$\sigma(yz)$	
$\mathbf{\Gamma_{2s} = A_g + B_{1u}}$	$\mathbf{\Gamma_{2s}}$	**2**	**2**	**0**	**0**	**0**	**0**	**2**	**2**
	A_g	1	1	1	1	1	1	1	1
	B_{1u}	1	1	−1	−1	−1	−1	1	1
$\mathbf{\Gamma_{2p_x} = B_{2g} + B_{3u}}$	$\mathbf{\Gamma_{2p_x}}$	**2**	**−2**	**0**	**0**	**0**	**0**	**2**	**−2**
	B_{2g}	1	−1	1	−1	1	−1	1	−1
	B_{3u}	1	−1	−1	1	−1	1	1	−1
$\mathbf{\Gamma_{2p_y} = B_{3g} + B_{2u}}$	$\mathbf{\Gamma_{2p_y}}$	**2**	**−2**	**0**	**0**	**0**	**0**	**−2**	**2**
	B_{3g}	1	−1	−1	1	1	−1	−1	1
	B_{2u}	1	−1	1	−1	−1	1	−1	1
$\mathbf{\Gamma_{2p_z} = A_g + B_{1u}}$	$\mathbf{\Gamma_{2p_z}}$	**2**	**2**	**0**	**0**	**0**	**0**	**2**	**2**
	A_g	1	1	1	1	1	1	1	1
	B_{1u}	1	1	−1	−1	−1	−1	1	1

Step 5. Sketch the SALCs

From the systematic process above, you have found the symmetries (the irreducible representations) of all eight SALCs under the D_{2h} point group. To sketch the SALC that corresponds to each irreducible representation, again we use the D_{2h} character table, and specifically the functions listed on the right side columns of the table.

Two A_g SALCs (one from s and one from p_z): The A_g SALCs are each singly degenerate and symmetric with respect to both the principal axis (z) and the inversion center (i) (based on its Mulliken Label). We can look at the functions in the D_{2h} character table that correspond to A_g and see that it is completely symmetric under the group (because the combination of x^2, y^2, z^2 shows that it is totally symmetric). This would be the same symmetry as an s orbital on the central atom. From this information, we know that these SALCs must have symmetry compatible with an s orbital on the central atom, and we can draw the two A_g SALCs shown in Figure 3.5.2.2.

Two B_{1u} SALCs (one from s and one from p_z): The Mulliken Label tells us that the B_{1u} SALCs are each antisymmetric with respect to both the principal axis and the inversion center. The function, z, appearing with B_{1u} in the character table tells us that these SALCs have the same symmetry as the z axis, or a p_z orbital on the central atom. From this information, we know that these two SALCs should be compatible with a p_z orbital on the central atom, and we can draw the two B_{1u} SALCs shown in Figure 3.5.2.2.

All other SALCs shown below are derived using a strategy similar to the one in the two cases described above.

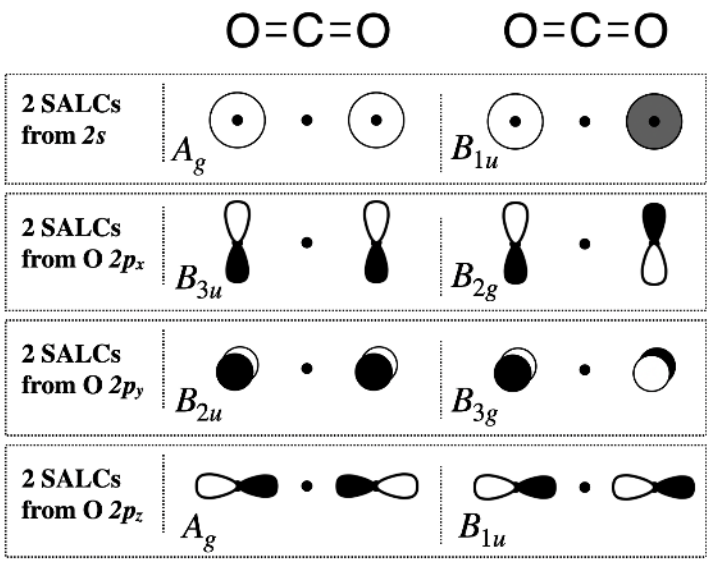


Figure 3.5.2.2: SALCs from the valence orbitals of oxygen atoms in CO_2. (CC-BY-NC-SA; Kathryn Haas)

Draw the MO diagram for CO_2

Step 6. Combine SALCs with AO's of like symmetry.

First we identify the valence orbitals on carbon: there are four including $2s$, $2p_x$, $2p_y$, and $2p_z$. Now we identify the symmetry of each using the D_{2h} character table. The symmetry of a central s orbital corresponds to the combination of functions x^2, y^2, and z^2 in the character table; this is A_g. The p_z orbital corresponds to the symmetry of the linear function z in the character table; this is B_{1u}. And so on... The symmetries of the C valence orbitals are listed below.

$$2s = A_g$$
$$2p_x = B_{3u}$$
$$2p_y = B_{2u}$$
$$2p_z = B_{1u}$$

Now that we have identified the symmetries of the eight oxygen SALCs and the four valence orbitals on carbon, we know which atomic orbitals and SALCs may combine based on compatible symmetries. We also need to know the relative orbital energy levels so that we can predict the relative strength of orbital interactions. The orbital ionization energies are listed in Section 5.3.

With knowledge of both orbital symmetries and energies, we can construct the molecular orbital diagram. The carbon atom goes on one side of the diagram while the oxygen SALCs are drawn on the opposite side. Molecular orbitals are drawn in the center column of the diagram:

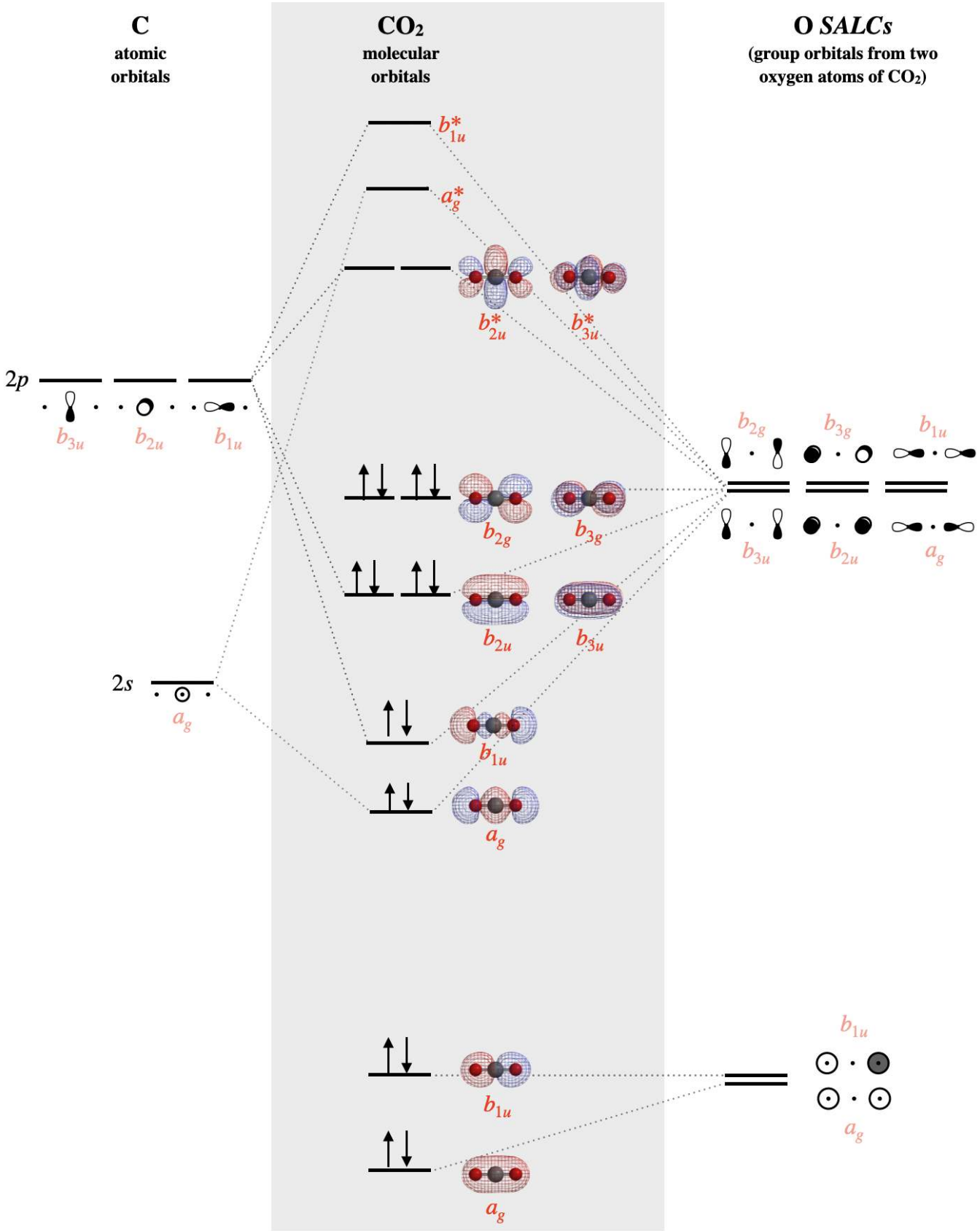


Figure 3.5.2.3: Molecular orbital diagram for carbon dioxide. (CC-BY-NC-SA; Kathryn Haas)

The SALCs on the right side of the diagram above are constructed from groups of either the $2s$ atomic orbitals of oxygen, or the $2p$ atomic orbitals of oxygen. Each SALC will combine with the atomic orbitals of carbon that have compatible symmetry; but the strength of the interaction depends on their relative energies. The individual valence atomic orbitals of oxygen have energies of $-32.36eV$ ($2s$) and $-15.87eV$ ($2p$), while the valence orbitals of carbon have energies of $-19.47eV$ ($2s$) and $-10.66eV$ ($2p$). The $2s$ orbitals of the oxygen are far lower in energy ($-32.36eV$) than all other valence orbitals, and so we should expect that molecular orbitals that are constructed from these oxygen $2s$ will be mostly non-bonding. These mostly non-bonding orbitals are the a_{1g} and b_{1g} orbitals shown at the bottom of Figure 3.5.2.3. The a_g orbital is lower in energy than the b_{1u} due to slight mixing with other orbitals of a_g symmetry.

The bonding orbitals of CO_2 include two $sigma$ molecular orbitals of a_g and b_{1u} symmetry and two π molecular orbitals of b_{2u} and b_{3u} symmetry. Each of these bonding molecular orbitals possesses a higher-energy antibonding partner. The b_{2g} and b_{3g} SALCs that are formed from oxygen $2p_x$ and $2p_y$ orbitals have no compatible match with carbon valence orbitals; thus they form two b_{2g} and b_{3g} molecular orbitals, which are truly non-bonding and mostly oxygen in character. Still, notice that each orbital is spread across both oxygen atoms at once, and again we see that each non-bonding electron pair in the HOMO is very different in molecular orbital theory compared to Lewis theory. Each non-bonding pair is distributed over both oxygen atoms at once in molecular orbital theory, while in Lewis theory each lone pair is isolated to one atom or to localized bonds attached to that atom.

This page titled 3.5.2: Carbon Dioxide is shared under a CC BY-NC-SA 4.0 license and was authored, remixed, and/or curated by Kathryn Haas.

- **5.4.2: Carbon Dioxide** by Kathryn Haas is licensed CC BY-SA 4.0.

3.5.3: H_2O

Construct SALCs and the molecular orbital diagram for H_2O.

This is the first example so far that is not a linear molecule. Water is a bent molecule, and so it is important to remember that interactions of pendant ligands are dependent on their positions in space. You should consider the positions of the three atoms in water to be essentially fixed in relation to each other. The process for constructing the molecular orbital diagram *for a non-linear molecule*, like water, is similar to the process for linear molecules. We will walk through the steps below to construct the molecular orbital diagram of water.

Preliminary Steps

Step 1. Find the point group of the molecule and assign Cartesian coordinates so that z is the principal axis.

The H_2O molecule is bent and its point group is C_{2v}. The z axis is collinear with the principal axis, the C_2 axis. There is no need to simplify this problem, as we had done for previous examples. The C_{2v} point group is simple enough.

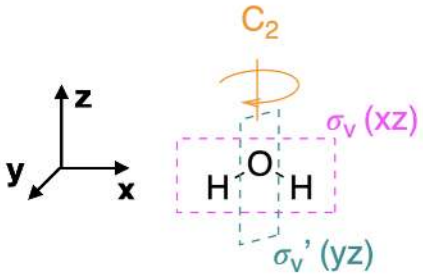


Figure **3.5.3.1**: The water molecular is in the C_{2v} point group. (CC-BY-NC-SA; Kathryn Haas)

Step 2. Identify and count the pendant atoms' valence orbitals.

Each of the two pendant hydrogen atoms has one valence orbital, the $1s$. Thus, we can expect a total of two SALCs from these two atoms.

Generate SALCs

The SALCs for H_2O are quite simple, yet we will systematically derive the SALCs here to demonstrate the process.

Step 3. Generate the Γ's

Use the C_{2v} character table to generate one reducible representation (Γ); in this case we need only one Γ because there is only one type of valence orbital (the $1s$). For each s orbital, assign a value of 1 if it remains in place during the operation or zero if it moves out of its original place. The Γ is given below:

C_{2v}	E	C_2	$\sigma_v(xz)$	$\sigma'_v(yz)$
Γ_{1s}	2	0	2	0

Step 4. Break Γ's into irreducible representations for individual SALCs

Reduce each Γ into its component irreducible representations. Using either of the processes described previously, we find that the Γ reduces to the two irreducible representations A_1 and B_1 under the C_{2v} point group.

C_{2v}	E	C_2	$\sigma_v(xz)$	$\sigma'_v(yz)$
Γ_{1s}	**2**	**0**	**2**	**0**
A_1	1	1	1	1
B_1	1	−1	1	−1

Step 5. Sketch the SALCs

From the systematic process above, you have found the symmetries (the irreducible representations) of both SALCs under the C_{2v} point group. To sketch the SALC that corresponds to each irreducible representation, again we use the C_{2v} character table, and

specifically the functions listed on the right side columns of the table.

One A_1 SALC: The A_1 SALC is singly degenerate and symmetric with respect to both the principle axis (z) and the inversion center (i) (based on its Mulliken Label). We can look at the functions in the C_{2v} character table that correspond to A_1 and see that it is completely symmetric under the group (because the combination of x^2, y^2, z^2 shows that it is totally symmetric). This would be the same symmetry as an s orbital on the central oxygen atom. From this information, we know that this SALC must have symmetry compatible with an s orbital on the central atom. We can also see from the character table that the z axis, and thus a p_z orbital on oxygen, also possesses A_1 symmetry. This tells us that in addition to being compatible with the oxygen s orbital, it should also be compatible with the oxygen p_z orbital. From this information we can draw the A_1 SALC shown in Figure **3.5.3.2**. *If it is not obvious how the A_1 sketch in Fig.* **3.5.3.2** *is compatible with the s and p_z orbitals of oxygen, inspect the drawings corresponding to molecular orbitals $2a_1$ and $3a_1$ in Fig.* **3.5.3.3**.

One B_1 SALC: The Mulliken Label tells us that the B_1 SALC is singly degenerate and antisymmetric with respect to both the principal axis and the inversion center. The function, x, appearing with B_1 in the character table tells us that this SALC has the same symmetry as the x axis, or a p_x orbital on the central oxygen atom. From this information, we know that this SALC should be compatible with a p_x orbital on the central atom, and we can draw the B_1 SALCs shown in Figure **3.5.3.2**. *If it is not obvious how the B_1 sketch in Fig.* **3.5.3.2** *is compatible with the p_x orbital of oxygen, inspect the drawing corresponding to molecular orbital $1b_1$ in Fig.* **3.5.3.3**.

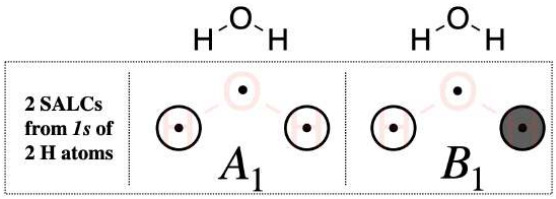


Figure **3.5.3.2**: Sketch of the A_1 and B_1 hydrogen SALCs of water. (CC-BY-NC-SA; Kathryn Haas)

Not convinced about the sketches of these SALCs? You can convince yourself by putting them to the test. Try the exercise below.

? Exercise 3.5.3.1

Perform all operations of the C_{2v} point group on the two sketches of H SALCs shown in Figure **3.5.3.2**, and convince yourself that each sketch does possess the A_1 and B_1 symmetries assigned to them, respectively, under the C_{2v} point group.

Answer

Add texts here. Do not delete this text first.

Draw the MO diagram for H_2O

Step 6. Combine SALCs with AO's of like symmetry.

First we must identify the valence orbitals on the central oxygen: there are four including $2s$, $2p_x$, $2p_y$, and $2p_z$. Now we identify the symmetry of each using the C_{2v} character table. The symmetry of a central $2s$ orbital corresponds to the combination of functions x^2, y^2, and z^2 in the character table; this is A_1. The p_z orbital also corresponds to A_1. And so on... The symmetries of oxygen valence orbitals are listed below.

$$2s = A_1$$
$$2p_x = B_1$$
$$2p_y = B_2$$
$$2p_z = A_1$$

Now that we have identified the symmetries of the two hydrogen SALCs and the four valence orbitals on oxygen, we know which atomic orbitals and SALCs may combine based on compatible symmetries. We also need to know the relative orbital energy levels so that we can predict the relative strength of orbital interactions. The orbital ionization energies are listed in Section 5.3.1.

With knowledge of both orbital symmetries and energies, we can construct the molecular orbital diagram. The valence orbitals of oxygen go on one side of the diagram while the hydrogen group orbitals are drawn on the opposite side. Molecular orbitals are

drawn in the center column of the diagram, as shown in Figure **3.5.3.3**:

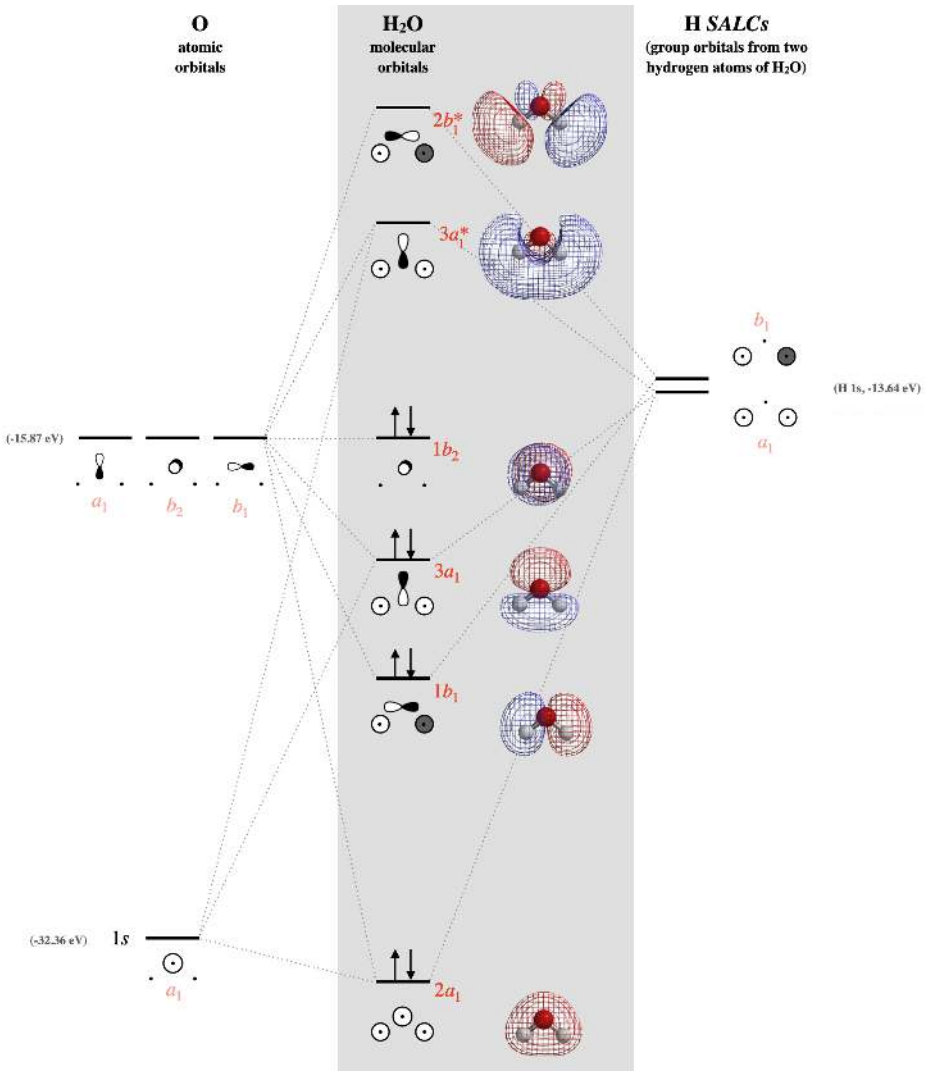


Figure **3.5.3.3**: The molecular orbital diagram of water. Molecular orbital surfaces calculated using Spartan software. The surface of the $3a_1^*$ orbital has been trimmed. (CC-BY-NC-SA; Kathryn Haas)

Example 3.5.3.1

In the previous examples shown for the molecular orbital diagrams of the bifluoride anion and carbon dioxide, we discussed differences in the understanding of those molecules from molecular orbital theory compared to Lewis structures. Water contains two lone pairs in its Lewis structure. Compare the predictions about water's lone pairs of electrons and its reactivity based on (1) the combination of elementary models (Lewis, Valence Bond, and Hybridized Orbital theories) and (2) Molecular Orbital theory. Specifically address and explain how the elementary models differ from molecular orbital theory in the following respects:

a. Where are the lone pairs in water?
b. Are the two lone pairs equivalent or are they different?
c. Where are sites on the molecule that will undergo reaction with electrophiles and nucleophiles?

Solution

1) Elementary models: The Lewis structure predicts that two lone pairs are (a) localized on the oxygen atom of water and that (b) both lone pairs are equivalent. The Lewis structure, combined with Valence Bond Theory, would predict that lone pairs occupy two equivalent hybridized sp^3 atomic orbitals on oxygen. (c) Lewis theory would predict that the oxygen lone pairs are

nucleophiles; thus an electrophile would react with the oxygen atom lone pairs. The polarized O-H bond leaves the H atoms as the most electrophilic locations on the water molecule; thus nucleophiles would react at the H atoms of water.

2) Molecular orbital theory: The molecular orbitals predict that (a) the two lone pairs of water are not equivalent, and that (b) each is distributed over the entire molecule. One lone pair is in the truly non-bonding $1b_2$ orbital (Figure **3.5.3.3**), which is also the HOMO. There is not another truly non-bonding orbital in the molecule, but the lowest-energy $2a_1$ orbital could be considered mostly non-bonding due to the large energy difference between it and other valence orbitals. (c) Although the $2a_1$ orbital can be considered mostly non-bonding, we cannot expect the electrons in $2a_1$ to react readily, as they are in the lowest-energy molecular orbital. Molecular orbital theory predicts that reactions occur at the HOMO and LUMO orbitals. The HOMO reacts with electrophiles, and in this case, the HOMO is distributed over the top and bottom faces of the molecule, and is centered on the oxygen atom. The LUMO would react with nucleophiles. The LUMO is the orbital labeled $3a_1^*$ in Figure **3.5.3.3**, and has a major lobe that is distributed more heavily over the H atoms, and from this we should predict H atoms to be the preferred site of reaction for nucleophiles.

Expressing molecular orbitals in terms of Ψ

The general expression for a molecular orbital, or the linear combination of atomic orbitals (LCAO), was given previously as $\Psi = c_a\psi_a + c_b\psi_b$. In this expression, the wavefunction of two atoms (ψ_a and ψ_b) is combined to form the wavefunction of the molecular orbital. The coefficients c_a and c_b quantify the contribution of each atomic ψ to the molecular Ψ.

$$\Psi = c_a\psi_a + c_b\psi_b$$

In the case of polyatomic orbitals, each LCAO is constructed of atomic orbitals from a central atom and group orbitals (SALCs) from the pendent atoms. In the case of water, the expression above could be modified to give the expression below.

$$\Psi = c_{oxygen}\,(\psi_{oxygen}) + c_{SALCs}\,(N(\psi_{H_a} \pm \psi_{H_b}))$$

N represents the normalizing requirement that was mentioned previously in reference to the requirements for electron wavefunctions and probability functions. The normalizing requirement simply stated is the requirement that the probability of finding the electron in any orbital, including group orbitals, is 1. In general, the value of N for a group orbital is...

$$N = \frac{1}{\sum c_i^2}$$

...where c_i is the coefficient of each unique atomic orbital that contributes to the group. For the hydrogen SALCs of water, there are two atomic orbitals that contribute to equally to each SALC, and so the coefficient on each of the two orbitals is 1. This gives $N = \left(\frac{1}{\sqrt{1^2+1^2}}\right) = \frac{1}{\sqrt{2}}$ for the H SALCs of water.

There are only two hydrogen SALCs: the one in which the hydrogen wavefunctions are added ($N(\psi_{H_a} + \psi_{H_b})$) has A_1 symmetry, and the one in which the hydrogen wavefunctions are subtracted ($N(\psi_{H_a} - \psi_{H_b})$) has B_1 symmetry.

The molecular orbitals from Figure **3.5.3.3** are expressed below in terms of their LCAO of individual wavefunctions. Yet, note that these expressions are simplifications that ignore orbital mixing. For example, as expressed below, they ignore contributions of oxygen $2s$ to the higher energy moelcular orbitals with A_1 symmetry (the $3a_1$ and $3a_1^*$ in Figure **3.5.3.3**).

MO		*OxygenAO*		*HydrogenSALC*	*Description*
Ψ_{2a_1}	=	$c_{(ox1)}\psi_{(2s)}$	+	$c_{(hy1)}[N(\psi_{H_a} + \psi_{H_b})]$	$c_{(hy1)}$ is positive; bonding, slightly nonbonding
Ψ_{1b_1}	=	$c_{(ox2)}\psi_{(2p_x)}$	+	$c_{(hy2)}[N(\psi_{H_a} - \psi_{H_b})]$	$c_{(hy2)}$ is positive; bonding
Ψ_{3a_1}	=	$c_{(ox3)}\psi_{(2p_z)}$	+	$c_{(hy3)}[N(\psi_{H_a} + \psi_{H_b})]$	$c_{(hy3)}$ is positive; bonding
Ψ_{1b_2}	=	$\psi_{(2p_y)}$			nonbonding
$\Psi^*_{3a_1}$	=	$c_{(ox4)}\psi_{(2p_z)}$	+	$c_{(hy4)}[N(\psi_{H_a} + \psi_{H_b})]$	$c_{(hy4)}$ is negative; antibonding
$\Psi^*_{1b_1}$	=	$c_{(ox5)}\psi_{(2p_x)}$	+	$c_{(hy5)}[N(\psi_{H_a} - \psi_{H_b})]$	$c_{(hy5)}$ is negative; antibonding

3.5.3: H_2O is shared under a CC BY-NC-SA 4.0 license and was authored, remixed, and/or curated by LibreTexts.

- **5.4.3: H_2O** is licensed CC BY-SA 4.0.

3.5.4: NH_3

Construct SALCs and the molecular orbital diagram for NH_3

This is the first example so far that has more than two pendant atoms and the first example in which the molecule has atoms that lie in three dimensions (i.e., it is not flat). Ammonia is a trigonal pyramidal molecule, with three pendant hydrogen atoms. The three-dimensional shape and the odd number of pendant atoms makes this example more complicated than the previous cases of water, carbon dioxide, and bifluoride. In this case, sketching the shapes (step 5) of pendant atom SALCs is less straightforward; rather, an alternative method, the **projection operator method**, is preferred for generating pictorial representations of the SALCs.

As in previous examples, it is important to remember that interactions of pendant ligands are dependent on their positions in three-dimensional space. You should consider the positions of the four atoms in ammonia to be essentially fixed in relation to each other. We will walk through the steps used to construct the molecular orbital diagram of ammonia. The first few steps are the same as you've seen before:

Step 1. Find the point group of the molecule and assign Cartesian coordinates so that z is the principal axis.

The NH_3 molecule is trigonal pyramidal and its point group is C_{3v}. The z axis is collinear with the principal axis, the C_3 axis.

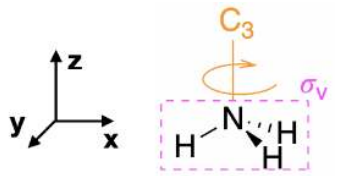


Figure **3.5.4.1**: The ammonia molecule is in the C_{3v} point group. (CC-BY-NC-SA; Kathryn Haas)

Step 2. Identify and count the pendant atoms' valence orbitals.

Each of the three pendant hydrogen atoms has one valence orbital; the $1s$. Thus, we can expect a total of three SALCs from these three atoms.

Step 3. Generate the Γ's

Use the C_{3v} character table to generate one reducible representation (Γ); in this case we need only one Γ because there is only one type of valence orbital (the $1s$). For each s orbital, assign a value of 1 if it remains in place during the operation or zero if it moves out of its original place. The Γ is given below:

C_{3v}	E	$2C_3$	$3\sigma_v$
Γ_{1s}	3	0	1

Step 4. Break Γ's into irreducible representations for individual SALCs

Reduce each Γ into its component irreducible representations. Using either of the processes described previously, we find that the Γ reduces to the two irreducible representations A_1 and E under the C_{3v} point group.

C_{3v}	E	$2C_3$	$3\sigma_v$
Γ_{1s}	3	0	2
A_1	1	1	1
E	2	−1	0

Notice that we only found TWO irreducible representations. But, in fact we have THREE different SALCs. The E irreducible representation is doubly degenerate, which in this context means that it corresponds to two degenerate SALCs. Thus, we have already found the symmetries of the three SALCs for ammonia: Two of the SALCs are degenerate with E symmetry under the C_{3v} point group, while the third SALC has A_1 symmetry.

Step 5. Sketch the SALCs using the PROJECTION OPERATOR METHOD

From the first four steps (described above), you have found the symmetries (the irreducible representations) of all three SALCs under the C_{3v} point group. To sketch the SALC that corresponds to each irreducible representation, again we use the C_{3v} character

table. But now we will introduce the **projection operator method** to derive the surface representation of each SALC.

Step 5.1: Label the pendent atoms

In the projection operator method, first **label each of the pendant atoms so that we can distinguish identical atoms from one another**; for example, identify the three hydrogen atoms on ammonia as H_a, H_b, and H_c (Figure 3.5.4.2).

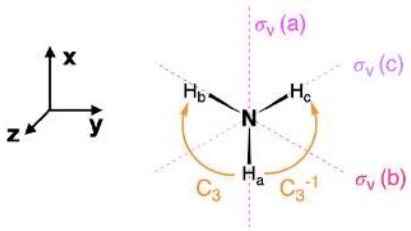


Figure 3.5.4.2: The three H's in NH_3 are chemically identical, but we can distinguish them using labels for the purpose of applying the projection operator method. In this figure, we have placed the z axis along the principal C_3 axis and placed the x axis colinear with one H. Each of the three H atoms has been labeled as H_a, H_b, or H_c. The σ_v that is coplanar with each H is labeled similarly (a, b, c) to keep account of each individual plane of symmetry. (CC-BY-NC-SA; Kathryn Haas)

Step 5.2: Create an expanded character table with one pendant atom's projected position after each operation

We will **perform each operation of the C_{3v} point group on this labeled molecule** and follow where one of the atoms is projected after the operation is complete. We will arbitrarily choose H_a. For example, upon performing the identity operation, E, the H_a atom is projected onto itself. On the other hand, H_a is projected onto H_b upon a clockwise C_3 rotation (as drawn in Figure 3.5.4.2). We take into account the result of each operation using an expanded character table (refer to the table below, 3.5.4.1). In the expanded character table, each operation within each class is written separately (i.e., $2C_3$ is accounted for separately as C_3 and C_3^{-1}).

Table 3.5.4.1: The expanded character table, and the projection of H_a by each operation is shown below.

$\mathbf{C_{3v}}$	E	C_3	C_3^{-1}	$\sigma_v(a)$	$\sigma_v(b)$	$\sigma_v(c)$
Projection of $\mathbf{H_a}$	H_a	H_b	H_c	H_a	H_c	H_b

(3.5.4.1)

Step 5.3: Find the contribution of each pendant atom to each SALC

Next, **create a linear combination of the projections for each of the SALCs** (the irreducible representations found in step 4). For each of the irreducible representations, multiply the projection by the respective character of the operation.

$$\text{Contribution of each atom to the SALC } = \sum(\text{Projection of } H_a \times \chi)$$

The linear combination for all irreducible representations of C_3v is shown below.

Table 3.5.4.2: The symmetry adapted linear combination (SALC) for each irreducible representation of C_3v is shown.

$\mathbf{C_{3v}}$	E	C_3	C_3^{-1}	$\sigma_v(a)$	$\sigma_v(b)$	$\sigma_v(c)$	Linear Combination
Projection of $\mathbf{H_a}$	$\mathbf{H_a}$	$\mathbf{H_b}$	$\mathbf{H_c}$	$\mathbf{H_a}$	$\mathbf{H_c}$	$\mathbf{H_b}$	
A_1	1	1	1	1	1	1	$= \mathbf{2H_a + 2H_b + 2H_c}$
A_2	1	1	1	−1	−1	−1	$= 0$
E	2	−1	−1	0	0	0	$= \mathbf{2H_a - H_b - H_c}$

(3.5.4.2)

Notice that there are only two irreducible representations that produce SALCs, and these are the same that were found in Step 4, above. This illustrates the fact that only the irreducible representations found through the reduction of the Γ will produce SALCs. We can ignore any irreducible representations that were not found in Step 4. Or, you can check your work in Step 4 by applying the projection operator to any irreducible representations not found in Step 4, and finding that they produce a sum of zero.

Step 5.4: Sketch the SALCs

The meaning of the linear combinations found in Table 3.5.4.2 is as follows:

- **Sketch the SALC with A_1 symmetry:** The linear combination $2H_a + 2H_b + 2H_c$ indicates all contributions to this SALC are of the same sign (of the wavefunction). Qualitatively, this means there is no node in this SALC. We can take this SALC almost literally to assume that all three H 1s wavefunctions contribute equally to the SALC. We can also use the fact that the A_1 representation possesses the full symmetry of the C_3v point group, is compatible with an s orbital on N, and thus is a totally symmetric SALC.

  Quantitatively, we can apply the normalizing factor, N, for this SALC. The linear combination for the A_1 SALC in Table 3.5.4.2 shows us that the coefficient for each orbital is 1. Thus, the normalizing factor for the A_1 SALC is $N = \left(\frac{1}{\sqrt{1^2+1^2+1^2}}\right) = \frac{1}{\sqrt{3}}$. This tells us that H_a, H_b, and H_c each contribute $\frac{1}{\sqrt{3}}$ to the normalized A_1 group orbital:

  $$A_1 \text{ group orbital } = \frac{1}{\sqrt{3}}\left[\psi_{H_a} + \psi_{H_b} + \psi_{H_c}\right]$$

  This is shown visually in Figure 3.5.4.3.
- **Sketch two SALCs with E symmetry:** The linear combination $2H_a - H_b - H_c$ indicates that there are contributions with both positive and negative sign to the wavefunction for each of the E group orbitals. Qualitatively, this tells us that there is a node within each of these two SALCs, and that the total contribution of the positive portion of the wavefunction is equal to the contribution of the negative portion.
  - **Finding the first E SALC:**
    For one of the SALCs, we can take the linear combination from Table 3.5.4.2 almost literally: The contribution from H_a is equal and opposite to the sum of the contributions from $H_b + H_c$. This would result in a SALC as shown in Figure 3.5.4.3 (E, left), that would have symmetry of the x axis and that would be compatible with the p_x orbital on N. The node exists in the yz plane and there is an equal contribution of positive and negative parts of the total wavefunction.

    We can also apply the normalizing factor, N, to find this SALC. The linear combination for the E SALC in Table 3.5.4.2 shows us that the coefficients for orbital contributions are 2, -1, and -1. Thus, the normalizing factor for the first E SALC is $N = \left(\frac{1}{\sqrt{2^2+(-1)^2+(-1)^2}}\right) = \frac{1}{\sqrt{6}}$. This normalized E group orbital is:

    $$\text{First } E \text{ group orbital } = \frac{1}{\sqrt{6}}\left[2\psi_{H_a} - \psi_{H_b} - \psi_{H_c}\right]$$

    This is shown visually in Figure 3.5.4.3 (E, left).
  - **Finding the second E SALC:**
    The second SALC is less obvious at first glance. We must use clues from the character table to help us determine what it should "look like". Since the E representation transforms as the group, (x, y), we know that one of the SALCs will have the symmetry of the x axis and p_x orbital on the central nitrogen atom, while the other should possess the symmetry of the y axis and be compatible with the p_y orbital on nitrogen. This alone could lead you to the sketch of the second SALC with E symmetry shown in Figure 3.5.4.3 (E, right). This second E SALC must have a node in the xz plane, and because H_a lies in this node, H_a cannot contribute to this group orbital. Retaining the fact that the positive and negative contributions of the linear combination must be equal, we can arrive at a SALC that has equal but opposite contributions of H_b and H_c, and no contribution by H_c (Figure 3.5.4.3, right).

    We can also apply the normalizing factor, N, to find this SALC. But we must apply the fact that H_a cannot contribute to the SALC with "y" symmetry. We remove the contribution of H_a, leaving us with coefficients of 0 for H_a and 1 for H_b and H_c. Thus, the normalizing factor for the second E SALC is $N = \left(\frac{1}{\sqrt{0^2+1^2+1^2}}\right) = \frac{1}{\sqrt{2}}$. To this, we must add positive and negative coefficients so that the entire wavefunction of this SALC is normalized. The result for this normalized E group orbital is:

    $$\text{Second } E \text{ group orbital } = \frac{1}{\sqrt{2}}\left[\psi_{H_b} - \psi_{H_c}\right]$$

    This is shown visually in Figure 3.5.4.3.

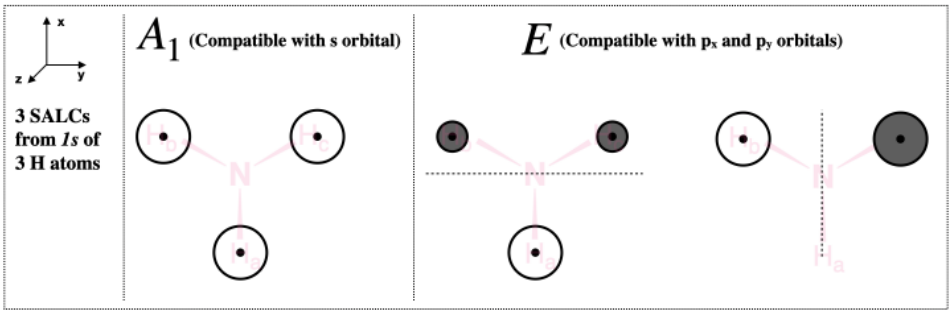


Figure 3.5.4.3: Sketches of H SALCs of ammonia from the perspective of the C_3 axiz (z axis). The A_1 SALC is shown at the left, while two degenerate SALCs with E symmetry are shown on the right. Nodes for E group orbitals are shown as dashed lines. (CC-BY-NC-SA; Kathryn Haas)

Step 6. Combine SALCs with AO's of like symmetry to draw the MO diagram for NH_3

First we must identify the valence orbitals on the central nitrogen: there are four including $2s$, $2p_x$, $2p_y$, and $2p_z$. Now we identify the symmetry of each using the C_{3v} character table. The symmetry of a central $2s$ orbital corresponds to the combination of functions x^2, y^2, and z^2 in the character table; this is A_1. The p_z orbital also corresponds to A_1. And so on... The symmetries of nitrogen valence orbitals are listed below.

$$2s = A_1$$
$$(2p_x,\ 2p_y) = E$$
$$2p_z = A_1$$

The next step is to get a sense of the relative energies of valence atomic orbitals for nitrogen and hydrogen, and then construct the molecular orbital diagram. The nitrogen $2s$ orbital is about 12 eV lower in energy than a H $1s$. This difference is an acceptable energy-match for the H orbitals to interact, but would not usually result in a strong interaction. On the other hand, the nitrogen 2p orbitals have an energy very close to the hydrogen 1s, different by only 0.5 eV. Knowledge of the relative energies of the atomic orbitals tells us that, when constructing a diagram, we can place the H SALCs at an energy similar to that of the N $2p$ orbitals, while the N $2s$ is much lower (Figure 3.5.4.4).

The $2s$ and $2p_z$ orbitals have A_1 symmetry and can combine with the A_1 SALC. These orbitals will give three molecular orbitals. The $2s$ orbital will not have strong interactions with the other orbitals of A_1 symmetry due to the large energy difference. The $2p_z$ orbital will not have good overlap with the wavefunctions for the three hydrogen orbitals due to their positions in space: The $2p_z$ orbital has half of its angular distribution pointed away from the hydrogen orbitals, and half pointed toward the center of a triangle formed by the three hydrogen atoms. The nitrogen $2s$ and $2p_z$ will combine with the hydrogen SALC of A_1 symmetry to give three molecular orbitals; one low-energy bonding orbital, one mid-energy non-bonding orbital, and one high-energy antibonding orbital. The mid-level non-bonding a_1 molecular orbital is close in energy to, and resembles, the nitrogen $2p_z$ orbital. The lowest energy a_1 molecular orbital will be lower in energy, but be similar to the nitrogen $2s$.

The remaining two $2p$ orbitals are degenerate and possess E symmetry under the C_{3v} point group. Although these orbitals are a good energy match, again, their orientation and positions in space do not allow for good orbital overlap, and their bonding and antibonding interactions are relatively weak compared to what we might otherwise expect from such a good energy match. The e atomic orbitals of nitrogen will combine with the e SALCs to give a set of two degenerate bonding molecular orbitals and a set of two degenerate antibonding orbitals (four total molecular orbitals of e symmetry). The MO diagram for NH_3 is shown in Figure 3.5.4.4, with calculated electron density surfaces of each MO shown.

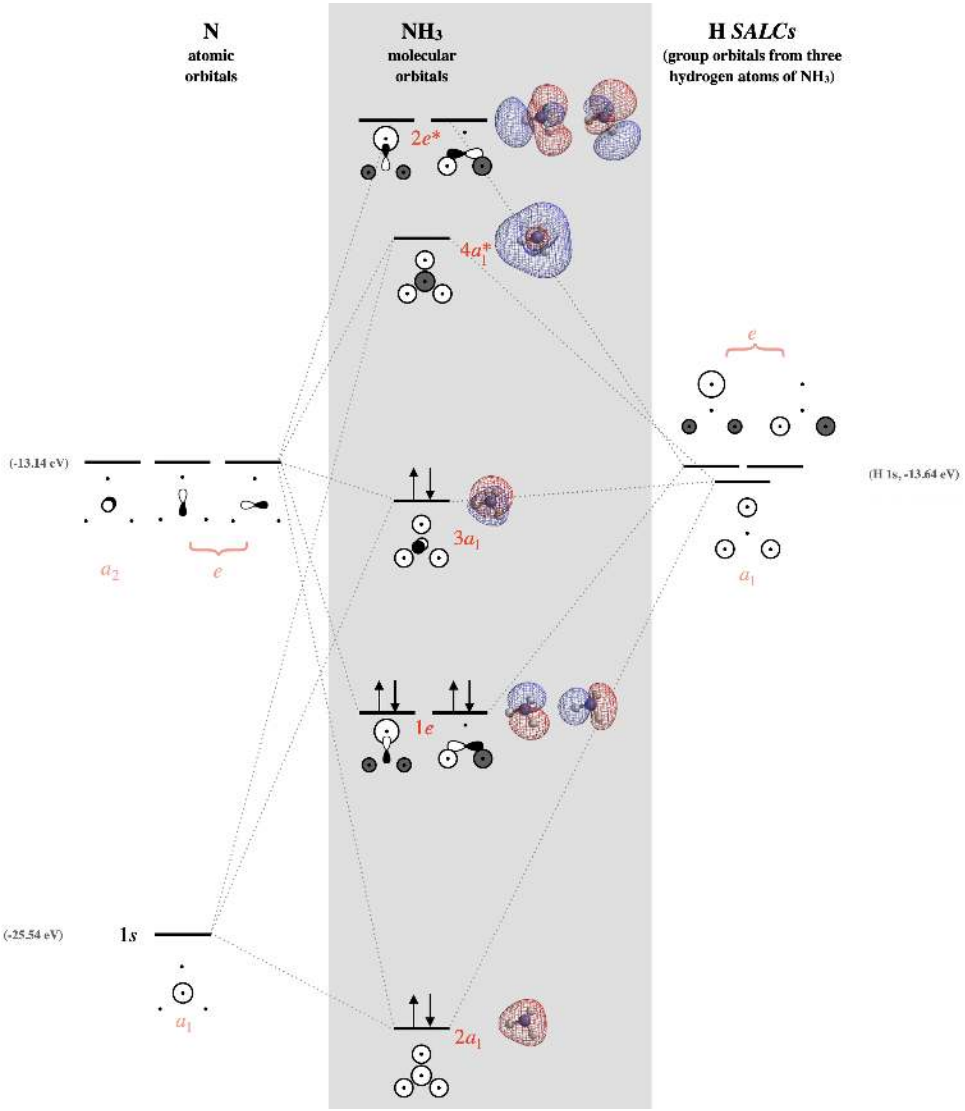


Figure **3.5.4.4**: The molecular orbital diagram of ammonia. Molecular orbitals surfaces calculated using Spartan software. (CC-BY-NC-SA; Kathryn Haas)

3.5.4: NH3 is shared under a CC BY-NC-SA 4.0 license and was authored, remixed, and/or curated by LibreTexts.

- **5.4.4: NH3** by Kathryn Haas is licensed CC BY-SA 4.0.

3.5.5: CO_2 (Revisted with Projection Operators)

The process for finding SALCs and constructing the molecular orbital diagram for carbon dioxide was described in a previous section (Section 5.4.2). However, we also just presented an alternative strategy, the projection operator method, to finding the shapes of SALCs in Section 5.4.4. Let's revisit carbon dioxide and demonstrate how you can use the projection operator method to find SALCs for carbon dioxide.

Just as before, we can simplify the problem by approximating the $D_{\infty h}$point group using D_{2h}. The first four steps for constructing the MO diagram would be the same as described in Section 5.4.2. and we will pick up from that point (with Step 5) to find what the SALCs look like using the projection operator method.

The projection operator method applied to CO_2

Step 5.1: Label the pendent atoms.

We can label the pendant atoms as O_a and O_b, as in Figure 3.5.5.1.

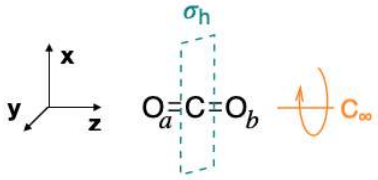


Figure 3.5.5.1: The structure of carbon dioxide with pendant oxygen atoms distinguished with labels a and b. Note that we will approximate the C_∞ axis as a C_2 axis to simplify the process of finding the SALCs. (CC-BY-SA; Kathryn Haas)

Step 5.2: Create an expanded character table with one pendant atom's projected position for each operation

The D_{2h} character table needs no expansion because each operation is in its own class. We will arbitrarily choose to determine the new position of O_a after each operation.

D_{2h}	E	$C_2(z)$	$C_2(y)$	$C_2(x)$	i	$\sigma(xy)$	$\sigma(xz)$	$\sigma(yz)$
Projection of O_a	O_a	O_a	O_b	O_b	O_b	O_b	O_a	O_a

Step 5.3: Find the contribution of each pendant atom to each SALC

Create a linear combination of the projections for each or the SALCs. The irreducible representations were found in step 4 in Section 5.4.2. Eight irreducible representations were found to be: $2A_g + 2B_{1u} + B_{2g} + B_{3u} + B_{3g} + B_{2u}$. For each of the irreducible representations, multiply the projection by the respective character of the operation.

$$\text{Contribution of each atom to the SALC } = \sum(\text{Projection of } H_a \times \chi)$$

The linear combination for all irreducible representations of D_{2h} are shown below.

Table 3.5.5.1: The symmetry adapted linear combination (SALC) for each irreducible representations of C_3v are shown.

D_{2h}	E	$C_2(z)$	$C_2(y)$	$C_2(x)$	i	$\sigma(xy)$	$\sigma(xz)$	$\sigma(yz)$	Linear Combination
Projection of O_a	O_a	O_a	O_b	O_b	O_b	O_b	O_a	O_a	
A_g	1	1	1	1	1	1	1	1	$= 4O_a + 4O_b$
B_{1u}	1	1	−1	−1	−1	−1	1	1	$= 4O_a - 4O_b$
B_{2g}	1	−1	1	−1	1	−1	1	−1	$= 0$
B_{3u}	1	−1	−1	1	−1	1	1	−1	$= 0$
B_{3g}	1	−1	−1	1	1	−1	−1	1	$= 0$
B_{2u}	1	−1	1	−1	−1	1	−1	1	$= 0$

(3.5.5.1)

Notice that there are only two irreducible representations that produce SALCs, the A_g and the B_{1u}. Since we found two of each ($2A_g + 2B_{1u}$) when we found the irreducible representations, we know that there will be two SALCs of A_g symmetry and two of B_{1u}

symmetry; that is four total SALCs from the pendant oxygens. This is the same as what we found in Section 5.4.2 using a different method.

Step 5.4: Sketch the SALCs

The SALCs with A_g symmetry: Quantitatively, we can apply the normalizing factor, N, for these SALCs. Each atom contributes equally to the SALCs, thus the normalizing factor for the A_g SALC is $N = \left(\frac{1}{\sqrt{1^2+1^2}}\right) = \frac{1}{\sqrt{2}}$. This tells us that each oxygen contributes $\frac{1}{\sqrt{2}}$ to each of the normalized A_g group orbitals:

$$A_g \text{ group orbital } = \frac{1}{\sqrt{2}}\left[\psi_{O_a} + \psi_{O_b}\right]$$

The linear combination $\mathbf{4O_a + 4O_b}$ indicates that wavefunctions from each oxygen atom contribute equally to each of the two SALCs, with the same sign of the wavefunction for each. Because we know that A_g is totally symmetric (all 1's in the characters), we can assume that the SALC's will look like a symmetric arrangement of oxygen orbitals. But which orbitals contribute? We could peek at the character table to get a hint. But we'll treat this problem systematically.

The SALCs with B_{1u} symmetry: The linear combination $\mathbf{4O_a - 4O_b}$ indicates that each oxygen atom contributes equally, but that they have opposite wavefunctions. Application of the normalizing factor would give us:

$$B_{1u} \text{ group orbital } = \frac{1}{\sqrt{2}}\left[\psi_{O_a} + \psi_{O_b}\right]$$

But how do we know what the SALCs look like? Again, the character table can give us some hints, but we'll use a systematic process, below.

What do the SALCs look like? One way to systematically derive the SALC shapes is to perform the projection (Step 5.3) on specific groups of orbitals on the oxygen atom. For example, if we replicate Table **3.5.5.1** using just the group of oxygen 2s orbitals and the A_g and B_{1u} representations, we get the following:

$\mathbf{D_{2h}}$	E	$C_2(z)$	$C_2(y)$	$C_2(x)$	i	$\sigma(xy)$	$\sigma(xz)$	$\sigma(yz)$	Linear Combination
Projection of 2s orbital of O_a	$\mathbf{O1s_a}$	$\mathbf{O1s_a}$	$\mathbf{O1s_b}$	$\mathbf{O1s_b}$	$\mathbf{O1s_b}$	$\mathbf{O1s_b}$	$\mathbf{O1s_a}$	$\mathbf{O1s_a}$	
A_g	1	1	1	1	1	1	1	1	$\mathbf{= 4O1s_a + 4O1s_b}$
B_{1u}	1	1	−1	−1	−1	−1	1	1	$\mathbf{= 4O1s_a - 4O1s_b}$

(3.5.5.2)

This tells us that one of the A_g SALCs looks like two oxygen 1s orbitals with equal signs and contributions. It also tells us that one of the B_{1u} SALCs looks like two s orbitals with opposite signs and equal magnitudes. These two SALCs are shown in Figure **3.5.5.2**.

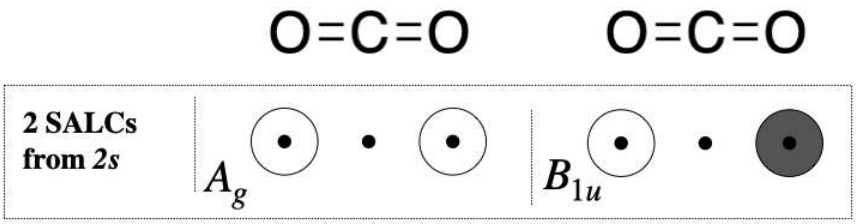


Figure **3.5.5.2**: SALCs derived from two oxygen **2s** orbitals from carbon dioxide. Compare to Section 5.4.2. (CC-BY-SA; Kathryn Haas)

If we do the same for the $2p_z$ orbitals, we need to pay attention to the orientation of the p orbital lobes. If the orbital is moved into the opposite orientation, it would get a negative sign in the projection (see below).

$\mathbf{D_{2h}}$	E	C_2 (z)	C_2 (y)	C_2 (x)	i	$\sigma(x$ $y)$	$\sigma(x$ $z)$	$\sigma(yz)$	Linear Combination
Projection of 2px orbital of O_a	$+O2$ pz_a	$+O2$ pz_a	$-O2$ pz_b	$+O2$ pz_b	$-O2$ pz_b	$-O2$ pz_b	$+O2$ pz_a	$+O2$ pz_a	
A_g	1	1	1	1	1	1	1	1	$= 4O2pz_a$ $- 4O2pz_b$
B_{1u}	1	1	−1	−1	−1	−1	1	1	$= 4O2pz_a$ $+ 4O2pz_b$

(3.5.5.3)

This tells us that one of the A_g SALCs is derived from two $2p_z$ orbitals of opposite sign but equal magnitude. In other words, the two p orbitals are pointing in opposite directions, but the lobes that are facing one another are of the same sign (see Figure **3.5.5.3**, left). This also tells us that one of the B_{1u} orbitals is derived from two p_z orbitals of equal magnitude and equal sign (pointing in the same directions, with lobes facing one another of opposite sign!) (see Figure **3.5.5.3**, right).

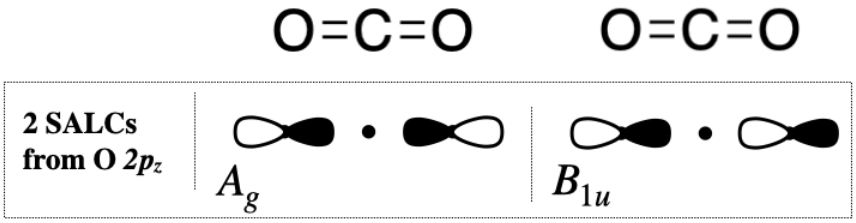


Figure **3.5.5.3**: SALCs derived from two oxygen $2p_z$ orbitals from carbon dioxide. Compare to Section 5.4.2. (CC-BY-SA; Kathryn Haas)

Now we have reached the same SALCs that we found previously in Section 5.4.2, but by an alternate method.

3.5.5: CO_2 (Revisted with Projection Operators) is shared under a CC BY-NC-SA 4.0 license and was authored, remixed, and/or curated by LibreTexts.

- **5.4.4: NH_3** by Kathryn Haas is licensed CC BY-SA 4.0.

3.5.6: BF_3

The case of boron trifluoride (BF_3) is an example of a molecule with one more layer of complexity than the other examples we have seen in previous sections in this chapter. (BF_3) is more complex than previous examples because it is the first case in which there are multiple types of valence orbitals on the pendant atoms. (BF_3) possesses s and p orbitals on *both* the central atom and all of the pendant atoms. We can follow the same steps that we have previously to derive other molecular orbital diagrams; however, there is one important difference: we will treat each type of pendant orbital as an individual set of SALCs.

Step 1. Find the point group of the molecule and assign Cartesian coordinates so that z is the principal axis.

The BH_3 molecule is trigonal planar, and its point group is D_{3h}. The z axis is colinear with the principle axis, the C_3 axis.

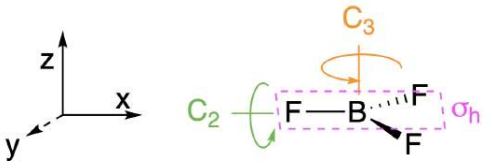


Figure 3.5.6.1: The molecule is in the D_{3h} point group. (CC-BY-NC-SA; Kathryn Haas)

Step 2. Identify and count the pendant atoms' valence orbitals.

Each of the three pendant fluorine atoms has four valence orbitals: one $2s$ and three $2p$ orbitals. Thus, we can expect a total of twelve SALCs from the three atoms. However, we will treat each type of orbital from the F atoms as its own set; each will have its own set of coordinates, with the y axis along the M-L bond. Thus we expect the following:

- One set of $2s$ SALCs: there is one 2s orbital on each of three atoms. This set will have three SALCs.
- One set of $2p_x$ SALCs: there is one $2p_x$ orbital on each of three atoms. Each of these individual orbitals is perpendicular to the M-L bond and coplanar with the molecule. This set will have three SALCs.
- One set of $2p_y$ SALCs: there is one $2p_y$ orbital on each of three atoms. Each of these individual orbitals is colinear with the M-L bond. This set will have three SALCs.
- One set of $2p_z$ SALCs: there is one $2p_z$ orbital on each of three atoms. Each of these individual orbitals is perpendicular to the M-L bond and parallel with the principal axis of the molecule. This set will have three SALCs.

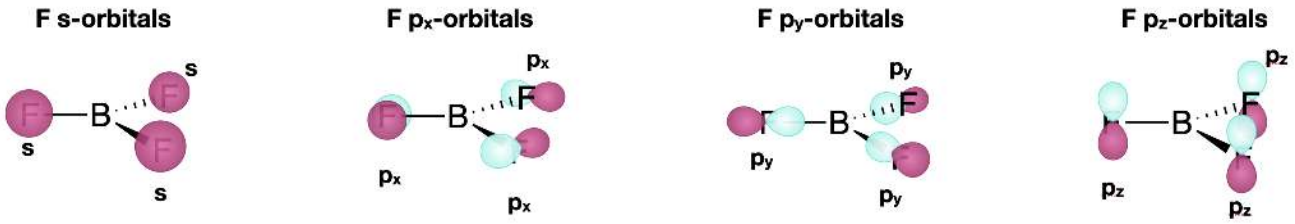


Figure 3.5.6.2: Individual sets of pendant fluorine atomic orbitals will create separate sets of SALCs. (CC-BY-SA; Kathryn Haas)

Step 3. Generate the Γ's for each set of SALCs

Use the D_{3h} character table to generate one reducible representation (Γ) for each of the four sets of pendant atomic orbitals shown in Figure 3.5.6.2; in this case we need four Γ because there are four types of valence orbital (the s, p_x, p_y, p_z).

- For the set of s orbitals: perform the operation for each class in the character table. Each s orbital is assigned a value depending on whether it moves or not: assign a value of 1 if it remains in place during the operation, or 0 (zero) if it moves out of its original place.
- for each set of p orbitals: Now there are phases (signs of the wavefunction), so a negative value is possible. Assign a value of 1 to each p orbital if it remains in place and in phase during the operation; assign a -1 if the atom's position remains, while the phase of the orbital is inverted (the positive lobe moves to the position of the negative lobe and vice versa); assign a 0 if it moves out of its original position.

The Γ for each type is given below:

$\mathbf{D_{3h}}$	E	$2C_3$	$3C_2$	σ_h	$2S_3$	$3\sigma_v$
$\mathbf{\Gamma_{2s}}$	3	0	1	3	0	1
$\mathbf{\Gamma_{2p_x}}$	3	0	−1	3	0	−1
$\mathbf{\Gamma_{2p_y}}$	3	0	1	3	0	1
$\mathbf{\Gamma_{2p_z}}$	3	0	−1	−3	0	1

Step 4. Break Γ's into irreducible representations for individual SALCs

Reduce each $\mathbf{\Gamma}$ into its component irreducible representations. Using either of the processes described previously, we find that each of the $\mathbf{\Gamma}$ reduces to two irreducible representations under the $\boldsymbol{D_{3h}}$ point group; in each case one is singly degenerate ($\boldsymbol{A}$) and the other doubly degenerate ($\boldsymbol{E}$). This equates to three SALCs for each $\mathbf{\Gamma}$ (orbital type) and a total of twelve SALCs. This should give us confidence! We were in fact expecting 12 SALCs because we found that there were twelve pendant atomic orbitals to start with.

D_{3h}	E	$2C_3$	$3C_2$	σ_h	$2S_3$	$3\sigma_v$
$\mathbf{\Gamma_{2s}}$	**3**	**0**	**1**	**3**	**0**	**1**
A_1'	1	1	1	1	1	1
E'	2	−1	0	2	−1	0

D_{3h}	E	$2C_3$	$3C_2$	σ_h	$2S_3$	$3\sigma_v$
$\mathbf{\Gamma_{2p_x}}$	**3**	**0**	**−1**	**3**	**0**	**−1**
A_2'	1	1	−1	1	1	−1
E'	2	−1	0	2	−1	0

D_{3h}	E	$2C_3$	$3C_2$	σ_h	$2S_3$	$3\sigma_v$
$\mathbf{\Gamma_{2p_y}}$	**3**	**0**	**1**	**3**	**0**	**1**
A_1'	1	1	1	1	1	1
E'	2	−1	0	2	−1	0

D_{3h}	E	$2C_3$	$3C_2$	σ_h	$2S_3$	$3\sigma_v$
$\mathbf{\Gamma_{2p_z}}$	**3**	**0**	**−1**	**−3**	**0**	**1**
A_2''	1	1	−1	−1	−1	1
E''	2	−1	0	−2	1	0

Step 5: Sketch the SALCs

We'll skip this step for now to make this problem simpler.

Step 6: Draw the MO diagram by combining SALCs with AO's of like symmetry.

We now know the symmetries of different pendant orbital SALCs - and it is helpful if we also know their relative energies, and the energies of the valence orbitals on the central boron atom. We can make predictions based on periodic trends, or we can use a table of ionization energies as a guide. The symmetries of the boron $\boldsymbol{2s}$ and $\boldsymbol{2p}$ orbitals can be found from the $\boldsymbol{D_{3h}}$ character table.

3.5.6: BF_3 is shared under a CC BY-NC-SA 4.0 license and was authored, remixed, and/or curated by LibreTexts.

- **5.4.4: NH_3** by Kathryn Haas is licensed CC BY-SA 4.0.

CHAPTER OVERVIEW

4: d Block Chemistry

4.1: Coordination Chemistry I - Structure and Isomers

4.2: Coordination Chemistry II - Bonding

4.1: Coordination Chemistry I - Structure and Isomers

4.1.1: History

4.1.2: Nomenclature and Ligands

4.1.3: Isomerism

4.1.4: Coordination Numbers and Structures

4.2: Coordination Chemistry II - Bonding

4.2.1: Evidence for Electronic Structures

4.2.1.1: Thermodynamic Data

4.2.1.2: Magnetic Susceptibility

4.2.1.3: Electronic Spectra

4.2.1.4: Coordination Number and Molecular Shapes

4.2.2: Bonding Theories

4.2.2.1: Crystal Field Theory

4.2.2.1.1: Crystal Field Theory

4.2.2.1.2: Colors of Coordination Complexes

4.2.2.1.3: Crystal Field Stabilization Energy

4.2.2.1.4: Factors That Affect the Magnitude of Δo

4.2.2.1.5: Jahn-Teller Distortions

4.2.2.1.6: Magnetic Moments of Transition Metals

4.2.2.1.7: Magnetism

4.2.2.1.8: Thermodynamics and Structural Consequences of d-Orbital Splitting

4.2.2.2: Ligand Field Theory

4.3: Ligand Exchange Reactions (Thermodynamics)

4.3.1: Associative Ligand Substitution

4.3.2: Dissociative Ligand Substitution

4.4: Electronic Spectra of Coordination Compounds

4: d Block Chemistry is shared under a not declared license and was authored, remixed, and/or curated by LibreTexts.

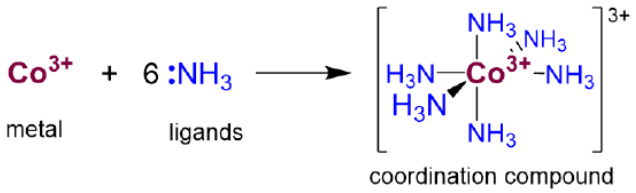
SECTION OVERVIEW

4.1: Coordination Chemistry I - Structure and Isomers

Coordination compounds are important to all areas of chemistry, engineering, the life and environmental sciences, and beyond. In the synthetic laboratory catalytic amounts of coordination compounds enable organic chemists to synthesize new compounds selectively and in high yield under mild condition. Applied industrially, coordination compound catalysts serve as vital catalysts that facilitate the conversion of raw petrochemical or bio-derived feedstocks into useful industrial and consumer products. Without them life as we know it would be impossible as many biochemical systems are coordination complexes. Examples include the hemoglobin which transports oxygen around our bodies and the myoglobin which stores it, the photosystems which harvest light and use light energy in photosynthesis, the constituents of the respiratory chain, and many of the enzymes involved in the expression and transmission of genetic information. In studying coordination chemistry you are about to take your first steps into a vast and exciting world.

What is a coordination compound?

Coordination compounds consist of one or more **metals** bound to one or more Lewis base **ligands**. For example, hexammineruthenium (3+) ion is a coordination complex in which six ammonia ligands coordinate a Co^{3+} ion, as shown in Scheme **4.1.I**.



Scheme 4.1.I. Formation of hexammineruthenium(3+) ion from Co^{3+} and NH_3. (CC BY 4.0; Stephen Contakes)

Such complexes are called coordination complexes because the ligand-metal bond may be thought of as a **coordinate covalent bond** in which both of the bonding electrons come from the ligand, which is then said to **coordinate** the metal. This coordinate covalent model is a very useful formalism for understanding the basic features of coordination chemistry, although it does not always accurately reflect the actual details of the bonding in every coordination complex. Nevertheless, even in those cases where the simple coordinate covalent bond model breaks down the coordinate covalent bond concept supplies the language sophisticated models employ to describe the more complex bonding involved.

Additional important terms

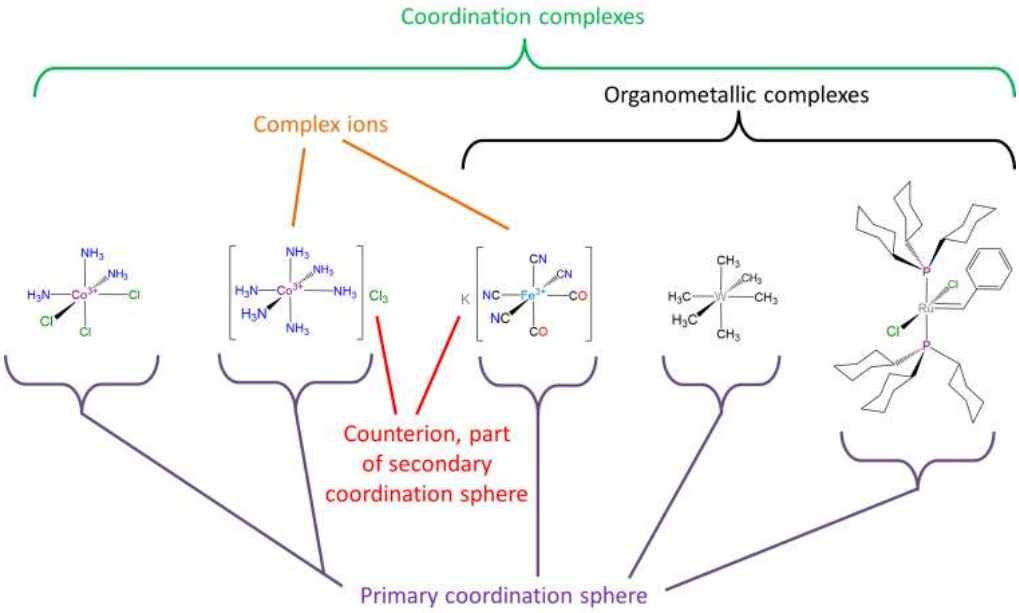
Some of the common widely terms that follow from the coordinate covalent model of bonding in coordination complexes include

- Coordination compounds are also called **coordination complexes**, **metal complexes**, or just **complexes**. The term **complex** refers to coordination compounds' composite nature, in that they may be thought of as comprised of multiple ligand and metal ion parts that can be restored by breaking the coordinate covalent bonds holding the complex together. This is in contrast to inorganic or organic molecules which are more commonly thought about as whole molecules held together by the sharing of electrons contributed by all the atoms.
- Coordination complexes that are ions are called **complex ions.**
- Ligands bound to the coordination complex are said to reside in the **primary** or **inner coordination sphere**. These bound ligands are not readily exchangeable, in contrast to nearby counterions and solvent molecules, which are said to reside in the **secondary** or **outer coordination sphere**.
- The portion of the complex contributing the electron pairs is said to be the **donor** and the portion which receives them the **acceptor**. In conventional coordination compounds the ligand is the donor and the metal the acceptor. In these cases it would be equally convenient to refer to the ligand donor as the Lewis base and the metal acceptor as the Lewis acid. However, in more

complex bonding scenarios there may be multiple electron pair donation and acceptance interactions taking place between each pair of atoms and donor-acceptor language will be more convenient.

- The number of ligand sites donating lone pairs to the central atom is referred to as the **coordination number**. For most complexes this will just be equal to the number of ligand atoms bound to the metal. In simple complexes it is just equal to the number of ligands. For instance, the cobalt in Scheme **4.1.I** has a coordination number of six.
- Although technically compounds with metal-carbon bonds are coordination complexes term coordination complex is sometimes used to refer to complexes which do not possess metal-carbon bonds in their primary coordination sphere. Complexes which possess metal-carbon bonds are called **organometallic compounds** instead. The use of the terms organometallic and coordination to distinguish organometallic compounds from other types of coordination compounds is often convenient since many organometallic ligands engage in more than simple σ donor acceptor coordinate covalent bond formation with the metal center. However, this is true of some wholly inorganic ligands too so it should always be kept in mind that organometallic compounds are just a type of coordination compound and that inorganic ligands can in principle be tuned in interact with a metal center in much the same way an organic ligand does.

A summary of some of the concepts and terms used to describe coordination compounds is given in Scheme **4.1.II**.



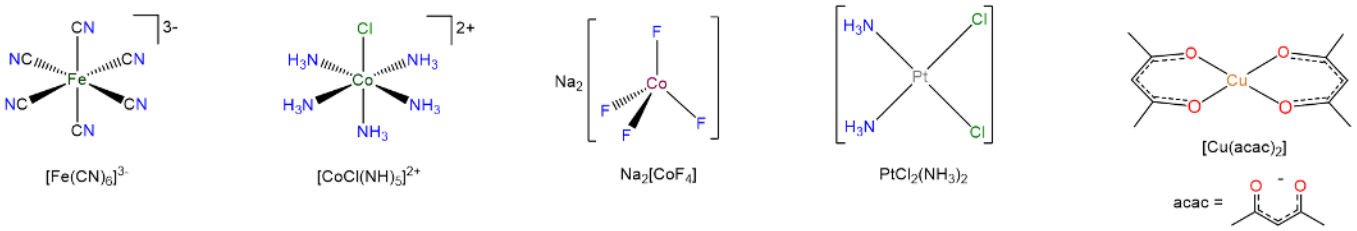
Scheme 4.1.II. Some terms used to describe coordination compounds. (CC BY 4.0; Stephen Contakes)

The formulae of coordination complexes

The way the formulae of coordination complexes are written reflects that it is often convenient to think of coordination compounds as a composite of metals and ligands. When writing the formulae of a complex

- the atoms of a ligand are not added to those of the rest of the compound. Instead, the ligand atoms are kept together, if necessary by enclosing the ligand formula in parentheses or giving an abbreviation for the ligand.
- For complex ions the metal and ligands are enclosed in square brackets. Sometimes this is also done for neutral coordination compounds as well. In either case the brackets enclose those parts of the compound which comprise the primary coordination sphere; anything else is in the secondary coordination sphere outside.

A careful perusal of the examples in Scheme **4.1.III** should make the important features of this system clear.



Scheme 4.1.III. Formulae of coordination compounds and complex ions. (CC BY 4.0; Stephen Contakes)

4.1.1: History

4.1.2: Nomenclature and Ligands

4.1.3: Isomerism

4.1.4: Coordination Numbers and Structures

Contributors and Attributions

- Stephen Contakes, Westmont College
- Unless otherwise noted, all line drawings on this page are by Stephen Contakes and licensed under a Creative Commons Attribution 4.0 International License.

4.1: Coordination Chemistry I - Structure and Isomers is shared under a not declared license and was authored, remixed, and/or curated by LibreTexts.

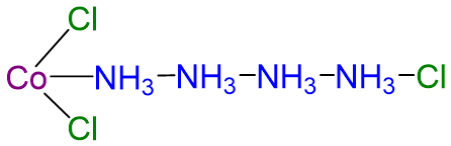
4.1.1: History

History of the Coordination Compounds

Coordination compounds have been known and used since antiquity; one of the oldest synthetic pigments is the blue pigment Egyptian blue, a copper complex of formula $CaCuSi_4O_{10}$ used by the Egyptians since the third Millenium B.C. (in ancient China the Ba analogue, Han blue, was discovered independently). The blue color of Egyptian blue is due to interlocked $Cu(Si_2O_7)_4$ units in which each copper is coordinated by four O atoms in a square planar arrangement. Later, in 1706, the Berlin painter Diesbach would discover another deep blue pigment, Prussian blue: $\mathbf{KFe_2(CN)_6}$.

Despite their long use, the chemical nature of coordination compounds was unclear for a number of reasons. For example, many compounds called “double salts” were known, such as $\mathbf{AlF_3 \cdot 3\,KF}$, $\mathbf{Fe(CN)_2 \cdot 4\,KCN}$, and $\mathbf{ZnCl_2 \cdot 2\,CsCl}$, which were combinations of simple salts in fixed and apparently arbitrary ratios. Why should $\mathbf{AlF_3 \cdot 3\,KF}$ exist but not $\mathbf{AlF_3 \cdot 4\,KF}$ or $\mathbf{AlF_3 \cdot 2\,KF}$? And why should a 3:1 KF:$\mathbf{AlF_3}$ mixture have different chemical and physical properties than either of its components? Similarly, adducts of metal salts with neutral molecules such as ammonia were also known—for example, $\mathbf{CoCl_3 \cdot 6\,NH_3}$, which was first prepared sometime before 1798. Like the double salts, the compositions of these adducts exhibited fixed and apparently arbitrary ratios of the components. For example, $\mathbf{CoCl_3 \cdot 6\,NH_3}$, $\mathbf{CoCl_3 \cdot 5\,NH_3}$, $\mathbf{CoCl_3 \cdot 4\,NH_3}$, and $\mathbf{CoCl_3 \cdot 3\,NH_3}$ were all known and had very different properties, but despite all attempts, chemists could not prepare $\mathbf{CoCl_3 \cdot 2\,NH_3}$ or $\mathbf{CoCl_3 \cdot NH_3}$.

Although the chemical composition of such compounds was readily established by existing analytical methods, their chemical nature was puzzling and highly controversial. The major problem was that what we now call valence (i.e., the oxidation state) and coordination number were thought to be identical. As a result, highly implausible (to modern eyes at least) structures were proposed for such compounds. Of these the most influential was the Blomstrand-Jørgensen chain theory of bonding in coordination compounds, which predicted the “Chattanooga choo-choo” model for $CoCl_3{\cdot}4NH_3$ shown in Scheme **4.1.1.I**.



Scheme **4.1.1.I**. Blomstrand-Jørgensen chain theory model of bonding in $CoCl_3{\cdot}4NH_3$.

Nevertheless, this theory was not wholly illogical and, in fact, explained much of the analytical data on coordination compounds available to chemists of the time. This data included the electrical conductivity of aqueous solutions of these compounds, which was roughly proportional to the number of ions formed per mole, and the number of free chloride ions present, which could be determined by precipitating them gravimetrically as AgCl. In the case of $CoCl_3{\cdot}4NH_3$, two ions and one chloride were produced when the compound was dissolved in water, which Jørgensen was able to explain using the chain structure shown above by postulating that chlorides attached to NH_3 could dissociate while those attached to Co could not. The modern theory of coordination chemistry, which overthrew the chain theory, is based largely on the work of Alfred Werner (1866–1919; Nobel Prize in Chemistry in 1913). In a series of careful experiments carried out in the late 1880s and early 1890s, he examined the properties of several series of metal halide complexes with ammonia. For example, five different “adducts” of ammonia with $PtCl_4$ were known at the time: $PtCl_4{\cdot}nNH_3$ (n = 2–6). Some of Werner’s original data on these compounds are shown in Table **4.1.1.1**. Werner’s data on $PtCl_4{\cdot}6NH_3$ in Table **4.1.1.1** showed that all the chloride ions were present as free chloride. In contrast, $PtCl_4{\cdot}2NH_3$, was a neutral molecule that did not give free chloride ions when dissolved in water.

Alfred Werner (1866–1919)

Werner, the son of a factory worker, was born in Alsace. He developed an interest in chemistry at an early age, and he did his first independent research experiments at age 18. While doing his military service in southern Germany, he attended a series of chemistry lectures, and he subsequently received his PhD at the University of Zurich in Switzerland, where he was appointed professor of chemistry at age 29. He won the Nobel Prize in Chemistry in 1913 for his work on coordination compounds, which he performed as a graduate student and first presented at age 26. Apparently, Werner was so obsessed with solving the riddle of the structure of coordination compounds that his brain continued to work on the problem even while he was asleep. In

1891, when he was only 25, he woke up in the middle of the night and, in only a few hours, had laid the foundation for modern coordination chemistry.

Table **4.1.1.1**: Werner's Data on Complexes of Ammonia with $PtCl_4$

Complex	Conductivity (ohm^{-1})	Number of Ions per Formula Unit	Number of Cl^- Ions Precipitated by Ag^+
$PtCl_4 \cdot 6NH_3$	523	5	4
$PtCl_4 \cdot 5NH_3$	404	4	3
$PtCl_4 \cdot 4NH_3$	299	3	2
$PtCl_4 \cdot 3NH_3$	97	2	1
$PtCl_4 \cdot 2NH_3$	0	0	0

These data led Werner to postulate that metal ions have two different kinds of valence: (1) a primary valence (oxidation state) that corresponds to the positive charge on the metal ion and (2) a secondary valence (coordination number) that is the total number of ligands bound to the metal ion. If Pt had a primary valence of 4 and a secondary valence of 6, Werner could explain the properties of the $PtCl_4 \cdot NH_3$ adducts by the following reactions, where the metal complex is enclosed in square brackets:

$$[Pt(NH_3)_6]Cl_4 \rightarrow [Pt(NH_3)_6]^{4+}(aq) + 4Cl^-(aq) \quad (4.1.1.1)$$

$$[Pt(NH_3)_5Cl]Cl_3 \rightarrow [Pt(NH_3)_5Cl]^{3+}(aq) + 3Cl^-(aq) \quad (4.1.1.2)$$

$$[Pt(NH_3)_4Cl_2]Cl_2 \rightarrow [Pt(NH_3)_4Cl_2]^{2+}(aq) + 2Cl^-(aq) \quad (4.1.1.3)$$

$$[Pt(NH_3)_3Cl_3]Cl \rightarrow [Pt(NH_3)_3Cl_3]^{+}(aq) + Cl^-(aq) \quad (4.1.1.4)$$

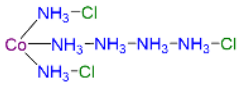
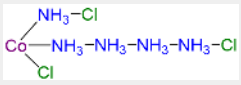
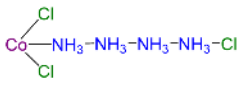
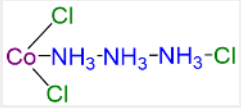
$$[Pt(NH_3)_2Cl_4] \rightarrow [Pt(NH_3)_2Cl_4]^{0}(aq) \quad (4.1.1.5)$$

Further work showed that the two missing members of the series—$[Pt(NH_3)Cl_5]^-$ and $[PtCl_6]^{2-}$—could be prepared as their mono- and dipotassium salts, respectively. Similar studies established coordination numbers of 6 for Co^{3+} and Cr^{3+} and 4 for Pt^{2+} and Pd^{2+}.

? Exercise 4.1.1.1. The $CoCl_3 xNH_3$ series.

The series $CoCl_3 \cdot xNH_3$ was particularly important in establishing the correctness of Werner's coordination theory over the rival chain theory. By ~1900 conductivity measurements suggested that the members of the series gave the number of ions shown in Table **4.1.1.1**.

Table **4.1.1.1**. The CoCl3·xNH3 series according to coordination theory, chain theory, and experiment.

Compound	Color	Werner formulation	Blomstrand-Jørgensen chain theory formulation	Number of ions in solution
$CoCl_3 \cdot 6NH_3$	yellow	$[Co(NH_3)_6]Cl_3$		4
$CoCl_3 \cdot 5NH_3$	violet	$[Co(NH_3)_5Cl]Cl_2$		3
$CoCl_3 \cdot 4NH_3$	green	$[Co(NH_3)_4Cl_2]Cl$		2
$CoCl_3 \cdot 3NH_3$	orange	$[Co(NH_3)_4Cl_3]$		0

What does this data suggest about the relative explanatory power of Werner's coordination theory and chain theory? Explain.

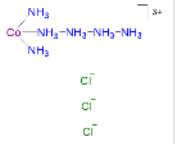
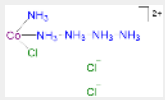
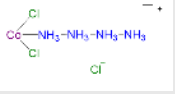
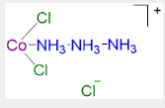
Answer

Remember that

- chain theory predicts that the number of ions is the number formed when the Cl atoms bound in a chain with NH_3 dissociate.
- coordination theory predicts the number of ions based on the number of complex ions and their counterions.

Based on this the predictions of coordination theory and chain theory can be compared with the experimental data, as is done in Table **4.1.1.2**.

Table **4.1.1.2**: Comparison of ions predicted for the $CoCl_3 \cdot xNH_3$ series by coordination theory and chain theory with the number observed experimentally.

Compound	Color	Ions predicted by Werner's coordination theory	Number of ions predicted by coordination theory	Ions predicted by Blomstrand-Jørgensen chain theory	Number of ions predicted by chain theory	Observed Number of ions in solution
$CoCl_3 \cdot 6NH_3$	yellow	$[Co(NH_3)_6]^{3+}$ Cl^- Cl^- Cl^-	4		4	4
$CoCl_3 \cdot 5NH_3$	violet	$[Co(NH_3)_5Cl]^{2+}$ Cl^- Cl^-	3		3	3
$CoCl_3 \cdot 4NH_3$	green	$[Co(NH_3)_4Cl_2]^+$ Cl^-	2		2	2
$CoCl_3 \cdot 3NH_3$	orange	None	0		2	0

As can be seen by comparing the number of ions predicted by coordination and chain theory in Table **4.1.1.2**, coordination theory successfully explains all the observed ion counts, while chain theory fails to explain the lack of ions observed for $CoCl_3 \cdot 3NH_3$.

Nevertheless, as is often the case when developing theoretical models using data from real experimental investigations, these observations did not convince Jørgensen, who could point to the experimental difficulty of determining the number of ions present from solution conductivity data.

What ultimately convinced Jørgensen of the correctness of Werner's coordination model over his own chain theory was how Werner's explanation of the structure of cobalt coordination complexes using an octahedral coordination geometry explained the existence of isomers in Co complexes containing Cl and NH_3 ligands. In the case of $[Co(NH_3)_4Cl_2]Cl$ two isomers were known: one red and the other green. Because both compounds had the same chemical composition and the same number of groups of the same kind attached to the same metal, there had to be something different about the arrangement of the ligands around the metal ion. Werner's key insight was that the six ligands in $[Co(NH_3)_4Cl_2]Cl$ had to be arranged at the vertices of an octahedron because that was the only structure consistent with the existence of two, and only two, stereoisomers (Figure **4.1.1.1**). His conclusion was also corroborated by the existence of two and only two stereoisomers of the next compound in the series: $Co(NH_3)_3Cl_3$.

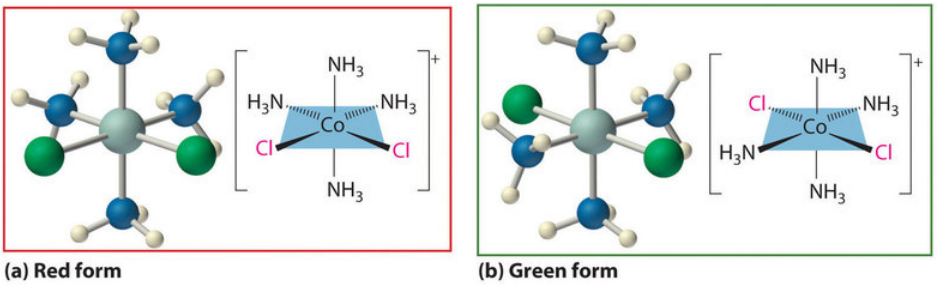


Figure **4.1.1.1**. The $[Co(NH_3)_4Cl_2]^+$ ion can have two different arrangements of the ligands, which results in different colors: if the two Cl^- ligands are next to each other (*cis*), the complex is red (a), but if they are opposite each other (*trans*), the complex is green (b).

✔ Example 4.1.1.1: Why did Werner propose an octahedral geometry for 6-coordinate complexes?

In Werner's time, many complexes of the general formula MA_4B_2 were known, but no more than two different compounds with the same composition had been prepared for any metal. To confirm Werner's reasoning that this suggests these complexes possess an octahedral geometry, calculate the maximum number of different structures possible for six-coordinate MA_4B_2 complexes with each of the three most symmetrical possible structures the ligands will form about the central metal - a hexagon, a trigonal prism, and an octahedron.

Assuming that the absence of evidence for additional compounds in this case serves as reasonable circumstantial evidence for their absence, what does the fact that no more than two forms of any MA_4B_2 complex were known suggest about the three-dimensional structures of these complexes?

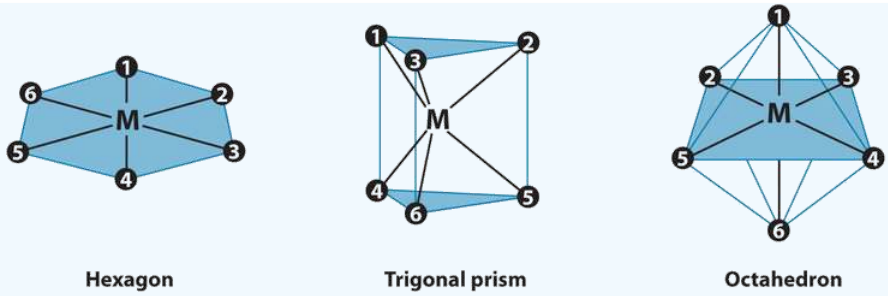
Solution

In this problem you are given

- the stochiometry of the complexes, MA_4B_2
- three possible coordination geometries - hexagonal, trigonal prismatic, and octahedral.

In order to calculate the number of isomers that could be present for each geometry it is best to follow a systematic approach. Since there are fewer B type ligands than A type ligands, the easiest way to do this for each geometry is to start by placing a B ligand at one vertex and then to determine how many different positions are available for the second B ligand.

The three regular six-coordinate structures are shown here, with each coordination position numbered so that we can keep track of the different arrangements of ligands. For each structure, all vertices are equivalent. We begin with a symmetrical MA_6 complex and simply replace two of the A ligands in each structure to give an MA_4B_2 complex:



For the hexagon, we place the first B ligand at position 1. There are now **three** possible places for the second B ligand:

- position 2 (or 6)
- position 3 (or 5)
- position 4

The (1, 2) and (1, 6) arrangements are chemically identical because the two B ligands are adjacent to each other. The (1, 3) and (1, 5) arrangements are also identical because in both cases the two B ligands are separated by an A ligand. Those of you who remember your ogranic chemistry might recognize that this situation is formally analogous to the *ortho-*, *meta-*, and *para-* isomerism in disubstituted benzenes.

Turning to the trigonal prism, we place the first B ligand at position 1. Again, there are three possible choices for the second B ligand:

- at position 2 or 3 on the same triangular face
- position 4 (on the other triangular face but adjacent to 1)
- position 5 or 6 (on the other triangular face but not adjacent to 1).

The (1, 2) and (1, 3) arrangements are chemically identical, as are the (1, 5) and (1, 6) arrangements.

In the octahedron, however, if we place the first B ligand at position 1, then we have only two choices for the second B ligand:

- position 2 (or 3 or 4 or 5)
- position 6.

In the latter, the two B ligands are at opposite vertices of the octahedron, with the metal lying directly between them. Although there are four possible arrangements for the former, they are chemically identical because in all cases the two B ligands are adjacent to each other.

The number of possible MA_4B_2 arrangements for the three geometries is thus: hexagon, 3; trigonal prism, 3; and octahedron, 2. The fact that only two different forms were known for all MA_4B_2 complexes that had been prepared suggested that the correct structure was the octahedron but did not prove it. For some reason one of the three arrangements possible for the other two structures could have been less stable or harder to prepare and had simply not yet been synthesized. When combined with analogous results for other types of complexes (e.g., MA_3B_3), however, the data were best explained by an octahedral structure for six-coordinate metal complexes.

? Exercise 4.1.1.1

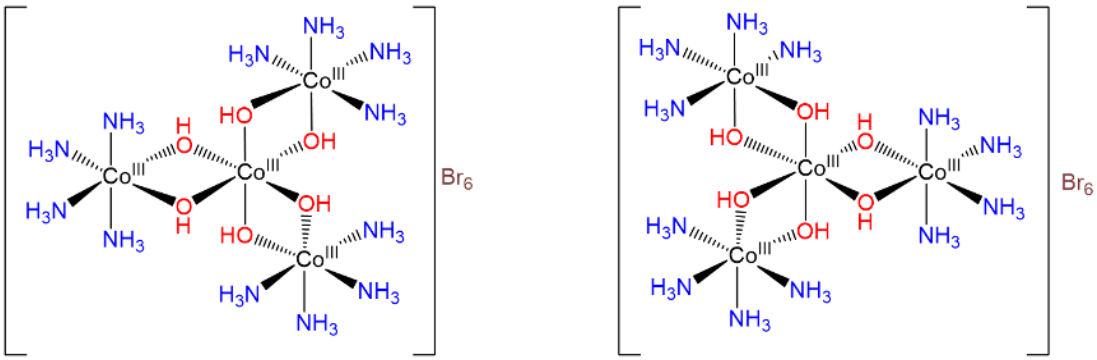
Determine the maximum number of structures that are possible for a four-coordinate MA_2B_2 complex with either a square planar or a tetrahedral symmetrical structure.

Answer

square planar, 2; tetrahedral, 1

Even Werner's explanation of isomerism in coordination complexes in terms of octahedral and other recognized coordination geometries did not convince all chemists until he was able to resolve a racemic mixture of *d*- and *l*-$[Co\{Co(NH3)_4(OH)_2\}_3]$ into its

enantiomers, which are shown in Scheme **4.1.1.II**. By doing so Werner demonstrated to chemists of his time (virtually none of whom knew group theory) that tetrahedral carbon atoms were not required for chirality; D_3 octahedral complexes were also chiral.



Scheme **4.1.1.II**: d- and l-enantiomers of [Co{Co(NH3)$_4$(OH)$_2$}$_3$], colloquially referred to as hexol. This work by Stephen Contakes is licensed under a Creative Commons Attribution 4.0 International License.

4.1.1: History is shared under a not declared license and was authored, remixed, and/or curated by LibreTexts.

- **24.1: Werner's Theory of Coordination Compounds** by Anonymous is licensed CC BY-NC-SA 4.0.

4.1.2: Nomenclature and Ligands

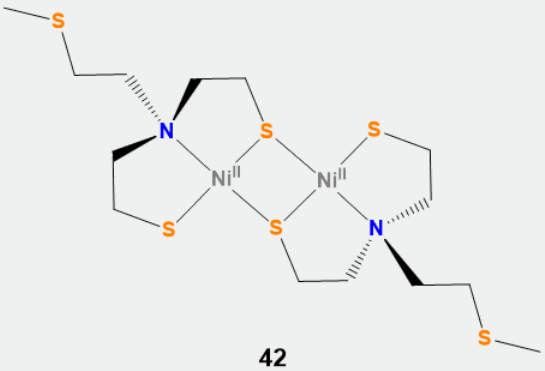
Systems of nomenclature and formulae are intended as tools, to be employed insofar as they are useful

There are well-established rules for both naming and writing the formulae of coordination compounds. The purpose of these rules is to facilitate clear and precise communication among chemists. As with all such rules, some are more burdensome than others to employ, and some serve more crucial roles in the communication process while others are more peripheral - and all are poorly used in the service of pedantic tyranny, especially when used against those who are otherwise doing good work. For this reason, you are urged to approach the rules in a spirit of generosity towards others in

- naming and writing formulas as reasonably accurately as you can so that ligands and metals are where readers expect them and thus can understand what you mean more easily.
- being gracious towards the many professional inorganic chemists who adhere loosely to some of the rules you are about to learn.
- recognizing that in cases when a structure is particularly complex and a picture may make be particularly useful, you should supply one (See the note below).

Note 4.1.2.1: Sometimes the most helpful name to give a compound is 42.

Even though the IUPAC nomenclature rules permit specification of even the most complex structures, it is often much easier and more effective to supply a numbered structure that can be referred to instead of the IUPAC name. Consider bis{[(μ-2-mercaptoethyl)(2-mercaptoethyl)-methylthioethylaminato (2-)]Nickel(II)}. Which is easier, to expect readers and hearers to work out the structure from that name or to just refer them to compound **42** in Scheme **4.1.2.I**?



42

Scheme **4.1.2.I**. Structure of bis{[(μ-2-mercaptoethyl)(2-mercaptoethyl)-methylthioethylaminato (2-)]Nickel(II)}. The authors of the synthesis of this compound in Inorganic syntheses1 may have had to figure out an IUPAC name for this compound but if you have this scheme in your paper and your instructor is OK with it you can just call it **42**

Coordination Complexes are named as the ligand derivatives of a metal

A variety of systems have been used for naming coordination compounds since the development of the discipline in the time of Alfred Werner. In this section the most common approaches as they are currently used by practicing chemists will be described. Those who need a more thorough and accurate acquaintance with the full IUPAC nomenclature rules are encouraged to consult the IUPAC brief guide to inorganic nomenclature followed by complete guidelines, commonly known as the IUPAC red book. If those are still not enough a careful read of note **4.1.2.1** is suggested.

The systems for naming coordination compounds used at present are additive, meaning that they consider coordination compounds as comprising a central metal to which are added ligands. To specify the structure and bonding in this metal-ligand complex then involves:

1. when there are several different ways of attaching the metal and ligands, specifying the structural or stereoisomer
2. systematically listing the ligands in a way that, as necessary, conveys information about how they are linked to the metal and their stereochemistry

3. providing the identity of the metal and its oxidation state, or if the oxidation state is unclear, at least the overall charge on the complex
4. specifying any counterions present

Since the stereochemistry of coordination compounds forms the subject of the next section, in this section it will be addressed by simply giving the prefixes that designate stereochemistry as if they were self-evident. Do not worry about these for now. They will make sense after you have learned more about stereochemistry in the next section. At that time, you can go back over the examples in that section to solidify your understanding of how to name coordination compounds.

However, in order to name coordination compounds accurately you will need to learn how to think about and name ligands first.

Ligands

Ligands are classified based on whether they bind to the metal center through a single site on the ligand or whether they bind at multiple sites. Ligands that bind through only a single site are called **monodentate** from the Latin word for tooth; in contrast, those which bind through multiple sites are called **chelating** after the Greek $\chi\alpha\lambda\epsilon$ for "claw". These relationships are summarized in Figure **4.1.2.1**.

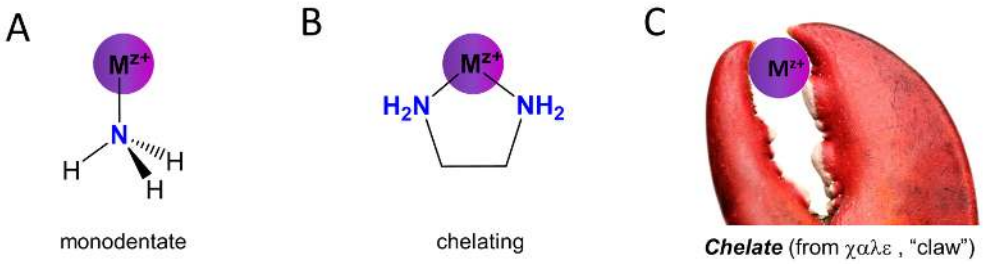
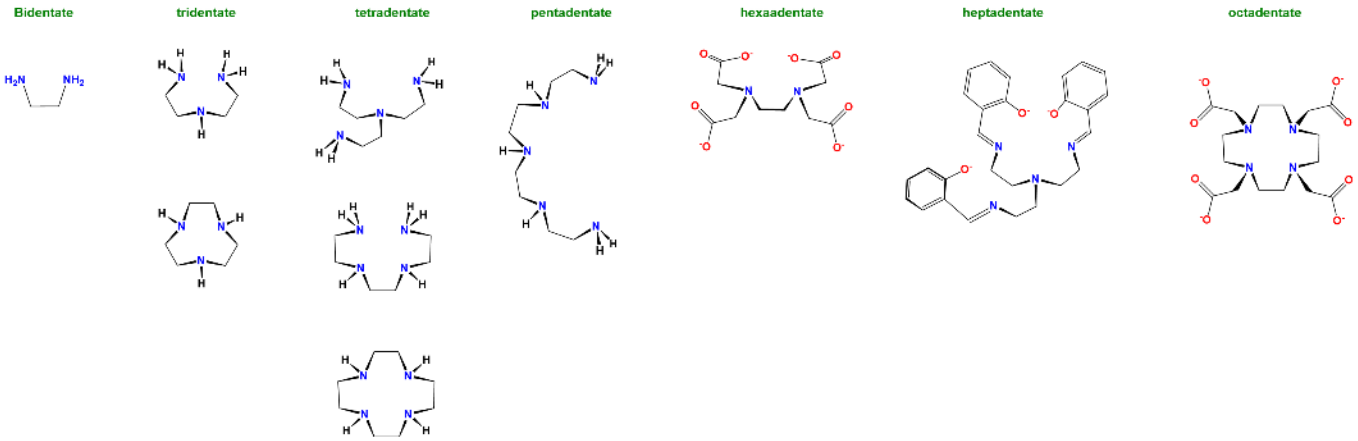


Figure **4.1.2.1**. (A) Ammonia is a monodentate ligand while (B) ethylene diamine is a chelating ligand owing to its capacity to bind metals via its two amine functional groups. (C) Chelating ligands act like a lobster claw in attaching to the metal via multiple sites. The lobster claw image is adapted from https://www.clipart.email/download/1127636.html. Otherwise this work by Stephen Contakes is licensed under a Creative Commons Attribution 4.0 International License.

Following naturally from the classification of non-chelating ligands as monodentate, chelating ligands are further classified according to the number of sites which they can use to bind a metal center. This number of binding sites is called the denticity and ligands are referred to as monodentate (non- chelating), bidentate, tridentate, etc., based on the number of sites available. Ligands with two binding sites have a denticity of two and are said to be bidentate; those with three are tridentate, four tetradentate, and so on. To illustrate this classification system examples of chelating ligands classified according to denticity are given in Scheme **4.1.2.I**.

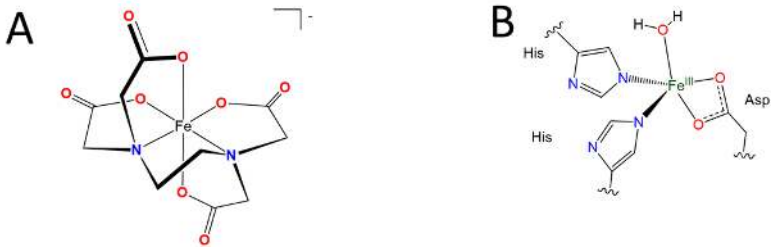
Scheme 4.1.2.I. A selection of chelating ligands classified according to denticity.



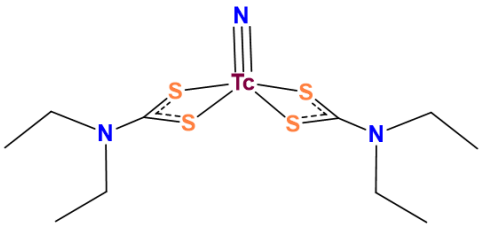
Scheme **4.1.2.IIA**. Because only one oxygen per carboxylate *typically* binds, only one is counted when assigning a ligand's denticity. This work by Stephen Contakes is licensed under a Creative Commons Attribution 4.0 International License.

Although only one carboxylate oxygen *usually* binds to a metal, it is still possible to bind for both oxygens to bind to a single metal. As shown in Scheme **4.1.2.IIB**, complexes in which both carboxylates bind to a metal are known, and in fact are common in the active sites of some enzymes. It is just that the binding of both oxygens gives a strained four-membered ring that is usually unstable.

Scheme 4.1.2.II. (A) Only one oxygen per carboxylate counts towards the denticity of EDTA since on binding the other oxygen generally points away from the metal center, as in the structure of $Fe(EDTA)^-$. (B) In some enzyme active sites both oxygens of a carboxylic acid (aspartate or Asp in this example) bind to a metal. The aspartate carboxylic acid group is bidentate while the EDTA carboxlic acid groups in A are monodentate. This work by Stephen Contakes is licensed under a Creative Commons Attribution 4.0 International License.



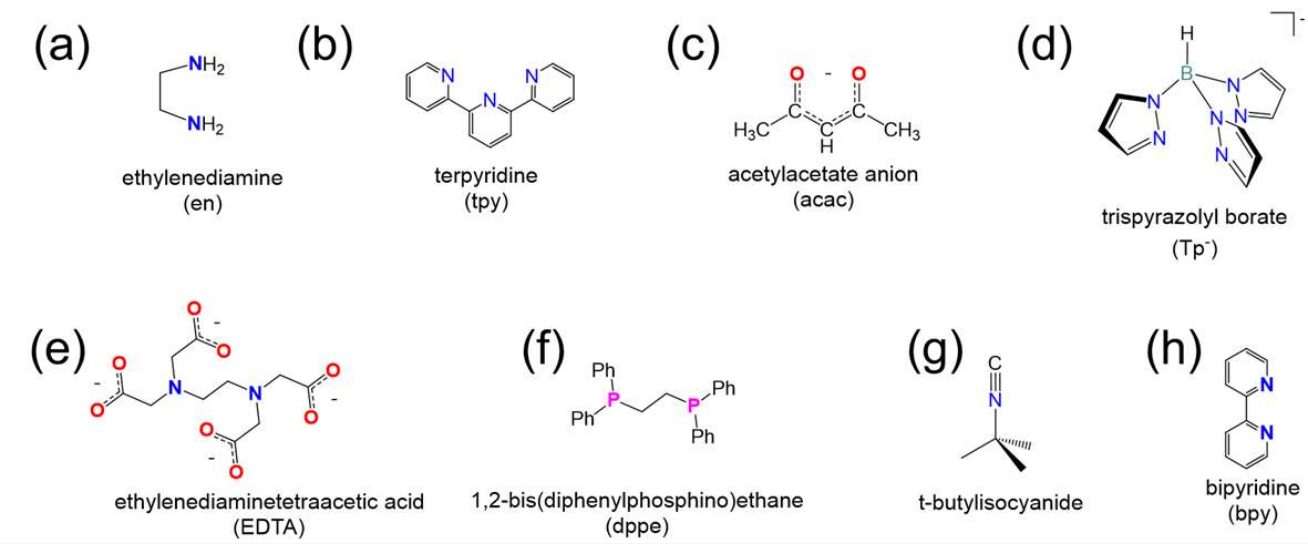
Scheme 4.1.2.III. As in this complex, dithiocarbamates commonly bind metals through both sulfur atoms. Consequently, dithiocarbamates are classified as bidentate. This work by Stephen Contakes is licensed under a Creative Commons Attribution 4.0 International License.



Because of these factors it is technically more correct to say that carboxylates *usually act as* monodentate ligands and dithiocarbamates bidentate ones than it is to say that carboxylates *are* monodentate ligands and dithiocarbamates bidentate ones. So in other words the ligand classifications presented here just represent common binding modes.

? Exercise 4.1.2.1

Determine the denticity of each ligand in the list below and classify them as monodentate, tridentate, etc.



Answer

(a) bidentate

(b) tridentate

(c) bidentate

(d) tridentate (only the lower N on each ring has a lone pair that can be used to bind the metal)

(e) hexadentate (remember that each carboxylate only counts as one point of attachment)

(f) bidentate

(g) monodentate (through the lone pair on the isocyanide C)

(h) bidentate

This experimentally-based classification of dithiocarbamates as bidentate and carboxylates as monodentate can be confusing to a beginner. Fortunately, such experimentally based classifications are embedded in the lists of common monodentate ligands as given in Table **4.1.2.1** and common chelating ligands in Table **4.1.2.2**.

A perusal of the ligands in Table **4.1.2.1** reveals that several can bind to a metal in multiple ways. For example, thiocyanate, SCN^- can bind metals through its S or N atoms. Such ligands are called **ambidentate ligands**. In naming an ambidentate ligand, the atom through which it attaches to the metal is commonly specified after the ligand name using the italicized element symbol or, more formally, a κ followed by the italicized element symbol. An example is given in Scheme **4.1.2.I**.[2]

Scheme 4.1.2.I. Two possible binding modes of nitrite acting as a ligand.[3]

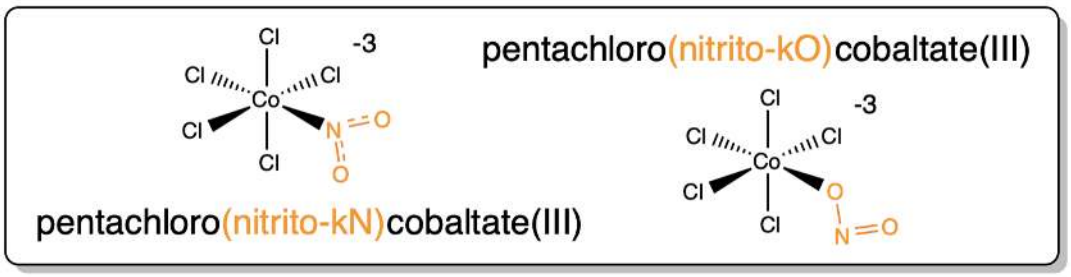
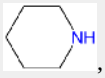
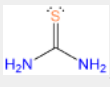
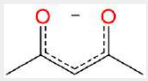
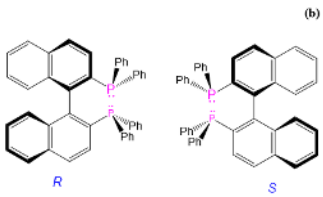
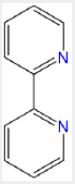
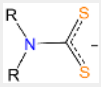
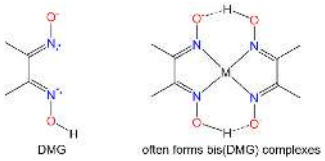
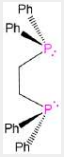
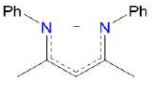


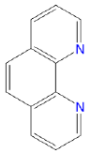
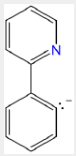
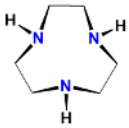
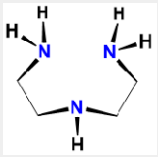
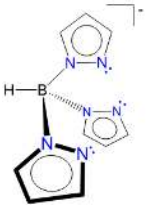
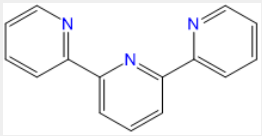
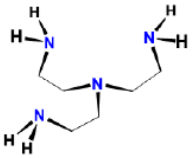
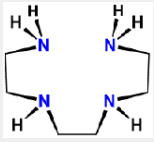
Table **4.1.2.1**. Common monodentate ligands. Most chemists still prefer common names over the IUPAC ones.

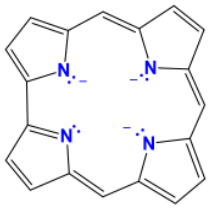
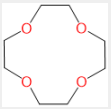
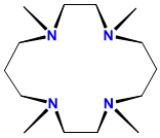
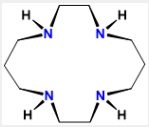
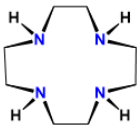
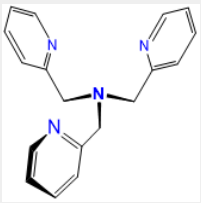
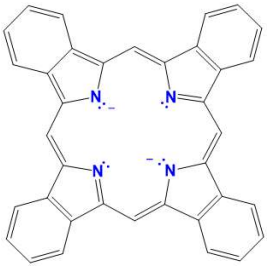
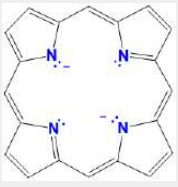
Ligand	Common name	IUPAC name
H^- (H ligands are always considered anions for naming purposes)	hydrido	hydrido
F^-	fluoro	fluorido
Cl^-	chloro	chlorido
Br^-	bromo	bromido
I^-	iodo	iodido
CN^-, as M-CN	cyano	cyanido or cyanido-κC or cyanido-*C*
CN^-, as M-NC	isocyano	isocyanido or cyanido-κN or cyanido-*N*
CH_3NC	methylisocyanide	methylisocyanide
N_3^-	azido	azido
SCN^-, *e.g.* thiocyanate as M-SCN	thiocyanato	thiocyanato-κS or thiocyanato-*S*
NCS^-, *e.g.* thiocyanate as M-NCS	isothiocyanato	thiocyanato-κN or thiocyanato-*N*
$CH_3CO_2^-$	acetato	ethanoato
N^{3-}	nitrido	nitrido
NH^{2-}	imido	azanediido
NH_2^-	amido	azanido
NH_3	ammine	ammine
RNH_2, R_2NH, R_3N	alkylamine, dialkylamine, trialkalyamine (*e.g.* methylamine for CH_3NH_2)	alkylamine, dialkylamine, trialkalyamine (*e.g.* methylamine for CH_3NH_2)
 , piperidine, abbreviated pip	piperidine	piperidine
 , pyridine, abbreviated py	pyridine	pyridine
CH_3CN, acetonitrile, abbreviated MeCN	acetonitrile	acetonitrile
P^{3-}	phosphido	phosphido
PH_3	phosphine	phosphane
PR_3	trialkylphosphine (*e.g.* trimethylphosphine for Me_3P)	trialkylphosphane (*e.g.* trimethylphosphane for Me_3P)
PAr_3	triarylphosphine (*e.g.* triphenylphosphine for Ph_3P)	triarylphosphine (*e.g.* triphenylphosphane for Ph_3P)
 , dimethylsulfoxide or DMSO or dmso	dimethylsulfoxide (sometimes called dimethylsulfoxo but this usage is rare and violates the nomenclature rules for neutral ligands)	(methanesulfinyl)methane or dimethyl(oxido)sulfur
 , thiourea or tu	thiourea	thiourea

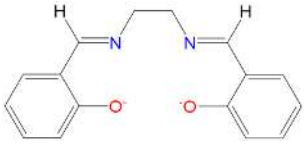
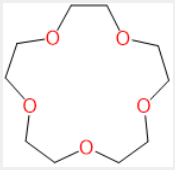
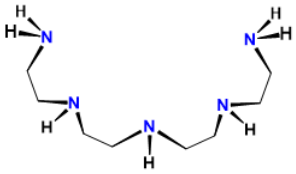
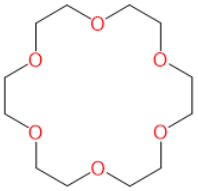
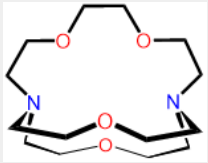
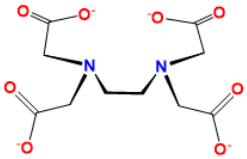
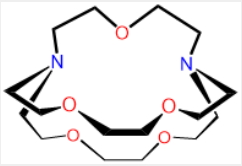
Ligand	Common name	IUPAC name
O^{2-}	oxo	oxido
OH^-	hydroxo	hydroxido
H_2O	aqua	aqua
S^{2-}	sulfo	sulfo
HS^-	hydrosulfido	hydrosulfido
RS^-	alkanethiolate (*e.g.* ethanthiolate for EtS^-)	thioalkanoate
H_2S	hydrogen sulfide	hydrogen sulfide
R_2S	alkylsulfanylalkane (*e.g.* ethylsulfanylethane for Et_2S)	dialkyl sulfide
O_2	dioxygen	dioxygen
O_2^-, superoxide	superoxido	dioxido(1-) or superoxido
O_2^{2-}, peroxide	peroxido	dioxido(2-) or peroxido
N_2	dinitrogen	dinitrogen
NO (are always considered neutral for naming purposes)	nitrosyl	nitrosyl
CO	carbonyl	carbonyl
CS	thiocarbonyl	thiocarbonyl
SO, as M-SO	sulfino	sulfur monoxide-κS or sulfur monoxide-*S*
NO_2, as M-NO_2	nitryl	nitrogen dioxide-κN or nitrogen dioxide-*N*
CO_3^{2-}	carbonato	carbonato
NO_2^-, as M-NO_2	nitro or nitrito-*N*	nitrito-κN or nitrito-*N*
NO_2^-, as M-ONO	nitrito or nitrito-*O*	nitrito-κO or nitrito-*O*
NO_3^-	nitrato	nitrato
SO_3^{2-}	sulfito	sulfito
SO_4^{2-}	sulfato	sulfato
$S_2O_3^{2-}$, as M-S-SO_2-O^-	thiosulfato-*S*	thiosulfato-κS or thiosulfato-*S*
$S_2O_3^{2-}$, as M-O-SO_2-S^-	thiosulfato-*O*	thiosulfato-κO or thiosulfato-*O*

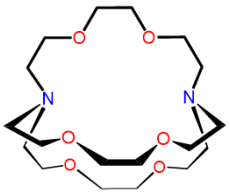
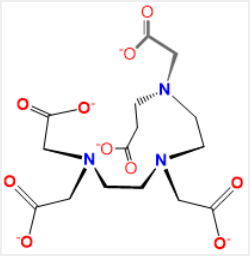
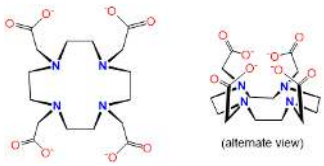
Table **4.1.2.2**. Common chelating ligands organized by denticity. Most chemists use the common names and abbreviations to describe these ligands.

Common Ligand name	IUPAC ligand name	abbreviation (if applicable)	structure or representative/parent structure (shown in the ionization state in which they bind to a metal)
bidentate ligands			
acetylacetonato	2,4-pentanediono	acac	
R-BINAP and *S*-BINAP	*R*- or *S*-2,2'-bis(diphenylphosphino)-1,1'-binapthyl	BINAP	
2,2'-bipyridine	2,2'-bipyridine	bpy or bipy	
cyclooctadiene	1,5-cyclooctadiene	COD	 (binding to the metal occurs through the alkene π cloud)
dialkyldithiocarbamato	dialkylcarbamodithiolato	$R_2NCS_2^-$ or dtc	
dimethylgloximato	butanedienedioxime	Hdmg or DMG	
diphenylphosphinoethane or 1,2-(diphenylphosphino)ethane	Ethane-1,2-diylbis(diphenylphosphane)	dppe	
ethylenediamine	Ethane-1,2-diamine	en	
ethylenedithiolato	Ethane-1,2-dithiolato	$C_2H_2S_2^{2-}$	
nacnac	*N*,*N*'-diphenyl-2,4-pentanediiminato	nacnac	
oxalato	oxalato	ox	

Common Ligand name	IUPAC ligand name	abbreviation (if applicable)	structure or representative/parent structure (shown in the ionization state in which they bind to a metal)
1,10-phenanthroline or *o*-phenanthroline	1,10-phenanthroline	phen or *o*-phen	
phenylpyridinato	2-phenylpyridinato-C^2,*N* or 2-phenylpyridinato-κC^2,*N*	ppy	
tridentate ligands			
triazacyclononane	1,4,7-triazacyclononane	tacn	
diethylenetriamine	1,4,7-triazaheptane	dien	
pyrazoylborato (scorpionate)	hydrotris(pyrazo-1-yl)borato	Tp	
terpyridine or 2,2';6',2"-terpyridine	1^2,2^2:2^6,3^2-terpyridine or 2,6-bis(2-pyridyl)pyridine, tripyridyl, 2,2′:6′,2″-terpyridine	tpy or terpy	
tetradentate ligands			
β, *β*', *β*"-triaminotriethylamine	*β*, *β*', *β*"-tris(2-aminoethyl)amine	tren	
triethylenetetramine	1,4,7,10-tetraazadecane	trien	

Common Ligand name	IUPAC ligand name	abbreviation (if applicable)	structure or representative/parent structure (shown in the ionization state in which they bind to a metal)
corroles	variable and generally not used	cor or Cor	
12-crown-4	1,4,7,10-tetraoxacyclododecane	12-crown-4	
tetramethylcyclam	1,4,8,11-tetramethyl-1,4,8,11-tetraazacyclotetradecane	TMC or cyclam	
cyclam	1,4,8,11-tetraazacyclotetradecane	cyclam	
cyclen	1,4,7,10-tetraazacyclododecane	cyclen	
tris(2-pyridylmethyl)amine	1-pyridin-2-yl-*N*,*N*-bis(pyridin-2-ylmethyl)methanamine	tpa or TPA	
phthalocyanines	variable and generally not used	variable, usually a modified Pc	
porphyrins	variable and generally not used	variable, usually a modified por, Por, or P (e.g. TPP = tetraphenylporphyrin)	

Common Ligand name	IUPAC ligand name	abbreviation (if applicable)	structure or representative/parent structure (shown in the ionization state in which they bind to a metal)
salen	2,2'-ethylenebis(nitrilomethylidene) diphenoxido	salen	
pentadentate ligands			
15-crown-5	1,4,7,10,13-Pentaoxacyclopentadecane	15-crown-5	
tetraethylenepentamine	1,4,7,10,13-pentaazatridecane	tepa or TEPA	
hexadentate ligands			
18-crown-6	1,4,7,10,13,16-hexaoxacyclooctadecane	18-crown-6	
2,1,1-cryptand	4,7,13,18-Tetraoxa-1,10-diazabicyclo[8.5.5]icosane	2,1,1-crypt or [2.1.1]-cryptand kryptofix 211 and variations thereof	
ethylenediaminetetraaceto	2,2′,2″,2‴-(Ethane-1,2-diyldinitrilo)tetraaceto	EDTA, edta, Y^{4-}	
heptadentate ligands			
2,2,1-cryptand	4,7,13,16,21-pentaoxa-1,10-diazabicyclo[8.8.5]icosane	2,2,1-crypt or [2.2.1]-cryptand kryptofix 221 and variations thereof	

Common Ligand name	IUPAC ligand name	abbreviation (if applicable)	structure or representative/parent structure (shown in the ionization state in which they bind to a metal)
octadentate ligands			
2,2,2-cryptand	4,7,13,16,21,24-Hexaoxa-1,10-diazabicyclo[8.8.8]hexacosan	2,2,2-crypt or [2.2.2]-cryptand kryptofix 222 and variations thereof	
pentetato acid or diethylenetriaminepentaacetato or DTPA	2-[bis[2-[bis(carboxylatomethyl)amino]ethyl]amino]acetato	DTPA	
DOTA or tetraxetan	1,4,7,10-Tetraazacyclododecane-1,4,7,10-tetraacetic acid	Dota, DOTA	

Rules for Naming Coordination Compounds

As explained above, the name of a coordination compound communicates

- as appropriate, information about isomerism
- systematically listing the ligands in a way that as necessary conveys information about their oxidation state and how they are linked to the metal
- the identity of the metal and its oxidation state
- any counterions present

Before going into these rules it is worth pointing out a few things.

1. It is easiest to learn these rules by starting with one or two of the rules, learning how to apply them, and then adding additional rules one at a time. To that end, instructors who wish to use a more programmed approach may find it convenient to first direct their students to this page which focuses on getting the names of the ligands and metal right, without worrying about isomerism or stereochemistry.

2. The rules also assume some familiarity with common coordination geometries and patterns of isomerism in metal complexes. Thus it might be easiest to learn about common coordination geometries first, followed by common patterns of isomerism in metal complexes before beginning this section. If you decide to dive right in to this section you might find it helpful to know that when applying nomenclature and formula rules most textbooks *assume*

- complexes in which the metal has a coordination number of six are octahedral
- complexes in which the metal has a coordination number of five are trigonal bipyramidal
- complexes in which Pt^{II} , Pd^{II} , or Rh^{I}, or Ir^{I} have a coordination number of four are square planar
- other complexes in which the metal has a coordination number of four are tetrahedral

Like all assumptions these don't always work in real life but they should be good enough to get you through your first inorganic chemistry course.

For the pedants among you, note that the complexes given as examples and in exercises on this page have been selected for pedagogical utility. Although many are well-known compounds, others are hypothetical.

Now on to the rules.

Rule 1: If ions are present, name the cation first, followed by the anion.

Examples:

$K_2[Pt^{II}Cl_4]$ potassium tetrachloroplatinate(2-)

$[Co^{III}(NH_3)_6](NO_3)_3$ hexaamminecobalt(3+) nitrate

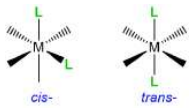
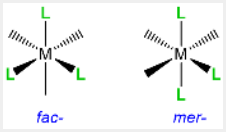
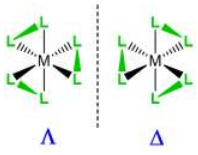
$[Co^{III}(NH_3)_6][Cr^{III}(C_2O_4)_3]$ hexaamminecobalt(3+) tris(oxalato)chromium(3-)

Rule 2: When multiple isomers are possible, designate the particular isomer in italics at the front of the name of each complex

If you have not yet learned about isomerism in coordination compounds skip this rule for now and return to it after you have.

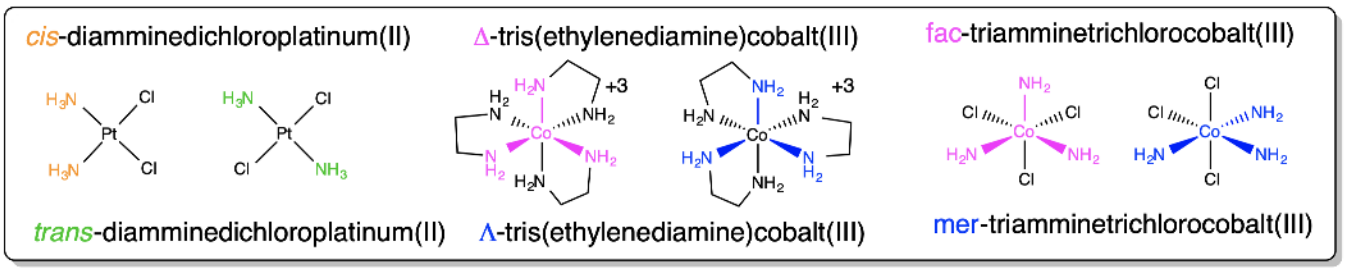
When a complex might exist as one of two stereoisomers, prefixes are commonly used to designate which isomer is present. The most common cases are listed in Table **4.1.2.3**.

Table **4.1.2.3**. Prefixes used to specify isomerism about a metal center when naming and writing coordination compounds' formulae.

Type of isomerism	Graphical reminder	Prefixes
Geometric, *cis-* , *trans-*		*cis-* or *trans-*
Geometric, *fac- /mer-*		*fac-* or *mer-*
Enantiomers, **Λ-**, **Δ-**		**Λ-** or **Δ-**

Examples of how isomerism about a metal center is designated are given in Scheme **4.1.2.II**.

Scheme 4.1.2.II. Application of nomenclature rules for stereosimerism about a metal.[3]



There are a number of other cases where it might be advisable to specify the stereochemistry of a complex. These cases involve specifying

- the coordination geometry about a metal center (octahedral, trigonal prismatic, tetrahedral, square planar, etc.)

- the geometry cannot be unambigouously described by a single *cis/trans* or *fac/mer* relaionship of ligands

These cases may also be handled by using a designator to specify the coordination geometry and, as necessary, giving the position of ligated atoms in terms of designated numbered positions for that geometry. See the IUPAC red book for details as such cases fall outside the scope of what is normally advisable for an undergraduate course.

Rule 3: Specify the identity, number, and as appropriate, isomerism of the ligands present in alphabetical order by ligand name.

Before specifying the metal, the ligands are written as prefixes of the metal.

In specifying the ligands several rules are followed.

1. The ligands are written in alphabetical order by the ligand name only; symbols are not considered and prefixes do not count in determining alphabetical order.

   Example: In the name of the complex ion $[Co(NH_3)_5Cl]^{2+}$, pentamminechlorocobalt(II), the ammine ligand is named before the chloro ligand because the order is alphabetical by the ligand name by virtue of which ammine comes before chloro.

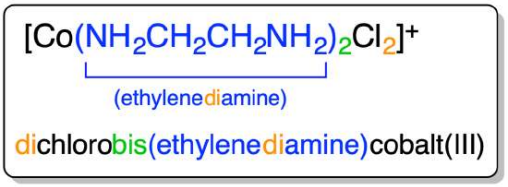
2. Prefixes are used to indicate the number of each ligand present. Specifically, *di-*, *tri-*, *tetra-* , *penta-*, *hexa-*, *etc.* prefixes are used to indicate multiple ligands of the same type EXCEPT when the ligand is polydentate or its name already has a *di-*, *tri-*, *tetra-* etc. In that case *bis-*,*tris-*, *tetrakis-*, etc. are used instead. These prefix rules are summarized in Table **4.1.2.3**.

Table **4.1.2.3**. Prefixes used to specify the number of a given ligand present.

Number of identical ligands	prefix used when the ligand name is simple	prefix used when the ligand is polydentate or its name already has a *di-*, *tri-*, *tetra-* etc.
2	di-	bis-
3	tri-	tris-
4	tetra-	tetrakis-
5	penta-	pentakis-
6	hexa-	hexakis-
7	hepta-	heptakis-
8	octa-	octakis-
9	nona-	nonakis-
10	deca-	decakis-

An example of the application of the prefix rule is given in Scheme **4.1.2.III**.

Scheme 4.1.2.III. Example of the use of prefixes to specify the number of ligands of each type in a complex.[3]



3. Ligand names are based on their charge.

   - Neutral and cationic ligand names are the same as the names of their neutral compounds with two caveats:

     i. names that involve spaces should either be put in parentheses or the spaces should be eliminated (preferred)

     Example: cis-dichlorobis(**dimethyl sulfoxide**)platinum(II) or *cis*-dichlorobis(**dimethylsulfoxide**)platinum(II)

ii. A few ligands are given common names.

- H_2O = aqua
- NH_3 = ammine (notice that there are two n's)
- CO = carbonyl
- CS = thiocarbonyl
- NO = nitrosyl

- For anionic ligands, the vowel at the end of their anion names is changed to an -"o"

  Examples: Cl^- = chloro, NH_2^- = amido, N_3^- = azido

  Caveat: some anionic ligands have common names that may also be used

  Examples:

  I^- = iodo or iodino

  CN^- = cyano or cyanido

  O^{2-} = oxo or oxido

The IUPAC and common names of many ligands are given in Tables **4.1.2.1**. and **4.1.2.2**.

4. When an ambidentate ligand is present, the atom through which it is bound to the metal is indicated by giving either its element symbol or a κ and its element symbol in italics after the ligand name.

   Example:

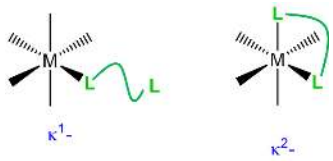
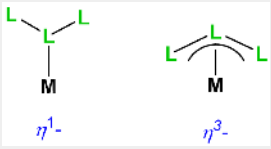
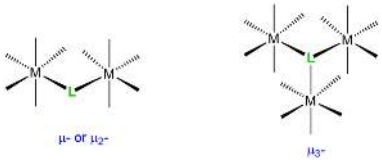
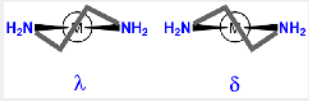
   M-SCN is thiocyanato-*S* or thiocyanato-κ*S*

   M-NCS = thiocyanato-*N or* thiocyanato-κ*N*

   The use of κ and an element symbol to indicate how a ligand and metal are linked is called a **k-term**. More complex k-terms might also involve specifying the atoms by number, though their use is outside the scope of this text.

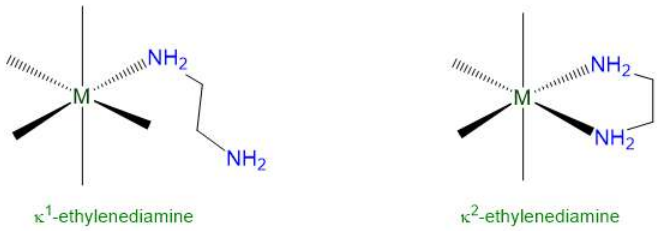
5. As appropriate, additional information about the way a ligand is bound to the metal center and/or its stereochemistry is specified using a prefix. The prefixes to provide linkage and stereochemistry for ligands are given in Table **4.1.2.4**.

Table **4.1.2.4**. Prefixes used to specify ligands' isomerism when naming and writing coordination compounds' formulae. Some of these types of isomerism will be discussed in later pages.

Type of isomerism	Graphical reminder	Prefixes
when a multidentate ligand binds through less than the full number of atoms		κ^n where n is the number of attached atoms; used when the attached atoms are not directly connected by a chemical bond. The metal-ligand bonding usually involves σ-type coordination.
hapticity		η^n where n is the number of attached atoms; used when the coordinated atoms are all connected by bonds. Usually the metal-ligand bonding involves π-type coordination. In speech, η^1=monohapto; η^2=dihapto; η^3=trihapto, etc.
bridging ligands		μ_n where n is the number of atoms bridged. The number n is usually omitted when n =2.
chelating ligand ring twist		λ- or δ-

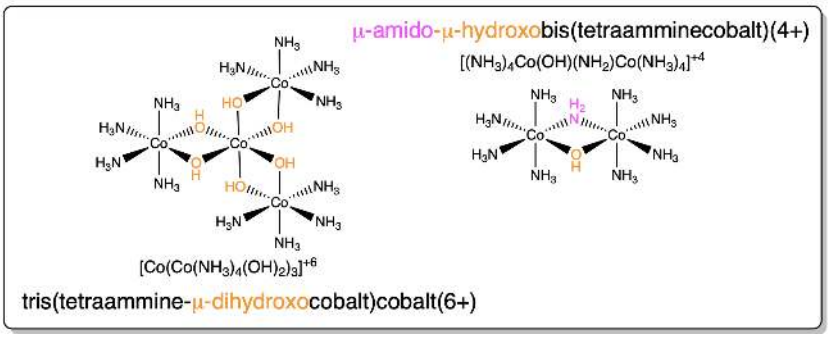
A example showing how the nomenclature rule is applied to a ligand that can have two coordination modes is given in Scheme 4.1.2.IV.

Scheme 4.1.2.IV. Use of the κ notation to specify the number of attached groups in a multidentate ligand.



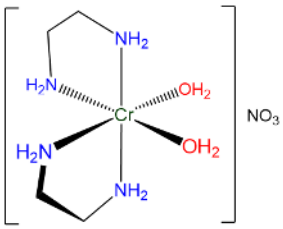
Scheme 4.1.2.V. The names of the complexes follow the rules described in 9.2.6: multinuclear coordination complexes.

Scheme 4.1.2.V. Use of the μ notation to specify bridging ligands in metal complexes.[3]



6. If desired, parentheses *may* be used to delineate a ligand name to make it easier to identify in the name of the complex. This can be particularly helpful when the entire name contains a lot of information to keep track of. An example is given in Scheme 4.1.2.VI.

Scheme 4.1.2.VI. When naming the complex shown, *cis*-diaquabis(ethylenediamine)chromium(III) nitrate is easier to read than *cis*-diaquabisethylenediaminechromium(III) nitrate.



Rule 4: Specify the identity of the metal

- In neutral and cationic complexes the metal's name is used directly

  - *e.g.* as in hexammineruthenium(III) for $[Ru(NH_3)_6]^{3+}$

- In anionic complexes, *-ate* replaces *-ium*, *-en*, or *–ese* or adds to the metal name,

  e.g., as in hexachloromanganate(IV) for $MnCl_6^{2-}$

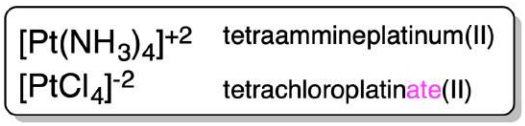
- In anionic complexes of some metals a Latin-derived name is used instead of the element's English name. These names are given in Table **4.1.2.5**.

Table **4.1.2.5**. Latin terms for select metal Ions. Redrawn from this page describing the nomenclature of coordination complexes.

Transition Metal	Latin
Copper	Cuprate
Gold	Aurate
Iron	Ferrate
Lead	Plumbate
Silver	Argentate
Tin	Stannate

An example of the application of the metal naming rules is given in Scheme \sf{\PageIndex{VII}}\).

Scheme 4.1.2.VII. Example of the application of the metal specification rules to a cationic and an anionic platinum complex.[3]



Rule 5: Specify the oxidation state of the metal.

Two different systems are used to specify the oxidation state of the metal.

1. In the **Stock system** the metal's oxidation state is indicated in Roman numerals after the metal name.

   Examples:

   $[CoCl(NH_3)_5]Cl_2$ = pentamminechlorocobalt(III) chloride

   $[PtBr_2(bpy)]$ = dibromobipyridineplatinium(II)

   $K[Ag(SCN)_2]$ = potassium di-*S*-thiocyanatoargentate(I)

2. In the **Ewing-Bassett system** the charge on the complex is specified in Arabic numerals after the complex name. This provides a way of specifying a complex even when the oxidation state of the metal isn't known and, in cases where it is known, the value

of the metal's oxidation state may be inferred from the complex ion's charge.

$[CoCl(NH_3)_5]Cl_2$ = pentamminechlorocobalt(2+) chloride

$[PtBr_2(bpy)]$ = dibromobipyridineplatinium(0)

$K[Ag(SCN)_2]$ = potassium di-*S*-thiocyanatoargentate(1-)

Summary of rules for naming coordination complexes.

A graphical summary of the **rules for naming complexes** along with a few examples that you can use to review the nomenclature rules is given in Figure **4.1.2.1**. This work by Stephen Contakes is licensed under a Creative Commons Attribution 4.0 International License.

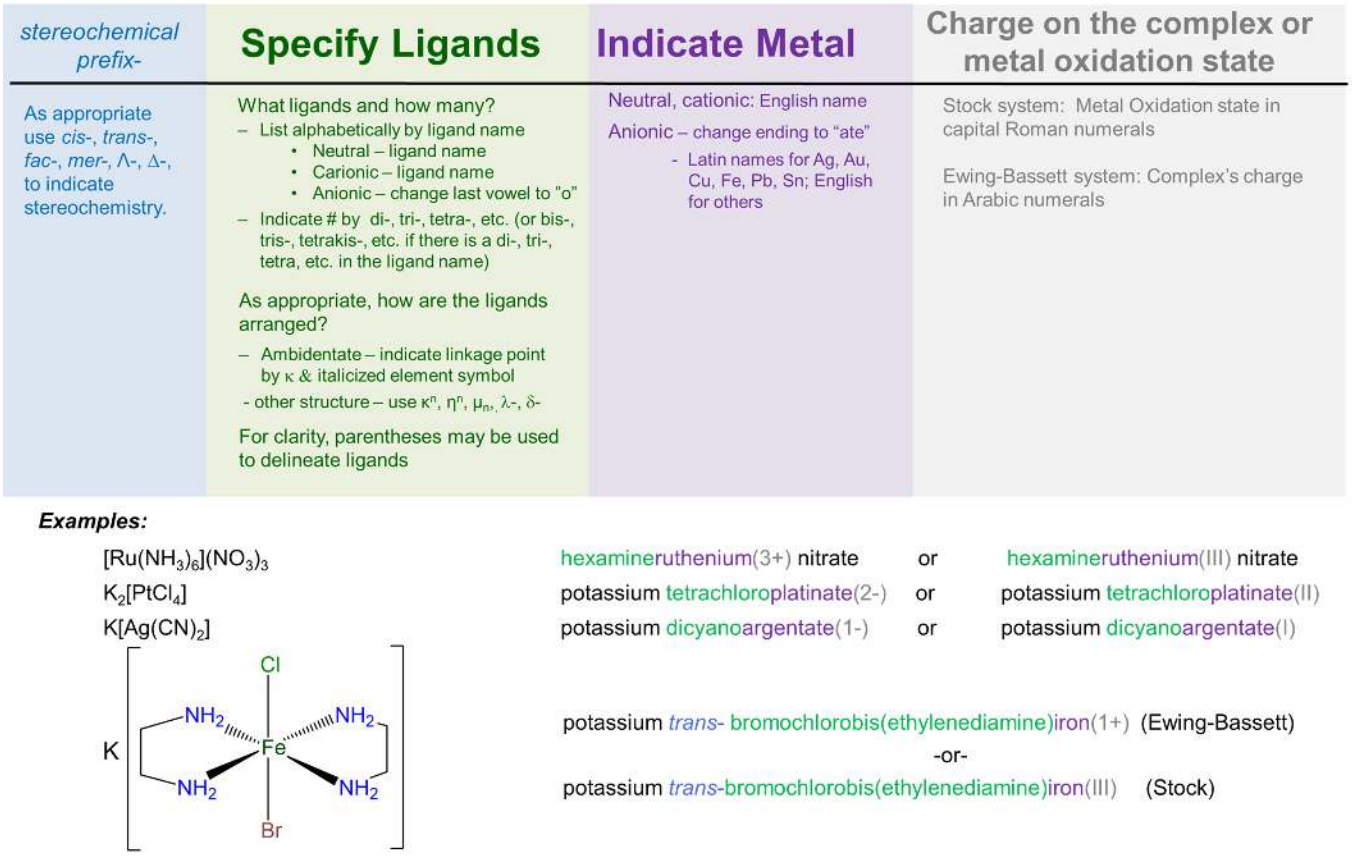


Figure **4.1.2.1**. Summary of nomenclature rules for coordination complexes along with a few examples of their application.

When learning chemical nomenclature, practice makes perfect. The following examples and exercises are provided to give you this practice. Additional examples and exercises on the https://chem.libretexts.org/ site include a set of simple examples with explained solutions, a set of simple exercises with solutions, and a set of more challenging exercises without solutions.

? Exercise **4.1.2.2**. Assigning metal oxidation states in a complex

In order to name a complex in the Stock system it is necessary to assign a formal oxidation state to the metal. For this reason it is important to be able to assign the oxidation state of a metal in a complex. Fortunately, this is easy to do if you remember

1. The sum of all atoms' oxidation states will equal the overall charge on the complex
2. When determining the metal's oxidation state the ligands can be treated as having an oxidation state equal to their charge - *i.e.*, the charge they possess in the form in which they coordinate the metal, so if they need to lose a proton to bind, don't forget to account for that.

Given the above, assign the oxidation state of the metal in the following real and hypothetical complexes.

a. $K_3[Fe(CN)_6]$

b. $[CoCl(NH_3)_5](NO_3)_2$
c. $K_2[PtCl_4]$
d. [MnCl(por)]
e. $[Ru(bpy)_3]Cl_2$
f. $[PdCl_2(dppe)]$
g. $[Mn(en)_2(SCN)_2]$

Answer for $K_3[Fe(CN)_6]^{3-}$.

This contains $[Fe(CN)_6]^{3-}$; so O.S.$_{Fe}$ + 6 x (-1) (for CN^-) = -3 (the complex's charge) so O.S.$_{Fe}$ = +3 or Fe^{3+}.

Answer for $[CoCl(NH_3)_5](NO_3)_2$.

This contains $[CoCl(NH_3)_5]^{2+}$; so O.S.$_{Co}$ + 1 x (-1) (for Cl^-) + 0 x 5 (for NH_3) = +2 (the complex's charge) so O.S.$_{Co}$ = +3 or Co^{3+}.

Answer for $K_2[PtCl_4]$.

This contains $2K^+$ and $[PtCl_4]^{2-}$; so O.S.$_{Pt}$ + 4 x (-1) (for Cl^-) = -2 (the complex's charge) so O.S.$_{Pt}$ = +2 or Pt^{2+}.

Answer for [MnCl(por)].

O.S.$_{Pt}$ + 1 x (-2) (for por; see table 9.2.2) + 1 x (-1) (for Cl^-) = +0 (the complex's charge) so O.S.$_{Mn}$ = +3 or Mn^{3+}.

Answer $[Ru(bpy)_3]Cl_2$.

The complex is $[Ru(bpy)3]^{2+}$ so O.S.$_{Ru}$ + 0 x 3 (for bpy) = +2 (the complex's charge) so O.S.$_{Ru}$ = +2 or Ru^{2+}.

Answer $[PdCl_2(dppe)]$.

O.S.$_{Pd}$ + 2 x (-1) (for Cl^-) + 0 x 3 (for dppe) = +0 (the complex's charge) so O.S.$_{Pd}$ = +2 or Pd^{2+}.

Answer $[Mn(en)_2(SCN)_2]$.

O.S.$_{Mn}$ + (2 x 0) (for en) + 2 x (-1) (for SCN^-) = +0 (the complex's charge) so O.S.$_{Mn}$ = +2 or Mn^{2+}.

? Exercise 4.1.2.3: Simple Nomenclature Problems.

Name the following compounds in both the Stock and Ewing-Bassett systems:

a. $[Ru(NH_3)_6](NO_3)_3$
b. $K_2[PtCl_4]$
c. $K[Ag(CN)_2]$
d. $Cs[CuBrCl_2F]$
e. $[Cu(acac)_2]$

Answer

	Complex	Stock system name	Ewing-Bassett System name
a	$[Ru(NH_3)_6](NO_3)_3$	hexammineruthenium(III) nitrate	hexammineruthenium(3+) nitrate
b	$K_2[PtCl_4]$	potassium tetrachloroplatinate(II)	potassium tetrachloroplatinate(2-)
c	$K[Ag(CN)_2]$	potassium dicyanoargentate(I)	potassium dicyanoargentate(1-)
d	$Cs_2[CuBrCl_2F]$	cesium bromodichlorofluorocuprate(II)	cesium bromodichlorofluorocuprate(2-)
e	$[Cu(acac)_2]$	bis(acetylacetonato)copper(II)	bis(acetylacetonato)copper(0)

Exercise 4.1.2.4: More simple nomenclature problems.

Name the following compounds and ions in both the Stock and Ewing-Bassett systems.

a. $Cu(OH)_4^-$
b. $[AuXe_4]^{2+}$
c. $AuCl_4^-$
d. $Fe(CN)_6^{3-}$
e. $K_4[Fe(CN)_6]$
f. *trans*-$[Cu(en)_2(NO_2)_2]$ (the N is bound to Cu)
g. cis-$IrCl_2(CO)(PPh_3)$ (ignore stereochemistry)
h. $IrCl(PPh_3)_3$

Answer

	Compound	Stock System Name	Ewing-Bassett System Name
a	$Cu(OH)_4^-$	tetrahydroxidocuprate(III) or tetrahydroxidocuprate(III)	tetrahydroxidocuprate(1-) or tetrahydroxidocuprate(1-)
b	$[AuXe_4]^{2+}$	tetraxenongold(II)	tetraxenongold(2+)
c	$AuCl_4^-$	tetrachloroaurate(III)	tetrachloroaurate(1-)
d	$Fe(CN)_6^{3-}$	hexacyanoferrate(III) or hexacyanidoferrrate(III)	hexacyanoferrate(3-) or hexacyanidoferrate(3-)
e	$K_4[Fe(CN)_6]$	potassium hexacyanoferrate(II) or potassium hexacyanidoferrrate(II)	potassium hexacyanoferrate(4-) or potassium hexacyanidoferrrate(4-)
f	*trans*-$[Cu(en)_2(NO_2)_2]$ (the N is bound to Cu)	bis(ethylenediamine)bisnitrocopper(II) or bis(ethylenediamine)bis(nitrito-*κN*)copper(II)	bis(ethylenediamine)bisnitrocopper(0) or bis(ethylenediamine)bis(nitrito-*κN*)copper(0)
g	*cis*-$IrCl_2(CO)(PPh_3)$	*cis*-dichlorocarbonyltriphenylphosphineiridium(I) or *cis*-dichloro(carbonyl)(triphenylphosphine)iridium(I)	*cis*-dichlorocarbonyltriphenylphosphineiridium(0) or *cis*-dichloro(carbonyl)(triphenylphosphine)iridium(0)
h	$IrCl(PPh_3)_3$	chlorotris(triphenylphosphine)iridium(I)	chlorotris(triphenylphosphine)iridium(0)

? Exercise 4.1.2.5: Even more simple nomenclature problems.

Name the following compounds and ions in both the Stock and Ewing-Bassett systems. Ignore prefixes for designating isomers if you haven't learned about those.

a. $Fe(acac)_3$
b. $K_2[CuBr_4]$
c. ReH_9
d. $[Ag(NH_3)_2]BF_4$
e. $[Ag(NH_3)_2][Ag(CN)_2]$
f. $[Ni(CN)_4]^{2-}$
g. $[Co(N_3)(NH_3)_5]SO_4$
h. $[CoBrCl(H_2O)(NH_3)]I$ (ignore stereochemistry)

Sample Answers

	Complex	Stock system name	Ewing-Bassett System name
a	$Fe(acac)_3$	tris(acetoacetato)iron(III)	tris(acetoacetato)iron(0)
b	$Na_2[CuBr_4]$	sodium tetrabromocuprate(II)	sodium tetrabromocuprate(2-)
c	$[Co(NH_3)_6][Co(ox)_3]$	hexamminecobalt(III) tris(oxalato)cobalt(III)	hexamminecobalt(3+) tris(oxalato)cobalt(3-)
d	$[Ag(NH_3)_2]BF_4$	diamminesilver(I) tetrafluoroborate	diamminesilver(1+) tetrafluoroborate
e	$[Ag(NH_3)_2][Ag(CN)_2]$	diamminesilver(I) dicyanoargentate(I) or diamminesilver(I) dicyanidoargentate(I)	diamminesilver(1+) dicyanoargentate(1-) or diamminesilver(1+) dicyanidoargentate(1-)
f	$[Ni(CN)_4]^{2-}$	tetracyanonickelate(II) or tetracyanonickelate(II) ion	tetracyanonickelate(2-) or tetracyanonickelate(2-) ion
g	$[Co(N_3)(NH_3)_5]SO_4$	pentammineazidocobalt(III) sulfate	pentammineazidocobalt(2+) sulfate
h	$[CoBrCl(H_2O)(NH_3)]I$ (ignore stereochemistry)	ammineaquabromochlorocobalt(III) iodide	ammineaquabromochlorocobalt(1+) iodide

? Exercise 4.1.2.6: Nomenclature problems, some of which involve consideration of isomerism.

Name the following compounds and ions in both the Stock and Ewing-Bassett systems. Ignore prefixes for designating isomers if you haven't learned about those.

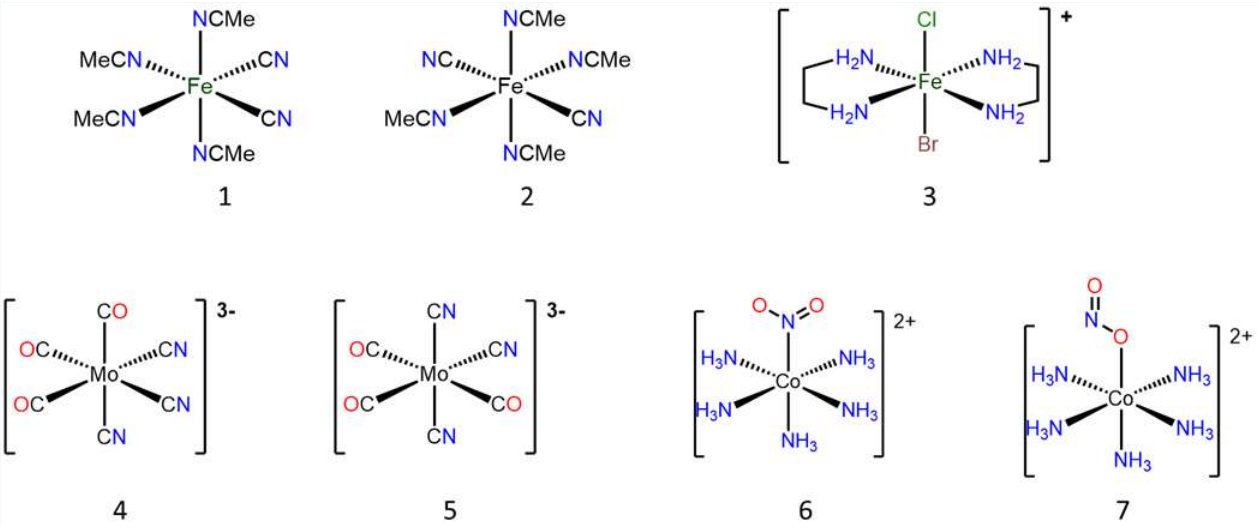
a. *trans*-$[Cu(dppe)_2(NO_2)_2]$ (the N is bound to Cu)
b. $[Pd(en)_2(SCN)_2]$, with the thiocyanates bound Pd-SCN
c. $[Mn(CO)_6]BPh_4$ (BPh_4 = tetraphenylborate)
d. $Rb[AgF_4]$
e. K_2ReH_9
f. K_3CrCl_6
g. $[Ru(H_2O)_6]Cl_2$
h. [*cis*-$Fe(CO)_4I_2$]
i. K_2[*trans*-$Fe(CN)_4(CO)_2$]
j. [*cis*-$MnCl(H_2O)_4(NH_3)](NO_3)$
k. K_3[*fac*-$RuCl_3(PMe_3)_3$]

Answer

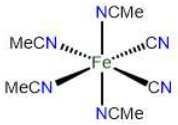
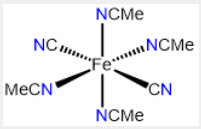
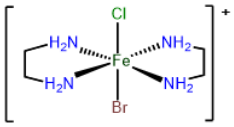
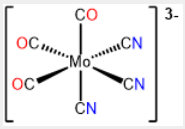
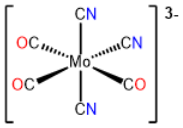
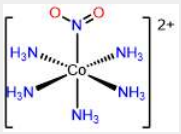
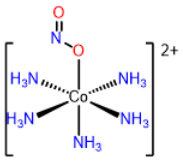
	Complex	Stock system name	Ewing-Bassett System name
a	*trans*-$[Cu(dppe)_2(NO_2)_2]$	*trans*-bis(diphenylphosphinoethane)bisnitrocopper(II) or *trans*-bis(diphenylphosphinoethane)bis(nitrito-κN)copper(II)	*trans*-bis(diphenylphosphinoethane)bisnitrocopper(0) or *trans*-bis(diphenylphosphino)ethane bis(nitrito-κN)copper(0)
b	$[Pd(en)_2(SCN)_2]$, with the thiocyanates bound Pd-SCN	bis(ethylenediamine)bisthiocyanatopalladium(II) or bis(ethylenediamine)bis(thiocyanato-*S*)palladium(II) or bis(ethylenediamine)bis(thiocyanato-κS)palladium(II)	bis(ethylenediamine)bisthiocyanatopalladium(0) or bis(ethylenediamine)bis(thiocyanato-*S*)palladium(0) or bis(ethylenediamine)bis(thiocyanato-κS)palladium(0)
c	$[Mn(CO)_6]BPh_4$	hexacarbonylmanganese(I) tetraphenylborate	hexacarbonylmanganese(1+) tetraphenylborate
d	$Rb[AgF_4]$	rubidium tetrafluoroargentate(III)	rubidium tetrafluoroargentate(1-)
e	K_2ReH_9	potassium nonahydridorhenium(VII)	potassium nonahydridorhenium(2-)
f	K_3CrCl_6 or $K_3[CrCl_6]$	potassium hexachlorochromium(III) or potassium hexachloridochromium(III)	potassium hexachlorochromium(3-) or potassium hexachloridochromium(3-)
g	$[Ru(H_2O)_6]Cl_2$	hexaaquaruthenium(II) chloride	hexaaquaruthenium(2+) chloride
h	[*cis*-$Fe(CO)_4I_2$]	*cis*-tetracarbonyldiiodoiron(II)	*cis*-tetracarbonyldiiodoiron(0)
i	K_2[*trans*-$Fe(CN)_4(CO)_2$]	potassium *trans*-dicarbonyltetracyanoferrate(II)	potassium *trans*-dicarbonyltetracyanoferrate(2-)
j	[*cis*-$MnCl(H_2O)_4(NH_3)$] (NO_3)	*cis*-amminetetraaquachloromanganese(0) nitrate	*cis*-amminetetraaquachloromanganese(1+) nitrate
k	K[*fac*-$RuCl_3(PMe_3)_3$]	potassium *fac*-trichlorotris(triphenylphosphine)ruthenium(II)	potassium *fac*-trichlorotris(triphenylphosphine)ruthenium(1-)

? Exercise 4.1.2.7

Name the compounds and ions below using both the Stock and Ewing-Bassett systems. Ignore prefixes for designating isomers if you haven't learned about those.


NCMe
MeCN
CN
Fe
MeCN
CN
NCMe
1
NCMe
NC
NCMe
Fe
MeCN
CN
NCMe
2
Cl
+
H2N
NH2
Fe
H2N
NH2
Br
3
CO
OC
CN
Mo
OC
CN
CN
3-
4
CN
OC
CN
Mo
OC
CO
CN
3-
5
O
N
O
2+
H3N
NH3
Co
H3N
NH3
NH3
6
O
N
O
2+
H3N
NH3
Co
H3N
NH3
NH3
7

Answer

#	Structure	Stock system name	Ewing-Bassett system name
1		*cis*-tetraacetonitriledicyanoiron(II) or *cis*-tetraacetonitriledicyanidoiron(II)	*cis*-tetraacetonitriledicyanoiron(0) or *cis*-tetraacetonitriledicyanidoiron(0)
2		*trans*-tetraacetonitriledicyanoiron(II) or *trans*-tetraacetonitriledicyanidoiron(II)	*trans*-tetraacetonitriledicyanoiron(0) or *trans*-tetraacetonitriledicyanidoiron(0)
3		*trans*-bromochlorobis(ethylenediamine)iron(III) or *trans*-bromidochloridobis(ethylenediamine)iron(III)	*trans*-bromochlorobis(ethylenediamine)iron(1+) or *trans*-bromidochloridobis(ethylenediamine)iron(1+)
4		*fac*-tricarbonyltricyanomolybdate(0) or *fac*-tricarbonyltricyanidomolybdate(0)	*fac*-tricarbonyltricyanomolybdate(3-) or *fac*-tricarbonyltricyanidomolybdate(3-)
5		*mer*-tricarbonyltricyanomolybdate(0) or *mer*-tricarbonyltricyanidomolybdate(0)	*mer*-tricarbonyltricyanomolybdate(3-) or *mer*-tricarbonyltricyanidomolybdate(3-)
6		pentamminenitrito-*N*-cobalt(III), pentamminenitrito-**κ***N*-cobalt(III), or pentamminenitrocobalt(III)	pentamminenitrito-*N*-cobalt(2+), pentamminenitrito-**κ***N*-cobalt(2+), or pentamminenitrocobalt(2+)
7		pentamminenitrito-*O*-cobalt(2+), pentamminenitrito-**κ***O*-cobalt(2+), or pentamminenitritocobalt(2+)	pentamminenitrito-*O*-cobalt(2+), pentamminenitrito-**κ***O*-cobalt(2+), or pentamminenitritocobalt(2+)

? Exercise 4.1.2.8

Draw structural formulae for the following compounds and ions. You may assume that

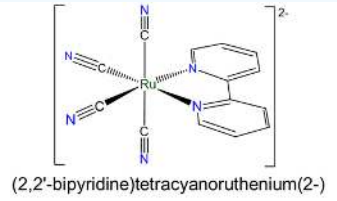
- complexes in which the metal has a coordination number of six are octahedral
- complexes in which the metal has a coordination number of five are trigonal bipyramidal

- complexes in which Pt^{II} , Pd^{II} , or Rh^{I}, or Ir^{I} have a coordination number of four are square planar
- other complexes in which the metal has a coordination number of four will be tetrahedral

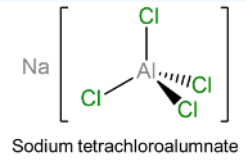
a. (2,2'-bipyridine)tetracyanoruthenium(2-)
b. sodium tetrachloroaluminate (note that since Al is a main group metal with a generally fixed oxidation state no oxidation state is given)
c. pentaamminechlorocobalt(2+) sulfate
d. carbonylhydridotris(triphenylphosphine)rhodium(I) (the ligands in this complex occupy sterically preferred positions)
e. bromotrichlorocobaltate(III)
f. hexaaquacopper(2+) sulfate
g. sodium tris(oxalato)cobalt(III)
h. *fac*-(1,10-phenanthroline)tricarbonylchlororhenium(I)
i. *mer*-triaquatrichlorochromium(III)
j. *trans*-dichlorobis(ethylenediamine)platinum(IV)

Answers

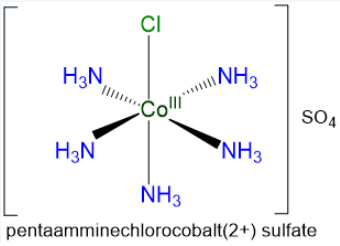
a



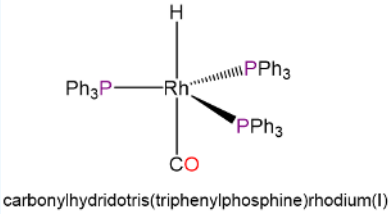
b



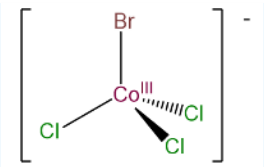
c



d

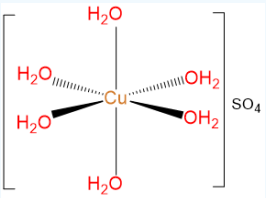


e



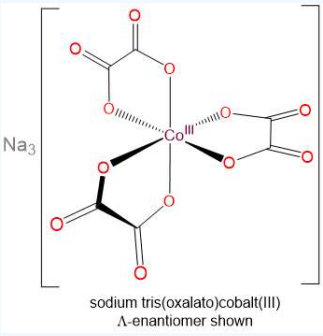
bromotrichlorocobaltate(III)

f



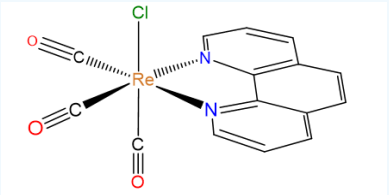
hexaaquacopper(2+) sulfate

g



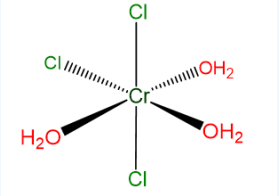
sodium tris(oxalato)cobalt(III)
Λ-enantiomer shown

h



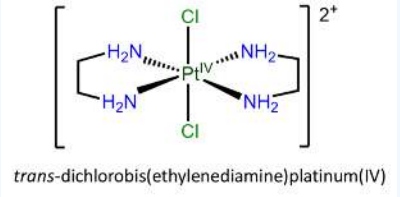
fac-(1,10-phenanthroline)tricarbonylchlororhenium(I)

i



mer-triaquatrichlorochromium(III)

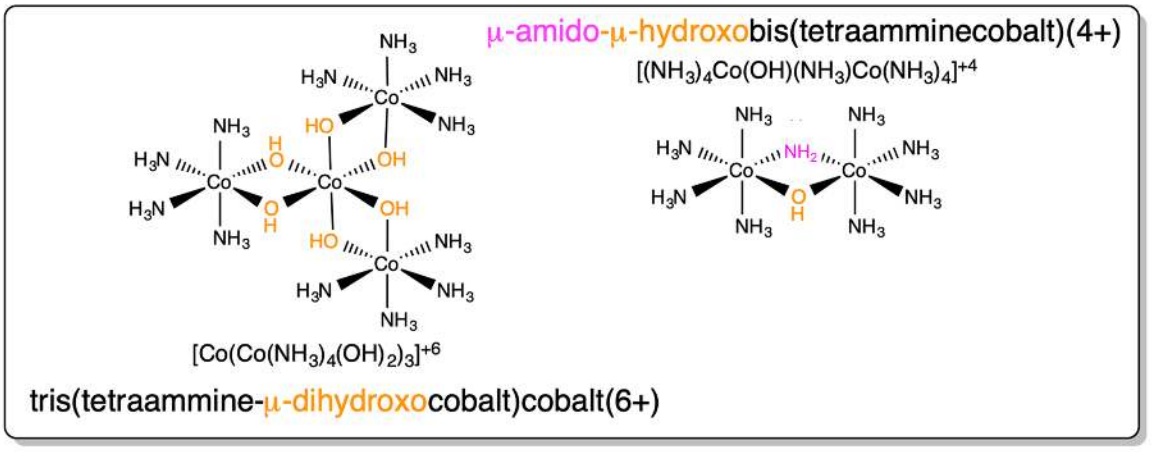
j



trans-dichlorobis(ethylenediamine)platinum(IV)

Exercise 4.1.2.9.

The name of the structure named tris(tetraammine-μ-dihydroxocobalt)cobalt(6+) in Scheme **4.1.2.III** (reproduced below) is incomplete. Give the complete name of the structure in both the Stock and Ewing-Basset systems.



Answer

Δ-tris(tetraammine-μ-dihydroxocobalt)cobalt(6+) or **Δ**-tris(tetraammine-μ-dihydroxocobalt(III)cobalt(III)

Note: Rules for Writing the Formulae of Coordination Copounds

Rules for writing the formulae of coordination compounds

As organized predictable formulae can be easier to read and understand than haphazardly written ones, the rules for writing the formulae of coordination compounds have value. To support those who wish to employ them they are given in this section. The rules as given here are adapted from a summary by Robert Lancashire.

The rules for writing the formulae of coordination compounds follow the same convention used to specify their names.

1. If there are multiple ions present list the cations before anions.
2. Enclose all the constituents of each complex ion in square brackets.
3. For each complex ion,
   - Give the **central metal** atom first.
   - Then **ligands** next, listed in alphabetical order, ignoring prefixes according to the first letters in the ligand's symbol as written. This is true regardless of whether the symbol is an element symbol (like C, N, O, etc.) or a symbol for the ligand name (bpy, en, MeCN, etc.). Contrary to widely-circulated myths, the ligand's charge does not matter.[4]
   - The formulae or abbreviations (*e.g.* en) for all polyatomic ligands should be enclosed in ordinary parentheses.
   - As appropriate, use italicized atom symbols to indicate linkage isomerism and prefixes such as *cis*-, *trans*-, *fac*-, *mer*-, **Λ**-, **Δ**-, κ^n, η^n , μ_n, **λ**-, or **δ**- to indicate stereochemistry.
   - When a ligand is bound to a metal through a particular atom, preferably place that atom closest to the metal - *e.g.*, $[Fe(CN)_6]^{3-}$ not $[Fe(NC)_6]^{3-}$ (Note: this rule is used primarily for ambidentate ligands; although IUPAC recommends that aqua ligands be written as OH_2 when the O would be closest to its coordinated metal, they are still usually written as H_2O).

These rules are graphically summarized in Figure **4.1.2.2**.

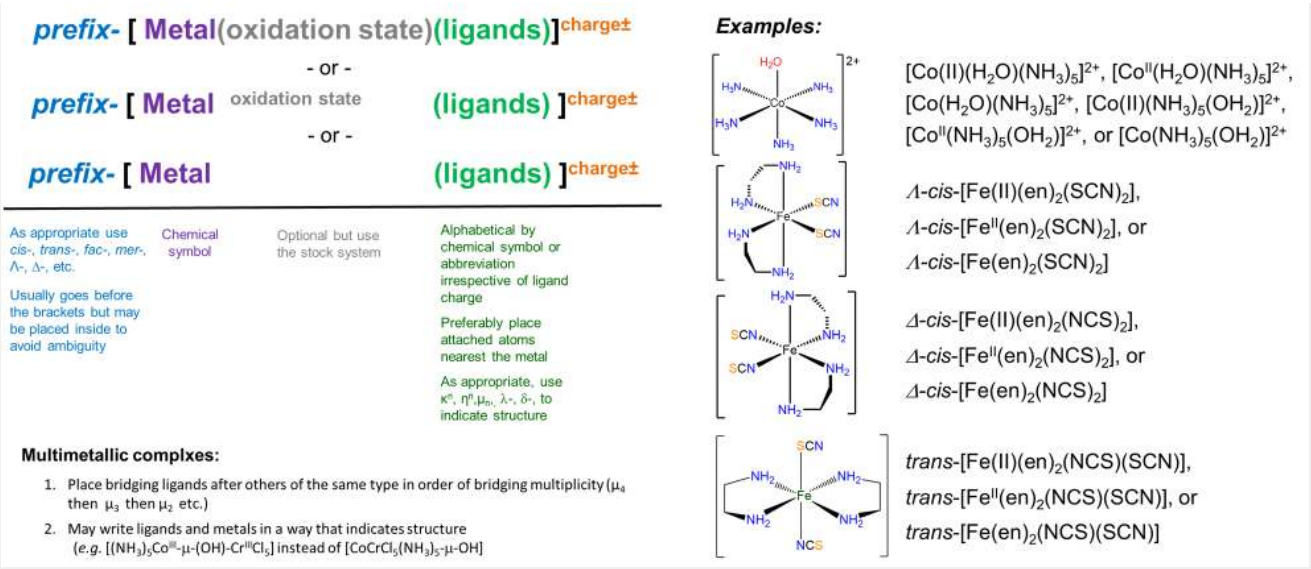
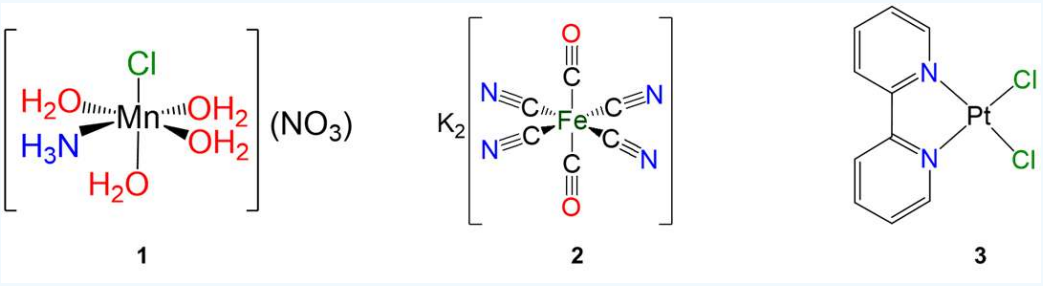


Figure **4.1.2.2**. Summary of the rules for writing the formula of a coordination complexes along with a few examples of their application. This work by Stephen Contakes is licensed under a Creative Commons Attribution 4.0 International License.

? Exercise 4.1.2.10

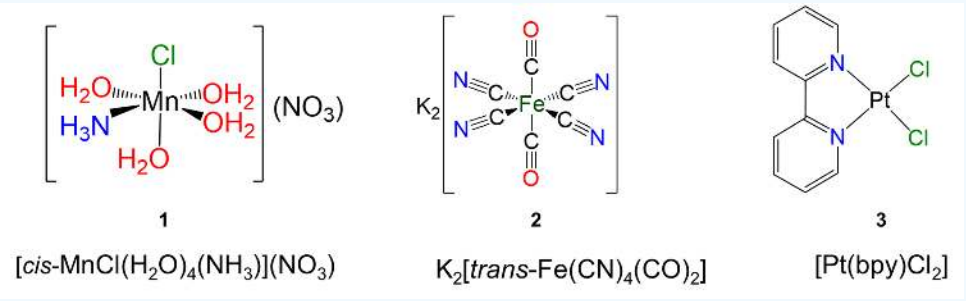
Give the formulae of the following complexes.



1 2 3

.

Answer



1 2 3

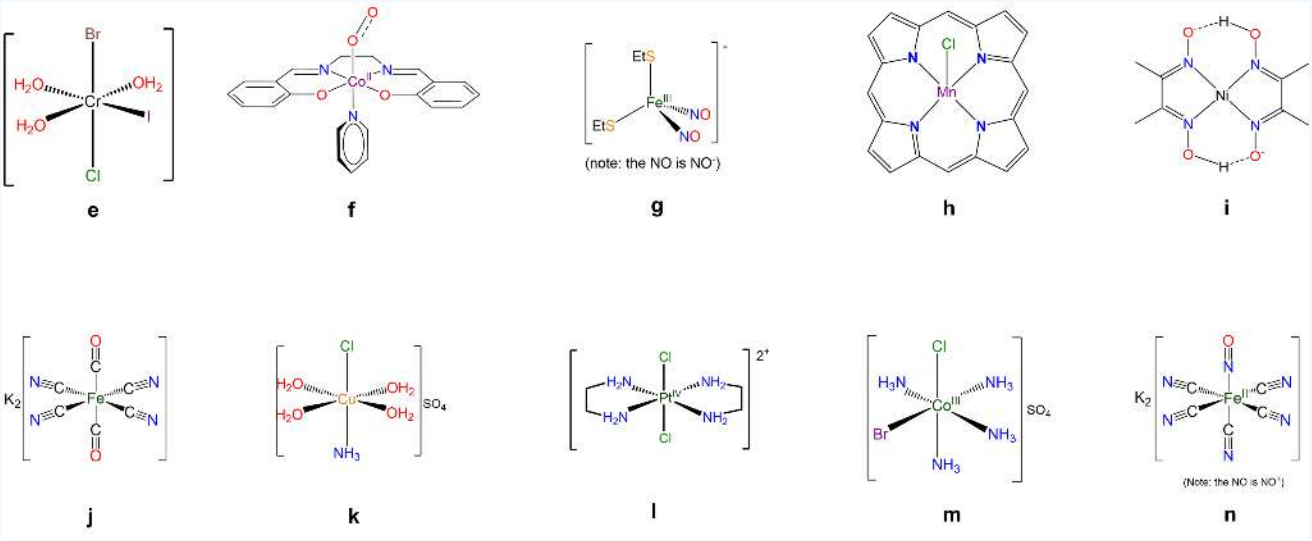
[*cis*-MnCl(H2O)4(NH3)](NO3) K2[*trans*-Fe(CN)4(CO)2] [Pt(bpy)Cl2]

? Exercise 4.1.2.11

Write formulae for each of the following compounds and ions. When multidentate ligands are present use suitable abbreviations.

a. pentaamminechlorocobalt(2+) sulfate
b. **Δ**-diamminebis(oxalato)manganate(III)
c. *trans*-tetraacetonitriledicyanoiron(II)

d. tricarbonyldichlorobis(triphenylphosphine)molybdenum



Answers

a.

$[CoCl(NH_3)_5](SO_4)$

b.

Δ-$[Mn(NH_3)_2(ox)_2]^-$

c.

trans-$[Fe(CN)_2(NCMe)_4]$

d.

$[MoCl_2(CO)_3(PPh_3)]$ or $MoCl_2(CO)_3(PPh_3)$

e.

mer-$[CrBrCl(H_2O)_3I]$

f.

$[Co(O_2)py(salen)]$

g.

$[Fe(NO)_2(SEt)_2]^-$

h.

$[MnCl(por)]^-$ or $[MnCl(porphyrin)]^-$

i.

$[Ni(DMG)_2]$ or $[Ni(Hdmg)_2]$

j.

potassium *trans*-$[Fe(CN)_2(CO)_4]$

k.

trans-$[CuCl(H_2O)_4(NH_3)]SO_4$

l.

trans-$[PtCl_2(en)_2]^{2+}$

m.

cis-$[CoBrCl(NH_3)_4]SO_4$

n.

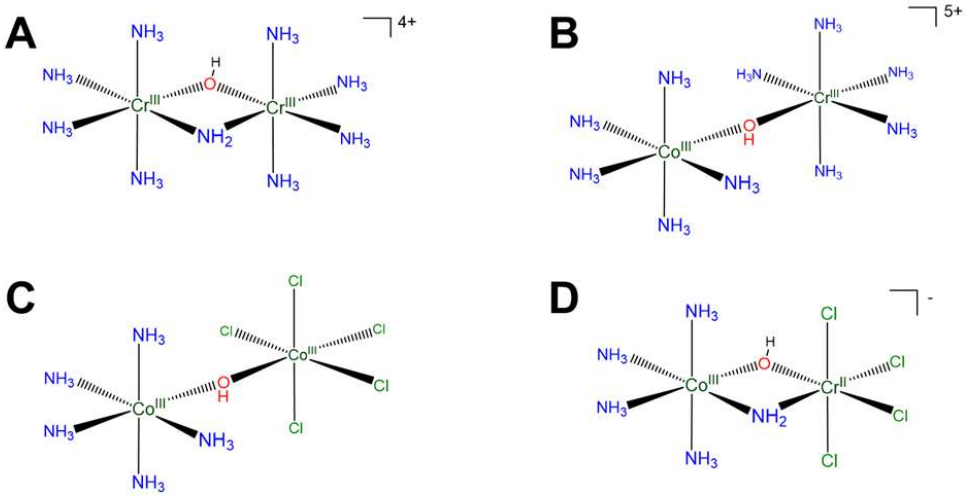
$K_2[Fe(CN)_5NO]$

Multinuclear coordination complexes

Multinuclear coordination complexes contain multiple metals connected by one or more bridging ligands. The structures of bridging complexes can usually be inferred from their μ-tagged ligands in their names and formulae. For the benefit of instructors who wish to have their students name multinuclear complexes, the rules are presented below.

Multinuclear complexes are named differently depending on whether the groups on either side of the bridging ligands are identical or different, as shown in Scheme **4.1.2.VIII**.

Scheme 4.1.2.VIII. Multinuclear coordination complexes may be named differently depending on whether the groups on either side of the bridging ligands are the same or different. The groups are the same if the metal, ligands, and ligand arrangement are identical. This is true in A but in B the metals differ, in C the ligands differ, and in D both the metal and ligands differ.



Naming multinuclear complexes

Let's look at the rules for naming symmetric and asymmetric multinuclear complexes.

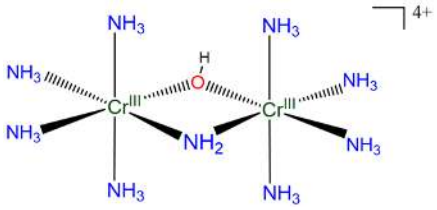
Application of the IUPAC system and variants thereof to symmetric complexes

The IUPAC naming system helpfully avoids the sort of ambiguities and *ad hoc* choices involved in most textbook-level nomenclature systems for multimetallic complexes. Unfortunately, it is correspondingly difficult for beginners to employ. Thus it will only be applied in depth to the case of symmetric complexes. Symmetric complexes are particularly easy to name in the IUPAC system and several of its variants that find common use. In these

1. The ligands are given in alphabetical order. When there are bridging and non-bridging ligands of the same type the bridging ligands are given first. When there are multiple bridging ligands of the same type but which use different bridging modes (*e.g.*, μ_4-, μ_3-, μ_2-), the bridging ligands are specified in decreasing order of bridging multiplicity, *e.g.*, μ_3 -sulfido-di-μ-sulfido.
2. The groups bridged are given afterwards using names that follow the ordinary rules. Generally this involves either
   a. naming all the ligands followed by all the metals, in both cases using prefixes to indicate the number of each, or
   b. naming each group of atoms individually as in the less formal naming system, using prefixes to indicate the number of ligands (this is an unofficial variant of the IUPAC system that some textbook authors seem to prefer).

These two rules are sufficient to describe simple symmetric bridging complexes.

Example: The compound in Scheme **4.1.2.VIIIA**



may be named

[μ-amido-μ-hydroxo-octaamminedichromium(4+)] ion

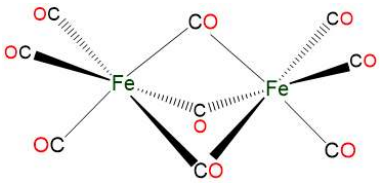
or

[μ-amido-μ-hydroxo-bis(tetraamminechromium(III))] ion

or

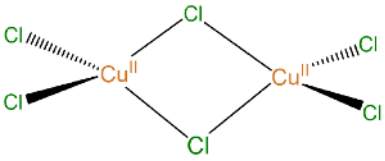
[μ-amido-μ-hydroxo-bis(tetraamminechromium)(4+)] ion

Example: The complex[5]



may be named [tri-μ-carbonyl-bis(tricarbonyliron)(0)], [tri-μ-carbonyl-bis(tricarbonyliron(0))], or [tri-μ-carbonyl-hexacarbonyldiiron)(0)]

Example: The complex



may be named di-μ-chlorido-tetrachloridodicopper(II), di-μ-chlorido-bis(dichlorocopper(II)), or di-μ-chlorido-bis(dichlorocopper)(0)

A note on the application of the IUPAC system and variants thereof to asymmetric complexes

For a symmetrical complex like the $[Cu_2Cl_4(\mu\text{-}Cl)_2]$ considered above it is enough to specify the existence of the two bridging and four terminal chloro ligands; there is no need to number the chloro ligands or to specify exactly which ones are involved in bridging or to clarify that the bridging involves κ^2 coordination of the chloro ligands. In cases where the two metal centers or the chloro ligands differ it is necessary to specify the exact ligands and metals involved and how they are connected.

For example, a more extensive IUPAC name for $[Cu_2Cl_4(\mu\text{-}Cl)_2]$ in which the chloro ligands are individually and more completely specified would read di-μ_2-chlorido-tetrachlorido-1κ^2Cl,2κ^2Cl-dicopper(II).

Even more extensive systems would involve numbering the metals and specifying how they are connected together too. The details of how this is done are typically beyond the level of most undergraduate and graduate courses in inorganic chemistry. Those who want to know the details should consult the red book. In many cases it is sufficient to reserve the use of formal IUPAC names for use in publications and to employ a convenient shorthand naming system for everyday use. An example of one type of system that is sometimes employed is given next.

Unofficial but commonly used methods applicable to complexes in which the groups bridged are identical or different.

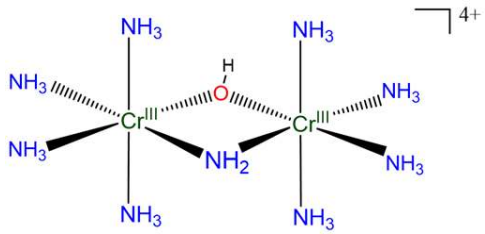
It can be quite complicated to use the IUPAC system to name asymmetric multinuclear coordination complexes. Fortunately it is rarely necessary and there are a variety of simpler somewhat *ad hoc* methods that work well for such cases. Since these methods

are commonly used by textbooks and inorganic instructors it is likely worth your while to learn about their general features. In these methods

1. A multinuclear complex is named as a derivative of one of the metal centers and the other metal centers and their ligands are treated as ligands to the prioritized metal center.
2. Unfortunately, most of the time the choice of which metals are part of the ligands and which one is central is made haphazardly. In other words, there is no agreed upon system for assigning which metal center is the central metal and which should be regarded as part of the ligands around it. One way to be more systematic about the selection of the central and ligand-embedded metals is to assign the central metal as the metal of highest priority in the IUPAC priority rules. In the IUPAC priority rules, the central metal is the highest priority metal alphabetically by name; then if there is a tie the ligands on each tied metal center are ranked alphabetically and the tied metal center with the highest priority (or most highest priority) ligands wins.
3. The metal centers not chosen as the primary metal center and all ligands around them, including those bridging to the winning metal center, are then treated as a single ligand that coordinates the winning metal center.
4. When naming the ligands and the overall complex, again there is much that is haphazard. However, in the best systems each coordination sphere is named using the same rules as for mononuclear complexes - *i.e.*, the ligands are given in alphabetical order, etc.
    - This is true of any metal center-containing ligands.
    - When there is a bridging and non-bridging ligand of the same type, the bridging ligands are given first. When there are multiple bridging ligands of the same type but which use different bridging modes (*e.g.* μ_4-, μ_3-, μ_2-), the ligands are specified in decreasing order of bridging multiplicity, *e.g.* μ_3 -sulfido-di-μ-sulfido.

Let's apply these rules to the examples in Scheme **4.1.2.VIII**.

Compound A:



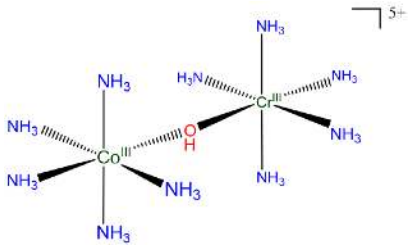
Using hydroxo for the OH^-, it may be named

[(μ-amido-tetraammine-μ-hydroxochromium(III))tetraamminechromium(III)] ion

or

[(μ-amido-tetraammine-μ-hydroxochromium)chromium(4+)] ion

Compound B:



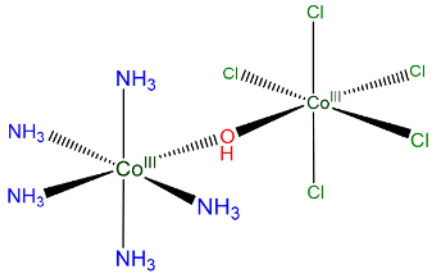
Using hydroxo for the OH^-, it may be named

[(pentaammine-μ-hydroxocobalt(III))tetraamminechromium(III)] ion

or

[(pentaammine-μ-hydroxocobalt)tetraamminechromium(5+)] ion

Compound C:



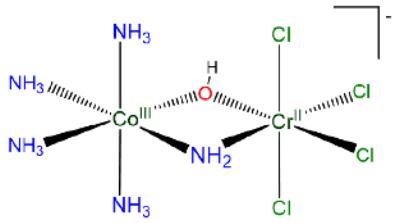
Using hydroxo for OH^-, it may be named

[pentaammine(pentachloro-μ-hydroxocobalt(III))cobalt(III)]

or

[pentaammine(pentachloro-μ-hydroxocobalt)cobalt](0)]

Compound D:



Using hydroxo for OH^- and chloro for Cl^-, it may be named

[pentaammine(pentachloro-μ-hydroxocobalt(III))chromate(III)] ion

or

[(tetrammine-μ-ammine-μ-hydroxocobalt)tetrachlorochromate](1-)] ion

As can be seen from the examples above this system gives serviceable names for multimetallic complexes but those names are not the IUPAC names and so should not be used to describe complexes outside of pedagogical and informal settings.

Writing and interpreting formulae for multinuclear complexes

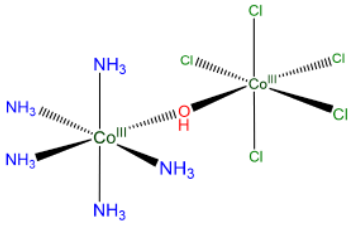
The rules for writing formulae for multinuclear complexes are the same as for mononuclear ones with two added details:

1. Write bridging ligands after nonbridging ligands of the same type. For example, Cu_2Cl_6 should be written as $[Cu_2Cl_4(\mu\text{-}Cl)_2]$
2. However, you may ignore that and other rules if you find it helpful to keep groups of metals and ligands together in a way that better conveys how the atoms are connected. Just as the structure of ethane may be more clearly conveyed as H_3CCH_3 instead of CH_3CH_3, the complex $[Cu_2Cl_4(\mu\text{-}Cl)_2]$ may be written as $[(Cl_2Cu)(\mu\text{-}Cl)_2(CuCl_2)]$.

Other Examples:

For dichromate write, $[Cr_2O_6(\mu\text{-}O)]^{2-}$ or $[O_5Cr\text{-}\mu\text{-}O\text{-}CrO_5]^{2-}$

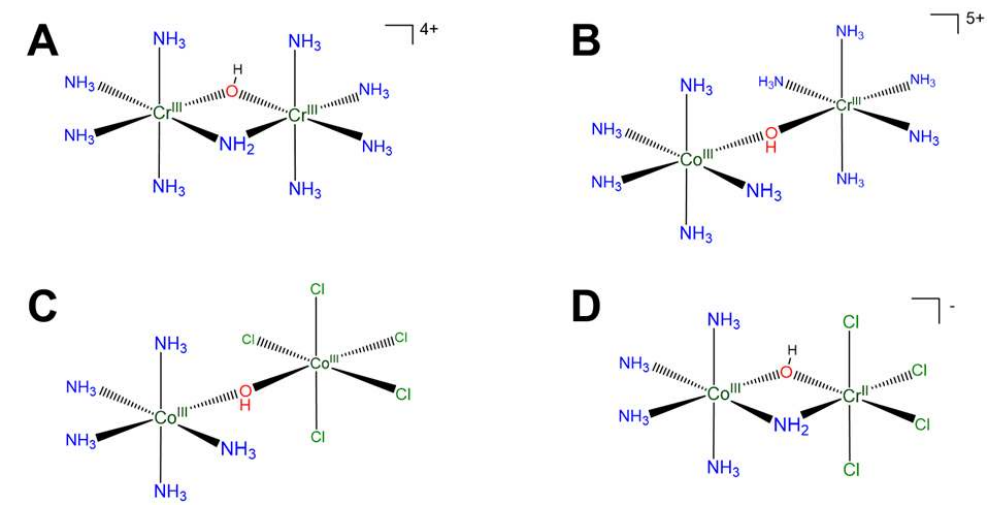
For compound C of Scheme **4.1.2.VIII**.



write $[Co_2Cl_5(NH_3)_5(\mu\text{-}OH)]$ or, even better, $[(H_3N)_5Co(\mu\text{-}OH)CoCl_5]$.

Exercise 4.1.2.10

Write reasonable formulae for complexes A, B, and D in Scheme **4.1.2.VIII**, which for convenience is reproduced below.



Sample answers for A

$[Cr_2(NH_3)_8\text{-}\mu(NH_2)\text{-}\mu(OH)]^{4+}$ or $[(H_3N)_4Cr^{III}\text{-}\mu(NH_2)\text{-}\mu(OH)\text{-}Cr^{II}(NH_3)_4]$ and variants thereof involving writing the H_3N as NH_3, μ as μ_2, etc.

Sample answers for B

$[CoCr(NH_3)_{10}\text{-}\mu(OH)]^{5+}$ or, better, $[(H_3N)_5Co^{III}\text{-}\mu(OH)\text{-}Cr^{III}(NH_3)_5]^{5+}$

Sample answers for C

This was already done as an example above, $[Co_2Cl_5(NH_3)_5\text{-}\mu(OH)]$ or, better, $[(NH_3)_5Co^{III}\text{-}\mu(OH)\text{-}Co^{III}Cl_5]$ and variants thereof

Sample answers for D

$[CoCrCl_4(NH_3)_4\text{-}\mu(NH_2)\text{-}\mu(OH)]$ or, better, $[(H_3N)_4Co^{III}\text{-}\mu(NH_2)\text{-}\mu(OH)\text{-}Cr^{II}Cl_4]$

References

1. International Union of Pure and Applied Chemistry *Nomenclature of Inorganic Chemistry* Cambridge, UK, 2005.

2. The structure and name is taken from Choudhury, S. B.; Allan, C. B.; Maroney, M.; Wodward, A. D.; Lucas, C. R. *Inorg. Synth.* **1998**, *32*, 98-107.

3. Haas, K. Naming Transition Metal Complexes. https://chem.libretexts.org/Courses/Saint_Mary's_College%2C_Notre_Dame%2C_IN/CHEM_342%3A_Bio-inorganic_Chemistry/Readings/Week_2%3A_Introduction_to_Metal-Ligand_Interactions_and_Biomolecules/2.1_Transition_metal_complexes/2.1.6%3A_Naming_Transition_Metal_Complexes

4. There is a widely-circulated myth that anionic ligands should be named before neutral ones. This myth is false. According to the IUPAC red book (bolding mine):

> IR-2.15.3.4: Ordering ligands in formulae and names in formulae of coordination compounds,
>
> The formulae or abbreviations representing the ligands **are cited in alphabetical order as the general rule**. Bridging ligands are cited immediately after terminal ligands of the same kind, if any, and in increasing order of bridging multiplicity. (See also Sections IR-9.2.3 and IR-9.2.5.)
>
> IR-9.2.3.1 Sequence of symbols within the coordination formula

(i) The central atom symbol(s) is (are) listed first.

(ii) The **ligand symbols (line formulae, abbreviations or acronyms) are then listed in alphabetical order** (see Section IR-4.4.2.2).5 Thus, CH_3CN, MeCN and NCMe would be ordered under C, M and N respectively, and CO precedes Cl because single letter symbols precede two letter symbols. **The placement of the ligand in the list does not depend on the charge of the ligand.**

(iii) More information is conveyed by formulae that show ligands with the donor atom nearest the central atom; this procedure is recommended wherever possible, even for coordinated water.

5. Technically organometallic complexes are named according to slightly different rules but the coordination compound naming system works here. Note that this complex was once thought to possess an Fe-Fe bond, in accordance with the predictions of the 18-electron rule. Consequently, older sources often give an [*Fe-Fe*] after the name to reflect the presence of that bond. However, as the complex is no longer thought to possess an Fe-Fe bond it is omitted here.

Contributors and Attributions

Stephen Contakes, Westmont College, to whom comments, corrections, and criticisms should be addressed.

with some examples taken from Naming Transition Metal Complexes by Kathryn Haas.

Consistent with the policy for original artwork made as part of this project, all unlabeled drawings of chemical structures are by Stephen Contakes and licensed under a Creative Commons Attribution 4.0 International License.

4.1.2: Nomenclature and Ligands is shared under a not declared license and was authored, remixed, and/or curated by LibreTexts.

- **9.3: Nomenclature and Ligands** by Stephen M. Contakes has no license indicated.

4.1.3: Isomerism

Metal complexes present a rich, interesting, and diverse structural chemistry. Major points of variation in the structural chemistry of metal complexes include

1. **coordination number** and **coordination geometry**, which involve differences in how many ligands surround a central metal and their overall geometric arrangement. Examples of the latter include the tetrahedral and square planar geometries commonly observed for four-coordinate metal centers. Tetrahedral, square planar, and octahedral coordination serve as a backdrop to the discussion of isomerism on this page. Readers who are unfamiliar with these structures might consider reading the section on coordination geometries before this one.
2. **structural iosmerism** involves differences in how potential ligand atoms are bound to metals in a complex. Possibilities for structural isomerism include
   - linkage or ambidentate isomerism
   - hydrate/solvate isomerism
   - ionization isomerism
   - coordination isomerism.

   Of these, linkage isomerism should always be considered when working with ambidentate ligands. As classifications, the last three forms of structural isomerism are mainly of academic interest since they represent permutations of ordinary structure patterns for solvates, salts, and coordination complexes, respectively.
3. **stereochemistry**, which includes
   - which coordination geometry is adopted for a metal with a given set of ligands in a particular oxidation state. For instance, $[Ni^{II}Cl_4]^{2-}$ is tetrahedral while $[Pt^{II}Cl_4]^{2-}$ is square planar. Since this geometry is usually fixed by the metal and ligands it is typically not a source of stereoisomeric varierty.
   - metal-centric stereoisomerism involving possible variations in where ligands are located relative to one another around the metal. The possibilities depend on the coordination number, geometry, and number of different types of ligands. For instance, square planar complexes can exhibit *cis-/trans-* isomerism while tetrahedral ones cannot. Tetrahedral complexes with four different ligands exhibit *R* and *S* chirality but complexes of that type are relatively rare. The more common cases include *cis* and *trans* isomerism in square planar complexes and *cis* & t*rans-*, *mer* & *fac-*, and Λ & Δ isomerism in octahedral ones, although some multidentate ligands present additional possibilities for stereochemical variation
   - Stereoisomerism centered on the ligands bound to a metal center. Possibilities include
     - stereoisomerism inherent to a ligand. This would include cases where the ligand itself is chiral or, as in the case of amines, exists as a rapidly interconverting mixture of isomers. Thus this sort of stereoisomerism is an extension of the isomerism encountered in ordinary organic and other main group compounds. The main new issues introduced by binding of such ligands to a metal center involve the creation of new possibilities for diastereoisomerism based on the stereochemistry of the metal center and the freezing out of stereocenter inversion on binding to a metal. The latter is particularly important for amines, which as free amines racemize rapidly by nitrogen inversion.
     - or conformational isomerism involving five-membered **chelate rings** created when a multidentate ligand binds to a metal. This isomerism is often called chelate ring twist since individual rings can exhibit one of two conformations depending on how they twist on binding.

A summary of these forms of isomerism is given in Figure **4.1.3.1**.

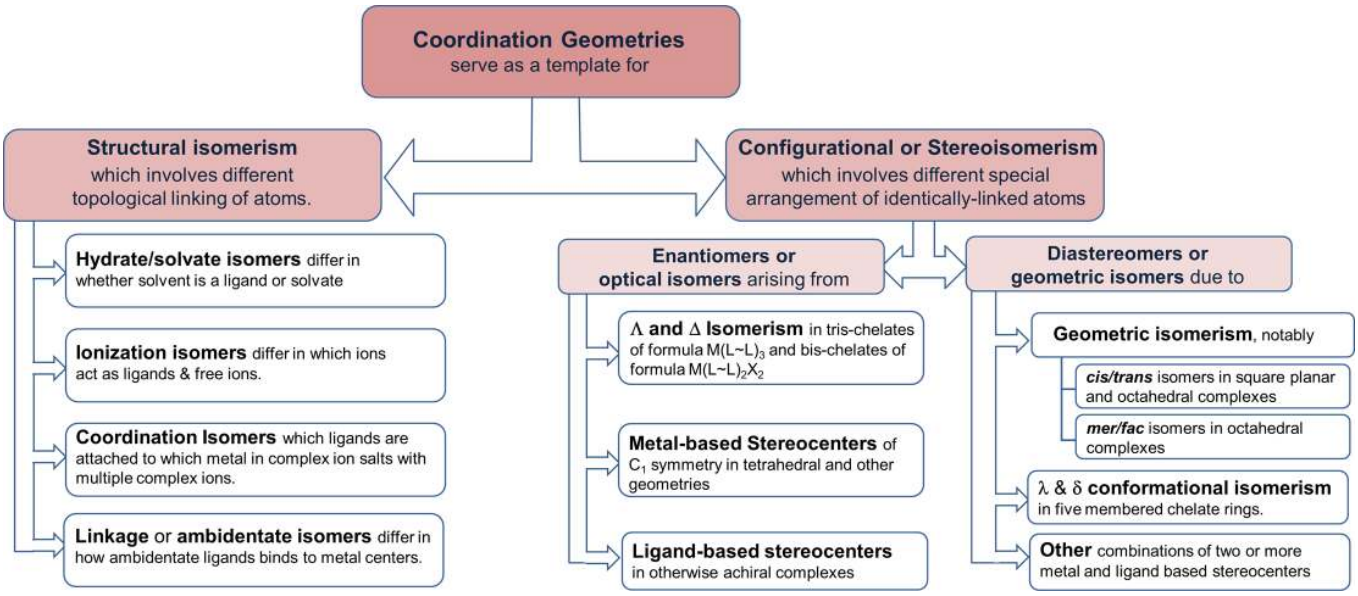


Figure **4.1.3.1**. Relationship among the common types of isomerism in metal complexes. This work by Stephen Contakes is licensed under a Creative Commons Attribution 4.0 International License.

Structural isomers

Structural isomerism involves different topological linkages of atoms. Differences in atomic linkages distinctive to coordination chemistry involve the linkages between metals and ligands. The main variations are:

1. Hydrate/solvate isomerism

Solvate isomers differ in terms of whether a molecule acts as a ligand or whether it acts as a solvate by occupying a lattice site in the crystal. Among solvate isomers, the case in which water is the ligand or solvate is the best known. The resulting isomers are called **hydrate isomers** after the term for water acting as a solvate, hydrate. A well-known example that illustrates how solvate isomerism works is the series $[CrCl_x(H_2O)_{6-x}]Cl_{3-x}{\cdot}xH_2O$, for which x = 0-2. The structures of the complex ions involved in this series are shown in Figure **4.1.3.2**.[1]

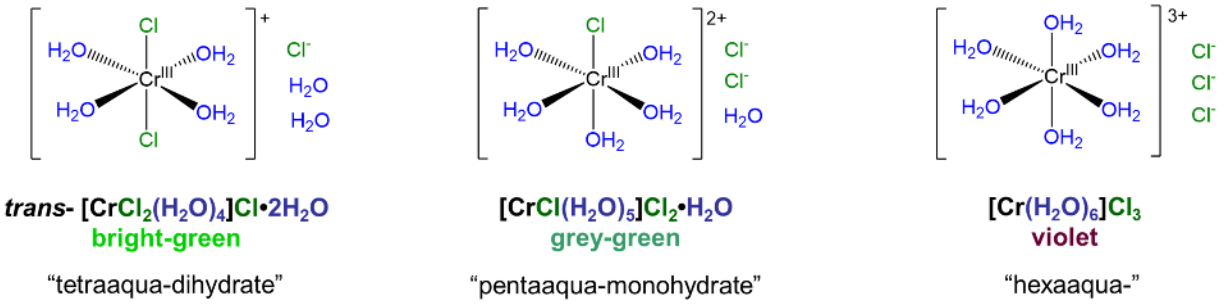


Figure **4.1.3.2**. Complexes of the hydrate isomer series $[CrCl_x(H_2O)_{6-x}]Cl_{3-x}{\cdot}xH_2O$ (x = 0-2). This work by Stephen Contakes is licensed under a Creative Commons Attribution 4.0 International License.

As can be seen from the compounds in Figure **4.1.3.2**, hydrate isomers differ both in terms of whether water acts as a ligand or hydrate *and* in terms of whether a potential counterion acts as a counterion or ligand. Thus, in *trans*-$[CrCl_2(H_2O)_4]Cl{\cdot}2H_2O$ two chlorides act as chloro ligands and four waters as aqua ligands while in $[CrCl(H_2O)_5]Cl_2{\cdot}H_2O$ five water molecules act as aqua ligands while only one chloride acts as a chloro ligand. In this way, solvate isomers simply represent cases in which two or more of the possible permutations for metal ligand binding among a set of solvent and counterion molecules are stable.

2. Ionization isomerism

In **ionization isomerism** there are two or more potential ions that can act as ligands. The ionization isomers differ in terms of which of these ions act as counterions and which act as ligands. Consider, for instance, the complexes shown in Figure **4.1.3.3**. These complexes differ in terms of whether the chloride or sulfate acts as a ligand, with the other acting as a counterion.

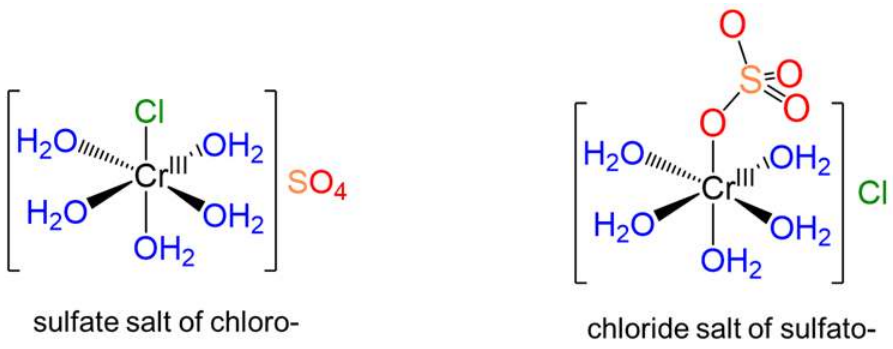


Figure **4.1.3.3**. Ionization isomers comprising a pentaaquachromium(III) fragment and the anions chloride and sulfate. As with all ionization isomers, the isomers differ in terms of which anion acts as a ligand and which a counterion. This work by Stephen Contakes is licensed under a Creative Commons Attribution 4.0 International License.

3. Coordination isomerism

Coordination isomers exist in compounds containing two or more complexes, each of which possesses a different set of ligands that can in principle be swapped with a ligand of the other complex. An example involves $[Co^{III}(NH_3)_6][Cr^{III}(ox)_3]$, depicted in Figure **4.1.3.4A**.[1] Coordination isomers of this complex involve swapping the ammine ligands around the Co^{3+} center for oxalato ligands surrounding the Cr^{3+} center. For instance, swapping all the ammine and oxalato ligands between the metal centers gives the coordination isomer $[Cr^{III}(NH_3)_6][Co^{III}(ox)_3]$ shown in Figure **4.1.3.4B**.

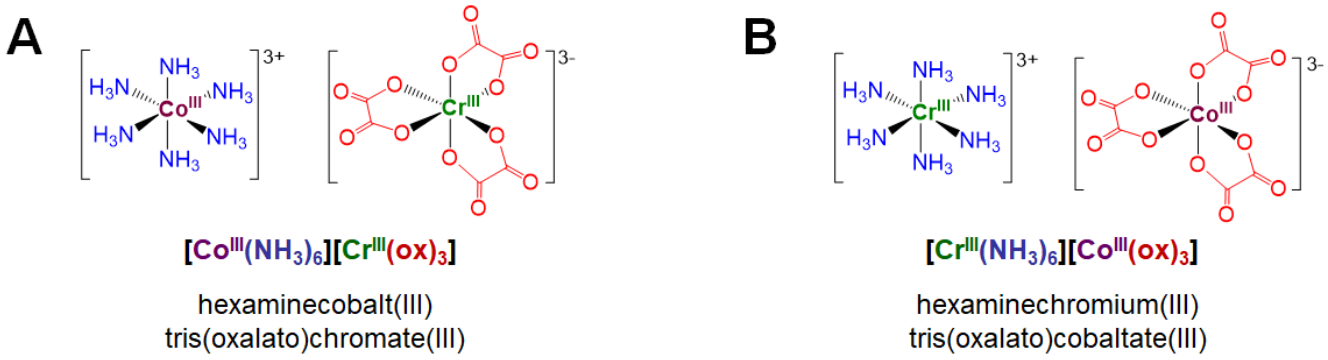
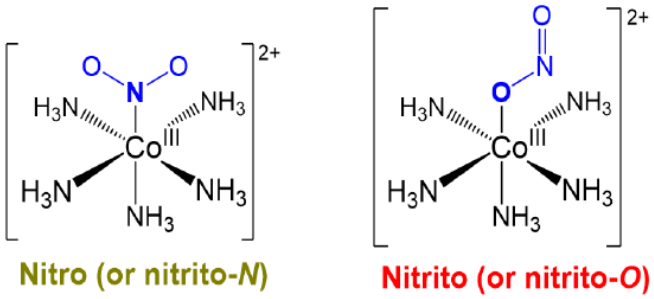


Figure **4.1.3.4**. Two coordination isomers comprising a Co^{3+} ,Cr^{3+}, six NH_3. and three oxalato ligands. The isomers differ in terms of which ligand type is bound to which metal. This work by Stephen Contakes is licensed under a Creative Commons Attribution 4.0 International License.

As classifications, hydrate/solvate, ionization, and coordination isomerism represent permutations of ordinary structure patterns for solvates, salts, and coordination complexes, respectively. As a result these forms of isomerism are rarely used as independent conceptual frameworks when thinking and talking about the structure of coordination compounds. Not so the final type of structural isomerism, linkage isomerism. That is because linkage isomerism has to do with the special *capacity* of ambidentate ligands to bind metals in multiple ways.

4. Linkage or ambidentate isomerism

Linkage or ambidentate isomers differ in how one or more ambidentate ligands bind to metal centers in a complex. The classic example dating from the work of Jørgensen and Werner is given in Scheme **4.1.3.I**.



Scheme **4.1.3.I**. Linkage isomers of penaamminenitritocobalt(III) ion. This work by Stephen Contakes is licensed under a Creative Commons Attribution 4.0 International License.

Just as alkenes exist as *E* and *Z* isomers, compounds possessing ambidentate ligands exist as one among the possible linkage isomers. As such, when working with ambidentate ligands the particular linkage isomer formed should be determined experimentally and considered when interpreting the complex's chemical and physical behavior.

The main ambidentate ligands which give rise to linkage isomerism are

- cyanide, CN^-
- thiocyanate, SCN^-, and the O and Se analogues, OCN^- and $SeCN^-$
- nitrite, NO_2^-
- sulfite, SO_3^-
- nitrosyl, NO

Although ambidentate ligands can bind metals in multiple ways, most exhibit a preferred binding mode (*i.e.*, prefer to bind metal centers in one of the possible ways). For instance, cyanide almost always binds through its carbon atom and thiocyanate almost always binds through its nitrogen (*μ-N*). However, the other binding mode can sometimes be formed kinetically or by using conditions that particularly favor its formation. Thus thiocyanate forms M-SCN^- linkages in the presence of exceptionally soft metal centers or in hard polar solvents (in which Lewis acid groups can stablize the terminal nitrogen of a bound thiocyanate ligand).

Ambidentate ligands are of significant research interest because many don't just bind to metal centers in two ways; the linkage isomers sometimes have significantly different physical properties. In addition, the possibility of two binding modes introduces the possibility of exploiting linkage isomerism to take advantage of some of these ligands:

a. different structural chemistry in different coordination modes. In mononuclear complexes the coordination mode influences which side of the ligand faces away from the complex and might be susceptible to stabilization by interaction with solvent. Additionally, the orientation of the ligand relative to the metal center might differ between one coordination mode and another. For instance, as predicted from the minor contributor to its resonance structure, thiocyanate binds nonlinearly via its S atom and linearly via its N (Figure **4.1.3.5**). Because of this the apparent steric bulk of the ligand around the metal center might differ between forms.

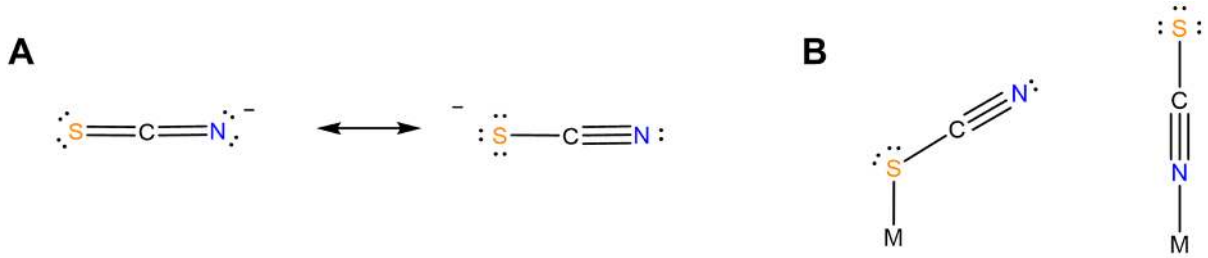


Figure **4.1.3.5**. Thiocyanate generally prefers to bind metals nonlinearly but in some cases forms linear M-SCN bonds. This work by Stephen Contakes is licensed under a Creative Commons Attribution 4.0 International License.

b. bind two different metal centers at the same time, linking them together. Perhaps the best-known examples involve thiocyanate and cyanide. The latter forms linkages of the type M-C≡N-M'. In the dye Prussian blue these take the form Fe^{II}-C≡N-Fe^{III}. An example from the author's graduate research involved tetrahedral clusters containing four metal atoms linked by six cyano ligands, as shown in Figure **4.1.3.6**.

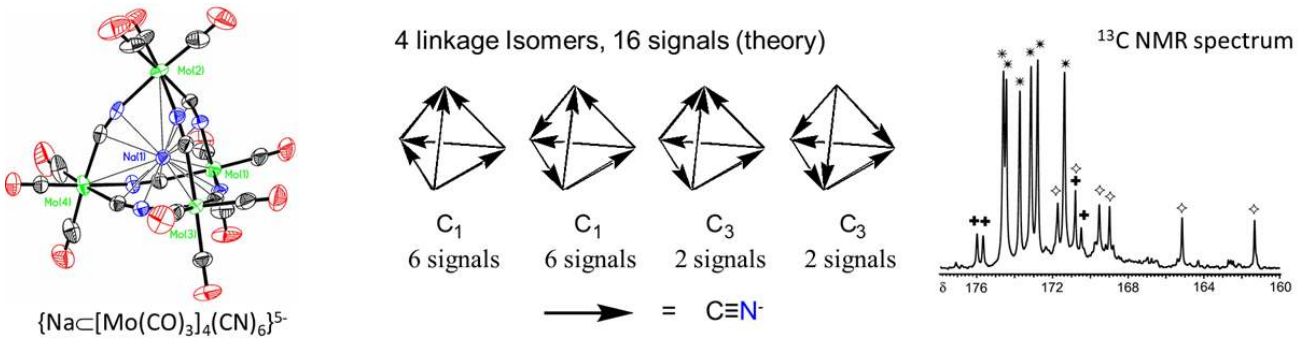


Figure **4.1.3.6**. (A) Structure of $\{Na@[Mo(CO)_3]_4(CN)_6\}$ showing the linking of four Mo centers by six CN ligands. Thermal ellipsoids for the C atoms are shown in black; those of the N atoms in blue. (B) The complex exists as a mixture of four linkage isomers in which the bridging CN^- ligands are oriented in different ways, as may be seen from the presence of the expected sixteen signals in its ^{13}C NMR spectrum. Based on work reported in reference 2.

c. can be induced to change from one binding mode to another in response to a stimulus. The classic example involves the light-driven transformation of the thermodynamically more stable yellow nitro complex of pentamminecobalt(III), $[Co(NH_3)_5NO_2]^{2+}$ to the less stable red *O*-nitrito complex, $[Co(NH_3)_5ONO]^{2+}$. Less stable cyanometallate coordination networks like those in the red $K\{Fe^{II}[Cr^{III}(CN)_6]\}$ transform into the more stable green $K\{Fe^{II}[Cr^{III}(NC)_6]\}$ form on heating, as shown in Figure **4.1.3.7**.[3]

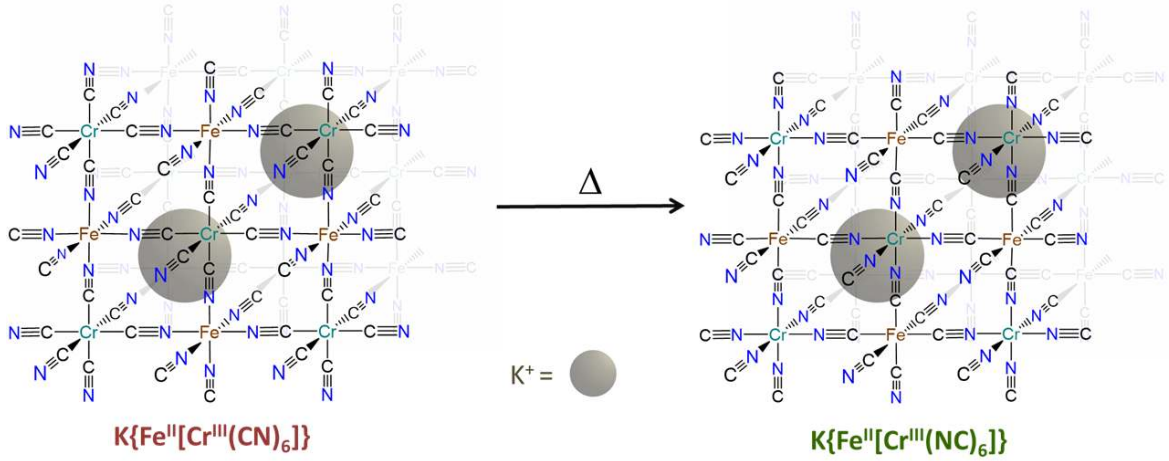


Figure **4.1.3.7**. Thermally-induced transformation of one $K\{Fe^{II}[Cr^{III}(CN)_6]\}$ into its more stable green linkage isomer $K\{Fe^{II}[Cr^{III}(NC)_6]\}$ involves "flipping" the cyano ligands. This work by Stephen Contakes is licensed under a Creative Commons Attribution 4.0 International License.

? Exercise 4.1.3.1: Bridging ambidentate ligands and the Hard-Soft Acid- Base Principle.

The hard-soft acid-base principle helps explain the preference of bridging ambidentate ligands for particular binding modes. How might the greater stability of the green $K\{Fe^{II}[Cr^{III}(NC)_6]\}$ over red $K\{Fe^{II}[Cr^{III}(CN)_6]\}$ be explained in terms of the hard and soft acid-base concept?

Answer

The greater stability of $K\{Fe^{II}[Cr^{III}(NC)_6]\}$ over $K\{Fe^{II}[Cr^{III}(CN)_6]\}$ reflects the greater stability of the Fe^{II}-CN-Cr^{III} linkages in the former over the Fe^{II}-NC-Cr^{III} linkages in the latter. This is consistent with the preference for hard-hard and soft-soft Lewis acid-base interactions of the Hard-Soft Acid-Base Principle.

The Fe^{II}-CN-Cr^{III} linkages are more stable because they possess bonds between

- the softer Lewis acid (Fe^{II}) and Lewis base (the C end of CN^-)
- the harder Lewis acid (Cr^{III}) and Lewis base (the N end of CN^-)

In contrast, the Fe^{II}-NC-Cr^{III} linkages in the less stable linkage isomer involve bonds between

- the softer base (the C end of CN^-) and harder acid (Cr^{III})
- the harder base (the N end of CN^-) and softer acid (Fe^{II})

Stereoisomerism

Optical Isomerism/Chirality

Molecules of D_n, C_n, or C_1 symmetry with only proper rotation axes (including $E = C_1$) are chiral and exhibit optical isomerism. As described in Figure **4.1.3.1**, the main sources of such optical isomerism in coordination chemistry are:

1. Chirality inherent to an organic or main group ligand.

   This type of isomerism is just an extension of the sort described in undergraduate organic texts and consequently does not merit separate discussion here, other than to note that some forms of optical isomerism which are of little importance in organic chemistry lead to optical activity in coordination compounds. In particular, the nitrogen inversion process which serves to rapidly racemize chiral amines is frozen out on formation of a metal-ligand bond. Because of this chiral amine, ligands bound to a metal form non-interconvertible *R* and *S* enantiomers, as shown in Figure **4.1.3.8**.

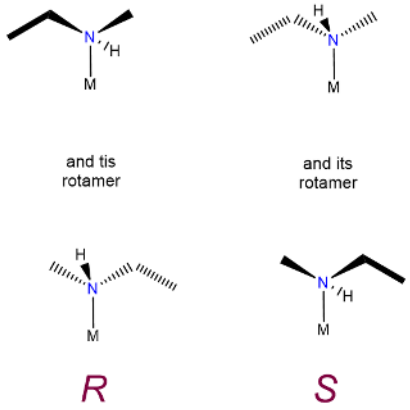


Figure **4.1.3.8**. Two views of *R* and *S* enantiomers formed when the chiral amine ethylmethylamine binds a metal that are commonly used to represent chiral amines in complexes. This work by Stephen Contakes is licensed under a Creative Commons Attribution 4.0 International License.

2. Chirality arising from the symmetry of ligands about a metal center.

   The two common situations through which such chirality arises involve:

   i. Chirality at a tetrahedral metal center surrounded by four different ligand attachment points.

   Such cases are often referred to as MABCD or Mabcd where M stands for the metal and a, b, c, and d the four different ligand attachment points. An example of such a complex is given in Figure **4.1.3.9A**. The chirality of such complexes is analogous to the chirality arising from a tetrahedral carbon stereocenter. There are two caveats, though. First, it is not enough to have a four-coordinate complex; the metal must possess tetrahedral symmetry since, as shown in Figure **4.1.3.9B**, square planar M complexes with four different ligands are identical to their mirror images. Second, such chirality is most easily realized using macrocyclic ligands like proteins. Metal ligand bonds involving sterically unhindered monodentate complexes like that in the example of Figure **4.1.3.9A** are in general weaker and more flexible than analogous carbon-carbon bonds. Consequently, in such cases it is likely that the enantiomers would interconvert through a fluxional process, making their resolution difficult if not impossible.

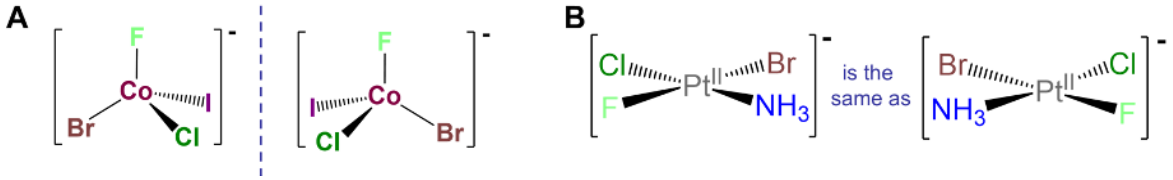


Figure **4.1.3.9**. (A) In principle tetrahedral metal centers surrounded by four different ligands (Mabcd) exhibit chirality analogous to the chirality of tetrahedral carbon stereocenters; (B) in contrast, square planar Macbd complexes like $[PtBrClF(NH_3)]^-$ are not chiral since they are the same as their mirror images. (It is easiest to see this by either working out its point group (C_s) or by rotating the left $[PtBrClF(NH_3)]^-$ structure clockwise 180 degrees to give its mirror image. This work by Stephen Contakes is licensed under a Creative Commons Attribution 4.0 International License.

ii. **Λ** and **Δ** isomerism at octahedral metal centers surrounded by two or three chelating ligands.

Specifically,

a. Octahedral tris-chelates of formula $M(L\sim L)_3$ exhibit D_3 symmetry.
b. cis-octahedral bis-chelates of formula $M(L\sim L)_2XY$ exhibit C_2 or C_1 symmetry: C_2 if X = Y and C_1 if $X \neq Y$.

As shown in Figure **4.1.3.10A**, octahedral tris-chelates like $[V(ox)_3]^{3-}$ are chiral and can exist as nonsuperimposable **Λ** and **Δ** enantiomers. The chirality of these tris-chelates is analogous to that of pinwheels. As shown in Figure **4.1.3.10B**, when looking directly at the head of any individual pinwheel from above, the blades will be angled from back to front going around the pinwheel in either the clockwise or counterclockwise direction. As shown in Figure **4.1.3.10C**, the case for which the blades are angled in the clockwise direction is analogous to the **Λ** enantiomer and the case when they are angled in the counterclockwise direction the **Δ**.

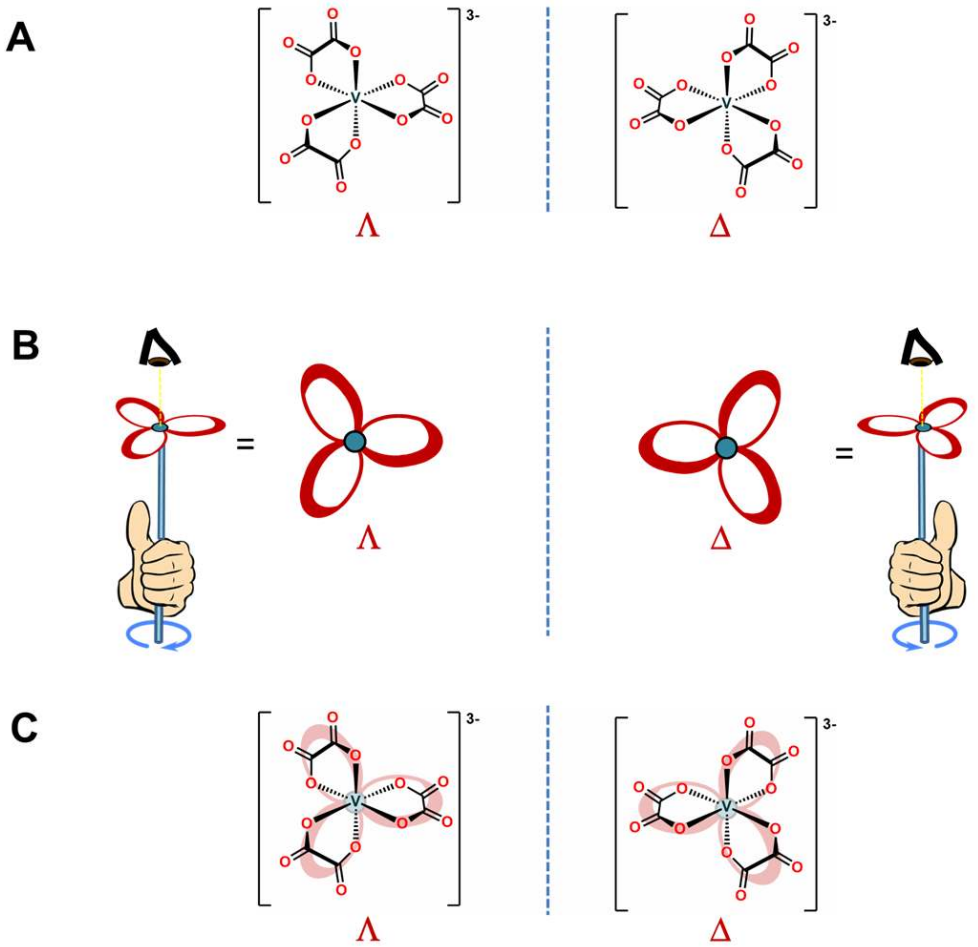


Figure **4.1.3.10**. (A) Octahedral tris-chelates like $[V(ox)_3]^{3-}$ are chiral and can exist as **Λ** and **Δ** enantiomers. (B) The chirality in these systems is analogous to that of a pinwheel, with the **Λ** enantiomer exhibiting the symmetry of a left-handed pinwheel and the **Δ** enantiomer that of a right handed one. (C) The pinwheel-like nature of **Λ** and **Δ** enantiomers is easiest to see by overlaying the structures of $[V(ox)_3]^{3-}$ from A with the pinwheel structures of B. One way to recognize **Λ** and **Δ** enantiomers is to draw them in these projections. If a left hand is curled around the **Λ** enantiomer with the thumb facing up the curl of the fingers will flow from the back of each ligand towards the front. The same will be true if the right hand is curled around the **Δ** enantiomer. Credits: Although the image is largely an original drawing, the hand images used in part B are adapted from an image by SVGguru / CC BY-SA (https://creativecommons.org/licenses/by-sa/4.0). Otherwise this work by Stephen Contakes is licensed under a Creative Commons Attribution 4.0 International License.

The **Λ** and **Δ** chirality in octahedral bis-chelates is analogous to that in the tris-chelates except this time the third chelating ligand is replaced by an arbitrary pair of ligands. This lowers the symmetry of the complex to either C_2 or C_1, as shown for the C_2 complex $[CoCl_2(en)_2]^+$ in Figure **4.1.3.11A**. In either case the result is that such complexes exist as **Λ** and **Δ** enantiomers analogous to those in the metal tris-chelates, as shown in Figure **4.1.3.11B**.

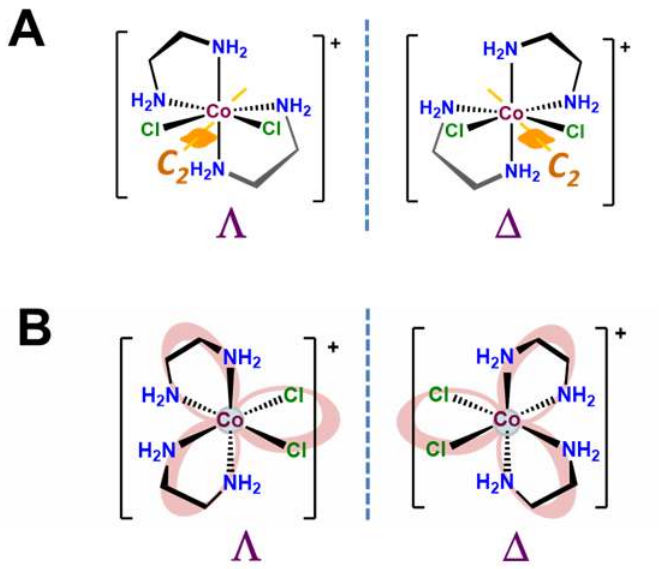


Figure **4.1.3.9C**. This work by Stephen Contakes is licensed under a Creative Commons Attribution 4.0 International License.

Octahedral complexes containing ligands with denticities of four or more also exhibit **Λ** and **Δ** chirality; it is just that in such cases the bound ligand defines multiple rings within the complex that can be defined as existing in either **Λ** or **Δ** orientations relative to each other. The procedure for making these assignments is beyond the scope of most introductory inorganic courses but the result is that such complexes are designated as **ΛΛ**, **ΔΔ**, **ΔΛ**, **ΔΔΔ**, etc., depending on the number of relationships involving the rings defined by the bound ligand. Interested readers should consult reference 4 for more details.

Circular dichroism may be used to characterize optically active metal complexes.

At the present the most definitive way to determine the absolute configuration of an optically active coordination compound is to determine its 3D molecular structure using single crystal X-ray crystallography.[5] However, as that is not always possible or convenient, the optical activity of coordination complexes is also commonly studied using circular dichroism (CD) spectroscopy. CD spectroscopy is used because, unlike most chiral organics, optically active coordination complexes possess low-energy electronic transitions that occur in the far UV and visible range. This means that it is often convenient to use the ability of a complex to refract and absorb different circular polarizations of light to derive information about both the configuration of an optically active complex and its electronic structure. The focus of this section will be to explain how the determination of absolute configuration by circular dichroism and optical rotatory dispersion work, as well as the relationship of these techniques to the more ordinary sort of polarimetry used to measure optical rotation in organic systems. Only brief notes will be made about the instrumental and electronic structure applications of these techniques since the electronic spectra of metal complexes will be discussed in Chapter 11: Coordination Chemistry III - Electronic Spectra and the instrumental aspects of CD are well-treated elsewhere.

Both polarimetry and circular dichroism spectroscopy are grounded in the recognition that plane polarized light is equivalent to a superposition of left and right circularly polarized light, as shown in Figure **4.1.3.12**.

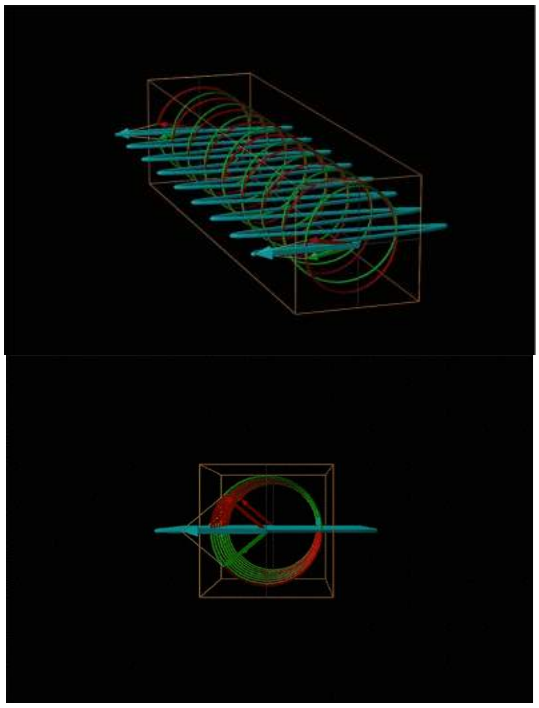


Figure **4.1.3.12**. Angled and front view of plane polarized light (light blue) as the vector sum of left circularly polarized light (red) and right circularly polarized light (green). Created using EMANIM Version 1.2 (2011 July) by Andras Szilagyi (www.enzim.hu/~szia/emanim). This work by Stephen Contakes is licensed under a Creative Commons Attribution 4.0 International License.

When plane polarized light passes through a chiral medium, its left and right circularly polarized components move at different rates (*i.e.*, have different indices of refraction). This causes the plane of polarization to rotate in the direction of the faster component according to the relationship

$$\alpha = \frac{n_l - n_r}{\lambda}$$

where α is the angle of rotation, λ the light's wavelength, and n_l and n_r the refractive indices experienced by left and right circularly polarized light.

An example of such a rotation is shown in Figure **4.1.3.13**.

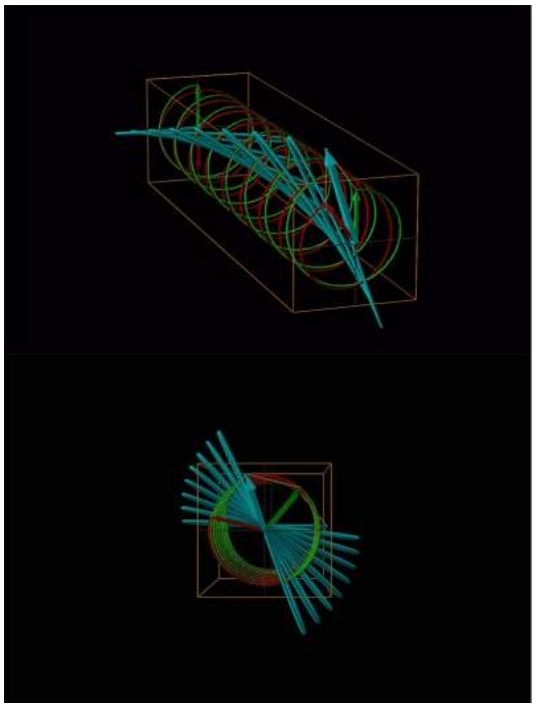


Figure **4.1.3.13**. Angled and front view of plane polarized light (light blue) as it passes through a medium (represented by the orange box) in which left circularly polarized light (red) experiences a higher refractive index (and so moves slower) than right circularly polarized light (green). Created using EMANIM Version 1.2 (2011 July) by Andras Szilagyi (www.enzim.hu/~szia/emanim) with a refractive index of 1.05 for left circularly polarized light and 1.00 for right circularly polarized light. This work by Stephen Contakes is licensed under a Creative Commons Attribution 4.0 International License.

Chemists typically call this rotation of light by a chiral medium optical rotation. In organic chemistry it is common to measure the optical rotation at the sodium D wavelength of 589.29 nm, a much longer wavelength than most organics are able to absorb. Because of this the optical rotations commonly measured by organic chemists are largely independent of absorption and mainly serve as a characteristic physical property similar to melting points or are used to establish the purity of a mixture of enantiomers. The sort of spectroscopic data used to characterize chiral coordination compounds more commonly makes use of the relationship between absorption and optical rotation.

In coordination chemistry the wavelength-dependence of optical rotation is used to discern information about compounds' electronic spectra. This measurement of the wavelength dependence of optical rotation is called **optical rotatory dispersion (ORD)** and the resulting plots are called optical rotatory dispersion or ORD spectra or curves. Such ORD curves are useful for characterizing the chiral environment in a coordination complex because the ORD curves exhibit a characteristic shape. This characteristic shape is because according to the **Cotton Effect,** the optical rotation changes sign at the absorption maximum of a chromophore in the compound. For one configuration the rotation will go from negative to positive with increasing wavelength and is called a **positive cotton effect**; for the other configuration the rotation will go from positive to negative or exhibit a **negative cotton effect**. This behavior is summarized in the top two curves of Figure **4.1.3.14**.

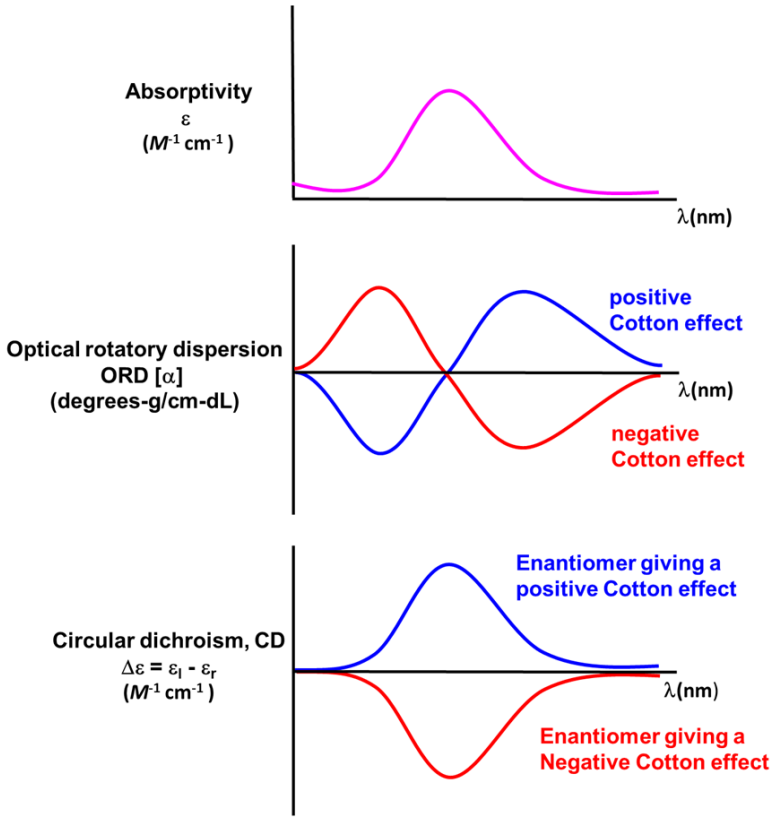


Figure 4.1.3.14. Idealized relationship between absorbance, ORD, and CD spectra for enantiomers exhibiting a positive and negative Cotton effect. This work by Stephen Contakes is licensed under a Creative Commons Attribution 4.0 International License.

A technique used even more often than ORD is **circular dichroism (CD)**, represented by the lowest spectrum in Figure 4.1.3.14. Circular dichroism arises from the differential absorption of left and right circularly polarized light by a chiral compound. This gives elliptically polarized light as shown in Figure 4.1.3.15.

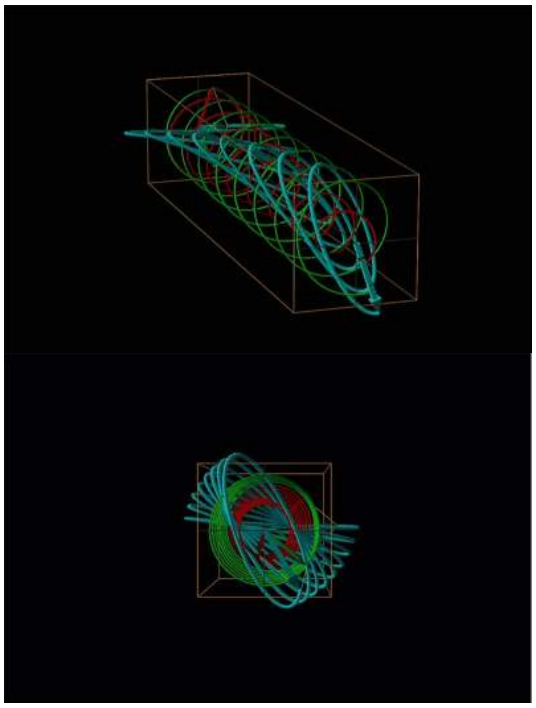


Figure **4.1.3.15**. Angled and front view of plane polarized light (light blue) as it passes through a medium (represented by the orange box) in which left circularly polarized light (red) both experiences a higher refractive index and greater absorption than right circularly polarized light (green). Created using EMANIM Version 1.2 (2011 July) by Andras Szilagyi (www.enzim.hu/~szia/emanim) with a refractive index of 1.05 and an extinction coefficient of 0.05 for left circularly polarized light and a refractive index of 1.00 and extinction coefficient of 0 for right circularly polarized light. This work by Stephen Contakes is licensed under a Creative Commons Attribution 4.0 International License.

In circular dichroism (CD) spectroscopy a sample is irradiated with polarized light resulting in the transmission of elliptically polarized light due to differential refraction and absorption of the polarized light's left and right circularly polarized components. For achiral molecules the handedness doesn't affect absorbance, but for chiral molecules, which chiral ground and excited states the handedness of an EM wave affects can determine how readily that wave can distort the chiral ground state into the chiral excited one. For this reason chiral molecules absorb left and right circularly polarized light differently.

In CD spectroscopy the magnitudes of the left and right circularly polarized components of light that is transmitted by the sample are measured and used to determine how much light of each was absorbed (just as in regular absorbance spectroscopy). The difference in absorption between left and right circularly polarized light constitutes the primary signal in CD spectroscopy. More specifically, circular dichroism spectra (CD spectra) show the difference in extinction coefficients for left and right circularly polarized light, $\Delta\epsilon$, as a function of wavelength, where

$$\Delta\epsilon = \epsilon_l - \epsilon_r$$

where Missing open brace for subscript and Missing open brace for subscript are the extinction coefficients observed with left and right circularly polarized light, respectively.

As with ORD spectra, the signs of the features in CD spectra like that of Δ–$[Co(en)_3]Cl_3$ given in Figure **4.1.3.16** are enantiomer-dependent. As illustrated in the lower spectrum in Figure **4.1.3.14** , the CD spectra of enantiomers mirror one another. Because of this difference in behavior it is possible in principle to determine the absolute configuration of a complex from its CD spectrum.

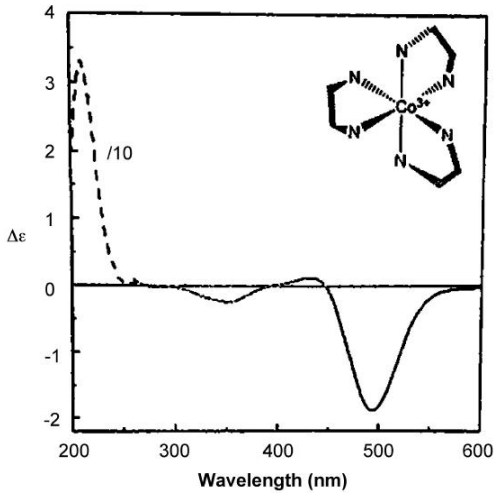


Figure **4.1.3.16**. CD spectrum of Δ–[Co(en)$_3$]Cl$_3$. Taken from reference 6.

There are several ways that ORD and CD spectra can be useful for determining the absolute configuration of a chiral complex.

1. First, the sign of the Cotton effect and peaks in CD spectra exhibited by a given absolute configuration is often consistent across a series of compounds. Thus if a new member of the series is isolated, its configuration can be determined based on which enantiomer has the same Cotton effect. For instance, if both the **Λ** isomer of a metal diimine complex like [Ru(bpy)$_3$]$^{2+}$ exhibit a positive Cotton effect and a newly resolved metal diimine exhibits a negative Cotton effect it might reasonably be inferred that the newly-resolved complex is in the opposite or **Δ** configuration.
2. Second, for some systems the expected sign of the Cotton effect and CD peaks for each enantiomer may be predicted semi-empirically based on the spatial locations of substituents relative to the chromophore (the part of the molecule that changes electronic structure during the transition), although the details are beyond the scope of the present discussion.
3. Consideration of interactions between multiple chromophores in a compound can be used to infer absolute configuration. Again, the details are beyond the scope of the present discussion. Interested readers are referred to reference 7 for details.

Common patterns of Diastereomerism

Geometric isomerism

Geometric isomerism involves differences in the geometric placement of atoms in a compound. In coordination chemistry, geometric isomerism involves differences in the relative placement of a set of ligands about a metal center. There are two main types:

cis and *trans* isomerism

This type of isomerism has to do with how two ligands are oriented relative to one another in a square planar or octahedral complex. As shown in Figure **4.1.3.17**, ligands that are next to one another with a L-M-L bond angle of 90° are said to be *cis*; those on opposite sides of the metal with a L-M-L bond angle of 180° are in the *trans* arrangement.



Figure **4.1.3.17**. *cis* and *trans* arrangement of ligands around (A) square planar and (B) octahedral metal centers. Since both types of complexes feature 90° L-M-L bond angles, the arrangements are fundamentally the same in both cases. This work by Stephen Contakes is licensed under a Creative Commons Attribution 4.0 International License.

Simple *cis* and *trans* geometric isomers can be identified when there are two identical ligands (A) or chelating ligands with distinguishable attachment points (A~B) oriented about either a square planar or octahedral center. Examples are given in Figure

4.1.3.18. Notice from the example given in Figure **4.1.3.18C** that multidentate ligands have the potential to constrain complexes to adopt a particular geometry.

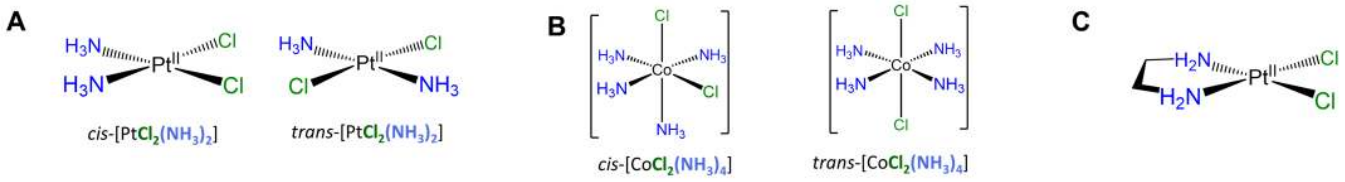


Figure **4.1.3.18**. Examples of square planar and octahedral *cis* and *trans* isomers. (A) *cis* and *trans* isomers of $[PtCl_2(NH_3)_2]$; the former is medicinally important. Sold under the name cisplatin, the *cis* isomer is used as a chemotheraphy against various forms of cancer. (B) *cis* and *trans* isomers of $[CoCl_2(NH_3)_4]$, a compound of more academic interest. (C) $PtCl_2$(en) only exists as the *cis* isomer because the chelating en ligand can only bind in a *cis* arrangement. This work by Stephen Contakes is licensed under a Creative Commons Attribution 4.0 International License.

Slightly more involved examples involve perturbations of the simple cases above in which there are multiple distinguishable *cis* and/or *trans* relationships. Two square planar examples are given in Figure **4.1.3.19**.

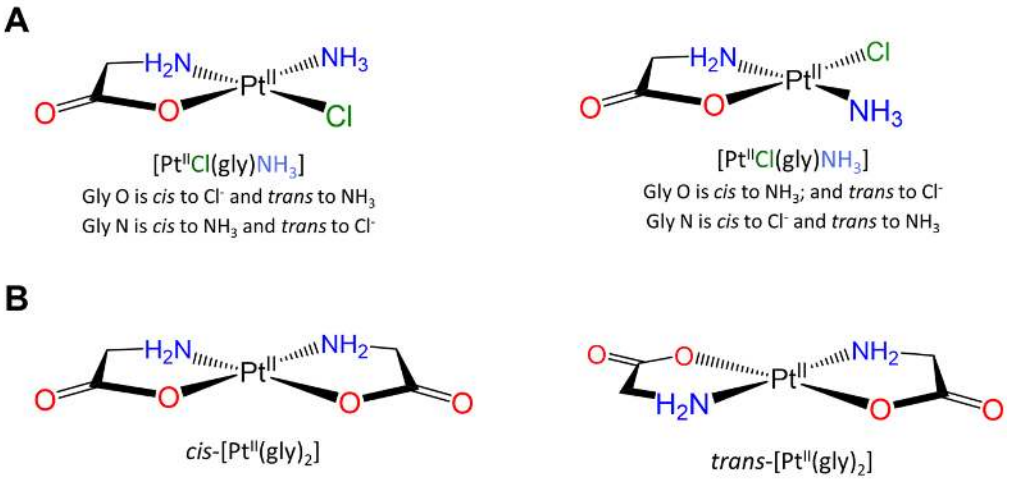


Figure **4.1.3.19**. Examples of more complex square planar systems. (A) Geometric isomers of $[PtCl(gly)NH_3]$, a MA_2BC system for which A = gly^-, B = Cl^-, and C = NH_3. Swapping of the ammine and chloro ligands changes both the *cis* and *trans* relationships involving the Gly ligand. (B) Geometric isomers of $[Pt(gly)_2]$, an $M(A\sim B)_2$ system for which A = the *κO* glycine carboxy group and B its *κN* amine. The only possible geometric isomerism involves swapping the orientation of one glycine relative to the other. For this reason the two complexes shown can be designated as *cis* and *trans* isomers based on whether the *κO* and *κ*N ends of the glycine are *cis* or *trans* to one another. This work by Stephen Contakes is licensed under a Creative Commons Attribution 4.0 International License.

More complex examples of *cis* and *trans* relationships between ligands in octahedral complexes are given in the exercises that conclude this page, which also demonstrates how a systematic approach may be used to identify isomers.

mer and *fac* isomerism

This type of isomerism has to do with how three ligands are oriented relative to one another in an octahedral complex. The arrangements are represented in Figure **4.1.3.20**.

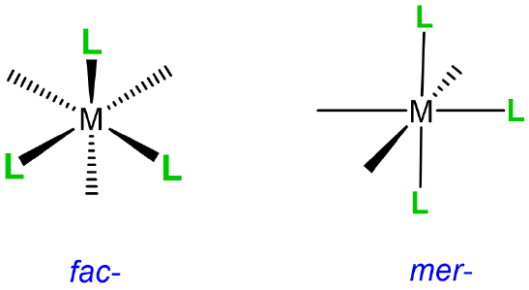


Figure **4.1.3.20**. Simple representation of the *fac* and *mer* arrangements of ligands around an octahedral metal center. This work by Stephen Contakes is licensed under a Creative Commons Attribution 4.0 International License.

Since it can help to visualize the *mer* and *fac* geometry from multiple points of view, several representations are given in Figure **4.1.3.21**. As shown in Figure **4.1.3.21**, in ***fac*** or **facial arrangements**, the ligands occupy the same "face" of the octahedral coordination sphere, while in the ***mer*** or **meridional geometry** the ligands form a T shape in the same plane or its "meridian."[8]

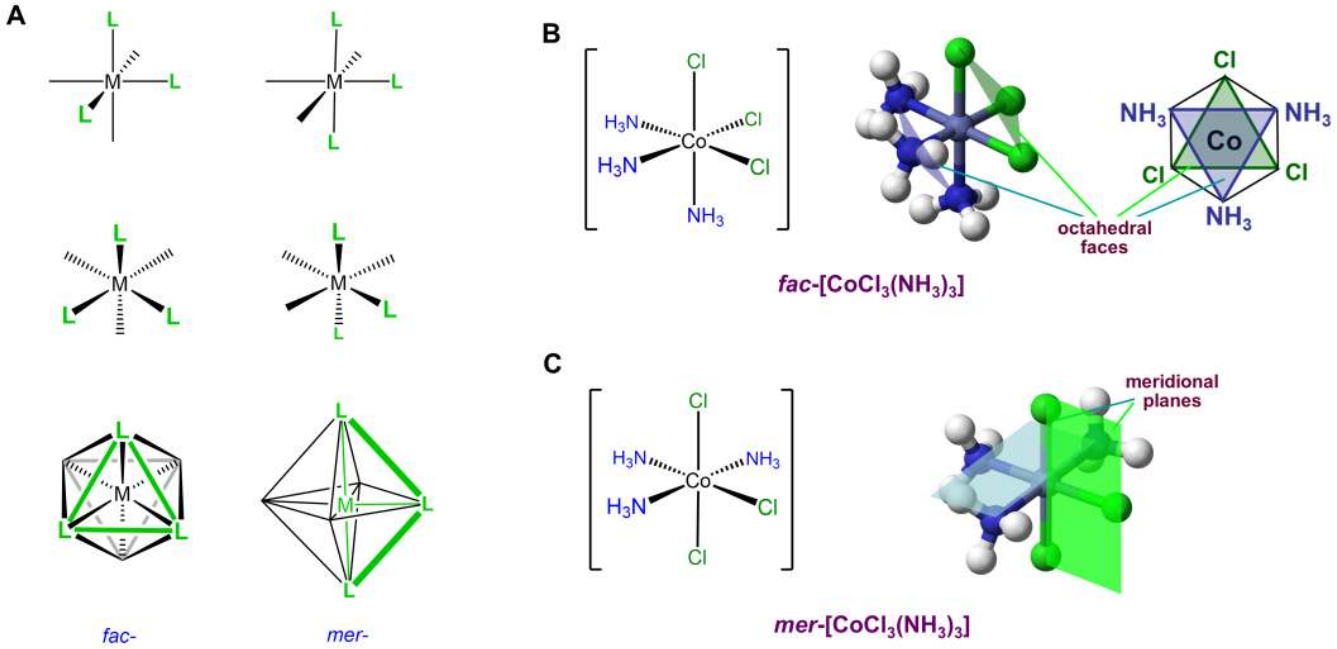
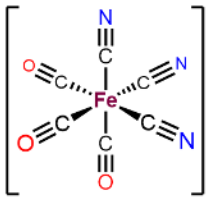
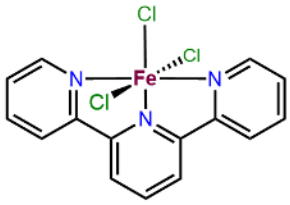
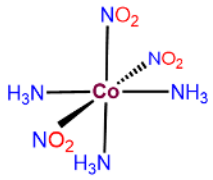


Figure **4.1.3.21**. (A) Three projections of *fac* and *mer* arrangements of ligands around an octahedral metal center emphasizing that in the *fac* arrangement the ligands are oriented along a face of the octahedron while in the *mer* arrangement they are oriented in a plane. (B) Structure of *fac*-$[CoCl_3(NH_3)_3]$ showing the octahedral faces occupied by the chloro and amine ligands. (C) Structure of *mer*-$[CoCl_3(NH_3)_3]$ showing the planar arrangement of the chloro and ammine ligands. The ball and stick models are modified from images by Benjah-bmm27 - Own work, Public Domain, https://commons.wikimedia.org/w/inde...?curid=1874872 and curid=1874873. Otherwise this work by Stephen Contakes is licensed under a Creative Commons Attribution 4.0 International License.

Octahedral complexes with three identical ligands oriented about an octahedral center can only exist in *mer* and *fac* arrangements. Consequently, such complexes can be designated as *mer* and *fac* isomers. Examples are given in Figure **4.1.3.22**.







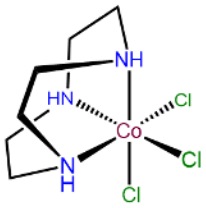


Figure **4.1.3.22**. Examples of *fac* and *mer* octahedral complexes. Note how some chelating ligands preferentially bind to the metal in a *fac* or *mer* arrangement and, in so doing, force the other ligands to also form a *mer* or *fac* arrangement. This work by Stephen Contakes is licensed under a Creative Commons Attribution 4.0 International License.

Diastereomerism arising from multiple ligand-associated chiral centers

Diastereomerism can also arise when two or more chiral ligands bind to a metal center. Such cases typically give rise to a complex mixture of isomers, as shown by the example in Figure **4.1.3.23**. As may be seen from Figure **4.1.3.23**, the differences between these isomers can arise from both changes in the stereochemical configuration of the ligand and the relationship of particular ligand centers relative to one another. For instance, the leftmost two structures in Figure **4.1.3.23** possess one *R* and *S* nitrogen center each but differ in whether the centers are oriented so that the *R* and *S* centers on the two ligands are *trans* or *cis* to one another.

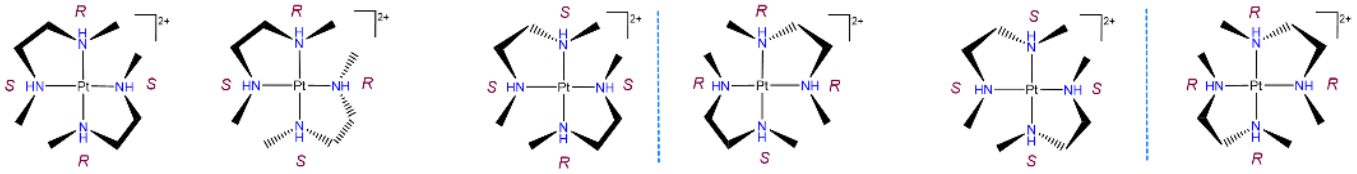


Figure **4.1.3.23**. Diastereomers that can in principle be formed when two *N*,*N*′-dimethylethylenediamine ligands coordinate a Pt^{2+} center. This work by Stephen Contakes is licensed under a Creative Commons Attribution 4.0 International License.

Diastereomerism arising from λ and δ ring conformation isomerism.

Chelate rings are formed when a chelating ligand binds a metal

As may also be seen from the structures in Figure **4.1.3.23**, when a multidentate ligand coordinates a metal, the ligand and metal center comprise one or more **chelate rings**. Examples of such chelate rings are shown in Figure **4.1.3.24**.

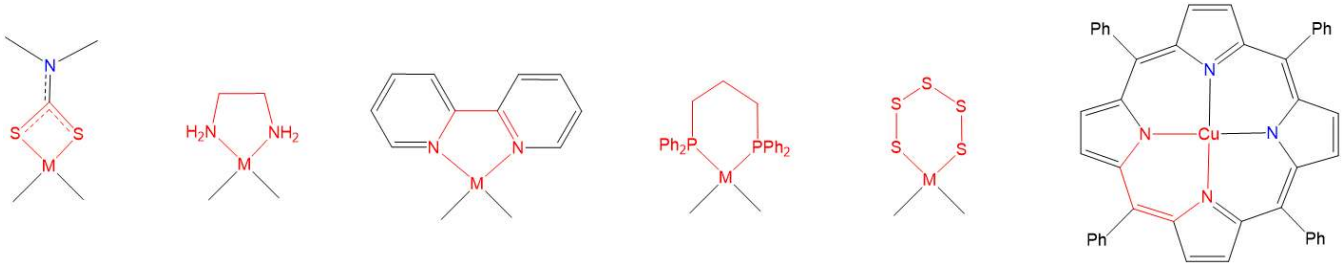


Figure **4.1.3.24**. Four, five, and six-membered chelate rings (shown in red) formed by coordination of selected bidentate ligands to a metal center. This work by Stephen Contakes is licensed under a Creative Commons Attribution 4.0 International License.

As may be inferred from the examples in Figure **4.1.3.24**, chelate rings may be of different sizes, although four, six, and especially five-membered rings are particularly common. Exactly which ring sizes will be more stable for a given system depends on the

coordination geometry and, due to differences in M-L bond lengths, to a lesser degree on the metal. As a result, for octahedral and square planar complexes with 90° L-M-L bond angles between *cis* ligands, *five-membered rings tend to be especially stable* (Figure **4.1.3.25**).

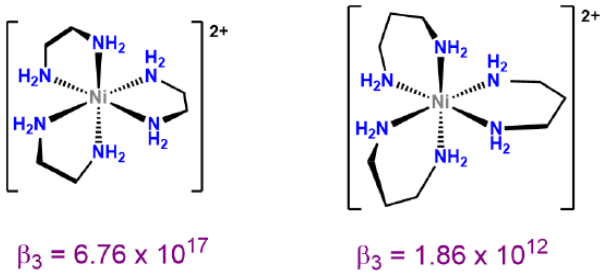


Figure **4.1.3.25**. The greater stability of five-membered chelate rings involving Ni^{2+} and organic ligands is reflected in the higher overall formation constant (β_3) for the five-membered chelate rings contained in $[Ni(en)_3]^{2+}$ compared to that of $[Ni(et)_3]^{2+}$, which has six-membered rings. The data in this figure is taken from Stability of Metal Complexes and Chelation by Robert Lancashire. This work by Stephen Contakes is licensed under a Creative Commons Attribution 4.0 International License.

Not all metal chelates prefer to form five-membered rings. The steric requirements of chelate rings depend on both the preferred coordination geometry of the metal center and the stereochemistry of the ligand. Both of these effects are typically considered in terms of preferred L-M-L bond angles. From the perspective of the metal center, the preferred bond angle is determined by the coordination geometry. Octahedral and square planar metals prefer 90° L-M-L bond amgles, trigonal bipyramidal systems 90 and 120° L-M-L bond angles, and tetrahedral complexes 109.5° L-M-L angles. The larger preferred bond angles in tetrahedral and trigonal bipyramidal systems often require the formation of larger six or seven-membered chelate rings for maximum stability. The size of the chelate ring actually formed between a metal and ligand is determined by the ligand's structure. As the contributor of all the atoms in the chelate ring but one, the ligand directly determines the chelate ring size. More subtly, ligands naturally prefer to coordinate metals at a particular L-M-L angle, called the **bite angle**, as shown in Figure **4.1.3.26A**. Ligands with bite angles corresponding to the ideal L-M-L angle for a metal's preferred geometry tend to form more stable complexes, although in turn ligand bite angles can cause metals with a weak coordination geometry preference to adopt the ligand's preferred geometry instead.[10] As may be seen from the values in Figure **4.1.3.26B**, bite angles roughly increase with the size of the chelate ring formed but are also influenced by the types of structures used to connect the ligand's Lewis base sites. This facilitates the use of diphosphine ligands to tailor the structure and reactivity of phosphine-containing organometallic catalysts.



Figure **4.1.3.26**. (A) Definition of the bite angle as the angle at which the ligand's preferred L-M-L angle when coordinating a metal center. (B) Bite angles of selected diphosphines.[9] The bite angles of many such diphosphines have been determined to facilitate the design of phosphine-containing organometallic catalysts. This work by Stephen Contakes is licensed under a Creative Commons Attribution 4.0 International License.

λ and δ isomerism involves differences in the conformation of nonplanar five-membered chelate rings

As shown in Figure **4.1.3.27**, some chelate ring systems are planar while others are not.

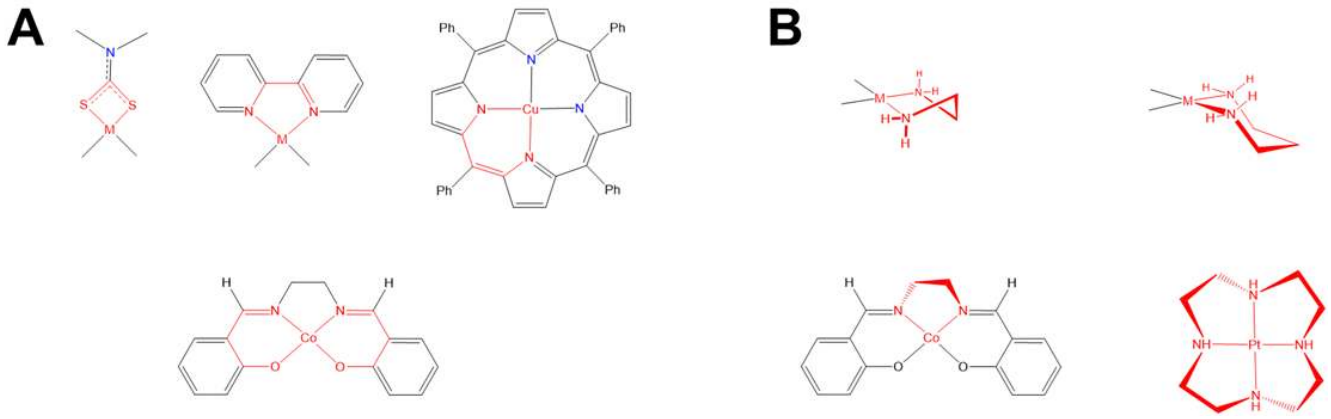


Figure 4.1.3.27. (A) Planar and (B) Nonplanar chelate rings shown highlighted in red. Notice how [Co(salen)] possesses a nonplanar chelate ring and two planar ones. This work by Stephen Contakes is licensed under a Creative Commons Attribution 4.0 International License.

Among the nonplanar chelate ring systems are ligands like en and dppe, which contain tetrahedral C, N, O, P, and S atoms. Because these atoms create kinks in the chelate ring they introduce additional opportunities for diastereomerism due to differences in the chelate ring conformation, called **ring twist**. Ring twist in nonplanar systems has been most extensively explored for five-membered chelates like those formed by dppe and by en and other chelating amines. Unlike the more rigid four-membered chelate rings, five-membered chelates tend to be conformationally flexible, but not so conformationally flexible that their conformers are rapidly interconverting at room temperature (at least not when the rings are substituted to introduce additional steric strain). This balance between flexibility and rigidity enables some five-membered chelate rings to exist as mixtures of distinguishable conformational isomers at room temperature.

To understand the two most stable conformers that five-membered chelates rings tend to form, it is helpful to think of five-membered chelate rings as involving two components (Figure 4.1.3.28):

- a planar L-M-L group, where L are the atoms directly attached to the metal, M, and
- the remaining two ring atoms, E, which form a rigid E-E bar across the back of the chelate ring.

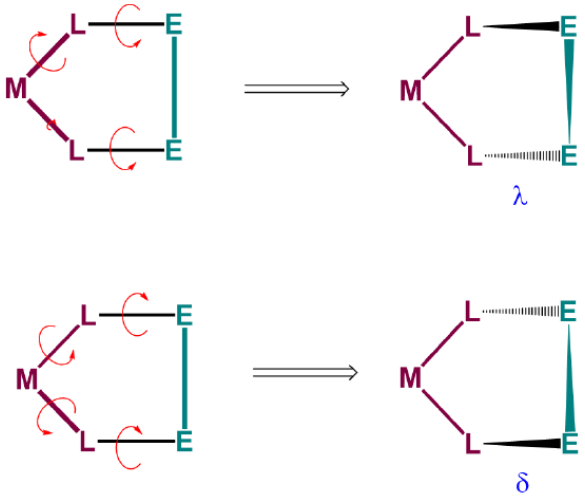


Figure 4.1.3.28. Five-membered chelate rings consist of a planar L-M-L group connected to a rigid E-E bar. Conformers arise as rotation about the M-L and L-E bonds causes twisting of the E-E bar relative to the L-M-L plane. This work by Stephen Contakes is licensed under a Creative Commons Attribution 4.0 International License.

As can be seen from Figure 4.1.3.28 , rotation about the M-L and L-E bonds causes twisting of the E-E bar relative to the L-M-L plane. The two most stable conformers produced by these motions are the λ or δ conformations as shown in Figures 4.1.3.29 and 4.1.3.29.

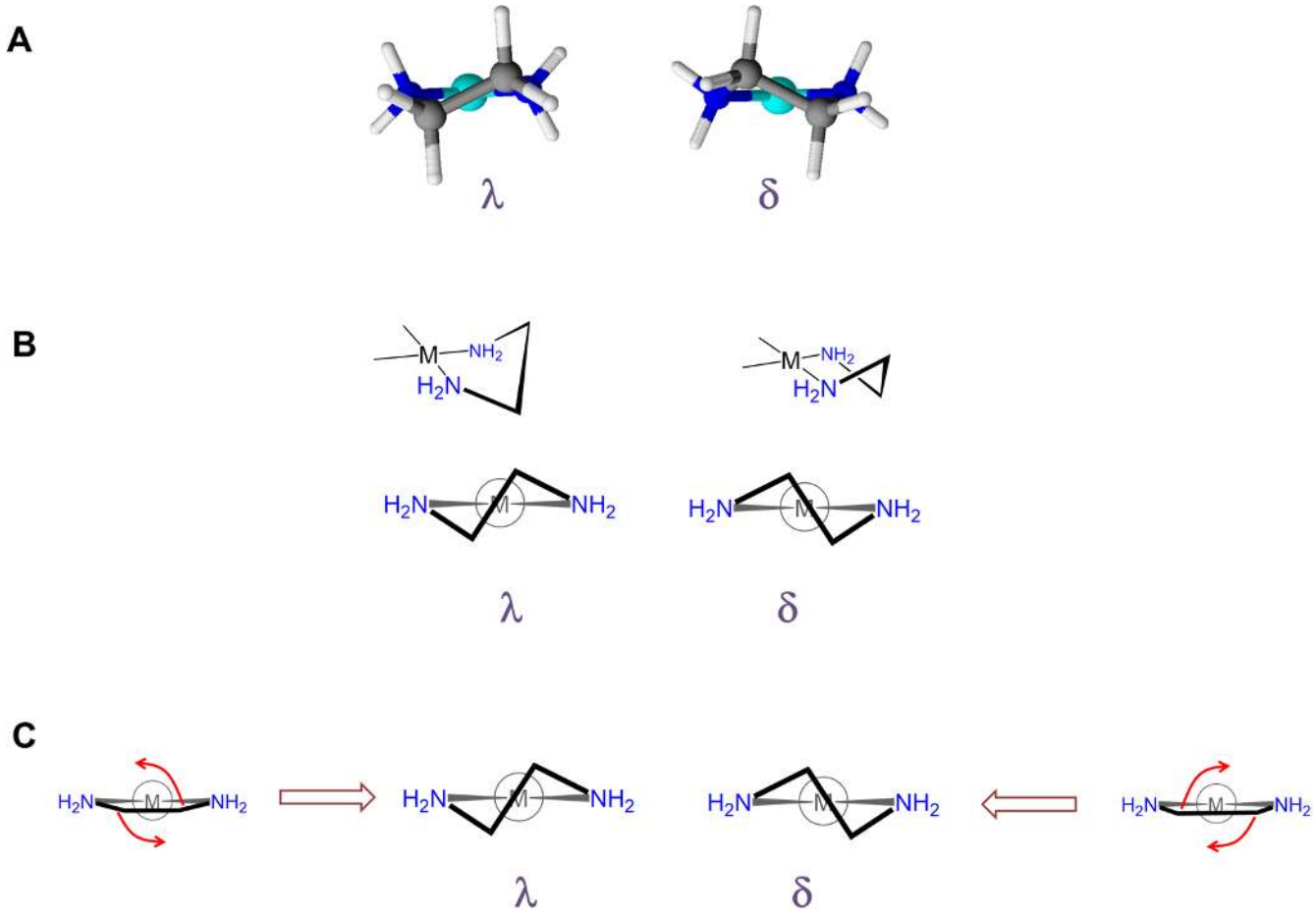


Figure **4.1.3.29**. (A) **λ** and ***δ*** ring twist in a square planar metal ethylenediamine complex (B) along with several ways to represent it in line drawing form. (C) Of these, the projection looking down an axis bisecting the chelate ring makes it easiest to see that, starting with a planar chelate ring the **λ** conformer corresponds to a counterclockwise twist of the CH_2CH_2 bond relative to the N-M-N plane and the ***δ*** conformer a clockwise twist relative to the N-M-N plane. This work by Stephen Contakes is licensed under a Creative Commons Attribution 4.0 International License.

The relative stability of the **λ** and ***δ*** conformers will depend on the configuration of any stereocenters present and steric factors. As with organic ring systems, steric effects tend to favor conformers in which bulky groups are placed in the less sterically strained equatorial positions while the configuration of the stereocenters present can serve to restrict the allowable ring twist conformations, as illustrated in Figure **4.1.3.30**. A detailed treatment of such systems is beyond the scope of this page. Interested readers are referred to reference 12 for more details.

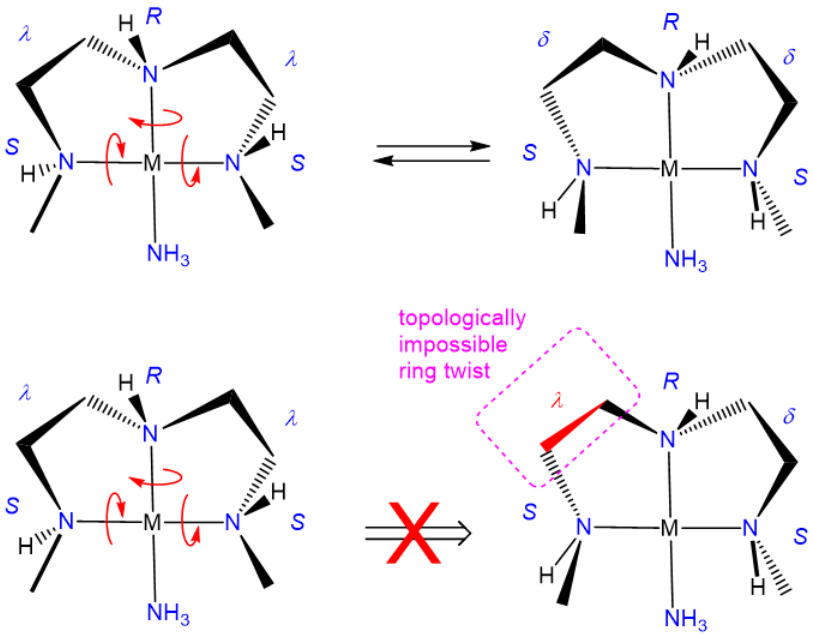


Figure 4.1.3.30. The configurations at nitrogen in the complex shown restrict the chelate ring conformations to either a λλ or δδ conformation because the rotations needed to enable a λδ configuration are topologically impossible. This work by Stephen Contakes is licensed under a Creative Commons Attribution 4.0 International License.

In closing, it should be noted that it might seem to be making much of small effects in pointing out that one source of diastereomerism in metal complexes involves the freezing out of chelate ring conformations. However, that would be to mistake the impacts that ring conformations can have on the steric accessibility of a coordination site and shaping the course of processes that might occur there. As illustrated in Figure 4.1.3.31, a simple shift in the conformation of one ring in a square planar, pyramidal, or octahedral complex containing coplanar ethylene diamine ligands can exert a significant effect on the steric profile of the complex perpendicular to the MN_4 square plane. Because of effects like these, ring conformation isomerism plays a role in the design of stereoselective transition metal catalysts.

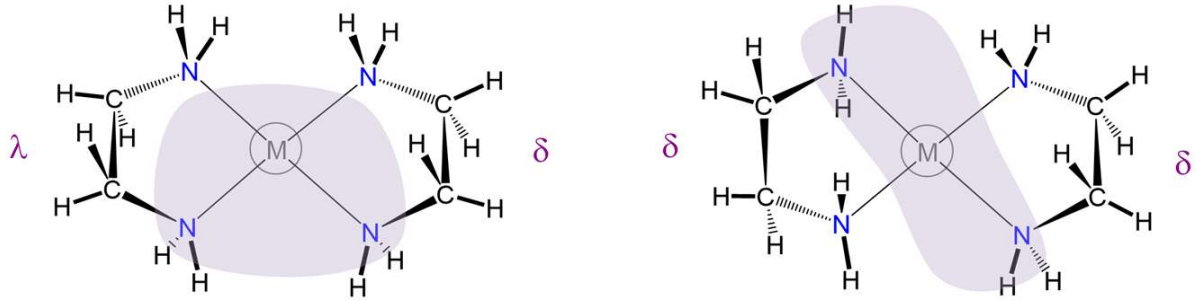


Figure 4.1.3.31. Schematic illustrating how the conformation of ethlyenediamine ligands bound to a metal center affects the steric accessibility of the metal (shown shaded in violet) to potential ligands attempting to bind from above the MN_4 plane. This work by Stephen Contakes is licensed under a Creative Commons Attribution 4.0 International License.

Exercises

? Exercise 4.1.3.1. Identify the type of isomerism

What type of isomers are

a. $[CoCl(NH_3)_5](NO_3)$ and $[Co(NH_3)_5(N\text{-}NO_2)]Cl$?
b. $[Co(NH_3)_5\text{-}CN\text{-}Ru(NH_3)_5]^{4+}$ and $[Co(NH_3)_5\text{-}NC\text{-}Ru(NH_3)_5]^{4+}$
c. $[Cr(CN)_5\text{-}CN\text{-}Co(NH_3)_5]$ and $[Co(CN)_5\text{-}CN\text{-}Cr(NH_3)_5]$
d. *cis*-$[Mn(en)_2(CN)_2]$ and *trans*-$[Mn(en)_2(CN)_2]$

Answer a.

Ionization isomers.

Answer b.

Linkage isomers.

Answer c.

Coordination isomers.

Answer d.

Geometric isomers, specifically *cis*/*trans* isomers.

? Exercise 4.1.3.2. Assigning metal oxidation states in a complex

Many properties of transition metal complexes depend on the metal's oxidation state. For instance,

- octahedral complexes of Co^{II} lose and gain ligands rapidly
- octahedral complexes of Co^{III} lose and gain ligands very slowly
- four-coordinate complexes are generally tetrahedral
- EXCEPT four-coordinate complexes of metals like Pt^{II} , Pd^{II} , Rh^{I}, and Ir^{I}, among others, are square planar

For this reason it is important to be able to estimate the formal oxidation state of a metal in a complex. Fortunately, this is easy to do if you remember

1. The sum of all atoms' oxidation states will equal the overall charge on the complex
2. When determining the metal's oxidation state, the ligands can be treated as having an oxidation state equal to their charge - *i.e.*, the charge they possess in the form in which they coordinate the metal - so if they need to lose a proton to bind, don't forget to account for that.

Given the above, estimate the oxidation state of the metal in the following real and hypothetical complexes.

a. $Na_4[Fe(CN)_6]$
b. $[Cu(phen)_2]BF_4$
c. $[PtF_4(NH_3)_2]$
d. $[Ni(en)_2]SO_4$
e. $Co(acac)_3$
f. [MnCl(O)(salen)]

Answer for $Na_4[Fe(CN)_6]$.

This contains $[Fe(CN)_6]^{4-}$; so $O.S._{Fe}$ + 6 x (-1) (for CN^-) = -4 (the complex's charge) so $O.S._{Fe}$ = +2 or Fe^{2+}.

Answer for $[Cu(phen)_2]BF_4$.

Since tetrafluoroborate is a monoanion, the complex is $[Cu(phen)_2]^+$ so $O.S._{Cu}$ + 0 x 2 (for phen) = +1 (the complex's charge) so $O.S._{Cu}$ = +1 or Cu^+.

Answer for $[PtF_4(NH_3)_2]$.

$O.S._{Pt}$ + 4 x (-1) (for F^-) + 0 x 2 (for NH_3) = +0 (the complex's charge) so $O.S._{Pt}$ = +4 or Pt^{4+}.

Answer $[Ni(en)_2]SO_4$.

The complex is $[Ni(en)_2]^+$ so $O.S._{Ni}$ + 0 x 2 (for en) = +2 (the complex's charge) so $O.S._{Ni}$ = +2 or Ni^{2+}.

Answer $Co(acac)_3$.

$O.S._{Co}$ + 3 x (-1) (for acac; see table 9.2.2) = +0 (the complex's charge) so $O.S._{Co}$ = +3 or Co^{3+}.

Answer [MnCl(O)(salen)].

$O.S._{Mn}$ + 1 x (-1) (for Cl^-) + 1 x (-2)(for oxo) + 1 x (-2) (for salen; see table 9.2.2) = +0 (the complex's charge) so $O.S._{Mn}$ = +5 or Mn^{5+}.

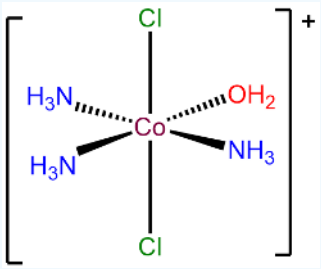
? Exercise 4.1.3.3. Drawing isomers from descriptions

Draw structures that match the descriptions given, assuming that

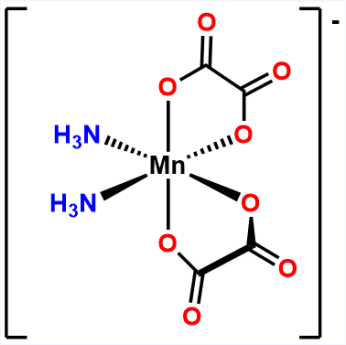
- complexes in which the metal has a coordination number of six are octahedral
- complexes in which the metal has a coordination number of five are trigonal bipyramidal
- complexes in which Pt^{II} , Pd^{II} , or Rh^{I}, or Ir^{I} have a coordination number of four are square planar
- other complexes in which the metal has a coordination number of four will be tetrahedral

a. *mer*-triammineaqua-*trans*-dichlorocobalt(III) ion
b. **Δ**-diaminebis(oxalato)manganate(III)
c. $[CoCl_4]^{2-}$
d. *trans*-diamminebis(ethylenediamine)Nickel(2+) tetracyanopalladate(2-)
e. **Λ**-bis(ethylenediamine)cobalt(III)- μ-amido μ-hydroxo-**Δ**-bis(ethylenediamine)cobalt(III)

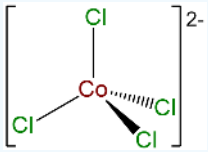
Answer a. *mer*-triammineaqua-*trans*-dichlorocobalt(III) ion.



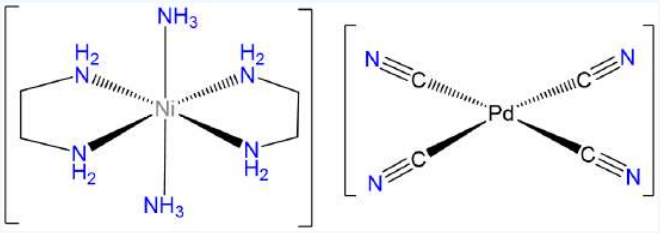
Answer b. Δ-diaminebis(oxalato)manganate(III).



Answer c. $[CoCl_4]^{2-}$.

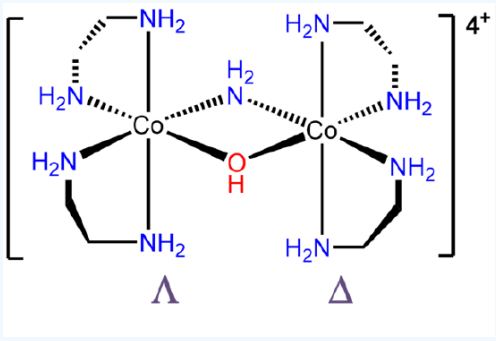


Answer d. *trans*-diamminebis(ethylenediamine)Nickel(2+) tetracyanopalladate(2-).



Note that since the Pd in $[Pd(CN)_4]^{2-}$ is Pd^{2+} it will be square planar.

Answer e. Λ-bis(ethylenediamine)cobalt(III)- μ-amido μ-hydroxo-Δ-bis(ethylenediamine)cobalt(III).



? Exercise 4.1.3.4. Stereoisomers of complexes containing only monodentate ligands.

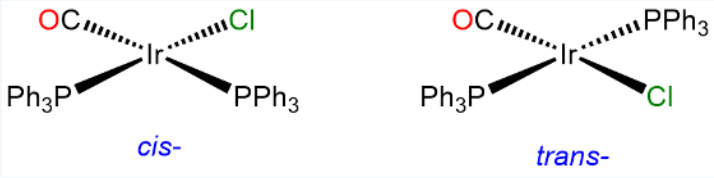
Draw all the stereoisomers of the following real and hypothetical complexes. You may assume that

- complexes in which the metal has a coordination number of six are octahedral
- complexes in which the metal has a coordination number of five are trigonal bipyramidal
- complexes in which Pt^{II} , Pd^{II} , or Rh^{I}, or Ir^{I} have a coordination number of four are square planar
- other complexes in which the metal has a coordination number of four will be tetrahedral

a. $[IrCl(CO)(PPh_3)_2]$
b. $[CoCl_3(NH_3)_3]$
c. $[CoCl_2(H_2O)_2(NH_3)_2]^+$
d. $[CoBrCl(H_2O)_2(NH_3)_2]^+$
e. $[CoBrClI(NH_3)_3]$

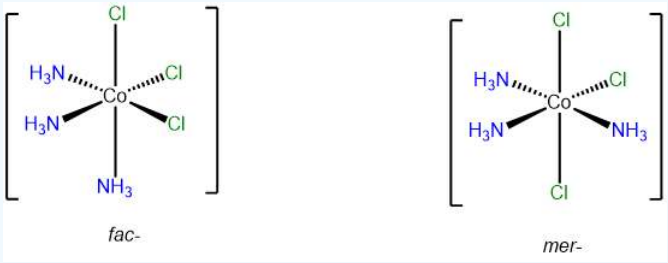
Answer a. $[IrCl(CO)(PPh_3)_2]$

This is a 4-coordinate Ir^{I} complex and, as such will be square planar. Since two of the ligands are identical, it will have *cis* and *trans* isomers. The *trans* isomer is famous for its ability to form adducts and is called Vaska's complex.



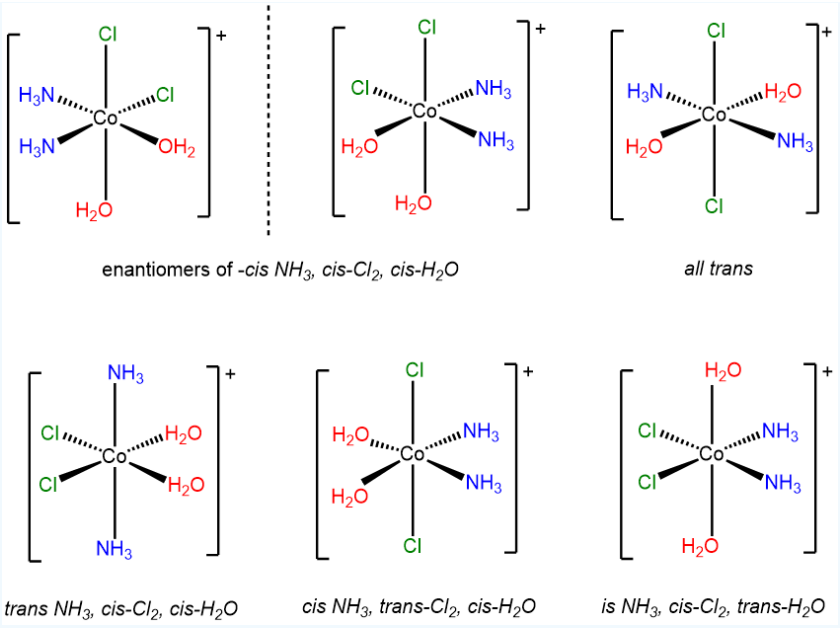
Answer b. $[CoCl_3(NH_3)_3]$

This complex contains three ammine and three chloro ligands and so will have *fac* and *mer* isomers.



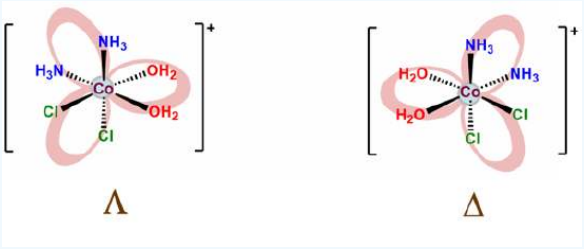
Answer c. $[CoCl_2(H_2O)_2(NH_3)_2]^+$

This is a case of an $MA_2B_2C_2$ system (A = Cl^-, B = H_2O, C = NH_3) involving multiple *cis* and *trans* relationships. The six stereoisomers are shown below.



Since it may not be obvious how to arrive at a set of isomers like the ones above, it is worth considering how one might work through the possibilities for a system of ligands like this one. Several systems may be used to systematically identify isomers. Once approach is the Macbdef system described in Note **4.1.3.1** at the end of these exercises. The solutions presented here and in subsequent problems employ a variant of that approach.

- Start by fixing one set of ligands. In this case the chloro ligands were first fixed as *cis* to one another. Then the remaining ligands might be *cis* or *trans* to one another, although since the *chloro* ligands are already *cis*, the ammine and aqua ligands cannot both be *trans* at the same time. Thus for *cis* chloro ligands the possibilities for the others are:
  - *cis*-H_2O ,*cis*-NH_3,
  - *cis*--H_2O, *trans*-NH_3
  - *trans*-H_2O, *cis*-NH_3
- Swap the configuration of the ligand set you started with. In this case it means placing the chloro ligands *trans* to one another. From that configuration, the possibilities for the ammine and aqua ligands are
  - *cis*-H_2O ,*cis*-NH_3,
  - *trans*-H_2O, *trans*-NH_3
- Check for enantiomers and create mirror images of any chiral complexes you drew. The easiest way to do this is to assign point groups. However, it turns out that the octahedral all-*cis* case is D_3 and formally equivalent to the symmetry of a tris chelate, as shown below.

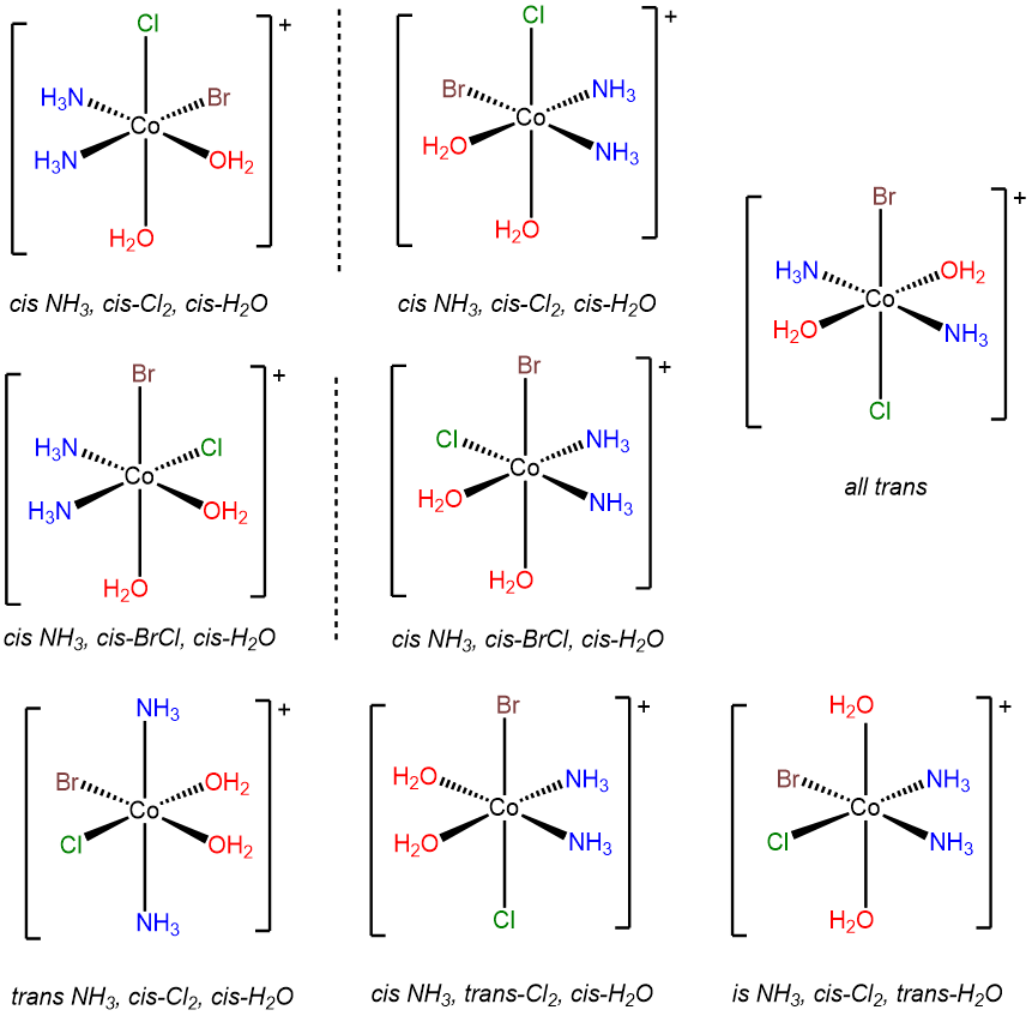


- finally, check to make sure you didn't include the same complex twice. Humans do make mistakes after all.

Answer d. $[CoBrCl(H_2O)_2(NH_3)_2]^+$

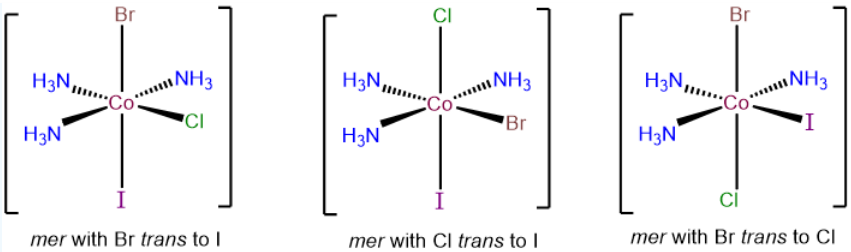
This problem is analogous to the one above except that this complex contains a bromo and chloro ligand in place of the two chloro ligands in $[CoCl_2(H_2O)_2(NH_3)_2]^+$. Consequently, when the bromo and chloro ligands are *cis* to one

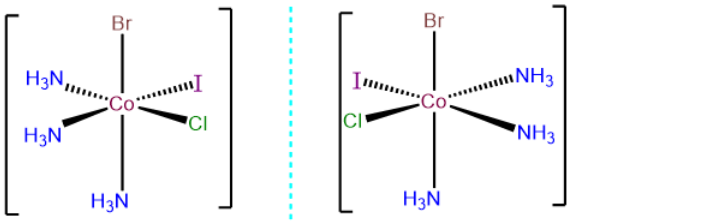
another, additional possibilities for isomers arise based on whether ammine or aqua ligands are *trans* to the chloro and bromo. The result is eight isomers.



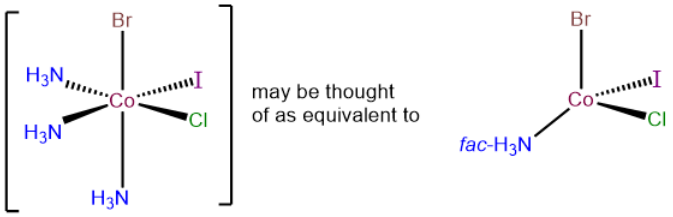
Answer e. [$CoBrClI(NH_3)_3$]

There are two possibilities for this complex - a *fac*-$(NH_3)_3$ and a *mer*-$(NH_3)_3$ arrangement. These may be taken as starting points for examining the possible permutations for the Cl^-, Br^-, and I^- ligands. The top row presents the three possibilities within the *mer*-$(NH_3)_3$ arrangement; each corresponds to a different ligand *trans* to an ammine ligand. The bottom row presents the two possible isomers with a *fac*-$(NH_3)_3$ arrangement. In each, the Cl^-, Br^-, and I^- ligands are *trans* to ammine ligands. However, the complexes possess C_1 symmetry and so are chiral and exist as enantiomers.





(C_1 symmetry or it you think of the *fac*-$(H_3N)_3$ as being "one uniform group" then the symmetry is equivalent to that of a chiral carbon)



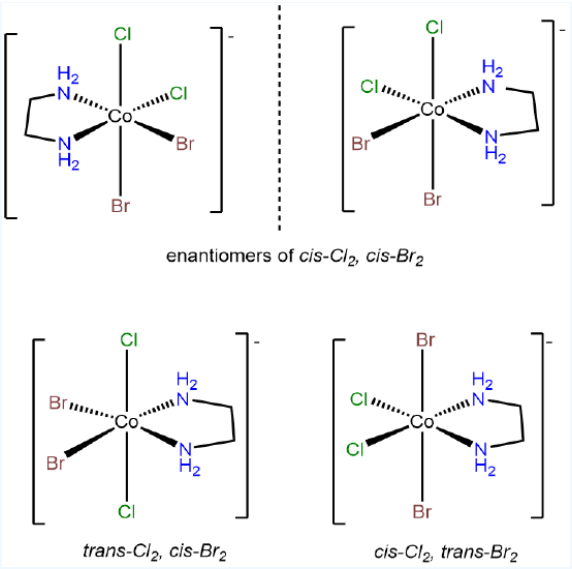
? Exercise 4.1.3.5. Stereoisomers of complexes with bidentate ligands (ignoring ring twist).

Ignoring ring twist, draw all the stereoisomers of the following real and hypothetical octahedral complexes.

a. $[CoBr_2Cl_2(en)]^-$
b. $[CoBrCl(en)_2]^+$
c. $[CoBrCl(gly)_2]^-$
d. $[Co(en)_3]^{3+}$
e. $[Co(gly)_3]$

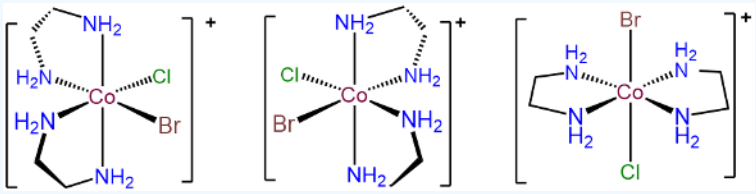
Answer a. $[CoBr_2Cl_2(en)]^-$

This complex is analogous to $[CoCl_2(H_2O)_2(NH_3)_2]^+$ in possessing pairs of identical ligating groups. The main difference is that in $[CoBr_2Cl_2(en)]^-$ the two amine ligating group of the en ligand are restricted to a *cis* arrangement. Under the MABCDEF system explained in Note **4.1.3.1**, $[CoCl_2(H_2O)_2(NH_3)_2]^+$ may be $MA_2B_2C_2$, but this complex, $[CoBr_2Cl_2(en)]^-$, is $M(AA)B_2C_2$. The isomers are:



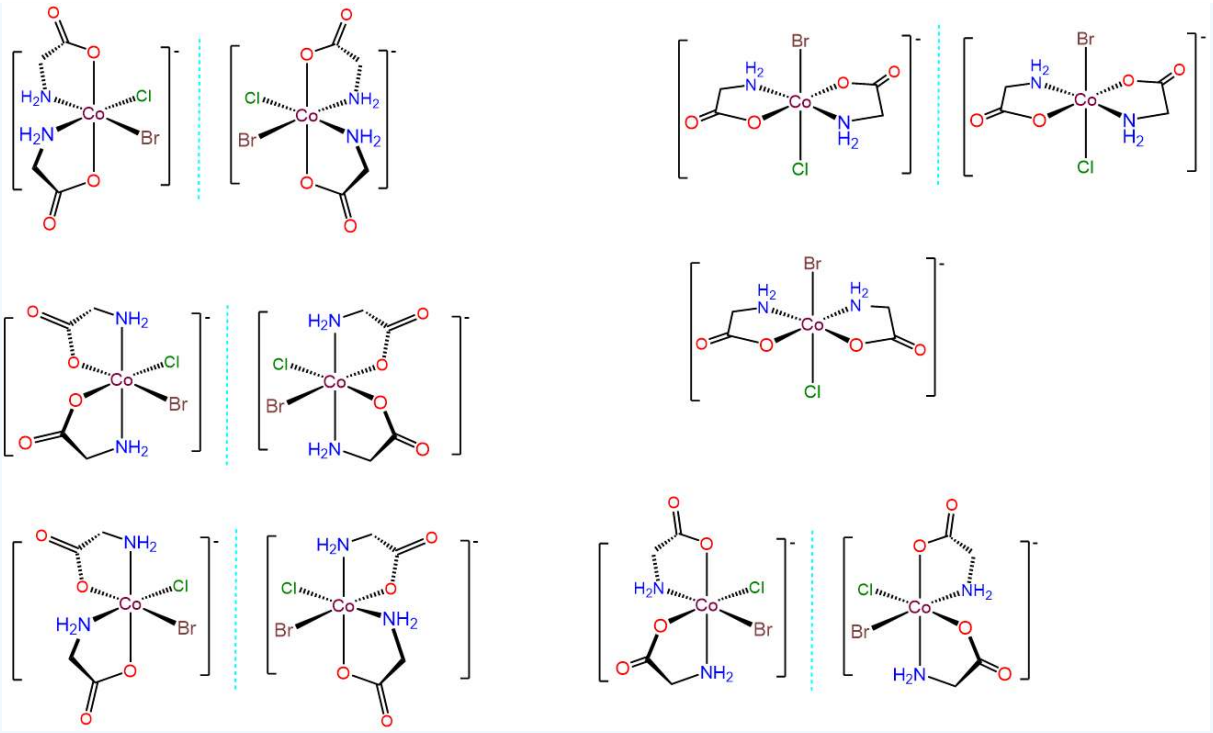
Answer b. $[CoBrCl(en)_2]^+$

The key to problems like this is to focus on the unique ligands, in this case Br^- and Cl^-. These can exist in either a *cis* or *trans* arrangement. The *trans* form is achiral, but in the case where Br^- and Cl^- are *cis*, **Λ** and **Δ** enantiomers are possible. The result is three isomers.



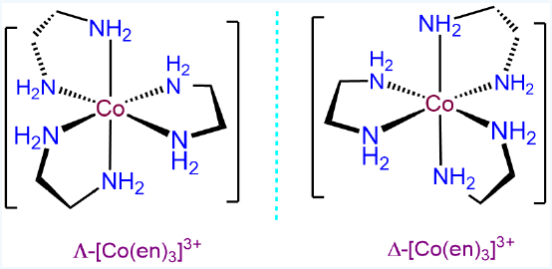
Answer c. $[CoBrCl(gly)_2]^-$

This case is analogous to the one above, but this time the bidentate ligand, gly, possesses distinguishable binding sites. Thus there are additional permutations involving how the gly ligands are bound relative to one another and/or whether the O or N end of the gly is bound *trans* to Br or Cl. The result is 11 different isomers, which are given below.



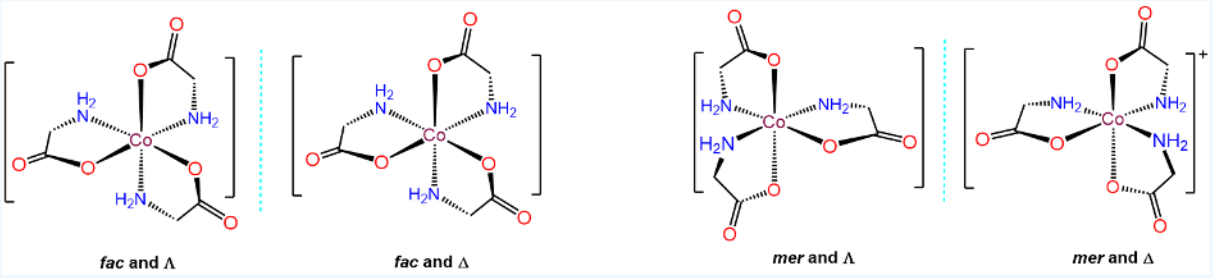
Answer d. $[Co(en)_3]^{3+}$

As a tris-chelate of symmetric bidentate ligands, ignoring ring twist, $[Co(en)_3]^{3+}$ will only exhibit **Λ** and **Δ** isomerism.



Answer e. $[Co(gly)_3]$

Since there are three gly ligands, each of which have carboxy and amine ends, the allowable arrangements involve whether the resulting three carboxy and three amine ends are oriented in a *mer* or *fac* arrangement. This gives two possibilities, each of which can exist as either the **Λ** or **Δ** enantiomer, for a total of four isomers, which are given below.



? Exercise 4.1.3.6. More stereoisomers: Now featuring linkage isomerism

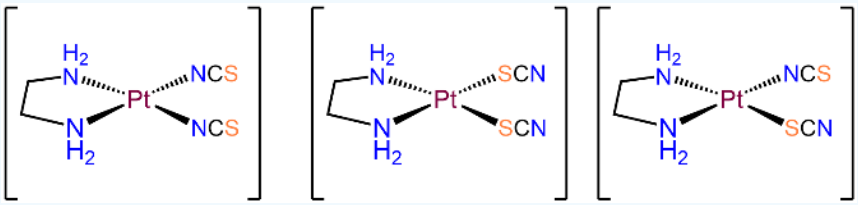
Ignoring ring twist, draw all chemically reasonable stereoisomers for the following real and hypothetical complexes. You may assume that

- complexes in which the metal has a coordination number of six are octahedral
- complexes in which the metal has a coordination number of five are trigonal bipyramidal
- complexes in which Pt^{II} , Pd^{II} , or Rh^{I}, or Ir^{I} have a coordination number of four are square planar
- other complexes in which the metal has a coordination number of four will be tetrahedral

a. $[Pt(en)(SCN)_2]$
b. $[Pt(NH_3)_2(SCN)_2]$
c. $[Co(en)_2(SCN)_2]^+$

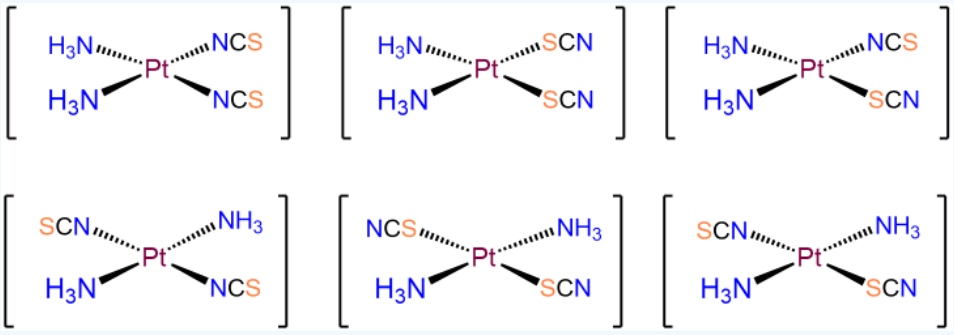
Answer a. $[Pt(en)(SCN)_2]$

The Pt in this neutral complex must be Pt^{2+} to balance the negative charges of the two SCN^- ligands. Complexes of Pt^{2+} are square planar and four coordinate, consistent with the bidentate en and two thiocyanato ligands. Of the ligands, the en ligand must bind in a *cis* arrangement. Consequently, the two SCN^- ligands will be in a *cis* arrangement as well. The isomers will therefore only differ in whether the two SCN^- bind κN or κS. The possibilities are:

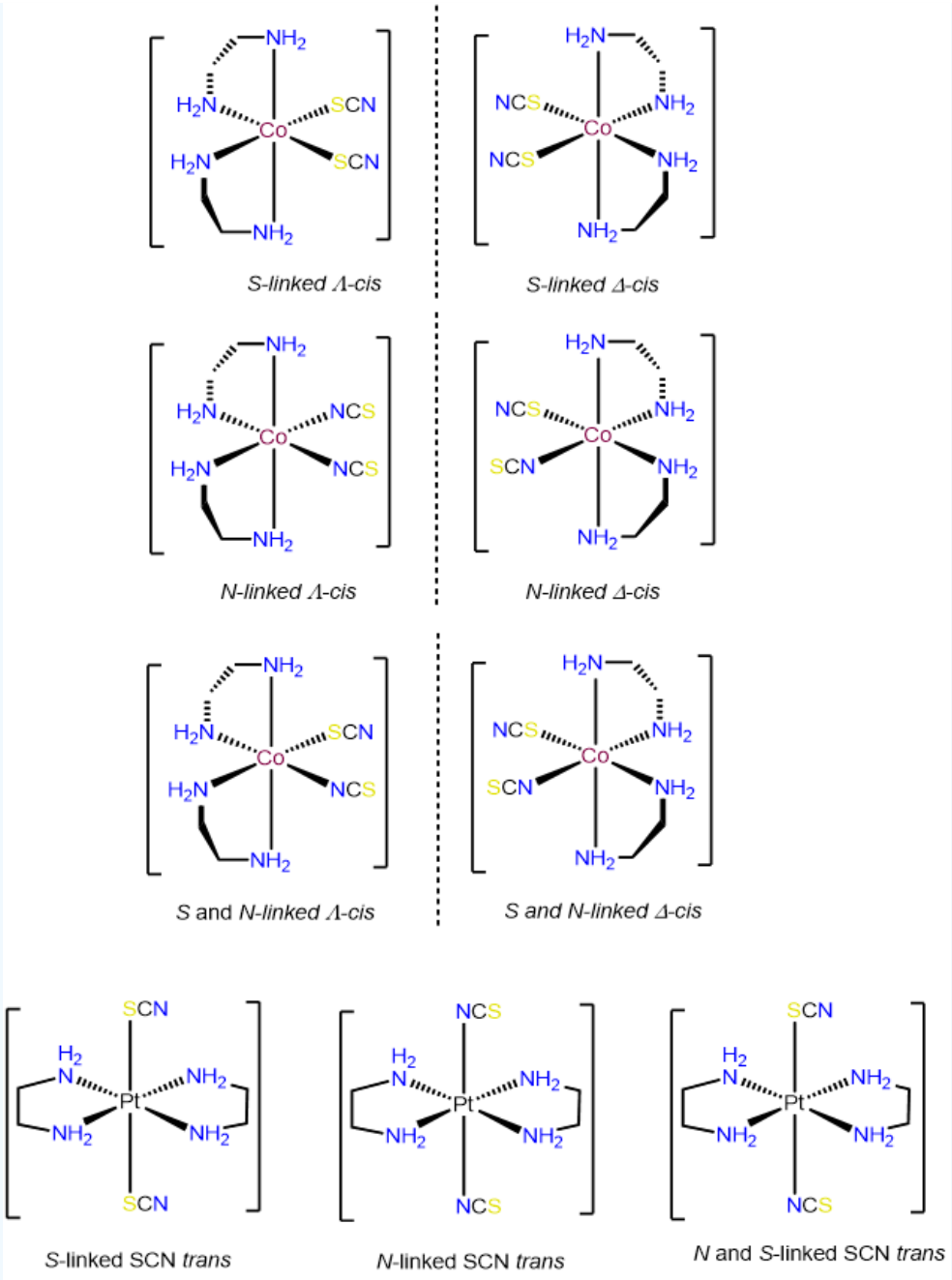


Answer b. $[Pt(NH_3)_2(SCN)_2]$

As with the preceding example, this will be a square planar Pt^{2+} complex. The main difference is that this time the coordinated nitrogens are not constrained to adopt a *cis* arrangement so there will be both *cis* and *trans* isomers.



Answer c. $[Co(en)_2(SCN)_2]^+$



? Exercise 4.1.3.7. Stereoisomer free for all.

Ignoring ring twist, draw all chemically reasonable stereoisomers for the following real and hypothetical complexes. You may assume that

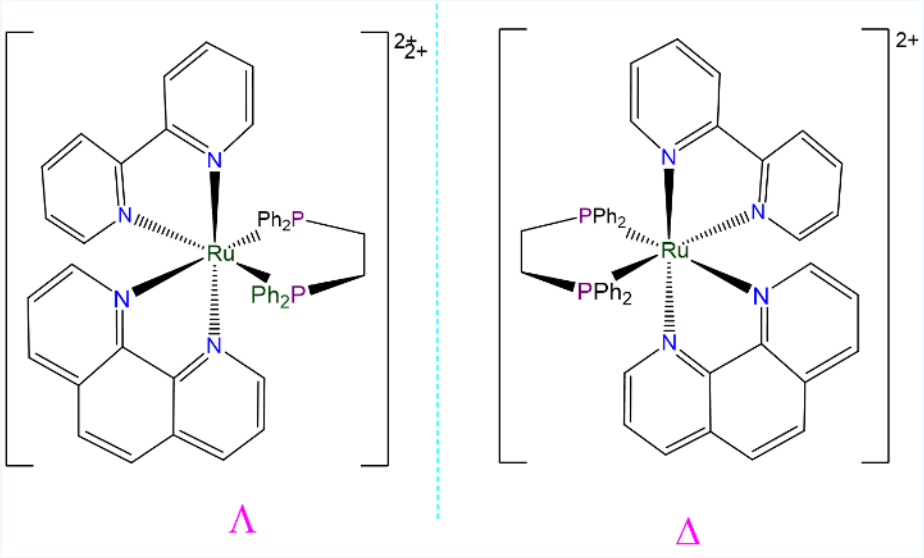
- complexes in which the metal has a coordination number of six are octahedral
- complexes in which the metal has a coordination number of five are trigonal bipyramidal
- complexes in which Pt^{II} , Pd^{II} , or Rh^{I}, or Ir^{I} have a coordination number of four are square planar
- other complexes in which the metal has a coordination number of four will be tetrahedral

a. $[Ru(bpy)(phen)(dppe)]^{2+}$
b. $[CoClF(PPh_3)(py)]^{-}$
c. $[Ni(en)_2(NO_2)_2]$

d. $[Fe(H_2O)_3(SCN)_3]$
e. $[PtClF(PPh_3)(py)]$
f. $[CoBr_2Cl(NH_3)_3]$

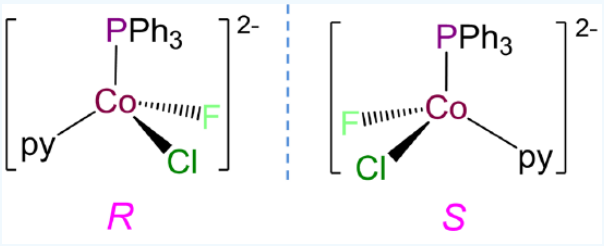
Answer a. $[Ru(bpy)(phen)(dppe)]^{2+}$

This complex is an octahedral tris-chelate containing symmetric ligands. As such it will exhibit **Λ** and **Δ** isomers:



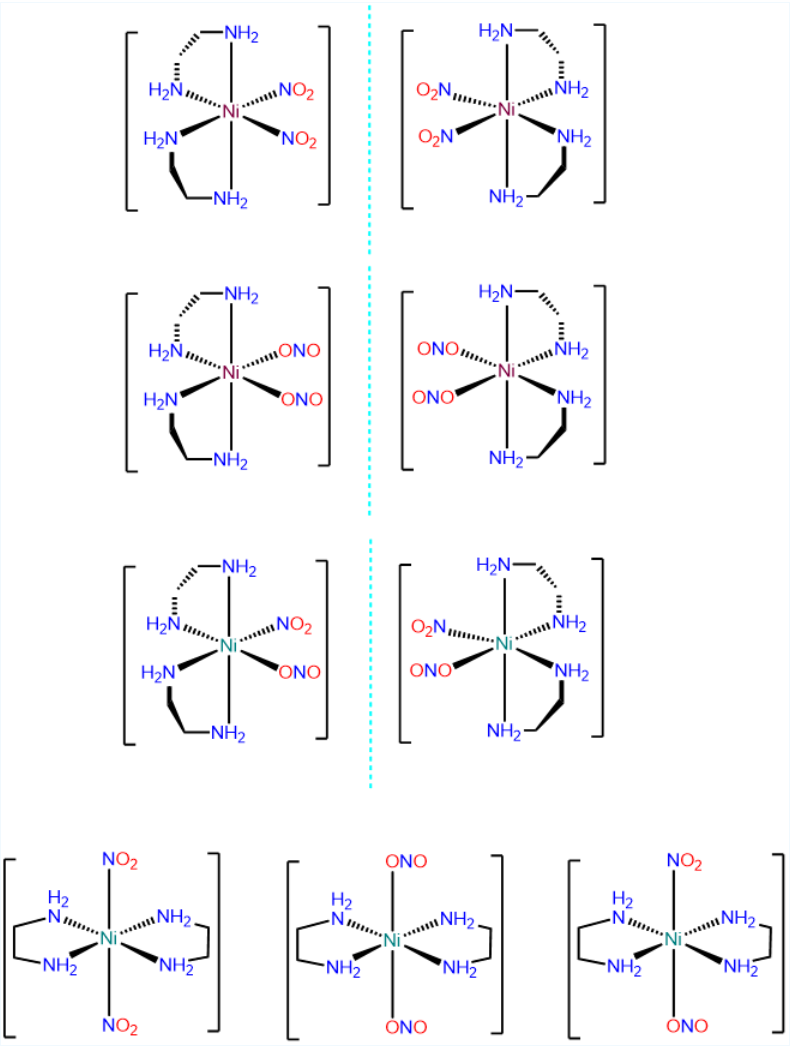
Answer b. $[CoClF(PPh_3)(py)]^-$

This complex has a coordination number of 4 and contains a Co^{2+} ion with a d^7 electron configuration, so a tetrahedral geometry is expected. Tetrahedral complexes like this one with four different ligands are chiral and can form *R* and *S* enantiomers.



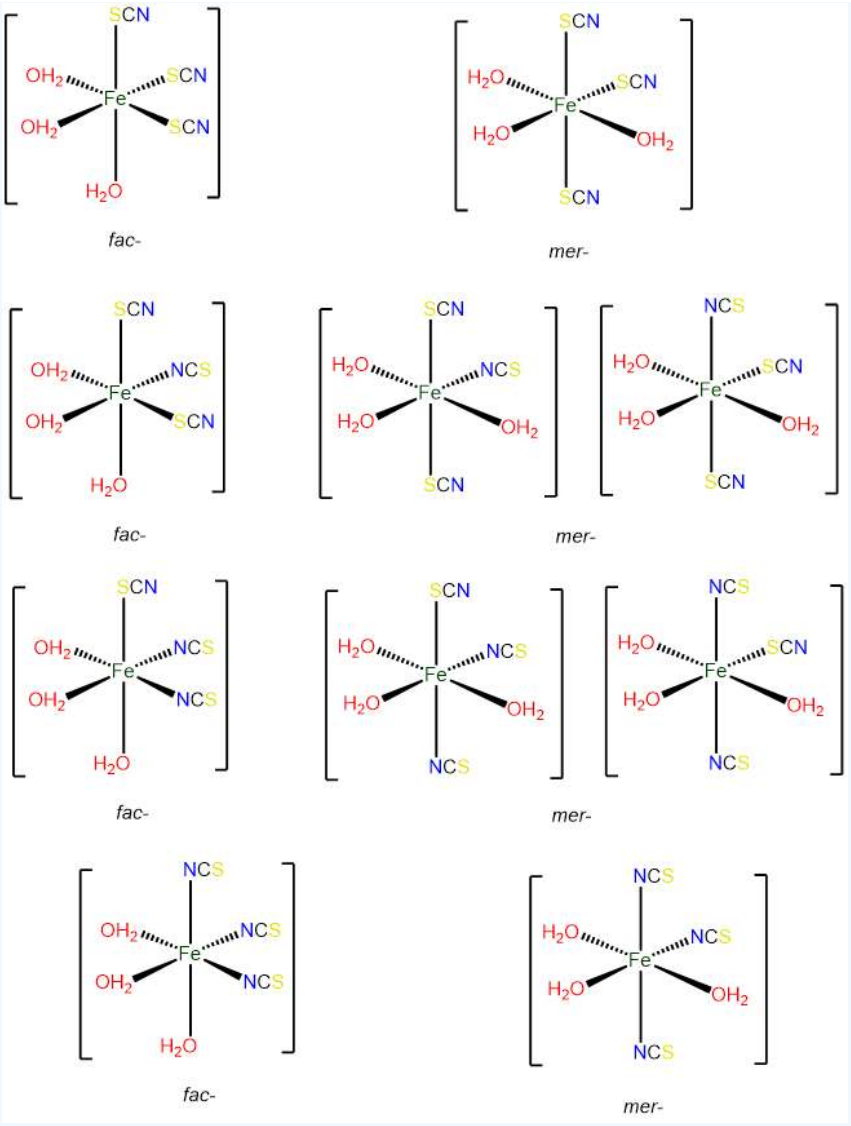
Answer c. $[Ni(en)_2(NO_2)_2]$

This is an octahedral bis-chelate and will exist in **Λ** and **Δ** configurations. Within each configuration the NO_2^- ligands can exist as ***κN*** and ***κO***, leading to the following possibilities:



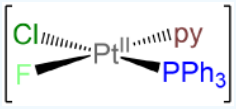
Answer d. $[Fe(H_2O)_3(SCN)_3]$

As an octahedral complex with three identical ligands it can exist in *mer* and *fac* configurations, with the ambidentate SCN ligand providing additional possibilities for isomerism.



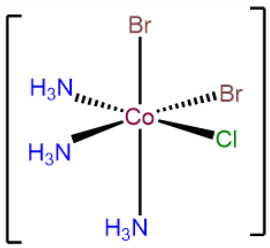
Answer e. [PtClF(PPh$_3$)(py)]

As a square planar complex with four nonidentical ligands, this complex exists as a single isomer.

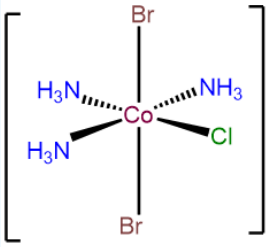


Answer f. [CoBr$_2$Cl(NH$_3$)$_3$]

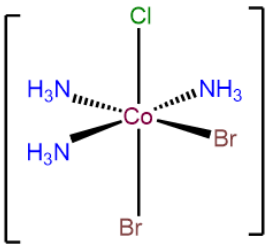
As an octahedral complex with three identical ligands it will exhibit *mer* and *fac* isomerism. In addition, it will have two *mer* configurations that differ in terms of the cis and trans relationships between the bromo and chloro ligands.



fac



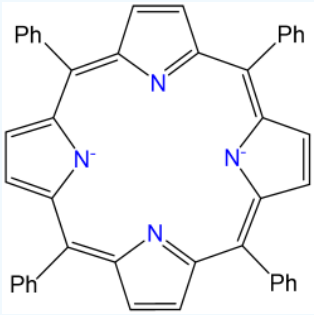
mer with Br *trans* to Br



mer with Cl *trans* to Br

Exercise 4.1.3.8

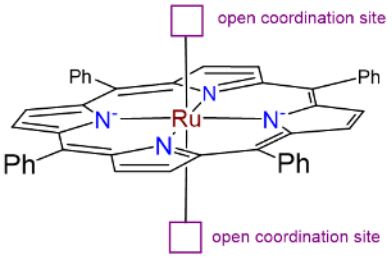
Complexes of formula Ru(TPP)py_2 have been prepared, in which TPP is tetraphenylporphyrin, which binds metals in the form given below. Draw all isomers of Ru(TPP)py_2.

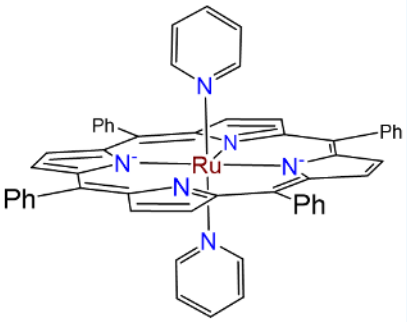


Answer

There is only one isomer. While normally complexes containing two identical ligands (in this case py) can exhibit *cis* and *trans* isomerism, in this case the planar tetraphenylporphyrin ring ligates the Ru^{2+} ion in a square planar arrangement, as shown at left in the image below. This leaves only a pair of *trans* coordination sites for the chloro ligands to occupy, giving the isomer shown at right below.

When TPP ligates Ru^{2+} it leaves only *trans* open coordination sites so only the *trans* isomer can form.

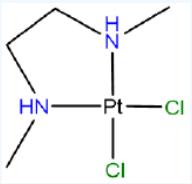




trans-[$Ru(py)_2(TPP)$]

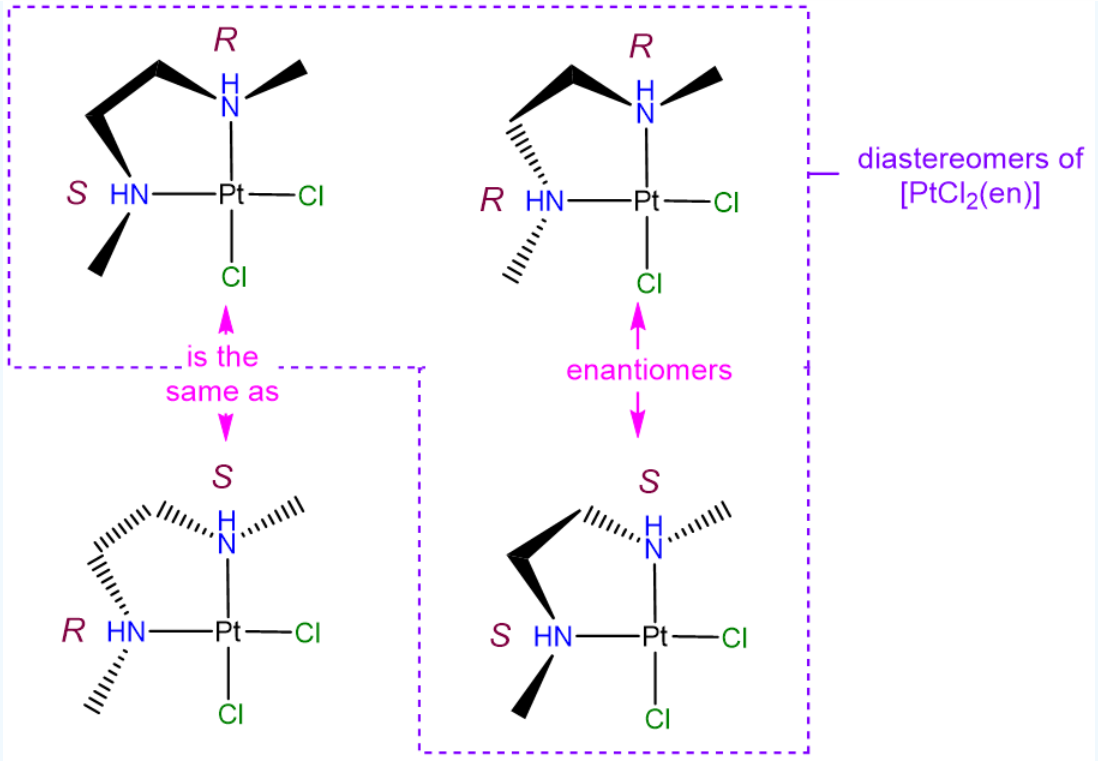
Exercise 4.1.3.9

Draw the diastereomers formed due to the chirality of the amine nitrogen atoms in [$PtCl_2$(*N*,*N*'-dimethylethane-1,2-diamine)] which has the atomic connectivity represented below



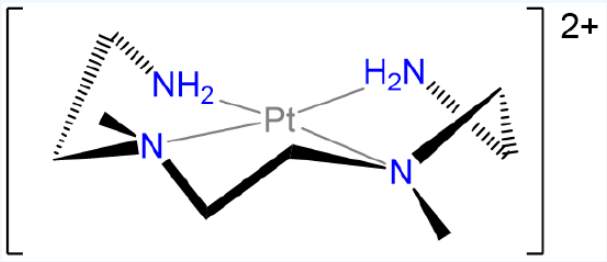
Answer

The diastereomers will differ in whether the N atoms adopt an *R* or *S* configuration at the nitrogen atoms. The possible permutations are (*R*,*R*), (S,*S*), (*R*,*S*), and (S,*R*). However, as may be seen from the image below, the (*R*,*S*) and (S,*R*) configurations are identical (the two projections shown can be interconverted through a C_2 rotation along an axis bisecting the Cl-Pt-Cl unit). As a result there are only three unique isomers. Of these, the (*R*,*R*) and (S,*S*) configurations are enantiomers (they are mirror images by reflection in the $PtCl_2N_2$ plane). Note that in solving problems like this one it can be helpful to keep track of possible isomers by assigning the stereochemistry at each chiral center as *R* or *S* using the Cahn-Ingold-Prelog-convention, though it is not strictly necessary to do so.

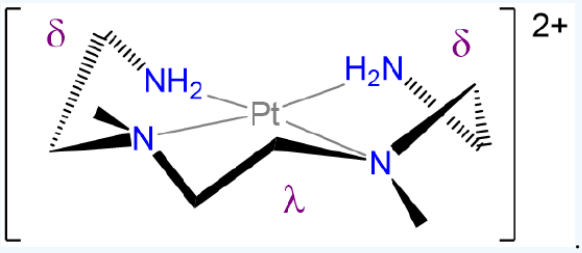


? Exercise 4.1.3.10

Label the conformations of all chelate rings in the structure below.



Answer



Appendix: The MABCDEF bookkeeping system for identifying isomers

The Mabcdef or MABCDEF system is one method for identifying the number of isomers in an octahedral complex, although since it is really just a bookkeeping and organizational system it can easily be extended to other geometries as well. The M in Mabcdef stands for metal and the other letters are used to stand in for ligands. The basic approach involves

- classifying the ligands as A, B, C, D, E, or F in order of multiplicity. Thus for

$[Cr(NH_3)_6]^{3+}$ A = NH_3; there are no B, C, D,E, or F ligands; and the complex is classified as MA_6

$[CoCl(NH_3)_5]^{2+}$ A = NH_3, B = Cl^-, and the complex is MA_5B

$[CrCl_2(H_2O)_2(NH_3)_2]^+$ A = Cl^-, B = H_2O, C = NH_3, and the complex is $MA_2B_2C_2$

- in the classification above, multidentate ligands are typically classified before monodentate ones and are designated AA, AB, ABC, ABA, etc. based on the symmetry of the attachment points. Thus

  en has identical attachment amine points and is AA

  gly has a carboxy and amine attachment points and is AB

  trien is ABA

  $CoCl_2(en)_2^+$ is $M(AA)_2B_2$

  $CoCl_2(gly)_2^-$ is $M(AB)_2C_2$

  $CoCl_2(en)(gly)$ is $M(AA)(AB)C_2$

- Systematically list out the possible *trans* arrangements of ligands by
  1. assigning one pair of ligands to be *trans* to one another.
  2. Then systematically list out the other possible *trans* pairs by permuting the remaining trans arrangements. It can help to organize the permutations in a table, such as that shown below for an MABCDEF complex where A and B are assigned *trans*. In looking at the table notice how the second set of trans permutations is systematically varied. This helps ensure that no possibility is skipped.
  3. Go through the list of isomers and remove any duplicates you generated so far. For instance, notice in the table below that the last three stereoisomers are identical with the first three (*e.g.*, stereoisomer 4 is identical to stereoisomer 3, 5 with 2, and 6 with 1).

Stereoisomer 1	Stereoisomer 2	Stereoisomer 3	Stereoisomer 4 (same as isomer 3)	Stereoisomer 5 (same as isomer 2)	Stereoisomer 6 (same as isomer 1)
trans AB (fixed)	*trans* AB (fixed)	*trans* AB (fixed)	*trans* AB (fixed)	*trans* AB (fixed)	*trans* AB (fixed)
trans CD	*trans* CE	*trans* CF	*trans* DE	*trans* DF	*trans* EF
trans EF	*trans* DF	*trans* DE	*trans* CF	*trans* CE	*trans* CD

  4. If the complex possesses multidentate ligands that demand that certain groups exist and *cis* pairs, then also remove any configurations which do not agree with the known binding capability of the ligand (*e.g.*, the two amine groups of ethylenediamine cannot be *trans* to one another, so if you have an en ligand, remove configurations like that from the list).

5. Next, swap or permute the original *trans* pair and repeat the process you just followed. In the case of Mabcdef this gives the following results:

Isomer	"fixed" trans pair	Additional trans pairs	
1	AB	CD	EF
2	AB	CE	DF
3	AB	CF	DE
4	AC	BD	EF
5	AC	BE	BF
6	AC	BF	DE
7	AD	BC	EF
8	AD	BE	CF
9	AD	BF	CE
10	AE	BC	DF
11	AE	BD	CF
12	AE	BF	CD
13	AF	BC	DE
14	AF	BD	CE
15	AF	BE	CD

- Since the procedure explained above only identifies isomers based on unique *trans* pairings, **it does not identify when a configuration is chiral and corresponds to a pair of enantiomers.** Any enantiomers can be identified by drawing out the complexes and either classifying their point groups or by drawing their mirror images and checking if they are superimposable. In the MABCDEF case - *i.e.*, where all the ligands are different - all of the isomers identified have C_1 symmetry so are chiral. This means there will be a pair of enantiomers for each, giving 15 x 2 = 30 different stereoisomers.

References

1. These examples are taken from http://wwwchem.uwimona.edu.jm/courses/inorgnom.html

2. Contakes S. M.; Rauchfuss, T.B. *Chem. Commun.* 2001, 553-554.

3. Shriver, D. F.; Shriver, S. A.; Anderson, S. E., *Inorg. Chem.* 1965, *4(5)*, 725-730.

4. Zelewsky, A. v., *Stereochemistry of Coordination Compounds* Wiley, 1996.

5. In the past it was difficult to determine absolute configurations from X-ray data alone, but recent advances have made it easier to do so.

6. Pavan M. V. Raja & Andrew R. Barron "Circular Dichroism Spectroscopy and its Application for Determination of Secondary Structure of Optically Active Species" in *Physical Methods in Chemistry and Nano Science* https://chem.libretexts.org/Bookshelves/Analytical_Chemistry/Book%3A_Physical_Methods_in_Chemistry_and_Nano_Science_(Barron)/07%3A_Molecular_and_Solid_State_Structure/7.07%3A_Circular_Dichroism_Spectroscopy_and_its_Application_for_Determination_of_Secondary_Structure_of_Optically_Active_Species

7. Berova, N.; Bari, L. D.; Pescitelli, G., *Chemical Society Reviews* 2007, 36 (6), 914-931.

8. Of course, if one set of ligands occupies a meridional plane, then the other three ligands will be oriented in an equatorial one. The reason they may both be considered meridional is because if the complex were rotated, the equatorial plane would be meridional and vice versa. From that point of view both might be considered meridional planes - albeit not at the same time.

9. Bite angles are taken from Mansell, S. M., Catalytic applications of small bite-angle diphosphorus ligands with single-atom linkers. Dalton Transactions 2017, 46 (44), 15157-15174.

10. Hancock, R. D., The pyridyl group in ligand design for selective metal ion complexation and sensing. Chemical Society Reviews 2013, 42 (4), 1500-1524.

11. Sasi, D.; Ramkumar, V.; Murthy, N. N., Bite-Angle-Regulated Coordination Geometries: Tetrahedral and Trigonal Bipyramidal in Ni(II) with Biphenyl-Appended (2-Pyridyl)alkylamine N,N'-Bidentate Ligands. ACS Omega 2017, 2 (6), 2474-2481.

12. Ehnbom, A.; Ghosh, S. K.; Lewis, K. G.; Gladysz, J. A., Octahedral Werner complexes with substituted ethylenediamine ligands: a stereochemical primer for a historic series of compounds now emerging as a modern family of catalysts. Chemical Society Reviews 2016, 45 (24), 6799-6811.

4.1.3: Isomerism is shared under a not declared license and was authored, remixed, and/or curated by LibreTexts.

- **9.4: Isomerism** by Stephen M. Contakes is licensed CC BY 4.0.

4.1.4: Coordination Numbers and Structures

Why do coordination complexes form the structures they do?

As with all chemical structure, coordination complexes form the structures they do so as to best stabilize the metal center and ligands through the formation of metal-ligand bonds while avoiding destabilizing interactions like steric repulsions. The issue then is how many metal-ligand bonds should be formed and how those bonds should be arranged spatially to give the largest net stabilization possible. This question will eventually be considered in detail in connection with the nature of bonding in coordination compounds. For now, it will be helpful to think about it in terms of seven factors:

The stabilizing effect of metal-ligand bond formation.

The driving force for complex formation is the stabilization of electrons in covalent chemical bonds. In the vast majority of cases, this largely involves stabilization of the ligand lone pair as it experiences the effective nuclear charge of the metal, although a few instances involve stabilization of metal electrons by ligand nuclei (inverse ligand fields). Regardless, metal-ligand bond formation is stabilizing and classified by the way it preferences the addition of ligands to the complex.

Steric effects, specifically steric repulsions between ligands.

One reason coordination numbers do not increase indefinitely is that only so many ligands can fit around a metal. Exactly how many depends on

- *the size of the metal center.* This is one of the more important factors. Many metals tend to exhibit preferred coordination numbers, which depend on their oxidation state and size as shown in Figure **4.1.4.1**. Larger inner transition metals like the Lanthanides and Actinides can accommodate 9-12 sterically undemanding ligands, while the smaller transition metals tend to accommodate up to six, although larger coordination numbers are more common for low valent metals and as size increases on moving from right to left across the transition metal block of the periodic table. Thus, the early transition metal molybdenum forms seven- and eight-coordinate $[Mo^{III}(CN)_7]^{4-}$ and $[Mo^{IV}(CN)_8]^{4-}$ with the sterically undemanding cyano ligand.
- *the size of the ligands.* As long as ligands are not excessively rigid and bulky, their size is less important than the size of the metal in determining the number of ligands that coordinate. Ligands' ability to donate electrons to the metal center also tends to influence coordination number more than ligand size. However, all other things being equal for a given metal and ligand donor ability, small ligands allow higher coordination numbers while fewer bulky ligands will fit around the metal center.
- *how the ligand bonds to the metal.* Again, all other things being equal, ligands that are more sterically demanding in the vicinity of the metal center tend to limit the ability of other ligands to bind more than those which bind through a small extended group. For example, a bulky isocyanide like t-BuCN will sterically crowd the metal less than a bulky phosphine like t-BuH_2P would. For this reason the effective size of a ligand is sometimes rated in terms of either a cone angle of space they are estimated to occupy around the metal (called the Tolman cone angle, it is commonly used to evaluate phosphines' steric bulk) or in terms of the percentage of the metal's coordination sphere the ligand occupies (called the percent buried volume, it is used to estimate the steric impact of *N*-heterocyclic carbenes).

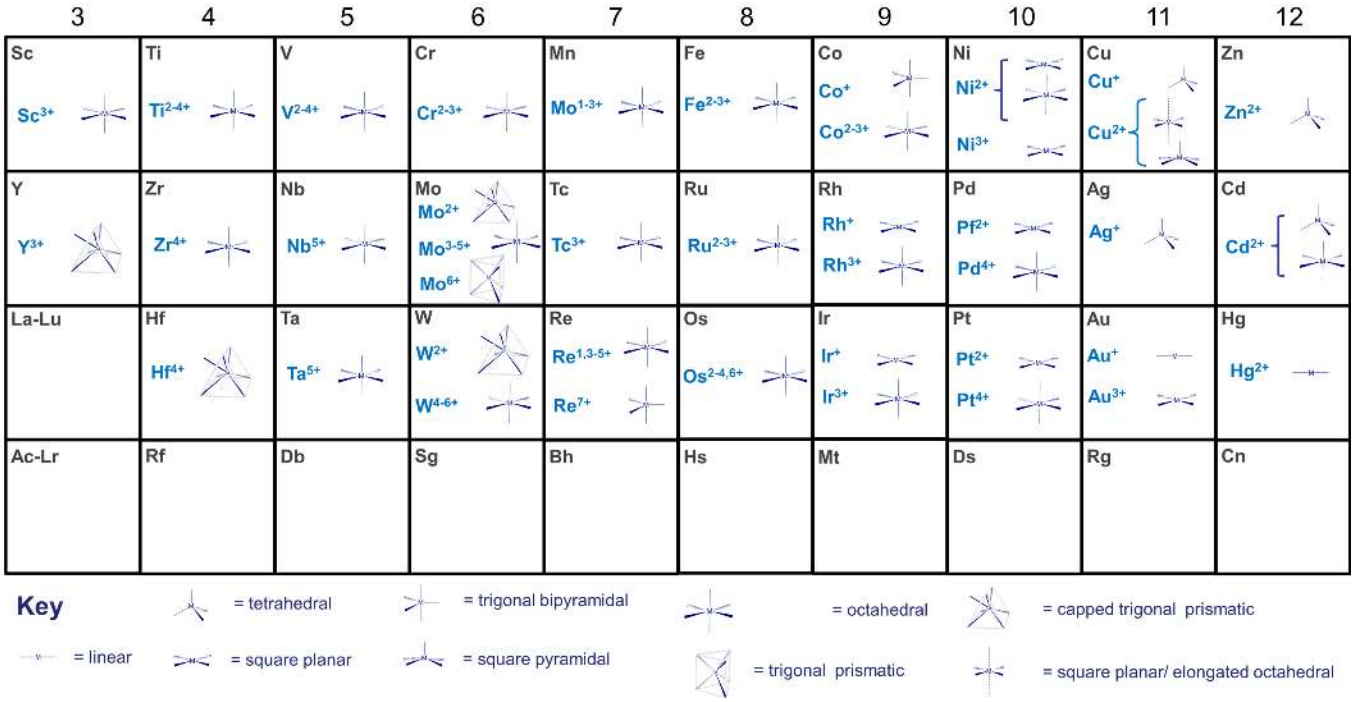


Figure **4.1.4.1**. Preferred coordination geometries of the transition elements. Assignments are as reported in reference 1 except for Cu^{2+}, which is assigned above as square planar/elongated octahedral instead of the square planar assignment given in that work. This work by Stephen Contakes is licensed under a Creative Commons Attribution 4.0 International License.

Repulsion between M-L bonding electrons on different ligands.

For many complexes, steric effects are neither the only effects nor the most important. Among the additional factors that should be considered are the repulsions that occur between the electrons that different ligands donate to the metal-ligand bonding. These electron-electron repulsions affect the

a. **Coordination number.** When a ligand donates its electrons to a metal center to form a new metal-ligand bond, the electron density around the metal increases, raising the overall energy of the other M-L bonding electrons. This increased repulsion often limits the number of coordinated ligands. As more ligands are added, the electron-electron repulsions keep increasing until the lowering of energy of the ligand electrons in the new bond is insufficient to compensate for the raising of energy of the existing M-L bonding electrons. Based on this effect alone,
   - larger metals tend to achieve higher coordination numbers than smaller ones because the electron-electron repulsions are spread across a larger coordination sphere.
   - With a given metal, ligands that are more electron donating have a greater tendency to form complexes with lower coordination numbers with a given metal than similar neutral ones do. This is why anionic ligands (which tend to be better electron donors) tend to give lower coordination numbers than comparable neutral ligands (which tend to be weaker donors). Thus Co^{2+} forms $CoCl_4^{2-}$ with chloro ligands but $[Co(H_2O)_6]^{2+}$ with aqua ligands.

b. **Coordination geometry.** In the **Kepert model** for the shapes of coordination complexes, this intraligand repulsion determines the most stable coordination geometry by causing the ligands to move as far apart from one another on the metal's coordination sphere as possible.

Formally, according to the **Kepert model**

- any of the metal's valence electrons not involved in metal-ligand bonds occupy (n-1)*d* orbitals and function as core electrons. As core electrons they do not influence the molecular shape.
- electrons involved in bonding to a given ligand constitute an electron group that repels all other electron groups around the metal.
- all other things being equal, the complex will form the geometry that maximizes the intra-electron group repulsions.

Notice the similarities of these postulates to those of VSEPR theory. In predicting coordination geometries in terms of electron-electron repulsions, the Kepert model is just an extension of VSEPR theory to coordination compounds. The difference between VSEPR theory and the Kepert model is that in the Kepert model, only electrons involved in metal-ligand bonds count.

Coordination geometries predicted by the Kepert model for coordination numbers two through nine are given in Figure **4.1.4.2**. As may be seen from the geometries listed in Figure **4.1.4.2**, these are just equivalent to VSEPR geometries for cases in which the number of electron groups is equal to the coordination number.

The difference between optimal and suboptimal coordination geometries is greater with few ligands, and becomes smaller as ligands become increasingly dispersed across the metal's coordination sphere. In complexes containing five, seven, eight, or higher coordinate metals, there are a number of geometries that are similar in energy to the preferred geometry. These geometries, which should be regarded as accessible, are also listed in Figure **4.1.4.2**.

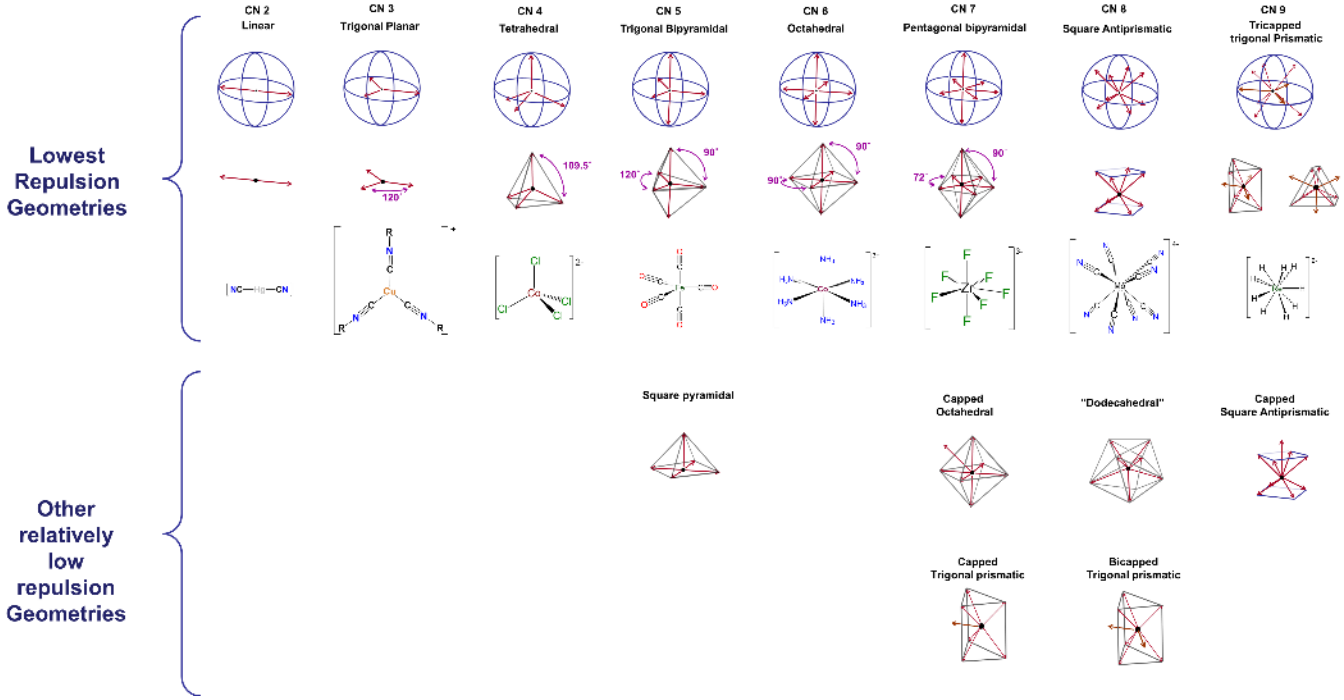


Figure **4.1.4.2**. Coordination geometries predicted by the Kepert model for coordination numbers two through nine along with other coordination geometries similar in energy to the lowest repulsion geometry. This work by Stephen Contakes is licensed under a Creative Commons Attribution 4.0 International License.

d-electron effects

A few coordination geometries are noticeably absent from the Kepert-preferred and Kepert-accessible geometries in Figure **4.1.4.1**. These include the trigonal prismatic geometries formed by compounds like $W(CH_3)_6$ and the very common square planar geometry illustrated by complexes like $[PtCl_4]^{2-}$ and $[IrClH(PPh_3)_2]$. One of the reasons the Kepert model fails to predict the existence of such structures is its neglect of directional interactions involving *d* electrons on the metal center. Metal *d* electrons exert a profound influence on almost all properties of transition metal complexes, including their structures. The way in which this occurs will be explored at length in the next chapter. For now, it is enough to note that both the ligand-donated electrons surrounding a metal center and the electrons occupying particular *d* orbitals on that metal are oriented in specific directions relative to one another. Because of this, the strength of the interactions between the ligand and metal *d* electrons depends on the number of *d* electrons present, how strongly metal-ligand binding affects their energy, and how the ligands are arranged about the metal center. The impact of these effects, here termed ligand field effects, differs from case to case and can include

- distortions of the complex's geometry. For instance, an ideal octahedral coordination geoemtry might be tetragonally distorted by flattening or elongating it.
- imparting a strong preference for non-Kepert coordination geometries. This is why, for example, 2nd and 3rd row complexes in which the metal has a d^8 electron configuration are almost always square planar.

- stabilizing non-Kepert geometries enough to permit complexes to adopt them in the presence of a rigid or semirigid ligand that prefers to coordinate the metal in that geometry.[3]

Because of these effects, square planar and trigonal prismatic geometries are also observed, and the list of coordination geometries given in Figure **4.1.4.2** may be extended to that shown in Figure **4.1.4.3**.

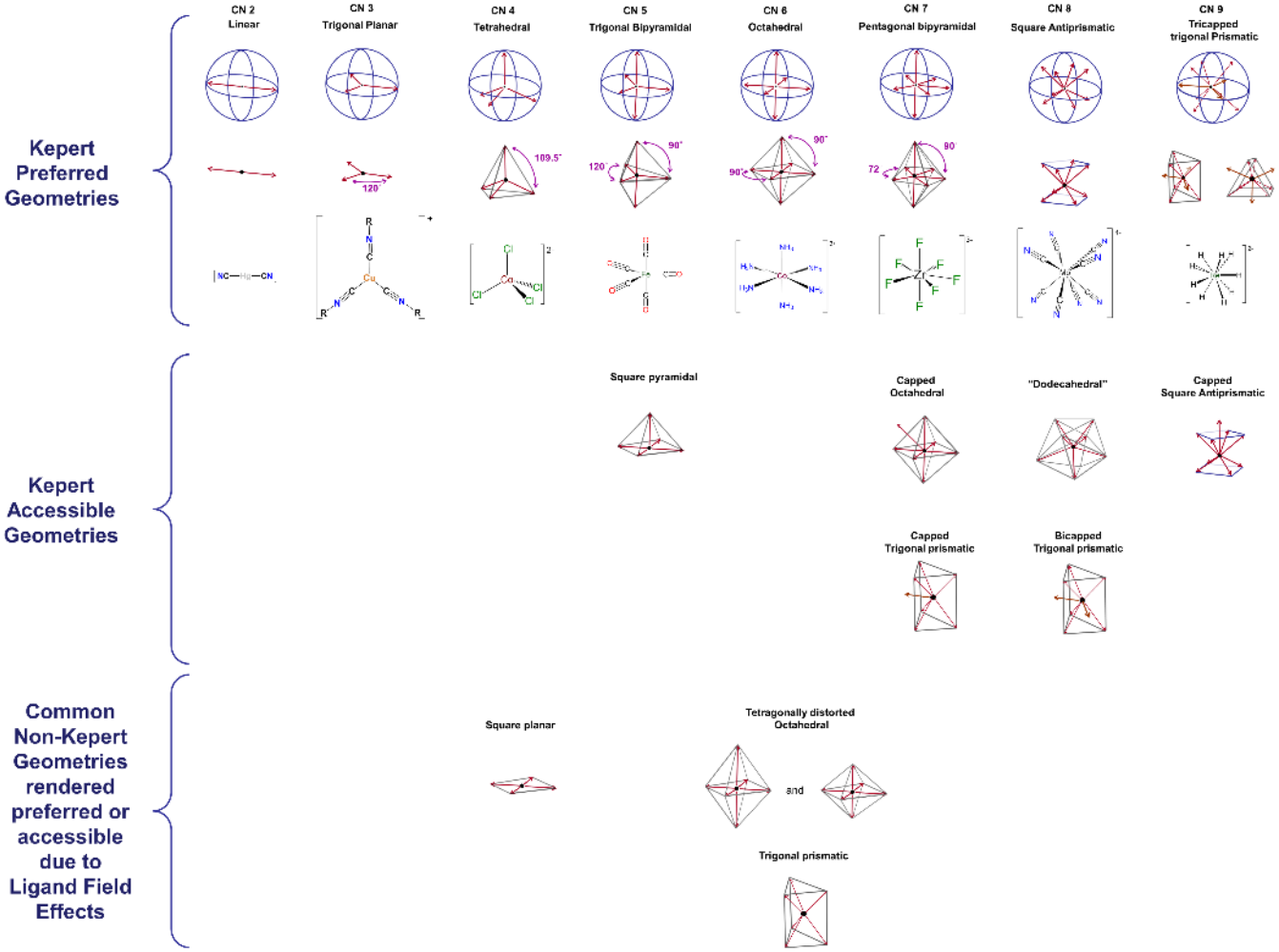


Figure **4.1.4.3**. Coordination geometries accessible for 2-9 coordinate complexes even without constraint by rigid or semirigid ligands. This work by Stephen Contakes is licensed under a Creative Commons Attribution 4.0 International License.

Ligand constraints imposed by rigid or semirigid ligands

Rigid or semirigid ligands influence the coordination geometry of metal complexes in two main ways:

a. Bulky rigid ligands that crowd the metal center prevent other ligands from binding. Thus such ligands are useful for preparing low-coordinate complexes.
b. Rigid and semirigid ligands can impose their preferred coordination geometry on a metal center. This is because these ligands energetically prefer to adopt a particular conformation when they bind a metal center. In doing so they shift the coordination geometry energy landscape toward that preferred geometry. If the shift is large enough relative to the native preference due to ligand repulsion and ligand field effects, the complex will either adopt the ligand-preferred geometry or be distorted in the direction of the ligand-preferred geometry. Examples are given in Figure **4.1.4.4**.

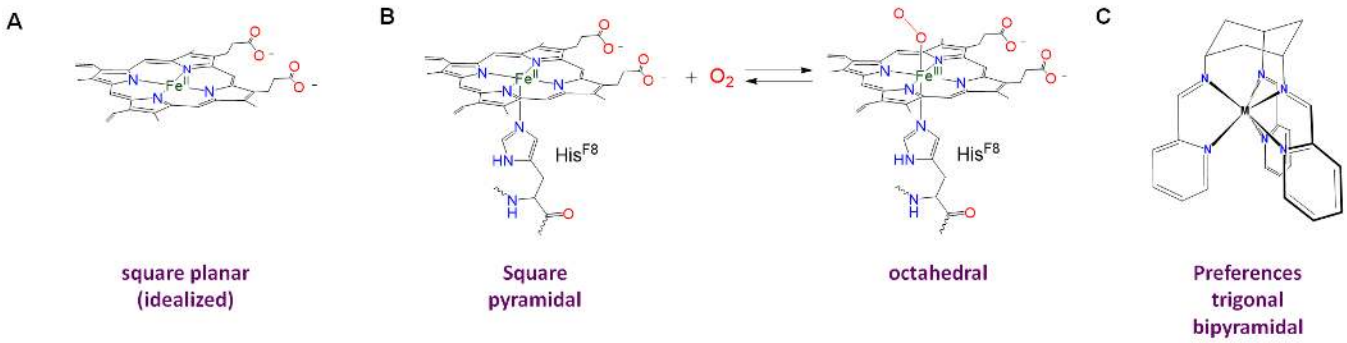


Figure **4.1.4.4**. Examples of rigid/semirigid ligands that can impose their preferred coordination geometry on a metal center. Porphyrins, phyhalocyanines and related macrocycles tend to impose a slightly bent square planar coordination geometry, although (B) many such complexes, including the iron of myoglobin's heme cofactor, coordinate additional ligands to give square planar or octahedral complexes. (C) Synthetic multidentate ligands have been developed to preference trigonal prismatic coordination geometries, including the one shown here. It forms roughly trigonal prismatic complexes with Co^{II} and $Zn^{II,}$ albeit imperfect ones.[3] This work by Stephen Contakes is licensed under a Creative Commons Attribution 4.0 International License.

The influence of ligands on coordination geometry is important in living systems, in which proteins and nucleic acids can act as rigid or semirigid ligands. The ability of these ligands to distort the coordination geometries of metal atoms in ways that enable them to perform specific functions is so common that the resulting distorted geometries are termed entactic states. A particularly spectacular case of an entactic state involves the blue copper proteins azurin and plastocyanin, the structure of which is given in Figure **4.1.4.5**.

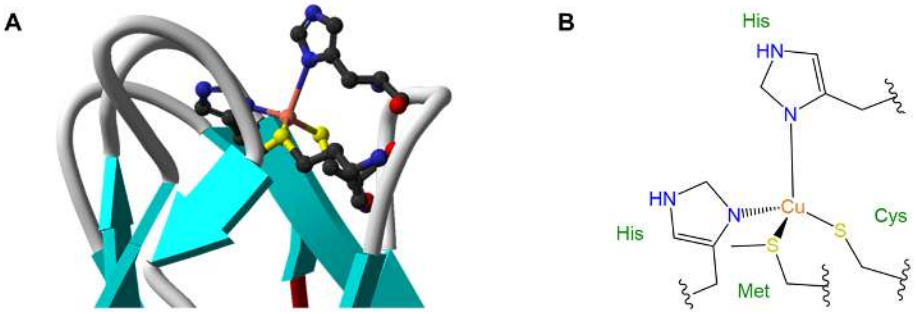


Figure **4.1.4.5**. (A) Structure and (B) schematic of the plastocyanin active site showing the distorted tetrahedral coordination environment that the protein imposes on the copper center (tan), which is most evident from the long vertically oriented Cu-Histidine bond. The image in part A is cropped from an original image by Ben Mills - Own work, Public Domain, https://commons.wikimedia.org/w/inde...?curid=6202620. The image in part B is by Stephen Contakes and licensed under a Creative Commons Attribution 4.0 International License.

As may be seen from the structure in Figure **4.1.4.5**, the copper in plastocyanin exibits a distorted tetrahedral coordination geometry. The protein is said to act like a medieval torture device called a rack in stretching the metal into its distorted geometry. This distortion makes it easier for the copper center to undergo facile redox reactions, enabling it to better function as an electron carrier.

Crystal packing effects, in which the energy-lowering packing of molecules and ions in a crystal drives the distortion of a complex's structure away from what it would adopt in the gas phase or solution

This effect is similar to that of ligand constraints except that in this case it arises not from the structure internal to a ligand but out of the forces involves in maximizing the stabilization energy of a crystal. With lower coordination number complexes, packing effects can shift the conformations of flexible ligands but only give rise to very small distortions of the overall coordination geometry. Packing effects can drive a shift in the overall coordination geometry of higher coordination number complexes, for which packing effects are significant relative to the small difference in energy between geometries. Thus while $[Mo(CN)_8]^{4-}$ has a square antiprismatic coordination geometry, in solution it exhibits a dodecahedral coordination geometry in the crystals of many of its salts.

Relativistic effects on orbital energies

The proximity of fast moving electrons to massive nuclei in the heavier transition elements results in relativistic expansion and contraction of orbitals. The net results are that

- heavier elements tend to be smaller than expected. This effect preferences lower coordination numbers.
- the relative energies of orbitals shift. Orbitals which become contracted are lowered in energy while those which are expanded increase in energy, as shown for the case of gold in Figure **4.1.4.6A**.

The combination of smaller sizes and altered orbital energies affects coordination preferences. Relativistic effects contribute to the greater tendency of Au^{I} relative to other group 11 metals to form linear two-coordinate complexes. As shown in Figure **4.1.4.6B**, the relative closeness in energy of the 6*s* and 5*d* orbitals of gold makes mixing of these orbitals more favorable, facilitating the ability of gold to form two-coordinate complexes with strong sigma bonds oriented 180/(^{\circ}\) from one another.

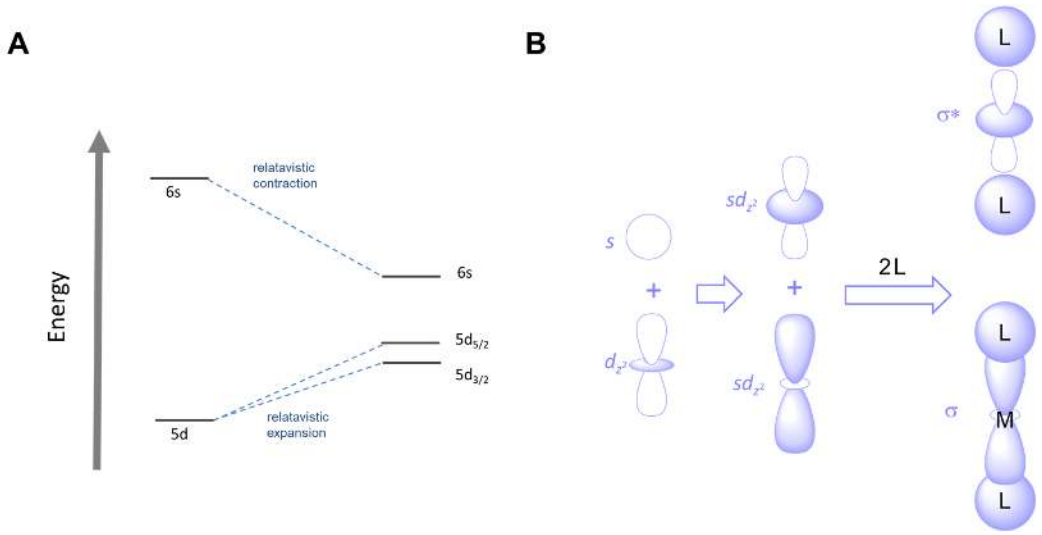


Figure **4.1.4.6**. (A) Gold experiences relativistic expansion and contraction of its 5*d* and 6*s* orbitals, resulting in shifts to their relative energies. (B) This makes mixing of these orbitals more favorable, facilitating the ability of gold to form two-coordinate complexes with strong sigma bonds that involve considerable sd_{z^2} character. This work by Stephen Contakes is licensed under a Creative Commons Attribution 4.0 International License.

What structures do coordination complexes form?

Metal complexes with coordination numbers ranging from one to 16 are known, although values greater than seven are rare for the transition metals. In this section, examples of common coordination geometries will be presented in order of coordination number.

Coordination Number 1.

Condensed phase monocoordinate complexes are unknown for the transition metals, although the post-transition metals Tl and In form monocoordinate complexes with the bulky ligands triazapentadienyl and 2,6-tris(2,4,6-triisopropylphenyl)benzene as shown in Figure **4.1.4.7**.

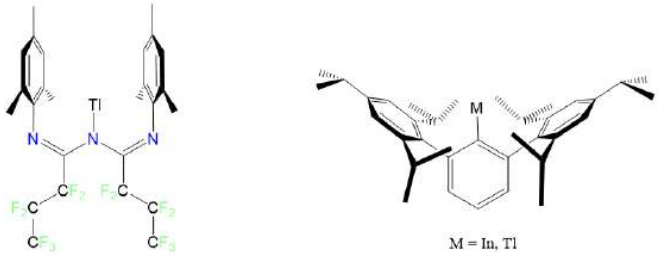
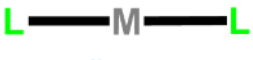


Figure **4.1.4.7**. No monocoordinate transition metal complexes are known, but Tl^{+} and In^{+} form monocoordinate complexes with extremely bulky ligands. This work by Stephen Contakes is licensed under a Creative Commons Attribution 4.0 International License.

Coordination Number 2.

A coordination number of 2 is rare outside of ***d*^{10} complexes of the group 11 metals and mercury**, specifically, Cu^+, Ag^+, Au^+, and Hg^{2+}. In accordance with the predictions of the Kepert model these give **linear complexes.**



linear

Among these,

- Cu^+ more commonly gives tetrahedral complexes but can be coaxed to give linear ones. The most prominent example is $[CuCl_2]^-$, which forms when CuCl is treated with concentrated HCl under anerobic conditions.
- Ag^+ also commonly forms tetrahedral or trigonal planar complexes but can give linear ones. The most prominent example is $[Ag(NH_3)_2]^+$, which can be formed by treating silver slats with concentrated aqueous or liquid ammonia.
- Au^+ almost always forms linear complexes, but many of these formally two-coordinate complexes associate as depicted in Figure **4.1.4.8**. The ability of Au^+ to form linear complexes with cyanide is even used to selectively extract metallic gold from low grade ores. The stability of $[Au(CN)_2]^-$ means that the dissolution of metallic gold in aqueous cyanide is thermodynamically favorable under aerobic conditions.

$$4\ Au + 8\ CN^- + O_2 + 2\ H_2O \longrightarrow 4\ [Au(CN)_2]^- + 4\ OH^-$$

- Hg^{2+}, like Au^+, benefits from relativistic effects and more commonly forms two-coordinate complexes with a linear geometry. Among these is $[Hg(CN)_2]$. However, its preference for linearity is not as rigid as for Au^+, and so complexes with a variety of coordination geometries are known.

And by means of honorary mention, the mercury(I) ion, Hg_2^{2+}, forms linear complexes of the type L-Hg-Hg-L, although since Hg_2^{2+} is often considered as a single unit, these aren't always considered to be two-coordinate complexes.

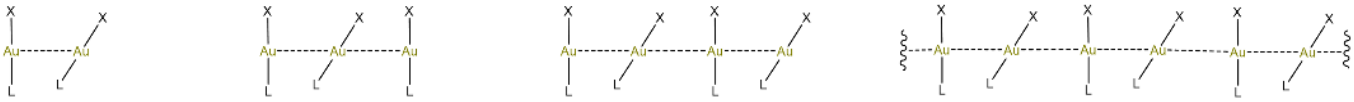
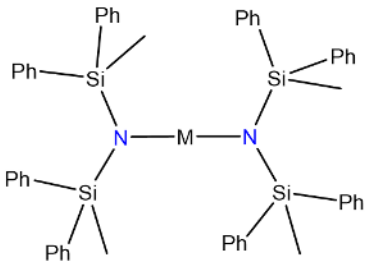


Figure **4.1.4.8**. Many "linear" gold complexes associate side-on to form dimers, trimers, tetramers, and chains. Although in this chapter L is usually taken to represent a generic ligand, in this scheme L represents a neutral ligand that donates two electrons to the metal (py, PR_3, CO, etc.) and X an anionic one (*e.g.*, Cl^-, CN^-, etc.). Exactly which structure forms depends on the identity of L and X. Redrawn from reference 5. This work by Stephen Contakes is licensed under a Creative Commons Attribution 4.0 International License.

Two-coordinate complexes may also be formed through the use of bulky ligands that only allow for the binding of two to the metal center. The classic examples are given in Figure **4.1.4.9**.



M = Mn, Fe, Co

Figure **4.1.4.9**. Two-coordinate complexes form between Mn^{2+}, Fe^{2+}, and Co^{2+} with $N(SiMePh_2)_2$.[6] This work by Stephen Contakes is licensed under a Creative Commons Attribution 4.0 International License.

Coordination Number 3

Three-coordinate complexes are similar to two-coordinate ones in that they are rare and, aside from the constraining influence of ligands, usually limited to d^{10} metal ions such as Cu^+ , Ag^+, Au^+, Hg^{2+}, and Pt(0). As expected from the Kepert model, in the absence of constraining ligands, three-coordinate complexes are trigonal planar.

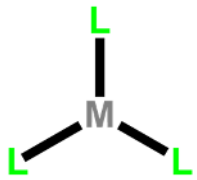


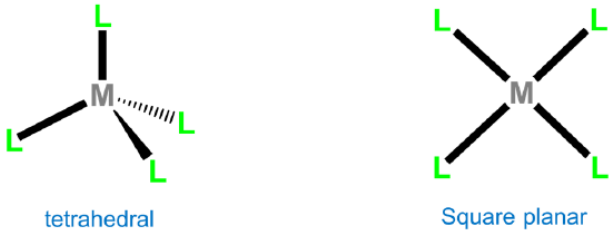
Figure **4.1.4.10**.



Figure **4.1.4.10**. Three-coordinate complexes prepared using bulky and semirigid ligands. This work by Stephen Contakes is licensed under a Creative Commons Attribution 4.0 International License.

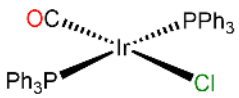
Coordination Number 4

The two common four-coordinate geometries are tetrahedral and square planar.



Tetrahedral complexes are commonly formed by metals possessing either a d^0 or d^{10} electron configuration. Monometallic examples of d^0 configurations include $TiCl_4$, VO_4^{3-}, WS_4^{2-}, MnO_4^-, CrO_4^{2-}, and OsO_4, while d^{10} examples are $[Ni(CO)_4]$, $[HgBr_4]^{2-}$, $[ZnCl_4]^{2-}$, and $[CdI_4]^{2-}$. For other electron configurations, tetrahedral complexes are known but much less common. Examples usually involve good donor ligands and include $[FeCl_4]^-$ (d^5), $[CoCl_4^{2-}]$ (d^6), and $[NiCl_4]^{2-}$ (d^7).

Second and third row transition metal centers with d^8 electron configurations like Rh^+, Ir^+, Pd^{2+}, Pt^{2+}, and Au^{3+} almost exclusively exhibit **square planar geometries**. Beyond this, square planar geometries are often formed by Ni^{2+} (d^8), Ni^{3+} (d^7), and Cu^{2+} (d^9). Examples of square planar complexes include $[Cu(acac)_2]$; $[PtCl_4]^{2-}$;Wilkinson's catalyst, $[RhCl(PPh_3)_3]$; and Vaska's complex, *trans*-$[Ir(CO)Cl(PPh_3)_2]$.



Coordination Number 5

The two common coordination geometries for five-coordinate complexes are trigonal bipyramidal and square pyramidal.



Figure **4.1.4.11**.

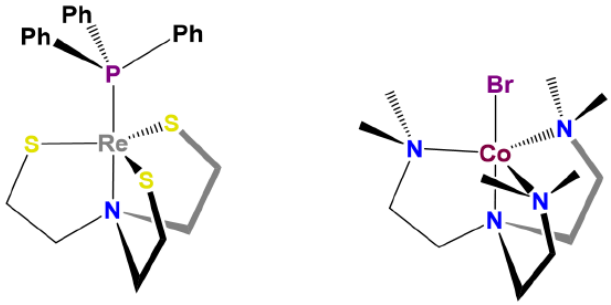


Figure **4.1.4.11**. Some tripodal ligands preference the formation of trigonal bipyramidal complexes. This work by Stephen Contakes is licensed under a Creative Commons Attribution 4.0 International License.

Homoleptic $[Ni(CN)_5]^{3-}$ possesses a square pyramidal structure, although the geometry is more common for macrocyclic complexes like the iron protoporphyrin of deoxymyoglobin shown in figure **4.1.4.4** and for complexes containing oxo and nitrido ligands, examples of which are shown in Figure **4.1.4.12**.

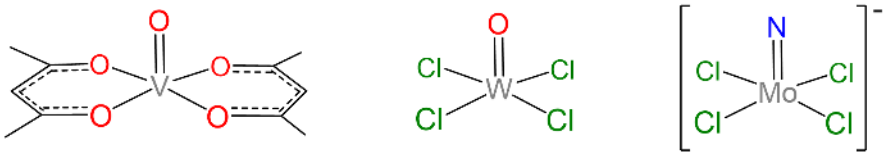


Figure **4.1.4.12**. Some square pyramidal oxo and nitrido complexes. This work by Stephen Contakes is licensed under a Creative Commons Attribution 4.0 International License.

In the absence of rigid constraining ligands, the relatively low energy difference between the trigonal bipyramidal and square pyramidal coordination geometries provides a mechanism for interconversion of the axial and equatorial ligands in a trigonal planar complex. For example, pentacarbonyliron(0) exhibits fluxionality involving a square pyramidal intermediate via a Berry pseudorotation mechanism, as shown in Figure **4.1.4.13**.

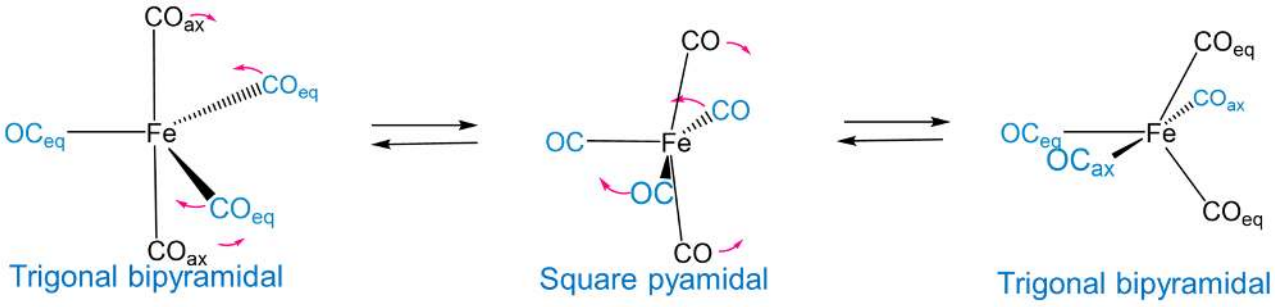


Figure **4.1.4.13**. Fluxionality in pentacarbonyliron(0) involves exchange of axial and equatorial carbonyl ligands via Berry pseudorotation. Interconversion of the axial and equatorial carbonyl groups occurs faster than the NMR timescale at room temperature. As a result the ^{13}C NMR spectrum of $Fe(CO)_5$ exhibits a single signal rather than two separate signals for the axial and equatorial carbonyl carbons. This work by Stephen Contakes is licensed under a Creative Commons Attribution 4.0 International License.

Coordination Number 6

The two common coordination geometries for coordination number 8 are octahedral and trigonal prismatic.

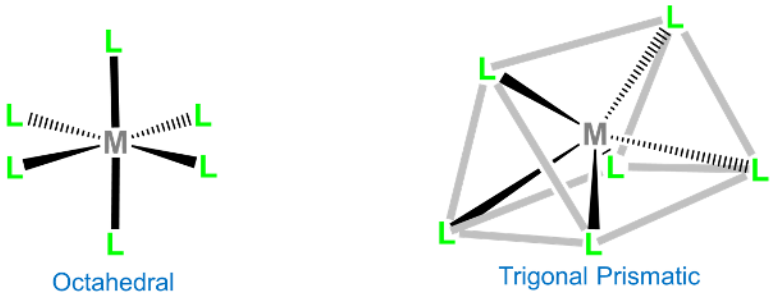


Figure **4.1.4.14**.

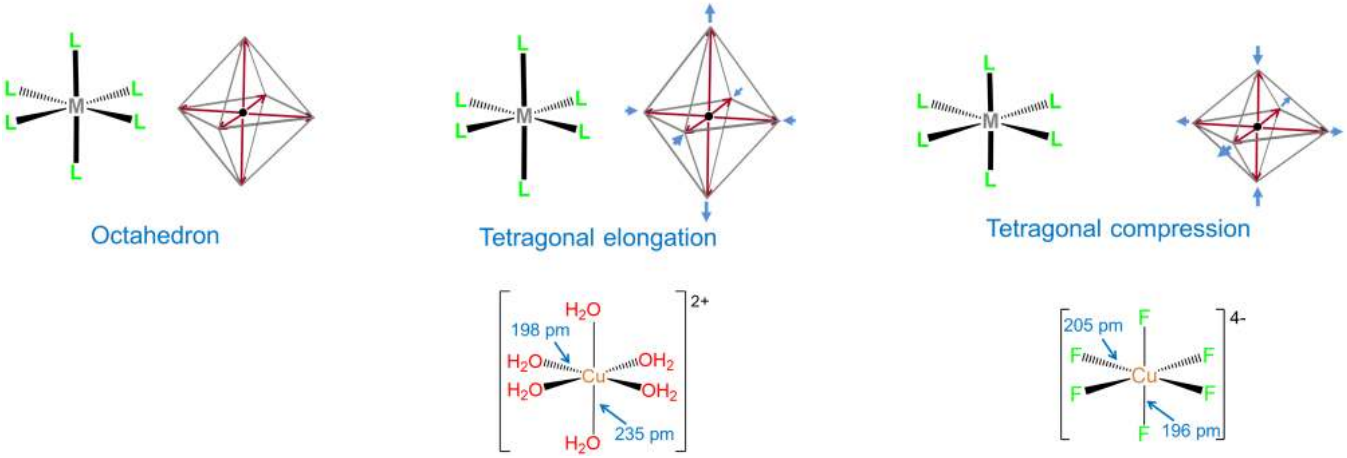


Figure **4.1.4.14**. Tetragonal distortions commonly occur for d^4, d^7 , and d^9 octahedral complexes. The most common type involves axial elongation in which the octahedron is stretched along a single *trans*-L-M-L axis, but axial compressions in which the octahedron is compressed along such an axis instead are sometimes observed. An example of an axial elongated complex is $[Cu(H_2O)_6]^{2+}$ in solution, while $[CuF_6]^{4-}$ is axially compressed when doped into a Ba_2ZrF_6 lattice (it is elongated when doped into a -----. Bond distances are taken from references 7 and 8. This work by Stephen Contakes is licensed under a Creative Commons Attribution 4.0 International License.

Trigonal prismatic coordination is related to octahedral coordination as shown in Figure **4.1.4.15**. As may be seen in Figure **4.1.4.15**, an octahedral coordination sphere is just a trigonal antiprism in which all edge lengths are identical. Rotation of one triangular face relative to its opposite until the two are eclipsed gives a trigonal prismatic geometry. In fact, since continuation of this rotation gives another octahedral complex, the trigonal prismatic geometry is an intermediate in isomerization reactions involving octahedral complexes.

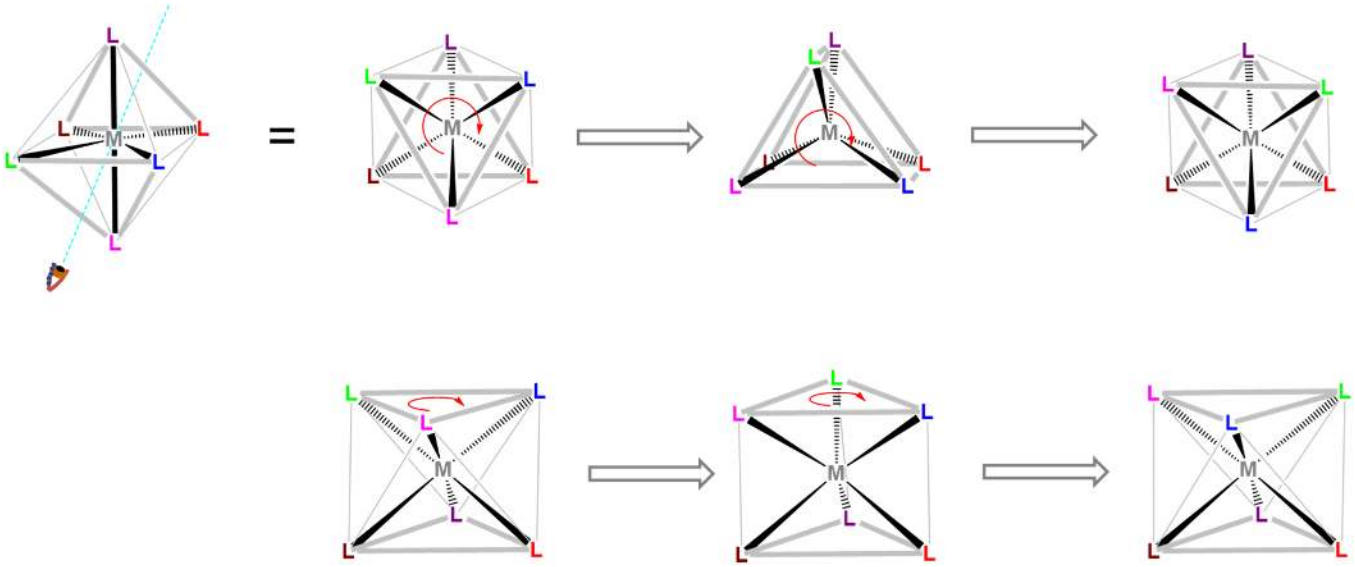


Figure 4.1.4.15. Since an octahedron is a trigonal antiprism, a trigonal prism may be produced by rotating or "twisting" one face of the octahedron relative to its opposite. Since continuation of the rotation gives an isomer of the original octahedron, when the energy landscape for twists like these is thermally or photochemically accessible, such twists provide one pathway for isomerization reactions involving octahedral complexes. In tris- and bis-chelates, such isomerizations are said to occur by Bailar and Ray-Dutt twists, which differ only in the relationship between the chelate rings and the faces twisted. Top: View looking down an axis bisecting a pair of opposing faces. Bottom: View perpendicular to that shown at top. This work by Stephen Contakes is licensed under a Creative Commons Attribution 4.0 International License.

In contrast to octahedral coordination geometries, trigonal prismatic coordination (and distorted versions thereof) are rare and occur mostly for d^0, d^1, and d^2 configurations. Examples of trigonal prismatic metal centers include the d^2 Mo^{4+} centers in MoS_2, d^1 $[Re(S_2C_2Ph_2)_3]^-$, and d^0 $[Ta(CH_3)_6]^-$, of which the latter two structures are given in Figure 4.1.4.16. Semirigid ligands like that shown in Figure 4.1.4.4C may be used to encourage the adoption of a trigonal prismatic geometry, although once the number of *d* electrons present exceeds two, the preference for octahedral coordination is too great for a trigonal prismatic geometry to occur.

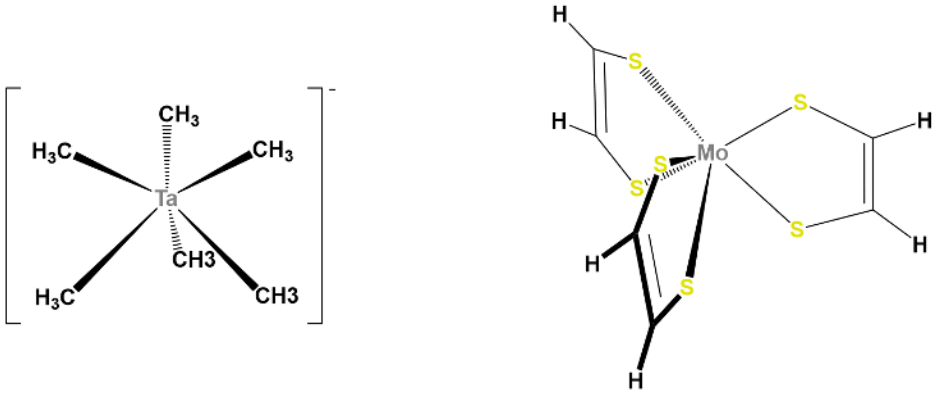
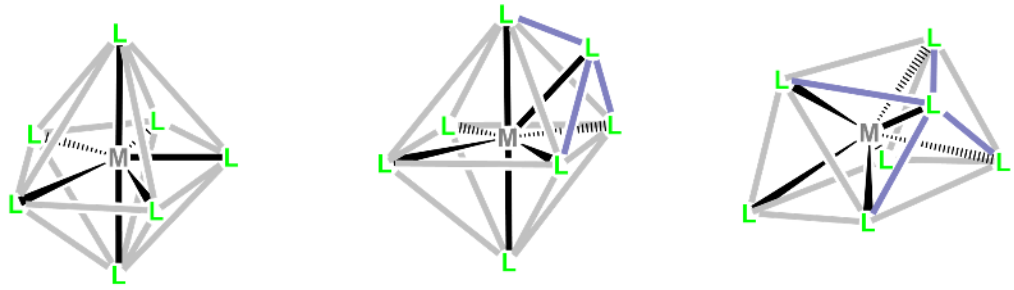


Figure 4.1.4.16. The complexes $[Ta(CH_3)_6]^-$ and $[Mo(S_2C_2H_2)_3]$ adopt a trigonal prismatic geometry. Trigonal prismatic coordination is common for d^0 and d^1 complexes with alkyl and dithiolene ligands. It is also typical for the dithiolene ligands to coordinate along the rectangular edges of the trigonal prism instead of the triangular ones. This work by Stephen Contakes is licensed under a Creative Commons Attribution 4.0 International License.

Coordination Number 7

Seven-coordinate complexes are rare outside of the relatively large early transition metals, lanthanides, and actinides. The three common seven-coordinate geometries are pentagonal bipyramidal, monocapped octahedral, and monocapped trigonal prismatic. The latter two are often called capped octahedral and capped trigonal prismatic, with the mono- prefix being understood.



Although intraligand repulsions are smaller in the pentagonal bipyramidal coordination geometry than the capped octahedral and capped trigonal prismatic geometries, the difference is small, and the three structures are often close in energy. As a result the structure observed is often dependent on ligand-based constraints, crystal packing, and solvent effects that preference one geometry over the others.

Heptacyano complexes are often pentagonal bipyramidal. Examples include $[Mo(CN)_7]^{3-}$, $[W(CN)_7]^{3-}$, and $[Os(CN)_7]^{3-}$. Seven-coordinate complexes containing oxo ligands commonly are pentagonal bipyramidal with the oxo ligand(s) in the less sterically hindered axial position. Examples include $[NbOF_6]^{3-}$ and, for the inner transition metals, $[UO_2F_5]^{3-}$. Ligands that have been used to promote formation of seven-coordinate species include 15-crown-5 and 2,2':6',2":6",2"'-quaterpyridine. Representative complexes are given in Figure **4.1.4.17**.

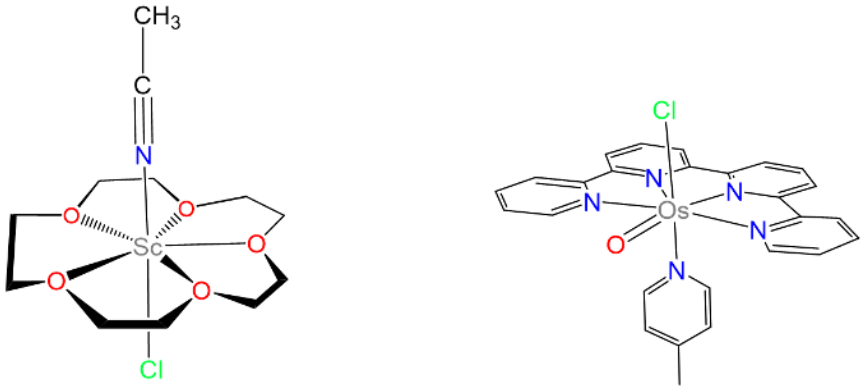


Figure **4.1.4.17**. Seven-coordinate complexes containing ligands that encourage the formation of seven-coordinate geometries. Note that while in $[NbOF_6]^{3-}$ and $[UO_2F_5]^{3-}$ the oxo ligands occupy axial positions, the Osmium complex shown possesses an oxo ligand in an equatorial position. This is likely because the parent octahedral complex, in which the oxo ligand is not present, possesses an expanded outer N-Os-N angle of 121.655° that opens to 154.161° to accommodate the oxo group. Drawn based on the structures reported in references 9 and 10. This work by Stephen Contakes is licensed under a Creative Commons Attribution 4.0 International License.

Capped trigonal prismatic geometries are common for complexes of the early transition metals. Examples include $[NbF_7]^{2-}$, $[TaF_7]^{2-}$, and $[ZrF_7]^{3-}$ in $(NH_4)_3[ZrF_7]$.

Capped octahedral geometries are found in $[MoMe_7]^-$, $[WMe_7]^-$, and $[WBr_3(CO)_4]$, which contains three pairs of *trans*-Br and CO with the final CO capping the octahedron's $(CO)_3$ face, as shown in Figure **4.1.4.18**.

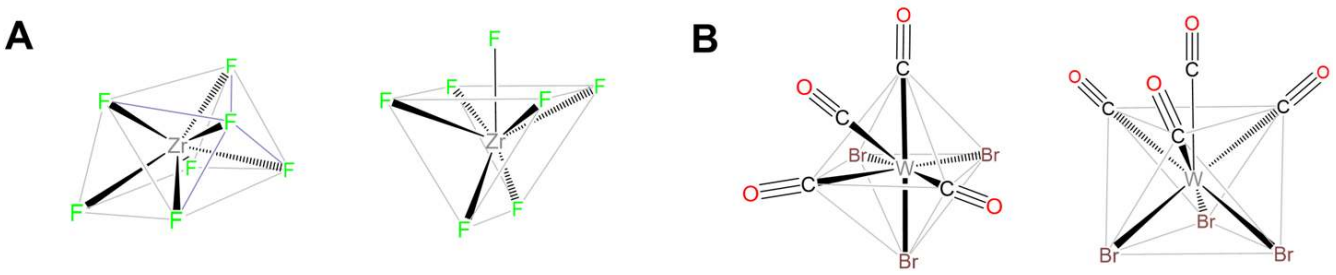


Figure **4.1.4.18**. Examples of complexes that adopt monocapped triconal prismatic and monocapped octahedral geometries.(A) Two views of the structure of (A) capped trigonalprismatic $[ZrF_7]^{3-}$ and (B) capped octahedral $[WBr_3(CO)_4]$. This work by Stephen Contakes is licensed under a Creative Commons Attribution 4.0 International License.

In seven- and higher-coordinate complexes, ligand and crystal packing effects frequently give distorted coordination geometries. These geometries are intermediate between two or more of the idealized seven coordinate geometries, making it difficult to tell exactly which structure they are a distortion of (Figure **4.1.4.19**).

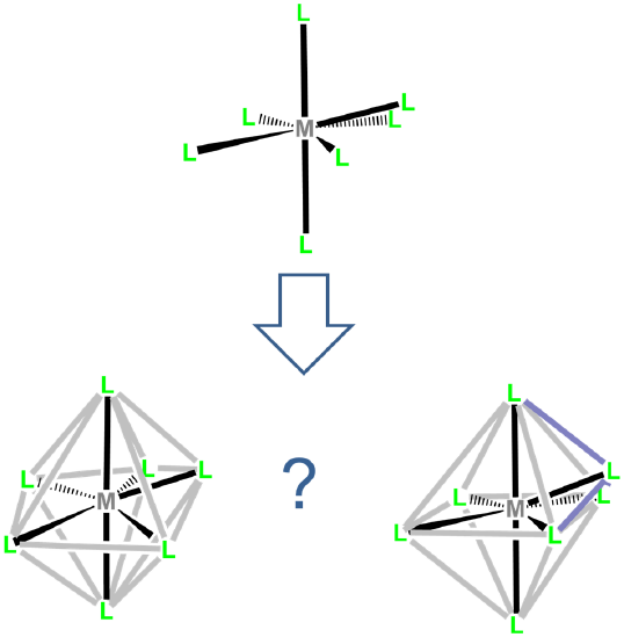


Figure **4.1.4.19**. Many seven-coordinate structures are distorted and can be difficult to classify. For example, how should the geometry of this complex be described - as distorted trigonal bipyramidal or distorted monocapped octahedral? This work by Stephen Contakes is licensed under a Creative Commons Attribution 4.0 International License.

Coordination Number 8

Eight-coordinate complexes are rare and occurs in discrete molecules and ions only for the relatively large early transition metals, lanthanides, and actinides. The three common eight-coordinate geometries are square antiprismatic, dodecahedral, and bicapped trigonal prismatic. In contrast, the cubic coordination geometry is only found in ionic lattices like that of CsCl and in complexes of the inner transition metals such as $Na_3[UF_8]$.

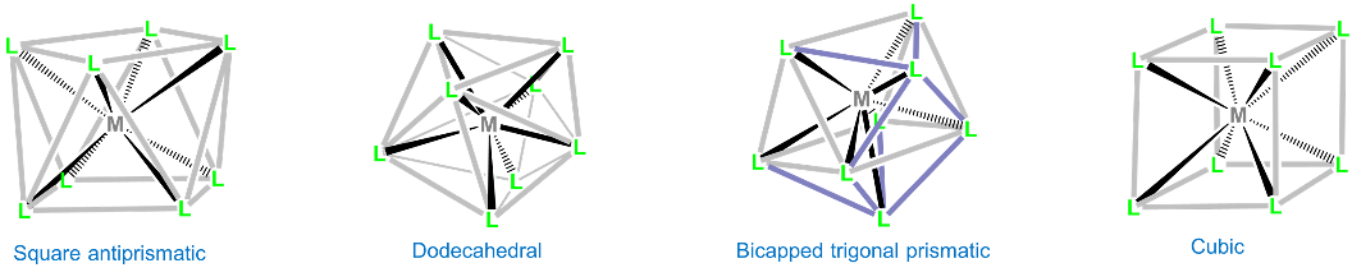


Figure **4.1.4.20**. The square antiprism may be made by twisting one face of a cube relative to another, and the dodecahedron by folding opposing faces towards one another.

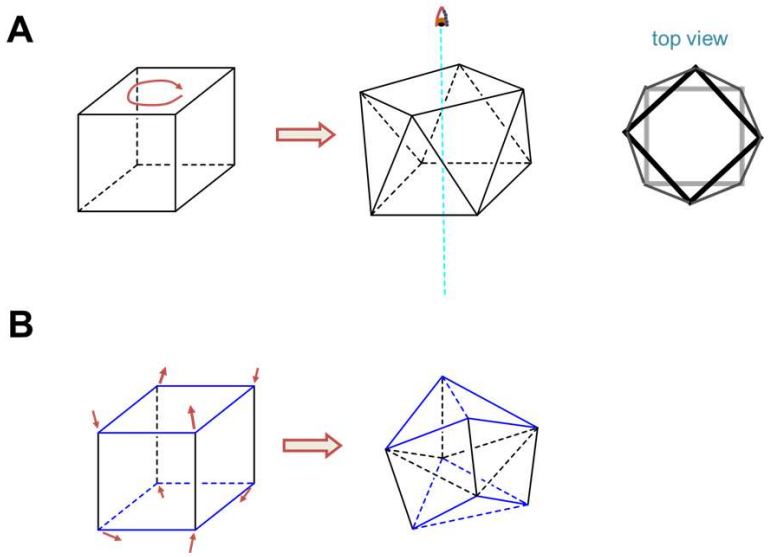


Figure 4.1.4.20. The (A) square antiprismatic and (B) dodecahedral coordination geometries are distorted cubic geometries. (A) The square antiprismatic coordination geometry is just a cubic coordination geometry in which one face has been rotated 45° relative to its opposite (and for which the distance between those faces need not be equal to the distance between adjacent atoms within a face) (B) The dodecahedral geometry may be thought of as a cube in which opposing faces are folded up and down relative to one another as shown. This work by Stephen Contakes is licensed under a Creative Commons Attribution 4.0 International License.

As with other high-coordinate structures, the energy difference between these eightfold coordination geometries is small enough that packing effects can significantly influence the observed structure. For example, octacyanomolybdates commonly adopt a square antiprismatic coordination geometry but depending on the counterions present can give dodecahedral or bicapped trigonal prismatic complexes. Examples are given in Figure 4.1.4.21.

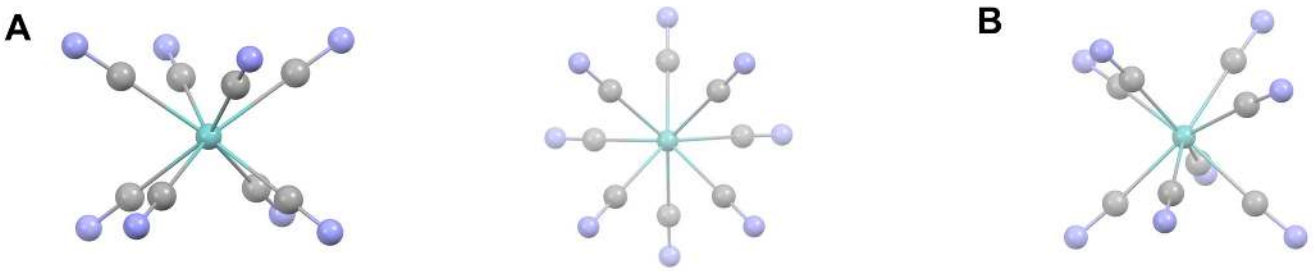


Figure 4.1.4.21: Structures reported for (A) square antiprismatic $[Mo(CN)_8]^{3-}$ as a solid 4,4'-Diazenediyldipyridinium salt and (B) dodecahedral $[Mo(CN)_8]^{4-}$ as a solid tetra-n-butylammonium salt.

Coordination Number 9

Again, nine-coordinate complexes typically require larger transition metals, lanthanides, and actinides. Coordination geometries are typically either tricapped trigonal prismatic or idiosyncratically determined by the ligands. Simple examples include the aqua complexes $[Sc(H_2O)_9]^{3+}$, $[Y(H_2O)_9]^{3+}$, and $[La(H_2O)_9]^{3+}$, as well as $[TcH_9]^{2-}$ and $[ReH_9]^{2-}$.

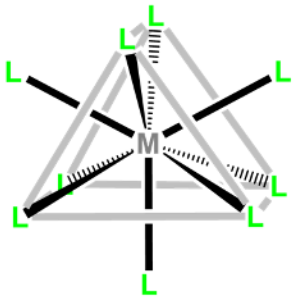


Figure **4.1.4.22**.

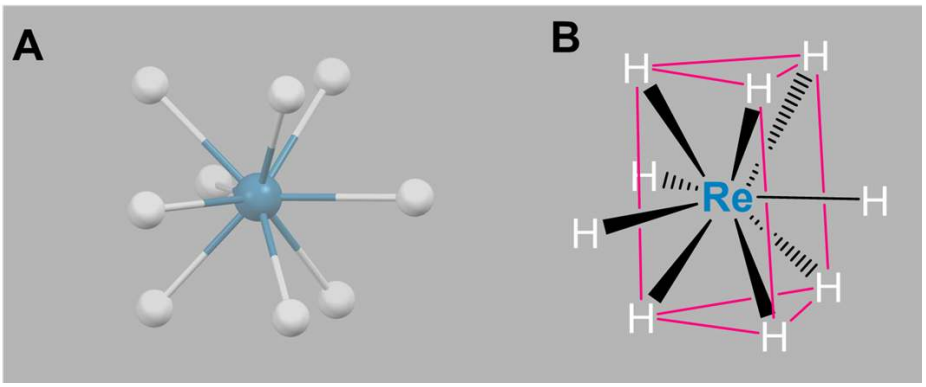


Figure **4.1.4.22**. (A) Structure of $[ReH_9]^{2-}$ in $K_2[ReH_9]$ and (B) schematic showing how the structure maps onto a tricapped trigonal pyramidal coordination geometry. This work by Stephen Contakes is licensed under a Creative Commons Attribution 4.0 International License.

Coordination Numbers 10-16

Coordination numbers higher than nine are extremely rare for compounds that bind in κ fashion (form conventional metal-ligand bonds)[14] and usually involve some combination of large metals, sterically undemanding ligands, and special ligand structures that promote higher coordination. Noteworthy examples include

1. Twelve-coordinate $[Hf(BH_4)_4]$, which illustrates how small multidentate ligands promote higher coordination numbers. As shown in Figure **4.1.4.23**, $[Hf(BH_4)_4]$ has a cubooctahedral structure in which BH_4^- acts as a tridentate ligand, with BH_3 units occupying triangular faces of the cubooctahedron to give a tetrahedron of BH_4^- ligands around the Hf.

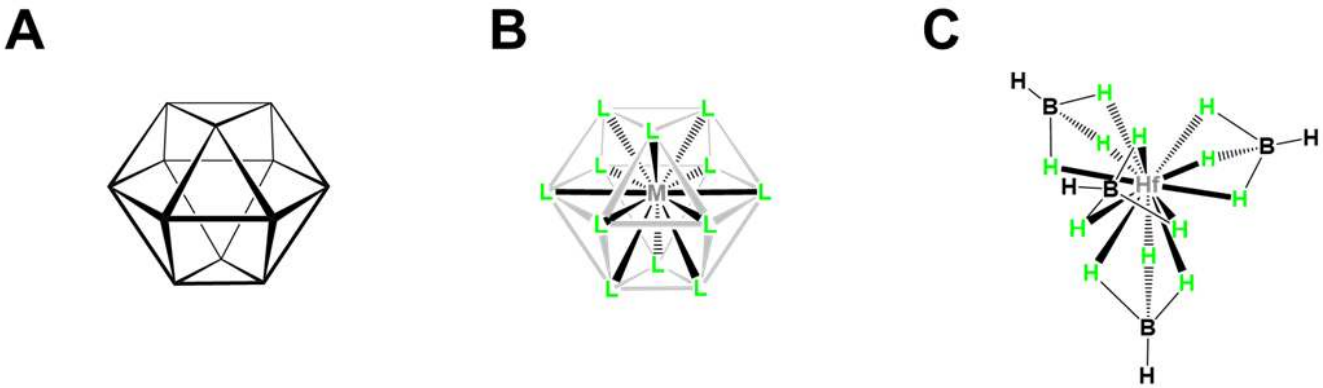


Figure **4.1.4.23**. The anticubooctahedral coordination geometry is observed for $[Hf(BH_4)_4]$. (A) An anticubooctahedron consists of a hexagonal ring capped with antiparallel triangles above and below the ring. (B) Idealized anticubooctahedral complex. (C) Structure of $[Hf(BH_4)_4]$. This work by Stephen Contakes is licensed under a Creative Commons Attribution 4.0 International License.

2. Twelve-coordinate $[Ce(NO_3)_6]^{2-}$, in which the nitrate oxygens define an icosahedral coordination geometry as shown in Figure **4.1.4.24**. The nitrates in the structure bind the Ce center in bidentate fashion in an octahedral array.

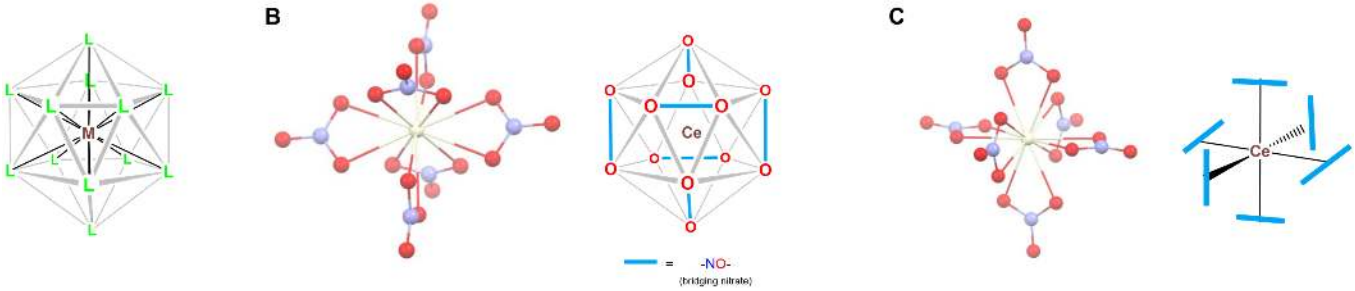


Figure **4.1.4.24**. Coordination geometry of $[Ce(NO_3)_6]^{2-}$ in $[Mg(H_2O)_6][Ce(NO_3)_6]\cdot H_2O$. (A) Idealized icosahedral coordination. (B) View of the structure of $[Ce(NO_3)_6]^{2-}$ showing how it maps onto the icosahedral coordination geometry. (C) The structure may also be thought of as comprising an octahedral geometry in which each vertex of the octahedron is occupied by a κ^2-NO_3^-. The structure of $[Ce(NO_3)_6]^{2-}$ is rendered in Mercury from the cif data in reference 15. This work by Stephen Contakes is licensed under a Creative Commons Attribution 4.0 International License.

3. Fifteen-coordinate $[Th(H_3BNMe_2BH_3)_4]$, which also uses bridging H-B-H units that occupy little of the coordination sphere. In $[Th(H_3BNMe_2BH_3)_4]$, three of the four $H_3BNMe_2BH_3$ ligands bind in κ^4 fashion and one binds κ^3, giving the fifteen fold coordination.[16]

4. Sixteen-coordinate $[CoB_{16}]^-$, which possesses the highest coordination number yet observed. Its structure is given in Figure **4.1.4.25**. The coordination geometry is an octahedral antiprism, and the complex should be considered to involve a Co center in the midst of a B_{16}^- "molecular drum" held together by cluster bonds.

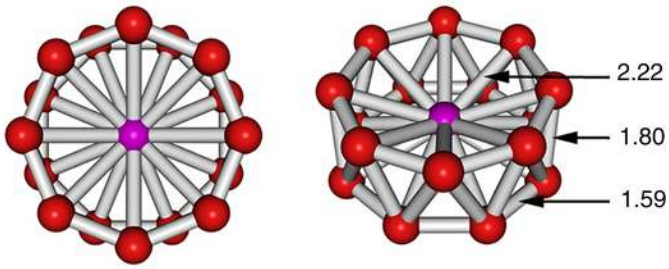


Figure 2A from Popov, I., Jian, T., Lopez, G. *et al.* Cobalt-centered boron molecular drums with the highest coordination number in the CoB_{16}^- cluster. *Nat Commun* **6,** 8654 (2015). https://doi.org/10.1038/ncomms9654, which is is licensed in that publication under a Creative Commons Attribution 4.0 International License.

References

1. Dudev, M.; Wang, J.; Dudev, T.; Lim, C., Factors Governing the Metal Coordination Number in Metal Complexes from Cambridge Structural Database Analyses. *The Journal of Physical Chemistry B* **2006**, *110(4)*, 1889-1895.
2. Kuppuraj, G.; Dudev, M.; Lim, C., Factors Governing Metal−Ligand Distances and Coordination Geometries of Metal Complexes. *The Journal of Physical Chemistry B* 2009, 113 (9), 2952-2960.
3. Cremades, E.; Echeverría, J.; Alvarez, S., The Trigonal Prism in Coordination Chemistry. *Chemistry – A European Journal* 2010, 16 (34), 10380-10396.
4. Xiong, X.-G.; Wang, Y.-L.; Xu, C.-Q.; Qiu, Y.-H.; Wang, L.-S.; Li, J., On the gold–ligand covalency in linear $[AuX_2]^-$ complexes. *Dalton Transactions* 2015, 44 (12), 5535-5546.
5. Concepción Gimeno, M. The Chemistry of Gold in Laguna, Antonio (ed.) *Modern Supramolecular Gold Chemistry: Gold-Metal Interactions and Applications*. Wiley, 2008.
6. Andersen, R. A.; Faegri, K.; Green, J. C.; Haaland, A.; Lappert, M. F.; Leung, W. P.; Rypdal, K., Synthesis of bis[bis(trimethylsilyl)amido]iron(II). Structure and bonding in M[N(SiMe3)2]2 (M = manganese, iron, cobalt): two-coordinate transition-metal amides. *Inorganic Chemistry* 1988, 27 (10), 1782-1786.
7. Persson, I., Hydrated metal ions in aqueous solution: How regular are their structures? Pure and Applied Chemistry 2010, 82*(10)*, 1901.

8. Aramburu, J. A.; García-Fernández, P.; García-Lastra, J. M.; Moreno, M., Jahn–Teller and Non-Jahn–Teller Systems Involving CuF_6^{4-} Units: Role of the Internal Electric Field in Ba2ZnF6:Cu2+ and Other Insulating Systems. *The Journal of Physical Chemistry C* 2017, *121(9)*, 5215-5224.
9. Brown, M. D.; Levason, W.; Murray, D. C.; Popham, M. C.; Reid, G.; Webster, M., Primary and secondary coordination of crown ethers to scandium(iii). Synthesis, properties and structures of the reaction products of ScCl3(thf)3, ScCl3·6H2O and Sc(NO3)3·5H2O with crown ethers. Dalton Transactions 2003, (5), 857-865.
10. Liu, Y.; Ng, S.-M.; Lam, W. W. Y.; Yiu, S.-M.; Lau, T.-C., A Highly Reactive Seven-Coordinate Osmium(V) Oxo Complex: [OsV(O)(qpy)(pic)Cl]2+. Angewandte Chemie International Edition 2016, 55 (1), 288-291.
11. Popov, I., Jian, T., Lopez, G. *et al.* Cobalt-centred boron molecular drums with the highest coordination number in the CoB_{16}^- cluster. *Nat Commun* **6,** 8654 (2015). https://doi.org/10.1038/ncomms9654
12. The structures are rendered from cif data reported in the following publications: (A) square antiprismatic $[Mo(CN)_8]^{3-}$: Wen-Yan Liu, Hu Zhou, Ai-Hua Yuan, *Acta Crystallographica Section E: Structure Reports Online*, 2008, 64, m1151, (B) dodecahedral $[Mo(CN)_8]^{4-}$: B.J.Corden, J.A.Cunningham, R.Eisenberg, *Inorganic Chemistry*, 1970, 9, 356.
13. The structure of ReH_9^{2-} is rendered from the structure reported in Abrahams, S.C.; Ginsberg, A.P.; Knox, K. Transition metal-hydrogen compounds. II. The crystal and molecular structure of potassium rhenium hydride, K_2ReH_9 *Inorganic Chemistry*, **1964**, *3*, 558-567.
14. There are other complexes in which a metal may be said to interact with more than sixteen "ligand atoms", but these are not usually considered to possess a higher coordination number. For example, in some π complexes like η^5-Cp_4U, technically there are 20 C atoms fastened to the U, but these complexes are better considered as 12-coordinate than twenty (since each cyclopentadienyl ring is isolobal with a *fac*-coordinated set of 3 L ligands), while the metal centers in endohedral fullerene species like $La@C_{60}$ do not interact with all sixty carbon atoms at once, and so are better thought of as a metal trapped in a spacious sixty-carbon cage.
15. Zalkin, A.; Forrester, J.D.; Templeton, D.H. Crystal structure of cerium magnesium nitrate hydrate *Journal of Chemical Physics*, **1963**, *39*, 2881-2891.
16. Daly, S. R.; Piccoli, P. M. B.; Schultz, A. J.; Todorova, T. K.; Gagliardi, L.; Girolami, G. S., Synthesis and Properties of a Fifteen-Coordinate Complex: The Thorium Aminodiboranate [Th(H3BNMe2BH3)4]. Angewandte Chemie International Edition 2010, 49 (19), 3379-3381.
17. Popov, I., Jian, T., Lopez, G., Boldyrev, A. I.; Wang, L-S. Cobalt-centred boron molecular drums with the highest coordination number in the CoB_{16}^- cluster. *Nat Commun* **6,** 8654 (2015).

4.1.4: Coordination Numbers and Structures is shared under a not declared license and was authored, remixed, and/or curated by LibreTexts.

- **9.5: Coordination Numbers and Structures** by Stephen M. Contakes is licensed CC BY 4.0.

SECTION OVERVIEW

4.2: Coordination Chemistry II - Bonding

4.2.1: Evidence for Electronic Structures

4.2.1.1: Thermodynamic Data
4.2.1.2: Magnetic Susceptibility
4.2.1.3: Electronic Spectra
4.2.1.4: Coordination Number and Molecular Shapes

4.2.2: Bonding Theories

4.2.2.1: Crystal Field Theory
4.2.2.1.1: Crystal Field Theory
4.2.2.1.2: Colors of Coordination Complexes
4.2.2.1.3: Crystal Field Stabilization Energy
4.2.2.1.4: Factors That Affect the Magnitude of Δo
4.2.2.1.5: Jahn-Teller Distortions
4.2.2.1.6: Magnetic Moments of Transition Metals
4.2.2.1.7: Magnetism
4.2.2.1.8: Thermodynamics and Structural Consequences of d-Orbital Splitting
4.2.2.2: Ligand Field Theory

4.2: Coordination Chemistry II - Bonding is shared under a not declared license and was authored, remixed, and/or curated by LibreTexts.

SECTION OVERVIEW

4.2.1: Evidence for Electronic Structures

This section describes the types of experimental data that give us hints about the electronic structure of coordination complexes (ie the molecular orbitals, their energy levels, and electron configurations). The types of experimental observations discussed here have been used to generate the theories of bonding that are described later in this chapter.

Introduction

The frontier (valence) electrons and orbitals define the chemical and physical properties of any compound. In the transition metals and their coordination compounds, the ***d*** orbitals and ***d*** electrons are the ones of interest. Thus, the ***d*** orbitals and electrons will be the focus of this chapter.

One of the first things you might notice about valence ***d*** orbitals is the order of orbital energy levels of atoms and ions in the transition metals. For example, in the first row of transition metals, the 4s orbital fills before the **3*d*** *in the atoms*. This indicates that **4*s*** is lower in energy than **3*d*** *in these atoms*. However, *in the ions* of the same elements, the **3*d*** orbital is occupied while the **4*s*** orbital is empty. This indicates the opposite, that the **3*d*** orbital is lower in energy than **4*s*** *in these ions*. The change in the relative energy levels of the **3*d*** and **4*s*** orbitals in atoms compared to ions is a result of the combined effects of shielding and penetration, as discussed in a previous chapter. The result is that the 3d and 4s orbital energy levels are close enough in energy that subtle changes in the environment can reverse the order.

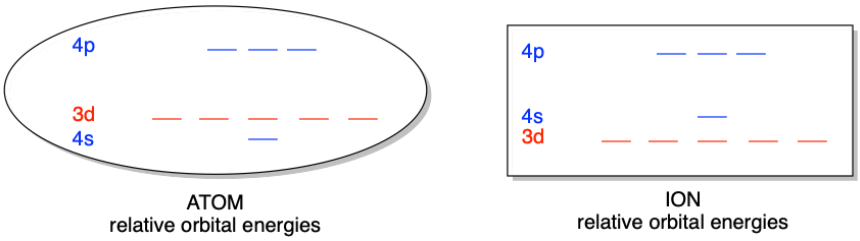


Figure **4.2.1.1**: In early period 4 of the periodic table, the **4*s*** orbital energy level is lower than **3*d*** for atoms. However, in the ions of the same elements, the **3*d*** is lower in energy than **4*s***. (CC-BY-NC; Chris Schaller)

Furthermore, you are going to see that once the atom is surrounded by ligands, the five ***d*** orbitals are no longer degenerate. In a coordination compound, with ligands bound in a specific geometry, the ***d*** orbitals become split into slightly different energy levels. The splitting pattern depends on where the ligands are in space; in other words it depends on the coordination geometry. The patterns of splitting for tetrahedral and octahedral geometries are shown below. Notice that the splitting is reversed between metals in a tetrahedral coordination environment compared to an octahedral environment.

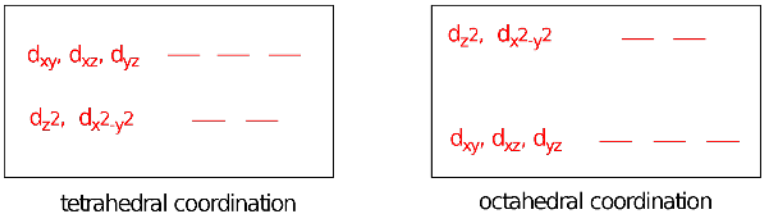


Figure **4.2.1.2**: Splitting of d orbitals for (left) tetrahedral and (right) octahedral ligand geometries. (CC-BY-NC; Chris Schaller)

When the orbitals of a coordination compound are filled with electrons, the electron configuration depends on the energy difference between the lower and higher energy levels. For example, given five ***d*** electrons in an octahedral environment, there are two possible electron configurations. All five electrons may occupy the lower level of ***d*** orbitals (Fig. **4.2.1.3**, left), so that some electrons are paired. Another possibility is that all the electrons will be unpaired if they populate both levels of the d orbitals (Fig. **4.2.1.3**, right).

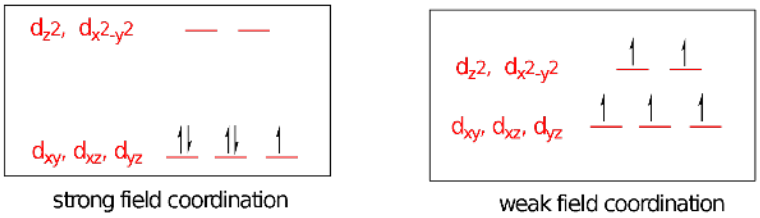


Figure **4.2.1.3**: Two possible electron configurations for five electrons in an octahedral ligand field. (CC-BY-NC; Chris Schaller)

A number of factors determine which case results, including the identity of the metal ion and the nature of the ligands involved. These different filling orders have consequences, too. The magnetic properties of the complex, its propensity to undergo reactions, and its optical properties all depend on the configuration of these frontier electrons.

This chapter is an exploration of the nature of the metal-ligand bond and how both geometry and the mode of bonding influence the properties of coordination complexes.

4.2.1.1: Thermodynamic Data

4.2.1.2: Magnetic Susceptibility

4.2.1.3: Electronic Spectra

4.2.1.4: Coordination Number and Molecular Shapes

This page titled 4.2.1: Evidence for Electronic Structures is shared under a CC BY-NC 3.0 license and was authored, remixed, and/or curated by Chris Schaller.

4.2.1.1: Thermodynamic Data

We can get some insight into the stability of coordination complexes by looking at their formation constants. The formation constant is the equilibrium constant for the reaction leading to the formation of a coordination complex. The greater the formation constant, the more thermodynamically stable the product complex compared to the reactant complex.

Many complexation reactions take place in aqueous solution by dissolving a metal ion in water to produce the "aqueous metal ion". An aqueous metal ion is one that is coordinated by a number of water molecules, and since it is charged, there must be counter ions to balance that charge. When an aqueous metal ion reacts to form a new complex, its formation constant indicates the stability of the product compared to the aqueous complex. Depending on the number of ligands that are replaced in the product compared to the reactant, the formation complex is defined as either a **stepwise formation constant** (K) or an **overall formation constant** (β).

For example, the formation of $[Cu(NH_3)(OH_2)_5]^{2+}$ complex ion from $Cu^{2+}_{(aq)}$ can be represented by the following *stepwise* reaction:[1]

$$[Cu(OH_2)_6]^{2+} + NH_3 \rightleftharpoons [Cu(NH_3)(OH_2)_5]^{2+} + H_2O \qquad K_1 = 1.9 \times 10^4$$

The formation constant, K_1, is a stepwise formation constant because it represents the substitution of a single aquo ligand (a coordinated water) by an ammine ligand. Another example is the reaction below that represents the substitution of four aquo ligands for four ammine ligands. The *overall* formation of the $[Cu(NH_3)_4(OH_2)_2]^{2+}$ complex ion from $Cu^{2+}_{(aq)}$ would be represented by this equation:

$$[Cu(OH_2)_6]^{2+} + 4\,NH_3 \rightleftharpoons [Cu(NH_3)_4(OH_2)_2]^{2+} + 4\,H_2O \qquad \beta_4 = 1.1 \times 10^{13}$$

This time, the formation constant represents the substitution of four ammine ligands for four aquo ligands. This transformation does not happen in one step, so the formation constant, β_4 is a composite of the equilibrium constants for four individual steps:

$$[Cu(OH_2)_6]^{2+} + NH_3 \rightleftharpoons [Cu(NH_3)(OH_2)_5]^{2+} + H_2O \qquad K_1 = \frac{[Cu(NH_3)(OH_2)_5{}^{2+}]}{[Cu(OH_2)_6{}^{2+}][NH_3]} = 1.9 \times 10^4$$

$$[Cu(NH_3)(OH_2)_5]^{2+} + NH_3 \rightleftharpoons [Cu(NH_3)_2(OH_2)_4]^{2+} + H_2O \qquad K_2 = \frac{[Cu(NH_3)_2(OH_2)_4{}^{2+}]}{[Cu(NH_3)(OH_2)_5{}^{2+}][NH_3]} = 3.9 \times 10^3$$

$$[Cu(NH_3)_2(OH_2)_4]^{2+} + NH_3 \rightleftharpoons [Cu(NH_3)_3(OH_2)_3]^{2+} + H_2O \qquad K_3 = \frac{[Cu(NH_3)_3(OH_2)_3{}^{2+}]}{[Cu(NH_3)_2(OH_2)_4{}^{2+}][NH_3]} = 1.0 \times 10^3$$

$$[Cu(NH_3)_3(OH_2)_3]^{2+} + NH_3 \rightleftharpoons [Cu(NH_3)_4(OH_2)_2]^{2+} + H_2O \qquad K_4 = \frac{[Cu(NH_3)_4(OH_2)_2{}^{2+}]}{[Cu(NH_3)_3(OH_2)_3{}^{2+}][NH_3]} = 1.5 \times 10^2$$

$$\beta_4 = K_1 \times K_2 \times K_3 \times K_4 = (1.9 \times 10^4)(3.9 \times 10^3)(1.0 \times 10^3)(1.5 \times 10^2) = 1.1 \times 10^{13}$$

(\beta\) notation

The β notation is used to distinguish an overall formation constant from a stepwise formation constant. However, sometimes alternative notation will be used. You may see other texts, the literature, or your instructor using alternative ways to distinguish an overall formation constant like β_4 from the stepwise formation constant, like K_4. The important thing is to understand the conventions used for whatever source you are reading.

In both the examples above, the equilibrium lies to the right (in other words, the formation constant is >> 1). Another way to interpret this is that Cu(II) has a higher affinity for ammonia than for water, and thus the ammine complex is more stable than the aqueous metal ion. In the case of the copper tetraammine complex, replacement of each individual water by ammonia is favorable, so the aggregate formation constant β_4 becomes very large. The preference of Cu(II) for ammonia can be explained by the increased basicity of ammonia compared to water.

Formation constants can provide valuable insight into factors that contribute to the stability of coordination complexes, but we may need a more extensive set of data to build a more complete picture. If we look at formation constants in a series of complexes that have something in common, we may get an idea about additional factors that play a role in complex stability. Take a look at these examples:[2]

$$\mathrm{Cu^+(aq) + 2\,Cl^- \rightleftharpoons [CuCl_2]^-} \quad K = 3.0 \times 10^5$$
$$\mathrm{Cu^+(aq) + 2\,Br^- \overset{CuBr_2}{\rightleftharpoons} -} \quad K = 8.0 \times 10^5$$
$$\mathrm{Cu^+(aq) + 2\,I^- \overset{CuI_2}{\rightleftharpoons} -} \quad K = 8.0 \times 10^8$$

The reactions above are simplified by abbreviating the aqueous metal ion, $\mathrm{[Cu(OH_2)n]^+}$ as $\mathrm{Cu^+(aq)}$. This time, we are dealing with Cu(I) rather than Cu(II). Note that basicity does not seem to play a role in this series. The pK_a's of the conjugate acids HCl, HBr, and HI are -6.7, -8.7, and -9.3, respectively. If basicity were important, chloride should bind most tightly, followed by bromide, and then iodide; that trend is reversed here. Instead, this case can be explained by an application of Pearson's hard-soft acid-base theory (HSAB). HSAB theory predicts that small, charge-dense bases will bind more tightly with small, charge-dense acids. Archetypically, hard bases have N, O, or F donor atoms. Conversely, larger, more polarizable bases bind more tightly with larger, more polarizable acids. Soft bases archetypically have P or S donor atoms. In this series of copper complexes, the iodide is the softest, most polarizable of the three halide ions shown, whereas the chloride is the hardest (although not as hard as fluoride). Cu(I) has a relatively low charge density, so it can be considered a soft acid. Soft acids and soft bases form strong bonds because of the pronounced covalency between the donor and acceptor. Of the three halides, iodide is the most capable of providing that soft-soft interaction with the Cu(I) ion.

Let's look at another major contributor to complex stability. In this case, aqueous nickel ion reacts with ammonia to produce the hexaammine complex, $\mathrm{[Ni(NH_3)_6]^{2+}}$. That's similar to the reaction of aqueous copper ion with ammonia; ammonia is a better donor in this case than water. However, ammine is easily displaced by ethylenediamine ($\mathrm{H_2NCH_2CH_2NH_2}$, abbreviated en) to provide an ethylenediamine complex, $\mathrm{[Ni(en)_3]_2^+}$.[2,3]

$$\mathrm{[Ni(OH_2)_6]^{2+} + 6\,NH_3 \overset{Ni(NH_3)_6}{\rightleftharpoons} {}^{2}+} \quad K = 2.0 \times 10^8$$
$$\mathrm{[Ni(NH_3)_6]^{2+} + 3\,en \overset{Ni(en)_3}{\rightleftharpoons} {}^{2} + + 6\,NH_3} \quad K = 4.7 \times 10^9$$

Once again, we see that an ammine ligand is a much more effective donor than an aquo ligand. The ethylenediamine ligand, however, binds exceptionally tightly, and can even displace ammine ligands. To gain insight into why a metal ion would have higher affinity toward $\mathrm{H_2NCH_2CH_2NH_2}$ (en) than $\mathrm{NH_3}$, despite the fact that the two ligands have similar donor atoms, we can look at the thermodynamic parameters (the entropy and enthalpy) of the reaction for the formation of $\mathrm{[Ni(en)_3]^{2+}}$ from $\mathrm{[Ni(NH_3)_6]^{2+}}$:

$$\begin{aligned} \Delta H^\circ &= -12.1\ \mathrm{kJ\ mol^{-1}} \\ \Delta S^\circ &= 184.9\ \mathrm{J\ mol^{-1}K^{-1}} \\ \text{and at 298 K}, -T\Delta S^\circ &= -55.1\ \mathrm{kJ\ mol^{-1}} \end{aligned}$$

That last term, $-T\Delta S^\circ$, is included for easier comparison to the enthalpy contribution, since these two factors are evaluated via the Gibbs free energy equation, $\Delta G = \Delta H - T\Delta S$. We see that the formation of $\mathrm{[Ni(en)_3]^{2+}}$ from $\mathrm{[Ni(NH_3)_6]^{2+}}$ is slightly favored enthalpically (by $\Delta H^\circ = -12.1\mathrm{kJ\ mol^{-1}}$), even though there are nitrogen atom donor ligands in both reactant and product complexes. However, this small preference is not likely the most important driving force for the large formation constant. The entropy factor is much larger in comparison ($T\Delta S^\circ = -55.1\ \mathrm{kJ\ mol^{-1}}$), indicating entropy is driving the huge formation constant for the ethylenediamine complex.

How do we interpret that large $T\Delta S^\circ$? The simplest approach to interpreting a change in entropy of a reaction is to evaluate the number of molecules in the reactants compared to the products. If there is an increase in the number of molecules, there is an increase in disorder (entropy).

In the replacement of aquo ligands with ammine ligands, there are seven species on either side of the equation:

$$\underset{\text{7 molecules}}{\mathrm{[Ni(OH_2)_6]^{2+} + 6\,NH_3}} \quad \rightleftharpoons \quad \underset{\text{7 molecules}}{\mathrm{[Ni(NH_3)_6]^{2+}}}$$

We might not expect this reaction to have a large entropic driving force because the number of molecules is the same in the reactants and products.

On the other hand, in the replacement of ammine ligands with ethylenediamine ligands, there are four molecules on the reactant side, and seven on the products side.

$$\underset{\text{4 molecules}}{[Ni(NH_3)_6]^{2+} + 3\,en} \rightleftharpoons \underset{\text{7 molecules}}{[Ni(en)_3]^{2+} + 6\,NH_3}$$

That means there is a net increase in the number of molecules in solution when the ethylenediamine replaces the ammines. An increase in the number of molecules represents an increase in the partitioning of energy, which is entropically favorable. The underlying reason for this difference is that each ethylenediamine ligand has two nitrogen donors, allowing one ethylenediamine to replace two ammines. The high formation constant for ligands that contain multiple donor atoms is called the **chelate effect**, from the Greek word for "crab" (which has two claws with which it can grab things). We call donors capable of binding through multiple atoms “polydentate” ligands (for “many-toothed”, indicating they can bite more strongly into the metal and hold on).

Formation constants of coordination complexes affect important processes ranging from industrial catalysis to biology. For example, most people are aware of carbon monoxide poisoning. Carbon monoxide leads to suffocation by displacing molecular oxygen from hemoglobin (Hb), the oxygen-carrying protein in blood cells. Hemoglobin has an Fe(II) ion bound in its active site which in turn coordinates molecular oxygen, increasing the oxygen-carrying capacity of a blood cell. The two relevant equilibria are:[4]

$$Hb + O_2 \rightleftharpoons HbO_2 \quad K = 3.2\ \mu M^{-1}$$
$$Hb + CO \rightleftharpoons HbCO \quad K = 750\ \mu M^{-1}$$

Here, Hb is just a shorthand for hemoglobin. The formation constants shown above indicate that carbon monoxide binds to hemoglobin hundreds of times more tightly than does oxygen. This difference can’t be caused by a chelate effect; both **CO** and O_2 are monodentate donors in this case. The origin for this difference comes from more subtle differences in metal-ligand binding that we will develop later in this chapter.

Problems

Exercise 4.2.1.1.1

Show how we can combine the formation constants given above for $[Ni(NH_3)_6]^{2+}$ and $[Ni(en)_3]^{2+}$ from $[Ni(HO_2)_6]^{2+}$ to determine the formation constant for the ethylenediamine complex from aqueous nickel ion.

$$[Ni(OH_2)_6]^{2+} + 3\,en \rightleftarrows [Ni(en)_3]^{2+} + 6\,H_2O \qquad K = ?$$

Answer

We know the formation constants of $[Ni(NH_3)_6]^{2+}$ and $[Ni(en)_3]^{2+}$. Let's call them "reactions i and j":

$$\text{Reaction } i: \quad [Ni(OH_2)_6]^{2+} + 6\,NH_3 \overset{Ni(NH_3)_6}{\rightleftharpoons} {}^{2+} \qquad K_i = \frac{[Ni(NH_3)_6]}{[Ni(OH_2)_6][NH_3]} = 2.0 \times 10^8$$

$$\text{Reaction } j: \quad [Ni(NH_3)_6]^{2+} + 3\,en \overset{Ni(en)_3}{\rightleftharpoons} {}^{2+} + 6\,NH_3 \qquad K_j = \frac{[Ni(en)_3][NH_3]^6}{[Ni(NH_3)_6][en]^3} = 4.7 \times 10^9$$

and we want to find the equilibrium constant for the formation of $[Ni(en)_3]^{2+}$ from $[Ni(HO_2)_6]^{2+}$. We'll call this "reaction k".

$$\text{Reaction } k: \quad [Ni(OH_2)_6]^{2+} + 3\,en \rightleftarrows [Ni(en)_3]^{2+} + 6\,H_2O \qquad K_k = ?$$

Reaction "k" is the sum of reaction "i" followed by reaction "j".

$$\begin{aligned} K_k &= K_i \times K_j \\ &= \frac{[Ni(NH_3)_6]}{[Ni(OH_2)_6][NH_3]} \times \frac{[Ni(en)_3][NH_3]^6}{[Ni(NH_3)_6][en]^3} = \frac{[Ni(en)_3]}{[Ni(OH_2)_6][en]^3} \\ &= (2.0 \times 10^8)(4.7 \times 10^9) = 9.4 \times 10^{17} \end{aligned}$$

Exercise 4.2.1.1.2

The formation constants shown below correspond to the substitution of one ligand on aqueous Cu(II) ion.[5] Propose a trend that explains the different stabilities of the complexes.

$$\begin{array}{ll} \mathrm{NH_3} & K = 2.0 \times 10^3 \\ \mathrm{F^-} & K = 8.0 \\ \mathrm{Cl^-} & K = 1.2 \\ \mathrm{Br^-} & K = 0.9 \end{array}$$

Answer

This trend could be explained by basicity, since ammonium ion is a weak base and the acidity of the hydrogen halides increase in the order HF < HCl < HBr. The ammine ligand is a better donor than any of the halides to the nickel ion, but fluoride is better than chloride and chloride is better than bromide. The reason for the acidity trend varies in the midst of this series. Among the halides, fluoride is the best donor because it is the least polarizable and least stable ion. However, in the second row of the periodic table, the nitrogen in ammonia is a better donor than fluoride because nitrogen is less electronegative than fluorine. This difference is enough to compensate for the fact that ammine is a neutral ligand, presumably with less Coulombic attraction to the copper ion than fluoride.

Note that this trend is very different for Cu(II) than for a similar series of ligands with Cu(I). Cu(II), with greater charge density, is harder in character than Cu(I). Thus, it doesn't necessarily bind more tightly to softer donors the way Cu(I) does.

? Exercise 4.2.1.1.3

Ethylenediamine can be displaced from nickel by tren, (NH2CH2CH2)3N, another polydentate ligand.[3]

$$[\mathrm{Ni(en)_2(OH_2)_2}]^{2+} + \text{tren} \rightleftarrows [\mathrm{Ni(tren)(H_2O)_2}]^{2+} + 2\,\text{en} \qquad K = 76$$

a. What is the denticity of tren?
b. It is reported that $\Delta H° = +13.0$ kJ mol^{-1} and $\Delta S° = 79.5$ J mol^{-1} K^{-1}. Propose a reason for the moderately large formation constant.

Answer

a) Tren has a denticity of 4; it is sometimes described as a tetradentate ligand.

b) The enthalpy of reaction $\Delta H° = +13.0$ kJ mol-1 and at 298 K, $-T\Delta S° = -23.7$ kJ mol-1. That means there are no arguments based on the donor-acceptor strength, such as HSAB or basicity, because the enthalpy of reaction is positive. The tightness of binding must result from the positive entropy, which comes from the net increase in the number of molecules as the reaction proceeds (the chelate effect).

The moderately positive enthalpy change is probably related to ring strain in the multidentate complex.

References

1. Complex-Ion Equilibria https://chem.libretexts.org/@go/page/516 (accessed Jun 25, 2021).
2. Complex Ion Formation Constants https://chem.libretexts.org/@go/page/6648 (accessed Jun 25, 2021).
3. Cotton, F.A.; Wilkinson, G. *Advanced Inorganic Chemistry*, 4th Ed. John Wiley & Sons: New York, 1980, pp 71-73.
4. Wilbur S, Williams M, Williams R, et al. Toxicological Profile for Carbon Monoxide. Atlanta (GA): Agency for Toxic Substances and Disease Registry (US); 2012 Jun. Table 3-12, Hemoglobin and Myoglobin Binding Kinetics and Equilibrium Constants for Oxygen and Carbon Monoxide. Available from: https://www.ncbi.nlm.nih.gov/books/NBK153687/table/T22/ (accessed Jun 26, 2021).
5. Miessler, G. L.; Fischer, P. J.; Tarr, D. A. *Inorganic Chemistry*, 5th Ed. Pearson: Upper Saddle River, NJ, p. 358.

This page titled 4.2.1.1: Thermodynamic Data is shared under a CC BY-NC 3.0 license and was authored, remixed, and/or curated by Chris Schaller.

- **10.1.1: Thermodynamic Data** by Chris Schaller is licensed CC BY-NC 4.0.

4.2.1.2: Magnetic Susceptibility

Electronic Structure

The electronic structure of coordination complexes can lead to several different properties that involve different responses to magnetic fields. These properties can vary between related compounds because of differences in electron counts, geometry, or donor strength. As a result, magnetic measurement of these materials can be used as a tool to provide insight into the structure of a coordination complex.

Diamagnetic and paramagnetic compounds are two common categories defined by interaction with a magnetic field. Diamagnetic compounds display a very slight repulsion from magnetic fields. The interaction is quite subtle and requires the proper instrumentation if it is to be observed; it's not something you would normally notice by waving a magnet in front of a vial of coordination complex. In contrast, paramagnetic compounds display a very slight attraction to magnetic fields. In terms of electronic structure, diamagnetic compounds have all of their electrons in pairs whereas paramagnetic compounds have one or more unpaired electrons. These definitions are not limited to coordination complexes. Atmospheric oxygen, O_2, is a common example of a paramagnetic compound. Atmospheric nitrogen, N_2, is a common example of a diamagnetic compound.

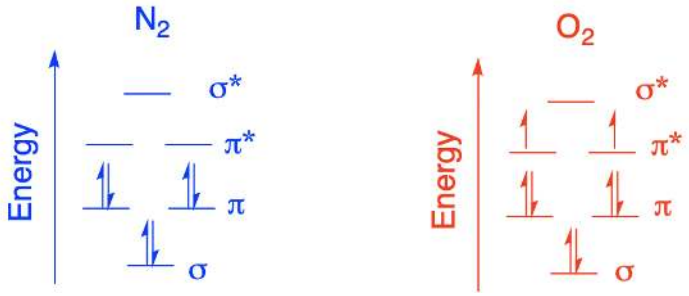


Figure **4.2.1.2.1**: Valence molecular orbital diagrams of N_2 and O_2 show that N_2 is diamagnetic while O_2 is paramagnetic. (CC-BY-NC; Chris Schaller)

These differences arise because of a quantum mechanical property of electrons and other subatomic particles: spin. Spin does not have a direct macroscopic analogy; physical chemists often urge caution about equating it to a phenomenon on the level at which we observe the universe. However, we do know that spin is related to magnetic phenomena. We can think of an electron as having a magnetic moment. There are two allowed values of this magnetic moment ($+\frac{1}{2}$ and $-\frac{1}{2}$) that differ in orientation; spin is a vector quantity. Normally, there is no preference for one orientation over the other. If a coordination complex has one unpaired electron, and we have a million of those coordination complexes in a very tiny sample, about 500,000 of the unpaired electrons would have spin = $+\frac{1}{2}$ and about 500,000 of them would have spin = $-\frac{1}{2}$. The spin of each electron is randomly oriented. As a result, the material would have no net magnetic moment. In the presence of a magnetic field, however, there is a small energy difference between those two spin states. As a result, a majority of the spins adopt the energetically more favorable orientation. Although the material by itself has no net magnetic field, one has temporarily been induced by the influence of an external magnetic field. This is what we mean by magnetic susceptibility.

Measuring Magnetic Susceptibility

All diamagnetic compounds have a roughly similar response to a magnetic field; either their electrons are all paired or they are not. Paramagnetic compounds, however, can respond quite differently to a magnetic field, depending on the number of unpaired electrons. The more unpaired electrons there are, the stronger the magnetic susceptibility will be, and so the stronger the attraction between the compound and the magnetic field. For this reason, measuring the strength of attraction of a compound for a magnetic field can reveal the number of unpaired electrons in the compound. This relationship is most straightforward for complexes of first row transition metals (**3*d*** metals), becoming a little more complicated for the **4*d*** and **5*d*** series.

A Guoy balance is probably the simplest example of a method for determining the presence of unpaired electrons in a coordination complex.[1] It uses a balance, a sample holder and a magnet. Essentially, the magnet is weighed in the presence and absence of the sample. The discrepancy between the two measurements arises because of the interaction of the sample with the magnetic field. Any diamagnetic sample causes slight downward repulsion, registering as a heavier weight. A paramagnetic sample suspended

between the poles of the magnet causes a slight upward pull on the magnet, which registers as a lighter weight. The more unpaired electrons there are, the greater the induced magnetic moment, and so the lighter the weight becomes.

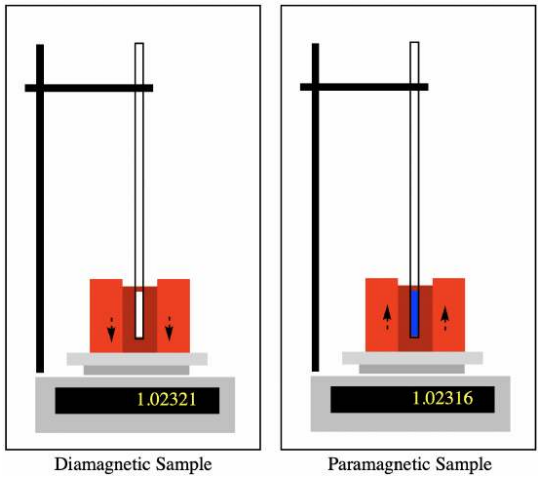


Figure 4.2.1.2.2: Diagram of a Guoy balance. A magnet (red) sits on a balance and a sample tube is placed in the center cavity of the magnet. (CC-BY-NC; Chris Schaller)

From that measurement, we can extract a parameter that we normally refer to as the effective magnetic moment of the material, μ_{eff}. The magnetic moment is expressed in units called Bohr magnetons. A Bohr magneton (BM or μ_B) is defined as:

$$1\text{BM} = \frac{eh}{4\pi mc}$$

in which e is the charge on an electron; h is Planck's constant; m is the mass of the electron; c is the speed of light.

This experimental quantity is fitted to a simple relationship that depends on the number of unpaired electrons. This mathematical model gives a prediction of the "spin-only" magnetic moment. If the magnetic moment arises purely from the number of unpaired electrons without additional complicating factors, the fit to the experimental data is pretty good.

$$\mu_{eff} \approx \mu_{so} = g\sqrt{S(S+1)}$$

Here, g is the gyromagnetic ratio, which is a proportionality constant between the angular momentum of the electron and the magnetic moment. It has a value of 2.00023, or approximately 2.0. The term $\sqrt{S(S+1)}$ is the value of the angular momentum, which depends on the number of unpaired electrons; S is the absolute value of the sum of the individual spins of the valence electrons. Of course, the spins would cancel out in electrons that were paired, because one would have $m_s = \frac{1}{2}$ and the other would have $m_s = -\frac{1}{2}$. For unpaired electrons, Hund's rule states that they would have parallel spins; for example, two unpaired electrons gives $S = 1$.

Number of unpaired electrons, n	Maximum total spin, S	Spin-only magnetic moment, $\mu_{so}(BM)$
1	$\frac{1}{2}$	1.73
2	1	2.83
3	$\frac{3}{2}$	3.87
4	2	4.90
5	$\frac{5}{2}$	5.92

The table above shows how the magnetic moment changes with the number of unpaired electrons. The maximum number of unpaired electrons given is five, because for a transition metal a sixth electron would have to pair up in a previously occupied orbital. In f-block elements, there could be seven unpaired electrons before pairing occurs because there are seven f orbitals rather than just five d orbitals.

Note that the expression for spin-only magnetic moment is sometimes written in an alternative way, based directly on the number of unpaired electrons, n, rather than S.

$$\mu_{eff} \approx \mu_{so} = \sqrt{n(n+2)}$$

There is an additional approximation in these cases, based on how the values of the spin-only magnetic moment correlate with the number of unpaired electrons. If we always round the value of μ_{so}, then it is one greater than the number of unpaired electrons. Thus, $\mu_{so} \approx n+1$, provided of course that there are any unpaired electrons at all; the relationship doesn't hold if n = 0 because then $\mu_{so} = 0$, not 1.

In reality, observed magnetic moments are slightly different than spin-only magnetic moments. In some cases, the observed magnetic moment is smaller than expected, but those cases are more complicated and we won't consider them here. Very often, the observed magnetic moments are larger than predicted because orbital angular momentum also plays a role in determining the magnitude of the overall magnetic moment. We may use a modified expression that takes this part into account.

$$\mu_{eff} \approx \mu_{s+L} = g\sqrt{S(S+1) + \frac{1}{4}L(L+1)}$$

Just as *S* is the absolute value of the sum of the spin quantum numbers in the ion, m_s, *L* is the absolute value of the sum of the orbital quantum numbers, m_l. There are five d orbitals, with $m_l = 2, 1, 0, -1, -2$, and the value of *L* has to be maximized according to Hund's rule. That means the value of *L* can be 3, 2, or 0.

As an example, suppose we have a Co^{2+} ion. Co^{2+} ion has a d^7 configuration. It has five d orbitals, so four of these electrons are paired, leaving only three unpaired electrons with parallel spins, so $S = 3/2$. In order to maximize the orbital quantum number, L, two electrons will be in an orbital with $m_l = 2$, two electrons will be in an orbital with $m_l = 1$, and one electron will be in each orbital with m_l = 0, -1, and -2. When we take the sum, we find $L = 2+2+1+1+0-1-2 = 3$. That gives us:

$$\mu_{s+L} = g\sqrt{3/2(3/2+1) + \frac{1}{4}3(3+1)} = 5.20$$

In comparison, $m_{so} = 3.87$ in this case. Observed values of μ_{eff} vary between different Co^{2+} complexes but are generally in the range 4.1 – 5.2 BM.[2] The orbital contribution is often smaller than expected, so magnetic susceptibilities frequently fall somewhere between μ_{so} and μ_{S+L}.

The use of a simple Guoy balance is an historically important method of determining magnetic susceptibility, and it is sometimes used in undergraduate laboratory experiments. Other methods are frequently used to measure magnetic susceptibility in the research laboratory. A magnetic susceptibility balance operates on a similar principle to the one behind the Guoy balance. A sample is placed within the poles of an electromagnet, causing the electromagnet to move very slightly. The current in the electromagnet is adjusted, changing its magnetic field, until the magnet comes back to its initial position. The magnitude of the current adjustment is proportional to the magnetic susceptibility of the sample.

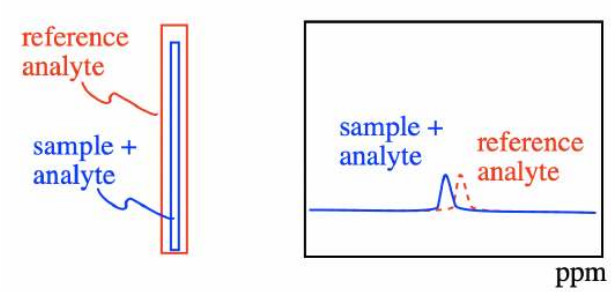


Figure **4.2.1.2.3**: The Evans Method uses chemical shifts (from NMR) to measure magnetic susceptibility. Left: A capillary tube containing sample and a reference analyte is bathed in a larger tube containing reference analyte solution. Right: The NMR signal of a reference analyte (red) is shifted when that analyte is mixed with a paramagnetic sample (blue). (CC-BY-NC; Chris Schaller)

A superconducting quantum interference device (SQUID) uses a superconducting loop in an external magnetic field to measure magnetic susceptibility of a sample.[3] The sample is mechanically moved though the superconducting loop, inducing a change in current and magnetic field that are proportional to the magnetic susceptibility of the sample. Commercially produced SQUID magnetometers often have variable temperature controls, allowing magnetic susceptibility to be measured across a range of temperatures.

The Evans NMR method is quite common because of the widespread availability of high-field NMR spectrometers in research labs. A capillary containing the paramagnetic sample and a reference analyte is placed in an NMR tube containing the same reference analyte but without the paramagnetic sample. The analyte in the presence of the paramagnetic material will experience a local, induced magnetic field owing to the effect of the superconducting magnet of the NMR instrument on the paramagnetic sample. Its NMR signals will shift as a result. The NMR signal of the analyte outside the capillary will undergo no such shift, and the difference in the two signals is an indicator of the magnetic susceptibility of the sample.

There are other types of magnetic behavior in addition to diamagnetism and paramagnetism. Ferromagnetic materials have long-range order with spins oriented parallel to each other, even in the absence of an external magnetic field. Common, permanent magnets are made from ferromagnetic materials. Antiferromagnetic materials also have long-range order, but the magnetic moments are arranged in opposing pairs. These three different magnetic behaviors are diagnosed by the temperature dependence of the magnetic susceptibility. Paramagnetic materials display magnetic susceptibility (χ_M, related to μ_{eff}) that increases with the inverse of temperature. Ferromagnetic materials have a critical temperature below which magnetic susceptibility rapidly rises. Antiferromagnetic materials have a critical temperature below which magnetic susceptibility rapidly falls. However, these behaviors are largely beyond the scope of the current discussion.

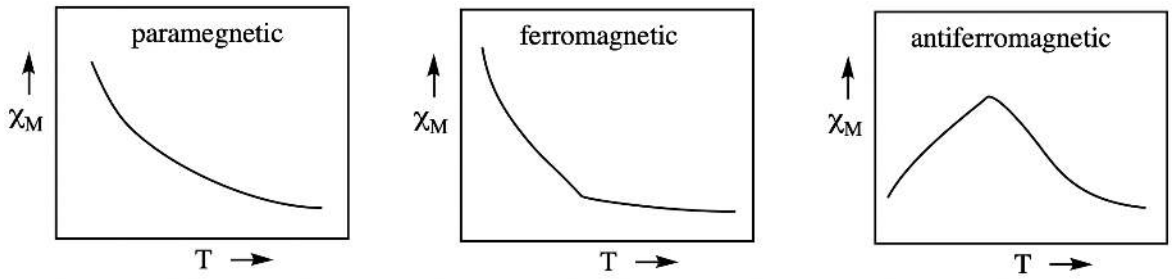


Figure **4.2.1.2.4**: Magnetic behavior depends on temperature. Shown are plots of magnetic behaviour in terms of magnetic susceptibility χ_M versus temperature (T). (CC-BY-NC; Chris Schaller)

Problems

? Exercise 4.2.1.2.1

Show that, given g = 2.0, then $g\sqrt{S(S+1)} = \sqrt{n(n+2)}$.

Answer

$$\begin{aligned}\mu_{so} &= g\sqrt{S(S+1)} \\ &= 2\sqrt{S(S+1)} \\ &= \sqrt{4S(S+1)} \\ &= \sqrt{2S(2S+2)}\end{aligned}$$

but $S = n(1/2)$ or $n = 2S$ then

$$\mu_{so} = \sqrt{n(n+2)}$$

? Exercise 4.2.1.2.2

Calculate the value of μ_{so} in the following cases:

a) V^{4+} b) Cr^{2+} c) Ni^{2+} d) Co^{3+} e) Mn^{2+} f) Fe^{2+}

Answer

a) V^{4+} is $d^1; n = 1; \sqrt{n(n+2)} = 1.73$
b) Cr^{2+} is $d^4; n = 4; \sqrt{n(n+2)} = 4.90$

c) Ni^{2+} is $d^8; n = 2; \sqrt{n(n+2)} = 2.83$
d) Co^{3+} is $d^6; n = 0; \sqrt{n(n+2)} = 0$
e) Mn^{2+} is $d^5; n = 5; \sqrt{n(n+2)} = 5.92$
f) Fe^{2+} is $d^6; n = 4; \sqrt{n(n+2)} = 4.90$
g) Cr^{3+} is $d^3; n = 3; \sqrt{n(n+2)} = 3.87$
h) V^{3+} is $d^2; n = 2; \sqrt{n(n+2)} = 2.83$

? Exercise 4.2.1.2.3

Calculate the value of μ_{eff} in the following cases:

a) V^{4+} b) Cr^{2+} c) Ni^{2+} d) Co^{3+} e) Mn^{2+} f) Fe^{2+}

g) Cr^{3+} h) V^{3+}

Answer

a) V^{4+} is $d^1; S = 1/2; L = 2; \mu_{s+L} = g\sqrt{1/2(1/2+1) + \frac{1}{4}2(2+1)} = 3.00$
b) Cr^{2+} is $d^4; S = 2; L = 2+1+0-1 = 2; \mu_{s+L} = g\sqrt{2(2+1) + \frac{1}{4}2(2+1)} = 5.48$
c) Ni^{2+} is $d^8; S = 1; L = 2+2+1+1+0+0-1-2 = 3; \mu_{s+L} = g\sqrt{1(1+1) + \frac{1}{4}3(3+1)} = 2.24$
d) Co^{3+} is $d^6; S = 2; L = 2+2+1+0-1-2 = 2; \mu_{s+L} = g\sqrt{(2+1) + \frac{1}{4}2(2+1)} = 5.48$
e) Mn^{2+} is $d^5; S = 5/2; L = 2+1+0-1-2 = 0; \mu_{s+L} = g\sqrt{5/2(5/2+1) + \frac{1}{4}0(0+1)} = 5.92$
f) Fe^{2+} is $d^6; S = 2; L = 2+2+1+0-1-2 = 2; \mu_{s+L} = g\sqrt{2(2+1) + \frac{1}{4}2(2+1)} = 5.48$
g) Cr^{3+} is $d^3; S = 3/2; L = 2+1+0 = 3; \mu_{s+L} = g\sqrt{3/2(3/2+1) + \frac{1}{4}3(3+1)} = 5.20$
h) V^{3+} is $d^2; S = 1; L = 2+1 = 3; \mu_{s+L} = g\sqrt{1(1+1) + \frac{1}{4}3(3+1)} = 2.24$

References

1. Lancashire, R. J. Magnetic Susceptibility https://chem.libretexts.org/Bookshelves/Inorganic_Chemistry/Map%3A_Inorganic_Chemistry_(Housecroft)/04%3A_Experimental_techniques/4.14%3A_Magnetism/Magnetic_Susceptibility_Measurements (accessed Jun 27, 2021).
2. Cotton, F.A.; Wilkinson, G. *Advanced Inorganic Chemistry*, 4th Ed. John Wiley & Sons: New York, 1980, p 628.
3. Raja, P. M. V.; Barron, A. R. Magnetism https://chem.libretexts.org/@go/page/55872 (accessed Jun 27, 2021).

This page titled 4.2.1.2: Magnetic Susceptibility is shared under a CC BY-NC 3.0 license and was authored, remixed, and/or curated by Chris Schaller.

- **10.1.2: Magnetic Susceptibility** by Chris Schaller is licensed CC BY-NC 4.0.

4.2.1.3: Electronic Spectra

The interaction of different wavelengths of electromagnetic radiation with matter provides a vast amount of information about material structure. The absorption of UV-visible light is connected to the excitation of electrons to higher orbitals. Inherently, this spectroscopy reveals information about the electronic structure of compounds, including coordination complexes. This topic is important enough that it is the subject of a later chapter.

This page titled 4.2.1.3: Electronic Spectra is shared under a CC BY-NC 3.0 license and was authored, remixed, and/or curated by Chris Schaller.

- **10.1.3: Electronic Spectra** by Chris Schaller is licensed CC BY-NC 4.0.

4.2.1.4: Coordination Number and Molecular Shapes

Examination of physical properties, such as electronic spectra or magnetic susceptibility, can often be used to distinguish between possible molecular geometries of coordination complexes. It can be difficult to predict the coordination number of a complex formed from a specific metal ion and a given set of ligands, to say nothing of its geometry. Steric crowding and valence electron count around the metal in the complex are just two of the factors that influence coordination number. Even for a given coordination number, there are sometimes different possible coordination geometries. For example, five-coordinate can adopt square pyramidal or trigonal bipyramidal geometry. In most cases, it is especially difficult to predict which geometry prevails. In fact, many complexes adopt a geometry somewhere between the two. Four-coordinate geometry offers a similar choice between square planar and tetrahedral geometry, although in this case it can be easier to predict which one is likely to occur. The energetic difference between these two possible geometries can often be explained based on the electronic structure of the complex.

This page titled 4.2.1.4: Coordination Number and Molecular Shapes is shared under a CC BY-NC 3.0 license and was authored, remixed, and/or curated by Chris Schaller.

- **10.1.4: Coordination Number and Molecular Shapes** by Chris Schaller is licensed CC BY-NC 4.0.

4.2.2: Bonding Theories

Coordination complexes caused great fascination among chemists during the nineteenth century, although it wasn't until the century's end that Alfred Werner determined the fundamental principles of their structure. A fuller understanding of their structures was developed over the first half of the twentieth century. This understanding developed in stages, with newer theories and models building on previous ones rather than replacing them completely.

Crystal Field Theory

In the early 1930's, American physicists John Hasbrouck van Vleck and Hans Bethe developed a theoretical treatment of crystalline transition metal compounds that explained their magnetic and optical properties. This treatment did not consider bonding in any way, but it did concern itself with the geometry of ligands, or counterions, around a central metal ion. Electrostatic considerations formed the basis of the theory, with attention to repulsive forces between ligand electrons and $\boldsymbol{d}$ electrons on the metal ion. The model gave good predictions about the effect of ligand geometry on the electronic structure of the metal ion.

Ligand Field Theory

During the 1950's, British chemists John Stanley Griffith and Leslie Orgel combined some aspects of crystal field theory with molecular orbital theory to produce a bonding model for coordination complexes. Rather than just considering electrostatic interactions between metal and ligand, this approach used orbital interactions to model the role of covalency in determining the electronic structure of the complex.

Angular Overlap Model

This model is a specific approach to considering how ligand and metal orbitals combine to produce molecular orbitals in a coordination complex. It uses the symmetry and orientation of atomic orbitals to determine what combinations of these orbitals should be considered.

Computational Chemistry

The three "pencil-and-paper models" described above for bonding in coordination complexes have been greatly augmented by the power of modern computational chemistry. Although based on the same principles, computational methods offer a much higher level of quantitative information about electronic energy and allow relatively easy assessment of possible structural features such as coordination geometry. Pioneering methods included extended Hückel theory, originally developed by Roald Hoffman and Robert Burns Woodward to study pericyclic reactions. The method was later adapted by Hoffman and others to investigate inorganic and organometallic complexes. More recently, developments such as density functional theory have greatly facilitated computational work on transition metal systems because of their simplified treatment of many-electron systems. These approaches and others like them allow for the prediction of coordination complex properties through a computer interface.

This page titled 4.2.2: Bonding Theories is shared under a CC BY-NC 3.0 license and was authored, remixed, and/or curated by Chris Schaller.

- **10.2: Bonding Theories** by Chris Schaller is licensed CC BY-NC 3.0.

SECTION OVERVIEW

4.2.2.1: Crystal Field Theory

One of the most striking characteristics of transition-metal complexes is the wide range of colors they exhibit. Crystal field theory (CFT) is a bonding model that explains many important properties of transition-metal complexes, including their colors, magnetism, structures, stability, and reactivity. The central assumption of CFT is that metal–ligand interactions are purely electrostatic in nature.

4.2.2.1.1: Crystal Field Theory

4.2.2.1.2: Colors of Coordination Complexes

4.2.2.1.3: Crystal Field Stabilization Energy

4.2.2.1.4: Factors That Affect the Magnitude of Δo

4.2.2.1.5: Jahn-Teller Distortions

4.2.2.1.6: Magnetic Moments of Transition Metals

4.2.2.1.7: Magnetism

4.2.2.1.8: Thermodynamics and Structural Consequences of d-Orbital Splitting

Template:HideTOC

4.2.2.1: Crystal Field Theory is shared under a not declared license and was authored, remixed, and/or curated by LibreTexts.

4.2.2.1.1: Crystal Field Theory

Crystal field theory (CFT) describes the breaking of orbital degeneracy in transition metal complexes due to the presence of ligands. CFT qualitatively describes the strength of the metal-ligand bonds. Based on the strength of the metal-ligand bonds, the energy of the system is altered. This may lead to a change in magnetic properties as well as color. This theory was developed by Hans Bethe and John Hasbrouck van Vleck.

Basic Concept

In Crystal Field Theory, it is assumed that the ions are **simple point charges** (a simplification). When applied to alkali metal ions containing a symmetric sphere of charge, calculations of bond energies are generally quite successful. The approach taken uses classical potential energy equations that take into account the attractive and repulsive interactions between charged particles (that is, Coulomb's Law interactions).

$$E \propto \frac{q_1 q_2}{r} \tag{4.2.2.1.1.1}$$

with

- E the bond energy between the charges and
- q_1 and q_2 are the charges of the interacting ions and
- r is the distance separating them.

This approach leads to the correct prediction that large cations of low charge, such as K^+ and Na^+, should form few coordination compounds. For transition metal cations that contain varying numbers of d electrons in orbitals that are NOT spherically symmetric, however, the situation is quite different. The shape and occupation of these d-orbitals then becomes important in an accurate description of the bond energy and properties of the transition metal compound.

Description of *d*-Orbitals

To understand CFT, one must understand the description of the lobes:

- d_{xy}: lobes lie in-between the x and the y axes.
- d_{xz}: lobes lie in-between the x and the z axes.
- d_{yz}: lobes lie in-between the y and the z axes.
- $d_{x^2-y^2}$: lobes lie on the x and y axes.
- d_{z^2}: there are two lobes on the z axes and there is a donut shape ring that lies on the xy plane around the other two lobes.

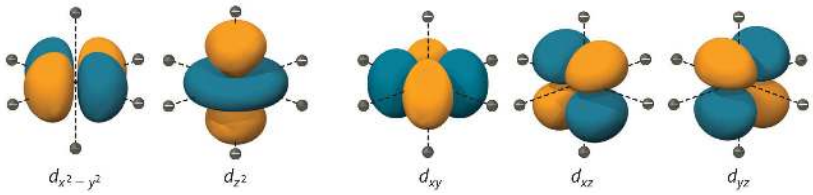


Figure **4.2.2.1.1.1**: Spatial arrangement of ligands in the an octahedral ligand field with respect to the five d-orbitals.

Octahedral Complexes

When examining a single transition metal ion, the five d-orbitals have the same energy (Figure **4.2.2.1.1.2**). When ligands approach the metal ion, some experience more opposition from the d-orbital electrons than others based on the geometric structure of the molecule. Since ligands approach from different directions, not all d-orbitals interact directly. These interactions, however, create a splitting due to the electrostatic environment.

For example, consider a molecule with octahedral geometry. Ligands approach the metal ion along the x, y, and z axes. Therefore, the electrons in the d_{z^2} and $d_{x^2-y^2}$ orbitals (which lie along these axes) experience greater repulsion. It requires more energy to have an electron in these orbitals than it would to put an electron in one of the other orbitals. This causes a splitting in the energy levels of the d-orbitals. This is known as **crystal field splitting**. For octahedral complexes, crystal field splitting is denoted by Δ_o (or Δ_{oct}). Any orbital that has a lobe on the axes moves to a higher energy level. The energies of the d_{z^2} and $d_{x^2-y^2}$ orbitals increase due to greater interactions with the ligands. The d_{xy}, d_{xz}, and d_{yz} orbitals decrease in energy with respect to the normal energy level and become more stable. This means that in an octahedral, the energy levels of e_g are higher (by $0.6\Delta_o$) while t_{2g} are lower (by $0.4\Delta_o$). It should be noted that the labels t_{2g} and e_g come from group theory and the octahedral point group. The energy difference between the t_{2g} and e_g orbitals dictates the energy that the complex will absorb causing electrons to move from one level to the next. For transition metal complexes, the absorbed energy is typically in the visible part of the spectrum and thus this will determine the color of the complex. Whether the complex is paramagnetic or diamagnetic will be determined by the spin state. If there are unpaired electrons, the complex is paramagnetic; if all electrons are paired, the complex is diamagnetic.

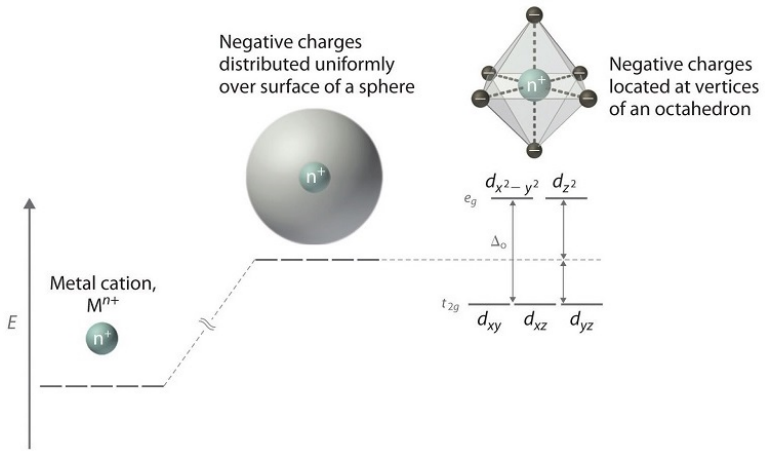


Figure **4.2.2.1.1.2**: (a) Distributing a charge of −6 uniformly over a spherical surface surrounding a metal ion causes the energy of all five d orbitals to increase due to electrostatic repulsions, but the five d orbitals remain degenerate. Placing a charge of −1 at each vertex of an octahedron causes the d orbitals to split into two groups with different energies: the $d_{x^2-y^2}$ and d_{z^2} orbitals increase in energy, while the, d_{xy}, d_{xz}, and d_{yz} orbitals decrease in energy. The average energy of the five d orbitals is the same as for a spherical distribution of a −6 charge, however. Attractive electrostatic interactions between the negatively charged ligands and the positively charged metal ion (far right) cause all five d orbitals to decrease in energy but does not affect the splittings of the orbitals. (b) The two e_g orbitals (left) point directly at the six negatively charged ligands, which increases their energy compared with a spherical distribution of negative charge. In contrast, the three t_{2g} orbitals (right) point between the negatively charged ligands, which decreases their energy compared with a spherical distribution of charge.

Electrons in Orbitals

According to the Aufbau principle, electrons are filled from lower to higher energy orbitals (Figure **4.2.2.1.1.3**). For the octahedral case above, this corresponds to the d_{xy}, d_{xz}, and d_{yz} orbitals. Following Hund's rule, electrons are filled in order to have the highest number of unpaired electrons. For example, if one had a d^3 complex, there would be three unpaired electrons. If one were to add an electron, however, it has the ability to fill a higher energy orbital (d_{z^2} or $d_{x^2-y^2}$) or pair with an electron residing in the d_{xy}, d_{xz}, or d_{yz} orbitals. This pairing of the electrons requires energy (spin pairing energy). If the pairing energy is less than the crystal field splitting energy, Δ_o, then the next electron will go into the d_{xy}, d_{xz}, or d_{yz} orbitals due to stability. This situation allows for the least amount of unpaired electrons, and is known as low spin. If the pairing energy is greater than Δ_o, then the next electron will go into the d_{z^2} or $d_{x^2-y^2}$ orbitals as an unpaired electron. This situation allows for the most number of unpaired electrons, and is known as high spin. Ligands that cause a transition metal to have a small crystal field splitting, which leads to high spin, are called weak-field ligands. Ligands that produce a large crystal field splitting, which leads to low spin, are called *strong field ligands*.

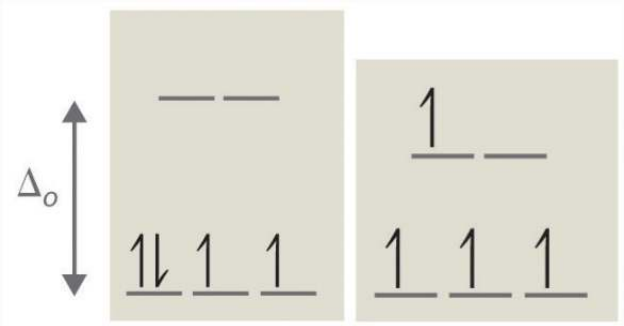


Figure **4.2.2.1.1.3**: Low Spin, Strong Field (Δ_o˃P) High Spin, Weak Field (Δ_o˂P)Splitting for a d^4 complex under a strong field (left) and a weak field (right). The strong field is a low spin complex, while the weak field is a high spin complex.

As mentioned above, CFT is based primarily on symmetry of ligands around a central metal/ion and how this anisotropic (properties depending on direction) ligand field affects the metal's atomic orbitals; the energies of which may increase, decrease or not be affected at all. Once the ligands' electrons interact with the electrons of the d-orbitals, the electrostatic interactions cause the energy levels of the d-orbital to fluctuate depending on the orientation and the nature of the ligands. For example, the valence and the strength of the ligands determine splitting; the higher the valence or the stronger the ligand, the larger the splitting. Ligands are classified as strong or weak based on the spectrochemical series:

$$I < Br < Cl < \underline{S}CN < F < OH < ox < \underline{O}NO < H_2O < SC\underline{N} < EDTA < NH_3 < en < \underline{N}O_2 < CN$$

Note that SCN and NO_2 ligands are represented twice in the above spectrochemical series since there are two different Lewis base sites (e.g., free electron pairs to share) on each ligand (e.g., for the SCN ligand, the electron pair on the sulfur or the nitrogen can form the bond to a metal). The specific atom that binds in such ligands is underlined.

Tetrahedral Complexes

In a tetrahedral complex, there are four ligands attached to the central metal. The d orbitals also split into two different energy levels. The top three consist of the d_{xy}, d_{xz}, and d_{yz} orbitals. The bottom two consist of the $d_{x^2-y^2}$ and d_{z^2} orbitals. The reason for this is due to poor orbital overlap between the metal and the ligand orbitals. The orbitals are directed on the axes, while the ligands are not.

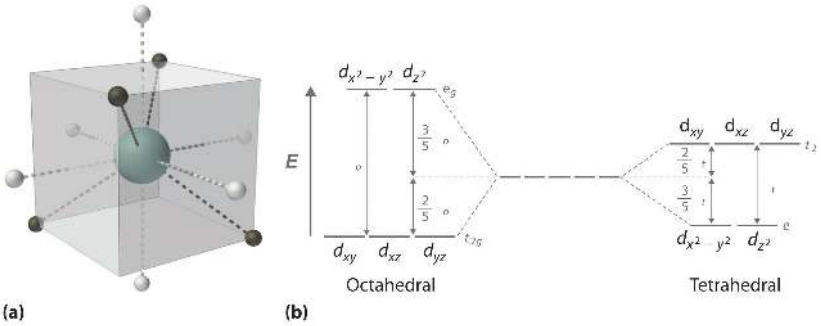


Figure 4.2.2.1.1.5: (a) Tetraheral ligand field surrounding a central transition metal (blue sphere). (b) Splitting of the degenerate d-orbitals (without a ligand field) due to an octahedral ligand field (left diagram) and the tetrahedral field (right diagram).

The difference in the splitting energy is tetrahedral splitting constant (Δ_t), which less than (Δ_o) for the same ligands:

$$\Delta_t = 0.44\,\Delta_o \tag{4.2.2.1.1.2}$$

Consequentially, Δ_t is typically smaller than the spin pairing energy, so tetrahedral complexes are usually **high spin**. As seen with octahedral compounds, the labels for the groups of orbitals, t_2 and e in this case, come from group theory and the tetrahedral point group.

Square Planar Complexes

In a square planar, there are four ligands as well. However, the difference is that the electrons of the ligands are only attracted to the xy plane. Any orbital in the xy plane has a higher energy level (Figure 4.2.2.1.1.6). There are four different energy levels for the square planar (from the highest energy level to the lowest energy level): $d_{x^2-y^2}$, d_{xy}, d_{z^2}, and both d_{xz} and d_{yz}.

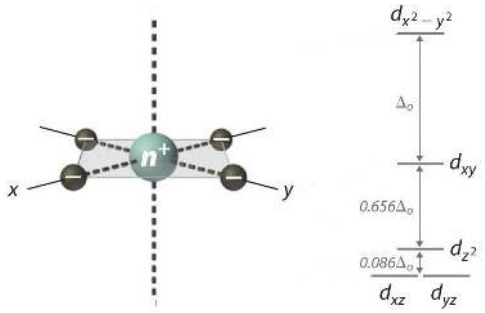


Figure 4.2.2.1.1.6: Splitting of the degenerate d-orbitals (without a ligand field) due to an square planar ligand field.

The splitting energy (from highest orbital to lowest orbital) is Δ_{sp} and tends to be larger then Δ_o

$$\Delta_{sp} = 1.74\,\Delta_o \tag{4.2.2.1.1.3}$$

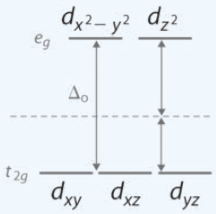
Moreover, Δ_{sp} is also larger than the pairing energy, so the square planar complexes are usually **low spin** complexes.

Exercise 4.2.2.1.1.1

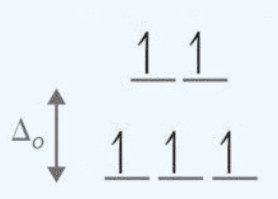
For the complex ion $[Fe(Cl)_6]^{3-}$ determine the number of d-electrons for Fe, sketch the d-orbital energy levels and the distribution of d electrons among them, list the number of lone electrons, and label whether the complex is paramagnetic or diamagnetic.

Answer

Step 1: Determine the valence of Fe. Here it is Fe(III). Based on its electron configuration, Fe(III) has **5 d-electrons**. Step 2: Determine the geometry of the ion. Here it is an octahedral which means the energy splitting should look like:



Step 3: Decide whether the ligand induces is a strong or weak field spin by looking at the spectrochemical series. Cl^- is a weak field ligand (i.e., it induces high spin complexes). Therefore, electrons will likely fill all orbitals before being paired.



Step four: Count the number of lone electrons. Here, there are **5 electrons**. Step five: The five unpaired electrons means this complex ion is **paramagnetic** (and strongly so).

Exercise 4.2.2.1.1.2

A *tetrahedral* complex absorbs at 545 nm. Estimate the octahedral crystal field splitting (Δ_o) for an octahedral compound of the same metal with the same ligands? What would be the color of the complex?

Answer

$$\Delta_t = \frac{hc}{\lambda} \tag{4.2.2.1.1.4}$$

$$\Delta_t = \frac{(6.626 \times 10^{-34} J \cdot s)(3 \times 10^8 m/s)}{545 \times 10^{-9} m} = 3.65 \times 10^{-19}\ J \tag{4.2.2.1.1.5}$$

However, the *tetrahedral* splitting (Δ_t) is ~4/9 that of the *octahedral* splitting (Δ_o).

$$\Delta_t = 0.44\Delta_o \tag{4.2.2.1.1.6}$$

$$\Delta_o = \frac{\Delta_t}{0.44} = \frac{3.65 \times 10^{-19} J}{0.44} = 8.30 \times 10^{-18} J \tag{4.2.2.1.1.7}$$

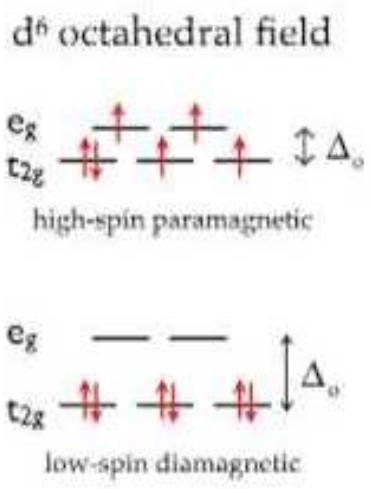
This is the energy needed to promote *one* electron in *one* complex. Often the crystal field splitting is given per mole, which requires this number to be multiplied by Avogadro's Number (6.022×10^{23}).

This complex appears red, since it absorbs in the complementary green color (determined via the color wheel).



Most ordinary materials have all electrons paired. Zero spin = diamagnetic (slight repulsion)

- Unpaired electrons have magnetic fields, so are attracted by an external field (paramagnetic)
- Permanently oriented spins are ferromagnetic



Video:

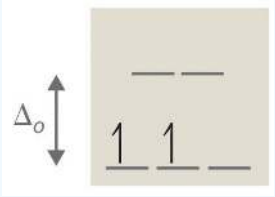
Exercise 4.2.2.1.1.3

For each of the following, sketch the d-orbital energy levels and the distribution of d electrons among them, state the geometry, list the number of d-electrons, list the number of lone electrons, and label whether they are paramagnetic or dimagnetic:

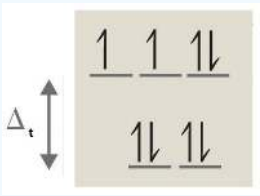
1. $[Ti(H_2O)_6]^{2+}$
2. $[NiCl_4]^{2-}$
3. $[CoF_6]^{3-}$ (also state whether this is low or high spin)
4. $[Co(NH_3)_6]^{3+}$ (also state whether this is low or high spin)

Answer

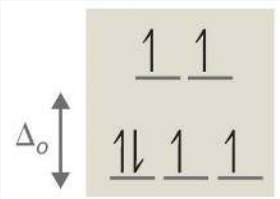
1. octahedral, 2, 2, paramagnetic



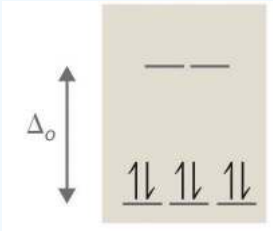
2. tetrahedral, 8, 2, paramagnetic (see Octahedral vs. Tetrahedral Geometries)



3. octahedral, 6, 4, paramagnetic, high spin



4. octahedral, 6, 0, diamagnetic, low spin



Contributors and Attributions

- Asadullah Awan (UCD), Hong Truong (UCD)
- Prof. Robert J. Lancashire (The Department of Chemistry, University of the West Indies)

4.2.2.1.1: Crystal Field Theory is shared under a CC BY-NC-SA 4.0 license and was authored, remixed, and/or curated by LibreTexts.

4.2.2.1.2: Colors of Coordination Complexes

The color for a coordination complex can be predicted using the Crystal Field Theory (CFT). Knowing the color can have a number of useful applications, such as the creation of pigments for dyes in the textile industry. The tendency for coordination complexes to display such a wide array of colors is merely coincidental; their absorption energies happen to fall within range of the visible light spectrum. Chemists and physicists often study the color of a substance not to understand its sheer appearance, but because color is an indicator of a chemical's physical proprieties on the atomic level.

The Electromagnetic Spectrum

The electromagnetic spectrum (EM) spectrum is made up of photons of different wavelengths. Photons, unique in displaying the properties of both waves and particles, create visible light and colors in a small portion of the EM spectrum. This visible light portion has wavelengths in approximately the 400-700 nanometer range (a nanometer, “nm,” is 10^{-9} meters). Each specific wavelength corresponds to a different color (Figure **4.2.2.1.2.1**), and when all the wavelengths are present, it appears as white light.

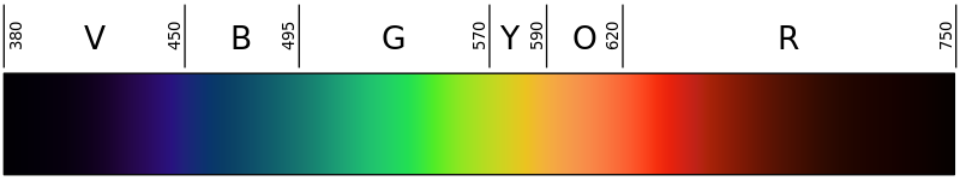


Figure **4.2.2.1.2.1**: A linear representation of the visible light spectrum. (Public Domain; Gringer via Wikipedia)

The wavelength and frequency of a wave are inversely proportional: as one increases, the other decreases; this is a consequence of all light traveling at the same speed.

$$\lambda = \nu^{-1} \qquad (4.2.2.1.2.1)$$

Because of this relationship, blue light has a much higher frequency and more energy than red light. In general, photons to the right of the EM spectrum have increasingly higher energy than photons to the left.

Perceiving Color

Color is perceived in two ways, through additive mixing, where different colors are made by combining different colors of light, and through subtractive mixing, where different wavelengths of light are taken out so that the light is no longer pure white. For colors of coordination complexes, subtractive mixing is considered. As shown in Figure **4.2.2.1.2.2**, the idea behind subtractive mixing is that white light (which is made from all the colors mixed together) interacts with an object. The object absorbs some of the light, and then reflects or transmits (or both, depending on the object) the rest of the light, which contacts the eye. The object is perceived as whichever color is not absorbed. In Figure **4.2.2.1.2.2**, white light (simplified as green, red, and blue bands) is shone through a solution. The solution absorbs the red and green wavelengths; however, the blue light is reflected and passes through, so the solution appears blue. This procedure takes place whenever an object displays visible color. If none of the light is absorbed, and all is reflected back off, the object appears white; if all of the light is absorbed, and there is none left to reflect or transmit through, the object appears black.

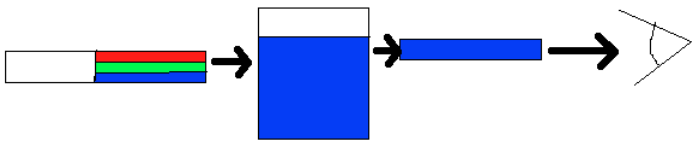


Figure **4.2.2.1.2.2**: Subtractive mixing

Colors of Coordination Complexes: Crystal Field Splitting

When ligands attach to a transition metal to form a coordination complex, electrons in the d orbital split into high energy and low energy orbitals. The difference in energy of the two levels is denoted as Δ, and it is a characteristic a property both of the metal and the ligands. This is illustrated in Figure **4.2.2.1.2.3**; the "o" subscript on the Δ indicates that the complex has octahedral geometry.

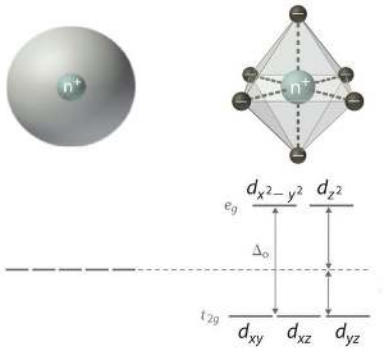


Figure **4.2.2.1.2.3**: d-Orbitals Splitting in an octahedral ligand field. (CC BY-SA-NC; anonymous by request)

If Δ_o is large, and much energy is required to promote electrons into the high energy orbitals, the electrons will instead pair in the lower energy orbitals, resulting in a "low spin" complex (Figure **4.2.2.1.2.4*A***); however, if Δ_o is small, and it takes little energy to occupy the higher orbitals, the electrons will do so, and remain unpaired (until there are more than five electrons), resulting in a “high spin” complex (Figure **4.2.2.1.2.4*B***). Different ligands are associated with either high or low spin —a "strong field" ligand results in a large Δ_o and a low spin configuration, while a "weak field" ligand results in a small Δ_o and a high spin configuration. For more details, see the Crystal Field Theory (CFT) page.

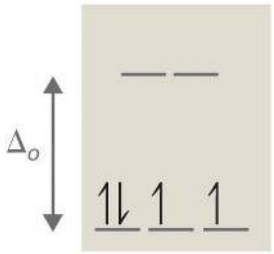


Figure **4.2.2.1.2.4*A***: Low Spin, Strong Field ($\Delta_o > P$). (CC BY-SA-NC; anonymous by request)

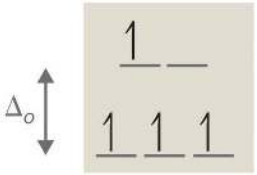


Figure **4.2.2.1.2.4*B***: High Spin, Weak Field ($\Delta_o < P$). (CC BY-SA-NC; anonymous by request)

A photon equal to the energy difference Δ_o can be absorbed, promoting an electron to the higher energy level. As certain wavelengths are absorbed in this process, subtractive color mixing occurs and the coordination complex solution becomes colored. If the ions have a noble gas configuration, and have no unpaired electrons, the solutions appear colorless; in reality, they still have a measured energy and absorb certain wavelengths of light, but these wavelengths are not in the visible portion of the EM spectrum and no color is perceived by the eye.

In general, a larger Δ_o indicates that higher energy photons are absorbed, and the solution appears further to the left on the EM spectrum shown in Figure **4.2.2.1.2.1**. This relationship is described in the equation

$$\Delta_o = hc/\lambda \qquad (4.2.2.1.2.2)$$

where h and c are constants, and λ is the wavelength of light absorbed.

Using a color wheel can be useful for determining what color a solution will appear based on what wavelengths it absorbs (Figure **4.2.2.1.2.6**). If a complex absorbs a particular color, it will have the appearance of whatever color is directly opposite it on the wheel. For example, if a complex is known to absorb photons in the orange range, it can be concluded that the solution will look blue. This concept can be used in reverse to determine Δ for a complex from the color of its solution.

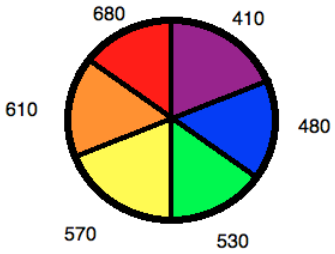


Figure 4.2.2.1.2.5

Relating the Colors of Coordination Complexes to the Spectrochemical Series

According to the Crystal Field Theory, ligands that have smaller Δ) values are considered "weak field" and will absorb lower-energy light with longer λ values (ie a "red shift"). Ligands that have larger Δ) values are considered "strong field" and will absorb higher-energy light with shorter λ values (ie a "blue shift"). This relates to the colors seen in a coordination complex. Weaker-field ligands induce the absorption of longer wavelength (lower frequency=lower energy) light than stronger-field ligands since their respective Δ_o values are **smaller** than the electron pairing energy.

The energy difference, Δ_o, determines the color of the coordination complex. According to the **spectrochemical series**, the high spin ligands are considered "weak field," and absorb longer wavelengths of light (weak Δ_o), while complexes with low spin ligands absorb light of greater frequency (high Δ_o). The color seen is the complementary color of the color associated with the absorbed wavelength. To predict which possible colors and their corresponding wavelengths are absorbed, the spectrochemical series can be used:

(Strong field/large Δ_0/low spin) (weak field/ small Δ_0/high spin)

CO, NO, CN>$\underline{N}O_2$>en>py≈NH_3>EDTA>SC$\underline{N}$>H_2O>ON$\underline{O}$>ox>OH>F>$\underline{S}$CN>Cl>Br>I

Exercise 4.2.2.1.2.1

If a solution with a dissolved octahedral complex appears yellow to the eye, what wavelength of light does it absorb? Is this complex expected to be low spin or high spin?

Answer

A solution that looks yellow absorbs light that is violet, which is roughly 410 nm from the color wheel. Since it absorbs high energy, the electrons must be raised to a higher level, and Δ_o is high, so the complex is likely to be low spin

Exercise 4.2.2.1.2.2

An octahedral metal complex absorbs light with wavelength 535 nm. What is the crystal field splitting Δ_o for the complex? What color is it to the eye?

Answer

To solve this question, we need to use the equation

$$\Delta_o = \frac{hc}{\lambda}$$

with

h is Planck's constant and is $6.625 \times 10^{-34} J \cdot s$ and c is the speed of light and is $2.998 \times 10^8 m/s$.

Note: the fact that the complex is octahedral makes no impact when solving this problem. Although the splitting is different for complexes of different structures, the mechanics of solving the problem are identical.

It is also important to remember that 1 nm is equal to 1×10^{-9} meters. With all this information, the final equation looks like this:

$$\Delta_o = \frac{(6.625 \times 10^{-34}\, J \cdot s)(2.998 \times 10^{8}\, m/s)}{(535 nm)\left(\frac{1\, m}{1 \times 10^{9}\, nm}\right)} = 3.712\, J/molecule$$

It is not necessary to use any equations to solve the second part of the problem. Light that is 535 nm is green, and because green light is absorbed, the complex appears red (refer to Figures **4.2.2.1.2.1** and **4.2.2.1.2.6** for this information).

Exercise 4.2.2.1.2.3

There are two solutions, one orange and one blue. Both solutions are known to be made up of a cobalt complex; however, one has chloride ions as ligands, while the other has ammonia ligands. Which solution is expected to be orange?

Answer

In order to solve this problem, it is necessary to know the relative strengths of the ligands involved. A sample ligand strength list is given here, but see Crystal Field Splitting for a more complete list:

$$CN > en > NH_3 > H_2O > F > SCN > Cl$$

From this information, it is clear that NH_3 is a stronger ligand than Cl, which means that the complex involving NH_3 has a greater Δ, and the complex will be low spin. Because of the larger Δ, the electrons absorb higher energy photons, and the solution will have the appearance of a lower energy color. Since orange light is less energetic than blue light, the NH_3 containing solution is predicted to be orange

References

1. Cox, P. A. Instant Notes Inorganic Chemistry. Second ed. Grand Rapids: Garland, Incorporated, 2004.
2. Nassau, Kurt. The Physics and Chemistry of Color : The Fifteen Causes of Color. Second ed. New York: Wiley-Interscience, 2001.
3. Petrucci, Ralph H., William S. Harwood, and Geoff E. Herring. General Chemistry : Principles and Modern Applications. Ninth ed. Upper Saddle River: Prentice Hall PTR, 2006.
4. Petrucci, Ralph H., Carey Bissonnette, F. Geoffrey Herring, Jeffrey D. Madura. General Chemistry: Principles and Modern Applications. Tenth Ed. Upper Saddle River: Pearson Education, Inc. 2011.

Contributors and Attributions

- Deyu Wang (UCD)

4.2.2.1.2: Colors of Coordination Complexes is shared under a not declared license and was authored, remixed, and/or curated by LibreTexts.

4.2.2.1.3: Crystal Field Stabilization Energy

A consequence of Crystal Field Theory is that the distribution of electrons in the d orbitals may lead to net stabilization (decrease in energy) of some complexes depending on the specific ligand field geometry and metal d-electron configurations. It is a simple matter to calculate this stabilization since all that is needed is the electron configuration and knowledge of the splitting patterns.

Definition: Crystal Field Stabilization Energy

The Crystal Field Stabilization Energy is defined as the energy of the electron configuration in the ligand field minus the energy of the electronic configuration in the isotropic field.

$$CFSE = \Delta E = E_{\text{ligand field}} - E_{\text{isotropic field}} \tag{4.2.2.1.3.1}$$

The CSFE will depend on multiple factors including:

- Geometry (which changes the d-orbital splitting patterns)
- Number of d-electrons
- Spin Pairing Energy
- Ligand character (via Spectrochemical Series)

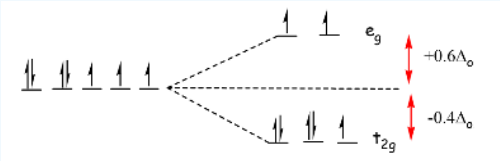
For an octahedral complex, an electron in the more stable t_{2g} subset is treated as contributing $-2/5\Delta_o$ whereas an electron in the higher energy e_g subset contributes to a destabilization of $+3/5\Delta_o$. The final answer is then expressed as a multiple of the crystal field splitting parameter Δ_o. If any electrons are paired within a single orbital, then the term P is used to represent the spin pairing energy.

Example 4.2.2.1.3.1: CFSE for a high Spin d^7 complex

What is the Crystal Field Stabilization Energy for a high spin d^7 octahedral complex?

Solution

The splitting pattern and electron configuration for both isotropic and octahedral ligand fields are compared below.



The energy of the isotropic field ($E_{\text{isotropic field}}$) is

$$E_{\text{isotropic field}} = 7 \times 0 + 2P = 2P$$

The energy of the octahedral ligand field $E_{\text{ligand field}}$ is

$$E_{\text{ligand field}} = (5 \times -2/5\Delta_o) + (2 \times 3/5\Delta_o) + 2P = -4/5\Delta_o + 2P$$

So via Equation 4.2.2.1.3.1, the CFSE is

$$\begin{aligned} CFSE &= E_{\text{ligand field}} - E_{\text{isotropic field}} \\ &= (-4/5\Delta_o + 2P) - 2P \\ &= -4/5\Delta_o \end{aligned}$$

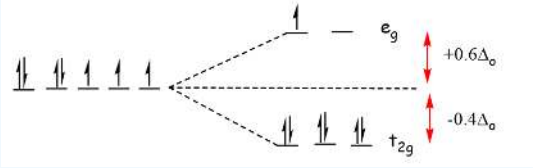
Notice that the Spin pairing Energy falls out in this case (and will when calculating the CFSE of high spin complexes) since the number of paired electrons in the ligand field is the same as that in isotropic field of the free metal ion.

Exercise 4.2.2.1.3.1

What is the Crystal Field Stabilization Energy for a low spin d^7 octahedral complex?

Answer

The splitting pattern and electron configuration for both isotropic and octahedral ligand fields are compared below.



The energy of the isotropic field is the same as calculated for the high spin configuration in Example 1:

$$E_{\text{isotropic field}} = 7 \times 0 + 2P = 2P$$

The energy of the octahedral ligand\) field $E_{\text{ligand field}}$ is

$$\begin{aligned} E_{\text{ligand field}} &= (6 \times -2/5\Delta_o) + (1 \times 3/5\Delta_o) + 3P \\ &= -9/5\Delta_o + 3P \end{aligned}$$

So via Equation 4.2.2.1.3.1, the CFSE is

$$\begin{aligned} CFSE &= E_{\text{ligand field}} - E_{\text{isotropic field}} \\ &= (-9/5\Delta_o + 3P) - 2P \\ &= -9/5\Delta_o + P \end{aligned}$$

Adding in the pairing energy since it will require extra energy to pair up one extra group of electrons. This appears more a more stable configuration than the high spin d^7 configuration in Example 4.2.2.1.3.1, but we have then to take into consideration the Pairing energy P to know definitely, which varies between $200-400\ kJ\ mol^{-1}$ depending on the metal.

Table 4.2.2.1.3.1: Crystal Field Stabilization Energies (CFSE) for high and low spin octahedral complexes

Total d-electrons	Isotropic Field	Octahedral Complex				Crystal Field Stabilization Energy	
		High Spin		Low Spin			
	$E_{\text{isotropic field}}$	Configuration	$E_{\text{ligand field}}$	Configuration	$E_{\text{ligand field}}$	High Spin	Low Spin
d^0	0	$t_{2g}0e_g0$	0	$t_{2g}^0e_g^0$	0	0	0
d^1	0	$t_{2g}1e_g0$	-2/5 Δ_o	$t_{2g}^1e_g^0$	-2/5 Δ_o	-2/5 Δ_o	-2/5 Δ_o
d^2	0	$t_{2g}2e_g0$	-4/5 Δ_o	$t_{2g}^2e_g^0$	-4/5 Δ_o	-4/5 Δ_o	-4/5 Δ_o
d^3	0	$t_{2g}3e_g0$	-6/5 Δ_o	$t_{2g}^3e_g^0$	-6/5 Δ_o	-6/5 Δ_o	-6/5 Δ_o
d^4	0	$t_{2g}3e_g1$	-3/5 Δ_o	$t_{2g}^4e_g^0$	-8/5 Δ_o + P	-3/5 Δ_o	-8/5 Δ_o + P
d^5	0	$t_{2g}3e_g2$	0 Δ_o	$t_{2g}^5e_g^0$	-10/5 Δ_o + 2P	0 Δ_o	-10/5 Δ_o + 2P
d^6	P	$t_{2g}4e_g2$	-2/5 Δ_o + P	$t_{2g}^6e_g^0$	-12/5 Δ_o + 3P	-2/5 Δ_o	-12/5 Δ_o + P
d^7	2P	$t_{2g}5e_g2$	-4/5 Δ_o + 2P	$t_{2g}^6e_g^1$	-9/5 Δ_o + 3P	-4/5 Δ_o	-9/5 Δ_o + P
d^8	3P	$t_{2g}6e_g2$	-6/5 Δ_o + 3P	$t_{2g}^6e_g^2$	-6/5 Δ_o + 3P	-6/5 Δ_o	-6/5 Δ_o
d^9	4P	$t_{2g}6e_g3$	-3/5 Δ_o + 4P	$t_{2g}^6e_g^3$	-3/5 Δ_o + 4P	-3/5 Δ_o	-3/5 Δ_o
d^{10}	5P	$t_{2g}6e_g4$	0 Δ_o + 5P	$t_{2g}^6e_g^4$	0 Δ_o + 5P	0	0

P is the spin pairing energy and represents the energy required to pair up electrons within the same orbital. For a given metal ion P (pairing energy) is constant, but it does not vary with ligand and oxidation state of the metal ion).

Octahedral Preference

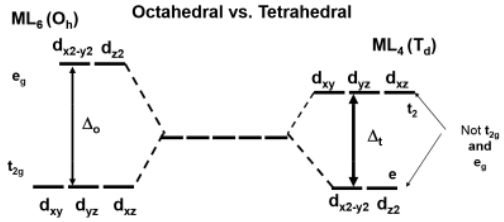
Similar CFSE values can be constructed for non-octahedral ligand field geometries once the knowledge of the d-orbital splitting is known and the electron configuration within those orbitals known, e.g., the tetrahedral complexes in Table **4.2.2.1.3.2**. These energies geoemtries can then be contrasted to the octahedral CFSE to calculate a thermodynamic preference (Enthalpy-wise) for a metal-ligand combination to favor the octahedral geometry. This is quantified via a Octahedral Site Preference Energy defined below.

Definition: Octahedral Site Preference Energies

The Octahedral Site Preference Energy (OSPE) is defined as the difference of CFSE energies for a non-octahedral complex and the octahedral complex. For comparing the preference of forming an octahedral ligand field vs. a tetrahedral ligand field, the OSPE is thus:

$$OSPE = CFSE_{(oct)} - CFSE_{(tet)} \tag{4.2.2.1.3.2}$$

The OSPE quantifies the preference of a complex to exhibit an octahedral geometry vs. a tetrahedral geometry.



Note: the conversion between Δ_o and Δ_t used for these calculations is:

$$\Delta_t \approx \frac{4}{9}\Delta_o \tag{4.2.2.1.3.3}$$

which is applicable for comparing octahedral and tetrahedral complexes that involve same ligands only.

Table 4.2.2.1.3.2: Octahedral Site Preference Energies (OSPE)

Total d-electrons	CFSE(Octahedral)	CFSE(Tetrahedral)	OSPE (for high spin complexes)**

Total d-electrons	CFSE(Octahedral)		CFSE(Tetrahedral)		OSPE (for high spin complexes)**
	High Spin	Low Spin	Configuration	**Always High Spin***	
d^0	0 Δ_o	0 Δ_o	e^0	0 Δ_t	0 Δ_o
d^1	-2/5 Δ_o	-2/5 Δ_o	e^1	-3/5 Δ_t	-6/45 Δ_o
d^2	-4/5 Δ_o	-4/5 Δ_o	e^2	-6/5 Δ_t	-12/45 Δ_o
d^3	-6/5 Δ_o	-6/5 Δ_o	$e^2t_2^1$	-4/5 Δ_t	-38/45 Δ_o
d^4	-3/5 Δ_o	-8/5 Δ_o + P	$e^2t_2^2$	-2/5 Δ_t	-19/45 Δ_o
d^5	0 Δ_o	-10/5 Δ_o + 2P	$e^2t_2^3$	0 Δ_t	0 Δ_o
d^6	-2/5 Δ_o	-12/5 Δ_o + P	$e^3t_2^3$	-3/5 Δ_t	-6/45 Δ_o
d^7	-4/5 Δ_o	-9/5 Δ_o + P	$e^4t_2^3$	-6/5 Δ_t	-12/45 Δ_o
d^8	-6/5 Δ_o	-6/5 Δ_o	$e^4t_2^4$	-4/5 Δ_t	-38/45 Δ_o
d^9	-3/5 Δ_o	-3/5 Δ_o	$e^4t_2^5$	-2/5 Δ_t	-19/45 Δ_o
d^{10}	0	0	$e^4t_2^6$	0 Δ_t	0 Δ_o

P is the spin pairing energy and represents the energy required to pair up electrons within the same orbital.

> Tetrahedral complexes are always high spin since the splitting is appreciably smaller than ***P*** (Equation 4.2.2.1.3.3).

After conversion with Equation 4.2.2.1.3.3. The data in Tables **4.2.2.1.3.1** and **4.2.2.1.3.2** are represented graphically by the curves in Figure **4.2.2.1.3.1** below for the high spin complexes only. The low spin complexes require knowledge of ***P*** to graph.

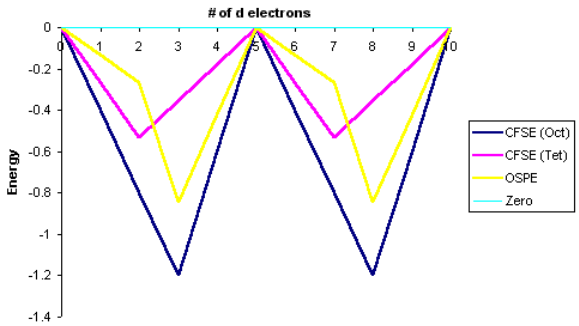


***Figure* 4.2.2.1.3.1:** *Crystal Field Stabilization Energies for both octahedral fields ($CFSE_{oct}$) and tetrahedral fields ($CFSE_{tet}$). Octahedral Site Preference Energies (OSPE) are in yellow. This is for high spin complexes.*

From a simple inspection of Figure **4.2.2.1.3.1**, the following observations can be made:

- The OSPE is *small* in d^1, d^2, d^5, d^6, d^7 complexes and other factors influence the stability of the complexes including steric factors
- The OSPE is *large* in d^3 and d^8 complexes which strongly favor octahedral geometries

Applications

The "double-humped" curve in Figure **4.2.2.1.3.1** is found for various properties of the first-row transition metals, including Hydration and Lattice energies of the M(II) ions, ionic radii as well as the stability of M(II) complexes. This suggests that these properties are somehow related to Crystal Field effects.

In the case of Hydration Energies describing the complexation of water ligands to a bare metal ion:

$$M^{2+}(g) + H_2O \rightarrow [M(OH_2)_6]^{2+}(aq) \qquad (4.2.2.1.3.4)$$

Table 4.2.2.1.3.3 and Figure 4.2.2.1.3.1 shows this type of curve. Note that in any series of this type not all the data are available since a number of ions are not very stable in the M(II) state.

Table 4.2.2.1.3.3: Hydration energies of M^{2+} ions

M	ΔH°/kJmol^{-1}	M	ΔH°/kJmol^{-1}
Ca	-2469	Fe	-2840
Sc	no stable 2+ ion	Co	-2910
Ti	-2729	Ni	-2993
>V	-2777	Cu	-2996
Cr	-2792	Zn	-2928
Mn	-2733		

Graphically the data in Table 2 can be represented by:

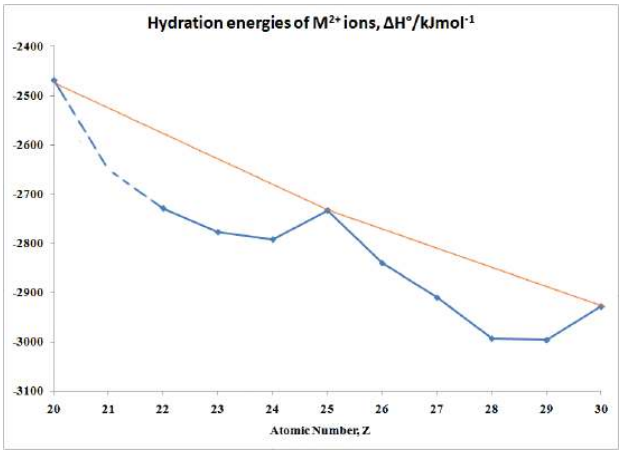


Figure* 4.2.2.1.3.2*: hydration energies of M^{2+} ions

Contributors and Attributions

- Prof. Robert J. Lancashire (The Department of Chemistry, University of the West Indies)

4.2.2.1.3: Crystal Field Stabilization Energy is shared under a not declared license and was authored, remixed, and/or curated by LibreTexts.

4.2.2.1.4: Factors That Affect the Magnitude of Δo

The magnitude of Δ_o dictates whether a complex with four, five, six, or seven d electrons is high spin or low spin, which affects its magnetic properties, structure, and reactivity. Large values of Δ_o (i.e., $\Delta_o > P$) yield a low-spin complex, whereas small values of Δ_o (i.e., $\Delta_o < P$) produce a high-spin complex. The magnitude of Δ_o depends on three factors: the valence of the metal, the principal quantum number of the metal (and thus its location in the periodic table), and the nature of the ligand(s). Values of Δ_o for some representative transition-metal complexes are given in Table **4.2.2.1.4.1**.

Table **4.2.2.1.4.1**: Crystal Field Splitting Energies for Some Octahedral (Δ_o)* and Tetrahedral (Δ_t) Transition-Metal Complexes

Octahedral Complexes	Δ_o (cm^{-1})	Octahedral Complexes	Δ_o (cm^{-1})	Tetrahedral Complexes	Δ_t (cm^{-1})
$[Ti(H_2O)_6]^{3+}$	20,300	$[Fe(CN)_6]^{4-}$	32,800	VCl_4	9010
$[V(H_2O)_6]^{2+}$	12,600	$[Fe(CN)_6]^{3-}$	35,000	$[CoCl_4]^{2-}$	3300
$[V(H_2O)_6]^{3+}$	18,900	$[CoF_6]^{3-}$	13,000	$[CoBr_4]^{2-}$	2900
$[CrCl_6]^{3-}$	13,000	$[Co(H_2O)_6]^{2+}$	9300	$[CoI_4]^{2-}$	2700
$[Cr(H_2O)_6]^{2+}$	13,900	$[Co(H_2O)_6]^{3+}$	27,000		
$[Cr(H_2O)_6]^{3+}$	17,400	$[Co(NH_3)_6]^{3+}$	22,900		
$[Cr(NH_3)_6]^{3+}$	21,500	$[Co(CN)_6]^{3-}$	34,800		
$[Cr(CN)_6]^{3-}$	26,600	$[Ni(H_2O)_6]^{2+}$	8500		
$Cr(CO)_6$	34,150	$[Ni(NH_3)_6]^{2+}$	10,800		
$[MnCl_6]^{4-}$	7500	$[RhCl_6]^{3-}$	20,400		
$[Mn(H_2O)_6]^{2+}$	8500	$[Rh(H_2O)_6]^{3+}$	27,000		
$[MnCl_6]^{3-}$	20,000	$[Rh(NH_3)_6]^{3+}$	34,000		
$[Mn(H_2O)_6]^{3+}$	21,000	$[Rh(CN)_6]^{3-}$	45,500		
$[Fe(H_2O)_6]^{2+}$	10,400	$[IrCl_6]^{3-}$	25,000		
$[Fe(H_2O)_6]^{3+}$	14,300	$[Ir(NH_3)_6]^{3+}$	41,000		

*Energies obtained by spectroscopic measurements are often given in units of wave numbers (cm^{-1}); the wave number is the reciprocal of the wavelength of the corresponding electromagnetic radiation expressed in centimeters: 1 cm^{-1} = 11.96 J/mol.

Source of data: Duward F. Shriver, Peter W. Atkins, and Cooper H. Langford, Inorganic Chemistry, 2nd ed. (New York: W. H. Freeman and Company, 1994).

Factor 1: Valence of the Metal

Increasing the valence of a metal ion has two effects: the radius of the metal decreases, and ligands are more strongly attracted to it. Both factors decrease the metal–ligand distance, which in turn causes the ligands to interact more strongly with the d-orbitals. Consequently, the magnitude of Δ_o increases as the valence of the metal increases. Typically, Δ_o for a M(III) is about 50% greater than for the M(II) of the same metal; for example, for $[V(H_2O)_6]^{2+}$, Δ_o = 11,800 cm^{-1}; for $[V(H_2O)_6]^{3+}$, Δ_o = 17,850 cm^{-1}.

Factor 2: Principal Quantum Number of the Metal

For a series of complexes of metals from the same group in the periodic table with the same charge and the same ligands, the magnitude of Δ_o increases with increasing principal quantum number: Δ_o (3d) < Δ_o (4d) < Δ_o (5d). The data for hexaammine complexes of the trivalent Group 9 metals illustrate this point:

$$[Co(NH_3)_6]^{3+}: \Delta_o = 22{,}900\ cm^{-1}$$

$$[Rh(NH_3)_6]^{3+}: \Delta_o = 34{,}100\ cm^{-1}$$

$$[Ir(NH_3)_6]^{3+}: \Delta_o = 40{,}000\ cm^{-1}$$

The increase in Δ_o with increasing principal quantum number is due to the larger radius of valence orbitals down a column. In addition, repulsive ligand–ligand interactions are most important for smaller metal ions. Relatively speaking, this results in shorter M–L distances and stronger d orbital–ligand interactions.

Factor 3: The Nature of the Ligands

Experimentally, it is found that the Δ_o observed for a series of complexes of the same metal ion depends strongly on the nature of the ligands. For a series of chemically similar ligands, the magnitude of Δ_o decreases as the size of the donor atom increases. For example, Δ_o values for halide complexes generally decrease in the order F > Cl > Br > I because smaller, more localized charges, such as we see for F, interact more strongly with the d-orbitals of the metal. In addition, a small neutral ligand with a highly localized lone pair, such as NH_3, results in significantly larger Δ_o values than might be expected. Because the lone pair points directly at the metal ion, the electron density along the M–L axis is greater than for a spherical anion such as F. The experimentally observed order of the crystal field splitting energies produced by different ligands is called the spectrochemical series which was presented in a previous section.

4.2.2.1.4: Factors That Affect the Magnitude of Δo is shared under a not declared license and was authored, remixed, and/or curated by LibreTexts.

4.2.2.1.5: Jahn-Teller Distortions

The Jahn-Teller effect is a geometric distortion of a non-linear molecular system that reduces its symmetry and energy. This distortion is typically observed among octahedral complexes where the two axial bonds can be shorter or longer than those of the equatorial bonds. This effect can also be observed in tetrahedral compounds. This effect is dependent on the electronic state of the system.

Introduction

In 1937, Hermann Jahn and Edward Teller postulated a theorem stating that "stability and degeneracy are not possible simultaneously unless the molecule is a linear one," in regards to its electronic state.[1] This leads to a break in degeneracy which stabilizes the molecule and by consequence, reduces its symmetry. Since 1937, the theorem has been revised which Housecroft and Sharpe have eloquently phrased as "any non-linear molecular system in a degenerate electronic state will be unstable and will undergo distortion to form a system of lower symmetry and lower energy, thereby removing the degeneracy."[2] This is most commonly observed with transition metal octahedral complexes, however, it can be observed in tetrahedral compounds as well.

For a given octahedral complex, the five d atomic orbitals are split into two degenerate sets when constructing a molecular orbital diagram. These are represented by the sets' symmetry labels: t_{2g} (d_{xz}, d_{yz}, d_{xy}) and e_g (d_{z^2} and $d_{x^2-y^2}$). When a molecule possesses a degenerate electronic ground state, it will distort to remove the degeneracy and form a lower energy (and by consequence, lower symmetry) system. The octahedral complex will either elongate or compress the z ligand bonds as shown in Figure **4.2.2.1.5.1** below:

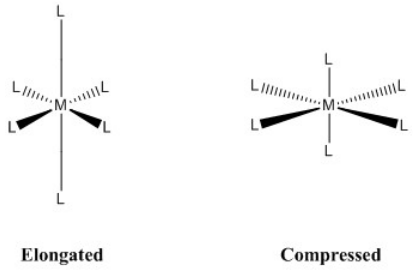


Figure **4.2.2.1.5.1**: Jahn-Teller distortions for an octahedral complex.

When an octahedral complex exhibits elongation, the axial bonds are longer than the equatorial bonds. For a compression, it is the reverse; the equatorial bonds are longer than the axial bonds. Elongation and compression effects are dictated by the amount of overlap between the metal and ligand orbitals. Thus, this distortion varies greatly depending on the type of metal and ligands. In general, the stronger the metal-ligand orbital interactions are, the greater the chance for a Jahn-Teller effect to be observed.

Elongation

Elongation Jahn-Teller distortions occur when the degeneracy is broken by the stabilization (lowering in energy) of the d orbitals with a z component, while the orbitals without a z component are destabilized (higher in energy) as shown in Figure **4.2.2.1.5.2** below:

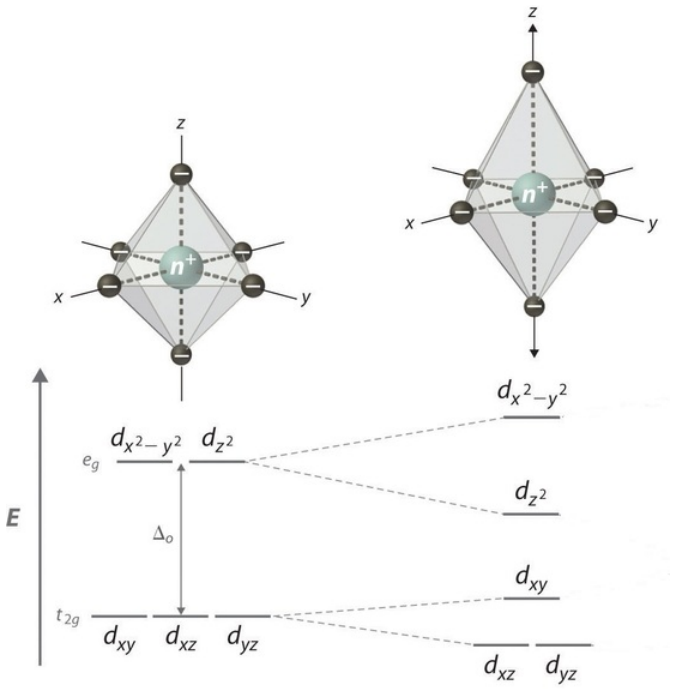


Figure **4.2.2.1.5.2**: Illustration of tetragonal distortion (elongation) for an octahedral complex.

This is due to the d_{xy} and $d_{x^2-y^2}$ orbitals having greater overlap with the ligand orbitals, resulting in the orbitals being higher in energy. Since the $d_{x^2-y^2}$ orbital is antibonding, it is expected to increase in energy due to elongation. The d_{xy} orbital is still nonbonding, but is destabilized due to the interactions. Jahn-Teller elongations are well-documented for copper(II) octahedral compounds. A classic example is that of copper(II) fluoride as shown in Figure **4.2.2.1.5.3**.

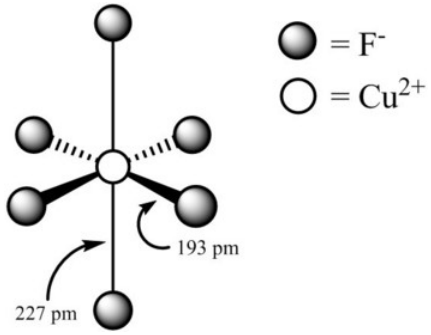


Figure **4.2.2.1.5.3**: Structure of octahedral copper(II) fluoride.[3]

Notice that the two axial bonds are both elongated and the four shorter equatorial bonds are the same length as each other. According the theorem, the orbital degeneracy is eliminated by distortion, making the molecule more stable based on the model presented in Figure **4.2.2.1.5.2**.

Compression

Compression Jahn-Teller distortions occur when the degeneracy is broken by the stabilization (lowering in energy) of the d orbitals *without* a *z* component, while the orbitals with a *z* component are destabilized (higher in energy) as shown in Figure **4.2.2.1.5.4** below:

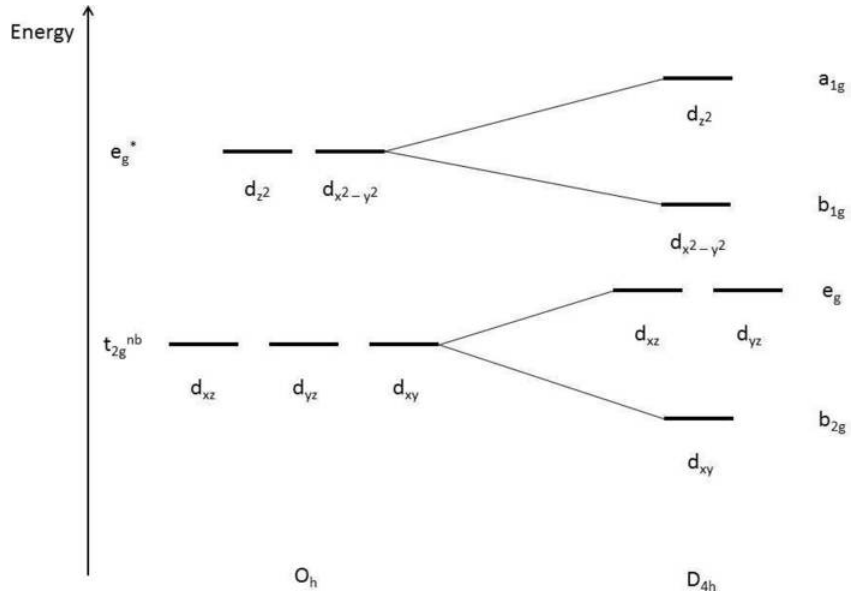


Figure **4.2.2.1.5.4**: Illustration of tetragonal distortion (compression) for an octahedral complex.

This is due to the *z*-component d orbitals having greater overlap with the ligand orbitals, resulting in the orbitals being higher in energy. Since the d_{z^2} orbital is antibonding, it is expected to increase in energy due to compression. The d_{xz} and d_{yz} orbitals are still nonbonding, but are destabilized due to the interactions.

Electronic Configurations

For Jahn-Teller effects to occur in transition metals there must be degeneracy in either the t_{2g} or e_g orbitals. The electronic states of octahedral complexes depend on the number of d-electrons and the splitting energy, **Δ**. When **Δ** is large and is greater than the energy required to pair electrons, electrons pair in t_{2g} before occupying e_g. On the other hand, when ***Delta*** small and is less than the pairing energy, electrons will occupy e_g before pairing in t_{2g}. The **Δ** of an octahedral complex is dictated by the chemical environment (ligand identity), and the identity and charge of the metal ion. If there electron configurations for any d-electron count is different depending on **Δ**, the configuration with more paired electrons is called low spin while the one with more unpaired electrons is called high spin.

The electron configurations diagrams for d1 through d10 with large and small ***δ*** are illustrated in the figures below. Notice that the electron configurations for d^1, d^2, d^3, d^8, d^9, and d^{10} are the same no matter what the magnitude of **Δ**. Low spin and high spin configurations exist only for the electron counts d^4, d^5, d^6, and d^7.

Large Δ

Figure **4.2.2.1.5.5** (below) shows the various electronic configurations for octahedral complexes with large **Δ**, including the low-spin configurations of d^4, d^5, d^6, and d^7:

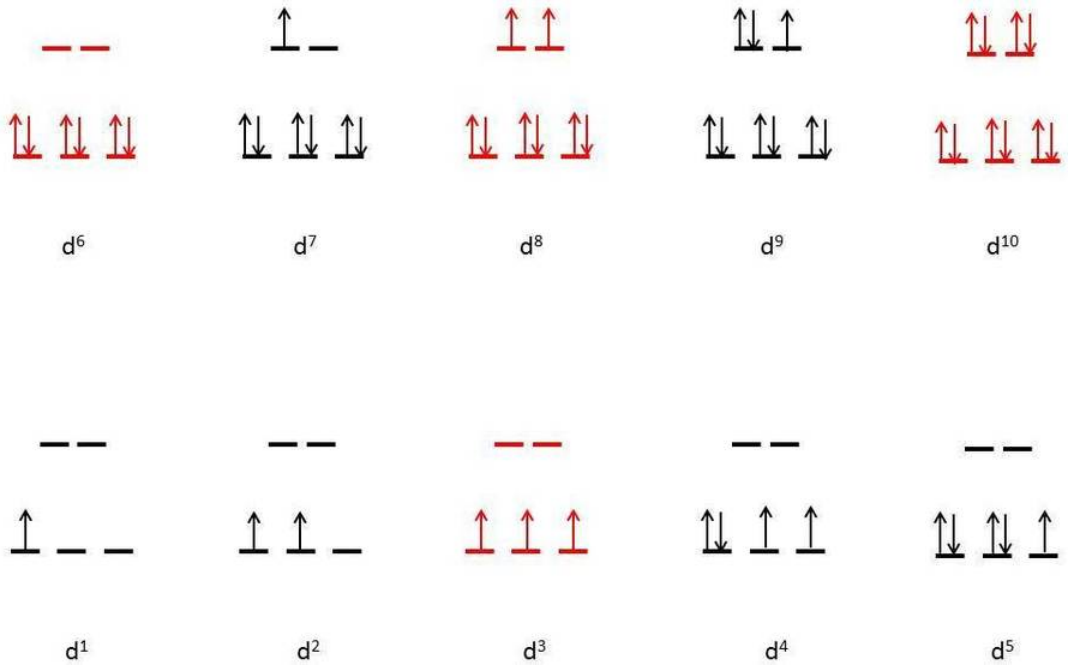


Figure 4.2.2.1.5.5: Electron configuration diagram of octahedral complexes (red indicates no degeneracies possible, thus no Jahn-Teller effects).

The figure illustrates the electron configurations in the case of large **Δ**. The electron configurations highlighted in red (d^3, low spin d^6, d^8, and d^{10}) **do not** exhibit Jahn-Teller distortions. On the other hand d^1, d^2, low spin d^4, low spin d^5, low spin d^7, and d^9, would be expected to exhibit Jhan-Teller distortion. These electronic configurations correspond to a variety of transition metals. Some common examples include Cr^{3+}, Co^{3+}, and Ni^{2+}.

Small Δ

Figure 4.2.2.1.5.6 (below) shows the various electronic configurations for octahedral complexes with small **Δ**, including the high-spin configurations of d^4, d^5, d^6, and d^7::

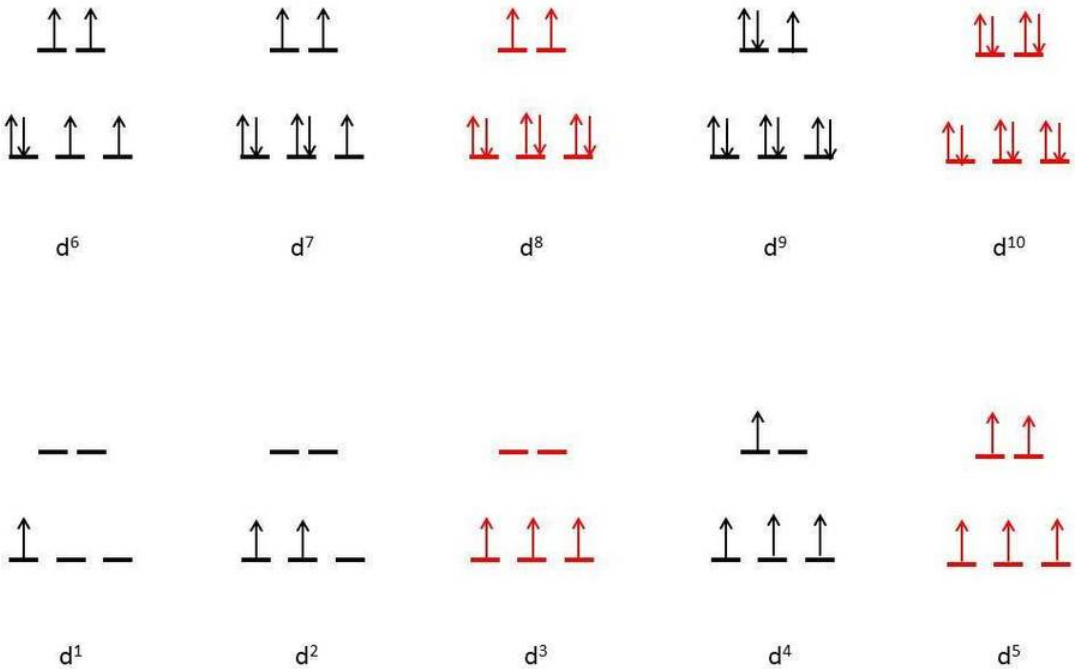


Figure 4.2.2.1.5.6: High spin octahedral coordination diagram (red indicates no degeneracies possible, thus no Jahn-Teller effects).

The figure illustrates the electron configurations in the case of small **Δ**. The electron configurations highlighted in red (d^3, high spin d^5, d^8, and d^{10}) **do not** exhibit Jahn-Teller distortions. In general, degenerate electronic states occupying the e_g orbital set tend to show stronger Jahn-Teller effects. This is primarily caused by the occupation of these high energy orbitals. Since the system is more stable with a lower energy configuration, the degeneracy of the e_g set is broken, the symmetry is reduced, and occupations at lower energy orbitals occur.

Spectroscopic Observation

Jahn-Teller distortions can be observed using a variety of spectroscopic techniques. In UV-VIS absorption spectroscopy, distortion causes splitting of bands in the spectrum due to a reduction in symmetry (O_h to D_{4h}). Consider a hypothetical molecule with octahedral symmetry showing a single absorption band. If the molecule were to undergo Jahn-Teller distortion, the number of bands would increase as shown in Figure **4.2.2.1.5.7** below:

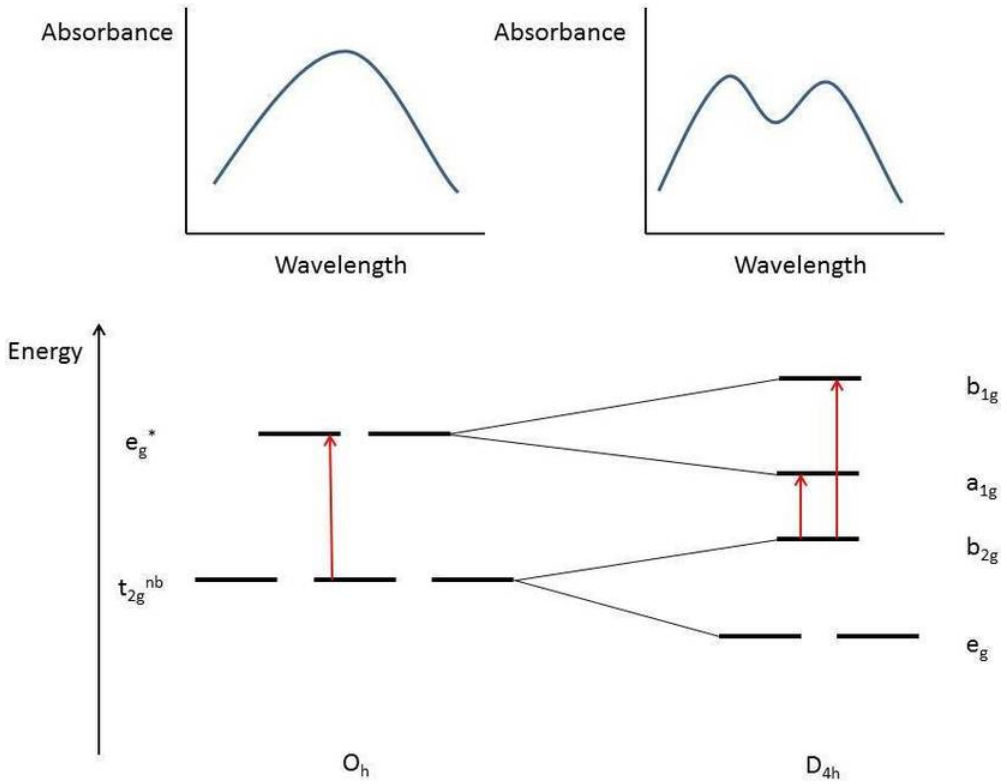


Figure **4.2.2.1.5.7**: Hypothetical absorption spectra of an octahedral molecule (left) and the same molecule with Jahn-Teller elongation (right). The red arrows indicate electronic transitions.

A similar phenomenon can be seen with IR and Raman vibrational spectroscopy. The number of vibrational modes for a molecule can be calculated using the 3n - 6 rule (or 3n - 5 for linear geometry) rule. If a molecule exhibits an O_h symmetry point group, it will have fewer bands than that of a Jahn-Teller distorted molecule with D_{4h} symmetry. Thus, one could observe Jahn-Teller effects through either IR or Raman techniques. This effect can also be observed in EPR experiments as long as there is at least one unpaired electron.

Table **4.2.2.1.5.1**: Examples of Jahn-Teller distorted complexes

$CuBr_2$	4 Br at 240 pm 2 Br at 318 pm
$CuCl_2$	4 Cl at 230 pm 2 Cl at 295 pm
$CuCl_2.2H_2O$	2 O at 193 pm 2 Cl at 228 pm 2 Cl at 295 pm
$CsCuCl_3$	4 Cl at 230 pm 2 Cl at 265 pm
CuF_2	4 F at 193 pm 2 F at 227 pm
$CuSO_4.4NH_3.H_2O$	4 N at 205 pm 1 O at 259 pm 1 O at 337 pm
K_2CuF_4	4 F at 191 pm 2 F at 237 pm
$KCuAlF_6$	2 F at 188 pm 4 F at 220 pm
CrF_2	4 F at 200 pm 2 F at 243 pm
$KCrF_3$	4 F at 214 pm 2 F at 200 pm
MnF_3	2 F at 209 pm 2 F at 191 pm 2 F at 179 pm

The Jahn-Teller Theorem predicts that distortions should occur for *any degenerate state*, including degeneracy of the t_{2g} level, however distortions in bond lengths are much more distinctive when the degenerate electrons are in the e_g level.

References

1. Jahn, H. A.; Teller, E. *Proc. R. Soc. London A*, **1937**, *161*, 220-235. DOI: 10.1098/rspa.1937.0142
2. Housecroft, C.; Sharpe, A. G. *Inorganic Chemistry*. Prentice Hall, 3rd Ed., 2008, p. 644. ISBN: 978-0-13-175553-6
3. Billy, C.; Haendler, H. A. *J. Am. Chem. Soc.*, **1957**, *79*, 1049–1051. DOI: 10.1021/ja01562a011

References

- Janes, R.; Moore, E. A. *Metal-ligand bonding*. The Open University, 2004, p. 23. ISBN 0-85404-979-7
- P.T.Miller, P.G.Lenhert and M.D.Joesten, *Inorg. Chem.*, 11, 2221, 1972.
- J.S.Wood, C.P.Keijzers and R.O.Day, *Acta Crystallogr., Sect.C (Cr. Str. Comm.)*, 40, 404, 1984.
- M.D.Joesten, M.S.Hussain and P.G.Lenhert, *Inorg. Chem.*, 9, 151, 1970.

Practice Questions

1. Why do d^3 complexes not show Jahn-Teller distortions?
2. Does the spin system (high spin v. low spin) of a molecule play a role in Jahn-Teller effects?
3. What spectroscopic method would one utilize in order to observe Jahn-Teller distortions in a diamagnetic molecule?
4. What spectroscopic method(s) would one utilize in order to observe Jahn-Teller distortions in a paramagnetic molecule?
5. Why are Jahn-Teller effects most prevalent in inorganic (transition metal) compounds?

Answers

1. Complexes with d^3 electron configurations do not show Jahn-Teller distortions because there is no ground state degeneracy.
2. Yes. Examining the d^5 electron configuration, one finds that the high spin scenario contains all singly occupied d orbitals (no degeneracy). However, the low spin d^5 electron configuration shows degeneracy, which then leads to possible Jahn-Teller effects.
3. UV-VIS absorption spectroscopy is one of the most common techniques for observing these effects. In general, it is independent of magnetism (diamagnetic v. paramagnetic). Thus, one would see the effect in the spectrum of UV-VIS absorption analysis. Note that EPR requires at least one unpaired electron, and therefore not EPR active.
4. Inorganic, specifically transition metal, complexes are most prevalent in showing Jahn-Teller distortions due to the availability of d orbitals. The most common geometry that the Jahn-Teller effect is observed is in octahedral complexes (see **Figures 2, 4, 5** and **6** above) due to the splitting of d orbitals into two degenerate sets. Due to stabilization, the degeneracies are removed, making a lower symmetry and lower energy molecule.

5. In addition to UV-VIS absorption, one can also employ EPR spectroscopy if a molecule possesses and unpaired electron.

Contributors and Attributions

- Kamran Ghiassi (UC Davis)
- Prof. Robert J. Lancashire (The Department of Chemistry, University of the West Indies)

4.2.2.1.5: Jahn-Teller Distortions is shared under a not declared license and was authored, remixed, and/or curated by LibreTexts.

- **Jahn-Teller Distortions** is licensed CC BY-NC-SA 4.0.

4.2.2.1.6: Magnetic Moments of Transition Metals

Magnetic moments are often used in conjunction with electronic spectra to gain information about the valence and stereochemistry of the central metal atom in coordination complexes. A common laboratory procedure for the determination of the magnetic moment for a complex is the Gouy method which involves weighing a sample of the complex in the presence and absence of a magnetic field and observing the difference in weight. A template is provided for the calculations involved.

For first row transition metal ions in the free ion state, i.e. isolated ions in a vacuum, all 5 of the 3d orbitals are degenerate.

A simple crystal field theory approach to the bonding in these ions assumes that when they form octahedral complexes, the energy of the d orbitals are no longer degenerate but are split such that two orbitals, the d_{x2-y2} and the d_{z2} (e_g subset) are at higher energy than the d_{xy}, d_{xz}, d_{yz} orbitals (the t_{2g} subset).

For octahedral ions with between 4 and 7 d electrons, this gives rise to 2 possible arrangements called either high spin/weak field or low spin/strong field respectively. The energy gap is dependent on the position of the coordinated ligands in the SPECTROCHEMICAL SERIES.

Note

A good starting point is to assume that all Co(III), d^6 complexes are octahedral and LOW spin, i.e. t_{2g}^6.

In tetrahedral complexes, the energy levels of the orbitals are again split, such that the energy of two orbitals, the $d_{x^2-y^2}$ and the d_{z^2} (e subset) are now at lower energy (more favored) than the remaining three d_{xy}, d_{xz}, d_{yz} (the t_2 subset) which are destabilized.

> *Tetrahedral complexes are ALL high spin since the difference between the 2 subsets of energies of the orbitals is much smaller than is found in octahedral complexes.*

The usual relationship quoted between them is:

$$\Delta_{tet} \approx \frac{4}{9}\Delta_{oct} \tag{4.2.2.1.6.1}$$

Square planar complexes are less common than tetrahedral and d^8 e.g. Ni(II), Pd(II), Pt(II), etc, have a strong propensity to form square planar complexes. As with octahedral complexes, the energy gap between the d_{xy} and $d_{x^2-y^2}$ is Δ_{oct} and these are considered strong field / low spin hence they are all diamagnetic, μ=0 Bohr Magneton (B.M.)

The formula used to calculate the spin-only magnetic moment can be written in two forms; the first based on the number of unpaired electrons, n, and the second based on the electron spin quantum number, S. Since for each unpaired electron, $n = 1$ and $S = 1/2$ then the two formulae are related and the answer obtained must be identical.

$$\mu_{so} = \sqrt{n(n+2)} \tag{4.2.2.1.6.2}$$

$$\mu_{so} = \sqrt{4S(S+1)} \tag{4.2.2.1.6.3}$$

Comparison of calculated spin-only magnetic moments with experimental data for some octahedral complexes

Metal	Config	μ_{so} / B.M.	μ_{obs} / B.M.
Ti(III)	d^1 (t_{2g}^1)	√3 = 1.73	1.6-1.7
V(III)	d^2 (t_{2g}^2)	√8 = 2.83	2.7-2.9
Cr(III)	d^3 (t_{2g}^3)	√15 = 3.88	3.7-3.9
Cr(II)	d^4 high spin (t_{2g}^3 e_g^1)	√24 = 4.90	4.7-4.9
Cr(II)	d^4 low spin (t_{2g}^4)	√8 = 2.83	3.2-3.3
Mn(II)/ Fe(III)	d^5 high spin (t_{2g}^3 e_g^2)	√35 = 5.92	5.6-6.1
Mn(II)/ Fe(III)	d^5 low spin (t_{2g}^5)	√3 = 1.73	1.8-2.1
Fe(II)	d^6 high spin (t_{2g}^4 e_g^2)	√24 = 4.90	5.1-5.7
Co(III)	d^6 low spin (t_{2g}^6)	0	0
Co(II)	d^7 high spin (t_{2g}^5 e_g^2)	√15 = 3.88	4.3-5.2
Co(II)	d^7 low spin (t_{2g}^6 e_g^1)	√3 = 1.73	1.8
Ni(II)	d^8 (t_{2g}^6 e_g^2)	√8 = 2.83	2.9-3.3
Cu(II)	d^9 (t_{2g}^6 e_g^3)	√3 = 1.73	1.7-2.2

Comparison of calculated spin-only magnetic moments with experimental data for some tetrahedral complexes

Ion	Config	μ_{so} / B.M.	μ_{obs} / B.M.
Cr(V)	d^1 (e^1)	√3 = 1.73	1.7-1.8
Cr(IV) / Mn(V)	d_2 (e^2)	√8 = 2.83	2.6 - 2.8
Fe(V)	d^3 (e^2 t_2^1)	√15 = 3.88	3.6-3.7
-	d^4 (e^2 t_2^2)	√24 = 4.90	-
Mn(II)	d^5 (e^2 t_2^3)	√35 = 5.92	5.9-6.2
Fe(II)	d^6 (e^3 t_2^3)	√24 = 4.90	5.3-5.5
Co(II)	d^7 (e^4 t_2^3)	√15 = 3.88	4.2-4.8
Ni(II)	d^8 (e^4 t_2^4)	√8 = 2.83	3.7-4.0
Cu(II)	d^9 (e^4 t_2^5)	√3 = 1.73	-

Contributors and Attributions

- Prof. Robert J. Lancashire (The Department of Chemistry, University of the West Indies)

4.2.2.1.6: Magnetic Moments of Transition Metals is shared under a not declared license and was authored, remixed, and/or curated by LibreTexts.

4.2.2.1.7: Magnetism

Movement of an electrical charge (which is the basis of electric currents) generates a magnetic field in a material. Magnetism is therefore a characteristic property of all materials that contain electrically charged particles and for most purposes can be considered to be entirely of electronic origin.

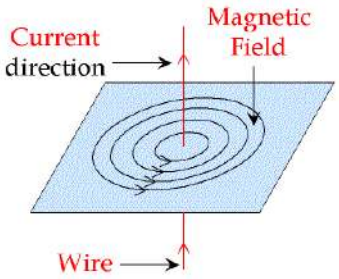


Figure **4.2.2.1.7.1**: The Right Hand Rule for an induced magnetic field

In an atom, the magnetic field is due to the coupled spin and orbital magnetic moments associated with the motion of electrons. The spin magnetic moment is due to the precession of the electrons about their own axes whereas the orbital magnetic moment is due to the motion of electrons around the nucleus. The resultant combination of the spin and orbital magnetic moments of the constituent atoms of a material gives rise to the observed magnetic properties.

Historically, magnetism has been recognized for thousands of years. An account, that is probably apochryphal, tells of a shepherd called Magnes in Crete who around 900 B.C discovered the naturally occurring magnet lodestone (a form of the the spinel magnetite, Fe_3O_4) in a region later named Magnesia. Supposedly while he was walking over a deposit, the lodestone pulled the nails out of his sandals and the metal tip from his staff.

The Classical Theory of Magnetism

The classical theory of magnetism was well developed before quantum mechanics. Lenz's Law states that when a substance is placed within a magnetic field, $\boldsymbol{H}$, the field within the substance, $\boldsymbol{B}$, differs from $\boldsymbol{H}$ by the induced field, $\boldsymbol{4\pi I}$, which is proportional to the intensity of magnetization, $\boldsymbol{I}$. That is;

$$\boldsymbol{B = H + 4\pi I} \tag{4.2.2.1.7.1}$$

where $\boldsymbol{B}$ is the magnetic field within the substance and $\boldsymbol{H}$ is the applied magnetic field and $\boldsymbol{I}$ is the intensity of magnetization

Lenz's Law (1834)

Lenz's Law can also be written as

$$\frac{\boldsymbol{B}}{\boldsymbol{H}} = 1 + \frac{\boldsymbol{4\pi I}}{\boldsymbol{H}} \tag{4.2.2.1.7.2}$$

or

$$\frac{\boldsymbol{B}}{\boldsymbol{H}} = 1 + \boldsymbol{4\pi\kappa} \tag{4.2.2.1.7.3}$$

where

- $\boldsymbol{B/H}$ is called the magnetic permeability of the material and
- $\boldsymbol{\kappa}$ is the magnetic susceptibility per unit volume, (I/H)

By definition, $\boldsymbol{\kappa}$ in a vacuum is zero, so under those conditions the equation would reduce to $\boldsymbol{B = H}$. It is usually more convenient to measure mass than volume and the mass susceptibility, $\boldsymbol{\chi_g}$, is related to the volume susceptibility, $\boldsymbol{\kappa}$, through the density.

$$\boldsymbol{\chi_g = \frac{\kappa}{\rho}} \tag{4.2.2.1.7.4}$$

where ρ is the density.

Finally to get our measured quantity on a basis that can be related to atomic properties, we convert to molar susceptibility

$$\chi_m = \chi_g \times RMM \tag{4.2.2.1.7.5}$$

Since this value includes the underlying diamagnetism of paired electrons, it is necessary to correct for the diamagnetic portion of χ_m to get a corrected paramagnetic susceptibility.

$$\chi'_m = \chi_m + \chi_{dia} \tag{4.2.2.1.7.6}$$

Examples of these corrections are tabulated below.

Table **4.2.2.1.7.1**: Table of Diamagnetic Corrections (Pascal's constants, 10^{-6} c.g.s. units)

Ion	DC	Ion	DC
Na^+	6.8	Co^{2+}	12.8
K^+	14.9	Co^{3+}	12.8
NH_4^+	13.3	Ni^{2+}	12.8
Hg^{2+}	40	VO^{2+}	12.5
Fe^{2+}	12.8	Mn^{3+}	12.5
Fe^{3+}	12.8	Cr^{3+}	12.5
Cu^{2+}	12.8	Cl^-	23.4
Br^-	34.6	SO_4^{2-}	40.1
I^-	50.6	OH^-	12
NO_3^-	18.9	$C_2O_4^{2-}$	34
ClO_4^-	32	OAc^-	31.5
IO_4^-	51.9	pyr	49.2
CN^-	13	Me-pyr	60
NCS^-	26.2	$Acac^-$	62.5
H_2O	13	en	46.3
$EDTA^{4-}$	~150	urea	33.4

these can be converted to S.I units of $m^3\ mol^{-1}$ by multiplying by $4\ \pi \times 10^{-7}$

There are numerous methods for measuring magnetic susceptibilities, including, the **Gouy, Evans and Faraday methods**. These all depend on measuring the force exerted upon a sample when it is placed in a magnetic field. The more paramagnetic the sample, the more strongly it will be drawn toward the more intense part of the field.

Determination of Magnetic Susceptibility

- **The Gouy Method:** The underlying theory of the Gouy method is described here and a form for calculating the magnetic moment from the collected data is available as well.
- **The Evans method:** The Evans balance measures the change in current required to keep a pair of suspended magnets in place or balanced after the interaction of the magnetic field with the sample. The Evans balance differs from that of the Gouy in that, in the former the permanent magnets are suspended and the position of the sample is kept constant while in the latter the position of the magnet is constant and the sample is suspended between the magnets.

Orbital contribution to magnetic moments

From a quantum mechanics viewpoint, the magnetic moment is dependent on both spin and orbital angular momentum contributions. The spin-only formula used last year was given as:

$$\mu_{s.o.} = \sqrt{4S(S+1)} \tag{4.2.2.1.7.7}$$

and this can be modified to include the orbital angular momentum

$$\mu_{S+L} = \sqrt{4S(S+1) + L(L+1)} \tag{4.2.2.1.7.8}$$

An orbital angular momentum contribution is expected when the ground term is triply degenerate (i.e. a triplet state). These show temperature dependence as well.

In order for an electron to contribute to the orbital angular momentum the orbital in which it resides must be able to transform into an exactly identical and degenerate orbital by a simple rotation (it is the rotation of the electrons that induces the orbital contribution). For example, in an octahedral complex the degenerate t_{2g} set of orbitals (d_{xz},d_{yx},d_{yz}) can be interconverted by a 90° rotation. However the orbitals in the e_g subset (d_{z^2},$d_{x^2-y^2}$) cannot be interconverted by rotation about any axis as the orbital shapes are different; therefore an electron in the e_g set does not contribute to the orbital angular momentum and is said to be quenched. In the free ion case the electrons can be transformed between any of the orbitals as they are all degenerate, but there will still be partial orbital quenching as the orbitals are not identical.

Electrons in the t_{2g} set do not always contribute to the orbital angular moment. For example in the d^3, t_{2g}^3 case, an electron in the d_{xz} orbital cannot by rotation be placed in the d_{yz} orbital as the orbital already has an electron of the same spin. This process is also called quenching.

Tetrahedral complexes can be treated in a similar way with the exception that we fill the e orbitals first, and the electrons in these do not contribute to the orbital angular momentum. The tables in the links below give a list of all d^1 to d^9 configurations including high and low spin complexes and a statement of whether or not a direct orbital contribution is expected.

- Octahedral complexes
- Tetrahedral complexes

Contributors and Attributions

- Prof. Robert J. Lancashire (The Department of Chemistry, University of the West Indies)

4.2.2.1.7: Magnetism is shared under a not declared license and was authored, remixed, and/or curated by LibreTexts.

4.2.2.1.8: Thermodynamics and Structural Consequences of d-Orbital Splitting

The energy level splitting of the d-orbitals due to their interaction with the ligands in a complex has important structural and thermodynamic effects on the chemistry of transition-metal complexes. Although these two types of effects are interrelated, they are considered separately here.

Structural Effects

There are two major kinds of structural effects: effects on the ionic radii of metal ions with regular octahedral or tetrahedral geometries, and structural distortions observed for specific electron configurations.

Ionic Radii

Figure **4.2.2.1.8.1** is a plot of the ionic radii of the divalent fourth-period metal ions versus atomic number. The dashed line represents the behavior predicted based on the effects of screening and variation in effective nuclear charge (Z_{eff}), assuming a spherical distribution of the 3d electrons. Because these radii are based on the structures of octahedral complexes and Cr^{2+} and Cu^{2+} do not form truly octahedral complexes, the points for these ions are shown as open circles.

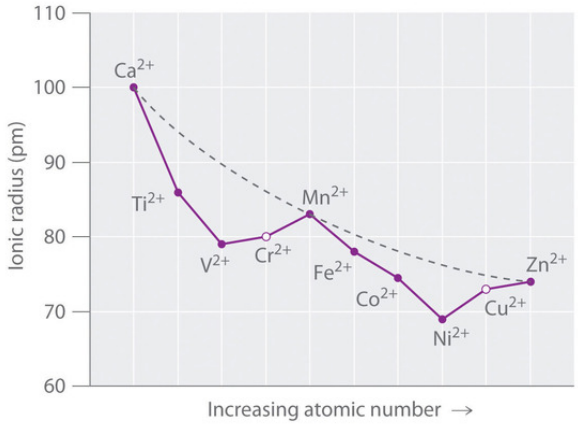


Figure **4.2.2.1.8.1**: The Effect of d-Orbital Splittings on the Radii of the Divalent Ions of the Fourth-Period Metals. Only $Ca^{2+}(d^0)$, Mn^{2+} (high-spin d^5), and Zn^{2+} (d^{10}) lie on the smooth dashed curve. All other divalent ions fall below this curve because they have asymmetrical distributions of d electrons. To explain why an asymmetrical distribution of d electrons makes a metal ion smaller than expected, consider the Ti^{2+} ion, which has a d^2 configuration with both electrons in the t_{2g} orbitals. Because the t_{2g} orbitals are directed between the ligands, the two d-electrons are unable to shield the ligands from the nuclear charge. Consequently, the ligands experience a higher effective nuclear charge than predicted, the metal–ligand distance is unusually short, and the ionic radius is smaller than expected. If instead the two electrons were distributed uniformly over all five d orbitals, they would be much more effective at screening the ligands from the nuclear charge, making the metal–ligand distances longer and giving the metal a larger ionic radius.

A similar effect is observed for the V^{2+} ion, which has a d^3 configuration. Because the three electrons in the t_{2g} orbitals provide essentially no shielding of the ligands from the metal, the ligands experience the full increase of +1 in nuclear charge that occurs from Ti^{2+} to V^{2+}. Consequently, the observed ionic radius of the V^{2+} ion is significantly smaller than that of the Ti^{2+} ion.

Skipping the Cr^{2+} ion for the moment, consider the d^5 Mn^{2+} ion. Because the nuclear charge increases by +2 from V^{2+} to Mn^{2+}, Mn^{2+} might be expected to be smaller than V^{2+}. The two electrons added from V^{2+} to Mn^{2+} occupy the e_g orbitals, however, which are oriented directly toward the six ligands. Because these electrons are localized directly between the metal ion and the ligands, they are effective at screening the ligands from the increased nuclear charge. As a result, the ionic radius actually increases significantly from V^{2+} to Mn^{2+}, despite the higher nuclear charge of the latter.

The same effects are observed in the second half of the first-row transition metals. In the Fe^{2+}, Co^{2+}, and Ni^{2+} ions, the extra electrons are added successively to the t_{2g} orbitals, resulting in increasingly poor shielding of the ligands from the nuclei and in abnormally small ionic radii. Skipping over Cu^{2+}, adding the last two electrons causes a significant increase in the ionic radius of Zn^{2+}, despite its greater nuclear charge.

The Jahn–Teller Effect

Because simple octahedral complexes are not observed for the Cr^{2+} and Cu^{2+} ions, only estimated values for their radii are shown in Figure **4.2.2.1.8.1**. Since both Cr^{2+} and Cu^{2+} ions have electron configurations with an odd number of electrons in the e_g orbitals. Because the single electron (in the case of Cr^{2+}) or the third electron (in the case of Cu^{2+}) can occupy either one of two degenerate e_g orbitals, both systems have degenerate ground states. The Jahn–Teller theorem states that such non-linear systems are not stable; they undergo a distortion that makes the complex less symmetrical and splits the degenerate states, which decreases the energy of the system. The distortion and resulting decrease in energy are collectively referred to as the Jahn–Teller effect. Neither the nature of the distortion nor its magnitude is specified, and in fact, they are difficult to predict. In principle, Jahn–Teller distortions are possible for many transition-metal ions; in practice, however, they are observed only for systems with an odd number of electrons in the e_g orbitals, such as the Cr^{2+} and Cu^{2+} ions.

Consider an octahedral Cu^{2+} complex, $[Cu(H_2O)_6]^{2+}$, which is elongated along the z axis. As indicated in Figure **4.2.2.1.8.2**, this kind of distortion splits both the e_g and t_{2g} sets of orbitals. Because the axial ligands interact most strongly with the d_{z^2} orbital, the splitting of the e_g set (δ_1) is significantly larger than the splitting of the t_{2g} set (δ_2), but both δ_1 and δ_2 are much, much smaller than the Δ_o. This splitting does not change the centerpoint of the energy within each set, so a Jahn–Teller distortion results in no net change in energy for a filled or half-filled set of orbitals. If, however, the e_g set contains one electron (as in the d^4 ions, Cr^{2+} and Mn^{3+}) or three electrons (as in the d^9 ion, Cu^{2+}), the distortion decreases the energy of the system. For Cu^{2+}, for example, the change in energy after distortion is $2(-\delta_1/2) + 1(\delta_1/2) = -\delta_1/2$. For Cu^{2+} complexes, the observed distortion is always an elongation along the z axis by as much as 50 pm; in fact, many Cu^{2+} complexes are distorted to the extent that they are effectively square planar. In contrast, the distortion observed for most Cr^{2+} complexes is a compression along the z axis. In both cases, however, the net effect is the same: the distorted system is more stable than the undistorted system.

Jahn–Teller distortions are most important for d^9 and high-spin d^4 complexes; the distorted system is more stable than the undistorted one.

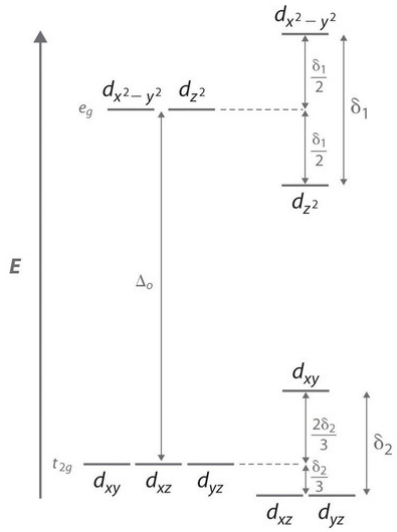


Figure **4.2.2.1.8.2**: The Jahn–Teller Effect

Increasing the axial metal–ligand distances in an octahedral d^9 complex is an example of a Jahn–Teller distortion, which causes the degenerate pair of e_g orbitals to split in energy by an amount δ_1; δ_1 and δ_2 are much smaller than Δ_o. As a result, the distorted system is more stable (lower in energy) than the undistorted complex by $\delta_1/2$.

Thermodynamic Effects

As previously noted, crystal field splitting energies (CFSEs) can be as large as several hundred kilojoules per mole, which is the same magnitude as the strength of many chemical bonds or the energy change in most chemical reactions. Consequently, CFSEs are important factors in determining the magnitude of hydration energies, lattice energies, and other thermodynamic properties of the transition metals.

Hydration Energies

The hydration energy of a metal ion is defined as the change in enthalpy for the following reaction:

$$M^{2+}_{(g)} + H_2O_{(l)} \rightarrow M^{2+}_{(aq)} \tag{4.2.2.1.8.1}$$

Although hydration energies cannot be measured directly, they can be calculated from experimentally measured quantities using thermochemical cycles. In Figure **4.2.2.1.8.3*a***, a plot of the hydration energies of the fourth-period metal dications versus atomic number forms a curve with two valleys. Note the relationship between the plot in Figure **4.2.2.1.8.3*a*** and the plot of ionic radii in Figure **4.2.2.1.8.1** the overall shapes are essentially identical, and only the three cations with spherically symmetrical distributions of d electrons (Ca^{2+}, Mn^{2+}, and Zn^{2+}) lie on the dashed lines. In Figure **4.2.2.1.8.3*a***, the dashed line corresponds to hydration energies calculated based solely on electrostatic interactions. Subtracting the CFSE values for the $[M(H_2O)_6]^{2+}$ ions from the experimentally determined hydration energies gives the points shown as open circles, which lie very near the calculated curve. Therefore, CFSEs are primarily responsible for the differences between the measured and calculated values of hydration energies.

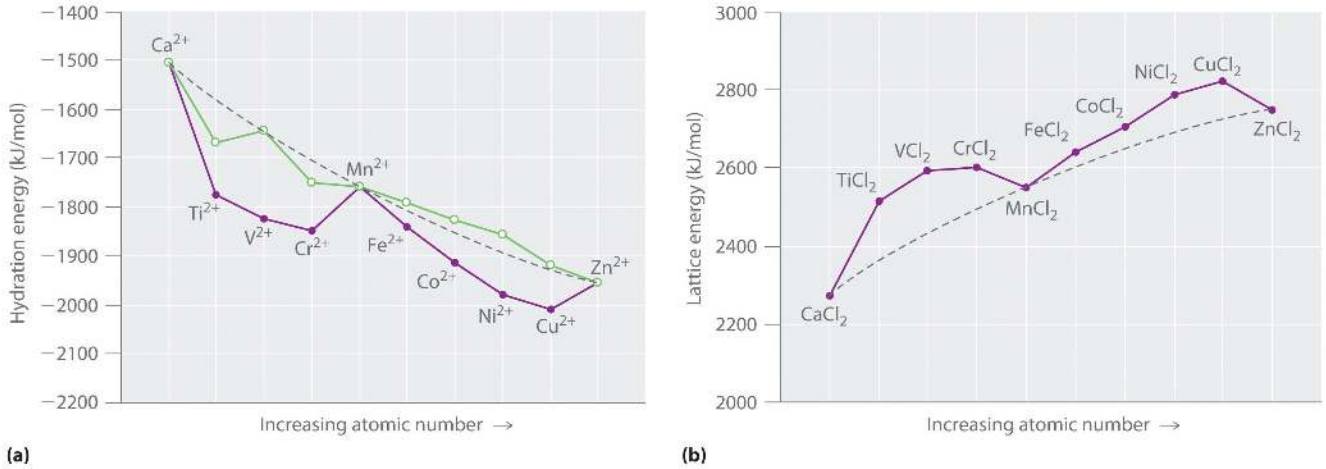


Figure **4.2.2.1.8.3**: Thermochemical Effects of d-Orbital Splittings. (a) A plot of the hydration energies of the divalent fourth-period metal ions versus atomic number (solid circles) shows large deviations from the smooth curve calculated, assuming a spherical distribution of d electrons (dashed line). Correcting for CFSE gives the points shown as open circles, which, except for Ti^{2+} and Cr^{2+}, are close to the calculated values. The apparent deviations for these ions are caused by the fact that solutions of the Ti^{2+} ion in water are not stable, and Cr^{2+} does not form truly octahedral complexes. (b) A plot of the lattice energies for the fourth-period metal dichlorides versus atomic number shows similar deviations from the smooth curve calculated, assuming a spherical distribution of d electrons (dashed lines), again illustrating the importance of CFSEs.

Lattice Energies

Values of the lattice energies for the fourth-period metal dichlorides are plotted against atomic number in part (b) of Figure **4.2.2.1.8.3**. Recall that the lattice energy is defined as the negative of the enthalpy change for the reaction below. Like hydration energies, lattice energies are determined indirectly from a thermochemical cycle.

$$M^{2+}(g) + 2Cl^-(g) \rightarrow MCl_2(s) \tag{4.2.2.1.8.2}$$

The shape of the lattice-energy curve is essentially the mirror image of the hydration-energy curve in part (a) of Figure **4.2.2.1.8.3**, with only Ca^{2+}, Mn^{2+}, and Zn^{2+} lying on the smooth curve. It is not surprising that the explanation for the deviations from the curve is exactly the same as for the hydration energy data: all the transition-metal dichlorides, except $MnCl_2$ and $ZnCl_2$, are more stable than expected due to CFSE.

Summary

Distorting an octahedral complex by moving opposite ligands away from the metal produces a tetragonal or square planar arrangement, in which interactions with equatorial ligands become stronger. Because none of the d orbitals points directly at the ligands in a tetrahedral complex, these complexes have smaller values of the crystal field splitting energy Δ_t. The crystal field stabilization energy (CFSE) is the additional stabilization of a complex due to placing electrons in the lower-energy set of d orbitals. CFSE explains the unusual curves seen in plots of ionic radii, hydration energies, and lattice energies versus atomic

number. The Jahn–Teller theorem states that a non-linear molecule with a spatially degenerate electronic ground state undergoes a geometrical distortion to remove the degeneracy and lower the overall energy of the system.

4.2.2.1.8: Thermodynamics and Structural Consequences of d-Orbital Splitting is shared under a CC BY-NC-SA 4.0 license and was authored, remixed, and/or curated by LibreTexts.

4.2.2.2: Ligand Field Theory

Ligand Field Theory (LFT) can be considered an extension of Crystal Field Theory such that all levels of covalent interactions can be incorporated into the model. LFT describes the bonding, orbital arrangement, and other characteristics of coordination complexes. It represents an application of molecular orbital theory to transition metal complexes. A transition metal has nine valence atomic orbitals: five nd, one (n+1)s, and three (n+1)p orbitals. These orbitals are of appropriate energy to form bonding interaction with ligands. The LFT analysis is highly dependent on the geometry of the complex, but will begin by examining octahedral complexes.

Treatment of the bonding in LFT is generally done using molecular orbital theory. A qualitative approach using generator functions and LGOs can be applied to these compounds just as we did previously. For the purpose of this discussion, we will consider the octahedral complex ion $[Co(NH_3)_6]^{3+}$. There are several assumptions that we must make in this approach.

1. The 4s, 4p and 3d orbitals are of the correct energy to interact with the nitrogen donor atoms of the NH_3 ligands.
2. As the NH_3 ligands are L-type ligands and will not participate in any π-bonding with the cobalt, we can treat the nitrogen atoms as though they were hydrogen atoms. This means our MO diagram will not account for any N-H bonding. As there are 18 N-H bonds in the complex, it certainly simplifies matters by choosing to ignore this.

Step 1 - Drawing the structure and determining the hybridization of the central atom

The geometry of the complex has already been specified and the structure of the complex is depicted below (Figure **4.2.2.2.1**).

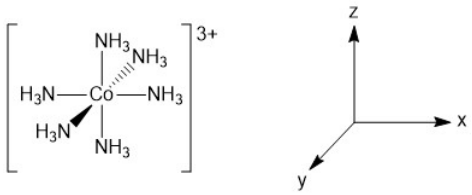


Figure 4.2.2.2.1. Structure and assigned axes for $[Co(NH_3)_6]^{3+}$.

Exercise 4.2.2.2.1

Using rules for VSEPR, what orbitals need to be used for hybridization of the central cobalt atom? Be as specific as possible about the orbitals.

Answer

The cobalt would be treated as AX_6E_0 and so would be sp^3d^2 hybridized.

The orbitals involved would be the 4s, 4p and two of the 3d orbitals. For the 3d orbitals, we can decide which ones to involve based on the assigned axes. As we are making σ-bonds, the orbitals involved must be pointing at the incoming ligands. In this geometry that means we much use the d_{z^2} and $d_{x^2-y^2}$ orbitals.

Step 2 - Determine the point group of the complex and assign the generator functions

The molecule is octahedral and so the point group is O_h. The O_h character table is rather robust and so only the abbreviated version will appear here.

O_h	Orbitals
A_{1g}	s
A_{2g}	
E_g	d_{z^2}, $d_{x^2-y^2}$
T_{1g}	
T_{2g}	d_{xy}, d_{yz}, d_{xz}
A_{1u}	
A_{2u}	
E_u	
T_{1u}	p_x. p_y, p_z
T_{2u}	

Exercise 4.2.2.2.2

What are the symmetry labels for the cobalt orbitals used to make $[Co(NH_3)_6]^{3+}$?.

Answer

s - a_{1g}

p_x - t_{1u}

p_y - t1u

p_z - t_{1u}

d_{z^2} - e_g

$d_{x^2-y^2}$ - e_g

Step 3 - Making the LGOs

As we have done previously, we will consider all of the potential interactions between the metal orbitals and ligand orbitals using a pictorial method. Based on the axes assigned above, the matching LGOs can be drawn as shown (Figure **4.2.2.2.2**).

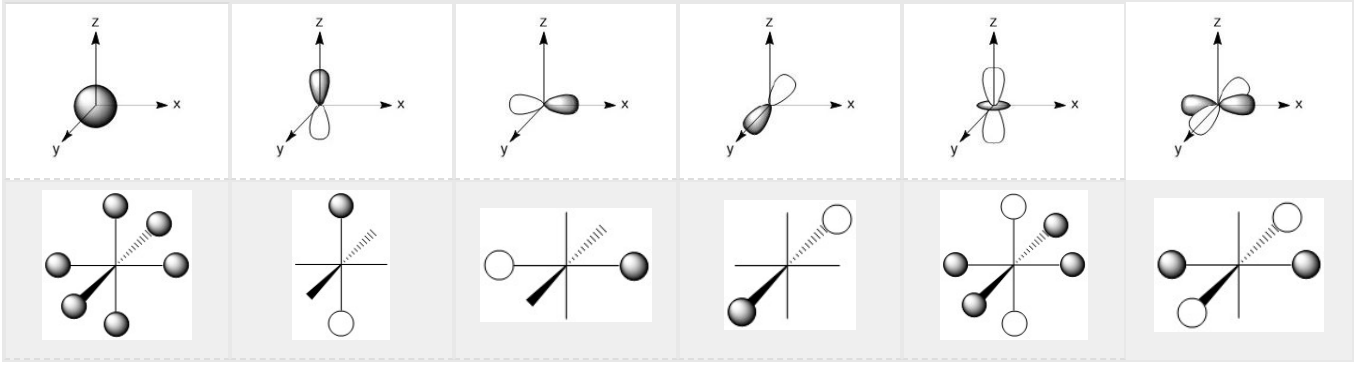


Figure 4.2.2.2.2. LGOs $[Co(NH_3)_6]^{3+}$.

Step 4 - Constructing the MO diagram

Previously when we were building MO diagrams we would start by looking at the orbital energies. In this case, doing this is a little more complicated. One complication is that the ligand is NH_3 and so we can not just use the orbital energy for nitrogen. Another complication is that the orbital energies for transition metals in various valence states are not as readily available. However, we can make some reasonable approximations. From WebMO, the orbital energies for Co(III) are 3d (-12.12 eV), 4s (-8.10 eV), and 4p (-5.290 eV). The lone pair in NH_3 would be the HOMO and from WebMO the energy of this orbital was calculated to be -13.702 eV. The general trend here is that the ligand orbitals are lower in energy than the metal orbitals. Once again we match the symmetry labels and if there is a match on the metal and the LGOs, we make bonding and antibonding orbitals. The t_{2g} orbitals on the metal do not have a match among the LGOs and so they will make non-bonding orbitals that do not change in energy much from the original metal d-orbitals. The rest of the metal orbitals have a match with the LGOs and so we get the diagram below (Figure **4.2.2.2.3**).

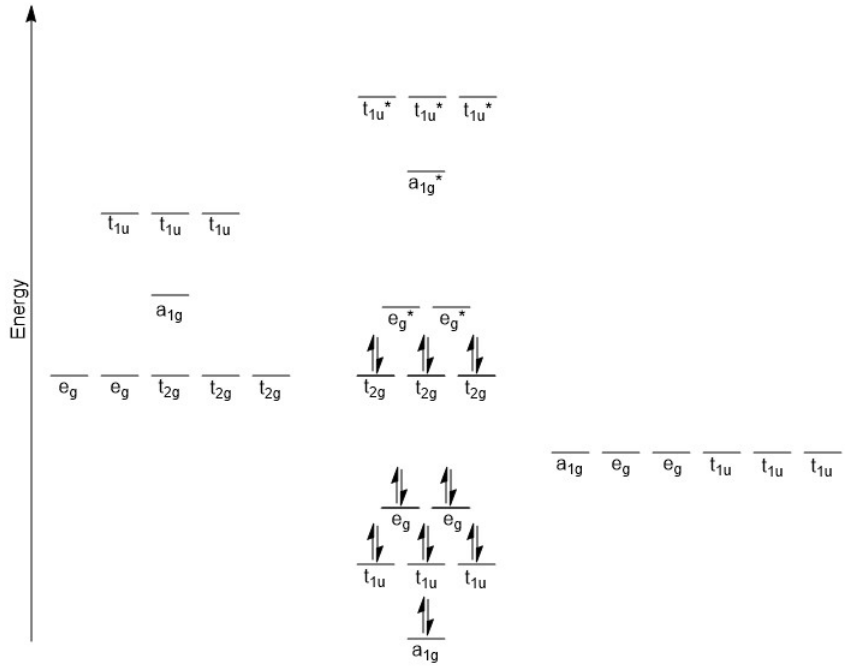


Figure 4.2.2.2.3. MO diagram for $[Co(NH_3)_6]^{3+}$.

This diagram likely raises a number of questions. One likely question would be the ordering of the bonding MOs. The e_g orbitals on the cobalt are the lowest energy, and yet they make the highest energy bonding MOs. Recall from our previous discussion that d-orbitals are not terribly good at forming bonding interactions. The s- and p-orbitals are much better at interacting with the incoming ligands and as such, give rise to lower energy bonding MOs. The a_{1g} orbital is based on the 4s orbital of cobalt which is lower in energy than the 4p orbitals which are t_{1u}. Somewhat similar logic can be applied to the antibonding orbitals. Since the e_g orbitals are not very good at forming bonding interactions, their antibonding interactions (e_g*) will not be quite as high in energy. The ordering of the a_{1g}* and t_{1u}* orbitals is a bit more difficult to rationalize. However, when considering the electron configuration of a cobalt atom ([Ar] $4s^2$ $3d^7$), the 4p orbitals are unoccupied. In fact, it may have seemed a bit odd to even consider these orbitals in the hybridization. They are certainly higher in energy and as the t_{1u}* orbitals are more localized on the cobalt, this could cause them to be higher in energy than the a_{1g}* orbital.

Another subtle point is that the d-orbital splitting that was previously discussed is found in this diagram. The MOs are labeled as t_{2g} and e_g*. The e_g* is slightly different than what we saw in the discussion on crystal field theory. However, these orbitals are closer in energy to the metal d-orbitals and as such are mostly metal d-orbital in character. It is common practice to refer to the t_{2g} and e_g* orbitals show in this diagram as the metal d-orbitals but realize there is antibonding character to the e_g* orbitals. In addition, this compound is drawn as being Low Spin, with the t_{2g} completely occupied and the e_g* unoccupied. Just building the

MO diagram there is no way to make that distinction. Looking at the spectrochemical series we see that NH_3 is towards the strong field end of the series so a Low Spin configuration is not unreasonable.

How did we do?

The calculations are a bit more involved for this complex. There are a total of 51 MOs for this complex cation, 18 from the 18 hydrogen atoms, 24 from the six nitrogen atoms and 9 from the cobalt. Pictorially, the 18 lowest energy MOs are mostly N-H in nature and will be ignored for this discussion. As there are multiple degenerate levels in the MO diagram, one representative orbital will be shown. The energy for the cobalt orbitals was calculated to be -13.180 eV (3d), -9.210 eV (4s) and -5.290 eV (4p). The energy of the HOMO for NH_3 was calculated to be -13.684 eV. This supports the idea that the orbitals from the ligands are lower in energy that those of the metal.

a_{1g}	t_{1u}	e_g	t_{2g}	e_g^*	a_{1g}^*	t_{1u}^*
						
-15.2 eV	-13.9 eV	-13.8 eV	-13.2 eV	-12.5 eV	20.7 eV	24.795 eV

Overall this isn't a bad match to our pictorial method. Overall the pictures help to visualize the orbitals and the energies do make sense with our rough approximations. The a_{1g}, t_{1u} and e_g orbitals are all lower in energy than the HOMO of NH_3. The t_{2g} orbitals are very similar to the energy of the 3d orbitals of cobalt. The e_g* orbitals are slightly higher in energy than the t_{2g} orbitals. The energy difference from this very rough calculation corresponds to an absorption of light with a wavelength of 1700 nm. While well outside the visible range and much larger than the actual value of approximately 470 nm displayed by the yellow $[Co(NH_3)_6]^{3+}$, this is a rough estimate made from fairly low level calculations.

Why did we choose NH_3?

The choice of NH_3 might seem a bit odd at first. Certainly a halide even with three lone pair would have been easier to deal with than NH_3. The choice of NH_3 was not by chance. The NH_3 ligand is purely σ-donating to the cobalt through the lone pair on the nitrogen atom. There are no other lone pair that could be donated to the cobalt to form and kind of π-bonding interaction. Although you may not think of halides as making π-bonds, the lone pair on the halides are capable of interacting in a π-bonding manner with an atom capable of accepting electrons. And it just so happens that the t_{2g} orbitals of a transition metal are of the proper symmetry and energy to interact with ligands capable of donating electrons to give a π-bonding interaction. While we would still draw a single bond (M-Cl) and not a double bond (M=Cl), we should appreciate that there is possibly some π-bonding interaction occurring in a M-Cl bond. In fact, all of the weak field ligands are capable of this sort of interaction to some extent.

An explanation for strong field ligands is also based on π-bonding arguments. However, in the case of strong field ligands, it is the metal that is providing the electrons in the π-bonding interaction. This interaction is a bit tougher to deal with. Unlike say the halide ligands, we never draw lone pair on metals. This means it is not always readily apparent that there are electrons on the metal available for π-bonding. However, as long as the metal does not have a d^0 configuration, we can consider that there are electrons in the t_{2g} orbitals that could be used for π-bonding. Even harder to visualize is how is the ligand going to be accepting these electrons. As we saw for weak field ligands, the key is that the ligand must have an orbital of the right symmetry and energy to be able to interact with a metal t_{2g} orbital. These orbitals are not readily apparent for many ligands. Consider the CO ligand which is called a carbonyl ligand (similar to an organic carbonyl, $R_2C{=}O$ but there are no groups on the carbon atom and so we draw a C≡O). The π-bonding interaction between the carbonyl and the metal involves the π* orbital of CO Figure **4.2.2.2.4**. Consider first the CO portion depicted. The orbitals are not drawn along the C-O bond axis. This tells us that we are dealing with some type of π-orbital. In the top half of the picture, the orbital is blue on the carbon atom and white on the oxygen atom. And these lobes point away from each other. The combination of the direction and the sign change indicate that this is a π* orbital. In addition (although it is a bit subtle in this picture), the lobes on the carbon atom are larger than the lobes on the oxygen atom. Antibonding orbitals are more localized on the LEAST electronegative atom where as bonding orbitals are localized on the more electronegative atom. This π* orbital of CO has the right symmetry and energy to give a boding interaction with a metal d-orbital. But way, we said this was a π* orbital. It

is...with respect to the carbon-oxygen bond. However, the interaction is bonding (as noted by the interaction of lobes with the same sign) with respect to the metal-carbon bond. In general, strong field ligands will share this ability to act as π-acceptors.

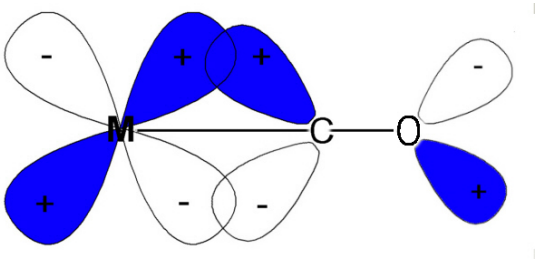


Figure 4.2.2.2.4. π interaction between a metal and a carbonyl ligand.

How does this impact our diagram for the metal d-orbitals? In both cases we consider the ligands to be interacting with the t_{2g} orbitals of the metal. In the case of a weak field ligand, the filled orbitals of the π-donating ligand are at a lower energy than the t_{2g} orbitals. The ligand orbitals and the t_{2g} orbitals interact to give π-bonding and π-antibonding orbitals. The π-antibonding orbitals will be more localized on the metal and they will get pushed up in energy relative to the starting t_{2g} orbitals. This will make them closer in energy to the e_g orbitals and therefore decrease Δ_o. With strong field ligands, the metal t_{2g} orbitals are lower in energy than the π-accepting orbitals of the ligands. These orbitals interact to give π-bonding and π-antibonding (with respect to the M-L) orbitals. The π-bonding orbital will go down in energy and be more metal in character. The moves it further away from the e_g orbitals and thus increases Δ_o. These interactions are illustrated below Figure **4.2.2.2.5**).

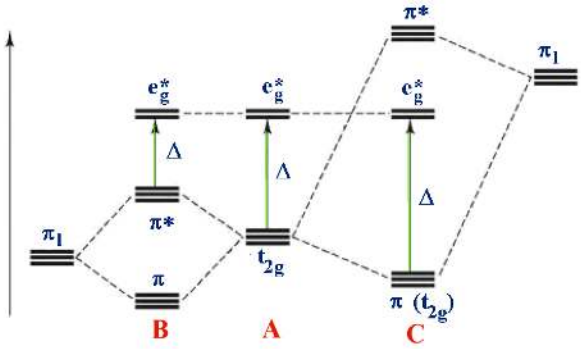


Figure 4.2.2.2.5. π interactions between a metal and its ligands (B: $[M(II)I_6]^{4-}$; A: $[M(II)(H_2O)_6]^{2+}$; C: $[M(II)(CN)_6]^{4-}$).

Contributors and Attributions

- Prof. Robert J. Lancashire (The Department of Chemistry, University of the West Indies)

4.2.2.2: Ligand Field Theory is shared under a not declared license and was authored, remixed, and/or curated by LibreTexts.

4.3: Ligand Exchange Reactions (Thermodynamics)

Replacing aqua ligands with ammine ligands

If you add ammonia solution to a solution containing hexaaquacopper(II) ions, $[Cu(H_2O)_6]^{2+}$, four of the water molecules are eventually replaced by ammonia molecules to give $[Cu(NH_3)_4(H_2O)_2]^{2+}$. This can be written as an equilibrium reaction to show the overall effect:

$$[Cu(H_2O)_6]^{2+} + 4\,NH_3 \rightleftharpoons [Cu(NH_3)_4(H_2O)_2]^{2+} + 4\,H_2O \tag{4.3.1}$$

In fact, the water molecules get replaced one at a time, and so this is made up of a series of part-reactions:

$$[Cu(H_2O)_6]^{2+} + NH_3 \rightleftharpoons [Cu(NH_3)(H_2O)_5]^{2+} + H_2O \tag{4.3.2}$$

$$[Cu(NH_3)(H_2O)_5]^{2+} + NH_3 \rightleftharpoons [Cu(NH_3)_2(H_2O)_4]^{2+} + H_2O \tag{4.3.3}$$

$$[Cu(NH_3)_2(H_2O)_4]^{2+} + NH_3 \rightleftharpoons [Cu(NH_3)_3(H_2O)_3]^{2+} + H_2O \tag{4.3.4}$$

$$[Cu(NH_3)_3(H_2O)_3]^{2+} + NH_3 \rightleftharpoons [Cu(NH_3)_4(H_2O)_2]^{2+} + H_2O \tag{4.3.5}$$

Although this can look a bit daunting at first sight, all that is happening is that first you have one, then two, then three, then four water molecules in total replaced by four ammine ligands.

Individual stability constants

Let's take a closer look at the first of these equilibria (Equation 4.3.2). Like any other equilibrium, this one has an equilibrium constant, K_c - except that in this case, we call it a stability constant. Because this is the first water molecule to be replaced, we call it K_1 and is given by this expression:

$$K_1 = \frac{[[Cu(NH_3)(H_2O)_5]^{2+}]}{[[Cu(H_2O)_6]^{2+}][NH_3]} \tag{4.3.6}$$

There are two points of possible confusion here - one minor, one more important!

- First, the square brackets have changed their meaning! Square brackets are often used to keep everything in a complex ion together and tidy. Here, they have reverted to their other use, which implies concentrations in mol dm^{-3}.
- In order to avoid complete confusion, the square brackets keeping the complexes together have been removed entirely.
- More importantly, if you compare the equilibrium constant expression with the equation, you will see that the water on the right-hand side hasn't been included. That is normal practice with these expressions.
- Because everything is dissolved in water, the water is present as a huge excess. Generating a little bit more during the reaction is going to make no effective difference to the total concentration of the water in terms of moles of water per dm^3.
- The concentration of the water is approximately constant. The equilibrium constant is defined so that you avoid having an extra unnecessary constant in the expression.

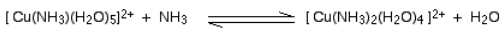
With that out of the way, let's go back to where we were - but introduce a value for K_1:

$$[Cu(H_2O)_6]^{2+} + NH_3 \rightleftharpoons [Cu(NH_3)(H_2O)_5]^{2+} + H_2O$$

$$K_1 = \frac{[Cu(NH_3)(H_2O)_5^{2+}]}{[Cu(H_2O)_6^{2+}]\,[NH_3]}$$

$$= 1.78 \times 10^4 \text{ mol}^{-1}\text{ dm}^3$$

The value of the equilibrium constant is fairly large, suggesting that there is a strong tendency to form the ion containing an ammonia molecule. A high value of a stability constant shows that the ion is easily formed. Each of the other equilibria above also has its own stability constant, K_2, K_3 and K_4. For example, K_2 is given by:



$$K_2 = \frac{[Cu(NH_3)_2(H_2O)_4^{2+}]}{[Cu(NH_3)(H_2O)_5^{2+}]\,[NH_3]} = 4.07 \times 10^3 \ mol^{-1}\ dm^3$$

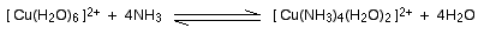
The ion with two ammonias is even more stable than the ion with one ammonia. You could keep plugging away at this and come up with the following table of stability constants:

ion	K_n	value (mol^{-1} dm^3)	log K_n
$[Cu(NH_3)(H_2O)_5]^{2+}$	K_1	1.78×10^4	4.25
$[Cu(NH_3)_2(H_2O)_4]^{2+}$	K_2	4.07×10^3	3.61
$[Cu(NH_3)_3(H_2O)_3]^{2+}$	K_3	9.55×10^2	2.98
$[Cu(NH_3)_4(H_2O)_2]^{2+}$	K_4	1.74×10^2	2.24

You will often find these values quoted as log K_1 or whatever. All this does is tidy the numbers up so that you can see the patterns more easily. The ions keep on getting more stable as you replace up to 4 water molecules, but notice that the equilibrium constants are gradually getting smaller as you replace more and more water ligands. This is common with individual stability constants.

Overall Formation constants

The overall stability constant is simply the equilibrium constant for the total reaction:



It is given by this expression:

$$\text{overall } K_{stab} = \frac{[Cu(NH_3)_4(H_2O)_2^{2+}]}{[Cu(H_2O)_6^{2+}]\,[NH_3]^4} = 1.20 \times 10^{13} \ mol^{-4}\ dm^{12}$$

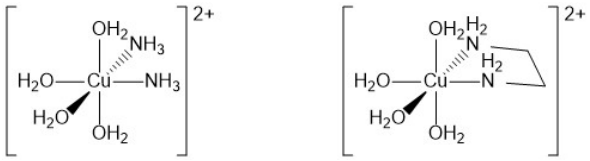
You can see that overall this is a very large equilibrium constant, implying a high tendency for the ammonia ligands to replace the water ligands. The "log" value is 13.1. This overall value is found by multiplying together all the individual values of K_1, K_2 and so on. To find out why that works, write down expressions for all the individual values (the first two are done for you above), and then multiply those expressions together. You will find that all the terms for the intermediate ions cancel out to leave you with the expression for the overall stability constant.

Summary

Whether you are looking at the replacement of individual water molecules or an overall reaction producing the final complex ion, a stability constant is simply the equilibrium constant for the reaction you are looking at. The **larger** the value of the stability constant, the further the reaction lies to the **right**. That implies that complex ions with large stability constants are more stable than ones with smaller ones.

Stability constants and entropy - the chelate effect

The chelate effect is an effect which happens when you replace water (or other simple ligands) around the central metal ion by multidentate ligands like 1,2-diaminoethane (en) or EDTA. Compare what happens if you replace two water ligands around a $[Cu(H_2O)_6]^{2+}$ ion with either 2 ammonia ligands or one en ligand.



Chelates are much more stable than complex ions formed from simple monodentate ligands. The overall stability constants for the two ions are:

ion	log K
$[Cu(NH_3)_2(H_2O)_4]^{2+}$	7.86
$[Cu(H_2O)_4(en)]^{2+}$	10.6

The reaction with the 1,2-diaminoethane could eventually go on to produce a complex ion $[Cu(en)_3]^{2+}$. The overall stability constant for this (as log K) is 18.7. Another copper-based chelate comes from the reaction with EDTA. This also has a high stability constant - log K is 18.8. However many examples you take, you always find that a chelated complex is more stable than one with only monodentate ligands. This is known as the chelate effect.

The reason for the chelate effect

If you compare the two equilibria below, the one with the en has the higher equilibrium (stability) constant (for values, see above).

$$[Cu(H_2O)_6]^{2+} + 2NH_3 \rightleftharpoons [Cu(NH_3)_2(H_2O)_4]^{2+} + 2H_2O$$

$$[Cu(H_2O)_6]^{2+} + en \rightleftharpoons [Cu(H_2O)_4(en)]^{2+} + 2H_2O$$

The enthalpy changes of the two reactions are fairly similar. You might expect this because in each case you are breaking two bonds between copper and oxygen atoms and replacing them by two bonds between copper and nitrogen atoms. However, when considering the reverse reaction there is a bit of a difference in enthalpy. If one Cu-N bond breaks, the NH_3 ligand can be replaced by a water ligand. However, for en to leave, both Cu-N bonds to the ligand must be broken. If only one Cu-N bond to en is broken, the unbound nitrogen atom remains in close proximity to the copper atom, making it very likely that it will just reform the Cu-N bond.

Another factor in the chelate effect is the difference has to do with the entropy change during each reaction.

Entropy is most easily thought of as a measure of disorder. Any change which increases the amount of disorder increases the tendency of a reaction to happen.

If you look again at the two equiilbria, you might notice that the en equilibrium does lead to an increase in the entropy. There are only two species on the left-hand side of the equation, but three on the right.

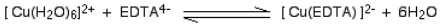
$$[Cu(H_2O)_6]^{2+} + en \rightleftharpoons [Cu(H_2O)_4(en)]^{2+} + 2H_2O$$

You can obviously get more entropy out of three species than out of only two. Compare that with the other equilibrium. In this case, there is no change in the total number of species before and after reaction, and so no useful contribution to an increase in

entropy.



In the case of the complex with EDTA, the increase in entropy is very pronounced.



Here, we are increasing the number of species present from two on the left-hand side to seven on the right. You can get a major amount of increase in disorder by making this change.

Reversing this last change is going to be far more difficult in entropy terms. You would have to move from a highly disordered state to a much more ordered one. That isn't so likely to happen, and so the copper-EDTA complex is very stable.

Summary

Complexes involving multidentate ligands are more stable than those with only monodentate ligands. The underlying reason for this is that each multidentate ligand displaces more than one water molecule. This leads to an increase in the number of species present in the system, and therefore an increase in entropy. An increase in entropy makes the formation of the chelated complex more favorable.

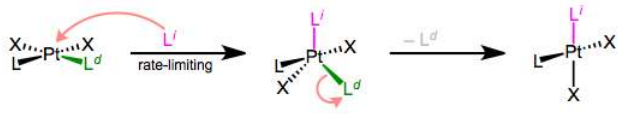
Contributors and Attributions

- Jim Clark (Chemguide.co.uk)

This page titled 4.3: Ligand Exchange Reactions (Thermodynamics) is shared under a CC BY-NC 4.0 license and was authored, remixed, and/or curated by Jim Clark.

4.3.1: Associative Ligand Substitution

A very common reaction for metal complexes is ligand substitution in which one ligand is exchanged with another. There are two common mechanisms for ligand substitution reactions the first of which is called the associative mechanism. In this mechanism the incoming ligand approaches the complex before departure of the leaving ligand. How can we spot an associative mechanism in experimental data, and what are some of the consequences of this mechanism?



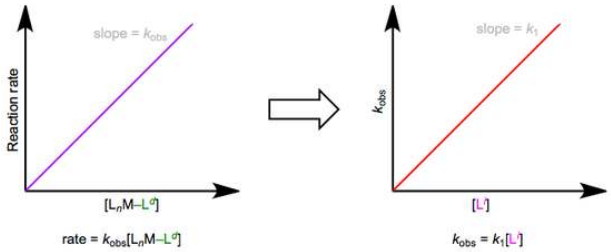
The prototypical mechanism of associative ligand substitution. The first step is rate-determining. A typical mechanism for associative ligand substitution is shown above. Let's begin by examining the kinetics of the reaction.

Reaction kinetics are commonly used to elucidate reaction mechanisms, and ligand substitution is no exception. Different mechanisms of substitution may follow different rate laws, so plotting the dependence of reaction rate on concentration of the species involved in the reaction often allows us to distinguish mechanisms. Associative substitution's rate law depends on the concentrations of both starting materials.

$$L_nM\text{–}L^d + L_i \rightarrow L_nM\text{–}L_i + L^d \tag{4.3.1.1}$$

$$\frac{d[L_nM\text{–}L^i]}{dt} = rate = k_1[L_nM\text{–}L^d][L^i] \tag{4.3.1.2}$$

The easiest way to determine this rate law is to use pseudo-first-order conditions. Although the rate law is second order overall, if we could somehow render the concentration of the incoming ligand unchanging, the reaction would appear first order. The observed rate constant under these conditions reflects the consistency of the incoming ligand's concentration ($k_{obs} = k_1[L^i]$, where both k_1 and $[Li]$ are constants). How can we make the concentration of the incoming ligand invariant, you ask? We can drown the reaction in ligand to achieve this. The small amount of the incoming ligand actually used up in the reaction has a negligible effect on the concentration of the "sea" of starting ligand we began with. The observed rate is equal to $k_{obs}[L_nM\text{–}L^d]$, as shown by the purple trace below. By determining k_{obs} at a variety of $[L^i]$ values, we can isolate k_1, the rate constant for the slow step. The red trace below at right shows the idea.



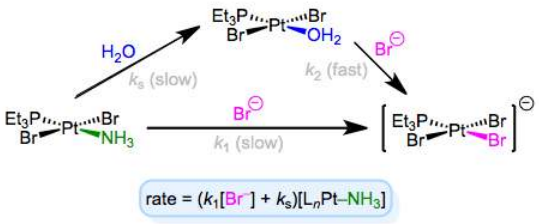
Associative substitution under pseudo-first-order conditions. The reaction is "swamped out" with incoming ligand.

In many cases, the red trace ends up with a non-zero y-intercept…curious, if we limit ourselves to the simple mechanism shown in the first figure of this post. A non-zero intercept suggests a more complex mechanism. We need to add a new term (called k_s for reasons to become clear shortly) to our first set of equations:

$$rate = (k_1[L_i] + k_s)[L_nM\text{–}L^d] \tag{4.3.1.3}$$

$$k_{obs} = k_1[L_i] + k_s \tag{4.3.1.4}$$

The full rate law suggests that some other step (with rate ks[LnM–Ld]) independent of incoming ligand is involved in the mechanism. To explain this observation, we can invoke the solvent as a reactant. Solvent can associate with the complex first in a slow step, then incoming ligand can displace the solvent in a fast step. Solvent concentration doesn't enter the rate law because, well, it's drowning the reactants and its concentration undergoes negligible change! An example of this mechanism iis shown below.



Associative substitution with solvent participation—a head-scratching mechanism for many an organometallic grad student!

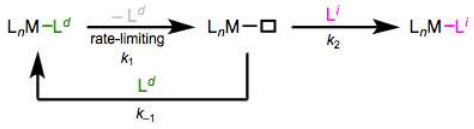
As an aside, it's worth mentioning that the entropy of activation of associative substitution is typically negative. Entropy decreases as the incoming ligand and complex come together in the rate-determining step.

Dr. Michael Evans (Georgia Tech)

This page titled 4.3.1: Associative Ligand Substitution is shared under a not declared license and was authored, remixed, and/or curated by Michael Evans.

4.3.2: Dissociative Ligand Substitution

The second mechanism for ligand substitution is the dissociative mechanism. In the slow step with positive entropy of activation, the departing ligand leaves, generating a coordinatively unsaturated intermediate. The incoming ligand then enters the coordination sphere of the metal to generate the product. The reverse of the first step, re-coordination of the departing ligand (rate constant k–1), is often competitive with dissociation.



A general scheme for dissociative ligand substitution. There's more to the intermediate than meets the eye!

Let's begin with the general situation in which k_1 and k_{-1} are similar in magnitude. Since k_1 is rate limiting, k_2 is assumed to be much larger than k_1 and k_{-1}. Most importantly, we need to assume that variation in the concentration of the unsaturated intermediate is essentially zero. This is called the steady state approximation, and it allows us to set up an equation that relates reaction rate to observable concentrations Hold onto that for a second; first, we can use step 2 to establish a preliminary rate expression.

$$\text{rate} = k_2[L_nM\text{–}\Diamond][Li] \tag{1}$$

Of course, the unsaturated complex is present in very small concentration and is unmeasurable, so this equation doesn't help us much. We need to remove the concentration of the unmeasurable intermediate from (1), and the steady state approximation helps us do this. We can express variation in the concentration of the unsaturated intermediate as (processes that make it) minus (processes that destroy it), multiplying by an arbitrary time length to make the units work out. All of that equals zero, according to the steady state approximation. Since Δt must not be zero, the other factor, the collection of terms, must equal zero.

$$\Delta[LnM\text{–}\Diamond] = 0 = (k1[LnM\text{–}L^d]\text{–}k\text{–}1[LnM\text{–}\Diamond][L^d]\text{–}k_2[LnM\text{–}\Diamond][Li])\Delta t \tag{2}$$

$$0 = k_1[LnM\text{–}Ld]\text{–}k_{-1}[LnM\text{–}\Diamond][Ld]\text{–}k_2[LnM\text{–}\Diamond][Li] \tag{3}$$

Rearranging to solve for [LnM–◊], we arrive at the following.

$$[LnM\text{–}\Diamond] = k_1\frac{[LnM\text{–}L_d]}{(k_{-1}[L_d] + k_2[Li]} \tag{4}$$

Finally, substituting into equation (1) we reach a verifiable rate equation.

$$\text{rate} = k_2k_1\frac{[LnM\text{–}Ld][Li]}{(k_{-1}[L_d] + k_2[Li]} \tag{5}$$

When k_{-1} is negligibly small, (5) reduces to the familiar equation (6), typical of dissociative reactions like S_N1.

$$\text{rate} = k_1[LnM\text{–}L_d] \tag{6}$$

Unlike the associative rate law, this rate does not depend on the concentration of incoming ligand. For reactions that are better described by (5), we can drown the reaction in incoming ligand to make $k_2[Li]$ far greater than $k_{-1}[Ld]$, essentially forcing the reaction to fit equation (6).

In general, introducing structural features that either stabilize the unsaturated intermediate or destabilize the starting complex can encourage dissociative substitution. Both of these strategies lower the activation barrier for the reaction. Other, quirky ways to encourage dissociation include photochemical methods, oxidation/reduction, and ligand abstraction.

Contributors and Attributions

- Dr. Michael Evans (Georgia Tech)

This page titled 4.3.2: Dissociative Ligand Substitution is shared under a not declared license and was authored, remixed, and/or curated by Michael Evans.

4.4: Electronic Spectra of Coordination Compounds

Term Splitting for Octahedral d^2 metal complexes

At first glance, one might think that there is only one possible transition for the d-electrons in an octahedral compound with a d^2 configuration when it absorbs light. That transition would be one of the electrons in a t_{2g} orbital raising in energy to one of the e_g orbitals. One example of this is shown below (Figure **4.4.1**). This might lead you to think there is only one band (peak) in the visible absorption spectrum for d^2 complexes, but that is not the case. In order to explain the additional bands, there would have to be other possible transitions. Perhaps you might think that since the electrons in the t_{2g} orbitals are equal in energy either of them could move to the e_g. Similarly, the e_g orbitals are degenerate, so the electron could go to either of those orbitals. That could give multiple transitions, but they would all be the same energy as the one depicted.

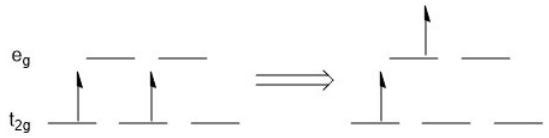


Figure 4.4.1. A possible transition for an electron in the t_{2g} orbital of a d^2 system.

What other transitions would be possible? The state shown above depicts the ground state electron configuration of a d^2 system. Remember back to general chemistry, the ground state follows Hund's rule in that the electrons are spread out and have the same spin. There are multiple possible excited states and these do not have to abide by Hund's rule, but they still must follow the Pauli exclusion principle. Several possible excited state configurations are shown below (Figure **4.4.2**).

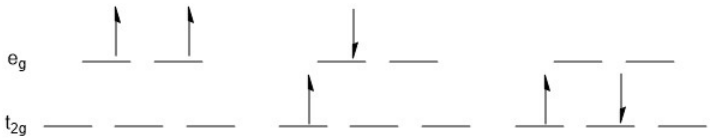


Figure 4.4.2. Additional possible excited states for a d^2 system.

To help keep track of all of the possible transitions, we use Term Symbols. Term Symbols are a method of accounting for electron-electron interactions in an atom. They are derived from the quantum numbers, in particular the values of m_l and m_s, associated with the electrons of interest. These term symbols take the form $^{2S+1}L_J$, where S represents the total spin angular momentum, L specifies the total orbital angular momentum, and J refers to the total angular momentum. How do we get these term symbols? The value of S comes from the sum of the m_s values for the electrons under consideration. As has typically been the case since general chemistry, the first electron we place is spin up or $+\frac{1}{2}$. So for the ground state shown in (Figure **4.4.1**) the value of S would be +1. The value of 2S+1 is called the multiplicity and in this example the multiplicity would equal three. This is referred to as a triplet or triplet state. The value of L comes from the sum of the m_l values. In the case above we are looking at d-orbitals. The possible m_l values are +2, +1, 0, -1 and -2. Standard practice is to begin filling the orbital with the highest value of m_l working to the lowest value. So for the ground state d^2 system, one electron would have a m_l or +2 and the other would be +1 giving a total of +3 as the value for L. However, L is not represented by this value, but rather a letter. This system is very similar to that used for the naming of atomic orbitals; an atomic orbital with an l value of 0 is an s-orbital while a term symbol with a L value of 0 would be an S term. This follows the same order as we learned for atomic orbitals, but it is very easy to get L values greater than 3, so after S, P, D, F the order proceeds G, H, K, I, etc. So far, this would make our ground state term for the d^2 system a ^3F term. The final value in the term symbol is J (which is why the letter J was skipped in the list above). This value comes from combinations of L and S.

The term symbols just described are known as free ion terms. This means we would be thinking about a d^2 metal ion in the gas phase. Things change a bit when you consider a metal with ligands. We move from the free ion terms to symbols that come from group theory. We also now have to deal with a wide range of ligands from weak field to strong field. As the ligands impact the separation of the t_{2g} and e_g orbitals, they should have an impact on the absorption of the complex. Doing much more with Term symbols is beyond the scope of this course. However, they do appear in the discussion below so it is important you have some appreciation of their source.

Selection Rules

In most cases the ligand field strength is in between the very weak and very strong case, and thus, we could expect very complicated spectra. Fortunately, nature does not make things quite as complicated, because not all possible electron transitions are quantum-mechanically allowed. The allowed transitions are defined by two rules: The spin selection rule and the Laporte rule.

The spin selection rule states that only transitions are allowed in which the total spin quantum number S does not change. Another way to say this is that only transitions between states with the same multiplicity are allowed. For example, it would be allowed to excite an electron from a triplet term to another triplet term, but not from a triplet term to a doublet or singlet term.

The Laporte rule state that transitions are only allowed when there is a change of parity. To fully appreciate this, we must define the terms gerade (symmetric with respect to inversion) and ungerade (not symmetric with respect to inversion). In thinking about this in terms of atomic orbitals, s-orbitals are completely spherical and as such are gerade. While it might take a little more to visualize it, d-orbitals are also gerade. On the other hand, p-orbitals, with the lobes having different signs are ungerade. This means that transitions between d-orbitals should not be allowed by the Laporte rule. However, in an octahedral geometry, it is possible that some terms may have a change in parity. So overall, a transition from a gerade (g) to an ungerade (u)-term and vice versa is possible, but not a transition from a g-term to another g-term, or the transition from a u-term to another u-term. For example the transition from a T_{2g} to a T_{1u} term would be allowed, but not the transition from a T_{2g} to a T_{1g} term.

Tanabe-Sugano diagram of a d^2 octahedral complex

In order to provide a somewhat quantitative way of representing the possible transitions for electrons in an octahedral compound, Tanabe-Sugano diagrams were developed (Figure **4.4.3**). The y-axis is energy divide by B, the Racah parameter. The Racah parameter is a quantum-mechanical energy unit for the electromagnetic interactions between the electrons. It is chosen because it provides “handy” numbers. Also on the y-axis one can find the free ion terms. The ground state is the lowest energy term. The x-axis is a measurement of the ligand field strength also given in terms of the Racah parameter. At 0, there are no ligands so we use the free ion terms. As the values on the x-axis increase so does the ligand field strength so weak-field ligands are towards the origin and strong field ligands are further away.

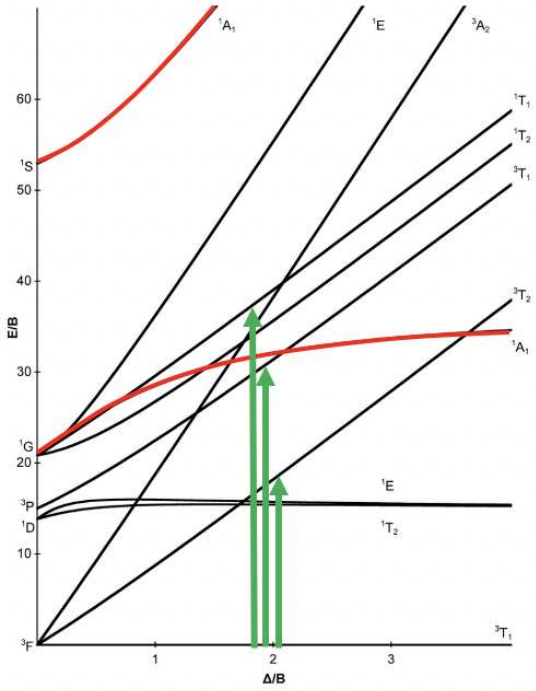


Figure 4.4.3. Tanabe-Sugano diagram for d^2 octahedral complexes.

You can see that some lines coming from the free ion terms in the diagram are bent, and some are straight. Bending of lines occurs when two terms interact with each other because they are close in energy and have the same symmetry. This is again an analogy to

orbitals. Like orbitals interact when they have the same symmetry and similar energy, terms interact when they have the same symmetry and the same energy. The closer the terms come to the point where they cross, the stronger their interactions, because their energies become more and more similar. The interactions lead to the fact that the terms bend away from each other, leading to bent curves. This means that curves for two terms of the same symmetry type will bend away in a Tanabe-Sugano diagram and never cross. For example the terms for the two $^1A_{1g}$ terms (in red above) bend away from each other and do not cross.

Next, let us think about which electron transitions would be allowed under the consideration of the spin selection and the Laporte rule. We notice that in the symmetry labels the "g" for gerade has been omitted. This is a common simplification made in the literature but all the terms shown are "g" terms. What does this mean for the allowance of electron transitions? It suggests that no electron transition should be allowed, and that would imply that the complex could not absorb light. The Laporte selection rule however does not hold strictly. It only says that the probability of the electron-transition is reduced, however, not forbidden. This means that an absorption band that disobeys the Laporte rule will have lower intensity compared to one that follows the Laporte rule, but it still can be observed. The spin-selection rule, however, holds strictly, and transitions between terms of different spin multiplicity are strictly forbidden, meaning that they have near zero probability to occur. Overall, we can therefore excite an electron from the $^3T_1$ ground state to other triplet terms, namely the $^3T_2$, $^3T_1$ and the $^3A_2$ terms.

Tanabe-Sugano diagram of d^3 octahedral complexes

Now, let us have a look at the Tanabe-Sugano diagram for a d^3 system in an octahedral ligand field (Figure **4.4.4**). What is the ground term? We can see the term designation on the horizontal line reads "$^4A_2$", therefore this term is the ground term. How many electron transitions from the ground state should we expect? To answer this question we need to count the number of other quartet terms. There is the $^4T_2$, the $^4T_1$, and the $^4T_1$. Thus, there are overall three electron transitions possible.

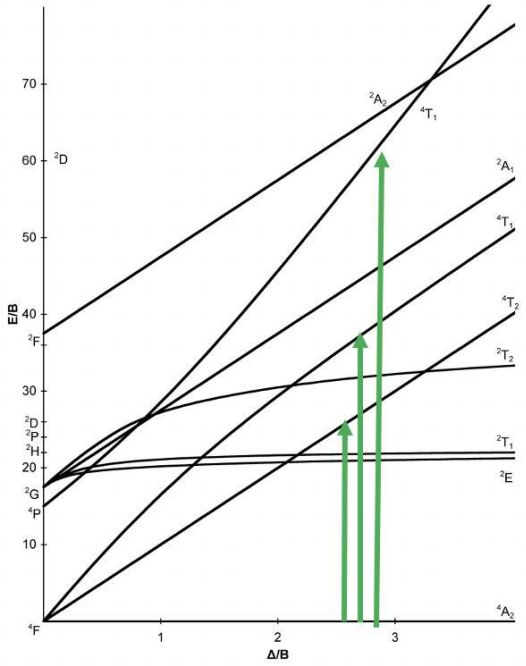


Figure 4.4.4. Tanabe-Sugano diagram for d^3 octahedral complexes.

Tanabe-Sugano diagram of d^4 octahedral complexes

Now let us look at the Tanabe-Sugano diagram for d^4 octahedral complexes (Figure **4.4.5**). You can see that this diagram is separated into two parts separated by a vertical line. The line indicates the ligand field strength at which the complex changes from a low sping complex to a high spin complex. At lower ligand field strengths, the ground term is a ^5E term. At higher field strength the ground term is a ^3T term. For a high spin complex there is only one allowed transition because there is only one other quintet term, namely the $^5T_2$ term. For the low spin complex, there are four transitions because there are four other triplet terms.

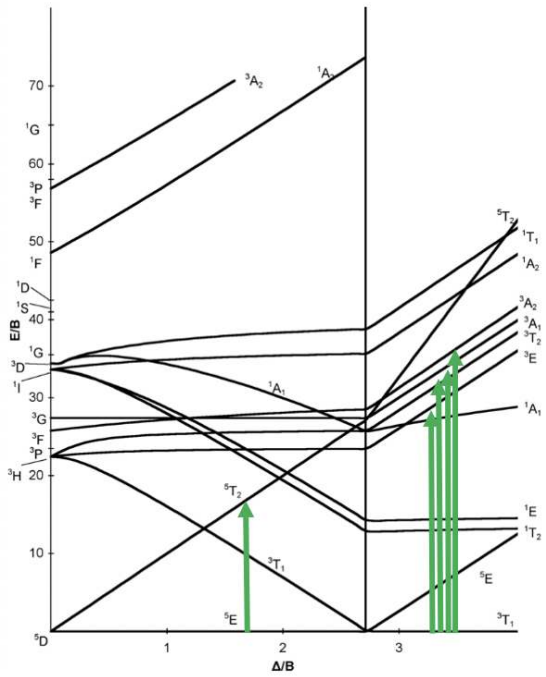


Figure 4.4.5. Tanabe-Sugano diagram for d^4 octahedral complexes.

Tananbe-Sugano diagram of d^5 octahedral complexes

The Tanabe-Sugano diagram for d^5 octahedral complexes is divided into two parts separated by a vertical line (Figure **4.4.6**). The left part reflects that high spin and the right part the low spin complex. The high spin ground state is a sextet term, and the low spin ground state is a doublet term. For the high-spin complex there are no other sextet terms, meaning that there is no electron transition possible. Hence, high-spin octahedral d^5-complexes are nearly colorless. An example for that is the hexaaqua manganese (2+) complex. A solution of this complex is near colorless, only very slightly pinkish. The slight color is because spin-forbidden transitions can occur albeit at a very low probability. For a d^5-low spin complex there are three additional doublet states, and thus there are three electron transitions possible.

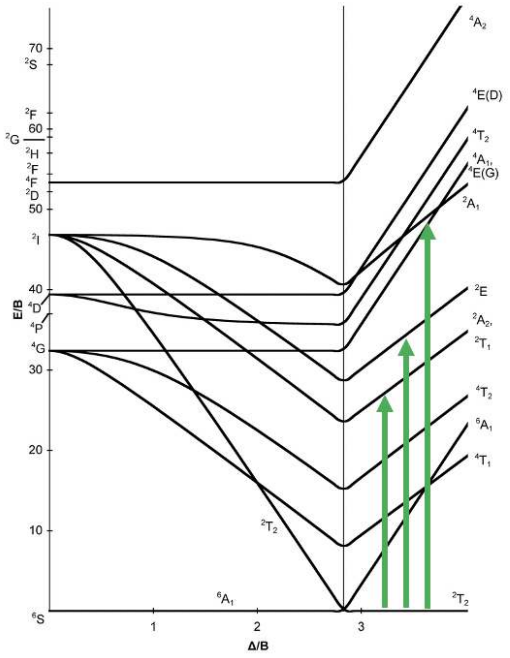


Figure 4.4.6. Tanabe-Sugano diagram for d^5 octahedral complexes.

Tanabe-Sugano diagram of d^6 octahedral complexes

The next diagram is the one for the d^6 electron configuration (Figure **4.4.7**). Again, the diagram is separated into parts for high and low spin complexes. There are dotted lines in the diagram. They indicate the terms that have a different spin multiplicity than the ground term. This way we can more easily see how many electron transitions are allowed. The ground term for the high-spin complex is the quintet $^5T_2$ term. The ground term for the low spin complex is a $^1A_1$ term. There is only transition allowed for the high-spin comples because the ^5E term is the only other quintet term. There are two transitions possible for the low-spin case because there are two additional singlet terms, namely the $^1T_1$ and the $^1T_2$.

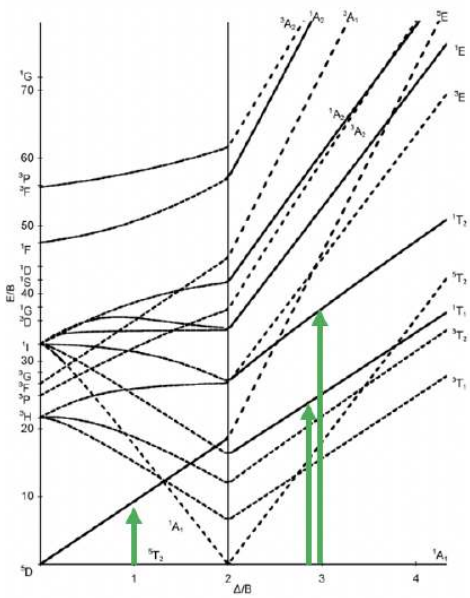


Figure 4.4.7. Tanabe-Sugano diagram for d^6 octahedral complexes.

Tanabe-Sugano diagram of d^7 octahedral complexes

Next, is the Tanabe-Sugano diagram for d^7 octahedral complexes (Figure **4.4.8**). In this case, the high spin complex has a $^4T_1$ ground term, and the low spin complex has a ^2E ground term. There are two other quartet terms, and two other doublet terms, hence there are two electrons transitions for the high-spin complex, and two for the low spin complex.

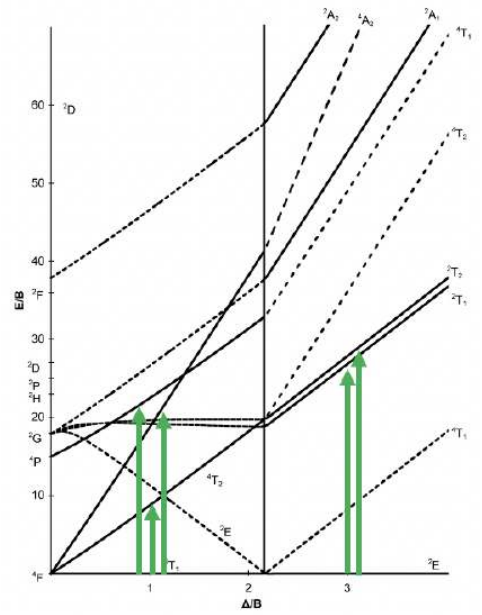


Figure 4.4.8. Tanabe-Sugano diagram for d^7 octahedral complexes.

Tanabe-Sugano diagram of d^8 octahedral complexes

Finally, we will examine the Tanabe-Sugano diagram for octahedral complexes with d^8 electron configuration (Figure **4.4.9**). For this electron configuration, there are no high and low spin complexes possible, therefore, the Tanabe-Sugano diagram is no longer divided into two parts. There is a single ground term of the type $^3A_2$. There are three other triplet states, namely the $^3T_2$ and two $^3T_1$ terms. Therefore, there are three electron transitions possible.

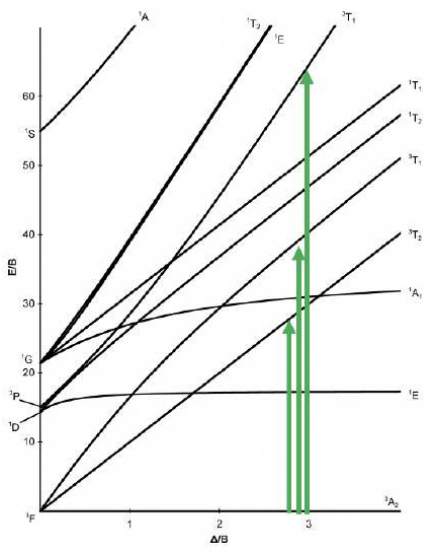


Figure 4.4.9. Tanabe-Sugano diagram for d^8 octahedral complexes.

You might wonder where are the Tanabe-Sugano diagrams for d^1, d^9, and d^{10}? For d^1 there are no electron-electron interactions, thus a simple orbital picture is sufficient. The ^2D term splits into T_{2g} and E_g terms, and there is only one electron transition possible. The d^9 electron configuration is the "hole-analog" of the d^1 electron configuration. It has also just one ^2D term which splits into a T_{2g} and an E_g term in the octahedral ligand field. Therefore, also in this case there is only one electron transition from the T_{2g} into the E_g term possible. In the case of d^{10} the orbitals are filled, and there is only the ^1S term which does not split in an octahedral ligand field. Therefore, there are no electron transitions in this case.

Finally, it should be mentioned that it is also possible to construct Tanabe-Sugano diagrams for other shapes such as the tetrahedral shape, but we will not discuss these further here.

Charge Transfer Transitions

Zn^{2+}		d^{10} ion	white
$[Cu(MeCN)_4]^+$	Cu(I)	d^{10} ion	colourless
$[Cu(phen)_2]^+$	Cu(I)	d^{10} ion	dark orange
TiF_4		d^0 ion	white
$TiCl_4$		d^0 ion	white
$TiBr_4$		d^0 ion	orange
TiI_4		d^0 ion	dark brown
$[MnO_4]^-$	Mn(VII)	d^0 ion	extremely purple
$[Cr_2O_7]^-$	Cr(VI)	d^0 ion	bright orange

Figure 8.2.19 d-d transitions

We are still not done with our electronic spectra. Thus, far we have only considered transitions of d-electrons between d-orbitals, and their terms. They are called d-d transitions. However, there are also so-called charge transfer transitions possible, that are not d-d transitions. We can easily see that there must be other transitions but d-d transitions when we look at the color of d^{10} and d^0 ions. For those, the are no d-d transitions possible. Therefore, they all should be colorless. However, that is not always true. Some of these ions are indeed colorless, but some are not. For example, Zn^{2+}, a d^{10} ion are always colorless in complexes, but not Cu(I) which is also d^{10}. While tetrakis(acetonitrile)copper (+) is colorless, bis(phenanthrene) copper(+) is dark orange. Similar is true for d0 ions. While TiF_4 and $TiCl_4$ are colorless, $TiBr_4$ is orange, and TiI_4 is brown. Some d^0 species are even extremely colorful, for example permanganate with Mn^{7+} which is extremely purple, and dichromate with Cr(VI) which is bright orange.

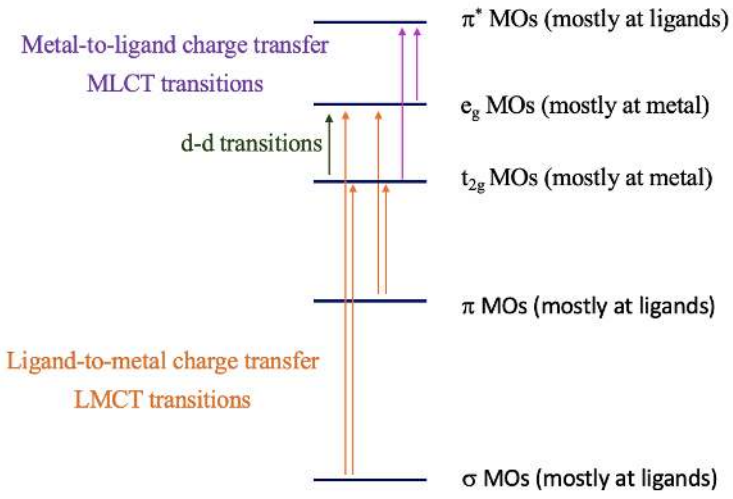


Figure 8.2.20 Charge-transfer transitions

The explanation of these phenomena are charge-transfer transitions. There are two types of charge-transfer transitions, the ligand-to-metal (LCMT) and the metal-to-ligand (MLCT) charge transfer transitions. For the ligand-to-metal transitions, electrons from bonding σ and π-orbitals get excited into metal d-orbitals in the ligand field, for example the t_{2g} and the e_g orbitals in an octahedral complex. If the energy difference between the σ/π-orbitals and the d-orbitals is small enough, then this electron-transition is associated with the absorption of visible light. The transition is called a ligand-to-metal transition because the ligand σ/π-orbitals

are mostly located at the ligands, while the metal-d-orbitals in a ligand field are mostly located at the metal. Vice versa, the metal-to-ligand transition involves the transition of an electron from metal d-orbitals in a ligand field to ligand π*-orbitals. This essentially moves electron density from the metal to the ligand, hance the name ligand-to-metal-charge transfer transition. If the energy-difference between the ligand π* and the metal orbitals is small enough, then the absorption occurs in the visible range. Charge-transfer transitions are usually both spin- and Laporte allowed, hence if they occur the color is often very intense. How can we distinguish between d-d and charge transfer transitions? Charge transfer transitions often change in energy as the solvent polarity is varied (solvatochromic) as there is a change in polarity of the complex associated with the charge transfer transition. This can be used to distinguish between d-d transitions and charge-transfer bands.

LMCT Transitions

Can we predict when the energy windows between the bonding molecular orbitals and the metal d-orbitals are small enough so that LMCT transitions in the visible can take place? Generally, it would be desirable if the energy of the metal orbitals was as low as possible and the energy of the bonding ligand orbitals are as high as possible. The energy of metal d-orbitals decreases with increasing positive charge at the metal because the effective nuclear charge on the metal increases. This means that very high oxidation states favor an LMCT transition. The d-orbitals should have few or no electrons, so that electrons can be promoted into the orbitals, and orbital energy increase due to electron-electron repulsion is minimized. Examples are Mn(VII), Cr(VI), and Ti(IV). The energy of MOs from bonding ligand orbitals increases when the ligand orbitals have high energy this is typically the case for π-donor ligand with negative charge.

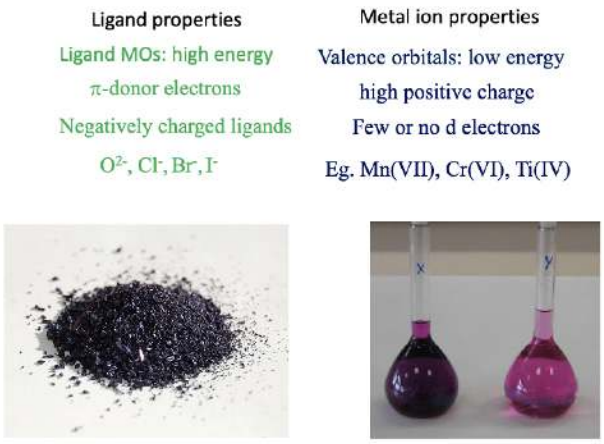


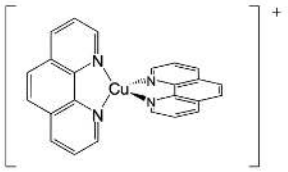
Figure 8.2.21 The properties of the metal ion and ligands in MnO_4^- (Attribution: Pradana Aumars / CC (https://commons.wikimedia.org/wiki/F...entrations.jpg))

Examples of ligands are oxo- and halo ligands. This explains for example the LMCT transitions in permanganate. The Mn is in the very high oxidation state +7, and the ligands are are oxo-ligands wich are π-donors with a 2- negative charge. The transitions are both Laporte and spin-allowed leading to very high intensity of light absorption, and thus color.

MLCT Transitions

What are favorable metal ion and ligand properties for a metal-to-ligand transition, then? In this case we would like to keep the energy of the metal orbitals as high as possible so that the energy difference between a metal d-orbital and a π*-orbital is minimized. This is accomplished when the positive charge at the metal ion is small, and there are many d-electrons that can repel each other, thereby increasing orbital energies, for examples Cu(I).

Metal ion properties	Ligand properties
low metal ion charge	π-acceptor ligand with low-lying π* orbitals
many electrons	
Cu(I), d^{10} ion	1,10-phenanthroline, CN^-, CO, SCN^-



$[Cu(phen)_2]^+$, dark orange

Figure 8.2.22 bis(phenanthroline) copper(+)

The ligand should be a π-acceptor with low-lying π*-orbitals, for example phenanthroline, CN^-, SCN^-, and CO. For instance, the bis(phenanthroline) copper(+) is dark-orange and has a MCLT absorption band a 458 nm. Also, the MLCT transfer is both spin and Laporte-allowed.

It should be mentioned that some complexes allow for both metal-to-ligand and ligand to metal transitions. For example, in the $Cr(CO)_6$ complex the σ-orbitals are high enough and the π*-orbitals are low enough in energy to allow for light absorption in the visible range. Finally, also intraligand bands are possible when the ligand is a chromophore.

Dr. Kai Landskron (Lehigh University). If you like this textbook, please consider to make a donation to support the author's research at Lehigh University: Click Here to Donate.

Tags recommended by the template: article:topic

This page titled 4.4: Electronic Spectra of Coordination Compounds is shared under a not declared license and was authored, remixed, and/or curated by Kai Landskron.

CHAPTER OVERVIEW

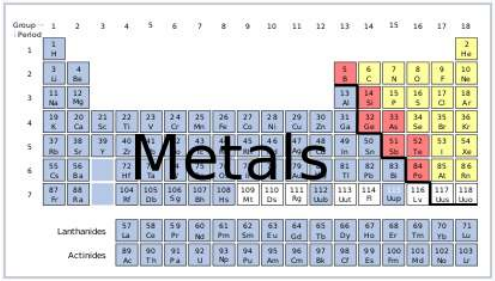
5: Solid State Chemistry

5.1: Prelude to Metals and Alloys
5.2: Unit Cells and Crystal Structures
5.3: Crystal Structures of Metals
5.3.1: Conduction in Metals
5.4: Atomic Orbitals and Magnetism
5.4.1: Ferro-, Ferri- and Antiferromagnetism
5.4.2: Hard and Soft Magnets
5.4.3: Defects in Metallic Crystals
5.5: X-ray Crystallography
5.5.1: Miller Indices (hkl)
5.5.2: Powder X-ray Diffraction
5.6: Prelude to Ionic and Covalent Solids - Structures
5.6.1: Close-packing and Interstitial Sites
5.6.2: Structures Related to NaCl and NiAs
5.6.3: Tetrahedral Structures
5.6.4: Layered Structures and Intercalation Reactions
5.6.5: Spinel, Perovskite, and Rutile Structures
5.7: Ionic Radii and Radius Ratios
5.8: Energetics of Crystalline Solids- The Ionic Model
5.8.1: Born-Haber Cycles for NaCl and Silver Halides
5.8.2: Lattice Energies and Solubility
5.8.3: Kapustinskii Equation
5.9: Electronic Properties of Materials - Superconductors and Semiconductors
5.9.1: Prelude to Electronic Properties of Materials - Superconductors and Semiconductors
5.9.2: Superconductors
5.9.3: Periodic Trends- Metals, Semiconductors, and Insulators
5.9.4: Semiconductors- Band Gaps, Colors, Conductivity and Doping
5.9.5: Semiconductor p-n Junctions
5.9.6: Diodes, LEDs and Solar Cells
5.9.7: References

5: Solid State Chemistry is shared under a not declared license and was authored, remixed, and/or curated by LibreTexts.

5.1: Prelude to Metals and Alloys

In the chemistry of molecular compounds, we are accustomed to the idea that properties depend strongly on structure. For example we can rationalize the polarity of the water molecule based on its shape. We also know that two molecules with the same composition (e.g., ethanol and dimethyl ether) have very different properties based on the bonding arrangements of atoms. It should come as no surprise that the properties of extended solids are also connected to their structures, and so to understand what they do we should begin with their crystal structures. Most of the metals in the periodic table have relatively simple structures and so this is a good place to begin.



Over 2/3 of the elements in the periodic table exist in their pure form as metals. All elemental metals (except the three - Cs, Ga, Hg - that are liquid) are crystalline solids at room temperature, and most have one of three simple crystal structures.

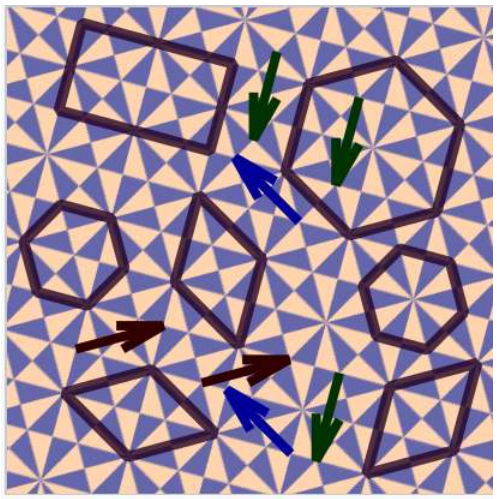
5.1: Prelude to Metals and Alloys is shared under a not declared license and was authored, remixed, and/or curated by LibreTexts.

- **6.1: Prelude to Metals and Alloys** by Chemistry 310 is licensed CC BY-SA 4.0. Original source: https://en.wikibooks.org/wiki/Introduction_to_Inorganic_Chemistry.

5.2: Unit Cells and Crystal Structures

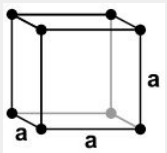
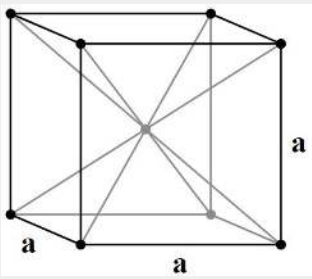
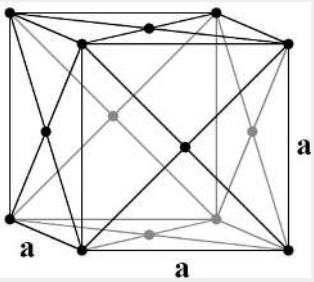
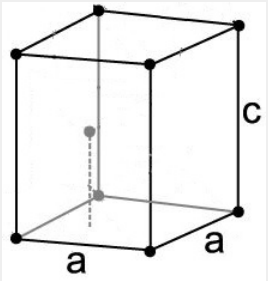
Crystals can be thought of as repeating patterns, much like wallpaper or bathroom tiles, but in three dimensions. The fundamental repeating unit of the crystal is called the **unit cell**. It is a three dimensional shape that can be repeated over and over by unit translations to fill space (and leave minimal gaps) in the structure. Some possible unit cells are shown in the tiling pattern at the right, along with arrows that indicate **unit translation vectors**. In three dimensions, the hexagonal or rhombic unit cells of this pattern would be replaced by three dimensional boxes that would stack together to fill all space. As shown in the figure, the origin of the unit cell is arbitrary. The same set of boxes will fill all space no matter where we define the origin of the lattice. We will see that pure metals typically have very simple crystal structures with cubic or hexagonal unit cells. However the crystal structures of alloys can be quite complicated.

When considering the crystal structures of metals and alloys, it is not sufficient to think of each atom and its neighboring ligands as an isolated system. Instead, think of the entire metallic crystal as a network of atoms connected by a sea of shared valence electrons. The **electrons are delocalized** because there are **not enough of them** to fill each "bond" between atoms with an electron pair. For example, in the crystal structures of s-block and p-block metals, each atom has either 8 or 12 nearest neighbors, but the maximum number of s + p electrons is 8. Thus, there are not enough to put two electrons between each pair of atoms. Transition metals can also use their d-orbitals in bonding, but again there are never enough electrons to completely fill all the "bonds."



Possible unit cells in a periodic tile pattern. The arrows connect translationally equivalent points (lattice points) in the pattern.

The atoms in a metal lattice arrange themselves in a certain pattern which can be represented as a 3D box structure known as the **unit cell** which repeats across the entire metal.

Simple Cubic	Body Centered Cubic	Face Centered Cubic	Hexagonal Close Packed
			
1 atom/cell	2 atoms/cell	4 atoms/cell	2 atoms/cell

Metal atoms can be approximated as spheres, and therefore are not 100 % efficient in packing, the same way a stack of cannonballs has some empty spaces between the balls. Different unit cells have different packing efficiencies. The number of atoms that is

included in the unit cell only includes the fractions of atoms *inside* of the box. Atoms on the corners of the unit cell count as ⅛ of an atom, atoms on a face count as ½, an atom in the center counts as a full atom. Using this, let's calculate the number of atoms in a simple cubic unit cell, a face centered cubic (fcc) unit cell, and a body centered cubic (bcc) unit cell.

Simple Cubic:

8 corner atoms × ⅛ = 1 atom/cell. The packing in this structure is not efficient (52%) and so this structure type is very rare for metals.

Body Centered Cubic, bcc:

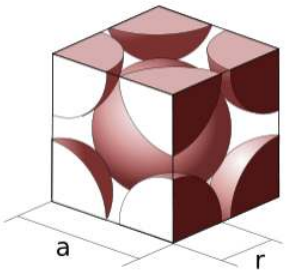
(8 corner atoms × ⅛) + (1 center atom × 1)= 2 atoms/cell. The packing is more efficient (68%) and the structure is a common one for alkali metals and early transition metals. Alloys such as brass (CuZn) also adopt these structures.

Face Centered Cubic, fcc (also called Cubic Close Packed, ccp):

(8 corner atoms × ⅛)+ (6 face atoms × ½)= 4 atoms/cell. This structure, along with its hexagonal relative (hcp), has the most efficient packing (74%). Many metals adopt either the fcc or hcp structure.

Hexagonal Close Packed, hcp:

Like the fcc structure, the packing density of hcp is 74%.

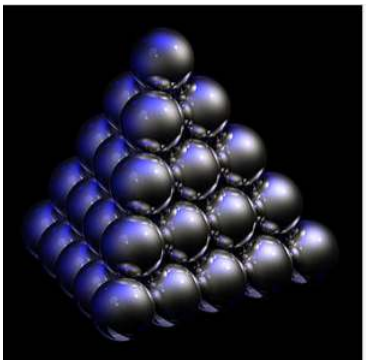


The unit cell of a bcc metal contains two atoms.

Calculating the packing fraction. The packing fractions of the crystal structures shown above can be calculated by dividing the volume of the atoms in the cell by the volume of the cell itself. The volume of the atoms in the cell is equal to the number of atoms/cell times the volume of a sphere, $(4/3)\pi r^3$. The volume of the cubic cells is found by cubing the side length. As an example, let's calculate the packing efficiency of a simple cubic unit cell. As we saw earlier in the section, a simple cubic unit cell contains one atom. The side length of the simple cubic unit cell is 2r, since the centers of each atom occupy the corners of the unit cell.

$$\text{Packing efficiency} = \frac{(1\ atom) \times (\frac{4}{3})\pi r^3}{(2r)^3} = 0.523 \qquad (5.2.1)$$

The same method can be applied to bcc and fcc structures.



Face-centered cubic stack of cannonballs.

5.2: Unit Cells and Crystal Structures is shared under a CC BY-SA license and was authored, remixed, and/or curated by LibreTexts.

- **6.2: Unit Cells and Crystal Structures** by Chemistry 310 is licensed CC BY-SA 4.0. Original source: https://en.wikibooks.org/wiki/Introduction_to_Inorganic_Chemistry.

5.3: Crystal Structures of Metals

Crystal structures

Most metals and alloys crystallize in one of three very common structures: body-centered cubic (bcc), hexagonal close packed (hcp), or cubic close packed (ccp, also called face centered cubic, fcc). In all three structures the coordination number of the metal atoms (i.e., the number of equidistant nearest neighbors) is rather high: 8 for bcc, and 12 for hcp and ccp. We can contrast this with the low coordination numbers (i.e., low valences - like 2 for O, 3 for N, or 4 for C) found in nonmetals. Atoms in metallic crystals have a tendency to pack in dense arrangments that fill space efficiently.

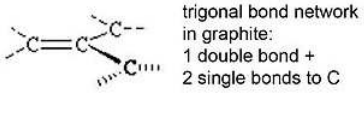
Periodic trends in structure and metallic behavior

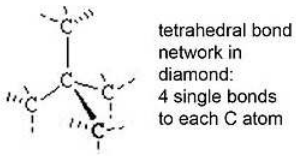
Remember where we find the metallic elements in the periodic table - everywhere except the upper right corner. This means that as we go down a group in the p-block (let's say, group IVA, the carbon group, or group VA, the nitrogen group), the properties of the elements gradually change from nonmetals to metalloids to metals. The carbon group nicely illustrates the transition. Starting at the top, the element carbon has two stable allotropes - graphite and diamond. In each one, the valence of carbon atoms is exactly satisfied by making four electron pair bonds to neighboring atoms. In graphite, each carbon has three nearest neighbors, and so there are two single bonds and one double bond. In diamond, there are four nearest neighbors situated at the vertices of a tetrahedron, and so there is a single bond to each one.

The two elements right under carbon (silicon and germanium) in the periodic table also have the diamond structure (recall that these elements cannot make double bonds to themselves easily, so there is no graphite allotrope for Si or Ge). While diamond is a good insulator, both silicon and germanium are semiconductors (i.e., metalloids). Mechanically, they are hard like diamond. Like carbon, each atom of Si and Ge satisfies its valence of four by making single bonds to four nearest neighbors.

The next element under germanium is tin (Sn). Tin has two allotropes, one with the diamond structure, and one with a slightly distorted bcc structure. The latter has metallic properties (metallic luster, malleability), and conductivity about 10^9 times higher than Si. Finally, lead (Pb), the element under Sn, has the ccp structure, and also is metallic. Note the trends in coordination number and conducting properties:

Element	Structure	Coord. no.	Conductivity
C	graphite, diamond	3, 4	semimetal, insulator
Si	diamond	4	semiconductor
Ge	diamond	4	semiconductor
Sn	diamond, distorted bcc	4, 8	semiconductor, metal
Pb	ccp	12	metal





The elements C, Si, and Ge obey the octet rule, and we can easily identify the electron pair bonds in their structures. Sn and Pb, on the other hand, adopt structures with high coordination numbers. They *do not have enough valence electrons* to make electron pair bonds to each neighbor (this is a common feature of metals). What happens in this case is that the valence electrons become "smeared out" or delocalized over all the atoms in the crystal. It is best to think of the bonding in metals as a crystalline arrangement of positively charged cores with a "sea" of shared valence electrons gluing the structure together. Because the electrons are not localized in any particular bond between atoms, they can move in an electric field, which is why metals conduct electricity well. Another way to describe the bonding in metals is nondirectional. That is, an atom's nearest neighbors surround it in every direction, rather than in a few particular directions (like at the corners of a tetrahedron, as we found for diamond). Nonmetals

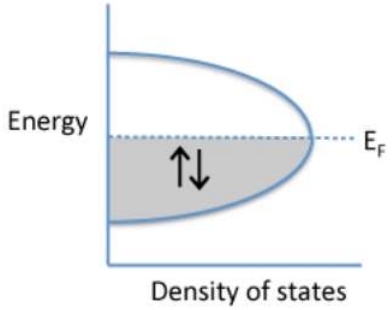
(insulators and semiconductors), on the other hand, have directional bonding. Because the bonding is non-directional and coordination numbers are high, it is relatively easy to deform the coordination sphere (i.e., break or stretch bonds) than it is in the case of a nonmetal. This is why elements like Pb are much more malleable than C, Si, or Ge.

5.3: Crystal Structures of Metals is shared under a CC BY-SA license and was authored, remixed, and/or curated by LibreTexts.

- **6.4: Crystal Structures of Metals** by Chemistry 310 is licensed CC BY-SA 4.0. Original source: https://en.wikibooks.org/wiki/Introduction_to_Inorganic_Chemistry.

5.3.1: Conduction in Metals

In metals, the valence electrons are in molecular orbitals that extend over the entire crystal lattice. Metals are almost always crystalline and the individual crystal grains are typically micron size. This means that the spatial extent of the orbitals is *very large* compared to the size of the atoms or the unit cell. The diagram shows a generic plot of electron energy vs. density of states for a metal such as Na, Cu, or Ag. In these cases, there are N orbitals for N electrons, and each orbital can accommodate two electrons. Therefore the Fermi level, which corresponds to the energy of the highest occupied MO at zero temperature, is somewhere in the middle of the band of orbitals. The energy level spacing between orbitals is very small compared to the thermal energy kT, so we can think of the orbitals as forming a continuous band.



Classically, if the electrons in this band were free to be thermally excited, we would expect them to have a specific heat of 3R per mole of electrons. However, experimentally we observe that C_p is only about 0.02 R per mole. This suggests that *only about 1%* of the electrons in the metal can be thermally excited at room temperature. However, essentially *all* of the valence electrons are free to move in the crystal and contribute to electrical conduction. To understand this apparent paradox, we need to recall that the electrons exist in *quantized energy levels.*

Because of quantization, electrons in metals have a Fermi-Dirac distribution of energies. In this distribution, most of the electrons are spin-paired, although the individual electrons in these pairs can be quite far apart since the orbitals extend over the entire crystal. A relatively small number of electrons at the top of the Fermi sea are unpaired by thermal excitation. This is the origin of the Pauli paramagnetism of metals.

How fast are electrons traveling in a typical metal? Because of the bell shape of the E vs. DOS curve, most of the electrons have $E \approx E_F$. At the midpoint energy (E_F) of the band, the MO's have one node for every two atoms. We can calculate the de Broglie wavelength as twice the distance between nodes and thus:

$\lambda = \mathbf{4a}$ at the midpoint of the band.

where **a** is the interatomic spacing. Since a typical value of **a** is about 2 Å, we obtain the **de Broglie wavelength λ ≈ 8 Å**.

Using the de Broglie relation p = h/λ, we can write:

$$\mathbf{p = \frac{h}{\lambda} = m_e v_F} \tag{5.3.1.1}$$

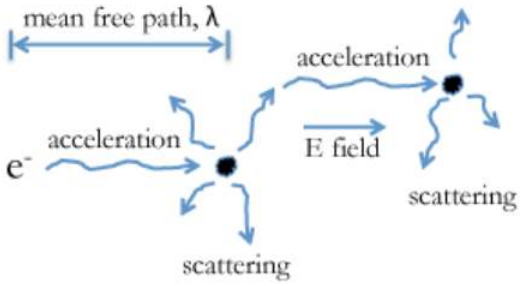
where $\mathbf{m_e}$ is the mass of the electron and $\mathbf{v_F}$ is the velocity of electrons with energy E_F.

Solving for $V_F = \frac{h}{m_e \lambda}$ we obtain $\mathbf{v_F = \frac{(6.62\times10^{-34} Js)}{(9.1\times10^{-31} kg)(8\times10^{-10} m)} = 1.0 \times 10^6 m/s}$

Experimental values of v_F are 1.07 x 10^6 and 1.39 x 10^6 m/s for Na and Ag, respectively, so our approximations are pretty good.

How fast are electrons moving in metals? Really, really fast!! **1,000,000 meters per second!** This is about 1/300 the speed of light, and about 3000 times the speed of sound in air (3 x 10^2 m/s).

However, the **drift velocity** of electrons in metals - the speed at which electrons move in applied electric field - is quite slow, on the order of 0.0001 m/s, or .01 cm/s. You can easily outrun an electron drifting in a metal, even if you have been drinking all night and have been personally reduced to a very slow crawl.



In order to understand the great disparity between the Fermi velocity and the drift velocity of electrons in metals, we need to consider a picture for the scattering of electrons, and their acceleration in an electric field, as shown at the left. If we apply a voltage across a metal (e.g., a metal wire), the electrons are subjected to an electric field **E**, which is the voltage divided by the length of the wire. This electric field exerts a force on the electron, causing it to accelerate. However, the electron is frequently scattered, mostly by phonons (lattice vibrations). Each time the electron is scattered its acceleration starts all over again. The time between scattering events is **τ** and the distance the electrons travel between scattering events is the **mean free path**, **λ**. (Note that this is NOT the same λ as the de Broglie wavelength, they just unfortunately have the same symbol!)

We can write the force on the electron as:

$$\mathbf{F = eE = m_e a = \frac{m_e v_{drift}}{\tau}} \tag{5.3.1.2}$$

In this equation, **a** is the acceleration in the electric field, $\mathbf{m_e}$ is the mass, and v_{drift} is the **drift velocity** of the electron.

Experimentally, the mean free path is typically obtained by measuring the scattering time. For an electron in Cu metal at 300 K, the scattering time τ is about 2 x 10^{-14} s. From this we can calculate the mean free path as:

$$\mathbf{\lambda = v_{avg}\tau \approx v_F\tau = (1 \times 10^6 m/s)(2 \times 10^{-14}) = 40nm} \tag{5.3.1.3}$$

The mean free path (40 nm = 400 Å) is quite long compared to the interatomic spacing (2 Å). To put it in perspective, if the interatomic spacing were scaled to the length of a football (0.3 m), the mean free path would be over half the length of the football field (60 m). Thus an electron travels a fairly long way between scattering events and scarcely notices the atomic structure of the metal in which it is traveling.

To summarize, electrons are traveling in metals at the Fermi velocity v_F, which is very, very fast (10^6 m/s), but the flux of electrons is the same in all directions. That is, they are *going nowhere fast*. In an electric field, a very small but directional *drift velocity* is superimposed on this fast random motion of valence electrons.

From F = ma, we obtain the acceleration (a) as:We can calculate the drift velocity of electrons as the acceleration in the electric field times the scattering time:

$$\mathbf{a = \frac{F}{m_e} = \frac{eE}{m_e}} \tag{5.3.1.4}$$

And thus,

$$\mathbf{v_{drift} = a\tau = \frac{eE\tau}{m_e}} \tag{5.3.1.5}$$

If we divide both sides of this equation by the magnitude of the electric field (**E**), we obtain the **mobility (μ)**:

$$\mathbf{\mu = \frac{v_{drift}}{E} = \frac{e\tau}{m_e}} \tag{5.3.1.6}$$

μ has units of velocity/field = cm/s / V/cm = cm^2/Vs

An important consequence of the calculation of v_{drift} is **Ohm's Law**, V = iR. From the equations above, we can see that the drift velocity increases linearly with the applied electric field. The drift velocity (cm/s) is proportional to the current (i, coul/s), and the electric field (E, V/cm) is proportional to the voltage (V):

$$\textbf{Current (i)} = \textbf{nev}_{\textbf{drift}} \times \textbf{area} \tag{5.3.1.7}$$

$$\textbf{Voltage (V)} = \textbf{E} \times \textbf{length} \tag{5.3.1.8}$$

Here **n** is the density of valence electrons (#/cm^3) and **e** is the charge of the electron (coul). Combining these equations with our equation for v_{drift} we obtain:

$$V = i(\frac{m_e}{ne^2\tau})\frac{(}{length}area) = iR \tag{5.3.1.9}$$

Thus, V = iR, where R is the combination of the two terms in parentheses. The first of these is the **resistivity**, ρ, and the second is a geometrical factor.

The **conductivity (σ)** of a metal, which is the inverse of ρ, is proportional to μ, which in turn is proportional to τ (and λ):

$$\sigma = \textbf{ne}\mu = \frac{\textbf{ne}^2\tau}{\textbf{m}_\textbf{e}} \tag{5.3.1.10}$$

We can use this equation to work out the conductivity of a specific metal (Cu), for which n = 8.5 x 10^{22} cm^{-3} and τ = 2 x 10^{-14} s. Putting in the numbers for m_e and e, we obtain σ = 7 x 10^5 Ω^{-1} cm^{-1} for Cu, in good agreement with the measured value (6 x 10^5 $\Omega^{-1}cm^{-1}$).

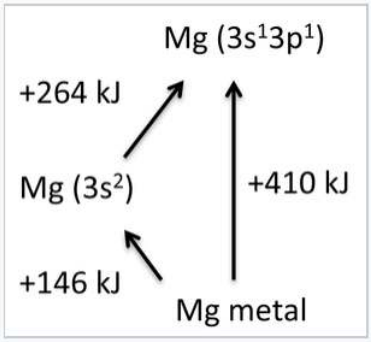
5.3.1: Conduction in Metals is shared under a CC BY-SA license and was authored, remixed, and/or curated by LibreTexts.

- **6.6: Conduction in Metals** by Chemistry 310 is licensed CC BY-SA 4.0. Original source: https://en.wikibooks.org/wiki/Introduction_to_Inorganic_Chemistry.

5.4: Atomic Orbitals and Magnetism

The MO picture we developed in Section 6.4 helps us rationalize the electrical conductivity of Na ($3s^1$), but what about Mg, which (as an atom in the gas phase) has a $3s^2$ electronic configuration? The two valence electrons are spin-paired in atomic Mg, as they are in the helium atom ($1s^2$). When the 3s orbitals of Mg combine to form a band, we would expect the band to be completely filled, since Mg has two electrons per orbital. By this reasoning, solid Mg should be an insulator. But Mg has all the properties of a metal: high electrical and thermal conductivity, metallic luster, malleability, etc. In this case the 3s and 3p bands are sufficiently broad (because of strong orbital overlap between Mg atoms) that they form a continuous band. This band, which contains a total of four orbitals (one 3s and three 3p) per atom, is only partially filled by the two valence electrons.

Another way to think about this is to consider the **hybridization** of the 3s and 3p electrons in Mg. Hybridization requires promotion from the $3s^23p^0$ ground state of an Mg atom to a $3s^13p^1$ excited state. The **promotion energy** (+264 kJ/mol) is more than offset by the **bonding energy** (-410 kJ/mol), the energy released when gaseous atoms in the excited state condense to form the metallic solid. The heat of vaporization, or the cohesive energy of a metal, is the difference between the bonding energy and the promotion energy. Experimentally, we can measure the vaporization energy (+146 kJ/mol) and the promotion energy and use them to calculate the bonding energy. From this we learn that each s or p electron is worth about 200 kJ/mol in bonding energy. The concepts of promotion energy and bonding energy are very useful in rationalizing periodic trends in the bond strengths and magnetic properties of metals, which are described below.

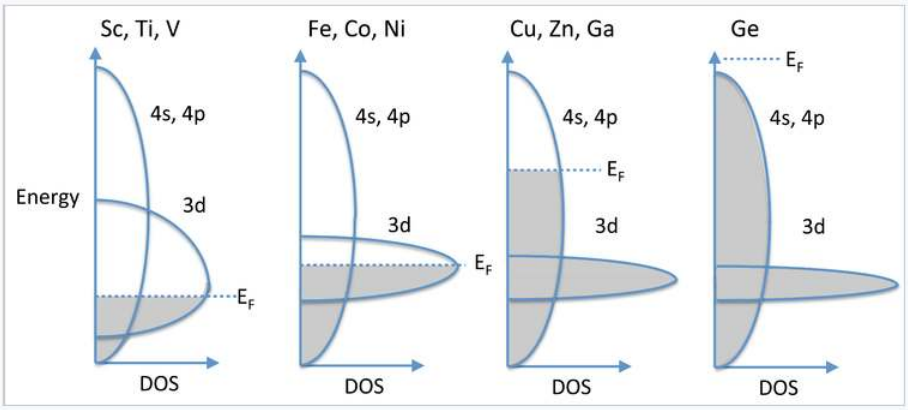


The cohesive energy of Mg metal is the difference between the bonding and promotion energies. The ground state of a gas phase Mg atom is [Ar]$3s^2$, but it can be promoted to the [Ar]$3s^13p^1$ state, which is 264 kJ/mol above the ground state. Mg uses two electrons per atom to make bonds, and the sublimation energy of the metal is 146 kJ/mol.

Filling of the 3d and 4s,4p bands

In the 3d series, we see magnetic behavior for elements and alloys between Cr and Ni. Past Ni, the elements (Cu, Zn, Ga,...) are no longer magnetic and they are very good electrical conductors, implying that their valence electrons are highly delocalized. We can understand this behavior by considering the overlap of 4s, 4p, and 3d orbitals, all of which are close in energy. The 4s and 4p have strong overlap and form a broad, continuous band. On the other hand, the 3d electrons are contracted and form a relatively narrow band. Progressing from the early 3d elements (Sc, Ti, V), we begin to fill the 3d orbitals, which are not yet so contracted that they cannot contribute to bonding. Thus, the valence electrons in Sc, Ti, and V are all spin-paired, except for a small number near the Fermi level that give rise to a weak Pauli paramagnetism. Moving across the 3d series to the magnetic elements (Fe, Co, Ni), the d-orbitals are now so contracted that their electrons unpair and we see cooperative ordering of spins (ferromagnetism and antiferromagnetism). Referring to the band diagram at the right, the 3d band is only partially filled and the Fermi level cuts through it. For Cu, Zn, and Ga, the 3d orbitals are even more contracted and the 3d band is thus more narrow, but now it is completely filled and the Fermi level is in the 4s,4p band. The strong orbital overlap in these bands results in spin pairing and a high degree of

electron delocalization. Consequently, metals in this part of the periodic table (Cu, Ag) are diamagnetic and are among the best electrical conductors at room temperature. Finally, at Ge, the 4s,4p band is completely filled and the solid is a semiconductor.



Progressive filling of the 3d and 4s,4p bands going across the periodic table from Sc to Ge.

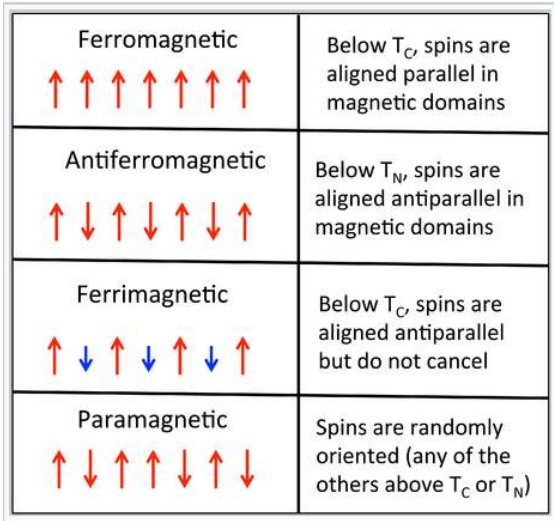
Materials are classified as diamagnetic if they contain no unpaired electrons. Diamagnetic substances are very weakly repelled from an inhomogeneous magnetic field. Molecules or ions that have unpaired spins are paramagnetic and are attracted to a magnet, i.e., they move towards the high field region of an inhomogeneous field. This attractive force results from the alignment of spins with the field, but in the case of paramagnetism each molecule acts independently. In metals, alloys, oxides, and other solid state compounds, the unpaired spins interact strongly with each other and can order spontaneously, resulting in the cooperative magnetic phenomena described below.

5.4: Atomic Orbitals and Magnetism is shared under a CC BY-SA license and was authored, remixed, and/or curated by LibreTexts.

- **6.7: Atomic Orbitals and Magnetism** by Chemistry 310 is licensed CC BY-SA 4.0. Original source: https://en.wikibooks.org/wiki/Introduction_to_Inorganic_Chemistry.

5.4.1: Ferro-, Ferri- and Antiferromagnetism

The magnetism of metals and other materials are determined by the orbital and spin motions of the unpaired electrons and the way in which unpaired electrons align with each other. All magnetic substances are **paramagnetic** at sufficiently high temperature, where the thermal energy (kT) exceeds the interaction energy between spins on neighboring atoms. Below a certain critical temperature, spins can adopt different kinds of ordered arrangements.



A pictorial description of the ordering of spins in ferromagnetism, antiferromagnetism, ferrimagnetism, and paramagnetism

Let's begin by considering an individual atom in the bcc structure of iron metal. Fe is in group VIIIb of the periodic table, so it has eight valence electrons. The atom is promoted to the $4s^1 3d^7$ state in order to make bonds. A localized picture of the d-electrons for an individual iron atom might look like this:



Since each unpaired electron has a spin moment of 1/2, the total spin angular momentum, **S**, for this atom is:

$\boldsymbol{S} = 3\frac{1}{2} = \frac{3}{2}$ (in units of h/2π)

We can think of each Fe atom in the solid as a little bar magnet with a spin-only moment **S** of 3/2. The spin moments of neigboring atoms can align in parallel (↑ ↑), antiparallel (↑ ↓), or random fashion. In bcc Fe, the tendency is to align parallel because of the positive sign of the exchange interaction. This results in **ferromagnetic** ordering, in which all the spins within a magnetic domain (typically hundreds of unit cells in width) have the same orientation, as shown in the figure at the right. Conversely, a negative exchange interaction between neighboring atoms in bcc Cr results in **antiferromagnetic** ordering. A third arrangement, **ferrimagnetic** ordering, results from an antiparallel alignment of spins on neighboring atoms when the magnetic moments of the neighbors are unequal. In this case, the spin moments do not cancel and there is a net magnetization. The ordering mechanism is like that of an antiferromagnetic solid, but the magnetic properties resemble those of a ferromagnet. Ferrimagnetic ordering is most common in metal oxides.

Magnetization and susceptibility

The **magnetic susceptibility**, **χ**, of a solid depends on the ordering of spins. Paramagnetic, ferromagnetic, antiferromagnetic, and ferrimagnetic solids all have $\chi > 0$, but the magnitude of their susceptibility varies with the kind of ordering and with temperature. We will see these kinds of magnetic ordering primarily among the **3d** and **4f** elements and their alloys and compounds. For example, Fe, Co, Ni, $Nd_2Fe_{14}B$, $SmCo_5$, and YCo_5 are all ferromagnets, Cr and MnO are antiferromagnets, and Fe_3O_4 and $CoFe_2O_4$ are ferrimagnets. Diamagnetic compounds have a weak *negative* susceptibility ($\chi < 0$).

Definitions

- H = applied magnetic field (units: Henry (H))
- B = induced magnetic field in a material (units: Tesla (T))
- M = magnetization, which represents the magnetic moments within a material in the presence of an external field H.

Magnetic susceptibility $\chi = M/H$

Usually, χ is given in *molar* units in the *cgs system*:

χ_M = molar susceptibility (units: cm^3/mol)

Typical values of χ_M:

Compound	Type of Magnetism	χ at 300K (cm^3/mol)
SiO_2	Diamagnetic	-3×10^{-4}
Pt metal	Pauli paramagnetic	$+2 \times 10^{-4}$
$Gd_2(SO_4)_3 \cdot 8H_2O$	Paramagnetic	$+5 \times 10^{-2}$
Ni-Fe alloy	Ferromagnetic	$+10^4 - 10^6$

To correlate χ with the number of unpaired electrons in a compound, we first correct for the small diamagnetic contribution of the core electrons:

$$\chi^{corr} = \chi^{obs} - \chi^{diamagnetic\ cores} \tag{5.4.1.1}$$

Susceptibility of paramagnets

For a paramagnetic substance,

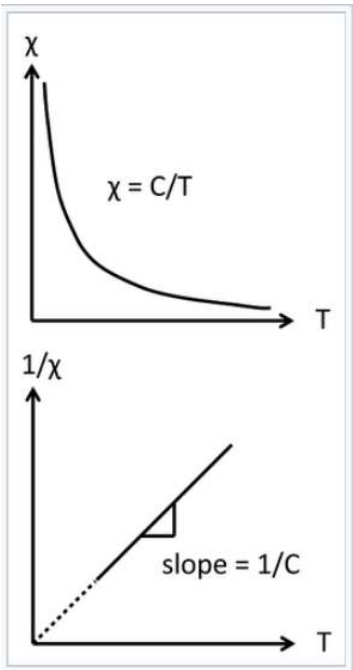
$$\chi_M^{corr} = \frac{C}{T} \tag{5.4.1.2}$$

The inverse relationship between the magnetic susceptibility and T, the absolute temperature, is called **Curie's Law**, and the proportionality constant C is the **Curie constant**:

$$C = \frac{N_A}{3k_B}\mu_{eff}^2 \tag{5.4.1.3}$$

Note that C is not a "constant" in the usual sense, because it depends on μ_{eff}, the **effective magnetic moment** of the molecule or ion, which in turn depends on its number of unpaired electrons:

$$\mu_{eff} = \sqrt{n(n+2)}\mu_B \tag{5.4.1.4}$$



Curie law behavior of a paramagnet. A plot of 1/χ vs. absolute temperature is a straight line, with a slope of 1/C and an intercept of zero.

Here μ_B is the Bohr magneton, a physical constant defined as $\mu_B = eh/4\pi m_e = 9.274 \times 10^{-21}$ erg/gauss (in cgs units).

In cgs units, we can combine physical constants,

$$\frac{N_A}{3k_B}\mu_B^2 = .125 \tag{5.4.1.5}$$

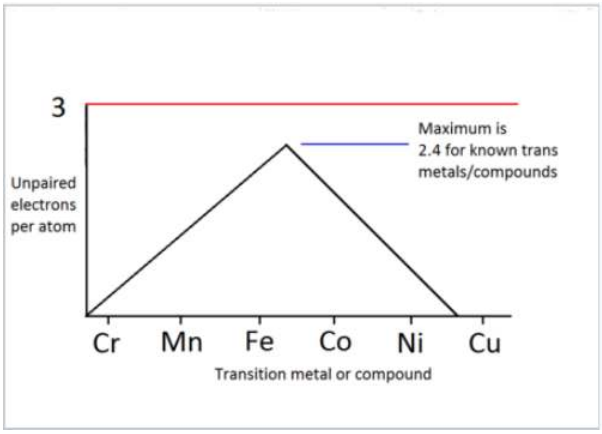
Combining these equations, we obtain

$$\chi_M^{corr} = \frac{.125}{T}\left(\frac{\mu_{eff}}{\mu_B}\right)^2 \tag{5.4.1.6}$$

These equations relate the molar susceptibility, a bulk quantity that can be measured with a magnetometer, to μ_{eff}, a quantity that can be calculated from the number of unpaired electrons, n. Two important points to note about this formula are:

- The magnetic susceptibility is inversely proportional to the absolute temperature, with a proportionality constant C (Curie's Law)

- So far we are talking only about paramagnetic substances, where there is no interaction between neighboring atoms.



Number of unpaired electrons per atom, determined from Curie constants of transition metals and their 1:1 alloys.

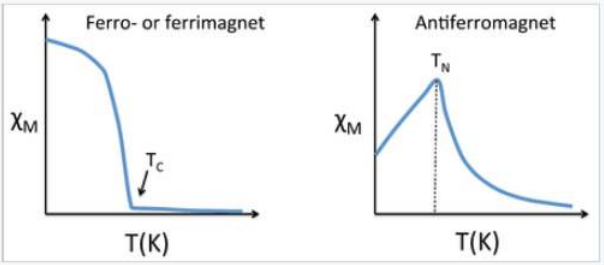
Returning to the isolated Fe atom with its three unpaired electrons, we can measure the Curie constant for iron metal (above the temperature of its transition to a paramagnetic solid) and compare it to the calculation of μ_{eff}. Since n = 3, we calculate:

$$\mu_{eff} = \sqrt{(3)(5)}\mu_B = 3.87\mu_B \tag{5.4.1.7}$$

The plot at the right shows the number of unpaired electrons per atom, calculated from measured Curie constants, for the magnetic elements and 1:1 alloys in the 3d series. The plot peaks at a value of 2.4 spins per atom, slightly lower than we calculated for an isolated iron atom. This reflects that fact that there is some pairing of d-electrons, i.e., that they do contribute somewhat to bonding in this part of the periodic table.

Susceptibility of ferro-, ferri-, and antiferromagnets

Below a certain critical temperature, the spins of a solid paramagnetic substance order and the susceptibility deviates from simple Curie-law behavior. Because the ordering depends on the short-range exchange interaction, this critical temperature varies widely. Metals and alloys in the 3d series tend to have high critical temperatures because the atoms are directly bonded to each other and the interaction is strong. For example, Fe and Co have critical temperatures (also called the Curie temperature, T_c, for ferromagnetic substances) of 1043 and 1400 K, respectively. The Curie temperature is determined by the strength of the magnetic exchange interaction and by the number of unpaired electrons per atom. The number of unpaired electrons peaks between Fe and Co as the d-band is filled, and the exchange interaction is stronger for Co than for Fe. In contrast to ferromagnetic metals and alloys, paramagnetic salts of transition metal ions typically have critical temperatures below 1K because the magnetic ions are not directly bonded to each other and thus their spins are very weakly coupled in the solid state. For example, in gadolinium sulfate, the paramagnetic Gd^{3+} ions are isolated from each other by SO_4^{2-} ions.

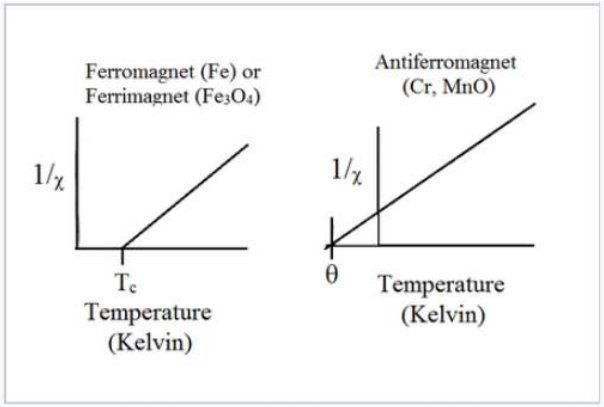


Magnetic susceptibility vs temperature (Kelvin) for ferrimagnetic, ferromagnetic, and antiferromagnetic materials

Above the critical temperature T_C, **ferromagnetic** compounds become paramagnetic and obey the **Curie-Weiss law:**

$$\chi = \frac{C}{T - T_c} \tag{5.4.1.8}$$

This is similar to the Curie law, except that the plot of $1/\chi$ vs. T is shifted to a positive intercept T_C on the temperature axis. This reflects the fact that ferromagnetic materials (in their paramagnetic state) have a greater tendency for their spins to align in a magnetic field than an ordinary paramagnet in which the spins do not interact with each other. Ferrimagnets follow the same kind of ordering behavior. Typical plots of χ vs. T and $1/\chi$ vs. T for ferro-/ferrimagnets are shown above and below.



Plots of $1/\chi$ vs. T for ferromagnets, ferrimagnets, and antiferromagnets.

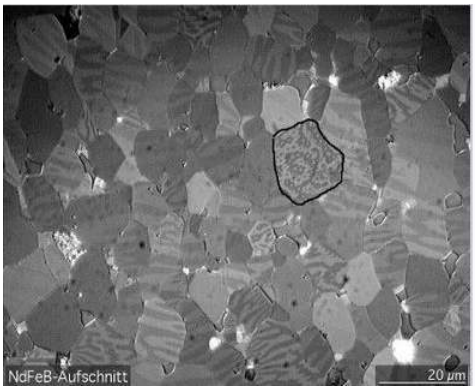
Antiferromagnetic solids are also paramagnetic above a critical temperature, which is called the Néel temperature, T_N. For antiferromagnets, χ reaches a maximum at T_N and is smaller at higher temperature (where the paramagnetic spins are further disordered by thermal energy) and at lower temperature (where the spins pair up). Typically, antiferromagnets retain some positive susceptibility even at very low temperature because of canting of their paired spins. However the maximum value of χ is much lower for an antiferromagnet than it is for a ferro- or ferrimagnet. The Curie-Weiss law is also modified for an antiferromagnet, reflecting the tendency of spins (in the paramagnetic state above T_N) to resist parallel ordering. A plot of $1/\chi$ vs. T intercepts the temperature axis at a negative temperature, $-\theta$, and the Curie-Weiss law becomes:

$$\chi = \frac{C}{T+\theta} \tag{5.4.1.9}$$

Ordering of spins below T_C

Below T_C, the spins align spontaneously in ferro- and ferrimagnets. Complex magnetization behavior is observed that depends on the history of the sample. For example, if a ferromagnetic material is cooled in the absence of an applied magnetic field, it forms a mosaic structure of magnetic domains that each have internally aligned spins. However, neighboring domains tend to align the opposite way in order to minimize the total energy of the system. This is illustrated in the figure at the left for a Nd-Fe-B magnet. The sample consists of 5-10 μm wide crystal grains that can be easily distinguished by the sharp boundaries in the image. Within

each grain are a series of lighter and darker stripes (imaged by using the optical Kerr effect) that are ferromagnetic domains with opposite orientations. Averaged over the whole sample, these domains have random orientation so the net magnetization is zero.



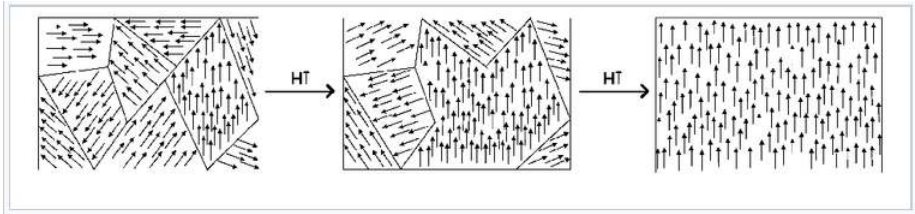
Microcrystalline grains within a piece of $Nd_2Fe_{14}B$ (the alloy used in neodymium magnets) with magnetic domains made visible with a Kerr microscope. The domains are the light and dark stripes visible within each grain.

When a sample like this one is magnetized (i.e., exposed to a strong magnetic field), the domain walls move and the favorably aligned domains grow at the expense of those with the opposite orientation. This transformation can be seen in real time in the Kerr microscope. The domain walls are typically hundreds of atoms wide, so movement of a domain wall involves a cooperative tilting of spin orientation (analogous to "the wave" in a sports stadium) and is a relatively low energy process.



The movement of domain walls in a grain of silicon steel is driven in this movie by increasing the external magnetic field in the "downward" direction, and is imaged using a Kerr microscope. White areas are domains with their magnetization directed up, dark areas - which eventually comprise the entire grain - are domains with their magnetization directed down.

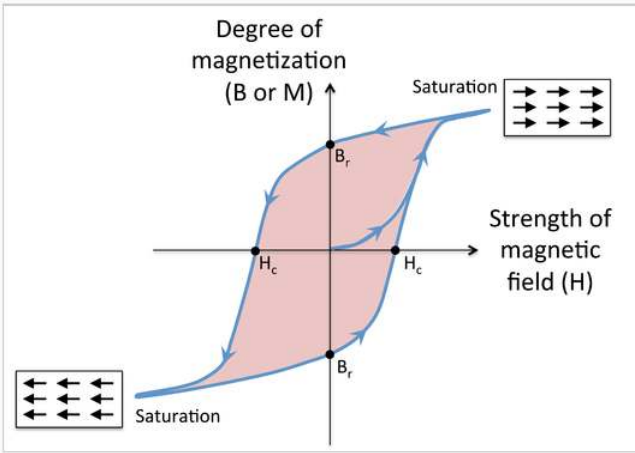
The process of magnetization moves the solid away from its lowest energy state (random domain orientation), so magnetization involves input of energy. When the external magnetic field is removed, the domain walls relax somewhat, but the solid (especially in the case of a "hard" magnet) can retain much of its magnetization. If you have ever magnetized a nail or a paper clip by using a permanent magnet, what you were doing was moving the walls of the magnetic domains inside the ferromagnet. The object thereafter retains the "memory" of its magnetization. However, annealing a permanent magnet destroys the magnetization by returning the system to its lowest energy state in which all the magnetic domains cancel each other.



Rotation of orientation and increase in size of magnetic domains in response to an externally applied magnetic field.

Magnetic hysteresis. Cycling a ferro- or ferrimagnetic material in a magnetic field results in hysteresis in the magnetization of the material, as shown in the figure at the left. At the beginning, the magnetization is zero, but it begins to rise rapidly as the magnetic field is applied. At high field, the magnetic domains are aligned and the magnetization is said to be saturated. When the field is removed, a certain **remanent magnetization** (indicated as the point $\mathbf{B_r}$ on the graph) is retained, i.e., the material is magnetized. Applying a field in the opposite direction begins to orient the magnetic domains in the other direction, and at a field $\mathbf{H_c}$ (the **coercive field**), the magnetization of the sample is reduced to zero. Eventually the material reaches saturation in the opposite direction, and when the field is removed again, it has remanent magnetization Br, but in the opposite direction. As the field continues to reverse, the magnet follows the hysteresis loop as indicated by the arrows. The area of colored region inside the loop is

proportional to the magnetic work done in each cycle. When the field cycles rapidly (for example, in the core of a transformer, or in read-write cycles of a magnetic disk) this work is turned into heat.



Magnetization of a ferro- or ferrimagnet vs. applied magnetic field H. Starting at the origin, the upward curve is the initial magnetization curve. The downward curve after saturation, along with the lower return curve, form the main loop. The intercepts Hc and Br are the coercivity and remanent magnetization.

5.4.1: Ferro-, Ferri- and Antiferromagnetism is shared under a CC BY-SA license and was authored, remixed, and/or curated by LibreTexts.

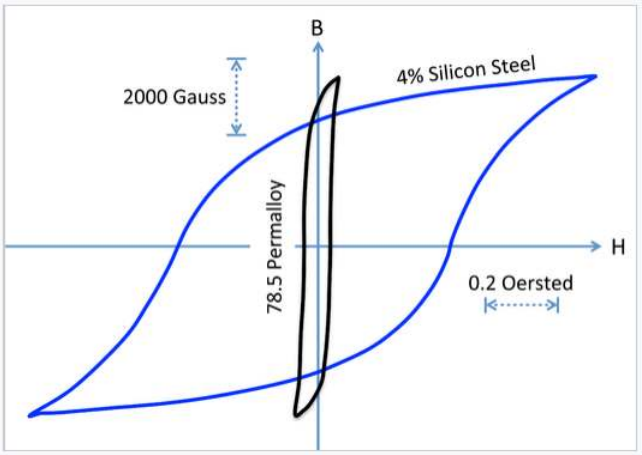
- **6.8: Ferro-, Ferri- and Antiferromagnetism** by Chemistry 310 is licensed CC BY-SA 4.0. Original source: https://en.wikibooks.org/wiki/Introduction_to_Inorganic_Chemistry.

5.4.2: Hard and Soft Magnets

Whether a ferro- or ferrimagnetic material is a **hard** or a **soft magnet** depends on the strength of the magnetic field needed to align the magnetic domains. This property is characterized by $\mathbf{H_c}$, the coercivity. Hard magnets have a high coercivity (H_c), and thus retain their magnetization in the absence of an applied field, whereas soft magnets have low values.

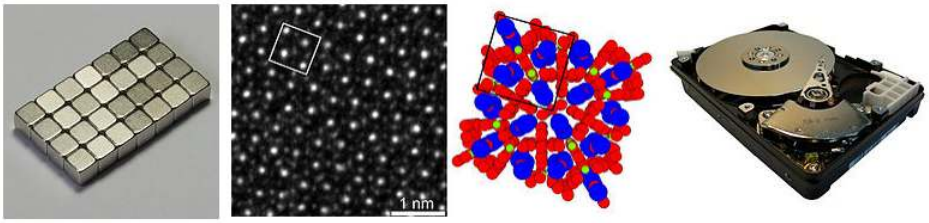
The figure at the right compares hysteresis loops for hard and soft magnets. Recall that the energy dissipated in magnetizing and demagnetizing the material is proportional to the area of the hysteresis loop. We can see that soft magnets, while they can achieve a high value of B_{sat}, dissipate relatively little energy in the loop. This makes **soft magnets** preferable for use in **transformer cores**, where the field is switched rapidly. **Permalloy**, an alloy consisting of about 20% Fe and 80% Ni, is a soft magnet that has very high magnetic permeability μ (i.e., a large maximum slope of the B vs. H curve) and a very narrow hysteresis loop.

Some materials, such as iron metal, can exist as either hard or soft magnets. Whether bcc iron is a hard or soft magnet depends on the crystal grain size. When crystal grains in iron are sub-micron size, and comparable to the size of the magnetic domains, then the magnetic domains are pinned by crystal grain boundaries. When the magnetic domains are pinned a stronger coercive magnetic field needs to be applied to cause them to re-align. When iron is annealed, the crystal grains grow and the magnetic domains become more free to align with applied magnetic fields. This decreases the coercive field and the material becomes a soft magnet.



Hysteresis loops comparing a hard magnet (iron-silicon steel) to a soft magnet (permalloy) on the same scale. H_c for permallloy is 0.05 Oe, about 10 times lower than that of the hard magnet. The remanent magnetizations of the two materials are comparable.

Hard magnets such as CrO_2, γ-Fe_2O_3, and cobalt ferrite ($CoFe_2O_4$) are used in magnetic recording media, where the high coercivity allows them to retain the magnetization state (read as a logical 0 or 1) of a magnetic bit over long periods of time. Hard magnets are also used in disk drives, refrigerator magnets, electric motors and other applications. Drive motors for hybrid and electric vehicles such as the Toyota Prius use the hard magnet $Nd_2Fe_{14}B$ (also used to make strong refrigerator magnets) and require 1 kilogram (2.2 pounds) of neodymium.[6]. A high-resolution transmission electron microscope image of $Nd_2Fe_{14}B$ is shown below and compared to the crystal structure with the unit cell marked.

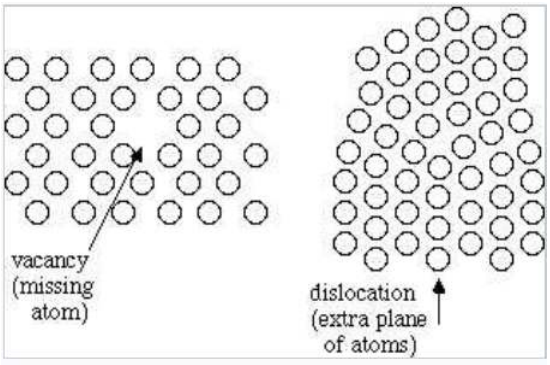


5.4.2: Hard and Soft Magnets is shared under a CC BY-SA license and was authored, remixed, and/or curated by LibreTexts.

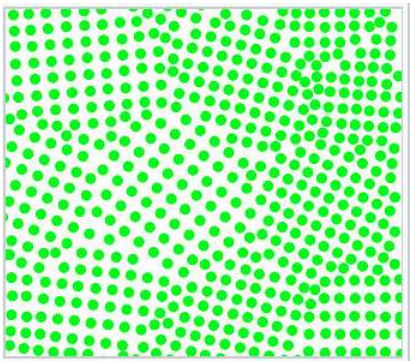
- **6.9: Hard and Soft Magnets** by Chemistry 310 is licensed CC BY-SA 4.0. Original source: https://en.wikibooks.org/wiki/Introduction_to_Inorganic_Chemistry.

5.4.3: Defects in Metallic Crystals

“Crystals are like people, it is the defects in them which tend to make them interesting!” - *Colin Humphreys.*



Metals, by virtue of their non-directional bonding, are more energetically tolerant of **defects** than are covalent network or ionic solids. Because there is no strong preference for one atomic position over another, the energy of a metallic crystal is not greatly impaired by the vacancy of a single atom or by the dislocation of a group of atoms. These kinds of "mistakes" in the packing of metal atoms within crystals are collectively called defects. The deformability of metals is the direct result of defects in the crystal structure. Defects in metals such as Al and Fe are responsible for the three orders of magnitude difference between the yield stress of annealed polycrystalline samples (i.e., normal articles of commerce) and perfect single crystals.



Grains and grain boundaries in a polycrystalline material

5.4.3: Defects in Metallic Crystals is shared under a CC BY-SA license and was authored, remixed, and/or curated by LibreTexts.

- **7.1: Defects in Metallic Crystals** by Chemistry 310 is licensed CC BY-SA 4.0. Original source: https://en.wikibooks.org/wiki/Introduction_to_Inorganic_Chemistry.

5.5: X-ray Crystallography

X-ray Crystallography is a scientific method used to determine the arrangement of atoms of a crystalline solid in three dimensional space. This technique takes advantage of the interatomic spacing of most crystalline solids by employing them as a diffraction gradient for x-ray light, which has wavelengths on the order of 1 angstrom (10^{-8} cm).

Introduction

In 1895, Wilhelm Rontgen discovered X-rays. The nature of X-rays, whether they were particles or electromagnetic radiation, was a topic of debate until 1912. If the wave idea was correct, researchers knew that the wavelength of this light would need to be on the order of 1 Angstrom (Å) (10^{-8} cm). Diffraction and measurement of such small wavelengths would require a gradient with spacing on the same order of magnitude as the light.

In 1912, Max von Laue, at the University of Munich in Germany, postulated that atoms in a crystal lattice had a regular, periodic structure with interatomic distances on the order of 1 Å. Without having any evidence to support his claim on the periodic arrangements of atoms in a lattice, he further postulated that the crystalline structure can be used to diffract X-rays, much like a gradient in an infrared spectrometer can diffract infrared light. His postulate was based on the following assumptions: the atomic lattice of a crystal is periodic, X-rays are electromagnetic radiation, and the interatomic distance of a crystal are on the same order of magnitude as X-ray light. Laue's predictions were confirmed when two researchers: Friedrich and Knipping, successfully photographed the diffraction pattern associated with the X-ray radiation of crystalline $CuSO_4$ • 5 H_2O. The science of X-ray crystallography was born.

The arrangement of the atoms needs to be in an ordered, periodic structure in order for them to diffract the X-ray beams. A series of mathematical calculations is then used to produce a diffraction pattern that is characteristic to the particular arrangement of atoms in that crystal. X-ray crystallography remains to this day the primary tool used by researchers in characterizing the structure and bonding of organometallic compounds.

Diffraction

Diffraction is a phenomena that occurs when light encounters an obstacle. The waves of light can either bend around the obstacle, or in the case of a slit, can travel through the slits. The resulting diffraction pattern will show areas of constructive interference, where two waves interact in phase, and destructive interference, where two waves interact out of phase. Calculation of the phase difference can be explained by examining Figure 1 below.

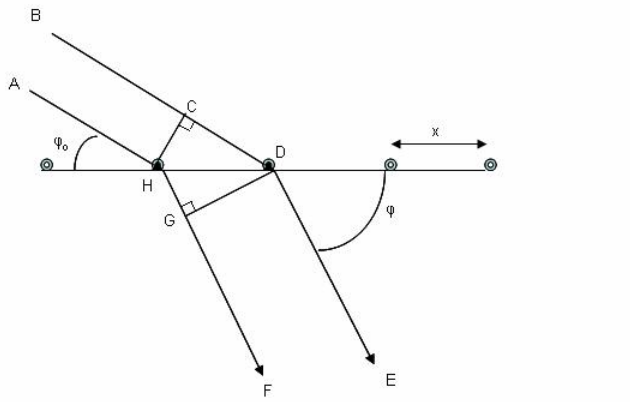


Figure 1: Scattering of light by a diffraction gratting

In the figure below, two parallel waves, BD and AH are striking a gradient at an angle θ_o. The incident wave BD travels farther than AH by a distance of CD before reaching the gradient. The scattered wave (depicted below the gradient) HF, travels father than the scattered wave DE by a distance of HG. So the total path difference between path AHGF and BCDE is CD - HG. To observe a wave of high intensity (one created through constructive interference), the difference CD - HG must equal to an integer number of

wavelengths to be observed at the angle psi, $CD - HG = n\lambda$, where λ is the wavelength of the light. Applying some basic trigonometric properties, the following two equations can be shown about the lines:

$$CD = x\cos(\theta o) \tag{5.5.1}$$

and

$$HG = x\cos(\theta) \tag{5.5.2}$$

where x is the distance between the points where the diffraction repeats. Combining the two equations,

$$x(\cos\theta_o - \cos\theta) = n\lambda \tag{5.5.3}$$

Bragg's Law

Diffraction of an X-ray beam, occurs when the light interacts with the electron cloud surrounding the atoms of the crystalline solid. Due to the periodic crystalline structure of a solid, it is possible to describe it as a series of planes with an equal interplaner distance. As an X-ray's beam hits the surface of the crystal at an angle, θ, some of the light will be diffracted at that same angle away from the solid (Figure 2). The remainder of the light will travel into the crystal and some of that light will interact with the second plane of atoms. Some of the light will be diffracted at an angle θ, and the remainder will travel deeper into the solid. This process will repeat for the many planes in the crystal. The X-ray beams travel different pathlengths before hitting the various planes of the crystal, so after diffraction, the beams will interact constructively only if the path length difference is equal to an integer number of wavelengths (just like in the normal diffraction case above). In the figure below, the difference in path lengths of the beam striking the first plane and the beam striking the second plane is equal to BG + GF. So, the two diffracted beams will constructively interfere (be in phase) only if $BG + GF = n\lambda$. Basic trigonometry will tell us that the two segments are equal to one another with the interplaner distance times the sine of the angle θ. So we get:

$$BG = BC = d\sin\theta \tag{5.5.4}$$

Thus,

$$2d\sin\theta = n\lambda \tag{5.5.5}$$

This equation is known as Bragg's Law, discovered in 1912. {C}{C}Bragg's Law relates the distance between two planes in a crystal and the angle of reflection to the X-ray wavelength. The X-rays that are diffracted off the crystal have to be in-phase in order to signal. Only certain angles that satisfy the following condition will register:

$$\sin\theta = \frac{n\lambda}{2d} \tag{5.5.6}$$

For historical reasons, the resulting diffraction spectrum is represented as intensity vs. 2θ.

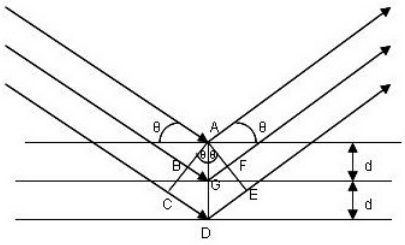


Figure 2: Incident X-ray strikes a set of planes (with an interplaner distance of d) at an angle of θ

Instrument Components

The main components of an X-ray instrument are similar to those of many optical spectroscopic instruments. These include a source, a device to select and restrict the wavelengths used for measurement, a holder for the sample, a detector, and a signal converter and readout. However, for X-ray diffraction; only a source, sample holder, and signal converter/readout are required.

The Source

X-ray tubes provides a means for generating X-ray radiation in most analytical instruments. An evacuated tube houses a tungsten filament which acts as a cathode opposite to a much larger, water cooled anode made of copper with a metal plate on it. The metal plate can be made of any of the following metals: chromium, tungsten, copper, rhodium, silver, cobalt, and iron. A high voltage is passed through the filament and high energy electrons are produced. The machine needs some way of controlling the intensity and wavelength of the resulting light. The intensity of the light can be controlled by adjusting the amount of current passing through the filament; essentially acting as a temperature control. The wavelength of the light is controlled by setting the proper accelerating voltage of the electrons. The voltage placed across the system will determine the energy of the electrons traveling towards the anode. X-rays are produced when the electrons hit the target metal. Because the energy of light is inversely proportional to wavelength ($E = hc = h(1/\lambda)$), controlling the energy, controls the wavelength of the X-ray beam.

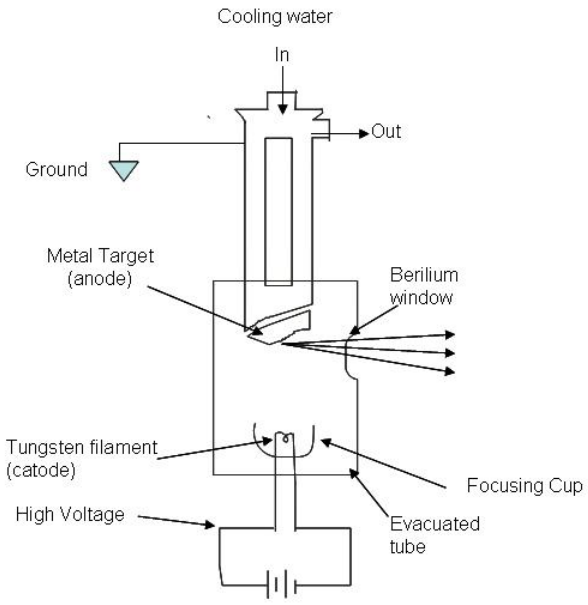


Figure 3: X-ray tube schematic

X-ray Filter

Monochromators and filters are used to produce monochromatic X-ray light. This narrow wavelength range is essential for diffraction calculations. For instance, a zirconium filter can be used to cut out unwanted wavelengths from a molybdenum metal target (see figure 4). The molybdenum target will produce X-rays with two wavelengths. A zirconium filter can be used to absorb the unwanted emission with wavelength $K\beta$, while allowing the desired wavelength, K_α to pass through.

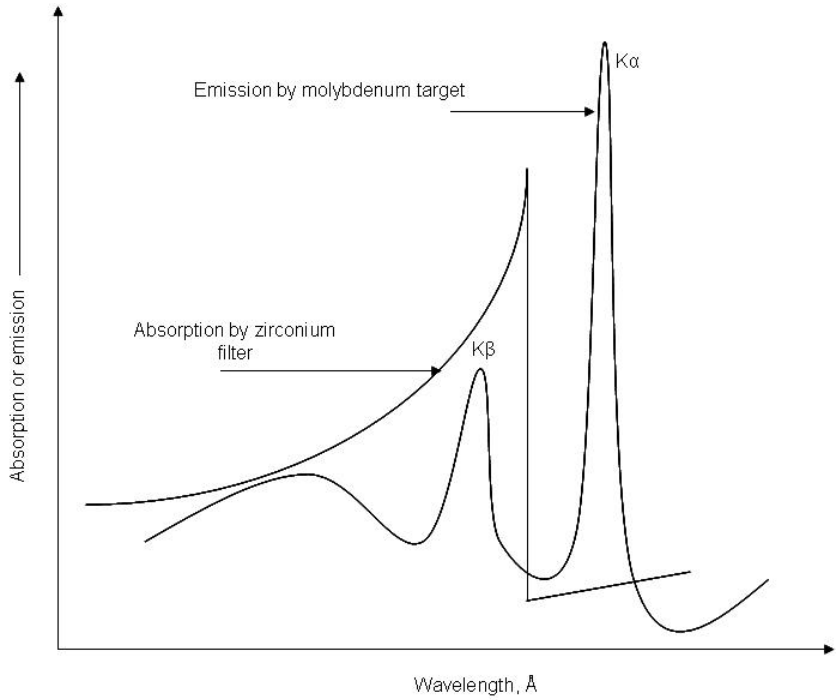


Figure 4: Monochromatic light produce by absorption of unwanted emissions.

Signal Converter

In x-ray diffraction, the detector is a transducer that counts the number of photons that collide into it. This photon counter gives a digital readout in number of photons per unit time.

References

1. Skoog, D . A.; Holler, F. J.; Stanley R. C.; Principles of Instrumental Analysis; Thomson Brooks/Cole: Belmont CA, 2007.
2. Sands, D. E.; Introduction to Crystallography; Dover Publications, Inc.; New York, 1975
3. Drenth, Jan. Principles of Protein x-ray Crystallography, 3rd edition. 2007, Springer Science + Business Media, LLC. pg. 14.
4. Rhodes, Gale. Crystallography Made Crystal Clear, 3rd edition. 2006, Elsevier Inc. pg. 33, 55 - 57.
5. Actual experimentation done of APS Kinase D63N *Penicillium Chrysogenum*.

Contributors and Attributions

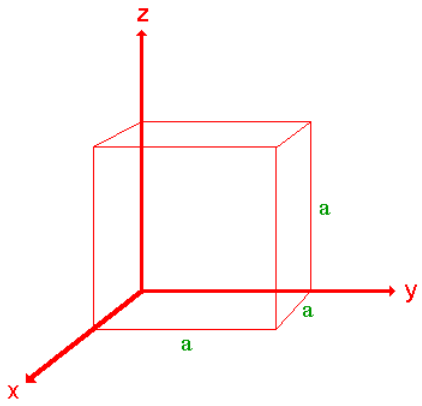
- Roman Kazantsev (UC Davis) and Michelle Towles (UC Davis)

5.5: X-ray Crystallography is shared under a not declared license and was authored, remixed, and/or curated by LibreTexts.

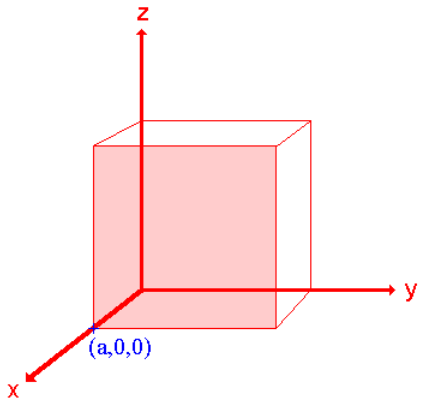
5.5.1: Miller Indices (hkl)

The orientation of a surface or a crystal plane may be defined by considering how the plane (or indeed any parallel plane) intersects the main crystallographic axes of the solid. The application of a set of rules leads to the assignment of the Miller Indices (*hkl*), which are a set of numbers which quantify the intercepts and thus may be used to uniquely identify the plane or surface.

The following treatment of the procedure used to assign the Miller Indices is a simplified one and only a **cubic** crystal system (one having a cubic unit cell with dimensions a x a x a) will be considered.



The procedure is most easily illustrated using an example so we will first consider the following surface/plane:



Step 1: *Identify the intercepts on the* x- , y- *and* z- *axes.*

In this case the intercept on the x-axis is at x = a (at the point (a,0,0)), but the surface is parallel to the y- and z-axes - strictly therefore there is no intercept on these two axes but we shall consider the intercept to be at infinity (∞) for the special case where the plane is parallel to an axis. The intercepts on the x- , y- and z-axes are thus **a , ∞ , ∞**.

Step 2: Specify the intercepts in fractional co-ordinates

Co-ordinates are converted to fractional co-ordinates by dividing by the respective cell-dimension - for example, a point (x,y,z) in a unit cell of dimensions a x b x c has fractional co-ordinates of (x/a , y/b , z/c). In the case of a cubic unit cell each co-ordinate will simply be divided by the cubic cell constant, a. This gives

Fractional Intercepts = **a/a , ∞/a, ∞/a** i.e. **1 , ∞ , ∞**.

Step 3: Take the reciprocals of the fractional intercepts

This final manipulation generates the Miller Indices which (by convention) should then be specified without being separated by any commas or other symbols. The Miller Indices are also enclosed within standard brackets (….) when one is specifying a unique

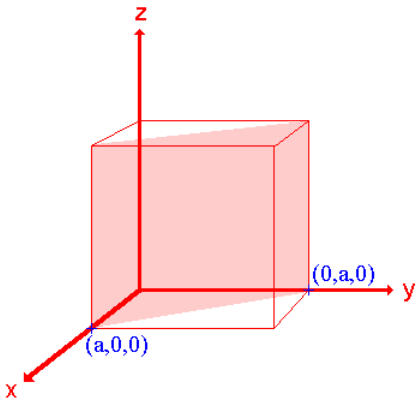
surface such as that being considered here.

The reciprocals of 1 and ∞ are 1 and 0 respectively, thus yielding Miller Indices **(100)**.

So the surface/plane illustrated is the (100) plane of the cubic crystal.

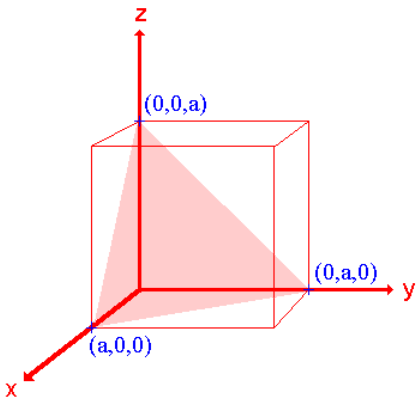
Other Examples

1. The (110) surface



Assignment
Intercepts: a , a , ∞
Fractional intercepts: 1 , 1 , ∞
Miller Indices: **(110)**

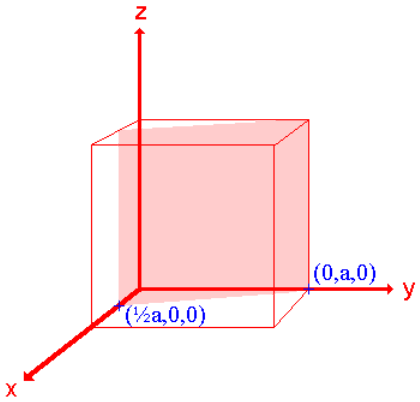
2. The (111) surface



Assignment
Intercepts: a , a , a
Fractional intercepts: 1 , 1 , 1
Miller Indices: **(111)**

The (100), (110) and (111) surfaces considered above are the so-called low index surfaces of a cubic crystal system (the "low" refers to the Miller indices being small numbers - 0 or 1 in this case). These surfaces have a particular importance but there an infinite number of other planes that may be defined using Miller index notation. We shall just look at one more …

3. The (210) surface



Assignment
Intercepts: ½ a , a , ∞
Fractional intercepts: ½ , 1 , ∞
Miller Indices: **(210)**

Further notes:

i. in some instances the Miller indices are best multiplied or divided through by a common number in order to simplify them by, for example, removing a common factor. This operation of multiplication simply generates a parallel plane which is at a different distance from the origin of the particular unit cell being considered. e.g. (200) is transformed to (100) by dividing through by 2 .
ii. if any of the intercepts are at negative values on the axes then the negative sign will carry through into the Miller indices; in such cases the negative sign is actually denoted by overstriking the relevant number. e.g. (00-1) is instead denoted by (00$\bar{1}$)
iii. in the *hcp* crystal system there are four principal axes; this leads to four Miller Indices e.g. you may see articles referring to an *hcp* (0001) surface. It is worth noting, however, that the intercepts on the first three axes are necessarily related and not completely independent; consequently the values of the first three Miller indices are also linked by a simple mathematical relationship.

Contributors and Attributions

- Roger Nix (Queen Mary, University of London)

This page titled 5.5.1: Miller Indices (hkl) is shared under a not declared license and was authored, remixed, and/or curated by Roger Nix.

5.5.2: Powder X-ray Diffraction

When an X-ray is shined on a crystal, it diffracts in a pattern characteristic of the structure. In powder X-ray diffraction, the diffraction pattern is obtained from a powder of the material, rather than an individual crystal. Powder diffraction is often easier and more convenient than single crystal diffraction since it does not require individual crystals be made. Powder X-ray diffraction (XRD) also obtains a diffraction pattern for the bulk material of a crystalline solid, rather than of a single crystal, which doesn't necessarily represent the overall material. A diffraction pattern plots intensity against the angle of the detector, 2θ.

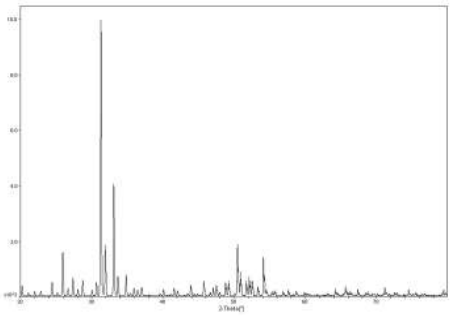
Introduction

Since most materials have unique diffraction patterns, compounds can be identified by using a database of diffraction patterns. The purity of a sample can also be determined from its diffraction pattern, as well as the composition of any impurities present. A diffraction pattern can also be used to determine and refine the lattice parameters of a crystal structure. A theoretical structure can also be refined using a method known as **Rietveld refinement**. The particle size of the powder can also be determined by using the Scherrer formula, which relates the particle size to the peak width. The Scherrer fomula is

$$t = \frac{0.9\lambda}{\sqrt{B_M^2 - B_s^2}\cos\theta} \tag{5.5.2.1}$$

with

- λ is the x-ray wavelength,
- B_M is the observed peak width,
- B_S is the peak width of a crystalline standard, and
- θ is the angle of diffraction.



To the left is an example XRD pattern for $Ba_{24}Ge_{100}$. The x axis is 2θ and the y axis is the intensity.

References

1. Dann, S.E. *Reactions and Characterization of SOLIDS.* Royal Society of Chemistry, USA (2002).
2. Skoog, D.A.; Holler, F.J.; Crouch, S.R. *Principles of Instrumental Analysis*. Sixth Edition, Thomson Brooks/Cole, USA (2007).

Contributors and Attributions

- Jason Grebenkemper

5.5.2: Powder X-ray Diffraction is shared under a not declared license and was authored, remixed, and/or curated by LibreTexts.

5.6: Prelude to Ionic and Covalent Solids - Structures

As we noted in our discussion of metal and alloy structures, there is an intimate connection between the structures and the physical properties of materials. As we "graduate" from simple metal structures based on sphere packings to more complex structures, we find that this is still true. In this section we will try to systematize the structures of inorganic solids - metal oxides, halides, sulfides, and related compounds - and develop some rules for which structures to expect based on electronegativity differences, hard-soft acid-base rules, and other periodic trends. We will see that many of these structures are related to the sphere packings that we learned about previously.



The morphology of twinned crystals of iron pyrite (FeS_2) is related to the underlying cubic symmetry of the unit cell. Like NaCl, the pyrite crystal structure can be thought of as a face-centered cubic array of anions (S_2^{2-}) with cations (Fe^{2+}) occupying all the octahedral holes.

Inorganic solids often have simple crystal structures, and some of these structures are adopted by large families of ionic or covalent compounds. Examples of the most common structures include NaCl, CsCl, NiAs, zincblende, wurtzite, fluorite, perovskite, rutile, and spinel. We will develop these structures systematically from the close packed and non-close packed lattices. Some layered structures, such as $CdCl_2$ and CdI_2, can be thought of as relatives of simple ionic lattices with some atoms "missing."

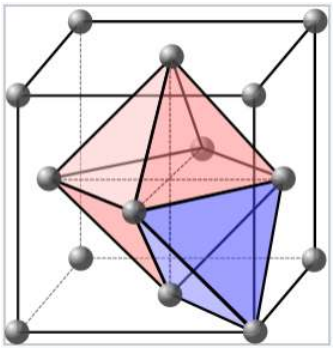
5.6: Prelude to Ionic and Covalent Solids - Structures is shared under a not declared license and was authored, remixed, and/or curated by LibreTexts.

- **8.1: Prelude to Ionic and Covalent Solids - Structures** by Chemistry 310 is licensed CC BY-SA 4.0. Original source: https://en.wikibooks.org/wiki/Introduction_to_Inorganic_Chemistry.

5.6.1: Close-packing and Interstitial Sites

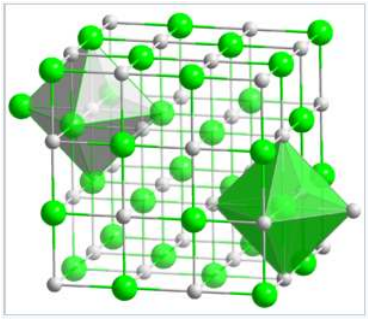
Many common inorganic crystals have structures that are related to cubic close packed (face-centered cubic) or hexagonal close packed sphere packings. These packing lattices contain two types of sites or "holes" that the interstitial atoms fill, and the coordination geometry of these sites is either **tetrahedral** or **octahedral**. An interstitial atom filling a tetrahedral hole is coordinated to four packing atoms, and an atom filling an octahedral hole is coordinated to six packing atoms. In both the hexagonal close packed and cubic close packed lattices, there is one octahedral hole and two tetrahedral holes per packing atom.

Question: Would anions or cations be better as packing atoms?
We might expect that anions, which are often larger than cations, would be better suited to the positions of packing atoms. While this is often true, there are many examples of structures in which cations are the packing atoms, and others in which the distinction is arbitrary. The NaCl structure is a good example of the latter.



One octahedral and one tetrahedral site in a face-centered cubic unit cell. Each cell contains four packing atoms (gray), four octahedral sites (pink), and eight tetrahedral sites (blue).

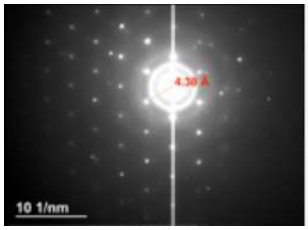
In the NaCl structure, shown on the right, the green spheres are the Cl^- ions and the gray spheres are the Na^+ ions. The octahedral holes in a face-centered cubic lattice can be found at fractional coordinates (1/2 1/2 1/2), (1/2 0 0), (0 1/2 0), and (0 0 1/2). There are four of these holes per cell, and they are filled by the chloride ions. The packing atoms (Na^+) have coordinates (0 0 0), (0 1/2 1/2), (1/2 1/2 0), and (1/2 0 1/2). Note that each of the Na^+ positions is related to a Cl^- position by a translation of (1/2 0 0). Another way of stating this is that the structure consists of **two interpenetrating fcc lattices**, which are related to each other by a translation of half the unit cell along any of the three Cartesian axes. We could have equivalently placed the Cl ions at the fcc lattice points and the Na ions in the octahedral holes by simply translating the origin of the unit cell by (1/2 0 0). Thus the distinction between packing and interstitial atoms in this case is arbitrary.



Crystal structure of NaCl. Both the Na^+ and Cl^- ions are octahedrally coordinated.

NaCl is interesting in that it is a three-dimensional checkerboard, and thus there are no NaCl "molecules" that exist in the structure. When this structure was originally solved (in 1913 by using X-ray diffraction) by W. L. Bragg, his interpretation met resistance by chemists who thought that precise integer stoichiometries were a consequence of the valency of atoms in molecules. The German chemist Pfeiffer noted in 1915 that ‘the ordinary notion of valency didn’t seem to apply’, and fourteen years later, the influential chemist Armstrong still found Bragg’s proposed structure of sodium chloride ‘more than repugnant to the common sense, not

chemical cricket'! Nevertheless, Bragg and his father, W. H. Bragg, persevered and used the then-new technique of X-ray diffraction to determine the structures of a number of other compounds, including diamond, zincblende, calcium fluoride, and other alkali halides. These experiments gave chemists their first real look at the atomic structure of solids, and laid the groundwork for X-ray diffraction experiments that later elucidated the structures of DNA, proteins, and many other compounds. For their work on X-ray diffraction the Braggs received the Nobel prize in Physics in 1915.

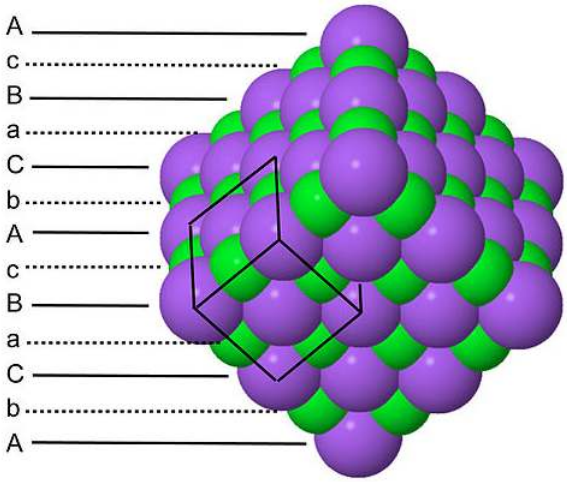


The lattice dimensions and positions of atoms in crystals such as NaCl are inferred from diffraction patterns.

Since each type of atom in the NaCl structure forms a face-centered cubic lattice, there are four Na and four Cl atoms per NaCl unit cell. It is because of this ratio that NaCl has a 1:1 stoichiometry. The shaded green and gray bipyramidal structures in the NaCl lattice show that the Na^+ ions are coordinated to six Cl^- ions, and vice versa. The NaCl structure can be alternatively drawn as a stacking of close-packed layer planes, AcBaCbAcBa... along the body diagonal of the unit cell. Here the uppercase letters represent the packing atoms, and the lower case letters are the interstitial atoms. This layered packing is illustrated below:

NaCl structure

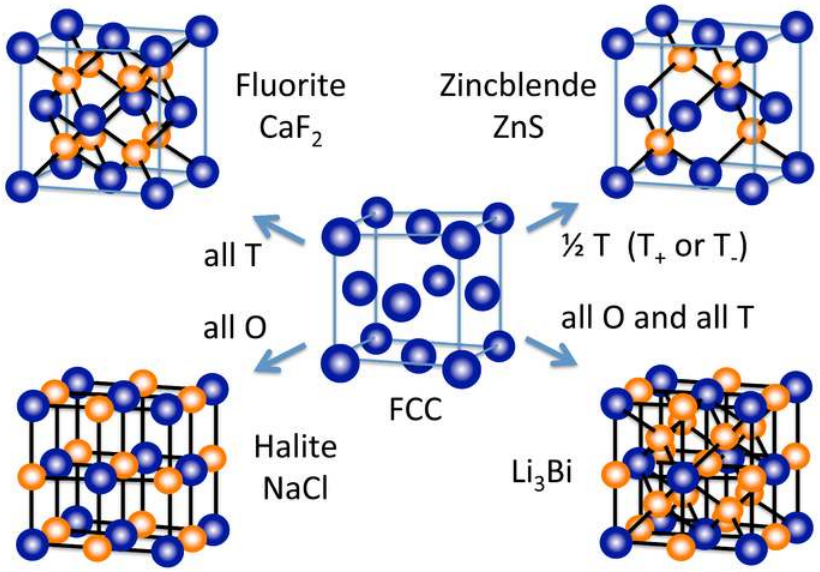
- ---------- A
- - - -c- - - -
- ---------- B
- - - -a- - - -
- ---------- C
- - - -b- - - -
- ---------- A
- - - -c- - - -
- ---------- B
- - - -a- - - -
- ---------- C
- - - -b- - - -
- ---------- A



Note that both the packing atoms and interstitials are stacked in the sequence A-B-C-A-B-C..., in keeping with the fact that each forms a cubic close-packed lattice.

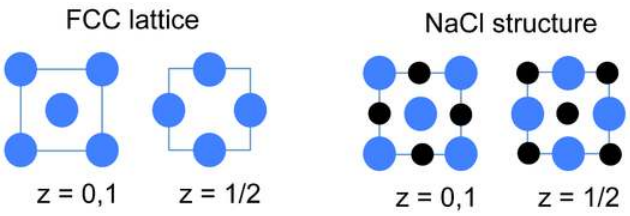
The NaCl structure is fairly common among ionic compounds:

- Alkali Halides (except CsCl, CsBr, and CsI)
- Transition Metal Monoxides (TiO, VO,..., NiO)
- Alkali Earth Oxides and Sulfides (MgO, CaO, BaS... except BeO and MgTe)
- Carbides and Nitrides (TiC, TiN, ZrC, NbC) -these are very stable refractory, interstitial alloys (metallic)



A number of other inorganic crystal structures are formed (at least conceptually) by filling octahedral and/or tetrahedral holes in close-packed lattices. The figure at the right shows some of the most common structures (fluorite, halite, zincblende) as well as a rather rare one (Li_3Bi) that derive from the fcc lattice. From the hcp lattice, we can make the NiAs and wurzite structures, which are the hexagonal relatives of NaCl and zincblende, respectively.

An alternative and very convenient way to represent inorganic crystal structures (especially complex structures such as Li_3Bi) is to draw the unit cell in slices along one of the unit cell axes. This kind of representation is shown at the left for the fcc lattice and the NaCl structure. Since all atoms in these structures have z-coordinates of either 0 or 1/2, only those sections need to be drawn in order to describe the contents of the unit cell. It is a useful exercise to draw some of the fcc compound structures (above) in sections.



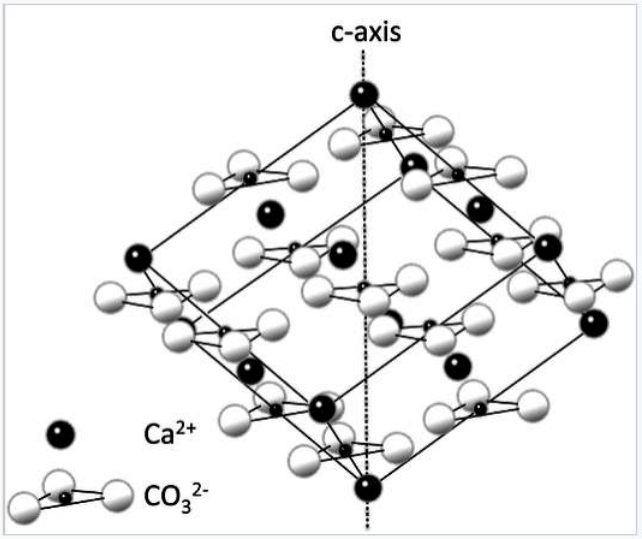
5.6.1: Close-packing and Interstitial Sites is shared under a CC BY-SA license and was authored, remixed, and/or curated by LibreTexts.

- **8.2: Close-packing and Interstitial Sites** by Chemistry 310 is licensed CC BY-SA 4.0. Original source: https://en.wikibooks.org/wiki/Introduction_to_Inorganic_Chemistry.

5.6.2: Structures Related to NaCl and NiAs

There are a number of compounds that have structures similar to that of NaCl, but have a lower symmetry (usually imposed by the geometry of the anion) than NaCl itself. These compounds include:

- FeS_2 (pyrite, "fools gold"): S_2^{2-} (disulfide) and Fe^{2+}
- CaC_2 (a salt-like carbide): Ca^{2+} and linear C_2^{2-} anions
- $CaCO_3$ (calcite, limestone, marble): Ca^{2+} and triangular CO_3^{2-}.



The rhombohedral unit cell of the calcite crystal structure. The hexagonal c-axis is shown.

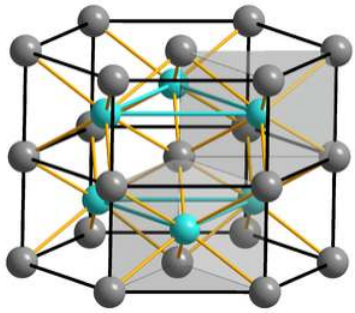
The **calcite** ($CaCO_3$) crystal structure is shown above. Triangular CO_3^{2-} ions fill octahedral holes between the Ca^{2+} ions (black spheres) in a distorted NaCl lattice. As in NaCl, each ion is coordinated by six of the other kind. From this image we can see why the $CaCO_3$ structure has a lower symmetry than that of NaCl. The fourfold rotation symmetry of the NaCl unit cell is lost when the spherical Cl^- ions are replaced by triangular CO_3^{2-} ions. Because of this symmetry lowering, transparent crystals calcite are birefringent, as illustrated below.



Calcite crystals are birefringent, meaning that their refractive indices are different along the two principal crystal directions. This gives rise to the phenomenon of double refraction.

NiAs structure

The NaCl structure can be described a face-centered cubic lattice with all of the octahedral holes filled. What if we start with a hexagonal-close packed lattice rather than a face-centered cubic lattice?



Nickel arsenide crystal structure. The Ni_6As trigonal prisms are shaded gray. One octahedron of six As atoms surrounding a Ni atom is shown in the center of the figure.

This is the structure adopted by **NiAs** and many other transition metal sulfides, phosphides, and arsenides. The cations are shown in gray while the anions are light blue in the figure at the right. The cations are in octahedral coordination, so each cation is coordinated to six anions. The anions are also coordinated to six cations, but they occupy trigonal prismatic sites. In terms of layer stacking, the NiAs structure is AcBcAcBc..., where the A and B sites (the hcp lattice) are occupied by the As atoms, and the c sites, which are eclipsed along the layer stacking axis, are occupied by Ni. Unlike the NaCl structure, where the anion and cation sites are interchangeable, NiAs has unique anion and cation sites. The layer stacking sequence for NiAs is shown below:

- ---------- A
- - - -c- - - -
- ---------- B
- - - -c- - - -
- ---------- A
- - - -c- - - -
- ---------- B
- - - -c- - - -

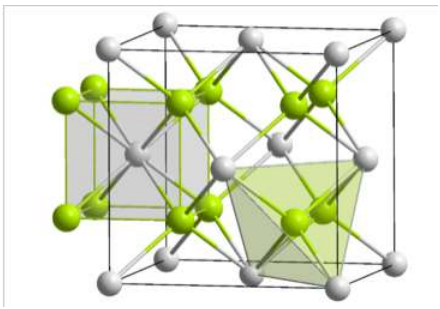
The NiAs structure cannot be adopted by ionic compounds because of the eclipsing cations, because the cation-cation repulsions would be internally destabilizing for an ionic compound. This structure is mainly adopted by covalent and polar covalent MX compounds, typically with "soft" X anions (S, Se, P, As,....) and low-valent transition metal cations. For example, some compounds with the NiAs structure are: MS, MSe, MTe (M=Ti, V, Fe, Co, Ni). Often these are nonstoichiometric or complex stoichiometries with ordered vacancies (Cr_7S_8, Fe_7S_8).

5.6.2: Structures Related to NaCl and NiAs is shared under a CC BY-SA license and was authored, remixed, and/or curated by LibreTexts.

- **8.3: Structures Related to NaCl and NiAs** by Chemistry 310 is licensed CC BY-SA 4.0. Original source: https://en.wikibooks.org/wiki/Introduction_to_Inorganic_Chemistry.

5.6.3: Tetrahedral Structures

In ccp and hcp lattices, there are two tetrahedral holes per packing atom. A stoichiometry of either M_2X or MX_2 gives a structure that fills all tetrahedral sites, while an MX structure fills only half of the sites. An example of an MX_2 structure is **fluorite**, CaF_2, whose structure is shown in the figure at the left. The packing atom in fluorite is Ca^{2+} and the structure is composed of three interpenetrating fcc lattices. It should be noted that the Ca^{2+} ion (gray spheres) as a packing atom defies our "rule" that anions are larger than cations and therefore must be the packing atoms. The fluorite structure is common for ionic MX_2 (MgF_2, ZrO_2, etc.) and M_2X compounds (Li_2O). In contrast, the hcp relative of the fluorite structure is quite rare because of unfavorable close contacts between like-charged ions.



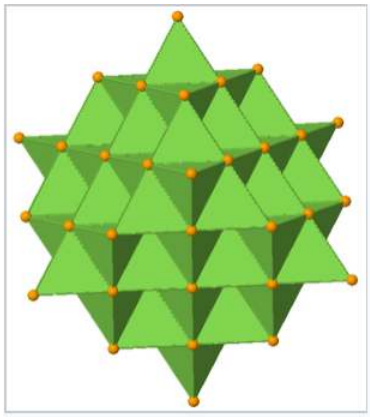
The fluorite (CaF_2) crystal structure showing the coordination environments of the Ca and F atoms

In terms of geometry, Ca^{2+} is in cubic coordination with eight F^- neighbors, and the fluoride ions are tetrahedrally coordinated by four Ca^{2+} ions. The 8:4 coordination geometry is consistent with the 1:2 Ca:F stoichiometry; in all crystal structures the ratio of the coordination numbers is the inverse of the stoichiometric ratio. The three interpenetrating fcc lattices have Ca at 0,0,0 , 1/2,1/2,0 , etc....F at 1/4,1/4,1/4 , 3/4,3/4,1/4 , etc... and F at 3/4,3/4,3/4 , 1/4,1/4/3/4 , etc.

Looking more closely at the tetrahedral sites in fluorite, we see that they fall into two distinct groups: T_+ and T_-. If a tetrahedron is oriented with a vertex pointing upwards along the stacking axis, the site is T_+. Likewise, a tetrahedron with a vertex oriented downward is T_-. The alternation of T_+ and T_- sites allows for efficient packing of ions in the structure. The layer stacking sequence in this structure (including fluoride ions in the T_+ and T_- sites) is:

- ---------- A
- - - -b- - - T_+
- - - -a- - - T_-
- ---------- B
- - - -c- - - T_+
- - - -b- - - T_-
- ---------- C
- - - -a- - - T_+
- - - -c- - - T_-
- ---------- A
- - - -b- - - T_+

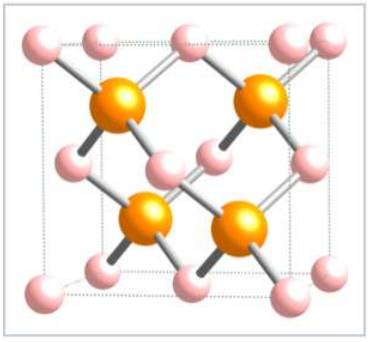
- - - -a- - - T_-



Polyhedral view of the fluorite crystal structure, showing T_+ and T_- Ca_4F tetrahedra. The Ca^{2+} ions are stacked ABCABC... along the body diagonal of the unit cell, which is the vertical direction in this image.

Tetrahedrally bonded compounds with a 1:1 stoichiometry (MX compounds) have only **half** of the tetrahedral sites (either the T_+ or T_- sites) filled. In this case, both the M and the X atoms are tetrahedrally coordinated. The **zincblende** and **wurtzite** structures of ZnS are 1:1 tetrahedral structures based on fcc and hcp lattices, respectively. Both structures are favored by p-block compounds that follow the octet rule, and these compounds are usually semiconductors or insulators. The zincblende structure, shown below, can be thought of as two interpenetrating fcc lattices, one of anions and one of cations, offset from each other by a translation of 1/4 along the body diagonal of the unit cell. Examples of compounds with the zincblende structure include CuCl, CuI, ZnSe, HgS, BeS, CdTe, AlP, GaP, SnSb, CSi, and diamond. Additionally, the compound $CuInSe_2$ is zincblende in an ordered, doubled unit cell (the chalcopyrite structure). The solid solution compounds $CuIn_{1-x}Ga_xSe_2$ with this structure are among the most widely studied materials for use in efficient thin film photovoltaic cells. Using ZnS as a representative of zincblende, the coordination of both Zn and S atoms is tetrahedral. The layer sequence, which is AbBcCaAbBcC..., results in non-planar, six-membered ZnS rings which allows for a relatively long distance between opposite atoms in the ring. The sequence of close-packed layers in zincblende, filling only the T_+ sites and leaving the T_- sites empty, is shown below:

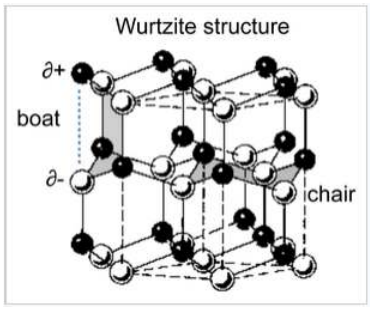
- ---------- A
- - - -b- - - T_+
- - - - - - T_-
- ---------- B
- - - -c- - - T_+
- - - - - - T_-
- ---------- C
- - - -a- - - T_+
- - - - - - T_-



The zincblende unit cell

The wurtzite structure is a close relative of zinc blende, based on filling half the tetrahedral holes in the hcp lattice. Like zincblende, wurtzite contains planes of fused six-membered rings in the chair conformation. Unlike zincblende, however, the rings joining these planes contain non-planar, six-membered rings. The structure aligns the anions so that they are directly above the cations in the structure, a less favorable situation sterically but a more favorable one in terms of electrostatics. As a result, the wurtzite structure tends to favor more polar or ionic compounds (e.g., ZnO, $NH_4^+F^-$) than the zincblende structure. As with zincblende, both ions are in tetrahedral (4:4) coordination and there are typically eight valence electrons in the MX compound. Examples of compounds with this structure include: BeO, ZnO, MnS, CdSe, MgTe, AlN, and NH_4F. The layered structure of wurtzite is AbBaAbB and the layer sequence with T_+ sites filled is illustrated below:

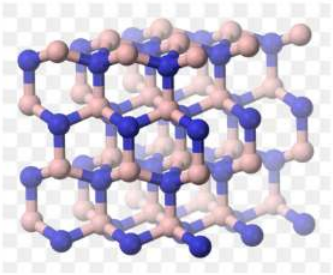
- ---------- A
- - - -b- - - T_+
- - - - - - - T_-
- ---------- B
- - - -a- - - T_+
- - - - - - - T_-
- ---------- A
- - - -b- - - T_+
- - - - - - - T_-
- ---------- B



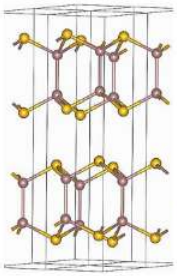
The chair and boat conformations of six-membered ZnS rings in the wurtzite structure.

An interesting consequence of the layer stacking in the wurtzite structure is that the crystals are polar. When cleaved along the c-axis (the stacking axis), crystals of ZnO, ZnS, and GaN have one negatively charged face and an opposite positively charged face. An applied electric field interacts with the crystal dipole, resulting in compression or elongation of the lattice along this direction. For this reason crystals of compounds in the wurtzite structure are typically piezoelectric (increasing the pressure on the material generates a voltage in the material).

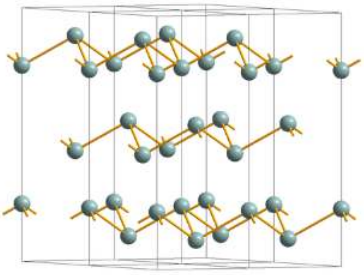
Some compounds are diamorphic and can have either the zincblende or wurtzite structure. Examples of these compounds that have intermediate polarities include CdS and ZnS. SiO_2 exists in polymorphs (crystobalite and tridymite) that resemble zincblende and wurtzite with O atoms midway between each of the Si atoms. The zincblende and wurtzite structures have efficient packing arrangements for tetrahedrally bonded networks and are commonly found in compounds that have tetrahedral bonding. Water, for example, has a tetrahedral hydrogen bonding network and is wurtzite-type. The undistorted wurtzite and zinc blende structures are typically found for AX compounds with eight valence electrons, which follow the octet rule. AX compounds with nine or ten electrons such as GaSe and GaAs crystallize in distorted variants of the wurtzite structure. In GaSe, the extra electrons form lone pairs and this creates layers in the structure, as can be seen in the figure below. To the right of GaSe, the structures of As, Sb, and SbAs show an ever further breakdown of the structure into layers as more valence electrons are added.



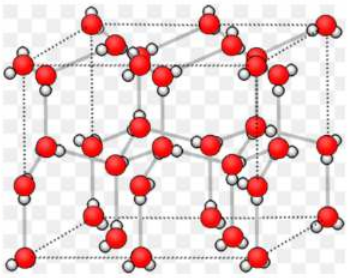
Wurtzite crystal structure



GaSe crystal structure



Crystal structure of Sb, SbAs, and gray As



Crystal structure of hexagonal ice

Hexagonal ice is the most stable polymorph of ice, which is obtained upon freezing at 1 atmosphere pressure. This polymorph (ice-I) has a hcp wurtzite-type structure. Looking at the structure shown at the right, we see that there are irregular arrangements of the O-H---O bonds. In the structure, hydrogen bonding enforces the tetrahedral coordination of each water molecule, resulting in a relatively open structure that is less dense than liquid water. For this reason, ice floats in water.

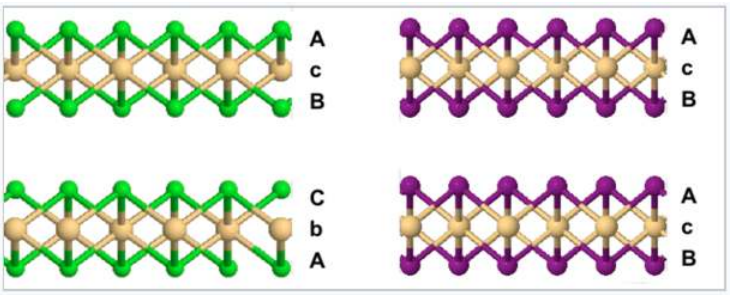
5.6.3: Tetrahedral Structures is shared under a CC BY-SA license and was authored, remixed, and/or curated by LibreTexts.

- **8.4: Tetrahedral Structures** by Chemistry 310 is licensed CC BY-SA 4.0. Original source: https://en.wikibooks.org/wiki/Introduction_to_Inorganic_Chemistry.

5.6.4: Layered Structures and Intercalation Reactions

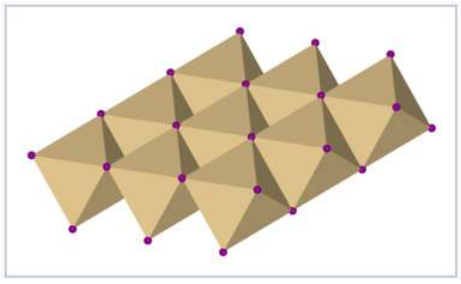
Layered structures are characterized by strong (and typically covalent) bonding between atoms in two dimensions and weaker bonding in the third. A broad range of compounds including metal halides, oxides, sulfides, selenides, borides, nitrides, carbides, and allotropes of some pure elements (B, C, P, As) exist in layered forms. Structurally, the simplest of these structures (for example binary metal halides and sulfides) can be described as having some fraction of the octahedral and/or tetrahedral sites are filled in the fcc and hcp lattices. For example, the $CdCl_2$ structure is formed by filling all the octahedral sites in alternate layers of the fcc lattice, and the CdI_2 structure is the relative of this structure in the hcp lattice.

In the **$CdCl_2$ structure**, the stacking sequence of anion layers is ABCABC...
In the **CdI_2 structure**, the anion stacking sequence is ABAB..., and all the cations are eclipsed along the stacking axis.



Comparison of the $CdCl_2$ (left) and CdI_2 (right) crystal structures

These are examples of **6-3 structures**, because the cations are coordinated by an octahedron of six anions, and the anions are coordinated by three cations to make a trigonal pyramid (like NH_3). Another way to describe these structures is to say that the MX_6 octahedra each share six edges in the MX_2 sheets.



Polyhedral drawing of one layer of the $CdCl_2$ or CdI_2 structure showing edge-sharing MX_6 octahedra

Because these structures place the packing atoms (the anions) in direct van der Waals contact, they are most stable for relatively **covalent** compounds. Otherwise, the electrostatic repulsion between contacting anions would destabilize the structure energetically. More ionic MX_2 compounds tend to adopt the fluorite (CaF_2) or rutile (TiO_2) structures, which are not layered.

Despite the fact that these two structure types are the same at the level of nearest and next-nearest neighbor ions, the CdI_2 structure is much more common than the $CdCl_2$ structure.

$CdCl_2$ structure:

MCl_2 (M = Mg, Mn, Fe, Co, Ni, Zn, Cd)

$NiBr_2$, NiI_2, $ZnBr_2$, ZnI_2

CdI_2 structure:

MCl_2 (M = Ti, V)

MBr_2 (M = Mg, Fe, Co, Cd)

MI_2 (M = Mg, Ca, Ti, V, Mn, Fe, Co, Cd, Ge, Pb, Th)

$M(OH)_2$ (M = Mg, Ca, Mn, Fe, Co, Ni, Cd)

MS_2 (M = Ti, Zr, Sn, Ta, Pt)

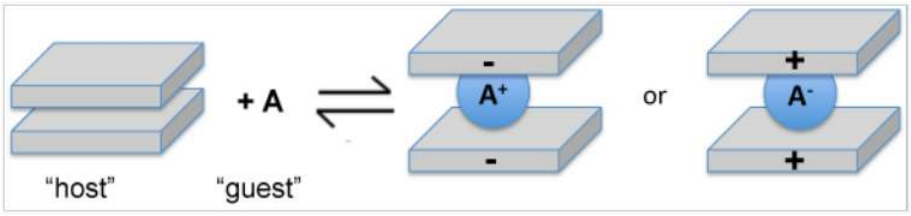
MSe_2 (M = Ti, Zr, Sn, V, Pt)

MTe_2 (M = Ti, Co, Ni, Rh, Pd, Pt)

Physically, layered compounds are **soft** and **slippery**, because the layer planes slide past each other easily. For example, graphite, MoS_2, and talc (a silicate) are layered compounds that are used widely as **lubricants** and lubricant additives.

An important reaction of layered compounds is **intercalation**. In intercalation reactions, guest molecules and ions enter the galleries that separate the sheets, usually with expansion of the lattice along the stacking axis. This reaction is typically reversible if it does not perturb the bonding within the sheets. Often the **driving force for intercalation is a redox reaction**, i.e., electron transfer between the host and guest. For example, lithium metal reacts with TiS_2, MoS_2, and graphite to produce $LiTiS_2$, Li_xMoS_2 ($x < 1$), and LiC_6. In these compounds, lithium is ionized to Li^+ and the sheets are negatively charged. Oxidizing agents such as Br_2, $FeCl_3$, and AsF_5 also react with graphite. In the resulting intercalation compounds, the sheets are positively charged and the intercalated species are anionic.

Intercalation reactions are especially important for electrochemical energy storage in **secondary batteries**, such as **lithium ion** batteries, **nickel-metal hydride** batteries, and **nickel-cadmium** batteries. The reversible nature of the intercalation reaction allows the electrodes to be charged and discharged up to several thousand times without losing their mechanical integrity. In lithium ion batteries, the negative electrode material is typically graphite, which is intercalated by lithium to make LiC_6. Several different oxides and phosphates containing redox active transition metal ions (Mn, Fe, Co, Ni) are used as the positive electrode materials.



Oxidative or reductive intercalation involves the placement of anions or cations between sheets.

Lithium ion batteries based on CoO_2 were first described in 1980[1] by John B. Goodenough's research group at Oxford. In batteries based on CoO_2, which has the CdI_2 structure, the positive electrode half-reaction is:

$$\mathrm{LiCoO_2 \leftrightharpoons Li_{1-x}CoO_2 + x\,Li^+ + xe^-} \tag{5.6.4.1}$$

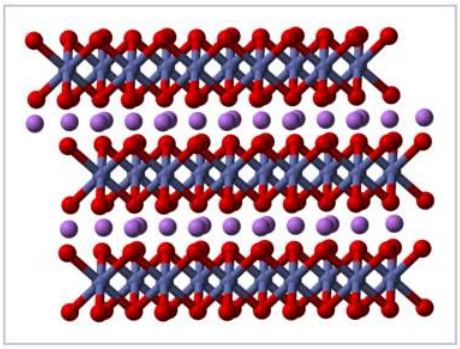
The negative electrode half reaction is:

$$\mathrm{x\,Li^+ + xe^- + x\,C_6 \leftrightharpoons x\,LiC_6} \tag{5.6.4.2}$$

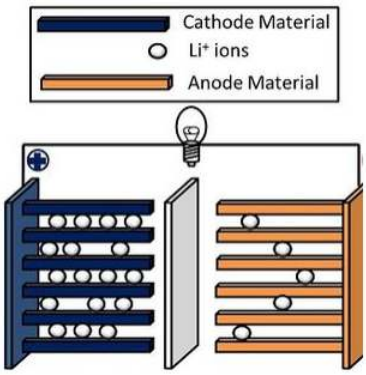
The battery is fully charged when the positive electrode is in the CoO_2 form and the negative electrode is in the LiC_6 form. Discharge involves the motion of Li^+ ions through the electrolyte, forming Li_xCoO_2 and graphite at the two electrodes.



Blue plaque erected by the Royal Society of Chemistry commemorating the development of cathode materials for the lithium-ion battery



Crystal structure of $LiCoO_2$[2]



The lithium ion battery is a "rocking chair" battery, so named because charging and discharging involve moving Li^+ ions from one side to the other. CoO_2 is one example of a positive electrode material that has been used in lithium ion batteries. It has a high energy density, but batteries based on CoO_2 have poor thermal stability. Safer materials include lithium iron phosphate ($LiFePO_4$), and $LiMO_2$ (M = a mixture of Co, Mn, and Ni). These batteries are used widely in laptop computers, portable electronics, cellular telephones, cordless tools, and electric and hybrid vehicles.

A similar intercalation reaction occurs in nickel-cadmium batteries and nickel-metal hydride batteries, except in this case the reaction involves the movement of protons in and out of the $Ni(OH)_2$ lattice, which has the CdI_2 structure:

$$NiO(OH) + H_2O + e^- \longrightarrow Ni(OH)_2 + OH^- \qquad (5.6.4.3)$$

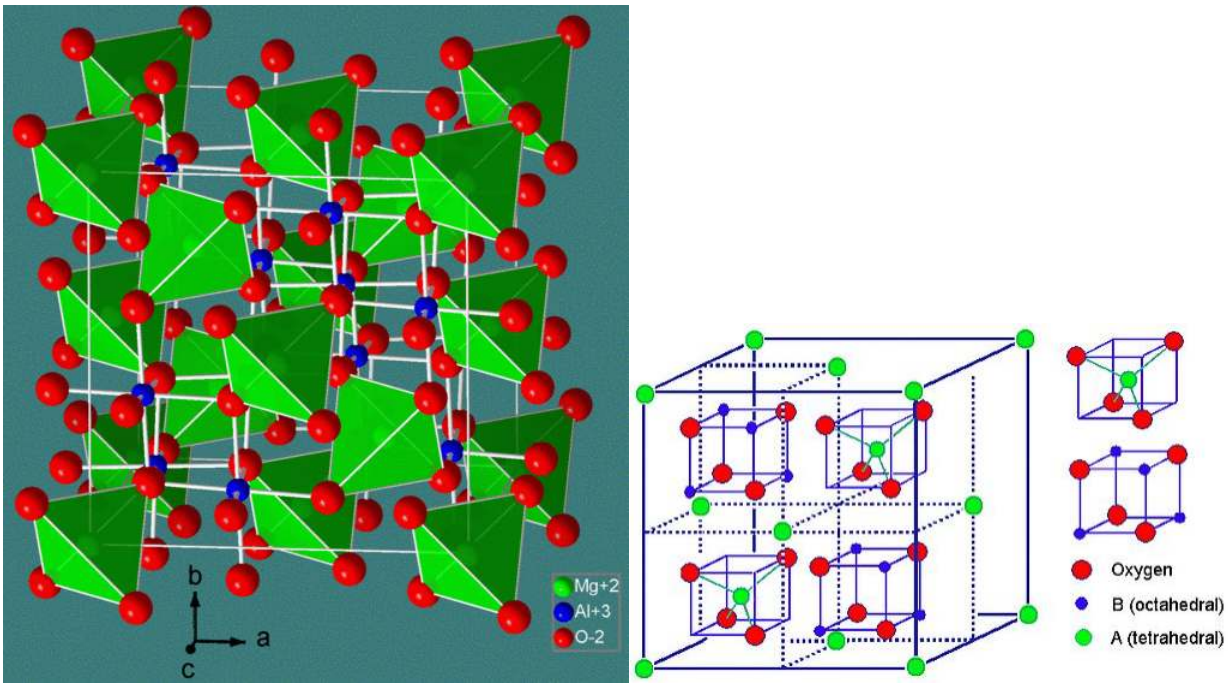
There are many layered compounds that cannot be intercalated by redox reactions, typically because some other stable product is formed. For example, the reaction of layered CdI_2 with Li produces LiI (NaCl structure) and Cd metal.

5.6.4: Layered Structures and Intercalation Reactions is shared under a CC BY-SA license and was authored, remixed, and/or curated by LibreTexts.

- **8.5: Layered Structures and Intercalation Reactions** by Chemistry 310 is licensed CC BY-SA 4.0. Original source: https://en.wikibooks.org/wiki/Introduction_to_Inorganic_Chemistry.

5.6.5: Spinel, Perovskite, and Rutile Structures

There are three more structures, which are derived from close-packed lattices, that are particularly important because of the material properties of their compounds. These are the **spinel** structure, on which ferrites and other magnetic oxides are based, the **perovskite** structure, which is adopted by ferroelectric and superconducting oxides, and the **rutile** structure, which is a common binary 6:3 structure adopted by oxides and fluorides.



The **spinel structure** is formulated MM'_2X_4, where M and M' are tetrahedrally and octahedrally coordinated cations, respectively, and X is an anion (typically O or F). The structure is named after the mineral $MgAl_2O_4$, and oxide spinels have the general formula AB_2O_4.

In the **normal spinel** structure, there is a close-packed array of anions. The A-site cations fill 1/8 of the tetrahedral holes and the B-site cations fill 1/2 of the octahedral holes. A polyhedral view of the normal spinel unit cell is shown at the left, and a simplified view (with the contents of the back half of the cell removed for clarity) is shown above. Each unit cell contains eight formula units and has a composition $A_8B_{16}O_{32}$.

Inverse spinels have a closely related structure (with the same large unit cell) in which the A-site ions and half of the B-site ions switch places. Inverse spinels are thus formulated $B(AB)O_4$, where the AB ions in parentheses occupy octahedral sites, and the other B ions are on tetrahedral sites. There are also mixed spinels, which are intermediate between the **normal** and **inverse** spinel structure.

Some spinel and inverse spinel AB combinations are:

$A^{2+}B^{3+}$, e.g., $MgAl_2O_4$ (normal spinel)

$A^{4+}B^{2+}$, e.g., $Pb_3O_4 = Pb^{II}(Pb^{II}Pb^{IV})O_4$ (inverse spinel)

$A^{6+}B^{+}$, e.g., Na_2WO_4 (normal spinel)

Many magnetic oxides, such as Fe_3O_4 and $CoFe_2O_4$, are spinels.

Normal vs. inverse spinel structure

For transition metal oxide spinels, the choice of the normal vs. inverse spinel structure is driven primarily by the **crystal field stabilization energy** (CFSE) of ions in the tetrahedral and octahedral sites. For spinels that contain 3d elements such as Cr, Mn, Fe,

Co, and Ni, the electron configuration is typically **high spin** because O^{2-} is a **weak field ligand**. We will learn more about these terms in the next section.

Ferrites are compounds of general formula $\mathbf{M^{II}Fe_2O_4}$. We can see that magnetite is one example of a ferrite (with M = Fe). Other divalent metals (M = Mg, Mn, Co, Ni, Zn) also form ferrites. Ferrites can be normal or inverse spinels, or mixed spinels, depending on the CFSE of the M^{II} ion. Based on their CFSE, Fe^{2+}, Co^{2+}, and Ni^{2+} all have a strong preference for the octahedral site, so those compounds are all inverse spinels. $ZnFe_2O_4$ is a normal spinel because the small Zn^{2+} ion (d^{10}) fits more easily into the tetrahedral site than Fe^{3+} (d^5), and both ions have zero CFSE. $MgFe_2O_4$ and $MnFe_2O_4$, in which all ions have zero CFSE and no site preference, are mixed spinels. **Chromite** spinels, $\mathbf{M^{II}Cr_2O_4}$, are always **normal spinels** because the d^3 Cr^{3+} ion has a strong preference for the octahedral site.

Examples of normal and inverse spinel structures:

> $\mathbf{MgAl_2O_4}$ is a **normal spinel** since both Mg^{2+} and Al^{3+} are non-transition metal ions and thus CFSE = 0. The more highly charged Al^{3+} ion prefers the octahedral site, where it is surrounded by six negatively charged oxygen atoms.
>
> $\mathbf{Mn_3O_4}$ is a **normal spinel** since the Mn^{2+} ion is a high spin d^5 system with zero CFSE. The two Mn^{3+} ions are high spin d^4 with higher CFSE on the octahedral sites ($3/5\ \Delta_O$) than on the tetrahedral site ($2/5\ \Delta_t \sim 1/5\ \Delta_O$).
>
> $\mathbf{Fe_3O_4}$ is an **inverse spinel** since the Fe^{3+} ion is a high spin d^5 system with zero CFSE. Fe^{2+} is a high spin d^6 system with more CFSE on an octahedral site than on a tetrahedral one.
>
> $\mathbf{NiFe_2O_4}$ is again an **inverse spinel** since Ni^{2+} (a d^8 ion) prefers the octahedral site and the CFSE of Fe^{3+} (a d^5 ion) is zero.
>
> $\mathbf{FeCr_2O_4}$ is a **normal spinel** since Fe^{2+} is high spin d^6 ion with $CFSE = [4(\frac{2}{5}) - 2(\frac{3}{5})]\Delta_o = \frac{2}{5}\Delta_o$ on an octahedral site, and Cr^{3+} is a d^3 ion with CFSE = $3(2/5)\ \Delta_O = 6/5\ \Delta_O$. Hence it is more energetically favorable for Cr^{3+} to occupy both of the octahedral sites.
>
> $\mathbf{Co_3O_4}$ is a **normal spinel**. Even in the presence of weak field oxo ligands, Co^{3+} is a low spin d^6 ion with very high CFSE on the octahedral sites, because of the high charge and small size of the Co^{3+} ion. Hence the Co^{3+} ions occupy both octahedral sites, and Co^{2+} occupies the tetrahedral site.

Magnetism of ferrite spinels

Ferrite spinels are of technological interest because of their magnetic ordering, which can be ferrimagnetic or antiferromagnetic depending on the structure (normal or inverse) and the nature of the metal ions. Fe_3O_4, $CoFe_2O_4$, and $NiFe_2O_4$ are all inverse spinels and are ferrimagnets. The latter two compounds are used in magnetic recording media and as deflection magnets, respectively.

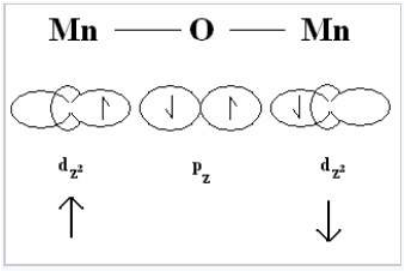
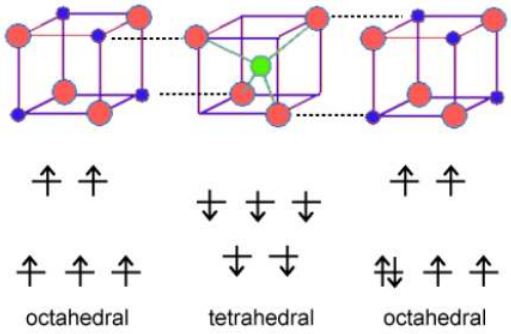


Illustration of antiferromagnetic superexchange between two transition metal cations through a shared oxygen atom.

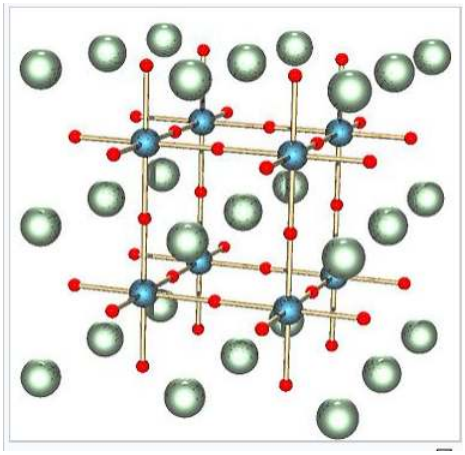
In order to understand the magnetism of ferrites, we need to think about how the unpaired spins of metal ions are coupled in oxides. If an oxide ion is shared by two metal ions, it can mediate the coupling of spins by superexchange as shown at the right. The coupling can be antiferromagnetic, as shown, or ferromagnetic, depending on the orbital filling and the symmetry of the orbitals involved. The **Goodenough-Kanamori rules** predict the local magnetic ordering (ferromagnetic vs. antiferromagnetic) that results from superexchange coupling of the electron spins of transition metal ions. For ferrites, the strongest coupling is between ions on neighboring **tetrahedral and octahedral sites**, and the ordering of spins between these two sites is reliably **antiferromagnetic**.



Because all the tetrahedral and octahedral sites in a spinel or inverse spinel crystal are coupled together identically, it works out that ions on the tetrahedral sites will all have one orientation (e.g., spin down) and ions on all the octahedral sites will have the opposite orientation (e.g., spin up). If the number of spins on the two sites is the same, then the solid will be antiferromagnetic. However, if the **number of spins is unequal** (as in the case of Fe_3O_4, $CoFe_2O_4$, and $NiFe_2O_4$) then the solid will be **ferrimagnetic**. This is illustrated above for Fe_3O_4. The spins on the Fe^{3+} sites cancel, because half of them are up and half are down. However, the four unpaired electrons on the Fe^{2+} ions are all aligned the same way in the crystal, so the compound is ferrimagnetic.

Perovskites are **ternary oxides** of general formula **ABO_3**. More generally, the perovskite formula is ABX_3, where the anion X can be **O, N, or halogen**. The A ions are typically large ions such as Sr^{2+}, Ba^{2+}, Rb^{+}, or a lanthanide 3+ ion, and the B ions are smaller transition metal ions such as Ti^{4+}, Nb^{5+}, Ru^{4+}, etc. The mineral after which the structure is named has the formula $CaTiO_3$.

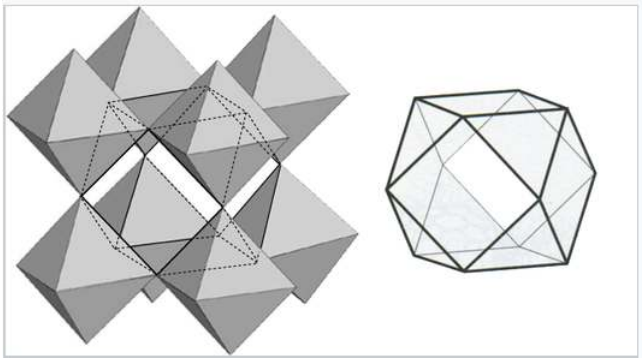
The perovskite structure has simple cubic symmetry, but is related to the fcc lattice in the sense that the A site cations and the three O atoms comprise a fcc lattice. The B-site cations fill 1/4 of the octahedral holes and are surrounded by six oxide anions.



ABX_3 perovskite structure. A, B, and X are white, blue, and red, respectively.

The coordination of the A ions in perovsite and the arrangement of BO_6 octahedra is best understood by looking at the ReO_3 structure, which is the same structure but with the A-site cations removed. In the polyhedral representation of the structure shown at the right, it can be seen that the octahedra share all their vertices but do not share any octahedral edges. This makes the ReO_3 and perovskite structures flexible, like three-dimensional wine racks, in that the octahedra can **rotate and tilt cooperatively**. Eight such

octahedra surround a large **cuboctahedral cavity**, which is the site of the A ions in the perovskite structure. Cations in these sites are coordinated by 12 oxide ions, as expected from the relationship between the perovskite and fcc lattices.



Polyhedral representation of the ReO_3 structure showing the large cuboctahedral cavity that is surrounded by 12 oxygen atoms

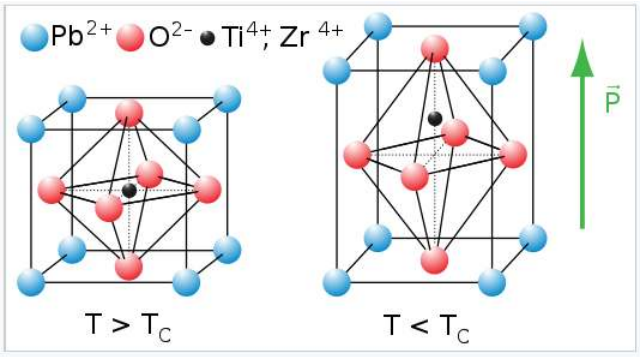
Because the A-site is empty in the ReO_3 structure, compounds with that structure can be reversibly **intercalated** by small ions such as **Li^+ or H^+**, which then occupy sites in the cuboctahedral cavity. For example, smart windows that darken in bright sunlight contain the **electrochromic** material WO_3, which has the ReO_3 structure. In the sunlight, a photovoltaic cell drives the reductive intercalation of WO_3 according to the reaction:

$$x\,H^+ + xe^- + WO_3 \leftrightharpoons H_xWO_3 \qquad (5.6.5.1)$$

WO_3 is a light yellow compound containing d^0 W(VI). In contrast, H_xWO_3, which is mixed-valent W(V)-W(VI) = d^1-d^0, has a deep blue color. Such coloration is typical of mixed-valence transition metal complexes because their d-electrons can be excited to delocalized conduction band levels by red light. Because the electrochemical intercalation-deintercalation process is powered by a solar cell, the tint of the windows can adjust automatically to the level of sunlight.

Ferroelectric perovskites

The flexibility of the network of corner-sharing BO_6 octahedra is also very important in ferroelectric oxides that have the perovskite structure. In some perovsites with small B-site cations, such as Ti^{4+} and Nb^{5+}, the cation is too small to fit symmetrically in the BO_6 octahedron. The octahedron distorts, allowing the cation to move off-center. These distortions can be **tetragonal** (as in the example shown at the right), **rhombohedral**, or **orthorhombic**, depending on whether the cation moves towards a vertex, face, or edge of the BO_6 octahedron. Moving the cation off-center in the octahedron creates an **electric dipole**. In ferroelectrics, these dipoles align in neighboring unit cells through cooperative rotation and tilting of octahedra. The crystal thus acquires a net electrical polarization.



Tetragonal distortion of the perovskite unit cell in the ferroelectric oxide PZT, $PbTi_xZr_{1-x}$

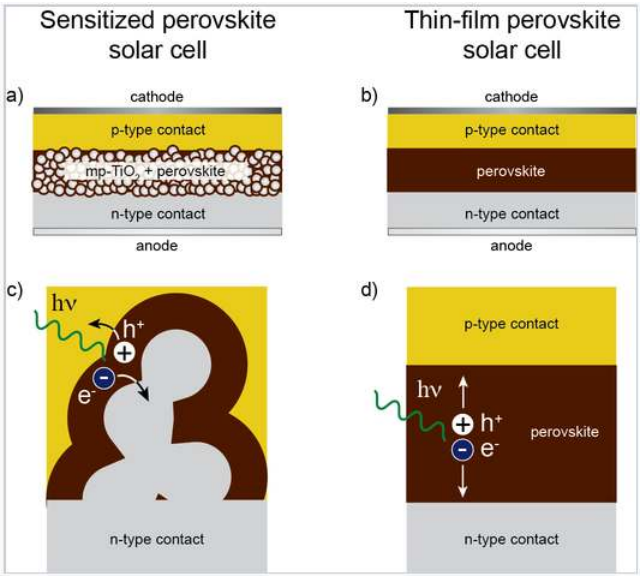
Ferroelectricity behaves analogously to **ferromagnetism**, except that the polarization is electrical rather than magnetic. In both cases, there is a **critical temperature (T_c)** above which the **spontaneous polarization** of the crystal disappears. Below T_c, the

electric polarization of a ferroelectric can be switched with a coercive field, and hysteresis loop of polarization vs. field resembles that of a ferromagnet. Above T_c, the crystal is **paraelectric** and has a high dielectric permittivity.

Ferroelectric and paraelectric oxides (along with piezoelectrics and pyroelectrics) have a wide variety of applications as switches, actuators, transducers, and dielectrics for capacitors. **Ferroelectric capacitors** are important in memory devices (FRAM) and in the tuning circuits of cellular telephones. **Multiferroics**, which are materials that are simultaneously ferroelectric and ferromagnetic, are rare and are being now intensively researched because of their potential applications in electrically adressable magnetic memory.

Halide perovskites (ABX_3, X = Cl, Br, I) can be made by combining salts of monovalent A ions ($A^+ = Cs^+$, NH_4^+, RNH_3^+) and divalent metal salts such as $PbCl_2$ or PbI_2. These compounds have sparked recent interest as light absorbers for **thin film solar cells** that produce electricity from sunlight. Lead and tin halide perovskites can be grown as thin films from solution precursors or by thermal evaporation at relatively low temperatures. In some lead halide perovskites, the mobility of electrons and holes is very high, comparable to that of more expensive III-V semiconductors such as GaAs, which must be grown as very pure single crystals at high temperatures for use in solar cells. Because of their high carrier mobility, some lead halide perovskites are also electroluminescent and are of interest as inexpensive materials for light-emitting diodes (LEDs).

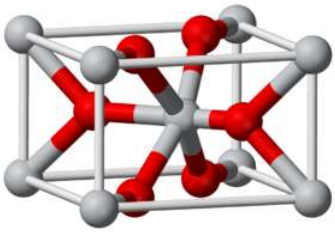
Tin and lead halide perovskites were first studied in the 1990s as materials for thin film electronics,[4] and more recently as light absorbers in dye-sensitized solar cells. Soon after the results on dye-sensitized perovskite cells were reported, it was discovered that halide perovskites could also be used in thin film solid state solar cells. The structures of these solar cells are shown schematically at the right. The highest reported solar power conversion efficiencies of perovskite solar cells have jumped from 3.8% in 2009 [5] to 10.2% in 2012[6] and a certified 20.1% in 2014.[7]. The highest performing cells to date contain divalent lead in the perovskite B cation site and a mixture of methylammonium and formamidinium ions in the perovskite A cation site.



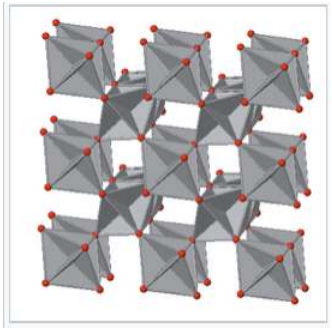
a) Solar cell architecture in which a lead halide perovskite absorber coats a layer of nanocrystalline anatase TiO_2. b) Thin-film solar cell, with a layer of lead halide perovskite sandwiched between two selective contacts. c) Charge generation and extraction in the sensitized architecture and d) in the thin-film architecture.

Despite their very impressive efficiency, perovskite solar cells are stable for relatively short periods of time and are sensitive to air and moisture. Current research is focused on understanding the degradation mechanisms of these solar cells and improving their stability under operating conditions.

The **rutile structure** is an important MX_2 (X = O, F) structure. It is a 6:3 structure, in which the cations are octahedrally coordinated by anions, and as such is intermediate in polarity between the CaF_2 (8:4) and SiO_2 (4:2) structures. The mineral rutile is one of the polymorphs of TiO_2, the others (anatase and brookite) also being 6:3 structures.



The rutile structure can be described as a distorted version of the NiAs structure with half the cations removed. Recall that compounds with the NiAs structure were typically metallic because the metal ions are eclipsed along the stacking axis and thus are in relatively close contact. In rutile, the MO_6 **octahedra share edges** along the tetragonal c-axis, and so some rutile oxides, such as **NbO_2, RuO_2 and IrO_2,** are also **metallic** because of **d-orbital overlap** along that axis. These compounds are important as electrolyzer catalysts and catalyst supports because they combine high catalytic activity with good electronic conductivity.



View down the tetragonal c-axis of the rutile lattice, showing edge-sharing MO_6 octahedra.

Rutile TiO_2, because of its high refractive index, is the base pigment for white paint. It is a wide bandgap semiconductor that has also been extensively researched as an electrode for water splitting solar cells and as a photocatalyst (primarily as the anatase polymorph) for degradation of pollutants in air and water. Self-cleaning glass exploits the photocatalytic properties of a thin film of TiO_2 to remove oily substances from the glass surface and improve the wetting properties of the glass.

5.6.5: Spinel, Perovskite, and Rutile Structures is shared under a CC BY-SA license and was authored, remixed, and/or curated by LibreTexts.

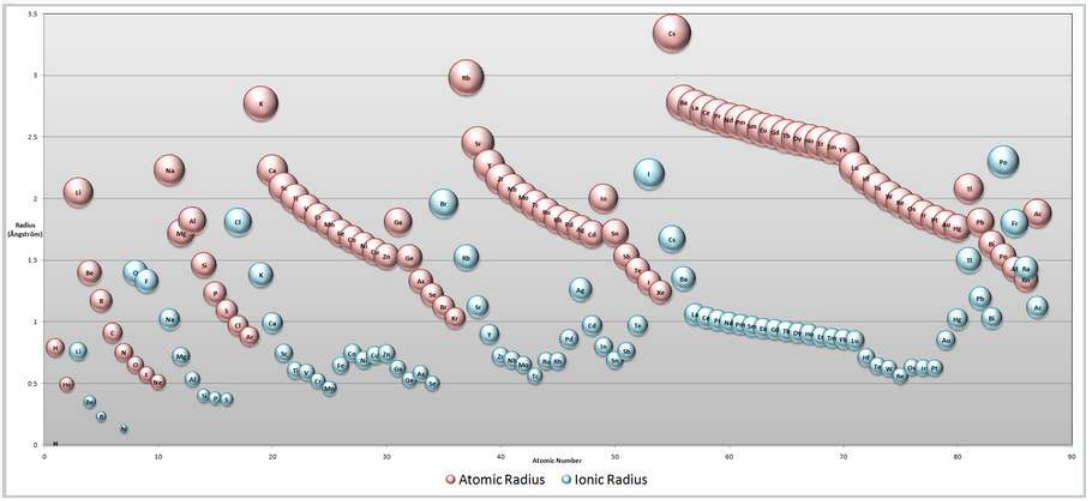
- **8.7: Spinel, Perovskite, and Rutile Structures** by Chemistry 310 is licensed CC BY-SA 4.0. Original source: https://en.wikibooks.org/wiki/Introduction_to_Inorganic_Chemistry.

5.7: Ionic Radii and Radius Ratios

Atoms in crystals are held together by electrostatic forces, van der Waals interactions, and covalent bonding. It follows that arrangements of atoms that can maximize the strength of these attractive interactions should be most favorable and lead to the most commonly observed crystal structures.

Radius ratio rules

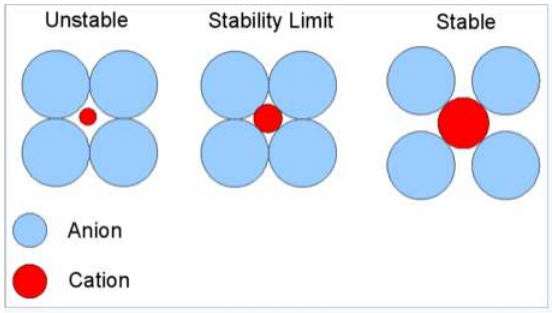
Early crystallographers had trouble solving the structures of inorganic solids using X-ray diffraction because some of the mathematical tools for analyzing the data had not yet been developed. Once a trial structure was proposed, it was relatively easy to calculate the diffraction pattern, but it was difficult to go the other way (from the diffraction pattern to the structure) if nothing was known *a priori* about the arrangement of atoms in the unit cell. It was (and still is!) important to develop some guidelines for guessing the coordination numbers and bonding geometries of atoms in crystals. The first such rules were proposed by Linus Pauling, who considered how one might pack together oppositely charged spheres of different radii. Pauling proposed from geometric considerations that the quality of the "fit" depended on the **radius ratio** of the anion and the cation.



Atomic and Ionic Radii. Note that cations are always smaller than the neutral atom (pink) of the same element, whereas anions are larger. Going from left to right across any row of the periodic table, neutral atoms and cations contract in size because of increasing nuclear charge. (click for larger image)

The basic idea of radius ratio rules is illustrated at the right. We consider that the anion is the packing atom in the crystal and the smaller cation fills interstitial sites ("holes"). Cations will find arrangements in which they can contact the largest number of anions. If the cation can touch all of its nearest neighbor anions, as shown at the right for a small cation in contact with larger anions, then the fit is good. If the cation is too small for a given site, that coordination number will be unstable and it will prefer a

lower coordination structure. The table below gives the ranges of cation/anion radius ratios that give the best fit for a given coordination geometry.



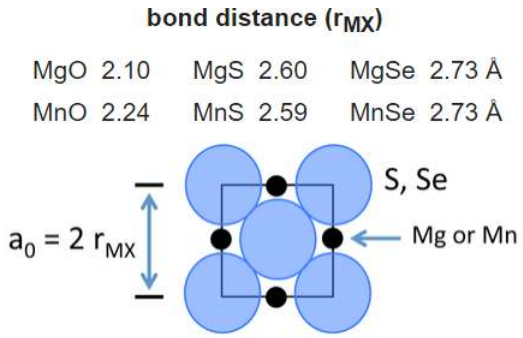
Critical Radius Ratio. This diagram is for coordination number six: 4 anions in the plane are shown, 1 is above the plane and 1 is below. The stability limit is at $r_C/r_A = 0.414$

Coordination number	Geometry	$\rho = r_{cation}/r_{anion}$
2	linear	0 - 0.155
3	triangular	0.155 - 0.225
4	tetrahedral	0.225 - 0.414
4	square planar	0.414 - 0.732
6	octahedral	0.414 - 0.732
8	cubic	0.732 - 1.0
12	cuboctahedral	1.0

There are unfortunately several challenges with using this idea to predict crystal structures:

- We don't know the radii of individual ions
- Atoms in crystals are not really ions - there is a varying degree of covalency depending electronegativity differences
- Bond distances (and therefore ionic radii) depend on bond strength and coordination number (remember Pauling's rule D(n) = D(1) - 0.6 log n)
- Ionic radii depend on oxidation state (higher charge => smaller cation size, larger anion size)

We can build up a table of ionic radii by assuming that the bond length is the sum of the radii ($r_+ + r_-$) if the ions are in contact in the crystal. Consider for example the compounds MgX and MnX, where X = O, S, Se. All of these compounds crystallize in the NaCl structure:



For the two larger anions (S^{2-} and Se^{2-}), the unit cell dimensions are the same for both cations. This suggests that the anions are in contact in these structures. From geometric considerations, the anion radius in this case is given by:

Extra close brace or missing open brace

and thus the radii of the S^{2-} and Se^{2-} ions are 1.84 and 1.93 Å, respectively. Once the sizes of these anions are fixed, we can obtain a self-consistent set of cation and anion radii from the lattice constants of many MX compounds.

How well does this model work? Let's consider the structures of tetravalent metal oxides (MO_2), using Pauling radii and the predictions of the radius ratio model:

Oxide MO_2	Radius ratio	Predicted coord. no.	Observed coord no. (structure)
CO_2	~0.1	2	2 (linear molecule)
SiO_2	0.32	4	4 (various tetrahedral structures)
GeO_2	0.43	4	4 (silica-like structures)
"	0.54	6	6 (rutile)
TiO_2	0.59	6	6 (rutile)
ZrO_2	0.68	6	7 (baddleyite)
"	0.77	8	8 (fluorite)
ThO_2	0.95	8	8 (fluorite)

Note that cations have different radii depending on their coordination numbers, and thus different radius ratios are calculated for Ge^{4+} with coordination numbers 4 and 6, and for Zr^{4+} with coordination numbers 6 and 8.

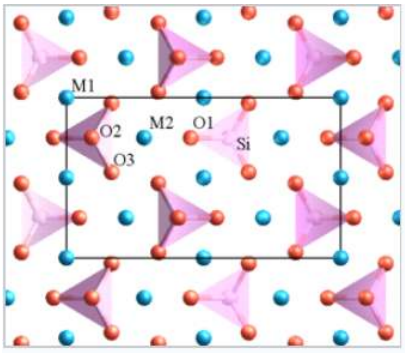
For this series of oxides, the model appears to work quite well. The correct coordination number is predicted in all cases, and borderline cases such as GeO_2 and ZrO_2 are found in structures with different coordination numbers. The model also correctly predicts the structures of BeF_2 (SiO_2 type), MgF_2 (rutile), and CaF_2 (fluorite).

What about the alkali halides NaCl, KBr, LiI, CsF, etc.? All of them have the NaCl structure except for CsCl, CsBr, and CsI, which have the CsCl (8-8) structure. In this case the radius ratio model fails rather badly. The Li^+ salts LiBr and LiI are predicted to have tetrahedral structures, and KF is predicted to have an 8-8 structure like CsCl. We can try adjusting the radii (e.g., making the cations larger and anions smaller), but the best we can do with the alkali halides is predict about half of their structures correctly. Since the alkali halides are clearly ionic compounds, this failure suggests that there is something very wrong with the radius ratio model, and its success with MO_2 compounds was coincidental.

In addition to the radius ratio rule, Linus Pauling developed other useful rules that are helpful in rationalizing and also predicting the structures of inorganic compounds. Pauling's rules[1] state that:

- Stable structures are **locally electroneutral**. For example, in the structure of the double perovskite Sr_2FeMoO_6, MO_6 (M = Fe^{2+}, Mo^{6+}) octahedra share all their vertices, and Sr^{2+} ions fill the cubooctahedral cavities that are flanked by eight MO_6 octahedra.[2] Each O^{2-} ion is coordinated to one Fe^{2+} and one Mo^{6+} ion in order to achieve local electroneutrality, and thus the FeO_6 and MoO_6 octahedra alternate in the structure.
- **Cation-cation repulsion** should be minimized. Anion polyhedra can share vertices (as in the perovskite structure) without any energetic penalty. Shared polyhedral edges, and especially shared faces, cause cation-cation repulsion and should be avoided. For example, in rutile, the most stable polymorph of TiO_2, the TiO_6 octahedra share vertices and two opposite edges, forming ribbons in the structure. In anatase TiO_2, each octahedron shares four edges so the anatase polymorph is less thermodynamically stable.

- **Highly charged cations** in anion polyhedra tend not to share edges or even vertices, especially when the coordination number is low. For example, in orthosilicates such as olivine (M_2SiO_4), there are isolated SiO_4^{4-} tetrahedra.



Structure of olivine. M (Mg or Fe) = blue spheres, Si = pink tetrahedra, O = red spheres.

As we will soon see, all of Pauling's rules are justified on the basis of lattice energy considerations. In ionic compounds, the arrangement of atoms that maximizes anion-cation interactions while minimizing cation-cation and anion-anion contacts is energetically the best.

5.7: Ionic Radii and Radius Ratios is shared under a CC BY-SA license and was authored, remixed, and/or curated by LibreTexts.

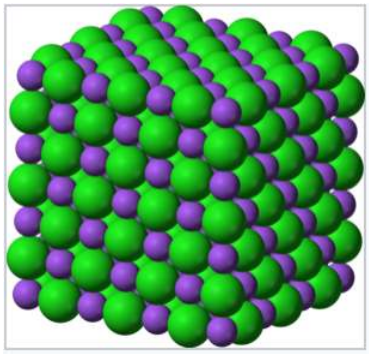
- **9.1: Ionic Radii and Radius Ratios** by Chemistry 310 is licensed CC BY-SA 4.0. Original source: https://en.wikibooks.org/wiki/Introduction_to_Inorganic_Chemistry.

5.8: Energetics of Crystalline Solids- The Ionic Model

Many ionic compounds have simple structures. Because the forces holding the atoms together are primarily electrostatic, we can calculate the cohesive energy of the crystal lattice with good accuracy. Interesting questions to ask about these lattice energy calculations are:

- How accurate are lattice energy calculations?
- What do they teach us about the chemical bonds in ionic crystals?
- Can we use lattice energies to predict properties such as solubility, stability, and reactivity?
- Can we use lattice energies to predict the crystal structures of ionic compounds?

Let's start by looking at the forces that hold ionic lattices together. There are mainly two kinds of force that determine the energy of an ionic bond.



The NaCl crystal structure is the archetype for calculating lattice energies and computing enthalpies of formation from Born-Haber cycles.

1) **Electrostatic Force** of attraction and repulsion (Coulomb's Law): Two ions with charges z_+ and z_-, separated by a distance r, experience a force F:

$$\mathbf{F} = -\frac{e^2}{4\pi\varepsilon_0}\frac{z_+z_-}{r^2} \tag{5.8.1}$$

where

e = 1.6022×10^{-19} C

4 π ε_0 = 1.112×10^{-10} C²/(J m)

This force is attractive for ions of opposite charge.

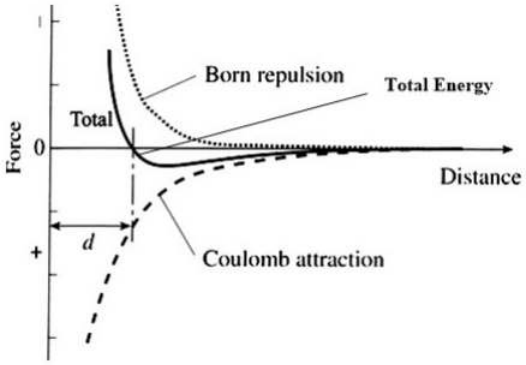
The electrostatic potential energy, E_{elec}, is then given by

$$\mathbf{E}_{elec}\int_{\infty}^{r} F(r)dr = \frac{e^2}{4\pi\varepsilon_0}\frac{z_+z_-}{r} \tag{5.8.2}$$

The sign of E_{elec} is negative for the attractive interaction between a cation and an anion. That is, the closer oppositely charged ions approach each other, the lower the potential energy.

2) **Closed-shell repulsion**. When electrons in the closed shells of one ion overlap with those of another ion, there is a repulsive force comes from the Pauli exclusion principle. A third electron cannot enter an orbital that already contains two electrons. This force is short range, and is typically modeled as falling off exponentially or with a high power of the distance r between atoms. For example, in the Born approximation, B is a constant and ρ is a number with units of length, which is usually empirically determined from compressibility data. A typical value of ρ is 0.345 Å.

$$\mathbf{E}_{repulsion} = Bexp(\frac{-r}{\rho}) \tag{5.8.3}$$



The energy of the ionic bond between two atoms is then calculated as the combination of net electrostatic and the closed-shell repulsion energies, as shown in the figure at the right. Note that for the moment we are ignoring the attractive van der Waals energy between ions, which we will explain below. For a pair of ions, the equilibrium distance between ions is determined by the minimum in the total energy curve. At this distance, the net force on each ion is zero.

Electrostatic energy of a crystal lattice

We can use these equations to calculate the lattice energy of a crystal by summing up the interactions between all pairs of ions. Because the closed-shell repulsion force is short range, this term is typically calculated only for interactions between neighboring ions. However, the Coulomb force is long range, and must be calculated over the entire crystal. This problem was first solved in 1918 by Erwin Madelung, a German physicist.[4]

Consider an ion in the NaCl structure labeled "O" in the diagram at the right. We can see that the nearest neighbor interactions (+ -) with ions labeled "1" are attractive, the next nearest neighbor interactions (- - and + +) are repulsive, and so on. In the NaCl structure, counting from the ion in the center of the unit cell, there are 6 nearest neighbors (on the faces of the cube), 12 next nearest neighbors (on the edges of the cube), 8 in the next shell (at the vertices of the cube), and so on. Their distances from ion "0" increase progressively: r_o, $\sqrt{2}\ r_o$, $\sqrt{3}\ r_o$, and so on, where r_o is the nearest neighbor distance.

We can now write the electrostatic energy at ion "O" as:

$$\mathbf{E}_{elec} = -6\frac{e^2}{4\pi\varepsilon_0}\frac{z_+z_-}{r_o} + 12\frac{e^2}{4\pi\varepsilon_0}\frac{z_+z_-}{\sqrt{2}r_o} - 8\frac{e^2}{4\pi\varepsilon_0}\frac{z_+z_-}{\sqrt{3}r_o} + \ldots \tag{5.8.4}$$

Factoring out constants and the nearest-neighbor bond distance r_o we obtain:

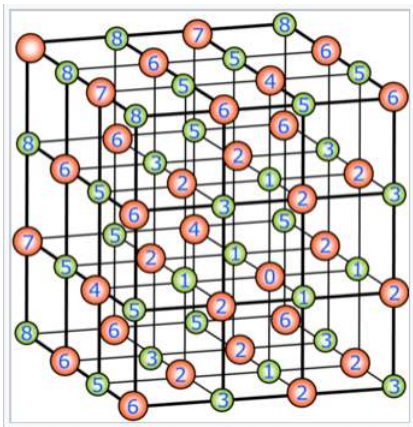
$$\mathbf{E}_{elec} = \frac{e^2}{4\pi\varepsilon_0}\frac{z_+z_-}{r_o}\left(6 - \frac{12}{\sqrt{2}} + \frac{8}{\sqrt{3}} - \frac{6}{\sqrt{4}} + \ldots\right) \tag{5.8.5}$$

Where the sum in parentheses, which is unitless, slowly converges to a value of A = 1.74756. Generalizing this formula for any three-dimensional ionic crystal we get a function:

$$\mathbf{E}_{elec} = \frac{e^2}{4\pi\varepsilon_0}\frac{z_+z_-}{r_o}NA \tag{5.8.6}$$

where N is Avogadro's number (because we are calculating energy per mole of ions) and A is called the *Madelung constant*. The **Madelung constant** depends only on the geometrical arrangement of the ions and so it varies between different types of crystal

structures, but within a given structure type it does not change. Thus MgO and NaCl have the same Madelung constant because they both have the NaCl structure. We will see more about the Madelung constant in an upcoming section.



The Madelung constant is calculated by summing up electrostatic interactions with ion labeled 0 in the expanding spheres method. Each number designates the order in which it is summed. For example, ions labeled 1 represent the six nearest neighbors (attractive interaction), ions labeled 2 are the 12 next nearest neighbors (repulsive interaction) and so on. Note that if the sum is carried out over shells 1-2-3..., it converges very slowly, but there are mathematical methods for summing it which give a rapidly converging series.

Total lattice energy of a crystal

Having in hand a formula for the electrostatic energy, we can now add in the closed-shell repulsion term to obtain an equation that gives us the total lattice energy.

$$E_L = \frac{e^2}{4\pi\varepsilon_0}\frac{z_+z_-}{r_o}NA + NBexp(\frac{-r}{\rho}) \tag{5.8.7}$$

At the equilibrium bond distance, the forces on all the ions are zero, and we can use this fact to eliminate the constant B:

$$[\frac{dE}{dr}]_{r=r_o} = 0 \tag{5.8.8}$$

Expressed this way, E_L is a negative number (because z_+ and z_- have opposite signs). It represents the energy change for forming one mole of solid salt from one mole of the gaseous ions, separated initially at an infinite distance.



Lithium fluoride (shown here as a large single crystal in a beaker of water) is the only alkali halide that is not freely soluble in water. The lattice energy of LiF is the most negative of the alkali fluorides because Li^+ and F^- are both small ions and E_L is proportional to $1/r_0$.

5.8: Energetics of Crystalline Solids- The Ionic Model is shared under a CC BY-SA license and was authored, remixed, and/or curated by LibreTexts.

- **9.3: Energetics of Crystalline Solids- The Ionic Model** by Chemistry 310 is licensed CC BY-SA 4.0. Original source: https://en.wikibooks.org/wiki/Introduction_to_Inorganic_Chemistry.

5.8.1: Born-Haber Cycles for NaCl and Silver Halides

Now that we have an equation for the lattice energy of an ionic crystal, we can ask the question of how accurate it is. Remember, we made several approximations in arriving at this formula. We assumed that the lattice was completely ionic, we ignored the van der Waals attractive energy of the ions, and we assumed that there was no covalent contribution to the bonding.

Let's consider the lattice energy of table salt (NaCl)

$$Na^+_{(g)} + Cl^-_{(g)} \longrightarrow NaCl_{(s)}$$

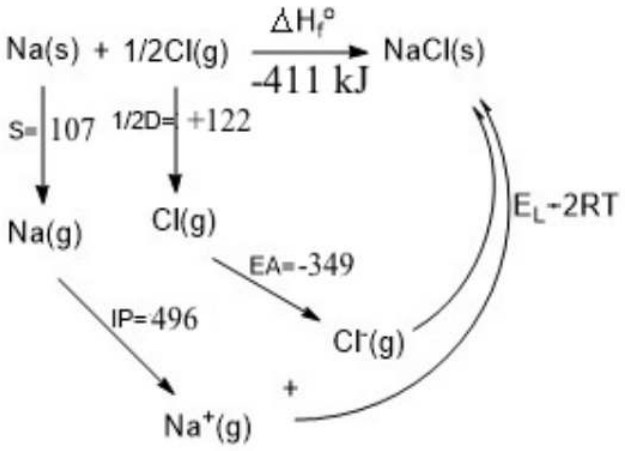
To calculate the lattice energy, we lump together the physical constants:

$$E_L(\frac{kJ}{mol}) = (1389.3)\frac{Aq_1q_2}{r_o}(1 - \frac{.345}{r_o}) \tag{5.8.1.1}$$

where r_o is expressed in Å. Now we can calculate the lattice energy for NaCl using r_o = 2.814 Å, as:

$$E_L = -(1389.3)\frac{1.7476}{2.814}(1 - \frac{.345}{2.814}) = -766.5\frac{kJ}{mol} \tag{5.8.1.2}$$

We can alternatively construct a **Born-Haber cycle** for the formation of NaCl from the elements and calculate the lattice energy as the "missing" term in the cycle.



S= Sublimation energy of Na(s)

IP= Ionization potential of Na(g)

D= Bond dissocation energy of Cl_2(g)

EA= Electron affinity of Cl(g)

E_L=Lattice energy of NaCl

R= Gas constant

T= Absolute temperature

From **Hess' Law:** $\Delta H_f = s + \frac{1}{2}D + IP + EA + E_L - 2RT = -396\frac{kJ}{mol}$

Here we have to subtract 2RT to convert our cycle of energies to a cycle of enthalpies, because we are compressing two moles of gas in making NaCl(s) and PΔV = ΔnRT, where Δn = -2.

Experimentally ΔH_f for NaCl is **-411 kJ/mol**

Because all the other numbers in the cycle are known accurately, the error in our calculation is only about 15 kJ (about 2% of E_L). The result is promising because we neglected the van der Waals term.

But....how did we get away with neglecting the van der Waals term?

This is because we used **energy minimization** to obtain the repulsion energy in the Born-Mayer equation. If we underestimate the attractive energy of the crystal lattice, the energy minimization criterion ensures that the repulsion energy is underestimated as well. The two errors partially compensate, so the overall error in the calculation is small.

We can do better by explicitly including the short-range van der Waals attractive energy between ions. The table below shows results of more detailed lattice energy calculations for ionic fluorides in which the van der Waals term is explicitly included. The errors in this case are only about 1% of E_L.

Compound	Calculated Lattice Energy (kJ/mol)	Experimental E_L from Born-Haber Cycle
MgF_2 (rutile structure)	-2,920	-2,908
CaF_2 (fluorite structure)	-2,586	-2,611
BaF_2 (fluorite structure)	-2,326	-2,368

Silver Halides

It is interesting to repeat this exercise for the silver halides, which have either the NaCl structure (AgF, AgCl, AgBr) or zincblende structure (AgI).

Silver Halide	Calculated	Cycle	Difference (kJ/mol)
AgF	-920	-954	34
AgCl	-833	-908	75
AgBr	-816	-900	84
AgI	-778	-883	105

Looking at the table, we see that the error is small for AgF and becomes progressively larger for the heavier silver halides. However we are still obtaining answers within about 12% error even for AgI. Should we interpret the good agreement with values calculated from the ionic model to mean that these compounds are ionic? Clearly, this description is inappropriate for AgI, where the electronegativity difference $\Delta\chi$ is only 0.6 (compare this value to 0.4 for a C-H bond, which we typically view as non-polar).



A drop of siver nitrate solution, when added to a dilute hydrochloric acid solution, results in the immediate formation of a white silver chloride precipitate. This reaction is used as a qualitative test for the presence of halide ions in solutions. The covalent bonding contribution to the lattice energies of AgCl, AgBr, and AgI makes these salts sparingly soluble in water.

Again, we can interpret the fortuitous agreement between the calculated and experimentally obtained energies in terms of compensating errors. Our lattice energy calculation *overestimates* the ionic contribution in the case of the heavier silver halides, but *underestimates* the covalent contribution. Of these compounds, only AgF is soluble in water and should be thought of as an ionic compound. The others are progressively more insoluble in water (K_{sp} is 10^{-10}, 10^{-13}, and 10^{-16} for AgCl, AgBr, and AgI), reflecting increasing covalency as $\Delta\chi$ decreases.

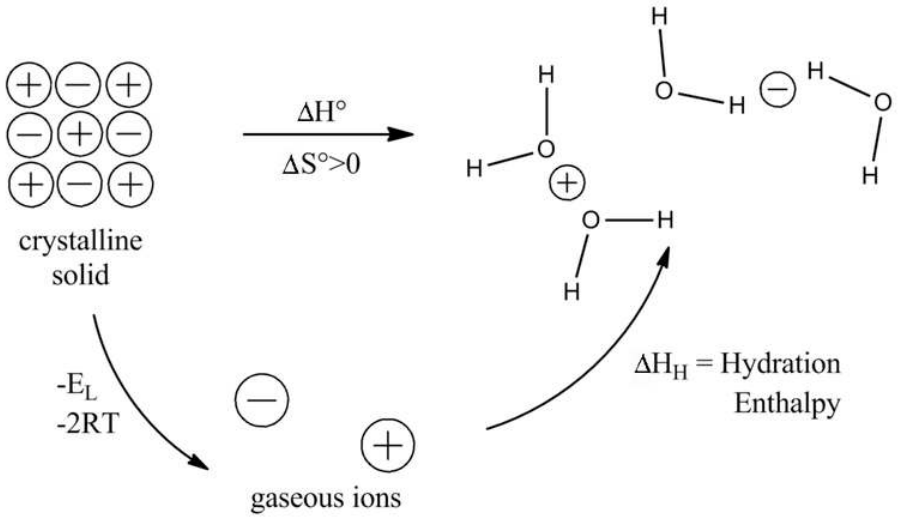
The moral of the story is that simple lattice energy calculations based on the ionic model work well, but *they do not necessarily imply that the compounds are ionic*!

5.8.1: Born-Haber Cycles for NaCl and Silver Halides is shared under a CC BY-SA license and was authored, remixed, and/or curated by LibreTexts.

- **9.4: Born-Haber Cycles for NaCl and Silver Halides** by Chemistry 310 is licensed CC BY-SA 4.0. Original source: https://en.wikibooks.org/wiki/Introduction_to_Inorganic_Chemistry.

5.8.2: Lattice Energies and Solubility

Lattice energies can also help predict compound solubilities. Let's consider a Born-Haber cycle for dissolving a salt in water. We can imagine this as the sum of two processes: (1) the vaporization of the salt to produce gaseous ions, characterized by the lattice enthalpy, and (2) the hydration of those ions to produce the solution. The enthalpy change for the overall process is the sum of those two steps. We know that the entropy change for dissolution of a solid is positive, so the solubility depends on the enthalpy change for the overall process.



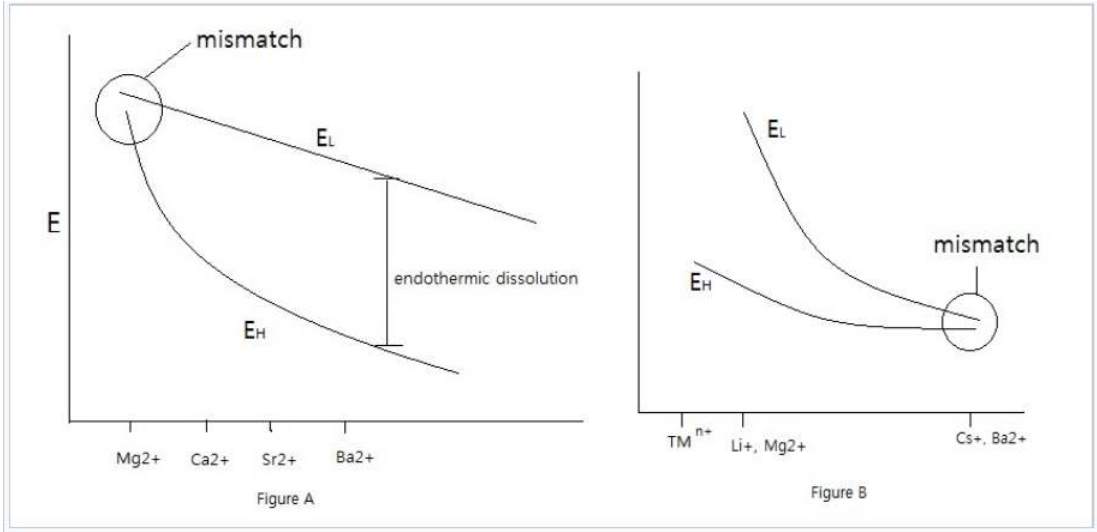
Here we need to consider the trends in both the lattice energy E_L and the hydration energy E_H. The lattice energy depends on the sum of the anion and cation radii ($r_+ + r_-$), whereas the hydration energy has separate anion and cation terms. Generally the solvation of small ions (typically cations) dominates the hydration energy because of the $1/r^2$ dependence.

$$E_L \alpha \frac{1}{r_+ + r_-} \tag{5.8.2.1}$$

$$E_H \alpha \frac{1}{r_+^2} + \frac{1}{r_-^2} \tag{5.8.2.2}$$

For salts that contain large anions, E_L doesn't change much as r_+ changes. That is because the anion dominates the $r_+ + r_-$ term in the denominator of the formula for E_L. On the other hand, E_H changes substantially with r_+, especially for small cations.

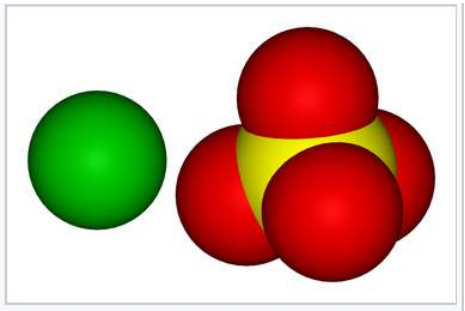
As a result, sulfate salts of small divalent cations, such as $MgSO_4$ (epsom salts), are soluble, whereas the lower hydration energy of Ba^{2+} in $BaSO_4$ makes that salt insoluble ($K_{sp} = 10^{-10}$).



Left: E_L diagram for sulfate salts. The large SO_4^{2-} ion is size-mismatched to small cations such as Mg^{2+}, which have large hydration energies, resulting soluble salts. With larger cations such as Ba^{2+}, which have lower E_H, the lattice energy exceeds the solvation enthalpy and the salts are insoluble.. Right: In the case of small anions such as F^- and OH^-, the lattice energy dominates with small cations such as transition metal ions (TM^{n+}), Mg^{2+}, and Li^+. Anion-cation size mismatch occurs with larger cations, such as Cs^+ and Ba^{2+}, which make soluble fluoride salts.

For small anions, E_L is more sensitive to r_+, whereas E_H does not depend on r_+ as strongly. For fluorides and hydroxides, LiF is slightly soluble whereas CsF is very soluble, and $Mg(OH)_2$ is insoluble whereas $Ba(OH)_2$ is very soluble.

Putting both trends together, we see that **low solubility** is most often encountered when the **anion and cation match well in their sizes**, especially when one or both are **multiply charged**.



Space-filling models showing the van der Waals surfaces of Ba^{2+} and SO_4^{2-}. The similarity in size of the two ions contributes to the low solubility of $BaSO_4$ in water.

Combining all our conclusions about solubility, we note the following trends:

1) Increasing **size mismatch** between the anion and cation leads to greater solubility, so CsF and LiI are the most soluble alkali halides.

2) Increasing **covalency** leads to lower solubility in the salts (due to larger E_L. For example, AgF, AgCl, AgBr, and AgI exhibit progressively lower solubility because of increasing covalency.

AgF > AgCl > AgBr > AgI

3) Increasing the **charge on the anion** lowers the solubility because the increase in E_L is large relative to the increase in E_H.

4) Small, polyvalent cations (having large E_H) make **soluble salts with large, univalent anions** such as I^-, NO_3^-, ClO_4^-, PF_6^-, and acetate.

Examples: Salts of transition metal and lanthanide ions

- Ln^{3+}: Nitrate salts are soluble, but oxides and hydroxides are insoluble.
- Fe^{3+}: Perchlorate is soluble, but sulfate is insoluble.

5) Multiple charged anions such as O^{2-}, S^{2-}, PO_4^{3-}, and SO_4^{2-} make insoluble salts with most M^{2+}, M^{3+}, and M^{4+} metals.

5.8.2: Lattice Energies and Solubility is shared under a CC BY-SA license and was authored, remixed, and/or curated by LibreTexts.

- **9.12: Lattice Energies and Solubility** by Chemistry 310 is licensed CC BY-SA 4.0. Original source: https://en.wikibooks.org/wiki/Introduction_to_Inorganic_Chemistry.

5.8.3: Kapustinskii Equation

From the discussion above, it is clear that the lattice energy, E_L, of an ionic crystal can be calculated with reasonable accuracy if the structure is known. But how can we calculate E_L for a new or hypothetical compound of unknown structure? Recall that the reduced Madelung constant is about the same for different crystal structures. Russian chemist A. F. Kapustinskii recognized this fact and devised a formula that allows one to calculate E_L for any compound if we know the univalent radii of the constituent ions. [5]

The Madelung constant, A, is proportional to the number of ions (n) in formula unit, so dividing by the n gives similar values as shown in the table below:

A/n ~ invariant

Structure	A/n
NaCl	0.874
CsCl	0.882
Rutile	0.803
Fluorite	0.800

Kapustinskii noticed that the difference in ionic radii between M^+ and M^{2+} (the monovalent vs. divalent radius) largely compensates for the differences in A/n between monovalent (NaCl, CsCl) and divalent (rutile, CaF_2) structures. He thus arrived at a lattice energy formula using an average Madelung constant, corrected to monovalent radii. In the **Kapustinskii formula**, the lattice energy (kJ/mol) is given by:

$$E_L = \frac{1213.8 z_+ z_- n}{r_+ + r_-}\left(1 - \frac{0.345}{r_+ + r_-}\right) \tag{5.8.3.1}$$

Here the sum of the monovalent radii is used in place of r_o, the bond distance in the Born-Mayer equation. The beauty of this formula is that it requires no knowledge of the structure of the compound. Therefore it can be used, in combination with Born-Haber cycles, to predict the stability of unknown compounds. As we show below, this is a broadly useful tool in guiding syntheses and predicting the reactivity of inorganic solids.

5.8.3: Kapustinskii Equation is shared under a CC BY-SA license and was authored, remixed, and/or curated by LibreTexts.

- **9.5: Kapustinskii Equation** by Chemistry 310 is licensed CC BY-SA 4.0. Original source: https://en.wikibooks.org/wiki/Introduction_to_Inorganic_Chemistry.

SECTION OVERVIEW

5.9: Electronic Properties of Materials - Superconductors and Semiconductors

Learning Objectives

- Explain the physical basis of the Hubbard and Mott models of metal-insulator transitions.
- Understand why good superconductors derive from bad metals.
- Know the structures and the periodic trends in band gaps and colors of semiconductors.
- Obtain the band gap of an intrinsic semiconductor from the temperature dependence of the conductivity.
- Predict the doping type when impurities or defects are introduced into a semiconductor.
- Correlate the band picture and Fermi level with n- or p-type doping.
- Understand the physical principles of operation of diodes, LEDs, solar cells, and FETs.
- Explain the differences in structures and electronic properties of crystalline and amorphous semiconductors.

The band model (like MO theory) is based on a *one-electron* model. This was an approximation we made at the very beginning of our discussion of MO theory: we used hydrogen-like (one-electron) solutions to the Schrödinger equation to give us the shapes of s, p, d, and f atomic orbitals. In a one-electron atom, these orbitals are degenerate within a given shell, and the energy differences between, e.g., 2s and 2p orbitals arise only when we consider the energy of an electron in the field of other electrons in the atom. Moving from atoms to molecules, we made linear combinations to generate one-electron molecular orbitals (and, in solids, one-electron energy bands). But as in multi-electron atoms, life is not so simple for real molecules and solids that contain many electrons. Electrons repel each other and so their movement in molecules and in solids is ***correlated***.

5.9.1: Prelude to Electronic Properties of Materials - Superconductors and Semiconductors

5.9.2: Superconductors

5.9.3: Periodic Trends- Metals, Semiconductors, and Insulators

5.9.4: Semiconductors- Band Gaps, Colors, Conductivity and Doping

5.9.5: Semiconductor p-n Junctions

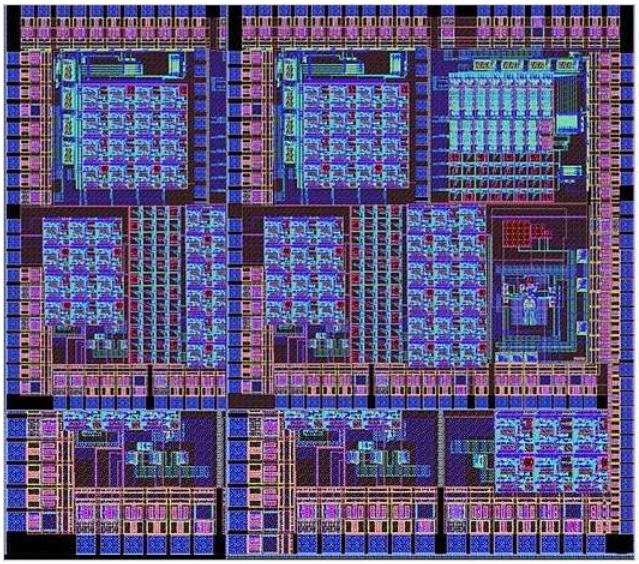
5.9.6: Diodes, LEDs and Solar Cells

5.9.7: References

5.9: Electronic Properties of Materials - Superconductors and Semiconductors is shared under a CC BY-SA license and was authored, remixed, and/or curated by LibreTexts.

5.9.1: Prelude to Electronic Properties of Materials - Superconductors and Semiconductors

In Chapter 6 we developed an energy band picture for metals, starting from atomic orbitals and building up the molecular orbitals of the solid metallic crystal. This treatment gave us a useful picture of how electrons behave in metals, moving at very fast speed between scattering events, and migrating in an electric field at a slow drift velocity. It also taught us that a metal is something with a partially filled band, meaning that the Fermi level cuts through one of its bands of orbitals. An insulator or a semiconductor has a similar band picture, except that the bands are either completely full or completely empty. In this case the Fermi level lies in the gap between fully occupied and unoccupied bands. We will see in this chapter that the properties of semiconductors (along with their useful electronic applications) depend on the addition of small amounts of impurities ("dopants") that change the position of the Fermi level, resulting in conduction by electrons or "holes."



Modern integrated circuits contain billions of nanoscale transistors and diodes that are essential for logic and memory functions. Both kinds of devices rely on junctions between crystalline silicon regions that contain a few parts per million of boron or phosphorus impurities.

While the band picture works well for most crystalline materials, it does not tell us the whole story of conduction in solids. That is because the band model (like MO theory) is based on a *one-electron* model. This was an approximation we made at the very beginning of our discussion of MO theory: we used hydrogen-like (one-electron) solutions to the Schrödinger equation to give us the shapes of s, p, d, and f atomic orbitals. In a one-electron atom, these orbitals are degenerate within a given shell, and the energy differences between, e.g., 2s and 2p orbitals arise only when we consider the energy of an electron in the field of other electrons in the atom. Moving from atoms to molecules, we made linear combinations to generate one-electron molecular orbitals (and, in solids, one-electron energy bands). But as in multi-electron atoms, life is not so simple for real molecules and solids that contain many electrons. Electrons repel each other and so their movement in molecules and in solids is ***correlated***. While this effect is weak in a "good" metal such as sodium - where the wavefunctions are highly delocalized - it can be quite important in other materials such as transition metal oxides. Correlated electron effects give rise to **metal-insulator transitions** that are driven by small changes in temperature, pressure, or composition, as well as to **superconductivity** - the passage of current with zero resistance at low temperatures. In this chapter we will develop some simple models to understand these interesting and important electronic properties of solids.

5.9.1: Prelude to Electronic Properties of Materials - Superconductors and Semiconductors is shared under a CC BY-SA license and was authored, remixed, and/or curated by LibreTexts.

- **10.1: Prelude to Electronic Properties of Materials - Superconductors and Semiconductors** by Chemistry 310 is licensed CC BY-SA 4.0. Original source: https://en.wikibooks.org/wiki/Introduction_to_Inorganic_Chemistry.

5.9.2: Superconductors

Superconductivity refers to the flow of electrical current in a material with zero resistance. Such materials are very important for use in electromagnets, e.g., in magnetic resonance imaging (MRI) and nuclear magnetic resonance (NMR) machines, because once the current starts flowing in the coils of these magnets it doesn't stop. Magnetic levitation using superconductors - which, below a critical field strength, are perfect diamagnets that are not penetrated by magnetic flux lines - is also potentially relevant to future technologies such as magnetically levitated trains.

The phenomenon of superconductivity, first discovered in Hg metal in 1911 by Onnes, continues to be only partially understood. It is of great interest to physicists as a macroscopic quantum phenomenon, and to chemists and materials scientists who try to make better superconductors (especially those that superconduct at higher temperatures) and devices derived from them, such as superconducting quantum interference devices (SQUIDs), which are extremely sensitive magnetometers.

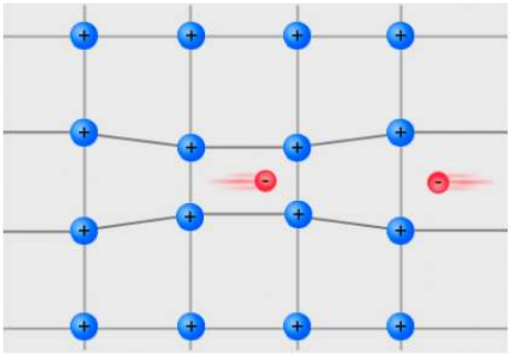


A magnet levitating above a high-temperature superconductor, cooled with liquid nitrogen. Persistent electric current flows on the surface of the superconductor, excluding the magnetic field of the magnet. This current effectively forms an electromagnet that repels the magnet.

Spin pairing and zero resistance

The transition from the metallic to the superconducting state is related to the quantum phenomena of Bose-Einstein condensation and superfluidity. Individual electrons have spin = 1/2, and as such are fermions (particles with half-integer spin). Because of the Pauli exclusion principle, no more than two fermions can occupy the same quantum state (such as an orbital in a molecule or a solid). The familiar consequence of this rule is the aufbau filling of orbitals with spin-paired electrons in each energy level. In contrast, particles with integer spins - which are called bosons - do not have this restriction, and any number of bosons can occupy the same quantized energy level.

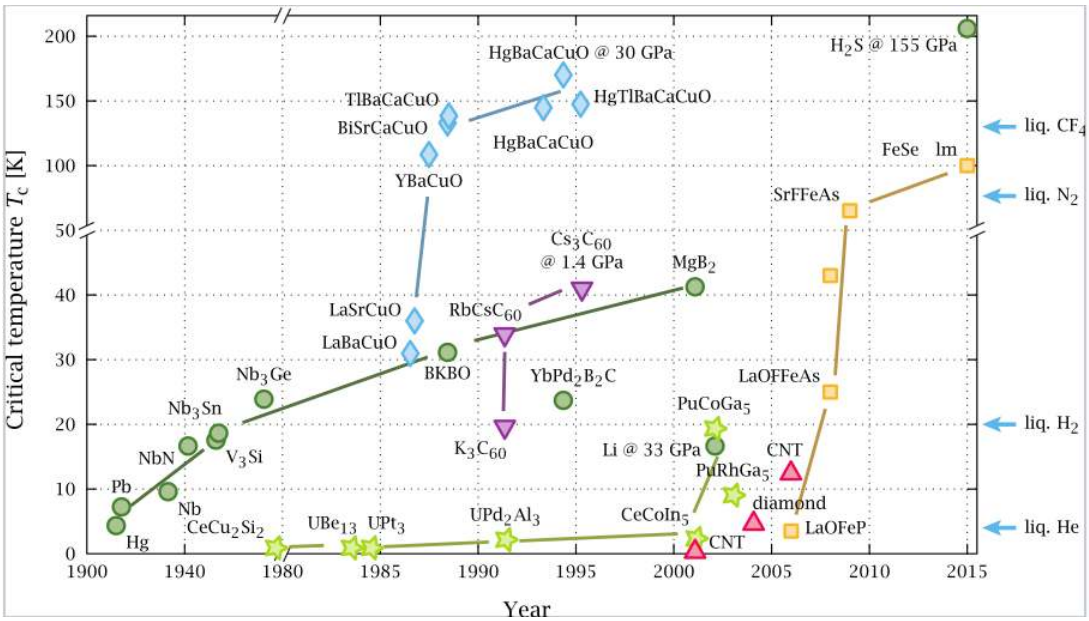
Superconductivity occurs when electrons spin pair into so-called Cooper pairs, which can travel through the lattice together. The electrons in a Cooper pair, although spin-paired, have a long-distance relationship: the spatial extent of a Cooper pair is a few nanometers in cuprate superconductors, and up to one micron in low T_c superconductors such as aluminum. Because its overall spin angular momentum is zero, a Cooper pair is a boson. When the temperature is low enough, the Cooper pairs "condense" into the lowest energy level. The second lowest energy level - which is typically a few meV above the ground state - is not accessible to them as long as the energy gap is larger than the thermal energy, kT. The scattering of electrons by the lattice then becomes forbidden by energy conservation because scattering dissipates energy, and the Cooper pairs cannot change their energy state. Thus the resistance (which arises from scattering, as we learned in Ch. 6) drops abruptly to zero below T_c. However, the Cooper pairs can be broken apart when they move fast, and thus superconductors turn back into normal metals (even below T_c) above some critical current density j_c. This phenomenon is also related to the critical magnetic field, H_c, that quenches superconductivity.



A trampoline for electrons

What causes electrons, which repel each other because of their negative charge, to pair up and travel together in superconductors? The mechanism - which must involve some kind of attractive interaction between electrons - is well understood for "conventional" superconductors which have relatively low transition temperatures, but is not yet known with certainty for high temperature oxide superconductors. In conventional, or BCS superconductors, the spin pairing is mediated by the lattice as shown in the figure at the left. A strong electron-lattice interaction causes a distortion in the lattice as an electron moves through. This elastic deformation is felt as an attractive force by a second electron moving in the opposite direction. This can be thought of as analogous to the interaction of two people jumping on a trampoline. The weight of the first person on the trampoline creates a "well" that attracts the second one, and they tend to move together (even if they don't like each other). Strange as this interaction seems, it is supported experimentally by isotope effects on T_c and by quantitative predictions of T_c values in conventional superconductors.

Bad metals make good superconductors. All superconductors are "normal" metals - with finite electrical resistance - above their critical transition temperature, T_c. If you ask where in the periodic table one might look for superconductors, the answer is surprising. The most conductive metals (Ag, Au, Cu, Cs, etc.) make the worst superconductors, i.e., they have the lowest superconducting transition temperatures, in many cases below 0.01 K. Conversely "bad" metals, such as niobium alloys, certain copper oxides, $K_xBa_{1-x}BiO_3$, MgB_2, FeSe, and alkali salts of C_{60}^{n-} anions, can have relatively high transition temperatures.

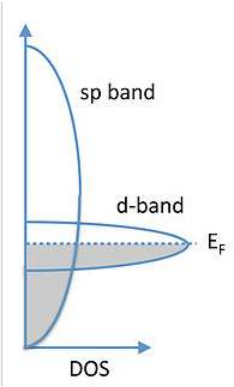


Timeline of superconducting materials, showing T_c vs. year of discovery.

We observe that most good superconductors appear in composition space very **near a metal-insulator transition**. In terms of our microscopic picture, orbital overlap in superconductors is poor, just barely enough to make them act as metals ($\Delta \approx U$) above T_c. In the normal state, superconductors with high T_c - which can be as high as 150 K - are typically "bad" metals. An important

characteristic of such metals is that the **mean free path** of electrons (in the normal state, above T_c) is on the order of the lattice spacing, i.e., **only a few Å**. In contrast, we learned in Ch. 6 that good metals such as Au, Ag, and Cu have electron mean free paths that are two orders of magnitude longer (ca. 40 nm). In a bad metal, the electron "feels" the lattice rather strongly, whereas in a good metal, the electrons are insensitive to small changes in the distance between metals atoms.

What does the band picture look like for a bad metal? The key point is that because orbital overlap is poor, the metal has a **high density of states** at the Fermi level. This is a universal property of high temperature superconductors and provides a clue of where to look for new and improved superconducting materials. Recall that transition elements in the middle of the 3d series (Cr, Fe, Co, Ni) were magnetic because of poor orbital overlap and weak d-d bonding. The elements below these - especially Nb, Ta, and W - have just barely enough d-d orbital overlap to be on the metallic side of the metal-insulator transition and to be "bad" metals. Carbides and nitrides of these elements are typically superconducting, with the carbon and nitrogen atoms serving to adjust the valence electron density, as illustrated in the table below.



Generic E vs. DOS for a bad metal.

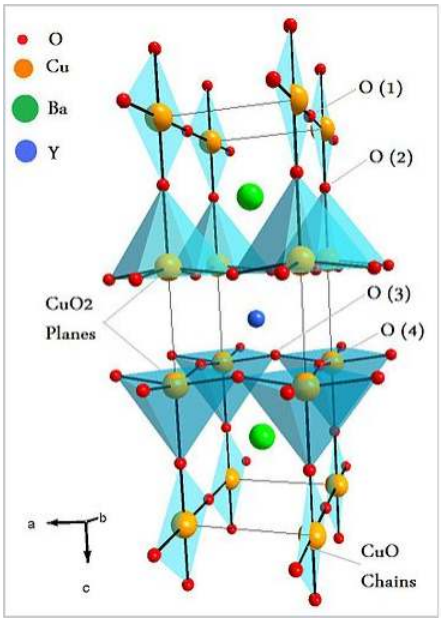
Compound	NbC	Mo_2N	TaC	VN	NbN	TaN	Nb_3Ge
T_c (K)	11.1	5.0	9.7	7.5	15.2	17.8	22.3

High T_c superconductors

In addition to having weak orbital overlap in the metallic state - which results in a high DOS at E_F - high temperature superconductors also typically contain elements in mixed oxidation states (for example, $Cu^{2+/3+}$ or $Bi^{3+/5+}$) that are close in energy to the O^{2-}/O^- couple in the lattice. At ambient pressure, cuprate superconductors have the highest known T_c values, ranging between about 35 and 150 K. The crystal structures of these materials are almost all variants of the perovskite lattice, as shown at the right for the 1-2-3 superconductor $YBa_2Cu_3O_{7-\delta}$. An ideal perovskite lattice would have formula $ABO_3 = A_3B_3O_9$. In $YBa_2Cu_3O_{7-\delta}$, Y and Ba occupy the A cation sites, Cu occupies the B sites, and two of the nine O atoms are missing.

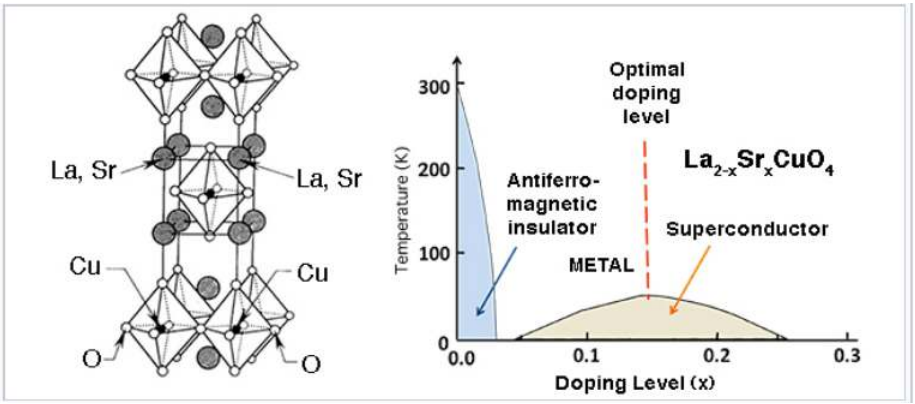
The $YBa_2Cu_3O_{7-\delta}$ lattice consists of mixed-valent copper(II/III) oxide sheets capped by oxygen atoms to form CuO_5 square pyramids. These sheets encapsulate the Y^{3+} cations. Copper(II) oxide ribbons that share the apical oxygen atoms of the square pyramids run in one direction through the structure. In $YBa_2Cu_3O_{7-\delta}$ and related materials, one component of the structure (here the Cu-O ribbons) acts as a **charge reservoir** to control the doping of the planar CuO_2 sheets, which are the elements of the structure

that carry the supercurrent. Cuprate superconductors with Bi, Tl, or Hg-containing charge reservoir layers and multiple, eclipsed CuO_2 sheets in the unit cell tend to have the highest T_c values.



Crystal structure of $YBa_2Cu_3O_{7-\delta}$ (YBCO), the first superconductor with T_c above the boiling point of liquid nitrogen.

The connection between the metal-insulator transtion and superconductivity is nicely illustrated in the phase diagram of $La_{2-x}Sr_xCuO_4$, the first cuprate superconductor, which was discovered in 1986 by Georg Bednorz and K. Alex Müller. This compound has a rather simple structure in which rocksalt La(Sr)O layers are intergrown with perovskite La(Sr)CuO_3 layers. Undoped La_2CuO_4 contains only Cu^{2+} ions and is an antiferromagnetic insulator. As a small amount of Sr^{2+} is substituted for La^{3+}, some of the Cu^{2+} is oxidized to Cu^{3+}, and the lattice is doped with holes. As the doping level increases, the antiferromagnetic phase undergoes a first-order phase transition to a "bad" metal, and at slightly higher doping density the superconducting phase appears. The proximity of the superconducting phase to the metal-insulator transition is a hallmark of cuprate superconductors. A maximum T_c of 35K is observed at x = 0.15. Doping at higher levels moves the Fermi level beyond the point of highest DOS in the d-band of Cu and the superconducting phase then gradually disappears. It is interesting to compare this phase diagram with that of V_2O_3 (above), which also undergoes an antiferromagnetic insulator to "bad" metal transition as it is doped.



Crystal structure and phase diagram of the cuprate superconductor $La_{2-x}Sr_xCuO_4$. (LSCO)

5.9.2: Superconductors is shared under a CC BY-SA license and was authored, remixed, and/or curated by LibreTexts.

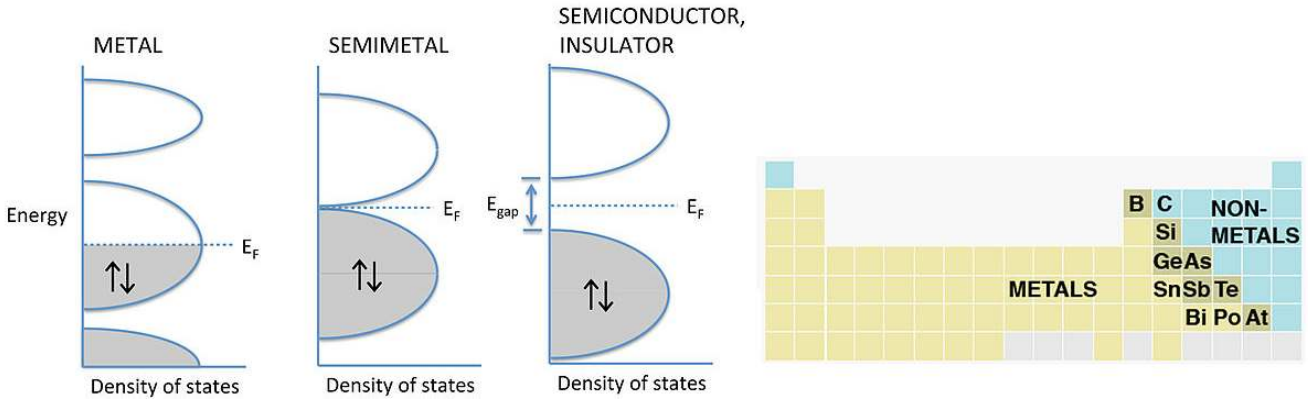
- **10.3: Superconductors** by Chemistry 310 is licensed CC BY-SA 4.0. Original source: https://en.wikibooks.org/wiki/Introduction_to_Inorganic_Chemistry.

5.9.3: Periodic Trends- Metals, Semiconductors, and Insulators

As we consider periodic trends in the electronic properties of materials, it is important to review some of the key bonding trends we have learned in earlier chapters:

- Going down the periodic table, atoms in solids tend to adopt structures with higher coordination numbers.
- The second row of the periodic table is special, with strong s-p hybridization and π-bonding between atoms.
- Electrons in higher quantum shells are less strongly bound, so the energy difference between bonding and antibonding orbitals becomes smaller for heavier atoms.

We also know that most of the elements in the periodic table are metals, but the elements in the top right corner are insulating under ordinary conditions (1 atm. pressure) and tend to obey the octet rule in their compounds.



At the transition between metals and non-metals in the periodic table we encounter a crossover in electronic properties, as well as in other properties such as the acidity of the oxides (see Ch. 3). The group of elements at the border is loosely referred to as the metalloids. Several of these elements (such as C, Sn, and As) can exist as different allotropes that can be metals, insulators, or something in between.

A more rigorous delineation of the electronic properties of these elements (and of many compounds) can be made by considering their band structures and the **temperature dependence of the electronic conductivity**. As we have previously discussed, metals have partially filled energy bands, meaning that the Fermi level intersects a partially filled band. With increasing temperature, metals become poorer conductors because lattice vibrations (which are called phonons in the physics literature) scatter the mobile valence electrons. In contrast, semiconductors and insulators, which have filled and empty bands, become better conductors at higher temperature, since some electrons are thermally excited to the lowest empty band. The distinction between insulators and semiconductors is arbitrary, and from the point of view of metal-insulator transitions, all semiconductors are insulators. We typically call an insulator a semiconductor if its band gap (E_{gap}) is less than about 3 eV. A semimetal is a material that has a band gap near zero, examples being single sheets of sp^2-bonded carbon (graphene) and elemental Bi. Like a narrow gap semiconductor, a semimetal has higher conductivity at higher temperature.

5.9.3: Periodic Trends- Metals, Semiconductors, and Insulators is shared under a CC BY-SA license and was authored, remixed, and/or curated by LibreTexts.

- **10.4: Periodic Trends- Metals, Semiconductors, and Insulators** by Chemistry 310 is licensed CC BY-SA 4.0. Original source: https://en.wikibooks.org/wiki/Introduction_to_Inorganic_Chemistry.

5.9.4: Semiconductors- Band Gaps, Colors, Conductivity and Doping

Semiconductors, as we noted above, are somewhat arbitrarily defined as insulators with **band gap energy ≤ 3.0 eV** (~290 kJ/mol). This cutoff is chosen because, as we will see, the conductivity of undoped semiconductors drops off exponentially with the band gap energy and at 3.0 eV it is very low. Also, materials with wider band gaps (e.g. $SrTiO_3$, E_{gap} = 3.2 eV) do not absorb light in the visible part of the spectrum

There are a number of places where we find semiconductors in the periodic table:

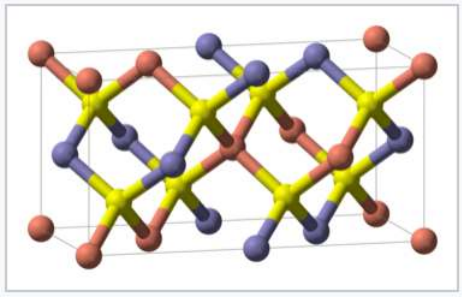
- Early transition metal oxides and nitrides, especially those with d^0 electron counts such as TiO_2, TaON, and WO_3
- Oxides of later 3d elements such as Fe_2O_3, NiO, and Cu_2O
- Layered transition metal chalcogenides with d^0, d^2 and d^6 electron counts including TiS_2, ZrS_2, MoS_2, WSe_2, and PtS_2
- d^{10} copper and sliver halides, e.g., CuI, AgBr, and AgI
- Zincblende- and wurtzite-structure compounds of the p-block elements, especially those that are isoelectronic with Si or Ge, such as GaAs and CdTe. While these are most common, there are other p-block semiconductors that are not isoelectronic and have different structures, including GaS, PbS, and Se.



A 2" wafer cut from a GaAs single crystal. GaAs, like many p-block semiconductors, has the zincblende structure.

The **p-block octet semiconductors** are by far the most studied and important for technological applications, and are the ones that we will discuss in detail.

Zincblende- and wurtzite-structure semiconductors have 8 valence electrons per 2 atoms. These combinations include 4-4 (Si, Ge, SiC,…), 3-5 (GaAs, AlSb, InP,…), 2-6 (CdSe, HgTe, ZnO,…), and 1-7 (AgCl, CuBr,…) semiconductors. Other variations that add up to an octet configuration are also possible, such as $Cu^{I}In^{III}Se_2$, which has the **chalcopyrite** structure, shown at the right.



The **chalcopyrite structure** is adopted by ABX_2 octet semiconductors such as $Cu^{I}In^{III}Se_2$ and $Cd^{II}Sn^{IV}P_2$. The unit cell is doubled relative to the parent **zincblende structure** because of the ordered arrangement of cations. Each anion (yellow) is coordinated by two cations of each type (blue and red).

How does the **band gap energy** vary with **composition**? There are two important trends

(1) Going **down a group** in the periodic table, the gap **decreases**:

C (diamond) > Si > Ge > α-Sn

E_{gap} (eV): 5.4 1.1 0.7 0.0

This trend can be understood by recalling that E_{gap} is related to the **energy splitting between bonding and antibonding orbitals**. This difference decreases (and bonds become weaker) as the principal quantum number increases.

(2) For isoelectronic compounds, **increasing ionicity** results in a **larger band gap**.

Ge < GaAs < ZnSe

0.7 1.4 2.8 eV

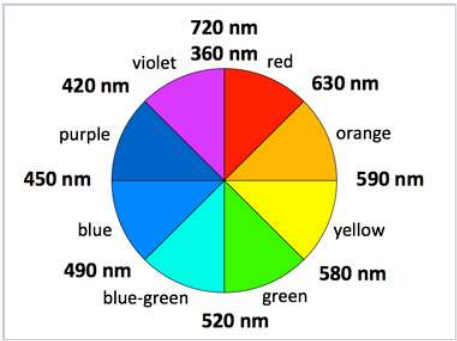
Sn < InSb < CdTe < AgI

0.0 0.2 1.6 2.8 eV

This trend can also be understood from a simple MO picture, as we discussed in Ch. 2. As the electronegativity difference Δχ increases, so does the energy difference between bonding and antibonding orbitals.

The band gap is a very important property of a semiconductor because it determines its color and conductivity. Many of the applications of semiconductors are related to band gaps:

- Narrow gap materials ($Hg_xCd_{1-x}Te$, VO_2, InSb, Bi_2Te_3) are used as infrared photodetectors and thermoelectrics (which convert heat to electricity).
- Wider gap materials (Si, GaAs, GaP, GaN, CdTe, $CuIn_xGa_{1-x}Se_2$) are used in electronics, light-emitting diodes, and solar cells.



Color wheel showing the colors and wavelengths of emitted light.

Semiconductor solid solutions such as $GaAs_{1-x}P_x$ have band gaps that are intermediate between the end member compounds, in this case GaAs and GaP (both zincblende structure). Often, there is a linear relation between composition and band gap, which is referred to as **Vegard's Law**. This "law" is often violated in real materials, but nevertheless offers useful guidance for designing materials with specific band gaps. For example, red and orange light-emitting diodes (LED's) are made from solid solutions with compositions of $GaP_{0.40}As_{0.60}$ and $GaP_{0.65}As_{0.35}$, respectively. Increasing the mole fraction of the lighter element (P) results in a larger band gap, and thus a higher energy of emitted photons.

Colors of semiconductors

The color of absorbed and emitted light both depend on the band gap of the semiconductor. Visible light covers the range of approximately 390-700 nm, or 1.8-3.1 eV. The **color of emitted light** from an LED or semiconductor laser corresponds to the band gap energy and can be read off the color wheel shown at the right.



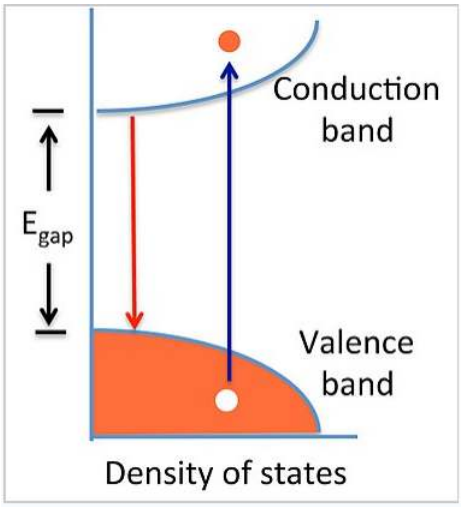
Fe_2O_3 powder is reddish orange because of its 2.2 eV band gap

The color of **absorbed light** includes the band gap energy, but also all colors of higher energy (shorter wavelength), because electrons can be excited from the valence band to a range of energies in the conduction band. Thus semiconductors with band gaps in the infrared (e.g., Si, 1.1 eV and GaAs, 1.4 eV) appear black because they absorb all colors of visible light. Wide band gap semiconductors such as TiO_2 (3.0 eV) are white because they absorb only in the UV. Fe_2O_3 has a band gap of 2.2 eV and thus absorbs light with $\lambda < 560$ nm. It thus appears reddish-orange (the colors of light reflected from Fe_2O_3) because it absorbs green, blue, and violet light. Similarly, CdS (E_{gap} = 2.6 eV) is yellow because it absorbs blue and violet light.

Electrons and holes in semiconductors

Pure (undoped) semiconductors can conduct electricity when electrons are promoted, either by heat or light, from the valence band to the conduction band. The promotion of an **electron** (e^-) leaves behind a **hole** (h^+) in the valence band. The hole, which is the absence of an electron in a bonding orbital, is also a mobile charge carrier, but with a positive charge. The motion of holes in the lattice can be pictured as analogous to the movement of an empty seat in a crowded theater. An empty seat in the middle of a row can move to the end of the row (to accommodate a person arriving late to the movie) if everyone moves over by one seat. Because the movement of the hole is in the opposite direction of electron movement, it acts as a positive charge carrier in an electric field.

The opposite process of excitation, which creates an electron-hole pair, is their recombination. When a conduction band electron drops down to recombine with a valence band hole, both are annihilated and energy is released. This release of energy is responsible for the emission of light in LEDs.



An electron-hole pair is created by adding heat or light energy E ≥ E_{gap} to a semiconductor (blue arrow). The electron-hole pair recombines to release energy equal to E_{gap} (red arrow).

At equilibrium, the creation and annihilation of electron-hole pairs proceed at equal rates. This dynamic equilibrium is analogous to the dissociation-association equilibrium of H^+ and OH^- ions in water. We can write a mass action expression:

$$n \times p = K_{eq} = n_i^2$$

where n and p represent the number density of electrons and holes, respectively, in units of cm^{-3}. The intrinsic carrier concentration, n_i, is equal to the number density of electrons or holes in an undoped semiconductor, where $n = p = n_i$.

Note the similarity to the equation for water autodissociation:

$$[H^+][OH^-] = K_w$$

By analogy, we will see that when we increase n (e.g., by doping), p will decrease, and vice-versa, but their product will remain constant at a given temperature.

Temperature dependence of the carrier concentration. Using the equations $K_{eq} = e^{(\frac{-\Delta G^o}{RT})}$ and $\Delta G^o = \Delta H^o - T\Delta S^o$, we can write:

$$n \times p = n_i^2 = e^{(\frac{\Delta S^o}{R})} e^{(\frac{-\Delta H^o}{RT})} \tag{5.9.4.1}$$

The entropy change for creating electron hole pairs is given by:

$$\Delta S^o = Rln(N_V) + Rln(N_V) = Rln(N_C N_V) \tag{5.9.4.2}$$

where N_V and N_C are the effective density of states in the valence and conduction bands, respectively.

and thus we obtain

$$n_i^2 = N_C N_V e^{(-\Delta H^o RT)} \tag{5.9.4.3}$$

Since the volume change is negligible, $\Delta H^o \approx \Delta E^o$, and therefore $\frac{\Delta H^o}{R} \approx \frac{E_{gap}}{k}$, from which we obtain

$$n_i^2 = N_C N_V e^{(\frac{-E_{gap}}{kT})} \tag{5.9.4.4}$$

and finally

$$\mathbf{n = p = n_i = (N_C N_V)^{\frac{1}{2}} e^{(\frac{-E_{gap}}{2kT})}} \tag{5.9.4.5}$$

For pure Si (E_{gap} = 1.1 eV) with N ≈ 10^{22}/cm^3, we can calculate from this equation a carrier density n_i of approximately 10^{10}/cm^3 at 300 K. This is about 12 orders of magnitude lower than the valence electron density of Al, the element just to the left of Si in the periodic table. Thus we expect the conductivity of pure semiconductors to be many orders of magnitude lower than those of metals.

Conductivity of intrinsic semiconductors

The conductivity (σ) is the product of the number density of carriers (n or p), their charge (e), and their mobility (μ). Recall from Chapter 6 that μ is the ratio of the carrier drift velocity to the electric field and has units of cm^2/Volt-second. Typically electrons and holes have somewhat different mobilities (μ_e and μ_h, respectively) so the conductivity is given by:

$$\sigma = ne\mu_e + pe\mu_h \tag{5.9.4.6}$$

For either type of charge carrier, we recall from Ch. 6 that the mobility μ is given by:

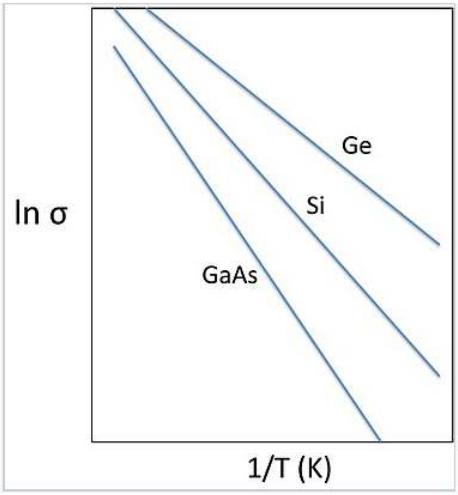
$$\mu = \frac{v_{drift}}{E} = \frac{e\tau}{m} \tag{5.9.4.7}$$

where e is the fundamental unit of charge, τ is the scattering time, and m is the effective mass of the charge carrier.

Taking an average of the electron and hole mobilities, and using n = p, we obtain

$$\sigma = \sigma_o e^{\left(\frac{-E_{gap}}{2kT}\right)},\ where\ \sigma_o = 2(N_C N_V)^{\frac{1}{2}} e\mu \tag{5.9.4.8}$$

By measuring the conductivity as a function of temperature, it is possible to obtain the activation energy for conduction, which is $E_{gap}/2$. This kind of plot, which resembles an Arrhenius plot, is shown at the right for three different undoped semiconductors. The slope of the line in each case is $-E_{gap}/2k$.



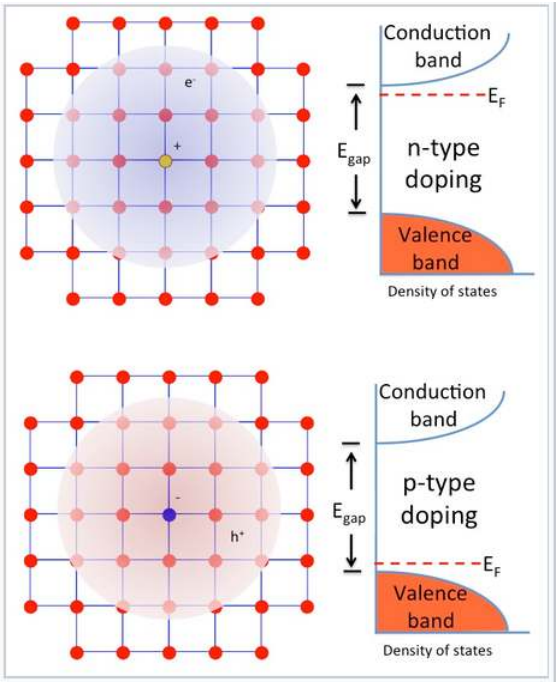
Plots of ln(σ) vs. inverse temperature for intrinsic semiconductors Ge (E_{gap} = 0.7 eV), Si (1.1 eV) and GaAs (1.4 eV). The slope of the line is $-E_{gap}/2k$.

Doping of semiconductors. Almost all applications of semiconductors involve controlled **doping**, which is the substitution of impurity atoms, into the lattice. Very small amounts of dopants (in the parts-per-million range) dramatically affect the conductivity of semiconductors. For this reason, very pure semiconductor materials that are carefully doped - both in terms of the concentration and spatial distribution of impurity atoms - are needed.

n- and p-type doping. In crystalline Si, each atom has four valence electrons and makes four bonds to its neighbors. This is exactly the right number of electrons to completely fill the valence band of the semiconductor. Introducing a phosphorus atom into the lattice (the positively charged atom in the figure at the right) adds an extra electron, because P has five valence electrons and only needs four to make bonds to its neighbors. The extra electron, at low temperature, is bound to the phosphorus atom in a hydrogen-like molecular orbital that is much larger than the 3s orbital of an isolated P atom because of the high dielectric constant of the semiconductor. In silicon, this "expanded" Bohr radius is about 42 Å, i.e., 80 times larger than in the hydrogen atom. The energy needed to ionize this electron – to allow it to move freely in the lattice - is only about 40–50 meV, which is not much larger

the thermal energy (26 meV) at room temperature. Therefore the Fermi level lies just below the conduction band edge, and a large fraction of these extra electrons are promoted to the conduction band at room temperature, leaving behind fixed positive charges on the P atom sites. The crystal is **n-doped**, meaning that the majority carrier (electron) is negatively charged.

Alternatively, boron can be substituted for silicon in the lattice, resulting in **p-type** doping, in which the majority carrier (hole) is positively charged. Boron has only three valence electrons, and "borrows" one from the Si lattice, creating a positively charged hole that exists in a large hydrogen-like orbital around the B atom. This hole can become delocalized by promoting an electron from the valence band to fill the localized hole state. Again, this process requires only 40–50 meV, and so at room temperature a large fraction of the holes introduced by boron doping exist in delocalized valence band states. The Fermi level (the electron energy level that has a 50% probability of occupancy at zero temperature) lies just above the valence band edge in a p-type semiconductor.



n- and p-type doping of semiconductors involves substitution of electron donor atoms (light orange) or acceptor atoms (blue) into the lattice. These substitutions introduce extra electrons or holes, respectively, which are easily ionized by thermal energy to become free carriers. The Fermi level of a doped semiconductor is a few tens of mV below the conduction band (n-type) or above the valence band (p-type).

As noted above, the doping of semiconductors dramatically changes their conductivity. For example, the intrinsic carrier concentration in Si at 300 K is about 10^{10} cm^{-3}. The mass action equilibrium for electrons and holes also applies to doped semiconductors, so we can write:

$$n \times p = n_i^2 = 10^{20} cm^{-6} \; at \; 300K \tag{5.9.4.9}$$

If we substitute P for Si at the level of one part-per-million, the concentration of electrons is about 10^{16} cm^{-3}, since there are approximately 10^{22} Si atoms/cm^3 in the crystal. According to the mass action equation, if n = 10^{16}, then p = 10^4 cm^{-3}. There are three consequences of this calculation:

- The density of carriers in the doped semiconductor (10^{16} cm^{-3}) is much higher than in the undoped material (~10^{10} cm^{-3}), so the conductivity is also many orders of magnitude higher.
- The activation energy for conduction is only 40–50 meV, so the conductivity does not change much with temperature (unlike in the intrinsic semiconductor)
- The minority carriers (in this case holes) do not contribute to the conductivity, because their concentration is so much lower than that of the majority carrier (electrons).

Similarly, for p-type materials, the conductivity is dominated by holes, and is also much higher than that of the intrinsic semiconductor.

Chemistry of semiconductor doping. Sometimes it is not immediately obvious what kind of doping (n- or p-type) is induced by "messing up" a semiconductor crystal lattice. In addition to substitution of impurity atoms on normal lattice sites (the examples given above for Si), it is also possible to dope with vacancies - missing atoms - and with interstitials - extra atoms on sites that are not ordinarily occupied. Some simple rules are as follows:

- For substitutions, adding an **atom to the right** in the periodic table results in **n-type** doping, and an atom to the **left** in **p-type** doping.

  For example, when TiO_2 is doped with Nb on some of the Ti sites, or with F on O sites, the result is n-type doping. In both cases, the impurity atom has one more valence electron than the atom for which it was substituted. Similarly, substituting a small amount of Zn for Ga in GaAs, or a small amount of Li for Ni in NiO, results in p-type doping.

- **Anion vacancies** result in **n-type** doping, and **cation vacancies** in **p-type** doping.

  Examples are anion vacancies in CdS_{1-x} and WO_{3-x}, both of which give n-type semiconductors, and copper vacancies in $Cu_{1-x}O$, which gives a p-type semiconductor.

- **Interstitial cations** (e.g. Li) donate electrons to the lattice resulting in **n-type** doping. Interstitial anions are rather rare but would result in p-type doping.

Sometimes, there can be both p- and n-type dopants in the same crystal, for example B and P impurities in a Si lattice, or cation and anion vacancies in a metal oxide lattice. In this case, the two kinds of doping **compensate** each other, and the doping type is determined by the one that is in higher concentration. A dopant can also be present on more than one site. For example, Si can occupy both the Ga and As sites in GaAs, and the two substitutions compensate each other. Si has a slight preference for the Ga site, however, resulting in n-type doping.

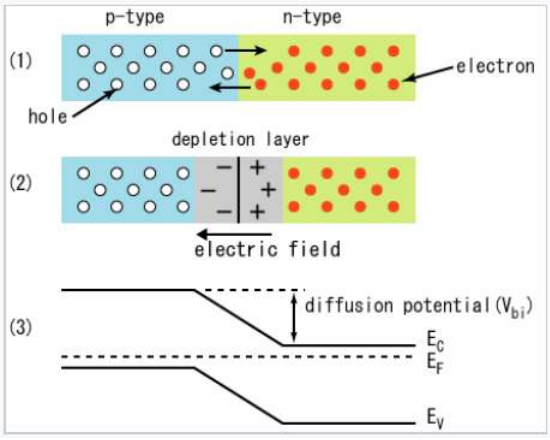
5.9.4: Semiconductors- Band Gaps, Colors, Conductivity and Doping is shared under a CC BY-SA license and was authored, remixed, and/or curated by LibreTexts.

- **10.5: Semiconductors- Band Gaps, Colors, Conductivity and Doping** by Chemistry 310 is licensed CC BY-SA 4.0. Original source: https://en.wikibooks.org/wiki/Introduction_to_Inorganic_Chemistry.

5.9.5: Semiconductor p-n Junctions

Semiconductor p-n junctions are important in many kinds of electronic devices, including diodes, transistors, light-emitting diodes, and photovoltaic cells. To understand the operation of these devices, we first need to look at what happens to electrons and holes when we bring p-type and n-type semiconductors together. At the junction between the two materials, mobile electrons and holes annihilate each other, leaving behind the fixed + and - charges of the electron donor and electron acceptor dopants, respectively. For example, on the n-side of a silicon p-n junction, the positively charged dopants are P^+ ions and on the p-side the negatively charged dopants are B^-. The presence of these uncompensated electrical charges creates an electric field, the **built-in field** of the p-n junction. The region that contains these charges (and a very low density of mobile electrons or holes) is called the **depletion region**.

The electric field, which is created in the depletion region by electron-hole recombination, repels both the electrons (on the n-side) and holes (on the p-side) away from the junction. The concentration gradient of electrons and holes, however, tends to move them in the opposite direction by diffusion. At equilibrium, the flux of mobile carriers is zero because the field-driven migration flux is equal and opposite to the concentration-driven diffusion flux.



When p-type and n-type semiconductors are joined, electrons and holes are annihilated at the interface, leaving a depletion region that contains positively and negatively charged donor and acceptor atoms, respectively. At equilibrium, the Fermi level (E_F) is uniform throughout the junction. E_F lies just above the valence band on the p-type side of the junction and just below the conduction band on the n-type side.

The width of the depletion layer depends on the screening length in the semiconductor, which in turn depends on the dopant density. At high doping levels, the depletion layer is narrow (tens of nanometers across), whereas at low doping density it can be as thick as 1 μm. The depletion region is the only place where the electric field is nonzero, and the only place where the bands bend. Elsewhere in the semiconductor the field is zero and the bands are flat.

In the middle of p-n junction, the Fermi level energy, E_F, is halfway between the valence band, VB, and the conduction band, CB, and the semiconductor is intrinsic ($n = p = n_i$)

5.9.5: Semiconductor p-n Junctions is shared under a CC BY-SA license and was authored, remixed, and/or curated by LibreTexts.

- **10.6: Semiconductor p-n Junctions** by Chemistry 310 is licensed CC BY-SA 4.0. Original source: https://en.wikibooks.org/wiki/Introduction_to_Inorganic_Chemistry.

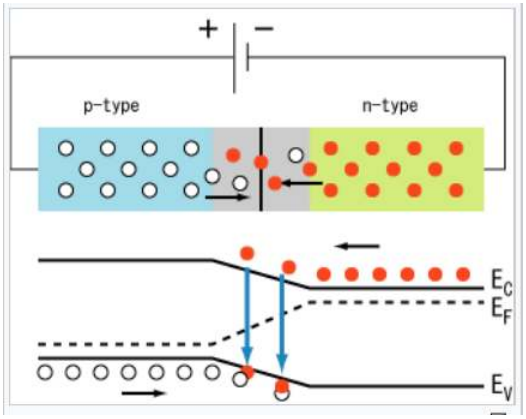
5.9.6: Diodes, LEDs and Solar Cells

Diodes are semiconductor devices that allow current to flow in only one direction. Diodes act as rectifiers in electronic circuits, and also as efficient light emitters (in LEDs) and solar cells (in photovoltaics). The basic structure of a diode is a junction between a p-type and an n-type semiconductor, called a p-n junction. Typically, diodes are made from a single semiconductor crystal into which p- and n- dopants are introduced.



Closeup of a diode, showing the square-shaped semiconductor crystal *(black object on left)* (John Maushammer, Wikipedia, CC-BY-SA)

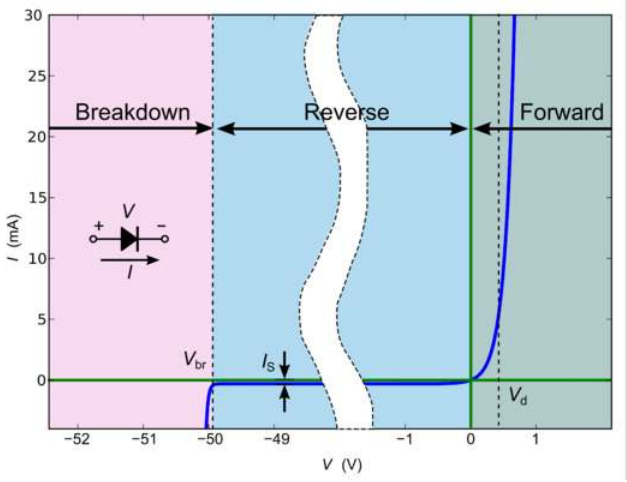
If the n-side of a diode is biased at positive potential and the p-side is biased negative, electrons are drawn to the n-side and holes to the p-side. This reinforces the built in potential of the p-n junction, the width of the depletion layer increases, and very little current flows. This polarization direction is referred to as "back bias." If the diode is biased the other way, carriers are driven into the junction where they recombine. The electric field is diminished, the bands are flattened, and current flows easily since the applied bias lowers the built-in potential. This is called "forward bias."



Electrons (red) and holes (white) in a forward-biased diode. (S-kei. Wikipedia, CC-BY-SA)

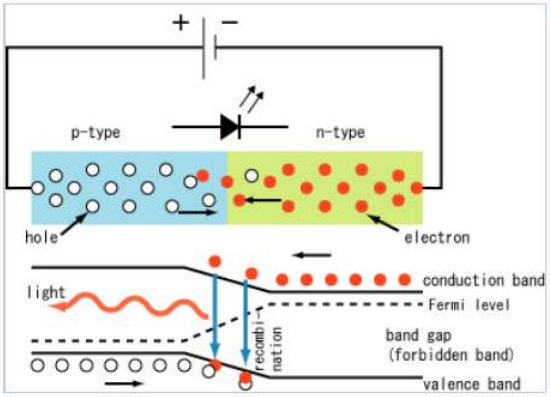
The figure on the left illustrates a forward-biased diode, through which current flows easily. As electrons and holes are driven into the junction (black arrows in lower left figure), they recombine (downward blue arrows), producing light and/or heat. The Fermi level in the diode is indicated as the dotted line. There is a drop in the Fermi level (equal to the applied bias) across the depletion layer. The corresponding diode i-V curve is shown on the right. The current rises exponentially with applied voltage in the forward

bias direction, and there is very little leakage current under reverse bias. At very high reverse bias (typically tens of volts) diodes undergo avalanche breakdown and a large reverse current flows.



Diode i-V curve

A **light-emitting diode** or **LED** is a kind of diode that converts some of the energy of electron-hole recombination into light. This radiative recombination process always occurs in competition with non-radiative recombination, in which the energy is simply converted to heat. When light is emitted from an LED, the photon energy is equal to the bandgap energy. Because of this, LED lights have pure colors and narrow emission spectra relative to other light sources, such as incandescent and fluorescent lights. LED lights are energy-efficient and thus are typically cool to the touch.



Light-emitting diode (LED). (S-kei. Wikipedia, CC-BY-SA)

Direct-gap semiconductors such as GaAs and GaP have efficient luminescence and are also good light absorbers. In direct gap semiconductors, there is no momentum change involved in electron-hole creation or recombination. That is, the electrons and holes originate at the same value of the momentum wavevector **k**, which we encountered in Ch. 6. **k** is related to the momentum (also a vector quantity) by **p** = h**k**/2π. In a direct-gap semiconductor, the top of the valence band and the bottom of the conduction band most typically both occur at **k** = 0. Since the momentum of the photon is close to zero, photon absorption and emission are strongly allowed (and thus kinetically fast). Polar semiconductors such as GaAs, GaN, and CdSe are typically direct-gap materials. **Indirect-gap** semiconductors such as Si and Ge absorb and emit light very weakly because the valence band maximum and conduction band minimum do not occur at the same point in k-space. This means that a lattice vibration (a phonon) must also be created or annihilated in order to conserve momentum. Since this "three body" (electron, hole, phonon) process has low probability, the radiative recombination of electrons and holes is slow relative to non-radiative decay - the thermalization of electron-hole

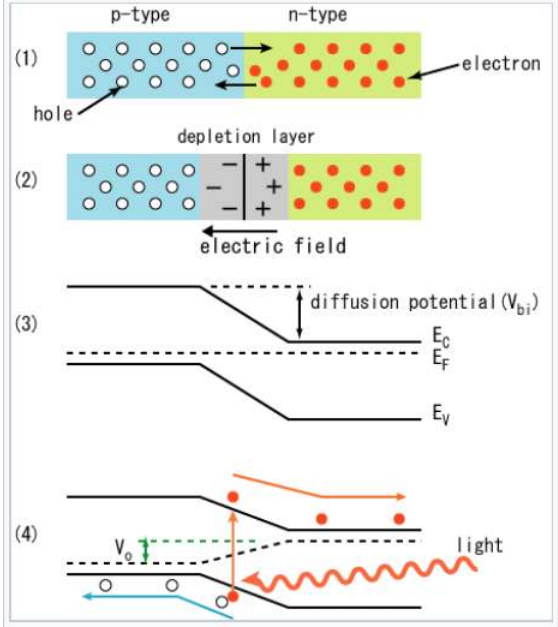
energy as lattice vibrations - in indirect-gap semiconductors. The momentum selection rule thus prevents light absorption/emission and there are no pure Si LEDs or Si-based lasers.



Prof. Shuji Nakamura holding a blue LED.

While red, orange, yellow, and green LEDs can be fabricated relatively easily from AlP-GaAs solid solutions, it was initially very difficult to fabricate blue LEDs because the best direct gap semiconductor with a bandgap in the right energy range is a nitride, GaN, which is difficult to make and to dope p-type. Working at Nichia Corporation in Japan, Shuji Nakamura succeeded in developing a manufacturable process for p-GaN, which is the basis of the blue LED. Because of the importance of this work in the development of information storage (Blu-Ray technology) and full-spectrum, energy-efficient LED lighting, Nakamura shared the 2014 Nobel Prize in Physics with Isamu Asaki and Hiroshi Amano, both of whom had made earlier contributions to the development of GaN diodes.

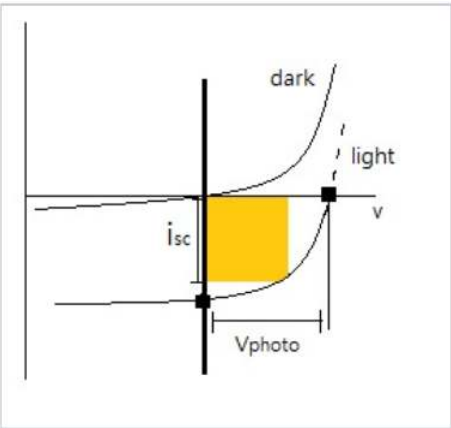
A **Solar cell**, or photovoltaic cell, converts light absorbed in a p-n junction directly to electricity by the photovoltaic effect. Photovoltaics is the field of technology and research related to the development of solar cells for conversion of solar energy to electricity. Sometimes the term solar cell is reserved for devices intended specifically to capture energy from sunlight, whereas the term photovoltaic cell is used when the light source is unspecified.



Photovoltaic effect in a semiconductor p-n junction. (S-kei. Wikipedia, CC-BY-SA)

Photocurrent in p-n junction solar cells flows in the diode reverse bias direction. In the dark, the solar cell simply acts as a diode. In the light, the photocurrent can be thought of as a constant current source, which is added to the i-V characteristic of the diode. The

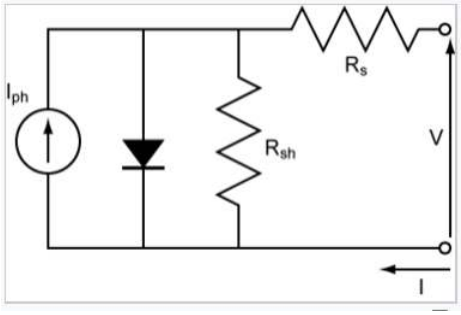
relationship between the dark and light current in a photovoltaic cell is shown in the diagram at the left.



Current-voltage characteristic of a solar cell in the dark and under illumination with band gap light. The short-circuit photocurrent is indicated as i_{sc}, and the open-circuit photovoltage is V_{photo}. The maximum power generated by the solar cell is determined by the area of the orange box.

The built-in electric field of the p-n junction separates e^- h^+ pairs that are formed by absorption of bandgap light in the depletion region. The electrons flow downhill, towards the n-type side of the junction, the holes flow uphill towards the p-side. If $h\nu \geq E_{gap}$, light can be absorbed by promoting an electron from the valence band to the conduction band. Any excess energy is rapidly thermalized. Light with $h\nu > E_g$ thus can store only E_g worth of energy in an e^- h^+ pair. If light is absorbed outside of depletion region, i.e., on the n- or p-side of the junction where there is no electric field, minority carriers must diffuse into the junction in order to be collected. This process occurs in competition with electron-hole recombination. Because impurity atoms and lattice defects make efficient recombination centers, semiconductors used in solar cells (especially indirect-gap materials such as Si, which must be relatively thick in order to absorb most of the solar spectrum) must be very pure. Most of the cost of silicon solar cells is associated with the process of purifying elemental silicon and growing large single crystals from the melt.

In the photodiode i-V curve above, V_{photo} is typically only about 70% of the bandgap energy E_{gap}. The photocurrent is limited by the photon flux, the recombination rate, and the re-emission of absorbed light.[6] The area of the orange rectangle indicates the power generated by the solar cell, which can be calculated as P = i x V. In good single crystal or polycrystalline solar cells made of Si, GaAs, CdTe, $CuIn_xGa_{1-x}Se_2$, or $(CH_3NH_3)PbI_3$ the quantum yield (the ratio of short circuit photocurrent to photon flux) is close to unity.

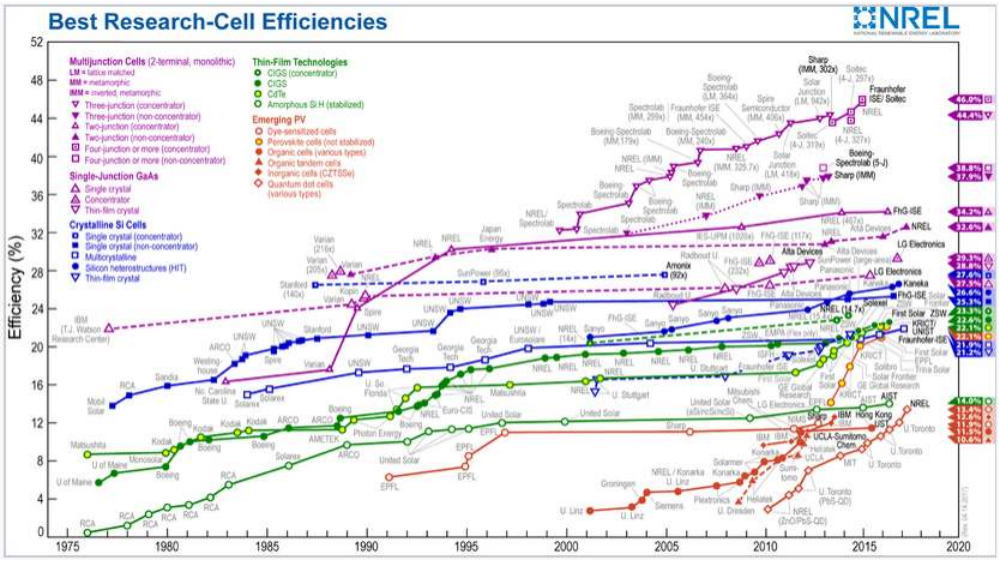


The equivalent circuit of a p-n junction solar cell, which results in the "light" i-V curve shown in the figure above. The solar cell is effectively a diode with a reverse-bias current source provided by light-generated electrons and holes. The shunt resistance (R_{sh}) in the equivalent circuit represents parasitic electron-hole recombination. A high shunt resistance (low recombination rate) and low series resistance (R_s) are needed for high solar cell efficiency.

Solar cells have many current applications. Individual cells are used for powering small devices such as electronic calculators. Photovoltaic arrays generate a form of renewable electricity, particularly useful in situations where electrical power from the grid is

unavailable such as in remote area power systems, Earth-orbiting satellites and space probes, remote radio-telephones and water pumping applications. Photovoltaic electricity is also increasingly deployed in grid-tied electrical systems.

The cost of installed photovoltaics (calculated on a per-watt basis) has dropped over the past decade at a rate of about 13% per year, and has already reached grid parity in Germany and a number of other countries.[7] Photovoltaic grid parity is anticipated in U.S. power markets in the 2020 timeframe.[8] A major driver in the progressively lower cost of photovoltaic power is the steadily increasing efficiency of solar cells, which is shown in the graphic at the right. Higher efficiency solar cells require less area to deliver the same amount of power, and this lowers the "balance of system" costs such as wiring, roof mounting, etc., which scale as the area of the solar panels. Progress towards higher efficiency reflects improved processes for making photovoltaic materials such as silicon and gallium arsenide, as well as the discovery of new materials. Silicon solar cells are a mature technology, so they are now in the flat part of the learning curve and are approaching their maximum theoretical efficiencies. Newer technologies such as organic photovoltaics, quantum dot solar cells, and lead halide perovskite cells are still in the rising part of the learning curve.

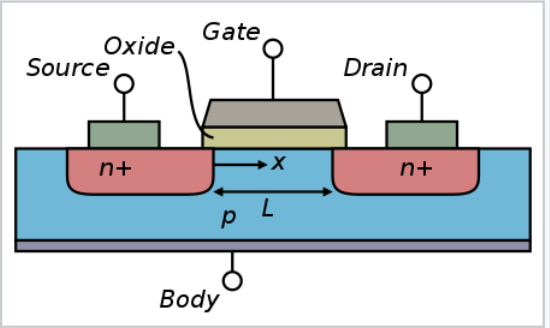


Reported timeline of solar cell energy conversion efficiencies since 1976 (National Renewable Energy Laboratory)

A **field effect transistor (FET)** is a transistor that uses an electric field to control the width of a conducting channel and thus the current in a semiconductor material. It is classified as unipolar transistor, in contrast to bipolar transistors.

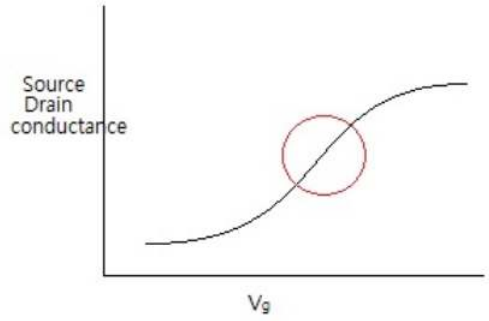
Field effect transistors function as current amplifiers. The typical structure of Si-based FETs is one in which two n-type regions (the source and the drain) are separated by a p-type region. An oxide insulator over the p-type region separates a metal gate lead from the semiconductor. This structure is called a metal-oxide-semiconductor FET (or MOSFET). When voltage is applied between source and drain, current cannot flow because either the n-p or the p-n junction is back-biased. When a positive potential is applied to the gate, however, electrons are driven towards the gate, and locally the semiconductor is "inverted" to n-type. Then the current flows easily between the n-type source and drain through the n-channel. The current flow between the source and drain is many

times larger than the current through the gate, and thus the FET can act as an amplifier. Current flow can also represent a logical "1," so FETs are also used in digital logic.



Cross section of an n-type MOSFET

In electronic devices such as microprocessors, field-effect transistors are kept in the off-state most of the time in order to minimize background current and power consumption. The FET shown above, which has n-type source and drain regions, is called an NMOS transistor. In a PMOS transistor, the source and drain regions are p-type and the gate is n-type. In **CMOS** (complementary metal-oxide semiconductor) integrated circuits, both NMOS and PMOS transistors are used. CMOS circuits are constructed in such a way that all PMOS transistors must have either an input from the voltage source or from another PMOS transistor. Similarly, all NMOS transistors must have either an input from ground or from another NMOS transistor. This arrangement results in low static power consumption.



Transistors are most useful in the range of gate voltage (indicated by the red circle in the figure at the left) where the source-drain current changes rapidly. In this region it is possible to effect a large change in current between source and drain when a small signal is applied to the gate. An important figure of merit for FETs is the **subthreshold slope**, which is the slope a plot of log(current) vs. V_{gate}. An ideal subthreshold slope is one decade of current per 60 mV of gate bias. Typically, a decade change in source-drain current can be achieved with a change in gate voltage of ~70 mV. The performance of FETs as switches and amplifiers is limited by the subthreshold slope, which in turn is limited by the capacitance of the gate. It is desirable to have a very high gate capacitance, which requires a thin insulating oxide, but also to have a small leakage current, which requires a thick oxide. A current challenge in the semiconductor industry is to continue to scale FETs to even smaller nanoscale dimensions while maintaining acceptable values of these parameters. This is being done by developing new gate insulator materials that have higher dielectric constants than silicon oxide and do not undergo redox reactions with silicon or with metal gate leads. Only a few known materials (such as hafnium oxynitride and hafnium silicates) currently meet these stringent requirements.

5.9.6: Diodes, LEDs and Solar Cells is shared under a CC BY-SA license and was authored, remixed, and/or curated by LibreTexts.

- **10.7: Diodes, LEDs and Solar Cells** by Chemistry 310 is licensed CC BY-SA 4.0. Original source: https://en.wikibooks.org/wiki/Introduction_to_Inorganic_Chemistry.

5.9.7: References

1. Hubbard, J. (1963). "Electron Correlations in Narrow Energy Bands". *Proceedings of the Royal Society of London* **276** (1365): 238–257. doi:10.1098/rspa.1963.0204. Bibcode: 1963RSPSA.276..238H.
2. T. Mizokawa, Metal-insulator transitions: orbital control, Nature Physics 9, 612–613 (2013), doi: doi:10.1038/nphys2769
3. N. F. Mott, (1961) "The Transition to the Metallic State," Phil. Mag. 6, 287. DOI: 10.1080/14786436108243318.
4. P. P. Edwards and M. J. Sienko (1982) "The Transition to the Metallic State," Acc. Chem. Res. 15, 87-93. DOI: 10.1021/ar00075a004
5. Recent data have disproven this assertion; MacDonalds has finally responded to public opinion and is offering breakfast after 10:30 AM. But the laws of thermodynamics remain immutable and eternal
6. E. Yablonovitch, O. Miller, and S. Kurtz, "Strong Internal and External Luminescence as Solar Cells Approach the Shockley–Queisser Limit," IEEE Journal of Photovoltaics, vol. 2, no. 3, pp. 303-311, July 2012.
7. "Recent facts about photovoltaics in Germany". Fraunhofer ISE. 7 January 2015. Retrieved 17 February 2015.
8. Energy Information Administration, (November 2010). Levelized Cost of New Generation Resources in the Annual Energy Outlook 2011.
9. Staebler, D. L. and Wronski, C. R. Optically induced conductivity changes in discharge-produced hydrogenated amorphous silicon. J. Appl. Physics. 51(6), June 1980.
10. Mishima, T., Taguchi, M., Sakata, H., Maruyama, E., 2011. Development status of high efficiency HIT solar cells. Sol. Energy Mater. Sol. Cell. 95, 18–21. doi:10.1016/j.solmat.2010.04.030

5.9.7: References is shared under a CC BY-SA license and was authored, remixed, and/or curated by LibreTexts.

- **10.11: References** by Chemistry 310 is licensed CC BY-SA 4.0. Original source: https://en.wikibooks.org/wiki/Introduction_to_Inorganic_Chemistry.

CHAPTER OVERVIEW

6: Organometallic Chemistry

6.1: 18 Valence Electron Rule

6.2: Synthesis and Stability

6.2.1: Transition Metal Alkyl Complexes

6.2.2: Metal-Carbenes

6.2.3: Metal Hydrides

6.2.4: Metal Carbonyls

6.2.5: Metal Phosphines

6.2.6: Complexes of π−bound Ligands

6.2.6.1: Metal Alkene Complexes

6.2.6.2: Metal Allyl and Diene Complexes

6.2.6.3: Metal Cyclopentadienyl Complexes

6.3: Reaction Mechanisms

6.3.1: Oxidative Addition and Reductive Elimination

6.3.2: Insertion and Elimination Reactions

6.3.3: Nucleophilic and Electrophilic Addition and Abstraction

6.4: Applications

6.4.1: Homogeneous Catalysis - I

6.4.2: Homogeneous Catalysis - II

6.4.3: Catalytic Applications of Organometallic Compounds- Alkene Metathesis

---

6: Organometallic Chemistry is shared under a not declared license and was authored, remixed, and/or curated by LibreTexts.

6.1: 18 Valence Electron Rule

Learning Objectives

In this section you will learn the following

- Have an insight about the stability of the transition metal complexes with respect to their total valence electron count.
- Be aware of the transition metal complexes that obey or do not obey the 18 Valence Electron Rule.
- Have an appreciation of the valence electron count in the transition metal organometallic complexes that arise out of the metal-ligand orbital interactions.

The transition metal organometallic compounds exhibit diverse structural variations that manifest in different chemical properties. Many of these transition metal organometallic compounds are primarily of interest from the prospectives of chemical catalysis. Unlike the main group organometallic compounds, which use mainly *ns* and *np* orbitals in chemical bonding, the transition metal compounds regularly use the $(n-1)d$, *ns* and *np* orbitals for chemical bonding (Figure **6.1.1**). Partial filling of these orbitals thus render these metal centers both electron donor and electron acceptor abilities, thus allowing them to participate in σ-donor/π-acceptor synergic interactions with donor-acceptor ligands like carbonyls, carbenes, arenes, isonitriles and etc,.

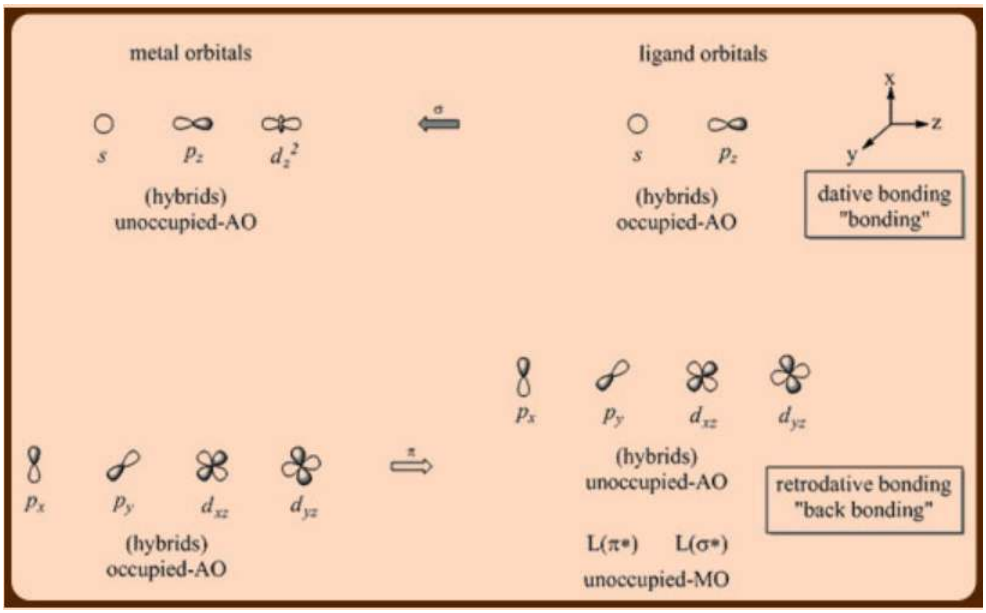
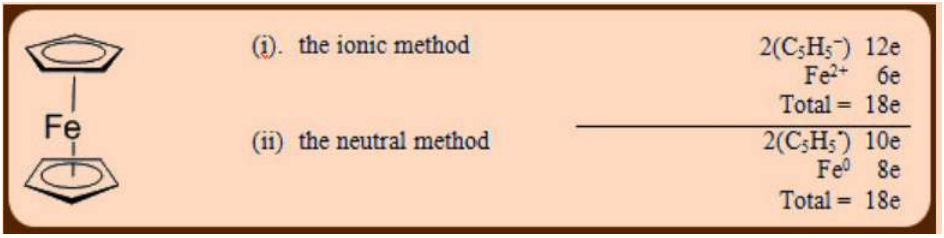


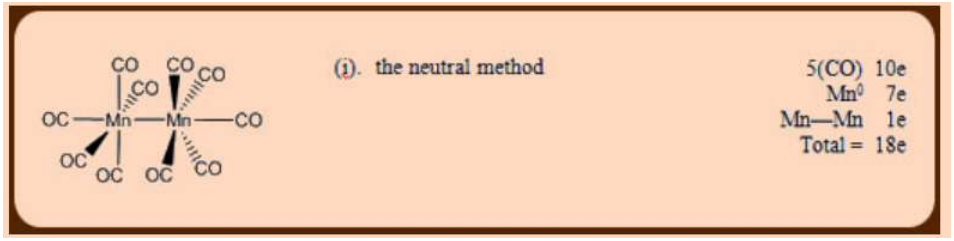
Figure **6.1.1**

The 18 Valence Electron (18 VE) Rule or The Inert Gas Rule or The Effective Atomic Number (EAN) Rule: The 18-valence electron (VE) rule states that thermodynamically stable transition metal compounds contain 18 valence electrons comprising of the metal *d* electrons plus the electrons supplied by the metal bound ligands. The counting of the 18 valence electrons in transition metal complexes may be obtained by following either of the two methods of electron counting, (*i*). the ionic method and (*ii*). the neutral method. Please note that a metal-metal bond contributes one electron to the total electron count of the metal atom. A bridging ligand donates one electron towards bridging metal atom.

Example 1: Ferrocene $Fe(C_5H_5)_2$



Example 2. $Mn_2(CO)_{10}$



Transition metal organometallic compounds mainly belong to any of the three categories.

a. **Class I** complexes for which the number of valence electrons do not obey the 18 VE rule.
b. **Class II** complexes for which the number of valence electrons do not exceed 18.
c. **Class III** complexes for which the valence electrons exactly obey the 18 VE rule.

The guiding principle which governs the classification of transition metal organometallic compounds is based on the premise that the antibonding orbitals should not be occupied; the nonbonding orbitals may be occupied while the bonding orbitals should be occupied.

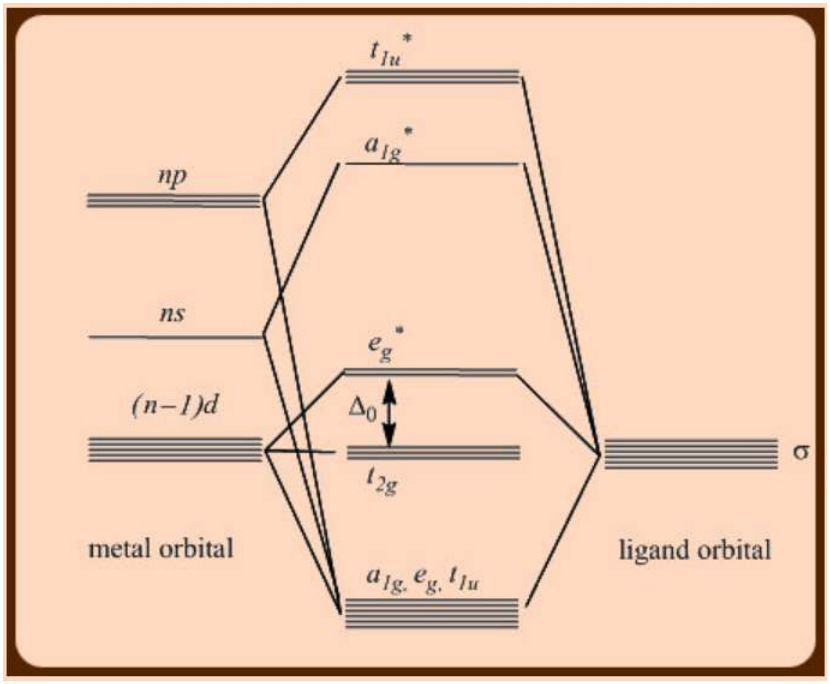


Figure **6.1.2**: A simplified molecular orbital diagram for an octahedral transition metal complex showing σ−interactions only.

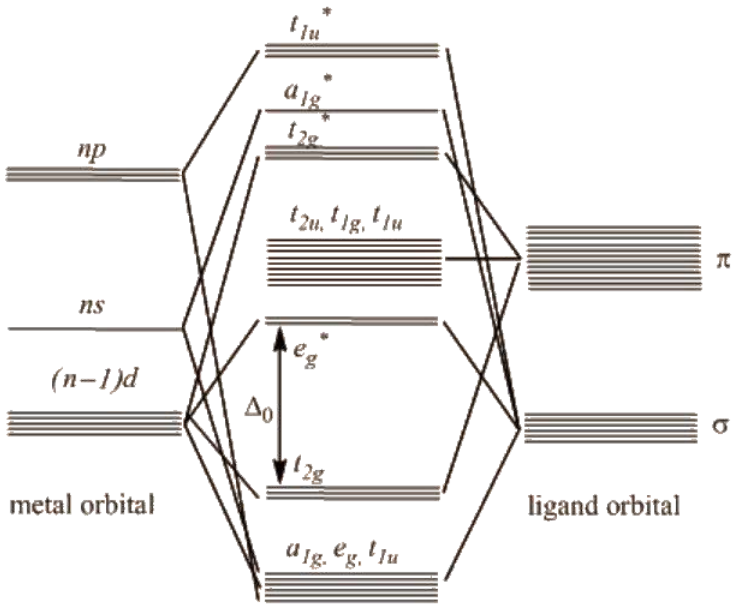


Figure **6.1.3**: A simplified molecular orbital diagram for an octahedral transition metal complex showing σ−and π−interactions only.

Class I:

In **class I** complexes, the Δ_o splitting is small and often applies to *3d* metals and σ ligands at lower end of the spectrochemical series. In this case the t_{2g} orbital is nonbonding in nature and may be occupied by 0−6 electrons (Figure **6.1.2**). The e_g* orbital is weakly antibonding and may be occupied by 0−4 electrons. As a consequence, 12−22 valence electron count may be obtained for this class of compounds. Owing to small Δ_{tetr} splitting energy, the tetrahedral transition metal complexes also belongs to this class.

Class II:

In **class II** complexes, the Δ_o splitting is relatively large and is applicable to *4d* and *5d* transition metals having high oxidation state and for σ ligands in the intermediate and upper range of the spectrochemical series. In this case, the t_{2g} orbital is essentially nonbonding in nature and can be filled by 0−6 electrons (Figure 3). The e_g* orbital is strongly antibonding and is not occupied at all. Consequently, the valence shell electron count of these type of complexes would thus be 18 electrons or less.

Class III:

In **class III** complexes, the Δ_o splitting is the largest and is applicable to good σ donor and π acceptor ligands like CO, PF_3, olefins and arenes located at the upper end of the spectrochemical series.

The t_{2g}orbital becomes bonding owing to interactions with ligand orbitals and should be occupied by 6 electrons. The e_g* orbital is strongly antibonding and therefore remains unoccupied.

Problems

State the oxidation state of the metal and the total valence electron count of the following species.

1. $V(C_2O_4)_3^{3-}$

Ans: +3 and 14

2. $Mn(acac)_3$

Ans: +3 and 16

3. $W(CN)_8^{3-}$

Ans: +5 and 17

4. $CpMn(CO)_3$

Ans: 0 and 18

5. $Fe_2(CO)_9$

Ans: 0 and 18

Self Assessment test

State the oxidation state of the metal and the total valence electron count of the following species.

1. TiF_6^{2-}

Ans: +4 and 12

2. $Ni(en)_3^{2+}$

Ans: +2 and 20

3. $Cu(NH_3)_6^{2+}$

Ans: +2 and 21

4. $W(CN)_8^{4-}$

Ans: +4 and 18

5. $CH_3Co(CO)_4$

Ans: 0 and 18

Summary

The transition metal complexes may be classified into the following three types.

i. The ones that do not obey the 18 valence electron rule are of class I type
ii. The ones that do not exceed the 18 valence electron rule are of class II and
iii. The ones that strictly follow the 18 valence electron rule.

Depending upon the interaction of the metal orbitals with the ligand orbitals and also upon the nature of the ligand position in spectrochemical series, the transition metal organometallic compounds can form into any of the three categories.

6.1: 18 Valence Electron Rule is shared under a CC BY-SA license and was authored, remixed, and/or curated by LibreTexts.

6.2: Synthesis and Stability

Learning Objectives

In this lecture you will learn the following

- Understand the role lead by ligands in stabilizing organometallic transition metal complexes.
- Know about various synthetic methods available for preparing the organometallic transition metal complexes.
- Understand the various factors like β-elimination and other bimolecular decomposition pathways that contribute to the observed instability of the organometallic transition metal complexes.
- Obtain insight about making stable organometallic transition metal complexes by suppression of the destabilizing factors mentioned.

Ligands play a vital role in stabilizing transition metal complexes. The stability as well as the reactivity of a metal in its complex form thus depend upon the number and the type of ligands it is bound to. In this regard, the organometallic carbon based ligands come in diverse varieties displaying a wide range of binding modes to a metal. In general, the binding modes of the carbon-derived ligands depend upon the hybridization state of the metal bound carbon atom. These ligands can thus bind to a metal in many different ways as depicted below. Lastly, these ligands can either be of *(a)* purely σ−donor type, or depending upon the capability of the ligand to form the multiple bonds may also be of *(b)* a σ−donor/π−acceptor type, in which the σ−interaction is supplemented by a varying degree of π−interaction.

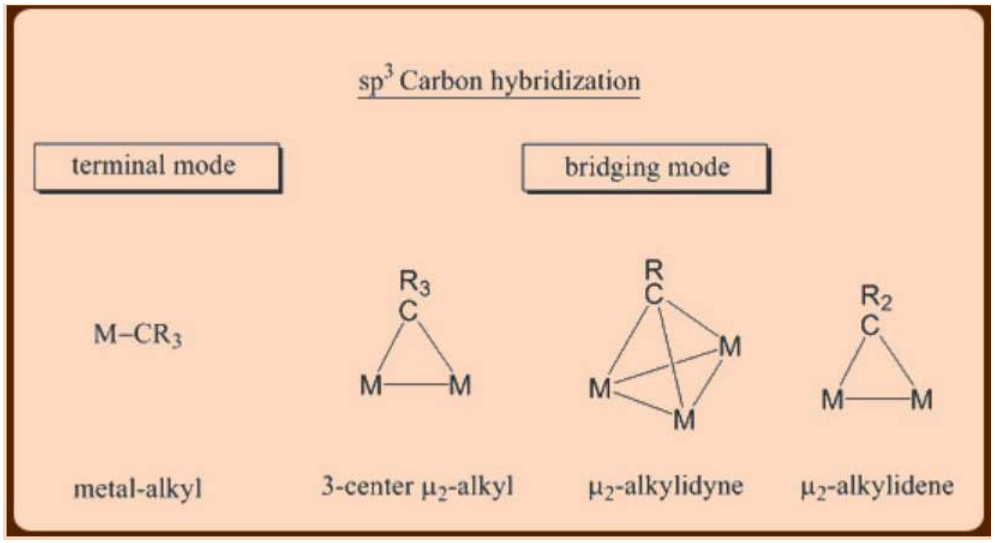


Figure 6.2.1

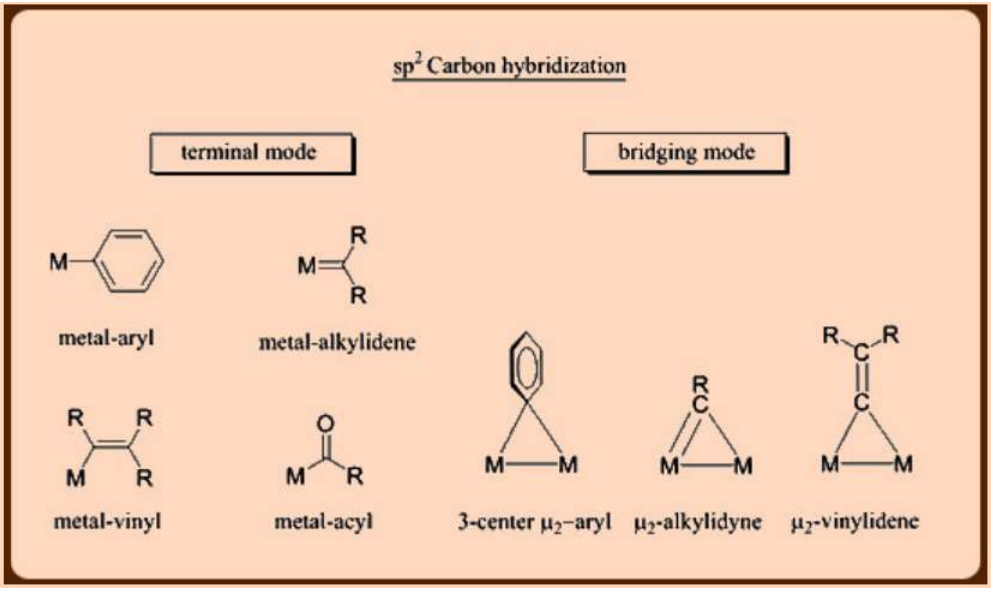


Figure **6.2.2**

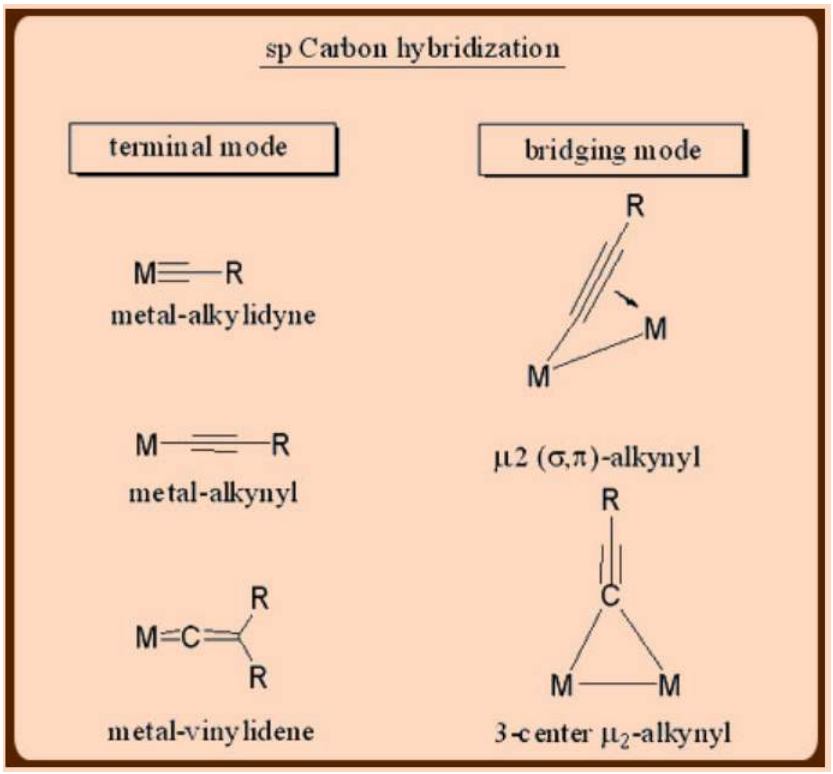


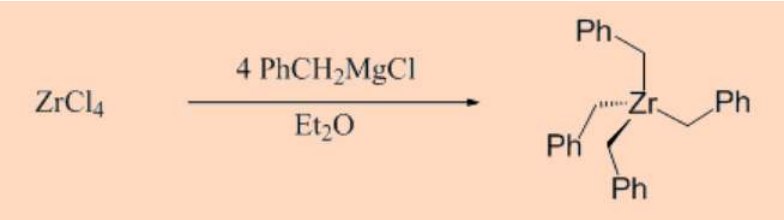
Figure **6.2.3**

Preparation of transition metal-alkyl and transition metal-aryl complexes

The transition metal−alkyl and transition−metal aryl complexes are usually prepared by the following routes discussed below,

a. Metathesis

This involves the reactions of metal halides with organolithium, organomagnesium, organoaluminium, organotin and organozinc reagents.



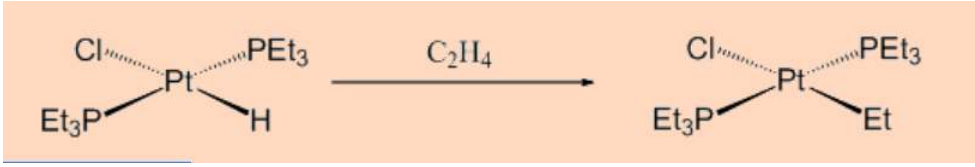
Of the different organoalkyl compounds listed above, the organolithium and organomagnesium compounds are strongly carbanionic while the remaining main group organometallics like the organoalkyl, organozinc and organotin reagents are relatively less carbanionic in nature. Thus, the main group organometallic reagents have attenuated alkylating power, that can be productively used in partial exchange of halide ligands.

$$TiCl_4 \xrightarrow{Al_2Me_6} MeTiCl_3$$

$$NbCl_5 \xrightarrow{ZnMe_2} Me_2NbCl_3$$

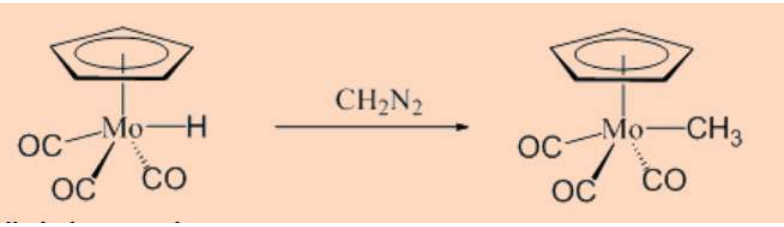
b. Alkene insertion or Hydrometallation

As the name implies, this category of reaction involves an insertion reaction between metal hydride and alkene as shown below. These type reactions are relevant to certain homogeneous catalytic processes in which insertion of an olefin to M−H bond is often observed.



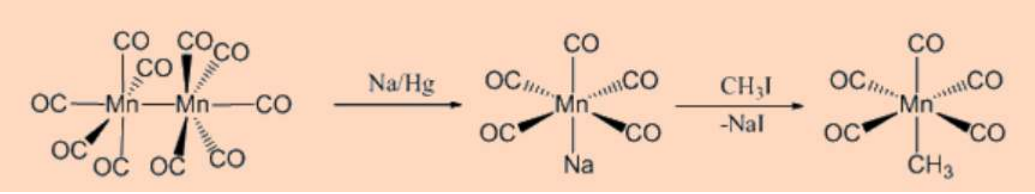
c. Carbene insertion

This category represents the reaction of metal hydrides with carbenes.



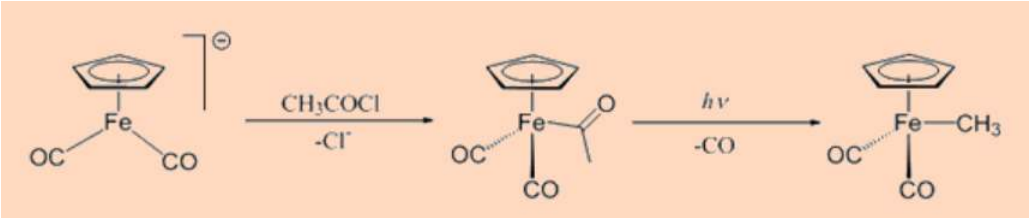
d. Metallate alkylation reaction

This category represents the reaction of carbonylate anions with alkyl halides as shown below.



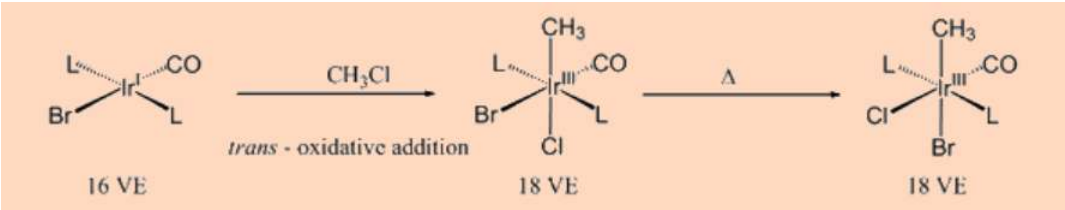
e. Metallate acylation reaction

This category involves the reaction of carbonylate anions with acyl halides



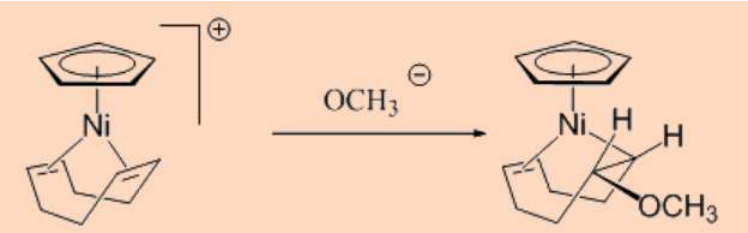
f. Oxidative addition reaction

Many unsaturated 16 VE transition metal complexes having d^8 or d^{10} configuration undergo oxidative addition reactions with alkyl halides. The oxidative addition reactions proceed with the oxidation state as well as coordination number of the metal increasing by +2.



g. Addition reaction

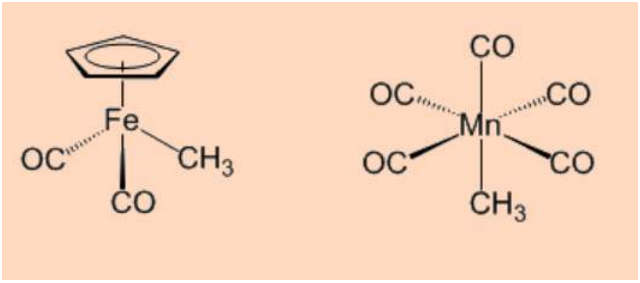
This category involves the reaction of an activated metal bound olefin complex with a nucleophile as shown below.



Thermodynamic Stability and Kinetic Lability

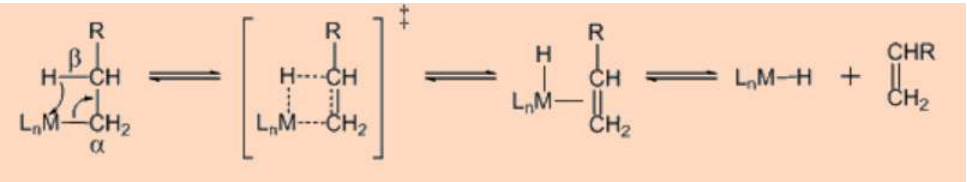
The transition metal organometallic compounds are often difficult to synthesize under ordinary laboratory conditions and require stringent experimental protocols involving the exclusion of air and moisture for doing so. As a consequence, many homoleptic binary transition metal−alkyl and transition metal−aryl compounds like, Et_2Fe or Me_2Ni cannot be made under normal laboratory conditions. More interestingly, most of the examples of transition metal−aryl and transition metal−alkyl compounds, known in the literature, invariably contain additional ligands like η^5-C_5H_5, CO, PR_3 or halides.

For example,

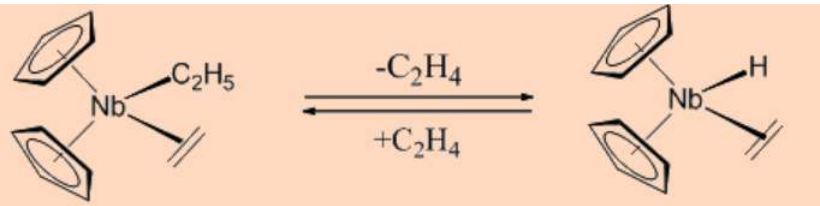


Transition metal−carbon (TM−C) bond energy values are important for understanding the instability of transition metal organometallic compounds. In general, the TM−C bonds are weaker than the transition metal−main group element (TM−MGE) bonds (MGE = F, O, Cl, and N) and more interestingly so, unlike the TM−MGE bond energies, the TM−C bond energy values increase with increasing atomic number. The steric effects of the ligands also play a crucial role in influencing the TM−C bond energies and thus have to be given due consideration.

Contrary to the popular belief, the difficulty in obtaining transition metal−aryl and transition metal−alkyl complexes does primarily arise from the thermodynamic reasons but rather the kinetic ones. β−elimination is by far the most general decomposition mechanism that contribute to the instability of transition metal organometallic compounds. β−elimination results in the formation of metal hydrides and olefin as shown below.



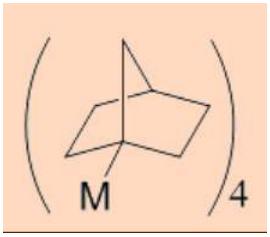
β−elimination can also be reversible as shown below.



The instability of transition metal organometallic compounds can arise out of kinetic lability like in the case of the β−elimination reactions that trigger decomposition of these complexes. Thus, the suppression of the decomposition reactions provides a viable option for the stabilization of the transition metal organometallic complexes. The β−elimination reactions in transition metal organometallic complexes may be suppressed under any of the following three conditions.

a. Formation of the leaving olefin becomes sterically or energetically unfavorable

In the course of β−elimination, this situation arises when the olefinic bond is formed at a bridgehead carbon atom or when a double bond is formed with the elements of higher periods. For instance, the norbornyl group is less prone to decomposition by β−elimination because that would require the formation of olefinic double bond at a bridgehead carbon atom in the subsequent olefin, *i.e*. norbornene, and which is energetically unfavorable.

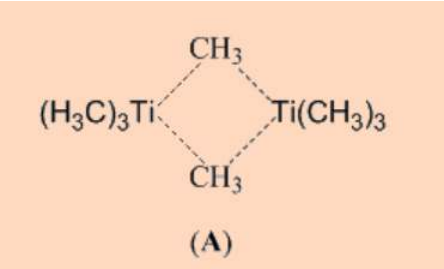


b. Absence of β−hydrogen atom in organic ligands

Transition metal bound ligands that do not possess β−hydrogen cannot decompose by β−elimination pathway and hence such complexes are generally more stable than the ones containing β−hydrogen atoms. For example, the neopentyl complex, $Ti[CH_2C(CH_3)_3]_4$ (m.p 90 °C), and the benzyl complex, $Zr(CH_2Ph)_4$ (m.p. 132 °C), exhibit higher thermal stability as both of the neopentyl and benzyl ligands lack β−hydrogens.

c. Central metal atom is coordinatively saturated

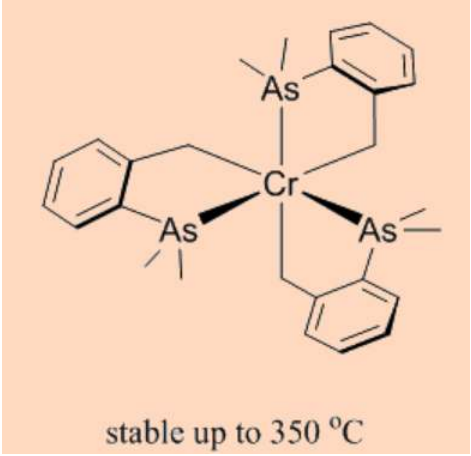
Transition metal organometallic complexes in which the central metal atom is coordinatively saturated tend to be more stable due to the lack of coordination space available around the metal center to facilitate β−elimination reaction or other decomposition reactions. Thus, the absence of free coordination sites at the metal is crucial towards enhancing the stability of the transition metal organometallic complexes. For example, $Ti(Me)_4$, which is coordinatively unsaturated can undergo a bimolecular decomposition reaction *via* a binuclear intermediate (**A**), is unstable and exhibits a decomposition temperature of –40 °C. On the contrary, $Pb(Me)_4$, that cannot undergo decomposition by such bimolecular pathway, is more stable and distills at 110 °C at 1 bar atmospheric pressure.



(A)

The $Ti(Me)_4$ decomposes by dimerization involving the formation of Ti−C (*3c−2e*) bonds. For $Pb(Me)_4$, such bimolecular decomposition pathway is not feasible, as being a main group element it has higher outer *d* orbital for extending the coordination number. If the free coordination site of $Ti(Me)_4$ is blocked by another ligand, as in $[(bipy)Ti(Me)_4]$, then the thermal stability of the complex, $[(bipy)Ti(Me)_4]$, increased significantly. Other bidentate chelating ligands like *bis*(dimethylphosphano)ethane (dmpe) also serve the same purpose.

Coordinative saturation thus brings in kinetic stabilization in complexes. For example, $Ti(Me)_4$is extremely reactive as it is coordinatively unsaturated, while $W(Me)_4$ is relatively inert for reasons of being sterically shielded and hence, coordinatively saturated. Thus, if all of the above discussed criteria for the suppression of β-elimination are taken care of, then extremely stable organometallic complexes can be obtained like the one shown below.



stable up to 350 °C

Problems

1. Arrange the following compounds in the order of their stability.

a. $Ti(Et)_4$
b. $Ti(Me)_4$ and
c. $Ti(6\text{-norbornyl})_4$

Ans: $Ti(Et)_4 < Ti(Me)_4 < Ti(6\text{-norbornyl})_4$

2. Predict the product of the reaction given below.

$$(BuP)CuCH_2CD_2C_2H_5 \longrightarrow$$

Ans: Equi molar amounts of $(Bu_3P)CuD$ and $CH_2{=}CDC_2H_5$

3. Will the compound β-eliminate,

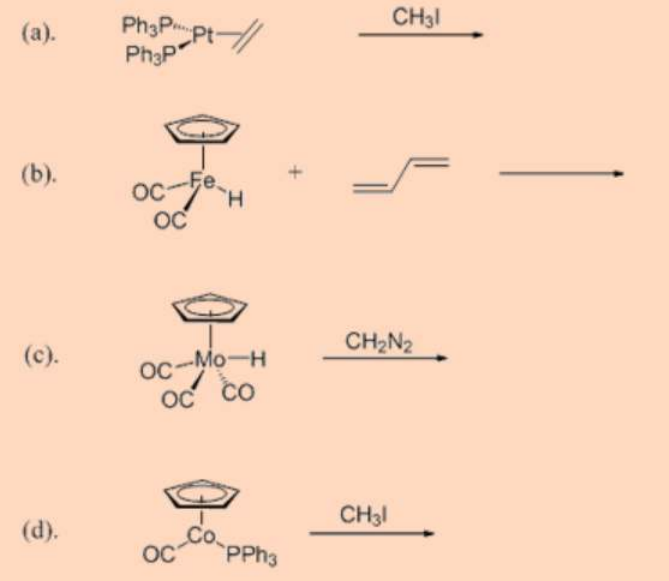
$$PtH(C{\equiv}CH)L_2 \xrightarrow{\text{Beta-elimination}}$$

(a). readily, (b). slowly and (c). not at all.
Explain your answer with proper reasoning.

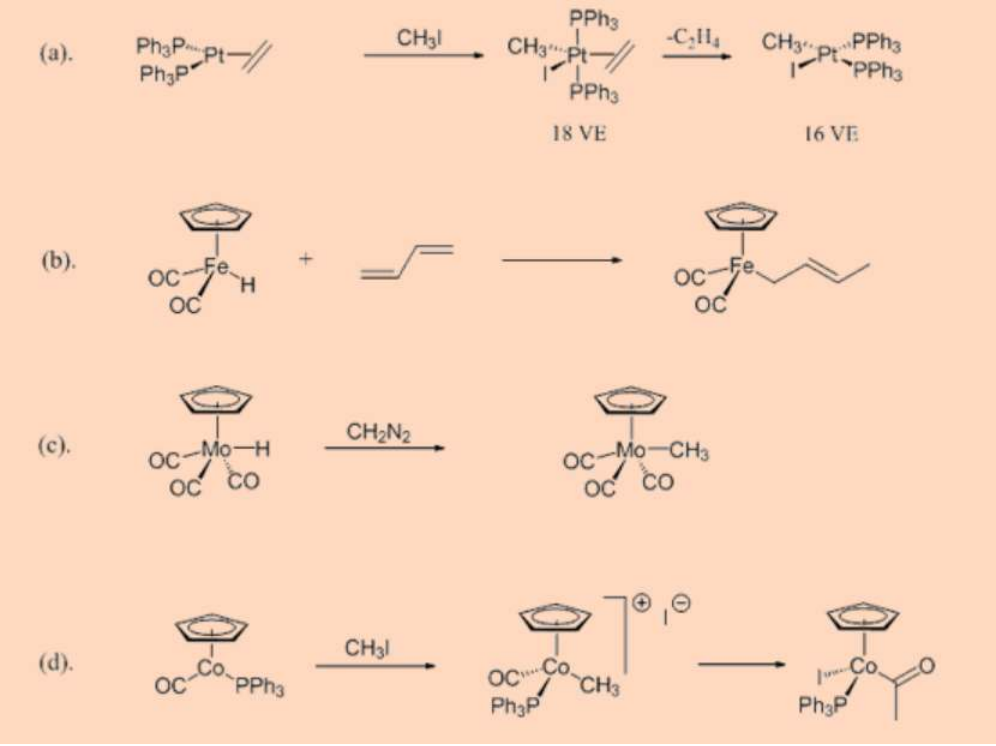
Ans: Not at all as the ß-hydrogens are pointing away from the metal and cannot participate in ß-elimination recation.

Self Assessment test

1. Write the product(s) of the reactions.



Ans:



Summary

Ligands assume a pivotal role in the stabilization of the organometallic transition metal complexes. There are several methods available for the preparation of the organometallic transition metal complexes. The observed instability of the organometallic transition metal complexes can be attributed to two main phenomena namely β-elimination and bimolecular decomposition reaction

that severely undermine the instability of these complexes. The suppression of these decomposition pathway thus pave way for obtaining highly stable organometallic transition metal complexes.

6.2: Synthesis and Stability is shared under a CC BY-SA license and was authored, remixed, and/or curated by LibreTexts.

- **6.2: Synthesis and Stability** by M. S. Balakrishna & Prasenjit Ghosh is licensed CC BY-NC-SA 4.0. Original source: https://nptel.ac.in/courses/104101006.

6.2.1: Transition Metal Alkyl Complexes

Learning Objectives

In this lecture you will learn the following

- Get a general prospective on the historical background of transition metal organometallic compounds with particular emphasis on metal alkyls.
- Know more about stable metal alkyls.
- Get introduced to transition metal agostic alkyls.
- Develop an understanding of reactions of relevance to metal alkyls like the reductive eliminations, oxidative additions and the halide eliminations.

Transition metal σ−bonded organometallic compounds like the metal alkyls, aryls and the hydrides derivatives are by for the most common organometallic species encountered in the world of chemistry. Yet, these compounds remained elusive till as late as the 1960s and the 1970s.

Historical background

Metal alkyls of the main group elements namely, Li, Mg, Zn, As and Al, have been known for a long time and which over the years have conveniently found applications in organic synthesis whereas development on similar scale and scope in case of the transition metal counterparts were missing till only recently. The origin of the organometallic compounds traces back to 1757, when Cadet prepared a foul smelling compound called cacodyl oxide from As_2O_3 and CH_3COOK, while working in a military pharmacy in Paris. Years later in 1840, R. W. Bunsen gave the formulation of cacodyl oxide as $Me_2As{-}O{-}AsMe_2$. The next known transition metal organometallic compound happens to be Et_2Zn, which was prepared serendipitously in 1848 from the reaction of ethyl iodide (EtI) and Zn with the objective of generating free ethyl radical. Frankland further synthesized alkyl mercury halides like, CH_3HgI, from the reaction of methyl iodide (CH_3I) and Hg in sunlight. It is important to note that the dialkyl mercury, R_2Hg, and the dialkyl zinc, R_2Zn, have found applications as alkyl transfer reagents in the synthesis of numerous main group organometallic compounds.

Another notable development of the time was of the preparation of Et_4Pb from ethyl iodide (EtI) and Na/Pb alloy by C. J. Lowig and M. E. Schweizer in 1852. They subsequently extended the same method for the preparation of the Et_3Sb and Et_3Bi compounds. In 1859, aluminumalkyliodides, R_2 AlI, were prepared by W. Hallwachs and A Schafarik from alkyl iodide (RI) and Al. The year 1863 saw the preparation of organochlorosilanes, $RmSiCl_{4-m}$, by C. Friedel and J. M. Crafts while the year 1866 saw the synthesis of halide-free alkyl magnesium compound, Et_2Mg, by J. A. Wanklyn from the reaction of Et_2Hg and Mg. In 1868, M. P. Schutzenberger reported the first metal−carbonyl complex in the form of $[Pt(CO)Cl_2]_2$. In 1890, the first binary metal−carbonyl compound, $Ni(CO)_4$ was reported by L. Mond, who later founded the well−known chemical company called ICI (Imperial Chemical Industries). In 1909, W. J. Pope reported the first σ−organotransition metal compound in the form of $(CH_3)_3PtI$. In 1917, the alkyllithium, RLi, compounds were prepared by W. Schlenk by transalkylation reactions. In 1922, T. Midgley and T. A. Boyd reported the utility of Et_4Pb as an antiknock agent in gasoline. A. Job and A. Cassal prepared $Cr(CO)_6$ in 1927. In 1930, K. Ziegler showed the utility of organolithium compounds as alkylating agent while in the following year in 1931, W. Heiber prepared $Fe(CO)_4H_2$ as the first transition metal−hydride complex. O. Roelen discovered the much renowned hydroformylation reaction in 1938, that went on to become a very successful industrial process worldwide.

The large scale production and the use of silicones were triggered by E. G. Rochow, when he reported the ‘direct synthesis’ from methyl chloride (CH_3Cl) and Si using Cu catalyst at 300 °C in 1943. The landmark compound, ferrocene $(C_5H_5)_2Fe$, known as the first sandwich complex was obtained by P. Pauson and S. A. Miller in 1951. H. Gilman introduced the important utility of organocuprates when he prepared $LiCu(CH_3)_2$, in 1952. In the subsequent year 1953, G. Wittig found a new method of synthesizing olefins from phosphonium ylides and carbonyl compounds that fetched him a Nobel prize in 1979. The year 1955 turned out to be a year of path breaking discoveries with E. O. Fischer reporting the rational synthesis of bis(benzene)chromium, $(C_6H_6)_2Cr$ while K. Ziegler and G. Natta announcing the ground breaking polyolefin polymerization process that subsequently gave them the Nobel prizes, E. O. Fischer sharing with G. Wilkinson in 1973 while K. Ziegler and G. Natta shared the same in 1963. In 1956, H. C. Brown reported hydroboration for which he too received the Nobel prize in 1979. In 1963, L. Vaska reported the famous Vaska’s complex, *trans*−$(PPh_3)_2Ir(CO)Cl$, that reversibly binds to molecular oxygen. In 1964, E. O. Fischer reported the

first carbene complex, $(CO)_5WC(OMe)Me$. In 1965, G. Wilkinson and R. S. Coffey reported the Wilkinson catalyst, $(PPh_3)_3RhCl$, for the hydrogenation of alkenes. In 1973, E. O. Fischer synthesized the first carbyne complex, $I(CO)_4Cr(CR)$.

After the early 1970s, there were tremendous outburst in activity, in the area of transition metal organometallic chemistry leading to phenomenal developments having far-reaching consequences in various branches of the main stream and interfacial chemistry. Several Nobel prizes that have been awarded to the area in recent times fully recognized the significance of these efforts with Y. Chauvin, R. R. Schrock, and R. H. Grubbs winning it in 2005 for olefin metathesis and Akira Suzuki, Richard F Heck and E. Negishi receiving the same for the Pd catalyzed C−C cross-coupling reactions in organic synthesis in 2010.

Metal alkyls

In day to day organic synthesis, particularly from the application point of view, the metal alkyls are often perceived as a source of stabilized carbanions for reactions with various electrophiles. The extent of stabilization of alkyl carbanions in metal alkyl complexes depend upon the nature of the metal cations. For example, the alkyls of electropositive metals like that of Group 1 and 2, Al and Zn are regarded as polar organometallics as the alkyl carbanions remain weakly stabilized while retaining strong nucleophilic and basic character of a free anion. These polar alkyls are extremely air and moisture sensitive as in their presence they often get hydrolyzed and oxidized readily. Similar high reactivity was also observed in case of the early transition metal organometallic compounds particularly of Ti and Zr. On the contrary the late transition metal organometallic compounds are much less reactive and stable. For example, the Hg−C bond of $(Me-Hg)^+$ cation is indefinitely stable in aqueous H_2SO_4 solution in air. Thus, on moving from extremely ionic Na alkyls to highly polar covalent Li and Mg alkyls and to essentially covalent late−transition metal alkyls, a steady decrease in reactivity is observed. This trend can be correlated to the stability of alkyl carbanions that also depended on the nature of hybridization of the carbon center, with sp^3 hybridized carbanions being the least stable and hence most reactive, followed by the sp^2 carbanions being moderately stable while the *sp* carbanions being the least reactive and most stable. The trend also correlates well with the respective p*K*a values observed for CH_4 (p*K*a = ~50), C_6H_6 (p*K*a = ~43) and RC≡CH (p*K*a = ~25).

Stable alkyls

As has been mentioned earlier, that the β−elimination is a crucial destabilizing influence on the transition metal organometallic complexes. Hence, inhibition of this decomposition pathway leads to increased stabilities of organometallic compounds. Thus, many stable alkyl transition metal complexes do not possesses β−hydrogens like, $W(Me)_6$ and $Ti(CH_2Ph)_4$. In some cases despite the presence of the β−hydrogens the organometallic complexes are stable as the β−hydrogens are deposed away from the metal center like in, $Cr(CHMe_2)_4$, and $Cr(CMe_3)_4$. In this category of stable transition metal organometallic compounds also falls the ones that contain β−hydrogens but cannot β−eliminate owing to the formation of a olefinic bond at a bridgehead, which is unfavorable, like in $Ti(6-norbornyl)_4$ and $Cr(1-adamantyl)_4$. Lastly, some 18 VE metal complexes are stable, again despite having β−hydrogens, for reasons of being electronically as well as coordinatively saturated at the metal center owing to attaining the stable 18 electron configuration.

Agostic alkyls

Agostic alkyls are extremely rare but very interesting species that represents a frozen point in a β−elimination pathway that have fallen short of the completion of the decomposition reaction. Thus, these agostic alkyl complexes can be viewed as snap shots of a β−elimination trajectory thereby providing valuable mechanistic understanding of the decomposition reaction. The agostic interaction has characteristic signatures in various spectroscopic techniques as observed from the decreasing J_{C-H}coupling constant values in the ^1H NMR and the ^{13}C NMR spectra and the lowering of the ν_{C-H}stretching frequencies in the IR spectroscopy. The agostic alkyl complexes can be definitively proven by X−ray diffraction or neutron diffraction studies. The agostic alkyls thus have activated C−H bonds which are of interest for their utility in chemical catalysis. Quite interestingly, many d^0 Ti agostic alkyl complexes do not β−eliminate primarily for the metal center being too electron deficient to donate electron to the σ* C−H orbital as required for the subsequent β−elimination process.

Reductive elimination

Reductive elimination represents a major decomposition pathway of the metal alkyls. Opposite of oxidative addition, the reductive elimination is accompanied by the decrease in the oxidation state and the valence electron count of the metal by two units. The

metal alkyl complexes may thus reductively eliminate with an adjacent hydrogen atom to yield an alkane, (R−H) or undergo the same with an adjacent alkyl group to give an even larger alkane (R−R) as shown below.

$$L_nMRH \longrightarrow R{-}H + L_nM$$

$$L_nMR_2 \longrightarrow R{-}R + L_nM$$

The reductive elimination is often facilitated by an electron deficient metal center and by sterically demanding ligand systems. Often d^8 metals like Ni(II), Pd(II), and Au(III) and d^6 metals in high oxidation state like, Pt(IV), Pd(IV), Ir(III), and Rh(III) exhibit reductive elimination.

Oxidative addition

Unlike the reductive elimination that represents a decomposition pathway of metal alkyls, the oxidative addition reaction represents a useful method for the formation of the metal alkyl complexes. The oxidative addition thus leads to increase in valence electron count and the oxidation state of the metal center by two units. The oxidative addition reactions are often facilitated by low valent electron rich metal centers and by less sterically demanding ligands.



Halide elimination

β−halide elimination is observed for the early transition metals and the *f*−block elements resulting in the formation of stable alkyl halides. The phenomenon is mostly seen in case of the metal fluorides and arise owing to the very high alkyl−fluoride bond strengths that favor the halide elimination.

Problems

1. Who elucidated the structure of cacodyl oxide?

Ans: R. W. Bunsen in 1840

2. Give the example of the first olefin bound transition metal complex?

Ans: Zeise's salt, $Na[PtCl_3(C_2H_4)]$

3. Who discovered olefin polymerization?

Ans: K. Ziegler and G. Natta

4. What kind of metal center promotes oxidative addition reactions?

Ans: Electron rich

5. The 18 VE complex would favor/disfavor oxidative addition reactions?

Ans: Disfavor

Self Assessment test

1. O. Roelen discovered which famous reaction?

Ans: Hydroformylation

2. What is the first binary metal−carbonyl complex?

Ans: $Ni(CO)_4$

3. Who discovered the hydroboration reaction?

Ans: H. C. Brown

4. Reductive elimination reaction is favored by what kind of ligands?

Ans: Sterically demanding

5. β−halide elimination is mainly observed for what type of metal halide complexes?

Ans: Metal fluorides

Summary

A broader outlook on metal alkyls is obtained from the study of its historical background thus dispelling many myths about these compounds like them being inherently unstable. It also establishes newer founding principles like these compounds indeed being thermodynamically stable under certain experimental conditions and thus facilitating further attempts to take up the synthesis of these compounds. Another important class of transition metal organometallic compounds are the agostic alkyls, which can be viewed as the ones that have proceeded along but have fallen short of the final sequence of the β−elimination step. While oxidative addition reaction remains a key method for synthesizing metal alkyls, the complementary reaction, *i.e*, the reductive elimination, represents a decomposition reaction of these compounds. β−halide elimination reactions are observed for early transition metal elements and *f*−block elements.

6.2.1: Transition Metal Alkyl Complexes is shared under a CC BY-SA license and was authored, remixed, and/or curated by LibreTexts.

- **7.1: Transition Metal Alkyl Complexes** by M. S. Balakrishna & Prasenjit Ghosh is licensed CC BY-NC-SA 4.0. Original source: https://nptel.ac.in/courses/104101006.

6.2.2: Metal-Carbenes

Learning Objectives

In this lecture you will learn the following

- The metal−ligand multiple bonding and their relevance in.
- The Fischer type carbene complexes.
- The Schrock type carbene complexes.

The organometallic compounds containing metal−ligand multiple bonds of the types, M=X and M≡X (X = C, N, O) are of current interest as they are valuable intermediates in many important catalytic cycles. In this regard, considerable attention has been paid towards developing an understanding of the metal−ligand multiply bonded systems like that of the metal carbene $L_nM{=}CR_2$ type complexes and of the metal carbyne $L_nM{\equiv}CR$ type complexes. A detailed account of the metal−carbene complexes is presented in this chapter.

Metal carbene complexes

Carbenes are highly reactive hexavalent species that exist in two spin states, *i.e.* (*i*) in a singlet form (═), in which two electrons are paired up and (*ii*) in a triplet form (═), in which the two electrons remain unpaired. Of the two, the singlet form is the more reactive one. The instability of carbene accounts for its unique reactivity like that of the insertion reaction, which has aroused significant interest in recent years. The singlet carbene and the triplet carbene bind differently to metals, with the singlet one yielding Fischer type carbene complexes while the triplet one yielding Schrock type carbene complexes (Figure **6.2.2.1**).

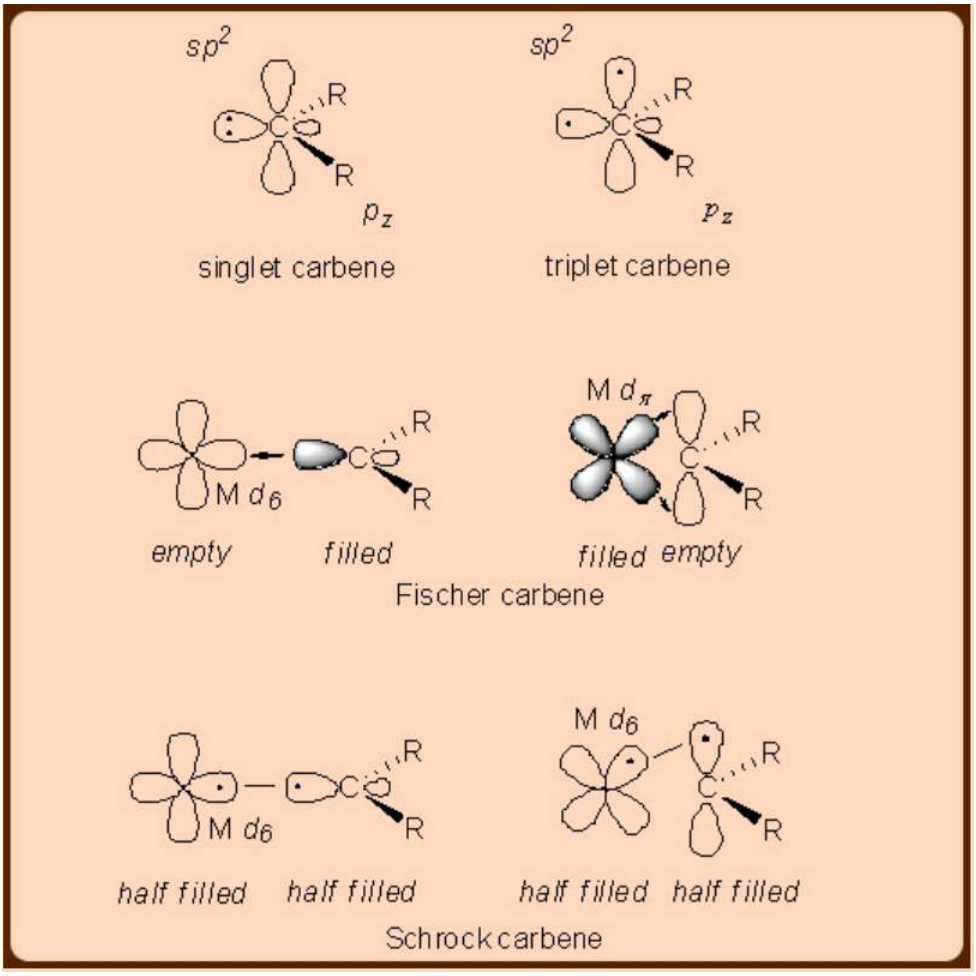


Figure **6.2.2.1**: Metal−ligand multiple bonding in the Fischer and Schrock carbene system.

The $L_nM{=}CR_2$ type Fischer carbene complexes comprise of two dative covalent interactions that include (*i*) a $L_nM{\leftarrow}CR_2$ type ligand to metal σ−donation and (*ii*) a $L_nM{\rightarrow}CR_2$ type metal to ligand π−back donation. The Fischer type carbene complexes are usually formed with metal centers at a low oxidation state. These are also commonly observed for the more electron rich late−transition metals that participate in the $L_nM{\rightarrow}CR_2$ type metal to ligand π−back donation. Another characteristic of the Fischer type carbene complex is the presence of the heteroatom substituents like R = OMe or NMe_2 on the carbene CR_2 moiety which makes the carbene carbon significantly cationic (δ^+) to facilitate the $L_nM{\rightarrow}CR_2$ type metal to ligand π−back donation.

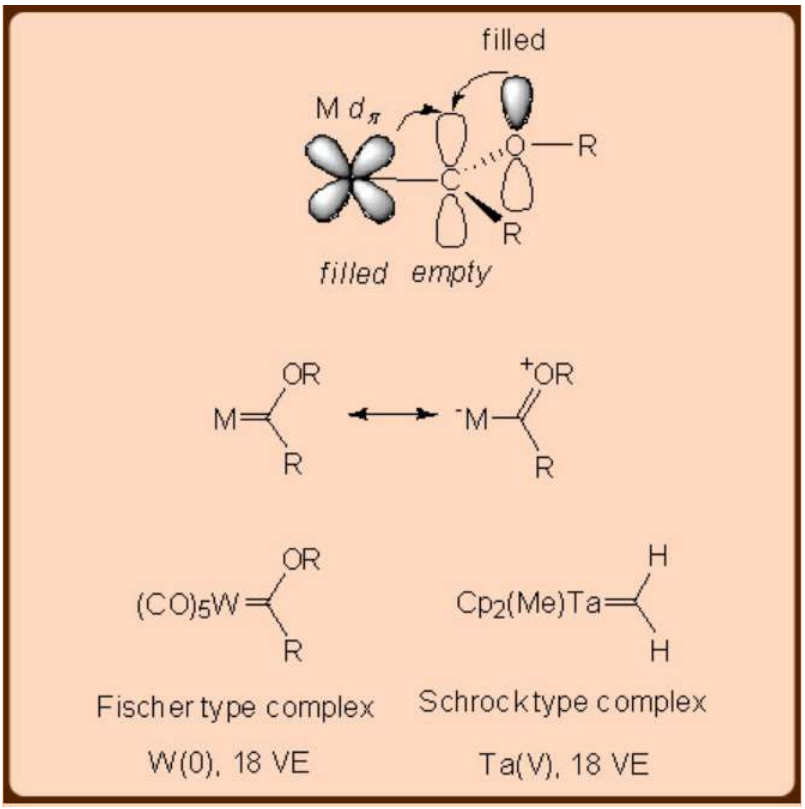
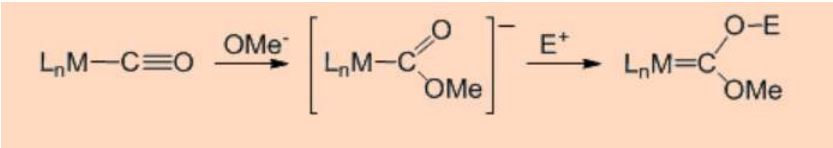


Figure **6.2.2.2**: Fischer and Schrock type complexes.

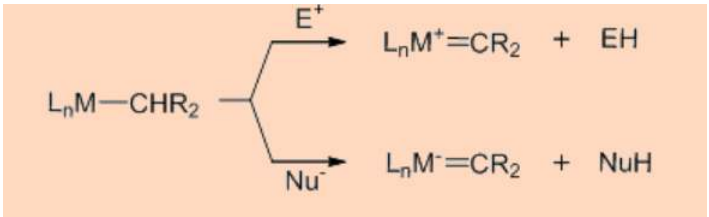
Similarly, the $L_nM{=}CR_2$ type Schrock carbene complexes comprise of two covalent interactions that involve one electron donation towards the σ−bond from each of the metal L_nM and the carbene CR_2fragments. Schrock carbene complexes are thus formed with the metal centers having high oxidation state and are usually observed for electron deficient early−transition metals (Figure **6.2.2.2**).

Carbene complexes can be prepared by the following methods.

i. by the reaction with electrophiles



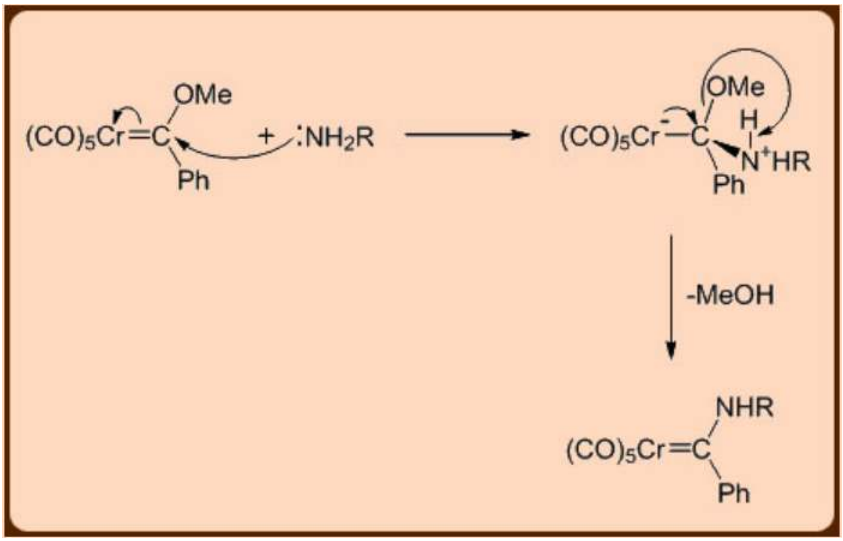
ii. by H^-/H^+ abstraction reactions as shown below



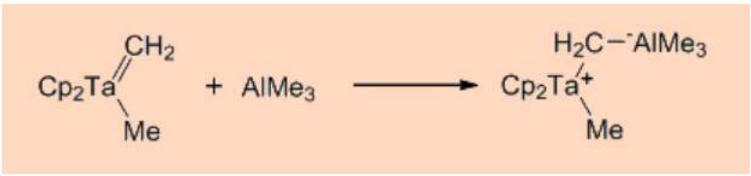
iii. from low−valent metal complexes

$$L_nM + CH_2N_2 \longrightarrow L_nMCH_2 + N_2$$

Because of the electronically different metal−ligand interaction that exist between the L_nM and the carbene CR_2 moiety, the reactivity of Fischer and Schrock carbene complexes are completely different. For example, the Fischer type carbene complexes undergo attack by nucleophiles at its carbene−C center.



The Schrock type carbene complexes on the other hand undergo attack by electrophiles at its carbene−C center.



Summary

The metal−ligand multiple bonding is of significant interest as many of the compounds containing such bonds are important intermediates in various catalytic cycles. The metal−ligand doubly bonded carbene systems can exist in two varieties like the Fischer type and the Schrock type carbene complexes. Due to their different electronic structures, the reactivities of these Fischer type and the Schrock type carbene complexes differ significantly, with the former undergoing nucleophilic attack while the later undergo electrophilic attack at their respective carbene−C centers.

6.2.2: Metal-Carbenes is shared under a CC BY-SA license and was authored, remixed, and/or curated by LibreTexts.

- **13.1: Metal-Carbenes** by M. S. Balakrishna & Prasenjit Ghosh is licensed CC BY-NC-SA 4.0. Original source: https://nptel.ac.in/courses/104101006.

6.2.3: Metal Hydrides

Learning Objectives

In this lecture you will learn the following

- Know about metal hydrides, their synthesis, characterization and their reactivity.
- Know about σ−complexes and their properties.
- Know about transition metal dihydrogen complexes.

Metal hydrides occupy an important place in transition metal organometallic chemistry as the M−H bonds can undergo insertion reactions with a variety of unsaturated organic substrates yielding numerous organometallic compounds with M−C bonds. Not only the metal hydrides are needed as synthetic reagents for preparing the transition metal organometallic compounds but they also are required for important hydride insertion steps in many catalytic processes. The first transition metal hydride compound was reported by W. Heiber in 1931 when he synthesized $Fe(CO)_4H_2$. Though he claimed that the $Fe(CO)_4H_2$ contained Fe−H bond, it was not accepted until 1950s, when the concept of normal covalent M−H bond was widely recognized.

The metal hydride moieties are easily detectable in ^1H NMR as they appear high field of TMS in the region between 0 to 60 ppm, where no other resonances appear. The hydride moieties usually couple with metal centers possessing nuclear spins. Similarly, the hydride moieties also couple with the adjacent metal bound phosphine ligands, if at all present in the complex, exhibiting characteristic *cis* (J = 15 − 30 Hz) and *trans* (J = 90 − 150 Hz) coupling constants. In the IR spectroscopy, the M−H frequencies appear between (1500 − 2200) cm^{-1} but their intensities are mostly weak. Crystallographic detection of metal hydride moiety is difficult as hydrogen atoms in general are poor scatterer of X−rays. Located adjacent to a metal atom in a M−H bond, the detection of hydrogen atom thus becomes challenging and as a consequence the X−ray crystallographic method systematically underestimates the M−H internuclear distance by ~ 0.1 Å. However, better data could be obtained by performing the X−ray diffraction studies at a low temperature in which the thermal motion of the atoms are significantly reduced. In light of these facts, the neutron diffraction becomes a powerful method for detection of the metal hydride moieties as hydrogen scatters neutrons more effectively and hence the M−H bond distances can be measured more accurately. A limitation of neutron diffraction method is that large sized crystals are required for the study.

Synthesis

Following reactions are employed for synthesizing metal hydrides.

i. Protonation reactions

For this reaction to occur the metal center has to be basic and electron rich.

$$[Fe(CO)_4]^{-2} \xrightarrow{H^+} [HFe(CO)_4]^- \xrightarrow{H^+} H_2Fe(CO)_4$$

ii. From hydride donors

Generally for this method, a main group hydride is reacted with metal halide.

$$WCl_6 + LiBEt_3H + PR_3 \longrightarrow WH_6(PR_3)_3$$

iii. Using dihydrogen (H_2) addition

This method involves oxidative addition of H_2 and thus requires metal centers that are capable of undergoing the oxidative addition step.

$$WMe_6 + PMe_2Ph \xrightarrow{H_2} WH_6(PMe_2Ph)_3$$

iv. From a ligand

This method takes into account the β−elimination that occur in a variety of metal bound ligand moieties, thereby yielding a M−H bond.

$$RuCl_2(PPh_3)_3 + KOCHMe_2 + PPH_3 \longrightarrow RuH_2(PPh_3)_4 + Me_2CO + KCl$$

Reactions of metal hydrides

Metal hydrides are reactive species kinetically and thus participate in a variety of transformations like the ones discussed below.

i. Deprotonation reactions

The deprotonation reaction can be achieved by a hydride moiety resulting in the formation of H_2gas as shown below.

$$WH_6(PMe_3)_3 + NaH \longrightarrow Na[WH_5(PMe_3)_3] + H_2$$

ii. Hydride transfer and insertion

In this reaction a hydride transfer from a metal center to formaldehyde resulting in the formation of a metal bound methoxy moiety is observed as shown below.

$$Cp_2 \cdot ZrH_2 + CH_2O \longrightarrow Cp_2 \cdot Zr(OMe)_2$$

iii. Hydrogen atom transfer reaction

An example of hydrogen atom transfer reaction is given below.

$$[Co(CN)_5H]^{3-} + PhCH{=}CHCOOH \longrightarrow [Co(CN)_5]^{3-} + PHCH{-}CH_2COOH$$

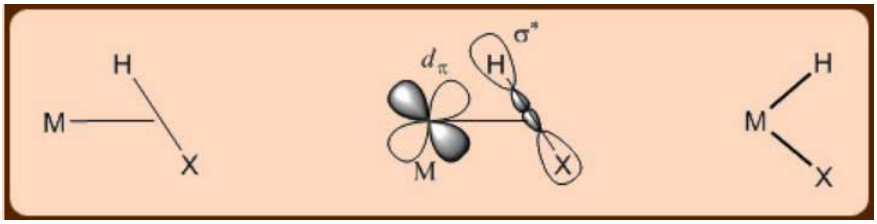
It is interesting to note that the nature of hydrogen atom in a M−H bond can vary from being protic in nature, when bound to electron deficient metal centers as in metal carbonyl compounds, to that of being hydridic in nature, when bound to more electropositive early transition metals. In the latter case, the hydride moieties tend to be basic and exhibit hydride transfer reactions with electrophiles like aldehydes or ketones. Furthermore, the protonation of these basic metal hydrides leads to the elimination of dihydrogen (H_2) gas along with the generation of a vacant coordination site at the metal center.

Bridging hydrides

The metal hydrides usually show two modes of binding, namely terminal and bridging. In case of the bridging hydrides, the hydrogen atom can bridge between two or even more metal centers and thus, the bridging hydrides often display bent geometries.

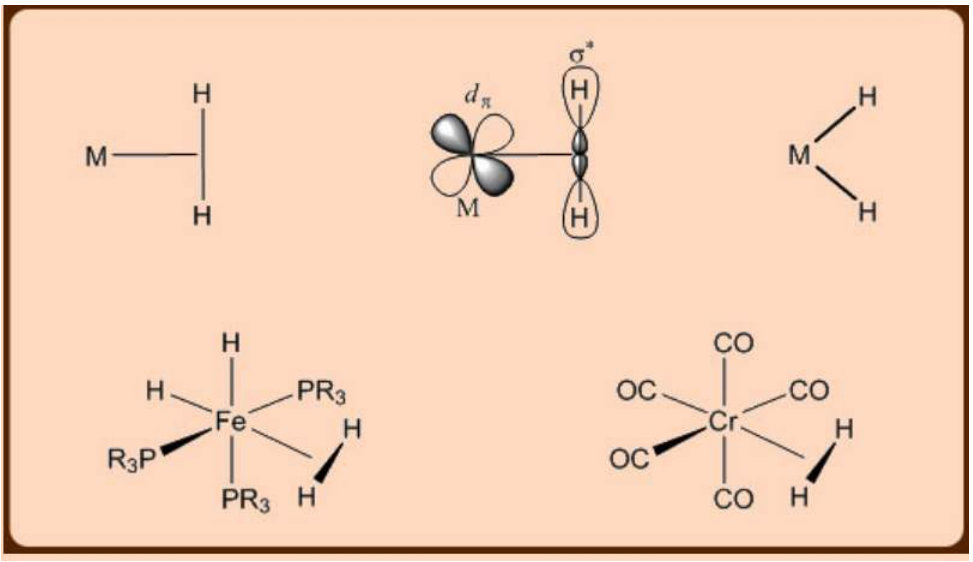
σ−complexes

σ−complexes are rare compounds, in which the σ bonding electrons of a X−H bond further participate in bonding with a metal center (X = H, Si, Sn, B, and P). The σ complexes thus exhibit an askewed binding to a metal center with the hydrogen atom, containing no lone pair, being more close to the metal center and thereby resulting in a side−on structure. Many times if the metal center is electron rich, then further back donation to the σ* orbital of the metal bound X−H moiety may occur resulting in a complete cleavage of the X−H bond.

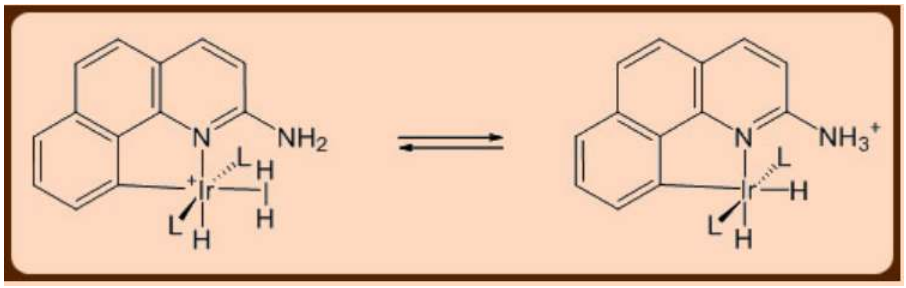


Metal dihydrogen complexes

The simplest variant of a σ−complex contains a dihydrogen ligand. The first dihydrogen complex was isolated by Kubas, after which many new ones were reported.



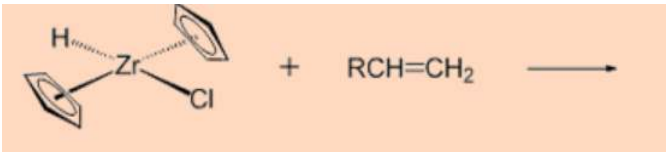
Quite expectedly, the dihydrogen moiety bound to a metal in a σ−complex is found to be more acidic (p*K*a = 0 − 20) when compared to the free dihydrogen molecule (p*K*a = 35). It is interesting to note that the p*K*a change associated with the binding of dihydrogen to a metal in a σ−complex relative to that of the free H_2 molecule is significantly larger than the change associated with binding of H_2O to metal. Owing to this inherent acidity, the deprotonation of the metal bound dihydrogen moiety by a base can thus be appropriately employed for heterolytic activation of the dihydrogen moiety as illustrated below.



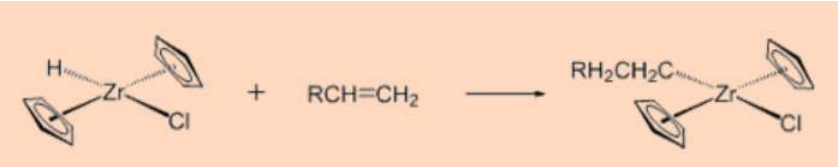
The dihydrogen complexes of metals are often referred to as nonclassical hydrides. The electron rich π basic metals are anticipated to split the metal bound dihydrogen moieties resulting in classical dihydride complexes. Along the same line of thinking, the electron deficient and less π basic metal would tend to stabilize a dihydrogen complex. The dihydrogen complexes can also be characterized by the X ray diffraction as well as neutron diffraction methods. In IR spectrum, the metal bound H−H stretch appear in the range (2300 − 2900) cm^{-1} while in the ^1H NMR spectrum the same appear between 0 to −10 ppm as a broad peak. The dihydrogen complexes are often characterized by isotopic labeling studies of metal bound H−D moiety that shows a coupling constant of 20 – 34 Hz as supposed to 43 Hz observed in case of the free H−D molecule.

Problems

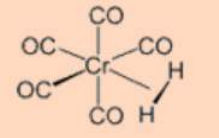
1. Predict the product of the reaction.



Ans:



2. Give the oxidation state and total valence electron count of the metal center.



Ans: Oxidation state 0 and 18 VE

3. What kind of metal centers would stabilize metal dihydrogen complexes?

Ans: Electron deficient and less π basic ligands

4. Specify whether the nature of hydrogen moiety in the complex, $HCo(CO)_4$ is acidic or basic?

Ans: Acidic

5. Where do the M−H stretching bands appear in the IR spectrum of metal hydride complexes?

Ans: 1500 to 2200 cm^{-1}

Self Assessment test

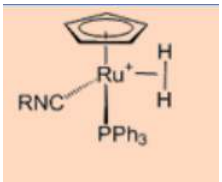
1. Predict the product of the reaction.

$$IrCl(Co)(Pph_3)_2 \xrightarrow{H_2}$$

Ans:

$$IrCl(CO)(PPh_3)_2 \xrightarrow{H_2} IrH_2Cl(CO)(PPh_3)_2$$

2. Give the oxidation state and total valence electron count of the metal center.



Ans: Oxidation state +2 and 18 VE

3. What kind of metal centers would stabilize classical dihydride complexes?

Ans: Electron rich and more p basic ligands

4. Specify whether the nature of hydrogen moiety in the complex, $IrH_5(PCy_3)_2$ is acidic or basic?

Ans: Basic

5. Between X−ray diffraction and neutron diffraction, which is a better method for the characterization of the M−H moiety?

Ans: Neutron diffraction

Summary

Metal hydrides are important compounds in the overall scheme of organometallic chemistry as they are involved in many crucial steps of numerous catalytic reactions. Apart from metal hydrides another important class of compounds are transition metal

σ−complexes whose simplest variant are the metal dihydrogen complexes. These σ−complexes and the metal dihydrogen complexes are important for the heterolytic activations of the respective metal bound H−heteroatom and the H−H bonds.

6.2.3: Metal Hydrides is shared under a CC BY-SA license and was authored, remixed, and/or curated by LibreTexts.

- **7.2: Metal Hydrides** by M. S. Balakrishna & Prasenjit Ghosh is licensed CC BY-NC-SA 4.0. Original source: https://nptel.ac.in/courses/104101006.

6.2.4: Metal Carbonyls

Learning Objectives

In this lecture you will learn the following

- The historical background of metal carbonyl complexes.
- The CO ligand and its binding ability to metal.
- Synergism between the ligand to metal forward σ–donation and the metal to ligand backward π–donation observed in a metal-CO interaction.
- The synthesis, characterization and their reactivity of the metal carbonyl compounds.

Metal carbonyls are important class of organometallic compounds that have been studied for a long time. Way back in 1884, Ludwig Mond, upon observing that the nickel valves were being eating away by CO gas in a nickel refining industry, heated nickel powder in a stream of CO gas to synthesize the first known metal carbonyl compound in the form $Ni(CO)_4$. The famous Mond refining process was thus born, grounded on the premise that the volatile $Ni(CO)_4$ compound can be decomposed to pure metal at elevated temperature. Mond subsequently founded the Mond Nickel Company Limited for purifying nickel from its ore using this method.

The carbonyl ligand (CO) distinguishes itself from other ligands in many respects. For example, unlike the alkyl ligands, the carbonyl (CO) ligand is unsaturated thus allowing not only the ligand to σ−donate but also to accept electrons in its π* orbital from d_π metal orbitals and thereby making the CO ligand π−acidic. The other difference lies in the fact that CO is a soft ligand compared to the other common σ−and π−basic ligands like H_2O or the alkoxides (RO−), which are considered as hard ligands.

Being π−acidic in nature, CO is a strong field ligand that achieves greater *d*−orbital splitting through the metal to ligand π−back donation. A metal−CO bonding interaction thus comprises of a CO to metal σ−donation and a metal to CO π−back donation (Figure **6.2.4.1**). Interestingly enough, both the spectroscopic measurements and the theoretical studies suggest that the extent of the metal to CO π−back donation is almost equal to or even greater than the extent of the CO to metal σ−donation in metal carbonyl complexes. This observation is in agreement with the fact that low valent−transition metal centers tend to form metal carbonyl complexes.

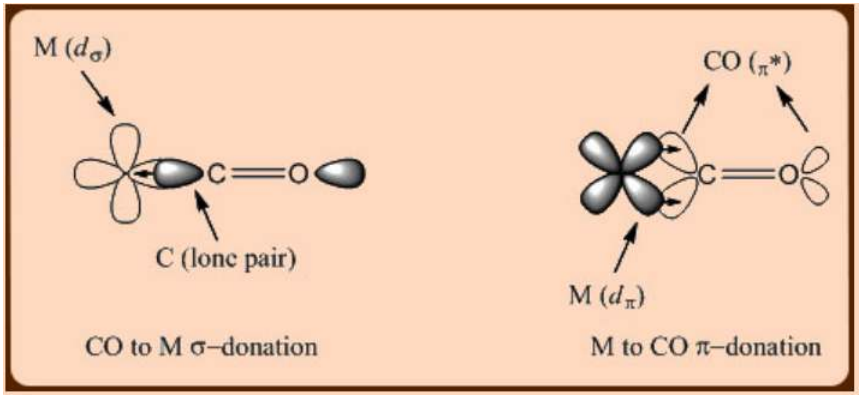


Figure **6.2.4.1**: Orbital diagram showing ligand to metal forward σ-donation and the metal to ligand backward π-donation in metal-CO interaction.

In the metal carbonyl complexes, the direct bearing of the π−back donation is observed on the M−C bond distance that becomes shorter as compared to that of a normal M−C single bond distance. For example, the $CpMo(CO)_3CH_3$ complex, exhibits two kind of M−C bond distances that comprise of a longer Mo−CH_3 distance (2.38 Å) and a much shorter Mo−CO distance (1.99 Å) arising out of a metal to ligand π−back donation. It becomes thus apparent that the metal−CO interaction can be easily characterized using X−ray crystallography. The infrared spectroscopy can also be equally successfully employed in studying the metal−CO interaction. Since the metal to CO π−back bonding involves a π−donation from the metal d_π orbital to a π* orbital of a C−O bond, significant shift of the ν(CO) stretching frequency towards the lower energy is observed in metal carbonyl complexes with respect to that of free CO (2143 cm^{-1}).

Preparation of metal carbonyl complexes

The common methods of the preparation of the metal carbonyl compounds are,

i. Directly using CO

$$Fe \xrightarrow{CO,\ 200\ atm,\ 200^{\circ}C} Fe(CO)_5$$

The main requirement of this method is that the metal center must be in a reduced low oxidation state in order to facilitate CO binding to the metal center through metal to ligand π−back donation.

ii. Using CO and a reducing agent

$$NiSO_4 + CO + S_2O_4^{2-} \longrightarrow Ni(CO)_4$$

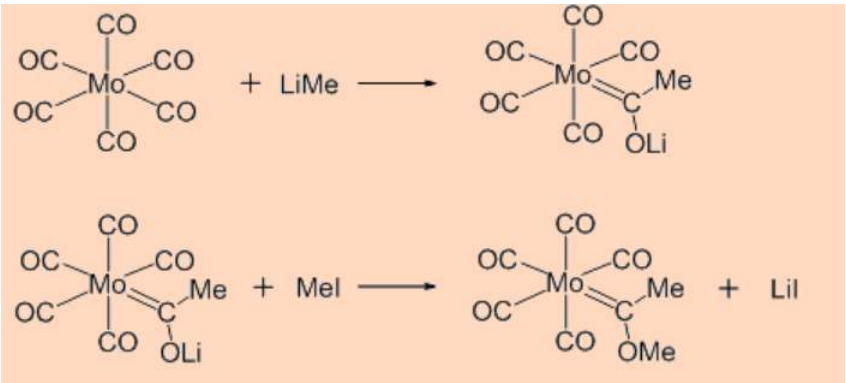
This method is commonly called reductive carbonylation and is mainly used for the compounds having higher oxidation state metal centers. The reducing agent first reduces the metal center to a lower oxidation state prior to the binding of CO to form the metal carbonyl compounds.

iii. From carbonyl compounds

This method involves abstraction of CO from organic compounds like the alcohols, aldehydes and CO_2.

Reactivities of metal carbonyls

i. Nucleophilic attack on carbon



The reaction usually gives rise to carbene moiety.

ii. Electrophilic attack at oxygen

$$Cl(PR_3)_4Re{-}CO + AlMe_3 \longrightarrow Cl(PR_3)_4Re{-}CO \longrightarrow AlMe_3$$

iii. Migratory insertion reaction

$$MeMn(CO)_5 + PMe_3 \longrightarrow (MeCO)Mn(CO)_4(PMe_3)$$

The metal carbonyl displays two kinds of bindings in the form of the terminal and the bridging modes. The infrared spectroscopy can easily distinguish between these two binding modes of the metal carbonyl moiety as the terminal ones show ν(CO) stretching band at *ca*. 2100-2000 cm^{-1} while the bridging ones appear in the range 1720−1850 cm^{-1}. The carbonyl moiety can bridge between more than two metal centers (Figure **6.2.4.2**).

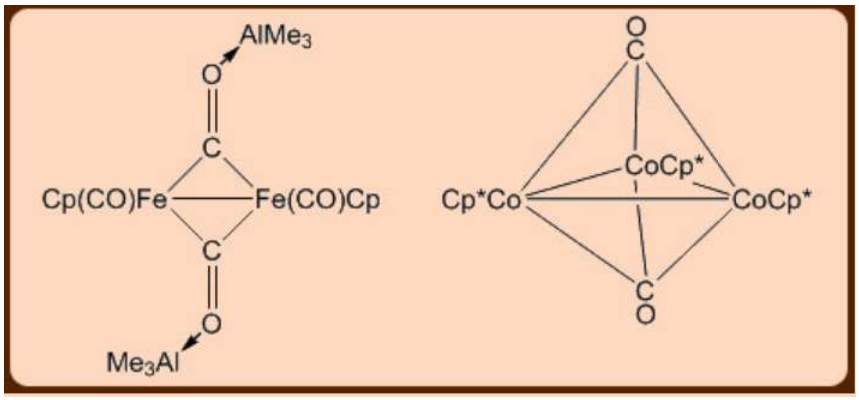


Figure **6.2.4.2**: Different bridging modes of the carbonyl binding to a metal is shown.

Problems

1. How many lone pairs are there in the CO molecule?

Ans: Three (one from carbon and two from oxygen).

2. Despite O being more electronegative than C, the dipole moment of CO is almost zero. Explain.

Ans: Because of the electron donation from oxygen to carbon.

3. What type of metal centers form metal carbonyl complexes?

Ans: Low−valent metal centers.

4. What are the two main modes of binding exhibited by CO ligand?

Ans: Terminal and bridging modes of binding.

Self Assessment test

1. Predict the product of the reaction?

$$\mathbf{Ni + CO_{Excess} \longrightarrow}$$

Ans: Three (one from carbon and two from oxygen).

2. Upon binding to a metal center the C−O stretching frequency increases/decreases with regard to that of the free CO?

Ans: Decreases.

3. Explain why do low−valent metal centers stabilize CO binding in metal carbonyl complexes?

Ans: Because metal to ligand π−back donation.

4. Give an example of a good σ−donor and π−donor ligand?

Ans: Alkoxides (RO^-).

Summary

CO is a hallmark ligand of organometallic chemistry. The metal carbonyl complexes have been studied for a long time. The CO ligands bind tightly to metal center using a synergistic mechanism that involves σ−donation of the ligand lone pair to metal and followed by the π−back donation from a filled metal *d* orbital to a vacant σ* orbital of C−O bond of the CO ligand. The metal carbonyl complexes are prepared by several methods. The metal carbonyl complexes are usually stabilized by metal centers in low oxidation states.

6.2.4: Metal Carbonyls is shared under a CC BY-SA license and was authored, remixed, and/or curated by LibreTexts.

- **8.1: Metal Carbonyls** by M. S. Balakrishna & Prasenjit Ghosh is licensed CC BY-NC-SA 4.0. Original source: https://nptel.ac.in/courses/104101006.

6.2.5: Metal Phosphines

Learning Objectives

In this lecture you will learn the following

- Know about metal phosphine complexes.
- Have an understanding of the steric and electronic properties of the phosphine ligands.
- Obtain a deeper insight about the metal phosphine interactions.
- Be introduced to other π−basic ligands.

Phosphines are one of the few ligands that have been extensively studied over the last few decades to an extent that the systematic fine tuning of the sterics and electronics can now be achieved with certain degree of predictability. Phosphines are better spectator ligands than actor ligands. Tolman carried out pioneering infrared spectroscopy experiments on the $PR_3Ni(CO)_3$ complexes looking at the $\nu_{(CO)}$stretching frequencies for obtaining an insight on the donor properties of the PR_3 ligands. Thus, a stronger σ−donor phosphine ligand would increase the electron density at the metal center leading to an enhanced metal to ligand π−back bonding and thereby lowering of the $\nu_{(CO)}$ stretching frequencies in these complexes. Another important aspect of the phosphine ligand is its size that has significant steric impact on its metal complexes. Thus, unlike CO ligand, which is small and hence many may simultaneously be able to bind to a metal center, the same is not true for the phosphine ligands as only a few can bind to a metal center. The number of phosphine ligands that can bind to a metal center also depends on the size of its R substituents. For example, up to two can bind to a metal center in case of the PCy_3 or $P(i\text{−}Pr)_3$ ligands, three or four for PPh_3, four for Me_2PH, and five or six for PMe_3. The steric effect of phosphine was quantified by Tolmann and is given by a parameter called *Cone Angle* that measures the angle at the metal formed by the PR_3 ligand binding to a metal (Figure **6.2.5.1**).

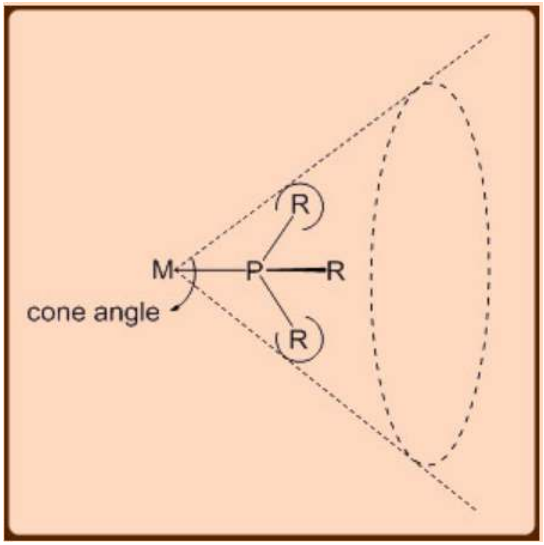


Figure **6.2.5.1**: Cone Angle in metal−phosphine complexes.

The *Cone Angle* criteria has been successfully invoked in rationalizing the properties of a wide range of metal phosphine complexes. One unique feature of the phosphine ligand is that it allows convenient change of electronic effect without undergoing much change in its steric effects. For example, PBu_3 and $P(O^iPr)_3$ have similar steric effects but vary in their electronic effects. The converse is also true as the steric effect can be easily changed without undergoing much change in the electronic effect. For example, PMe_3 and $P(o\text{−}tolyl)_3$ have similar electronic effect but differ in their steric effects. Thus, the ability to conveniently modulate the steric and the electronic effects make the phosphine ligands a versatile system for carrying out many organometallic catalysis.

Structure and Bonding

Phosphines are two electron donors that engage a lone pair for binding to metals. These are thus considered as good σ−donors and poor π−acceptors and they belong to the same class with the aryl, dialkylamino and alkoxo ligands. In fact they are more π−acidic

than pure σ−donor ligands like $NH_3$and, more interestingly so, their π−acidity can be varied significantly by systematic incorporation of substituents on the P atom. For example, PF_3 is more π−acidic than CO. Analogous to what is observed in case of the benchmark π−acidic CO ligand, in which the metal d_π orbital donates electron to a π* orbital of a C−O bond, in the case of the phosphines ligands, such π−back donation occurs from the metal d_π orbital occurs on to a σ* orbital of a P−R bond (Figure **6.2.5.2**). In phosphine ligands, with the increase of the electronegativity of R both of the σ and the σ* orbitals of the P−R bond gets stabilized. Consequently, the contribution of the atomic orbital of the P atom to the σ*−orbital of the P−R bond increases, which eventually increases the size of the σ* orbital of the P−R bond. This in turn facilitates better overlap of the σ* orbital of the P−R bond with the metal d_π orbital during the metal to ligand π−back donation in these metal phosphine complexes.

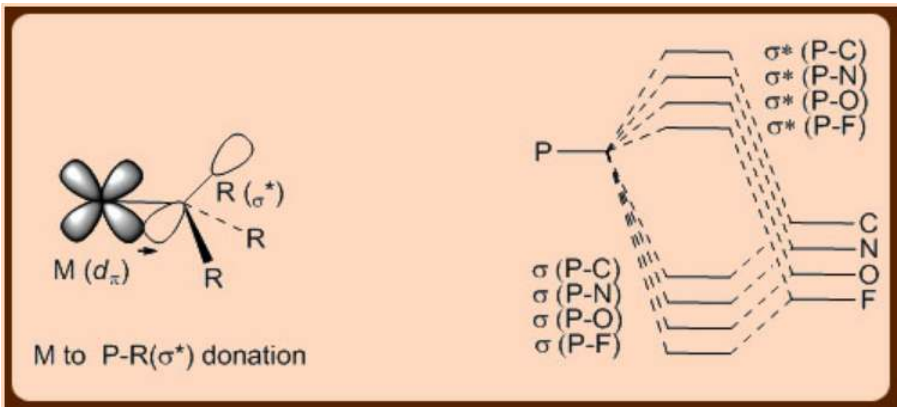


Figure **6.2.5.2**: Back donation from the metal d_π orbital to a σ* orbital of a P−R bond.

Starting from CO, which is a strong π−acceptor ligand, to moving to the phosphines, which are good σ−donors and poor π−acceptor ligands, to even going further to other extreme to the ligands, which are both good σ−donors as well as π−donors, a rich variety of phosphine ligands thus are available for stabilizing different types of organometallic complexes. In this context the following ligands are discussed below.

π-basic ligands

Alkoxides (RO^-) and halides like F^-, Cl^- and Br^- belong to a category of π−basic ligands as they engage a second lone pair for π−donation to the metal over and above the first lone pair partaking σ−donation to the metal. Opposite to what is observed in the case of π−acidic ligands, in which the π* ligand orbital stabilizes the d_π metal orbital and thereby affecting a larger ligand field splitting, as consistent with the strong field nature of these ligands (Figure 3), in the case of the π−basic ligands, the second lone pair destabilizes the d_π metal orbitals leading to a smaller ligand field splitting, which is in agreement with the weak field nature of these ligands. The orbitals containing the lone pair of the ligands are usually located on the more electronegative heteroatoms and so they are invariably lower in energy than the metal d_π orbitals. Hence, the destabilization of the metal d_π orbitals occurs due to the repulsion of the filled ligand lone pair orbital with the filled metal d_π orbitals. In case of the situations in which the metal d_π orbitals are vacant, like in d^0 systems of Ti^{4+} ions, the possibility of the destabilization of the metal d_π orbitals do not arise but instead stabilization occurs through the donation of the filled ligand lone pair orbital electrons to the empty metal d_π orbitals as seen in the case of TiF_6 and $W(OMe)_6$. Thus, this scenario in π−basic ligands is opposite to that observed in case of the π−acidic ligands, for which the empty π* ligand orbitals are higher in energy than the filled metal d_π orbitals.

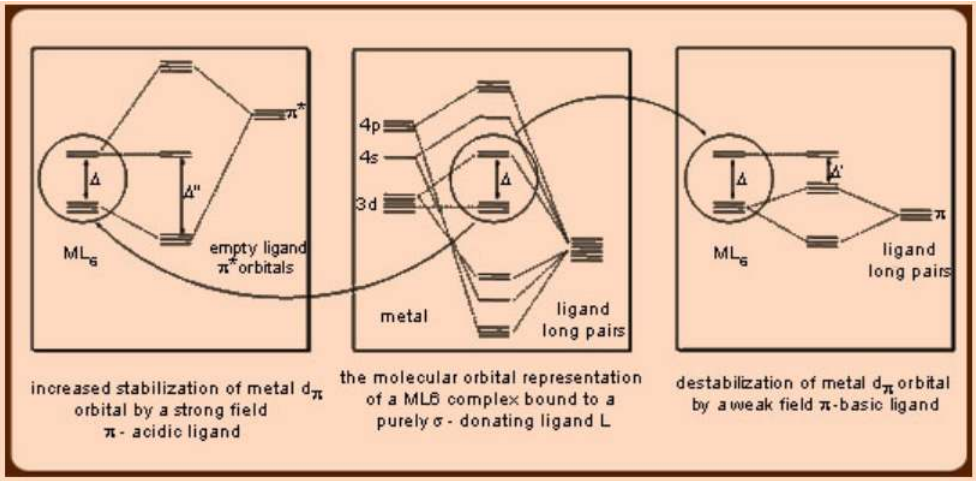


Figure **6.2.5.3**: Orbital interactions in the presence of the π−acceptor, (pure) σ−donor and π−basic ligands are shown.

6.2.5: Metal Phosphines is shared under a CC BY-SA license and was authored, remixed, and/or curated by LibreTexts.

- **8.2: Metal Phosphines** by M. S. Balakrishna & Prasenjit Ghosh is licensed CC BY-NC-SA 4.0. Original source: https://nptel.ac.in/courses/104101006.

SECTION OVERVIEW

6.2.6: Complexes of π−bound Ligands

6.2.6.1: Metal Alkene Complexes

6.2.6.2: Metal Allyl and Diene Complexes

6.2.6.3: Metal Cyclopentadienyl Complexes

6.2.6: Complexes of π−bound Ligands is shared under a CC BY-SA license and was authored, remixed, and/or curated by LibreTexts.

6.2.6.1: Metal Alkene Complexes

Learning Objectives

In this lecture you will learn the following

- The metal alkene complexes.
- The metal−olefin bonding interactions.
- The synthesis and reactivities of the metal−olefin complexes.
- The *umpolung* reactivities of olefins in the metal alkene complexes.

Though the first metal olefin complex dates back a long time to the beginning of 19th century, its formulation was established only a century later in the 1950s. While reacting $\mathbf{K_2PtCl_4}$ with EtOH in 1827, the Danish chemist Zeise synthesized the famous **Zeise's salt** $\mathbf{K[PtCl_3(C_2H_4)]\cdot H_2O}$ containing a Pt bound ethylene moiety and which incidentally represented the first metal−olefin complex (Figure **6.2.6.1.1**).

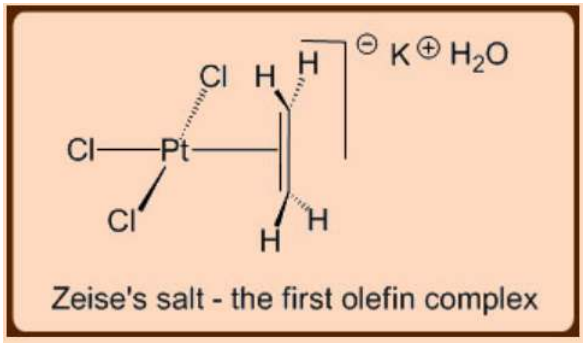


Figure **6.2.6.1.1**: Zeise's salt

The metal−olefin bonding interaction is best explained by the *Dewar−Chatt* model, that takes into account two mutually opposing electron donation involving σ−donation of the olefinic C=C π−electrons to an empty d_π metal orbital followed by π−back donation from a filled metal d_π orbital into the unoccupied C=C π* orbital. Quite understandably so, for the d^0 systems, the formations of metal−olefin complexes are not observed. The extent of the C=C forward π-donation to the metal and the subsequent π−back donation from the filled d_π orbital to the olefinic C=C π* orbital have a direct bearing on the C=C bond of the metal bound olefinic moiety in form of bringing about a change in hybridization as well as in the C−C bond distance (Figure **6.2.6.1.2**).

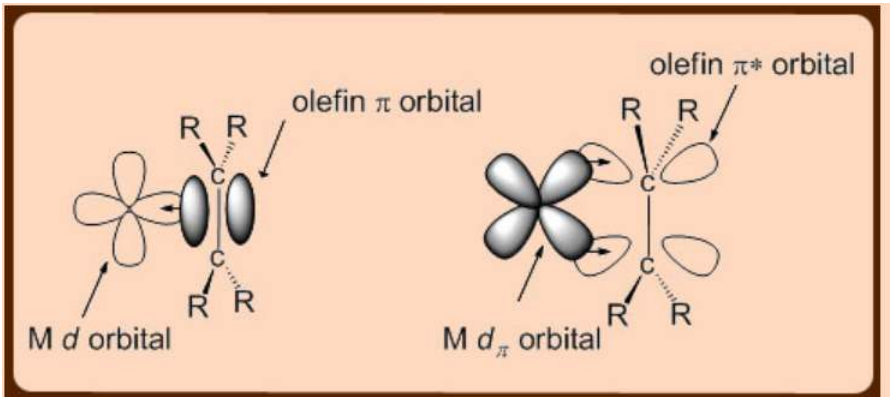


Figure **6.2.6.1.2**: Metal olefin bonding interactions.

If the metal to ligand π−back donation component is smaller than the ligand to metal σ−donation, then the lengthening of the C−C bond in the metal bound olefin moiety is observed. This happens primarily because of the fact that the alkene to metal σ−donation removes the C=C π−electrons away from the C−C bond of the olefin moiety and towards the metal center, thus, decreasing its bond order and increasing the C−C bond length. Additionally, as the metal to ligand π−back donation increases, the electron donation of the filled metal d_π orbital on to the π* orbital of the metal bound olefin moiety is enhanced. This results in an increase in the C−C bond length. The lengthening of the C−C bond in metal bound olefin complex can be correlated to the π−basicity of the metal. For

example, for a weak π−basic metal, the C−C bond lengthening is anticipated to be small while for a strong π−basic metal, the C−C lengthening would be significant.

Another implication of ligand−metal π−back donation is in the observed change of hybridization at the olefinic C atoms from pure sp^2, in complexes with no metal to ligand π−back donation, to sp^3, in complexes with significant metal to ligand π−back donation, is observed. The change in hybridization from sp^2 to sp^3 centers of the olefinic carbon is accompanied by the substituents being slightly bent away from the metal center in the final metalacyclopropane form (Figure **6.2.6.1.3**). This change in hybridization can be conveniently detected by ^{1}H and ^{13}C NMR spectroscopy. For example, in case of the metalacyclopropane systems, which have strong metal to ligand π−back donation, the vinyl protons appear 5 ppm (in the ^{1}H NMR) and 100 ppm (in the ^{13}C NMR) high field with respect to the respective position of the free ligands.

An interesting fallout of the metal to ligand π−back bonding is the tighter binding of the strained olefins to the metal center as observed in the case of cyclopropene and norbornene. The strong binding of these cyclopropene and norbornene moieties to the metal center arise out of the relief of ring strain upon binding to the metal. Lastly, in the metal−olefin complexes having very little π−back bonding component, the chemical reactivities of the metal bound olefin appear opposite to that of a free olefin. For example, a free olefin is considered electron rich by virtue of the presence of π−electrons in its outermost valence orbital and hence it undergoes an electrophilic attack. However, the metal bound olefin complexes having predominantly σ−donation of the olefinic π−electrons and negligible metal to ligand π−back donation, the olefinic C becomes positively charged and hence undergoes a nuclophilic attack. This nature of reversal of olefin reactivity is called *umpolung* character.

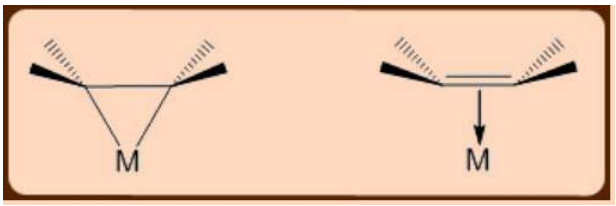


Figure **6.2.6.1.3**: Metalacyclopropane system and *Dewar−Chatt* model

Synthesis

Metal alkene complexes are synthesized by the following methods.

i. Substitution in low valent metals

$$AgOSO_2CF_3 + C_2H_4 \longrightarrow (C_2H_4)AgOSO_2CF_3$$

ii. Reduction of high valent metal in presence of an alkene

$$(cod)PtCl_2 + C_2H_4 \longrightarrow [PtCl_3(C_2H_4)]^- + Cl^-$$

iii. From alkyls and related species

$$Cp_2TaCl_3 + n\text{-}BuMgX \longrightarrow Cp2TaBu3$$

$$Cp2TaBu3 \xrightarrow[\text{reductive elimination}]{\text{Beta-elimination}} Cp_2TaH(1\text{-}Butene) + Butene + Butane$$

Reaction of alkenes

The metal alkene complexes show the following reactivities.

i. Insertion reaction

These reactions are commonly displayed by alkenes as they insert into metal−X bonds yielding metal alkyls. The reaction occurs readily at room temperature for X = H, whereas for other elements (X = other atoms), such insertions become rare. Also, the strained alkenes and alkynes undergo such insertion readily.

$$PtHCl(PEt_3)_2 + C_2H_4 \rightleftharpoons PtElCl(PEt_3)_2$$

ii. *Umpolung* reactions

Umpolung reactions are observed only for those metal−alkene complexes for which the metal center is a poor π−base and as a result of which the olefin undergoes a nuclophilic attack.

iii. Oxidative addition

Alkenes containing allylic hydrogens undergo oxidative addition to give a allyl hydride complex.

? Exercise 6.2.6.1.1

Predict the product of the reaction.

$$\mathbf{AuMe(PPh_3) + CF_2{=}CF_2 \longrightarrow A \longrightarrow B}$$

Answer

A = {(CF_2=CF_2)AuMe(PPh_3)} and

B = Au(CF_2-CF_2Me)(PPh_3)

? Exercise 6.2.6.1.2

Specify whether the lengthening/shortening of the C−C bond distance in the metal bound olefin moiety is observed as a result of metal to ligand π−back donation?

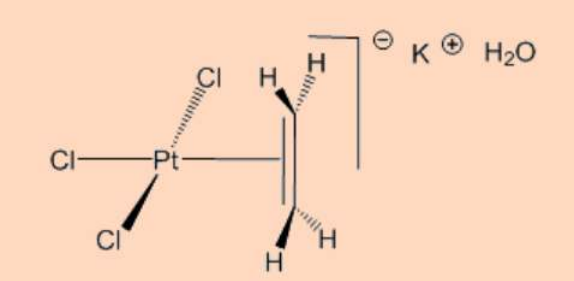
Answer

Lengthening

? Exercise 6.2.6.1.3

Draw the structure of Zeise's salt.

Answer



? Exercise 6.2.6.1.4

The change in hybridization at the olefinic C from sp^2 to sp^3 primarily arise due to?

Answer

Metal-ligand π-back donation.

Self Assessment test

1. Predict the product of the reaction.

$$\mathbf{PtCl_2^- + C_2H_4 \longrightarrow}$$

Ans: $[PtCl_3(C_2H_4)]^-$ and Cl^-

2. Specify whether the lengthening/shortening of the C−C bond distance in the metal bound olefin moiety is observed as a result of ligand to metal σ− donation?

Ans: Lengthening.

3. Metalacyclopropane intermediate in a metal bound olefin complex is primarily formed due to which kind of interaction?

Ans: Metal−ligand π−back donation

4. The oxidation state of Pt in Zeise's salt is?

Ans: Pt^{II}

Summary

Alkenes are an important class of unsaturated ligands that bind to a metal by σ−donating its C=C π−electrons and also accepts electrons from the metal in its π* orbital of C=C bond. These symbiotic σ−donation and π−back donation in metal bound olefin complexes have a significant impact on their structure and reactivity properties. Quite importantly, the structural manifestations arising out of these forward σ−donation and π−back donation can be characterized by using ^1H, ^{13}C NMR and IR spectroscopic methods.

6.2.6.1: Metal Alkene Complexes is shared under a CC BY-SA license and was authored, remixed, and/or curated by LibreTexts.

- **9.1: Metal Alkene Complexes** by M. S. Balakrishna & Prasenjit Ghosh is licensed CC BY-NC-SA 4.0. Original source: https://nptel.ac.in/courses/104101006.

6.2.6.2: Metal Allyl and Diene Complexes

Learning Objectives

In this lecture you will learn the following

- The metal−allyl complexes.
- The metal−diene complexes.
- The metal−cyclobutadiene complexes.
- The respective metal−ligand interactions.

The allyl ligand is often referred to as an “actor” ligand rather than a “spectator” ligand. It binds to metals in two ways *i.e.* in a η^1 (monohapto) form and a η^3 (trihapto) form (Figure **6.2.6.2.1**). (*i*). In its monohapto (η^1) form, it behaves as an anionic *1e−donor* X type of a ligand analogous to that of a methyl moiety while (*ii*) in a trihapto (η^3) form, it acts as an anionic *3e−donor* LX type of a ligand.

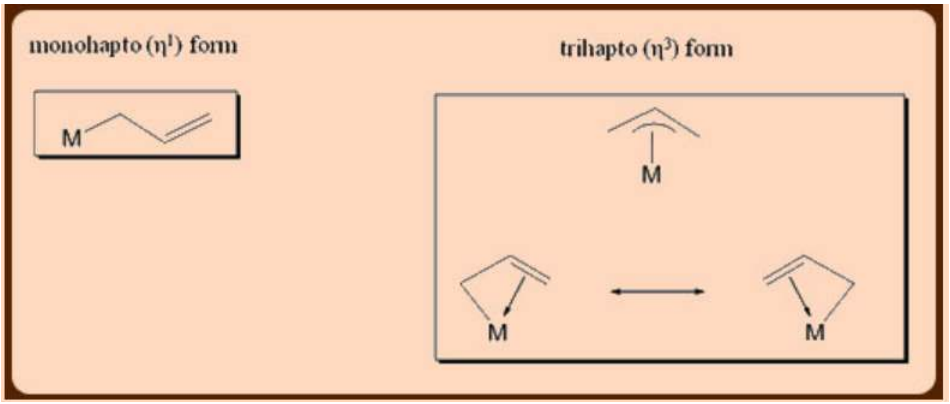


Figure **6.2.6.2.1**: Metal−allyl interaction.

Metal−allyl interaction

Of particular interest are the molecular orbitals namely Ψ_1, Ψ_2 and Ψ_3 of the allyl ligand that interact with the metal in a metal allyl complex. The energy of these molecular orbitals increase with the increase in the number of nodes. Of the three, the Ψ_1 and Ψ_2 orbitals usually engage in ligand to metal σ−donation, with Ψ_1 involving in a dative L−type bonding and Ψ_2 participating in a covalent X−type bonding with the metal *d* orbitals (Figure **6.2.6.2.2**).

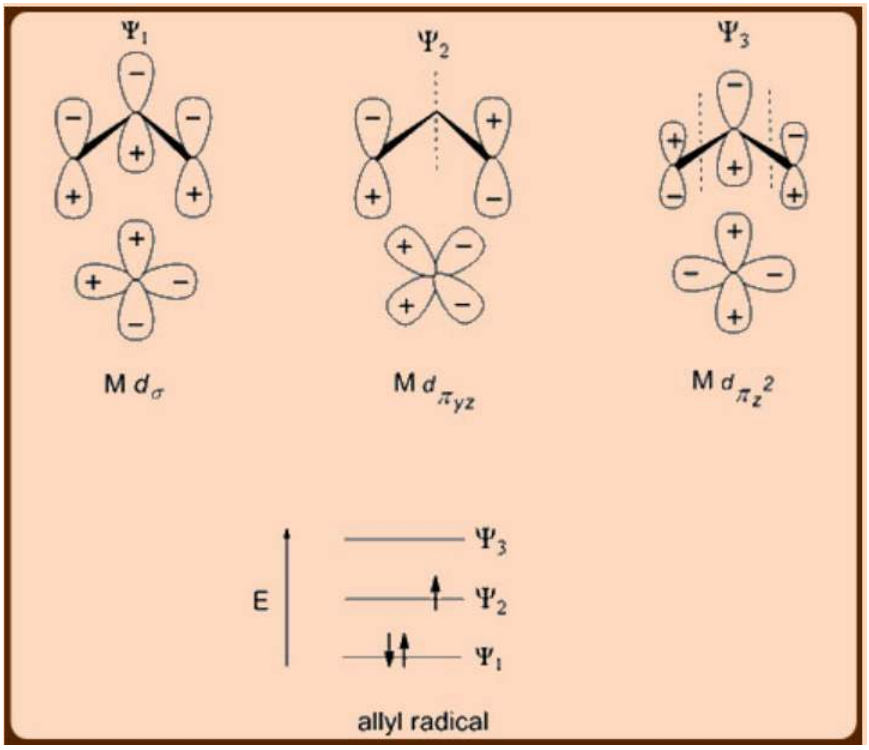


Figure **6.2.6.2.2**: Metal−allyl interactions.

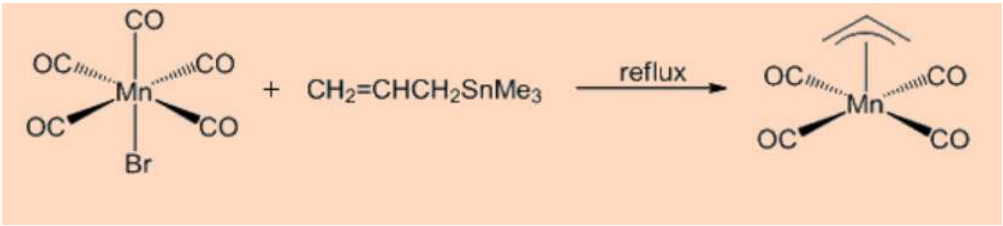
Synthesis of the metal allyl complexes

The metal allyl complexes are synthesized by the following methods.

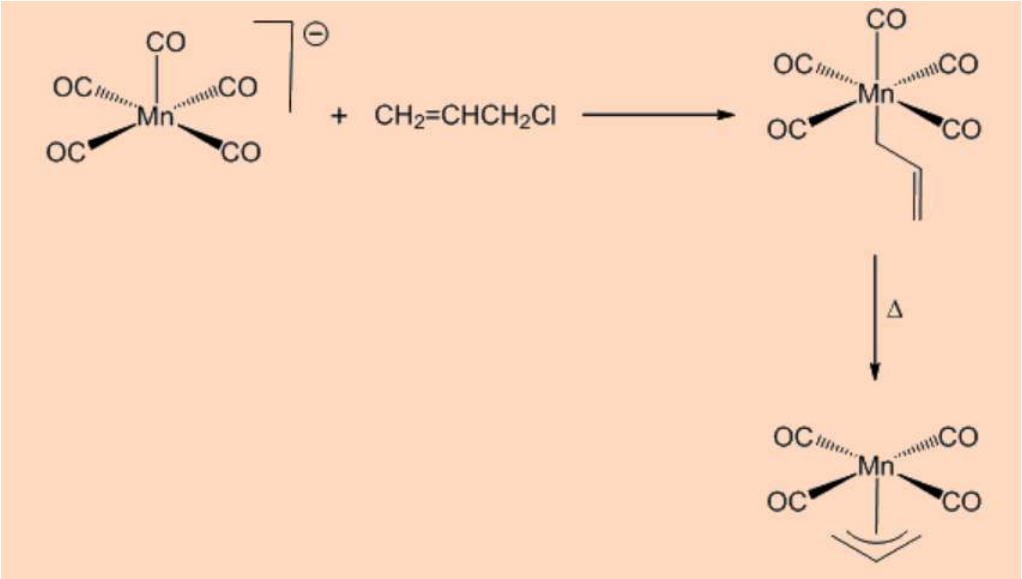
i. From an alkene complex as shown below.

$$\mathrm{Mo(dpe)_2(\eta_2\ -propene)} \rightleftharpoons \mathrm{Mo(dpe)_2(\ \eta_3\text{-allyl)H}}$$

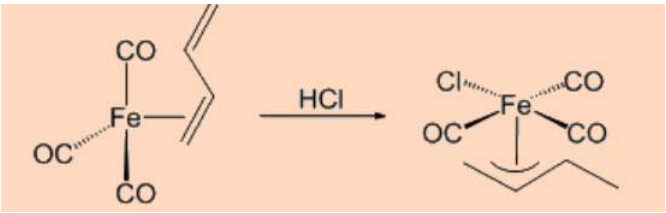
ii. By a nucleophilic attack of an allyl compound as shown below.



iii. By an electrophilic attack of an allyl compound as shown below.



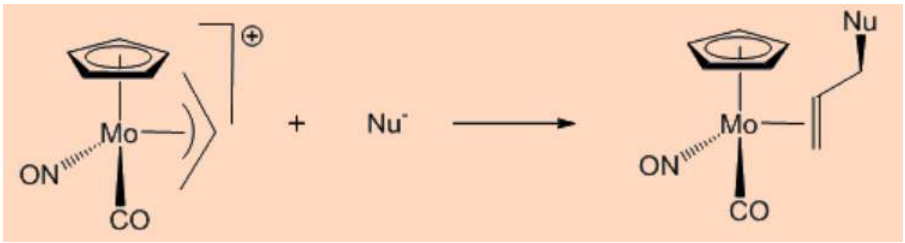
iv. From a diene complex as shown below.



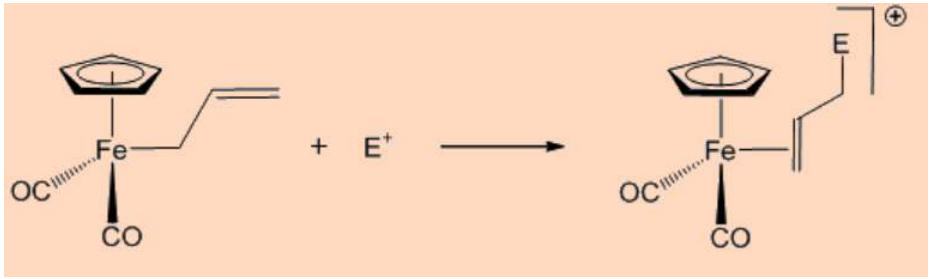
Reactions of metal allyl complexes

The reactivities of the metal allyl complexes toward various species are illustrated below.

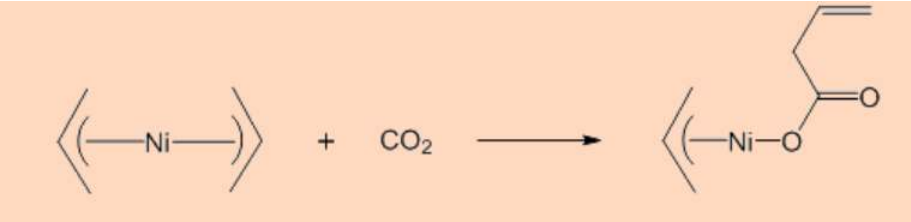
i. Reaction with nucleophiles



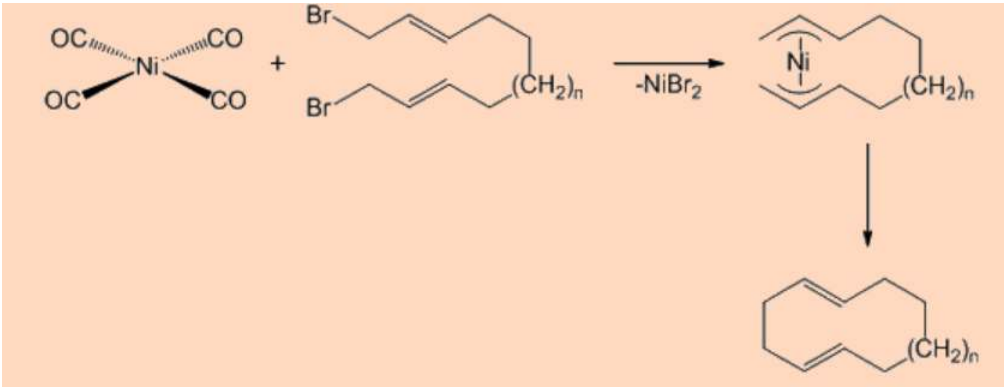
ii. Reaction with electrophiles



iii. Insertion reaction



iv. Reductive elimination



Diene complexes

1,3−Butadiene is a *4e−donor* ligand that binds to a metal in a *cisoid* conformation. The *Dewar−Chatt* model, when applied to 1,3−butadiene, predicts that the ligand may bind to metal either as a L_2 (π_2) donor type, similar to that of an alkene, or as an LX_2 ($\sigma_2\pi$) donor type, similar to that of a metalacyclopropane form. The L_2 binding of 1,3−butadiene is rare, *e.g.* asin (butadiene)$Fe(CO)_3$, while the LX_2 type binding is more common, *e.g.* as in $Hf(PMe_3)_2Cl_2$. An implication of the LX_2 type binding is in the observed shortening of the C_2−C_3 (1.40 Å) distance alongside the lengthening of the C_1−C_2(1.46 Å) and C_3−C_4 (1.46 Å) distances (Figure **6.2.6.2.3**).

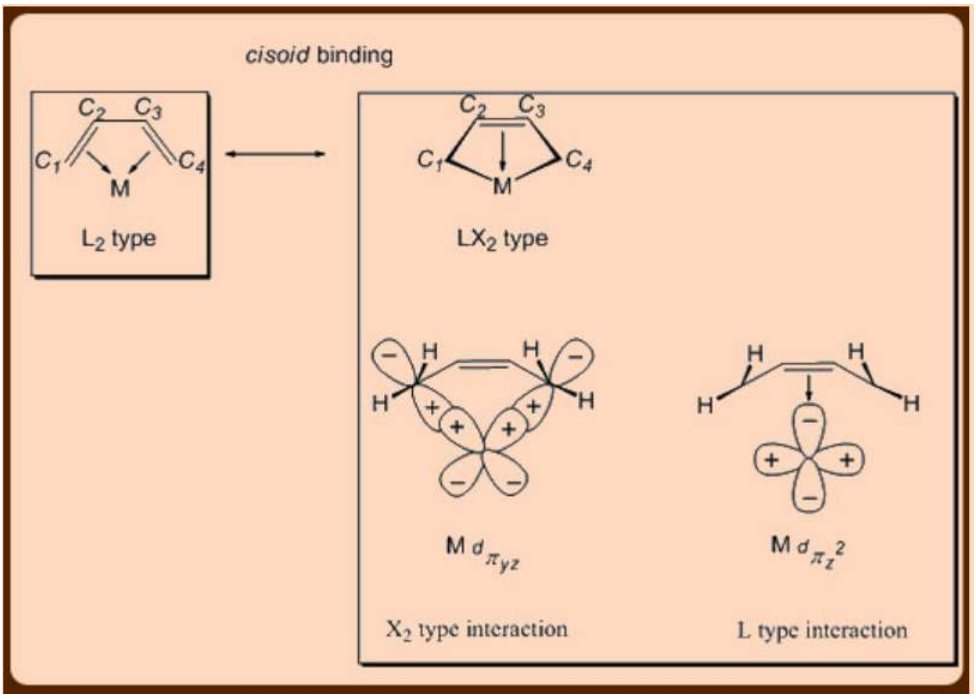


Figure **6.2.6.2.3**: Metal−diene interaction in *cisoid* binding.

The molecular orbitals of the 1,3−butadiene ligand comprises of two filled Ψ_1 (HOMO−1) and Ψ_2(HOMO) orbitals and two empty Ψ_3 (LUMO) and Ψ_4 (LUMO+1) orbitals. In a metal−butadiene interaction the ligand to metal σ−donation occurs from the filled Ψ_2 orbital of the 1,3−butadiene ligand while the metal to ligand π−back donation occurs on to the empty Ψ_3 orbital of the 1,3−butadiene ligand (Figure **6.2.6.2.4**).

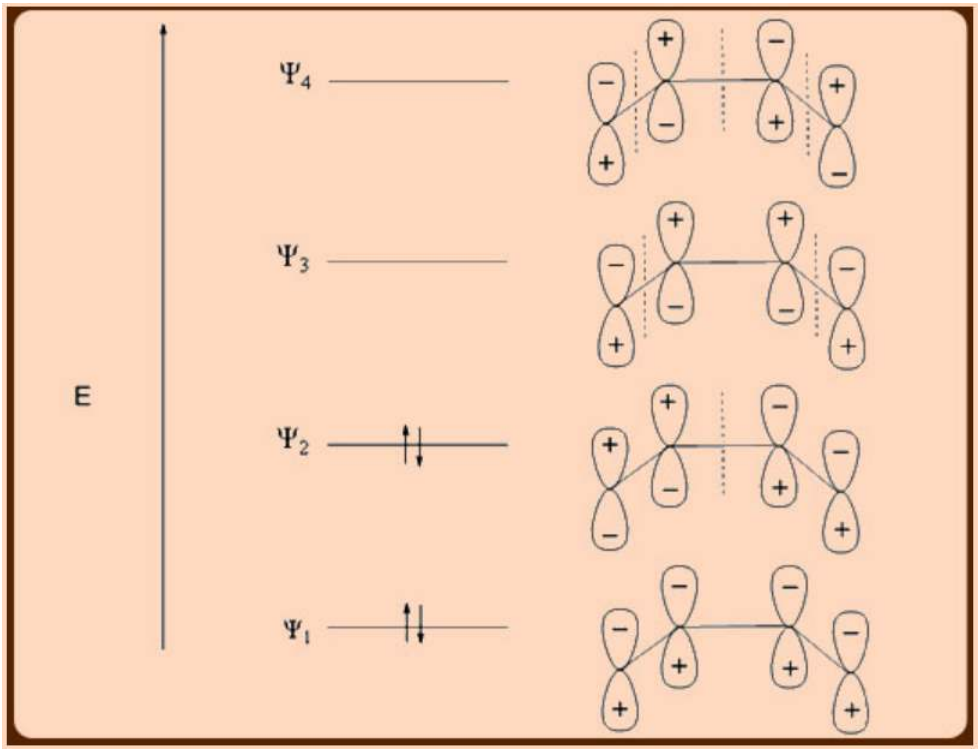


Figure **6.2.6.2.4**: Metal−diene interaction.

Though *cisoid* binding is often observed in metal butadiene complexes, a few instances of *transoid*binding is seen in dinuclear, *e.g.* as in $Os_3(CO)_{10}(C_4H_6)$, and in mononuclear complexes *e.g.* as in $Cp_2Zr(C_4H_6)$ (Figure **6.2.6.2.5**).

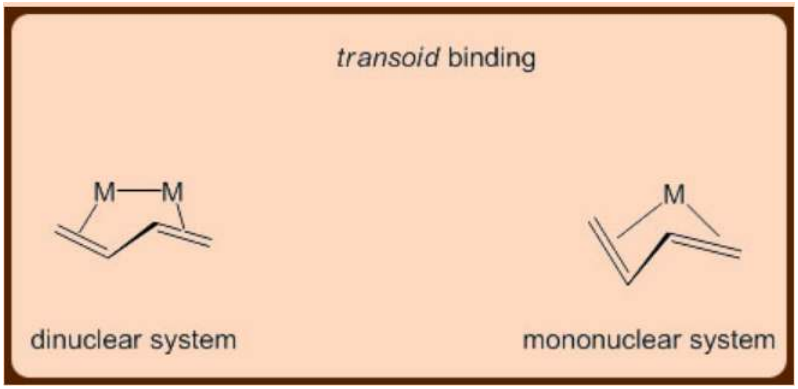
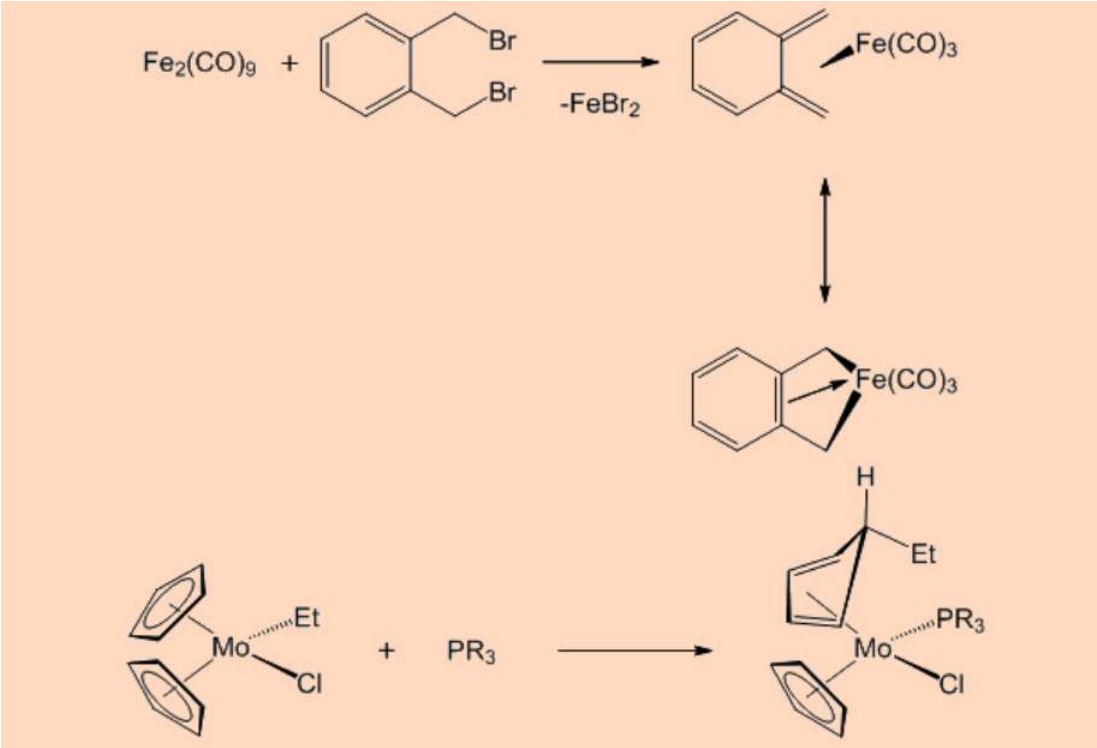


Figure **6.2.6.2.5**: Metal−diene interaction in *transoid* binding.

Synthesis of metal butadiene complex

Metal butadiene complexes are usually prepared by the same methods used for synthesizing metal alkene complexes. Two noteworthy synthetic routes are shown below.



Metal cyclobutadiene complexes

Cyclobutadiene is an interesting ligand because of the fact that its neutral form, being anti−aromatic (*4π*−electrons), is unstable as a free molecule (Figure **6.2.6.2.6**), but its dianionic form is stable because of being aromatic (*6π*−electrons). Consequently, the cyclobutadiene ligand is stabilized by significant metal to ligand π−back donation to the vacant ligand orbitals.

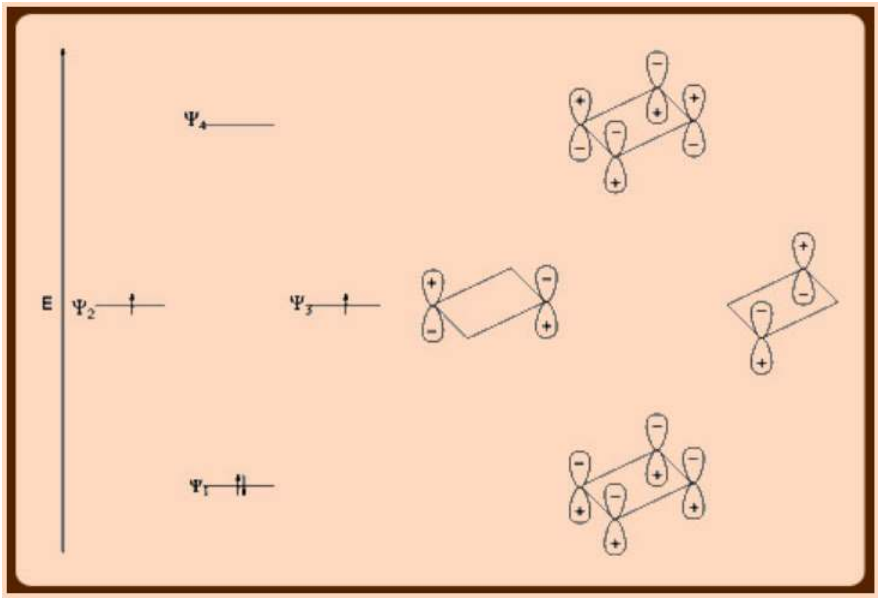
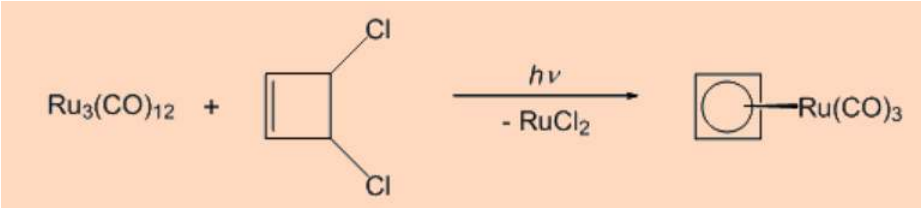


Figure **6.2.6.2.6**: Electronic structure of cyclobutadiene ligand.

A synthetic route to metal cyclobutadiene complex is shown below.



Problems

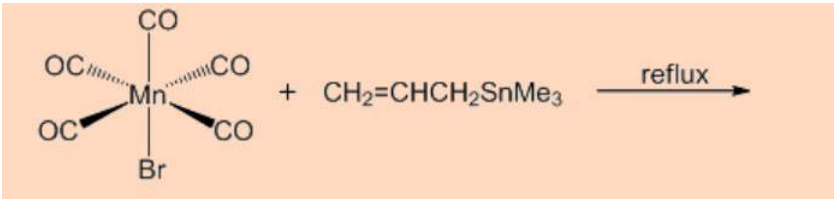
1. The hapticities displayed by an allyl moiety in binding to metals are?

Ans: 1 and 3.

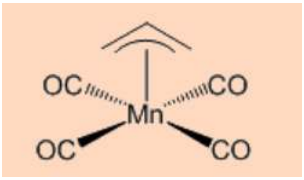
2. Identify which molecular orbitals of an allyl moiety engage in σ−interaction with a suitable *d* orbital of a metal in a η^3−metal allyl complex?

Ans: Ψ_1 and Ψ_2.

3. Predict the product of the reaction.



Ans:

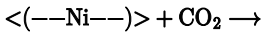


4. Identify which molecular orbitals of a butadiene moiety engage in σ−interaction with a suitable *d*orbital of a metal in a η^4−metal butadiene complex?

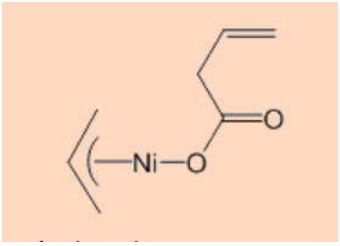
Ans: Ψ_2.

Self Assessment test

1. Predict the product of the reaction.



Ans:



2. Identify which molecular orbitals of a butadiene moiety engage in π−interaction with a suitable *d*orbital of a metal in a η^4−metal allyl complex?

Ans: Ψ_3.

3. Mention the type of orientations displayed by butadiene ligands for binding to metal.

Ans: Cisoid (common) and transoid (rare).

4. Comment on the number of π−electrons present in the cyclobutadiene moiety of a metal cyclobutadiene complex.

Ans: 6 π−electrons.

Summary

Allyl, 1,3−butadiene and cyclobutadiene together constitute an important class of σ−donor/π−acceptor ligands that occupy a special place in organometallic chemistry. The complexes of these ligands with metals are important intermediates in many catalytic cycles and hence an understanding of their interaction with metal is of significant importance. In this context, the synthesis, characterization and the reactivities of the organometallic complexes of these ligands are described alongside the respective metal−ligand interactions.

6.2.6.2: Metal Allyl and Diene Complexes is shared under a CC BY-SA license and was authored, remixed, and/or curated by LibreTexts.

- **9.2: Metal Allyl and Diene Complexes** by M. S. Balakrishna & Prasenjit Ghosh is licensed CC BY-NC-SA 4.0. Original source: https://nptel.ac.in/courses/104101006.

6.2.6.3: Metal Cyclopentadienyl Complexes

Learning Objectives

In this lecture you will learn the following

- The cyclopentadienyl ligands.
- The synthesis and reactivity of metal−cyclopentadienyl complexes.
- The metal−cyclopentadienyl interaction.

Cyclopentadienyl moiety acts as an important “spectator” ligand and is quite ubiquitous in organometallic chemistry. It remains inert to most nucleophiles and electrophiles and solely engages in stabilizing organometallic complexes. The cyclopentadienyl ligands form a wide array of organometallic compounds exhibiting different formulations that begin with the so-called “piano stool” $CpML_n$ (n = 2,3 or 4) type ones and extends to the most commonly observed “metallocene” Cp_2M type ones to even go beyond further to the “bent metallocene” Cp_2MX_n (n = 1,2 or 3) type ones. In the “piano stool” $CpML_n$ structure, the cyclopentadienyl (Cp) ligand is regarded as the “seat” of the piano stool while the remaining L ligands are referred to as the “legs” of the piano stool. Though the cyclopentadienyl ligand often binds to metal in a η^5 (pentahapto) fashion, *e. g.* as in ferrocene, the other form of binding to metal at lower hapticities, like that of the η^3 (trihapto) binding *e. g.* as in $(\eta^5\text{−Cp})(\eta^3\text{−Cp})W(CO)_2$ and that of the η^1 (monohapto) binding *e. g.* as in $(\eta^5\text{−Cp})(\eta^1\text{−Cp})Fe(CO)_2$, are also seen on certain rare occasions.

The binding modes of the cyclopentadienyl ligand in metal complexes can be ascertained to a certain degree by ^1H NMR in the diamagnetic metal complexes, in which the Cp−protons appear as a singlet between 5.5−3.5 ppm while the β and γ hydrogens come at 7−5 ppm.

Cyclopentadienyl−metal interaction

The frontier molecular orbital of the cyclopentadienyl ligand contains 5 orbitals (Ψ_1–Ψ_5) residing in three energy levels (Figure 9.3.1). The lowest energy orbital Ψ_1 does not contain any node and is represented by an a_1 state, followed by a doubly degenerate e_1 states that comprise of the Ψ_2 and $\Psi_3$orbitals, which precede another doubly degenerate e_2 states consisting of Ψ_4 and Ψ_5 orbitals.

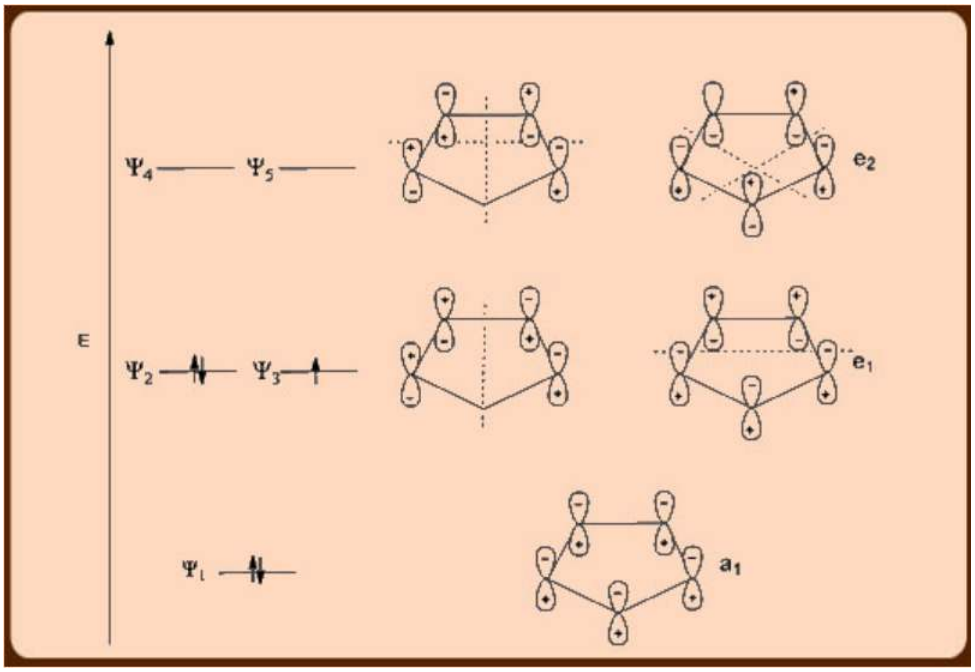


Figure 9.3.1 : Molecular orbital diagram of cyclopentadienyl ligand.

The above frontier molecular orbital diagram becomes more intriguing on moving over to the metallocenes that contain two such cyclopentadienyl ligands. Specifically, in the Cp_2M system, (*e. g.* ferrocene) each of these above five molecular orbital of the two

cyclopentadienyl ligands combines to give ten ligand molecular orbitals in three energy levels (Figure 9.3.2). Of these, the orbitals that subsequently interact with the metal orbitals to generate the overall molecular orbital correlation diagram for the Cp_2M type of complexes are shown below (Figure 9.3.3).

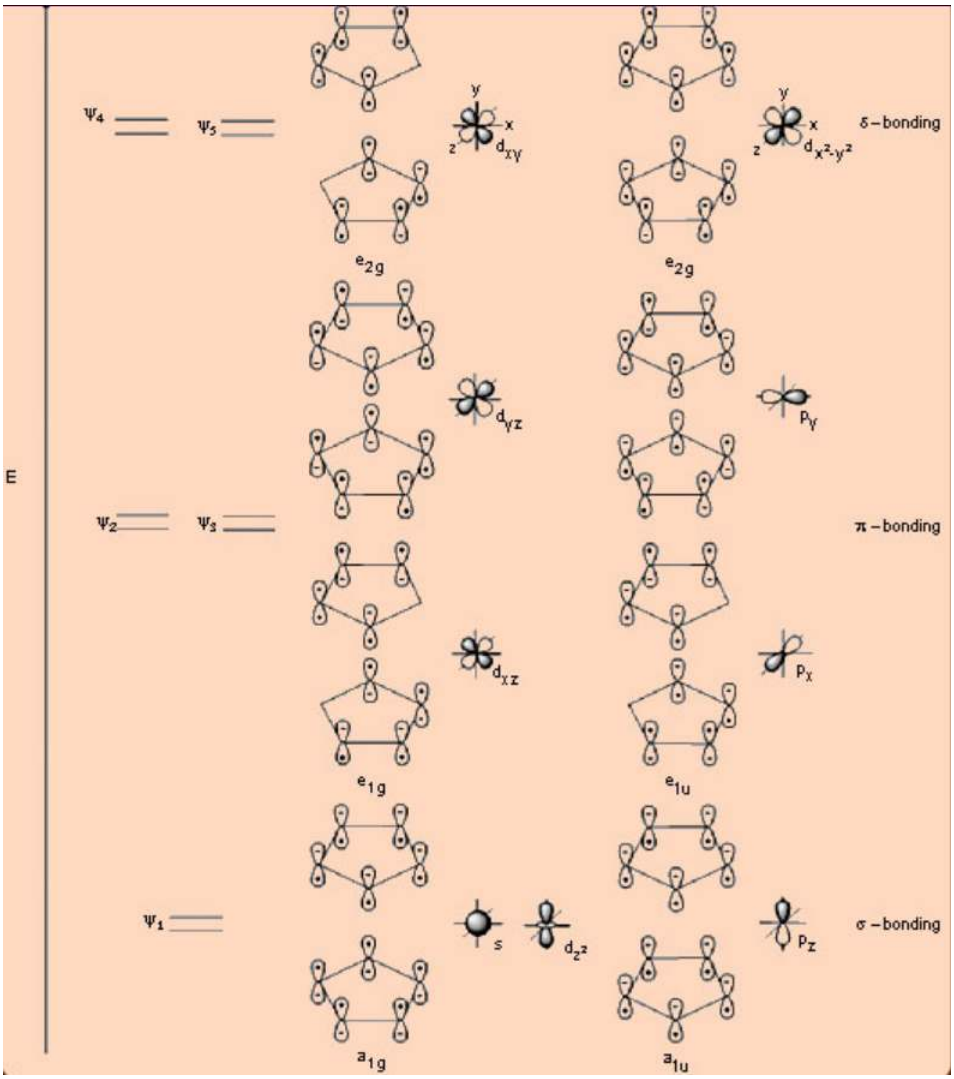


Figure 9.3.2 : Metal−cyclopentadienyl Bonding interactions.

https://chem.libretexts.org/@go/page/360911

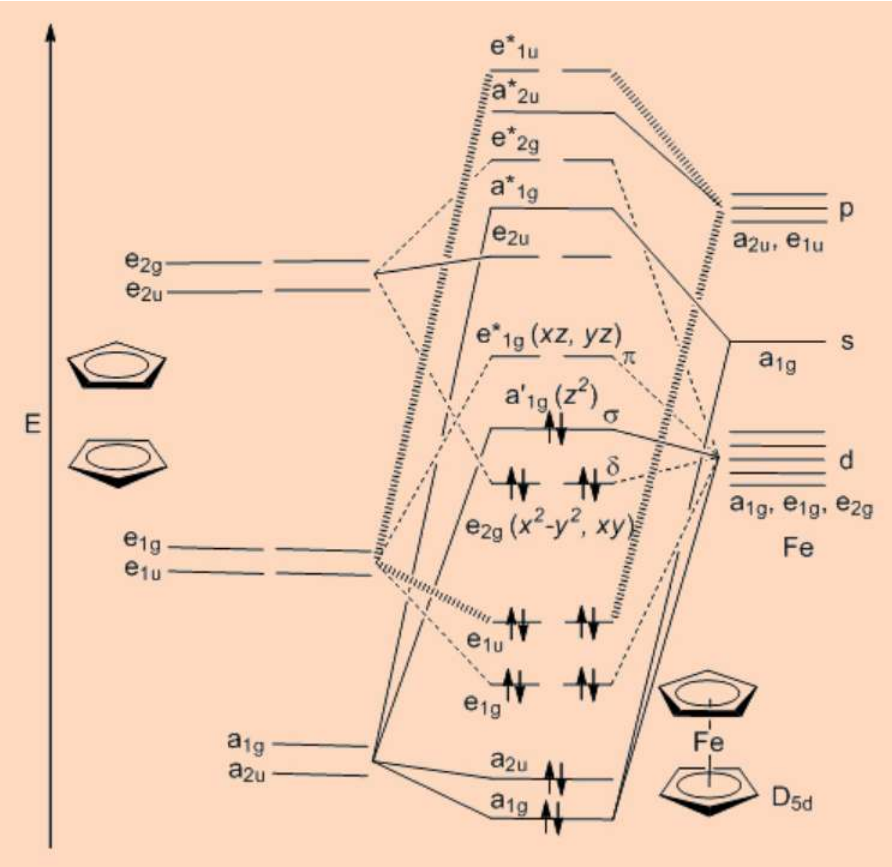


Figure 9.3.3 : MO diagram of ferrocene.

Generic metallocene Cp_2M type complexes are formed for many from across the 1st row transition metal series along Sc to Zn. The number of unpaired electrons thus correlates with the number unpaired electrons present in the valence orbital of the metal (Figure 4). Of the complexes of the 1st row transition metal series, the manganocene exists in two distinct forms, one in a high-spin form with five unpaired electrons, *e.g.* as in Cp_2Mn and the other in a low-spin form with one unpaired electron, *e.g.* as in Cp^*_2Mn owing to the higher ligand field strength of the Cp* ligand. Cobaltocene, Cp_2Co, has 19 valence electrons (VE) and thus gets easily oxidized to the diamagnetic 18 VE valence electron species, Cp_2Co^+. Of these metallocenes, the much-renowned ferrocene, Cp_2Fe is a diamagnetic 18 VE complex, whose molecular orbital diagram is shown above (Figure 9.3.3).

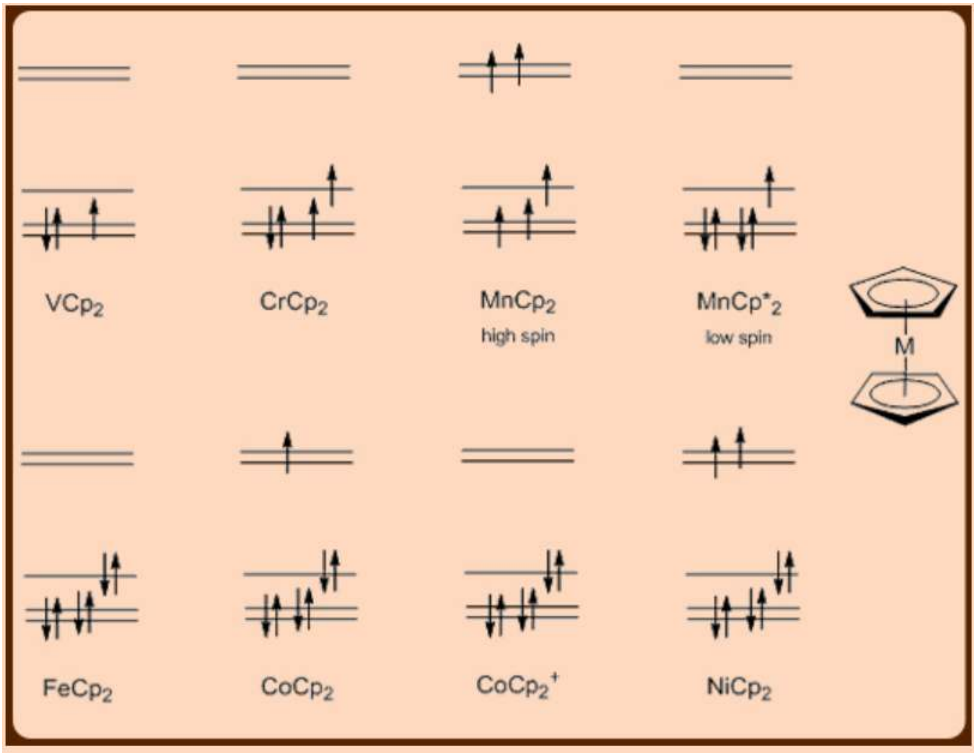


Figure 9.3.4 : Metallocene

Bent metallocenes

Bent metallocenes are Cp_2MX_n type complexes formed of group 4 and the heavier elements of groups 5−7. In these complexes the frontier doubly degenerate e_2g orbitals of Cp_2M fragment interacts with the filled lone pair orbitals of the ligand (Figure 9.3.5).

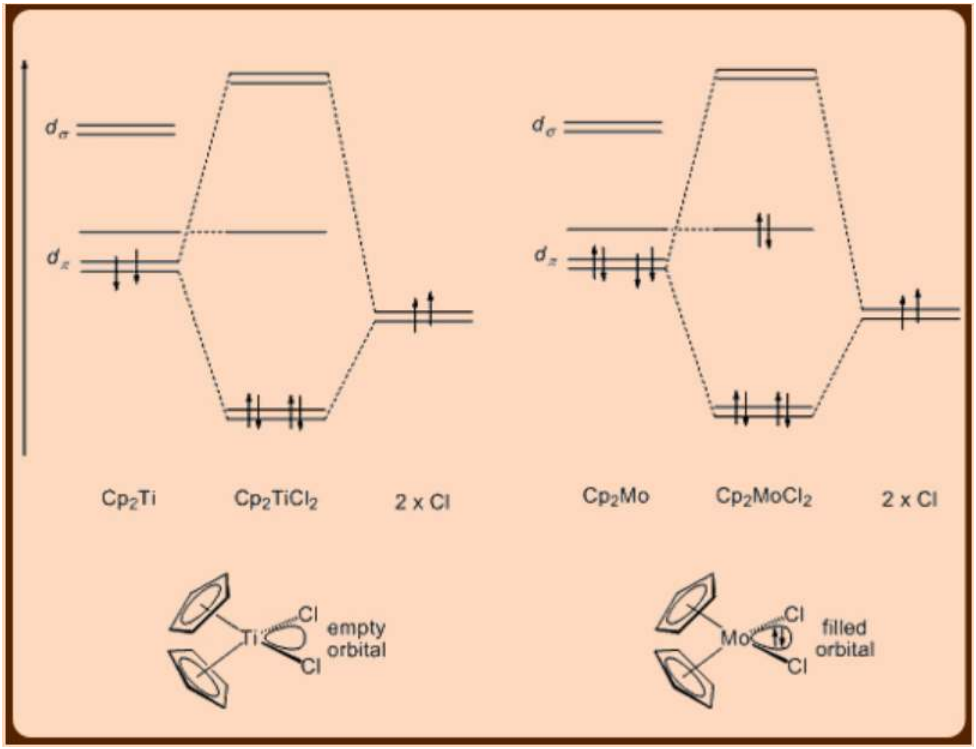
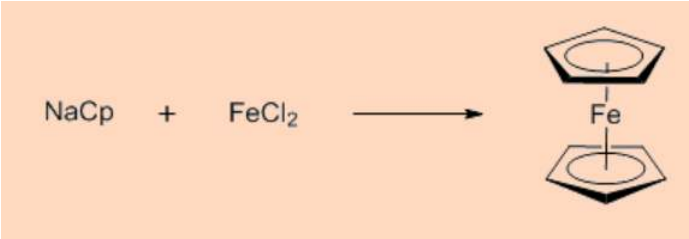


Figure 9.3.5 : Bent metallocene.

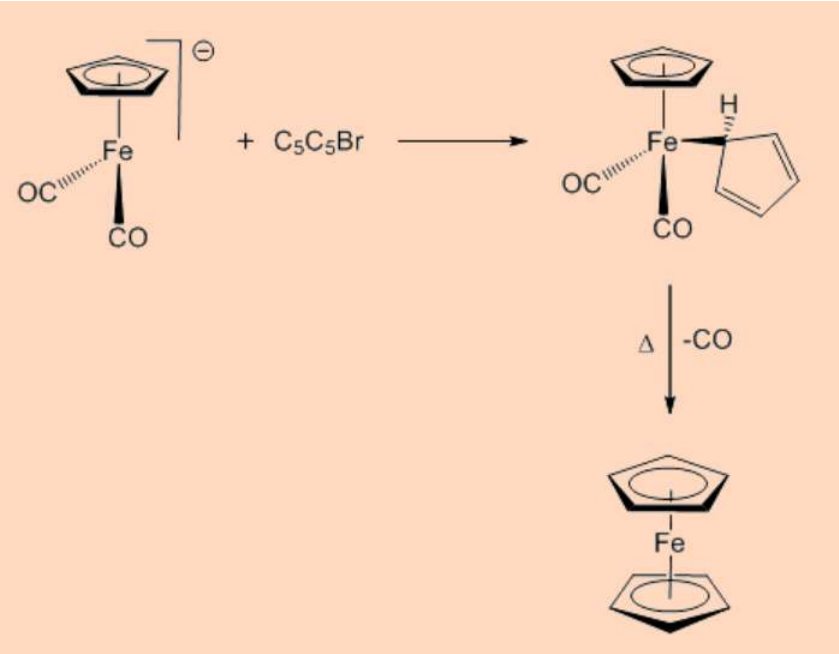
Synthesis of cyclopentadienyl-metal complexes

The metal−cyclopentadienyl complexes are synthesized by the following methods.

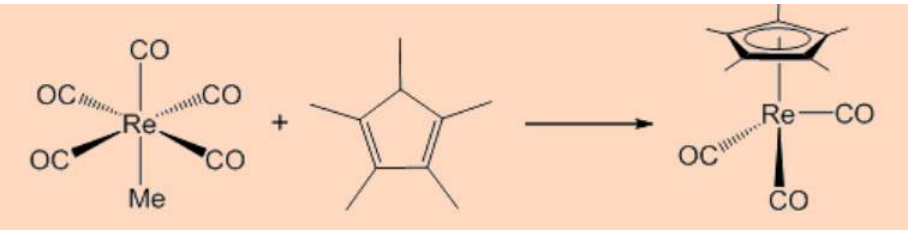
i. from Cp−



ii. from Cp+



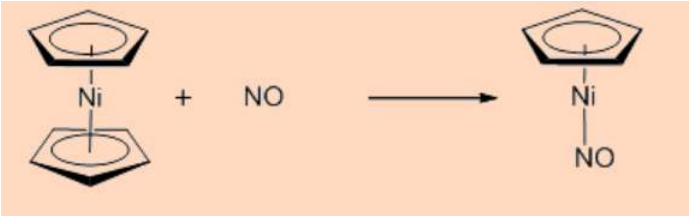
iii. from hydrocarbon



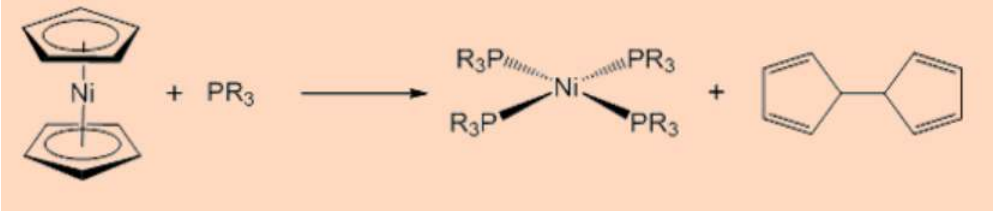
Reactivity of cyclopentadienyl-metal complexes

The reactivity of cyclopentadienyl−metal complexes of the type Cp_2M is shown for a representative nickellocene complex.

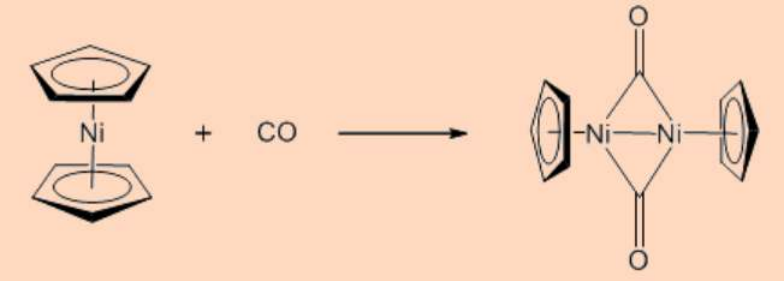
i. reaction with NO



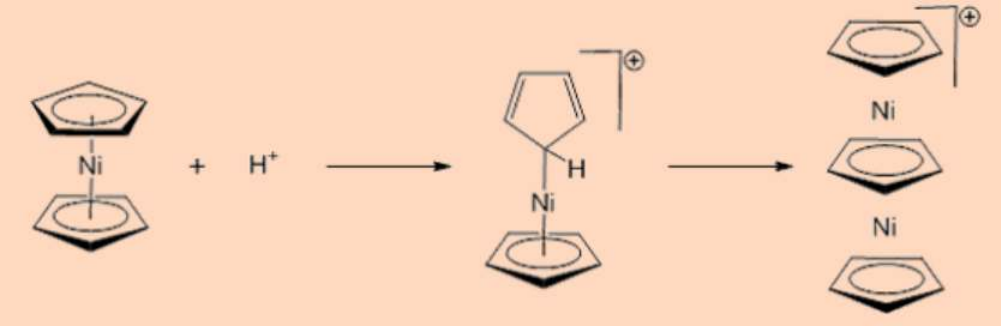
ii. reaction with PR_3



iii. reaction with CO



iv. reaction with H^+



Problems

1. Comment on the p−acceptor property of the cyclopentadienyl ligand.

Ans: The ligand being anionic shows very little π-acceptor properties.

2. Give the total valence electron count at the metal in a nickellocene complex.

Ans: 20 electrons.

3. Explain why the metal center in cobalticene gets easily oxidized.

Ans: 19 electrons cobalticene gets easily oxidized to 18 electron Cp_2Co^+.

4. Specify the number unpaired electrons present in chromocene.

Ans: 2

Self Assessment test

1. Specify the number of unpaired electron present in vanadocene.

Ans: The ligand being anionic shows very little π-acceptor properties.

2. What different hapticities are exhibited by cyclopentadienyl ligand?

Ans: 1, 3, and 5.

3. Specify the hapticities of the cyclopentadienyl ligands in $Cp_2W(CO)_2$.

Ans: 5 and 3.

4. Specify the hapticity of the cyclopentadienyl ligands in $CpRh(CO)_2(PMe_3)$.

Ans: 3.

Summary

Cyclopentadienyl moiety is almost synonymous with the transition metal organometallic complexes as the ligand played a pivotal role at the early developmental stages of the field of organometallic chemistry in the 1960s and 1970s. An important quality of the cyclopentadienyl ligand is that it behaves as an extremely good “spectator” ligand being inert to nucleophiles and electrophiles and displays uncanny ability towards stabilizing metal complexes of elements from across the different parts of the periodic table. Cyclopentadienyl moiety thus forms several types of complexes of different formulations like that of the “piano stool” $CpML_n$ (n = 2,3 or 4) types, the metallocene Cp_2M types and the bent metallocene Cp_2MX_n (n = 1,2 or 3) types. Cyclopentadienyl metal complexes make valuable catalysts for many chemical transformations of interest to academia and industries alike. The cyclopentadienyl moiety participates in a complex interaction with the metal involving ligand frontier molecular orbitals and the metal valence orbitals. Cyclopentadienyl metal complexes can be accessed by many methods.

6.2.6.3: Metal Cyclopentadienyl Complexes is shared under a CC BY-SA license and was authored, remixed, and/or curated by LibreTexts.

- **9.3: Metal Cyclopentadienyl Complexes** by M. S. Balakrishna & Prasenjit Ghosh is licensed CC BY-NC-SA 4.0. Original source: https://nptel.ac.in/courses/104101006.

SECTION OVERVIEW

6.3: Reaction Mechanisms

6.3.1: Oxidative Addition and Reductive Elimination

6.3.2: Insertion and Elimination Reactions

6.3.3: Nucleophilic and Electrophilic Addition and Abstraction

---

6.3: Reaction Mechanisms is shared under a CC BY-SA license and was authored, remixed, and/or curated by LibreTexts.

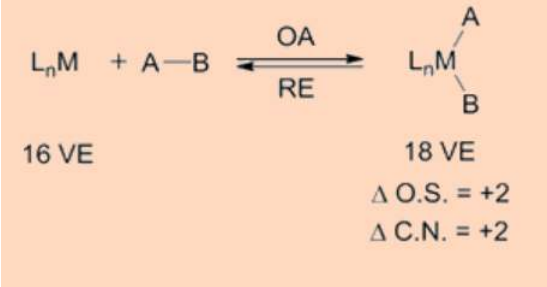
6.3.1: Oxidative Addition and Reductive Elimination

Learning Objectives

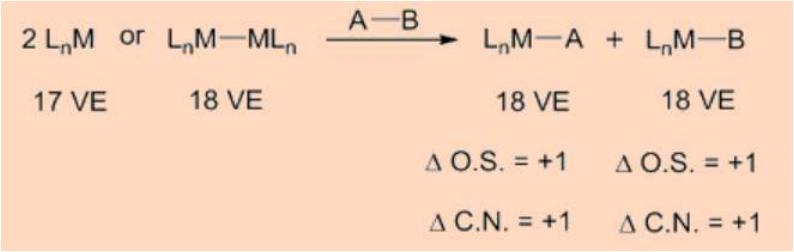
In this lecture you will learn the following

- The oxidative addition reactions.
- The reductive elimination reactions.
- Various mechanistic pathways prevalent for these reactions.

Oxidative addition (OA) is a process that adds two anionic ligands *e. g*. A and B, that originally are a part of a A-B molecule, like in H_2 or Me−I, on to a metal center and is of significant importance from the perspective of both synthesis and catalysis. The exact reverse of the same process, in which the two ligands, A and B, are eliminated from the metal center forming back the A−B molecule, is called the reductive elimination (RA). As A and B are anionic X type ligands, the oxidative addition is accompanied by an increase in the coordination number, valence electron count as well as in the formal oxidation state of the metal center by two units. The oxidative addition step may proceed by a variety of pathways. It requires the metal center to be both coordinatively unsaturated and electron deficient.



Oxidative addition transfers a single mononuclear metal center having 16 VE to a 18 VE species upon oxidative addition. Another frequently observed pathway is that a 18 VE complex looses a ligand to become a 16 VE species which then undergoes an oxidative addition. Apart from above two types, another possible pathway for oxidative addition proceeds as a binuclear oxidative addition in which each of the two metal centers undergo change in oxidation state, electron count and coordination number by one unit instead of two. This type of a binuclear oxidative addition is observed for a 17 VE metal complex or for a binuclear 18 VE metal complex having a metal−metal bond and, for which the metal has a stable oxidation state at a higher positive oxidation state by one unit.



It is interesting to note that in the oxidative addition the breakage of A−B σ−bond occurs as a result of a net transfer of electrons from the metal center to a σ*−orbital of the A−B bond, thus resulting in the formation of the two new M−A and M−B bonds. The oxidative addition is facilitated by electron rich metal centers having low oxidation state whereas the reductive elimination is facilitated by metal centers in higher oxidation state.

Table 6.3.1.1. Common types of oxidative addition reactions.

Change in d^n Configuration	Change in Coordination Geometry	Examples	Group
$d^{10} \rightarrow d^8$	Lin. $\xrightarrow{X_2}$ Sq. Pl.	Au(I) → (III)	11
	Tet. $\xrightarrow{-2L,\ X_2}$ Sq. Pl.	Pt, Pd(0) → (II)	10
$d^8 \rightarrow d^6$	Sq. Pl. $\xrightarrow{X_2}$ Oct.	Pt, Pd(II) → (IV)	10
		Rh, Ir(I) → (III)	9
		Pt, Pd(0) → (II)	8
	TBP. $\xrightarrow{-L,\ X_2}$ Oct.	Pt, Pd(I) → (III)	9
		Pt, Pd(0) → (II)	8
$d^7 \rightarrow d^6$	2Sq. Pyr. $\xrightarrow{X_2}$ 2Oct.	2Co(II) → (III)	8
	2Oct. $\xrightarrow{-L,\ X_2}$ 2Oct.	2Co(II) → (III)	8
$d^6 \rightarrow d^4$	Oct. $\xrightarrow{X_2}$ 7-c	Re(I) → (III)	7
		Pt, Pd(0) → (II)	6
		V(-I) → (I)	5
$d^4 \rightarrow d^3$	2Sq. Pyr. $\xrightarrow{X_2}$ 2Oct.	2Cr(II) → (III)	6
	2Oct. $\xrightarrow{-L,\ X_2}$ 2Oct.	2Cr(II) → (III)	6
$d^4 \rightarrow d^2$	Oct. $\xrightarrow{X_2}$ 8-c	Mo, W(II) → (IV)	6
$d^2 \rightarrow d^0$	Various	Pt, Pd(III) → (V)	5
		Pt, Pd(II) → (IV)	4

Abbreviations: Lin. = linear, Tet. = tetrahedral, Oct. = octahedral, Sq. Pl. = square planar, TBP = trigonal bipyramidal, Sq. Pyr. = square pyramidal: 7-c, 8-c = 7- and 8-coordinate.

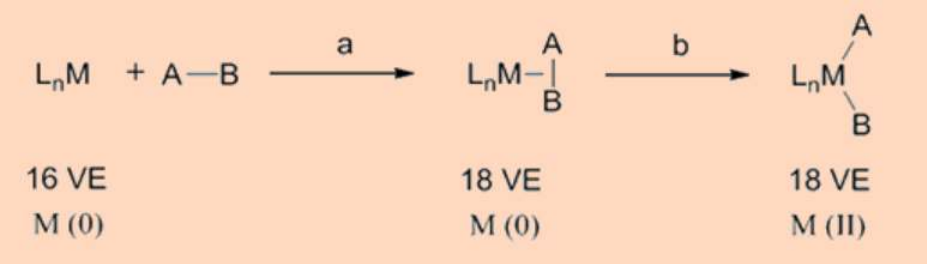
In principle, the oxidative addition is the reverse of reductive elimination, but in practice one may dominate over the other. Thus, the favorability of one over the other is depends on the position of equilibrium, which is further dependent on the stability of the two oxidation states of the metal and on the difference of bond strengths of A−B versus that of the M−A and M−B bonds. For example, metal hydride complexes frequently undergo reductive elimination to give alkanes but rarely an alkane undergoes oxidative addition to give an alkyl hydride complex. Along the same line, alkyl halides frequently undergo oxidative addition to a metal giving metal−alkyl halide complexes but these complexes rarely reductively eliminate to give back alkyl halides. Usually the oxidative addition is more common for 3rd row transition metals because they tend to possess stronger metal ligand bond strengths. The oxidative addition is also favored by strong donor ligands, as they stabilize the higher oxidation state of the metal. The oxidative addition reaction can expand beyond transition metals as observed in the case of the Grignard reagents as well as for some main group elements.

Oxidative addition may proceed by several pathways as discussed below.

Concerted oxidative addition pathway

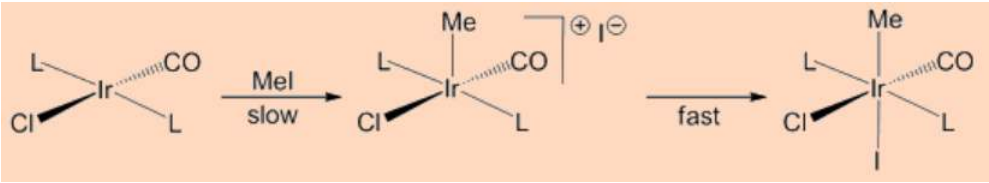
Oxidative addition may proceed by a **concerted 3−centered associative mechanism** involving the incoming ligand with the metal center. Specifically, the addition proceeds by the formation of a σ−complex upon binding of an incoming ligand say, H_2, followed by the cleavage of the H−H bond as a result of the back donation of electrons from the metal to the σ*−orbital of the H−H bond. Such type of addition is common for the H−H, C−H and Si−H bonds. As expected these proceed by two steps (*i*) the formation of a

σ−complex and (*ii*) the oxidation step. For example, the oxidative addition of H_2 to Vaska's complex $(PMe_3)_2Ir(CO)Cl$ proceeds by this pathways.



S_N2 pathway

This pathway of oxidative addition is operational for the polarized AB type of ligand substrates like the alkyl, acyl, allyl and benzyl halides. In this mechanism, the L_nM fragment directly donates electrons to the σ*−orbital of the A−B bond by attacking the least electronegative atom, say A, of the AB molecule and concurrently initiating the elimination of the most electronegative atom of the AB molecule in its anionic form, B^-. These reactions proceed *via* a polar transition state that is accompanied by an inversion of the stereochemistry at the atom of attack by the metal center and are usually accelerated in polar solvents.



Radical pathway

This type of oxidative addition proceeds *via* a by radical pathway that generally are vulnerable to the presence of impurities. The radical processes can be of non−chain and chain types. In a non−chain type of mechanism, the metal (M) transfer one electron to the σ*−orbital of the RX bond resulting in the formation of a radical cation $M^{+\bullet}$ and a radical anion $RX^{-\bullet}$. The generation of the two radical fragments occurs by the way of the elimination of the anion X^- from the radical anion $RX^{-\bullet}$ leaving behind the radical $R^\bullet$ while the subsequent reaction of X^- anion with the radical cation $M^{+\bullet}$ generates the other radical $MX^\bullet$ in the course of the reaction. Such type of non−chain type of oxidative addition is observed for the addition of the alkyl halide to $Pt(PPh_3)_3$ complexes.

$$PtL_3 \xrightarrow{fast} PtL_2$$

$$PtL_2 + RX \longrightarrow {}^\bullet PtL_2 + {}^{\bullet-}RX \xrightarrow{slow} {}^\bullet PtXL_2 + {}^\bullet R$$

$${}^\bullet PtXL_2 + {}^\bullet R \xrightarrow{fast} RPtXL_2$$

The other type in this category is the chain radical type reaction that is usually observed for the oxidative addition of EtBr and $PhCH_2Br$ to the $(PMe_3)_2Ir(CO)Cl$ complex. For this process a radical initiator is required and the reaction proceeds along a series of known steps common to a radical process.

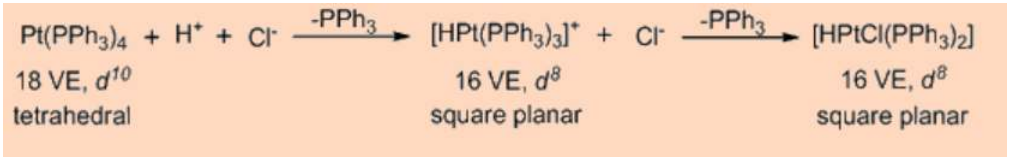
$$R^\bullet + IR^{I}Cl(CO)L_2 \longrightarrow RIr^{II\bullet}Cl(CO)L_2$$

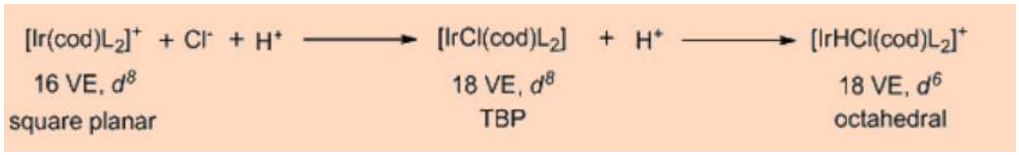
$$RIr^{II\bullet}Cl(CO)L_2 + RX \longrightarrow RXIr^{III}Cl(CO)L_2 + R^\bullet$$

$$2\,R^\bullet \longrightarrow R_2$$

Ionic pathway

This is kind of pathway for the oxidative addition reaction is common to the addition of hydrogen halides (HX) in its dissociated H^+ and X^- forms. The ionic pathways are usually of the following two types (*i*) the ones in which the starting metal complex adds to H^+ prior to the addition of the halide $X^-$and (*ii*) the other type, in which the halide anion X^- adds to the starting metal complex first, and then the addition of proton H^+ occurs on the metal complex.





Reductive Elimination

The r**eductive eliminations** are reverse of the oxidative addition reactions and are accompanied by the reduction of the formal oxidation state of the metal and the coordination numbers by two units. The reductive eliminations are commonly observed for d^8 systems, like the Ni(II), Pd(II) and Au(III) ions and the d^6 systems, like the Pt(IV), Pd(IV), Ir(III) and Rh(III) ions. The reaction may proceed by the elimination of several groups.

$$L_nMRH \longrightarrow L_nM + R{-}H$$

$$L_nMR_2 \longrightarrow L_nM + R{-}R$$

$$L_nMH(COR) \longrightarrow L_nM + RCHO$$

$$L_nMR(COR) \longrightarrow L_nM + R_2CO$$

$$L_nMR(SiR_3) \longrightarrow L_nM + R{-}SiR_3$$

Binuclear Reductive Elimination

Similar to what has been observed in the case of binuclear oxidative addition, the binuclear reductive elimination is also observed in some instances. As expected, the oxidation state and the coordination number decrease by one unit in the binuclear reductive elimination pathway.

$$2\,MeCH{=}CHCu(PBu_3) \xrightarrow{heat} MeCH{=}CHCH{=}CHMe$$

$$ArCOMn(CO)_5 + HMn(CO)_5 \longrightarrow ArCHO + Mn_2(CO)_{10}$$

Problems

1. What kind of metal centers favor oxidative addition?

Ans: Electron rich low valent metal centers.

2. Complete the sentence correctly.

(a) Reductive elimination is frequently observed in coordinatively saturated/unsaturated metal complexes.
(b) Reductive elimination is accompanied by increase/decrease in the oxidation state of the metal.
(c) Oxidative addition is accompanied by increase/decrease in the coordination number of the metal

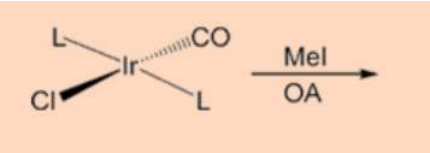
Ans:

(a) Saturated.
(b) Decrease in the oxidation state by two units.
(c) Increase in the coordination number by two units

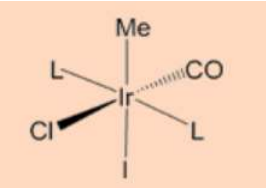
3. State the various mechanistic pathways involved in oxidative addition reactions.

Ans: Concerted oxidative addition, S_N2 mechanism, radical and ionic mechanism.

4. Complete the reaction.



Ans:



Self Assessment test

1. What kind of metal centers favor reductive elimination?

Ans: Electron deficient high valent metal centers

2. Complete the sentence correctly.

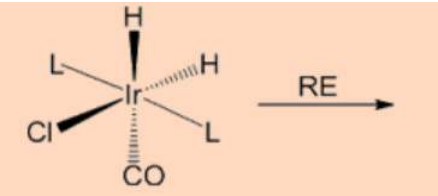
(a) Oxidative addition is frequently observed in coordinatively saturated/unsaturated metal complexes.
(b) Oxidative addition is accompanied by increase/decrease in the oxidation state of the metal.
(c) Reductive elimination is accompanied by increase/decrease in the coordination number of the metal.

Ans:
(a) Unsaturated.
(b) Increase in the oxidation state by two units.
(c) Decrease in the coordination numbers by two units.

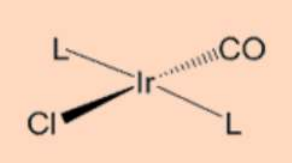
3. How does the geometry of the square planar complexes change upon oxidative addition reactions?

Ans: Square planar to octahedral.

4. Complete the reaction.



Ans:



Summary

The oxidative addition and the reductive elimination reactions are like the observe and reverse of the same coin. The oxidative addition is generally observed for metal centers with low oxidation state and is usually accompanied by the increase in the oxidation state, the valence electron count and the coordination number of the metal by two units. Being opposite, the reductive elimination is seen in the case of the metal centers with higher oxidation state and is accompanied by the decrease in the oxidation state, the valence electron count and the coordination number of the metal by two units. The oxidative addition may proceed by a

variety of pathways that involve concerted, ionic and the radical based mechanisms. More interestingly, the oxidative addition and reductive elimination reactions are not solely restricted to the mononuclear metal complexes but can also be observed for the binuclear complexes.

6.3.1: Oxidative Addition and Reductive Elimination is shared under a CC BY-SA license and was authored, remixed, and/or curated by LibreTexts.

- **10.1: Oxidative Addition and Reductive Elimination** by M. S. Balakrishna & Prasenjit Ghosh is licensed CC BY-NC-SA 4.0. Original source: https://nptel.ac.in/courses/104101006.

6.3.2: Insertion and Elimination Reactions

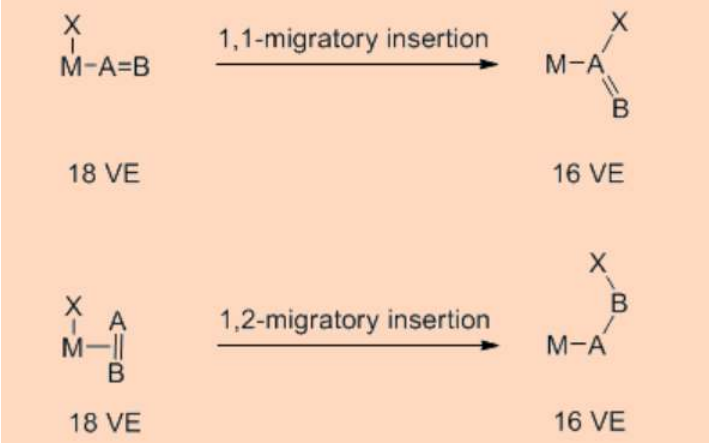
Learning Objectives

In this lecture you will learn the following

- The insertion and elimination reactions.
- The various mechanistic pathways by which these reactions proceed.
- Their relevance in some important catalytic cycles.

Unlike what we have learned about the oxidative addition and the reductive elimination reactions, that facilitate the addition or removal of 1−electron and 2−electron ligands on to a metal center, the insertion and the elimination reactions perform the subsequent transformation of these ligands from within the same coordination sphere of a metal. Thus, in an insertion reaction a metal bound 2 electron A=B type of a ligand can insert on to a M−X bond resulting in a new metal bound 1−electron ligand like, M−A−B−X, which is formed as a result of the formations of the M−A and B−X bonds. The insertion reaction thus leads to the generation of one vacant site created at the initial metal bound A=B site. Thus a primary requirement for reverse elimination reaction to occur is the presence of a *cis* vacant site.

Insertions are of two types, 1,1−insertion and 1,2−insertion. In 1,1−insertion both the metal M and the ligand X of the M−X bond end up on the same atom like in the M−A(X)−B moiety formed after the insertion of the A=B molecule in the M−X bond, whereas in the 1,2−insertion, these end up on the adjacent atoms like in the M−A−B−X moiety formed after the insertion of the A=B molecule in the M−X bond. The type of insertion depends on the type of the ligand undergoing the insertion like η^1−ligand showing 1,1−insertion and η^2−ligands showing 1,2−insertion. For example, the CO ligand exclusively undergoes 1,1−insertion while the C_2H_4 ligand undergoes 1,2−insertion. The SO_2 ligand remains the only exception as it can bind by both η^1−(by S−donor site) and η^2−(by S− and O−donor sites) modes and thus shows both type of insertions.

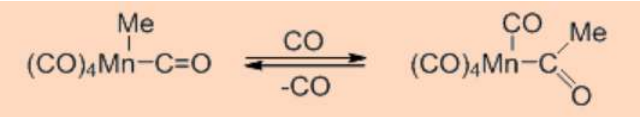


Though the insertion and the elimination reactions are mutually reversible, owing to the thermodynamical reasons one is favored over the other. For example, SO_2 is known to insert into the M−R bond with no report of its elimination is known of it, while for N_2 ligand, no report of its insertion is known but it's elimination from a M−N=N−R bond is known.

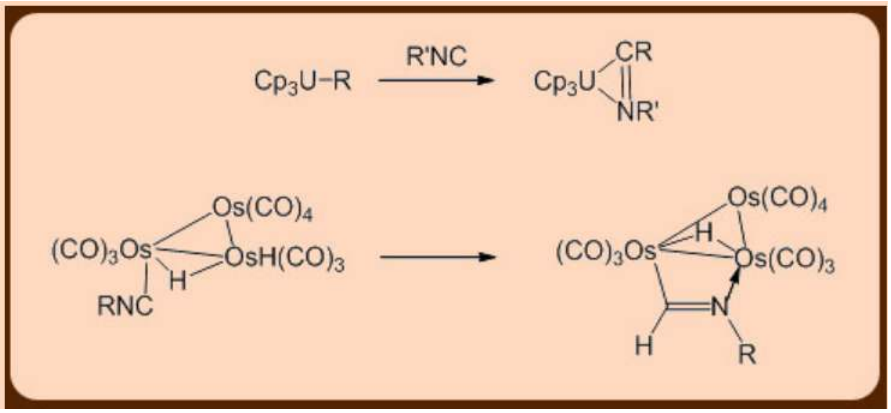
$$\mathbf{M{-}R + SO_2 \longrightarrow M{-}SO_2R}$$

$$\mathbf{M{-}N{=}N{-}Ar \longrightarrow M{-}Ar = N_2}$$

The CO ligand inserts readily into a metal−alkyl bond. Sterically demanding substituents (R) is found to accelerate the reaction as a bulky R group in an acyl moiety in the final M−CO−R bond is far removed from the metal center than that in the starting M−R bond.



Isonitriles readily insert into M−R and M−H bonds giving η^2-bound iminoacyls.

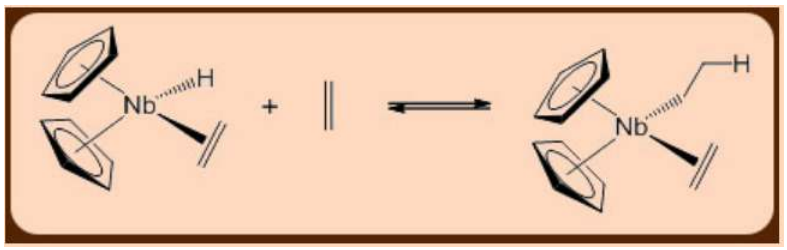


Olefins usually inserts across a M−H bond and such insertions are of relevance to the commercially important olefin polymerization process. In certain cases the 1,2−insertions of olefins give species exhibiting agostic insertions.



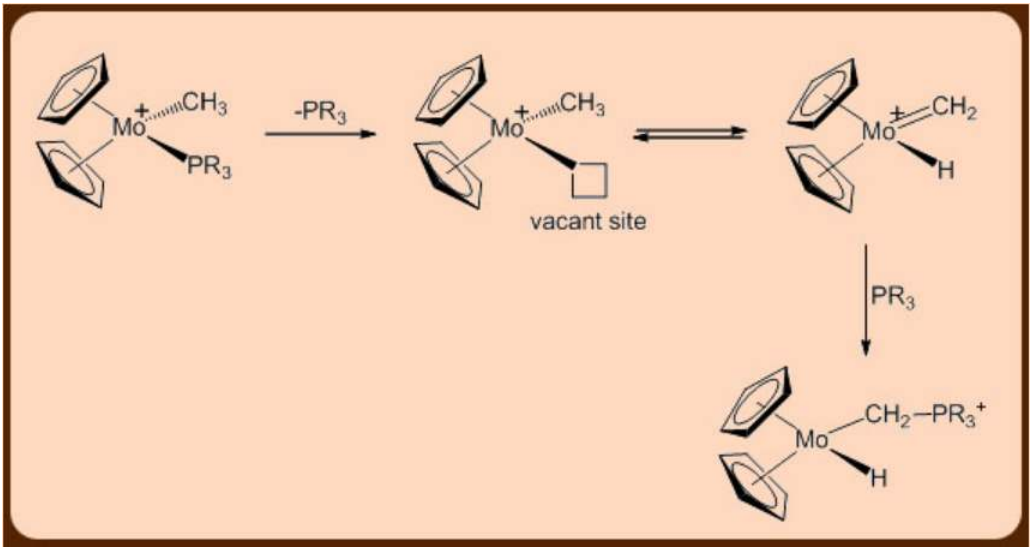
ß-Elimination

β−elimination is just a reverse of 1,2−insertion and is a major cause of decomposition of metal alkyl bond having a b−hydrogen atom. A pre-requisite for the β−elimination reaction to occur is the presence of an adjacent vacant site next to the metal alkyl bond undergoing the β−elimination. The β−elimination step results in the formation of a metal hydride species that also contain a metal bound olefin moiety.



α-elimination

In absence of a β−hydrogen, a metal bound alkyl moiety may undergo the cleavage of a C−H bond at the α, γ and δ positions. For example, a methyl moiety may α−eliminate to give a metal bound methylene hydride moiety.



Problems

1. Give an example of a ligand that undergo 1,1−insertion.

Ans: CO

2. Give an example of a ligand that undergo 1,2−insertion.

Ans: C_2H_4

3. Give an example of a ligand that undergo both the 1,1−insertion and the 1,2−insertion reactions.

Ans: C_2H_4

Self Assessment test

1. On what type of bonds does CO insertion usually occur?

Ans: Metal−alkyl (M−R) bonds.

2. On what type of bonds does isonitrile insertion usually occur?

Ans: Metal-alkyl (M-R) and the metal-hydride (M-H) bonds.

3. On what type of bonds does C_2H_4 insertion usually occur?

Ans: Metal-hydride (M-H) bonds.

4. State an important requirement for the occurrence of an elimination reaction.

Ans: The presence of an adjacent vacant site.

Summary

Insertion and elimination reactions are important sequences that carryout transformation of the metal bound ligands to the corresponding product from within the same coordination sphere of the metal center and thus together represent key steps of an overall catalytic cycle. The insertions are highly ligand dependent and may proceed by 1,1−insertion and 1,2−insertion mechanisms. Elimination reactions are just reverse of the insertion reactions and they too may proceed by several pathways. The two pathways that are commonly observed are the β−elimination and the α−eliminations, even though other type of elimination pathways exists.

6.3.2: Insertion and Elimination Reactions is shared under a CC BY-SA license and was authored, remixed, and/or curated by LibreTexts.

- **10.2: Insertion and Elimination Reactions** by M. S. Balakrishna & Prasenjit Ghosh is licensed CC BY-NC-SA 4.0. Original source: https://nptel.ac.in/courses/104101006.

6.3.3: Nucleophilic and Electrophilic Addition and Abstraction

Learning Objectives

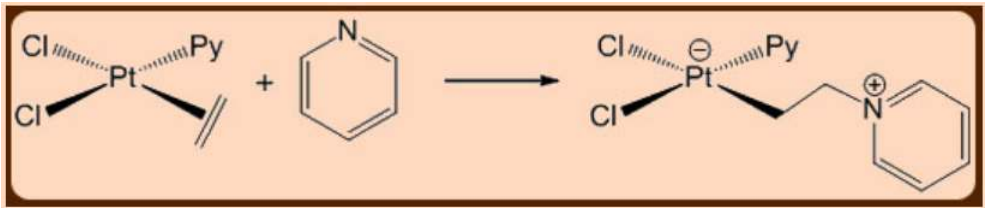
In this lecture you will learn the following

- Ligand activation by metal that leads to a direct external attack at the ligand.
- Nucleophilic addition and nucleophilic abstraction reactions.
- Electrophilic addition and electrophilic abstraction reactions.

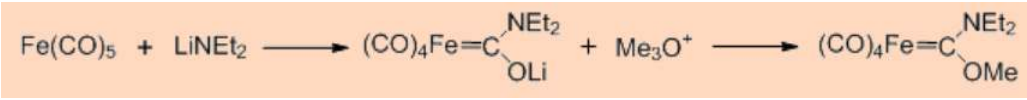
The nucleophilic and electrophilic substitution and abstraction reactions can be viewed as ways of activation of substrates to allow an external reagent to directly attack the metal activated ligand without requiring prior binding of the external reagent to the metal. The attacking reagent may be a nucleophile or an electrophile. The nucleophilic attack of the external reagent is favored if the L_nM fragment is a poor π−base and a good σ−acid *i.e.*, when the complex is cationic and/or when the other metal bound ligands are electron withdrawing such that the ligand getting activated gets depleted of electron density and can undergo an external attack by a nucleophile Nu^-, like LiMe or OH^-. The attack of the nucleophiles may result in the formation of a bond between the nucleophiles and the activated unsaturated substrate, in which case it is called nucleophilic addition, or may result in an abstraction of a part or the whole of the activated ligand, in which case it is called the nucleophilic abstraction. The nucleophilic addition and the abstraction reactions are discussed below.

Nucleophilic addition

An example of a nucleophilic addition reaction is shown below.

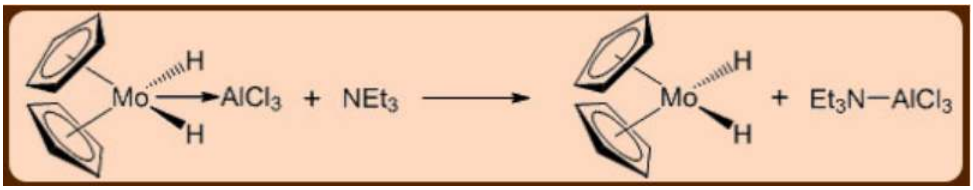


Carbon monoxide (CO) as a ligand can undergo nucleophilic attack when bound to a metal center of poor π−basicity, as the carbon center of the CO ligand is electron deficient owing to the ligand to metal σ−donation not being fully compensated by the metal to ligand π−back donation. Thus, activated CO ligand undergoes nucleophilic attack by the lithium reagent to give an anionic acyl ligand, which upon alkylation generates the famous Fischer carbene complex.



Nucleophilic abstraction

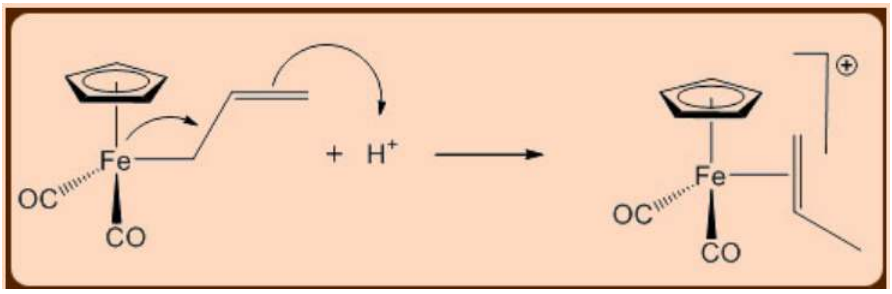
An example of a nucleophilic abstraction reaction is shown below.



Electrophilic addition

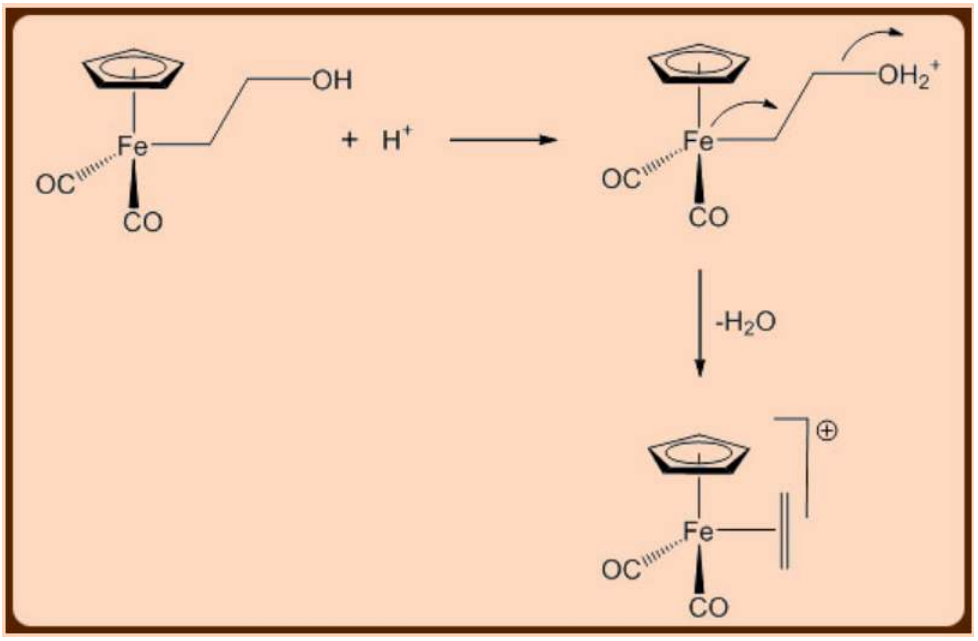
Similar to the nucleophilic addition and abstraction reactions, the electrophilic counterparts of these reactions also exist. An electrophilic attack is favored if the L_nM fragment is a good π−base and a poor σ−acid *i.e.*, when the complex is anionic with the metal center at low−oxidation state and/or when the other metal bound ligands are electron donating such that the ligand getting

activated becomes electron rich from the π−back donation of the metal center and thus can undergo an external attack by an electrophile E^+ like H^+ and CH_3I. The attack of the electrophiles may result in the formation of a bond between the electrophile and the activated unsaturated substrate, in which case it is called electrophilic addition, or may result in an abstraction of a part or the whole of the activated ligand, in which case it is called the electrophilic abstraction.

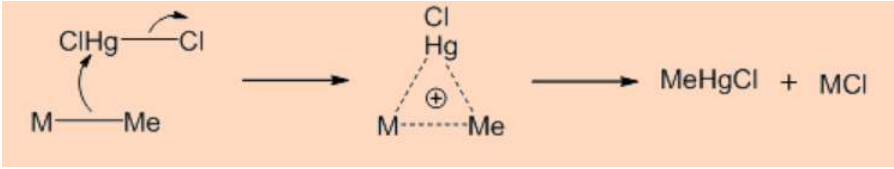


Electrophilic abstraction

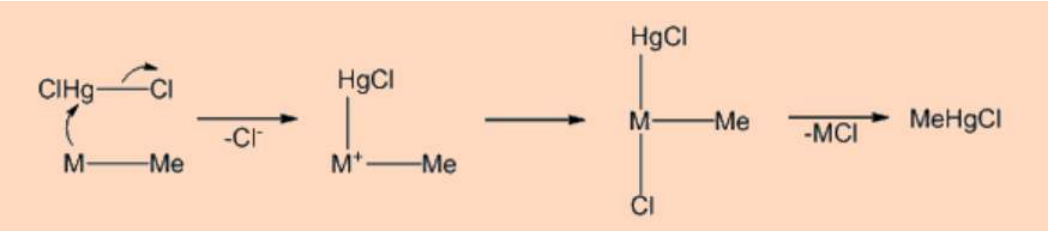
An example of an electrophilic abstraction reaction is shown below.



Alkyl abstractions are often achieved by Hg^{2+} that can proceed in two ways, (*i*) by an attack at the α−carbon of a metal alkyl bond leading to an inversion of configuration at the alkyl carbon and (*ii*) by an attack at the metal center leading to retention of configuration at the alkyl carbon. The inversion of configuration proceeds by the following pathway.



The retention of configuration proceeds by the following pathway.



6.3.3: Nucleophilic and Electrophilic Addition and Abstraction is shared under a CC BY-SA license and was authored, remixed, and/or curated by LibreTexts.

- **10.3: Nucleophilic and Electrophilic Addition and Abstraction** by M. S. Balakrishna & Prasenjit Ghosh is licensed CC BY-NC-SA 4.0. Original source: https://nptel.ac.in/courses/104101006.

SECTION OVERVIEW

6.4: Applications

6.4.1: Homogeneous Catalysis - I

6.4.2: Homogeneous Catalysis - II

6.4.3: Catalytic Applications of Organometallic Compounds- Alkene Metathesis

6.4: Applications is shared under a CC BY-SA license and was authored, remixed, and/or curated by LibreTexts.

6.4.1: Homogeneous Catalysis - I

Learning Objectives

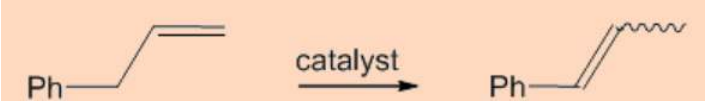
In this lecture you will learn the following

- The application of organometallic complexes in homogeneous catalysis.
- Alkene isomerization.
- Alkene and the arene hydrogenations.
- Transfer hydrogenation.

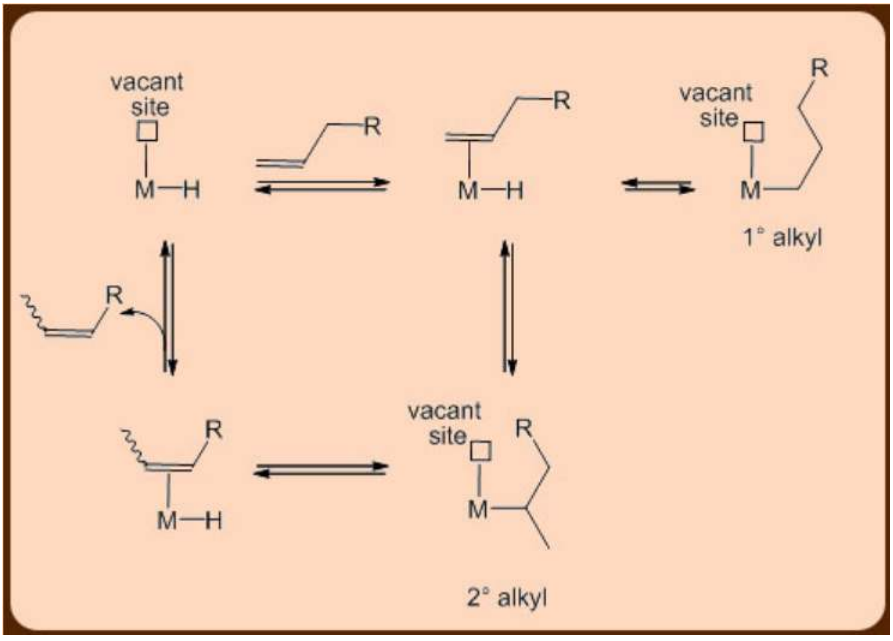
One of the most important exploits of the organometallic chemistry is its application in the area of homogeneous catalysis. The field has now expanded its territory to accommodate in equal measures many large-scale industrial processes as well as numerous small scale reactions of the day-to-day organic synthesis. A few representative examples of organometallic catalysis are outlined below.

Alkene Isomerization

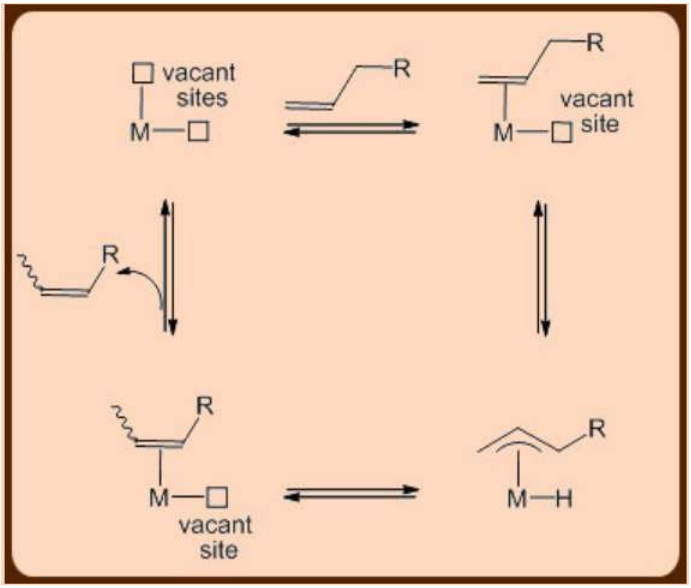
Alkene isomerization is a transformation that involve a shift of a double bond to an adjacent position followed by 1,3−migration of a H atom. The isomerization reaction is transition metal catalyzed.



The alkene isomerization reaction may proceed by two pathways, (*i*) one through a η^1−alkyl intermediate and (*ii*) the other through η^3−allyl intermediate. In the η^1−alkyl pathway, an alkene first binds to a metal at a vacant site next to M−H bond and then subsequently undergoing an insertion into the M−H bond thus creating back the vacant site. The resultant species then undergoes a H atom transfer from the alkyl moiety to give the isomerized olefin along with the regeneration of the M−H species.



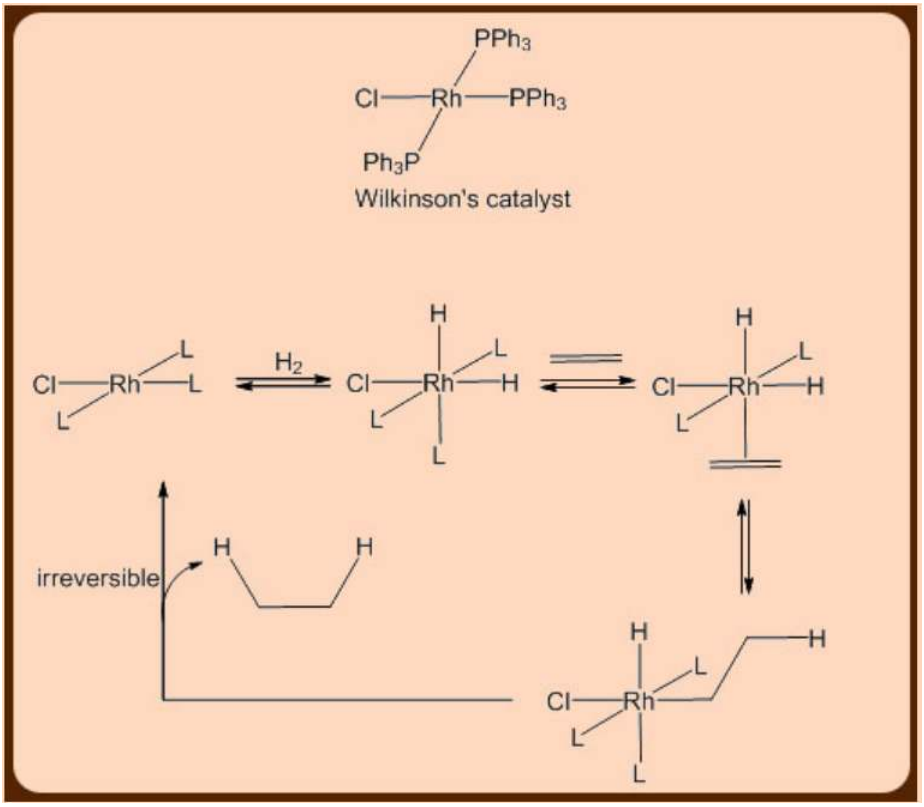
The η^3−allyl mechanism requires the presence of two vacant sites. This mechanism goes through a η^3−allyl intermediate formed by a C−H activation at the allylic position of the olefin formed after binding to the metal and alongside leads to the formation of a M−H bond. Subsequent H transfer from the metal back to the η^3−allyl moiety leads to the alkene isomerized product.



Alkene Hydrogenation

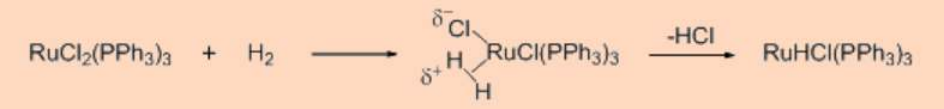
The transition metal catalyzed alkene hydrogenation reactions are of significant industrial and academic interest. These reactions involve the H_2 addition on a C=C bond of olefins to give alkenes. The alkene hydrogenation may proceed by three different pathways namely the (*i*) oxidative addition (*ii*) heterolytic activation and (*iii*) the homolytic activation of the H_2 molecule.

The oxidative addition pathway is commonly observed for the Wilkinson's catalyst $(PPh_3)_3RhCl$ and is the most studied among all of the three pathways that exist. The catalytic cycle initiates with the oxidative addition of H_2 followed by alkene coordination. The resultant species subsequently get converted to the hydrogenated product.

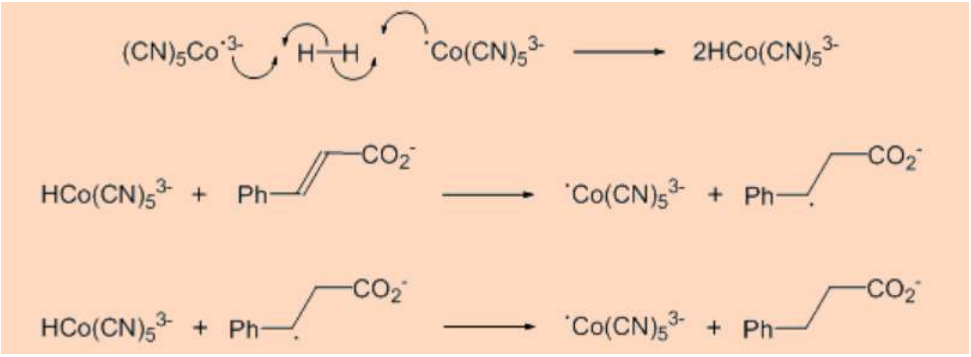


The second pathway proceeds by the heterolytic activation of the H_2 molecule and requires the presence of a base like NEt_3, which facilitates the heterolytic cleavage by abstracting a proton from the H_2 molecule and leaving behind a hydride H^- ion that participates in the hydrogenation reaction. This type of mechanism is usually followed by the $(PPh_3)_3RuCl_2$ type of complexes.

$$X{-}Y + M{-}Z \longrightarrow M{-}X + Y{-}Z$$

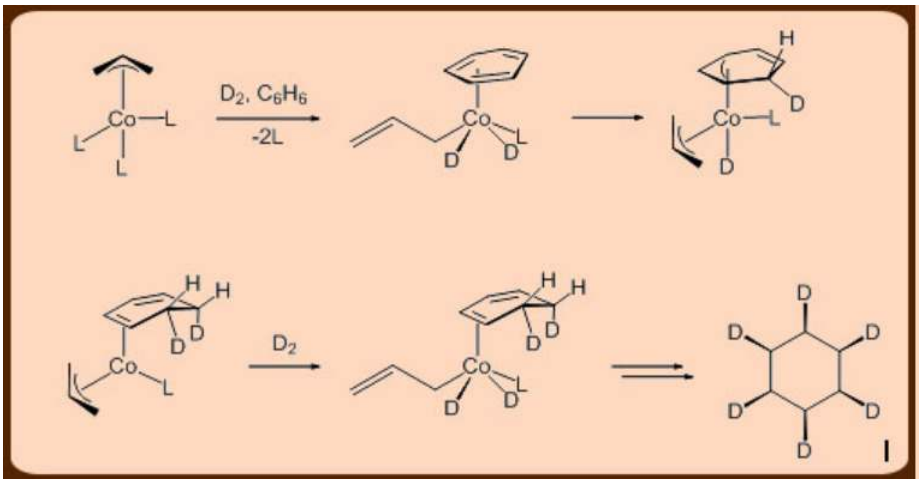


Homolytic cleavage of H_2 is the third pathway for the alkene hydrogenation. It is the rarest of all the three methods and proceeds mainly in a binuclear pathway. Paramagnetic cobalt based $Co(CN)_5^{3-}$ type catalysts carries out alkene hydrogenation by this pathway *via* the formation of the $HCo(CN)_5^{3-}$species.



Arene hydrogenations

Examples of homogeneous catalysts for arene hydrogenation are rare though it is routinely achieved using catalysts like Rh/C under the heterogeneous conditions. A representative example of a homogeneous catalyst of this class is $(\eta^3{-}allyl)Co[P(OMe)_3]_3$ that carry out the deuteration of benzene to give the all-*cis*-$C_6H_6D_6$ compound.



Transfer hydrogenation

This is a new kind of a hydrogenation reaction in which the source of the hydrogen is not the H_2molecule but an easily oxidizable substrate like isopropyl alcohol. The method is particularly useful for the reduction of ketones and imines but not very effective for the olefins.

$$Me_2CHOH + RCH{=}CH_2 \longrightarrow Me_2C{=}O + RCH_2CH_3$$

Summary

The applications of organometallic compounds in homogeneous catalysis have transcend the boundaries of industry to meet the day-to-day synthesis in laboratory scale reactions. The alkene isomerization is one such application of homogeneous catalysis by the transition metal organometallic complexes. The hydrogenation reactions of alkene, arene, ketone and imine substrates are achieved by several types of the transition metal organometallic catalysts. They also proceed by different mechanisms involving oxidative addition, heterolytic and homolytic cleavages of the H−H bond. The transfer hydrogenation reaction uses easily oxidizable substrates like *i*−PrOH instead of H_2 as the hydrogenation source.

6.4.1: Homogeneous Catalysis - I is shared under a CC BY-SA license and was authored, remixed, and/or curated by LibreTexts.

- **11.1: Homogeneous Catalysis - I** by M. S. Balakrishna & Prasenjit Ghosh is licensed CC BY-NC-SA 4.0. Original source: https://nptel.ac.in/courses/104101006.

6.4.2: Homogeneous Catalysis - II

Learning Objectives

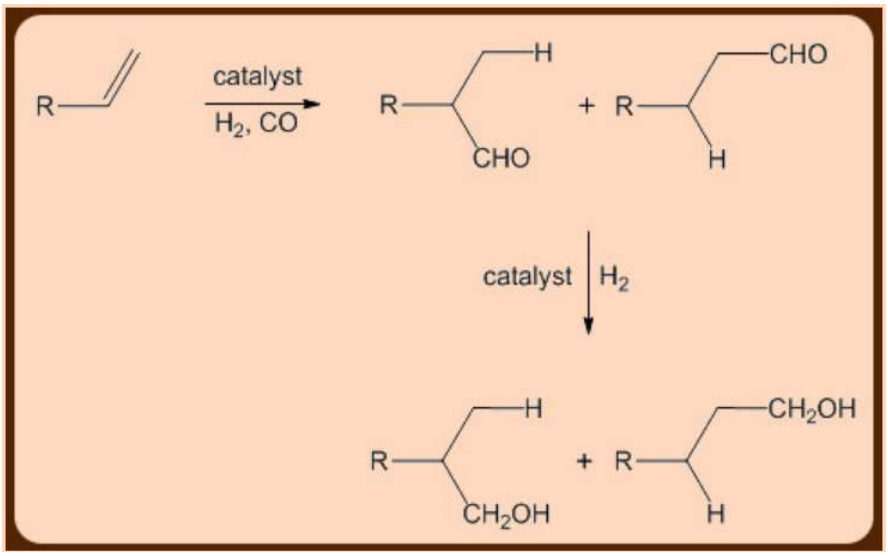
In this lecture you will learn the following

- The hydroformylation reaction and its mechanism.
- The C−C cross-coupling reactions and their mechanisms.

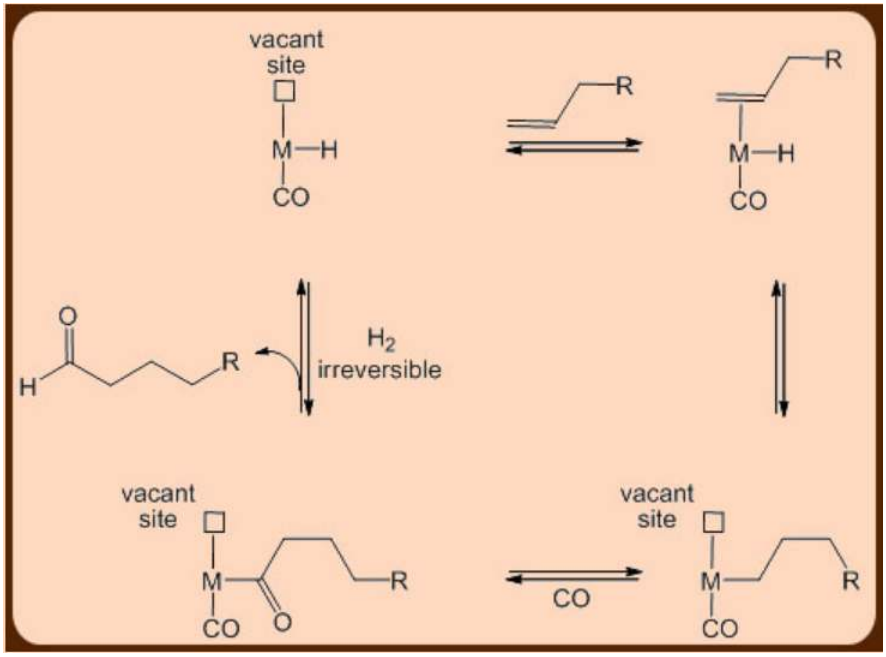
It is truly an exciting time for the field of organometallic chemistry as its potentials in homogeneous catalysis are being realized in an unprecedented manner. The growth in the field organometallic chemistry has been rightly acknowledged by the award of three Nobel prizes in over a decade in the areas of asymmetric hydrogenation (Nyori and Knowles in 2001), olefin metathesis (Grubbs, Schrock and Chauvin in 2006) and palladium mediated C−C cross coupling reactions (Suzuki, Negishi and Heck, 2010). A few representative examples of such landmark discoveries of homogeneous catalysis by organometallic compounds are discussed below.

Hydroformylation reaction

Hydroformylation, popularly known as the "oxo" process, is a Co or Rh catalyzed reaction of olefins with CO and H_2 to produce the value-added aldehydes.



The reaction, discovered by Otto Roelen in 1938, soon assumed an enormous proportion both in terms of the scope and scale of its application in the global production of aldehydes. The metal hydride complexes namely, the rhodium based $HRh(CO)(PPh_3)_3$ and the cobalt based $HCo(CO)_4$ complexes, catalyzed the hydroformylation reaction as shown below.



C−C cross-coupling reactions

The palladium catalyzed cross-coupling reactions are a class of highly successful reactions with applications in the organic synthesis to have emerged recently. The reactions carry out a coupling of the aryl, vinyl or alkyl halide substrates with different organometallic nucleophiles and as such encompasses a family of C−C cross-coupling reactions that are dependent on the nature of nucleophiles like that of the B based ones in the Suzuki-Miyuara coupling, the Sn based ones in the Stille coupling, the Si based ones in the Hiyama coupling, the Zn based ones in the Negishi coupling and the Mg based ones in the Kumada coupling reactions (Figure 6.4.2.1).

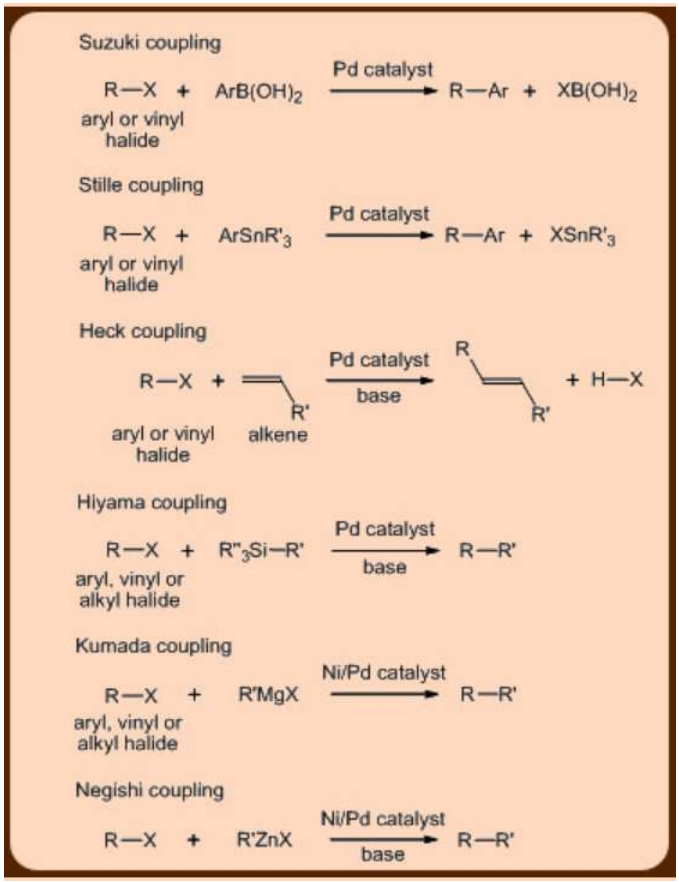


Figure **6.4.2.1**: Various types of the palladium mediated C−C cross-coupling reactions.

An unique feature of these reactions is the exclusive formation of the cross-coupled product without the accompaniment of any homo-coupled product. Another interesting feature of these coupling reactions is that they proceed *via* a common mechanism involving three steps that include the oxidative addition, the transmetallation and the reductive elimination reactions (Figures **6.4.2.2** and **6.4.2.3**).

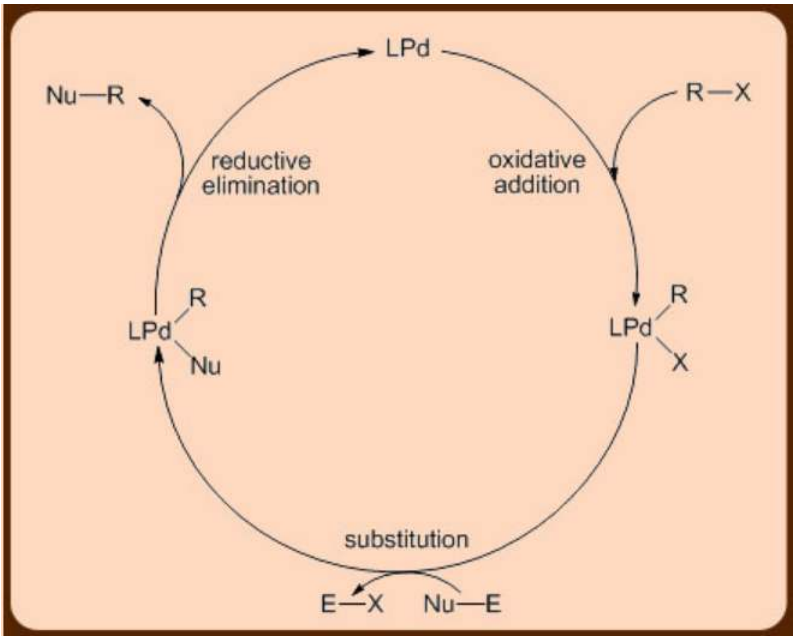


Figure **6.4.2.2**: A general catalytic cycle for the palladium mediated C−C cross-coupling reactions.

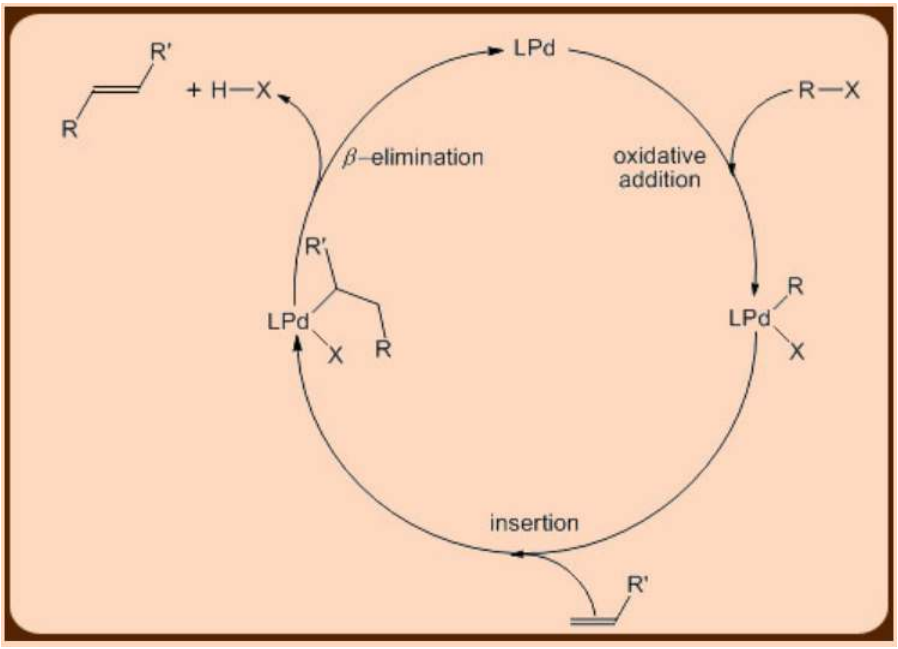


Figure **6.4.2.3**: A catalytic cycle for the palladium mediated Heck coupling reaction.

Summary

Organometallic complexes play a pivotal role in several successful homogeneous catalysis reactions like that of the hydroformylation and the C−C cross-coupling reactions. These reactions are important because of the fact that both of the hydroformylation and the C−C cross-coupling reactions give more value added products compared to the starting reactants. The palladium catalyzed C−C cross-coupling reactions are a class of highly successful reactions that have permanently impacted the area of organic synthesis in a profound way to an extent that the 2010 Nobel prize has been conferred on one of these reactions thereby recognizing the importance of the C−C cross-coupling recations.

6.4.2: Homogeneous Catalysis - II is shared under a CC BY-SA license and was authored, remixed, and/or curated by LibreTexts.

- **11.2: Homogeneous Catalysis - II** by M. S. Balakrishna & Prasenjit Ghosh is licensed CC BY-NC-SA 4.0. Original source: https://nptel.ac.in/courses/104101006.

6.4.3: Catalytic Applications of Organometallic Compounds- Alkene Metathesis

Learning Objectives

In this lecture you will learn the following

- The alkene metathesis reactions and their different variants.
- The application of metal carbenes in alkene metathesis reactions.
- The functional group tolerance, air and moisture sensitivity and high efficiency as important catalyst attributes for the alkene metathesis reactions.

The application of organometallic chemistry in homogenous catalysis is progressively increasing with the fast pace of discovery of new catalysts in the area. The benefits of organometallic catalysis have now percolated to all facets of the chemical world that span from the confines of the industry to the day-to-day small scale use in organic synthesis in academic laboratories. Quite a few of these applications of organometallic complexes in homogeneous catalysis have made a permanent imprint on the ever going developmental process that is constantly transforming our day-to-day life. An example of such a success story is of alkene metathesis, which is described in this chapter.

Alkene metathesis

Alkene metathesis reactions are gaining wide popularity in synthesizing unsaturated olefinic compounds as well as the unsaturated polymeric counterparts. Central to this catalysis is a metal carbene intermediate that reacts with olefins to give different olefinic compounds or even the unsaturated olefinic polymers depending upon the reaction conditions of the metathesis reaction. Metathesis is an unusual transformation in which a C=C is broken and also formed during catalysis to generate new unsaturated olefins.

$$\mathrm{RCH{=}CHR + R'CH{=}CHR' \rightleftharpoons 2\,RCH{=}CHR'}$$

Though a large variety of metal−carbene catalysts have been developed for the metathesis reaction, only a few have been found to be functional group tolerant. Thus a critical step in broadening the utility of metathesis reaction has been in developing catalysts that are functional group tolerant. In this regard, the early-transition metal based carbene catalysts like that of the Ti based ones are highly oxophilic and hence are intolerant to the functional groups. On the other hand, the more electron-rich Mo and W based catalysts are of intermediate character. Finally, the late-transition metal based Ru catalysts are found to be exceptionally tolerant toward functional groups but all the while exhibiting high reactivity toward olefinic bonds. In this context notable are the Grubb's Ru catalyst, which is easy to handle, and the Schrock's Mo catalyst, which display high activity.

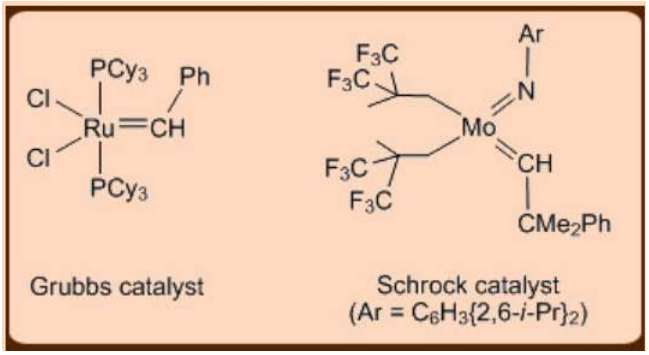
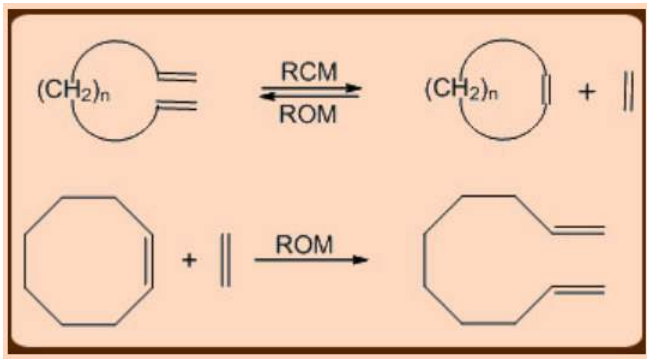


Figure **6.4.3.1**: The Grubb's and the Schrock's catalyst.

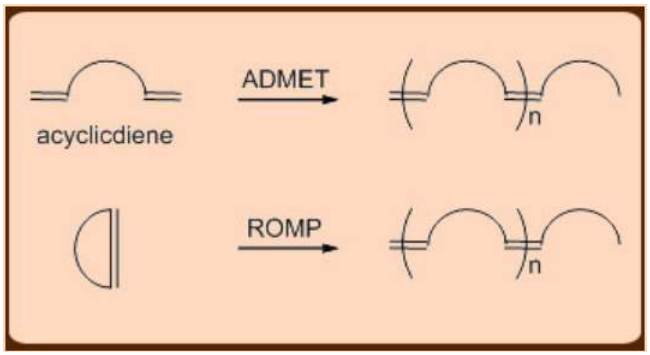
The metathesis reaction as such stands for a family of related reactions all of which involve a "cutting and stitching" of olefinic bonds leading to different unsaturated products. When two different olefin substrates are used, the reaction is called the "cross metathesis" owing to the fact that the olefinic ends are exchanged.

$$\mathrm{RCH{=}CHR + R'CH{=}CHR' \rightleftharpoons 2\,RCH{=}CHR'}$$

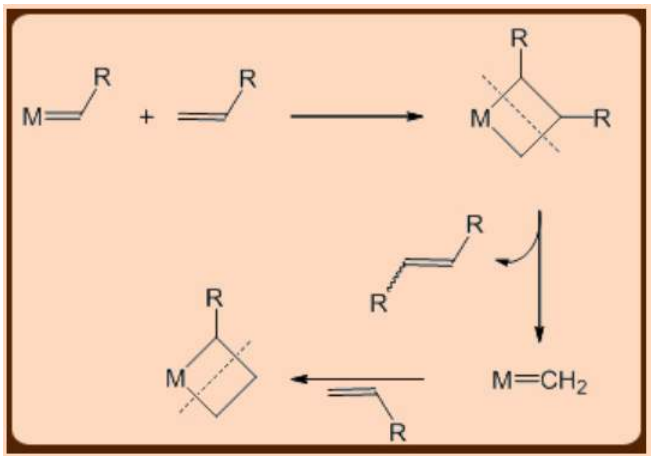
The metathesis reactions can even extend further to the conjugated dienes that can undergo Ring Closing Metathesis (RCM) in systems where the ring strain is not too high in the final product. The reverse of Ring Closing Metathesis (RCM) is called the Ring Opening Metathesis (ROM), and which is usually favored in the presence of large excess of C_2H_4.



The variants of metathesis often used in producing polymers are, (*i*) the Acyclic Diene Metathesis (ADMET) and (*ii*) the Ring Opening Metathesis Polymerization (ROMP), in which the relief of ring-strain of cycloalkenes drives the polymerization reaction forward. Both of these reactions, produce long chain polymers in a living fashion and as a result of which these reactions are useful for producing block copolymers $-(AAABBBB)_n-$.



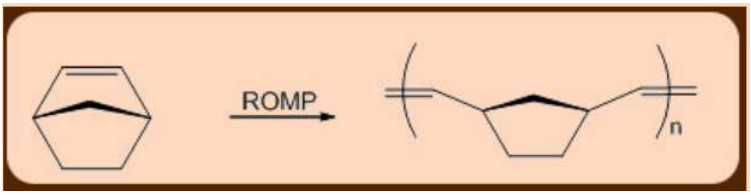
Though several possibilities have been debated for the mechanism of the metathesis reaction, the one proceeding *via* a metalacyclobutane intermediate has gained credence.



Several important industrial applications have emerged out of the metathesis reaction like that of the commercial synthesis of the housefly pheromone.

$$Me(CH_2)_7CH{=}CH_2 + Me(CH_2)_{12}CH{=}CH_2 \longrightarrow Me(CH_2)_7CH{=}C(CH_2)_{12}Me\ [\text{housefly pheromone}] + C_2H_4 + \text{other products}$$

Similarly, the polycyclopentadiene polymer, which is formed from the Ring Opening Metathesis Polymerization (ROMP) of dicyclopentadiene substrate, is used for bullet proof related applications because of its exceptional strength owing to its cross-linked nature.



Summary

Alkene metathesis represents a distinct class of related chemical reactions that involve the “cutting and stitching” of olefinic bonds to give unsaturated organic products. Depending upon the nature of the product formed, different type of alkene metathesis reactions exist like the alkene metathesis, cross-metathesis, Ring Closing Metathesis (RCM), Ring Opening Metathesis (ROM), Acyclic Diene Metathesis (ADMET), and the Ring Opening Metathesis Polymerization (ROMP). A commonality that runs through all of these different varieties of the metathesis reaction is its mechanism that involves a catalytically active metal−carbene species. The mechanism is said to be proceed *via* a 4−membered metalacyclobutane intermediate. The alkene metathesis has found important applications in organic synthesis as well as in the chemical industry.

6.4.3: Catalytic Applications of Organometallic Compounds- Alkene Metathesis is shared under a CC BY-SA license and was authored, remixed, and/or curated by LibreTexts.

- **14.1: Catalytic Applications of Organometallic Compounds- Alkene Metathesis** by M. S. Balakrishna & Prasenjit Ghosh is licensed CC BY-NC-SA 4.0. Original source: https://nptel.ac.in/courses/104101006.

CHAPTER OVERVIEW

7: Bioinorganic Chemistry

7.1: Biological Significance of Iron, Zinc, Copper, Molybdenum, Cobalt, Chromium, Vanadium, and Nickel
7.2: Introduction to Amino Acids and Proteins
7.3: Overview of Hemoglobin and Myoglobin
7.3.1: Myoglobin, Hemoglobin, and their Ligands
7.3.2: Oxygen Transport by the Proteins Myoglobin and Hemoglobin
7.4: Ferrodoxins, Hydrogenases, and Nitrogenases - Metal-Sulfide Proteins
7.4.1: Iron-sulfur Proteins and Models
7.4.2: Iron-sulfur Proteins and Models (Part 2)
7.4.3: Iron-sulfur Proteins and Models (Part 3)
7.4.4: Iron-sulfur Proteins and Models (Part 4)
7.5: The Reaction Pathways of Zinc Enzymes and Related Biological Catalysts
7.5.1: About Carbonic Anhydrase
7.5.2: Catalytic Mechanism
7.5.3: Metal Substitution
7.6: Metals in Medicine
7.6.1: Metal Deficiency and Disease
7.6.2: Toxic Effects of Metals
7.6.3: Aspects of Platinum Binding to DNA
7.6.4: Survey of Metals Used for Diagnosis and Chemotherapy
7.6.5: Platinum Anticancer Drugs- A Case Study
7.6.6: Mapping the Major Adducts of cis- and trans-DDP on DNA; Sequence Specificity
7.6.7: Structure of Platinum-DNA Complexes
7.6.8: Site-specifically Platinated DNA \(\;^{154}\)
7.6.9: Bioinorganic Chemistry of Platinum Anticancer Drugs- How Might They Work?
7.6.10: Bioinorganic Chemistry of Platinum Anticancer Drugs; How Might They Work? (Part 2)
7.6.11: Design of New Inorganic Anticancer Drugs

7.5: The Reaction Pathways of Zinc Enzymes and Related Biological Catalysts

7.6: Metals in Medicine

7: Bioinorganic Chemistry is shared under a not declared license and was authored, remixed, and/or curated by LibreTexts.

7.1: Biological Significance of Iron, Zinc, Copper, Molybdenum, Cobalt, Chromium, Vanadium, and Nickel

The transition metals are among the least abundant metal ions in sea water from which contemporary organisms are thought to have evolved (Table 1.1).[1-5] For many of the metals, the concentration in human blood plasma greatly exceeds that in sea water. Such data indicate the importance of mechanisms for accumulation, storage, and transport of transition metals and zinc in living organisms.

Table 1.1: Concentrations of transition metals and zinc in sea water and human plasma.a*Data from References 1 - 5 and 12

Element	Sea Water (M) x 10^8	Human Plasma (M) x 10^8
Fe	0.005 - 2	2230
Zn	8.0	1720
Cu	1.0	1650
Mo	10.0	1000
Co	0.7	0.0025
Cr	0.4	5.5
V	4.0	17.7
Mn	0.7	10.9
Ni	0.5	4.4

The metals are generally found either bound directly to proteins, found in cofactors, or part of clusters that are in turn bound by a protein. The ligands usually contain O, N, S, or C donor atoms. Proteins with transition metals are most commonly associated with the catalysis involving the intramolecular or intermolecular rearrangement of electrons. Although the redox properties of the metals are important in many of the reactions, in others the metal appears to contribute to the structure of the active state, e.g., zinc in the Cu-Zn dismutases and some of the iron in the photosynthetic reaction center. Sometimes equivalent reactions are catalyzed by proteins with different metal centers; the metal binding sites and proteins have evolved separately for each type of metal center.

Iron is the most common transition metal in biology.[6,7] Its use has created a dependence that has survived the appearance of dioxygen in the atmosphere ca. 2.5 billion years ago, and the concomitant conversion of ferrous ion to ferric ion and insoluble rust. All plants, animals, and bacteria use iron, except for a lactobacillus that appears to maintain high concentrations of manganese instead of iron. The processes and reactions in which iron participates are crucial to the survival of terrestrial organisms, and include ribonucleotide reduction (DNA synthesis), energy production (respiration), energy conversion (photosynthesis), nitrogen reduction, oxygen transport (respiration, muscle contraction), and oxygenation (e.g., steroid synthesis, solubilization and detoxification of aromatic compounds). Among the transition metals used in living organisms, iron is the most abundant in the environment. Whether this fact alone explains the biological predominance of iron or whether specific features of iron chemistry contribute is not clear.

Many of the other transition metals participate in reactions equivalent to those involving iron, and can sometimes substitute for iron, albeit less effectively, in natural Fe-proteins. Additional biological reactions are unique to nonferrous transition metals.

Zinc is relatively abundant in biological materials.[8,9] The major location of zinc in the body is metallothionein, which also binds copper, chromium, mercury, and other metals. Among the other well-characterized zinc proteins are the Cu-Zn superoxide dismutases (other forms have Fe or Mn), carbonic anhydrase (an abundant protein in red blood cells responsible for maintaining the pH of the blood), alcohol dehydrogenase, and a variety of hydrolases involved in the metabolism of sugars, proteins, and nucleic acids. Zinc is a common element in nucleic-acid polymerases and transcription factors, where its role is considered to be structural rather than catalytic. Interestingly, zinc enhances the stereoselectivity of the polymerization of nucleotides under reaction conditions designed to simulate the environment for prebiotic reactions. Recently a group of nucleic-acid binding proteins, with a

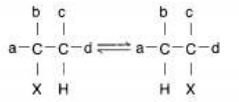
repeated sequence containing the amino acids cysteine and histidine, were shown to bind as many as eleven zinc atoms necessary for protein function (transcribing DNA to RNA).[10] Zinc plays a structural role, forming the peptide into multiple domains or "zinc fingers" by means of coordination to cysteine and histidine. A survey of the sequences of many nucleic-acid binding proteins shows that many of them have the common motif required to form zinc fingers. Other zinc-finger proteins called steroid receptors bind both steroids such as progesterone and the progesterone gene DNA . Much of the zinc in animals and plants has no known function, but it may be maintaining the structures of proteins that activate and deactivate genes.[11]

Copper and iron proteins participate in many of the same biological reactions:

1. reversible binding of dioxygen, e.g., hemocyanin (Cu), hemerythrin (Fe), and hemoglobin (Fe);
2. activation of dioxygen, e.g., dopamine hydroxylase (Cu) (important in the synthesis of the hormone epinephrine), tyrosinases (Cu), and catechol dioxygenases (Fe);
3. electron transfer, e.g., plastocyanins (Cu), ferredoxins, and c-type cytochromes (Fe);
4. dismutation of superoxide by Cu or Fe as the redox-active metal (superoxide dismutases).

The two metal ions also function in concert in proteins such as cytochrome oxidase, which catalyzes the transfer of four electrons to dioxygen to form water during respiration. Whether any types of biological reactions are unique to copper proteins is not clear. However, use of stored iron is reduced by copper deficiency, which suggests that iron metabolism may depend on copper proteins, such as the serum protein ceruloplasmin, which can function as a ferroxidase, and the cellular protein ascorbic acid oxidase, which also is a ferrireductase.

Cobalt is found in vitamin B_{12} , its only apparent biological site.[12] The vitamin is a cyano complex, but a methyl or methylene group replaces CN in native enzymes. Vitamin-B_{12} deficiency causes the severe disease of pernicious anemia in humans, which indicates the critical role of cobalt. The most common type of reaction in which cobalamin enzymes participate results in the reciprocal exchange of hydrogen atoms if they are on adjacent carbon atoms, yet not with hydrogen in solvent water:



(An important exception is the ribonucleotide reductase from some bacteria and lower plants, which converts ribonucleotides to the DNA precursors, deoxyribonucleotides, a reaction in which a sugar -OH is replaced by -H. Note that ribonucleotide reductases catalyzing the same reaction in higher organisms and viruses are proteins with an oxo-bridged dimeric iron center.) The cobalt in vitamin B_{12} is coordinated to five N atoms, four contributed by a tetrapyrrole (corrin); the sixth ligand is C, provided either by C5 of deoxyadenosine in enzymes such as methylmalonyl-CoA mutase (fatty acid metabolism) or by a methyl group in the enzyme that synthesizes the amino acid methionine in bacteria.

Nickel is a component of a hydrolase (urease), of hydrogenase, of CO dehydrogenase, and of S-methyl CoM reductase, which catalyzes the terminal step in methane production by methanogenic bacteria. All the Ni-proteins known to date are from plants or bacteria.[13,14] However, about 50 years elapsed between the crystallization of jack-bean urease in 1925 and the identification of the nickel component in the plant protein. Thus it is premature to exclude the possibility of Ni-proteins in animals. Despite the small number of characterized Ni-proteins, it is clear that many different environments exist, from apparently direct coordination to protein ligands (urease) to the tetrapyrrole F430 in methylreductase and the multiple metal sites of Ni and Fe-S in a hydrogenase from the bacterium *Desulfovibrio gigas*. Specific environments for nickel are also indicated for nucleic acids (or nucleic acid-binding proteins), since nickel activates the gene for hydrogenase.[15]

Manganese plays a critical role in oxygen evolution catalyzed by the proteins of the photosynthetic reaction center. The superoxide dismutase of bacteria and mitochondria, as well as pyruvate carboxylase in mammals, are also manganese proteins.[16,17] How the multiple manganese atoms of the photosynthetic reaction center participate in the removal of four electrons and protons from water is the subject of intense investigation by spectroscopists, synthetic inorganic chemists, and molecular biologists.[17]

Vanadium and chromium have several features in common, from a bioinorganic viewpoint.[18a] First, both metals are present in only small amounts in most organisms. Second, the biological roles of each remain largely unknown.[18] Finally, each has served as a probe to characterize the sites of other metals, such as iron and zinc. Vanadium is required for normal health, and could act *in vivo* either as a metal cation or as a phosphate analogue, depending on the oxidation state, V(lV) or V(V), respectively. Vanadium in a

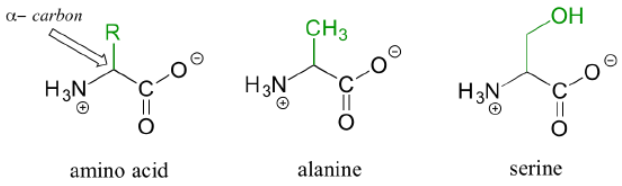
sea squirt (tunicate), a primitive vertebrate, is concentrated in blood cells, apparently as the major cellular transition metal, but whether it participates in the transport of dioxygen (as iron and copper do) is not known. In proteins, vanadium is a cofactor in an algal bromoperoxidase and in certain prokaryotic nitrogenases. Chromium imbalance affects sugar metabolism and has been associated with the glucose tolerance factor in animals. But little is known about the structure of the factor or of any other specific chromium complexes from plants, animals, or bacteria.

Molybdenum proteins catalyze the reduction of nitrogen and nitrate, as well as the oxidation of aldehydes, purines, and sulfite.[19] Few Mo-proteins are known compared to those involving other transition metals. Nitrogenases, which also contain iron, have been the focus of intense investigations by bioinorganic chemists and biologists; the iron is found in a cluster with molybdenum (the iron-molybdenum cofactor, or FeMoCo) and in an iron-sulfur center (Chapter 7). Interestingly, certain bacteria (*Azotobacter*) have alternative nitrogenases, which are produced when molybdenum is deficient and which contain vanadium and iron or only iron. All other known Mo-proteins are also Fe-proteins with iron centers, such as tetrapyrroles (heme and chlorins), Fe-sulfur clusters, and, apparently, non-heme/non-sulfur iron. Some Mo-proteins contain additional cofactors such as the Havins, e.g., in xanthine oxidase and aldehyde oxidase. The number of redox centers in some Mo-proteins exceeds the number of electrons transferred; reasons for this are unknown currently.

7.1: Biological Significance of Iron, Zinc, Copper, Molybdenum, Cobalt, Chromium, Vanadium, and Nickel is shared under a not declared license and was authored, remixed, and/or curated by LibreTexts.

7.2: Introduction to Amino Acids and Proteins

Proteins are polymers of **amino acids**, linked by amide groups known as **peptide bond**s. An amino acid can be thought of as having two components: a 'backbone', or 'main chain', composed of an ammonium group (H_3N^+-C), an 'alpha-carbon' bonded to the nitrogen atom, a carboxylate (COO^-), and a variable 'side chain' (in green below) bonded to the alpha-carbon (Figure **7.2.1**).



(Figure 7.2.1). Structures of amino acids.

There are twenty different side chains in naturally occurring amino acids, and it is the identity of the side chain that determines the identity of the amino acid: for example, if the side chain is a $-CH_3$ group, the amino acid is alanine, and if the side chain is a $-CH_2OH$ group, the amino acid is serine. Many amino acid side chains contain a functional group (the side chain of serine, for example, contains a primary alcohol), while others, like alanine, lack a functional group, and contain only a simple hydrocarbon group.

The two 'hooks' on an amino acid monomer are the ammonium and carboxylate groups. Proteins (polymers of ~50 amino acids or more) and peptides (shorter polymers) are formed when the amino group of one amino acid monomer reacts with the carboxylate carbon of another amino acid to form an amide linkage, which in protein terminology is a **peptide bond**. Which amino acids are linked, and in what order - the protein **sequence** - is what distinguishes one protein from another. This sequence is coded for by an organism's DNA. Protein sequences are written in the ammonium terminal (N-terminal) to carboxylate terminal (C-terminal) direction, with either three-letter or single-letter abbreviations for the amino acids. Below is a four amino acid peptide with the sequence "cysteine - histidine - glutamate - methionine". Using the single-letter code, the sequence is abbreviated CHEM (Figure **7.2.2**).

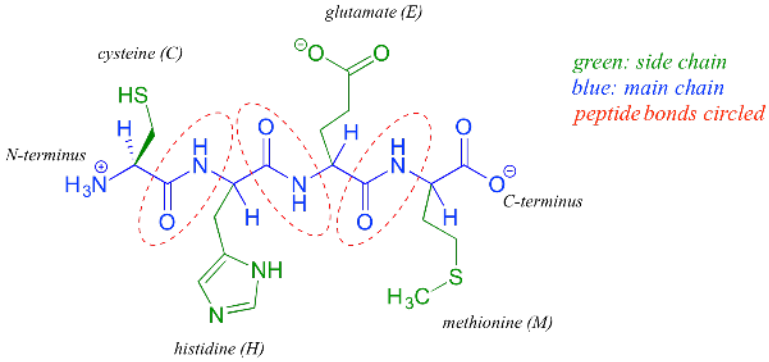


Figure 7.2.2. The CHEM peptide.

When an amino acid is incorporated into a protein it loses a molecule of water and what remains is called a **residue** of the original amino acid. Thus we might refer to the 'glutamate residue' at position 3 of the CHEM peptide above.

Once a protein polymer is constructed, it in many cases folds up very specifically into a three-dimensional structure, which often includes one or more 'binding pockets' in which other molecules can be bound. It is this shape of this folded structure, and the precise arrangement of the functional groups within the structure (especially in the area of the binding pocket) that determines the function of the protein.

Enzymes are proteins which catalyze biochemical reactions. One or more reacting molecules - often called **substrates** - become bound in the **active site** pocket of an enzyme, where the actual reaction takes place. **Receptors** are proteins that bind specifically to

one or more molecules - referred to as **ligands** - to initiate a biochemical process. For example, we saw in the introduction to this chapter that the TrpVI receptor in mammalian tissues binds capsaicin (from hot chili peppers) in its binding pocket and initiates a heat/pain signal which is sent to the brain.

Contributors and Attributions

- Organic Chemistry With a Biological Emphasis by Tim Soderberg (University of Minnesota, Morris)

This page titled 7.2: Introduction to Amino Acids and Proteins is shared under a CC BY-NC-SA 4.0 license and was authored, remixed, and/or curated by Tim Soderberg.

SECTION OVERVIEW

7.3: Overview of Hemoglobin and Myoglobin

7.3.1: Myoglobin, Hemoglobin, and their Ligands

7.3.2: Oxygen Transport by the Proteins Myoglobin and Hemoglobin

---

7.3: Overview of Hemoglobin and Myoglobin is shared under a not declared license and was authored, remixed, and/or curated by LibreTexts.

7.3.1: Myoglobin, Hemoglobin, and their Ligands

Hemoglobin:

- 1st. protein whose molecular weight was determined
- 1st protein to be assigned a specific function - dioxygen transport
- has a prosthetic group (non-amino acid) heme group (protoporphyrin IX with a ferrous ion) covalently attached to the protein. The heme group binds dioxygen.
- 1st protein in which a point mutation (single base pair charge) causes a single amino acid change in the protein, marking the start of molecular medicine
- 1st protein with high resolution x-ray structure
- theory for dioxygen binding explain control of enzyme activity
- the binding of dioxygen is regulated by binding of H^+, CO_2, and bisphosphoglcyerate which bind to sites (allosteric) distant from oxygen binding site.
- crystals of deoxy-Hb shatter on binding dioxygen, indicating significant conformational changes on binding.

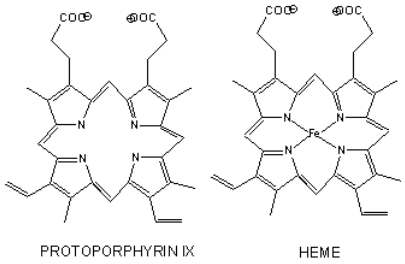


Figure 7.3.1.1. The heme group contains protoporphyrin IX, with four tetrapyrrole rings linked by methene bridges. Attached to the tetrapyrrole structure are four methyl, two vinyl, and two proprionate groups. These can be arranged in 15 ways, only one (IX) occurs in biological systems.

The heme fits into a hydrophobic crevice in the proteins with the proprionate groups exposed to solvent. The Fe^{2+} ion is coordinated to 4 N's on the 4 pyrrole rings, The 5th ligand is a supplied by proximal His (the 8th amino acid on helix F) of the protein. In the absence of dioxygen, the 6 ligand is missing. and the geometry of the complex is square pyramidal with the Fe above the plane of the heme ring. A distal His (E7) is on the opposite side of the heme ring, but too far to coordinate with the Fe. When dioxgen binds, it occupies the 6th coordination site and pulls the Fe into the plane of the ring, leading to octahedral geometry. CO, NO, and H_2S also bind to the 6th site, but with higher affinity than dioxygen, which can lead to CO poisoning. The distal His keeps these ligands (including dioxygen) bound in a bent, non-optimal geometry. This minimizes the chances of CO poisoning.

Myoglobin

- Myoglobin is a relatively small protein that contains 150 amino acids.
- Mb is extremely compact, and consists of 75% alpha helical structure.
- The interior amino acids are almost entirely nonpolar. The only polar amino acids found completely buried are the two His (proximal and distal) found at the active site of dioxygen binding.

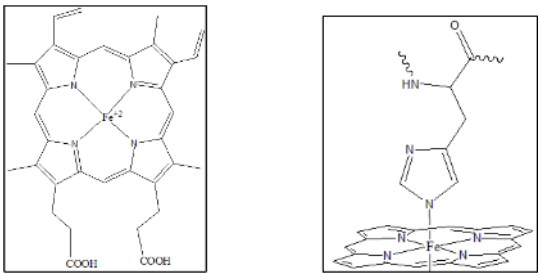


Figure 7.3.1.2. The skeletal structure of the heme prosthetic group found within the structure of myoglobin. The porphyrin ring contains four pyrrole nitrogens bound to a ferrous (Fe(II)) ion center. There are six coordination sites in the Fe(II) ion; four are occupied by the pyrrole nitrogens, one is occupied by a proximal histidine, one site can be occupied by a dioxygen molecule (not shown).

Difference between Hb and Mb

Hb is a tetramer of two α and two β subunits held together by IMF's (an example of quarternary protein structure), and 4 bound hemes, each of which can bind a dioxygen. In a fetus, two other subunits make up Hb (two zeta - ζand two epsilion - ε subunits - analogous to the two αand two β subunits, respectively). This changes in fetuses to two α and two γ subunits. Fetal Hb has higher affinity for dioxygen than adult Hb. Mb is a single polypeptide chains which has higher affinity for dioxygen than Hb.

The α and β chains are similar to Mb, which is unexpected since only 24 of 141 residues in the α and β chains of Hb are identical to amino acids in Mb. This suggests that different sequences can fold to similar structures. The globin fold of Mb and each chain of Hb is common to vertebrates and must be nature's design for dioxygen carriers. A comparison of the sequence of Hb from 60 species show much variability of amino acids, with only 9 identical amino founds. These must be important for structure/function. All internal changes are conservative (e.g. changing a nonpolar for a nonpolar amino acid). Not even Pro's are conserved, suggesting there are different ways to break helices. The two active site His are conserved, as is Gly B6 (required for a reverse turn).

This page titled 7.3.1: Myoglobin, Hemoglobin, and their Ligands is shared under a CC BY-NC-SA 4.0 license and was authored, remixed, and/or curated by Henry Jakubowski.

7.3.2: Oxygen Transport by the Proteins Myoglobin and Hemoglobin

Oxygen Transport

Many microorganisms and most animals obtain energy by respiration, the oxidation of organic or inorganic molecules by O_2. At 25°C, however, the concentration of dissolved oxygen in water in contact with air is only about 0.25 mM. Because of their high surface area-to-volume ratio, aerobic microorganisms can obtain enough oxygen for respiration by passive diffusion of O_2 through the cell membrane. As the size of an organism increases, however, its volume increases much more rapidly than its surface area, and the need for oxygen depends on its volume. Consequently, as a multicellular organism grows larger, its need for O_2 rapidly outstrips the supply available through diffusion. Unless a transport system is available to provide an adequate supply of oxygen for the interior cells, organisms that contain more than a few cells cannot exist. In addition, O_2 is such a powerful oxidant that the oxidation reactions used to obtain metabolic energy must be carefully controlled to avoid releasing so much heat that the water in the cell boils. Consequently, in higher-level organisms, the respiratory apparatus is located in internal compartments called mitochondria, which are the power plants of a cell. Oxygen must therefore be transported not only to a cell but also to the proper compartment within a cell.

Myoglobin and Hemoglobin

Myoglobin is a relatively small protein that contains 150 amino acids. The functional unit of myoglobin is an **iron–porphyrin complex** that is embedded in the protein (Figure 4.2.1). In myoglobin, the heme iron is five-coordinate, with only a single histidine imidazole ligand from the protein (called the proximal histidine because it is near the iron) in addition to the four nitrogen atoms of the porphyrin. A second histidine imidazole (the distal histidine because it is more distant from the iron) is located on the other side of the heme group, too far from the iron to be bonded to it. Consequently, the iron atom has a vacant coordination site, which is where O_2 binds.

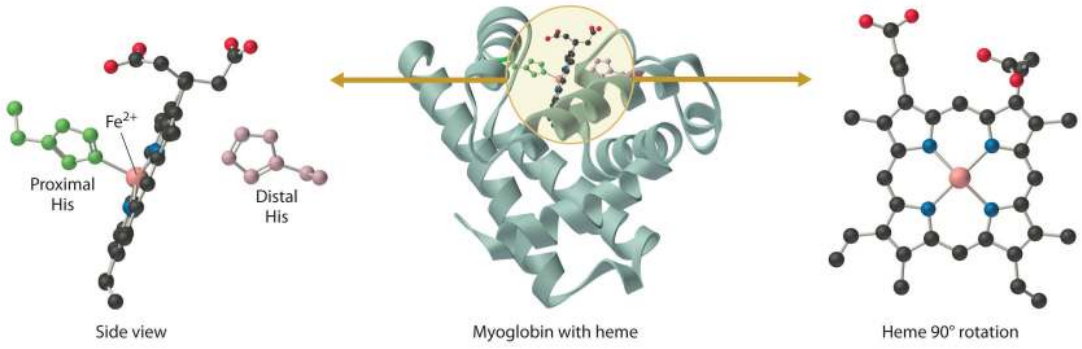


Figure 7.3.2.1. The Structure of Deoxymyoglobin, Showing the Heme Group. The iron in deoxymyoglobin is five-coordinate, with one histidine imidazole ligand from the protein. Oxygen binds at the vacant site on iron.

In the ferrous form (deoxymyoglobin), the iron is five-coordinate and high spin. Because high-spin Fe^{2+} is too large to fit into the "hole" in the center of the porphyrin, it is about 60 pm above the plane of the porphyrin. When O_2 binds to deoxymyoglobin to form oxymyoglobin, the iron is converted from five-coordinate (high spin) to six-coordinate (low spin; Figure 4.2.2). Because low-spin Fe^{2+} and Fe^{3+} are smaller than high-spin Fe^{2+}, the iron atom moves into the plane of the porphyrin ring to form an octahedral complex. The O_2 pressure at which half of the molecules in a solution of myoglobin are bound to O_2 ($P_{1/2}$) is about 1 mm Hg (1.3×10^{-3} atm).

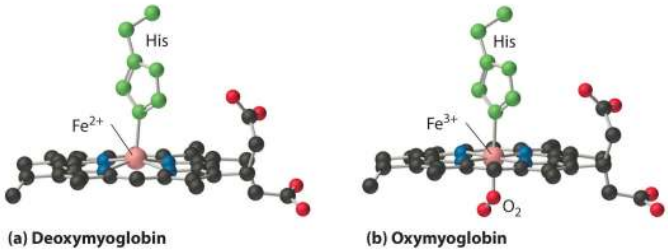


Figure 7.3.2.2. Oxygen Binding to Myoglobin and Hemoglobin. (a) The Fe^{2+} ion in deoxymyoglobin is high spin, which makes it too large to fit into the "hole" in the center of the porphyrin. (b) When O_2 binds to deoxymyoglobin, the iron is converted to low-spin Fe^{3+}, which is smaller, allowing the iron to move into the plane of the four nitrogen atoms of the porphyrin to form an octahedral complex.

Hemoglobin consists of two subunits of 141 amino acids and two subunits of 146 amino acids, both similar to myoglobin; it is called a tetramer because of its four subunits. Because hemoglobin has very different O_2-binding properties, however, it is not simply a "super myoglobin" that can carry four O_2 molecules simultaneously (one per heme group). The shape of the O_2-binding curve of myoglobin can be described mathematically by the following equilibrium:

$$MbO_2 \rightleftharpoons Mb + O_2 \tag{7.3.2.1}$$

$$K_{diss} = \frac{[Mb]\,[O_2]}{[MbO_2]} \tag{7.3.2.2}$$

The O_2-binding curve of hemoglobin is S shaped (Figure 4.2.3). As shown in the curves, at low oxygen pressures, the affinity of deoxyhemoglobin for O_2 is substantially lower than that of myoglobin, whereas at high O_2 pressures the two proteins have comparable O_2 affinities. The physiological consequences of unusual S-shaped O_2-binding curve of hemoglobin are enormous. In the lungs, where O_2 pressure is highest, the high oxygen affinity of deoxyhemoglobin allows it to be completely loaded with O_2, giving four O_2 molecules per hemoglobin. In the tissues, however, where the oxygen pressure is much lower, the decreased oxygen affinity of hemoglobin allows it to release O_2, resulting in a net transfer of oxygen to myoglobin.

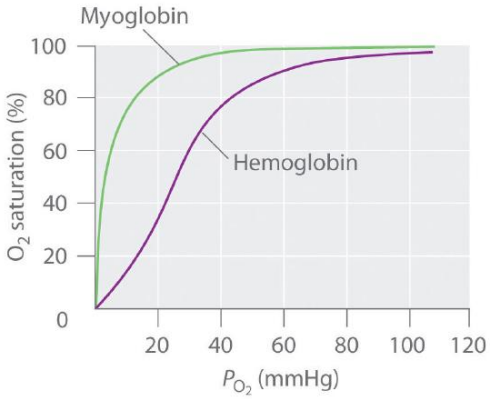


Figure 4.2.3: The O_2-Binding Curves of Myoglobin and Hemoglobin. Plots of Y (fractional saturation) vs L (pO2) are hyperbolic for Mb, but sigmoidal for Hb, suggesting cooperative binding of oxygen to Hb (binding of the first oxygen facilitates binding of second, etc).

The S-shaped O_2-binding curve of hemoglobin is due to a phenomenon called **cooperativity**, in which the affinity of one heme for O_2 depends on whether the other hemes are already bound to O_2. Cooperativity in hemoglobin requires an interaction between the four heme groups in the hemoglobin tetramer, even though they are more than 3000 pm apart, and depends on the change in structure of the heme group that occurs with oxygen binding. The structures of deoxyhemoglobin and oxyhemoglobin are slightly different, and as a result, deoxyhemoglobin has a much lower O_2 affinity than myoglobin, whereas the O_2 affinity of oxyhemoglobin is essentially identical to that of oxymyoglobin. Binding of the first two O_2 molecules to deoxyhemoglobin causes the overall structure of the protein to change to that of oxyhemoglobin; consequently, the last two heme groups have a much higher affinity for O_2 than the first two.

The affinity of Hb, but not of Mb, for dioxygen depends on pH. This is called the **Bohr effect**, after the father of Neils Bohr, who discovered it.

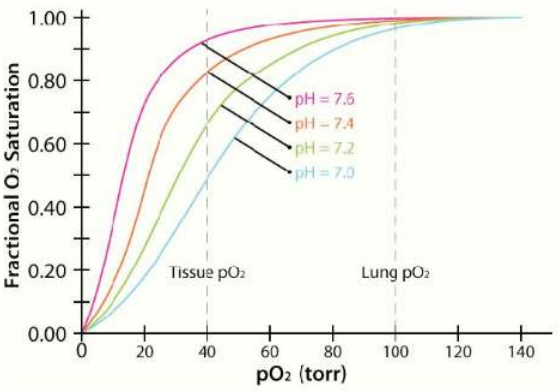


Figure 4.2.4: The Bohr Effect

Decreasing pH shifts the oxygen binding curves to the right (to decreased oxygen affinity). Increased [H^+] will cause protonation of basic side chains. In the pH range for the Bohr effect, the mostly likely side chain to get protonated is His (pKa around 6), which then becomes charged. The mostly likely candidate for protonation is His 146 (on the β chain - CH_3) which can then form a salt bridge with Asp 94 of the β(FG1) chain. This salt bridge stabilizes the positive charge on the His and raises its pKa compared to the oxyHb state. Carbon dioxide binds covalently to the N-terminus to form a negatively charge carbamate which forms a salt bridge with Arg 141 on the alpha chain. BPG, a strongly negatively charged ligand, binds in a pocket lined with Lys 82, His 2, and His 143 (all on the beta chain). It fits into a cavity present between the β subunits of the Hb tetramer in the T state. Notice all these allosteric effectors lead to the formation of more salt bridges which stabilize the T or deoxy state. The central cavity where BPG binds between the β subunits become much smaller on oxygen binding and the shift to the oxy or R state. Hence BPG is extruded from the cavity.

The binding of H^+ and CO_2 helps shift the equilibrium to deoxyHb which faciliates dumping of oxygen to the tissue. It is in respiring tissues that CO_2 and H^+ levels are high. CO_2 is produced from the oxidation of glucose through glycolysis and the Krebs cycle. In addition, high levels of CO_2 increase H^+ levels through the following equilibrium:

$$\mathbf{H_2O + CO_2 \rightleftharpoons H_2CO_3 \rightleftharpoons H^+ + HCO_3^-} \tag{7.3.2.3}$$

In addition, H^+ increases due to production of weak acids such as pyruvic acid in glycolysis .

Hb, by binding CO_2 and H^+, in addition to O_2, serves an additional function: it removes excess CO_2 and H^+ from the tissues where they build up. When deoxyHb with bound H^+ and CO_2 reaches the lungs, they leave as O_2 builds and deoxyHb is converted to oxyHb.

Contributors

Prof. Henry Jakubowski (College of St. Benedict/St. John's University)

Contributed by OpenStax, General Biology at OpenStax CNX

Dr. Kevin Ahern and Dr. Indira Rajagopal (Oregon State University)

7.3.2: Oxygen Transport by the Proteins Myoglobin and Hemoglobin is shared under a not declared license and was authored, remixed, and/or curated by LibreTexts.

SECTION OVERVIEW

7.4: Ferrodoxins, Hydrogenases, and Nitrogenases - Metal-Sulfide Proteins

Transition-metal/sulfide sites, especially those containing iron, are present in all forms of life and are found at the active centers of a wide variety of redox and catalytic proteins. These proteins include simple soluble electron-transfer agents (the ferredoxins), membrane-bound components of electron-transfer chains, and some of the most complex metalloenzymes, such as nitrogenase, hydrogenase, and xanthine oxidase. In this chapter we first review the chemistry of the Fe-S sites that occur in relatively simple rubredoxins and ferredoxins, and make note of the ubiquity of these sites in other metalloenzymes. We use these relatively simple systems to show the usefulness of spectroscopy and model-system studies for deducing bioinorganic structure and reactivity. We then direct our attention to the hydrogenase and nitrogenase enzyme systems, both of which use transition-metalsulfur clusters to activate and evolve molecular hydrogen.

7.4.1: Iron-sulfur Proteins and Models

7.4.2: Iron-sulfur Proteins and Models (Part 2)

7.4.3: Iron-sulfur Proteins and Models (Part 3)

7.4.4: Iron-sulfur Proteins and Models (Part 4)

References

1. F. Armstrong, in A. G. Sykes, ed., *Advances in Inorganic and Bioinorganic Mechanisms*, Vol. **I**, Academic Press, 1982.
2. H. Beinert and S. P. J. Albracht, *Biochim. Biophys. Acta* **683** (1982), 245.
3. A. V. Xavier, J. J. G. Moura, and I. Moura, in J. B. Goodenough *et al.*, eds., *Structure and Bonding*, Springer-Verlag, **43** (1981), 187-213.
4. D. C. Yoch and R. P. Carithers, *Microbiol. Rev*. **43** (1979), 384.
5. H. B. Dunford *et aI.*, eds., *The Biological Chemistry of Iron: A Look at the Metabolism of Iron and Its Subsequent Uses in Living Organisms*, Reidel, 1981.
6. R. K. Thauer and P. Schönheit, in Reference 8, p. 329.
7. A. Bezkorovainy, *Biochemistry of Nonheme Iron*, Plenum, 1980, pp. 343-393.
8. T. G. Spiro, ed., *Iron-Sulfur Proteins*, Wiley-Interscience, 1985.
9. W. Lovenberg, ed., *Iron-Sulfur Proteins*, Vol. I, Academic Press, 1973.
10. Reference 9, Vol. II, Academic Press, 1973.
11. Reference 10, Vol. III, Academic Press, 1977.
12. Nomenclature, *Eur. J. Biochem.* **93** (1979), 427.
13. Nomenclature, *Biochim. Biophys. Acta* 549 (1979), 101.
14. C. F. Yocum, J. N. Sadow, and A. San Pietro, in Reference 9, p. 112.
15. B. B. Buchanan, in Reference 9, p. 129.
16. T. P. Singer and R. R. Ramsay, in A. N. Martonosi, ed., *The Enzymes of Biological Membranes*, Plenum, 1985, pp. 301-332.
17. T. Yagi, H. Inokuchi, and K. Kimura, *Acc. Chem. Res.* **16** (1983), 2; Y. Higuchi *et al.*, *J. Mol. Biol.* **172** (1984), 109.
18. R. Lemberg and J. Barrett, *Cytochromes*, Academic Press, 1973.
19. H. Beinert, in Reference 9, p. 1.
20. K. K. Rao and D. O. Hall, in G. V. Leigh, ed., *Evolution of Metalloenzymes, Metalloproteins, and Related Materials*, 1977, p. 39.
21. D. O. Hall, R. Cammack, and K. K. Rao, *Nature* **233** (1977), 136.
22. T. Ohnishi and J. C. Salerno, in Reference 8, p. 285.
23. F. A. Cotton and G. Wilkinson, *Advanced Inorganic Chemistry*, Wiley, 1980.
24. D. E. McRee *et al.*, *J. Biol. Chem.* **261** (1986), 10277.

25. S. J. N. Burgmayer and E. I. Stiefel, *J. Chem. Educ.* **62** (1985), 943.
26. W. Lovenberg and B. E. Sobel, *Proc. Natl. Acad. Sci. USA* **54** (1965), 193.
27. E. T. Lode and M. J. Coon, in Reference 9, pp. 173-191.
28. I. C. Gunsalus and J. D. Lipscomb, in Reference 11, p. 151.
29. R. W. Estabrook *et al*., in Reference 9.
30. I. Moura *et al*., *Biochem. Biophys. Res. Commun*. **75** (1977), 1037.
31. I. Moura *et al*., *J. Biol. Chem.* **255** (1980), 2493. a) J. LeGall *et al*., *Biochemistry* **27** (1988), 1636.
32. K. D. Watenpaugh, L. C. Sieker, and L. H. Jensen, *J. Mol. Biol*. **138** (1980), 615.
33. E. T. Adman *et al*., *J. Mol. Biol.* **112** (1977), 113. a) C. D. Stout, in Reference 8, p. 97.
34. K. D. Watenpaugh *et al*., *Acta Cryst*. **B29** (1973), 943.
35. R. G. Shulman *et al*., *Proc. Natl. Acad. Sci. USA* **72** (1975), 4003.
36. R. G. Shulman *et al*., *J. Mol. Biol.* **124** (1978), 305.
37. W. D. Phillips *et al*., *Nature* **227** (1970), 574.
38. J. C. Rivoal *et aI*., *Biochim. Biophys. Acta* **493** (1977), 122.
39. D. E. Bennett and M. K. Johnson, *Biochim. Biophys. Acta* **911** (1987), 71. a) M. S. Gebhard *et al*.,*J. Am. Chem. Soc*. **112** (1990), 2217. b) K. D. Butcher, M. S. Gebhard, and E. I. Solomon, *Inorg. Chem*. **29** (1990), 2067.
40. M. C. W. Evans, in Reference 8, p. 249.
41. W. A. Eaton and W. J. Lovenberg, *J. Am. Chem. Soc*. **92** (1970), 7195.
42. M. K. Johnson, A. E. Robinson, and A. J. Thomson, in Reference 8, p. 367.
43. P. J. Stephens *et aI*., *Proc. Natl. Acad. Sci. USA* **75** (1978), 5273.
44. J. Peisach *et al*., *J. Biol. Chem.* 246 (1971), 5877.
45. P. M. Champion and A. J. Siever, *J. Chem. Phys.* **66** (1977), 1819; D. Coucouvanis *et al*., *J. Am. Chem Soc.* **101** (1979), 3392.
46. R. Cammack, D. S. Patil, and V. M. Fernandez, *Biochem. Soc. Trans.* **13** (1985), 572.
47. B. L. Trumpower, *Biochim. Biophys. Acta* **639** (1981), 129.
48. H. Beinert, *Biochem. Soc. Trans.* **13** (1985), 542.
49. G. Palmer, *Biochem. Soc. Trans.* **13** (1985), 548.
50. R. Malkin and A. J. Bearden, *Biochim. Biophys. Acta* **505** (1978), 147.
51. C. E. Johnson, *J. Inorg. Biochem.* **28** (1986), 207.
52. E. Münck and T. A. Kent, *Hyperfine Interactions* **27** (1986), 161.
53. K. K. Rao *et al*., *Biochem. J.* **129** (1972), 1063.
54. I. Bertini and C. Luchinat, eds., *NMR of Paramagnetic Molecules in Biological Systems*, Benjamin/ Cummings, 1986.
55. G. N. La Mar, W. D. Horrocks, Jr., and R. H. Holm, NMR *of Paramagnetic Molecules*, Academic Press, 1973.
56. M. T. Werth *et al*., *J. Am. Chem. Soc.* **109** (1987), 273.
57. T. G. Spiro *et al*., in Reference 8, p. 407. a) T. V. Long and T. M. Loehr, *J. Am. Chem. Soc.* **92** (1970), 6384.
58. G. Christou, B. Ridge, and H. N. Rydon, *J. Chem. Soc. Chem. Commun.* (1979), 20.
59. S. W. May and J.-Y. Kuo, *Biochemistry* **17** (1978), 3333.
60. S. W. May *et al*., *Biochemistry* **23** (1984), 2187.
61. P. Saint-Martin *et al*., *Proc. Natl. Acad. Sci. USA* **85** (1988), 9378.
62. R. W. Lane *et al*., *Proc. Natl. Acad. Sci. USA* **72** (1975), 2868.
63. R. W. Lane *et al*., *J. Am. Chem. Soc.* **99** (1977), 84.
64. D. G. Holah and D. Coucouvanis, *J. Am. Chem. Soc.* **97** (1975), 6917.
65. D. Coucouvanis *et al*., *J. Am. Chem. Soc.* **93** (1976), 5721.
66. M. Millar *et al*., *lnorg. Chem.* **21** (1982), 4105.
67. S. A. Koch and L. E. Madia, *J. Am. Chem. Soc.* **105** (1983), 5944.
68. M. Millar, S. A. Koch, and R. Fikar, *lnorg. Chim. Acta* **88** (1984), L15.
69. J. C. Deaton *et al*., *J. Am. Chem. Soc.* **110** (1988), 6241.
70. D. B. Knaff, *Trends Biochem. Sci.* **13** (1988), 461. a) T. Tsukihara *et al*., *J. Biochem.* **90** (1981), 1763.
71. D. R. Ort and N. E. Good, *Trends Biochem. Sci.* **13** (1988), 467.
72. V. Massey, in Reference 9, p. 301.
73. M. K. Johnson *et al*., *J. Biol. Chem.* **260** (1985), 7368.

74. J. C. Salerno *et al*., *J. Biol. Chem.* **254** (1979), 4828.
75. T. P. Singer, M. Gutman, and V. Massey, in Reference 9, p. 225.
76. H. Twilfer, F.-H. Bernhardt, and K. Gersonde, *Eur. J. Biochem.* **119** (1981), 595.
77. L. Petersson, R. Cammack, and K. Krishna Rao, *Biochim. Biophys. Acta* **622** (1980), 18.
78. B.-K. Teo and R. G. Shulman, in Reference 8, p. 343.
79. T. Tsukihara *et al*., in K. Kimura, ed., *Molecular Evolution, Protein Polymorphism and the Neutral Theory*, Japan Scientific Societies Press and Springer-Verlag, 1982, p. 299.
80. T. Tsukihara *et al*., *BioSystems* **15** (1982), 243.
81. D. Petering and G. Palmer, *Arch. Biochem. Biophys*. **141** (1970), 456.
82. J. F. Gibson *et aI*., *Proc. Natl. Acad. Sci. USA* **56** (1966), 987.
83. W. A. Eaton *et al*., *Proc. Natl. Acad. Soc. USA* **68** (1971), 3015. a) L. B. Dugad *et al*., *Biochemistry* **29** (1990), 2663.
84. J. Rawlings, O. Siiman, and H. B. Gray, *Proc. Natl. Acad. Sci. USA* **71** (1974), 125.
85. I. Salmeen and G. Palmer, *Arch. Biochem. Biophys.* **150** (1972), 767.
86. J. J. Mayerle *et al*., *Proc. Natl. Acad. Sci. USA* **70** (1973), 2429.
87. J. L. Markley *et al*., *Science* **240** (1988), 908. a) L. Banci, I. Bertini, and C. Luchinat, *Structure and Bonding* **72** (1990), 113.
88. V. K. Yachandra *et al*., *J. Am. Chem. Soc.* **105** (1983), 6462.
89. S. Hwa, R. S. Czernuszewicz, and T. G. Spiro, *J. Am. Chem. Soc*. **111** (1989), 3496.
90. S. Hwa *et al*., *J. Am. Chem. Soc.* **111** (1989), 3505.
91. J. R. Rieske, D. H. MacLennan, and R. Coleman, *Biochem. Biophys. Res. Commun*. **15** (1964), 338.
92. W. D. Bonner, Jr., and R. C. Prince, *FEBS Lett.* **177** (1984), 47.
93. J. F. Cline *et al*., *J. Biol. Chem.* **260** (1985), 3251.
94. H.-T. Tsang *et al*., *Biochemistry* **28** (1989), 7233.
95. R. C. Prince, S. J. G. Linkletter, and P. L. Dutton, *Biochem. Biophys. Acta* **635** (1981), 132.
96. J. G. Reynolds and R. H. Holm, *lnorg. Chem*. **19** (1980), 3257; **20** (1981), 1873. a) J. J. Mayerle *et al*., *J. Am. Chem. Soc*. **97** (1977), 1032. b) Y. Do, E. D. Simhon, and R. H. Holm, *lnorg. Chem.* **22** (1983), 3809. c) S. Han, R. Czernuszewicz, and T. G. Spiro, *lnorg. Chem.* **25** (1986), 2276. d) H. Strasdeit, B. Krebs, and G. Henkel, *lnorg. Chim. Acta* **89** (1989), LII.
97. P. K. Mascharak *et al*., *J. Am. Chem. Soc.* **103** (1981), 6110.
98. P. Beardwood *et al*., *J. Chem. Soc.* Dalton Trans. (1982), 2015.
99. D. Coucouvanis *et al*., *J. Am. Chem. Soc*. **106** (1984), 6081.
100. P. Beardwood and J. F. Gibson, *J. Chem. Soc. Chem. Commun.* **102** (1985), 490 and 1345.
101. L. C. Sieker, E. Adman, and L. H. Jensen, *Nature* **235** (1971), 40.
102. J. M. Berg, K. O. Hodgson, and R. H. Holm, *J. Am. Chem. Soc*. **101** (1970), 4586.
103. P. J. Stephens *et al*., *Proc. Natl. Acad. Sci. USA* **82** (1985), 5661.
104. M. W. W. Adams and L. E. Mortenson, in Reference 235a.
105. L. W. Lim *et al*., *J. Biol. Chem.* **261** (1986), 15 and 140.
106. J. C. Salerno *et al*., *Biochem. Biophys. Res. Commun.* **73** (1976), 833.
107. G. Strahs and J. Kraut, *J. Mol. Biol.* **35** (1968), 503.
108. C. W. Carter, Jr., *et al*., *Proc. Natl. Acad. Sci. USA* **69** (1972), 3526.
109. C. W. Carter, Jr., *et al*., *J. Biol. Chem*. **249** (1974), 4212.
110. K. Fukuyama, *J. Mol. Biol.* 199 (1988), 183. a) K. Fukuyama *et al*., *J. Mol. Biol.* **210** (1989), 383.
111. G. H. Stout *et al*., *Proc. Natl. Acad. Sci. USA* **85** (1988), 1020.
112. C. D. Stout, *J. Biol. Chem.* **263** (1988), 9256.
113. A. H. Robbins and C. D. Stout, *Proc. Natl. Acad. Sci. USA* **86** (1989), 3639.
114. E. T. Adman, L. C. Sieker, and L. H. Jensen, *J. Biol. Chem.* **248** (1973), 3987.
115. R. C. Prince and M. W. W. Adams, *J. Biol. Chem.* **262** (1987), 5125.
116. L. E. Mortenson, R. C. Valentine, and J. E. Carnahan, *Biochem. Biophys. Res. Commun.* **7** (1962), 448.
117. W. Lovenberg, B. B. Buchanan, and J. C. Rabinowitz, *J. Biol. Chem*. **254** (1979), 4499.
118. R. Mathews *et al*., *J. Biol. Chem.* **249** (1974), 4326.
119. A. J. Thomson, in P. M. Harrison, ed., *Metalloproteins, Part I: Metal Proteins with Redox Roles*, Verlag Chemie, 1985, pp. 79-120.

120. R. Cammack, *Biochem. Biophys. Res. Commun.* **54** (1973), 548.
121. M. J. Carney *et al.*, *Inorg. Chem.* **27** (1988), 346.
122. M. J. Carney *et al.*, *J. Am. Chem. Soc.* **110** (1988), 6084.
123. L. Noodleman, D. A. Case, and A. Aizman, *J. Am. Chem. Soc.* **110** (1988), 1001.
124. L. Noodleman, *Inorg. Chem.* 27 (1988), 3677.
125. J.-M. Moulis, J. Meyer, and M. Lutz, *Biochemistry* **23** (1984), 6605. a) W. D. Phillips and M. Poe, in Reference 10, p. 255. b) E. L. Packer *et al.*, *J. Biol. Chem.* **252** (1977), 2245. c) J. Bertini *et al.*, *Inorg. Chem.* **29** (1990), 1874. d) B.-K. Teo *et al.*, *J. Am. Chem. Soc.* **101** (1979), 5624.
126. T. Herskovitz *et al.*, *Proc. Natl. Acad. Sci. USA* **69** (1972), 2437.
127. B. A. Averill *et al.*, *J. Am. Chem. Soc.* **95** (1973), 3523.
128. J. M. Berg and R. H. Holm, in Reference 8, p. I.
129. G. B. Wang, M. A. Bobrick, and R. H. Holm, *Inorg. Chem.* **17** (1978), 578.
130. D. Coucouvanis *et al.*, *J. Am. Chem. Soc.* **104** (1982), 1874.
131. A. Müller and N. Schladerbeck, *Chimia* **39** (1985), 23.
132. A. Müller, N. Schladerbeck, and H. Bagge, *Chimia* **39** (1985), 24.
133. S. Rutchik, S. Kim, and M. A. Walters, *Inorg. Chem.* **27** (1988), 1513.
134. W. E. Cleland *et al.*, *J. Am. Chem. Soc.* **105** (1983), 6021.
135. M. G. Kanatzidis *et al.*, *J. Am. Chem. Soc.* **106** (1984), 4500.
136. M. G. Kanatzidis *et al.*, *Inorg. Chem.* **22** (1983), 179.
137. R. E. Johnson *et al.*, *J. Am. Chem. Soc.* **105** (1983), 7280.
138. M. G. Kanatzidis *et al.*, *J. Am. Chem. Soc.* **107** (1985), 4925. a) K. S. Hagen, J. G. Reynolds, and R. H. Holm, *J. Am. Chem. Soc.* **103** (1981), 4054. b) G. Christou and C. D. Gamer, *J. Chem. Soc. Dalton Trans.* (1979), 1093. c) M. J. Carney *et al.*, *Inorg. Chem.* **27** (1988), 346. d) P. Barbaro *et al.*, *J. Am. Chem. Soc.* **112** (1990), 7238.
139. E. J. Laskowski *et al.*, *J. Am. Chem. Soc.* **100** (1978), 5322.
140. E.1. Laskowski *et al.*, *J. Am. Chem. Soc.* **101** (1979), 6562.
141. T. O'Sullivan and M. Millar, *J. Am. Chem. Soc.* **107** (1985), 4096.
142. M. Millar, private communication.
143. T. D. P. Stack and R. H. Holm, *J. Am. Chem. Soc.* **110** (1989), 2484. a) T. D. P. Stack, M. J. Carney, and R. H. Holm, *J. Am. Chem. Soc.* **111** (1989), 1670. b) S. Ciurli *et al.*, *J. Am. Chem. Soc.* **112** (1990), 2654. c) P. R. Challen *et al.*, *J. Am. Chem. Soc.* **112** (1990), 2455.
144. L. Que, Jr., R. H. Holm, and L. E. Mortenson, *J. Am. Chem. Soc.* **97** (1975), 463.
145. N. R. Bastian *et al.*, in Reference 10, p. 227.
146. H. Beinert and A. J. Thomson, *Arch. Biochem. Biophys.* **222** (1983), 333.
147. M. H. Emptage *et al.*, *J. Biol. Chem.* **255** (1980), 1793.
148. W. W. Sweeney, J. C. Rabinowitz, and D. C. Yoch, *J. Biol. Chem.* **250** (1985), 7842.
149. B. A. Averill, J. R. Bal, and W. H. Orme-Johnson, *J. Am. Chem. Soc.* **100** (1978), 3034.
150. C. D. Stout, *Nature* **279** (1979), 83.
151. D. Ghosh *et al.*, *J. Biol. Chem.* **256** (1981), 4185.
152. D. Ghosh *et al.*, *J. Mol. Biol.* **158** (1982), 73.
153. M. K. Johnson *et al.*, *J. Am. Chem. Soc.* **105** (1983), 6671.
154. H. Beinert and A. J. Thomson, *Arch. Biochem. Biophys.* **222** (1983), 333.
155. M. R. Antonio *et al.*, *J. Biol. Chem.* **257** (1982), 6646.
156. E. Miinck, in Reference 8, p. 147.
157. C. E. Johnson, *J. Inorg. Biochem.* **207** (1986), 28.
158. B. H. Huynh *et al.*, *J. Biol. Chem.* **255** (1980), 3242.
159. J. J. G. Moura *et al.*, *J. Biol. Chem.* **257** (1982), 6259. a) H. Beinert and M. C. Kennedy, *Eur. J. Biochem.* **186** (1989), 1865.
160. C. R. Kissinger *et al.*, *J. Am. Chem. Soc.* **110** (1988), 8721. a) S. Ciurli and R. H. Holm, *Inorg. Chem.* **28** (1989), 1685.
161. T. A. Kent *et al.*, *J. Biol. Chem.* **260** (1985), 6871.
162. A. H. Robbins and C. D. Stout, *J. Biol. Chem.* **260** (1985), 2328.
163. M. K. Johnson *et al.*, *J. Biol. Chem.* **258** (1983), 12771.

164. M. C. Kennedy *et al.*, *J. Biol. Chem.* **258** (1983), 11098.
165. J. TeIser *et al.*, *J. Biol. Chem.* **261** (1986), 4840.
166. D. H. Flint, M. H. Emptage, and J. R. Guest, *J. Inorg. Biochem.* **36** (1989), 306. a) R. L. Switzer, *BioFactors* **2** (1989), 77.
167. H. Beinert *et al.*, *Proc. Natl. Acad. Sci. USA* **80** (1983), 393.
168. M. K. Johnson *et al.*, *J. Biol. Chem.* **256** (1981), 9806.
169. T. R. Halbert *et al.*, *J. Am. Chem. Soc.* **106** (1984),1849.
170. G. N. George and S. J. George, *Trends Biochem. Sci.* **13** (1988), 369. a) I. Moura *et al*., *J. Am. Chem. Soc.* **108** (1986), 349. b) K. K. Surerus *et al.*, *J. Am. Chem. Soc.* **109** (1987), 3805. c) R. C. Conover *et al.*, *J. Am. Chem. Soc.* **112** (1990), 4562. d) J. K. Money, J. C. Huffman, and G. Christou, *Inorg. Chem.* **27** (1988), 507.
171. B. H. Huynh *et al*., *Proc. Natl. Acad. Sci. USA* **81** (1984), 3728.
172. T. R. Hawkes and B. E. Smith, *Biochem. J.* 223 (1984), 783.
173. M. A. Whitener *et al.*, *J. Am. Chem. Soc.* **108** (1986), 5607.
174. K. S. Hagen and R. H. Holm, *J. Am. Chem. Soc.* **104** (1982), 5496.
175. K. S. Hagen, A. D. Watson, and R. H. Holm, *J. Am. Chem. Soc.* **105** (1983), 3905. a) J.-J. Girard *et al.*, *J. Am. Chem. Soc.* **106** (1984), 5941.
176. M. C. Kennedy *et al.*, *J. Biol. Chem.* 259 (1984), 14463. a) H. Strasdeit, B. Krebs, and G. Henkel, *Inorg. Chem*. **23** (1983), 1816.
177. M. G. Kanatzidis *et al.*, *J. Chem. Soc. Chem. Commun.* (1984), 356.
178. M. G. Kanatzidis, A. Salifoglou, and D. Coucouvanis, *J. Am. Chem. Soc.* **107** (1985), 3358; *Inorg. Chem*. **25** (1986), 2460.
179. S. Pohl and W. Saak, *Angew. Chem. Int. Ed. Engl.* **23** (1984), 907. a) S. A. AI-Ahmand *et al.*, *Inorg. Chem.* **29** (1990), 927.
180. F. Cecconi, C. A. Ghilardi, and S. Midolini, *J. Chem. Soc. Chem. Commun.* (1981), 640.
181. A. Agresti *et al.*, *Inorg. Chem.* **24** (1985), 689.
182. K. S. Hagen, J. M. Berg, and R. H. Holm, *Inorg. Chim. Acta* **45** (1980), L17. a) B. S. Snyder and R. H. Holm, *Inorg. Chem.* **27** (1988), 1816. b) B. S. Synder *et al.*, *Inorg. Chem.* **27** (1988), 595. c) M. S. Reynolds and R. H. Holm, *Inorg. Chem.* **27** (1988), 4494. d) B. S. Snyder and R. H. Holm, *Inorg. Chem*. **29** (1990), 274.
183. I. Noda, B. S. Snyder, and R. H. Holm, *Inorg. Chem.* **25** (1986), 3851. a) J.-F. You, B. S. Snyder, and R. H. Holm, *J. Am. Chem. Soc.* **110** (1988), 6589. b) J.-F. You *et al.*, *J. Am. Chem. Soc.* **112** (1990), 1067. c) W. R. Hagen, A. J. Pierik, and C. Veeger, *J. Chem. Soc., Faraday Trans. I* **85** (1989), 4083.
184. E. I. Stiefel *et al*., *Adv. Chem. Ser.* **162** (1977), 353. a) I. Moura and J. J. G. Moura, in Reference 5, p. 179. b) J. R. Lancaster, Jr., ed., *The Bioinorganic Chemistry of Nickel*, VCH Publishers, 1988. c) H. J. Grande *et al.*, in Reference 5, p. 193. d M. W. W. Adams, L. E. Mortenson, and J.-S. Chen, *Biochim. Biophys. Acta* **594** (1981), 105. e) J. LeGall and H. D. Peck, Jr., in Reference 5, p. 207. f) J. LeGall *et al.*, in Reference 8, p. 177. g) S. P. Ballantine and D. H. Boxer, *Eur. J. Biochem.* **156** (1986), 276. h) W. H. Onne-Johnson and N. R. Onne-Johnson, in Reference 8, p. 67.
185. B. Bowien and H. G. Schlegel, *Annu. Rev. Microbiol.* **35** (1981), 401.
186. C. R. Bowers and D. P. Weitekamp, *J. Am. Chem. Soc.* **109** (1987), 5541.
187. T. C. Eisenschmid *et al.*, *J. Am. Chem. Soc.* **109** (1987), 8089.
188. M. W. W. Adams *et al.*, *Biochimie* **68** (1986), 35.
189. R. Cammack, V. M. Fernandez, and K. Schneider, in Reference 184b, p. 167. 189a. M. W. W. Adams, *Biochem. Biophys. Acta* **1020** (1990),115.
190. H. J. Grande *et al.*, *Eur. J. Biochem.* **136** (1983), 201.
191. M. W. W. Adams and L. E. Mortenson, *J. Biol. Chem.* **259** (1984), 7045.
192. S. W. Ragsdale and L. G. L. Ljungdahl, *Arch. Microbial*. **139** (1984), 361.
193. C. R. Woese, *Microbial. Rev.* **81** (1987), 221.
194. M. W. W. Adams, E. Eccleston, and J. B. Howard, *Proc. Natl. Acad. Sci. USA* **86** (1989), 4932.
195. D. S. Patil *et al*., *J. Am. Chem. Soc.* **110** (1988), 8533.
196. A. T. Kowal, M. W. W. Adams, and M. K. Johnson, *J. Biol. Chem.* **264** (1989), 4342.
197. W. R. Hagen *et al.*, *FEBS Lett.* **203** (1986), 59.
198. I. C. Zambrano *et al.*, *J. Biol. Chem.* **264** (1989), 20974.
199. M. W. W. Adams, *J. Biol. Chem.* **262** (1987), 15054.
200. T. V. Morgan, R. C. Prince, and L. E. Mortenson, *FEBS Lett*. **206** (1986), 4.

201. W. R. Hagen *et al.*, *FEBS Lett.* **201** (1986), 158.
202. F. M. Rusnak *et al.*, *J. Biol. Chem.* **262** (1987), 38.
203. G. Wang *et al.*, *J. Biol. Chem.* **259** (1984), 14328.
204. J. Telser *et al.*, *J. Biol. Chem.* **262** (1987), 6589.
205. J. Telser *et al.*, *J. Biol. Chem.* **261** (1986), 15536.
206. H. Thomann, M. Bernardo, and M. W. W. Adams, *J. Am. Chem. Soc.* **113** (1991), 7044.
207. A. J. Thomson *et al.*, *Biochem. J.* **227** (1985), 333.
208. K. A. Macor *et al.*, *J. Biol. Chem.* **282** (1987), 9945.
209. G. N. George *et al.*, *Biochem. J.* **259** (1989), 597.
210. R. Cammack, *Adv. Inorg. Chem.* **32** (1988), 297.
211. J. J. G. Moura *et al.*, in Reference 5, p. 191.
212. J. R. Lancaster, *FEBS Lett.* **115** (1980), 285.
213. M. Teixeira *et al.*, *J. Biol. Chem.* **260** (1985), 8942.
214. J. W. Van der Zwaan *et al.*, *FEBS Lett.* **179** (1985), 271.
215. M. K. Eidsness, R. J. Sullivan, and R. A. Scott, in Reference 184b, p. 73.
216. M. K. Eidsness *et al.*, *Proc. Natl. Acad. Sci. USA* **86** (1989), 147.
217. P. A. Lindahl *et al.*, *J. Am. Chem. Soc.* **106** (1984), 3062.
218. R. A. Scott *et al.*, *J. Am. Chem. Soc.* **106** (1984), 6864.
219. S. P. J. Albracht *et al.*, *Biochim. Biophys. Acta* **874** (1986), 116.
220. A. Chapman *et al.*, *FEBS Lett.* **242** (1988), 134.
221. S. L. Tau *et al.*, *J. Am. Chem. Soc.* **106** (1984), 3064.
222. G. J. Kubas *et al.*, *J. Am. Chem. Soc.* **106** (1984), 451.
223. G. J. Kubas and R. R. Ryan, *Polyhedron* **5** (1986), 473.
224. G. J. Kubas *et al.*, *J. Am. Chem. Soc.* **108** (1986), 7000.
225. M. Rakowski DuBois *et al.*, *J. Am. Chem. Soc.* **102** (1980), 7456.
226. C. Bianchini *et al.*, *Inorg. Chem.* **25** (1986), 4617.
227. W. Tremel *et al.*, *Inorg. Chem.* **27** (1988), 3886.
228. W. Tremel and G. Henkel, *Inorg. Chem.* **27** (1988), 3896.
229. I. Dance, *Polyhedron* **5** (1986), 1037; P. J. Blower and J. R. Dilworth, *Coord. Chem. Rev.* **76** (1987), 121.
230. C. L. Coyle and E. I. Stiefel, in Reference 184b, p. 1.
231. M. Kumar *et al.*, *J. Am Chem. Soc.* **111** (1989), 5974.
232. M. Kumar *et al.*, *J. Am. Chem. Soc.* **111** (1989), 8323.
233. T. H. Blackburn, in W. E. Krumbein, ed., *Microbial Geochemistry*, Blackwell Scientific, 1983, p. 63.
234. J. R. Postgate, *Fundamentals of Nitrogen Fixation*, Cambridge University Press, 1982.
235. R. W. F. Hardy, *Treatise on Dinitrogen Fixation*, Wiley, 1979, Section I. a) T. G. Spiro, ed., *Molybdenum Enzymes*, Wiley-Interscience, 1985.
236. W. J. Brill, *NATO Adv. Sci. Inst., Ser. A* **63** (1983), 231.
237. R. Haselkorn, *Annu. Rev. Microbial.* **40** (1986), 525.
238. A. C. Robinson, D. R. Dean, and B. K. Burgess, *J. Biol. Chem.* **262** (1987), 14327.
239. P. J. Stephens, in Reference 235a, p. 117.
240. A. H. Gibson and W. E. Newton, eds., Current *Perspectives in Nitrogen Fixation*, Australian Academy of Science, 1981.
241. E. I. Stiefel, in W. E. Newton and C. Rodriquez-Barrucco, eds., in *Recent Progress in Nitrogen Fixation*, Academic Press, 1977, p. 69.
242. C. Veeger and W. E. Newton, eds., *Advances in Nitrogen Fixation Research*, Nijhoff/Junk, 1984.
243. H. J. Evans, P. J. Bottomley, and W. E. Newton, eds., *Nitrogen Fixation Research Progress*, Martinus Nijhoff, 1985. a) A. Braaksma *et al.*, in Reference 5, p. 223. b) B. H. Huynh, E. Münck, and W. H. Orme-Johnson, in Reference 5, p. 241.
244. E. I. Stiefel, in Reference 240, p. 55.
245. R. V. Hageman and R. H. Burris, *Proc. Natl. Acad. Sci. USA* **75** (1978), 2699.
246. V. Sundaresan and F. M. Ausubel, *J. Biol. Chem.* **256** (1981), 2808. a) R. P. Hausinger and J. B. Howard, *J. Biol. Chem.* **258** (1983), 13486. b) M. M. Georgiadis, P. Chakrabarti, and D. C. Rees, *SSRL Annual Report* (1989), p. 94.

247. L. E. Mortenson, M. N. Walker, and G. A. Walker, in W. E. Newton and C. J. Nyman, eds., *Proceedings of the First International Conference on Nitrogen Fixation*, Washington State University Press (1976), p. 117.
248. W. H. Orme-Johnson et al., in W. E. Newton, J. R. Postgate, and C. Rodriguez Barrucco, eds., *Recent Developments in Nitrogen Fixation*, Academic Press, 1977, p. 131.
249. G. D. Watt and J. W. McDonald, *Biochemistry* **24** (1985), 7226.
250. W. R. Hagen *et al.*, *FEBS Lett.* **189** (1986), 250.
251. L. Noodleman *et al.*, *J. Am. Chem. Soc.* **107** (1985), 3418.
252. G. D. Watt, Z.-C. Wang, and R. R. Knotts, *Biochemistry* **25** (1986),8156; J. Cordewener *et al.*, *Eur. J. Biochem.* **148** (1985), 499.
253. L. E. Mortenson and R. N. F. Thorneley, *Annu. Rev. Biochem.* **48** (1979), 387.
254. A. V. Kulikov *et al.*, *Dokl. Akad. Nauk SSR* **262** (1981), 1177.
255. R. N. F. Thorneley and D. J. Lowe, in Reference 235, p. 221. a) F. A. Schultz, S. F. Gheller, and W. E. Newton, Proc. *Int. Symp. Redox Mech. Interfacial Prop. Mol. Biol. Importance* **3** (1988), 203.
256. B. K. Burgess and W. E. Newton, in A. Müller and W. E. Newton, eds., *Nitrogen Fixation: The Chemical-Biochemical-Genetic Interface*, Plenum, 1983, p. 83.
257. E. I. Stiefel and S. P. Cramer, in Reference 235, p. 88.
258. V. Shah and W. J. Brill, *Proc. Natl. Acad. Sci. USA* **74** (1977), 3249.
259. S. D. Conradson *et al.*, *J. Am. Chem. Soc.* **109** (1987), 7507. a) P. A. McLean *et al.*, *Biochemistry* **28** (1989), 9402. b) D. A. Wink *et al.*, *Biochemistry* **28** (1989), 9407.
260. M. A. Walters, S. K. Chapman, and W. H. Orme-Johnson, *Polyhedron* **5** (1986), 561.
261. P. A. McLean and R. A. Dixon, *Nature* **292** (1981), 655.
262. P. A. McLean and B. E. Smith, *Biochem. J.* **211** (1983), 589.
263. T. R. Hawkes, P. A. McLean, and B. E. Smith, *Biochem. J.* **217** (1984), 317.
264. T. R. Hoover *et al.*, *Biochemistry* **27** (1988), 3647.
265. T. R. Hoover *et al.*, *Biochemistry* **28** (1989), 2768. a) J. Liang *et al.*, *Biochemistry* **29** (1990), 8377. b) M. S. Madden *et al.*, *Proc. Natl. Acad. Sci. USA* **87** (1990), 6517.
266. A. C. Robinson, D. Dean, and B. K. Burgess, *J. Biol. Chem.* **262** (1989), 14327. a) A. C. Robinson *et al.*, *J. Biol. Chem.* **264** (1989), 10088. b) D. J. Scott *et al.*, *Nature* **343** (1990), 188. c) H. M. Kent *et al.*, *Biochem. J.* **264** (1989), 257.
267. W. R. Hagen *et al.*, *Eur. J. Biochem*. **169** (1987), 457.
268. P. A. McLean *et al.*, *J. Biol. Chem.* **262** (1987), 12900.
269. P. A. Lindahl *et al.*, *J. Biol. Chem.* **263** (1988), 19442.
270. G. D. Watt, A. Burns, and D. L. Tennent, *Biochemistry* **20** (1981), 7272; G. D. Watt and Z. C. Wang, *Biochemistry* **25** (1986), 5196.
271. R. Zimmermann *et al.*, *Biochim. Biophys. Acta.* **537** (1978), 185.
272. D. M. Kurtz *et al.*, *Proc. Natl. Acad. Sci. USA* **76** (1979), 4986.
273. R. A. Venters *et al.*, *J. Am. Chem. Soc*. **108** (1986), 3487. a) J. Bolin, in P. M. Gresshoff, L. E. Roth, G. Stacey, and W. E. Newton, eds., *Nitrogen Fixation: Achievements and Objectives*, Chapman and Hall, 1990, p. 111.
274. B. M. Hoffman, J. E. Roberts, and W. H. Orme-Johnson, *J. Am. Chern. Soc.* **104** (1982), 860.
275. A. E. True *et al.*, *J. Am. Chem. Soc.* **110** (1988), 1935. a) A. E. True *et al.*, *J. Am. Chem. Soc.* **112** (1990), 651.
276. G. N. George *et aI.*, *Biochem. J.* **262** (1989), 349.
277. W. B. Mims and J. Peisach, in R. G. Shulman, ed., *Biological Applications of Magnetic Resonance*, Academic Press, 1980, p. 221.
278. W. H. Orme-Johnson *et al.*, in Reference 8, p. 79.
279. H. Thomann *et al.*, *J. Am. Chem. Soc.* **109** (1987), 7913.
280. H. Thomann *et al.*, *Proc. Natl. Acad. Sci. USA*, **88** (1991), 6620.
281. B. H. Huynh, E. Munck, and W. H. Orme-Johnson, *Biochim. Biophys. Acta* **527** (1979), 192.
282. B. H. Huynh *et aI.*, *Biochim. Biophys. Acta* **623** (1980), 124.
283. E. Münck *et al.*, *Biochim. Biophys. Acta* **400** (1975), 32. a) W. E. Newton *et al.*, *Biochem. Biophys. Res. Commun*. **162** (1989), 882.
284. S. D. Conradson, B. K. Burgess, and R. H. Holm, *J. Biol. Chem*. **263** (1988), 13743.

285. W. R. Dunham *et aI*., *Eur. J. Biochem.* **146** (1985), 497.
286. S. P. Cramer *et al*., *J. Am. Chem. Soc*. **100** (1978), 3398.
287. M. K. Eidsness *et al*., *J. Am. Chem. Soc*. **108** (1986), 2746.
288. S. D. Conradson *et aI*., *J. Am. Chem. Soc.* **107** (1985), 7935; Reference 259.
289. B. Hedman *et al*., *J. Am. Chem. Soc*. **110** (1988), 3798.
290. M. R. Antonio *et al*., *J. Am. Chem. Soc.* **104** (1982), 4703.
291. J. M. Arber *et al*., *Biochem. J.* **252** (1988), 421.
292. M. S. Weininger and L. E. Mortenson, *Proc. Natl. Acad. Sci. USA* **79** (1982), 378.
293. N. I. Sosfenov *et al*., *Dokl. Akad. Nauk. SSSR* **291** (1986), 1123.
294. T. Yamane *et al*., *J. Biol. Chem.* **257** (1982), 1221.
295. A. M. Flank *et aI*., *J. Am. Chem. Soc.* **108** (1986), 1049.
296. J. F. Rubinson *et aI*., *Biochemistry* **24** (1985), 273.
297. E. I. Stiefel, *Proc. Natl. Acad. Sci. USA* **70** (1973), 988.
298. K. L. Hadfield and W. A. Bulen, *Biochemistry* **8** (1969), 5103.
299. F. B. Simpson and R. Burris, *Science* **224** (1984), 1095.
300. B. K. Burgess *et al*., *Biochemistry* **20** (1981), 5140.
301. S. Wherland *et aI*., *Biochemistry* **20** (1981), 5132.
302. J. H. Guth and R. H. Burris, *Biochemistry* **22** (1983), 5111.
303. Z.-c. Wang and G. D. Watt, *Proc. Natl. Acad. Sci. USA* **81** (1984), 376.
304. B. E. Smith *et al*., *Phil. Trans. Roy. Soc. London* **B317** (1987), 131.
305. R. N. F. Thorneley, R. R. Eady, and D. J. Lowe, *Nature* **272** (1978), 557.
306. S. Wherland *et al*., *Biochemistry* **20** (1981), 5132.
307. B. K. Burgess *et al*., *Biochemistry* **20** (1981), 5140.
308. H. Bortels, *Arch. Mikrobiol*. **1** (1930), 333.
309. R. C. Bray, *Quart. Rev. Biophys*. **21** (1988), 299.
310. H. Bortels, *Zentbl. Bakt. Parasiten Abt. II* **95** (1935), 193.
311. C. E. McKenna, J. R. Benemann, and T. G. Traylor, *Biochem. Biophys. Res. Commun.* **41** (1970), 1501.
312. R. C. Burns, W. H. Fuchsman, and R. W. F. Hardy, *Biochem. Biophys. Res. Commun.* **42** (1971), 353.
313. J. R. Benemann *et al*., *Biochim. Biophys. Acta* **264** (1972), 25.
314. P. E. Bishop, D. M. L. Jarlenski, and D. R. Hetherington, *Proc. Natl. Acad. Sci. USA* **77** (1980), 7342.
315. P. E. Bishop *et al*., *Science* **232** (1986), 92.
316. B. J. Hales, D. J. Langosch, and E. E. Case, *J. Biol. Chem.* **261** (1986), 15301.
317. B. J. Hales *et al*., *Biochemistry* **26** (1987), 1795.
318. J. Morningstar *et al*., *Biochemistry* **26** (1987), 1795.
319. R. L. Robson *et al*., *Nature* **322** (1986), 388.
320. R. R. Eady *et al*., *Biochem. J.* **244** (1987), 197.
321. M. J. Dilworth *et al*., *Nature* **327** (1987), 167.
322. R. N. Pau, *Trends Biochem. Res.* **14** (1989), 186; P. E. Bishop and R. D. Joerger, *Annu. Rev. Plant Physiol. Plant Mol. Biol*. **41** (1990), 109.
323. J. E. Morningstar and B. J. Hales, *J. Am. Chem. Soc.* **109** (1987), 6854.
324. J. M. Arber *et al*., *Nature* **372** (1987), 325.
325. G. N. George *et al*., *J: Am. Chem. Soc.* **110** (1988), 4057.
326. R. R. Eady *et al*., *Recueil des Travaus Chim. des Pays-Bas* **106** (1987), 175.
327. M. J. Carney *et al*., *J. Am. Chem. Soc.* **108** (1986), 3519.
328. R. H. Holm, *Chem. Soc. Rev.* (1981), 455.
329. G. Christou and C. D. Gamer, *J. Chem. Soc. Dalton Trans.* (1980), 2354.
330. C. D. Gamer *et al*., *Phil. Trans. Roy. Soc. Land.* **A308** (1982), 159. a). R. H. Holm and E. D. Simhon, in Reference 235a, p. 1.
331. W. H. Armstrong, P. K. Mascharak, and R. H. Holm, *Inorg. Chem.* **21** (1982),1699.
332. R. E. Palermo and R. H. Holm, *J. Am. Chem. Soc.* **105** (1983), 4310. a) D. Coucouvanis, E. D. Simhon, and N. C. Baenziger, *J. Am. Chem. Soc.* **102** (1980), 6644. b) G. D. Friesen *et al*., *Inorg. Chem.* **22** (1983), 2203. c) P. Stremple, N. C. Baenziger, and D.

Coucouvanis, *J. Am. Chem. Soc.* **103** (1981), 4601. d) D. Coucouvanis *et al.*, *J. Am. Chem. Soc.* **102** (1980), 1732. e) A. Müller *et al.*, *Inorg. Chim. Acta* **148** (1988), 11. f) A. Müller *et al.*, *Angew. Chem. Int. Ed. Engl.* **21** (1982), 860. g) D. Coucouvanis *et al.*, *Inorg. Chem.* **27** (1988), 4066. h) P. A. Eldridge *et al.*, *J. Am. Chem. Soc.* **110** (1988), 5573. i) K. S. Bose *et al.*, *J. Am. Chem. Soc.* **111** (1989), 8953. j) J. A. Kovacs, J. K. Bashkin, and R. H. Holm, *Polyhedron* **6** (1987), 1445.

333. R. D. Sanner *et al.*, *J. Am. Chem. Soc.* **98** (1972), 8351. a) M. B. O'Regan *et al.*, *J. Am. Chem. Soc.* **112** (1990), 4331.
334. G. Pez, P. Apgar, and R. K. Crissey, *J. Am. Chem. Soc.* **104** (1982), 462.
335. K. Jones *et al.*, *J. Am. Chem. Soc.* **98** (1976), 74.
336. G. J. Leigh, *J. Mol. Catal.* **47** (1988), 363.
337. R. A. Henderson, G. J. Leigh, and C. J. Pickett, *Adv. Inorg. Chem. Radiochem.* **27** (1984), 198. a) M. Hidai and Y. Mizobe, in P. S. Braterman, ed., *Reactions of Coordinated Ligands*, Plenum, **2** (1989),53. b) T. Yoshida *et al.*, *J. Am. Chem. Soc.* **110** (1988), 4872. c) T. Yoshida, T. Adachi, and T. Ueda, *Pure Appl. Chem.* **62** (1990), 1127.
338. D. Sellmann *et al.*, *Angew. Chem. Int. Ed. Engl.* **28** (1989), 1271.
339. A. E. Shilov, in M. Gratzel, ed., *Energy Resources through Chemistry and Catalysis*, Academic Press, 1983, p. 533.
340. W. E. Newton *et al.*, *Inorg. Chem.* **19** (1980), 1997.
341. T. R. Halbert, W.-H. Pan, and E. I. Stiefel, *J. Am. Chem. Soc.* **105** (1983), 5476.
342. M. Rakowski DuBois *et al.*, *J. Am. Chem. Soc.* **101** (1979), 5245.
343. R. H. Crabtree, *Inorg. Chim. Acta* **125** (1986), 27.
344. W. B. Mims and J. Peisach, in J. Berliner and J. Reuben, eds., *Biological Magnetic Resonance*, Plenum, **3** (1981), 213.
345. T. Yamane *et al.*, *J. Biol. Chem.* **257** (1982), 1221.
346. D. C. Rees and J. B. Howard, *J. Biol. Chem.* **2587** (1983), 12733.
347. R. B. Frankel *et al.*, *J. de Physique* **37** (1976), C6.
348. C. E. Johnson, *J. Appl. Phys.* **42** (1971), 1325.
349. P. Middleton *et al.*, *Eur. J. Biochem.* **88** (1978), 135.
350. K. Tagawa and D. I. Amon, *Biochim. Biophys. Acta* **153** (1968), 602.
351. G. Palmer, R. H. Sands, and L. E. Mortenson, *Biochim. Biophys. Acta* **23** (1966), 357.
352. R. H. Sands and W. R. Dunham, *Quart. Rev. Biophys.* **4** (1975), 443.
353. R. Cammack, in M. J. Allen and P. N. R. Usherwood, eds., *Charge and Field Effects in Biosystems*, Abacus Press, 1984, p. 41.
354. J. Cardenas, L. E. Mortenson, and D. C. Yoch, *Biochim. Biophys. Acta* **434** (1976), 244.
355. R. Cammack, M. J. Barber, and R. C. Bray, *Biochem. J.* **157** (1976), 469.
356. R. C. Bray, in *The Enzymes*, 3d ed., **12** (1975), 299.
357. J. A. Fee *et al.*, *J. Biol. Chem.* **259** (1984), 124.
358. R. N. Mullinger *et al.*, *Biochem. J.* **151** (1975), 75.
359. R. Cammack *et al.*, *Biochim. Biophys. Acta* **490** (1977), 311.
360. F. A. Armstrong *et al.*, *FEBS Lett.* **234** (1988), 107.
361. W. R. Hagen *et al.*, *Biochim. Biophys. Acta* **828** (1985), 369.
362. E. deGryse, N. Glandsdorff, and A. Piérard, *Arch. Microbiol.* **117** (1978), 189.
363. V. M. Fernandez, E. C. Hatchikian, and R. Cammack, *Biochim. Biophys. Acta* **832** (1985), 69.
364. V. Niviére, *Biochem. Biophys. Res. Commun.* **139** (1986), 658.
365. M. Teixeira *et al.*, *Biochimie* **68** (1986), 75.
366. D. J. Lowe, B. E. Smith, and R. R. Eady, in N. S. Subba Rao, ed., *Recent Advances in Biological Nitrogen Fixation*, Arnold, 1980, p. 34.
367. R. C. Bums, R. D. Holsten, and R. W. F. Hardy, *Biochem. Biophys. Res. Commun.* **39** (1970), 90.
368. M. G. Yates and K. Planque, *Eur. J. Biochem.* **60** (1975), 467.
369. T. C. Huang, W. G. Zumft, and L. E. Mortenson, *J. Bact.* **113** (1973), 884.
370. P. C. Hallenback, P. J. Kostel, and J. R. Benemann, *Eur. J. Biochem.* **98** (1979), 275.
371. S. Norlund, U. Erikson, and H. Baltscheffsky, *Biochim. Biophys. Acta* **504** (1978), 248.
372. B. K. Burgess *et al.*, in Reference 242.
373. S. D. Conradson *et aI.*, *J. Am. Chem. Soc.* **109** (1987), 7507.
374. S. A. Vaughn and B. K. Burgess, *Biochemistry* **28** (1989), 419.
375. R. W. Miller and R. R. Eady, *Biochim. Biophys. Acta* **952** (1988), 290.

376. B. K. Burgess, in Reference 235a, p. 161.
377. B. J. Hales *et al.*, *Biochemistry* **25** (1986), 7251.
378. M. M. Georgiadis *et al.*, *Science* **257** (1992), 1653.
379. J. T. Bolin *et al.*, in P. M. Greshoff et al., eds., *Nitrogen Fixation: Achievements and Objectives*, Chapman and Hall, 1990, p. 117.
380. J. Kim and D. C. Rees, *Science* **257** (1992), 1677.
381. J. Kim and D. C. Rees, *Nature* **360** (1992), 553.
382. For allowing us to see and quote their work prior to publication, we are grateful to Prof. M. W. W. Adams, Prof. B. K. Burgess, Dr. R. Cammack, Prof. D. Coucouvanis, Prof. S. P. Cramer, Dr. S. J. George, Prof. J. N. Enemark, Prof. J. Lancaster, Dr. Michelle Millar, Prof. M. Maroney, Prof. W. E. Newton, Prof. D. C. Rees, Prof. Dieter Sellman, Prof. A. E. Shilov, Dr. Barry E. Smith, Dr. R. N. F. Thorneley, and Prof. G. D. Watt. We thank Pat Deuel for her superb efforts under difficult circumstances in the preparation of this manuscript.

Contributors and Attributions

- Edward I. Stiefel (Exxon Research and Engineering Company)
- Graham N. George (Exxon Research and Engineering Company)

7.4: Ferrodoxins, Hydrogenases, and Nitrogenases - Metal-Sulfide Proteins is shared under a not declared license and was authored, remixed, and/or curated by LibreTexts.

7.4.1: Iron-sulfur Proteins and Models

Iron sulfide proteins involved in electron transfer are called *ferredoxins* and *rubredoxins*.* The ferredoxins were discovered first, and were originally classified as bacterial (containing Fe_4S_4 clusters) and plant (containing Fe_2S_2 clusters) ferredoxins. This classification is now recognized as being not generally useful, since both Fe_2S_2 and Fe_4S_4 ferredoxins are found in plants,[14,15] animals,[2,6,16] and bacteria.[4] Ferredoxins are distinguished from rubredoxins by their possession of acid-labile sulfide; i.e., an inorganic S^{2-} ion that forms H_2S gas upon denaturation at low pH. Rubredoxins have no acid-labile sulfide, and generally have a single iron in a more or less isolated site. Despite their lack of acid-labile sulfide, rubredoxins are included in this chapter because they have sequences much like those of the ferredoxins, and because their simple mononuclear Fe^{2+} and Fe^{3+} sites provide convenient illustrations of key structural and spectroscopic features.

In most ferredoxins, and in all rubredoxins, the protein ligands are cysteines, which provide four thiolate donors to the 1Fe, 2Fe, or 4Fe center. Additionally, the existence of 3Fe centers and of Fe-S sites that contain a second metal (i.e., heteronuclear clusters) make the Fe-S class a broad and multifunctional one.

Simple cytochromes and simple iron-sulfide proteins are similar, in that both can undergo one-electron transfer processes that are generally uncoupled from proton-, atom-, or group-transfer processes. Some of these proteins, such as cytochrome c_3 from *Desulfovibrio* with four hemes[17] or ferredoxin from *Clostridium pasteurianum* with two Fe_4S_4 centers,[6] can transfer more than one electron, because they have multiple copies of a one-electron transfer group. The cytochromes were discovered in 1886 by McMunn,[18] and their role in metabolism was discovered in the 1920s by Keilin (Chapter 6). The intense optical absorbance of these heme-containing proteins contributed singularly to their discovery and biochemical characterization. In contrast, the iron-sulfur proteins, although red to red-brown, absorb far more weakly in the visible region than do the cytochromes. Their presence is sometimes obscured by the cytochromes, and their frequent air instability made their initial recognition and isolation more difficult. It was not until the early 1960s that discoveries by several research groups[19] led to the isolation, recognition, and characterization of the ferredoxins. The use of EPR spectroscopy and its application to biological systems had a profoundly stimulating effect on the field (see below).

Although cytochromes were discovered first, the ferredoxins are likely to be the older proteins from an evolutionary perspective.[20] Ferredoxins have relatively low-molecular-weight polypeptide chains, require no organic prosthetic group, and often lack the more complex amino acids. In fact, the amino-acid composition in clostridial ferredoxin is close to that found in certain meteorites.[21]

The various Fe-S sites found in electron-transfer proteins (ferredoxins) are also found in many enzymes,[6,11,22.23] where these centers are involved in intraor interprotein electron transfer. For example, sulfite reductase contains a siroheme and an Fe_4S_4 center,[24] which are strongly coupled and involved in the sixelectron reduction of SO_3^{2-} to H_2S. Xanthine oxidase (see Figure 7.1) has two identical subunits, each containing two different Fe_2S_2 sites plus molybdenum and FAD sites. In xanthine oxidase, the Mo(VI) site carries out the two-electron oxidation of xanthine to uric acid, being reduced to Mo(IV) in the process.[25] The Mo(VI) site is regenerated by transferring electrons, one at a time, to the Fe_2S_2 and flavin sites, thereby readying the Mo site for the next equivalent of xanthine. Although the Fe_2S_2 sites do not directly participate in substrate reactions, they are essential to the overall functioning of the enzyme system. The Fe_2S_2 centers in xanthine oxidase play the same simple electron-transfer role as the Fe_2S_2 ferredoxins play in photosynthesis.

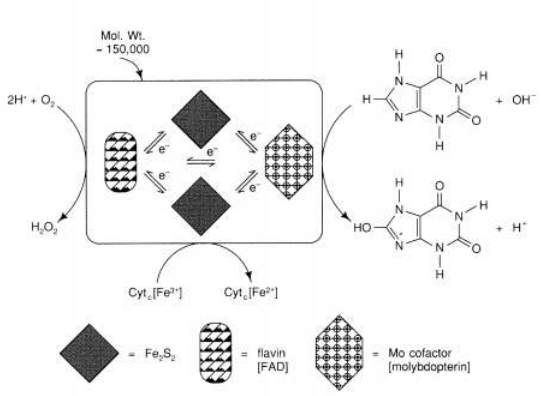


Figure 7.1 - A schematic drawing of xanthine oxidase illustrating the Mo, flavin, and Fe_2S_2 sites and interaction of the enzyme with substrate and oxidant(s).

Structurally, all the iron-sulfur sites characterized to date are built up of (approximately) tetrahedral iron units (see Figure 7.2). In rubredoxins the single iron atom is bound in tetrahedral coordination by four thiolate ligands provided by cysteine side chains. In two-iron ferredoxins the Fe_2S_2 site consists of two tetrahedra doubly bridged through a pair of sulfide ions, i.e., $Fe_2(\mu_2\text{-}S)_2$, with the tetrahedral coordination of each Fe completed by two cysteine thiolates. In four-iron or eight-iron ferredoxins, the 'thiocubane' Fe_4S_4 cluster consists of four tetrahedra sharing edges with triply bridging S^{2-} ions, i.e., $Fe_4(\mu_3\text{-}S)_4$, with each Fe completing its tetrahedron by binding to a single cysteine thiolate. Finally, for Fe_3S_4 clusters, which are now being found in more and more proteins, the well-established structure has one triply bridging and three doubly bridging sulfide ions, $Fe_3(\mu_3\text{-}S)(\mu_2S)_3$. The Fe_3S_4 unit can be thought of as derived from the 'thiocubane' Fe_4S_4 unit by the removal of a single iron atom.

In what follows we will introduce these structures in the order 1Fe, 2Fe, 4Fe, and 3Fe. For each, we will first discuss the physiological role(s) of the particular proteins, then the structural features, followed by the spectroscopic properties and model systems.

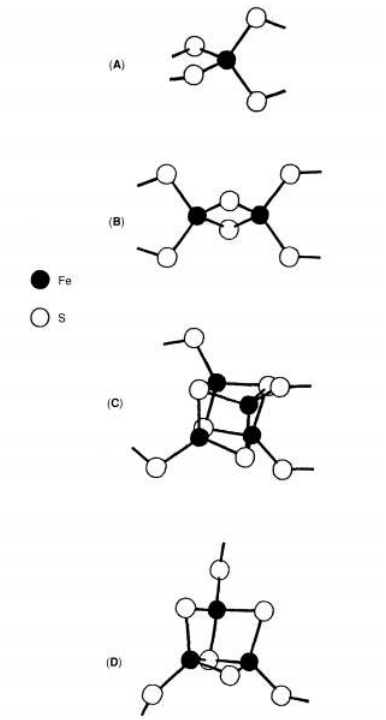


Figure 7.2 - Structural systematics of Fe-S units found in proteins: (A) rubredoxin single Fe center; (B) Fe_2S_2 unit; (C) Fe_4S_4 unit; (d) Fe_3S_4 unit.

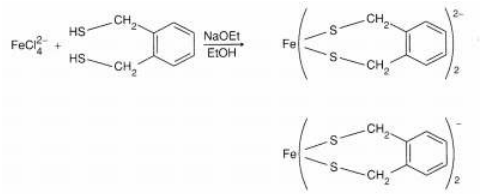
* For review articles, see References 1-11. For a discussion of nomenclature, see References 12 and 13.

7.4.1: Iron-sulfur Proteins and Models is shared under a not declared license and was authored, remixed, and/or curated by LibreTexts.

7.4.2: Iron-sulfur Proteins and Models (Part 2)

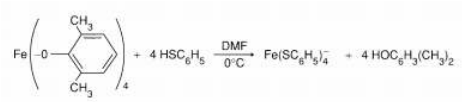
Rubredoxin Model Systems

The simple mononuclear tetrahedral site of Rd has been chemically modeled in both its reduced and its oxidized forms. The bidentate o-xylyl-α,α'-dithiolate ligand forms bis complexes of Fe(II) and Fe(III) that have spectroscopic features quite similar to those of the protein.[62,63] The preparative procedure is relatively straightforward (Equation 7.1).



The UV-visible-NIR spectra, Mössbauer spectra, and magnetic susceptibility differ only slightly from those of oxidized and reduced rubredoxins.

The monodentate benzenethiolate (thiophenolate) ligand, $C_6H_5S^-$, similarly forms the ferrous $Fe(SC_6H_5)_4^{2-}$ complex.[64,65] Although for some time it was felt that the oxidized form, $Fe(SC_6H_5)_4^-$, was inherently unstable, the sterically hindered monothiolate ligand 2,3,5,6-tetramethylbenzenethiolate was found to form[66-68] a stable, quite symmetric Fe(III) tetrathiolate anion. Armed with this information, the preparation of the tetrakis(benzenethiolate) Fe(III) complex was reinvestigated, and the complex successfully synthesized[67] (Equation 7.2).



The Fe(III) and Fe(II) tetrathiolate species now serve as excellent structural models for the Fe sites of both oxidized and reduced Rd.[69]

The structural parameters for the oxidized rubredoxin analogues are very similar to those of the oxidized Rd iron site. The reduced complexes reveal a lengthening of the average Fe-S bond from 2.27 to 2.36 Å, consistent with the change in oxidation state from ferric to ferrous. The addition of an electron has a more profound structural effect in this single-iron center than in some of the multiiron clusters, where electrons are more delocalized.

Clearly, for the single-Fe sites, the dominant structural feature is their near-tetrahedral tetrathiolate coordination. The dominant electronic structural feature is the presence of high-spin Fe^{3+} and Fe^{2+} sites. The important mode of chemical reactivity is a simple one-electron transfer. Each of these features carries over to the 2Fe, 4Fe, and 3Fe sites discussed below.

Fe_2S_2 Ferredoxins

The simple 2Fe-2S proteins are sometimes referred to as "plant" or "plant-type" ferredoxins. The protein from spinach, which serves as an electron acceptor in the photosynthetic apparatus,[14,15,50,70] was among the first to be wellcharacterized and widely studied, and could be considered the prototypical 2Fe-2S ferredoxin, However, 2Fe-2S proteins are also well-known in bacteria.[4] The protein from the cyanobacterium (blue-green alga) *Spirulina platensis* has been structurally elucidated by x-ray crystallography.[47] Putidaredoxin, from *Pseudomonas putida*, which serves as a donor to the P-450 camphor monooxygenase system, has been extensively studied.[28] Fe_2S_2 centers are also well-established in mammalian proteins. Adrenodoxin[29] serves as the electron donor to the P-450 monooxygenase system that carries out the 11-β-hydroxylation of steroids, The so-called "Rieske proteins" are found in the bc_1 complex of mitochondria[47] as well as in the bd complex of the photosynthetic apparatus of plants.[71] In addition, Fe_2S_2 centers are well-known constituents of such redox proteins as xanthine oxidase,[25,72] CO oxidase,[25] succinate dehydrogenase,[73-75] and putidamonooxin.[76] Table 7.1 lists some of the Fe_2S_2 proteins and their properties.

The x-ray crystal structure of only the single 2Fe-2S protein mentioned above has been determined;[70a] the 2Fe-2S ferredoxin from the blue-green alga Spirulina platensis[6,22,47,77,78] shows significant sequence identity with chloroplast ferredoxins typical of higher plants.[79,80] As Figure 7.8 shows, the Fe_2S_2 unit in this 11-kDa protein is bound by Cys-41, Cys-46, Cys-49, and Cys-79, The

binuclear iron cluster is found in a largely hydrophobic region of the protein, but is within 5 Å of the protein surface.[6] The sulfur atoms of the cluster, both inorganic and cysteinyl, are hydrogen-bonded to six peptide NH groups and one serine OH group, which presumably stabilize the cluster/protein complex, The serine involved in the H-bonding, Ser-40, is conserved in all plant and algal 2Fe-2S ferredoxins sequenced, which implies that it plays a crucial structural or functional role.

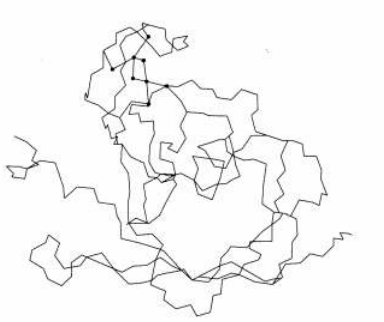


Figure 7.8 - The x-ray crystal structure of the Fe_2S_2 ferredoxin from Spirulina platensis.[70a]

The structure of the 2Fe-2S core in Figure 7.2 reveals a tetrahedron of S ligands surrounding each Fe atom. The two tetrahedra share an edge defined by the two bridging sulfide ions, and the core structure is designated $Fe_2(\mu_2\text{-}S)_2$. Fe-S distances and angles cannot be measured accurately in the structure at the present 2.5-Å resolution;[70a] so we will later discuss these details in terms of model compounds.

The Fe_2S_2 center shows nicely how spectroscopy can be used to deduce the structure of an active site. Indeed, in this case the now well-established active-site structure was deduced by a combination of chemical, spectroscopic, and magnetic methods, and the site was successfully modeled long before the first protein crystallographic study was reported. The presence of acid-labile, inorganic sulfide is a key feature of both the Fe_2S_2 and the Fe_4S_4 centers. The 1:1 stoichiometry between iron and acid-labile sulfide was eventually established analytically for Fe_2S_2 centers.[9-11] Care must be taken to ensure that both the protein and its active-site complement are homogeneous. Although protein homogeneity is usually established by electrophoretic methods, these methods may not distinguish between pure proteins and those with absent or incomplete active centers. Fortunately, absorption at 420 nm is due solely to the Fe_2S_2 cluster, whereas the 275-nm absorption is dominated by the protein. Therefore a good criterion for active-site saturation and homogeneity is the ratio of the absorbances at 420 and 275 nm, $A_{420\ nm}/A_{275\ nm}$, which is ~0.48 for pure spinach ferredoxin.[81] Once homogeneous protein is obtained, the Fe_2S_2 composition of the "plant" ferredoxins can be correctly deduced analytically.

The Fe_2S_2 center displays two redox states that differ by a single electron. The potential range for the couple is -250 to -420 mV, revealing the highly reducing nature of the ferredoxin. The correct structure of the Fe_2S_2 center was first proposed in 1966 based on EPR studies.[82] The reduced state of the cluster shows a rhombic EPR signal with g values of 1.88, 1.94, and 2.04 (Figure 7.6B) characteristic of an $S = \frac{1}{2}$ center. The oxidized state is EPR-silent. The weakness of the sulfur ligand field causes the iron atoms to be high-spin. But how can two sulfur-ligated iron atoms, each with a tendency to be high-spin, produce a state with a single unpaired electron?

The individual Fe atoms in the Fe_2S_2 cluster resemble those in rubredoxin quite closely. The two redox states of the Fe_2S_2 protein correspond to an Fe^{3+}-Fe^{3+} and an Fe^{3+}-Fe^{2+} pair, respectively, as shown in Figure 7.9. In the all-ferric oxidized state, the two Fe^{3+} sites are antiferromagnetically coupled; i.e., the spins of the five d electrons on the two iron atoms are oppositely aligned, such that their pairing produces an effective S = 0, diamagnetic ground state. In the reduced form, a single unpaired electron is present, because the $S = \frac{5}{2}$ Fe^{3+} and S = 2 Fe^{2+} sites are antiferromagnetically coupled, leaving one net unpaired spin and an $S = \frac{1}{2}$ ground state. The profound difference between the electronic properties of rubredoxin and Fe_2S_2 ferredoxin arises because the latter has two Fe atoms in close proximity, which allows for their magnetic coupling.

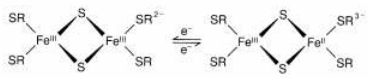


Figure 7.9 - Redox states of Fe_2S_2 proteins: (A) reduced; (B) oxidized.

Strong support for the spin-coupling model in Fe_2S_2 ferredoxins comes from a detailed analysis of their absorption and circular dichroism spectra.[83] As with rubredoxin (see Figure 7.5), we expect no low-energy spin-allowed d-d bands for the ferric site in either the oxidized or the reduced state. Indeed, the oxidized state containing all Fe^{3+} shows no low-energy bands; the reduced state containing a single Fe^{2+} displays low-energy, low-intensity bands in the region 4,000-9,000 cm^{-1}, in close analogy to the situation in reduced rubredoxin. The combined EPR and optical spectra leave little doubt about the structural assignment: two coupled high-spin ferric ions in the oxidized state, and coupled high-spin ferric and ferrous ions in the reduced state. Moreover, the spectra are consistent only with a localized model, i.e., one in which the Fe(II) site is associated with a single iron.[83,83a] The Fe_2S_2 site is inherently asymmetric, and inequivalence of the Fe(llI) sites is spectroscopically detectable in the all-ferric oxidized form.[84] In fact, the localized valence trapping is present in reduced model compounds that contain no ligand asymmetry.

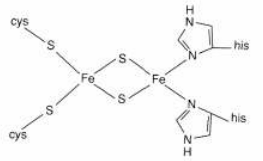
Mössbauer spectra provide additional and striking confirmation of the structural assignment. The spectrum of the oxidized ferredoxin (Figure 7.7) resembles strongly that of oxidized rubredoxin, indicating the presence of high-spin Fe^{3+}, even though the net spin is zero. In the reduced form, the Mössbauer spectrum involves the superposition of signals from a high-spin Fe^{2+} and a high-spin Fe^{3+}, i.e., a reduced and an oxidized rubredoxin, respectively. Clearly, the simplest interpretation of this result consistent with the S = $\frac{1}{2}$ spin state required by the EPR is the localized Fe^{2+}-Fe^{3+} antiferromagnetic coupling model discussed above.

NMR studies of oxidized Fe_2S_2 proteins reveal broad isotropically shifted resonances for the CH_2 protons of the cysteine ligands.[85] Despite the coupling of the irons, the net magnetism at room temperature is sufficient to lead to large contact shifts (-30 to -40 ppm downfield from TMS). The assignment of the resonance was confirmed with the synthesis and spectroscopic analysis of model compounds.[86] Extensive NMR studies of the Fe_2S_2 proteins have been reported.[87,87a]

Resonance Raman spectra of Fe_2S_2 sites[88,89,90] reveal many bands attributable to Fe-S stretching. Detailed assignments have been presented for the four bridging and four terminal Fe-S modes. A strong band at 390 cm^{-1}, which shifts on ^{34}S sulfide labeling, is assigned to the A_{1g} "breathing" mode; another band at 275 cm^{-1} is assigned to B_{3u} symmetry in point group D_{2h}.[57,88] Spectroscopic differences in the terminal, Fe-S(Cys) stretches between plant ferredoxins and adrenodoxin (which also differ somewhat in redox potential) seem to reflect different conformations of the cysteine ligands in the two classes. Evidence for asymmetry of the iron atoms is found in the intensity of the resonance enhancement of certain modes.

Rieske Centers

Within the class of Fe_2S_2 ferredoxins there is a subclass called the Rieske proteins, or the Rieske centers.[47,91,92] The Rieske iron-sulfur centers are found in proteins isolated from mitochondria and related redox chains.[47,92] In addition, the phthalate dioxygenase system from *Pseudomonas cepacia*[93,94] contains one Fe_2S_2 Rieske center as well as one additional nonheme Fe atom. Although the Rieske centers appear to contain an Fe_2S_2 core, there is extensive evidence for nonsulfur ligands coordinated to at least one of the Fe atoms. The proposed model in Scheme (7.3) has two imidazole ligands bound to one Fe atom. The nitrogen atoms are seen in ENDOR (Electron Nuclear Double Resonance) experiments,[93] and are manifest in EXAFS spectra, which are consistent with the presence of a low-Z (atomic number) ligand bound to iron.[94] The potentials for the Rieske proteins range from +350 to -150 mV,[47] in contrast to the plant-type Fe_2S_2 centers, which range from -250 to -450 mV. The strong dependence of redox potential on pH[95] suggests a possible role in coupling protonand electron-transfer processes.



Fe_2S_2 Models

Although spectroscopic studies led to the correct deduction of the structure of the Fe_2S_2 core, the synthesis of model compounds containing this core provided unequivocal confirmation. The model compounds allowed detailed structural analysis unavailable for the proteins. Moreover, by using a uniform set of peripheral ligands, properties inherent to the Fe_2S_2 core could be discerned.

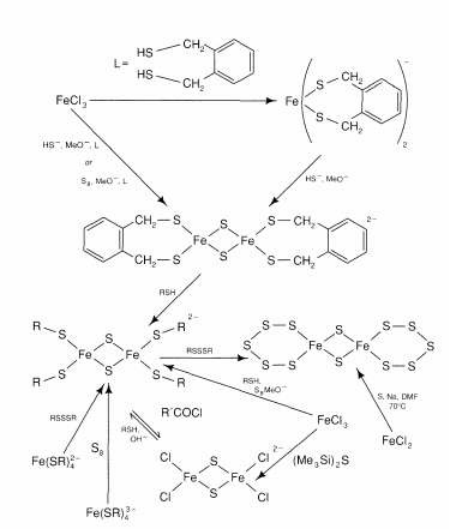


Figure 7.10: Preparative schemes leading to complexes containing the Fe_2S_2 core.[128]

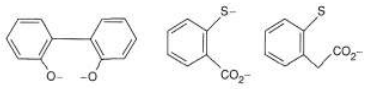
The Fe_2S_2 core has been synthesized by several routes[86,96a,b,c,d] (see Figure 7.10). For example, the reaction of $Fe(SR)_4^{2-}$, the ferrous rubredoxin model, with elemental sulfur produces the complex $Fe_2S_2(SR)_4^{2-}$. In this reaction the sulfur presumably oxidizes the Fe^{2+} to Fe^{3+}, being reduced to sulfide in the process. The Fe_2S_2 core has been prepared with a variety of peripheral S-donor ligands. Metrical details for $Fe_2S_2(SC_6H_4\text{-}p\text{-}CH_3)_4^{2-}$ are given in Table 7.3. Notable distances are the Fe-S (bridging) distance of 2.20 Å, the Fe-S (terminal) distance of 2.31 Å, and the Fe-Fe distance of 2.69 Å.

Table 7.3: Structural parameters for $Fe_2S_2(SC_6H_4-p-CH_3)_4^{2-}$. a) Data from Reference 211.

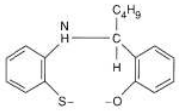
Atoms[a]	Distance Å	Atoms[a]	Angle[a]
Fe-Fe	2.691 (1)	Fe-S-Fe	75.3
Fe-S1 (bridge)	2.200 (1)	S-Fe-S	104.6
Fe-S2 (bridge)	2.202 (1)	S-Fe-S	115.1
Fe-S3	2.312 (1)	S-Fe-S	105.4

To date, all analogue systems structurally characterized contain the Fe^{3+}-Fe^{3+} fully oxidized form. Attempts to isolate the Fe^{3+}-Fe^{2+} form have so far failed. However, the mixed-valence Fe_2S_2 form can be generated and trapped by freezing for spectroscopic examination.[97,98] Mössbauer spectroscopy reveals the presence of distinct Fe^{2+} and Fe^{3+} ions, as found in the proteins, clearly showing that "trapped" valence states are an inherent characteristic of the $Fe_2S_2^{2+}$ core and are *not* enforced by the protein.[97,98]

The existence of noncysteine-bound Fe_2S_2 cores in Rieske-type proteins has led to attempts to synthesize complexes with oxygen and nitrogen ligands.[99-101] Characterized species include $Fe_2S_2(OC_6H_5)_4^{2-}$, $Fe_2S_2(OC_6H_4\text{-}p\text{-}CH_3)_4^{2-}$, $Fe_2S_2(C_4H_4N)_4^{2-}$, and $Fe_2S_2(L)_2^{2-}$, where L is a bidentate ligand.



The potentially tridentate ligand



acts in a bidentate fashion, binding through S and O but not N.

No Fe_2S_2 complexes containing mixed S,N terminal ligands, such as those suggested for the Rieske site, have been prepared. The Se^{2-} bridged analogue has been prepared for some of the complexes.[102,103]

7.4.2: Iron-sulfur Proteins and Models (Part 2) is shared under a not declared license and was authored, remixed, and/or curated by LibreTexts.

7.4.3: Iron-sulfur Proteins and Models (Part 3)

Fe_4S_4 Ferredoxins (including HiPIPs)

We now turn our attention to proteins containing the Fe_4S_4 center. Historically, within this class a strong distinction was made between the "ferredoxins," which are low-potential (as low as -600 mV in chloroplasts) iron-sulfur proteins, and the "HiPIPs" = High Potential Iron Proteins, which have positive redox potentials (as high as +350 mV in photosynthetic bacteria). Although the HiPIP designation is still useful, proteins of both high and low potential are considered ferredoxins, whose key defining feature is the presence of iron and acid-labile sulfide.[13]

The Fe_4S_4 proteins participate in numerous electron-transfer functions in bacteria, and in some organisms (such as *Clostridium*) are the immediate electron donors for the nitrogenase and/or hydrogenase enzymes. The function of the HiPIPs seems obscure at present. In addition, Fe_4S_4 centers have been shown or postulated to occur in numerous microbial, plant, and mammalian redox enzymes, including nitrate reductase,[104] sulfite reductase,[24] trimethylamine dehydrogenase,[105] succinate dehydrogenase,[73,106] hydrogenase, and, possibly, in altered forms, nitrogenase. Table 7.1 lists some of the Fe_4S_4 ferredoxins and their properties.

In the Fe_2S_2 ferredoxins, combined spectroscopic, analytical, and model-system work led to an unequivocal assignment of the structural nature of the active site long before the crystallography was done. In contrast, for Fe_4S_4 systems and in particular the 8Fe-8S = $2Fe_4S_4$ systems from bacteria, the initial chemical suggestions were fallacious, and even the number and stoichiometry of the clusters were in doubt. In these cases, crystallography provided the definitive structural information.

The first indication of the presence of the "thiocubane" structure came in 1968, when a 4-Å resolution study[107] indicated a compact cluster of potentially tetrahedral Fe_4 shape in the HiPIP from *Chromatium vinosum*. This finding did not lead to much excitement, since it was not yet appreciated that HiPIPs and ferredoxins were structurally similar. In 1972, the high-resolution structure solution of both *Chromatium* HiPIP[108] and the 8Fe ferredoxin from *Peptococcus aerogenes* (formerly *Microbacter aerogenes*)[101] confirmed the presence of virtually identical thiocubane clusters in the two proteins.[108] Moreover, the structures for both oxidized and reduced HiPIP were deduced, and these revealed that the Fe_4S_4 cluster remained intact during the redox interconversion.[109] Subsequently, four-iron clusters have been crystallographically confirmed in an Fe_4S_4 ferredoxin from *Bacillus thermoproteolyticus*,[110,110a] in *Azotobacter vinelandii* ferredoxin I (also previously called Shethna Fe-S protein II), which also contains a 3Fe-4S cluster,[111,112] in the active form of aconitase,[113] and in sulfite reductase, where the cluster is probably bridged by cysteine sulfur to a siroheme.

In all the proteins characterized to date, the Fe_4S_4 clusters adopt the thiocubane structure,[108] which is discussed at greater length in the section on models. The clusters are usually bound to their proteins by four cysteine residues. As shown in Figure 7.11, in the *P. aerogenes* protein the two Fe_4S_4 clusters are bound by cysteines numbered 8, 11, 14, 18, 35, 38, 41, and 45.[101,114] The presence of the Cys-x-x-Cys unit is again apparent. However, this sequence seems prominent in all Fe-S proteins, and so is not specific for a particular Fe-S site. At first glance one might expect one cluster to be bound by cysteines 8,11,14, and 18, the other by cysteines 35, 38, 41, and 45. Actually, one cluster is bound by cysteines 8, 11, 14, and 45, the other by cysteines 35, 38, 41, and 18. The binding of a given cluster by cysteine residues from different portions of the polypeptide chain apparently helps stabilize the tertiary structure of the protein and brings the two clusters into relatively close proximity, the center-center distance being 12 Å.[114]

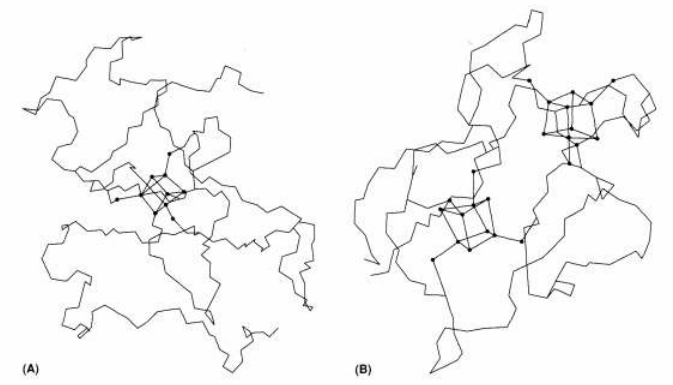


Figure 7.11 - The x-ray crystal structures of (A) *Chromatium vinosum* HiPIP[108] and (B) the 8Fe-8S ferredoxin from *Peptococcus aerogenes*.[101]

The *C. pasteurianum* protein displays weak magnetic coupling, which leads to an unusual EPR spectrum[115] consistent with the 12-Å cluster-cluster separation. However, the redox potentials for the two sites seem virtually identical at -412 mV, thus allowing the 8Fe ferredoxin to deliver two electrons at this low redox potential.[115] Significant sequence identity indicates the likelihood that other 8Fe ferredoxins, such as the well-studied one from *C. pasteurianum*,[116-118] have quite similar structures.

The thiocubane unit of Fe_4S_4 proteins can exist in proteins in at least three stable oxidation states. This so-called three-state model[74,109,119,120] contrasts dramatically with the situation for Rd(1Fe), Fe_2S_2, and Fe_3S_4 systems, in which only two oxidation states are accessible through simple electron transfer for each center. For the thiocubane structure, the three accessible states can be designated $Fe_4S_4^{3+}$, $Fe_4S_4^{2+}$, and $Fe_4S_4^{+}$, corresponding to $[Fe(III)_2Fe(II)]$, $[Fe(III)_2Fe(II)_2]$, and $[Fe(III)Fe(II)_3]$ valence-state combinations, respectively. It is crucial to note that, in sharp contrast to the Fe_2S_2 and Fe_3S_4 sites, the oxidation states are not localized in the Fe_4S_4 clusters. In most cases, each Fe atom behaves as if it had the same average oxidation level as the other Fe atoms in the cluster. The redox interconversion of the Fe4S4 sites is shown in Figure 7.12. The $Fe_4S_4^{3+} \rightleftharpoons Fe_4S_4^{2+}$ couple is the high-potential redox couple characteristic of HiPIPs; the $Fe_4S_4^{2+} \rightleftharpoons Fe_4S_4^{+}$ couple is responsible for the low-potential process characteristic of the classical ferredoxins. In any given protein under physiological conditions, only one of the two redox couples appears to be accessible and functional.

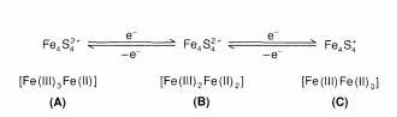


Figure 7.12 - The redox interconversions of Fe_4S_4 sites illustrating the three-state model. The states are found in (A) oxidized HiPIP; (B) reduced HiPIP and oxidized ferredoxin; (C) reduced ferredoxin.

Both the $Fe_4S_4^{+}$ and the $Fe_4S_4^{3+}$ states of the thiocubane cluster are paramagnetic and display characteristic EPR spectra (Figure 7.6C,D). The $Fe_4S_4^{3+}$ site in reduced ferredoxins[46,48,49,119] displays a rhombic EPR signal (Figure 7.6C) with g = 1.88, 1.92, and 2.06. The oxidized form of low-potential ferredoxins is EPR-silent, and attempts to "superoxidize" it to achieve the $Fe_4S_4^{3+}$ state invariably lead to irreversible cluster decomposition, probably through a 3Fe-4S structure. The $Fe_4S_4^{3+}$ signal is usually referred to as the HiPIP signal (Figure 7.6D) and shows distinct g values at 2.04($g_\perp$) and 2.10($g_\parallel$); it is present in oxidized HiPIP but absent in reduced HiPIP.[46,119] Reduction of HiPIP to a "super-reduced" state apparently occurs under partially denaturing conditions in aqueous DMSO.[108] The observed axial EPR signal with g = 1.94 and 2.05 is assigned to the $Fe_4S_4^{+}$ state characteristic of reduced ferredoxins. This result[108] is consistent with structural and spectroscopic identity of the HiPIP and Fd sites, as required by the three-state model of the Fe_4S_4 proteins (Figure 7.12).

In Fe_4S_4 centers at each level of oxidation, electronic transitions give rise to characteristic visible and UV spectra, although the delocalized nature of the electronic states makes detailed assignment difficult. MCD spectra of clusters in the three states of oxidation are clearly distinguishable from each other and from MCD of Fe_2S_2 clusters.[43,119] MCD, magnetic susceptibility, and Mössbauer spectra provide evidence that the S = $\frac{1}{2}$ state, whose EPR signal is so distinct in reduced ferredoxins, may coexist at higher T with S = $\frac{3}{2}$ and perhaps even higher spin states. Indeed, recent studies with model systems[121,122] and theoretical treatments[123,124] clearly support the ability of the Fe_4S_4 cluster to display a number of spin states that are in labile equilibria, which are influenced, perhaps quite subtly, by local structural conditions. The iron protein of nitrogenase also displays this behavior.

The Mössbauer spectra of Fe_4S_4 centers of ferredoxins reveal the equivalence of the Fe sites, and quadrupole splittings and isomer shifts at averaged values for the particular combination of oxidation states present.[3,51,52] Representative spectra are shown in Figure 7.7. Magnetic coupling is seen for the paramagnetic states.

Resonance Raman spectra (and IR spectra) have been extensively investigated in *C. pasteurianum* ferredoxin and in model compounds.[57,125] Selective labeling of either thiolate sulfur or sulfide sulfur with ^{34}S allows modes associated with the Fe_4S_4 core to be distinguished from modes associated with the FeSR ligands. The band at 351 cm^{-1} is assigned to Fe-SR stretching, and Fe_4S_4 modes occur at 248 and 334 cm^{-1} in reduced ferredoxin from *C. pasteurianum.* There is little difference between the oxidized and reduced spectra, although an extra band at 277 cm^{-1} seems present in the oxidized protein. The Fe_4Se_4 substituted protein has also been studied.[125]

As in the 1Fe and 2Fe proteins, ^1H NMR spectra reveal resonances from contact-shifted-CH_2-groups of cysteinyl residues.[125a] However, unlike the other proteins, where all states are at least weakly magnetic, only the reduced ferredoxin and the oxidized HiPIP states show contact shifts.[87a,125a,b,c]

EXAFS studies on proteins and on model compounds clearly identify the Fe-S distance of ~2.35 Å and an Fe-Fe distance of 2.7 Å. These distances, as expected, vary only slightly with state of oxidation.[125d]

Fe_4S_4 Models

Judging from the ease with which models of Fe_4S_4 are prepared under a variety of conditions and their relative stability, the $Fe_4S_4^{2+}$ core structure seems to be a relatively stable entity, a local thermodynamic minimum in the multitude of possible iron-sulfide-thiolate complexes. The initial preparation and structural characterization[126,127] of the models showed that synthetic chemistry can duplicate the biological centers in far-simpler chemical systems, which can be more easily studied in great detail.

The general synthetic scheme for Fe-S clusters is shown in Figure 7.13. Many different synthetic procedures can be used to obtain complexes with the Fe_4S_4 core.[126-138,138a,b] The multitude of preparative procedures is consistent with the notion that the $Fe_4S_4^{2+}$ core is the most stable entity present and "spontaneously self-assembles" when not limited by stoichiometric constraints.

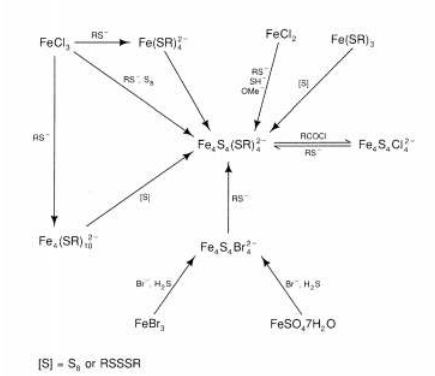


Figure 7.13 - Preparative schemes leading to complexes containing the Fe_4S_4 core.[128]

The thiocubane structure can be viewed as two interpenetrating tetrahedra of 4Fe and 4S atoms. The 4S tetrahedra are the larger, since the S-S distance is ~3.5 Å, compared with the Fe-Fe distance of ~2.7 Å. The S_4 tetrahedron encloses ~2.3 times as much volume as does the Fe_4 tetrahedron.[128] Key distances and angles for $Fe_4S_4(SCH_2C_6H_5)_4^{2-}$ given in Table 7.4 are extremely similar to those found in oxidized ferredoxin and reduced HiPIP centers in proteins.[127]

Table 7.4 - Structural parameters for $Fe_4S_4(SCH_2C_6H_5)_4^{2-}$.

a) Data from References 126 and 127.

Atoms[a]	Average Distances	Number of Bonds	Type
Fe(1)-S(3)	2.310 (3)	8	Sulfide
Fe(1)-S(2)	2.239 (4)	4	Sulfide
Fe(1)-S(5)	2.251 (3)	4	Thiolate
Fe(1)-Fe(2)	2.776 (10)	2	
Fe-Fe(other)	2.732 (5)	4	

Atoms[a]	Average Distances	Number of Bonds	Type
Fe-S-Fe	73.8 (3)	12	
S-Fe-S	104.1 (2)	12	Sulfide-Fe-Sulfide
S-Fe-S	111.7-117.3	12	Sulfide-Fe-Thiolate

The idealized symmetry of $Fe_4S_4^{2+}$ model systems is that of a regular tetrahedron, i.e., T_d. Though the distortion of the cube is quite pronounced, all known examples of the Fe_4S^{2+} core show distortion, which lowers the symmetry at least to D_{2d}. In most Fe_4S^{2+} core structures, this distortion involves a tetragonal compression, which leaves four short and eight long Fe-S bonds.

Complexes with non-S-donor peripheral ligands have been prepared and studied. The halide complexes $Fe_4S_4X_4^{2-}$ (X = Cl^-, Br^-, I^-) have been prepared, and serve as useful starting points for further syntheses.[129-133] The complex $Fe_4S_4(OC_6H_5)_4^{2-}$ can be prepared[134] from the tetrachloride (or tetrathiolate) thiocubane by reaction with $NaOC_6H_5$ (or HOC_6H_5). There are a few examples of synthetic $Fe_4S_4^{2+}$ cores in which the peripheral ligands are not identical. For example, $Fe_4S_4Cl_2(OC_6H_5)_2^{2-}$ and $Fe_4S_4Cl_2(SC_6H_5)_2^{2-}$ have structures characterized by D_{2d} symmetry.[135] The complexes $Fe_4S_4(SC_6H_5)_2[S_2CN(C_2H_5)_2]^{2-}$ and $Fe_4S_4(SC_6H_4OH)_4^{2-}$ are similarly asymmetric, containing both four- and five-coordinate iron.[136-138] The presence of five-coordinate iron in the Fe_4S_4 cluster is notable, since it offers a possible mode of reactivity for the cluster wherever it plays a catalytic role (such as in aconitase). Complexes with Fe_4Se^{2+} and $Fe_4Te_4^{2+}$ cores have also been prepared.[138c,d]

One structural analysis of $Fe_4S_4(SC_6H_5)_4^{3-}$, which contains the reduced $Fe_4S_4^+$ core, revealed a tetragonal elongation[139] in the solid state. In contrast, analysis of $Fe_4S_4(SCH_2C_6H_5)_4^{3-}$ revealed a distorted structure possessing C_{2v} symmetry.[102] It would appear that the $Fe_4S_4^+$ clusters maintain the thiocubane structure, but are nevertheless highly deformable. Interestingly, when the solidstate C_{2v} structure, $Fe_4S_4(SCH_2C_6H_5)_4^{3-}$, is investigated in solution, its spectroscopic and magnetic behavior change to resemble closely those of the $Fe_4S_4(SC_6H_5)_4^{3-}$ cluster,[140] which does not change on dissolution. The simplest interpretation assigns the elongated tetragonal structure as the preferred form for $Fe_4S_4^+$ cores with deformation of sufficiently low energy that crystal packing (or, by inference, protein binding forces) could control the nature of the distortions in specific compounds.[128] The elongated tetragonal structure has four long and eight short bonds in the core structure. The terminal (thiolate) ligands are 0.03-0.05 Å longer in the reduced structure, consistent with the presence of 3Fe(ll) and 1Fe(III) in the reduced form, compared to 2Fe(II) and 2Fe(III) in the oxidized form. There is no evidence for any valence localization.[128]

The oxidized $Fe_4S_4^{3+}$ core defied isolation and crystallization in a molecular complex prior to the use of sterically hindered thiolate ligands. With 2,4,6 tris(isopropyl)phenylthiolate, the $Fe_4S_4L_4^-$ complex could be isolated and characterized.[141] The structure is a tetragonally compressed thiocubane with average Fe-S and Fe-SR distances 0.02 and 0.04 Å shorter than the corresponding distances in the $Fe_4S_4L_4^{2-}$ complex. Again, there is no evidence for Fe inequivalence or more profound structural distortion in this 3Fe(III)-1Fe(II) cluster. Clearly, the Fe_4S_4 clusters have highly delocalized bonding.

Evidence from model systems using sterically hindered thiolate ligands indicates the existence of an $Fe_4S_4^{4+}$, i.e., all-ferric fully oxidized cube.[142] The existence of the complete series $Fe_4S_4[(Cy)_3C_6H_2S]_4^n$ (Cy =cyclohexyl; n = 0, -1, -2, -3) is implied by reversible electrochemical measurements. Clearly, five different states of the Fe_4S_4 core—including the (at least) transient fully oxidized state and the all-ferrous fully reduced state—may have stable existence. Although only the central three states have been shown to exist in biological contexts, one must not rule out the possible existence of the others under certain circumstances.

Recently, specifically designed tridentate ligands have been synthesized that bind tightly to three of the four Fe atoms in the thiocubane structure.[143,143a,b] The remaining Fe atom can then be treated with a range of reagents to produce a series of subsite-differentiated derivatives and variously bridged double-cubane units. These derivatives illustrate the potential to synthesize complexes that mimic the more unusual features of Fe_4S_4 centers that are bound specifically and asymmetrically to protein sites. The recently synthesized complex ion $[(Cl_3Fe_4S_4)_2S]^{4-}$, containing two Fe_4S_4 units bridged by a single S^{2-} ligand, illustrates the potential coupling of known clusters into larger aggregates.[143c]

The model-system work has made an important contribution to our understanding of the Fe_4S_4 centers. The existence of three states, the exchange of ligands, the redox properties, the metrical details of the basic Fe_4S_4 unit, and the subtleties of structural distortion can each be addressed through the study of models in comparison with the native proteins.

7.4.3: Iron-sulfur Proteins and Models (Part 3) is shared under a not declared license and was authored, remixed, and/or curated by LibreTexts.

7.4.4: Iron-sulfur Proteins and Models (Part 4)

Core Extrusion/Cluster Displacement Reactions

Synthetic model-system work led to the realization that the cluster cores can exist outside the protein and undergo relatively facile ligand-exchange reactions.[128] This behavior of the purely inorganic complexes allowed core extrusion reactions[128,144] to be developed. The basic assumption behind these reactions is that the cluster core retains its integrity when it is substituted by low-MW thiolates, especially aryl thiolates, which replace the cysteinyl ligands that bind it to the protein. In order to free the cluster from the protein, one must at least partially denature the protein, usually by using ~80 percent aqueous solution of a polar aprotic solvent, such as DMSO or HMPA. The resulting inorganic clusters can be identified and quantified by measurement of their characteristic electronic absorption or NMR spectra. An alternative approach involves transferal of the unknown cluster in question to an apoprotein that binds a cluster of known type.[145]

Since the 1Fe, 2Fe, and 4Fe sites are each usually bound to the protein by four cysteine residues, it is perhaps not surprising that there have been reports[58] of interconversion of cluster types bound to a given protein. Specifically, in 90 percent aqueous DMSO, the single Fe site in rubredoxin from *C. pasteurianum* is converted to an Fe_4S_4 cluster by the addition of sodium sulfide, ferrous chloride, and ferric chloride in ratio 4:2:1. Presumably the spacing and geometric disposition of the cysteines are suitable to bind a single Fe or the Fe_4S_4 cluster, which is readily formed under the reaction conditions. Another example of cluster rearrangement involves the three-iron center discussed below that does *not* extrude as an Fe_3S_4 center. Rather, at least under *certain* conditions, the Fe_{3Sx} center rearranges to form Fe_2S_2 centers.[146] The facile interconversion of the Fe clusters demonstrated the lability of Fe-S systems, and indicates that caution must be exercised in interpreting the results of cluster-displacement reactions.

Fe_3S_4 Centers

Three-iron centers are a comparatively recent finding,[119,146] and the full scope of their distribution is not yet known. Although they have now been confirmed in dozens of proteins, it often remains uncertain what physiological role these centers play. Indeed, since Fe_3S_4 centers can be produced as an artifact upon oxidation of Fe_4S_4 centers, it has been suggested that 3Fe centers may not be truly physiological, and could be side products of aerobic protein isolation. This caveat notwithstanding, the 3Fe sites are being found in more and more proteins and enzymes. Their physiological *raison d' être* may be more subtle than that of their 1, 2, and 4Fe cousins; we should certainly try to find out more about them. Some proteins containing Fe_3S_4 centers are listed in Table 7.1.

The 3Fe center was first recognized[147] in the protein ferredoxin I from the anaerobic nitrogen-fixing bacterium *Azotobacter vinelandii*. The protein is called *Av* FdI for short. It is instructive to sketch historically the evolution of our understanding of this protein. *Av* ferredoxin I was reported to have 6 to 8 Fe atoms and was first thought to resemble the clostridial 8Fe ferredoxins. However, unlike the clostridial protein, the *Av* FdI clusters appeared to have two quite different redox couples at +320 and -420 mV. Although it might have been thought that this protein contained one HiPIP-type and one Fd- or "ferredoxin"-type Fe_4S_4 cluster, the protein as isolated had an EPR signal with g = 2.01, which differed significantly (Figure 7.6) from that of an oxidized HiPIP or a reduced Fd.[148] Cluster extrusion reactions also seemed to indicate the presence of an unusual cluster type.[149]

Fortunately, the protein was crystallized, and could be studied by x-ray diffraction. Unfortunately, the initial conclusions[150] and subsequent revisions[151,152] of the crystal-structure analysis have proven to be wrong, teaching us in the process that protein x-ray crystallography, taken alone, does not always provide definitive results. Specifically, the first crystallographic report suggested the presence of a conventional Fe_4S_4 cluster and a smaller packet of electron density that was assigned as a 2Fe-2S center.[150] However, upon further refinement, and following the formulation of the 3Fe center by Mössbauer spectroscopy,[147] a 3Fe-3S center was identified and refined.[151,152] The "refined" Fe_3S_3 center was a six-membered alternating iron-sulfide ring with an open, almost flat, twistedboat conformation (Figure 7. 14). The Fe-Fe separation of 4.1 Å and the structural type was unprecedented, and did not agree with the results of resonance Raman spectroscopy,[153] with x-ray absorption spectroscopy on the native protein or on samples from which the Fe_4S_4 center was removed,[103] or even with stoichiometry, which eventually led to the reformulation[154] of the cluster as Fe_3S_4. The x-ray absorption studies (EXAFS) clearly led to the assignment of a 2.7-Å Fe-Fe distance for the 3Fe cluster.[103]

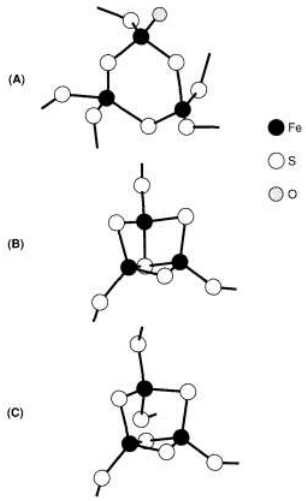


Figure 7.14 - Fe_3S_n structures: (A) open Fe_3S_3 structure proposed from initial x-ray studies (now shown to be in error); (B) the thiocubane fragment structure believed present in most Fe_3S_4 proteins; (C) open Fe_3S_4 structure (not found to date).

In parallel with the studies on *Av* FdI, two additional proteins played key roles in the resolution of the nature of the Fe_3 cluster. These are FdII from *Desulfovibrio gigas* and aconitase from beef heart. Each contains (under certain conditions) only Fe_3S_4 sites, thus enabling more definitive structural, stoichiometric, and spectral information to be acquired. Studies on these proteins using EXAFS,[155] Mössbauer,[52,156,157] EPR,[146] and resonance Raman (to which we will return briefly) clearly favor the closed structure shown in Figure 7.14C. Indeed, x-ray crystallography on aconitase by the same group that did the initial x-ray work on *Av* FdII revealed the compact structure in agreement with the spectroscopy.[20]

In 1988 the structural error in the crystallography of *Av* FdI was found by two groups, and a new refinement in a corrected space group led to a structure in agreement with the spectroscopy.[111,112] The Fe_3S_4 cluster has the apoFe thiocubane structure, with each iron atom bound to the protein by a single cysteinyl thiolate. Clearly, even x-ray crystallography is potentially fallible, and its findings must be critically integrated with the data from other techniques in arriving at full structural definition of metalloenzyme sites.

The studies on the ferredoxins from *D. gigas* present an interesting lesson on the lability of the Fe-S cluster systems. Two distinct proteins from *D. gigas*, FdI and FdII, contain the same polypeptide chain (6 kDa) in different states of aggregation,[158,159] Whereas FdI is a trimer containing three Fe_4S_4 clusters, FdII is a tetramer that contains four Fe_3S_4 clusters. The ferredoxins differ in their redox potentials and appear to have different metabolic functions in *D. gigas*. The oxidation of *D. gigas* FdI with $Fe(CN)_6^{3-}$ leads to FdII, and treatment of FdII with iron salts leads to FdI. The *D. gigas* system reveals the lability and interconvertibility of Fe-S clusters. The recently reported[160] crystal structure of *D. gigas* FdII shown in Figure 7.15 confirms the partial (apoFe) thiocubane Fe_3S_4 center. The iron atoms are ligated by three cysteinyl residues from protein side chains. The cube missing an iron is now firmly established as a viable structural type.

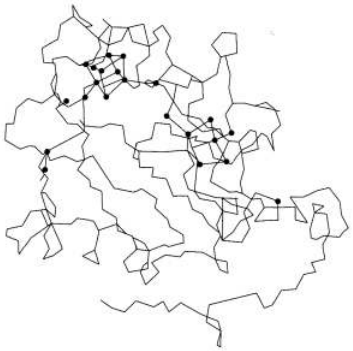
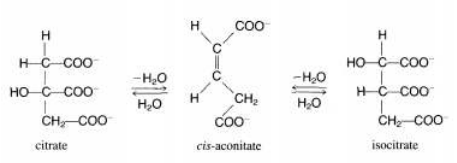


Figure 7.15 - The x-ray crystal structure of D.gigas FdII, illustrating the Fe_4S_4 and Fe_3S_4 centers in this protein.[160]

The aconitase system presents yet another fascinating story.[159a] Aconitase is a key enzyme in the Krebs cycle, catalyzing the conversion of citrate and isocitrate through the intermediacy of cis-aconitate, as shown in Equation (7.6).



This is a hydrolytic nonredox process, and for some time it was thought that aconitase was a simple Fe^{2+} protein wherein the ferrous iron was involved in the Lewis-acid function of facilitating the hydrolytic reaction. Indeed, aconitase is inactive when isolated from mitochondria, and requires the addition of Fe^{2+} to achieve activity.

Surprisingly, the isolated aconitase was found by analysis and Mossbauer spectroscopy to possess an Fe_3S_4 site in its inactive form.[161] Low-resolution crystallographic study supports the presence of an apo-Fe thiocubane, Fe_3S_4 structure in aconitase.[162] Resonance Raman[163] and EXAFS[103,155] studies clearly fingerprint the Fe_3S_4 cluster. The current hypothesis for aconitase activation involves the Fe_3S_4 thiocubane fragment reacting with Fe^{2+} to complete the cube, which is the active form of the enzyme.[164] Recent crystallographic studies[113] confirm the presence of a complete cube in the activated aconitase. The dimensions and positioning of the Fe_3S_4 and Fe_4S_4 centers in the cube are virtually identical. The added Fe^{2+} iron atom is ligated by a water (or hydroxide) ligand, consistent with the absence of any cysteine residues near the exchangeable iron. Since this water (or a hydroxide) is also present in the Fe_3S_4 system, one wonders whether a small ion such as Na^+ might be present in the Fe_3S_4 aconitase system.

Questions of detailed mechanism for aconitase remain open. ENDOR spectroscopy[165] shows that both substrate and water (or OH^-) can bind at the cluster. Does one of its Fe-atom vertices play the Lewis-acid role necessary for aconitase activity? Is the $Fe_3S_4 \rightleftharpoons Fe_4S_4$ conversion a redox- or iron-activated switch, which works as a control system for the activity of aconitase? These and other questions will continue to be asked. If aconitase is indeed an Fe-S enzyme with an iron-triggered control mechanism, it may be representative of a large class of Fe_3/Fe_4 proteins. Other hydrolytic enzymes containing similar Fe-S centers have recently been reported.[166,166a]

Spectroscopically, the Fe_3S_4 center is distinct and clearly distinguishable from 1Fe, 2Fe, and 4Fe centers. The center is EPR-active in its oxidized form, displaying a signal (Figure 7.6) with g = 1.97, 2.00, and 2.06 (*D. gigas* FdII).[158] The Mössbauer spectrum (Figure 7.7) shows a single quadrupole doublet with ΔQ = 0.53 nm/s and isomer shift of 0.27 nm, suggesting the now familiar highspin iron electronic structure.[158,159] In its reduced form, the center becomes EPR-silent, but the Mössbauer spectrum now reveals two quadrupole doublets of intensity ratio 2:1. The suggestion of the presence of a 3Fe center was first made based on this observation.[147] The picture of the reduced Fe_3S_4 state that has emerged involves a coupled, delocalized Fe^{2+}/Fe^{3+} unit responsible for the outer doublet, with a single Fe^{3+} unit responsible for the inner doublet of half the intensity. The oxidized state contains all Fe^{3+} ions, which are coupled in the trinuclear center.

EXAFS studies were consistent and unequivocal in finding an Fe-Fe distance of ~2.7 Å in all putative Fe_3S_4 proteins.[103,155,167] Resonance Raman spectra compared with those of other proteins and of model compounds with known structures[168,169] for other metals also favored the structure of Figure 7.14B. Clearly, what has been termed the spectroscopic imperative[170] has been crucial in the successful elucidation of the 3Fe structure. An interesting excursion has led to isolation of what are presumed to be $ZnFe_3S_4$, $CoFe_3S_4$, and $NiFe_3S_4$ thiocubane structures by adding Zn^{2+}, Co^{2+}, or Ni^{2+}, respectively, to proteins containing reduced Fe_3S_4 cores.[170a,b,c] These modified proteins provide interesting electronic structural insights and, potentially, new catalytic capabilities.

Fe_3 Model Systems

To date, the Fe_3S_4 center is the only structurally characterized biological iron-sulfide center that does not have an analogue in synthetic Fe chemistry. In fact, the closest structural analogue[21,170d] is found in the $Mo_3S_4^{4+}$ or $V_3S_4^{3+}$ core in clusters such as $Mo_3S_4(SCH_2CH_2S)_3^{2-}$, whose structure is shown in Figure 7.16.

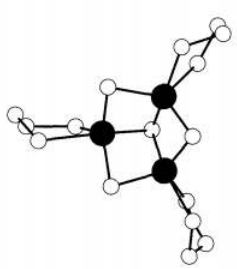


Figure 7.16 - The x-ray crystal structure of $Mo_3S_4(SCH_2CH_2S)_3^{2-}$. (From Reference 10a.)

The resonance Raman spectrum[169] of this complex bears a close resemblance to that of the *D. gigas* ferredoxin II. Since the vibrational bands responsible for the resonance Raman spectrum are not strongly dependent on the electronic properties, it is not surprising that an analogue with a different metal can be identified using this technique.

In synthetic Fe chemistry, although there is no precise structural analogue, it is instructive to consider three types of trinuclear and one hexanuclear center in relation to the three-iron biocenter.

The trinuclear cluster $Fe_3S[(SCH_2)C_6H_4]_3^{2-}$ is prepared[171,172] by the reaction of $FeCI_3$, $C_6H_4(CH_2SH)_2$, $Na^+OCH_3^-$, and p-CH_3-C_6H_4-SH in CH_3OH. As shown in Figure 7.17A, this cluster has, like the biocluster, a single triply bridging sulfide ion but, unlike the biocluster, it uses the sulfur atoms of the ethane 1,2-dithiolate as doubly bridging, as well as terminal, groups. The inorganic ring $Fe_3(SR)_3S_6^{3-}$ (X = CI, Br) has a planar $Fe_3(SR)_3$ core, which resembles the now-discredited structure for *Av* FdI[173] (Figure 7. 14A).

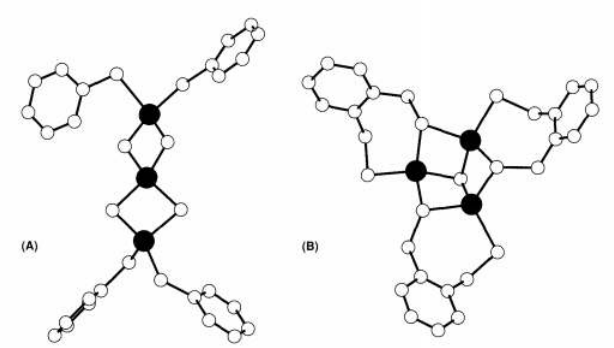


Figure 7.17 - The x-ray crystal structures of trinuclear Fe complexes: (A) $Fe_3S_4(SR)_4^{3-}$; (B) $Fe_3S[(SCH_2)_2C_6H_4]_3^{2-}$. (Data from References 171, 172, 174, 175.)

The complex $Fe_3S_4(SR)_4^{3-}$ is prepared[174,175] by reaction of $Fe(SR)_4^{2-}$ with sulfur. The x-ray-determined structure reveals two tetrahedra sharing a vertex with the linear Fe-Fe-Fe array shown in Figure 7.17B. This complex has distinctive EPR, Mössbauer, and NMR spectra that allow it to be readily identified[174,175,175a] Interestingly, after the complex was reported, a study of (denatured) aconitase at high pH (>9.5) revealed that the thiocubane fragment Fe_3S_4 site in that enzyme rearranged to adopt a structure that was spectroscopically almost identical with that of the linear complex.[176] Although the state may not have any physiological significance, it does show that Fe-S clusters different from the common (conventional) ones already discussed could be important in proteins under certain physiological conditions or in certain organisms; i.e., iron centers first identified synthetically may yet prove to be present in biological systems.

A synthetic cluster that displays features related to the biological Fe_3S_4 cluster is the hexanuclear cluster $Fe_6S_9(SR)_2^{4-}$ shown in Figure 7.18. This cluster contains two Fe_3S_4 units bridged through their diiron edges by a unique quadruply bridging S^{2-} ion (μ_4-S^{2-}) and by two additional μ_2S^{2-} bridges. The inability of synthetic chemists to isolate an Fe_3S_4 analogue may indicate that in proteins this unit requires strong binding. Significant sequestration by the protein may be needed to stabilize the Fe_3S_4 unit against oligomerization through sulfide bridges or, alternatively, rearrangement to the stable Fe_4S_4 center.

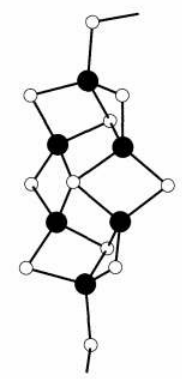


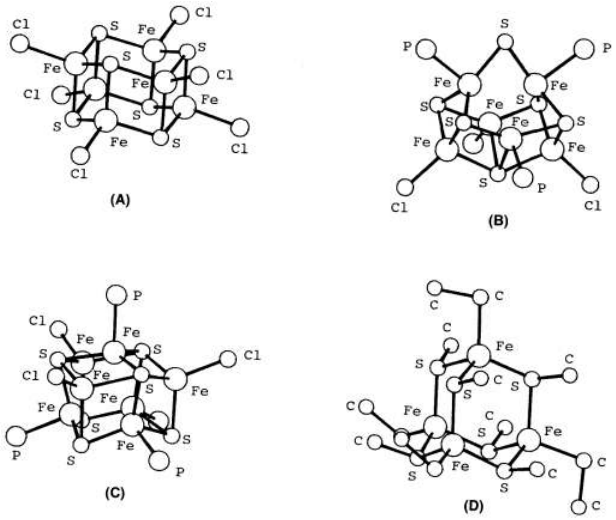
Figure 7.18 - The x-ray crystal structure[176a,b] of $Fe_6S_9(SR)_2^{4-}$.

Fe-S Chemistry: Comments and New Structures

The first successful model system for an iron-sulfur protein was an analogue of the Fe_4S_4 system, i.e., the system with the largest presently established biological Fe cluster. The reactions used to synthesize the cluster shown in Figure 7.13 are said to involve self-assembly, meaning that starting materials are simply mixed together, and thermodynamic control causes the cluster to assemble in its stable form. Interestingly, the Fe_4S_4-containing proteins, such as those of *C. pasteurianum*, are considered to be among the most ancient of proteins. Perhaps on the anaerobic primordial Earth, Fe-S clusters self-assembled in the presence of protein ligands to form the progenitors of the modem ferredoxins.

Much progress has been made in synthetic chemistry, and it is clear that both understanding and control of Fe-S chemistry are continuing to grow. New preparations for known clusters continue to be found, and new clusters continue to be synthesized, Although many of the new clusters appear to be abiological, we should not ignore them or their potential. They add to our understanding of Fe-S chemistry in general, and serve as starting points in the study of heteronuclear clusters, There is also the distinct possibility that one or more of these synthetic clusters represent an existing biological site that has not yet been identified in an isolated system.

Among the "nonbiological" structures that have been synthesized are complexes with $Fe_6S_6^{3+/2+}$ cores[177,178] including the thioprismanes,[108,109,177-179] the octahedron/cube $Fe_6S_8^{3+}$ cores,[180,181] the $Fe_6S_9^{2-}$ cores[176a,b] discussed above, the adamantane-like $Fe_6(SR)_{10}^{4-}$ complexes related to Zn and Cu structures in metallothioneins,[182] basket $Fe_6S_6^{2+}/Fe_6S_6^{+}$ cores,[182a,b,c,d] monocapped prismatic $Fe_7S_6^{3+}$ cores,[183] the cube/octahedron $Fe_8S_6^{5+}$ cores,[179] and the circular Na^+-binding $Fe_{18}S_{30}^{10-}$ unit.[183a,b] Representative ions are shown in Figure 7.19. Some of these cores are stabilized by distinctly nonbiological phosphine ligands. Nevertheless, one should not *a priori* eliminate any of these structures from a possible biological presence. Indeed, recently a novel, apparently six-iron protein from *Desulfovibio gigas* has been suggested[183c] to have the thioprismane core structure first found in model compounds.



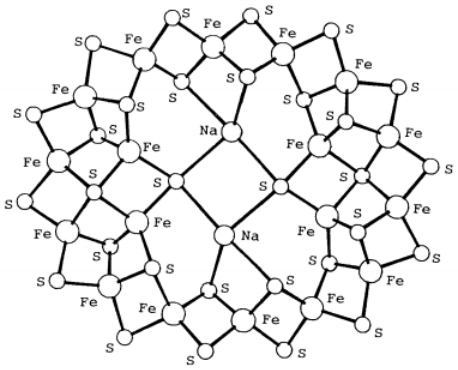


Figure 7.19 - Structures of "to date nonbiological" Fe-S clusters: (A) the thioprismane structure;[177] (B) basket-handle structure;[182a] (C) monocapped prismatic structure;[183] (D) adamantane structure;[182] (E) circular $Fe_{18}S_{30}^{10-}$ core unit.[183a,b]

Detection of Fe-S Sites

Several recent reviews have concentrated on the ways in which the various Fe-S centers can be identified in newly isolated proteins.[5,6,184] It is instructive to summarize the central techniques used in the identification of active sites. Optical spectra are usually quite distinctive, but they are broad and of relatively low intensity, and can be obscured or uninterpretable in complex systems. MCD spectra can give useful electronic information, especially when the temperature dependence is measured. EPR spectra, when they are observed, are distinctive, and are usually sufficiently sharp to be useful even in complex systems. Mössbauer and resonance Raman spectroscopies have each been applied with good effect when they can be deconvoluted, and NMR and magnetic susceptibility have given important information in some simple, lower-MW protein systems. X-ray absorption spectra, especially EXAFS, give accurate Fe-S and Fe-Fe distances when a single type of Fe atom is present. Analytical and extrusion data complement the spectroscopic and magnetic information. Extrusion data must be viewed with considerable caution, because of possible cluster-rearrangement reactions. Even x-ray crystallography has led to incorrect or poorly refined structures. In general, no one technique can unequivocally identify a site except in the very simplest systems, and there is continued need for synergistic and collaborative application of complementary techniques to a given system.

Redox Behavior

Figure 7.20 shows the ranges of redox behavior known for Fe-S centers. Clearly, the Fe-S systems can carry out low-potential processes. The rubredoxins cover the mid-potential range, and the HiPIPs are active in the high-potential region. The lack of extensive Fe-S proteins in the positive potential region may reflect their instability under oxidizing conditions and their preemption by Mn, Cu, or heme-iron sites (such as in cytochrome c), which function in this region.

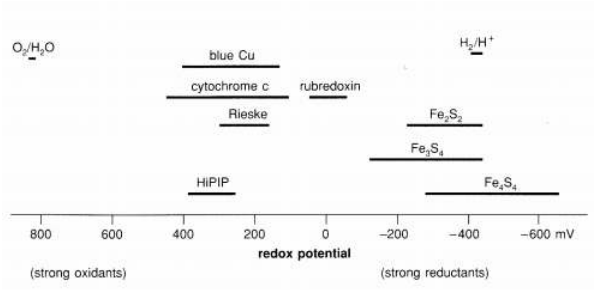


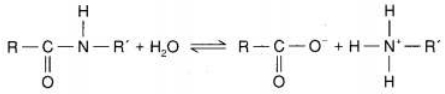
Figure 7.20 - A schematic diagram of the redox potential of the various FeS centers in comparison with other known redox centers.

7.4.4: Iron-sulfur Proteins and Models (Part 4) is shared under a not declared license and was authored, remixed, and/or curated by LibreTexts.

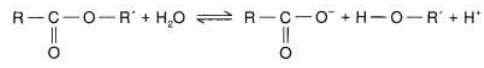
7.5: The Reaction Pathways of Zinc Enzymes and Related Biological Catalysts

I. Introduction

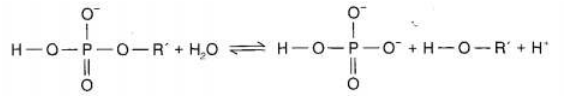
This chapter deals with metalloenzymes wherein the metal acts mainly as a Lewis acid; i.e., the metal does not change its oxidation state nor, generally, its protein ligands. Changes in the coordination sphere may occur on the side exposed to solvent. The substrate interacts with protein residues inside the active cavity and/or with the metal ion in order to be activated, so that the reaction can occur. Under these circumstances the catalyzed reactions involve, as central steps with often complex reaction pathways, the following bond-breaking and/or formation processes:



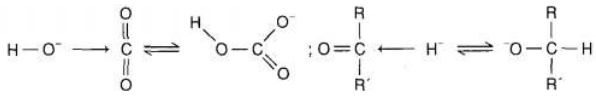
Peptide Hydrolysis



Carboxylic Ester Hydrolysis

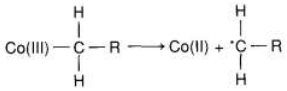


Phosphoric Ester Hydrolysis



Nucleophilic Addition of OH^- and H^-

Scheme (2.3) also pertains to the reactions which need ATP hydrolysis to promote endoenergetic reactions. We will also briefly deal with coenzyme B_{12}; this is a cobalt(III) complex that, by interacting with a number of proteins, produces an R-CH_2 radical by homolytic breaking of the Co-C bond as follows:



After an R-CH_2 radical is formed, it initiates a radical reaction. This is the only system we treat in which the oxidation state changes.

II. The Natural Catalysts

III. Strategies for the Investigation of Zinc Enzymes

A. Why Zinc?

1. The Groups to Which Zinc(II) is Bound
2. The Reactivity of Zinc(II) in Cavities
3. The Investigation of Zinc Enzymes

B. Metal Substitution

IV. Elucidation of Structure-Function Relationships: Carbonic Anhydrase as an Example

A. About the Enzyme

B. Steady-State and Equilibrium Kinetics of Carbonic Anhydrase-Catalyzed CO_2/HCO_3^- Interconversion

C. What Do We Learn from Cobalt Substitution?

1. Acid-base Equilibria
2. Coordination Geometries
3. Coordinated Water and NMR
4. pH Dependence of Inhibitor Binding

D. What Do We Learn from Copper Substitution?

E. What Do We Learn from Manganese and Cadmium Substitution?

F. Catalytic Mechanism

G. Model Chemistry

V. Other Enzymatic Mechanisms and Model Chemistry

A. Peptide Hydrolysis

B. Ester Hydrolysis and Phosphoryl Transfer

C. Nucleophilic Addition of OH^- and H^-

D. Group Transfer and Vitamin B_{12}

1. Group Transfer Enzymes
2. The B_{12}-dependent Enzymes

VI. Perspectives

Although a great deal is known about the biophysical characteristics of the various enzyme derivatives mentioned in this chapter, we are still far from a clear understanding of their mechanisms of action, especially if we take into consideration the role of each amino-acid residue inside the active-site cavity. Although we can successfully discuss why certain metal ions are used in certain biological reactions, we still do not know why nickel(II), for example, is involved in the enzymatic hydrolysis of urea.[199,200] If we are content with the explanations given in Sections III.A or V.D, we would need model compounds that are good catalysts and perform the job in several steps. This latter requirement would make the various models much more interesting, and would represent a new objective in the investigation of the structure-function relationship of catalytically active molecules. Indeed, the synthesis of large polypeptides may in principle provide such models. In this respect we need to know more about protein folding, for which emerging techniques like protein computer graphics and molecular dynamics are very promising.

Chemical modifications of proteins like the alkylation of carboxylate[124,201] or histidine[202] residues have been performed for a long time. A newer approach toward modeling the function of a protein, and understanding the role of the active site, involves cleaving part of a naturally occurring protein through enzymatic or chemical procedures, and then replacing it with a synthetic polypeptide. The use of modem techniques of molecular genetics has allowed site-directed mutagenesis to become in principle a very powerful technique for changing a single residue in a cavity. Site-directed mutagenesis is a very popular approach, and its principal limitation with respect to the synthetic polypeptide route is that only natural amino acids can be used (aside from the technical difficulties in both approaches). Small quantities of site-directed mutants have been obtained for CPA[125-127] and AP,[203] whereas the expression of CA[204,205] is now satisfactory.

Predictions of the changes in structure needed to affect the reaction pathway can nowadays be made with the aid of computers. The occurrence of the predicted change can be checked through x-ray analysis and NMR. The latter spectroscopy is today well-

recognized as being able to provide structural information on small (≲20 kDa) proteins through 2- or 3-dimensional techniques.[206-208] These techniques are increasingly being applied to paramagnetic metalloproteins such as many of those discussed here.[208,209] The advantage of handling a paramagnetic metalloprotein is that we can analyze signals shifted far away from their diamagnetic positions, which correspond to protons close to the metal ion,[69] even for larger proteins. It is possible to monitor the distances between two or more protons under various conditions, such as after the addition of inhibitors or pseudosubstrates, chemical modification, or substitution of a specific amino acid.

VII. References

1. H. Sigel and A. Sigel, eds., *Metal Ions in Biological Systems*, Dekker, **26** (1990).
2. R. K. Andrews, R. L. Blakeley, and B. Zemer, in Reference 1, **23** (1988).
3. K. Doi, B. C. Antanaitis, and P. Aisen, *Struct. Bonding* **70** (1988), I.
4. M. M. Werst, M. C. Kennedy, H. Beinert, and B. M. Hoffman, *Biochemistry* **29** (1990), 10526, and references therein.
5. A. G. Orpen *et al.*, *J. Chem. Soc., Dalton Trans.* **S1** (1989).
6. F. H. Westheimer, *Spec. Publ. Chem. Soc.* **8** (1957), I.
7. F. Basolo and R. G. Pearson, *Mechanisms of Inorganic Reactions*, Wiley, 2d ed., 1967.
8. L. G. Sillen and A. E. Martell, *Stability Constants of Metal-Ion Complexes*, Spec. Publ. Chern. Soc., London, **25**, 1971.
9. E. J. Billo, *Inorg. Nucl. Chem. Lett.* **11** (1975), 491.
10. I. Bertini, G. Canti, C. Luchinat, and F. Mani, *Inorg. Chem.* **20** (1981), 1670.
11. S. Burki, Ph.D. Thesis, Univ. Basel, 1977.
12. P. Wolley, *Nature* **258** (1975), 677.
13. J. T. Groves and R. R. Chambers, *J. Am. Chem. Soc.* **106** (1984), 630.
14. J. T. Groves and J. R. Olson, *Inorg. Chem.* **24** (1985), 2717.
15. L. J. Zompa, *Inorg. Chem.* **17** (1978), 2531.
16. E. Kimura, T. Koike, and K. Toriumi, *Inorg. Chem.* **27** (1988), 3687; E. Kimura *et al.*, *J. Am. Chem. Soc.* **112** (1990), 5805.
17. R. S. Brown *et al.*, *J. Am. Chem. Soc.* **104** (1982), 3188.
18. I. Bertini *et al.*, *Inorg. Chem* **29** (1990), 1460.
19. R. J. P. Williams, *Coord. Chem. Rev.* **100** (1990), 573.
20. D. W. Christianson, *Adv. Prot. Chem.* **42** (1991), 281.
21. I. Bertini, C. Luchinat, and M. S. Viezzoli, in I. Bertini *et al.*, eds., *Zinc Enzymes*, Birkhauser, 1986, p.27.
22. D. S. Auld and B. L. Vallee, in Reference 21, p. 167.
23. G. Formicka-Kozlowska, W. Maret, and M. Zeppezauer, in Reference 21, p. 579.
24. I. Bertini and C. Luchinat, in Reference 30, p. 101.
25. I. Bertini and C. Luchinat, *Adv. Inorg. Biochem.* **6** (1984), 71.
26. H. Sigel, ed., *Metal Ions in Biological Systems*, Dekker, **12** (1981).
27. T. G. Spiro, ed., *Copper Proteins*, Wiley, 1981.
28. J. E. Coleman and P. Gettins, in Reference 21, p. 77.
29. J. E. Coleman and D. P. Giedroc, in Reference 1, **25** (1989).
30. H. Sigel, ed., *Metal Ions in Biological Systems*, Dekker, **15** (1983).
31. N. U. Meldrum and F. J. W. Roughton, *J. Physiol.* **75** (1932), 4.
32. D. Keilin and T. Mann, *Biochem. J.* **34** (1940), 1163.
33. S. Lindskog, in T. G. Spiro, ed., *Zinc Enzymes: Metal Ions in Biology*, Wiley, **5** (1983), 78; D. N. Silverman and S. Lindskog, *Acc. Chem. Res.* **21** (1988), 30.
34. J.-Y. Liang and W. N. Lipscomb, *J. Am. Chem. Soc.* **108** (1986), 5051.
35. K. M. Merz, *J. Am. Chem. Soc.* **112** (1990), 7973.
36. (a) G. Sanyal, *Ann. N. Y. Acad. Sci.* **429** (1984), 165; (b) G. Sanyal and T. H. Maren, *J. Biol. Chem.* **256** (1981), 608.
37. T. Kararli and D. N. Silverman, *J. Biol. Chem.* **260** (1985), 3484.
38. A. Liljas *et al.*, *Nature* **235** (1972), 131.
39. K. K. Kannan *et al.*, *Proc. Natl. Acad. Sci. USA*, **72** (1975), 51.
40. E. A. Eriksson *et al.*, in Reference 21, p. 317.
41. S. Lindskog in Reference 21, p. 307.

42. E. Clementi *et al.*, *FEBS Lett.* **100** (1979), 313.
43. B. P. N. Ko *et al.*, *Biochemistry* **16** (1977), 1720.
44. A. Ikai, S. Tanaka, and H. Noda, *Arch. Biochem. Biophys.* **190** (1978), 39.
45. I. Bertini, C. Luchinat, and A. Scozzafava, *Struct. Bonding* **48** (1982), 45.
46. A useful review by W. W. Cleland on pH-dependent kinetics can be found in *Methods Enzymol.*, 1987, 390.
47. Y. Pocker and S. Sarkanen, *Adv. Enzymol.* **47** (1978), 149.
48. I. Bertini and C. Luchinat, *Acc. Chern. Res.* **16** (1983), 272.
49. S. Lindskog and I. Simonsson, *Eur. J. Biochem.* **123** (1982), 29.
50. B.-H. Jonsson, H. Steiner, and S. Lindskog, *FEBS Lett.* **64** (1976), 310.
51. H. Steiner, B.-H. Jonsson, and S. Lindskog, *Eur. J. Biochem.* **59** (1975), 253.
52. D. N. Silverman *et al.*, *J. Am. Chem. Soc.* **101** (1979), 6734.
53. S. H. Koenig *et al.*, *Pure Appl. Chem.* **40** (1974), 103.
54. I. Simonsson, B.-H. Jonsson, and S. Lindskog, *Eur. J. Biochem.* **93** (1979), 4.
55. T. J. Williams and R. W. Henkens, *Biochemistry* **24** (1985), 2459.
56. I. Bertini, C. Luchinat, and M. Monnanni, in Reference 99, p. 139.
57. I. Bertini *et al.*, in Reference 21, p. 371.
58. I. Bertini *et al.*, *Inorg. Chem.* **24** (1985), 301.
59. I. Bertini *et al.*, *J. Am. Chem. Soc.* **100** (1978), 4873.
60. R. C. Rosenberg, C. A. Root, and H. B. Gray, *J. Am. Chem. Soc.* **97** (1975), 21.
61. B. Holmquist, T. A. Kaden, and B. L. Vallee, *Biochemistry* **14** (1975), 1454, and references therein.
62. M. W. Makinen and G. B. Wells, in H. Sigel, ed., *Metal Ions in Biological Systems*, Dekker, **22** (1987).
63. M. W. Makinen *et al.*, *J. Am. Chem. Soc.* **107** (1985), 5245.
64. A. E. Eriksson, Uppsala Dissertation, Faculty of Science, n. 164, 1988.
65. A. E. Eriksson, A. T. Jones, and A. Liljas, *Proteins* **4** (1989), 274.
66. A. E. Eriksson *et al.*, *Proteins* **4** (1989), 283.
67. I. Bertini *et al.*, *Inorg. Chem.*, **31** (1992), 3975.
68. P. H. Haffner and J. E. Coleman, *J. Biol. Chem.* **248** (1973), 6630.
69. I. Bertini and C. Luchinat, *NMR of Paramagnetic Molecules in Biological Systems*, Benjamin/Cummings, 1986.
70. R. D. Brown III, C. F. Brewer, and S. H. Koenig, *Biochemistry* **16** (1977), 3883.
71. I. Bertini, C. Luchinat, and M. Messori, in Reference 62, vol. 21.
72. I. Solomon, *Phys. Rev.* **99** (1955), 559.
73. I. Bertini *et al.*, *J. Magn. Reson.* **59** (1984), 213.
74. L. Banci, I. Bertini, and C. Luchinat, *Magn. Res. Rev.*, **11** (1986), 1.
75. I. Bertini *et al.*, *J. Am. Chem. Soc.*, **103** (1981), 7784.
76. T. H. Maren, A. L. Parcell, and M. N. Malik, *J. Pharmacol. Exp. Theor.* **130** (1960), 389.
77. J. E. Coleman, *J. Biol. Chem.* **243** (1968), 4574.
78. S. Lindskog, *Adv. Inorg. Biochem.* **4** (1982), 115.
79. G. Alberti *et al.*, *Biochim. Biophys. Acta* **16** (1981), 668.
80. J. I. Rogers, J. Mukherjee, and R. G. Khalifah, *Biochemistry* **26** (1987), 5672.
81. C. Luchinat, R. Monnanni, and M. Sola, *Inorg. Chim. Acta* **177** (1990), 133.
82. L. Morpurgo *et al.*, *Arch. Biochem. Biophys.* **170** (1975),360.
83. I. Bertini and C. Luchinat, in K. D. Karlin and J. Zubieta, eds., *Biological and Inorganic Copper Chemistry,* vol. 1, Adenine Press, 1986.
84. I. Bertini *et al.*, *J. Chem. Soc., Dalton Trans.* (1978), 1269.
85. P. H. Haffner and J. E. Coleman, *J. Biol. Chem.* **250** (1975), 996.
86. I. Bertini *et al.*, *J. Inorg. Biochem.* **18** (1983), 221.
87. I. Bertini, E. Borghi, and C. Luchinat, *J. Am. Chem. Soc.* **102** (1979), 7069.
88. I. Bertini *et al.*, *J. Am. Chem. Soc.* **109** (1987), 7855.
89. P. Yeagle, Y. Lochmtiller, and R. W. Henkens, *Proc. Natl. Acad. Sci. USA* **48** (1975), 1728.
90. P. J. Stein, S. T. Merrill, and R. W. Henkens, *J. Am. Chem. Soc.* **99** (1977), 3194.

91. P. S. Hubbard, *Proc. Roy. Soc. London* **291** (1966), 537.
92. A. Lanir and G. Navon, *Biochemistry* **11** (1972), 3536.
93. J. J. Led and E. Neesgard, *Biochemistry* **26** (1987), 183.
94. N. B.-H. Johnsson *et al.*, *Proc. Natl. Acad. Sci. USA* **77** (1980), 3269.
95. J. L. Evelhoch, D. F. Bocian, and J. L. Sudmeier, *Biochemistry* **20** (1981), 4951.
96. J.-Y. Liang and W. N. Lipscomb, *Proc. Natl. Acad. Sci. USA* **87** (1990), 3675.
97. K. M. Merz, *J. Mol. Biol.* **214** (1990), 799.
98. C. A. Fierke, T. L. Calderone, and J. F. Krebs, *Biochemistry* **30** (1991) 11054.
99. M. Aresta and G. Forti, eds., *Carbon Dioxide as a Source of Carbon*, Reidel, 1987.
100. M. Aresta and J. V. Schloss, eds., *Enzymatic and Model Carboxylation and Reduction Reactions for Carbon Dioxide Utilization*, Kluwer, 1990.
101. C. K. Tu and D. N. Silverman, *J. Am. Chem. Soc.* **108** (1986), 6065.
102. E. Chaffee, T. P. Dasgupta, and J. M. Harris, *J. Am. Chem. Soc.* **95** (1973), 4169.
103. J. B. Hunt, A. C. Rutenberg, and H. Taube, *J. Am. Chem. Soc.* **74** (1983), 268.
104. R. S. Brown, N. J. Curtis, and J. Huguet, *J. Am. Chem. Soc.* **103** (1981), 6953.
105. I. Tabushi and Y. Kuroda, *J. Am. Chem. Soc.* **106** (1984), 4580.
106. I. Bertini *et al.*, *Gazz. Chim. Ital.* **118** (1988), 777.
107. L. Meriwether and F. H. Westheimer, *J. Am. Chem. Soc.* **78** (1956), 5119.
108. D. A. Buckingham, D. M. Foster, and A. M. Sargeson, *J. Am. Chem. Soc.* 92 (1970), 6151.
109. M. L. Bender, R. J. Bergeron, and M. Komiyama, *The Bioorganic Chemistry of Enzymatic Catalysis*, Wiley, 1984.
110. B. Anderson *et al.*, *J. Am. Chem. Soc.* **99** (1977), 2652.
111. M. L. Bender and B. W. Tumquest, *J. Am. Chem. Soc.* **77** (1955), 4271.
112. D. L. Miller and F. H. Westheimer, *J. Am. Chem. Soc.* **88** (1966), 1514.
113. H. Kroll, *J. Am. Chem. Soc.* **74** (1952), 2036.
114. D. A. Buckingham, D. M. Foster, and A. M. Sargeson, *J. Am. Chem. Soc.* **90** (1968), 6032.
115. R. Breslow, in R. F. Gould, ed., *Bioinorganic Chemistry (Advances in Chemistry Series*, vol. **100**), American Chemical Society, 1971; Chapter 2.
116. A. Schepartz and R. Breslow, *J. Am. Chem. Soc.* **109** (1987), 1814.
117. J. T. Groves and R. R. Chambers, Jr., *J. Am. Chem. Soc.* **106** (1984), 630.
118. M. A. Wells and T. C. Bruice, *J. Am. Chem. Soc.* **99** (1977), 5341.
119. H. Sigel, ed., *Metal Ions in Biological Systems*, Dekker, **5** (1976).
120. N. E. Dixon and A. M. Sargeson, in Reference 33.
121. R. W. Hay, G. Wilkinson, R. D. Gillard, and J. A. McCleverty, eds., in *Comprehensive Coordination Chemistry*, Pergamon Press, 1987.
122. D. C. Rees, M. Lewis, and W. N. Lipscomb, *J. Mol. Biol.* **168** (1983), 367.
123. D. C. Rees *et al.*, in Reference 21, p. 155.
124. D. S. Auld, K. Larson, and B. L. Vallee, in Reference 21, p. 133.
125. W. J. Rutter, personal communication.
126. D. Hilvert et al., *J. Am. Chem. Soc.* **108** (1986), 5298.
127. S. J. Gardell *et al.*, *J. Biol. Chem.* **262** (1987), 576.
128. D. S. Auld *et al.*, *Biochemistry*, **31** (1992), 3840; W. L. Mock and J. T. Tsay, *J. Biol. Chem.* **263** (1988), 8635.
129. G. Shoham, D. C. Rees, and W. N. Lipscomb, *Proc. Natl. Acad. Sci. USA* **81** (1984), 7767.
130. K. F. Geoghegan *et al.*, *Biochemistry* **22** (1983), 1847.
131. I. Bertini *et al.*, *J. Inorg. Biochem.* **32** (1988), 13.
132. C. Luchinat *et al.*, *J. Inorg. Biochem.* **32** (1988), 1.
133. R. Bicknell *et al.*, *Biochemistry* **27** (1988), 1050.
134. I. Bertini *et al.*, *Biochemistry* **27** (1988), 8318.
135. M. E. Sander and H. Witzel, in Reference 21, p. 207.
136. M. W. Makinen, in Reference 21, p. 215.
137. D. W. Christianson and W. N. Lipscomb, *Acc. Chem. Res.* **22** (1989), 62.

138. D. W. Christianson *et al.*, *J. Biol. Chem.* **264** (1989), 12849.
139. B. W. Matthews, *Acc. Chem. Res.* **21** (1988), 333, and references therein.
140. B. S. Cooperman, in Reference 119.
141. D. M. Blow, J. J. Birktoft, and B. S. Hartley, *Nature* **221** (1969), 337.
142. R. C. Nordlie, in P. D. Boyer, ed., *T he Enzymes*, Academic Press, 3d ed., **4** (1975), 543.
143. R. Breslow *et al.*, *Proc. Natl. Acad. Sci. USA* **80** (1983), 4585.
144. H. W. Wyckoff *et al.*, *Adv. Enzymol.* **55** (1983), 453.
145. E. E. Kim and H. W. Wyckoff, *J. Mol. Biol.* **218** (1991), 449.
146. L. Banci *et aI.*, *J. Inorg. Biochem.* **30** (1987), 77.
147. P. Gettins and J. E. Coleman, *J. Biol. Chem.* **259** (1984), 11036.
148. I. Bertini *et al.*, *Inorg. Chem.* **28** (1989), 352.
149. A. Chaidaroglou *et al.*, *Biochemistry* **27** (1988), 8338.
150. E. C. Dinovo and P. D. Boyer, *J. Biol. Chem.* **246** (1971), 4586.
151. H. Dutler, A. Ambar, and J. Donatsch, in Reference 21, p. 471.
152. H. Eklund and C.-I. Bränden, in *Biological Macromolecules and Assemblies*, Wiley, 1985.
153. C.-I. Branden *et al.*, *The Enzymes* **11** (1975), 104.
154. E. S. Cedergren-Zeppezauer, in Reference 21, p. 393.
155. H. Theorell, *Feder. Proc.* **20** (1961), 967.
156. M. W. Makinen and W. Maret, in Reference 21, p. 465.
157. J. Kvassman and G. Pettersson, *Eur. J. Biochem.* **103** (1980), 565.
158. P. F. Cook and W. W. Cleland, *Biochemistry* **20** (1981),1805.
159. I. Bertini *et al.*, *J. Am. Chem. Soc.* **106** (1984), 1826.
160. W. Maret *et al.*, *J. Inorg. Biochem.* **12** (1980), 241.
161. H. B. Gray and E. I. Solomon, in Reference 27, p. 1.
162. J. S. Valentine and M. W. Pantoliano, in Reference 27, p. 291.
163. M. F. Dunn, A. K. H. MacGibbon, and K. Pease, in Reference 21, p. 486.
164. I. Bertini *et al.*, *Eur. Biophys. J.* **14** (1987), 431.
165. W. Maret and M. Zeppezauer, *Biochemistry* **25** (1986), 1584.
166. C. Sartorius, M. Zeppezauer, and M. F. Dunn, *Rev. Port. Quim.* **27** (1985), 256; C. Sartorius *et al.*, *Biochemistry* **26** (1987), 871.
167. G. Pettersson, in Reference 21, p. 451.
168. E. Garces and W. W. Cleland, *Biochemistry* **8** (1969), 633.
169. B. Edlund *et al.*, *Eur. J. Biochem.* **9** (1969), 451.
170. R. K. Crane, in M. Horkin and E. H. Stotz, eds., *Comprehensive Biochemistry*, Elsevier, **15** (1964), 200.
171. B. M. Babior and J. S. Krouwer, *CRC Crit. Rev. Biochem.* **6** (1979), 35.
172. C. Brink-Shoemaker *et al.*, *Proc. Roy. Soc. London, Ser. A* **278** (1964), 1.
173. B. T. Golding and P. J. Sellars, *Nature* (1983), p. 204.
174. D. Lexa and J. M. Saveant, *Acc. Chem. Res.* **16** (1983), 235.
175. R. A. Firth *et al.*, *Chem. Commun.* (1967), 1013.
176. G. N. Schrauzer and L. P. Lee, *J. Am. Chem. Soc.* **90** (1968), 6541.
177. R. A. Firth *et al.*, *Biochemistry* **6** (1968), 2178.
178. V. B. Koppenhagen and J. J. Pfiffner, *J. Biol. Chem.* **245** (1970), 5865.
179. H. A. O. Hill, in G. L. Eichhorn, ed., *Inorganic Biochemistry*, Elsevier, **2** (1973), 1067.
180. J. Halpern, *Pure. Appl. Chem.* **55** (1983), 1059.
181. J. Halpern, S. H. Kim, and T. W. Leung, *J. Am. Chem. Soc.* **106** (1984), 8317.
182. R. G. Finke and B. P. Hay, *Inorg. Chem.* **23** (1984), 3041; B. P. Hay and R. G. Finke, *Polyhedron* **4** (1988), 1469; R. G. Finke, in C. Bleasdale and B. T. Golding, eds., *Molecular Mechanisms in Bioorganic Processes*, The Royal Society of Chemistry; Cambridge, England (1990).
183. B. P. Hay and R. G. Finke, *J. Am. Chem. Soc.* **108** (1986), 4820.
184. B. P. Hay and R. G. Finke, *J. Am. Chem. Soc.* **109** (1987), 8012.
185. J. M. Pratt, *Quart. Rev.* (1984), 161.

186. J. Halpern, *Science* **227** (1985), 869.
187. B. M. Babier, *Acc. Chem. Res.* **8** (1975), 376.
188. B. T. Golding, in D. Dolphin, ed., B_{12} , Wiley, **2** (1982), 543.
189. N. Bresciani-Pahor *et al.*, *Coord. Chem. Rev.* **63** (1985), 1.
190. J. M. Pratt, *J. Mol. Cat.* **23** (1984), 187.
191. S. M. Chennaly and J. M. Pratt, *J. Chem. Soc., Dalton Trans.* (1980), 2259.
192. *Ibid*., p. 2267.
193. *Ibid*., p. 2274.
194. L. G. Marzilli *et al.*, *J. Am. Chem. Soc.* **101** (1979), 6754.
195. J. Glusker, in Reference 188, **1** (1982), 23.
196. G. De Alti *et al.*, *Inorg. Chim. Acta* **3** (1969), 533.
197. K. Geno and J. Halpern, *J. Am. Chem. Soc.* **109** (1987), 1238.
198. C. Mealli, M. Sabat, and L. G. Marzilli, *J. Am. Chem. Soc.* **109** (1987), 1593.
199. *Nickel and its Role in Biology*, vol. 23 of Reference 62.
200. C. T. Walsh and W. H. Orme-Johnson, *Biochemistry* **26** (1987), 4901.
201. J. F. Riordan and H. Hayashida, *Biochem. Biophys. Res. Commun.* **41** (1970), 122.
202. R. G. Khalifah, J. I. Rogers, and J. Mukherjee, in Reference 21, p. 357.
203. A. Chaidaroglou *et al.*, *Biochemistry* **27** (1988), 8338.
204. C. Forsman *et al.*, *FEBS Lett.* **229** (1988), 360; S. Lindskog *et al.*, in *Carbonic Anhydrase*, F. Botre, G. Gros, and B. T. Storey, eds., VCH, 1991.
205. C. A. Fierke, J. F. Krebs, and R. A. Venters, in *Carbonic Anhydrase*, F. Botre, G. Gros, and B. T. Storey, eds., VCH, 1991.
206. K. Wüthrich, *NMR in Biological Research*, Elsevier-North Holland, 1976.
207. K. Wüthrich, *NMR of Proteins and Nucleic Acids*, Wiley, 1986.
208. I. Bertini, H. Molinari, and N. Niccolai, eds., *NMR and Biomolecular Structure*, Verlag Chemie, 1991.
209. J. T. J. LeComte, R. D. Johnson, and G. N. La Mar, *Biochim. Biophys. Acta* **829** (1985), 268.
210. Recently, ^{67}Zn has been used as a relaxing probe to monitor the binding of ^{13}C-enriched cyanide to zinc in carbonic anhydrase (see Section IV.C).
211. Recent work on HCA II has improved the resolution to 1.54 Å (K. Hakan *et al.*, *J. Mol. Biol.* **227** (1993), 1192). Mutants at positions 143 (R. S. Alexander, S. K. Nair, and D. W. Christianson, *Biochemistry* **30** (1991), 11064) and 200 (1. F. Krebs et al., Biochemistry 30 (1991),9153; Y. Xue *et al.*, *Proteins* **15** (1993), 80) also have been characterized by x-ray methods.
212. An x-ray study of the cyanate and cyanide derivatives of the native enzyme has shown that the anions sit in the cavity without binding to the metal ion (M. Lindahl, L.A. Svensson, and A. Liljas, *Proteins* **15** (1993), 177). Since NCO^- has been shown to interact with the paramagnetic cobalt(II) center, and ^{13}C-enriched cyanide has been shown to interact with ^{67}Zn-substituted CA (see Reference 67), it appears that the structures in the solid state and solution are strikingly different.
213. Recent x-ray data on the adduct of 1,2,4-triazole with HCA II confirm H-bonding with Thr-200 (S. Mangani and A. Liljas, *J. Mol. Biol.* **232** (1993), 9).
214. An HCO_3^--complex of the His-200 mutant of HCA II has been studied by x-ray methods. The data are consistent with the coordinated oxygen being protonated and H-bonded to Thr-199 (Y. Xue *et al.*, *Proteins* **15** (1993), 80).

Contributors and Attributions

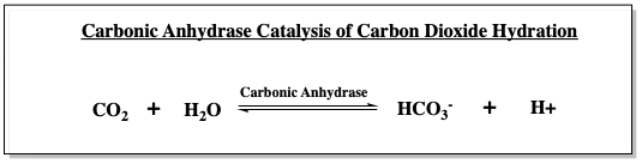
- Ivano Bertini (University of Florence, Department of Chemistry)
- Claudio Luchinat (University of Bologna, Institute of Agricultural Chemistry)

7.5: The Reaction Pathways of Zinc Enzymes and Related Biological Catalysts is shared under a not declared license and was authored, remixed, and/or curated by LibreTexts.

7.5.1: About Carbonic Anhydrase

Introduction

Carbon-dioxide (CO2) hydration and its mechanism in living systems are of fundamental importance for bioinorganic chemistry. In 1932 the existence of an enzyme catalyzing CO2 hydration in red blood cells was established,31 The enzyme was named carbonic anhydrase (abbreviated CA). In 1939 the enzyme was recognized to contain zinc (Zn).32 Because CO2 is either the starting point for photosynthesis or the endpoint of substrate oxidation, carbonic anhydrases are now known to be ubiquitous, occurring in animals, plants, bacteria, and fungi. Different enzymes from different sources, catalyzing the same reaction and usually having homologous structures, are termed isoenzymes. Thus far, a total of 7 distinct classes of CAs have been identified based upon organism: alpha, beta, gamma, delta, zeta, eta, and theta. Each class may contain multiple isoenzymes. Sometimes the same organism has more than one isoenzyme for a particular function, as is true for human carbonic anhydrase. Humans have 15 CAs that belong to the alpha class; these isozymes vary by location in the body and by catalytic activity. CA is a classic example of a hydrolytic enzyme, one that catalyzes addition or removal of water to a substrate molecule. More specifically, CA catalyzes the reversible conversion of carbon dioxide (CO2) to bicarbonate (HCO3-), also referred to as carbonic acid.



Although hydration of CO2 is spontaneous in water at pH 7, the reaction is kinetically slow (k = 10-1 s-1), too slow to convert all CO2 produced in respiration. Only above pH 9 does the uncatalyzed reaction become fast, owing to direct attack of OH-, which is a much better nucleophile than H2O (k = 104 M-1 s-1, where M-1 refers to the OH- concentration). The figure below compares nucleophilic attack of water versus hydroxide (OH-) on CO2.

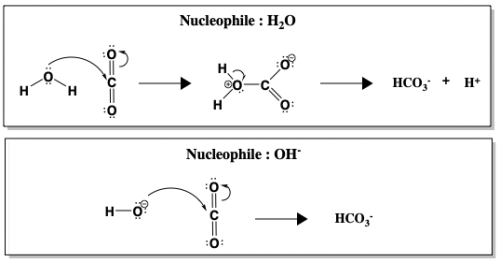


Figure: This figure depicts nucleophilic attack on carbon in carbon dioxide (CO2) in the formation of bicarbonate (HCO3-). In the top panel, H2O is the nucleophile. The bottom panel shows the reaction with hydroxide (OH-) as the nucleophile. Since the OH- is a stronger nucleophile, HCO3- formation is faster when OH- is the nucleophile.

Between H2O and OH-, formation of HCO3- occurs faster when OH- is the nucleophile. A faster reaction at higher pH, when more OH- ions are present, suggests OH- is involved in the rate determining step. However, realistically, the pH of human blood cannot be changed to speed up hydration of CO2. Instead, humans use carbonic anhydrase to catalyse the reaction. When CA is present, the reaction is sped up to a rate of k = 106 s-1.

The ubiquity of CA in different organisms reflects the importance of these enzymes in sustaining life. The speed of CA-catalyzed CO2 hydration is essential to meet the needs of living cells. Some physiological CA functions include pH regulation, electrolyte secretion, ion transport, and CO2 homeostasis. In the digestive tract, CAs plays a role in the secretion of acid and keep saliva neutral by modulating pH.G,H Among these functions, CA most notably plays a role in transport of CO2 and HCO3- related to respiration, the process of atmospheric oxygen and carbon dioxide exchange that occurs when humans inhale oxygen and exhale carbon dioxide. With low solubility, CO2 must be converted to a more soluble form, HCO3-, for transport throughout the body. Bicarbonate ion (HCO3-) eventually reaches the lungs, gets converted back to CO2, and exits the body through exhalation.C

Medical research revolving around CA focuses on the Zn-containing active site as a therapeutic target for various disease treatments; both CA inhibitors and activators are incorporated in drug design. CA inhibitors are used as treatment for epilepsy, ulcers, cancer, obesity, and other neurological disorders. In the eye, CA produces hydrogen ions that maintain optic pressure.

However, too much pressure in the eye can damage the optic nerve and cause glaucoma. CA activity can create a concentration gradient that drives the transport of water to the optical nerve. When too much water is around the optical nerve, pressure around the nerve increases causing damage. Inhibition of CA has become a key treatment of glaucoma.

Beyond pharmaceutical applications, CA has also been investigated for its utility in carbon capture and carbon sensor applications. Carbon capture and storage happens as CAs convert CO2 to bicarbonate. Increased availability of bicarbonate in the presence of calcium ions (Ca2+) causes precipitation of calcite (CaCO3). This process, called bio-mineralization, may be a viable mode of long term storage of CO2 in calcite to mitigate CO2 emissions.

Details about the structure and function of CA's Zn-containing active site have been elucidated over 80 years of research. The current article delves into the metalloenzyme active site using bioinorganic concepts.

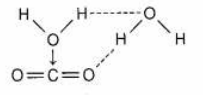
Old Text Below ----------

Carbon-dioxide hydration and its mechanism in living systems are of fundamental importance for bioinorganic chemistry. In 1932 the existence of an enzyme catalyzing CO_2 hydration in red blood cells was established,[31] The enzyme was named carbonic anhydrase (abbreviated CA). In 1939 the enzyme was recognized to contain zinc.[32] Because CO_2 is either the starting point for photosynthesis or the endpoint of substrate oxidation, carbonic anhydrases are now known to be ubiquitous, occurring in animals, plants, and several bacteria. Different enzymes from different sources, catalyzing the same reaction and usually having homologous structures, are termed isoenzymes. Sometimes the same organism has more than one isoenzyme for a particular function, as is true for human carbonic anhydrase.

CO_2 gas is relatively soluble in water (3×10^{-2} M at room temperature under p_{CO2} = 1 atm), equilibrating with hydrogen carbonate at pK_a 6.1:

$$CO_2 + H_2O \rightleftharpoons HCO_3^- + H^- \tag{2.6}$$

The uncatalyzed reaction is kinetically slow around physiological pH ($k \simeq 10^{-1}\ s^{-1}$), whereas, in the presence of the most efficient isoenzyme of CA, the maximal CO_2 turnover number (i.e., the number of substrate molecules transformed per unit time by each molecule of enzyme)[33] is $\simeq 10^6\ s^{-1}$. The uncatalyzed attack by water on CO_2 may be facilitated by two hydrogen-bonded water molecules, one of which activates the carbon by means of a hydrogen bond to a terminal CO_2 oxygen, the other of which binds the carbon atom via oxygen: [34,35]



Only above pH 9 does the uncatalyzed reaction become fast, owing to direct attack of OH^-, which is a much better nucleophile than H_2O ($k \simeq 10^4\ M^{-1}s^{-1}$, where M^{-1} refers to the OH^- concentration):

$$CO_2 + OH^- \rightleftharpoons HCO_3^- \tag{2.8}$$

On the other hand, the rate constant in the presence of the enzyme, called k_{cat}, is pH-independent above pH 8 in every CA isoenzyme (Figure 2.2).[33,36]

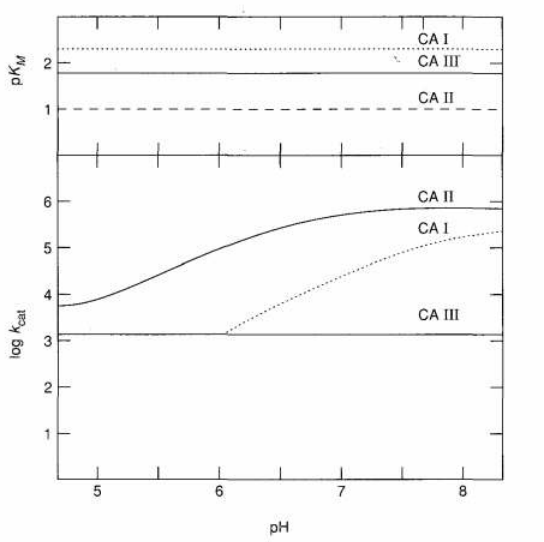


Figure 2.2 - pH dependence of k_{cat} and K_m values for CO_2 hydration catalyzed by carbonic anhydrase I, II, and III isoenzymes.[33,36]

In vitro, carbonic anhydrase is quite versatile, catalyzing several reactions that involve both OH^- and H^+, such as the hydrolysis of esters and the hydration of aldehydes. The various isoenzymes have been characterized to different degrees of sophistication. High-activity forms are labeled II ($k_{cat} \simeq 10^6\ s^{-1}$ at 25 °C); low-activity forms I ($k_{cat} \simeq 10^5\ s^{-1}$), and the very-low-activity forms III ($k_{cat} \simeq 10^3\ s^{-1}$).[37] X-ray structural information at nominal 2 Å resolution is available for HCA I[38] and HCA II,[39] where H indicates human. The structure of HCA II has been refined recently.[40] High-resolution structures of mutants and of their substrate and inhibitor derivatives are being reported.[211] All isoenzymes are single-chain polypeptides, with M.W. about 30 kDa and one zinc ion per molecule. They have the shape of a rugby ball with a crevice 16 Å deep running through the south pole (Figure 2.3 See color plate section, page C-2.). At the bottom of the crevice, the zinc ion is anchored to the protein by three histidine nitrogen atoms and is exposed to solvent. Two histidines (His-94 and His-96, HCA I numbering) are bound to zinc via their Nϵ2 atoms, whereas one (His-119) is bound via its Nδ1 atom (Figure 2.4). It is quite general that histidines bind zinc equally well by either of the two histidine nitrogens, the preference being probably dictated by the steric constraints imposed by the protein folding. The three histidine NH protons are all engaged in H-bonding (Figure 2.4). Histidine-119 is involved in H-bonding with a glutamate residue. As mentioned, this could be a way of controlling the basicity of the metal ligands. A solvent molecule bound to zinc is involved in an H-bond with Thr-199, which in turn is H-bonded to Glu-106. This H-bonding network is important for understanding the subtle structural changes that occur with pH changes; these could, in principle, account for the pH-dependent properties. Although the structure of crystals grown at pH 8 in sulfate-containing buffer gives some indication of a single solvent molecule bound to zinc (Figures 2.3 and 2.5 See color plate section, pages C2, C3.), theoretical studies indicate that two water molecules can be at bonding distances.[42] Such a finding is consistent with spectroscopic studies on other derivatives and with the concept that attachment and detachment of substrates occur through five coordination.

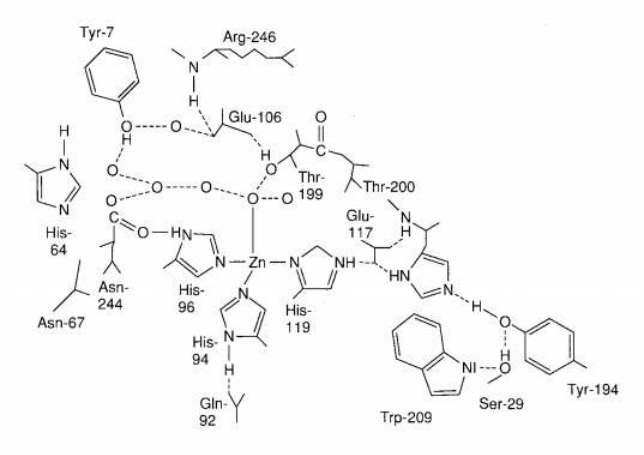


Figure 2.4 - Schematic representation of the active site of human carbonic anhydrase II. Hydrogen bonds (---) and ordered water molecules (o) are indicated.[41]

Just as is true for every zinc enzyme in which zinc is at the catalytic site, activity is lost if the metal is removed, and is restored by zinc uptake. The tertiary structure of carbonic anhydrase is maintained in the absence of zinc; even the denatured apoprotein can refold spontaneously from a random coil to a native-like conformation. Although such a process is accelerated by zinc,[43,44] the presence of the metal does not seem to be an absolute requirement for the correct folding of CA, whereas it is an absolute requirement for several other metalloproteins.[23,29,30]

Anions are attracted in the metal cavity by the positive $Zn(N_3OH_2)^{2+}$ moiety, and are believed to bind to zinc in carbonic anhydrase very effectively; so their use should be avoided as much as possible if the goal is to study the enzyme as it is. When the protein is dialyzed against freshly doubly distilled or carefully deionized water under an inert atmosphere, the pH of the sample approaches the isoelectric point, which is below 6 for HCA I and bovine (BCA II) enzymes. The pH can then be adjusted by appropriate additions of NaOH. All the measurements reported in the literature performed in acetate, phosphate, imidazole, or tris sulfate buffers are affected by the interference of the anion with the metal ion. However, buffer species containing large anions like Hepes (4[(2-hydroxyethyl)-l-piperazinyl]ethanesulfonic acid) can be used,[45] since these anions do not enter the cavity.

There are many indications that zinc in the high-pH form of CA is four-coordinate with an OH group in the fourth coordination site. At low pH the enzyme exists in a form that contains coordinated water; the coordination number can be four (one water molecule) or five (two water molecules). Of course, the occurrence of the low-pH species depends on the pK_a's of the complex acid-base equilibria.

7.5.1: About Carbonic Anhydrase is shared under a not declared license and was authored, remixed, and/or curated by LibreTexts.

7.5.2: Catalytic Mechanism

All the above structural and kinetic information obtained under a variety of conditions with different metal ions can be used to propose a catalytic cycle for carbonic anhydrase (Figure 2.21), As shown by studies on the pH-dependent properties of native and metal-substituted CAs, both type-I and type-II proteins have two acidic groups, the zinc-coordinated water and a free histidine. At physiological pH the enzyme is essentially in the Zn—OH form (step A in Figure 2.21). A Zn—OH moiety is a relatively good nucleophile, poised for nucleophilic attack on carbon dioxide. It is possible that the hydrogen bond with Thr-199, which seems to be consistent with an sp^3 oxygen, orients the OH for attack at the substrate CO_2 . Studies of the copper derivative indicated that the concentration of CO_2 in the cavity is higher than in bulk solution (step B).

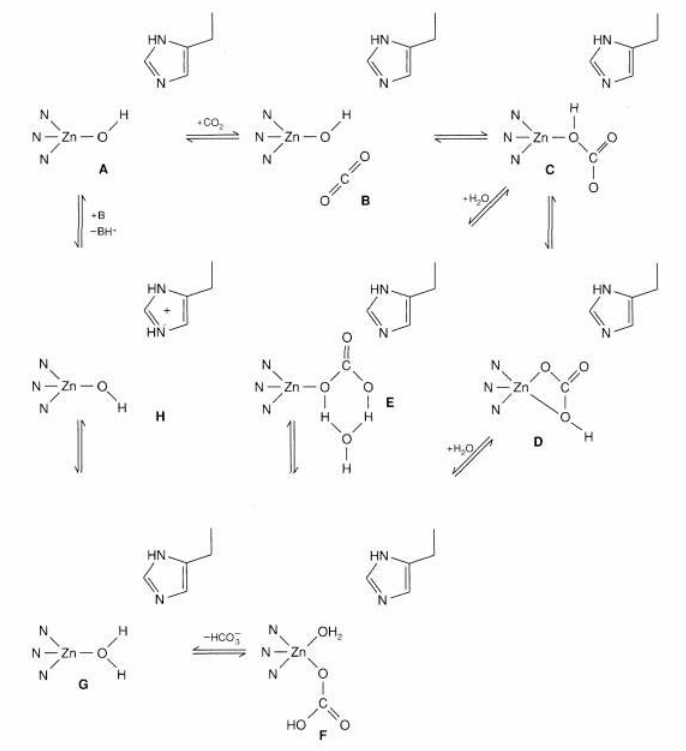


Figure 2.21 - Proposed catalytic cycle of CA.

Molecular dynamics calculations have shown that there are either three[96] or two[97] potential wells for CO_2 in the hydrophobic pocket. It was shown[98] that when Val-143 is replaced by the much larger Phe, the activity decreases by a factor of 10^3. Apparently the large Phe residue does not leave space within the cavity to accomodate CO_2.

It would also be nice if the enzyme were able to activate CO_2. There is no evidence that it does, even though the positive charge around zinc and the NH of Thr-199 would represent two electrostatic attraction points that could activate CO_2. It is well-known that CO_2's interactions with positive charges activate the carbon for nucleophilic attack.[99,100] The positioning of CO_2 between zinc and the peptide NH of Thr-199 would be ideal for the OH attack. Merz[97] locates it as shown in Figure 2.22.

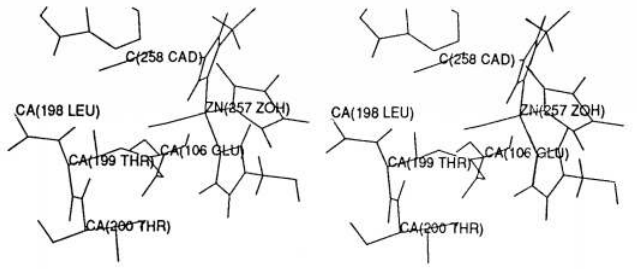


Figure 2.22 - Stereo view of the site of activation of CO_2 in the cavity of CA as proposed by Merz.[97]

It was believed that, once bicarbonate is formed (C), the proton has to transfer to a terminal oxygen atom, either via an intermediate in which bicarbonate is bidentate (D) or via a hydrogen-bond network (E). Indeed, in model compounds one would expect HCO_3^- to bind through a nonprotonated oxygen. However, the possibility of restoring the hydrogen bond with Thr-199 as in sulfonamide adducts could justify the presence of the hydrogen on the coordinating oxygen.[214] The bicarbonate derivative is presumably in equilibrium between four- and five-coordinate species (F), as shown by the electronic spectra of the cobalt derivative.[59] The five-coordinate species provides a low barrier for the substrate detachment step via an associative mechanism involving coordination of a water molecule (G). A possible five-coordinate species would contain bicarbonate in the B site and water in the C site (Figure 2.12). It is reasonable that the measured K_m for the reaction of bicarbonate dehydration is the thermodynamic dissociation constant of the M—HCO_3^- species. Anionic or neutral inhibitors are competitive with bicarbonate because they tend to bind at the same site. At this stage the second substrate, which is H^+, has to be released (H). It is reasonable that the water proton transfers to a group inside the cavity, e.g. , the free histidine mentioned above, and subsequently to the solvent. In the absence of buffers the latter step is rate-limiting for the high-activity isoenzymes, since the diffusion rate cannot exceed the product of the concentration times the diffusion coefficient, i.e., 10^{-7} M x 10^{11} $M^{-1}s^{-1}$. Such a limit is then 10^4 s^{-1}, whereas the turnover rate is 10^6 s^{-1}. The presence of buffer can assist in proton transfer at this stage, in such a way that the rate-limiting step becomes the internal proton transfer. The release of H^+ from the Zn—OH_2 moiety is also the rate-limiting step for the low-activity CA III, as nicely shown by the electronic spectra of CoCA III. These spectra change from the basic form at the beginning of the reaction to the acidic form upon CO_2 addition (Figure 2.23).[101] After the interconversion of CO_2 into bicarbonate, there is an accumulation of the $CoOH_2$ species, the deprotonation of which is slower than the release of HCO_3^-.

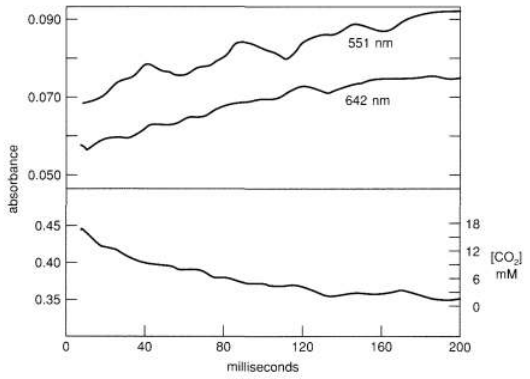


Figure 2.23 - Time dependence of $\epsilon_{15.6}$ and $\epsilon_{18\cdot1}$ of cobalt(II)-substituted CA III after addition of CO_2 to a buffered enzyme solution at pH 8. The initial drop of absorbance reflects the accumulation of a $CoOH_2$ intermediate.[101]

7.5.2: Catalytic Mechanism is shared under a not declared license and was authored, remixed, and/or curated by LibreTexts.

7.5.3: Metal Substitution

With zinc enzymes, metallosubstitution is a convenient tool for monitoring the protein and its function by means of spectroscopic techniques. Furthermore, it is interesting to learn how reactivity depends on the nature of the metal ion and its coordination properties, because much of it depends on the protein structure, which seemingly remains constant. As discussed, zinc enzymes can be studied by replacing zinc with other spectroscopically useful metal ions, whose activities have been checked, and by transferring the information obtained to the native enzyme. The strategy of metal substitution is not limited to zinc enzymes, since it has been used for magnesium-activated enzymes and, occasionally, other metalloenzymes as well.

By dialyzing a protein solution against chelating agents, such as EDTA, 1,10-phenanthroline, or 2,6-dipicolinic acid at moderately acidic pH, or by reversibly unfolding the protein with denaturing agents (as has been done with alkaline phosphatase), one can cause zinc proteins to release their metal ions, giving rise to the corresponding but inactive apoprotein. Sometimes (e.g., by using alcohol dehydrogenase) dialysis against chelating agents can be applied to a suspension of protein microcrystals. In this way the chelating agent is still able to reach and remove the active site metal by slowly diffusing in the crystals through the hydration water, while the apoprotein is maintained in the native conformation by the crystal packing forces and denaturation is avoided. After the chelating agent is dialyzed out, often against a high-salt (e.g., ClO_4^-) buffer to reduce nonspecific binding, a new metalloprotein can obtained by addition of the appropriate metal salt.[23]

Cobalt(II)-substituted zinc proteins often show about as much activity as the native zinc enzymes (Table 2.4). This is a general characteristic of the cobalt-substituted zinc enzymes,[24] since the coordination chemistry of cobalt(II) is very similar to that of zinc(II). The two ions also show virtually identical ionic radii. Cobalt(II) derivatives generally display useful electronic spectra. High-spin cobalt(II) ions are paramagnetic, containing three unpaired electrons ($S = \frac{3}{2}$); thus they can also give rise to EPR spectra. The electronic relaxation times, i.e., the average lifetimes of the unpaired electrons in a given spin state of the S manifold ($-\frac{3}{2}$, $-\frac{1}{2}$, $\frac{1}{2}$, $\frac{3}{2}$), are very short (10^{-11} to 10^{-12} s) at room temperature. In order to detect EPR spectra, the sample temperature is usually decreased, often down to liquid helium temperature, to increase the electronic relaxation times and sharpen the EPR linewidths. On the other hand, as the paramagnetic broadening of the NMR lines in such systems is inversely proportional to the electronic relaxation times (see Section IV.C.3), room-temperature ^1H NMR spectra of cobalt(II) complexes can be easily detected, even in the absence of chemical exchange. Therefore cobalt(II) is an exceptional probe to monitor the structure and reactivity of zinc enzymes. Of course, the transfer of information from the artificial to the native enzyme must be done with caution. However, if we can understand the functioning of the cobalt enzyme, we then have a reference frame by which to understand the kinetic properties of the native enzyme. The spectroscopic properties of cobalt(Il) in cobalt-substituted proteins have been reviewed.[25]

Copper(Il)-substituted zinc proteins are generally inactive with respect to the natural and most artificial substrates (Table 2.4). In model compounds copper(Il) is often principally four-coordinate, with at most two more ligands present at metal-ligand distances that are longer than normal coordination bonds. As a consequence, the ability of zinc to switch between four- and five-coordinate species without any appreciable barrier and with usual metal-donor distances is not mimicked by copper. Furthermore, binding at the four principal coordination positions is generally stronger for copper than for zinc. It follows that substrates may have slow detachment kinetics. These properties are unfavorable for catalysis.

Copper(II) can be easily and meaningfully studied by means of electronic spectroscopy. Moreover, the EPR spectra can be recorded even at room temperature because of the long electronic relaxation times, which are of the order of 10^{-9} s. Because a protein is a macromolecule, it rotates slowly, and the EPR spectra in solution at room temperature look like those of crystalline powders or frozen solutions (powder-like spectra). ENDOR spectra are also easily obtained for copper proteins at low temperatures, because at low temperature the electronic relaxation times are even longer, and saturation of the EPR lines (which is a requirement to obtain ENDOR spectra) is easy to accomplish. The long electronic relaxation times make the broadening effects on the NMR lines of nuclei sensing the metal ion too severe; so these lines, unlike those of cobalt(Il) complexes, generally escape detection. However, if the nucleus under investigation is in fast exchange between a free species in large excess and a bound species, the line may be observed, because the broadening effects are scaled down by a factor equal to the molar fraction of bound species. The nuclear relaxation parameters contain precious structural and/or dynamic information (see Section IV.C.3). The spectroscopic properties of copper(II) in proteins have been extensively reviewed.[26,27]

Cadmium-substituted zinc proteins may also be active (Table 2.4), although usually at higher pH. This observation is readily explained in terms of the pK_a of a coordinated water, which is expected to be higher than that of analogous zinc complexes because

the cadmium ion is larger and polarizes the Cd-OH_2 bond less.

^{113}Cd and ^{111}Cd are nuclei with relatively high sensitivity for NMR spectroscopic study. The ^{113}Cd chemical shift spans from -200 to 800 ppm relative to $CdSO_4$ in H_2O, depending on the number and nature of donor atoms.[24,28] Sulfur donor atoms cause larger downfield shifts than oxygens or nitrogens, and the downfield shift increases with decreasing number of donor atoms. Therefore, ^{113}Cd NMR probes have been used extensively to study zinc enzymes, metal-storage proteins like thioneins, and other proteins with cysteine ligands, and chemical shifts in various cadmium proteins, together with the proposed ligand donor set, have been obtained (Figure 2.1).

Manganese(II)-containing proteins give rise to detectable EPR signals; however, their interpretation in terms of structure and dynamics is not always informative. The electronic relaxation times of Mn^{2+} are the longest among metal ions, of the order of 10^{-8} s at room temperature and at the magnetic fields of interest. This property and the large S = $\frac{5}{2}$ value account for a large NMR linewidth, even larger than in copper(II) systems. Manganese(II)- and nickel(II)- substituted zinc proteins have often been reported to have fractional activity (Table 2.4).[24] Several efforts have been devoted to Mn(II) derivatives, especially by studying the NMR signals of nuclei in molecules that exchange rapidly with the metalloprotein.

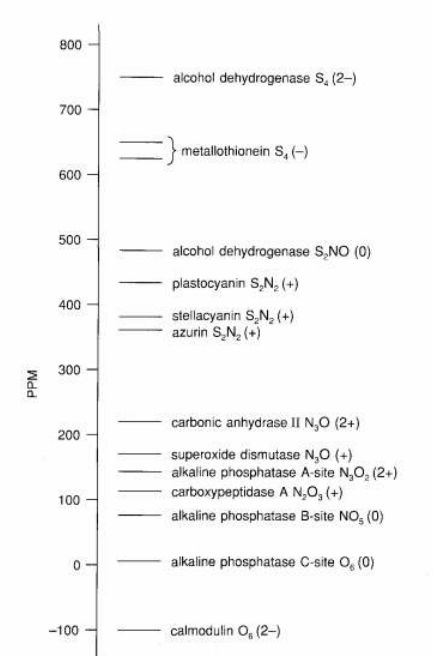


Figure 2.1 - ^{113}Cd chemical shifts in cadmium(II)-substituted metalloproteins. [24,28] Donor sets and overall charges (in parentheses) of the complexes are indicated.

Finally, several other metal-substituted zinc metalloprotein derivatives have been prepared, including those of VO^{2+} , Fe(II), Co(III), Pt(II), and $HgCl_2$. Although these systems add little directly to our understanding of the relationship between structure and function of the enzymes, nonetheless they represent new bioinorganic compounds and are of interest in themselves, or can add information on the coordinating capabilities, and reactivity in general, of the residues present in the active cavity.

Under the heading *zinc enzymes* there are several enzymes in which zinc is essential for the biological function, but is not present in the catalytic site. Among the most-studied enzymes, zinc has a structural role in superoxide dismutase, where the ligands are three histidines and one aspartate. In alcohol dehydrogenase there is a zinc ion that has a structural role, besides the catalytically active one. The former zinc has four cysteine ligands. Cysteine ligands are also present in zinc thioneins, which are zinc-storage proteins. The recently discovered class of genetic factors containing "zinc fingers" are zinc proteins in which the metal has an essentially structural role.[29] Such a role may consist of lowering the folding enthalpy of a protein to induce an active conformation or to stabilize a particular quaternary structure.

Zinc may also have a regulatory role; i.e., it does not participate in the various catalytic steps, but its presence increases the catalytic rate. This is a rather loose but common definition. Typically, zinc in the B site of alkaline phosphatase (Section V.B) has such a role, and the ligands are histidines, aspartates, and water molecules.

The enzymes in which zinc plays a structural or regulatory role will not be further discussed here, because they do not participate in the catalytic mechanisms; see the broader review articles.[23] ,[29,30] Rather, we will describe in some detail the enzyme carbonic anhydrase, in order to show how researchers have investigated such complicated systems as enzymes. We will discover as we look at the details of the structures and mechanisms of enzymes that there are large differences between reactivities in solution and in enzymatic cavities. The fundamental properties underlying these differences are still not fully understood.

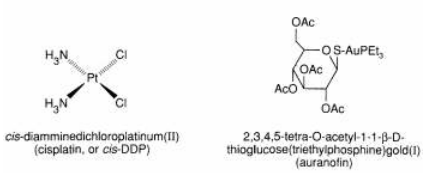
7.5.3: Metal Substitution is shared under a not declared license and was authored, remixed, and/or curated by LibreTexts.

7.6: Metals in Medicine

Metal ions are required for many critical functions in humans. Scarcity of some metal ions can lead to disease. Well-known examples include pernicious anemia resulting from iron deficiency, growth retardation arising from insufficient dietary zinc, and heart disease in infants owing to copper deficiency. The ability to recognize, to understand at the molecular level, and to treat diseases caused by inadequate metal-ion function constitutes an important aspect of medicinal bioinorganic chemistry.

Metal ions can also induce toxicity in humans, classic examples being heavy-metal poisons such as mercury and lead. Even essential metal ions can be toxic when present in excess; iron is a common household poison in the United States as a result of accidental ingestion, usually by children, of the dietary supplement ferrous sulfate. Understanding the biochemistry and molecular biology of natural detoxification mechanisms, and designing and applying ion-specific chelating agents to treat metal overloads, are two components of a second major aspect of the new science that is evolving at the interface of bioinorganic chemistry and medicine.

Less well known than the fact that metal ions are required in biology is their role as pharmaceuticals. Two major drugs based on metals that have no known natural biological function, Pt (cisplatin) and Au (auranofin), are widely used for the treatment of genitourinary and head and neck tumors and of rheumatoid arthritis, respectively. In addition, compounds of radioactive metal ions such as ^{99m}Tc and complexes of paramagnetic metals such as Gd(III) are now in widespread use as imaging agents for the diagnosis of disease. Many patients admitted overnight to a hospital in the U.S. will receive an injection of a ^{99m}Tc compound for radiodiagnostic purposes. Yet, despite the obvious success of metal complexes as diagnostic and chemotherapeutic agents, few pharmaceutical or chemical companies have serious in-house research programs that address these important bioinorganic aspects of medicine.



This chapter introduces three broad aspects of metals in medicine: nutritional requirements and diseases related thereto; the toxic effects of metals; and the use of metals for diagnosis and chemotherapy. Each area is discussed in survey form, with attention drawn to those problems for which substantial chemical information exists. Since there is only a primitive understanding at the molecular level of the underlying biochemical mechanisms for most of the topics, this field is an important frontier area of bioinorganic chemistry. The major focus of this chapter is on the platinum anticancer drug cisplatin, which is presented as a case study exemplifying the scope of the problem, the array of methodologies employed, and the progress that can be made in understanding the molecular basis of a single, if spectacular, metal complex used in medicine today.

II. Metal Deficiency and Disease[1]

A. Essential Metals

B. Anemia and Iron[2]

C. Causes and Consequences of Zinc Deficiency[4-6]

D. Copper Deficiency[7]

E. Summary

III. Toxic Effects of Metals

A. Two Classes of Toxic Metal Compounds

B. Copper Overload and Wilson's Disease[8]

C. Iron Toxicity[9]

D. Toxic Effects of Other Essential Metals[10,11]

E. Plutonium: A Consequence of the Nuclear Age[12]

F. Mercury Toxicity[13] and Bacterial Resistance[14-17]

G. Cadmium and Lead Toxicity[18]

H. Metals as Carcinogens[19,20]

I. Summary

IV. Survey of Metals Used for Diagnosis and Chemotherapy

A. Radiodiagnostic Agents[21,22]

B. Magnetic Resonance Imaging (MRI)[27]

C. Lithium and Mental Health[28-31]

D. Gold and Rheumatoid Arthritis[23,32,33]

E. Anticancer Drugs

1. Platinum Ammine Halides[34,35]
2. Metallocenes and Their Halides: Ti, V, Fe[36,37]
3. Gold and Other Metal Phosphines[39]
4. Other Main Group and Transition-Metal Compounds[36,40,41]

F. Miscellaneous Metals in Medicine

G. Summary and Prospectus

V. Platinum Anticancer Drugs: A Case Study

A. History of Discovery[47]

B. Principles that Underlie Drug Development

1. Strategic Considerations
2. Pre-clinical and Clinical Trials[49]
3. Mechanism of Action Studies

C. Clinical Picture for Cisplatin and Carboplatin[49,52]

1. Responsive Tumors and Combination Chemotherapy
2. Dose-limiting Problems; Toxicology
3. Pharmacology[49,52]

D. Bioinorganic Chemistry of Platinum Anticancer Drugs; How Might They Work?

1. Reactions of *cis*-DDP and Related Compounds in Aqueous, Biological, and Other Media
2. Evidence that DNA is the Target
3. Aspects of Platinum Binding to DNA
4. Mapping the Major Adducts of *cis*- and *trans*-DDP on DNA; Sequence Specificity

5. Structure of Platinum-DNA Complexes
6. Effects of DNA Structure on Platinum Binding
7. Speculations About the Molecular Mechanism
8. Site-Specifically Platinated DNA[154]

E. Design of New Inorganic Anticancer Drugs

1. Objectives
2. Strategies for Drug Development
3. Second- and Third-generation Platinum Anticancer Drugs
4. Nonplatinum Antitumor Metal Complexes

VI. Restrospective

The topics discussed in this chapter are helping to expand bioinorganic chemistry from a subject that arose chiefly from spectroscopic analysis of metal centers in proteins, because they were uniquely convenient functional groups, to a discipline where fundamental knowledge about metal functions and the application of metals as diagnostic and chemotherapeutic agents are making important contributions to medicine. As the case study of cisplatin is intended to demonstrate, progress in understanding how metals function in chemotherapy can be made only by the combined efforts of many disciplines, including synthetic and physical inorganic and organic chemistry, molecular and cell biology, immunology, pharmacology, toxicology, and clinical medicine. Although we have not yet reached the day where chemotherapeutic agents can be rationally designed from knowledge of a molecular mechanism, such a concept does not seem that farfetched. If nothing else, knowledge of fundamental bioinorganic processes related to metal-macromolecule interactions will continue to grow enormously through efforts to achieve this ultimate goal.

VII. References

1. H. Sigel, ed., *Metal Ions in Biological Systems*, Dekker, vol. 14, 1982.
2. D. A. Brown, *Metal Ions Biol. Syst.* **14** (1982), 125.
3. A. D. Young and R. W. Noble, *Methods Enzymol*. **76** (1981), 792.
4. D. A. Phipps, *Metals and Metabolism*, Oxford University Press, 1976, p. 63.
5. G. J. Brewer, *Metal Ions Biol. Syst*. **14** (1982), 57.
6. A. S. Prasad, *Metal Ions Biol. Syst.* **14** (1982), 37.
7. J. R. J. Sorenson, *Metal Ions Biol. Syst.* 14 (1982), 77.
8. D. R. Williams, *An Introduction to Bioinorganic Chemistry*, C. C. Thomas, 1976, p. 327.
9. Reference 8, p. 371.
10. Reference 4, p. 56.
11. Reference 8, p. 372.
12. K. N. Raymond and W. L. Smith, *Struct. Bonding* **43** (1981), 159.
13. Reference 8, p. 366.
14. C. T. Walsh *et al*., *FASEB* **2** (1988), 124.
15. J. G. Wright *et al.*, *Prog. Inorg. Chem*. **38** (1990), 323.
16. J. D. HeImann, L. M. Shewshuck, and C. T. Walsh, *Adv. Inorg. Biochem.* **8** (1990), 331.
17. M. J. Moore *et al*., *Acc. Chem. Res*. **23** (1990), 301.
18. Reference 8, p. 363.
19. Reference I, vol. 10, 1980.
20. K. E. Wetterhahn. *J. Am. Coll. Toxicol.* **8** (1989), 1275.
21. C. J. Mathias *et al.*, *Nucl. Med. Biol.* **15** (1988), 69.
22. A. Yokoyama and H. Saji, *Metal Ions Biol. Syst.* **10** (1980), 313.
23. R. C. Elder and M. K. Eidness, *Chem. Rev*. **87** (1987), 1027.
24. J. C. Dabrowiak, *Adv. lnorg. Chem*. **4** (1982), 70.
25. J. Stubbe and J. W. Kozarich, *Chem. Rev*. **87** (1987), 1107.
26. C. F. Meares and T. G. Wensel, *Acc. Chem. Res*. **17** (1984), 202.

27. R. B. Laufer, *Chem. Rev*. **87** (1987), 901.
28. N. J. Birch, *Metal Ions Biol. Syst.* **14** (1982),257.
29. S. Avissar *et al*., *Nature* **331** (1988), 440.
30. M. C. Espanol and D. Mota de Freitas, *Inorg. Chem*. **26** (1987), 4356.
31. P. F. Worley *et al*., *Science* **239** (1988), 1428.
32. B. M. Sutton, in Reference 159, p. 355.
33. K. C. Dash and H. Schmidbauer, *Metal Ions Biol. Syst.* **14** (1982), 179.
34. M. J. Cleare and J. D. Hoeschele, *Bioinorg. Chem.* **2** (1973), 187.
35. B. Rosenberg *et al*., *Nature* **222** (1969), 385.
36. P. Köpf-Maier and H. Köpf, *Chem. Rev.* **87** (1987), 1137.
37. P. Köpf-Maier and H. Köpf, *Struct. Bonding* **70** (1988), 105.
38. J. H. Toney, C. P. Brock, and T. J. Marks, *J. Am. Chem. Soc.* **108** (1986), 7263.
39. S. J. Bemers-Price and P. J. Sadler, in Reference 41, p. 527.
40. Reference 1, vol. 11, 1980.
41. M. Nicolini, ed., *Platinum and Other Metal Coordination Compounds in Cancer Chemotherapy*, Nijhoff, 1988.
42. Reference 8, p. 316.
43. Reference 4, p. 60.
44. C. C. Hinckley *et aI.*, in Reference 159, p. 421.
45. D. D. Perrin and H. Stiinzi, *Metal Ions Biol. Syst.* **14** (1982), 207.
46. C. Hill, M. Weeks, and R. F. Sehinazi, *J. Med. Chem.* **33** (1990), 2767.
47. B. Rosenberg, *Metal Ions in Biol.* **1** (1980), 1.
48. S. J. Lippard, *Science* **218** (1982), 1075.
49. B. Rosenberg, *Metal Ions Biol. Syst*. **11** (1980), 127.
50. J. M. Paseoe and J. J. Roberts, *Biochem. Pharmacol*. **23** (1974), 1345.
51. J. K. Barton and S. J. Lippard, *Metal Ions in Biol.* **1** (1980), 31.
52. P. J. Loehrer and L. H. Einhorn, *Ann. Intern. Med*. **100** (1984), 704.
53. R. F. Boreh, in Reference 41, p. 216.
54. L. R. Kelland *et al*., *Cancer Res*. **52** (1992), 822.
55. M. E. Howe-Grant and S. J. Lippard, *Metal Ions Biol. Syst.* **11** (1980), 63.
56. R. Faggiani *et al*., *J. Am. Chem. Soc*. **99** (1977), 777.
57. R. Faggiani *et al*., *Inorg. Chem*. **16** (1977), 1192.
58. T. G. Appleton, 1. R. Hall, and S. F. Ralph, in Reference 41, p. 634.
59. M. C. Lim and R. B. Martin, *J. Inorg. Nucl. Chem.* **38** (1976), 1911.
60. S. K. Mauldin *et al*., *Cancer Res*. **48** (1988), 5136.
61. W. I. Sundquist *et al*., *Inorg. Chem*. **26** (1987), 1524.
62. H. C. Harder and B. Rosenberg, *Int. J. Cancer* **6** (1970), 207.
63. J. H. Howle and G. R. Gale, *Biochem. Pharmacol*. **19** (1970), 2757.
64. S. Reslova, *Chem.-Biol. Interact*. **4** (1971), 66.
65. S. Reslova-Vasilukova, in T. A. Connors and J. J. Roberts, eds., *Recent Results in Cancer Research*, Springer, 1974, p. 105.
66. J. J. Roberts and A. J. Thomson, *Prog. Nucl. Acids Res. Mol. Biol*. **22** (1979), 71.
67. D. P. Bancroft, C. A. Lepre, and S. J. Lippard, *J. Am. Chem. Soc*. **112** (1990), 6860.
68. J.-P. Macquet, J.-L. Butour, and N. P. Johnson, in Reference 159, p. 75.
69. N. P. Johnson *et al*., *J. Am. Chem. Soc.* **107** (1985), 6376.
70. R. B. Ciccarelli, unpublished results.
71. J. C. Caradonna and S. J. Lippard, *Inorg. C*hem. **27** (1988), 1454.
72. K. Inagaki and Y. Kidani, *J. Inorg. Biochem.* **11** (1979), 39.
73. B. K. Teo *et al*., *J. Am. Chem. Soc.* **100** (1978), 3225.
74. H. M. Ushay, Ph.D. Dissertation, Columbia University, 1984.
75. A. B. Robins and M. O. Leach, *Cancer Treat. Rep*. **67** (1983), 245.
76. P. Bedford *et al*., *Cancer Res*. **48** (1988), 3019.

77. W. Bauer *et al.*, *Biochemistry* **17** (1978), 1060.
78. J. Filipski *et al.*, *Science* **204** (1979), 181.
79. K. M. Comess, C. E. Costello, and S. J. Lippard, *Biochemistry* **29** (1990), 2102.
80. W. A. Rembers, in *Antineoplastic Agents*, Wiley, 1984; p. 83.
81. S. E. Sherman and S. J. Lippard, *Chem. Rev.* **87** (1987), 1153.
82. J.-P. Macquet and T. Theophanides, *Bioinorg. Chem.* **5** (1975), 59.
83. D. M. L. Goodgame *et al.*, *Biochim. Biophys. Acta* **378** (1975), 153.
84. L. A. Zwelling *et al.*, *Cancer Res.* **38** (1978), 1762.
85. R. B. Ciccarelli *et al.*, *Biochemistry* **24** (1985), 7533.
86. S. J. Lippard and J. D. Hoeschele, *Proc. Natl. Acad. Sci. USA* **76** (1979), 6091.
87. G. L. Cohen *et al.*, *Science* **203** (1979), 1014.
88. S. J. Lippard, *Acc. Chem. Res.* **11** (1978), 211.
89. M. Howe-Grant *et al.*, *Biochemistry* **15** (1976), 4339.
90. J.-L. Butour and J.-P. Macquet, *Eur. J. Biochemistry* **78** (1977), 455.
91. J.-P Macquet and J.-L. Butour, *Biochimie* **60** (1978), 901.
92. S. F. Bellon and S. J. Lippard, *Biophys. Chem.* **35** (1990), 179.
93. J. A. Rice *et aI.*, *Proc. Natl. Acad. Sci. USA* **85** (1988), 4158.
94. H.-M. Wu and D. M. Crothers, *Nature* **308** (1984), 509.
95. S. F. Bellon, J. H. Coleman, and S. J. Lippard, *Biochemistry* **30** (1991), 8026.
96. W. Heiger-Bernays, J. M. Essigmann, and S. J. Lippard, *Biochemistry* **29** (1990), 8461.
97. J. J. Roberts *et al.*, in Reference 41, p. 16.
98. M. F. Pera, C. J. Rawlings, and J. J. Roberts, *Chem.-Biol. Interact.* **37** (1981), 245.
99. A. M. J. Fichtinger-Schepman *et al.*, in Reference 41, p. 32.
100. D. J. Beck *et al.*, *Nucleic Acids Res.* **13** (1985), 7395.
101. J. D. Page *et al.*, *Biochemistry* **29** (1990), 1016.
102. G. A. Curt, N. J. Clendeninn, and B. A. Chabner, *Cancer Treat. Rep.* **68** (1984), 87.
103. W. H. DeJong *et al.*, *Cancer Res.* **43** (1983), 4927.
104. A. Eastman and N. Schulte, *Biochemistry* **27** (1988), 4730.
105. A. Eastman *et al.*, in Reference 41, p. 178.
106. V. M. Richon, N. Schulte, and A. Eastman, *Cancer Res.* **47** (1987), 2056.
107. B. A. Donahue *et al.*, *Biochemistry* **29** (1990), 5872.
108. P. J. Stone, A. D. Kelman, and F. M. Sinex, *J. Mol. Biol.* **104** (1976), 793.
109. P. J. Stone, A. D. Kelman, and F. M. Sinex, *Nature* **251** (1974), 736.
110. H. M. Ushay, T. D. Tullius, and S. J. Lippard, *Biochemistry* **20** (1981), 3744.
111. T. D. Tullius and S. J. Lippard, *J. Am. Chem. Soc.* **103** (1981), 4620.
112. B. Royer-Pokora, L. K. Gordon, and W. A. Haseltine, *Nucleic Acids Res.* **9** (1981), 4595.
113. M. C. Poirier *et al.*, *Proc. Natl. Acad. Sci USA* **79** (1982), 6443.
114. S. J. Lippard *et al.*, *Biochemistry* **22** (1983), 5165.
115. E. Reed *et al.*, *J. Clin. Invest.* **77** (1986), 545.
116. M. C. Poirier *et al.*, *Environ. Health Persp.* **62** (1985), 49.
117. W. L Sundquist, S. J. Lippard, and B. D. Stollar, *Proc. Natl. Acad. Sci. USA* **84** (1987), 8225.
118. A. Eastman, *Biochemistry* **25** (1986), 3912.
119. A. M. J. Fichtinger-Schepman *et al.*, *Biochemistry* **24** (1985), 707.
120. A. M. J. Fichtinger-Schepman *et al.*, *Chem.-Biol. Interact.* **55** (1975), 275.
121. A. C. M. Plooyetal., *Carcinogenesis* **6** (1985), 561.
122. A. M. J. Fichtinger-Schepman *et al.*, *Cancer Res.* 47 (1987), 3000.
123. J. C. Dewan, *J. Am. Chem. Soc.* **106** (1984), 7239.
124. T. W. Hambly, *J. Chem. Soc. Chem. Comm.* (1988), 221.
125. J. H. J. den Hartog *et al.*, *J. Biomol. Struct. Dynam.* **2** (1985), 1137.
126. B. van Hemelryck *et al.*, *Biochem. Biophys. Res. Comm.* **138** (1986), 758.

127. L. S. Hollis *et al.*, in Reference 41, p. 538.
128. R. M. Wing *et al.*, *EMBO* **3** (1984), 1201.
129. J. R. Rubin, M. Sabat, and M. Sundaralingam, *Nucleic Acids Res.* **11** (1983), 6571.
130. S. E. Sherman *et al.*, *Science* **230** (1985), 412.
131. G. Admiraal *et al.*, *J. Am. Chem. Soc.* **109** (1987), 592.
132. S. F. Bellon, T. Takahara, and S. J. Lippard, unpublished results.
133. J. Kozelka *et al.*, *Biopolymers* **26** (1987), 1245.
134. B. Lippert, Prog, Inorg. Chem. 37 (1989), 1.
135. A. L. Pinto and S. J. Lippard, *Proc. Natl. Acad. Sci. USA* **82** (1985), 4616.
136. C. A. Lepre, K. G. Strothkamp, and S. J. Lippard, *Biochemistry* **26** (1987), 5651.
137. D. Gibson and S. J. Lippard, *Inorg. Chem.* **26** (1987), 2275.
138. J. L. van der Veer *et al.*, *J. Am. Chem. Soc.* **108** (1986), 3860.
139. C. A. Lepre *et al.*, unpublished results.
140. W. Saenger, *Principles of Nucleic Acid Structure*, Springer, 1984.
141. B. Malfoy, B. Hartman, and M. Leng, *Nucleic Acids Res.* **9** (1981), 5659.
142. T. D. Tullius and S. J. Lippard, *Proc. Natl. Acad. Sci. USA* **79** (1982), 3489.
143. B. E. Bowler and S. J. Lippard, *Biochemistry* **25** (1986), 3031.
144. B. E. Bowler, Ph.D. Dissertation, Massachusetts Institute of Technology, 1987.
145. J.-M Malinge, A. Schwartz, and M. Leng, *Nucleic Acids Res.* **15** (1987), 1779.
146. W. I. Sundquist *et al.*, *J. Am. Chem. Soc.* **112** (1990), 1590.
147. W. I. Sundquist *et al.*, *J. Am. Chem. Soc.* **110** (1988),8559.
148. D. P. Bancroft *et al.*, *J. Am. Chem. Soc.*, in press.
149. K. M. Comess, *Biochemistry* **25** (1992), 3975.
150. S. L. Bruhn, J. H. Toney, and S. J. Lippard, *Prog. Inorg. Chem.* **38** (1990), 477.
151. A. Sancar and G. B. Sancar, *Annu. Rev. Biochem.* **57** (1988), 29.
152. J. H. Toney *et al.*, *Proc. Natl. Acad. Sci. USA* **86** (1990), 8328; S. L. Bruhn *et al.*, *Proc. Natl. Acad. Sci. USA* **89** (1992), 2307; P. M. Pil and S. J. Lippard, *Science* **256** (1992), 234.
153. S. J. Brown, P. J. Kellett, and S. J. Lippard, *Science* **261** (1993), 603.
154. L. J. Naser *et al.*, *Biochemistry* **27** (1988), 4357.
155. S. E. Sherman *et al.*, *J. Am. Chem. Soc.* **107** (1988), 7368.
156. E. Rotondo *et al.*, *Tumori* **69** (1983), 31.
157. V. Brabec, O. Vrana, and V. Kleinwachter, *Studia Biophys.* **114** (1986), 199.
158. G. E. Plum and V. A. Bloomfield, *Biopolymers* **27** (1988), 1045.
159. J. K. Barton, *Chem. Eng. News* **66** (Sept. 26, 1988), 30.
160. S. J. Lippard, *Platinum, Gold. and Other Metal Chemotherapeutic Agents*, American Chemical Socicty, 1983.
161. W. I. Sundquist and S. J. Lippard, *Coord. Chem. Rev.* **100** (1990), 293.
162. I am grateful to the Alexander von Humboldt Foundation for a U.S. Senior Scientist Award, Massachusetts Institute of Technology for sabbatical leave time, and Prof. Drs. W. Herrmann and K. Wieghardt for their kind hospitality, all of which were essential for the preparation of the first draft of this chapter during the spring of 1988. I very much appreciate help from the following individuals: A. Davison, for providing Figure 9.2, and D. L. Bancroft, S. F. Bellon, S. L. Bruhn, J. N. Burstyn, K. M. Comess, G. B. Jameson, C. A. Lepre, and J. T. Toney for commenting critically on the manuscript. I also thank M. Mason for typing the first draft.

Contributors and Attributions

- Stephen J. Lippard (Massachusetts Institute of Technology, Department of Chemistry)

Thumbnail: Cisplatin, $PtCl_2(NH_3)_2$ A platinum atom with four ligands. (Public Domain; Benjah-bmm27).

7.6: Metals in Medicine is shared under a not declared license and was authored, remixed, and/or curated by LibreTexts.

7.6.1: Metal Deficiency and Disease

Essential Metals

Four main group (Na, K, Mg, and Ca) and ten transition (V, Cr, Mn, Fe, Co, Ni, Cu, Zn, Mo, and Cd) metals are currently known or thought to be required for normal biological functions in humans. Table 9.1 lists these elements, their relative abundances, and the medical consequences of insufficient quantities where known. The nutritional requirements for selected members of the essential metals are discussed in the following sections.

Table 9.1 - Essential metals and medical consequences resulting from their deficiency.[a]

a) Data taken from E.-i. Ochiai, *Bioinorganic Chemistry*, Allyn & Bacon, 1977, p. 6

Metal	Abundance	Abundance	Diseases Resulting from Metal Deficiency
	Sea Water mg/1 (ppm)	Earth's Crust mg/1 (ppm)	
Na	1.05×10^{4}	2.83×10^{4}	
K	380	2.59×10^{4}	
M-	1.35×10^{4}	2.09×10^{4}	
Ca	400	3.63×10^{4}	bone deterioration
V	2×10^{-3}	135	
Cr	5×10^{-3}	100	glucose tolerance (?)
Mn	2×10^{-5}	950	
Fe	1×10^{-2}	5.00×10^{4}	anemia
Co	1×10^{-4}	25	anemia
Ni	2×10^{-4}	75	
Cu	3×10^{-3}	55	brain disease, anemia, heart disease
Zn	1×10^{-2}	70	growth retardation, skin changes
Mo	1×10^{-2}	1.5	
Cd	1.1×10^{-4}	0.2	

Anemia and Iron[2]

Anemia results from insufficient oxygen supply, often because of a decrease in hemoglobin (Hb) blood levels. Approximately 65 to 70 percent of total body iron resides in Hb. In the U.S., many foods, especially those derived from flour, are enriched in iron. In third-world countries, however, scarcity of dietary iron is a major contributor to anemia. This information illustrates one important fact about disease that results from metal deficiency, namely, the need for an adequate supply of essential metals in food. A related aspect, one of greater interest for bioinorganic chemistry, is the requirement that metals be adequately absorbed by cells, appropriately stored, and ultimately inserted into the proper environment to carry out the requisite biological function. For iron, these tasks, among others, are performed by specific iron-chelating agents, the storage protein ferritin and the transport protein transferrin, the bioinorganic chemistry of which is extensively discussed in Chapter 1.

Another cause of anemia exists in individuals who have a mutant variety of hemoglobin, HbS, in which valine has been substituted for glutamic acid in the sixth position of the β subunits.[3] Interestingly, extensive studies have shown that this phenomenon, which

leads to sickling of the red blood cells, does not result from failure of the protein to bind heme or from changes in the O_2 binding constant of the iron atom. Rather, deoxy HbS polymerizes into soluble, ordered fibrous structures that lower the ability of blood to carry oxygen effectively to the tissues. These results illustrate the importance of structural features remote from the metal-binding domain in determining the functional characteristics of a metalloprotein.

Causes and Consequences of Zinc Deficiency[4-6]

The average adult contains ~ 2 g of zinc and requires a daily intake of 15 to 20 mg, only half of which is absorbed, to maintain this level. Although food in many technologically advanced societies contains sufficient zinc to afford this balance, zinc deficiencies occur in certain populations where there is either an unbalanced diet or food that inhibits zinc absorption. An especially interesting example of the latter phenomenon is found in certain villages in the Middle East where phytates, organic phosphates present in unleavened bread, chelate zinc ion and render it inaccessible. Zinc deficiency produces growth retardation, testicular atrophy, skin lesions, poor appetite, and loss of body hair. Little is known about the biochemical events that give rise to these varied consequences, although the three most affected enzymes are alkaline phosphatase, carboxypeptidase, and thymidine kinase. About 30 percent of zinc in adults occurs in skin and bones, which are also likely to be affected by an insufficient supply of the element. Zinc deficiency is readily reversed by dietary supplements such as $ZnSO_4$, but high doses (>200 mg) cannot be given without inducing secondary effects of copper, iron, and calcium deficiency.

Copper Deficiency[7]

More copper is found in the brain and heart than in any other tissue except for liver, where it is stored as copper thionein and released as ceruloplasmin or in the form of a complex with serum albumin. The high metabolic rate of the heart and brain requires relatively large amounts of copper metalloenzymes including tyrosinase, cytochrome c oxidase, dopamine-β-hydroxylase, pyridoxal-requiring monamine oxidases, and Cu-Zn superoxide dismutase. Copper deficiency, which can occur for reasons analogous to those discussed above for Fe and Zn, leads to brain disease in infants, anemia (since cytochrome oxidase is required for blood formation), and heart disease. Few details are known about the molecular basis for copper uptake from foods.

Summary

From the above anecdotal cases, for which similar examples may be found for the other metals in Table 9.1, the biological consequences of metal deficiency are seen to result from a breakdown in one or more of the following steps: adequate supply in ingestible form in foodstuffs; absorption and circulation in the body; uptake into cells; insertion into critical proteins and enzymes requiring the element; adequate storage to supply needed metal in case of stress; and an appropriate mechanism to trigger release of the needed element under such circumstances. Only for iron, and to a lesser extent copper and zinc, is there a reasonably satisfying picture of the molecular processes involved in this chain of events. The elucidation of the detailed mechanisms of these phenomena, for example, the insertion of iron into ferritin, remains an exciting challenge for the bioinorganic chemist (see Chapter 1).

7.6.1: Metal Deficiency and Disease is shared under a not declared license and was authored, remixed, and/or curated by LibreTexts.

7.6.2: Toxic Effects of Metals

Two Classes of Toxic Metal Compounds

As intimated in the previous section, the presence of excess quantities of an essential metal can be as deleterious as insufficient amounts. This situation can arise from accidental ingestion of the element or from metabolic disorders leading to the incapacitation of normal biochemical mechanisms that control uptake and distribution phenomena. These possibilities constitute one major class of metal toxicity. The other broad class results from entry of nonessential metals into the cell through food, skin absorption, or respiration. The toxicities associated with this latter class have received much recent attention because of the public health risks of chemical and radioisotopic environmental pollutants.

In this section, we survey examples of both categories, and discuss ways in which bioinorganic chemistry can contribute to the removal of toxic metals and restoration of normal function. One way involves chelation therapy, in which metal-specific chelating agents are administered as drugs to complex and facilitate excretion of the unwanted excess element. The use of desferrioxamine to treat iron poisoning is one example of this approach. A second role of bioinorganic chemistry is to identify fundamental biological mechanisms that regulate metal detoxification, and to apply the principles that emerge to help control the toxic effects of metal ions in the environment. Recent studies of mercury resistance and detoxification in bacteria provide an elegant example of the way in which biochemistry and molecular biology can be used to elucidate events at the molecular level. This work, which has uncovered the existence of metalloregulatory proteins, is described in some detail in Section III.F below. It represents a benchmark by which other investigations into the mechanisms of metal-detoxification phenomena may be evaluated.

Copper Overload and Wilson's Disease[8]

Wilson's disease results from a genetically inherited metabolic defect in which copper can no longer be tolerated at normal levels. The clinical manifestations are liver disease, neurological damage, and brown or green (Kayser-Fleischer) rings in the cornea of the eyes. Patients suffering from Wilson's disease have low levels of the copper-storage protein ceruloplasmin; the gene and gene products responsible for the altered metabolism have not yet been identified. Chelation therapy, using $K_2Ca(EDTA)$, the Ca^{2+} ion being added to replenish body calcium stores depleted by EDTA coordination, 2,3-dimercaptopropan-1-ol (BAL, British Anti-Lewisite), or d-penicillamine to remove excess copper, causes the symptoms to disappear. The sulfhydryl groups of the latter two compounds presumably effect removal of copper as Cu(I) thiolate complexes. Wilson's disease offers an excellent opportunity for modem methodologies to isolate and clone the gene responsible for this altered Cu metabolism, ultimately providing a rational basis for treatment.

Iron Toxicity[9]

Chelation therapy is also used to treat iron overload. Acute iron poisoning, such as that resulting from accidental ingestion of $FeSO_4$ tablets, results in corrosion of the gastrointestinal tract. Chronic iron poisoning, or hemochromatosis, arises from digestion of excess iron usually supplied by vessels used for cooking. A classic case of the latter is siderosis induced in members of the Bantu tribe in South Africa, who consume large quantities of beer brewed in iron pots and who suffer from deposits of iron in liver, kidney, and heart, causing failure of these organs. The chelating agent of choice for iron toxicity is the siderophore desferrioxamine, a polypeptide having a very high affinity for Fe(III) but not for other metals. Ferrioxamine chelates occur naturally in bacteria as iron-transport agents. Attempts to mimic and improve upon the natural systems to provide better ligands for chelation therapy constitutes an active area of bioinorganic research (see Chapter 1).

Toxic Effects of Other Essential Metals[10,11]

When present in concentrations above their normal cellular levels, most of the other metals listed in Table 9.1 are toxic. Calcium levels in the body are controlled by vitamin D and parathyroid hormones. Failure to regulate Ca^{2+} leads to calcification of tissue, the formation of stones and cataracts, a complex process about which little is understood (see Chapter 3). Chronic manganese poisoning, which can occur following ingestion of metal-oxide dust, e.g., among miners in Chile, produces neurological symptoms similar to Parkinson's disease. Neuron damage has been demonstrated. Although Zn toxicity is rare, it can lead to deficiencies in other essential metals, notably calcium, iron, and copper. Cobalt poisoning leads to gastrointestinal distress and heart failure. Metal poisoning by those elements has been treated by chelating agents, most frequently CaNaiEDTA), but the selectivity offered by the

ferrioxamine class of ligands available for iron has not even been approached. Fortunately, there are few cases involving these metals.

Plutonium: A Consequence of the Nuclear Age[12]

Some of the chelating agents developed to treat iron toxicity have found application as therapeutics for plutonium poisoning. Diethylenetriaminepentaacetic acid (DTPA) salts and siderophores are especially effective. Some improvement over the naturally occurring chelates has been made by tailoring the ligand to encapsulate completely the eight-coordinate Pu(IV) center. Although few individuals have been affected, ingestion of ^{239}Pu, for example, as small particles of PuO_2, at nuclear-reactor sites can have dire consequences. ^{239}Pu emits high energy ex particles, leading to malignancies of bone, liver, lung and lymph nodes, to which tissues it is transported by transferrin. With a maximum tolerated dose of only 1.5 μg, plutonium is among the most toxic metals known. We turn now to other, more classic examples of such industrial pollutants.

Mercuy Toxicity[13] and Bacterial Resistance[14-17]

Mercury is released into the environment as Hg(II) ions through weathering of its most common ore, HgS, red cinnabar. Organomercurials of general formula RHgX used in agriculture have also entered the environment as toxic waste. Both RHgX and HgX_2 compounds bind avidly to sulfhydryl groups in proteins, which can lead to neurological disease and kidney failure. Metallothionein is a favored protein target, which may help to limit mercury toxicity. A highly publicized case occurred in 1953 at Minimata, Japan, where 52 people died after eating mercury-contaminated fish and crustaceans near a factory waste outlet. The volatile, elemental form of mercury, Hg(0), is reportedly nontoxic, but its conversion to alkylmercury compounds by anaerobic microorganisms utilizing a vitamin B-12 biosynthetic pathway constitutes a serious health hazard.

Because of the high affinity of mercury for sulfur-donor ligands, mercury poisoning is treated by BAL; N-acetylpenicillamine has also been proposed. Recently, a very interesting natural detoxification system has been discovered in bacteria resistant to mercury; this system, when fully elucidated, might provide important strategies for treating heavy-metal poisoning in humans.

Presumably under environmental pressure, bacteria have developed mechanisms of resistance to HgX_2 and RHgX compounds in which mercury is recycled back to Hg(0). At least five gene products are involved in the bacterial mercury-resistance mechanism. MerT and MerP mediate the specific uptake of mercury compounds. MerB, organomercury lyase, and MerA, mercuric reductase, catalyze two of the reactions, given in Equations (9.1) and (9.2). Plasmids encoding the genes for these two proteins have been isolated. A typical arrangement of genes in the *mer* operon

$$RHgX + H^+ + X^- \xrightarrow[lyase]{organomercury} HgX_2 + RH \tag{9.1}$$

$$Hg(SR)_2 + NADPH + H^+ \xrightarrow[reductase]{mercuric} Hg(0) + NADP^+ + 2RSH \tag{9.2}$$

region of these plasmids is shown in Figure 9.1. The most thoroughly studied gene product is MerR, a metalloregulatory protein that controls transcription of the *mer* genes. In the absence of Hg(II) the MerR protein binds to DNA as a repressor, preventing transcription of the *merT, P, A*, and *B* genes (Figure 9.1) and negatively autoregulating its own synthesis. When Hg(II) is present, transcription of these genes is turned on. Interestingly, the MerR protein remains bound to the same site on DNA whether acting as an activator in the presence of Hg(II) or as a repressor in its absence. Random and site-specific mutagenesis studies implicate several cysteine residues in the carboxyl terminal region of the protein as candidates for the mercury-binding site.

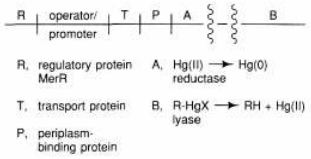
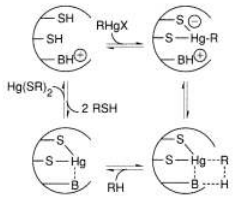


Figure 1, Reference 14).

Organomercury lyase, encoded by the *merB* gene, achieves the remarkable enzymatic step of breaking Hg-C bonds (Equation 9.1). It is a 22-kDa protein with no metals or cofactors. Two cysteine-sulfhydryl groups on the protein have been postulated to effect this chemistry, as depicted in Equation (9.3). Stereochemical studies of the Hg-C bond cleavage revealed retention of configuration, indicating that cleavage of the Hg-C bond probably does not proceed by a radical pathway. A novel concerted S_E2 mechanism has

been suggested. The enzyme turnover numbers, ranging from 1 min^{-1} for CH_3HgCl to 240 min^{-1} for butenylmercuric chloride, although slow, are ~10^5-10^8-fold faster than the nonenzymatic rate.



Mercuric ion reductase, the FAD-containing *merA* gene product, has several pairs of conserved cysteines. From site-specific mutagenesis studies, cysteine residues in the sequence 134-Thr-Cys-Val-Asn-Val-Gly-Cys-140 are known to comprise a redox-active disulfide group; in addition, a redox-inactive pair of cysteines near the carboxyl terminus is also required for the selective reduction of Hg(II). Exactly how the enzyme achieves the chemistry shown in Equation (9.2) is currently uncertain, but the redox activities of the flavin and disulfide/ thiol centers are undoubtedly involved. This enzyme serves both to detoxify mercury supplied directly from the environment as Hg(II) salts and to complete clearance of Hg^{2+} generated by the MerB protein from RHgX compounds. Clearly, Nature has invented a remarkable system to detoxify mercury in this fascinating class of Hg-resistant bacteria.

Cadmium and Lead Toxicity[18]

Gastrointestinal, neurological, and kidney toxicity are among the symptoms experienced by acute or chronic exposure to these heavy metals. The use of unleaded gasoline and the removal of lead-containing pigments from paint have substantially diminished the quantity of this element released to the environment each year. Cadmium sources include alkaline batteries, pigments, and plating. Lead poisoning can be treated by chelation therapy using $CaNa_2$(EDTA) (acute) or penicillamine (chronic). Although both Cd(II) and Pb(II) bind to sulfhydryl groups in thionein, we have little information at the molecular level on the mechanisms by which these elements induce toxicity.

Metals as Carcinogens[19,20]

Although most metal ions have been reported to be carcinogenic, the three most effective cancer-causing metals are Ni, Cr, and, to a lesser extent, Cd. Nickel subsulfide, Ni_2S_3, found in many nickel-containing ores, has been extensively studied and shown to be carcinogenic in humans and other animals. In short-term bioassays including mutagenesis, enhanced infidelity of gene replication *in vitro* and altered bacterial DNA repair were observed. Chromium is most carcinogenic as chromate ion (CrO_4^{2-}), which enters cells by the sulfate uptake pathway and is ultimately reduced to Cr(III) via a Cr(V)-glutathione intermediate species. The latter complex binds to DNA to produce a kinetically inert and potentially damaging lesion. Despite the fact that much information is available about metal-DNA interactions, molecular mechanisms of metal-induced carcinogenesis have not been elucidated. Two aspects of the problem are tumor initiation and tumor development, which are likely to involve different pathways. As new methods become available for studying the molecular events responsible for cancer (oncogenesis), it should be possible for bioinorganic chemists to unravel details of how metals act as carcinogens and as mutagens. Since cancer has genetic origins, metal/nucleic-acid chemistry is likely to be prominent in such mechanisms. As discussed later, metal-DNA interactions are an important aspect of the antitumor drug mechanism of *cis*-$[Pt(NH_3)_2Cl_2]$.

Summary

Toxicity can arise from excessive quantities of either an essential metal, possibly the result of a metabolic deficiency, or a nonessential metal. Both acute and chronic exposure can be treated by chelation therapy, in which hard-soft acid-base relationships are useful in the choice of chelating agent. Since chelates can also remove essential metals not present in toxic amounts, ligands with high specificity are greatly desired. The design and synthesis of such ligands for chelation therapy remains an important objective for the medicinal bioinorganic chemist. Until recently, studies of the toxic effects of metals and their removal, sometimes categorized under "environmental chemistry," have been empirical, with little insight at the molecular level. Application of the new tools of molecular biology to these problems has the potential to change this situation, as illustrated by rapid progress made in cloning the genes and studying the gene products of the mercury-resistance phenotype in bacteria. The discovery of such resistance

phenomena in mammalian cells, and even the remote prospect of transferring Hg-resistant genes from bacteria to humans, are exciting possibilities for the future.

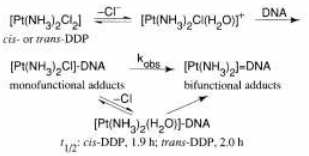
7.6.2: Toxic Effects of Metals is shared under a not declared license and was authored, remixed, and/or curated by LibreTexts.

7.6.3: Aspects of Platinum Binding to DNA

Given that DNA is a major target of platinum binding in cells, it is incumbent upon the bioinorganic chemist to investigate the nature of these interactions and their biological consequences. Of all the ligands studied in coordination chemistry, DNA is surely among the most complex. In the ensuing discussion, we first present experiments that delineate the chemical steps involved in *cis*- and *trans*-DDP binding to DNA as well as the chemical consequences of the adducts formed. We next describe the physical changes in the double helix that accompany platinum binding, and then we discuss the biological consequences that attend the platination of DNA. Subsequent sections describe the major adducts formed, in other words the regiospecificity of the drug, the three-dimensional structures of the adducts, and the way in which different structures within DNA can modulate platinum binding. Finally, we consider the response of the cell to Pt-DNA adducts, including studies with site-specifically modified DNA, and speculate about how this chemistry might relate to the antitumor drug mechanism.

a. Kinetics of Platinum Binding to DNA

The binding of *cis*- and *trans*-DDP to DNA has been studied[67] by ^{195}Pt NMR spectroscopy with the use of isotopically enriched ^{195}Pt, which has a nuclear spin I = $\frac{1}{2}$. The DNA used in this experiment was obtained from chicken red blood cell chromosomes that had been enzymatically degraded to relatively small pieces ranging from 20 to 60 base pairs in length (molecular-weight range 13 to 30 kDa). Since the ^{195}Pt chemical shifts are very sensitive to chemical environment, this NMR study provided important details about the kinetics and mechanism of platinum binding to the biopolymer. The rate-determining step in platination of the DNA is loss of chloride ion (Equation 9.5) to form the monoaqua complex, which rapidly coordinates to a nitrogen donor on the nucleic acid. The identification of the coordinating atom as nitrogen was possible because the ^{195}Pt chemical shift is characteristic of species having one chloride and three nitrogen ligands bound to Pt(II).[67] The spectroscopic changes that accompany the formation of the family of monofunctional adducts are shown in Figure 9.8. Subsequent hydrolysis of the second chloride ion leads to the formation of a second bond with DNA. This sequence of events affords bifunctional adducts and is similarly accompanied by discrete ^{195}Pt spectral changes (Figure 9.8). From the ^{195}Pt chemical-shift range of the final products, it was apparent that the *cis*-$\{Pt(NH_3)_2\}^{2+}$ moiety is bound primarily to two nitrogen donors on the nucleic acid. This chemistry is summarized in Equation (9.10), together with the half-lives for the mono-functional adducts. The half-lives were calculated from a kinetic analysis of the time-dependence of the ^{195}Pt spectral changes. As can be seen, the rates of closure of mono- to bifunctional adducts for the two isomers are quite similar, suggesting that their different biological properties are not a consequence of the kinetics of binding to DNA.



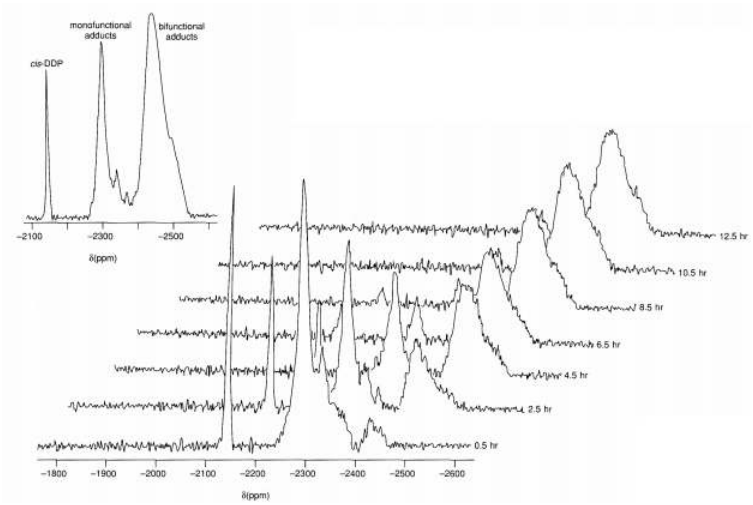


Figure 9.8 - Time course of the reaction between double-stranded chicken erythrocyte DNA and cis-$[Pt(NH_3)_2(H_2O)Cl]^+$ at a D/N = 0.07, in 3 mM NaCl and 1 mM NaH_2PO_4, 37 °C, pH 6.5. Each spectrum consists of 200,000 transients. The inset shows the sum of the individual spectra (reproduced by permission from Reference 67).

The next logical question to address is what donor atoms on DNA are coordinating to platinum in the mono- and bifunctional adducts. This important issue is discussed in considerable detail in Sections V.D.4 and V.D.5. As will be shown, the N7 atoms of the purine bases adenine and guanine are the principal binding sites. Alkylation of DNA at these positions facilitates depurination. Platinum binding to N7 atoms of purines (Figure 9.9), however, stabilizes the glycosidic (N9-C1') linkage.[68-70] Presumably the positive charge is better distributed over the platinum atom and its ligands in the adduct than over a purine alkylated at N7. On the other hand, platinum binding to N7 of guanine does perturb the charge distribution in the purine ring, as evidenced by the lowering of the pK_a of N1 by ≈ 2 units from its value in the unplatinated nucleotide (usually from $pK_a \approx 10$ to $pK_a \approx 8$).[71,72] This effect has been used to assign platinum binding sites in DNA fragments, as discussed below.

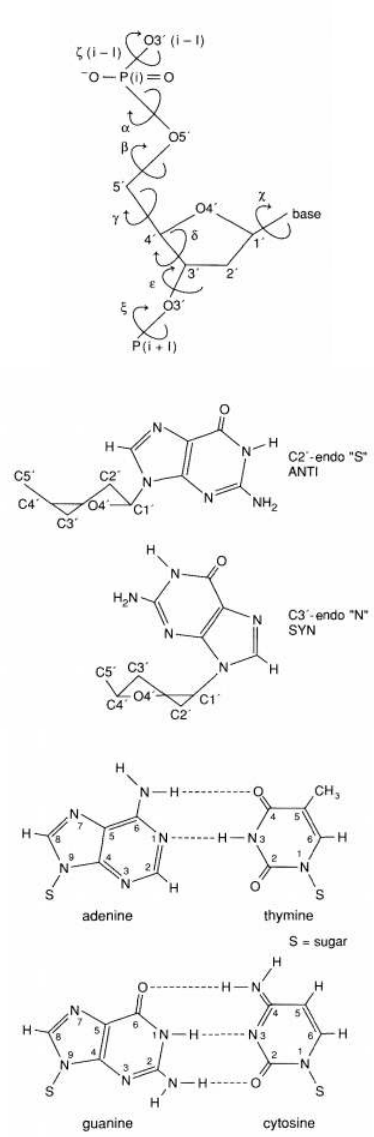


Figure 9.9 - Structural components of DNA. The left panel shows a schematic of the DNA backbone, including the deoxyribose ring numbering scheme and torsion angles. The center panel gives the two main classes of sugar pucker and base orientations. The right panel gives the bases in their Watson-Crick, A-T, and G-C pairs and the base numbering scheme, viewed down the helix axis, with the major grooves pointing toward the top of the figure and the minor grooves toward the bottom.

What are the chemical changes at the platinum center when *cis*-DDP binds to DNA? Both chloride ions are lost from the coordination sphere, as already indicated. Platinum EXAFS studies of calf-thymus DNA modified with *cis*-DDP revealed no chlorine backscattering features characteristic of Pt-CI bonds.[73] The spectra were consistent with the presence of four Pt-N/O linkages, since the technique is unable to distinguish between the two low-Z elements oxygen and nitrogen. Various studies reveal that, under most circumstances, the NH_3 ligands are not lost from DNA upon the binding of platinum ammine halides. For example, when ^{14}C-Iabeled *cis*-[$Pt(NH_2CH_3)_2Cl_2$] was allowed to bind to T7 (47 percent GC content) or *M. luteus* (73 percent GC content) DNA, no loss of radiolabel was found to accompany platinum binding.[74] *In vivo*, however, loss of amine ligands has been observed. Injection of ^{195m}Pt and ^{14}C doubly labeled [$Pt(en)CI_2$] into tumor-bearing mice resulted in unequal distribution of the two labels in various biochemical fractions, but there is no reason to believe that this result is relevant to the antitumor mechanism.[75] Metabolic inactivation of the drug could occur in a variety of ways unrelated to anticancer activity. The best evidence that ammine loss does not occur at the critical biological target of cisplatin is the finding, by using antibodies specific for *cis*-$\{Pt(NH_3)_2\}^{2+}$ nucleotide complexes (see Section V.D.4.c), that DNA, extracted from cells in culture or from human cancer patients treated with *cis*-DDP and subsequently degraded, contains intact Pt-NH_3 Iinkages.[76]

Once bonds are made between Pt and its targets on DNA, they are relatively inert kinetically. Platinum-DNA complexes can be subjected to various physical methods of separation and purification, including gel electrophoresis, ethanol precipitation, centrifugation, and chromatography, as well as to enzymatic and even chemical degradation procedures that digest the DNA, without releasing the platinum. Platinum can be removed, however, either by use of cyanide ion, to form the very stable ($K \sim 10^{41}$) $[Pt(CN)_4]^{2-}$ complex, or by excess thiourea.[77,78] These properties have proved to be extremely valuable in facilitating localization and characterization of the major *cis*- and *trans*-DDP binding sites on DNA.

Although Pt-DNA linkages are, generally speaking, kinetically inert, sometimes a particular adduct will rearrange into a more stable linkage isomer. One interesting example is the product of the reaction of *trans*-DDP with the dodecanucleotide 5'-d(TCTACGCGTTCT).[79] Initially the platinum coordinates to the two guanosine residues, forming a *trans*-$[Pt(NH_3)_2\{d(GCG)\}]$ 1,3-intrastrand crosslink. This complex rearranges to a more stable trans-$[Pt(NH_3)_2\{d(CGCG)\}]$ 1,4-intrastrand crosslink with a half-life of 129 h at 30 °C or 3.6 h at 62 °C. In this rearrangement product the platinum is coordinated to a cytosine and a guanosine residue.

As just described, the binding of bifunctional platinum complexes to DNA proceeds in a stepwise fashion. The second step is sufficiently slow (a few hours), however, that various reagents such as NH_3, nucleobases, and low concentrations of thiourea can coordinate to the fourth site and trap the monoadducts. Generally speaking, however, given sufficient time both *cis*- and *trans*-DDP will bind DNA in a bifunctional manner. As such, they bear some resemblance to organic alkylating agents, such as the nitrogen mustards, which have been employed as anticancer agents.[80]

b. Crosslinking Reactions of Platinum Complexes

There are three broad classes of DNA adducts that can be made by bifunctional platinum complexes. As illustrated for *cis*-DDP in Figure 9.10, they are DNA-protein crosslinks, interstrand DNA-DNA crosslinks, and intrastrand crosslinks,[81] A fourth possibility for platinum complexes is bidentate chelate ring formation utilizing two donor atoms on a nucleotide. For many years, a favored such postulated mode of binding was chelation by the N7-O6 positions of the guanine base (Figure 9.9), since this structure could be formed only by *cis*- and not by *trans*-DDP.[82,83]

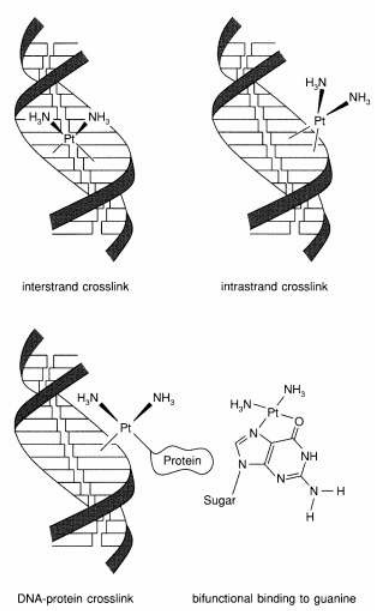


Figure 9.10 - Possible bifunctional binding modes of cis-DDP with DNA (reproduced by permission from Reference 81).

Such a structure has never been observed for *cis*-DDP binding to DNA, however. DNA-protein and interstrand crosslinks formed by platinum complexes have been the focus of many attempts to explain cytotoxicity and antitumor behavior.[84] The technique of alkaline elution, in which crosslinked DNA-DNA strands or DNA-protein molecules bind to filter paper following denaturation under basic conditions, sensitively and easily reveals such adducts. *trans*-DDP forms such adducts more rapidly than the *cis* isomer, perhaps because of its faster chloride-ion hydrolysis rates (see above) and a more favorable geometry, but they also seem to be repaired more rapidly in cells. As will be shown, interstrand and DNA-protein crosslinks are a small minority of adducts formed by

cisplatin, and their contribution to the cytotoxic and anticancer properties of the drug remains to be established. In studies of SV40 replication *in vivo*, DNA-protein crosslinking by *cis*- and *trans*-DDP was shown not to be correlated with the inhibition of DNA replication.[85]

What proteins form crosslinks to DNA? One possibility is the histones that make up the spools around which DNA is wound when packaged into chromatin in the nucleus. Studies[86] of *cis*- and *trans*-DDP binding to nucleosome core particles (each particle made up of eight histone proteins; around each particle is wound a 146-bp piece of DNA in a shallow superhelix of 1.75 turns) revealed the DNA binding to be little affected by the protein core. Both DNA-protein and specific histone crosslinked species were observed; from the latter it was suggested that DDP complexes might be useful crosslinking probes of biological structures. Other proteins likely to form crosslinks to DNA in the presence of platinum complexes are DNA-processing enzymes, or enzymes requiring a DNA template for normal function. In the *in vivo* SV40 study, for example, T antigen was one of the proteins found to be crosslinked to SV40 DNA by cisplatin.[85] Other nuclear proteins such as the high-mobility group (HMG) class are also crosslinked to DNA in the presence of *cis*-DDP. In all cases so far, DNA-protein crosslinking has occurred when platinum was added to cells. There is as yet no evidence that transfection of platinated DNA into cells results in such crosslinking or that crosslinks form during *in vitro* enzymatic digestions of platinated DNAs.

c. Physical Effects of Platinum-DNA Binding

(i). Unwinding, Shortening, and Bending of the Double Helix

Early studies of *cis*- and *trans*-DDP binding to DNA employed closed and nicked circular plasmids.[87] As was described in more detail in Chapter 8, closed circular DNAs are topologically constrained such that any change in the number of helical turns must result in an equal and opposite number of superhelical turns. Any reagent that unwinds the double helix reduces the number of helical turns. Consider, for example, a stretch of DNA that is 360 base pairs (bp) long. Normal B-DNA has ≈ 10.5 bp per turn or a helical winding angle of ≈ 34.3° per bp. Suppose the DNA is unwound, so that there are now 12 bp per turn or a winding angle of ≈ 30°. Instead of 34.3 helical turns (360 ÷ 10.5), the DNA now has only 30 (360 ÷ 12). If this DNA molecule were in the form of a covalently closed circle, the helical unwinding of -4.3 turns would be accompanied by a superhelical winding of +4.3 turns.

Planar organic dyes such as ethidium bromide (EtdBr) and inorganic complexes such as $[Pt(terpy)(HET)]^{+}$ (Figure 9.11) bind to DNA by intercalation, inserting between the base pairs and unwinding the double helix by ~ 26° per molecule bound (Figure 9.12).[88] This unwinding can be measured by monitoring changes in the superhelicity of closed circular DNA. This kind of DNA is subjected to certain topological constraints that lead to the formation of supercoils and superhelical winding that dramatically alter the hydrodynamic properties of the DNA. Either gel electrophoresis or analytical ultracentrifugation can be used to measure this phenomenon. The platinum complexes *cis*- and *trans*-DDP also produce changes in the superhelix density when bound to closed circular DNA.[87] As shown in Figure 9.13, increasing concentrations of platinum bound per nucleotide on the DNA first retard its mobility and then increase its mobility through the gel. These interesting alterations in gel mobility occur because the negatively coiled superhelix unwinds first into an open, or untwisted, form and then into a positively supercoiled form. The conformational changes, which are depicted in Figure 9.14, are directly proportional to the drug-per-nucleotide, or $(D/N)_b$, ratio. In addition to superhelical winding, both platinum complexes increase the mobility of nicked circular DNA in the gels (Figure 9.13). Nicked DNA has one or more breaks in the sugar-phosphate backbone, which relieve the topological constraint and prohibit the DNA from twisting into superhelical structures.

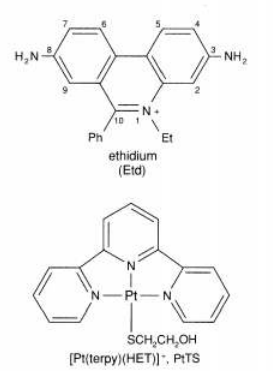


Figure 9.11 - Organic (top) and inorganic (bottom) intercalators.

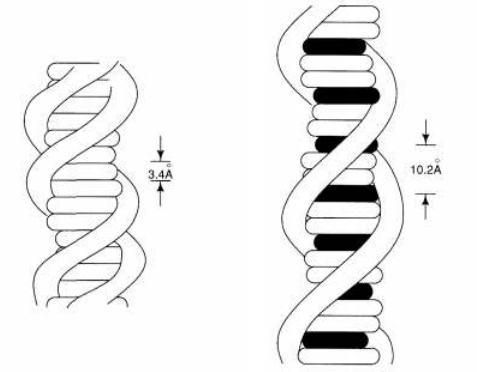


Figure 9.12 - Schematic representation of double-stranded DNA without (left) and with (shaded area, right) a bound intercalator (reproduced with permission from Reference 51).

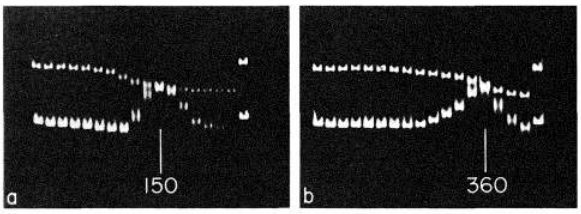


Figure 9.13 - Electrophoresis in 1 percent agarose gels of nicked and closed circular PSMI DNA incubated with (a) cis- and (b) trans-$[Pt(NH_3)_2Cl_2]$ as function of time. After electrophoresis, gels were stained with ethidium bromide. Reproduced with permission from Reference 51.

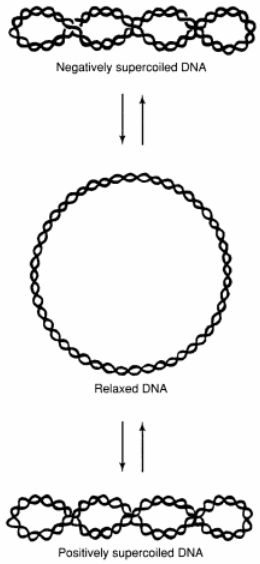


Figure 9.14 - Topological forms of closed circular DNA.

What could be the cause of these physical changes in the DNA structure upon *cis*- or *trans*-DDP binding? Intercalation can be excluded, not only because the compounds do not have the aromatic character normally associated with intercalators (Figure 9.11), but also through studies of the manner by which these and other platinum complexes inhibit the intercalative binding of EtdBr to DNA.[89,90] Platinum metallointercalators such as $[Pt(terpy)(HET)]^+$ are competitive inhibitors of EtdBr binding, as measured by fluorescence Scatchard plots, whereas the non-intercalators *cis*- and *trans*-DDP are not. Moreover, intercalation tends to lengthen and stiffen the double helix, whereas the mobility changes of nicked circular DNAs upon binding of *cis*- or *trans*-DDP were shown by electron microscopy experiments to arise from a pronounced shortening of the DNA with increased Pt binding.

One manner by which *cis*- or *trans*-DDP might produce these physical alterations in DNA structure is by kinking the double helix at or near the binding site. Such an effect could be produced by the bidentate attachment of platinum; the monofunctional $[Pt(dien)Cl]^+$ complex does not have these pronounced effects on DNA secondary structure.[91] Recently, it has been demonstrated that *cis*-DDP binding to DNA does indeed produce a pronounced bend in the helix axis.[92,93] The proof employed a gel-electrophoretic method of analysis that had previously been used to study DNA bending at naturally occurring specific sequences called A-tracts, consisting of five or six adenosine nucleosides in a row followed by about the same number of thymidine residues.[94] When these $d(A_5T_5)_2$ sequences are positioned in the center of a DNA restriction fragment of, say, 150 bp, the mobility of the DNA through polyacrylamide electrophoresis gels is greatly retarded compared to that of a similar DNA fragment where the A-tract is at the end. For the former fragment, the bent molecules presumably cannot snake their way through the pores of the polyacrylamide as well as the molecules whose bends are at the ends and have little effect on the linear structure. It was further shown that A-tracts bend the duplex toward the minor groove of the DNA. Moreover, in a DNA containing multiple A-tracts, the bends must be separated by integral numbers of helical turns (~ 10.5 bp) or else the effect will cancel and the gel mobility will be that of normal DNA of similar length. This latter phenomenon has been referred to as phasing.

With this background information in mind, we can now discuss the experiments with *cis*-DDP that demonstrated bending.[92,93] By methods described in Section V.D.8, a 22-bp oligonucleotide (22-mer) containing self-complementary overhanging ends ("sticky ends") was synthesized with a single *cis*-diammineplatinum(II) moiety linking adjacent guanosine residues (Figure 9.15A). A 22-mer was chosen since it has approximately two helical turns, accounting for some platinum-induced unwinding, and will thus have phased bends when polymerized. This platinated DNA was then labeled with ^{32}P and treated with the enzyme DNA ligase, which seals the ends, producing oligomers of the 22-mer having lengths 22, 44, 66, 88, 110, etc., bp. In these oligomers, the platinum atoms are spaced apart approximately by integral numbers of helical turns. As shown in Figure 9.15, studies of this family of oligomers by gel electrophoresis revealed a pronounced retardation compared to the mobility of unplatinated DNA oligomers of comparable size (line P22 in Figure 9.15B). The plots in this figure show the relative mobilities (R_L) of the different length multimers, compared to a control in which the top strand is not platinated, as a function of the length in base pairs. From the resulting curves may be extracted the extent of cooperative bending. When oligomers of a platinated DNA fragment in which the

metal atoms were spaced apart by 27 bp were examined, their relative mobilities were found to be nearly the same as unplatinated control molecules (line P27 in Figure 9.15B). These experiments unequivocally established that platinum kinks the double helix. As with A-tract-induced bends, the platinum atoms must be phased in order to induce cooperative bending. Comparison of the magnitudes of the gel mobility changes made it evident that *cis*-$\{Pt(NH_3)_2\}^{2+}$ binding produces a bend comparable to that of two A-tracts, ≈ 34°.

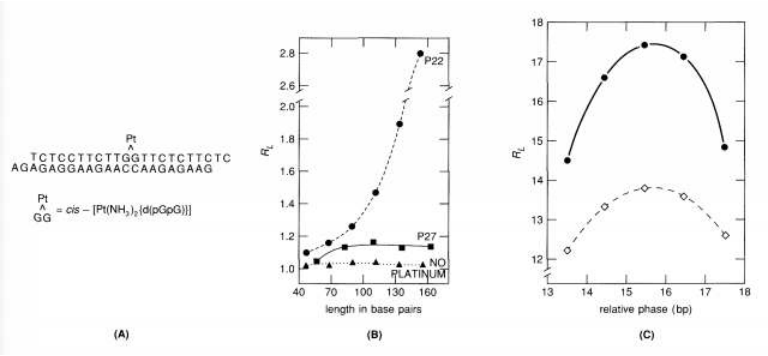


Figure 9.15 - Experiment to demonstrate that cis-$[Pt(NH_3)_2\{d(pGpG)\}]$ intrastrand crosslinks bend duplex DNA by ≈ 34°. Panel A shows the platinated 22-mer sequence, panel B the effect of platination on the gel-electrophoresis mobility of the 22-mer (P22) and a control 27-mer (P27) oligomers, and panel C the mobility of copolymerized DNAs containing cis-DDP and A-tract induced bends (●), 128-bp Pt + A-tract DNA; ♢ , 96-bp Pt + A-tract DNA) that maximize at approximately halfintegral helical turns corresponding to their phasing. For more detail consult Reference 93.

In a related series of experiments,[93] the platinated 22-mer was copolymerized with various A-tract-containing Il-mers to produce ladders of oligomers in which the phasing of Pt with respect to the center of the A-tract was varied, but the Pt atoms were always in phase. The results of these studies showed that maximum gel-mobility retardation occurred when the Pt and A-tract center were spaced apart by half-integral numbers of helical turns (Figure 9.15C). Since A-tracts bend the DNA into the minor groove, this result implies that platinum bends the DNA into the major groove. Only when phased by n/2 (n = integer) turns will copolymers of species situated alternatively in the major and minor grooves of DNA exhibit such cooperative bending. It will be shown later that helix bending of *cis*-DDP-DNA adducts into the major groove is in accord with their known structures.

The ability to prepare site-specifically platinated oligonucleotides (see Section V.D.8) has provided a means for measuring the extent to which *cis*-DDP produces local unwinding of the double helix.[95] When the platinum atoms are positioned with respect to one another, or phased, by exactly integral numbers of helical turns, the retardation of the DNA multimers in the gel is maximized. This phenomenon is illustrated in Figure 9.16, where the R_L values are plotted as a function of the interplatinum spacing for oligonucleotides containing the *cis*-$\{Pt(NH_3)_2d(GpG)\}$ intrastrand crosslink. When the resulting curve was analyzed, the maximum was found to occur at 21.38 bp. Since normal B-DNA has a helical repeat of 10.5 bp, one can compute the effect of platination from the expression [(21.38 - 2(10.5)] bp = 0.38 bp. From the fact that one helical turn of DNA comprises 360° and 10.5 bp, the unwinding of the DNA double helix due to the presence of a single *cis*-$\{Pt(NH_3)_2d(GpG)\}$ intrastrand crosslink can be calculated as

$$\left(\frac{0.38}{10.5}\right) \times 360 = 13^{o}. \qquad (7.6.3.1)$$

Similar studies of DNA platinated with *trans*-DDP have been carried out. In these, oligonucleotides containing the 1,3-*trans*-{Pt(NH3hd(GpNpG)} intrastrand crosslink were examined. The electrophoresis gels of polymerized 15-mers and 22-mers containing this adduct showed cooperative bending. This result indicates that bends at the sites of platination by *trans*-DDP are not phase sensitive, and has been interpreted to imply the formation of a "hinge joint" at these positions.[92,95] The directed bends and local unwinding of DNA produced by cisplatin could be an important structural element that triggers a response by cellular proteins. This subject is discussed in greater detail in Section V.D.7.d.

d. Biological Consequences of Platinum-DNA Binding

(i). Inhibition of Replication

Binding of *cis*-DDP to DNA inhibits replication both *in vivo* and *in vitro*, as shown by a variety of assays. Inhibition of replication of SV40 viral DNA in African green monkey cells as a function of the concentration of added *cis*-DDP is shown in Figure 9.17.

When SV40 virus infects monkey cells, it does not integrate its DNA into the genome of the host. Instead, it forms its own chromosomes in the cell nucleus. These so-called mini-chromosomes consist of ≈ 20 nucleosomes, fundamental chromosome building blocks. SV40 has its own life cycle, using virally encoded and cellular proteins to replicate and, ultimately, reassemble virus particles before lysing the cell and departing to infect neighboring cells.

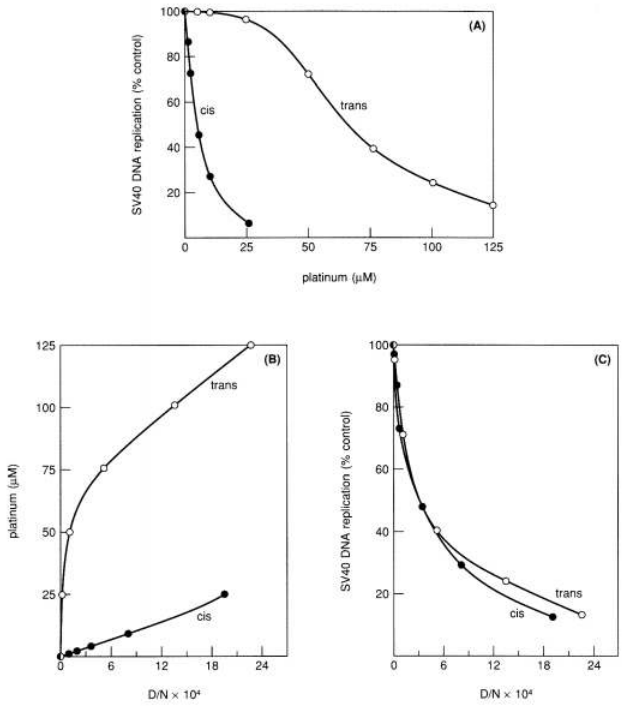


Figure 9.17 - SV40 DNA replication in CV-1 cells as a function of platinum concentration in the medium (panel A) or D/N (panel C). In panel B, DIN is plotted as a function of platinum concentration in the medium. SV40-infected cells were treated with cis-DDP (●) *or trans-DDP* (o) *at the indicated concentrations for 40 h. SV40 DNA replication relative to control (untreated) cells was measured by incorporation of [^{3}H]thymidine, added after the first 24 h of platinum treatment, and Pt in isolated SV40 chromosomes was measured by AAS. The data shown are from a representative experiment. Experiments were carried out in quadruplicate. Reproduced by permission from Reference 85.*

In the experiment shown in Figure 9.17, the SV40-infected cells were treated with cisplatin. After 24 h, [^{3}H]thymidine was added and, after 24 more hours, the cells were harvested, and SV40 DNA was isolated; the amount of DNA synthesis was recorded by comparing incorporated radiolabel with results from control experiments where no platinum was present. The data show that, when 25 μM platinum was present, SV40 DNA replication was reduced to about 5 percent of control. Quantitation reveals that, at ≈ 2 platinum atoms bound per thousand nucleotides (drug-per-nucleotide, or $(D/N)_b$, = 0.002), synthesis is only 10 percent that of control.

Recently, a related series of experiments has been carried out that can monitor DNA synthesis from templates platinated *in vitro*.[96] In this work, DNA plasmids containing the SV40 origin of replication are added to cellular extracts prepared from human kidney cells previously infected with adenovirus. In the presence of large T antigen, a virally encoded protein required for replication, SV40 DNA is synthesized from the plasmid templates. Synthesis can be conveniently monitored by [^{32}P]dATP incorporation. At a $(D/N)_b$ ratio of only 1.7 x 10^{-3}, DNA synthesis is about 5 percent of control, in agreement with the results of the *in vivo* study.

The binding of *cis*-DDP to DNA has also been measured for normal and tumor cells implanted in nude mice and in cells obtained from the ascites fluid of patients with ovarian carcinoma 24 h after their last dose.[97] The data for mouse bone marrow and a human pancreatic tumor xenograft show that, at a dose of 10 mg/kg, (D/Nh platinum binding levels of 3.3 x 10^{-6} and 1.82 x 10^{-6} reduce survival to 20 and 10 percent of control, respectively. These ratios are in good accord with platinum levels required to inhibit DNA synthesis in mammalian cells, as revealed by various studies, but substantially less than that needed for replication inhibition in the SV40 experiments described above. The difference can be readily explained, illustrating an important point. The SV40 genome, like most other DNAs of viral or plasmid origin, consists of only 15,000 nucleotides whereas the nuclear DNA of mammals has about 10^9 nucleotides. Thus, $(D/N)_b$ levels of ~ 10^{-6} would leave 99 out of 100 SV40 DNA molecules with no platinum at all, and

replication would hardly be affected. For the mammalian genome, $(D/N)_b$ values of 10^{-6} place 10^3 platinum atoms on each DNA genome, sufficient to inhibit replication and reduce cell survival. Platinum-DNA binding levels of this magnitude are found for ovarian ascites cells taken from patients receiving cisplatin chemotherapy.[97]

(ii). Mutagenesis and Repair

Apart from inhibition of DNA synthesis, what are the other biological consequences of cisplatin binding to DNA? One such consequence is mutagenesis, in which a normal base in the sequence is replaced by a different base. This phenomenon has been demonstrated for *cis*-DDP-treated cells in a variety of studies. What brings about such mutagenesis? There are several possibilities. One is that errors are introduced in DNA strands during attempts of the replication apparatus to synthesize past a platinum lesion. Another is that the platinum-damaged DNA is recognized by cellular repair systems that, in attempting to eliminate the platinated stretch of DNA, incorporate one or more incorrect nucleotides. Platinum-induced mutagenesis can lead to deleterious long-term health problems in patients treated with cisplatin. It is therefore important to understand the mechanism by which cellular DNA becomes mutated following platination, and to devise strategies for minimizing or eliminating this mutagenesis.

The foregoing considerations bring up another biological consequence of *cis*-DDP binding, namely, DNA repair. Removal of platinum from DNA by cellular repair mechanisms has been demonstrated by several groups. For example, in studying cis-DDP-treated human fibroblast cells in culture, it was found that the amount of bound platinum per nucleotide decreased according to first-order kinetics, from $(D/N)_b$ of 2.3×10^{-5} to 3.3×10^{-6} over a six-day period. Since Pt-DNA adducts are stable with respect to dissociation from DNA under physiological conditions (see above discussion), loss of platinum was attributed to DNA repair.[98]

How does the cell remove platinum from DNA? One mechanism is by a process known as excision repair, whereby the sugar-phosphate backbone on the platinated strand is hydrolyzed ("nicked") on either side of the damage and the remaining, unplatinated strand is used as a template for new DNA synthesis. The platinated oligonucleotide is displaced and the resulting gap filled in. In support of this picture is the fact that, in xeroderma pigmentosum (XP) human fibroblast cells, known to be deficient in excision repair, there is very little removal of platinum during post-treatment incubation.[99] Recent studies of *in vitro* repair of cisplatin-DNA adducts by a defined enzyme system, the ABC excision nuclease of *E. coli*, have provided some details at the molecular level about the process.[100,101] [^{32}P]-Labeled double-stranded DNA fragments containing $\{Pt(NH_3)_2\}^{2+}$ or $\{Pt(en)\}^{2+}$ adducts at random or defined sites were incubated with the enzyme. Cleavage of the platinated strand occurred at the 8th phosphodiester bond 5', and the 4th phosphodiester bond 3', to the GG or AG intrastrand crosslink. Further details about the identification and construction of such specific crosslinks will be given later in this chapter.

(iii). Drug Resistance

Another biological consequence of DNA-platinum interactions, probably related to the repair phenomenon, is resistance. Resistance of a cell to a chemotherapeutic agent, which can be inherent or acquired, is a phenotypical ability of the cell to tolerate doses of a drug that would be toxic to normal, or parent, cells.[102] Resistance is often acquired by prolonged exposure of cells in culture to the drug or, in patients, to repeated doses of drug therapy. There is not yet any direct proof that platinum-DNA interactions are responsible for acquired resistance to cisplatin. Studies of sensitive and resistant tumors in rats have shown, however, that after intravenous injection of 10 mg/kg of the drug, the platinum levels were the same after an hour, but after 24 hours a larger proportion of adducts had been removed in the resistant cells.[103] Similar results have been found for studies of Pt-DNA adducts in cultured L1210 cells of varying levels of resistance to cisplatin where, in the 18 h following a 6-hour incubation with the drug, the resistant cells had up to fourfold more platinum removed than the sensitive cells.[104]

Experiments have also been carried out showing that *cis*-DDP binding to DNA inhibits transcription, the formation of RNA from a gene, and that this phenomenon is less efficiently reversed for parent versus resistant L1210 cells in culture.[105] The assay involves transfection (the process whereby free or viral DNA or RNA is taken into a cell) of pRSVcat plasmid DNA into L1210 cells. The plasmid contains the bacterial *cat* gene in a position that permits its expression in mammalian cells. The *cat* gene encodes the enzyme chloroamphenicol acyltransferase (CAT), an activity readily measured following lysis of the cells. Transfection of the *cis*-DDP-damaged plasmid into resistant L1210 cells showed that up to eight times the amount of platinum was required in the resistant versus sensitive cells to produce a mean lethal hit (63 percent reduction in activity). This result is consistent with greater repair of platinum-DNA adducts in the resistant cells.

These results should not be construed to mean that DNA repair is the only mechanism of cisplatin resistance. There is evidence that relative amounts of glutathione are increased in cisplatin-resistant cells.[106] Glutathione presumably uses its thiol moiety to

coordinate platinum and diminish the amount that can bind to DNA. Reduced influx or increased efflux of a drug constitutes additional mechanisms by which cells become resistant. Further studies are required to ascertain which of these possibilities is most important for the cisplatin resistance phenomenon.

The discovery that cells can become resistant to cisplatin by repairing DNA lesions suggests a way to explain the selectivity of the drug for certain tumor tissue, and even the selective cytotoxicity of the drug for tumor versus normal cells of the same tissue. Tumor cells that cannot repair platinum-DNA adducts would be most affected by *cis*-DDP. This idea forms one of the central hypotheses about the molecular mechanism of action of *cis*-DDP, details of which can be probed by bioinorganic chemists. Specifically, it is important to inquire what DNA adducts formed by *cis*-DDP are both cytotoxic and repairable, what enzymes are responsible for such repair in mammalian cells, by what mechanisms these enzymes operate, and how this knowledge can be used to design better metal-based antitumor drugs and chemotherapeutic protocols.

(iv). DNA-protein Interactions

Most of the phenomena discussed in this section, inhibition of replication, DNA repair, drug resistance, and mutagenesis, probably involve interaction of a protein or group of proteins with platinated DNA. These interactions are clearly important in determining the biological consequences of DNA templates containing bound platinum. Very recent experiments have uncovered the existence of proteins from a variety of mammalian sources that bind specifically to DNA platinated with *cis*- but not *trans*-DDP.[107] Identifying the nature and function of these factors may provide important clues about the mechanisms of antitumor activity, drug resistance, or repair. Study of protein-DNA-drug interactions is an essential feature of the bioinorganic chemistry of platinum chemotherapeutic agents.

7.6.3: Aspects of Platinum Binding to DNA is shared under a not declared license and was authored, remixed, and/or curated by LibreTexts.

7.6.4: Survey of Metals Used for Diagnosis and Chemotherapy

Radiodiagnostic Agents[21,22]

Metal complexes having radioactive nuclei find many applications in medicine, such as in organ, and tissue imaging, Early detection of cancer, for example, by selective and imaging of the tumor using a radioactive metal compound can facilitate surgical removal or chemotherapeutic treatment before the disease reaches an advanced stage. radioisotopes used for diagnostic purposes be emit low-energy γ and no α or β particles. Table 9.2 lists the radionuclides most commonly employed for purpose in nuclear medicine. Among these, ^{99m}Tc is perhaps the most desirable,[23] for it gives off a 140-keV γ ray that is detected scintillation cameras and produces clear images. radionuclide is prepared from an alumina column loaded with $^{99}MoO_4^{2-}$, which decays to form $^{99m}TcO_4^-$, which in turn may be selectively eluted from the column with saline owing to its lower charge. treatment with a reducing agent in the presence of the appropriate ligands produces radiopharmaceuticals with desired water stability, and properties. Such complexes may be injected at concentrations of 10^{-6}-10^{-8} M. For example, isocyanide complexes such as $[Tc(CNR)_6]^+$= t-Bu, $CH_2CO_2Bu^t$, etc.) have been found to be taken up selectively into heart tissue and thus have the potential to be used as heart-imaging agents. Figure 9.2 displays bone as imaged a ^{99m}Tc bone agent. The dark correspond to surface areas of metabolic which can be used to diagnose or disease. One goal of research in this field is to images of myocardial infarcts or clogged arteries for physicians who can watch the patient's heart on a video surgery. Although chemical details responsible for the selective tissue of Tc isocyanide, and other complexes are largely synthetic modifications are and have many new compounds for evaluation.

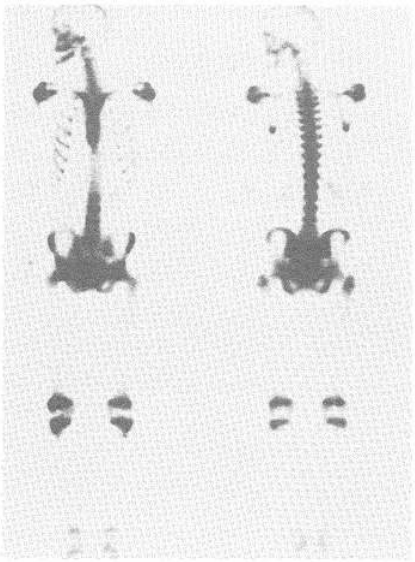


Figure 9.2 - Human skeleton (bone) imaged with ^{99m}Tc. Both anterior (left) and posterior (right) views are shown.

Table 9.2 - Radionuclides most commonly employed in diagnostic nuclear medicine.[a]

a) Data are from Table of the Isotopes in D. R. Lide, ed., *CRC Handbook of Chemistry and Physics*, CRC Press, 71 st ed., 1990-91, pp. 11-33 ff.

Radionuclide	Half-Life	Energy (keV)
^{57}Co	271 d	836
^{67}Ga	78 h	1,001
^{99m}Tc	6 h	140
^{111}In	67 h	172, 247
^{113m}In	104 m	392
^{123}I	13 h	1,230
^{169}Yb	32 d	207
^{197}Hg	64 h	159
^{201}Tl	72 h	135, 167

Among the few known to be absorbed selectively tumor cells is the antitumor antibiotic bleomycin (BLM),[24,25] the structure of which is portrayed in Figure 9.3. binds most radioactive metal ions, but the $^{57}Co(III)$ complex has the best tumor-to-blood ratio. Unfortunately, the long ^{57}Co (Table 9.2) has limited its clinical utility. Attempts to prepare ^{99m}Tc complexes of BLM with selective uptake properties approaching that of the cobalt have not yet been successful, although the target molecule would be a most valuable radiodiagnostic agent. One imaginative solution[26] to this problem was achieved by covalent attachment of an EDTA moiety to the terminal thiazole ring of BLM (Figure 9.3). The resulting Co(III) BLM-EDTA molecule was radiolabeled with $^{111}In^{3+}$ and found to be useful for diagnosis of cancer in humans. Also used for tumor imaging are ^{99m}Tc and ^{67}Ga citrate complexes, the latter being the agent of choice for many applications. Again, there is little known at the molecular level about the mechanism of tumor-cell specificity

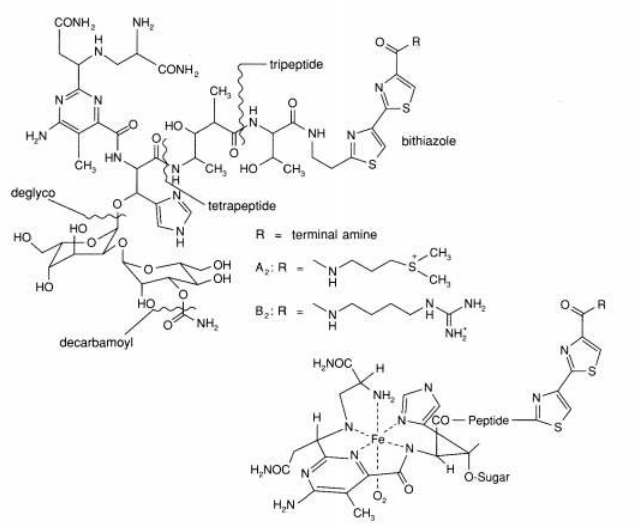


Figure 9.3 - Structure of bleomycin and its proposed iron complex (reproduced by permission from Reference 25).

An alternative approach to radionuclide-based tumor-imaging agents for diagnosis of disease is to modify, with metal chelating agents, antibodies raised against a biological substance, such as a tumor-cell antigen, hormone, or other target. Antibodies are proteins that are synthesized by specialized cells of the immune system in response to an external stimulant, or antigen. The high specificity and affinity of antibodies for the antigen can be used to target the antibody to a particular biological site, such as a site on the membrane of a particular cell type. Chelating agents are now routinely attached to antibodies and used to bind radioactive metal ions. The resulting radionuclide-labeled products are currently under extensive study in diagnostic medicine.[26]

Magnetic Resonance Imaging (MRI)[27]

Nuclear magnetic resonance (NMR) spectroscopy can be used to image specific tissues of biological specimens because of differences in the relaxation times of water proton resonances, usually brought about by paramagnetic metal ions. An early, pioneering example was the demonstration that Mn(lI) salts localize in normal heart-muscle tissue in dogs rather than in regions affected by blocked coronary arteries. Since the paramagnetism of the d^5 Mn(lI) ions alters the relaxation rate of nearby water protons, the normal and diseased tissue could be distinguished. Of the various metal ions surveyed in attempts to provide clinically useful NMR images in humans, Gd(III), Fe(III) , and Mn(lI) were found to give the best proton-relaxation enhancements. The gadolinium complex $[Gd(DTPA)(H_2O)]^{2-}$,an agent currently used in the clinic, has been successfully employed to image brain tumors. Ferric chloride improves gastrointestinal tract images in humans and, as already mentioned, manganous salts can be used for heart imaging. NMR imaging methodologies have advanced to the stage where increases as small as 10 to 20 percent in T_1^{-1}, the inverse nuclear-spin relaxation time, can be detected. As with radionuclide labeling, the complexes must be soluble and stable in biological fluids and relatively nontoxic, and are of greatest value when able to target a specific tissue. Even more important than targeting, however, is that proton relaxivity be maximally enhanced, an objective that depends not only upon the local binding constant but also upon large magnetic moments, long electron-spin relaxation (T_{le}) values, access to and the residence lifetime in the inner and outer coordination spheres by water molecules, and the rotational correlation time of the complex at its binding site. An obvious advantage of paramagnetic NMR over radioisotopic imaging agents is that there is no possibility of radiation damage; on the other hand, the need for 10-100 μM concentrations at the site of imaging is a distinct drawback. Both methods are likely to continue to be used in the future, and both will benefit from the design of new stable chelates that are selectively absorbed by the tissue to be diagnosed.

Lithium and Mental Health[28-31]

One in every 1,000 people in the United States currently receives lithium, as Li_2CO_3, for the treatment and prophylaxis of manic-depressive behavior. Doses of 250 mg to 2 g per day are administered in order to maintain a 0.5 to 2.0 mM concentration window, outside of which the drug is either toxic or ineffective. The detailed molecular mechanism by which Li^+ ion brings about its remarkable chemotherapeutic effects is largely unknown, but there are various theories. One theory proposes that lithium binds to inositol phosphates, inhibiting their breakdown to inositol, and so reducing inositol-containing phospholipids. A consequence of this chain of events would be disruption of the neurotransmission pathway based on inositol 1,4,5-triphosphate and 1,2-diacylglycerol, reducing neuronal communication, which is most likely hyperactivated in the manic state. This theory does not account for the antidepressive action of the drug, however. An alternative explanation is that lithium inhibits cyclic adenosine monophosphate (AMP) formation, again interfering with neurotransmission by intercepting this key intracellular signaling molecule. Recent experiments indicate that lithium affects the activation of G-proteins, a class of guanosine triphosphate (GTP)-binding proteins involved in information transduction. Possibly these effects result from displacement by Li^+ of Mg^{2+} from GTP and/or from protein-binding sites normally required for activation. Use of ^{7}Li NMR spectroscopy to study lithium transport in human erythrocytes suggests that it might be possible to apply this method to unravel details of the bioinorganic chemistry of lithium associated with the management of manic depression.

Gold and Rheumatoid Arthritis[23,32,33]

Gold compounds have been used in medicine for centuries, an application known as chrysotherapy. Since 1940, however, complexes of gold have been used most successfully to treat arthritic disorders in humans and other animals. Au(I) compounds are currently the only class of pharmaceuticals known to halt the progression of rheumatoid arthritis.

Until recently, gold compounds used to treat arthritis were painfully administered as intramuscular injections. Included were colloidal gold metal, colloidal gold sulfides, $Na_3[Au(S_2O_3)_2]$ (Sanocrysin), gold thiomalate and its sodium and calcium salts (Myochrisin), and polymeric gold thioglucose (Solganol, approved by the FDA). It was discovered, however, that triethylphosphinegold(l) tetra-O-acetylthioglucose (auranofin, Figure 9.4, approved by the FDA) was equally effective against rheumatoid arthritis and could be orally administered. The availability of this compound has sparked many studies of its biodistribution, stability, and possible metabolism that lead to antiarthritic activity. The mode of action of antiarthritic gold drugs is largely unknown, but it may involve binding of Au(I) to protein thiol groups, a process that inhibits the formation of disulfide bonds, and could lead to denaturation and subsequent formation of macroglobulins.

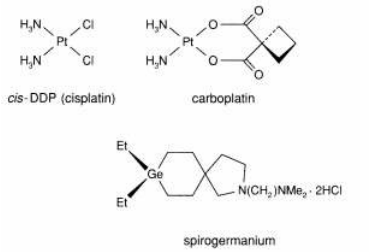


Figure 9.4 - Structures and trivial names of metal-based antitumor drugs.

Anticancer Drugs

1. Platinum Ammine Halides[34,35]

The discovery that *cis*-diamminedichloroplatinum(Il), *cis*-DDP or cisplatin (Figure 9.4), has anticancer activity in mice, and its subsequent clinical success in the treatment of genitourinary and head and neck tumors in humans, constitutes the most impressive contribution to the use of metals in medicine. Given in combination chemotherapy as an intravenous injection together with large amounts of saline solution to limit kidney toxicity, cisplatin treatment results in long-term (>5 yr) survival for more than 90 percent of testicular cancer patients. In a typical course, ~ 5 mg/kg body weight of the drug is administered once a week for four weeks. Extensive studies of platinum ammine halide analogues led to a series of empirical rules governing their chemotherapeutic potential. Specifically, it was concluded that active compounds should:

1. be neutral, presumably to facilitate passive diffusion into cells;
2. have two leaving groups in a *cis* configuration;
3. contain nonleaving groups with poor trans-Iabilizing ability, similar to that of NH_3 or organic amines;
4. have leaving groups with a "window of lability" centered on chloride.

These early structure-activity relationships have had to be modified somewhat, however, since chelating dicarboxylate ligands such as 1,1-dicarboxylatocyclobutane can replace the two chloride ions, and since cationic complexes with only one labile ligand, specifically, *cis*-$[Pt(NH_3)_2CI(4\text{-}X\text{-}py)]^+$, where X = H, Br, CH_3, etc., showed activity in some tumor screens. The two compounds shown in Figure 9.4, cisplatin and carboplatin (Figure 9.4), were the first to be approved for clinical use. Of particular interest to the bioinorganic chemist is that complexes having a *trans* disposition of leaving groups are inactive *in vivo*. This difference suggests the presence of a specific cellular receptor that, when identified, should facilitate the design of new, metal-based anticancer drugs. Present evidence strongly points to DNA as being the relevant cellular target molecule. Section V of this chapter expands on this topic in considerable detail.

2. Metallocenes and Their Halides: Ti, V, Fe[36,37]

Several compounds in this category, including $[(C_5H_5)_2TiX_2]$ (X = CI, Br, O_2CCl_3), $[(C_5H_5)_2VCl_2]$, $[(C_5H_5)_2NbCl_2]$, $[(C_5H_5)_2MoCl_2]$, and $[(C_5H_5)_2Fe]^+$ salts, exhibit significant activity against experimental animal tumors. Higher quantities (200 mg/kg) of these compounds than of *cis*-DDP can be tolerated with fewer toxic side effects, but their failure in two mouse leukemia screens commonly used to predict the success of platinum anticancer agents appears to have delayed their introduction into human clinical trials. Studies of Ehrlich ascites tumor cells treated with $[(C_5H_5)_2VCl_2]$ *in vitro* revealed selective inhibition of incorporation of radiolabeled thymidine, versus uridine or leucine, indicating that the complex blocks DNA replication. Unlike cisplatin, however, metallocene halides undergo rapid hydrolysis reactions in aqueous media, forming oxobridged and aqua complexes that may have a higher affinity for phosphate oxygen atoms than the heterocyclic nitrogen atoms of the bases in DNA.[38] Exactly how the ferrocenium ion might bind to DNA is even more obscure, although partial metallointercalation and groove binding are more likely than covalent attachment of the chemically unmodified cation. From the limited information available, metallocenes and their halides appear to behave fundamentally differently from platinum antitumor compounds. As a class, they provide a promising new opportunity to expand the scope of metal complexes used in cancer chemotherapy.

3. Gold and Other Metal Phosphines[39]

Following the successful entry of the soluble gold-phosphine complex auranofin (Figure 9.4) into the metal-based pharmaceuticals industry, several gold-phosphine complexes were examined for possible anticancer activity. Although auranofin itself was active in only a small fraction of the mouse tumor models tested, biological activity approaching that of cisplatin was discovered for many

analogues, most notably the diphosphine bridged complex [ClAu($PPh_2CH_2CH_2$ PPh_2)AuCI]. Attempts to replace the phosphine with As or S donor ligands, to increase or decrease the length of the 2-carbon bridge, or to replace the phenyl with alkyl groups all led to diminished activity. Most noteworthy is that the diphosphine ligands themselves have activity very similar to that of their gold complexes, and that Ag(I) and Cu(I) analogues are also effective. These results strongly imply that the phosphine ligands are the chemical agents responsible for the anticancer properties of these compounds. Coordination to a metal presumably serves to protect phosphines against oxidation to the phosphine oxides, which independent investigations have proved to be ineffective. A possible role for the metal in the cytotoxicity of the compounds cannot be ruled out, however.

4. Other Main Group and Transition-metal Compounds[36,40,41]

Several main group metal complexes exhibit anticancer activity. Gallium(III) nitrate is active against human lymphomas, but with dose-limiting side effects on the kidneys and gastrointestinal tract. Tin complexes of general formula $R_2L_2SnX_2$, where R = alkyl or phenyl, L_2 = py_2, bpy, or phen, and X_2 = two *cis*-oriented halide or pseudohalide leaving groups, are active against the mouse P388 leukemia tumor. The *cis* disposition of the leaving groups suggests a possible mechanism analogous to that of cisplatin (see below). Organo-gennanium compounds are also active, notably the derivative spirogermanium shown in Figure 9.4. Nothing is known about the mechanism of action of any of these compounds.

Following the discovery of activity for cisplatin, several thousand platinum and nearly 100 other transition-metal complexes have been screened in various tumor model systems in the hope of achieving better activity against a broader range of tumors. Among the classes of nonplatinum compounds showing some activity are ruthenium complexes *cis*-[$RuCl_2(DMSO)_4$], [$Ru(NH_3)_5$(Asc)] (CF_3SO_3), where Asc is ascorbate dianion, and *fac*-[$Ru(NH_3)_2Cl_4$] , all of which are believed to bind to DNA; binuclear rhodium complexes [$Rh_2(O_2CR)_4L_2$]; octahedral Pd(IV) complexes such as *cis*-[$Pd(NH_3)_2CI_4$]; and such miscellaneous molecules as the iron(II) complex of 2-formylpyridine thiosemicarbazone, the site of action of which is thought to be ribonucleotide reductase. These examples illustrate the broad scope encompassed by this field, which has a potential for developing fundamental infonnation about metal-biomolecule interactions as well as novel anticancer drugs. Much remains to be explored.

Miscellaneous Metals in Medicine

Numerous other anecdotal and some fairly elaborate studies have been reported for metal complexes as medicinal agents. The use of zinc applied topically to promote the healing of wounds dates back to around 1500 B.C., and silver is now commonly applied to prevent infection in bum patients.[42,43] Osmium carbohydrate polymers have been reported to have antiarthritic activity.[44] Transition-metal complexes have a long history of use as antibacterial and antiviral agents; for example, Zn^{2+} is used to treat herpes, possibly by inhibiting the viral DNA polymerase.[45] Early transition-metal (e.g., tungsten) polyoxoanions have been employed to treat AIDS patients.[46] Numerous reports have appeared detailing the anti-inflammatory, antiulcer, and analgesic activities of copper carboxylate complexes.[7] As in the previous section, these reports and others like them require more serious attention from bioinorganic chemists to elucidate the molecular events responsible for such a fascinating menu of biologically active metal complexes.

Summary and Prospectus

The clinical successes of platinum anticancer and gold antiarthritic drugs have changed the attitudes of many who doubted that heavy-metal compounds, notorious for their deleterious effects on human health, would ever playa serious role in chemotherapy. Indeed, we have seen that Hg^{2+}, Pb^{2+}, and Cd^{2+} are toxic elements. Even essential metals can be highly toxic if present in excess, either because of chronic or acute poisoning or because of metabolic defects that deregulate their control in the cell. An important common theme running throughout this discussion is selectivity. For a drug to be effective, it must be selectively toxic to diseased tissue while leaving nonnal tissue alone; or it must selectively kill harmful microorganisms at levels where it fails to deplete helpful ones. For a chelating agent to be useful in the toxic effects of metals, it must bind as selectively as possible to the deleterious ion while coordinating only weakly, if all, to others. For a diagnostic metal complex to be it must be taken up (or excluded) selectively from diseased cells relative to normal ones, or to one tissue type versus another. Rarely has such selectivity been designed in advance of the discovery of a useful metal-based pharmaceutical, although spectacular advances in biology, such as monoclonal antibodies, may be hastening the day when such an objective be common. Interestingly, the successes of such unlikely as *cis*-[$Pt(NH_3)_2Cl_2$] and [(Et_3P)Au(OAc_4-thioglucose)] in chemotherapy were driven by the personal involvement of individuals like B. Rosenberg for the former and B. Sutton for the latter. Like Hollywood producers, these men mustered every conceivable resource

to promote the compounds for testing, introduction into human clinical trials, and eventually approval by the FDA. Such zeal requires years, usually more than a decade, of sustained personal effort, and may be the reason why other metal complexes, such as those mentioned above, have not had the impact of a cisplatin or an auranofin. On average, only one of 7,000 such compounds makes it from the laboratory bench to the patient, at an average cost of 250 million dollars and a time interval of 13 years.

Another component of the evolving field of metals in medicine, however, is that, once a has proved its in the clinic, how does it work? This question is deceptively for coordination chemistry *in vivo*, and the of cells to respond to unnatural external stimuli such as metal complexes, are matters about which we are beginning to learn. As progress is made in this latter area, it should become possible to design drugs in a rational way to achieve the required selectivity.

The remainder of this chapter focuses on a case study where some progress in unraveling the molecular mechanism of a metal-based drug, cisplatin being made. If nothing else, this discussion will elucidate strategic guidelines that may be employed to attack similar questions about other chemotherapeutic metal compounds discussed earlier in this section. Unfortunately, there is very little information available about the molecular mechanisms of these other complexes. At this transition in our discussion, we move from general considerations to a specific, analysis. The reader must here take time to become familiar with the biological aspects of the new material.

7.6.4: Survey of Metals Used for Diagnosis and Chemotherapy is shared under a not declared license and was authored, remixed, and/or curated by LibreTexts.

7.6.5: Platinum Anticancer Drugs- A Case Study

History of the Discovery[47]

cis-[Pt(NH3hCh], a molecule known since the mid-19th century, has been a subject of considerable importance in the of inorganic stereochemistry and substitution reaction kinetics.[48] Its biological was discovered by accident. In the mid-1960s, biophysicist Barnett Rosenberg, at Michigan State University, was studying the effects of electric fields on the growth of *Escherichia coli* cells in culture. They had hypothesized that, during cell division, the orientation of the mitotic be affected by local electric which they hoped to perturb. Instead, they observed growth without cell division, the result being elongated, spaghetti-like bacterial filaments approaching 1 cm in length. After much detective work, they realized that small amounts of platinum from the electrodes used to apply the electric fields had reacted with NH_4CI in their buffer to produce various platinum ammine halide compounds. Two of these, *cis*-$[Pt(NH_3)_2Cl_2]$ and *cis*-$[Pt(NH_3)_2CI_4]$, were capable of inducing filamentous growth in the absence of any electric field. Since chemicals that produce filamentation in bacteria had been known to exhibit antitumor activity, Rosenberg was eager to have his platinum compounds tested. Unable to convince existing agencies like the National Cancer Institute (who to their credit later spearheaded the development of cisplatin) that a heavy-metal complex could actually be beneficial to animals, the Michigan State group set up their own animal-tumor screens. The results were nothing short of spectacular. Injection of *cis*-DDP directly into the abdominal cavity of mice into which a solid Sarcoma-180 tumor had been implanted led within a few days to a blackening (necrosis), reduction in size, and eventual disappearance of the tumor (Figure 9.5). The cured mouse enjoyed a normal lifespan. From these and other animal studies, physicians became convinced that administering platinum compounds to cancer patients might be worthwile, and a new field involving bioinorganic chemistry and cancer chemotherapy was born. The drug, marketed as Platinol with the generic name cisplatin, received FDA approval in 1979 and is today one of the leading anticancer agents.

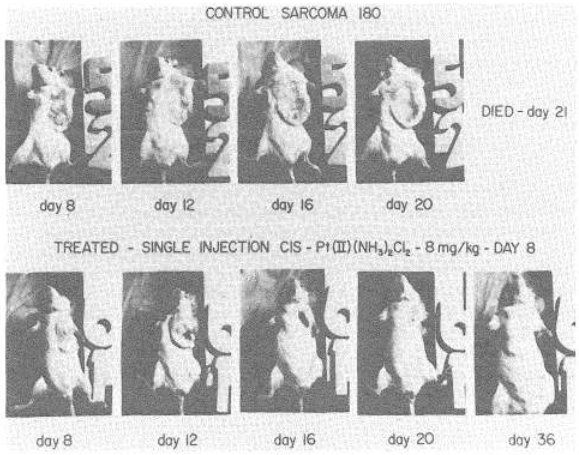


Figure 9.5 - Photographic demonstration of the dramatic ability of cisplatin to cure a Sarcoma-180murine tumor (reproduced by permission from Reference 47).

Principles that Underlie Drug Development

1. Strategic Considerations

There are two general routes to the development of inorganic complexes, and indeed most chemical compounds, as drugs. One, illustrated by cisplatin, arises from an empirical observation of biological activity followed by attempts to optimize the efficacy through investigations of structure-activity relationships (SAR). The goals are to minimize toxicity, to develop cell culture and animal screens for testing related compounds, and ultimately to elucidate the molecular mechanism. Knowledge of the molecular mechanism might evenlead to a rational strategy for designing better drugs.

The second general approach to drug design begins with known biochemistry. For example, ribonucleotide reductase is required in the first committed step in the biosynthesis of DNA, the conversion of ribo- to deoxyribonucleoside dir)hclsphat.es. The mammalian enzyme contains a binuclear non-heme iron center required for activity. Compounds that would selectively inhibit this enzyme by destroying this center are potentially useful as antiviral or antitumor agents. Another example is the enzyme reverse Iranscriptase, encoded by the HIV (AIDS) virus and required for its integration into the genome of the host cell. Compounds like

3'-azidothymidine (AZT) are accepted by the enzyme as substrates but, when added to the growing DNA chain, cannot be linked to the next nucleotide. Chain termination therefore occurs and the replication process becomes permanently interrupted. Attempts to find organic molecules or inorganic complexes that are more effective chain terminators than AZT constitute a rational strategy for developing new anti-AIDS drugs.

In the remainder of this chapter we describe research that has evolved following the discovery of biological activity for cisplatin. Although the initial breakthrough was serendipitous, subsequent studies have revealed many aspects of the molecular mechanism. From this known biochemistry we may one day be in a position to design more effective anticancer drugs and therapies based upon the fundamental bioinorganic chemistry of cisplatin.

2. Pre-clinical and Clinical Trials[49]

Predicting the chemotherapeutic potential of an inorganic compound such as *cis*-DDP prior to its introduction into human cancer patients is an important objective. Compounds are most easily tested for their cytotoxic effects on bacterial or mammalian cells in culture. Shown in Figure 9.6 are results for the survival of cultured L1210 cells in the presence of increasing amounts of *cis*- or *trans*-DDP.[50,51] The data reveal the markedly greater toxicity of the *cis* isomer, which is a much better anticancer agent than its stereoisomer. Unfortunately, no single assay has yet been found that can predict the chemotherapeutic potential of platinum compounds in humans. The best that can be obtained are results relative to those for *cis*-DDP, in which case toxicity at low dose is usually scored positive.

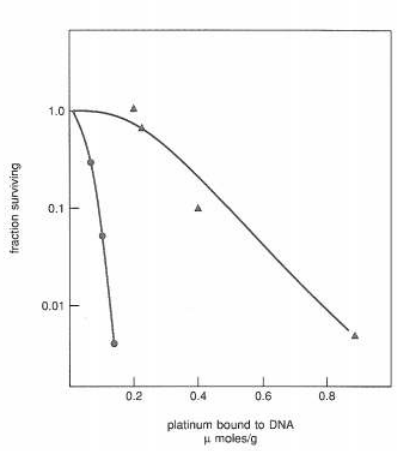


Figure 9.6 - Differential toxicity of cis- (●) and trans-DDP (▲) on HeLa cells growing in culture (reproduced by permission from Reference 51).

The next level of testing, often employed directly without first examining cell-culture results, involves animal (usually mammals, excluding human) screens.[49] Among the most popular measures of the chemotherapeutic activity of platinum compounds has been their ability to prolong the survival of mice bearing the L1210 or P388 leukemia. A suspension of cells is inoculated intraperitoneally (i.p., in the abdominal cavity), producing a leukemia that eventually progresses to the generalized disease. In one commonly used protocol, platinum compounds are dissolved in physiological saline (0.85 percent NaCl) or sterile H_2O and injected i.p. 24 h, 5, 9, and 13 days after inoculation of the leukemia cells. Several indices of antitumor activity and toxicity have been defined. The percent I.L.S., or increased lifespan measures the mean survival of treated versus control animals that were given no platinum drug. A related index is the median survival, percent T/C (Test/Control), which is 100 + percent I.L.S. The LD_{50} value measures toxicity as mean lethal dose,the amount of drug (usually in mg/kg body weight) required to kill half the animals. Potency is defined by lD_{90}, the inhibiting dose at which 90 percent of the tumor cells are killed. From these values, a therapeutic index (TI) = LD_{50}/lD_{90} is sometimes defined, which should be substantially greater than one. Typical values for *cis*-DDP are 85 percent I.L.S. at 8 mg/kg for the L1210 tumor, 13.0 mg/kg LD_{50}, and 1.6 mg/kg lD_{90} resulting in a TI of 8.1.

In addition to being tested in mice, cisplatin and related compounds have been screened in other mammals, specifically dogs and monkeys, mainly to look for possible dose-limiting side effects. Severe vomiting, once thought to be an insurmountable obstacle, was monitored by using ferrets. None of the animal screens can substitute for the ultimate test, however, which is human clinical trials. In 1972, such trials were initiated using terminally ill cancer patients. It was determined that intravenous (i.v.) injection,

rather than i.p. or oral administration, was the preferred method for giving the drug. Further details of the clinical development of cisplatin are discussed in a later section.

From the animal screens emerged the set of structure-activity relationships enumerated earlier (Section IV.E.1). Both cisplatin and carboplatin conform to these rules, and to date no compounds with demonstrably better antitumor activity have been tested in humans. The decision to move an experimental drug into the clinic is a difficult one, however, and it may be that molecules such as cis- $[Pt(NH_3)_2(4\text{-Br-py})Cl]Cl$ (see Section V.D.7.c) would be effective for tumors that are refractive to cisplatin chemotherapy. In any case, the foregoing chain of events, from studying the effects of a compound on cells in culture through animal screens and eventually to humans, constitutes the principal route for introducing a new anticancer drug. The process can take more than a decade.

3. Mechanism of Action Atudies

Once a class of compounds has been identified as biologically active, studies to elucidate the molecular mechanism of action can be undertaken. A first step is to identify the major cellular target or targets responsible for the chemotherapeutic properties of the drug. These investigations must also focus on chemical transformations that might take place in the solutions being administered and in the biological fluids that transport the drug to its ultimate target site. The next major step is to characterize the adduct or family of adducts made with the biological target molecule. The structure and kinetic lifetime of these adducts need to be investigated. Once this information is in hand, the effect of the adducts on the structure, stability, and function of the biological target molecule must be studied. Here many powerful new methodologies of modern molecular biology, genetics, and immunology can be brought to bear on the problem. The ultimate goals are to translate the molecular events elucidated into a realistic mechanism for how the drug molecule brings about its toxic effects selectively at the sites responsible for the disease and to use this information to design even better drugs.

Having progressed this far, we next need to bridge the gap between fundamental knowledge gained in studies of the mechanism of action and the SAR gleaned through pre-clinical and clinical trials. Whether such a happy situation can be reached for cisplatin remains to be seen, but there are encouraging signs, as we hope to demonstrate in the following discussion.

Clinical Picture for Cisplatin and Carboplatin[49,52]

1. Responsive Tumors and Combination Chemotherapy

It was an early observation that the best responses to cisplatin occurred in patients with genitourinary tumors. For testicular cancer, once a leading cause of death for males of age 20-40, cisplatin cures nearly all patients with stage A (testes alone) or B (metastasis or retroperitoneal lymph nodes) carcinomas. Platinum is usually given in combination with other drugs, commonly vinblastine and bleomycin for testicular cancer. This combination chemotherapy, as it is known, has several objectives. Some tumors have a natural or acquired resistance to one class of drugs and, by applying several, it is hoped that an effective reduction in tumor mass can be achieved. In addition, various drugs are known to affect different phases of the cell cycle, so several are applied simultaneously to allow for this possibility. Finally, synergism, where the response is greater than expected from simple additive effects, can occur, although it is rare. In addition to testicular cancer, platinum chemotherapy has produced responses in patients with ovarian carcinomas (>90 percent), head and neck cancers, non-small-cell lung cancer, and cervical cancer. Cisplatin is also effective when combined with radiation therapy.

2. Dose-limiting Problems; Toxicology

An early and quite worrisome adverse side effect of cisplatin was kidney toxicity. This problem, not commonly encountered with the older cancer drugs, nearly prevented its widespread use and eventual FDA approval. The major breakthrough here was made by E. Cvitkovic, who, while working at Sloan-Kettering Memorial Hospital in New York, administered large quantities of water by intravenous injection to patients, together with an osmotic diuretic agent such as D-mannitol. The rationale was that such hydration could ameliorate kidney toxicity by flushing out the heavy-metal complex. This simple idea worked, and the dose of the platinum compound could be increased threefold without accompanying nephrotoxicity. Hydration therapy is now commonly employed when cisplatin is administered. Among the other toxic effects encountered in cisplatin chemotherapy are nausea and vomiting, but this problem has also been controlled by use of antiemetic agents. Patients have also been known to experience bone-marrow suppression, a ringing in the ears, and occasional allergic reactions.

More recently, attempts have been made to extend cisplatin treatment to other broad classes of tumors by raising the dose above the ~5 mg/kg body weight levels given by i.v. injection every few weeks. Direct injection into the peritoneal cavity has been employed for refractory ovarian tumors. These more aggressive therapeutic protocols have been frustrated by drug resistance, a phenomenon by which cells learn to tolerate a toxic agent and for which many mechanisms exist, and by the return of the usual cisplatin side effects, most notably kidney toxicity and neurotoxicity. In order to combat toxic effects to the kidneys, chemoprotector drugs have been introduced. Based on the known affinity of platinum(II) complexes for sulfur-donor ligands, sodium diethyldithiocarbamate (DDTC) has been given both to experimental animals and to humans by i.v. infusion over about an hour following cisplatin administration.[53] DDTC inhibits many of the toxic side effects, particularly to the kidneys and bone marrow, without itself producing long-term side effects or apparently inhibiting the antitumor properties of *cis*-DDP. Similar efforts have been made to reduce the toxic effects of cisplatin with other sulfur-containing compounds including thiosulfate and the naturally occurring biomolecules glutathione, cysteine, and methionine. The relative amounts of the latter three molecules can be controlled by drugs that affect their normal cellular concentrations.

Another approach to reducing cisplatin toxicity is to develop new classes of platinum drugs or different routes of their administration. Carboplatin (Figure 9.4) is one result of these efforts. The bidentate chelating dicarboxylate leaving group in carboplatin presumably retards the rates of reactions leading to toxicity, but does not adversely interfere with the chemistry required for antitumor activity. Recently, promising platinum compounds for oral administration have been developed.[54] In Pt(IV) complexes of the kind *cis*, *trans*, *cis*-$[Pt(NH_3)(C_6H_{11}NH_2)\bullet(O_2CCH_3)_2Cl_2]$, where $C_6H_{11}NH_2$ is cyclohexylamine, have been found to be effective in preclinical screens. The greater kinetic inertness of these complexes apparently renders them sufficiently stable to the chemically harsh environment of the gastrointestinal tract. Once absorbed into the bloodstream, these compounds are metabolized to the Pt(II) analogues, *cis*-$[Pt(NH_3)(C_6H_{11}NH_2)Cl_2]$, which are presumed to be the active form of the drug. The Pt(IV) compound has recently entered clinical trials.

Although impressive inroads have been made in the management of human tumors by platinum chemotherapy, the fact remains that, apart from testicular and to a lesser extent ovarian cancer, the median survival times are measured in months. Clearly, there is much room for improvement.

3. Pharmacology[49,52]

Solutions of cisplatin are usually given in physiological saline (NaCl), since hydrolysis reactions occur that can modify the nature of the compound and its reactions *in vivo* (see below). Cisplatin is rapidly cleared from the plasma after injection, 70-90 percent of the platinum being removed within the first 15 minutes. It has been found that more than half the platinum binds to serum proteins and is excreted. Most of the platinum exits the body via the urine within a few days. These results account for the use of multiple-dose chemotherapy at intervals of several weeks. Animal studies employing *cis*-DDP labeled with ^{195m}Pt, a 99 keV γ-emitter with a 4.1-day half-life, reveal retention half-times in various tissues of 8.4 (kidney), 6.0 (ileum), 4.1 (liver), 2.8 (tumor), and 1.9 (serum) days following a single dose. Platinum distributes widely to all tissue, with kidney, uterus, liver, and skin having the most, and muscles, testes, and brain the least amount of the compound. There is no evidence for selective uptake into normal versus tumor cells.

7.6.5: Platinum Anticancer Drugs- A Case Study is shared under a not declared license and was authored, remixed, and/or curated by LibreTexts.

7.6.6: Mapping the Major Adducts of cis- and trans-DDP on DNA; Sequence Specificity

As we have seen, the antitumor activity of cisplatin is most likely the result of its DNA-binding properties. But what are the adducts? The human genome has more than a billion nucleotides. Does platinum recognize any special regions of the DNA or any particular sequences? In other words, is binding simply random or is there at least a regioselectivity? In this section, we discuss the best strategies for answering these questions, strategies that evolved in pursuit of learning how *cis*-DDP binds to DNA. We also illustrate their power in elucidating the DNA-binding properties of other metal complexes of interest to bioinorganic chemists.

a. Early Strategic Approaches

The first experiments to imply the sequence preferences of *cis*-DDP binding to DNA employed synthetic polymers.[108,109] Specifically, the buoyant density of poly(dG)•poly(dC), poly(dG•dC), and their *cis*-DDP adducts was studied in the analytical ultracentrifuge. The greatest shift in buoyant density was seen for the platinum adducts of poly(dG)•poly(dC), from which it was concluded that platinum forms an intrastrand crosslink between two neighboring guanosine nucleosides on the same strand. This interpretation was suggested by the known preference of metal ions, and especially platinum, for binding at the N7 position on the guanine base (Figure 9.9), information available from model studies of metal-nucleobase chemistry. Although other interpretations of the buoyant-density shift were possible, especially since the amount of platinum bound was not quantitated, the conclusion proved to be correct, as confirmed by later investigations. Interestingly, *trans*-DDP did not selectively increase the buoyant density of poly(dG)•poly(dC).

Following these initial experiments, the regioselectivity of *cis*-DDP binding was investigated by studying the inhibition of enzymatic digestion of platinated DNA. For example, the platinum complex inhibits the cleavage of DNA by restriction enzymes that recognize specific sequences and cut both strands of the double helix.[110] The resulting fragments are readily identified on electrophoresis gels. One such restriction enzyme is Bam HI. As shown by the arrows in Scheme (9.11), Bam HI cleaves a six-bp palindromic sequence at the phosphodiester bonds between two guanosine nucleosides. Formation of an intrastrand crosslink between the two adjacent guanosine nucleosides inhibits digestion by the enzyme. Another method, termed exonuclease mapping, involves digestion of the strands of duplex DNA from its 3'-ends.[111,112] When the enzyme encounters a bound platinum atom, it is unable to proceed further. Analysis of the digestion products by gel electrophoresis reveals the presence of discrete bands caused by the inhibition of digestion by bound platinum at specific sequences. Results from experiments of this kind were the most definitive at this time in demonstrating the profound regioselectivity of cisplatin for adjacent guanosines, and strongly supported the earlier conclusion that the drug was making an intrastrand d(GpG) crosslink.



Figure 9.18. Platinum is first bound to a single-stranded DNA template, in this example from bacteriophage M13mp18, to which is next annealed a short, complementary oligonucleotide termed a "primer" for DNA synthesis. Addition of the large (Klenow) fragment of *E. coli* DNA polymerase I and deoxynucleoside triphosphates, one of which bears a ^{32}P label, [α-^{32}P]dATP, initiates replication. When the enzyme encounters a platinum adduct, the chain is terminated. By running out the newly synthesized DNA strands on a sequencing gel, the sites of platinum binding can be detected by comparing the positions of the radiolabeled fragments with those obtained from sequencing ladders. The results of this procedure, which has been termed "replication mapping," confirmed that *cis*-DDP binds selectively to $(dG)_n$ ($n \geq 2$) sequences. In addition, they showed that *trans*-DDP blocks replication, in a much less regioselective manner, in the vicinity of sequences of the kind d(GpNpG), where N is an intervening nucleotide. These data afforded the first clear insight into the sequence preferences for *trans*-DDP on DNA. A control experiment run with DNA platinated by the monofunctional complex $[Pt(dien)CI]^+$ gave the interesting result that DNA synthesis was virtually unaffected.

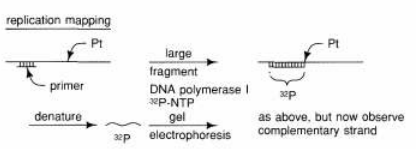


Figure 9.18 - Diagram illustrating the replication mapping experiment. To a single-stranded, platinated template is annealed a short primer for DNA synthesis using DNA polymerase I (Klenow fragment) and radiolabeled nucleotides. Sites of platinum binding are revealed as bands on gel electrophoresis where chain termination occurs (see text for details).

In yet another approach to the problem, DNA containing *cis*- or *trans*-DDP adducts was electrostatically coupled to bovine serum albumin, to enhance its antigenicity, and injected into rabbits.[113,114] The resulting antisera and antibodies were then studied for their ability to recognize and bind specifically to platinated DNAs having defined sequences, such as poly(dG)•poly(dC) and poly[d(GC)]•poly[d(GC)].

From experiments of this kind, the major *cis*-DDP adduct recognized by the antibody was found to be *cis*-[$Pt(NH_3)_2${d(GpG)}], in accord with the findings of the enzymatic mapping experiments. Unplatinated DNA was not recognized, nor was DNA platinated with *trans*-DDP. On the other hand, the antibody recognized DNA platinated with antitumor-active compounds [$Pt(en)Cl_2$] and [Pt(DACH)(CP)], where DACH = 1,2-diaminocyclohexane and CP = 4-carboxyphthalate. This result revealed that the antibody recognized the structural change in DNA that accompanies formation of d(GpG) intrastrand crosslinks, irrespective of the diamine ligand in the coordination sphere of the platinum atom. The antibody is also capable of distinguishing adducts formed by active versus inactive platinum complexes. Most importantly, DNA isolated from the cells of mice bearing the L1210 tumor five hours after cisplatin injection, was recognized.[113,115] Subsequent studies[116] revealed that these antibodies could detect cisplatin-DNA adducts formed in the white blood cells of patients receiving platinum chemotherapy. Thus, the antibody work linked the regiospecificity of platination chemistry *in vitro* with that occurring *in vivo* and in a clinically relevant manner.

Additional studies with monoclonal antibodies generated using DNA platinated with *cis*- or *trans*-DDP further confirmed and extended these results.[117] This later work indicated that intrastrand crosslinked d(ApG) and d(GpG) sequences possess a common structural determinant produced by *cis*-DDP platination, and that carboplatin is also capable of inducing the same DNA structure. For *trans*-DDP-platinated DNA, a monoclonal antibody was obtained that appeared to have the intrastrand d(GpTpG) adduct as its major recognition site. In all these studies, the primary structural determinant appears to be DNA duplex opposite the site of platination, since fairly major stereochemical changes could be made in the amine ligands with no appreciable effect on antibody binding.

b. Degradation, Chromatographic Separation, and Quantitation of DNA Adducts

Experiments in which DNA platinated with *cis*-DDP is degraded to chromatographically separable, well-defined adducts have been invaluable in revealing the spectrum of products formed. In a typical experiment, platinated DNA is digested with DNAse I, nuclease P1, and alkaline phosphatase. These enzymatic digestions degrade DNA into nucleosides that can be readily separated by high-performance liquid chromatography (HPLC). Detection of the adducts can be accomplished by the UV absorption of the nucleoside bases at 260 nm or, for platinum complexes containing a radioactively labeled ligand such as [^{14}C]ethylenediamine,[118] by monitoring counts. In addition to peaks corresponding to dA, dC, dG, and dT, the chromatographic trace contains additional peaks corresponding to specific platinum nucleobase adducts such as *cis*-[$Pt(NH_3)_2(dG)_2$]. The precise nature of these adducts was established by comparison with chemically synthesized compounds structurally characterized by NMR spectroscopy.[118-121] An alternative method for identifying the adducts employed antibodies raised against specific platinum-nucleobase complexes.[122]

This approach has revealed the relative amounts of various adducts formed by a variety of platinum complexes; selected results are summarized in Table 9.4. Usually, for cisplatin, the relative amounts of the various adducts formed varies according to the series *cis*-[$Pt(NH_3)_2${d(pGpG)}] > *cis*-[$Pt(NH_3)_2${d(pApG)}] > *cis*-[$Pt(NH_3)_2${d(GMP)}$_2$] > monofunctional adducts. Only when the total incubation time was short, less than an hour, were the monofunctional adducts more prevalent, as expected from the kinetic studies of *cis*-DDP binding to DNA discussed previously. It is noteworthy that no d(pGpA) adducts were detected. This result, which is consistent with information obtained by enzymatic mapping, can be understood on stereochemical grounds.[123] If the guanosine nucleoside N7 position is the most-preferred binding site on DNA, closure to make an N7,N7 intrastrand crosslink between two adjacent purine nucleotides is more feasible in the 5' direction along the helix backbone (N7•••N7 distance of ≈ 3 Å) than in the 3' direction (N7•••N7 distance ≈ 5 Å). In addition, molecular-mechanics modeling studies[124] indicate that a highly unfavorable steric

clash occurs between the 6-amino group of the 3'-adenosine residue in a d(pGpA) crosslink and the platinum ammine ligand, whereas in the platinated d(pApG) sequence, the 6-oxo group forms a stabilizing hydrogen bond to this ligand. A 28 kJ mol^{-1} preference of *cis*-DDP for binding d(pApG) over d(pGpA) was calculated.

Table 9.4 - Geometric features of the platinum coordination spheres of *cis*- [$Pt(NH_3)_2${d(pGpG)}].

a) Bond distances are in Angstroms and angles are in degrees.

b) Conventions used for assigning Base/Base and Base/PtN4 dihedral angles can be found in J. D. Orbell, L. G. Marzilli, and T. J. Kistenmacher, *J. Am. Chem. Soc.* **103** (l981), 5126. The numbers in square brackets refer to the corresponding N(ammine)•••O6 distance, in Å (see text).

Bond Distances and Angles[a]	Molecule 1	Molecule 2	Molecule 3	Molecule 4
Pt-N1	2.03(2)	2.01(2)	2.08(2)	2.08(2)
Pt-N2	2.03(3)	2.09(2)	2.04(3)	2.06(3)
Pt-N7A	2.01(2)	2.02(2)	1.91(3)	1.93(3)
Pt-N7B	2.05(2)	1.95(3)	2.00(3)	2.06(3)
N7A-Pt-N1	88.6(9)	90.3(9)	91.0(1)	88.4(9)
N7A-Pt-N2	179(1)	173.3(8)	178(1)	177(1)
N7A-Pt-N7B	89.1(9)	90.0(1)	85(1)	89(1)
N1-Pt-N2	92(9)	90.8(9)	91(1)	93(1)
qN1-Pt-N7B	176.5(9)	179.0(1)	173(1)	175(1)
N2-Pt-N7B	90.3(9)	89.0(1)	93(1)	89(1)

Dihedral Angles[b] Molecule	3'-Gua/5'-Gua	5'-Gua/PtN_4	3'-Gua/PtN_4
1	76.2(5)	110.6(5) [3.30(3)]	86.1(5)
2	81.0(5)	110.8(5) [3.49(3)]	95.5(5)
3	86.8(6)	81.0(6)	58.0(6) [3.11(4)]
4	80.6(5)	76.6(6)	59.6(6) [3.18(4)]

There are two likely sources of *cis*-[$Pt(NH_3)_2${d(GMP)}$_2$] in the spectrum of adducts. This species could arise from long-range intrastrand crosslinks, where the two coordinated guanosines are separated by one or more nucleotides. In support of this possibility is the fact that digestion of chemically synthesized *cis*-[$Pt(NH_3)_2${d(GpNpG)}], where N = C or A, led to *cis*-[$Pt(NH_3)_2${d(Gua)}-{d(GMP)}] and mononucleotides.[118,119,121] The other source of this product is interstrand crosslinked DNA, known to occur from the alkaline elution studies.

As indicated in Table 9.4, in all the experiments there was platinum that was unaccounted for in the quantitation procedures, which employed either antibodies, platinum atomic absorption spectroscopy, or a radiolabeled ethylenediamine ligand. Some of this material was assigned to oligonucleotides having high platinum content, resistant to enzymatic degradation.

Two important points emerge from the quantitation of adducts by this method. One is that intrastrand d(GpG) and d(ApG) crosslinks constitute the major adducts (>90 percent of total platination) made by cisplatin on DNA *in vivo*. Because they were identified by an antibody specific for their structures, no chemical change brought about by cellular metabolism has occurred. Secondly, the preponderance of these adducts far exceeds the frequency of adjacent guanosine or guanosine/adenosine nucleosides in DNA. This latter result implies a kinetic preference for, or recognition of, d(pGpG)- and d(pApG)-containing sequences by cisplatin.

c. Postscript: A Comment on Methodologies

With few exceptions, none of the experimental studies described in this section could have been carried out in 1969, when Rosenberg first demonstrated the anticancer activity of *cis*-DDP. The techniques of DNA sequencing, monoclonal antibody formation, oligonucleotide synthesis, HPLC, FPLC, and many of the higher resolution gel electrophoresis methodologies employed were the result of later developments driven by rapid advances in the fields of molecular biology and immunology. Future progress in elucidating the molecular mechanisms of action of cisplatin and other inorganic pharmaceuticals will no doubt benefit from new technological discoveries and inventions of this kind yet to come.

7.6.6: Mapping the Major Adducts of cis- and trans-DDP on DNA; Sequence Specificity is shared under a not declared license and was authored, remixed, and/or curated by LibreTexts.

7.6.7: Structure of Platinum-DNA Complexes

a. NMR Studies of Platinated Oligonucleotides

Once the major spectrum of adducts formed by *cis*- and *trans*-DDP with DNA began to emerge, it was of immediate interest to learn to what positions on the nucleobases the platinum atom was coordinated. Proton NMR spectroscopy soon proved to be an invaluable tool for obtaining this information.[71,125,126] Several ribo- and deoxyribooligonucleotides containing GG, AG, or GNG sequences were synthesized, and allowed to react with *cis*-DDP or its hydrolysis products, and the resulting complexes were purified by chromatography. All GG-containing oligomers formed intrastrand crosslinks with the $\{Pt(NH_3)_2\}^{2+}$ moiety coordinated to the N7 atoms. This structure was deduced from several criteria. Most frequently studied were the nonexchangeable base protons H8 and H2 of adenine, H6 of thymine, H8 of guanine, and H5 and H6 of cytosine (Figure 9.9). Coordination of platinum to N7 of guanine causes a downfield shift of the H8 proton resonance. More importantly, however, it also lowers the pK_a of the N1 proton by ~ 2 units, because platination adds positive charge to the base. Thus, titration of the platinated oligonucleotide over a pH range, and comparison of the results to those obtained for the unplatinated oligomer, reveals a difference in the midpoint of the transition in chemical shift of the H8 proton by 2 pH units if coordination occurs at N7. This effect is illustrated in Figure 9. 19 for the adduct *cis*- $[Pt(NH_3)_2\{d(ApGpGpCpCpT)\}N7\text{-}G(2),N7\text{-}G(3)]$, where the pK_a of N1 is seen to shift from ~ 10 to ~ 8 upon platination.[71] The pH titration in this example also reveals the pH-dependent chemical shift of the cytosine ^1H resonances at a pH of ~ 4.5, corresponding to protonation of the N3 atoms. The protonation of adenine N7 (pK_a ~ 4) is also frequently observed in these studies. These results conclusively demonstrate platinum coordination at N7 of the two guanosine nucleosides.

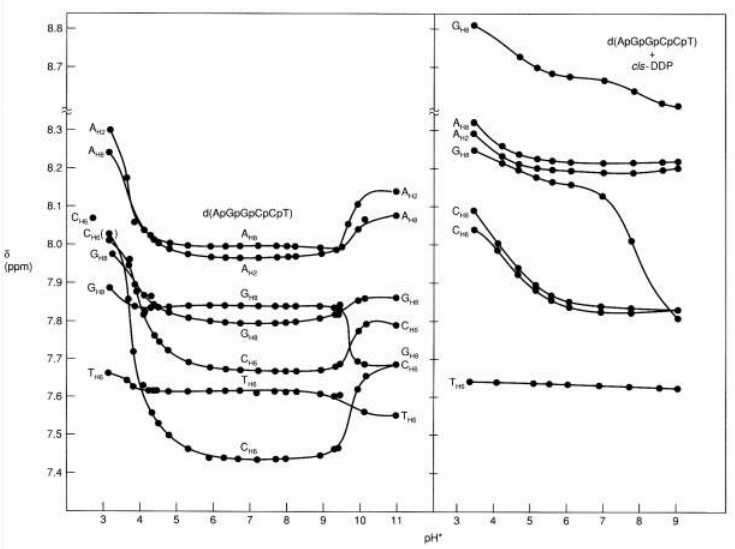


Figure 9.19 - Chemical shift (***δ***) vs. pH* of the nonexchangeable base protons of D_2O solutions of $[d(ApGpGpCpCpT)]_2$ (3.5 mM, 35 °C) and its cis-DDP adduct (2.5 mM, 70 °C). The pyrimidine resonances of the latter sample show no chemical shift changes with temperature over the range 35 < T < 70 °C while the purine resonances show a slight temperature-dependent chemical shift change of up to 0.1 ppm. Tetramethylammonium chloride was used as the internal standard (***δ*** 3.180). Reproduced by permission from J. C. Caradonna, S. J. Lippard, M. J. Gait, and M. Singh, J. Am. Chem. Soc. **104** (1982), 5793.

Although several of the oligonucleotides studied have self-complementary sequences, such that they can form a double helix when unplatinated, in no such case was a duplex observed for their platinated forms. The presence of the platinum-induced crosslink presumably decreases the stability of the doublestranded form of the oligonucleotide. Another interesting result is that all intrastrand $\{Pt(NH_3)_2\}^{2+}$ adducts of d(GpG) or d(ApG) have an altered deoxyribosesugar ring conformation. In normal, unplatinated form, these single-stranded or duplex oligonucleotides have a C2'-endo sugar pucker (Figure 9.9). Upon platination, the 5'-nucleotide switches to C3'-endo. This change is readily monitored by the ring proton-coupling constants $J_{H1'\text{-}H2'}$ and $J_{H1'\text{-}H2''}$. These protons constitute an ABX spin system such that the sum, $\Sigma^3J = {}^3J_{1'2'} + {}^3J_{1'2'}$, is most easily measured as the separation between the outermost peaks in the multiplet. For the C2'-endo conformation, a pseudotriplet occurs with Σ^3J = 13.6 Hz, and for C3'-endo, Σ^3J = 7.5 Hz. The 3'-guanosines in the adducts show greater conformational flexibility, having ~ 70 to 80 percent C2'-endo sugar puckers, depending upon the temperature.

Another conformational feature that could be deduced from ^{1}H NMR studies of all *cis*-DDP-platinated oligonucleotides containing an embedded d(GpG) sequence is that both guanosine nucleosides retain the anti orientation of the base around the C1'-N9 glycosidic linkage (Figure 9.9). This result was deduced from the lack of a pronounced nuclear Overhauser effect (NOE) between H8 and the H1' protons, such as would occur in the syn conformation. An NOE between H8 resonances on the two coordinated nucleosides was observed for adducts of d(ApTpGpG) and d(CpGpG), indicating that the two bases are in a head-to-head orientation with respect to the platinum coordination plane. In other words, both O6 atoms lie on the same side of that plane. Two oligonucleotides containing *cis*-$[Pt(NH_3)_2(ApG)]$ adducts have been examined; their structural properties closely resemble those of the (GpG) adducts, with platinum coordinated to N7 of both purine bases.

In order to study double-stranded DNAs platinated on one strand, it was necessary to adopt a special strategy. First, the desired oligonucleotide is synthesized. It is preferable that the DNA strands not be self-complementary, since the affinity of such an oligomer for itself is so much greater than that for its platinated form that the desired, singly platinated duplex will not form. After the platinated single strand is synthesized and purified, the complementary strand is added. Several duplex oligonucleotide-containing *cis*-$[Pt(NH_3)_2\{d(pGpG)\}]$-embedded adducts prepared in this manner have been studied by ^{1}H NMR spectroscopy. With the use of two-dimensional and temperature-dependent techniques, both the nonexchangeable base and sugar protons as well as the exchangeable (guanine N1 and thymine N3) N-H (imino) proton resonances were examined. The last are useful, since they give some measure of the extent to which the double helix remains intact. When not base-paired to their complements in the other strand, these protons exchange more rapidly with solvent (water) protons, leading at moderate exchange rates to broadening of the resonances and, at high exchange rates ($>10^{7}$ s^{-1}), disappearance of the signals. Several interesting results were obtained in these studies. In all of them, platination of the d(GpG) sequence brought about the same C2'-endo → C3'-endo sugar-ring pucker switch for the 5'-guanosine as seen in the single-stranded adducts. Head-to-head, anti conformations were also observed. At low temperatures, below the melting transition temperature, above which the duplex becomes single-stranded, the imino proton resonances were observed. This result was interpreted to mean that normal, Watson-Crick base pairs can still exist between the *cis*-DDP d(GpG) adduct and the d(CpC) sequence on the complementary strand. In the case of [d(TpCpTpCpG*pG*pTpCpTpC)]•[d(GpApGpApCpCpGpApGpA)], where the asterisks refer to the sites of platination, the imino proton resonances were assigned with the assistance of NOE experiments.[125] Temperature-dependent studies showed that, in the range - 4° < T < 46 °C, the imino resonances of the coordinated guanosine nucleosides broadened first with increasing temperature. Apparently the base pairs of the intrastrand crosslinked, platinated duplex DNA are disrupted, or "melted," outward from the point of platination as well as from the ends. Since the amino hydrogen atoms involved in base pairing were not observed in this study, a completely definitive structural analysis was not possible. Nevertheless, the authors proposed that the duplex would be kinked by an angle of ~ 60° at the *cis*-DDP binding site in order to preserve full duplex character.

Another useful NMR nucleus for monitoring *cis*-DDP-DNA interactions is ^{195}Pt, which is 34 percent abundant with I = $\frac{1}{2}$. When used in conjunction with ^{15}N (I = $\frac{1}{2}$) enriched NH_3 ligands, ^{195}Pt NMR resonances provide a powerful means for characterizing complexes in solution. The ^{195}Pt and ^{15}N chemical shifts are both sensitive to the ligand trans to the NH_3 group, as is the ^{195}Pt-^{15}N coupling constant.[127] ^{195}Pt NMR studies of *cis*-DDP binding have been carried out using nucleobases, small oligonucleotides, and even double-stranded fragments of 20 to 40 bp in length, as previously described (Section V.D.l). The major contribution of this method is to show whether platinum coordinates to a nitrogen or an oxygen donor atom on the DNA, since the ^{195}Pt chemical shift is sensitive to this difference in ligation.

b. X-ray Structural Studies

In recent years several oligonucleotide duplexes have been crystallized and characterized by x-ray diffraction methods. The probability of forming suitable single crystals of DNA fragments is disappointingly low, however, with only 1 in 10 such attempts being successful. Correspondingly, it has been difficult to crystallize platinated oligonucleotides. An alternative approach has been to soak nucleic-acid crystals of known structure with the platinum reagent in the hope of forming an isomorphous derivative, the structure of which could be obtained by using the changes in phases from the native material. In attempts to characterize a *cis*-DDP nucleic acid adduct, crystals of $tRNA^{Phe}$ and the self-complementary dodecamer d(CpGpCpGpApApTpTpCpGpCpG) were soaked with cisplatin solutions in the hope of obtaining useful metric information.[123,128,129] These efforts have thus far failed to produce a high-resolution structure, although they confirm the predilection for platinum to coordinate to the N7 position of purine rings. Addition of *cis*-DDP tends to disorder the crystal, with platinum going to several sites of partial occupancy.

A more fruitful approach has been to crystallize a purified oligonucleotide containing the coordinated *cis*-$\{Pt(NH_3)_2\}^{2+}$ moiety. The first x-ray structure to be deciphered through such a strategy was that of *cis*-$[Pt(NH_3)_2\{d(pGpG)\}]$.[130] This compound crystallizes with water solvent and glycine buffer molecules in the lattice. The crystals were grown at pH 3.8, where the terminal phosphate is monoprotonated in order to provide a neutral complex of diminished solubility. Two crystalline forms have been obtained, and both structures solved, one to 0.94 Å resolution. The latter contains four crystallographically independent molecules, which, although complicating the structure solution, afforded four independent views of the major adduct formed by *cis*-DDP with DNA. The four molecules form an aggregate, held together by hydrogen bonding and intermolecular base-base stacking interactions (Figure 9.20). There are two conformationally distinct classes that comprise molecules 1 and 2, and molecules 3 and 4; within each class, the molecules are related by an approximate C_2 symmetry axis.

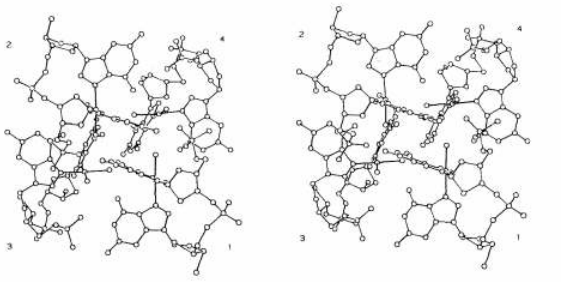


Figure 9.20 - Stereoview of aggregate of four cis-$[Pt(NH_3)_2\{d(pGpG)\}]$ molecules (reproduced by permission from Reference 130).

The molecular structure of molecule 1 is displayed in Figure 9.21; geometric information about all four molecules is contained in Table 9.4. As expected from the NMR studies, platinum coordinates to N7 atoms of the guanine bases, which are completely destacked (dihedral angles range from 76.2 to 86.7°), to form a square-planar geometry. The bases have a head-to-head configuration and conformational angles χ (Table 9.4 and Figure 9.9) that fall in the anti range. The sugar puckers of the 5'-deoxyribose rings for all four molecules have a C3'-endo conformation, and some of the 3'-sugar carbon atoms exhibit large thermal parameters suggestive of a less well-ordered structure. These results further demonstrate the similarity of the structure as detected in the solid state by x-ray diffraction and in the solution state by NMR spectroscopy.

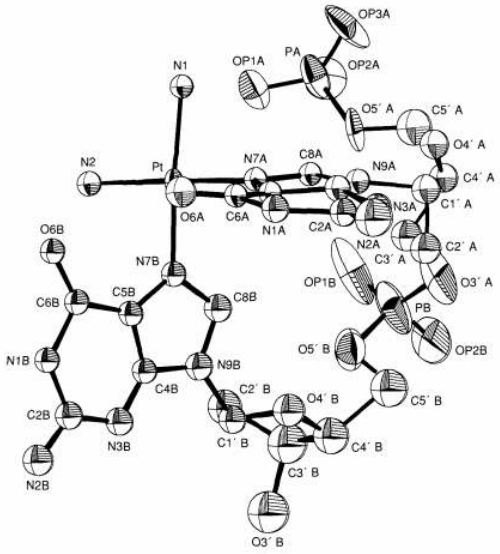


Figure 9.21 Molecular structure of cis-$[Pt(NH_3)_2d(pGpG)\}]$.

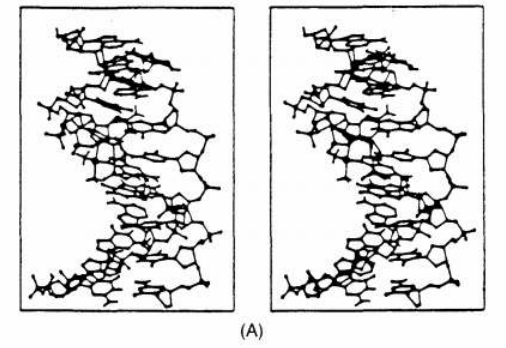
An interesting additional feature of the *cis*-$[Pt(NH_3)_2\{d(pGpG)\}]$ crystal structure is a hydrogen bonding interaction between an ammine ligand and the oxygen atom of the terminal phosphate group (OP1A•••N1, Figure 9.21). This intramolecular hydrogen bond is prominent in three of the four molecules in the asymmetric unit. Although the relevance of this hydrogen bonding interaction to the solution structure and molecular mechanism of cisplatin is presently unknown, it is interesting to note that the antitumor activity of platinum amine halide complexes is reduced when protons on coordinated NH_3 are replaced by alkyl groups.[34]

A second *cis*-DDP-oligonucleotide adduct characterized by x-ray crystallography is the neutral molecule *cis*-[$Pt(NH_3)_2${d(CpGpG)}].[131] Here again, there are several (three) molecules in the asymmetric unit. Although determined at lower resolution, the structure is similar in most respects to that of *cis*-[$Pt(NH_3)_2${d(pGpG)}] except for the presence of some weak NH_3•••O6(guanosine) intramolecular hydrogen bonding interactions and a few unusual sugar-phosphate backbone torsional angles. Also, no NH_3(H)••• phosphate(O) hydrogen bonds were observed.

From the foregoing discussion, it is apparent that adequate x-ray structure information is available for the *cis*-$\{Pt(NH_3)_2\}^{2+}$/d(pGpG) intrastrand crosslink. What is needed now are structures of the minor adducts and, most importantly, of adducts in double-stranded DNA. Very recently, dodecanucleotide duplexes containing *cis*-$\{Pt(NH_3)_2\}^{2+}$/d(pGpG) adducts have been crystallized, the structures of which are currently being investigated.[132]

c. Molecular Mechanics Calculations on Platinated Duplexes

As a supplement to x-ray structural information on double-stranded oligonucleotides containing an embedded *cis*-[$Pt(NH_3)_2${d(pGpG)}] adduct, several models have been constructed by using a molecular mechanics approach.[133] In this work, a set of coordinates was first obtained by amalgamation of structural information about standard double-helical DNAs and the platinated d(pGpG) fragment. Various starting structures were assumed, both linear and bent. The models were then refined according to various charge and stereochemical constraints built into the calculation. The results, which can reveal only what is feasible and not necessarily what actually happens, for both linear and bent structures are depicted in Figure 9.22 for two of the duplex sequences studied. In the linear model, the 5'-coordinated guanosine is rotated out of the stack, and its hydrogen bonding to the cytosine on the complementary strand is seriously disrupted. The imino N-H group is still involved in H-bonding, however; so this structure is not inconsistent with the NMR results. Two classes of kinked platinated duplex structures were encountered, with bending angles of 61 and 50°. In one of these, all Watson-Crick hydrogen bonds remain intact. These kinked structures are supported most strongly by the gel-electrophoresis experiments discussed in Section V.D.3.b.v.



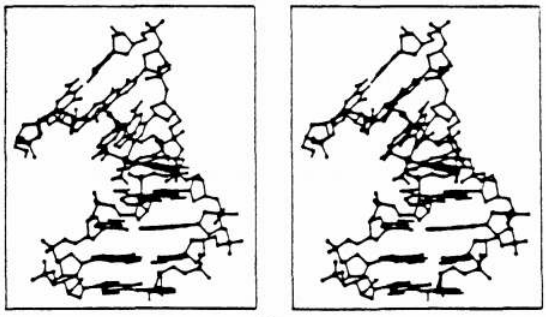


Figure 9.22 - (A) Stereoscopic view of the unkinked, platinated model of duplex d(TpCpTpCpG*pG*pTpCpTpC) from molecular-mechanics calculations. Counter ions used to stabilize the negative charge of the phosphates are not shown. (B) Stereoscopic view of the "high-salt" kinked, platinated model of duplex d(GpGpCpCpG*pG*pCpC) from molecular-mechanics calculations. Counter-ions are not depicted, with the exception of the bridging ion. (C) Stereoscopic view of the "low-salt" kinked, platinated model of duplex d(GpGpCpCpG*pG*pCpC). Counter-ions are not depicted. Reproduced with permission from Reference 133.

Molecular mechanics and the related molecular dynamics calculations are a potentially valuable tool for the bioinorganic chemist interested in how metal complexes might perturb the structures of biopolymers. Analysis of the results for cisplatin-DNA binding reveals that, compared with the sum of all contributions from the biopolymer, the Pt-DNA interactions constitute a small part of the overall energy. For the most accurate results, it is important to know the charge distributions on the metal and its ligands as well as the effects of solvent interactions. Much work needs to be done in these areas before the results of molecular mechanics and dynamics calculations can be used reliably to predict or analyze structures. At present, however, they are far superior to examination of space-filling molecular models, for example, and produce quantitatively revealing structural diagrams.

d. Platinum-Nucleobase Model Complexes

Several studies have been carried out of the *cis*-diammineplatinum(II) moiety coordinated to nucleobases in which the N9 (purine) or N3 (pyrimidine) positions either have been alkylated, to simulate the glycosidic linkages, or in which the actual nucleotide (AMP, dGMP, etc.) is employed.[134] These investigations are in many respects analogous to the synthesis and characterization by bioinorganic chemists of model complexes for the active site of a metalloenzyme. Their purpose is to simplify the problem, revealing kinetic, thennodynamic, and structural preferences of the primary building blocks involved in the metallodrug-biopolymer interaction, without the profound stereochemical constraints of the latter. Early studies of *cis*- and *trans*-DDP adducts with nucleobases (i) revealed the kinetic preferences for platinum binding to GMP and AMP, (ii) mapped out the preferred sites of platination (N7 of A and G; N1 of A; N3 of C; no N7-O6 chelate; no ribose or deoxyribose binding; only rare binding to phosphate oxygen atoms), (iii) demonstrated that Pt-N7 binding to G lowered the pK_a of N1-H by ~ 2 units, and (iv) led to the discovery of interesting new classes of coordination complexes such as the *cis*-diammineplatinum pyrimidine blues and metal-metal bonded diplatinum(III) complexes.

Attempts to model the intrastrand d(GpG) crosslink with nucleobases have met with only moderate success. Usually the O6 atoms of the two guanosine rings are on opposite sides of the platinum coordination plane ("head-to-tail" isomer). Only for *cis*-$[Pt(NH_3)_2(9\text{-EtG})_2]^{2+}$ was the correct isomer obtained. Nucleobase complexes of the *cis*-diammineplatinum(II) moiety have been valuable for testing the controversial proposal of N7,O6 chelate formation, which to date has not been observed. Several interesting discoveries of metal-nucleobase chemistry are that metal binding can stabilize rare tautomers, for example, the 4-imino, 2-oxo form of cytosine, through N4 binding, that coordination of platinum often produces unusual base pairing, and that metal migration from one donor site to another on an isolated nucleobase can occur. These model studies will continue to provide valuable insights into the possible chemistry of platinum antitumor drugs with DNA.

e. trans-DDP-DNA Adducts

Because *trans*-DDP is biologically inactive, it has received less attention than the *cis* isomer. Nevertheless, knowledge of its binding to DNA is important to have as a reference point for mechanistic comparison with the active compounds. Shortly after replication mapping experiments established that *trans*-DDP binds preferentially to d(GpNpG) and d(ApNpG) sequences,[135] several synthetic oligonucleotides containing such sequences were prepared and used to investigate reactions with the *trans* isomer.[136-138] Kinetic studies of *trans*-DDP with d(GpCpG) and d(ApGpGpCpCpT) revealed the presence of, presumably

monofunctional, intermediates that closed to form both intra- and interstrand products. In the reaction with d(GpCpG), the 1,3-intrastrand G-G chelate accounted for 70 percent of the product, and 21 percent of the remaining material was unreacted oligonucleotide. Proton NMR studies of purified *trans*-[$Pt(NH_3)_2${d(GpCpG)}] as well as the d(GpTpG) analog established platinum binding to N7 positions of the two trans guanosine nucleosides. As with the *cis*-[$Pt(NH_3)_2${d(pGpG)}] adducts, the 5'-guanosine residue no longer retained the normal B-DNA type conformation; instead, the sugar ring pucker switched to C3'-endo. A fairly detailed ^1H NMR characterization of *trans*- [$Pt(NH_3)_2${d(ApGpGpCpCpT)-N7-A(1),N7-G(3)}] revealed very similar features. This example nicely illustrates the different stereoselectivity of *cis*- and *trans*-DDP binding to DNA. The *cis* isomer forms exclusively an intrastrand d(GpG) crosslink, whereas the *trans* isomer makes a 1,3-d(A*pGpG*) adduct. A schematic depiction of the *trans*-$\{Pt(NH_3)_2\}^{2+}$ adduct is shown in Figure 9.23. As can be seen, the two purine rings enclose a large, 23-membered ring, the central guanosine residue is "bulged out," and the 5'-residue has a C3'-endo sugar pucker. This structure may be compared with that of *cis*-[$Pt(NH_3)_2${d(pGpG)}] (Figure 9.21), where the platinum is part of a smaller, 17-membered ring. Both space-filling model building studies and molecular mechanics calculations reveal that it would be stereochemically very unfavorable for the *trans*-$\{Pt(NH_3)_2\}^{2+}$ fragment to replace the *cis* analogue in an intrastrand crosslinked d(GpG) structure of the kind shown in Figure 9.21. Thus, for bidentate adducts, it seems clear that the important difference between *cis*- and *trans*-DDP binding to single-stranded DNA is revealed by the structures shown in Figures 9.21 and 9.23, respectively.

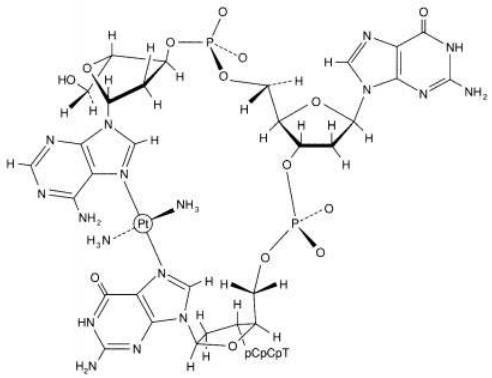


Figure 9.23 - Structure of the intrastrand 1,3-d(A*pGpG*) crosslink formed in the reaction of trans-DDP with d(ApGpGpCpCpT). Reproduced by permission from Reference 136.

Information about *trans*-DDP binding to double-stranded DNA is scanty, but very recent studies indicate that the *trans*-[$Pt(NH_3)_2${d(GpApG)-N7-G(1),N7-G(3)}] intrastrand crosslinked fragment can be embedded in duplex dodecamers.[139] Interestingly, for one sequence the melting temperature (T_M) of this duplex is not reduced over that of the unplatinated DNA fragment, in contrast to results for *cis*-DDP intrastrand d(GpG) adducts. This intriguing result, which agrees with earlier T_M studies of DNA platinated by *trans*-DDP, does not yet have a structural rationale. It is possibly relevant to the processing of bifunctional *trans*-DDP-DNA adducts *in vivo*.

f. Effects of Platination on DNA Structure

It is valuable to summarize at this stage all that has been learned concerning the changes in DNA structure that occur upon *cis*- or *trans*-DDP binding. *cis*-DDP intrastrand crosslinks result in unstacking of neighboring bases and a switch in the sugar pucker of the 5'-nucleoside from C2'-endo, the standard B-DNA conformation, to C3'-endo, a conformation encountered in A-DNA. These various forms of DNA have already been introduced in the previous chapter. Watson-Crick base pairing, although weakened, is probably maintained. Evidence that base pairing is altered comes from studies with antinucleoside antibodies that bind appreciably better to DNA platinated with *cis*-DDP than to unmodified DNA. These antibodies recognize the nucleobases much better in platinated than in unplatinated DNA, presumably because platination disrupts the double helix. Additional support for base-pair disruption comes from gradient gel-denaturation experiments using sitespecifically platinated DNA (see Section V.D.8.b). Intrastrand crosslinking by *cis*-DDP also bends the helix by about 34° and unwinds the duplex by 13°. When *trans*-DDP forms 1,3-intrastrand crosslinks, the nucleotides situated between the platinated residues may be bulged out; consistent with this picture is the fact that they present an especially good target for antinucleoside antibodies. In 1,3-intrastrand d(GpNpG) or d(ApNpG) adducts, the 5'-nucleoside sugar pucker is altered to C3 I-endo. Intrastrand crosslink formation by *trans*-DDP also leads to DNA bending,

but the platinum serves as the locus for a hinge joint and not for cooperative bending. These different effects of platination on DNA structure brought about by the two isomers are likely to be related to their different biological activities.

7.6.7: Structure of Platinum-DNA Complexes is shared under a not declared license and was authored, remixed, and/or curated by LibreTexts.

7.6.8: Site-specifically Platinated DNA 154

a. The Problem

Much of the information obtained about the mechanism of action of cisplatin has been derived from experiments where Pt-DNA binding has occurred *in vivo* or *in vitro*, with the use of random-sequence DNA having all available targets for the drug. In these studies, platination is controlled by the inorganic chemistry of *cis*-DDP in the medium and the accessibility of target sites on the DNA, as already discussed in considerable detail. As such, this situation best represents drug action as it actually occurs in the tumor cell. On the other hand, the resultant spectrum of DNA adducts makes it difficult, if not impossible, to understand the structural and functional consequences of any specific adduct. In order to address this problem, a methodology has been developed in which a single platinum adduct is built into a unique position in the genome. This approach is powerful and has the potential to be extended to the study of many other metal-based drugs. In this section, we discuss the strategy used to construct such site-specifically platinated DNA molecules and the information obtained thus far from their study. Some uses have already been discussed.

b. Synthesis and Characterization

Figure 9.29 displays the map of a genome constructed by insertion of platinated or unplatinated dodecanucleotide duplexes d(pTpCpTpApGpGpCpCpTpTpCpT)•d(pApGpApApGpGpCpCpTpApGpA) into DNA from bacteriophage M13mp18. This genome was constructed in the following manner.[154] Double-stranded DNA from M13mp18 was first digested with Hinc II, a restriction enzyme that recognizes a unique six-base-pair sequence in the DNA and cleaves the double helix there, leaving a blunt-ended (no overhanging bases) cleavage site. The unplatinated dodecamer duplex was next ligated into the Hinc II site, and the DNA amplified *in vivo*. The dodecamer can insert into the genome in two different orientations, the desired one of which, termed M13-12A-Stu I, was identified by DNA sequencing. The presence of the insert in the new DNA was checked by its sensitivity to the restriction enzyme Stu I, which cleaves at the d(AGGCCT) sequence uniquely situated in the dodecamer insert, and the absence of cleavage by Hinc II the site for which was destroyed. Next, Hinc II-linearized M13mp18 replicative form (RF) DNA was allowed to form a heteroduplex with excess viral DNA (which has only the + strand in the presence of the denaturant formamide which was dialyzed away during the experiment. The resulting circular DNA has a gap in the minus strand into which the platinated d(TCTAG*G*CCTTCT) was ligated (Figure 9.30). The latter material was prepared by the methods described in Section V.D.5.a and characterized by ^{1}H NMR spectroscopy. The resulting site-specifically platinated DNA contains a single *cis*-[$Pt(NH_3)_2${d(pGpG)}] intrastrand crosslink built into a unique position. The methodology is general, and has been used to create other known platinum-DNA adducts site-specifically in M13mp18.

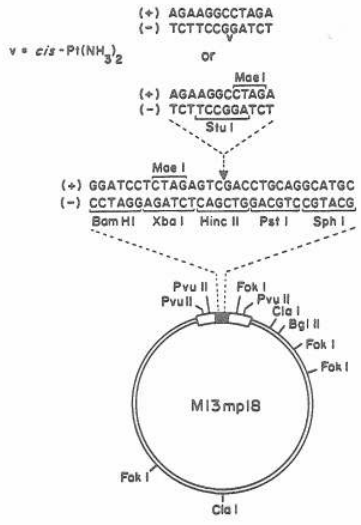


Figure 9.29 - Map of the genome created by insertion of cis-DDP platinated or unplatinated d(TpCpTpApGpGpCpCpTpTpCpT)-d(ApGpApApGpGpCpCpTpApGpA) into the Hinc II restriction site of bacteriophage M13mp18 DNA.

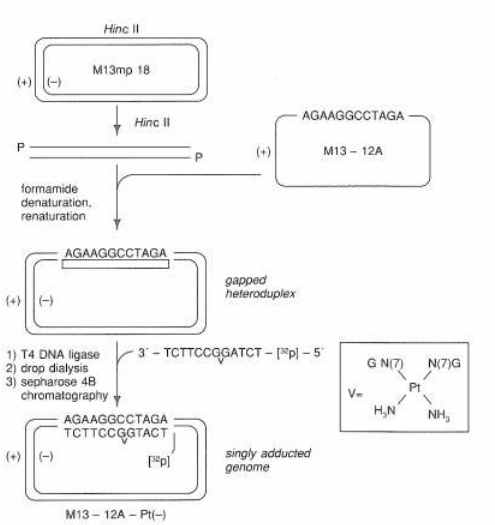


Figure 9.30 - Scheme for constructing site-specifically platinated genomes via gapped heteroduplex synthesis (reproduced by permission from Reference 154).

The chemical properties of the platinated DNA, termed M13-12A-Pt(-)-Stu I, were investigated by enzymatic, digestion and gel electrophoresis experiments. Platinum completely inhibits cleavage of the DNA by Stu I, as expected from the earlier restriction enzyme mapping studies. In addition, the *cis*- [$Pt(NH_3)_2${d(pGpG)}] and *cis*-[$Pt(NH_3)_2${d(pApG)}] intrastrand crosslinks were found to inhibit a variety of DNA polymerases, with only a small amount of bypass of the platinum lesion.[149] These results indicate that the most abundant adducts of cisplatin on DNA are able to block replication efficiently.

c. Biological Properties

When M13-12A-Pt(-)-Stu I DNA was introduced into *E. coli* cells by transformation, DNA synthesis was uninterrupted, because the cell can both repair the damage and use the unmodified (+) strand for synthesis. Consequently, a slightly different strategy was used to construct single-stranded M13-12A-Pt(+)-Stu I DNA, the details of which are available elsewhere.[154] This platinated template, in which the damage can neither be repaired nor bypassed by known mechanisms *in vivo*, was then transformed into *E. coli* cells co-plated with GW5100 cells. Under these conditions, viral DNA replication is detected by the expression of the *β*-galactosidase gene, which, in the presence of appropriate reagents in the medium, leads to formation of blue plaques on a clear background. The results clearly indicate that many fewer plaques appear when M13-12A-Pt(+) is introduced into the cells than when M13-12A-u(+) was employed, where u stands for unmodified DNA. In three repeats of this experiment, survival of DNA containing only a single *cis*-[Pt(NH3h{d(pGpG)}] crosslink was only 11 ± 1 percent.

These data provide unambiguous proof that the most frequent DNA adduct formed by cisplatin is toxic, capable of inhibiting replication when only a single such lesion is present on a natural DNA template of 7,167 nucleotides. The fact that as many as 10 percent of the transformed cells can bypass or repair the lesion is also of interest, and parallels the results found *in vitro*. In related work, it was found that the *cis*-[$Pt(NH_3)_2${d(pGpG)}] intrastrand crosslink is not very mutagenic, but that *cis*-[$Pt(NH_3)_2${d(pApG)}] intrastrand adducts are considerably more so. This finding is important, since mutations could lead to long-term secondary tumor production in patients treated with cisplatin. The methodology affords a way to screen new compounds that one would like to be equally effective at inhibiting replication but less mutagenic. In addition, by using repairdeficient mutant cell lines, as well as cisplatin resistant cells, one can study the effects of varying the properties of the host cells. Incorporation of site-specifically platinated DNA sequences into appropriate shuttle vectors will also facilitate investigation of toxicity, repair, and resistance in mammalian cells.

d. Prospectus

The foregoing discussion illustrates the power of site-specifically platinated DNAs as a probe of the molecular mechanism of the drug. We recall that similar strategies were employed to obtain uniquely modified DNA in the bending[92,93] and unwinding[95] experiments discussed previously. In principle, this technique can be applied to examine other aspects of the molecular mechanism of other metallochemotherapeutic agents. The requirements are a synthetic route to the uniquely modified genome, for which both

the inorganic coordination chemistry and molecular biology must be amenable, an adduct stable to the biological conditions for DNA synthesis, and a method (usually genetic) for scoring the biological effects being investigated. Site-specifically platinated DNAs allow the bioinorganic chemist to have maximal control over the genetics and should continue to provide valuable information about the molecular mechanism of action of cisplatin.

7.6.8: Site-specifically Platinated DNA [154] is shared under a not declared license and was authored, remixed, and/or curated by LibreTexts.

7.6.9: Bioinorganic Chemistry of Platinum Anticancer Drugs- How Might They Work?

The material in this section constitutes the major portion of this chapter. One important goal of the discussion is to illustrate, by means of an in-depth analysis of a single case history, the questions that must be addressed to elucidate the molecular mechanism of an inorganic pharmaceutical. Another is to introduce the techniques that are required to answer these questions, at least for the chosen case. The inorganic chemist reading this material with little or no biological background may find the experience challenging, although an attempt has been made to explain unfamiliar terms as much as possible. It is strongly advised that material in Chapter 8 be read before this section. Toward the end of this section, the results obtained are used to speculate about a molecular mechanism to account for the biological activity of the drug. Experiments directed toward evaluating the various hypotheses are delineated. Once the mechanism or mechanisms are known, it should be possible to design new and better antitumor drugs which, if successful, would be the ultimate proof of the validity of the hypotheses. This topic is discussed in the next and final section of the chapter. Such an analysis could, in principle, be applied to probe the molecular mechanisms of the other metals used in medicine described previously. In fact, it is hoped that the approach will prove valuable to students and researchers in these other areas, where much less information is currently available at the molecular level.

The material in this section has been organized in the following manner. First we discuss the relevant inorganic chemistry of platinum complexes in biological media. Next we summarize the evidence that DNA is a major target of cisplatin in the cancer cell, responsible for its antitumor activity. The chemical, physical, and biological consequences of damaging DNA by the drug are then described, followed by a presentation of the methodologies used to map its binding sites on DNA. The detailed structures of the DNA adducts of both active and inactive platinum complexes are then discussed, together with the way in which the tertiary structure of the double helix can modulate these structures. Finally, the response of cellular proteins to cisplatin-damaged DNA is presented, leading eventually to hypotheses about how tumor cells are selectively destroyed by the drug. Together these events constitute our knowledge of the' 'molecular mechanism," at least as it is currently understood.

1. Reactions of *cis*-DDP and Related Compounds in Aqueous, Biological, and Other Media

cis-Diamminedichloroplatinum(II) is a square-planar d^8 complex. As such, it belongs to a class of compounds extensively investigated by coordination chemists.[55] Typically, such compounds are relatively inert kinetically, do not usually expand their coordination numbers, and undergo ligand substitution reactions by two independent pathways with the rate law as given by Equation (9.4). The rate constants k_1 and k_2 correspond to first-order (solvent-assisted) and second-order (bimolecular) pathways;

$$Rate = (k_1 + k_2[Y])[complex] \tag{9.4}$$

[Y] is the concentration of the incoming ligand. Usually, $k_1 << k_2$ by several orders of magnitude. In biological fluids, however, the concentration of a potential target molecule could be ~10^{-6} M, in which case $k_1 \simeq k_2[Y]$. Substitution of ligands in *cis*-DDP, required for binding to a cellular target molecule, is therefore likely to proceed by the solvent-assisted pathway. Such a pathway is assumed in the ensuing discussion.

For the hydrolysis of the first chloride ion from *cis*- or *trans*-DDP,

$$[Pt(NH_3)_2Cl_2] + H_2O \rightleftharpoons [Pt(NH_3)_2Cl(OH_2)]^+ + Cl^- \tag{9.5}$$

the k_1 values at 25 °C are 2.5 x 10^{-5} and 9.8 x 10^{-5} s^{-1}, respectively.[55] These hydrolyzed complexes can undergo further equilibrium reactions, summarized by Equations (9.6) to (9.9).

$$[Pt(NH_3)_2Cl(OH_2)]^+ \rightleftharpoons [Pt(NH_3)_2Cl(OH)] + H^+ \tag{9.6}$$

$$[Pt(NH_3)_2Cl(OH_2)]^+ + H_2O \rightleftharpoons [Pt(NH_3)_2(OH_2)_2]^{2+} + Cl^- \tag{9.7}$$

$$[Pt(NH_3)_2(OH_2)_2]^{2+} \rightleftharpoons [Pt(NH_3)_2(OH_2)(OH)]^+ + H^+ \tag{9.8}$$

$$[Pt(NH_3)_2(OH_2)(OH)]^+ \rightleftharpoons [Pt(NH_3)_2(OH)_2] + H^+ \tag{9.9}$$

The formation of dimers such as $[Pt(NH_3)_2(OH)]_2^{2+}$ and higher oligomers can also occur,[56,57] but such reactions are unlikely to be important at the low platinum concentrations encountered in biological media, Reactions (9.5) to (9.9), which depend on pH and the chloride-ion concentrations, have been followed by ^{195}Pt (I = $\frac{1}{2}$, 34.4 percent abundance) and ^{15}N (using enriched compounds)

NMR spectroscopy. The latter method has revealed for the *cis*-diammine complexes pK_a values of 6.70 ± 0.10 at 25 °C for Reaction (9.6) and of 5.95 ± 0.1 and 7.85 ± 0.1 at 5 °C for Reactions (9.8) and (9.9), respectively.[58]

The effects of pH and Cl^- ion concentration on the species distribution of platinum compounds have been used to fashion the following plausible argument for the chemistry of *cis*-DDP *in vivo*.[59] With the use of thermodynamic data for the ethylenediamine (en) analogue $[Pt(en)Cl_2]$ the relative concentrations of hydrolyzed species at pH 7.4 were estimated (see Table 9.3) for blood plasma and cytoplasm (Figure 9.7). The higher chloride ion concentration in plasma preserves the complex as the neutral molecule cis-DDP, which passively diffuses across cell membranes. The lower intracellular chloride ion concentration facilitates hydrolysis reactions such as Equations (9.5) to (9.9), thereby activating the drug for binding to its biological target molecules. There is, of course, a reasonable probability that *cis*-DDP and species derived from it will encounter small molecules and macromolecules *in vivo* that divert it from this route to the target. We have already seen such cases; cisplatin binds to serum proteins, and there is good evidence that intracellular thiols react with the drug.[60] Glutathione, for example, is present in millimolar concentrations in cells. How, one might ask, does cisplatin swim through such a sea of sulfur donors to find its target in the tumor cell? Is it possible that a modified form of the drug, in which a Pt-CI bond has been displaced by thiolate to fonn a Pt-S bond, is the actual species responsible for its activity? Although these questions have not yet been satisfactorily answered, there is reason to believe that such reactions are not directly involved in the molecular mechanism of action. As evident from structure-activity relationship studies, the most active compounds have two labile ligands in *cis* positions. If Pt-S bonds were required, then compounds already having such linkages would be expected to exhibit activity and they do not. Rather, it seems most likely that the antitumor activity of cisplatin results from surviving species of the kind written in Equations (9.5) to (9.9) that find their way to the target molecule, and that the induced toxicity must arise from a significantly disruptive structural consequence of drug binding. Since only *cis* complexes are active, it is reasonable for the coordination chemist to infer that the stereochemistry of this interaction is of fundamental importance.

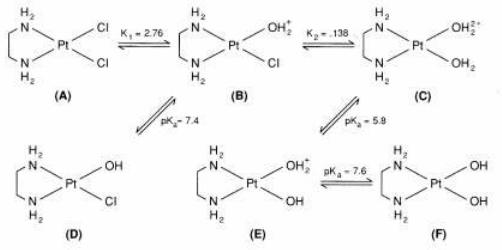


Figure 9.7 - Hydrolysis reactions of antitumor platinum complexes and an estimate of the species present in plasma and cytoplasm (reproduced by permission from Reference 51).

Table 9.3 - Distribution of various adducts formed between *cis*-DDP or $[^3H][Pt(en)Cl_2]$[a] and DNA *in vitro* and *in vivo*.[118-122]

a) A radiolabeled analogue of *cis*-DDP, [^{3}H]dichloroethylenediamineplatinum(II).

b) A_2 represents either $(NH_3)_2$ or ethylenediamine.

c) By difference.

d) Percentage of adducts based on total amount of platinum eluted from the separation column.

e) Percentage of adducts based on total amount of radioactivity eluted from the separation column.

f) Not given.

g) Chinese hamster ovary cells treated with 83 μM *cis*-DDP.

h) Results from ELISA.

i) Results from AAS. Where the signal was too weak for reliable quantitation, the maximal amount possible is given. Adapted from Table 1 in Reference 81.

D/N Ratio	Total Incubation Time	Adducts Formed			Mono-functional Adducts	Remaining Platinum[c]
		cis-[PtA_2{d(pGpGl}][b]	*cis*-[PtA_2{d(pApG}][b]	*cis*-[PtA_2{d(GMP)}$_2$][b]		
In vitro						
0.055[c]	5 h (50 °C)	47-50%	23-28%	8-10%	2-3%	10%
0.022[d]	5 h (50 °C)	60-65%	20%	~4%	~2%	9-14%
0.01[e]	16 h (37 °C)	62%	21%	7%	—	10%
[ef]	30 m (37 °C)	36%	3%	8%	40%	13%
[ef]	2 h (37 °C)	54%	9%	9%	14%	14%
[ef]	3 h (37 °C)	57%	15%	9%	4%	15%
In vivo						
[dg]	1 h (37 °C)	35.9 ± 4.7%[h]	<34%[i]	3.1 ± 1.6%[h]	38.5%[i]	~22%
[dg]	25 h (37 °C)	46.6 ± 6.8%[h]	<48%[i]	3.0 ± 0.9%[h]	<14.5%[i]	~50%

Reactions of platinum compounds with components in media used to dissolve them can give and undoubtedly have given rise to misleading results, both in fundamental mechanistic work and in screening studies. A particularly noteworthy example is dimethylsulfoxide (DMSO), which even recently has been used to dissolve platinum compounds, presumably owing to their greater solubility in DMSO compared to water. As demonstrated by ^{195}Pt NMR spectroscopy, both *cis*- and *trans*-DDP react rapidly ($t_{1/2}$ = 60 and 8 min at 37 °C, respectively) to form $[Pt(NH_3)_2CI(DMSO)]^+$ complexes with chemical and biological reactivity different from those of the parent ammine halides.[61]

2. Evidence that DNA is the Target

Two early sets of experiments pointed to interactions of cisplatin with DNA, rather than the many other possible cellular receptors, as an essential target responsible for cytotoxicity and antitumor properties.[62,63] Monitoring the uptake of radiolabeled precursors for synthesizing DNA, RNA, and proteins, showed that [^{3}H]thymidine incorporation was most affected by therapeutic levels of cisplatin for both cells in culture and Ehrlich ascites cells in mice. Since independent studies showed that *cis*-DDP binding to DNA polymerase does not alter its ability to synthesize DNA, it was concluded that platination of the template and not the enzyme was responsible for the inhibition of replication.

In a second kind of experiment demonstrating that DNA is a target of cisplatin, hydrolyzed forms of the drug in low concentrations were added to a strain of *E. coli* K12 cells containing a sex-specific factor F.[64,65] After free platinum was removed, these F^+ cells were conjugated with a strain of *E. coli* K12 cells lacking this factor that had previously been infected with lambda bacteriophage. Addition of *cis*-DDP, but not *trans*-DDP, directly to the latter infected F^- cells had been shown in a separate study to accelerate cell lysis. Conjugation with the platinum-treated F^+ cells produced the same effect, strongly suggesting that Pt had been transferred from the F^+ to the F^- cells. Since only DNA is passed between the F^+ and F^- strains, it was concluded that Pt was attached to the DNA and that this modification was essential for the observed lysis of the cell. Further studies showed a good correlation between cell lysis by platinum compounds and their antitumor properties.

Various other observations are consistent with the notion that platinum binding to DNA in the cell is an event of biological consequence.[66] The filamentous bacterial growth observed in the original Rosenberg experiment is one such piece of evidence, since other known DNA-damaging agents, for example, alkylating drugs and x-irradiation, also elicit this response. Another is the greater sensitivity toward *cis*-DDP of cells deficient in their ability to repair DNA. Finally, quantitation of the amount of platinum bound to DNA, RNA, and proteins revealed that, although more Pt was bound to RNA per gram biomolecule, much more Pt was on the DNA when expressed as a per-molecule basis. In the absence of any selective interaction of Pt with a specific molecule, only

one out of every 1,500 protein molecules (average M.W. ~60 kDa) in a cell will contain a single bound platinum atom, whereas hundreds or thousands of Pt atoms are coordinated to DNA (M.W. ~10^{11}). If the replication apparatus cannot bypass these lesions, then cell division will not occur, and tumor growth is inhibited.

Although these and other results all point to DNA as an important cellular target of cisplatin, most likely responsible for its anticancer activity, this information does not explain why tumor cells are more affected by *cis*-DDP than non-tumor cells of the same tissue. Moreover, why is *trans*-DDP, which also enters cells, binds DNA, and inhibits replication, albeit at much higher doses (see discussion below), not an active anticancer drug? What causes cisplatin to kill cells and not merely to arrest tumor growth? The latter can be explained by DNA synthesis inhibition, but not necessarily the former. Very recent studies have begun to address these questions using powerful new methodologies of molecular and cell biology, as described in subsequent sections of this chapter. The results, although preliminary, continue to point to DNA as the most important cellular target of cisplatin.

7.6.9: Bioinorganic Chemistry of Platinum Anticancer Drugs- How Might They Work? is shared under a not declared license and was authored, remixed, and/or curated by LibreTexts.

7.6.10: Bioinorganic Chemistry of Platinum Anticancer Drugs; How Might They Work? (Part 2)

6. Effects of DNA Structure on Platinum Binding

a. A-, B-, and Z-DNA[140]

As discussed in more detail in Chapter 8, double-helical DNA can adopt different polymorphic forms depending on the conditions in solution or polycrystalline fiber. Even within a given DNA molecule, there can be sequence-dependent local secondary and tertiary structural differences that constitute important signals for cellular DNA binding and processing molecules. An example already discussed is the recognition of palindromic sequences by type II restriction endonucleases. As shown in Figure 9.24, three such DNA polymorphs are the right-handed A- and B- and the left-handed Z-forms. Most commonly encountered in solution is B-DNA, characterized by well-classified major and minor grooves designated by arrows in Figure 9.24. The targets of platinum binding, guanine N7 atoms, are situated in the major groove.

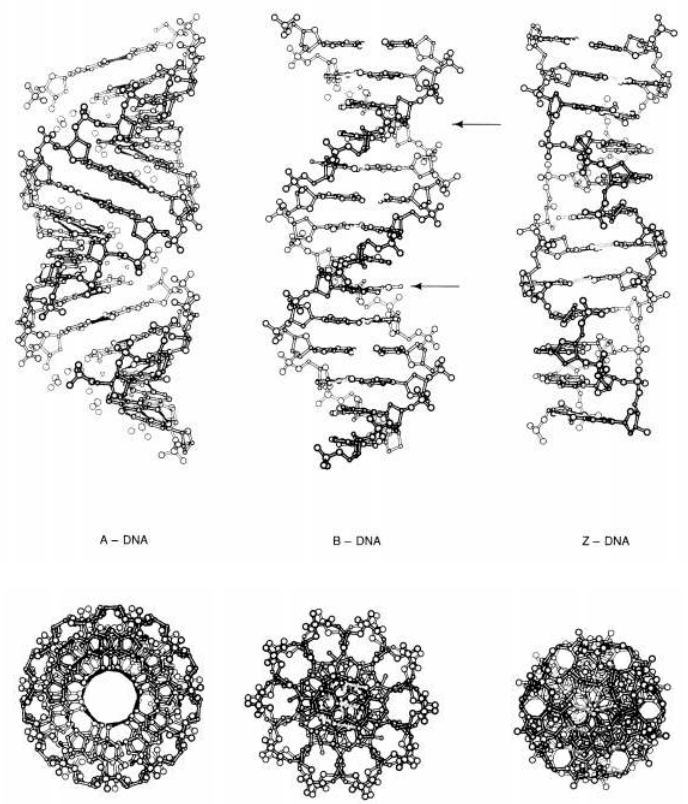


Figure 9.24 - Representations of side (above) and top (below) views of three major classes of double-stranded DNA. For B-DNA, arrows near the top and bottom of the helix designate the minor and major grooves, respectively. Reproduced with permission from Reference 140.

To what extent do sequence-dependent local structural modulations affect platinum binding? Although no general answer to this question can be given, there are several interesting anecdotal pieces of information worth mentioning. Z-DNA, a form favored by alternating purine-pyrimidine sequences such as in poly d(GC), does not constitute a particularly good target for *cis*-DDP binding. For one thing, it lacks the preferred d(GpG) or d(ApG) sequences. The monofunctional $[Pt(dien)Cl]^{+}$ complex, however, facilitates the B-DNA → Z-DNA conformational transition, as demonstrated by circular dichroism and ^{31}P NMR spectroscopic data.[141] In Z-DNA, the guanosine nucleoside adopts the syn conformation (Figure 9.9), which is presumably favored by placing a bulky $\{Pt(dien)\}^{2+}$ moiety on N7. Moreover, the local charge density on DNA is greater in Z- than B-DNA, owing to the closer proximity of the phosphate groups, and the former is presumably stabilized by the +2 charge on the platinum complex.

b. Effects of Local Sequence and of Free and Linked Intercalators on Platinum Binding

Of more interest perhaps to anticancer drug-DNA interactions is the fact that some d(GpG), d(ApG), and even d(GpA) targets for *cis*-DDP binding are very sensitive to the sequences in which they are embedded. This phenomenon was first discovered during exonuclease III mapping studies of cisplatin binding to a 165-bp restriction fragment from pBR322 DNA.[142] Although *cis*-DDP binding stops the enzyme at G_3, G_5, and GAGGGAG sequences, at a $(D/N)_b$ ratio of 0.05 there is little evidence for coordination to an apparently favored G_6CG_2 sequence (Figure. 9.25, lane 8). When platination was carried out in the presence of the DNA intercalator EtdBr (Figure 9.11), however, the G_6CG_2 sequence became a Pt binding site (Figure 9.25, lanes 9-12). A more extensive exonuclease III mapping study of this phenomenon suggested that d(CGG)-containing sequences in general are less well platinated by *cis*-DDP.[143,144] Moreover, only EtdBr, and not other acridine or phenanthridinium type intercalators, was able to promote an enzyme-detectable *cis*-DDP binding to these sequences. A suggested explanation for these results is that local d(purCGG) sequences might have an A-DNA-type structure (Figure 9.24) in which the major groove is narrow, inhibiting access of platinum to N7 of guanosine nucleosides. In the presence of the intercalator EtdBr, the local DNA structure might be altered in such a manner as to permit binding.[143,144]

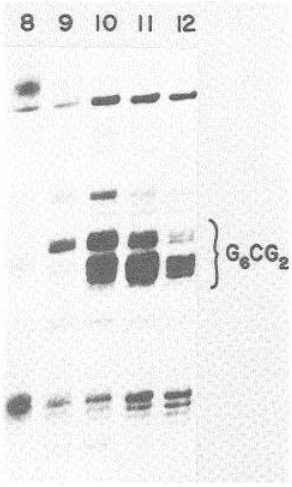


Figure 9.25 - Autoradiograph of Exo III mapping results for cis-DDP binding to a 165-bp DNA restriction fragment. The Pt/nucleotide ratio is 0.05. Lanes 8-12 contain DNA platinated in the presence of 0, 0.012, 0.057, 0.12, and 0.23 Etd/nucleotide, respectively. For more details, see Reference 142.

In accord with this interpretation, and further to delineate a possible reason why acridines and deaminated ethidium cations do not promote cisplatin binding to d(purCGG) sequences, NMR studies were performed that revealed the mean residence time of EtdBr on DNA to be 6 to 21 times longer than that of any of the other intercalators examined.[144] Thus, for these latter intercalators, the local DNA structure presumably can relax back to one unfavored for cisplatin binding before it can diffuse to the site. Moreover, when acridine orange (AO), one of the five intercalators studied that does not promote cisplatin binding to excluded sites, was covalently attached to dichloroethylenediamineplatinum(ll) (Figure 9.26) via a hexamethylene linker chain, the resulting AO-Pt molecule was able to bind to all d(CpGpG) sites, as determined by exonuclease III mapping. In the tethered molecule, the high local concentration near the intercalator binding site facilitates attachment of the $\{Pt(en)\}^{2+}$ moiety to DNA before the acridine orange fragment can diffuse away and the structure can relax to reform the excluded site.

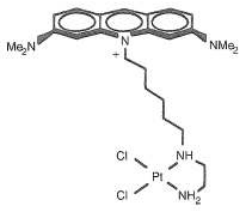


Figure 9.26 - Structure of AO-Pt in which the $\{Pt(en)C_{12}\}$ moiety is linked by a hexamethylene chain to acridine orange.

Subsequently, the excluded site phenomenon was found for *cis*-DDP binding, as assayed by the 3'-5'-exonuclease activity of T4 DNA polymerase.[145] Enzyme stopping sites were observed at all d(GpG) sequences, but only weakly when at a d(GTGGTC) site.

Similarly, d(ApG) was not modltled when embedded in pyGAGCpy and pyGAGCA sequences. Although most d(GpA) sequences were not platinated, as detected by T4 mapping, a few were. These results further underscore the importance of local sequence modulation of cisbinding to DNA.

c. DNA-Promoted Reaction Chemistry

In the EtdBr-enhanced binding of *cis*-DDP to DNA, a small fraction (< 5 percent) of the intercalator is strongly bound and can be dialyzed out only very slowly.[145] The detailed structure of this DNA-cisplatin-EtdBr ternary complex has been established, and involves *cis*-$\{Pt(NH_3)_2\}^{2+}$ binding to the exocyclic amino groups of ethidium as well as to donor sites on DNA.[146] This assignment was proved by synthesizing *cis*- $[Pt(NH_3)_2CEtd)CI]^{2+}$ complexes in dimethylformamide solution and then allowing them to react with DNA. The optical spectra of the resulting adducts were identical to that of the ternary complex. The reaction of *cis*-DDP, and DNA to form the ternary complex is promoted by the favorable orientation of the exocyclic amino group of intercalated Etd with respect to the coordination plane of bound to the double helix. The N-8 exocyclic amino group of ethidium, bound intercalatively at a site adjacent to a purine N-7 coordinated *cis*-$\{Pt(NH_3)_2CI\}^{+}$ moiety, is positioned above the platinum atom in a structure resembling the transition state for a square-planar substitution reaction. The structure of this transition state has been modeled in a molecular mechanics calculation (Figure 9.27 See color plate section, page C-16.),[147] and evidence has been obtained that indicates selective binding of platinum to the Etd N-8 amino position.[148]

Since cisplatin is usually administered in combination chemotherapy with other drugs, many of which contain intercalating functionalities, strong covalent, DNA-promoted interactions between drug molecules at a target site must be considered as possibly relevant to the molecular mechanism of action. In such a situation, there must be a strong binding preference for both drug molecules for the same target sequences, since on probability grounds alone it is unlikely that both would migrate to the same site by random diffusion at the low concentrations found *in vivo*.

d. Effects of DNA Function on Platinum Binding

Although there is yet little known about this topic for cisplatin, it is worth pointing out that other DNA-targeted drugs, such as bifunctional alkylating agents, bind preferentially to actively transcribed genes. It is therefore possible that platinum exhibits such preferences, for example, to single-stranded DNA at or beyond the transcription fork, compared to duplex DNA in chromatin structures. Or, perhaps, it too binds selectively to actively transcribed DNA. Investigation of these possibilities seems worthwhile.

7. Speculations About the Molecular Mechanism

a. Is There a Single Mechanism?

Most investigators now agree that DNA is the cytotoxic target of cisplatin. We have seen that the drug inhibits DNA replication by binding to the template and halting the processive action of DNA polymerase. Less well-studied is the inhibition of transcription by platinum-DNA adducts, but recent evidence clearly indicates that they can do so. Studies of the effects of platinum on cells growing in culture reveal that DNA replication and cell growth can continue without cell division in the presence of low levels (1 μ g/mL) of *cis*-DDP cells are arrested at the G2 phase, the stage of cell growth just preceding division.[105] G2 arrest was reversible, but at higher cisplatin levels (8 μg/mL), cell death occurred. These observations led to the speculation that, perhaps, post-replication DNA repair can handle the toxicity associated with a platinum-damaged template, at least for DNA synthesis, but that there is no known pathway by which transcription can circumvent Pt-DNA lesions. Possibly, inhibition of transcription is ultimately a more lethal event than inhibition of replication. This idea is inconsistent with the well-established fact that thymidine incorporation into DNA is more affected by low levels of cisplatin than is uridine incorporation into RNA. Might there be more than one biochemical pathway by which cisplatin manifests its anticancer activity? Further work is necessary to address this intriguing question.

b. Is There a "Critical Lesion"?

We now have an excellent understanding of the major DNA adducts made by *cis*-DDP, their structures, and the corresponding DNA distortions. Information about adducts made by the inactive *trans* isomer, though not as complete, is also substantial. During the period when this knowledge was being accumulated, it was of interest to learn whether a "critical lesion," a specific DNA adduct with a unique molecular structure might be responsible for the antitumor activity of the drug. At present, it appears that all bidentate adducts made by *cis*- and *trans*-DDP can inhibit replication, although they may not be equally efficient at doing so.[149]

Even monofunctional adducts of the kind formed by *cis*-$[Pt(NH_3)_2(4\text{-Br-py})Cl]^+$ can block replication.[96] Thus, it be better to think about the concept of "critical lesion" in a functional sense, where the rates of adduct formation, removal, and enzyme inhibition together determine which family of adducts will exhibit antitumor activity and which will not. Here the biochemistry of the host cell will also be an important determinant. Clearly, more studies are required to delineate these possibilities.

c. Replication and Repair in the Tumor Cell[150]

If the anticancer activity of cisplatin arises from damaged DNA templates, then the drug could be selectively toxic to cancer versus normal cells of the same tissue if repair of DNA damage occurred more efficiently in the latter. The best way to study this phenomenon would be to measure the platinum-DNA levels and list the spetrum of adducts formed in tumor versus normal biopsy tissue obtained from patients undergoing cisplatin chemotherapy. As described previously, methodologies are now reaching the point where such experiments can be carried out in order to test the key hypotheses about the mechanism of action of cisplatin. In addition, powerful new methods have recently been developed to screen for DNA bmdlnlg proteins. If one could identify proteins that bind selectively to *cis*-DDP-platinated DNA and determine function, further insights into cellular replication and repair phenomena would be forthcoming. Such cellular factors that bind selectively to DNA containing cisplatin adducts have, in fact, recently been discovered.[107] The experiments that led to this finding and their possible implications for the molecular mechanism of cisplatin are described in the next section.

d. Structure-Specific (or Damage) Recognition Proteins[150]

If selective repair of platinum-DNA adducts in cells of different origin is an integral part of the anticancer mechanism of *cis*-DDP, then it is important to identify the cullular factors associated this phenomenon. In bacteria, *cis*-DDP adducts on DNA are removed by excision repair, a process in which the lesion is first identified and then excised by the uvrABC excinuclease system.[151] In this process, the uvrA protein first binds to the adducted DNA. Subsequently, the uvrB and C proteins excise the damaged strand, which additional cellular proteins rebuild by copying the genetic information from the remaining strand.

The repair of *cis*-DDP intrastrand crosslinks in mammalian cells is much less well understood. Under the assumption that an analogue of the uvrA protein might exist in such cells, experiments were carried out to try to isolate and clone the gene for such a protein. In particular, the mobility of platinated DNA restriction fragments of defined length was found to be substantially retarded in electrophoresis gels following incubation extracts from human HeLa cells.[107] This gel-mobility shift was attributed to the binding of factors termed "damage recognition proteins" (or DRPs). Subsequent studies with site-specifically platinated oligonucleotides (see V.D.8) revealed that the cisplatin DRP binds specifically to DNA containing the intrastrand *cis*-$[Pt(NH_3)_2\{d(pGpG)\}]$ or *cis*-$[Pt(NH_3)_2\{d(pApG)\}]$ crosslink. In parallel work, the gene encoding for a DRP was cloned[152] and used to demonstrate the occurrence of such a in nearly all eukaryotic cells. Since binding of the DRP to platinated DNA is not specific for the ammine ligands opposite the crosslinked nucleobases, the interaction is thougllt to involve recognition of local changes in the twist and bending of the double helix. Figure 9.28 depicts one possible structure for the complex formed between *cis*-DDP platinated DNA and a DRP. More recently, the cloned proteins were found to contain a high mobility group (HMG) protein box, and even HMG 1 itself binds to cisplatin-modified DNA.[152] The class of proteins was renamed "structure-specific recognition proteins" (SSRPs).

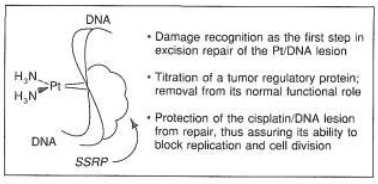


Figure 9.28 - Model depicting the binding of an SSRP to cisplatin-damaged DNA and several hypotheses for its role in the molecular mechanism.

The discovery of SSRPs that bind specifically to cisplatin-modified DNA raises several questions that are the subjects of current study. The first is to determine whether the proteins are an integral component in the mechanism of action of the drug. Although it has not yet been possible to induce the proteins by treating cells with cisplatin, nor have elevated or suppressed levels been found in platinum-resistant cells, deletion of an SSRP gene in yeast has re(~enltlv afforded a mutant strain less sensitive to cisplatin than wild-type cells.[153] This result links a yeast SSRP with cellular sensitization to the drug. Such a protein could contribute to the molecular mechanism in one of several ways (Figure 9.28). It might be the analogue of uvrA, which, as mentioned above,

recognizes damage and signals the cell to perform excision repair. If so, then one would like to depress the levels of the protein in cancer cells to make them more sensitive to the drug. A second possibility is that the true role of the SSRP is to serve as a tumor-cell activator, and that cisplatin lesions titrate it away from its functionally active sites on the DNA. Alternatively, binding of the protein could protect cisplatin adducts from repair, preserving their lethality at the time of cell division and leading to the arrest of tumor growth. This last hypothesis would require more of the SSRP in cells sensitive to the drug. Studies are currently in progress to delineate these three and other hypotheses, and to learn whether the discovery of the SSRPs has heralded the final chapter in the quest for the molecular mechanism of cisplatin or merely been an entertaining sidelight.

e. Drug Resistance: What Do We Know?[150]

Perhaps the most serious problem for successful chemotherapy of tumors is drug resistance.[102] In most tumors there exists a subpopulation of cells that are naturally resistant to a given drug; as the sensitive cells are killed, these refractory clones take over. In addition, resistance can be acquired by tumor cells following repeated application of the drug. Attempts to identify mechanisms responsible for cisplatin resistance have therefore been the subjects of considerable research activity. Other DNA-damaging agents sometimes amplify genes as a mechanism of drug resistance. An example is the multidrug resistance phenomenon, in which a gene encoded for a P-glycoprotein is amplified in cells resistant to agents such as daunomycin. This protein is believed to increase efflux of the drug through the cell membrane by an ATP-dependent, energy-driven pump. There is currently an intensive search underway to see whether the cisplatin resistance phenomenon has a genetic origin. If a cisplatin resistance gene could be cloned and its phenotype identified, a powerful new avenue would be opened to overcome drug resistance.

7.6.10: Bioinorganic Chemistry of Platinum Anticancer Drugs; How Might They Work? (Part 2) is shared under a not declared license and was authored, remixed, and/or curated by LibreTexts.

7.6.11: Design of New Inorganic Anticancer Drugs

1. Objectives

Although chemotherapy has made significant contributions to cancer treatment, the effect of cisplatin on testicular cancer being a showcase example, early detection and surgical removal of all neoplastic tissue still remain the preferred means of combating most forms of the disease. What steps need to be taken to devise better chemotherapeutic agents? One answer is to understand the biochemical mechanisms that underlie the transformation of normal into neoplastic cells and to attack the disease on the basis of that knowledge. The value of this approach is indisputable, but it need not be the only one. We have seen that *cis*-$[Pt(NH_3)_2Cl_2]$, a simple third-row transition-metal complex containing no carbon atoms, can contribute significantly to cancer chemotherapy. This example alone should lead us to search for improved inorganic drugs based on the evolving knowledge of the mechanism of action of *cis*-DDP. What then should our objectives be? Three answers are immediately apparent. First, we need to find compounds that are active against resistant cells. Such compounds are termed "second-generation" platinum drugs, and are the focus of much activity in the pharmaceutical industry. Their development will be facilitated by understanding the fundamental biochemistry of cisplatin drug resistance, designing complexes to circumvent the cellular resistance mechanisms. Second, there needs to be an improved spectrum of activity, to be provided by the so-called "third-generation" compounds. The major cancers of the colon, breast, and lung are not effectively diminished by cisplatin chemotherapy. Finally, cisplatin toxicity is often dose-limiting, and there is a need for agents with a greater chemotherapeutic index-to-toxicity ratio. Some of these objectives may ultimately be met by modifying the mode of delivery of cisplatin, for example, by encapsulating the drug in a tumor-seeking liposome or attaching it to a tissue-specific monoclonal antibody. A major step in alternative delivery has recently been taken with the development of a class of oral platinum complexes that have just entered clinical trials.[54] These complexes are platinum(IV) cycloalkylamine species of the kind *cis*, *trans*, *cis*-$[Pt(NH_3)(C_6H_5NH_2)(O_2CCH_3)_2Cl_2]$. The prospects are reasonably good that new platinum and other metal anticancer drugs can be designed in a bioinorganic chemical approach to the problem.

2. Strategies for Drug Development

a. Can We Build on Our Knowledge About Cisplatin?

If we consider what is known about the molecular mechanism of cisplatin, what properties are desirable in the design of new metal complexes for testing? The molecules should be reasonably stable kinetrically and soluble in biological fluids, cross the cell membrane, bind covalently to DNA, and inhibit gene function. As described previously in this section of the chapter, powerful methods are now available to screen compounds for these properties in a relatively short time. But there are additional factors required for metallodrug anticancer activity, above and beyond these criteria; *trans*-DDP, after all, has all five of the above properties and is not active. Probably one should add to the list the requirement that the complex have two substitutionally labile *cis* sites for intrastrand crosslinking of adjacent DNA nucleotides; such a criterion would, of course, rule out molecules like *trans*-DDP. Recall, however, that *cis*-$[Pt(NH_3)_2(4\text{-X-py})CI]^+$ complexes (X = Br, Me) are active. These cations have the five properties listed above, but, as far as is currently known, bind only monofunctionally to DNA. The pyridine ring moiety of a covalently attached platinum atom could possibly intercalate into a neighboring interbase pair site on the DNA, making a pseudointrastrand crosslinked adduct structurally similar to the *cis*-DDP-d(pGpG) structure. Further information is required about these active, monofunctional cations before any firm conclusions can be drawn. Nevertheless, it is useful to remember that if the requirement of two substitutionally labile *cis* ligands had been rigorously followed, this new class of monofunctional platinum complexes would not have been discovered.

Another rationale for designing new platinum or other metal antitumor drugs could emerge with a better understanding of the SSRPs in the mechanism of action of cisplatin. For example, if they serve to protect cisplatin lesions on DNA from repair, one would want to design complexes that form adducts that bind even more strongly to the purified protein. The strength of this binding interaction, having been a serendipitous discovery, surely cannot have been maximized. A tighter SSRP-platinated DNA complex would require the use of less platinum, and thus afford lower toxicities.

b. Is Platinum Uniquely Suited?

Given the above criteria, platinum is the only metal to be chosen for further drug development? The answer to this question is "probably not" but a few points need to be kept in mind. Given the assumption that the geometry of the *cis*-$[Pt(NH_3)_2\{d(GpG)\}]$

intrastrand crosslink was important for the antitumor activity of cisplatin, computer graphics methods were employed to probe the stereochemical consequences of modifying this structure.[155] Addition of axial chloride or water ligands in fifth and sixth coordination positions to form pseudo-octahedral adducts, for example, introduces several steric clashes with the guanosine O6 atoms. An octahedral complex, for example *cis*,*cis*,*cis*-$[Pt(NH_3)_2Cl_2(OH)_2]$, bifunctionally coordinated to DNA either would not form an intrastrand d(GpG) crosslink or would form an adduct structurally different from that made by *cis*-DDP. This octahedral complex Pt(IV), known as "tetraplatin" in the pharmaceutical industry, is active, but is believed to be reduced *in vivo* to platinum(II) before coordinating to DNA.[156,157] These considerations might imply that the best strategy for inorganic drug development would be to employ square-planar d^8 complexes. Clearly there are as yet no definitive answers. Nevertheless, the criteria derived from the mechanism of action studies of cisplatin represent an excellent starting point for designing new antitumor metallodrugs.

c. How Important are Amine Ligands?

Here again, the answer is not unequivocal, but amines (including NH_3) are probably ideally suited ligands for covalent DNA-binding metal complexes. Even completely inert complexes such as $[Co(NH_3)_6]^{3+}$ show sequence and DNA polymorph binding preferences,[158] suggesting that the N-H bonds orient toward the phosphate and heterocyclic nitrogen atoms in the major groove, forming hydrogen-bonding interactions. This chemistry is analogous to the binding and recognition of organic amines and polyamines, such as spermine and spermidine, by nucleic acids. Apart from amines, hydrophobic groove-binding and/or intercalating ligands such as o-phenanthroline and its derivatives should be considered. Molecules such as $[Rh(DIP)_3]^{3+}$, where DIP = 4,7-diphenyl-1,10penanthroline, bind to DNA and have proved to be useful structural probes (Chapter 8). Recent work has shown that $[Rh(DIP)_2Cl_2]^+$ binds preferentially to d(GpG) sequences, like cisplatin, although its antitumor properties have not yet been investigated.[159]

3. Second and Third-generation Platinum Anticancer Drugs

Improvements over cisplatin have been made, most notably the molecule carboplatin (Figure 9.4), which is less nephrotoxic and has been reported to be effective in some patients where cisplatin chemotherapy has failed. These properties come solely from the dicarboxylate leaving group, which is kinetically more inert to substitution. Studies with monoclonal antibodies have shown the DNA adducts of carboplatin to be identical with those formed by *cis*-DDP.[117]Other platinum compounds that have undergone clinical trials are close analogues of *cis*-$[PtA_2X_2]$, or tetraplatin, *cis*,*cis*,*cis*-$[PtA_2X_2Y_2]$, that obey the classic structure-activity relationships. The activity of cationic triamines, *cis*-$[Pt(NH_3)_2LCI]CI$, where L is pyridine, a substituted pyridine, pyrimidine, or purine, against S180 ascites and L1210 tumors in mice opens a new vista of possible structures to be tried. The intercalator-linked complex AO-Pt (Figure 9.26) has also been found to show activity in the S180 ascites system, suggesting a further class of complexes that could be studied. The oral compounds, *cis*,*trans*,*cis*-$[Pt(NH_3)(C_6H_5NH_2)(O_2CCH_3)_2Cl_2]$, survive the digestive tract, are taken across the gastrointestinal mucosa, and metabolize to *cis*-$[Pt(NH_3)(C_6H_5NH_2)Cl_2]$, a cisplatin analogue.[54] As such they are effective pro-drugs that could become the major platinum agent in clinical use. Until these recent advances, there was a general impression that, by chance, the best compound discovered was the first one, cisplatin. There is now sufficient reason to expect that innovative experimentation will lead to improved drugs, bearing in mind the comment made earlier (Section IV.G.) that sustained individual effort for up to a decade can be required to move a compound from the laboratory bench into the clinic.

4. Nonplatinum Antitumor Metal Complexes

a. Soft Metals

As mentioned in Section IV.E., some compounds of Pd(II), Au(I), Rh(II), and Ru(II or III) have been screened for antitumor activity, but much more work needs to be done in this arena. The higher metal-ligand exchange rates of Pd(II), ~10^5 faster than those of Pt(Il), make these complexes potentially more toxic, as some preliminary animal studies have shown. By use of chelating or organometallic complexes, however, this problem might be avoided. The properties of Ru, Rh, and to a lesser extent Au amine and polypyridine complexes would seem to make them attractive candidates, and indeed there appears to be renewed interest in these molecules.[160] Inorganic chemists interested in pursuing drug development with these metals need to forge alliances with biological colleagues equipped to do the necessary animal screening and to develop in-house expertise for cell culture and related biochemical work. The techniques are not all that difficult and it is actually fun to undertake studies of the biological consequences of metallodrug chemistry.

b. Metallocenes and Metallocene Dihalides[36-37]

Although complexes such as $[(C_5H_5)_2TiCl_2]$ are superficially analogous to *cis*-DDP, in being potentially bifunctional DNA crosslinking agents, their hydrolytic reactions are sufficiently different to cast doubt on the value of this comparison. The fact that antitumor activity has been found for this very different class of inorganic compound, however, suggests that perhaps bioinorganic chemists have explored only a very small sample of possible metallodrugs.

7.6.11: Design of New Inorganic Anticancer Drugs is shared under a not declared license and was authored, remixed, and/or curated by LibreTexts.

Index

A

active site
7.2: Introduction to Amino Acids and Proteins
Agostic alkyls
6.2.1: Transition Metal Alkyl Complexes
amino acids
7.2: Introduction to Amino Acids and Proteins
ammine ligands
4.3: Ligand Exchange Reactions (Thermodynamics)
aqua ligands
4.3: Ligand Exchange Reactions (Thermodynamics)
Associative Substitution
4.3.1: Associative Ligand Substitution
Aufbau principle
1.2.2.3: Aufbau Principle

B

bent
1.3.2: Valence Shell Electron-Pair Repulsion
Berry pseudorotation
4.3.1: Associative Ligand Substitution
birefringence
5.6.2: Structures Related to NaCl and NiAs
block diagonal
2.3.2: Representations of Point Groups
bond angle
1.3.2: Valence Shell Electron-Pair Repulsion
Bragg equation
5.5: X-ray Crystallography
Bridging hydrides
6.2.3: Metal Hydrides

C

Carbene insertion
6.2: Synthesis and Stability
character (matrix)
2.3.2: Representations of Point Groups
character table
2.3.3: Character Tables
chelate effect
4.3: Ligand Exchange Reactions (Thermodynamics)
compression
4.2.2.1.5: Jahn-Teller Distortions
coordination complex
4.2.2.1.2: Colors of Coordination Complexes
coordination complexes
4.2.2.1.2: Colors of Coordination Complexes
crystal field splitting
4.2.2.1.3: Crystal Field Stabilization Energy
crystal field stabilization energy
4.2.2.1.3: Crystal Field Stabilization Energy
crystal field theory
4.2.2.1: Crystal Field Theory
4.2.2.1.2: Colors of Coordination Complexes
4.2.2.1.3: Crystal Field Stabilization Energy
4.3.2: Dissociative Ligand Substitution

D

Dewar−Chatt model
6.2.6.1: Metal Alkene Complexes
Diode
5.9.6: Diodes, LEDs and Solar Cells
5.9.7: References
dipole moment
1.3.2: Valence Shell Electron-Pair Repulsion
1.3.3: Molecular Polarity
Dissocative Substitution
4.3.2: Dissociative Ligand Substitution
dissociation
4.3.2: Dissociative Ligand Substitution
Dissociative Ligand Substitution
4.3.2: Dissociative Ligand Substitution
Drago and Wayland's EC Model
1.2.3.4.1: Quantitative Measures of Hardness, Softness, and Acid-Base Interactions from a Hard Soft Acid-Base Principle perspective involve orbital energies and or apportioning acid-base bonding in terms of electrostatic and covalent factors

E

electromagnetic spectrum
4.2.2.1.2: Colors of Coordination Complexes
electronegativity (Mulliken)
1.2.3.4.1: Quantitative Measures of Hardness, Softness, and Acid-Base Interactions from a Hard Soft Acid-Base Principle perspective involve orbital energies and or apportioning acid-base bonding in terms of electrostatic and covalent factors
Electronic Configurations
4.2.2.1.5: Jahn-Teller Distortions
elongation
4.2.2.1.5: Jahn-Teller Distortions
enzymes
7.2: Introduction to Amino Acids and Proteins

F

fluorite (structure)
5.6.3: Tetrahedral Structures
formal charge
1.3.1.3: Formal Charge
Formation Constants
4.3: Ligand Exchange Reactions (Thermodynamics)

G

Grubb's catalyst
6.4.3: Catalytic Applications of Organometallic Compounds- Alkene Metathesis

H

high spin
4.2.2.1.3: Crystal Field Stabilization Energy
4.2.2.1.5: Jahn-Teller Distortions
hybrid orbital
1.3.6: Hybrid Atomic Orbitals
hybridization
1.3.6: Hybrid Atomic Orbitals
hydration
4.2.2.1.3: Crystal Field Stabilization Energy
hydroformylation reaction
6.4.2: Homogeneous Catalysis - II
hydrogen bonding
1.3.4: Hydrogen Bonding
hypervalency
1.3.1: Lewis Electron-Dot Diagrams
hypovalency
1.3.1: Lewis Electron-Dot Diagrams

K

Kapustinskii equation
5.8.3: Kapustinskii Equation

L

Lancashire
4.2.2.1.5: Jahn-Teller Distortions
Lenz's Law
4.2.2.1.7: Magnetism
ligand
4.3.1: Associative Ligand Substitution
4.3.2: Dissociative Ligand Substitution
Ligand Close Packing (LCP)
1.3.2.4: Ligand Close Packing
Ligand Exchange Reactions
4.3: Ligand Exchange Reactions (Thermodynamics)
linear
1.3.2: Valence Shell Electron-Pair Repulsion
low spin
4.2.2.1.3: Crystal Field Stabilization Energy
4.2.2.1.5: Jahn-Teller Distortions

M

magnetic moments
4.2.2.1.6: Magnetic Moments of Transition Metals
magnetic permeability
4.2.2.1.7: Magnetism
magnetism
4.2.2.1.7: Magnetism
Metal Carbonyls
6.2.4: Metal Carbonyls
metal hydrides
6.2.3: Metal Hydrides
miller indicies
5.5.1: Miller Indices (hkl)

N

node
1.3.5: Valence Bond Theory

O

octahedral
1.3.2: Valence Shell Electron-Pair Repulsion
Octahedral Preference
4.2.2.1.3: Crystal Field Stabilization Energy
Octahedral Site Preference Energy
4.2.2.1.3: Crystal Field Stabilization Energy
orbital mixing
3.3.2: Orbital Mixing

organometallic
4.3.1: Associative Ligand Substitution
overlap
1.3.5: Valence Bond Theory

P

Pearson's absolute hardness
1.2.3.4.1: Quantitative Measures of Hardness, Softness, and Acid-Base Interactions from a Hard Soft Acid-Base Principle perspective involve orbital energies and or apportioning acid-base bonding in terms of electrostatic and covalent factors
Peptide bond
7.2: Introduction to Amino Acids and Proteins
philosopher's stone
1.1.3: History of Inorganic Chemistry
pi bond
1.3.5: Valence Bond Theory
proteins
7.2: Introduction to Amino Acids and Proteins

R

rate law
4.3.1: Associative Ligand Substitution
reaction kinetics
4.3.1: Associative Ligand Substitution
4.3.2: Dissociative Ligand Substitution
resonance
1.3.1.1: Resonance
resonance structures
1.3.1.1: Resonance
rotation axis
2.3.2: Representations of Point Groups

S

SALC
3.5.2: Carbon Dioxide
Schrock's catalyst
6.4.3: Catalytic Applications of Organometallic Compounds- Alkene Metathesis
seesaw
1.3.2: Valence Shell Electron-Pair Repulsion
sigma bond
1.3.5: Valence Bond Theory
sp hybrid orbital
1.3.6: Hybrid Atomic Orbitals
sp2 hybrid orbital
1.3.6: Hybrid Atomic Orbitals
sp3 hybrid orbital
1.3.6: Hybrid Atomic Orbitals
sp3d hybrid orbital
1.3.6: Hybrid Atomic Orbitals
sp3d2 hybrid orbital
1.3.6: Hybrid Atomic Orbitals
spectrochemical series
4.2.2.1.2: Colors of Coordination Complexes
spin pairing energy
4.2.2.1.3: Crystal Field Stabilization Energy
square pyramidal
1.3.2: Valence Shell Electron-Pair Repulsion
Stability Constants
4.3: Ligand Exchange Reactions (Thermodynamics)
steady state approximation
4.3.2: Dissociative Ligand Substitution
stereochemistry
4.3.1: Associative Ligand Substitution
4.3.2: Dissociative Ligand Substitution
substitution
4.3.1: Associative Ligand Substitution
substrate
7.2: Introduction to Amino Acids and Proteins
superconductor
5.9.2: Superconductors
symmetry elements
2.1: Symmetry Elements and Operations
symmetry operation
2.3.2: Representations of Point Groups
symmetry operations
2.1: Symmetry Elements and Operations

T

tetrahedral
1.3.2: Valence Shell Electron-Pair Repulsion
thermodynamics
4.3: Ligand Exchange Reactions (Thermodynamics)
trigonal bipyramidal
1.3.2: Valence Shell Electron-Pair Repulsion
trigonal planar
1.3.2: Valence Shell Electron-Pair Repulsion
trigonal pyramidal
1.3.2: Valence Shell Electron-Pair Repulsion

U

Unsaturated Intermediate
4.3.2: Dissociative Ligand Substitution

V

valence bond theory
1.3.5: Valence Bond Theory
valence shell electron pair repulsion theory
1.3.2: Valence Shell Electron-Pair Repulsion
VSEPR
1.3.2: Valence Shell Electron-Pair Repulsion

Z

Zeise's salt
6.2.6.1: Metal Alkene Complexes

Glossary

Sample Word 1 | Sample Definition 1

Detailed Licensing

Overview

Title: CHEM 361: Inorganic Chemistry (Watson)

Webpages: 185

Applicable Restrictions: Noncommercial

All licenses found:

- Undeclared: 54.1% (100 pages)
- CC BY-SA 4.0: 23.8% (44 pages)
- CC BY-NC-SA 4.0: 16.2% (30 pages)
- CC BY-NC 3.0: 3.2% (6 pages)
- CC BY 4.0: 1.1% (2 pages)
- CC BY-NC 4.0: 1.1% (2 pages)
- Public Domain: 0.5% (1 page)

By Page

- CHEM 361: Inorganic Chemistry (Watson) - *Undeclared*
  - Front Matter - *Undeclared*
    - TitlePage - *Undeclared*
    - InfoPage - *Undeclared*
    - Table of Contents - *Undeclared*
    - Licensing - *Undeclared*
  - 1: Intro, Review, and Effective Nuclear Charge - *Undeclared*
    - 1.1: Introduction to Inorganic Chemistry - *Undeclared*
      - 1.1.1: What is Inorganic Chemistry? - *Undeclared*
      - 1.1.2: Inorganic vs Organic Chemistry - *Undeclared*
      - 1.1.3: History of Inorganic Chemistry - *CC BY-NC-SA 4.0*
    - 1.2: Atomic Structure - *Undeclared*
      - 1.2.1: Historical Development of Atomic Theory - *Undeclared*
        - 1.2.1.1: The Periodic Table - *Undeclared*
        - 1.2.1.2: Discovery of Subatomic Particles and the Bohr Atom - *Undeclared*
      - 1.2.2: The Schrödinger equation, particle in a box, and atomic wavefunctions - *CC BY-NC-SA 4.0*
        - 1.2.2.1: Particle in a Box - *CC BY-NC-SA 4.0*
        - 1.2.2.2: Quantum Numbers and Atomic Wave Functions - *CC BY-NC-SA 4.0*
        - 1.2.2.3: Aufbau Principle - *Public Domain*
        - 1.2.2.4: Shielding - *CC BY-NC-SA 4.0*
      - 1.2.3: Periodic Properties of Atoms - *Undeclared*
        - 1.2.3.1: Ionization energy - *Undeclared*
        - 1.2.3.2: Electron Affinity - *Undeclared*
        - 1.2.3.3: Covalent and Ionic Radii - *Undeclared*
        - 1.2.3.4: Hard and Soft Acids and Bases - *Undeclared*
          - 1.2.3.4.1: Quantitative Measures of Hardness, Softness, and Acid-Base Interactions from a Hard Soft Acid-Base Principle perspective involve orbital energies and or apportioning acid-base bonding in terms of electrostatic and covalent factors - *Undeclared*
          - 1.2.3.4.2: Hard-Hard and Soft-Soft preferences may be explained and quantified in terms of electrostatic and covalent and electronic stabilization on the stability of Lewis acid-base adducts - *Undeclared*
    - 1.3: Simple Bonding Theory - *Undeclared*
      - 1.3.1: Lewis Electron-Dot Diagrams - *Undeclared*
        - 1.3.1.1: Resonance - *Undeclared*
        - 1.3.1.2: Breaking the octet rule with higher electron counts (hypervalent atoms) - *Undeclared*
        - 1.3.1.3: Formal Charge - *Undeclared*
        - 1.3.1.4: Lewis fails to predict unusual cases-Boron and Beryllium - *Undeclared*
      - 1.3.2: Valence Shell Electron-Pair Repulsion - *CC BY-NC-SA 4.0*
        - 1.3.2.1: Lone Pair Repulsion - *Undeclared*

- 1.3.2.2: Multiple Bonds - *Undeclared*
- 1.3.2.3: Electronegativity and Atomic Size Effects - *Undeclared*
- 1.3.2.4: Ligand Close Packing - *Undeclared*
- 1.3.3: Molecular Polarity - *Undeclared*
- 1.3.4: Hydrogen Bonding - *Undeclared*
- 1.3.5: Valence Bond Theory - *CC BY 4.0*
- 1.3.6: Hybrid Atomic Orbitals - *CC BY 4.0*

2: Molecular Symmetry and Point Groups - *Undeclared*

- 2.1: Symmetry Elements and Operations - *Undeclared*
- 2.2: Point Groups - *Undeclared*
  - 2.2.1: Groups of Low and High Symmetry - *Undeclared*
  - 2.2.2: Other Groups - *Undeclared*
- 2.3: Properties and Representations of Groups - *Undeclared*
  - 2.3.1: Matrices - *Undeclared*
  - 2.3.2: Representations of Point Groups - *Undeclared*
  - 2.3.3: Character Tables - *Undeclared*
- 2.4: Examples and Applications of Symmetry - *Undeclared*
  - 2.4.1: Molecular Vibrations - *Undeclared*
  - 2.4.2: Chirality - *CC BY-NC 4.0*

3: Molecular Orbital Theory - *Undeclared*

- 3.1: Prelude to Molecular Orbital Theory - *Undeclared*
- 3.2: Formation of Molecular Orbitals from Atomic Orbitals - *CC BY-NC-SA 4.0*
  - 3.2.1: Molecular Orbitals from s Orbitals - *CC BY-NC-SA 4.0*
  - 3.2.2: Molecular Orbitals from p Orbitals - *CC BY-NC-SA 4.0*
  - 3.2.3: Molecular orbitals from d orbitals - *CC BY-NC-SA 4.0*
  - 3.2.4: Nonbonding Orbitals and Other Factors - *CC BY-NC-SA 4.0*
- 3.3: Homonuclear Diatomic Molecules - *CC BY-NC-SA 4.0*
  - 3.3.1: Molecular Orbitals - *CC BY-NC-SA 4.0*
  - 3.3.2: Orbital Mixing - *CC BY-NC-SA 4.0*
  - 3.3.3: Diatomic Molecules of the First and Second Periods - *CC BY-NC-SA 4.0*
  - 3.3.4: Photoelectron Spectroscopy - *CC BY-NC-SA 4.0*
- 3.4: Heteronuclear Diatomic Molecules - *CC BY-NC-SA 4.0*
  - 3.4.1: Polar bonds - *CC BY-NC-SA 4.0*
  - 3.4.2: Ionic Compounds and Molecular Orbitals - *CC BY-NC-SA 4.0*
- 3.5: Larger (Polyatomic) Molecules - *CC BY-NC-SA 4.0*
  - 3.5.1: Bifluoride anion - *CC BY-NC-SA 4.0*
  - 3.5.2: Carbon Dioxide - *CC BY-NC-SA 4.0*
  - 3.5.3: H_2O - *CC BY-NC-SA 4.0*
  - 3.5.4: NH_3 - *CC BY-NC-SA 4.0*
  - 3.5.5: CO_2 (Revisted with Projection Operators) - *CC BY-NC-SA 4.0*
  - 3.5.6: BF_3 - *CC BY-NC-SA 4.0*

4: d Block Chemistry - *Undeclared*

- 4.1: Coordination Chemistry I - Structure and Isomers - *Undeclared*
  - 4.1.1: History - *Undeclared*
  - 4.1.2: Nomenclature and Ligands - *Undeclared*
  - 4.1.3: Isomerism - *Undeclared*
  - 4.1.4: Coordination Numbers and Structures - *Undeclared*
- 4.2: Coordination Chemistry II - Bonding - *Undeclared*
  - 4.2.1: Evidence for Electronic Structures - *CC BY-NC 3.0*
    - 4.2.1.1: Thermodynamic Data - *CC BY-NC 3.0*
    - 4.2.1.2: Magnetic Susceptibility - *CC BY-NC 3.0*
    - 4.2.1.3: Electronic Spectra - *CC BY-NC 3.0*
    - 4.2.1.4: Coordination Number and Molecular Shapes - *CC BY-NC 3.0*
  - 4.2.2: Bonding Theories - *CC BY-NC 3.0*
    - 4.2.2.1: Crystal Field Theory - *Undeclared*
      - 4.2.2.1.1: Crystal Field Theory - *CC BY-NC-SA 4.0*
      - 4.2.2.1.2: Colors of Coordination Complexes - *Undeclared*
      - 4.2.2.1.3: Crystal Field Stabilization Energy - *Undeclared*
      - 4.2.2.1.4: Factors That Affect the Magnitude of Δo - *Undeclared*
      - 4.2.2.1.5: Jahn-Teller Distortions - *Undeclared*
      - 4.2.2.1.6: Magnetic Moments of Transition Metals - *Undeclared*
      - 4.2.2.1.7: Magnetism - *Undeclared*
      - 4.2.2.1.8: Thermodynamics and Structural Consequences of d-Orbital Splitting - *CC BY-NC-SA 4.0*

        - 4.2.2.2: Ligand Field Theory - *Undeclared*
    - 4.3: Ligand Exchange Reactions (Thermodynamics) - *CC BY-NC 4.0*
        - 4.3.1: Associative Ligand Substitution - *Undeclared*
        - 4.3.2: Dissociative Ligand Substitution - *Undeclared*
    - 4.4: Electronic Spectra of Coordination Compounds - *Undeclared*
- 5: Solid State Chemistry - *Undeclared*
    - 5.1: Prelude to Metals and Alloys - *Undeclared*
    - 5.2: Unit Cells and Crystal Structures - *CC BY-SA 4.0*
    - 5.3: Crystal Structures of Metals - *CC BY-SA 4.0*
        - 5.3.1: Conduction in Metals - *CC BY-SA 4.0*
    - 5.4: Atomic Orbitals and Magnetism - *CC BY-SA 4.0*
        - 5.4.1: Ferro-, Ferri- and Antiferromagnetism - *CC BY-SA 4.0*
        - 5.4.2: Hard and Soft Magnets - *CC BY-SA 4.0*
        - 5.4.3: Defects in Metallic Crystals - *CC BY-SA 4.0*
    - 5.5: X-ray Crystallography - *Undeclared*
        - 5.5.1: Miller Indices (hkl) - *Undeclared*
        - 5.5.2: Powder X-ray Diffraction - *Undeclared*
    - 5.6: Prelude to Ionic and Covalent Solids - Structures - *Undeclared*
        - 5.6.1: Close-packing and Interstitial Sites - *CC BY-SA 4.0*
        - 5.6.2: Structures Related to NaCl and NiAs - *CC BY-SA 4.0*
        - 5.6.3: Tetrahedral Structures - *CC BY-SA 4.0*
        - 5.6.4: Layered Structures and Intercalation Reactions - *CC BY-SA 4.0*
        - 5.6.5: Spinel, Perovskite, and Rutile Structures - *CC BY-SA 4.0*
    - 5.7: Ionic Radii and Radius Ratios - *CC BY-SA 4.0*
    - 5.8: Energetics of Crystalline Solids- The Ionic Model - *CC BY-SA 4.0*
        - 5.8.1: Born-Haber Cycles for NaCl and Silver Halides - *CC BY-SA 4.0*
        - 5.8.2: Lattice Energies and Solubility - *CC BY-SA 4.0*
        - 5.8.3: Kapustinskii Equation - *CC BY-SA 4.0*
    - 5.9: Electronic Properties of Materials - Superconductors and Semiconductors - *CC BY-SA 4.0*
        - 5.9.1: Prelude to Electronic Properties of Materials - Superconductors and Semiconductors - *CC BY-SA 4.0*
        - 5.9.2: Superconductors - *CC BY-SA 4.0*
        - 5.9.3: Periodic Trends- Metals, Semiconductors, and Insulators - *CC BY-SA 4.0*
        - 5.9.4: Semiconductors- Band Gaps, Colors, Conductivity and Doping - *CC BY-SA 4.0*
        - 5.9.5: Semiconductor p-n Junctions - *CC BY-SA 4.0*
        - 5.9.6: Diodes, LEDs and Solar Cells - *CC BY-SA 4.0*
        - 5.9.7: References - *CC BY-SA 4.0*
- 6: Organometallic Chemistry - *Undeclared*
    - 6.1: 18 Valence Electron Rule - *CC BY-SA 4.0*
    - 6.2: Synthesis and Stability - *CC BY-SA 4.0*
        - 6.2.1: Transition Metal Alkyl Complexes - *CC BY-SA 4.0*
        - 6.2.2: Metal-Carbenes - *CC BY-SA 4.0*
        - 6.2.3: Metal Hydrides - *CC BY-SA 4.0*
        - 6.2.4: Metal Carbonyls - *CC BY-SA 4.0*
        - 6.2.5: Metal Phosphines - *CC BY-SA 4.0*
        - 6.2.6: Complexes of π−bound Ligands - *CC BY-SA 4.0*
            - 6.2.6.1: Metal Alkene Complexes - *CC BY-SA 4.0*
            - 6.2.6.2: Metal Allyl and Diene Complexes - *CC BY-SA 4.0*
            - 6.2.6.3: Metal Cyclopentadienyl Complexes - *CC BY-SA 4.0*
    - 6.3: Reaction Mechanisms - *CC BY-SA 4.0*
        - 6.3.1: Oxidative Addition and Reductive Elimination - *CC BY-SA 4.0*
        - 6.3.2: Insertion and Elimination Reactions - *CC BY-SA 4.0*
        - 6.3.3: Nucleophilic and Electrophilic Addition and Abstraction - *CC BY-SA 4.0*
    - 6.4: Applications - *CC BY-SA 4.0*
        - 6.4.1: Homogeneous Catalysis - I - *CC BY-SA 4.0*
        - 6.4.2: Homogeneous Catalysis - II - *CC BY-SA 4.0*
        - 6.4.3: Catalytic Applications of Organometallic Compounds- Alkene Metathesis - *CC BY-SA 4.0*
- 7: Bioinorganic Chemistry - *Undeclared*
    - 7.1: Biological Significance of Iron, Zinc, Copper, Molybdenum, Cobalt, Chromium, Vanadium, and Nickel - *Undeclared*
    - 7.2: Introduction to Amino Acids and Proteins - *CC BY-NC-SA 4.0*
    - 7.3: Overview of Hemoglobin and Myoglobin - *Undeclared*
        - 7.3.1: Myoglobin, Hemoglobin, and their Ligands - *CC BY-NC-SA 4.0*

- 7.3.2: Oxygen Transport by the Proteins Myoglobin and Hemoglobin - *Undeclared*
- 7.4: Ferrodoxins, Hydrogenases, and Nitrogenases - Metal-Sulfide Proteins - *Undeclared*
  - 7.4.1: Iron-sulfur Proteins and Models - *Undeclared*
  - 7.4.2: Iron-sulfur Proteins and Models (Part 2) - *Undeclared*
  - 7.4.3: Iron-sulfur Proteins and Models (Part 3) - *Undeclared*
  - 7.4.4: Iron-sulfur Proteins and Models (Part 4) - *Undeclared*
- 7.5: The Reaction Pathways of Zinc Enzymes and Related Biological Catalysts - *Undeclared*
  - 7.5.1: About Carbonic Anhydrase - *Undeclared*
  - 7.5.2: Catalytic Mechanism - *Undeclared*
  - 7.5.3: Metal Substitution - *Undeclared*
- 7.6: Metals in Medicine - *Undeclared*
  - 7.6.1: Metal Deficiency and Disease - *Undeclared*
  - 7.6.2: Toxic Effects of Metals - *Undeclared*
  - 7.6.3: Aspects of Platinum Binding to DNA - *Undeclared*
  - 7.6.4: Survey of Metals Used for Diagnosis and Chemotherapy - *Undeclared*
  - 7.6.5: Platinum Anticancer Drugs- A Case Study - *Undeclared*
  - 7.6.6: Mapping the Major Adducts of cis- and trans-DDP on DNA; Sequence Specificity - *Undeclared*
  - 7.6.7: Structure of Platinum-DNA Complexes - *Undeclared*
  - 7.6.8: Site-specifically Platinated DNA \(\;^{154}\) - *Undeclared*
  - 7.6.9: Bioinorganic Chemistry of Platinum Anticancer Drugs- How Might They Work? - *Undeclared*
  - 7.6.10: Bioinorganic Chemistry of Platinum Anticancer Drugs; How Might They Work? (Part 2) - *Undeclared*
  - 7.6.11: Design of New Inorganic Anticancer Drugs - *Undeclared*
- Back Matter - *Undeclared*
  - Index - *Undeclared*
  - Glossary - *Undeclared*
  - Detailed Licensing - *Undeclared*